

65TH INTERNATIONAL
CONFERENCE FOR STUDENTS OF
PHYSICS AND NATURAL SCIENCES
MARCH 15th-18th

OPEN READINGS

2022

ABSTRACT BOOK

Vilnius University
VILNIUS UNIVERSITY PRESS

Editors
Šarūnas Mickus
Simona Pūkienė
Lukas Naimovičius

Cover and Interior design
Milda Stancikaitė

Vilnius University Press
9 Saulėtekio Av., III Building, LT-10222 Vilnius
info@leidykla.vu.lt, www.leidykla.vu.lt/en/
www.knygynas.vu.lt, www.journals.vu.lt

Bibliographic information is available
on the Lithuanian Integral Library Information System (LIBIS) portal ibiblioteka.lt.

ISBN 978-609-07-0722-7 (PDF)
© Vilnius University, 2022

Dear participants,

The 65th international conference for students of Physics and Natural sciences Open Readings 2022 brings together young researchers from all over the world. Open Readings 2022 is a virtual event where the conference attendees can share their work and ideas on an extensive range of topics and connect with one another. We hope that the conference participants will enjoy memorable lectures from world-class speakers and presentations from eager young scientists.

We wish you good luck in your scientific journey. Stay curious and creative.

Yours sincerely,

Open Readings 2022 Organizing Team



Conference Chair:

Vaida Marčiulionytė, *Faculty of Physics, Vilnius University, Optica & SPIE Chapter of Vilnius University*

Organizing Committee:

Gabrielė Kareivaitė, *Faculty of Physics, Vilnius University, Optica & SPIE Chapter of Vilnius University*

Simona Pūkienė, *Center for Physical Sciences and Technology, Optica Chapter of Vilnius University*

Bernadeta Labžentienė, *Faculty of Physics, Vilnius University, SPIE Chapter of Vilnius University*

Lukas Naimovičius, *Faculty of Physics, Vilnius University, SPIE Chapter of Vilnius University*

Rimantė Bandzevičiūtė, *Faculty of Physics, Vilnius University, Optica & SPIE Chapter of Vilnius University*

Živilė Čerškutė, *Faculty of Physics, Vilnius University, Optica & SPIE Chapter of Vilnius University*

Šarūnas Mickus, *Faculty of Physics, Vilnius University, SPIE Chapter of Vilnius University*

Aleksandra Širvinskytė, *Faculty of Physics, Vilnius University, SPIE Chapter of Vilnius University*

Laura Tauraitė, *Faculty of Physics, Vilnius University, Optica & SPIE Chapter of Vilnius University*

Jonas Banys, *Faculty of Physics, Vilnius University, SPIE Chapter of Vilnius University*

Erikas Atkočaitis, *Faculty of Physics, Vilnius University, Optica & SPIE Chapter of Vilnius University*

Dovilė Lengvinaitė, *Faculty of Physics, Vilnius University*

Rasa Platakytė, *Faculty of Physics, Vilnius University*

Martynas Velička, *Faculty of Physics, Vilnius University*

Gabrielė Stanionytė, *Faculty of Physics, Vilnius University*

Milda Stancikaitė, *Faculty of Physics, Vilnius University*

Programme Committee:

dr. Linas Vilčiauskas, *Department of Chemical Engineering and Technology, Center for Physical Sciences and Technology*

prof. Tomas Tamulevičius, *Institute of Materials Science of Kaunas University of Technology*

dr. Danielis Rutkauskas, *Department of Molecular Compound Physics, Center for Physical Sciences and Technology*

dr. Julius Vengelis, *Laser Research Center, Faculty of Physics, Vilnius University*

dr. Rasa Pauliukaitė, *Department of Nanoengineering, Center for Physical Sciences and Technology*

dr. Andrius Gelžinis, *Institute of Chemical Physics, Faculty of Physics, Vilnius University*

dr. Jurga Juodkazytė, *Department of Chemical Engineering and Technology, Center for Physical Sciences and Technology*

dr. Justinas Čeponkus, *Institute of Chemical Physics, Faculty of Physics, Vilnius University*

dr. Vytautas Jakštas, *Department of Physical Technologies, Center for Physical Sciences and Technology*

dr. Tomas Šalkus, *Institute of Applied Electrodynamics and Telecommunications, Faculty of Physics, Vilnius University*

dr. Ilja Ignatjev, *Department of Organic chemistry, Center for Physical Sciences and Technology*

dr. Ieva Matulaitienė, *Department of Organic chemistry, Center for Physical Sciences and Technology*

dr. Jurga Būdienė, *Department of Organic chemistry, Center for Physical Sciences and Technology*

dr. Algirdas Mikalkėnas, *Institute of Biosciences, Life Science Center*

Aidas Sadauskas, *Department of Fundamental Research, Center for Physical Sciences and Technology*

Enrika Celitan, *Institute of Biosciences, Life Science Center*

dr. Povilas Šimonis, *Department of Functional Materials and Electronics, Center for Physical Sciences and Technology*

dr. Aldona Balčiūnaitė, *Department of Catalysis, Center for Physical Sciences and Technology*

dr. Brigita Abakevičienė, *Institute of Materials Science of Kaunas University of Technology*

dr. Darius Gailevičius, *Laser Research Center, Faculty of Physics, Vilnius University*

dr. Jonas Berzinš, *Light Conversion*

dr. Paulius Baronas, *Institute of Photonics and Nanotechnology, Vilnius University*

dr. Mindaugas Kamarauskas, *Department of Physical Technologies, Center for Physical Sciences and Technology*

dr. Virginijus Bukauskas, *Department of Physical Technologies, Center for Physical Sciences and Technology*

dr. Irena Nedveckytė, *Institute of Biosciences, Life Science Center, Vilnius University*

dr. Martynas Velička, *Faculty of Physics, Vilnius University*

dr. Virginija Kalcienė, *Institute of Biosciences, Life Science Center, Vilnius University*

dr. Rasa Sabaliauskaitė, *Laboratory of Genetic Diagnostic, National Cancer Institute*

Chairmen:

dr. Kristijonas Genevičius, *Department of Solid State Electronics, Vilnius University*

prof. Tomas Tamulevičius, *Institute of Materials Science of Kaunas University of Technology*

dr. Paulius Baronas, *Institute of Photonics and Nanotechnology, Vilnius University*

dr. Vytautas Klimavičius, *Institute of Chemical Physics, Vilnius University*

prof. Audrius Dubietis, *Laser Research Center, Vilnius University*

dr. Audrius Alkauskas, *Electronic Structure Theory Laboratory, Center for Physical Sciences and Technology*

dr. Martynas Velička, *Faculty of Physics, Vilnius University*

dr. Linas Jonušauskas, *Vital3D Technologies, Vilnius, Lithuania*

dr. Renata Butkutė, *Department of Optoelectronics, Center for Physical Sciences and Technology*

Rasa Platakytė, *Institute of Chemical Physics, Faculty of Physics, Vilnius University*

dr. Mažena Mackoit-Sinkevičienė, *Faculty of Physics, Vilnius University*

Dovydas Banevičius, *Institute of Photonics and Nanotechnology, Vilnius University*

Andrius Žemaitis, *Department of Laser Technologies, Center for Physical Sciences and Technology*

dr. Sergėjus Balčiūnas, *Institute of applied electrodynamics and telecommunications, Faculty of Physics, Vilnius University*

dr. Andrius Gelžinis, *Institute of Chemical Physics, Faculty of Physics, Vilnius University*

dr. Virginijus Bukauskas, *Department of Physical Technologies, Center for Physical Sciences and Technology*

dr. Aldona Balčiūnaitė, *Department of Catalysis, Center for Physical Sciences and Technology*

dr. Jurga Būdienė, *Department of Organic chemistry, Center for Physical Sciences and Technology*

dr. Algirdas Mikalkėnas, *Institute of Biosciences, Life Science Center*

Enrika Celitan, *Institute of Biosciences, Life Science Center*

dr. Wanessa De Cassia Martins Antunes De Melo, *Department of Functional Materials and Electronics, Center for Physical Sciences and Technology*

SENSING AT THE ZEPTOMOLAR CONCENTRATION LEVEL WITH LARGE AREA BIOELECTRONIC INTERFACES

Luisa Torsi[1]

[1]Dipartimento di Chimica, Università degli Studi di Bari Aldo Moro, Via Orabona 4, 70125 Bari, Italy
luisa.torsi@uniba.it

Nanosized interfaces have been the favoured route to single-molecule detections so far. However, because of the so-called diffusion-barrier issue, such near-field approaches, encompassing nano-wire transistors but also nanopores and many others, are, not able to detect at concentrations lower than nanomolar. Bioelectronic field-effect transistors endowed with large-area (mm2 wide) detecting interfaces, are perceived as unsuited too, because the footprint of a single molecule is negligible when compared to a large detecting interface. This is challenging as it would be like detecting a single droplet impacting on a kilometer-wide surface. However, many different groups have published data proving that field-effect large-area biosensors can detect at limit-of-detection of femtomolar and below.

Moreover, these single-molecule large-area bioelectronic based technologies can involve small readers, are fast, easy to operate directly in the fluid to be analyzed, and the electronic outputs are already in a convenient digital form so that an easy transfer to app is possible. Moreover, they can be fabricated by cost-effective technologies including printing and other direct-writing processes. Hence, ultrasensitive large area bioelectronic sensors are likely to have a bright future in healthcare. This lecture will give an overview of this field, discussing device architectures, materials used, and target analytes that can be selectively detected as well as the sensing mechanisms.

---

[1] The 2021 flexible and printed electronics roadmap, Yvan Bonnassieux at al. Flexible and Printed Electronics, volume 6 (2), article number: 023001 (2022) DOI: 10.1088/2058-8585/abf986

[2] Electrolyte-gated transistors for enhanced performance bioelectronics, Fabrizio Torricelli et al. Nature Reviews Methods Primers, volume 1, Article number: 66 (2021) DOI:10.1038/s43586-021-00065-8

2D QUANTUM MATERIALS ON DEMAND: TWISTING, STACKING & DEFECT ENGINEERING

Ursula Wurstbauer[1]

[1]Institute of Physics, University of Münster, Wilhelm-Klemm-Str. 10, 48149 Münster, Germany
wurstbauer@wwu.de

Quantum materials are of increasing interest and relevance for technological applications as well as in fundamental sciences. Quantum materials host controllable quantum states and emerging phases driven by various interactions resulting in novel ground states that can only be described by quantum mechanics. For real quantum technological applications towards quantum computation, information or sensing, quantum states and phase are often hosted by solid state materials. Those materials can be precisely tailored and integrated in existing technology platforms. However, for conventional solid-state platforms it is challenging to reliably achieve a high level of control of a quantum states due to interactions with thousands of atoms around.

In this lecture we will introduce two-dimensional materials as highly promising quantum materials hosting quantum light sources, emerging quantum phases such as magnetism, superconductivity, superfluidity or Mott insulator. Interactions in those systems can be engineered by stacking different materials together, precisely adjusting the twist angles in between or by selectively inducing defects. In-situ control can be realized by external stimuli such as electric and magnetic fields, charge doping in field effect structures or strain. Followed by a general introduction to two-dimensional materials, we will focus on two recent developments of two-dimensional quantum materials: (I) Quantum light sources on demand by defect engineering and (II) competing phases and Mott-Hubbard physics in moiré superlattice structures such as magic angle graphene or twisted two-dimensional semiconductors hosting competing quantum phases. In those structures superconducting, magnetic ordered and Mott insulating ground states are close by and the systems can be tuned from one phase into the other e.g. in field effect structures.

UNEXPECTED CONNECTIONS IN PURE AND APPLIED RESEARCH

John Dudley[1]

[1]Université Bourgogne Franche-Comté, CNRS Institute FEMTO-ST, Besancon, France
john.dudley@univ-fcomte.fr

There is currently intense international debate concerning optimal ways to manage interactions between fundamental and applied research. However, although there is sometimes a tendency to view this as a modern problem, the same issues have occurred frequently during the history of scientific development. This talk will review some particular examples from nonlinear science, discussing unappreciated aspects of research in nonlinear soliton physics, spanning the 19th century laying of the transatlantic cable, the Manhattan Project, the 2005 and 2009 Nobel Prizes in physics, the latest techniques in medical diagnostics and the detection of extra-solar planets. We will also see how these developments are leading to dramatic developments in nonlinear optics and fundamental advances in the understanding of nonlinear light - matter interactions, new approaches for ultrafast laser design, and leading to some surprising applications in other fields of physics. The talk will consider technical aspects of wave propagation and nonlinear photonics, but will be sprinkled with historical anecdotes and thus will be suitable for a general audience.

MOLECULAR SOLAR THERMAL ENERGY STORAGE SYSTEMS

Kasper Moth-Poulsen[1]

[1]Department of Chemistry and Chemical Engineering, Chalmers University of Technology, Gothenburg, Sweden
Kasper.moth-poulsen@chalmers.se

Norbornadiene (NBD) and its derivatives undergo photoisomerisation to the highly strained quadricyclane (QC). The system is being optimized towards solar energy storage applications, and the best NBD derivatives fulfil several of the requirements for a functional system,[1-5] such as high photoisomerisation quantum yield (up to 99%), red-shifted absorption, high energy storage densities (up to 1 MJ/kg)3, very long half-life, up to 18 years of storage time[2] and a record temperature gradient of 63°C (83°C measured)[1]. However, several key challenges remain; for example, substituents needed to improve the solar spectrum match and quantum yield of unsubstituted norbornadiene typically reduce the energy density. While unsubstituted norbornadiene is a liquid, most of the higher performing derivatives are solids at room temperature, and the characterization has typically only been done in dilute solution for practical reasons.[4,5] The use of solvents dilutes the effective energy densities of the systems significantly. In this presentation, our efforts in improving the NBD/QC system towards efficient energy storage systems including new ways to improve solar spectrum match and energy storage time without making compromises on energy storage densities will be presented.[5] Moreover, I will present device concepts for lab scale demonstration of solar energy capture (up to 900 cm^2 devices) as well as heat release devices based on molecular photoswitches that perhaps one day can be used in real life application in solar energy storage.

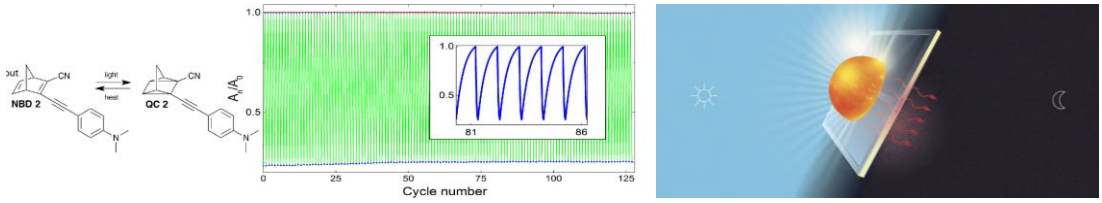


Fig. 1. (Left) Molecular structure of on NBD/QC photoswitch system. (Centre) Stability test performed at 60°C through 127 energy storage cycles (right) Illustration of a future MOST window concept.

[1] Zhihang Wang et al. "Macroscopic Heat Release in a Molecular Solar Thermal Energy Storage System" Energy and Environmental Science, 2019, 12, 187-193. (cover)
[2] Martyn Jevric et al. "Norbornadiene-based photoswitches with exceptional combination of solar spectrum match and long term energy storage" Chemistry a European Journal 2018 24 (49), 12767-12772. (frontispiece)
[3] Mads Mansø et al. "Molecular Solar Thermal Energy Storage in photoswitch oligomers increases energy densities and storage times" Nature Communications 2018, 9:1945.
[4] Ambra Dreos et al. "Liquid Norbornadiene Photoswitches for Solar Energy Storage" Advanced Energy Mater. 2018, 8 (18), 1703401. (cover)
[5] Ambra Dreos et al. "Exploring the potential of a hybrid device combining solar water heating and molecular solar thermal energy storage" Energy and Environmental Science 2017, 10, 728-734. (cover)
[6] Anne Ugleholdt Petersen et al. "Solar energy storage by molecular Norbornadiene-Quadricyclane photoswitches: polymer film devices" Advanced Science, 2019, 1900367.

NETWORKS POWERED BY QUANTUM ENTANGLEMENT: FROM A LOOPHOLE-FREE BELL TEST TO A QUANTUM INTERNET

Ronald Hanson[1]

[1]QuTech and Kavli Institute of Nanoscience, Delft University of Technology, The Netherlands
R.Hanson@tudelft.nl

Entanglement – the property that particles can share a single quantum state - is arguably the most counterintuitive yet potentially most powerful element in quantum theory. The non-local features of quantum theory are highlighted by the conflict between entanglement and local causality discovered by John Bell. Decades of Bell inequality tests, culminating in a series of loophole-free tests in 2015, have confirmed the non-locality of nature [1].

Future quantum networks [2] may harness these unique features of entanglement in a range of exciting applications, such as blind quantum computation, secure communication, enhanced metrology for astronomy and time-keeping as well as fundamental investigations. To fulfil these promises, a strong worldwide effort is ongoing to gain precise control over the full quantum dynamics of multi-particle nodes and to wire them up using quantum-photonic channels.

Here I will briefly introduce the field of quantum networks. I will then discuss our most recent work [3], demonstrating the realization of the first multi-node network wired by quantum entanglement, based on optically connected solid-state chips, including first primitive network protocols, and provide an outlook towards the coming years.

---

[1] For a popular account of these experiments, see e.g. Ronald Hanson and Krister Shalm, Scientific American 319, 58-65 (2018).

[2] Quantum internet: A vision for the road ahead, S Wehner, D Elkouss, R Hanson, Science 362 (6412), eaam9288 (2018).

[3] Realization of a multi-node quantum network of remote solid-state qubits, M. Pompili, S.L.N. Hermans, S. Baier et al., Science 372, 259-264 (2021).

HYBRID MATERIALS: FROM EXOTIC STRUCTURAL PHASES TO QUANTUM EFFECTS

Mantas Šimėnas[1,2*], Sergejus Balčiūnas[1], Šarūnas Svirskas[1], Martynas Kinka[1], Vidmantas Kalendra[1], Anna Gągor[3], Adam Sieradzki[4], Robertas Grigalaitis[1], Andreas Pöppl[5], Gunnar Jeschke[6], Aron Walsh[7], Miroslaw Mączka[3], Jūras Banys[1]

[1] Faculty of Physics, Vilnius University, Sauletekio 9, LT-10222 Vilnius, Lithuania
[2] London Centre for Nanotechnology, University College London, 17–19 Gordon Street, London WC1H 0AH, UK
[3] Polish Academy of Sciences, Institute of Low Temperature and Structure Research, PL-50-950 Wroclaw 2, Poland
[4] Wroclaw University of Science and Technology, Wybrzeze Wyspianskiego 27, 50-370 Wroclaw, Poland
[5] Leipzig University, Felix Bloch Institute for Solid State Physics, Linnestrasse 5, D-04103 Leipzig, Germany
[6] ETH-Zürich, Department of Chemistry and Applied Biosciences, Vladimir-Prelog-Weg 2, 8093 Zürich, Switzerland
[7] Imperial College London, Thomas Young Centre and Department of Materials, SW72AZ London, UK
mantas.simenas@ff.vu.lt

Recently, hybrid organic-inorganic materials attracted exceptional attention due to their remarkable gas sorption, optoelectronic, multiferroic, barocaloric and other functional properties originating from a tight interplay between the organic and inorganic motifs.

A highly promising class of such materials is AMX_3 hybrid perovskites, where A denotes an organic molecular cation, M is a metal ion, and X represents an organic or inorganic anionic linker. Among hybrid perovskites, metal formate frameworks $[A][M(HCOO)_3]$ and lead halides $APbX_3$ (X = Cl, Br, I) (see Fig. 1) are the most promising families due to their multiferroic and photovoltaic properties, respectively. The majority of these compounds exhibit structural phase transitions followed by the molecular cation ordering and framework deformation [1].

Another class of interesting hybrid materials is metal-organic frameworks (MOFs), which exhibit remarkable porosity utilizable for gas absorption, catalysis and chemical sensing. The organic linkers in MOFs are embedded in a porous crystalline lattice providing a handle to tune their dynamic behaviour, which in turn can affect the chemical and physical properties of these compounds [1].

Here, we use a multitechnique experimental and theoretical approach to study the aforementioned phenomena in hybrid perovskites and MOFs. The EPR and dielectric spectroscopies are used to elucidate the cation dynamics, phase transition mechanism, lattice distortion and possible ferroelectric nature of metal formate frameworks. In addition, we show that EPR spectroscopy can be used to excite and read the methyl group tunnel coherence in this class of compounds [2]. We also use the broadband dielectric, ultrasonic and vibrational spectroscopies to probe frustration of electric dipoles and determine phase diagrams of mixed-cation lead halide perovskites revealing signatures of a peculiar dipolar glass phase [3,4].

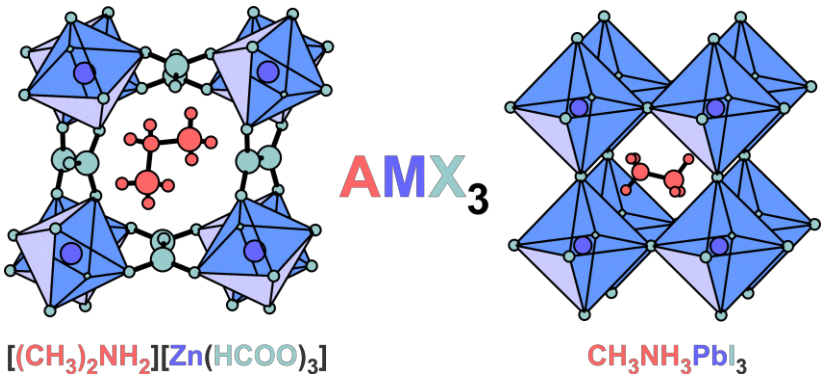


Fig. 1. Representatives of formate (left) and lead halide (right) hybrid perovskites investigated in this work.

[1] M. Ptak, A. Sieradzki, M. Šimėnas, M. Maczka, Molecular spectroscopy of hybrid organic-inorganic perovskites and related compounds, Coord. Chem. Rev. **448**, 214180 (2021).
[2] M. Šimėnas, D. Klose, M. Ptak, K. Aidas, M. Mączka, J. Banys, A. Pöppl, G. Jeschke, Magnetic excitation and readout of methyl group tunnel coherence, Sci. Adv. **6**, eaba1517 (2020).
[3] M. Šimėnas, S. Balčiūnas, S. Svirskas, M. Kinka, M. Ptak, V. Kalendra, A. Gągor, D. Szewczyk, A. Sieradzki, R. Grigalaitis, A. Walsh, M. Mączka, J. Banys, Phase Diagram and Cation Dynamics of Mixed $MA_{1-x}FA_xPbBr_3$ Hybrid Perovskites, Chem. Mater. **33**, 5926 (2021).
[4] M. Šimėnas, S. Balčiūnas, J. N. Wilson, S. Svirskas, M. Kinka, A. Garbaras, V. Kalendra, A. Gagor, A. Szewczyk, A. Sieradzki, M. Maczka, V. Samulionis, A. Walsh, R. Grigalaitis, J. Banys, Suppression of phase transitions and glass phase signatures in mixed cation halide perovskites, Nat. Comm. **11**, 5103 (2020).

SHINING NEW LIGHT INTO SOIL SYSTEMS: ADVANCED SPECTROSCOPY METHODS HELP US TACKLE ENVIRONMENTAL CHALLENGES

Milda Pučetaitė[1]

[1]Department of Biology, Lund University, Lund, Sweden
milda.pucetaite@biol.lu.se

Human activity-induced climate change, among many other environmental challenges, is not anymore a distant future, but a threatening reality. While grants and rewards are offered for carbon capture and storage solutions which could reduce net CO2 emissions, not many of us know that the biggest carbon pool lies directly under our feet. Soils store more carbon than the atmosphere and the biosphere combined, and research suggests that they could serve as reservoirs for further carbon sequestration and climate change mitigation. Increased understanding of biotic and abiotic biogeochemical processes taking place in soils is, therefore, key to identify cultivation and management techniques that will both secure soil fertility and increase its carbon sink potential.

High physical and chemical heterogeneity, variability both at the micro- and macroscale, and lack of optical access makes soils extremely difficult to study. Various advanced spectroscopy methods, particularly in combination with microfluidic technology that literally serves as a window to the underground, are now providing new opportunities to look into the biogeochemistry of soils. With soil microbes governing many of the related processes, in my research I use synchrotron-based X-ray techniques as well as vibrational microspectroscopy to answer questions such as: what are the chemical responses of the microbes to environmental triggers and how do they influence soil functioning under the changing climate? How do environmental factors influence microbial decomposition and thus carbon dynamics in soils? And more generally, what are the necessary analytical developments to gain better insights into soil systems and their potential to tackle environmental challenges.

15 March, TUESDAY

09:00 Luisa Torsi
SENSING AT THE ZEPTOMOLAR CONCENTRATION LEVEL WITH LARGE AREA BIOELECTRONIC INTERFACES

10:00 BREAK

ORAL SESSION O1

10:15	Vladislovas Čižas, Kirill Alekseev, Gintaras Valušis EXPERIMENTAL EVIDENCE OF THE NONDEGENERATE PARAMETRIC GAIN IN QUANTUM SUPERLATTICES	O1-1	30
10:30	Juzef Kučinski, Hsin Tseng, Lina Mikoliūnaitė, Karl Leo, Hans Kleemann STATISTICAL ANALYSIS OF ORGANIC ELECTROCHEMICAL TRANSISTORS WITH PHOTOPATTERNABLE SOLID ELECTROLYTE	O1-2	31
10:45	Andrea Zelioli, Arnas Pukinskas, Algirdas Jasinskas, Simona Pūkienė, Silvija Keraitytė, Arnas Naujokaitis, Martynas Skapas, Monika Jokubauskaitė, Evelina Dudutienė, Artūras Suchodolskis, Bronislovas Čechavičius, Renata Butkutė OPTIMIZATION OF QUANTUM WELL GROWTH TECHNOLOGY FOR APPLICATIONS IN NEAR INFRARED VERTICAL-EXTERNAL-CAVITY SURFACE-EMITTING LASERS	O1-3	32
11:00	Vytautas Žalandauskas, Marek Maciaszek, Lukas Razinkovas, Audrius Alkauskas THE APPLICATION OF THE SCAN DENSITY FUNCTIONAL TO COLOUR CENTRES IN DIAMOND	O1-4	33
11:15	Elena Valkiūnaitė, Jūras Mickevičius STUDY OF LUMINESCENCE SPECTRA DECAY IN NONPOLAR INGAN/GAN MQWS	O1-5	34

ORAL SESSION O2

10:15	Agnieszka Domagała, Ewa Machalska, Grzegorz Zając, Małgorzata Barańska ECD-RAMAN EFFECT AS A NEW PHENOMENON IN CHIROPTICAL SPECTROSCOPY	O2-1	35
10:30	Katarzyna Gorczowska, Ewa Machalska, Malgorzata Baranska RAMAN OPTICAL ACTIVITY OF POLYENE ANTIBIOTICS: PRE-RESONANCE SIGNAL ENHANCEMENT DUE TO AGGREGATION PROCESS	O2-2	36
10:45	Eglė Tankelevičiūtė, Paulius Baronas, Regimantas Komskis, Povilas Adomėnas, Ona Adomėnienė, Saulius Juršėnas INVESTIGATION OF INTERSYSTEM CROSSING IN OLIGOYNES	O2-3	37
11:00	Jasper Ristkok, Indrek Jõgi, Peeter Paris FULFILLMENT OF LOCAL THERMODYNAMIC EQUILIBRIUM IN ARGON ENVIRONMENT FOR CALIBRATION-FREE LIBS MEASUREMENT OF HYDROGEN ISOTOPES	O2-4	38
11:15	Natalia Chorąży, Magdalena Sternak, Agnieszka Kaczor, Stefan Chlopicki, Marta Pacia LIPID DROPLETS IN ACTIVATED ENDOTHELIUM IN ISOLATED BLOOD VESSELS - IMAGING OF BIOCHEMICAL ALTERATIONS USING RAMAN SPECTROSCOPY AND FLUORESCENCE MICROSCOPY	O2-5	39

11:30 BREAK

ORAL SESSION O3

11:45	Did not participate	O3-1	40
12:00	Matas Tartėnas, Kastytis Zubovas A MORE REALISTIC BLACK HOLE ACCRETION TREATMENT FOR NUMERICAL SIMULATIONS	O3-2	41
12:15	Marcos Muñiz Cueli, Laura Bonavera, Joaquin Gonzalez-Nuevo, David Crespo, José Manuel Casas, Andrea Lapi, Tommaso Ronconi, Marina Migliaccio COSMOLOGICAL CONSTRAINTS FROM A TOMOGRAPHIC ANALYSIS OF THE SUBMILLIMETER GALAXY MAGNIFICATION BIAS	O3-3	42
12:30	Martynas Laužikas, Kastytis Zubovas EVOLUTION OF MOLECULAR CLOUDS ABLATED BY AGN-DRIVEN OUTFLOWS: EFFECT OF TURBULENCE	O3-4	43
12:45	Kristers Nagainis, Ilgmārs Eglītis NEO OBSERVATIONS AND THEIR ROTATION PERIOD DETERMINATION	O3-5	44
13:00	Cormac Larkin, Scott Trager, Kristiina Verro, Anaïs Gonneau FUNDAMENTAL STELLAR PARAMETERS FOR 222 B-TYPE STARS FOR THE X-SHOOTER SPECTRAL LIBRARY	O3-6	45

ORAL SESSION O4

11:45	Yatinkumar Patel, Arvydas Palevicius, Giedrius Janusas FABRICATION AND CHARACTERIZATION OF NANOPOROUS ANODIC ALUMINA MEMBRANE FOR NANOFILTRATION APPLIATION	O4-1	46
12:00	Kernius Vilkevičius, Evaldas Stankevičius SINGLE-PULSE FEMTOSECOND LASER FABRICATION OF CONICAL AND ANTENNA-LIKE STRUCTURES ON THIN GOLD FILM	O4-2	47
12:15	Daniela Kujawa, Daria Szewczyk, Vitalii Boiko, Damian Bęben, Paweł Głuchowski EFFECT OF GRAPHENE ADDITION ON THE THERMAL AND PERSISTENT LUMINESCENCE PROPERTIES OF THE GD2.994CE0.006GA3AL2O12 AND GD2.964CE0.006DY0.03GA3AL2O12 CERAMICS	O4-3	48
12:30	Yaraslau Padrez, Lena Golubewa, Tatsiana Kulahava, Boris Zousman, Olga Levinson, Renata Karpicz, Yuri Svirko, Polina Kuzhir STEADY-STATE SPECTROSCOPIC PROPERTIES OF MAGNETIC NANODIAMONDS	O4-4	49
12:45	Maciej Nowagiel, Tomasz K. Pietrzak, Tomasz Płociński, Julien Trébosc, Olivier Lafon, Marek Wasiucionek, Jerzy E. Garbarczyk THERMAL NANOCRYSTALLIZATION OF BISMUTH OXIDE GLASSES	O4-5	50
13:00	Magdalena Bartolewska, Monika Biernat, Maciej Mazur, Marcin Wasylewski POLY (LACTIC ACID)/HYDROXYAPATITE (PLA/HAP) POROUS COMPOSITE WITH INORGANIC NANOPARTICLES FOR BONE REGENERATION	O4-6	51

13:15 **TIME FOR INDUSTRY**

15:00 BREAK

15:15-16:00 **POSTER SESSION P1**

16:00 BREAK

16:15-17:00 **POSTER SESSION P2**

16 March, WEDNESDAY

09:00 Ursula Wurstbauer
2D QUANTUM MATERIALS ON DEMAND: TWISTING, STACKING & DEFECT ENGINEERING

10:00 BREAK

ORAL SESSION O5

10:15	Wafaa Khater, Anton Kunčinas, Odd Magne Øgreid, Per Osland, Margarida Nesbitt Rebelo DARK MATTER IN THREE-HIGGS-DOUBLET MODELS WITH S3 SYMMETRY	O5-1	52
10:30	Einaras Sipavičius, Kęstutis Aidas MOLECULAR DYNAMICS MODELLING OF INTERMOLECULAR STRUCTURE OF AQUEOUS MIXTURES OF 1-BUTYL-3-METHYLIMIDAZOLIUM NITRATE IONIC LIQUID	O5-2	53
10:45	Joanna Marciniak, Wojciech Marciniak, Mirosław Werwiński MAGNETIC PROPERTIES OF BULK AND THIN FILMS OF FEPT L10 PHASE FROM DENSITY FUNCTIONAL THEORY CALCULATIONS	O5-3	54
11:00	Ewelina Lange, Grzegorz Chimczak, Anna Kowalewska-Kudłaszyk CLASSICAL AND QUANTUM EXCEPTIONAL POINTS IN NON-HERMITIAN BOSONIC SYSTEMS	O5-4	55
11:15	Marcin Klempka, Sebastian Wilman, Magdalena Elantkowska, Jarosław Ruczkowski SEMI-EMPIRICAL PREDICTIONS OF ENERGY LEVELS AND HYPERFINE STRUCTURE FOR THE ODD-PARITY CONFIGURATIONS SYSTEM OF HO II	O5-5	56

ORAL SESSION O6

10:15	Andrius Pakalniškis, Ramūnas Skaudžius, Dmitry Karpinsky, Gediminas Niaura, Aivaras Kareiva INVESTIGATION OF HIGH-PRESSURE EFFECTS ON STRUCTURAL AND MAGNETIC PROPERTIES OF MULTIFERROIC SM DOPED BIFEO3	O6-1	57
10:30	Karolina Olszewska, Izebella Jastrzębska, Rosa Santillan, Tomasz Runka RAMAN SPECTROSCOPY INVESTIGATION OF MOLECULAR ROTORS WITH STEROIDAL STATORS, AND 1,4-DIETHYNYLPHENYLENE ROTATOR SUBSTITUTED WITH FLUORINE	O6-2	58
10:45	Taras Zhezhera, Pawel Gluchowski, Marek Nowicki, Maciej Chrunik, Andrzej Majchrowski and Dobroslawa Kasprowicz SPECTROSCOPIC PROPERTIES OF BI3TEBO9 MICROCRYSTALLINE POWDERS DOPED WITH RARE EARTH IONS	O6-3	59
11:00	Jurga Jeršovaitė, Ugnė Šarachovaitė, Arnoldas Solovjovas, Daiva Baltriukienė, Mangirdas Malinauskas OPTICAL PRINTING OF 3D MICROPOROUS SCAFFOLDS, THEIR BIOCOMPATIBILITY EVALUATION AND ENHANCEMENT IN VITRO	O6-4	60
11:15	Maliha Parvin, Milda Petrulevičienė, Irena Savickaja, Arnas Naujokaitis, Vidas Pakštas,Jurga Juodkazytė WO3 PHOTOANODE FOR ADVANCED OXIDATION PROCESSES.	O6-5	61

11:30 BREAK

ORAL SESSION O7

11:45	Carl A. Fogarty, Aoife M. Harbison, Toan K. Phung, Akash Satheesan, Benjamin L. Schulz, Elisa Fadda FINE-TUNING THE SPIKE: ROLE OF THE NATURE AND TOPOLOGY OF THE GLYCAN SHIELD IN THE STRUCTURE AND DYNAMICS OF SARS-COV-2	O7-1	62
12:00	Marta Lotka EEG SIGNAL SEGMENTATION FOR HUMAN RESPONSE DETECTION	O7-2	63
12:15	Pedro Oliveira Corda, Joana Vieira Silva, Sara Catarina Pereira, Alberto Barros, Marco Alves, Margarida Fardilha THROUGHS THE CRYOPRESERVED SPERM PROTEOME: A BIOINFORMATIC APPROACH TO IDENTIFY RELEVANT DIFFERENTIALLY EXPRESSED PROTEINS	O7-3	64
12:30	Mariia Oleksiivna Yurchikova, Daria Sergiivna Ponomariova, Anatoliy Ivanovich Dragan STUDY OF SARS-COV-2 SPECIFIC MPRO PROTEASE AND INTERACTIONS OF ITS CATALYTIC CENTER WITH POTENTIAL INHIBITORS	O7-4	65
12:45	Dr. John Healy, Dr. Orla Slattery, Dr. Joan O'Keeffe, and Michela Caprani (Myself, Ph.D.) AN INVESTIGATION INTO THE BIOCHEMICAL AND PHYSIOCHEMICAL FREQUENCIES DISTRIBUTIONS OF AMP FAMILIES.	O7-5	66
13:00	Daria Ponomariova, Mariia Yurchikova, Anatoliy Dragan STUDY OF SARS COV 2 MPRO DIMERIZATION SITE AND ITS INTERACTIONS WITH POTENTIAL INHIBITORS	O7-6	67

ORAL SESSION O8

11:45	Domantas Vizbaras, Kęstutis Ikamas, Andrey A. Generalov, Alvydas Lisauskas TRUE ZERO-BIAS THZ DETECTOR WITH GRAPHENE FIELD-EFFECT TRANSISTOR	O8-1	68
12:00	Lukas Naimovičius, Edvinas Radiunas, Barbara Chatinovska, Augustina Jozeliūnaitė, Edvinas Orentas, Karolis Kazlauskas MODIFIED DIKETOPYRROLOPYRROLE EMITTERS FOR TUNABLE NIR-TO-VISIBLE PHOTON UPCONVERSION	O8-2	69
12:15	Kazimieras Badokas, Dominykas Augulis, Arūnas Kadys, Jūras Mickevičius, Ilja Ignatjev, Benjaminas Šebeka, Martynas Skapas, Giedrius Juška, Tadas Malinauskas MOVPE OF GAN ON GRAPHENE-COVERED GAN/SAPPHIRE TEMPLATES	O8-3	70
12:30	Arnas Pukinskas, Nerijus Jurkūnas, Silvija Keraitytė, Algirdas Jasinskas, Andrea Zelioli, Simona Pūkienė, Andrius Bičiūnas, Bronislovas Čechavičius, Arnas Naujokaitis, Martynas Skapas, Monika Jokubauskaitė, Evelina Dudutienė, and Renata Butkutė IN-SITU QUANTUM DOTS FORMATION IN MBE USING SEGREGATION PROCESS	O8-4	71
12:45	Ewelina Nowak, Alicja Stachowiak, Daria Piechowiak, Jan Raczyński, Edyta Chłopocka THE COPPER INFLUENCE ON ZNO STRUCTURAL AND OPTICAL PROPERTIES	O8-5	72
13:15	BREAK		
14:00	John Dudley UNEXPECTED CONNECTION IN PURE AND APPLIED RESEARCH		
15:00	BREAK		
15:15-16:00	**POSTER SESSION P3**		
16:00	BREAK		
16:30	Isaiah Hankel SUCCESSFUL CAREER AFTER THE UNIVERSITY STUDIES		

17 March, THURSDAY

09:00	Kasper Moth-Poulsen MOLECULAR SOLAR THERMAL ENERGY STORAGE SYSTEMS		
10:00	BREAK		
	ORAL SESSION O9		
10:15	Ernesta Bužavaitė-Vertelienė, Ieva Plikusienė, Vincentas Mačiulis, Audrius Valavičius, Almira Ramanavičienė, Zigmas Balevičius TAMM PLASMONS AND CAVITY MODES FOR BIOSENSING APPLICATION IN A COMBINED SPECTROSCOPIC ELLIPSOMETRY AND QUARTZ CRYSTAL MICROBALANCE METHOD	O9-1	73
10:30	Evaldas Kažukauskas, Simas Butkus, Vytautas Jukna, Domas Paipulas and Valdas Sirutkaitis NUMERICAL SIMULATIONS AND EXPERIMENTAL ANALYSIS OF SCANNING TECHNIQUES FOR LOW-ROUGHNESS SURFACES USING UV FEMTOSECOND PULSES	O9-2	74
10:45	Marius Navickas, Robertas Grigutis, Gintaras Tamošauskas, Vytautas Jukna, Audrius Dubietis FEMTOSECOND LASER-INDUCED PERIODIC SURFACE STRUCTURES ON FUSED SILICA WITH TUNABLE-WAVELENGTH PULSES	O9-3	75
11:00	Gaudenis Jansonas, Rimantas Budriūnas, Arūnas Varanavičius NUMERICALLY PROCESSED INTERFEROMETRIC NONLINEAR REFRACTIVE INDEX MEASUREMENTS IN THE SPECTRAL RANGE FROM 1MM TO 3MM	O9-4	76
	ORAL SESSION O10		
10:15	Karolina Maleckaitė, Domantas Narkevičius, Rugilė Žilėnaitė, Jelena Dodonova-Vaitkūnienė, Stepas Toliautas, Sigitas Tumkevičius, Aurimas Vyšniauskas THE IMPACT OF ELECTRON-DONATING/-WITHDRAWING GROUPS ON RED-FLUORESCENT BODIPY MOLECULAR ROTOR	O10-1	77
10:30	Julija Grigorjevaite, Arturas Katelnikovas OPTICAL PROPERTIES IVESTIGATION OF K2GD(PO4)(WO4):10% YB3+ 20% TB3+, XEU3+ AS A FUNCTION OF EU3+	O10-2	78
10:45	Agata Jarocka, Paweł Dębowski, Bartosz Fetliński, Tomasz Karol Pietrzak, Marek Wasiucionek CONTROL OF THE EUROPIUM OXIDATION STATES IN THE GLASS MATRIX AND ITS INFLUENCE ON THE PHOTOLUMINESCENCE SPECTRA	O10-3	79
11:30	BREAK		
	ORAL SESSION O11		
11:45	Dominyka Stonytė, Vytautas Jukna, Domas Paipulas RESULTS ON ABLATION OF WIDE BAND-GAP MATERIALS WITH FEMTOSECOND UV LASER PULSES AT LINEAR ABSORPTION REGIME	O11-1	80

12:00	Rodrigas Liudvinavičius, Evaldas Stankevičius LASER DIRECT WRITING FOR THE FORMATION OF LARGE-SCALE SILVER MICROBUMPS ARRAYS	O11-2	81
12:15	Jonas Banys, Ona Balachninaitė, Viktorija Tamulienė, Vygandas Jarutis, Justina Savickytė, Simona Armalytė, Julius Vengelis PERFORMANCE INVESTIGATION OF OPTICAL PARAMETRIC GENERATOR BASED ON PERIODICALLY POLED LITHIUM NIOBATE CRYSTAL PUMPED BY SUBNANOSECOND MICRO-LASER PULSES	O11-3	82
12:30	Karolis Adomavičius, Austėja Trečiokaitė, Dawid Borycki, Slawomir Tomczewski, Piotr Wegrzyn, Ieva Žičkienė, Maciej Wojtkowski, Egidijus Auksorius CROSSTALK REDUCTION WITH A MULTIMODE FIBER IN FOURIER-DOMAIN FULL-FIELD OPTICAL COHERENCE TOMOGRAPHY	O11-4	83
12:45	Aivaras Kazakevičius, Raimundas Burokas, Audrius Zaukevičius, Rokas Danilevičius, Andrejus Michailovas 10 MJ, 20 HZ SUB-PICOSECOND HYBRID LASER SYSTEM	O11-5	84
	ORAL SESSION O12		
11:45	Radka Lencová, Andrea Frejlachová, Jan Ženka CANCER IMMUNOTHERAPY OF PANCREATIC ADENOCARCINOMA: EFFICACY, LIMITATIONS, AND SIDE EFFECTS	O12-1	85
12:00	Ewa Michalska CHANGES IN PLANT DISTRIBUTION IN THE FACE OF CLIMATE CHANGE - THE CASE OF ORCHIDS	O12-2	86
12:15	Margarita Kazak, Dovilė Bukauskaitė, Rimgaudas Treinys, Rasa Bernotienė TRYPANOSOMATIDS IN WILD-CAUGHT BITING MIDGES (CULICOIDES) FROM THE NESTS OF RAPTOR BIRDS	O12-3	87
12:30	Eglė Žalytė, Jonas Cicėnas STARVATION MEDIATES PANCREATIC CANCER CELL SENSITIVITY TO FERROPTOSIS VIA ERK1/2, JNK AND CHANGES IN CELL MESENCHYMAL STATE	O12-4	88
12:45	Karolina Barčauskaitė, Ieva Čalkaitė, Antony Szumny, Vita Tilvikienė HARVEST TIME EFFECT ON CANNABINOIDS PROFILE CHANGES IN CANNABIS SATIVA L. PLANTS	O12-5	89
13:00	Justyna Rewak-Soroczynska, Paulina Sobierajska, Rafal J. Wiglusz ANTIMICROBIAL ACTIVITY OF NANOCRYSTALLINE HYDROXYAPATITES DOPED AND CO-DOPED WITH ZN2+ AND CU2+ IONS AGAINST GRAM-NEGATIVE BACTERIA	O12-6	90
13:15	BREAK		
14:00	Ronald Hanson NETWORKS POWERED BY QUANTUM ENTANGLEMENT: FROM A LOOPHOLE-FREE BELL TEST TO A QUANTUM INTERNET		
15:00	BREAK		
15:15-16:00	**POSTER SESSION P4**		
16:00	BREAK		
16:15-17:00	**POSTER SESSION P5**		

18 March, FRIDAY

09:00	Mantas Šimėnas HYBRID MATERIALS: FROM EXOTIC STRUCTURAL PHASES TO QUANTUM EFFECTS		
10:00	BREAK		
	ORAL SESSION O13		
10:15	Sergej Charkavliuk, Veronika Borutinskaitė STUDY OF POTENTIAL NEW DRUG COMBINATIONS FOR TREATMENT OF RESISTANT LEUKEMIA CASES	O13-1	91
10:30	Veronika Malyško-Ptašinskė, Eivina Radzevičiūtė DYNAMIC NUMERICAL MODELLING OF TUMOR TISSUE ELECTROPORATION	O13-2	92
10:45	Monika Navickaitė, Ramunė Stanevičienė, Juliana Lukša, Elena Servienė, Jolanta Sereikaitė PURIFICATION AND THE IDENTIFICATION OF PHYSICAL AND CHEMICAL PROPERTIES OF SACCHAROMYCES CEREVISIAE K2 TOXIN	O13-3	93
11:00	Edvinas Navakauskas, Simona Strazdaitė HOW DOES DEUTERATION OF THE PHOSPHOLIPID AFFECT ITS MONOLAYERS PROPERTIES?	O13-4	94
11:15	Kristupas Paulius, Aleksandras Konovalovas, Saulius Serva BIO-POTPOURRI OF SACCHAROMYCETALES KILLER YEASTS	O13-5	95

ORAL SESSION O14

10:15	Barbara Chatinovska, Edvinas Orentas TOWARDS THE SCALABLE TOTAL SYNTHESIS OF SARPAGINE FAMILY ALKALOIDS	O14-1	96
10:30	Monika Baublytė, Denis Sokol, Ramūnas Skaudžius SYNTHESIS AND ANALYSIS OF GDPO4·H2O:EU MODIFIED WOOD	O14-2	97
10:45	Greta Inkrataitė, Meldra Kemere, Anatolijs Sarakovskis, Ramūnas Skaudžius THE EFFECT OF BORON DOPING ON LUMINESCENCE OF YAG AND LUAG POWDER, CERAMIC AND THIN FILMS	O14-3	98
11:00	Dovydas Karoblis, Aleksej Žarkov, Ramūnas Diliautas, Kęstutis Mažeika, Dalis Baltrūnas, Gediminas Niaura, Martynas Talaikis, Edita Garškaitė, Aldona Beganskienė, Aivaras Kareiva STRUCTURAL, MORPHOLOGICAL, AND MAGNETIC INVESTIGATION OF VARIOUS PEROVSKITE-TYPE SOLID SOLUTIONS	O14-4	99
11:15	Sukomol Barua, Aldona Balčiūnaitė, Loreta Tamašauskaite-Tamašiūnaitė, Eugenijus Norkus THREE-DIMENSIONAL AU(NIMO)/TI CATALYSTS FOR EFFICIENT OXYGEN EVOLUTION	O14-5	100
11:30	BREAK		

ORAL SESSION O15

11:45	Wojciech Marciniak, Joanna Marciniak, Jonasz Łasut-Balcerzak, Karolina Olszewska, Arkadiusz Ptak COMBINED RAMAN SPECTROSCOPY AND BROAD RANGE DENSITY FUNCTIONAL THEORY ANALYSIS OF INOSITOL PHOSPHATES AND THEIR CONFORMATIONS	O15-1	101
12:00	Veronika Prepilková, Katarína Trnková, Juraj Poništ THE BACTERIAL POPULATION IN DRAINAGE WATER FROM TAILINGS POND IN HODRUŠA-HÁMRE (SLOVAKIA)	O15-2	102
12:15	Greta Gančytė, Povilas Šimonis, Arūnas Stirkė ENHANCEMENT AND REVERSION OF IRREVERSIBLE ELECTROPORATION VIA OSMOTIC SHOCK TREATMENT	O15-3	103
12:30	Alėja Marija Daugėlaitė, Greta Jarockytė, Artiom Skripka, Vilius Poderys, Vitalijus Karabanovas, Fiorenzo Vetrone, Ričardas Rotomskis HUMAN DERMAL MESENCHYMAL STEM CELLS AS NANOPARTICLES VEHICLES	O15-4	104
12:45	Neringa Barauskaitė, Paulius Ruzgys, Vitalij Novickij, Saulius Šatkauskas BYSTANDER EFFECT TRIGGERED BY CALCIUM ELECTROPORATION, BLEOMYCIN ELECTROTRANSFER AND IRREVERSIBLE ELECTROPORATION	O15-5	105
13:00	Kseniia Yutilova, Elena Shved THE EFFECT OF STRUCTURE OF TERTIARY AMINE ON THE ACETOLYSIS OF 2-(CHLOROMETHYL)OXIRANE: AB INITIO AND EXPERIMENTAL STUDY	O15-6	106

ORAL SESSION O16

11:45	Milica G. Bogdanović, Nikola D. Radnović, Marko V. Rodić. SYNTHESIS AND STRUCTURE OF {[ZN(HL)2] × 4 DMF} N (H2L = 2,2′-DIAMINOBIPHENYL 4,4′-DICARBOXYLIC ACID)	O16-1	107
12:00	Touqeer Gill, Julija Pauraitė, Steigvilė Byčenkienė and Kristina Plauškaitė CORRELATION STUDY OF 5-YEARS SUBMICRON ORGANIC AEROSOLS WITH TEMPERATURE IN THE RURAL ENVIRONMENT	O16-2	108
12:15	Mariia Stanitska, Malek Mahmoudi, Nazariy Pokhodylo, Roman Lytvyn, Dmytro Volyniuk, Ausra Tomkeviciene, Rasa Keruckiene, Mykola Obushak, Juozas Vidas Grazulevicius EXIPLEX-FORMING COMPOUNDS CONTAINING 1H-1,2,3-TRIAZOLE AND CARBAZOLE MOIETIES FOR SOLUTION PROCESSED WHITR OLEDS	O16-3	109
12:30	Natalia Hachlica, Aleksandra Wajda, Klaudia Rachwał, Aleksandra Szymczyk, Agnieszka Kaczor CHIROPTICAL SPECTROSCOPY IN STUDIES OF PROTEIN AGGREGATION	O16-4	110
12:45	Ainis Jarusaitis, Matas Matulevicius, Ali Jafarov, Alexandra Elsakova, Ieva Galdikaite, Arunas Ramanavicius, Ausra Baradoke DETECTION OF IGM ANTIBODIES AGAINST THE SARS-COV-2 VIRUS VIA COLLOIDAL GOLD - BASED ELECTROCHEMICAL ASSAY	O16-5	111
13:00	Did not participate	O16-6	112
13:15	BREAK		
14:00	Milda Pučetaitė SHINING NEW LIGHT INTO SOIL SYSTEMS: ADVANCED SPECTROSCOPY METHODS HELP US		
15:00	BREAK		
15:15-16:00	**POSTER SESSION P6**		
16:00	BREAK		
16:15-17:00	**POSTER SESSION P7**		
17:00	Closing remarks		

List of poster presentations

15 March, TUESDAY

15:15-16:00 POSTER SESSION P1

		page
Vytautas Zutautas, Tadas Jelinskas, Rasa Pauliukaite APPLICATION OF POLY(FOLIC ACID) MODIFIED ELECTRODES FOR PH MONITORING	P1-1	113
Pija Gadonaitė, Gediminas Usevičius, Vidmantas Kalendra, Jūras Banys, Mantas Šimėnas ELECTRON SPIN RESONANCE OF PARAMAGNETIC IMPURITIES IN CEO2	P1-2	114
Daria Kuchynska, Olena Ishchenko, Viktoriia Plavan, Mariia Kuchynska, Irina Liashok ELECTROSPINNING NONWOVEN MATERIALS WITH ANTISEPTIC PROPERTIES	P1-3	115
Did not participate	P1-4	116
Deimante Rosliuk, Dovile Liudvinaviciute, Ramune Rutkaite, Anne Loron, Véronique Coma THE BIOACTIVE PROPERTIES OF CHITOSAN AND GREEN COFFEE BEAN OR ARTICHOKE EXTRACT COMPLEXES	P1-5	117
Vesta Navikaite-Snipaitiene, Simona Sukackaite, Dovile Liudvinaviciute, Ramune Rutkaite IMMOBILIZATION OF ESSENTIAL OILS IN MODIFIED STARCH FOR ACTIVE PACKAGING APPLICATIONS	P1-6	118
Patricija Lapienytė, Šarūnas Svirskas, Lucjan Kozielski, Juras Banys FERROELECTRIC PROPERTIES OF BARIUM CALCIUM TITANATE DOPED WITH RARE EARTH METALS	P1-7	119
Eglė Šlinkšytė, Šarūnas Svirskas, Eriks Birks, Stanislav Kamba, Jūras Banys DIELECTRIC SPECTROSCOPY OF TIN DOPED BARIUM TITANATE	P1-8	120
Zygimantas Augys, Vesta Navikaite-Snipaitiene, Ramune Rutkaite ENCAPSULATION OF VACCINIUM MYRTILLUS L. ANTHOCYANINS INTO LIPOSOMES	P1-9	121
Did not participate	P1-10	122
Rugile Grabauskaite, Dovile Liudvinaviciute, Vesta Navikaite-Snipaitiene, Ramune Rutkaite, Joana Bendoraitiene FORMATION OF COMPLEXES BETWEEN ANTHOCYANINS AND CROSS-LINKED PECTIN	P1-11	123
Domantas Čiapas, Šarūnas Svirskas, Lucjan Kozielski, Jūras Banys DIELECTRIC PROPERTIES OF BA0.9CA0.1ZRXTI1-XO3 CERAMICS	P1-12	124
Did not participate	P1-13	125
Migle Babelyte, Ramune Rutkaite, Volodymyr Samaryk SYNTHESIS OF CHITOSAN AND N-ISOPROPYLACRYLAMIDE GRAFT COPOLYMERS	P1-14	126
Gabrielė Saulėnienė, Monika Kirsnytė, Wanessa De Cassia Martins Antunes De Melo, Arūnas Stirkė POLYLACTIC ACID MODIFICATIONS WITH FULLERENES FOR BIOFILM TREATMENT WITH PHOTODYNAMIC THERAPY	P1-15	127
Did not participate	P1-16	128
Did not participate	P1-17	129
Laura Peciulyte, Ugne Naruseviciute, Ramune Rutkaite HYDROPHOBIC AND THERMAL PROPERTIES OF ACETYLATED STARCH OCTENYL SUCCINATES	P1-18	130
Milda Grendaitė, Dainius Michelevičius, Sigitas Radzevičius INSIGHTS INTO STRUCTURE OF SEDIMENTARY SUCCESSION OF WESTERN LITHUANIA BASED ON INTERPRETATION OF NEW SEISMIC DATA	P1-19	131
Andrius Ambrutis DEVELOPMENT OF CFD-SUITABLE ANN MODEL OF LAMINAR BURNING VELOCITY	P1-20	132
Justas Kvedaravicius, Aleksejus Kononovicius SCALING OF EMPIRICAL COMPARTMENTAL DISTRIBUTIONS	P1-21	133
Justas Dilys THE UNSCENTED KALMAN FILTER IMPLEMENTATION FOR THE SENSORLESS SPEED CONTROL OF A PERMANENT MAGNET SYNCHRONOUS MOTOR	P1-22	134
Did not participate	P1-23	135
Rokas Garbačauskas, Thomas Gajdosik RENORMALISATION GROUP FLOW OF THE GRIMUS NEUFELD MODEL AT ONE LOOP LEVEL	P1-24	136
Did not participate	P1-25	137
Did not participate	P1-26	138
Did not participate	P1-27	139
Nomeda Tvaskaitė, Marijus Ambrozas DRELL-YAN PROCESS BACKGROUND ESTIMATION USING EM METHOD.	P1-28	140
Simas Jankauskas, Thomas Gajdosik THE GRIMUS-LAVOURA APPROXIMATION FOR A LOW SEESAW SCALE	P1-29	141
Tomas Klinavičius, Tomas Tamulevičius RIGOROUS MODELLING OF DIFFRACTION GRATING DIFFRACTION EFFICIENCY UNDER MULTIPLE ANGLE ILLUMINATION	P1-30	142
Did not participate	P1-31	143
Simona Armalytė, Viktorija Tamulienė THEORETICAL INVESTIGATION OF OPTICAL PARAMETRIC GENERATOR AND AMPLIFIER BASED ON PERIODICALLY POLED LITHIUM NIOBATE PUMPED BY SUBNANOSECOND LASER PULSES	P1-32	144
Gabrielė Stanionytė, Viktorija Tamulienė, Julius Vengelis, Rimantas Grigonis CONSTRUCTION AND INVESTIGATION OF BBO SUBNANOSECOND OPTICAL PARAMETRIC AMPLIFIER	P1-33	145
Jokūbas Pimpė, Julius Vengelis, Vygandas Jarutis, Miglė Kuliešaitė MEASUREMENT OF NONLINEAR REFRACTIVE INDEX AND ITS DISPERSION IN PHOTONIC CRYSTAL FIBER	P1-34	146
Tomas Montvydas, Vytautas Jukna, Audrius Dubietis SELF-FOCUSING IN NONLINEAR PHOTONIC CRYSTALS	P1-35	147

Aivaras Labžentis, Simas Butkus, Vytautas Jukna, Valdas Sirutkaitis SIMULATION AND DESIGN OF FLAT-TOP INTENSITY DISTRIBUTION GENERATING PHASE MASKS	P1-36	148
Darija Astrauskytė, Mantas Drazdys, Ramutis Drazdys, Darius Gailevičius, Lina Grinevičiūtė THE FORMATION OF OPTICAL COATINGS ON HYBRID POLYMER SZ2080 USING ATOMIC LAYER DEPOSITION TECHNOLOGY	P1-37	149
Gustė Dolmantaitė, Lukas Ramalis, Rytis Buzelis, Tomas Tolenis LASER INDUCED DAMAGE STUDY OF SCULPTURED THIN FILM BASED ALL-SILICA MIRRORS EXPOSED TO VARIOUS ENVIRONMENTS	P1-38	150
Bernadeta Labžentienė, Simas Butkus, Domas Paipulas and Valdas Sirutkaitis ABLATION OF MICROCHANNELS IN GLASS USING 206 NM – 1030 NM WAVELENGTH FEMTOSECOND PULSES	P1-39	151
Karolis Mundrys, Sergejus Orlovas, Paulius Ševas CONTROLLED GENERATION OF AIRY BEAMS USING PHASE ELEMENTS	P1-40	152
Evelina Stonytė, Dominyka Stonytė, Domas Paipulas MICROSTRUCTURING OF TRANSPARENT SURFACES FOR EFFICIENT DIFFRACTIVE OPTICAL ELEMENTS	P1-41	153
Varis Karitans IMPLEMENTING THE GERCHBERG-SAXTON ALGORITHM IN DIGITAL SIGNAL PROCESSORS	P1-42	154
Ignas Lukošiūnas, Darius Gailevičius, Kęstutis Staliūnas LEAKY MODES OF MODULATED WAVEGUIDES FOR SPATIAL FILTERING	P1-43	155
Justina Anulytė, Ernesta Bužavaitė-Vertelienė, Zigmas Balevičius MODELLING OF PLASMON – EXCITON STRONG COUPLING IN SILVER/GOLD FILM WITH RHODAMINE 6G DYE IN POLYMETHYL METHACRYLATE LAYER	P1-44	156
Arnoldas Solovjovas, Marius Navickas, Gabriele Gudaitiene, Mindaugas Masaitis, Mangirdas Malinauskas SCALING IGNALINA NUCLEAR POWER PLANT TO CENTIMETERS AND MICRO-METERS BY USING 3D PRINTING TECHNOLOGIES	P1-45	157
Andrius Kamarauskas, Laurynas Staišiūnas, Gediminas Šlekas, Dalius Seliuta, Žilvinas Kancleris GRAPHENE CAPACITOR FOR FABRY-PEROT RESONANCE CONTROL	P1-46	158
Laura Tauraitė, Ernestas Nacius, Orestas Ulčinas, Sergej Orlov, Vytautas Jukna RADIALLY SPLIT AXICON PHASE OPTIMISATION FOR ELONGATED BESSEL BEAM PEAK GENERATION FOR TRANSPARENT MATERIAL DICING	P1-47	159
Vaida Marčiulionytė, Vytautas Jukna, Gintaras Tamošauskas, Audrius Dubietis SUPERCONTINUUM GENERATION WITH BURSTS OF FEMTOSECOND LASER PULSES	P1-48	160
Justina Savickytė, Jonas Banys, Ona Balachninaitė, Viktorija Tamulienė, Julius Vengelis SUBNANOSECOND OPTICAL PARAMETRIC GENERATOR BASED ON PERIODICALLY POLED LITHIUM NIOBATE CRYSTAL	P1-49	161

16:15-17:00 POSTER SESSION P2

Did not participate	P2-1	162
Gazy Khatmi Rodowan, Mohamed Ahmed Baba, Martynas Simanavičius, Laimis Silimavičius, Agnė Barkauskienė, Gintautas Gylys, Tomas Tamulevičius DIRECT FEMTOSECOND LASER ABLATION OF NITROCELLULOSE MEMBRANES	P2-2	163
Miglė Kuliešaitė, Julius Vengelis, Vygandas Jarutis SUPERCONTINUUM GENERATION IN DIFFERENT LENGTH PHOTONIC CRYSTAL FIBERS	P2-3	164
Simonas Driukas, Vidmantas Gulbinas, Danielis Rutkauskas PHOTOLUMINESCENCE DYNAMICS OF MAPI PEROVSKITE FILMS INDUCED BY LATERAL ELECTRIC FIELD	P2-4	165
Carlos Marcuello, Anabel Lostao ATOMIC FORCE MICROSCOPY AS VERSATILE TOOL TO DISCERN THE PHYSICO-CHEMICAL PROPERTIES OF PROTEINS AT THE NANOSCALE	P2-5	166
Alejandro Iglesias Jiménez, Gema Artiaga, Estefanía Moreno, Milagros Gómez COULD SENPS REVERT SIDE EFFECTS OF CISPLATIN CHEMOTHERAPY? INSIGHTS FROM MASS SPECTROMETRY AND CHROMATOGRAPHY ANALYSIS	P2-6	167
Paulius Gaigalas, Arūnas Jagminas INTERCALATION OF HISTIDINE INTO MOLYBDENUM DISULFIDE FILMS FOR EFFICIENT HYDROGEN EVOLUTION REACTION	P2-7	168
Urtė Ciganė, Arvydas Palevičius DEVELOPMENT OF AN ELECTROCHEMICAL REACTOR FOR THE FABRICATION OF NANOPOROUS AAO MEMBRANES	P2-8	169
Rūta Aukštakojytė, Justina Gaidukevič, Rasa Pauliukaitė, Jurgis Barkauskas SYNTHESIS AND CHARACTERISATION OF THERMALLY REDUCED GRAPHENE OXIDE AND ITS APPLICATION AS A NOVEL ELECTRODE MATERIAL FOR DOPAMINE DETECTION	P2-9	170
Jadranka Milikić, Kristina Radinović, and Biljana Šljukić SODIUM BOROHYDRIDE OXIDATION AT GOLD SILVER NANOPARTICLES ON REDUCED GRAPHENE OXIDE	P2-10	171
Ana Nastasić, Jadranka Milikić, Sara Knežević and Biljana Šljukić EFFICIENT COBALT SILVER ELECTROCATALYST FOR OXYGEN REDUCTION REACTION IN ALKALINE MEDIA	P2-11	172
Edita Daublytė, Tatjana Charkova FUNCTIONALIZATION OF SILVER NANOPARTICLES WITH 4-MERCAPTOBENZOIC ACID FOR IRON (II) DETECTION	P2-12	173
Šarūnas Jankauskas, Rimantas Gudaitis, Algirdas Lazauskas, Šarūnas Meškinis CATALYST-LESS AND TRANSFER-LESS SYNTHESIS OF GRAPHENE ON SI(100) USING DIRECT MICROWAVE PLASMA ENHANCED CHEMICAL VAPOR DEPOSITION AND PROTECTIVE ENCLOSURES	P2-13	174
Aleksandar M. Đorđević, Jadranka Milikić, and Biljana Šljukić DETECTION OF NITROBENZENE DERIVATIVES USING SILVER COPPER ELECTRODE ON REDUCED GRAPHENE OXIDE IN NEUTRAL MEDIA	P2-14	175
Kevon Kadiwala , Edgars Butanovs, Andrejs Ogurcovs, Martins Zubkins, Boris Polyakov COMPARATIVE STUDY OF WSE2 THIN FILMS SYNTHESIZED VIA PRE-DEPOSITED WO3 AND W PRECURSOR MATERIAL SELENIZATION	P2-15	176
Jaunius Mykolaitis, Tomas Tamulevičius, Asta Tamulevičienė FEMTOSECOND LASER ABLATED SILVER NANOPARTICLE MORPHOLOGY DEPENDENCE ON THE APPLIED LIQUID	P2-16	177

Vincentas Mačiulis, Ieva Plikusienė, Silvija Juciutė, Justina Liesytė, Saulius Balevičius, Arūnas Ramanavičius, Vilius Vertelis, Almira Ramanavičienė ASSESSMENT OF ZNO NANOWIRES APPLICATION FOR THE COVALENT PROTEINS IMMOBILIZATION BY TOTAL INTERNAL REFLECTION ELLIPSOMETRY	P2-17	178
Gytis Babaitis, Darius Dobrovolskas INVESTIGATION OF CORRELATION BETWEEN PHOTOLUMINESCENCE INTENSITY AND WAVELENGTH IN INGAN MQWS ON SUB-MICROMETER SCALE	P2-18	179
Vita Petrikaitė, Evaldas Stankevičius SYNTHESIS OF HYBRID GOLD-SILVER NANOPARTICLES FROM THIN BIMETALLIC COATINGS USING LASER ABLATION	P2-19	180
Did not participate	P2-20	181
Maciej Nowagiel, Mateusz J. Samsel, Aldona Zalewska, Tomasz K. Pietrzak SODIUM-ION BATTERIES: HIGHLY-CONDUCTING NANOCRYSTALLIZED GLASS-CERAMIC CATHODE MATERIALS	P2-21	182
Viktorija Lisyte, Eimantas Bucmys, Anton Popov, Almira Ramanaviciene MULTICOLOR COLORIMETRIC ASSAY FOR CYANIDE DETECTION	P2-22	183
Greta Olimpija Remeikytė, Zenonas Kuodis, Olegas Eicher-Lorka MICROWAVE-ASSISTED SYNTHESIS OF 3D METAL OXIDE MAGNETO-PLASMONIC NANOPARTICLES	P2-23	184
Ernesta Lubinaite, Vincentas Maciulis, Ieva Plikusiene, Kristina Sobol, Almira Ramanaviciene GOLD NANOPARTICLES FOR SENSITIVE HEPARIN DETECTION BY OPTICAL AND ACOUSTIC SIGNAL REGISTRATION METHODS	P2-24	185
Did not participate	P2-25	186
Did not participate	P2-26	187
Daria Pashneva, Steigvilė Byčenkienė, Ieva Uogintė, Julija Pauraitė, Agnė Minderytė, Lina Davulienė, Kristina Plauškaitė, Martynas Skapas, Vadimas Dudoitis, Jelena Andriejauskiene, Vidmantas Ulevicius, Dalia Jasinevičienė, Valda Araminienė, Eugenija Farid THE ROLE OF TREE FOLIAGE ON BLACK CARBON DEPOSITION AN URBAN BACKGROUND IN VILNIUS	P2-27	188
Gerda Anužienė, Rimantė Bandzevičiūtė, Eglė Lastauskienė, Justinas Čeponkus ATR IR SPECTROSCOPY APPLICATION FOR THE IDENTIFICATION OF PATHOGENIC BACTERIA AND FUNGI	P2-28	189
Vaidas Pudzaitis, Martynas Talaikis and Gediminas Niaura ATR-SEIRAS PROBES DIELECTRIC ENVIRONMENT OF THE SUBMEMBRANE LAYER OF THETETHERED BILAYER LIPID MEMBRANES (TBLMS)	P2-29	190
Jogilė Mačytė, Rasa Platakyte, Justinas Čeponkus, Gamil A.Guirgis, Valdas Šablinskas CONFORMATIONAL STUDY OF 1-METHYL-GERMACYCLOHEXANE BY MEANS OF VIBRATIONAL SPECTROSCOPY	P2-30	191
Inna Hutsalo, Svitlana Litvynchuk, Antonina Boiko, Lyubov Zakidysheva COMPARISON OF METHODS FOR DETERMINATION OF OLEIC ACID IN SUNFLOWER SEEDS	P2-31	192
Eidvidas Šatkauskas, Sergejus Balčiūnas, Jūras Banys DIELECTRIC SPECTROSCOPY OF X(BI(ZN2/3NB1/3)O3)-(1-X)BATIO3 CERAMICS	P2-32	193
Kristiāna Rancāne, Anda Ābola A COMPARISON OF THE SPECTRAL PROPERTIES IN THE UV REGION OF ARSENIC HIGH FREQUENCY ELECTRODELESS LAMPS AND HOLLOW CATHODE LAMPS	P2-33	194
Morta Stadulytė, Rimantė Bandzevičiūtė, Justinas Čeponkus, Marius Snicorius, Arūnas Želvys, Valdas Šablinskas. INFRARED SPECTROSCOPY OF URINARY DEPOSITS	P2-34	195
Rimantė Bandzevičiūtė, Katja Liedel, Christian Teske, Carina Riediger-Schweipert, Justinas Čeponkus, Valdas Šablinskas, Gerald Steiner APPLICATION OF FIBER ATR IR SPECTROSCOPY FOR TUMOROUS LIVER TISSUE IDENTIFICATION	P2-35	196
Rugilė Lukaševičiūtė, Lena Golubewa, Tatsiana Kulahava, Renata Karpicz CYTOTOXICITY OF BORON NITRIDE QUANTUM DOTS ON RED BLOOD CELLS	P2-36	197
Did not participate	P2-37	198
Volodymyr Vyshniak, Svitlana Litvynchuk, Kateryna Boatri IR SPECTROSCOPY OF FOOD MIXTURES CONTAINING BEE POLLEN	P2-38	199
Marta Wujczyk, Sara Targonska, Philippe Boutinaud, Adam Watras and Rafal J. Wiglusz EMISSION ENHANCEMENT BY ENERGY TRANSFER IN YP0.5V0.5O4: BI3+, EU3+	P2-39	200
Mantas Jakučionis, Darius Abramavičius MODELING MOLECULAR AGGREGATES USING DIRAC-FRENKEL VARIATIONAL METHOD	P2-40	201
Patrycja Dawiec, Patrycja Leszczenko, Anna M. Nowakowska, Paulina Laskowska, Aleksandra Borek-Dorosz, Adriana Adamczyk, Justyna Jakubowska, Marta Ząbczyńska, Agata Pastorczak, Kinga Ostrowska, Maciej Szydłowski, Piotr Mrówka, Małgorzata Barańska, Katarzyna Majzner DIFFUSE LARGE B-CELL LYMPHOMA (DLBCL) SUBTYPES DISTINGUISHED USING RAMAN IMAGING	P2-41	202
Dionysios Gakis REGOLITH AS RADIATION PROTECTIVE MATERIAL FOR ASTRONAUTS ON MARS	P2-42	203
Algita Stankevičiūtė, Joachim Borowicz, Łukasz Wyrzykowski NACO ADAPTIVE OPTICS: THE KEY EXPLORATION OF BLACK HOLE LENSES	P2-43	204
Rūta Urbonavičiūtė, Erika Pakštienė VARIABLE STARS IN BINARY SYSTEMS	P2-44	205
Jorge Perez Gonzalez, Nicolas Carrizosa Arias, Andres Cadenas Blanco VARSTAR DETECT, A PYTHON LIBRARY DEDICATED TO THE SEMI-AUTOMATIC DETECTION OF STELLAR VARIABILITY	P2-45	206
José Manuel Casas González, Laura Bonavera, Joaquín González-Nuevo González CENN: A FULLY CONVOLUTIONAL NEURAL NETWORK FOR CMB RECOVERY IN REALISTIC MICROWAVE SKY SIMULATIONS	P2-46	207
Did not participate	P2-47	208
Aikaterini Niovi Triantafyllaki, Alessia Longobardi TESTS OF HIERARCHICAL FORMATION IN THE VIRGO CLUSTER	P2-48	209
Carlos Vytautas Diamond Manikas, Vygandas Jarutis, Domas Paipulas, Simas Butkus, Vytautas Jukna INVESTIGATION OF AMORPHIZATION RINGS GENERATED ON SILICON SURFACE VIA ULTRASHORT LASER PULSES	P2-49	210

16 March, WEDNESDAY

15:15-16:00 **POSTER SESSION P3**

Kamilė Kandrotaitė, Steigvilė Byčenkienė, Vadimas Dudoitis, Ieva Uogintė, Kristina Plauškaitė Šukienė, Francis Pope, Peter Strizak AEROSOL FILTRATION EFFICIENCY OF HOUSEHOLD MATERIALS WITH ANTIMICROBIAL HYDROPHOBIC COATING	P3-1	211
Mindaugas Ilickas, Simas Račkauskas ZNO NANOTETRAPODS FOR ROOM TEMPERATURE UV SENSORS	P3-2	212
Benjaminas Togobickij, Mantas Povilaitis, Gediminas Stankūnas DEVELOPMENT OF MCNP MODEL AND PRELIMINARY SIMULATION OF LIEBE PROTON TARGET	P3-3	213
Aukse Navaruckiene, Egidija Rainosalo, Jolita Ostrauskaite VANILLIN ACRYLATE-BASED SHAPE MEMORY POLYMERS	P3-4	214
Rasa Karalkeviciene, Eva Raudonyte-Svirbutavičiene, Aleksej Zarkov, Aivaras Kareiva HYDROXYAPATITE FORMATION BY SOLVOTHERMAL TREATMENT OF ALPHA-TRICALCIUM PHOSPHATE WITH WATER-ALCOHOL SOLUTION	P3-5	215
Sigita Grauželienė, Brigita Kazlauskaitė, Jolita Ostrauskaitė UV-CURABLE RESINS FROM RENEWABLE RESOURCES FOR SYNTHESIS OF VITRIMERS	P3-6	216
Gustas Petrusevičius, Marek Kolenda PRISM COUPLING TECHNIQUE FOR PLANAR GAN WAVEGUIDES	P3-7	217
Denys Baklan, Oleksiy Myronyuk, Jia Zilong CRUSHED PERLITE AS A MICROSTRUCTURAL FILLER FOR SUPERHYDROPHOBIC COATINGS	P3-8	218
Agnese Spustaka, Ernests Einbergs, Donāts Millers, Edgars Vanags THE LUMINISCENT PROPERTIES OF ZNS:MN THIN FILMS	P3-9	219
Augustine Nana Sekyi Appiah, Oktawian Bialas, Marcelina Jedrzejczyk, Natalia Ciemamala, Lucja Wantuch, Marcin Zuk, Artur Czuprynski, Marcin Adamiak HARDFACING OF MILD STEEL WITH WEAR-RESISTANT NI-BASED POWDERS CONTAINING WC PARTICLES USING PPTAW TECHNOLOGY	P3-10	220
Justas Ciganas, Giedrius Janušas HOT STAMPING AND VIBRATION BASED INNOVATIVE MICROSTRUCTURE FORMATION TECHNOLOGY	P3-11	221
Ada Steponavičiūtė, Aušra Selskienė, Ričardas Petkus, Karolis Stravinskas BIMETALLIC STRUCTURE FORMATION BY LASER ADDITIVE MANUFACTURING	P3-12	222
Romuald Petkevič, Giedrius Jočbalis, Sergejus Borodinas, Genrik Mordas INVESTIGATION OF POWDER FLOW FOR METAL DEPOSITION NOZZLE	P3-13	223
Yuliia Bardadym, Edward Sporyagin FEATURES INFLUENCE OF THE PHYSICAL FIELDS ON THE STRUCTURE AND PHYSICAL PROPERTIES OF POLYMER MATERIALS WITH METAL OXIDES	P3-14	224
Marijus Ambrozas, Stefano Mersi CALIBRATION OF PIXEL DETECTOR PROTOTYPES FOR THE PHASE-2 CMS INNER TRACKER UPGRADE	P3-15	225
Mantas Drazdys, Darija Astrauskytė, Ramutis Drazdys, Tadas Paulauskas MODELING AND DEPOSITION OF ANTIREFLECTIVE COATING FOR III-IV MULTI-JUNCTION SOLAR CELLS USING ATOMIC LAYER DEPOSITION	P3-16	226
Tomas Grigaitis, Karolis Bacevičius PASSIVATION OF THE HYDROGEN-TERMINATED DIAMOND SURFACE WITH ORGANIC MATERIALS	P3-17	227
Linda Krauze, Tatjana Pladere, Vita Konosonoka, Gunta Krumina EYE TRACKER CALIBRATION FOR THE ASSESSMENT OF MULTI-PLANE DISPLAY'S USER EXPERIENCE	P3-18	228
Justinas Jaras, Aukse Navaruckiene, Jolita Ostrauskaite PHOTORHEOMETRICAL STUDY OF VANILLIN ACRYLATE-BASED PHOTORESINS	P3-19	229
Dominykas Augulis, Kazimieras Badokas, Arūnas Kadys, Benjaminas Šebeka, Ilja Ignatjev, Jūras Mickevičius and Tadas Malinauskas EXFOLIATION OF GAN THIN FILMS GROWN BY MOVPE VIA GRAPHENE	P3-20	230
Paulius Sakalauskas, Pranciškus Vitta INVESTIGATION OF LEDS AND THEIR MODULATION CIRCUIT FOR VISUAL LIGHT COMMUNICATIONS	P3-21	231
Maria Skrodzka, Magdalena Łabowska THE PROBLEM OF WATER LOSS OF ALGINATE HYDROGELS: A LITERATURE REVIEW AND AN INTRODUCTION TO OWN RESEARCH	P3-22	232
Did not participate	P3-23	233
Justina Žemgulytė, Paulius Ragulis, Gediminas Šlekas, Romualdas Trusovas, Karolis Ratautas, Rimantas Simniškis, Žilvinas Kancleris, Gediminas Račiukaitis RADIO FREQUENCY ENERGY HARVESTER	P3-24	234
Gabrielė Kareivaitė, Renata Karpič, Mindaugas Mačernis, Darius Abramavičius, Leonas Valkūnas FLUORESCENCE DYNAMICS OF TRANS-STILBENE DUE TO THE PRESENCE OF AGGREGATES	P3-25	235
Did not participate	P3-26	236
Gintarė Gečė, Jurgis Pilipavičius, Jurga Juodkazytė, Linas Vilčiauskas NA4FEV(PO4)3 –ALTERNATIVE CATHODE FOR AQUEOUS SODIUM ION BATTERIES	P3-27	237
Kristine Kalnica-Dorosenko, Dzmitry Viarenich, Andrei Karol, Aliaksei Haraks, Artsem Makarau, Aliaksandr Katolik, Aiga Svede DEVELOPMENT OF A COMPUTERISED METHODOLOGY FOR THE TREATMENT OF AMBLYOPIA	P3-28	238
Mantas Slipkauskas, Emanuelis Lazauskas, Tomas Tolenis, Lina Grinevičiūtė THE SIGNATURES OF ACHROMATIC RETARDANCE IN MULTILAYER ANISOTROPIC COATINGS	P3-29	239
Šarūnas Mickus, Vytautas Vosylius, Evaldas Kvietkauskas, Viktorija Vrubliauskaitė, Karolis Ratautas SURFACE MODIFICATION OF POLYTETRAFLUOROETHYLENE (PTFE) POLYMER BY ULTRASHORT PULSE LASER RADIATION TO IMPROVE THE SURFACE ADHESION OF CHEMICALLY DEPOSITED COPPER	P3-30	240
Ieva Morkūnaitė, Kęstutis Ikamas, Dmytro B. But, Alvydas Lisauskas THE STUDY OF EMISSION SPECTRUM OF VOLTAGE-CONTROLLED OSCILLATORS	P3-31	241
Nicole Nowak, Tomasz Gebarowski, Rafal Jakub Wiglusz COLLAGEN BASED SCAFFOLD WITH HYDROXYAPATITE DOPED WITH RUBIDIUM IONS ENHANCES VIABILITY AND FORMING OF CELLULAR NETWORK OF DENTAL PULP STEM CELLS	P3-32	242

Ignas Bitinaitis, Anna Sytchkova, Naglis Kyžas, Rimantas Simniškis, Ramutis Drazdys, Alexandr Belosludtsev DETAILED INVESTIGATIONS FROM NANOSCALE TO BULK OF SILVER FILM GROWTH	P3-33	243
Monika Jokubauskaitė, Arnas Pukinskas, Evelina Dudutienė, Bronislovas Čechavičius, Nerijus Jurkūnas, Arnas Naujokaitis, Martynas Skapas, Renata Butkutė PHOTOLUMINESCENCE INTENSITY BOOST IN GAASBI PARABOLIC QUANTUM WELLS	P3-34	244
Urol Makhmanov, Abdulmutallib Kokhkharov, Shaxboz Esanov, Ulugbek Turdaliev BEHAVIOR OF FULLERENE C60 MOLECULES IN A SOLVENT SYSTEM	P3-35	245
Liudmyla Omelchenko, Eugene Petrenko, Andrei Solovjov, Ruslan Vovk EXCESS CONDUCTIVITY AND PSEUDOGAP IN SINGLE CRYSTALS UNDER PRESSURE UP TO 1.7 GPA	P3-36	246
Eugene Petrenko, Lyudmila Omelchenko, Andrei Solovjov MAGNETOCONDUCTIVITY STUDY IN YBCO MONOLAYERS	P3-37	247
Oleksandr Masalskyi, Jonas Gradauskas, Steponas Ašmontas, Algirdas Sužiedėlis, Aldis Šilėnas, Aurimas Čerškus, Ihor Zharchenko HOT CARRIERS IN PHOTORESPONSE FORMATION ACROSS GAAS P-N JUNCTION	P3-38	248
Justinas Turčak, Gediminas Usevičius, Jūras Banys, Mantas Šimėnas EXPLORING POTENTIAL SPIN QUBITS OF GROUP-VI DONORS IN SILICON	P3-39	249
Aleksandra Širvinskytė, Jūras Mickevičius PHOTOLUMINESCENCE STUDY OF INGAN/GAN QUANTUM WELLS WITH A SUPERLATTICE UNDERLAYER	P3-40	250
Malek Mahmoudi, Ervinas Urbonas, Dalius Gudeika, Dmytro Volyniuk, Juozas V. Grazulevicius PLUSES AND MINUSES OF DIFFERENTLY SUBSTITUTED INDOLOCARBAZOLE ISOMERS USED IN NON-DOPED ORGANIC LIGHT EMITTING DIODES	P3-41	251
Rokas Silkinis, Lukas Razinkovas, Audrius Alkauskas THEORETICAL MODELING OF LUMINESCENCE LINESHAPE IN SILICON DUE TO A CARBON-CARBON PAIR COMPLEX	P3-42	252
Karolis Redeckas, Ignas Grigelionis, Vladislovas Čižas, Vytautas Jakštas, Renata Butkutė, Andrius Bičiūnas, Linas Minkevičius QUANTUM WELL INFRARED PHOTODETECTOR OPERATING AT ROOM TEMPERATURE	P3-43	253
Žyginta Einorytė, Greta Majauskaitė, Kęstutis Aidas A COMPUTATIONAL QM/MD NMR STUDY OF MOLECULAR ASSOCIATION IN BINARY MIXTURES OF ACETIC ACID AND DIMETHYL SULFOXIDE	P3-44	254
Miglė Mackevičiūtė, Juozas Dudutis, Paulius Gečys INVESTIGATION OF REAR SIDE GLASS MILLING USING NANOSECOND LASER PULSES	P3-45	255
Aida Kamarauskienė , Vygailė Dudkaitė, Jorūnas Dobilas, Edvinas Orentas, Gintautas Bagdžiūnas SYNTHESIS AND MAGNETIC PROPERTIES OF CYCLODEXTRINS-FERROCENE INCLUSION COMPLEXES	P3-46	256
Paulina Verbaitytė, Gediminas Usevičius, Vidmantas Kalendra, Jūras Banys, Mantas Šimėnas COUPLING OF MICROWAVES TO A PLANAR EPR MICRORESONATOR VIA A 3D CAVITY	P3-47	257

17 March, THURSDAY

15:15-16:00 POSTER SESSION P4

Aistė Galinskaitė, Rūta Gruškienė, Jolita Pachaleva, Edita Kodytė, Jolanta Sereikaitė ENCAPSULATION EFFICIENCY OF NISIN LOADED FUCOIDAN PARTICLES	P4-1	258
Jurga Andreja Kazlauskaite, Jurga Bernatoniene B-CYCLODEXTRIN ASSISTED EXTRACTION OF DAIDZEIN AND GENISTEIN FROM TRIFOLIUM PRATENSE L.	P4-2	259
Did not participate	P4-3	260
Aušra Kondrataitė, Inga Matijošytė, Rimantas Šiekštelė INVESTIGATION OF KLUYVEROMYCES MARXIANUS AS A HOST FOR THE EXPRESSION OF THE HETEROLOGOUS GENES FOR THE BIOCATALYSTS PRODUCTION	P4-4	261
Justinas Babinskas, Jerica Sabotič, Inga Matijošytė STABILITY AND TOXICITY INVESTIGATION OF A NOVEL AROMATIC AMINE FOR LACCASE ACTIVITY SCREENING ON HIGH-THROUGHPUT AGAR PLATES	P4-5	262
Karolina Lankaitė, Rūta Mickienė, Vilma Kaškonienė, Audrius Sigitas Maruška ANALYSIS OF ANTIMICROBIAL PROPERTIES OF MEDICAL PLANTS LEVANDULA L. AND HELICHRYSUM L.	P4-6	263
Algimantas Kaminskas, Asta Kausaite-Minkstimiene SINGLE ENZYME BIOFUEL CELL POWERED BY GLUCOSE	P4-7	264
Lavija Žibutytė, Gintaras Zaleskis SOLUBLE AND LIPOSOMAL DOXORUBICIN UPTAKE IN CANCER CELLS AFTER SHORT TERM EXPOSURE.	P4-8	265
Rokas Statkevičius, Justas Vaitekūnas, Renata Gasparavičiūtė, Jonita Stankevičiūtė, Rolandas Meškys SCREENING AND CHARACTERIZATION OF AMINOTRANSFERASES FOR ASYMMETRIC SYNTHESIS OF CHIRAL AMINES	P4-9	266
Aida Šermukšnytė, Ilona Jonuškienė, Kristina Kantminienė, Ingrida Tumosienė SYNTHESIS OF BIOLOGICALLY ACTIVE 1,2,4-TRIAZOLE-3-THIOL DERIVATIVES BEARING HYDRAZONE MOIETY	P4-10	267
Tarik Corbo, Abdurahim Kalajdzic, Naris Pojskic IN SILICO INTERACTION OF ONOSMONE AND TRUXILLIC ACID AGAINST THE MAIN PROTEASE OF SARS-COV-2	P4-11	268
Lukas Asanavičius, Vilma Kaškonienė, Nicola Tiso, Audrius Sigitas Maruška OPTIMISATION OF BEE POLLEN FERMENTATION TIME BY FERMENTING WITH TIBICO AND KOMBUCHA CULTURES.	P4-12	269
Gintarė Dalmantaitė, Kamilė Jonynaitė VALUABLE COMPOUNDS EXTRACTION FROM MICROALGAE CULTIVATED IN AQUACULTURE WASTEWATER USING COLD PLASMA AND PULSED ELECTRIC FIELDS	P4-13	270
Agnė Mikelevičiūtė, Tautvydas Kojis, Aurelija Mickevičiūtė, Lina Baranauskienė PRODUCTION OF RECOMBINANT MOUSE CARBONIC ANHYDRASES PROTEINS	P4-14	271
Aušrinė Navickaitė, Vilmantas Pupkis, Saulius Bagdonas APPLICATION OF FLUORESCENCE SPECTROSCOPY FOR INVESTIGATION OF PH BANDING IN NITELLOPSIS OBTUSA	P4-15	272
Aurelija Kondratavičiūtė, Vilma Kaškonienė, Rūta Mickienė, Audrius Maruška EVALUATION OF THE IMPACT OF OAK (QUERCUS SPP.) ACORNS TREATMENT ON PHENOLIC COMPOUNDS AND FLAVONOIDS	P4-16	273
Enrika Vyčaitė, Edita Sužiedėlienė, Saulius Bagdonas, Irina Buchovec INACTIVATION OF ACINETOBACTER BAUMANNII BIOFILMS BY ANTIMICROBIAL PHOTODYNAMIC THERAPY	P4-17	274
Kamile Mikalauskaite, Mantas Ziaunys, Andrius Sakalauskas, Vytautas Smirnovas INTERPLAY BETWEEN EPIGALLOCATECHIN-3-GALLATE AND IONIC STRENGTH DURING AMYLOID AGGREGATION	P4-18	275
Did not participate	P4-19	276
Karyna Savchenko, Vadym Lisovyi, Dmytro Oliinyk, Daryna Taran, Galyna Kuzmina, Volodymyr Bessarabov DESIGN OF AN ANESTHETIC MEDICINE PROLONGED ACTION BASED ON NOVOCAINE	P4-20	277
Justė Tamošiūnaitė, Simona Streckaitė, Jevgenij Chmeliov, Andrius Gelžinis, Leonas Valkūnas CONCENTRATION QUENCHING OF CHLOROPHYLL A AND ZINC PHTHALOCYANINE IN THIN POLYSTYRENE FILMS	P4-21	278
Aurimas Greičius, Agnė Savickaitė, Renata Gudiukaitė ANALYSIS OF SITE-DIRECTED MUTANT (ASP94ALA) OF STREPTOMYCES SCABIEI 87.22 CUTINASE	P4-22	279
Gabriele Sejonaite, Alisa Gricajeva IDENTIFICATION AND ANTIMICROBIAL PHOTODYNAMIC INACTIVATION OF MOLDS ISOLATED FROM STRAWBERRIES	P4-23	280
Rugile Chmieliauskaite, Natalija German THE COMPARISON OF GLUCOSE BIOSENSORS MODIFIED BY ENZYME-ASSISTED POLYANILINE NANOCOMPOSITES WITHOUT AND WITH GOLD DERIVATIVES.	P4-24	281
Dominyka Gabulaitė, Baltramiejus Jakštys, Saulius Šatkauskas EVALUATION OF ELECTROPORATION EFFICIENCY, PORE RESEALING AND CELL VIABILITY USING TITANIUM VS STAINLESS-STEEL ELECTRODES	P4-25	282
Mindaugas Matukaitis, Lukas Zlatkus, Deividas Masaitis AUTOMATIC SUBSTRATE FEEDING SYSTEM FOR NON-GROWTH-LIMITING FED-BATCH CULTIVATION PROCESSES OF RECOMBINANT E. COLI IN INDUSTRIAL BIOTECHNOLOGY	P4-26	283
Emilija Januškaitė, Agnė Kalnaitytė, Saulius Bagdonas THE PHOTOSTABILITY OF CUINS/ZNS-COOH QUANTUM DOTS IN BIOLOGICAL MEDIA	P4-27	284
Did not participate	P4-28	285
Inga Matulyte, Jurga Bernatoniene THE INFLUENCE OF GLYCEROL ON CHEWABLE GEL TABLETS PROPERTIES	P4-29	286
Ernesta Lisauskaitė, Audrius Sigitas Maruška, Mantas Stankevičius, Kristina Bimbiraitė-Survilienė DEVELOPMENT AND APPLICATION OF GELS FOR CHIRAL CAPILLARY ELECTROCHROMATOGRAPHY	P4-30	287
Sabina Pavliukovič, Povilas Šimonis, Greta Gančytė, Rasa Garjonytė , Arūnas Stirkė EVALUATION OF ELECTROPORATION AND YEAST CELL DEATH BY AMPEROMETRY	P4-31	288

Brygida Serebriakova, Edita Sužiedėlienė, Saulius Bagdonas, Irina Buchovec A SPECTROSCOPIC STUDY ON PORPHYRINS' COMPOSITION IN 5-AMINOLEVULINIC ACID INDUCED ACINETOBACTER BAUMANNII AND STENOTROPHOMONAS MALTOPHILIA	P4-32	289
Jolita Jagelavičiūtė, Gustė Staniulytė, Dalia Čižeikiene, Loreta Bašinskienė TECHNOLOGICAL PROPERTIES OF ENZYMATICALLY HYDROLYSED APPLE POMACE AND THEIR IMPACT ON WHEAT BREAD PROPERTIES	P4-33	290
Varun P. Talati , Virupaksha A. Bastikar 3D STRUCTURE MODELING OF HUMAN TELOMERASE REVERSE TRANSCRIPTASE	P4-34	291
Viktorija Juščenko, Arūnas Stirkė and Wanessa de Cássia Martins Antunes de Melo SYNERGISTIC EFFECT OF APDT & ELECTROPORATION AGAINST CANDIDA ALBICANS BIOFILM	P4-35	292
Indrė Krastinaitė, Enrika Celitan, Saulius Serva OPTIMIZATION OF RECOMBINANT L-BC GAG PROTEIN SYNTHESIS IN S. CEREVISIAE	P4-36	293
Evelina Jankaitytė, Andrius Sakalauskas, Vytautas Smirnovas, Rima Budvytytė, Gintaras Valinčius STUDY OF THE INTERACTION BETWEEN BIOMIMETIC LIPID BILAYER AND AMYLOID-B PEPTIDE	P4-37	294
Ugnė Borinskytė, Neringa Barauskaitė, Paulius Ruzgys, Vitalij Novickij, Saulius Šatkauskas THE INVESTIGATION OF BYSTANDER EFFECT AFTER BLEOMYCIN ELECTROTRANSFER OR IRREVERSIBLE ELECTROPORATION IN BETWEEN CELL LINES	P4-38	295
Eliza Hartel, Adrianna Cieślak, Magdalena B. Łabowska, Agnieszka Podwin, Jerzy Detyna TECHNOLOGY AND PROPERTIES OF HYDROGEL LAB-ON-CHIP PLATFORM FOR BIOMEDICAL POTENTIAL APPLICATIONS CONCERNING MAGNETIC FIELD EFFECTS ON CANCER CELL LINES.	P4-39	296
Karyna Savchenko, Vadym Lisovyi, Nazar Zderko, Volodymyr Bessarabov, Galyna Kuzmina, Nadia Matvieieva, Hanna Kharytonenko RESEARCH OF ANTI-INFLAMMATORY PROPERTIES CICHORIUM INTYBUS EXTRACT	P4-40	297
Gabrielė Vasiliauskaitė, Povilas Šimonis, Arūnas Stirkė INVESTIGATION OF NANOSECOND PULSED ELECTRIC FIELD TREATMENT EFFECTS ON YEAST CELLS	P4-41	298
Antonina Rachkovska, Daryna Krenytska, Olexiy Savchuk LEVELS OF FGF-2 IN BLOOD PLASMA OF PATIENTS SUFFERED FROM COVID-19	P4-42	299
Did not participate	P4-43	300
Viktoriia Lyzhniuk, Vadym Lisovyi, Roman Smishko, Volodymyr Bessarabov, Galyna Kuzmina PROSPECTIVE METHODS OF PREVENTING POISONING BY PHOSPHORORGANIC COMPOUNDS USING COMPOUNDS OF NATURAL ORIGIN	P4-44	301
Vadym Lisovyi, Artem Kharchenko, Nazar Zderko, Olga Kovalevska, Volodymyr Bessarabov CENTRIFUGAL FORMATION OF FIBERS OF SOLID DISPERSED SYSTEM OF POLYMER WITH HESPERIDINE	P4-45	302
Iryna Pashchenko, Vadym Lisovyi, Viktor Kostyuk, Nadia Matvieieva, Volodymyr Bessarabov ARTEMISIA TILESII LEDEB EXTRACT INHIBITS 15-LIPOXYGENASE ENZYME	P4-46	303
Did not participate	P4-47	304
Tetiana Marynenko, Tetiana Halenova, Olexii Savchuk, Ludmyla Ostapchenko MONITORING OF SOLUBLE FIBRIN MONOMER COMPLEXES AND VITAMIN K-DEPENDENT PROTEINS IN PATIENTS WITH CORONARY ARTERY DISEASE	P4-48	305
Guoda Kolkatovaitė, Rūta Mickienė, Vilma Kaškonienė, Audrius Sigitas Maruška CHANGES IN MICROBIOTA AND PH VALUES OF CREOSOTE-TREATED WOOD DURING MYCOREMEDIATION	P4-49	306
Did not participate	P4-50	307

16:15-17:00 POSTER SESSION P5

Inga Garšvaitė, Edita Sužiedėlienė, Saulius Bagdonas, Irina Buchovec INACTIVATION OF ANTIBIOTIC RESISTANT OPPORTUNISTIC PATHOGENS STENOTROPHOMONAS MALTOPHILIA BY ANTIMICROBIAL PHOTODYNAMIC THERAPY	P5-1	308
Justė Narmontaitė, Ilona Jonuškienė, Rima Stankevičienė, Neringa Petrašauskienė ANTIOXIDANT PROPERTIES OF TAGETES PATULA IN VIVO AND IN VITRO EXTRACTS	P5-2	309
Rimgailė Tamulytė, Evelina Jankaitytė, Zigmantas Toleikis, Marija Jankunec S100A9 PROTEIN INTERACTION WITH BIOMIMETIC LIPID MEMBRANES	P5-3	310
Ernesta Augustiniene, Ingrida Kutraite, Naglis Malys IDENTIFICATION AND CHARACTERIZATION OF P-COUMARATE AND FERULATE-INDUCIBLE SYSTEMS FOR TRANSCRIPTION FACTOR-BASED BIOSENSORS DEVELOPMENT	P5-4	311
Povilas Petras Stepanenko, Zita Sukackienė, Arnas Naujokaitis, Loreta Tamašauskaitė-Tamašiūnaitė, Eugenijus Norkus COBALT AND NICKEL COATINGS WITH MANGANESE AND MOLYBDENUM AS EFFICIENT CATALYSTS FOR HYDROGEN GENERATION	P5-5	312
Anton Popov, Gabija Agasarjanaite, Neda Zenkeviciute, Viktorija Lysite, Asta Kausaite-Minkstimiene, Almira Ramanaviciene THE INVESTIGATION OF SPECIFIC ANTIBODIES INTERACTION WITH CD44 PROTEIN	P5-6	313
Did not participate	P5-7	314
Yuliia Khmelnytska, Olena Perepelytsina, Anna Prokopchuk, Mykhailo Sydorenko INVESTIGATION OF CELL POPULATIONS ON BREAST CANCER CELL MODELS	P5-8	315
Vladimír Koštál, Robert Grgac, Jaroslava Korbelová DELAYED MORTALITY AND SUBLETHAL EFFECTS OF COLD STRESS IN DROSOPHILA MELANOGASTER	P5-9	316
Gabrielė Dzimitravičiūtė, Gintarė Naskauskienė, Žydrūnė Visockienė, Kristina Daniūnaitė DIABETES RELATED MIRNA ANALYSIS IN BLOOD OF PREGNANT WOMEN DIAGNOSED WITH GESTATIONAL DIABETES	P5-10	317
Eivina Radzevičiūtė, Veronika Malyško-Ptašinskė, Irutė Girkontaitė, Vitalij Novickij EFFECTS OF ELECTROCHEMOTHERAPY ON MURINE LEWIS LUNG CARCINOMA CELL LINE	P5-11	318
Paulius Gibieža, Emilija Ratkevičiūtė, Girstautė Dabkevičiūtė, Vilma Petrikaitė RAB11 AND RAB35 REGULATED CYTOKINESIS EVENT THAT AFFECTS PHENOTYPE OF CANCER CELLS	P5-12	319
Aurelija Cicilionytė, Joanna Kaczorowska, Lia van der Hoek INVESTIGATION OF MOTHER-TO-CHILD TRANSMISSION OF HUMAN ANELLOVIRUSES	P5-13	320
Ieva Vaicekauskaitė, Diana Žilovič, Rūta Čiurlienė, Juozas Rimantas Lazutka, Rasa Sabaliauskaitė, Sonata Jarmalaitė NOTCH AND WNT GENE EXPRESSION SIGNATURE IN HIGH GRADE SEROUS OVARIAN CANCER	P5-14	321

Gintarė Mockevičienė, Jurga Turčinavičienė, Asta Križanauskienė, Jekaterina Havelka, Mantas Adomaitis DETECTION OF BABESIA SP. (APICOMPLEXA, PIROPLASMIDA, BABESIIDAE) IN TICKS AND DOGS: COMPARISON OF MOLECULAR AND MORPHOLOGICAL METHODS	P5-15	322
Anastasija Borisova, Danutė Labeikytė, Julija Armalytė PHENOTYPIC AND MOLECULAR CHARACTERIZATION OF ACINETOBACTER BAUMANNII ISOLATES FROM LITHUANIAN NATIONAL CANCER INSTITUTE HOSPITAL (2013-2019)	P5-16	323
Aistė Gerulaitytė, Justina Gaizevska, Monika Drobnienė, Rasa Sabaliauskaitė, Sonata Jarmalaitė STAT3 SIGNALING PATHWAY AS A POTENTIAL THERAPEUTIC TARGET IN TRIPLE NEGATIVE BREAST CANCER	P5-17	324
Jovita Gružaitė, Katryna Pampuščenko, Vytautas Smirnovas, Ramunė Morkūnienė INVESTIGATION OF SYNERGISTIC NEUROTOXIC EFFECT OF AMYLOIDOGENIC PROTEINS ON PRIMARY BRAIN CELL CULTURES	P5-18	325
Gerda Skinderytė, Saulius Serva, Aleksandras Konovalovas TRANSPOSITION FREQUENCY IN YEAST SACCHAROMYCES CEREVISIAE: ROLE OF SCV-LA VIRUS	P5-19	326
Girstautė Dabkevičiūtė, Elias Maccioni, Vilma Petrikaitė ANTICANCER ACTIVITY OF SUNITINIB ANALOGUES IN BRAIN CANCER MODELS	P5-20	327
Karolis Krinickis, Laurita Klimkaitė, Julija Armalytė, Edita Sužiedėlienė ISOLATION OF OPPORTUNISTIC PATHOGEN STENOTROPHOMONAS MALTOPHILIA FROM ENVIRONMENTAL SOURCES	P5-21	328
Justina Gaizevska, Rasa Sabaliauskaite, Augustinas Matulevicius, Albertas Ulys, Feliksas Jankevicius, Sonata Jarmalaite MULTIGENE TESTING FOR PROSTATE CANCER RISK ASSESSMENT AND DIAGNOSIS	P5-22	329
Gabija Mončiūtė, Asta Stapulionytė RESEARCH OF THE EFFECT OF SILICON DIOXIDE AND POLYSTYRENE NANOPARTICLES IN ALLIUM CEPA ROOT CELLS BY CYTOGENETIC AND MOLECULAR METHODS	P5-23	330
Tatjana Ščavlinskaja, Asta Stapulionytė, Ingrida Prigodina-Lukošienė, Eglė Lastauskienė OPTIMIZATION OF CULTIVATION, DNA PURIFICATION AND PCR-RAPD CONDITIONS FOR PUCCINIA SP.	P5-24	331
Žilvinas Survila, Gintaras Zaleskis MODELING OF LOCAL ANTICANCER THERAPIES USING DU-145 PROSTATE CANCER CELLS AND MONOCLONAL ANTIBODY ATEZOLIZUMAB	P5-25	332
Rugilė Pranskūnaitė, Rytis Rugienius, Danas Baniulis. CELL SUSPENSION CULTIVATION OF TRANSGENIC NICOTIANA TABACUM L. FOR BIOMASS PRODUCTION	P5-26	333
Sandra Saunoriūtė, Ona Ragažinskienė, Liudas Ivanauskas, Mindaugas Marksa VARIATION OF ESSENTIAL OIL FROM ARTEMISIA VULGARIS (L.) DURING DIFFERENT VEGETATION STAGES	P5-27	334
Rūta Kiseliūnaitė, Emilija Vasiliūnaitė, Alma Gedvilaitė SYNTHESIS OF NOVEL RODENT POLYOMAVIRUSES VIRUS-LIKE PARTICLES IN YEAST	P5-28	335
Ugnė Rickevičiūtė, Alisa Gricajeva SEARCH FOR PYRETHROIDS-DEGRADING MICROORGANISMS	P5-29	336
Emilija Vasiliūnaitė, Albertas Timinskas, Alma Gedvilaitė GOTTA CATCH 'EM ALL: DESIGNING UNIVERSAL PRIMERS FOR POLYOMAVIRUS DETECTION	P5-30	337
Milda Babonaitė, Veronika Dedonytė, Juozas Rimantas Lazutka ANALYSIS OF IN VITRO GENOTOXICITY OF DIFFERENTLY SIZED COBALT OXIDE NANOPARTICLES IN HUMAN LYMPHOCYTES	P5-31	338
Guoda Varnelytė, Bazilė Ravoitytė, Stanislavas Tracevičius, Elena Servienė DYNAMICS OF CULTIVABLE MICROORGANISMS IN COMMERCIALLY REARED BLACK SOLDIER FLY LARVAE	P5-32	339
Paulina Jonutė, Elias Maccioni, Vilma Petrikaitė ACTIVITY OF NEW SUNITINIB ANALOGUES ON HUMAN BREAST CANCER CELL MIGRATION IN NORMOXIA AND HYPOXIA	P5-33	340
Kornelija Rauduvytė, Agnė Šeštokaitė, Monika Drobnienė, Rasa Sabaliauskaitė, Sonata Jarmalaitė URINARY MIRNA ASOSCIATION WITH TREATMENT RESISTANCE IN TRIPLE-NEGATIVE BREAST CANCER	P5-34	341
Daira Paškevičiūtė, Birutė Gricienė CUMULATIVE EXPOSURE FROM COMPUTED TOMOGRAPHY SCANS. ASSESSMENT OF RECURRENT EXAMINATIONS	P5-35	342
Emilija Dešč, Gintarė Sauliutė, Arvydas Markuckas TOXICITY EVALUATION OF POLYSTYRENE NANOPLASTICS IN SALMONID EMBRYOS	P5-36	343
Ema Lomsargyte, Kristina Snipaitiene, Benita Buragaite-Staponkiene, Adomas Rovas, Egle Punceviciene, Raminta Vaiciuleviciute, Eiva Bernotiene, Irena Butrimiene, Alina Puriene, Sonata Jarmalaite INHIBITION OF MIRNA TO TREAT PERIODONTITIS	P5-37	344
Liudmyla Lastovetska, Valeriia Maslak, Olga Iungin COMBINED ANTIBIOTIC THERAPY CARRIED IN COLLAGEN MATRIX FOR OPPORTUNISTIC PATHOGENS TREATMENT	P5-38	345
Evelina Kaminskienė, Justina Snegiriovaitė MOLECULAR CHARACTERIZATION OF LAELAPS AGILIS MITES (MESOSTIGMATA: LAELAPIDAE) FROM SMALL RODENTS	P5-39	346
Andrea Frejlachova, Radka Lencova, Anna Venhauerova, Marketa Skalickova, Jan Zenka TREATMENT OF ADVANCED MURINE PANCREATIC ADENOCARCINOMA BY THE COMBINATION OF MBTA IMMUNOTHERAPY WITH A GLUTAMINE ANTAGONIST	P5-40	347
Laura Tamkutė, Audrius Pukalskas, Petras Rimantas Venskutonis FRACTIONATION OF CHOKEBERRY POMACE LIPIDS BY SUPERCRITICAL CARBON DIOXIDE EXTRACTION	P5-41	348
Miglė Urbonaitė, Andrius Merkys UNSUPERVISED NAMING OF CHEMICAL COMPOUNDS	P5-42	349
Marcel Jakubowski, Mariusz Sandomierski, Adam Voelkel X AND Y TYPE ZEOLITES IN ZINC FORM AS CARRIERS FOR 6 - MERCAPTOPURINE	P5-43	350

18 March, FRIDAY

15:15-16:00 POSTER SESSION P6

Gintarė Rimkutė, Mantvydas Gudaitis, Jurgis Barkauskas, Justina Gaidukevič, Gediminas Niaura SYNTHESIS AND ANALYSIS OF GRAPHITE INTERCALATION COMPOUND GRAPHITE BISULFATE	P6-1	351

Raminta Beresneviciute, Mangey Ram Nagar, Abhijeet Choudhury, Daiva Tavgeniene, Dovydas Blazevicius, Vygintas Jankauskas, Krishar Kumar, Subrata Banik, Subrata Ghosh, Greta Jacunskaite, Saulius Grigalevicius, Jwo-Huei Jou NEW PHENOTHIAZINE AND PHENOXAZINE SUBSTITUED FLUORENE CORED HOLE TRANSPORTING MATERIALS FOR HIGH-EFFICIENCY OLEDS	P6-2	352
Diana Griesiute, Erlandas Kabasinskas, Eva Raudonyte-Svirbutaviciene, Gabriele Klydziute, Aivaras Kareiva, Aleksej Zarkov THE EFFECT OF ANNEALING CONDITIONS ON CA/P RATIO AND PHASE TRANSFORMATIONS IN BULK CALCIUM PHOSPHATES	P6-3	353
Raman Novikau, Galina Lujanienė ADSORPTION MECHANISM OF CAESIUM AND COBALT ON MUSCOVITE MICA CLAY-GRAPHENE OXIDE-Γ FE2O3/FE3O4 COMPOSITE	P6-4	354
Lukas Dvylys, Rasa Keruckiene, Juozas Vidas Grazulevicius SYNTHESIS AND PROPERTIES OF QUINOXALINE-BASED COMPOUNDS FOR OPTOELECTRONIC APPLICATIONS	P6-5	355
Abdullah Khan, Muhammad Afzaal, Steigvilė Byčenkienė, Touqeer Gill and Muhammad Bilal CONCENTRATIONS OF AIRBORNE PM10 AND LEAD IN MAJOR BUS TERMINALS OF LAHORE AND PESHAWAR, PASKITAN	P6-6	356
Gerardas Laurinavičius, Vilius Poškus SYNTHESIS AND INVESTIGATION OF SELECTIVE SOLID PHASE MICROEXTRACTION SORBENT	P6-7	357
Gediminas Usevičius, Vidmantas Kalendra, Jūras Banys, Andreas Pöppl, Mantas Šimėnas QUANTUM TUNNELING OF METHYL GROUPS IN CO2+-DOPED DIMETHYLAMMONIUM ZINC FORMATE USING PULSED EPR	P6-8	358
Dawid Janasik RATIOMETRIC PH-RESPONSIVE 19F MRI CONTRAST AGENTS BASED ON HYDRAZONE SWITCHES	P6-9	359
Víctor Galileo Almendro Vedia, Marcin Makowski, Castor Salgado Soneira, José Osio Barcina, Manuel N. Melo, Iván López Montero ACRIDINE ORANGE DERIVATIVES TO PROMOTE MEMBRANE FUSION: MECHANISM BENEATH THE PROCESS	P6-10	360
Šarūnė Daškevičiūtė-Gegužienė, Yi Zhang, Kasparas Rakštys, Marytė Daškevičienė, Vygintas Jankauskas, Mohammad Khaja Nazeeruddin, Vytautas Getautis GREEN CHEMISTRY INSPIRED CARBAZOLE-FLANKED CYCLOBUTANES AS HOLE SELECTIVE MATERIALS FOR SOLAR CELLS AND MODULES	P6-11	361
Tavgeniene Daiva, Korzec Mateusz, Samuel Nizy Sara, Krucaite Gintare, Pająk Agnieszka Katarzyna, Kotowicz Sonia, Vasylieva Marharyta, Gnida Paweł, Malecki Jan Grzegorz, Grigalevicius Saulius, Schab-Balcerzak Ewa SYNTHESIS AND THERMAL, PHOTOPHYSICAL, ELECTROCHEMICAL PROPERTIES OF 3,3-DI[3-ARYLCARBAZOL-9-YLMETHYL] OXETANE DERIVATIVES	P6-12	362
Anabel Villalonga, Borja Vegas, Gonzalo Paniagua, Marcos Eguílaz, Beatriz Mayol, Concepción Parrado, Gustavo Rivas, Paula Díez, Reynaldo Villalonga CARCINOEMBRYONIC ANTIGEN-SPECIFIC APTASENSOR BASED ON A REDUCED GRAPHENE OXIDE/GOLD NANOPARTICLE MODIFIED ELECTRODE	P6-13	363
Raimonda Boguzaite, Vilma Ratautaite, Ernestas Brazys, Almira Ramanaviciene, Arunas Ramanavicius TOWARDS ELECTROCHEMICAL POLYMERIZATION OF POLYPYRROLE/POLY(METHYLENE BLUE) LAYER DOPED BY POLYSACCHARIDES	P6-14	364
Tatjana Stanković, Jadranka Milikić, Sara Knežević, Miloš Ognjanović, Dalibor Stanković and Biljana Šljukić COBALT (III) OXIDE AND MIXED COBALT(III) OXIDE - TIN OXIDE FOR OXYGEN EVOLUTION REACTION IN ALKALINE MEDIA	P6-15	365
Silvija Juciute, Ieva Plikusiene, Vincentas Maciulis, Saulius Balevicius, Rimantas Slibinskas, Arunas Ramanavicius, Almira Ramanaviciene REAL TIME MONITORING AND MATHEMATICAL MODELLING OF SARS-COV-2 SPIKE PROTEIN AND SPECIFIC ANTIBODY INTERACTION KINETICS BY TOTAL INTERNAL REFLECTION ELLIPSOMETRY	P6-16	366
Patryk Janasik, Malgorzata Czichy, Mieczyslaw Lapkowski ELECTROCHEMICAL AND SPECTROELECTROCHEMICAL PROPERTIES OF 10H-PYRROLO[1,2-A]PERIMIDIN-10-ONE	P6-17	367
Povilas Luizys, Vytautas Getautis, Kasparas Rakstys, Vygintas Jankauskas, Egidijus Kamarauskas SYNTHESIS AND CHARACTERISTICS OF ORGANIC SEMICONDUCTORS WITH N-CARBAZOLYL-BASED CHROMOPHORES LINKED VIA ALIPHATIC CHAIN	P6-18	368
Did not participate	P6-19	369
Gabrielė Klydžiūtė, Eva Raudonytė-Svirbutavičienė, Laura Lukavičiūtė, Aldona Beganskienė, Aleksej Žarkov, Aivaras Kareiva HYDROTHERMAL SYNTHESIS OF HYDROXYAPATITE FROM A-TCP USING DIVALENT CATIONS AS MORPHOLOGY-CONTROLLING AGENTS	P6-20	370
Povilas Virbickas, Gerda Žižiūnaitė, Aušra Valiūnienė PRUSSIAN BLUE-BASED ELECTROCHEMICAL BIOSENSOR FOR HG2+ IONS	P6-21	371
Branislava Tenjović, Dušan Živković, Tijana Jakica, Dušan Škorić, Andrea Nikolić SYNTHESIS AND IN SILICO ADMET PREDICTION OF NEW 17-HYDRAZINYLIDENE-16,17-SECOANDROST-5-ENE DERIVATIVES	P6-22	372
Did not participate	P6-23	373
Ernestas Brazys, Vilma Ratautaitė, Raimonda Bogužaitė, Arūnas Ramanavičius MOLECULARLY IMPRINTED POLYPYRROLE BASED SENSOR FOR THE DETECTION OF SARS-COV-2 SPIKE GLYCOPROTEIN	P6-24	374
Sandra Barysaitė, Andrius Gelzinis, Jevgenij Chmeliov, Leonas Valkunas MODELING OF CONCENTRATION QUENCHING IN 2D AND 3D CHLOROPHYLL SYSTEMS	P6-25	375
Agne Kizalaite, Erlandas Kabasinskas, Diana Griesiute, Hanna Klipan, Gabriele Klydziute, Aleksej Zarkov SYNTHESIS OF NOVEL CALCIUM PHOSPHATES WITH WHITLOCKITE STRUCTURE VIA DISSOLUTION-PRECIPITATION PROCESS	P6-26	376
Aistė Jegorovė, Cristina Momblona, Marytė Daškevičienė, Artiom Magomedov, Rimgailė Degutytė, Abdullah M. Asiri, Vygintas Jankauskas, Albertus Adrian Sutanto, Mohammad Khaja Nazeeruddin, Vytautas Getautis MOLECULAR ENGINEERING OF THE FLUORENE-BASED HOLE TRANSPORTING MATERIALS FOR EFFICIENT PEROVSKITE SOLAR CELLS	P6-27	377
Milica Ilić, Marija Sakač, Ivana Kuzminac DETERMINING THE SUITABILITY OF IN SILICO TOXICOLOGY PREDICTION TOOLS FOR APPLICATION ON STEROIDAL DRUG CANDIDATES	P6-28	378

Ivana Zorić, Ksenija Pavlović SYNTHESIS AND IN SILICO ADMET PROPERTIS OF B-RING-MODIFIED HYODEOXYHOLIC ACID	P6-29	379
Irma Sanvaitytė, Ingrida Tumosienė, Kristina Kantminienė REACTION OF 1-(4-(PHENYLAMINO)PHENYL)-5-OXOPYRROLIDINE3-CARBOHYDRAZIDE WITH AROMATIC ALDEHYDES	P6-30	380
Julius Petrulevičius, Marytė Daškevičienė, Egidijus Kamarauskas, Vygintas Jankauskas, Vytautas Getautis SYNTHESIS AND PROPERTIES OF FLUORENE DERIVATIVES AS HOLES AND ELECTRONS TRANSPORTING MATERIALS	P6-31	381
Iveta Žukaitė, Ingrida Tumosienė, Kristina Kantminienė, Zigmuntas Jonas Beresnevičius SYNTHESIS OF 1,2,4-TRIAZOLE-3-THIONE DERIVATIVES BEARING 2-AMINOPYRIDINE MOIETY	P6-32	382
Giedrė Gaidamavičienė, Artūras Žalga STRONTIUM SUBSTITUTION EFFECT ON THE STRUCTURE, SURFACE MORPHOLOGY AND THERMOANALYTICAL PROPERTIES OF LA2MO2O9 SYSTEM	P6-33	383
Zane Čerpakovska, Artis Kons, Agris Bērziņš MECHANOCHEMICAL PREPARATION OF DIFFERENT CRYSTAL FORMS OF PHARMACEUTICAL SUBSTANCES	P6-34	384
Nojus Radzevicius, Linas Vilciauskas MOLECULAR DYNAMICS STUDY OF CATION DYNAMICS IN THE [(CH3)2NH2][ZN(HCOO)3] HYBRID PEROVSKITE FRAMEWORK	P6-35	385
Pranas Juknevičius, Andrius Gelžinis, Jevgenij Chmeliov USING NEURAL NETWORKS TO DESCRIBE THE DYNAMICS OF ELECTRONIC EXCITATION IN TWO DIMENSIONAL SYSTEMS	P6-36	386
Indrė Misiūnaitė, Raminta Bajarūnaitė, Ieva Žutautė, Algirdas Brukštus INVESTIGATION OF GOLD-CATALYZED NUCLEOPHILIC CYCLIZATION OF DIFFERENT ALKYNYL 2-THIOIMIDAZOLES	P6-37	387
Gintare Krucaite, Daiva Tavgeniene, Dovydas Blazevicius, Baohua Zhang, Aivars Vembris, Saulius Grigalevicius, Raminta Beresneviciute ELECTROACTIVE POLYMERS CONTAINING ELECTRONICALLY ISOLATED 4,7-DIARYLFLUORENE FRAGMENTS FOR OLEDS	P6-38	388
Nerijus Karlonas COMPARISON OF SILYLATING REAGENTS IN DERIVATIZATION REACTIONS OF SEDATIVE-HYPNOTIC DRUGS PRIOR TO FAST GAS CHROMATOGRAPHY-MASS SPECTROMETRY	P6-39	389
Michael Haletskyi, Nataliia Simurova SYNTHESIS OF NEW 1,2,4-TRIAZOLE DERIVATIVES CONTAINING 1,2,4-OXADIAZOLE FRAGMENT	P6-40	390
Maryia Drobysh, Viktorija Liustrovaite, Alma Rucinskiene, Ausra Baradoke, Almira Ramanaviciene, Ieva Plikusiene, Urte Samukaite-Bubniene, Roman Viter, Chien-Fu Chen, Arunas Ramanavicius THE DETECTION OF ANTIBODIES AGAINST SARS-COV-2 BY ELECTROCHEMICAL METHODS	P6-41	391
Olha Maikovych, Natalya Nosova, Natalya Bukartyk, Zoriana Nadashkevych, Serhii Varvarenko SYNTHESIS AND STUDY OF PROPERTIES OF COMBINED ALGINATE/GELATIN HYDROGELS	P6-42	392
Diana Masiulionytė, Kotryna Laučiškytė, Monika Čekavičiūtė, Laura Pečiulytė, Joana Bendoraitienė, Karolina Almonaitytė THE EFFICIENCY OF POLYETHYLENE TEREPHTALATE GLYCOLYSIS REACTION USING MAYENITE AS A CATALYST	P6-43	393
Andrijana Vukojević, Sanja J. Armaković STABILITY AND PHOTOCHEMICAL FATE OF NADOLOL IN WATER	P6-44	394
Roberta Gelminauskaitė, Birutė Grybaitė SYNTHESIS OF NEW N-(4-METHOXY-2-NITRO)-B-ALANINE DERIVATIVES	P6-45	395

16:15-17:00 POSTER SESSION P7

Aleksandra Orlef, Aleksandra Wajda, Ewa Stanek, Krzysztof Czamara, Agnieszka Kaczor ENCAPSULATION AS A WAY TO DELIVER APOLAR ACTIVE COMPOUNDS TO ADIPOCYTES	P7-1	396
Gabriele Rankelyte, Jevgenij Chmeliov EXCITATION ANNIHILATION IN MOLECULAR AGGREGATES	P7-2	397
Gediminas Jakubauskas, Neringa Petrašauskienė, Edita Paluckienė, Eglė Ūsovienė INVESTIGATION OF DIFFERENT METHODS OF CADMIUM SELENIDE THIN FILM DEPOSITION ON FTO/ZNO SUBSTRATE FROM AQUEOUS SOLUTIONS	P7-3	398
Eglė Ūsovienė, Edita Paluckienė, Neringa Petrašauskienė, Gediminas Jakubauskas FORMATION OF CDS LAYERS ON ZNO/FTO SUBSTRATES AND UV/VIS INVESTIGATION	P7-4	399
Evgeniia Bakhalova, Elena Shved, Anna Mishchenko, Liliia Lisova EFFECT OF STRUCTURE OF BENZOIC ACIDS ON CATALYTIC ACIDOLYSIS OF 2-(CHLOROMETHYL) OXYRANE	P7-5	400
Audrius Sadaunykas, Audrius Zolumskis, Evaldas Naujalis DEVELOPMENT AND TESTING OF CRYOFOCUSING ADD-ON FOR GAS CHROMATOGRAPHY	P7-6	401
Gabija Kavaliauskaitė, Povilas Virbickas, Aušra Valiūnienė PRUSSIAN BLUE AS REDOX MEDIATOR IN YEAST-BASED BIOFUEL CELL	P7-7	402
Edvin Parafjanovič, Martynas Malikėnas, Viktoras Masevičius THE SYNTHESIS OF L-HOMOCYSTINE DERIVATIVES AS PRECURSORS TO MODIFIED S-ADENOSYL-L-METHIONINE ANALOGUES	P7-8	403
Paulina Kaziukonytė, Kamilė Venskūnaitė, Tomas Venslauskas, Algirdas Brukštus SYNTHESIS OF 1,5-DISUBSTITUTED IMIDAZOLES AS POTENTIAL HSP90 INHIBITORS	P7-9	404
Anna Stasiuk, Volodymyr Lyakh, Nataliia Fihurka, Iryna Dron, Volodymyr Samaryk INFLUENCE OF PHOSPHATE GROUP INTRODUCTION ON PROPERTIES OF PSEUDO-POLY(AMINO ACID)S OF POLYESTER TYPE.	P7-10	405
Greta Pilvenytė, Raimonda Bogužaitė, Vilma Ratautaitė, Aušra Baradokė, Arūnas Ramanavičius CONDUCTING POLYMERS IN THE DESIGN OF BIOSENSORS	P7-11	406
Oleksandra Yu. Mariichak, Anna O. Zaharchuk, Olena Yu. Popovska, Georgii M. Rozantsev, Serhii V. Radio SYNTHESIS AND CRYSTAL STRUCTURES OF NA9[EU(W5O18)2]·35H2O WITH PLATE-LIKE MORPHOLOGY	P7-12	407
Ligitas Vinciūnas, Mindaugas Mačernis MOLECULAR DYNAMICS ANALYSIS FOR POTENTIAL ENERGY SURFACES OF BACTERIORHODOPSIN ACTIVE CENTER	P7-13	408

Gytautė Sirgėdaitė, Paulina Nemaniutė, Dalia Bražinskienė, Svajus J. Asadauskas INFLUENCE OF LAYERED DOUBLE HYDROXIDE ON POLYADDITION OF AROMATIC ISOCYANATE AND MACRODIOL	P7-14	409
Rokas Žvirblis, Aurimas Vyšniauskas, Jelena Dodonova-Vaitkūnienė SYNTHESIS AND INVESTIGATION OF MESO-FORMYL BODIPY MODIFIED WITH PHENYL RINGS AT 2,6-POSITIONS	P7-15	410
Did not participate	P7-16	411
Mindaugas Matijūnas, Rasa Alaburdaitė STUDY OF FORMATION OF CADMIUM SULFIDE LAYERS ON POLYPROPYLENE FILM USING DIFFERENT CADMIUM SALTS	P7-17	412
Agnė Minderytė, Julija Pauraite, Steigvilė Byčenkienė AIR QUALITY ASSESSMENT IN RELATION WITH INCREASING CONTRIBUTION OF TRANSPORT-RELATED BLACK CARBON	P7-18	413
Greta Majauskaitė, Kęstutis Aidas INTERMOLECULAR STRUCTURE AND NMR PARAMETERS IN BINARY MIXTURES OF TRIFLUORACETIC ACID AND N, N–DIMETHYLFORMAMIDE MODELLED BY QM/MD APPROACHES	P7-19	414
Greta Majauskaitė, Kęstutis Aidas INTERMOLECUAR STRUCTURE AND NMR SPECTRA OF AQUEOUS MIXTURES OF [C4MIM][BF4] IONIC LIQUID: A QM/MD STUDY	P7-20	415
Did not participate	P7-21	416
Eglė Šidlauskaitė, Antanas Vaitkus, Andrius Merkys DERIVATION OF A COVALENT RADII TABLE FROM OPEN CRYSTALLOGRAPHIC DATA	P7-22	417
Audrė Kalinauskaitė, Inga Garbarienė, Agnė Minderytė, Julija Pauraite, Vadimas Dudoitis, Lina Davulienė, Kristina Plauškaitė-Šukienė, Vitalij Kovalevskij, Mindaugas Gaspariūnas, Steigvilė Byčenkienė INVESTIGATION OF MULTIELEMENTAL CONTENTS OF PM1 IN INDOOR AND OUTDOOR AIR	P7-23	418
Tetiana Tortykh, Oleg Shyniruk, Arkadiy Petukhov STUDY OF MELT FLOW INDEX FOR POST-CONSUMER MIXED POLYOLEFINS AFTER ADDITIONAL FILTRATION	P7-24	419
Ieva Bagamulskytė, Kristina Bunevičienė EFFECTS OF WOOD BIOFUEL ASH ON THE CHEMICAL COMPOSITION AND QUALITY OF MAIZE GROWN	P7-25	420
Lukas Graibus, Rita Butkutė, Juozas Vidas Gražulevičius SYNTHESIS AND INVESTIGATION OF PHENANTHROIMIDAZOLE DERIVATIVES FOR ORGANIC LIGHT EMITTING DIODES	P7-26	421
Nadežda Traškina, Jurgis Pilipavičius, Jurga Juodkazytė, Linas Vilčiauskas ADJUSTING ELECTROLYTE FOR HYDROGEN EVOLUTION SUPPRESSION IN NA-ION AQUEOUS BATTERIES	P7-27	422
Karolina Aleknaite, Laura Peciulyte, Deimante Rosliuk, Ramune Rutkaite MICROGRANULAR STARCH ACETATES AND CROSS-LINKED STARCH ACETATES FOR ADSORPTION OF ALKYL PARABENS	P7-28	423
Paulina Nemaniutė, Marijus Jurkūnas, Dalia Bražinskienė, Svajus J. Asadauskas VISCOSITY VARIATION DURING ADDITION OF POLYGLYCOLS TO TRIFUNCTIONAL ISOCYANATE	P7-29	424
Joanna Janus, Aleksandra Kołodziejczyk, Aleksandra Wajda, Krzysztof Czamara, Agnieszka Kaczor BINDING OF ASTAXANTHIN TO BOVINE SERUM ALBUMIN AND ITS INFLUENCE ON CAROTENOID TRANSPORT TO ADIPOCYTES – ECD SPECTROSCOPY AND RAMAN IMAGING STUDIES	P7-30	425
Laura Michailova, Irena Savickaja, Vidas Pakštas, Jurga Juodkazytė, Milda Petrulevičienė INFLUENCE OF TEMPERATURE ON FORMATION OF BIVO4 PHOTOANODE	P7-31	426
Sonata Pleskytė, dr. Ieva Uogintė SEASONAL VARIATION OF MICROPLASTIC ABUNDANCE AND CHARACTERISTICS IN SEWAGE SLUDGE	P7-32	427
Kasparas Kižys, Inga Morkvėnaitė-Vilkončienė, Wojciech Nogala ELECTROCHEMICAL IMAGING OF SACCHAROMYCES CEREVISIAE BY SCANNING ELECTROCHEMICAL MICROSCOPY	P7-33	428
Viktorija Reinikovaitė, Eivydas Andriukonis, Arūnas Ramanavičius POLYDOPAMINE AND POLYPYRROLE APPLICATION IN YEAST BIOFUEL CELLS: A SHORT POLYMER SYNTHESIS FOR BETTER FUNCTION	P7-34	429
Pavlo Sivolapov, Oleksiy Myronyuk, Denis Baklan, Valentyn Svidersky INFLUENCE OF SOLVENT POLARITY ON STOBER PARTICLES SIZE	P7-35	430
Karolina Karalevičiūtė, Galina Lujanienė CHITOSAN-CLAY-BASED COMPOSITES FOR SORPTION OF CS, CO, EU FROM AQUEOUS SOLUTIONS	P7-36	431
Karolina Almonaityte, Joana Bendoraitiene, Diana Masiulionyte, Ramune Rutkaite SYNTHESIS AND USE OF CATIONIC POTATO STARCH FLOCCULANTS FOR WASTEWATER SLUDGE SEPARATION	P7-37	432
Goda Gudinskaitė, Rasa Šlinkšienė, Rasa Paleckienė INFLUENCE OF AMINO ACIDS ON THE PROPERTIES OF LIQUID FERTILIZERS	P7-38	433
Davit Tediashvili, Linas Vilčiauskas CHARACTERIZATION OF MN-BASED PHOSPHATE FRAMEWORKS AS AQUEOUS NA-ION BATTERY CATHODES	P7-39	434
Augustas Antanaitis, Aldona Balčiūnaitė, Loreta Tamašauskaitė-Tamašiūnaitė, Eugenijus Norkus. 3D COATED GOLD(NICKEL, MOLYBDENUM)/TITANIUM CATALYST FOR THE GLUCOSE OXIDATION	P7-40	435
Monika Bertašiūtė, Vytautas Mickevičius SYNTHESIS OF NEW 1,3-DISUBSTITUTED PYRROLIDINONES WITH BENZIMIDAZOLE MOIETY	P7-41	436
Žana Činčienė, Aldona Balčiūnaitė, Loreta Tamašauskaitė-Tamašiūnaitė, Jūratė Vaičiūnienė, Eugenijus Norkus CUNI CATALYSTS MODIFIED WITH AU AND PT NANOPARTICLES FOR DIRECT BOROHYDRIDE FUEL CELLS	P7-42	437
Kristaps Saršūns, Toms Reķis, Agris Bērziņš SOLID SOLUTION FORMATION AMONG METHYL 4-HALOGENBENZOATE DERIVATIVES - EXPERIMENTAL AND COMPUTATIONAL INVESTIGATION	P7-43	438
Milana Kudus, Annu Sharma, Nikola Kanas, Subramshu Bhattacharya, Maria Uzelac, Stevan Armaković, Sanja J. Armaković PHOTOCATALYTIC PROPERTIES OF SR0.9LA0.1TIO3 AND SR0.25CA0.25NA0.25PR0.25TIO3 NANO-SIZED POWDERS	P7-44	439
Jolita Stabrauskienė, Jurga Bernatonienė, Mindaugas Marksa QUANTIFICATION OF FLAVANONES FROM THE FRESH FRUITS PARTS OF CITRUS XPARADISI.L USING DIFFERENT EXTRACTION AND HYDROLYSIS METHODS	P7-45	440

EXPERIMENTAL EVIDENCE OF THE NONDEGENERATE PARAMETRIC GAIN IN QUANTUM SUPERLATTICES

Vladislovas Čižas[1], Kirill Alekseev[1], Gintaras Valušis[1]

[1] Department of Optoelectronics, Center for Physical Sciences and Technology, Sauletėkio al. 3, Vilnius, Lithuania
vladislovas.cizas@ftmc.lt

Despite constantly increasing demand for small, powerful and cost-efficient THz radiation sources, there still is a significant lack of such emitters operating at room temperature. Invention of quantum semiconductor superlattices by Esaki and Tsu [1], allows employing them as a platform for high-frequency parametric generation or amplification. Although the theoretical explanation of these processes was noticeably developed throughout almost 50 years, there was no experimental evidence, leading to the unconformity of theoretical assumptions [2, 3].

In this work, experimental evidence of parametric gain in GaAs/AlGaAs superlattice was observed for the first time. It resulted in generation of harmonics, sub-harmonics and fractional frequencies corresponding to the multiphoton generation process described by

$$\omega_1 \pm \omega_2 = n_{\pm}\omega_0; \qquad 2\omega_1 = n_0\omega_0 \tag{1}$$

equations [4, 5]. As each of the spectral line in the recorded dataset can be assigned to participation in several multiphoton processes (with different $n_{\pm}$) simultaneously, it shows the need to upgrade the existing theoretical model which does not take into account simultaneous occurrence of several multiphoton processes. This argument was also confirmed by the discrepancy between the experimental power profile and the theoretical gain profiles.

Matching of superpositioned theoretical multi-photon gain profile and the experimental emission power dependency on static field strength was performed for one of the frequency datasets (Fig.1). Such superposition becomes possible due to existance of profile peculiarities, allowing to express and manipulate superpositioned gain profile using the equation

$$\left(\frac{\mu}{\mu_0}\right)_{total} = \sum_{n=1,2,3\ldots} C_n \cdot \frac{\mu_n}{\mu_0}\,, \tag{2}$$

where C_n is the weight coefficient. The fit performed for n=1,2,3 processes resulted in pecularity-matching gain profile. Inverse weight coefficient proportionality to n also meets theoretical considerations showing that processes with smaller n values have bigger influence on the final gain profile.

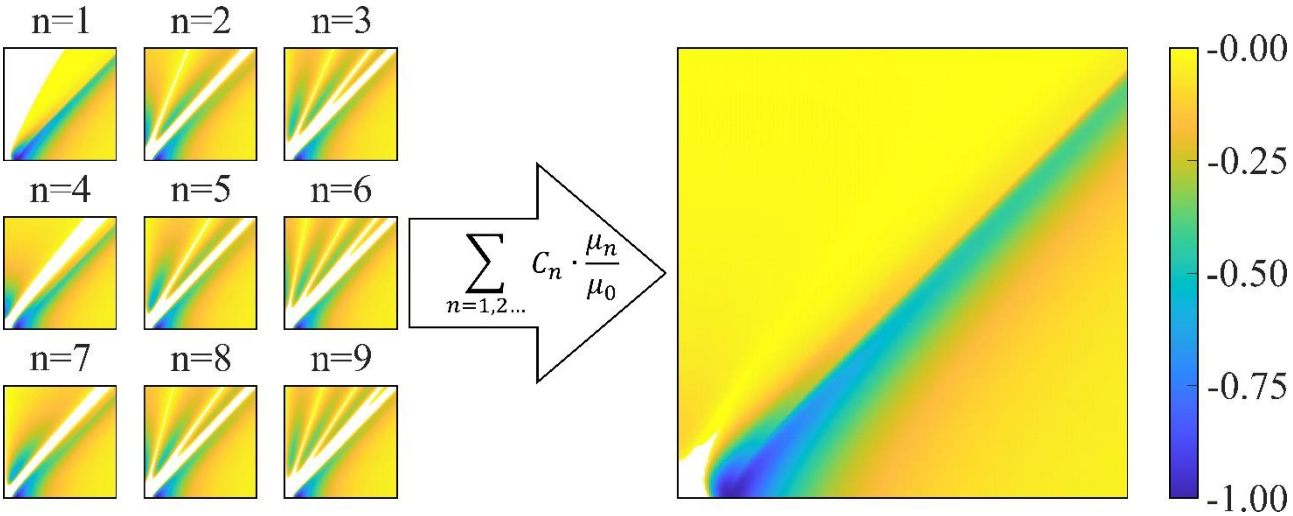


Fig. 1. Process of single multiphoton parametric gain profile superposition to illustrate multiphoton generation/amplification processes.

Such upgrade of the theoretical model allows to confirm obtained experimental results for the dissipative parametric high-frequency generation/amplification in quantum semiconductor superlattices.

[1] L. Esaki and R. Tsu, Superlattice and negative differential conductivity in semiconductors, IBM Journal of Research and Development **14-1**, 61-65 (1970).
[2] T. Hyart, A.V. Shorokhov and K.N. Alekseev, Theory of parametric amplification in superlattices, PRL **98-22**, 220404 (2007).
[3] T. Hyart, N.V. Alexeeva, A. Leppanen and K.N. Alexeev, Terahertz parametric gain in semiconductor superlattices in the absence of electric domains, APL **89**, 132105 (2006).
[4] Y.A. Romanov and J.Y. Romanova, Self-oscillations in semiconductor superlattices, JETP **91-5**, 1193-1206 (2000)
[5] J.Isohätälä and K.N. Alexeev, arXiv:1201.6280; Jukka Isohätälä, PhD Thesis, University of Oulu (2012).

STATISTICAL ANALYSIS OF ORGANIC ELECTROCHEMICAL TRANSISTORS WITH PHOTOPATTERNABLE SOLID ELECTROLYTE

Juzef Kučinski[1], Hsin Tseng[2], Lina Mikoliūnaitė[1], Karl Leo[2], Hans Kleemann[2*]

[1] Faculty of Chemistry and Geosciences, Vilnius University, Lithuania
[2] Dresden Integrated Center for Applied Physics and Photonic Materials, Dresden University of Technology, Germany
juzef.kucinski@chgf.stud.vu.lt

In the last twenty years, organic electronics have been rapidly developed and it is expected to replace inorganic semiconductors in a number of uses in the near future [1]. Organic photovoltaics, organic light-emitting diodes, and organic thin-film transistors are highly advanced and already available commercially. Recently, organic electrochemical transistors (OECTs) are being researched and promise us breakthroughs in flexible printed sensors, electronic skin, OECTs based logic circuits, and implantable sensors [2, 3]. An OECT consists of an organic semiconductor film that is in contact with an electrolyte, in which the gate electrode is immersed. Applying a potential to the gate electrode can make semiconductor film more or less conductive by reducing or oxidizing it (doping/de-doping). Because of that, OECTs can be used in sensor signal amplification and ion-to-electron transduction. Organic semiconductor films used in OECTs are often based on conductive polymers, mostly poly(3,4-ethylenedioxythiophene) polystyrene sulfonate (PEDOT:PSS).

Even though developed PEDOT:PSS-based OECTs (Fig.1. (a)) achieve excellent performance with on-off ratios of 10^5, a threshold voltage of 200 mV, and a sub-threshold swing of 61 mV dec^{-1}, however, OECTs have to be reliable to use it in circuits [4]. It is essential to have transistors with stable and reproducible parameters: threshold voltage, on-off current, subthreshold slope, and transconductance. These values tend to differ a lot from sample to sample and because of that, it is crucial to understand the underlying problem in the fabrication process. This can be achieved by quantifying the variation of parameters and, in a second step, improving the fabrication process.

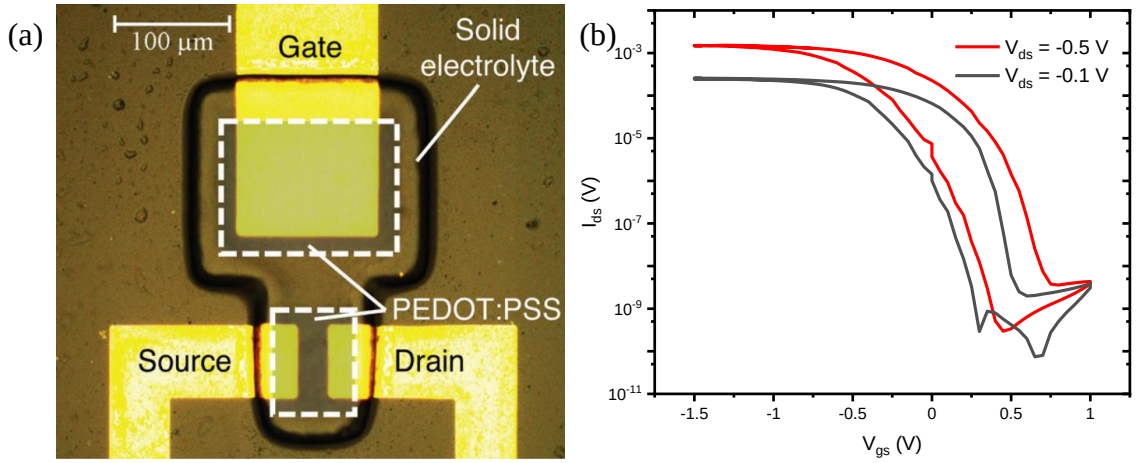


Fig. 1. (a) Micrograph of an OECT with patterned solid electrolyte [4]. (b) Transfer characteristics of OECTs with different drain voltages. Transfer curves are used to calculate threshold voltage, on-off current, subthreshold slope, and transconductance.

Discussed OECTs were developed in advance by co-workers and can be fabricated using well established 3-step lithography. We constructed solid-state OECTs with various geometrical parameters and collected data for statistical analysis by measuring transfer characteristics (Fig.1. (b)) of an OECTs using different drain voltages (V_{ds} = - 0.1 V; - 0.5 V; - 1 V; - 1.5 V). Mean values and standard deviation were calculated, Grubs and normality tests were used to describe the data. Using the collected data, we adjusted the fabrication process to lower standard distribution and increase the reproducibility of PEDOT:PSS based OECTs.

[1] Rivnay, J., Inal, S., Salleo, A., Owens, R. M., Berggren, M., & Malliaras, G. G. (2018). Organic electrochemical transistors. In Nature Reviews Materials (Vol. 3). Nature Publishing Group. https://doi.org/10.1038/natrevmats.2017.86
[2] Marquez, A. V., McEvoy, N., & Pakdel, A. (2020). Organic Electrochemical Transistors (OECTs) Toward Flexible and Wearable Bioelectronics. In Molecules (Basel, Switzerland) (Vol. 25, Issue 22). NLM (Medline). https://doi.org/10.3390/molecules25225288
[3] Tseng, H., Cucchi, M., Weissbach, A., Leo, K., & Kleemann, H. (2021). Membrane-Free, Selective Ion Sensing by Combining Organic Electrochemical Transistors and Impedance Analysis of Ionic Diffusion. ACS Applied Electronic Materials. https://doi.org/10.1021/acsaelm.1c00486
[4] Weissbach, A., Bongartz, L. M., Cucchi, M., Tseng, H., Leo, K., & Kleemann, H. (2022). Photopatternable solid electrolyte for integrable organic electrochemical transistors: operation and hysteresis. Journal of Materials Chemistry C. https://doi.org/10.1039/d1tc04230k

OPTIMIZATION OF QUANTUM WELL GROWTH TECHNOLOGY FOR APPLICATIONS IN NEAR INFRARED VERTICAL-EXTERNAL-CAVITY SURFACE-EMITTING LASERS

Andrea Zelioli[1], Arnas Pukinskas[1], Algirdas Jasinskas[1], Simona Pūkienė[1], Silvija Keraitytė[1, 2], Arnas Naujokaitis[1], Martynas Skapas[1], Monika Jokubauskaitė[1], Evelina Dudutienė[1], Artūras Suchodolskis[1], Bronislovas Čechavičius[1] and Renata Butkutė[1, 2]

[1] Center for Physical Sciences and Technology, Vilnius, Lithuania

[2] Institute of Photonics and Nanotechnology, Faculty of Physics, Vilnius University, Lithuania

andrea.zelioli@ftmc.lt

Several types of lasers, such as, solid-state, semiconductor, gas, excimer, and dye lasers, have been developed. Today lasers are used in many fields, particularly in optical fiber communication, optical digital recording, material processing, biology and medicine, spectroscopy, imaging, entertainment, and many others. Due to exceptional material properties and/or investigation conditions various application require unique set of laser parameters - emission wavelength, its tunability, beam quality, operation temperature, optical output power, as well as convenient method of laser excitation, power consumption, high-speed modulation and device size is very important.

Vertical-external-cavity surface-emitting lasers (VECSEL) also called optically pumped semiconductor lasers (OPSL) or semiconductor disk laser (SDL) belong to relatively new laser family that combines many of the desirable properties. VECSELs were developed to overcome key problems typical to conventional semiconductor lasers. In comparison to both types of electrically pumped Vertical-cavity surface-emitting lasers (VCSELs), which emit circular fundamental transverse mode beam but exhibit low power and edge emitting lasers (Fabry-Perot and DFB) that can reach high output power but an asymmetric beam with strong angular divergence, VECSELS are capable to generate high optical power with circular beam quality.

In this work the main activity was focused to investigation of the technological parameters required to grow high quality GaAsBi quantum structures, balance the strain during the growth procedure, obtain sharp interfaces and investigate photoluminescence properties. The multiple quantum well structures were grown using solid-source MBE system (Veeco GENxplor R&D) equipped with standard cells for metallic Al, Ga, Bi and unique As design source generating arsenic dimers flux. The semi-insulating GaAs substrate oriented in (001) crystalline plane was selected for the growth of the structures. During this work the thickness of the quantum wells has been kept constant at 10nm.Fig.1 demonstrates two different geometries of quantum wells investigated in this work. The design of sample shown in Fig. 1a consists of two separated quantum wells with parabolic barriers of AlGaAs. While sample b contains three quantum wells separated by usual shape GaAs barriers enclosed by AlGaAs parabolic barriers.

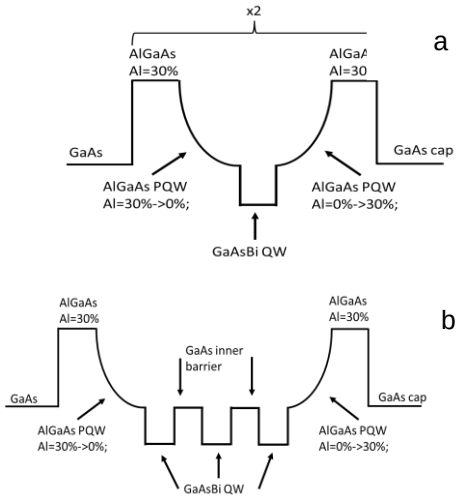


Fig. 1. Two types of multiple GaAsBi/GaAs/AlGaAS quantum well designs.

To obtain high crystalline quality and enhanced optical properties of MQW structures the temperature of the substrate was varied from 420 ºC to 425 ºC, and the beam equivalent pressure ratios of Bi/Ga as well As/Ga were changed in the ranges of 1.05-1.10 and 0.4-3.0, respectively.

The HR-TEM and STEM investigation evidenced that GaAsBi QWs with AlGaAs PQBs were formed successfully (see Fig. 2). The profiling of atomic composition measured along growth direction (orange line) confirmed the parabolic Al increase and decrease in barriers and step-like Bi profile in QW. The microscopy pictures presented in Figure 2 shows typical cross-sections of GaAsBi QW surrounded by parabolic AlGaAs barriers and zoomed TEM picture of GaAsBi QW. Visible atomic columns in fig. 2 left picture illustrates the highest crystalline quality of grown samples with no defects and dislocations.

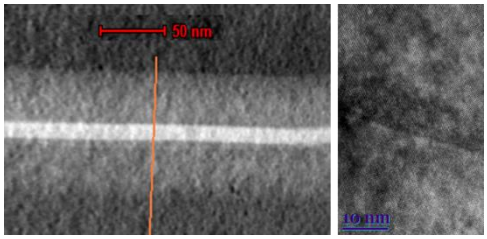


Fig. 2 The cross-section picture of the samples containing two parabolic QW investigated by STEM (on the left), and HR-TEM (on the right).

The photoluminescence measurements determined the relationship between the growth conditions and emission energy and intensity and highlighted the crucial growth parameters - As/Ga beam equivalent pressure ratio, Bi flux, growth rate and substrate temperature.

THE APPLICATION OF THE SCAN DENSITY FUNCTIONAL TO COLOUR CENTRES IN DIAMOND

Vytautas Žalandauskas[1], Marek Maciaszek[1], Lukas Razinkovas[1], Audrius Alkauskas[1]

[1] Department of Fundamental Research, Center for Physical Sciences and Technology (FTMC), Lithuania
vytautas.zalandauskas@ftmc.lt

Over the past decades, the Kohn-Sham density functional theory (DFT) [1] has become the main tool to investigate the atomic and the electronic structure of solids. While being in principle exact, the theory needs to invoke approximations to the so-called exchange-correlation (XC) contribution to the total energy, as the exact form of this contribution is unknown. Currently, the most popular functionals applied to solids are semilocal functionals based on the generalized-gradient approximation (GGA), in particular the Perdew-Burke-Ernzerhof (PBE) functional [2], and hybrid functionals that incorporate a fraction of (screened) Fock exchange, especially the Heyd-Scuseria-Ernzerhof (HSE) [3]. The biggest drawback of the GGA functionals is the well-known under-estimation of the band gap of semiconductors and insulators. Hybrid functionals provide a much improved description of the electronic structure, including the band gap, albeit at a much increased computational cost.

In 2015, a new semilocal meta-GGA class functional SCAN was introduced [4]. The advantages offered by the SCAN functional are particularly relevant for point defects in solids. These systems are most conveniently modelled using the supercell-approach. The supercells typically contain a few hundreds of atoms, and computational efficiency is important here, especially when analyzing many point defects. In addition, a better description of the band gap of the host material leads to a better description of defect levels that are situated in the band gap. However, despite an increasing popularity of the SCAN functional in modeling bulk materials [5], its application to defects has been scarce so far [6]. Thus, the benefits of the SCAN functional in the modelling of defects are currently little known.

In this work, we benchmarked the SCAN density functional for colour centres in diamond. Our chosen defects were: the nitrogen-vacancy (NV) centre, the silicon-vacancy (SiV) centre, and the germanium-vacancy (GeV) centre. Over the past two decades, these colour centres have gained prominence in various quantum-technological applications, in particular in quantum sensing, quantum communication, and even quantum computing. Our goal was to compare the parameters computed with the SCAN functional with those obtained using more traditional PBE and HSE functionals. These parameters were: formation energies, charge-state transition levels, optical excitation energies, lattice relaxation energies, as well as Jahn-Teller parameters. As a prerequisite, we applied the SCAN functional to bulk diamond, and compare the obtained results with PBE and HSE functionals. Our results show that the meta-GGA functionals SCAN and rSCAN yield very good results for modelling of colour centres in diamond and are often good alternatives to hybrid functionals.

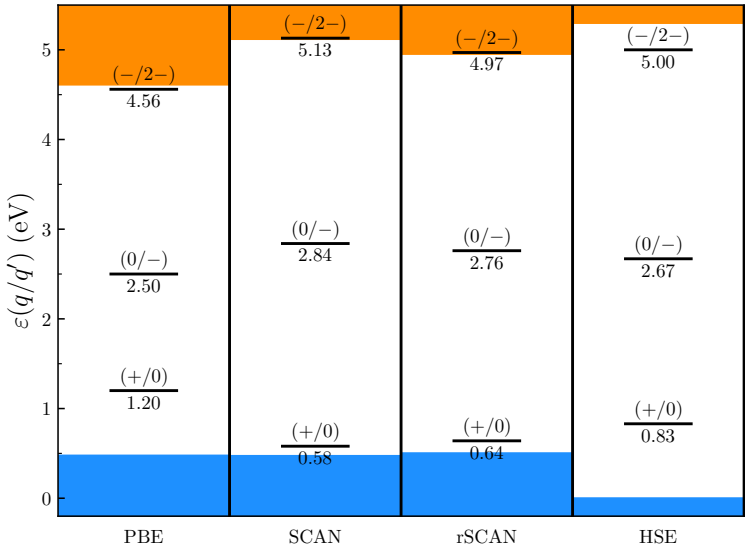


Fig. 1. Charge-state transition levels of the nitrogen-vacancy (NV) centre in diamond calculated with various functionals, aligned with respect to the average electrostatic potential.

[1] R. M. Martin, Electronic structure. Basic theory and practical methods, Cambridge University Press (2004).
[2] J. P. Perdew, K. Burke, and M. Ernzerhof, Physical Review Letters **77**, 3865 (1996).
[3] J. Heyd, G. Scuseria, and M. Ernzerhof, Journal of Chemical Physics **118**, 8207 (2003).
[4] J. Sun, A. Ruzsinszky, and J. P. Perdew, Physical Review Letters **115**, 036402 (2015).
[5] J. H. Yang, D. A. Kitchaev and G. Ceder, Physical Review B **100**, 035132 (2019).
[6] T. Rauch, F. Munoz, M. A. L. Marques, and S. Botti, Physical Review B **104**, 064105 (2021).

STUDY OF LUMINESCENCE SPECTRA DECAY IN NONPOLAR InGaN/GaN MQWs

Elena Valkiūnaitė, Jūras Mickevičius

[1] Institute of Photonics and Nanotechnology, Faculty of Physics, Vilnius University, Lithuania
elena.valkiunaite@ff.vu.stud.lt

Nonpolar (a- or m-plane) InGaN/GaN multiple quantum wells (MQWs) attract attention due to the absence of polarization-related electric field, which should improve the optical performance, and capability to emit highly polarized light. On the other hand, non-polar InGaN structures often exhibit two bands in the photoluminescence (PL) spectrum, with their origin still unclear. To gain more insight about the origin of double-band emission, the time evolution of the two PL bands was studied by time-resolved photoluminescence spectroscopy (TRPL).

In this work, we present the study of PL decay in non-polar InGaN/GaN MQWs with the main focus on the decay of different PL bands. The PL spectra of seven m-plane InGaN/GaN samples were measured at different delay times under several excitations. The seven samples under study can be categorized into three groups: i) structures having the same QW and barrier thicknesses of 8 and 9 nm, respectively, but with different In content from 9% to 13%; ii) structures with the same In content of 13% in the QWs, but having different QW and barrier thicknesses; and iii) additional pair of samples with In content of 14% and QW width of 4 nm, deposited at slightly different growth conditions.

All the studied m-plane InGaN structures showed double-band emission, except for one sample with 9% of In. The typical time dependence of spectrally-integrated PL intensity is shown in Fig. 1. A clear nonexponential decay is observed for all excitations. In this case, the PL dynamics can be characterized by two decay times - fast and slow components of bi-exponential function. The characteristic time of the fast initial decay is similar to the laser pulse duration of 4 ns. Meanwhile, the slow component of PL intensity decays with characteristic time of ~200 ns and might be attributed to the radiative recombination of deeply localized carriers and/or defects. For the studied samples, the PL intensity decay at highest excitation varies around 200 ns and decreases to approximately 170 ns for lower excitations. The longest decay time (~250 ns) is reached in the sample with 13% In content, 8 nm QW width and 15 nm barriers. Analysis of the individual PL bands revealed their different decay rates: the short-wavelength band decayed faster. Such behaviour was attributed to the carrier capture to localized states and/or defects.

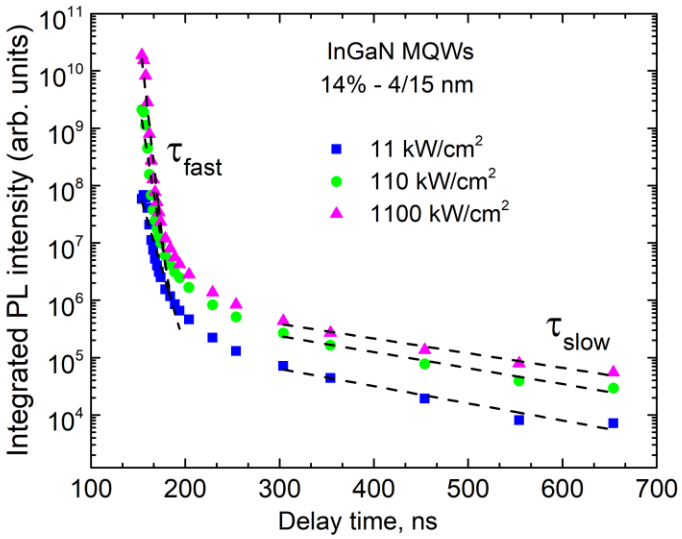


Fig. 1 Time-resolved PL kinetics of m-plane InGaN MQWs with varying excitation.

ECD-RAMAN EFFECT AS A NEW PHENOMENON IN CHIROPTICAL SPECTROSCOPY

Agnieszka Domagała[1], Ewa Machalska[1,2], Grzegorz Zając[2], Małgorzata Barańska[1,2]

[1] Faculty of Chemistry, Jagiellonian University, Gronostajowa 2, 30-387 Cracow, Poland
[2] Jagiellonian Centre for Experimental Therapeutics (JCET), Jagiellonian University, Bobrzynskiego 14, 30-348 Cracow, Poland
agnieszka.domagala@student.uj.edu.pl

Chiroptical spectroscopy techniques are becoming more and more popular due to their wide application in the study of structure of chiral compounds as well as supramolecular systems. They can detect even small changes that are impossible to observe using conventional spectroscopic methods. Chiroptical spectroscopies include Electronic Circular Dichroism (ECD), Raman Optical Activity (ROA), Vibrational Circular Dichroism (VCD) and Circularly Polarized Luminescence (CPL). [1]

In our research ECD and ROA were used as well as their non-chiroptical analogues, UV-Vis Spectroscopy and Raman Spectroscopy. Electronic Circular Dichroism measures a difference between left and right circularly polarized absorbed light due to chiral compounds. It is a very sensitive tool that provides rich information about the ground electronic state of molecules. Raman Optical Activity is based on inelastic scattering of light. It measures a difference between right and left circularly polarized Raman scattered light due to chiral compounds. It is much less sensitive than ECD, therefore it is necessary to prepare very well purified samples in high concentrations and do measurements with high laser power and long time of spectrum accumulation. [2]

Recently, a new phenomenon of interference of Electronic Circular Dichroism and Raman Optical Activity was discovered. It is known as ECD-Raman effect and occurs for chiral samples that absorb laser light and have an ECD band in the wavelength range of the laser line used in ROA measurements (in our research it was 532 nm). As shown in Figure 1, the ECD-Raman effect is related to the polarization of the laser beam after passing through the chiral sample, and then additional polarization of the scattered light. [1,3] The effect is possible to observe at ROA spectra because it is enriched with an additional, sometimes dominant, component for both the achiral solvent and chiral solute bands. Recognition of ECD-Raman effect and its minimization is important for the correct interpretation of the ROA spectra and appropriate concluding about the molecular structure of measured compounds.

In our research we carried out the spectroscopic analysis of chiral naphthalene diimide derivatives [4] dissolved in achiral organic solvents (i.e., chloroform, $CHCl_3$ and dimethylsulfoxide, DMSO). For each of the compounds, the vibrational spectra were dominated by achiral solvent bands and chiral solute bands was barely seen. The sign of the ROA spectra was complied with the sign of ECD band in range of the excitation laser line. These observations proved the ECD-Raman effect occurrence.

This work was supported by National Science Centre in Poland (Grant No. 2020/39/B/ST4/01670 and Grant No. 2019/33/N/ ST4/01986).

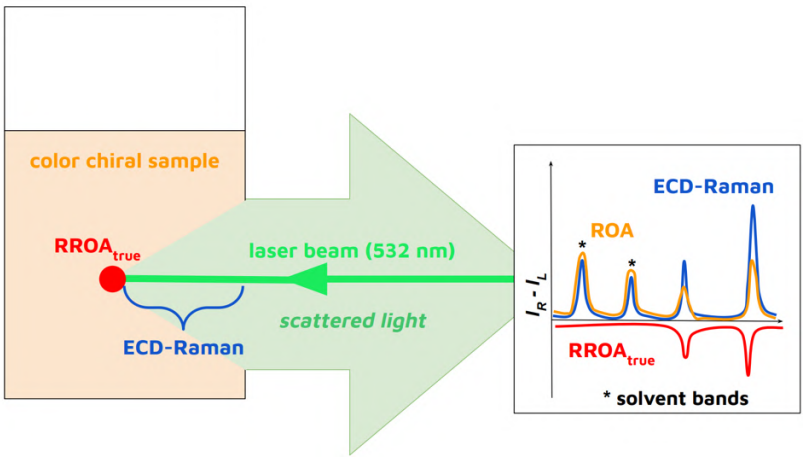


Fig. 1. Interference of ECD and ROA and its effect on the ROA spectrum.

[1] E. Machalska, G. Zajac et al., Recognition of the True and False Resonance Raman Optical Activity, Angew. Chem. Int. Ed. 2021, **60**, 21205–21210.
[2] G. Zajac, P. Bouř, Measurement and Theory of Resonance Raman Optical Activity for Gases, Liquids, and Aggregates. What It Tells about Molecules, J. Phys. Chem. B 2021, XXX, XXX-XXX.
[3] T. Wu et al., Two Spectroscopies in One: Interference of Circular Dichroism and Raman Optical Activity, Angew. Chem. Int. Ed., 2020, **59**, 21895 –21898.
[4] E. Machalska et al., On Raman optical activity sign-switching between the ground and excited states leading to an unusual resonance ROA induced chirality, Chem. Sci., 2021, **12**, 911–916.

RAMAN OPTICAL ACTIVITY OF POLYENE ANTIBIOTICS: PRE-RESONANCE SIGNAL ENHACEMENT DUE TO AGGREGATION PROCESS

Katarzyna Gorczowska[1], Ewa Machalska[1,2], Malgorzata Baranska[1,2]

[1] Faculty of Chemistry, Jagiellonian University, Gronostajowa 2, 30-387 Cracow, Poland
[2] Jagiellonian Centre for Experimental Therapeutics (JCET), Jagiellonian University, Bobrzynskiego 14, 30-348 Cracow, Poland
katarzyna.gorczowska@student.uj.edu.pl

Amphotericin B (AmB) is an antibiotic that is a golden standard in the treatment of fungal infections [1]. It's exceptional effectiveness in therapeutic action is accompanied by significant side effects. Despite many years of using this drug the mechanism of the therapeutic and toxic effect has not been thoroughly understood, which makes AmB subject of numerous scientific studies [2]. The antibiotic's amphiphilic properties results in the ability of AmB to self-association and self-aggregation into numerous molecular structures which affects the way the antibiotic works and the dependence of these processes on many environmental factors makes the topic more complex [3].

In the present study, we analyzed various molecular forms of AmB by means of spectroscopic methods like UV-Vis absorption spectroscopy, Raman spectroscopy and chiroptical methods, such as Electronic Circular Dichroism (ECD) and Raman Optical Activity (ROA). It was confirmed that the aggregation process of the antibiotic is highly sensitive to environmental conditions but also to the method of sample preparation. The research has shown that AmB can occur in the form of J and H aggregates, showing characteristic bato- and hypsochromic band shifts on the UV-Vis and ECD spectra. Additionally, spectroscopic changes in the Raman spectra were analyzed and marker bands of aggregation process were identified. An extremely important research aspect was the statement that supramolecular aggregates of AmB generate a pre-resonance ROA signal unlike the monomer form. It is caused by the process of self-assembly of molecules into larger systems. Because of that, Aggregation-Induced Resonance ROA (AIRROA) may be a very useful method to obtain the ROA signal. Pre-resonance ROA spectra of AmB monomer and super-aggregate confirming that statement were shown in Fig. 1.

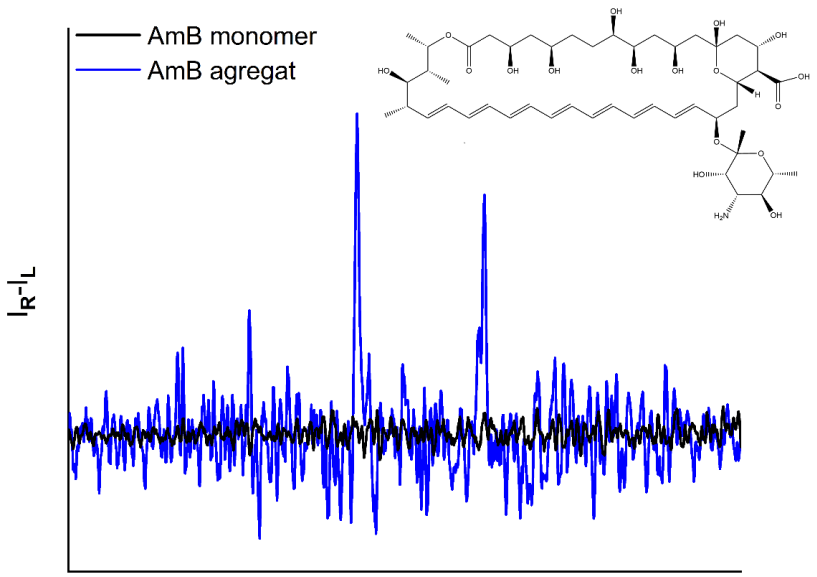


Fig. 1. Pre-ROA spectra of AmB monomer (black line) and aggregate (blue line).

This work was supported by National Science Centre in Poland (Grant No. 2019/33/N/ ST4/01986).

[1] H. G. Brittain Circular Dichroism Studies of the Self-Association of Amphotericin B, CHIRALITY, 6:665-669 (1994).
[2] M. Gagoś, M. Arczewska, W. I. Gruszecki, Raman Spectroscopic Study of Aggregation Process of Antibiotic Amphotericin B Induced by H+, Na+, K+ Ions, J. Phys. Chem. B **115**, 5032–5036 (2011).
[3] L. P. Jameson, S. V. Dzyuba, Effect of Imidazolium Room-temperature Ionic Liquids on Aggregation of Amphotericin B: A Circular Dichroism Study, RSC Adv. **5**, 80325–80329 (2015).

INVESTIGATION OF INTERSYSTEM CROSSING IN OLIGOYNES

Eglė Tankelevičiūtė[1], Paulius Baronas[1], Regimantas Komskis[1], Povilas Adomėnas[2], Ona Adomėnienė[2], and Saulius Juršėnas[1]

[1] Institute of Photonics and Nanotechnology, Vilnius University, Vilnius, Lithuania
[2] Fine Synthesis, Ltd., Kalvarijų g. 201E, LT-08311, Vilnius, Lithuania
egle.tankeleviciute@ff.stud.vu.lt

Compounds with strong spin-orbit coupling (SOC) and fast intersystem crossing (ISC) are important for organic light emitting diodes and photosensitizers used for photo-dynamic therapy [1]. However, achieving a high ISC rate usually requires heavy atoms, such as Pt or Ru, thus making materials of this kind not cost-efficient. Here, we propose a concept to enhance SOC in carbon-only structures by taking advantage of helical molecular orbitals (Hel-MOs) [2]. Intersystem crossing dynamics in bifluorenes were investigated by means of pump-probe measurements, which indicated that minor modifications of the molecule (extended alkyne bridge) cause considerable (25-fold) increase of ISC rate. Furthermore, theoretical calculations were performed to confirm the helical shape of the MO in the dialkyne bridge unit in rotational conformers and to evaluate their parameters. Theoretical ISC rate suggested conformers are a must when explaining strong spin-orbit coupling. Formation of helical molecular orbitals results in enhanced SOC leading to an increased ISC rate.

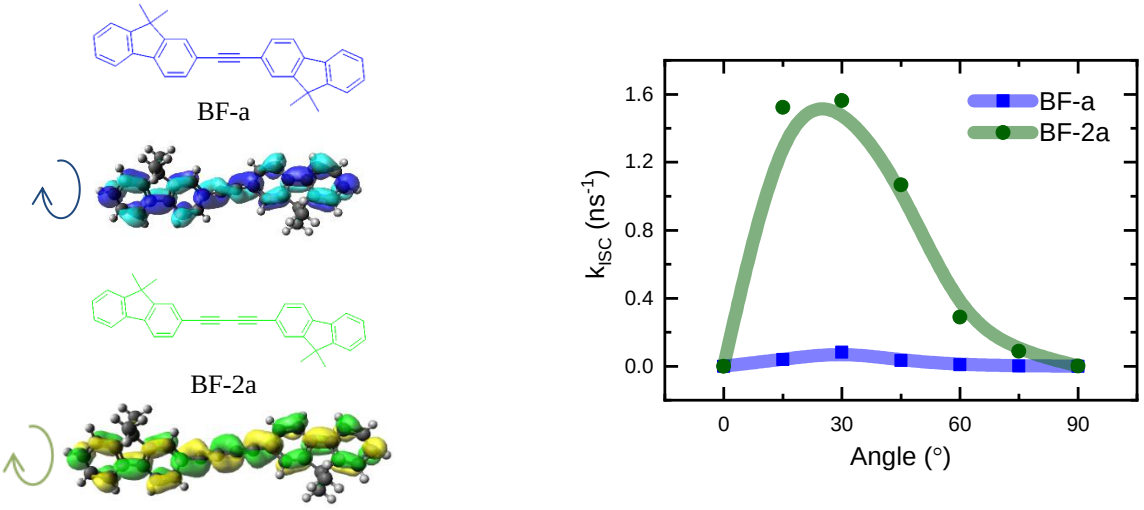


Fig. 1. Bifluorene molecules and their calculated ISC rates

[1] D. Sasikumar, A. T. John, J. Sunny, M. Hariharan, Chem. Soc. Rev. 2020, 49, 6122.
[2] P. Baronas, R. Komskis, E. Tankelevičiūtė, P. Adomėnas, O. Adomėnienė, S. Juršėnas, J. Phys. Chem. Lett. 2021, 12(29), 6827–6833.

FULFILLMENT OF LOCAL THERMODYNAMIC EQUILIBRIUM IN ARGON ENVIRONMENT FOR CALIBRATION-FREE LIBS MEASUREMENT OF HYDROGEN ISOTOPES

Jasper Ristkok[1], Indrek Jõgi[1], Peeter Paris[1]

[1] Institute of Physics, University of Tartu, Estonia
jasper.ristkok@ut.ee

To counter the rising energy demand of humanity a new energy source – fusion – is being researched. A new fusion reactor ITER is being built in France with first plasma scheduled in 2025. ITER tokamak is unique because it will have tenfold return of energy thus being the first fusion reactor to have positive net power. [1]

The fuel to be used in ITER will be deuterium (D) and tritium (T) mixture. Safety regulations require observations of T retention in plasma facing components since T is radioactive [2]. Therefore, it is necessary to develop diagnostical methods to measure fuel retention in walls of ITER. One such method suitable for use in ITER is laser-induced breakdown spectroscopy (LIBS).

LIBS apparatus uses a powerful laser pulse which is focused on a small spot on the investigated material. A small amount of the material is ablated and heated into plasma plume. The plume emits light characteristic to the investigated material and the emission spectrum of the plume is then used to determine the elemental composition of the material.

Calibration-free LIBS (CF-LIBS) is considered because exact calibration of LIBS for ITER conditions is very difficult. However, application of CF-LIBS requires the fulfilment of certain conditions in the laser-induced plasma and deviation from these conditions might lead to erroneous results. The aim of this work is to estimate the fulfilment of one such necessary condition for CF-LIBS: local thermodynamic equilibrium (LTE).

Experiments were carried out in argon environment at different pressures. The investigated material was molybdenum with hydrogen impurities to simulate ITER-relevant materials. Spectra were recorded at delay times from 200 ns to 6 µs after the laser pulse and at different distances from the target depending on the plume expansion.

Occasionally CF-LIBS might determine erroneous hydrogen isotope concentrations. The experiments show that one source of errors is the deviation from LTE. Three criteria for the existence of LTE were considered (Fig. 1). Under no conditions were all criteria completely fulfilled. Further research is needed to characterize the relation between CF-LIBS accuracy and the relative fulfilment of LTE.

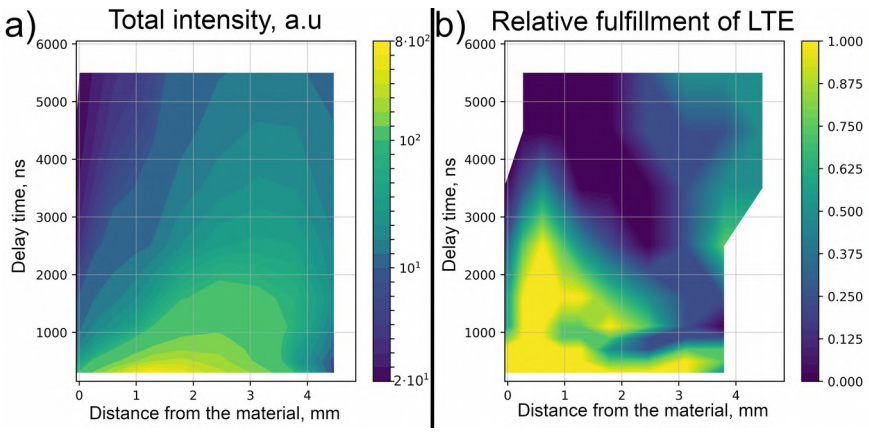


Fig. 1. a) Logarithmic heatmap of total intensity of the plasma plume. This can be used to estimate the location and size of the plasma plume. b) Qualitative heatmap for relative fulfillment of 3 necessary conditions for LTE. Value of 1 means best fulfilled LTE (not necessarily fulfilled LTE) and 0 means least fulfilled LTE.

This work has been carried out within the framework of the EUROfusion Consortium, funded by the European Union via the Euratom Research and Training Programme (Grant Agreement No 101052200 — EUROfusion). Views and opinions expressed are however those of the author(s) only and do not necessarily reflect those of the European Union or the European Commission. Neither the European Union nor the European Commission can be held responsible for them.

[1] ITER Organization, What is ITER?, https://www.iter.org/proj/inafewlines, (© 2022, used: 20.01.2022).
[2] G. De Temmerman, M.J. Baldwin, D. Anthoine et al., Efficiency of thermal outgassing for tritium retention measurement and removal in ITER, Nuclear Materials and Energy **12**, 267-272 (2017).

LIPID DROPLETS IN ACTIVATED ENDOTHELIUM IN ISOLATED BLOOD VESSELS – IMAGING OF BIOCHEMICAL ALTERATIONS USING RAMAN SPECTROSCOPY AND FLUORESCENCE MICROSCOPY

Natalia Chorazy[1,2], Magdalena Sternak[1], Agnieszka Kaczor[2], Stefan Chlopicki[1,3], Marta Pacia[1]

[1]Jagiellonian Centre for Experimental Therapeutics (JCET), Jagiellonian University, 14 Bobrzynskiego Str., 30-348 Krakow, Poland
[2]Faculty of Chemistry, Jagiellonian University, 2 Gronostajowa Str., 30-387 Krakow, Poland
[3]Chair of Pharmacology, Jagiellonian University, 16 Grzegorzecka Str., 31-531 Krakow, Poland
natalia.chorazy@student.uj.edu.pl

The endothelium covers the innermost layer of blood and lymphatic vessels, and fulfils many functions maintaining cardiovascular homeostasis, e.g. regulates the vessel diameter, takes part in the immune system functioning, and regulates an endothelial inflammation [1]. The endothelial dysfunction is recognized as a critical condition in the development of various diseases, e.g. hypertension, type 2 diabetes or atherosclerosis [2]. The endothelial inflammation may be triggered by pro-inflammatory factors, e.g. tumor necrosis factor (TNF), lipopolysaccharides (LPS) or angiotensin II, and also by hypoxia. In this work, we showed that activation of the vascular endothelium and the subsequent overexpression of intercellular adhesion molecule-1 (ICAM-1) is the common result of the action of aforementioned pro-inflammatory factors and hypoxia. What is more important, we demonstrated that formation and content of lipid droplets (LDs) is the marker of the endothelial inflammation in the isolated murine aorta.

The LDs, as a small, lipid-rich organelles, play a significant role in the development of obesity and atherosclerosis [3]. Although, the general knowledge on endothelial LDs is growing, neither the precise function of LDs, nor the pathway of their biogenesis have been completely revealed. Raman and fluorescence imaging provide information about the LDs structure, biochemical composition and general abundance, enabling LDs characterization under inflammatory conditions [4]. Here we demonstrated that in the TNF-, LPS-, angiotensin II- or hypoxic condition-activated vascular endothelium in the isolated murine aorta, the endothelial LDs are formed but are quickly metabolized. LDs are also formed in smooth muscle cells, which makes them difficult to detect in *en face* aorta preparation. To overcome this limitations for characterization of LDs in isolated aorta we used atglistatin – a selective inhibitor of adipose triglyceride lipase (ATGL) – which suppressed the lipolysis of the endothelial LDs. The rapidly metabolized LDs in TNF-, LPS- or angiotensin II-activated endothelium stood in the opposition to the formation of stable LDs in the endothelial cells in the isolated blood vessel upon hypoxic condition, when the atglistatin usage was not necessary for observation of stable LDs. Additionally, by comparing the Raman signature of endothelial LDs under hypoxic conditions in the presence or absence of atglistatin, we showed that atglistatin does not affect the biochemical composition of LDs.

The analysis of Raman spectra of LDs in the isolated vessels stimulated by TNF-, LPS- angiotensin II-or hypoxia uncovered that they were all rich in highly unsaturated lipids and had a negligible content of phospholipids and cholesterols. Accordingly, LDs biochemical composition in activated endothelium was similar for all types of pro-inflammatory stimuli and hypoxia. In conclusion, the spectroscopic and microscopic characterization of LDs suggest that LDs formation and their content in the isolated vessel represents a universal response to vascular pro-inflammatory insult, despite various cellular signalling events responsible for triggering vascular inflammation and could be also mimicked by hypoxia.

This work was supported by the National Science Centre, Poland, SONATINA1 No.: DEC-2017/24/C/ST4/00075.

[1] Aird W.C., Laubichler M.D., Endothelial biomedicine; Chapter 2 –Introductory Essay: Evolution, comparative biology, and development, *Cambridge University Press*, 2007, 23-28
[2] Sessa W.C., Pober J.S., Evolving functions of endothelial cells in inflammation*, Nature Reviews,* 2007, 7, 803-815
[3] Kuo, A., Lee, M. Y., Sessa, W. C., Lipid Droplet Biogenesis and Function in the Endothelium*, Circulation Research*, 2017, 120, 1289–1297
[4] Pacia, M. Z., Sternak, M., Mateuszuk, L., Stojak, M., Kaczor, A., Chlopicki, S., Heterogeneity of chemical composition of lipid droplets in endothelial inflammation and apoptosis, *Biochimica et Biophysica Acta (BBA) - Molecular Cell Research,* 2020, 1867, 1-24

O3-1

DID NOT PARTICIPATE

.

A MORE REALISTIC BLACK HOLE ACCRETION TREATMENT FOR NUMERICAL SIMULATIONS

Matas Tartėnas[1], Kastytis Zubovas[1,2]

[1]Department of Fundamental Research, Center for Physical Sciences and Technology, Lithuania
[2]Astronomical Observatory, Vilnius University, Lithuania
matas.tartenas@gmail.com

The large galactic scales seem to be connected to the many orders of magnitude smaller supermassive black hole (SMBH) scales by an episodic cycle of feeding and feedback [1]. The connection and possible interaction between the infalling/outflowing ISM makes it important to correctly address the timescales involved in SMBH feedback, but the large difference in relevant spatial scales makes the problem difficult to model directly.

One of the ways to address this issue in hydrodynamical simulations is to implement a "two-stage" sub-grid prescription for SMBH accretion. Matter swallowed by the SMBH particle is added to a separate reservoir coupled to the SMBH instead of directly feeding the black hole [2]. This allows one to delay the accretion and feedback by an arbitrary amount, changed by setting the timescale of reservoir depletion.

We extend the usual two-stage model to include a simple α-accretion disc model [3] coupled to the SMBH sink particle. The disc is evolved viscously with a separate timestep criterion from the simulation as a whole, but is synchronized at SMBH timesteps. Feedback is directly determined by the accretion disc, with radiation efficiency naturally approaching $\eta \approx 0.0625$ [4]. This allows us to determine the accretion timescale self-consistently and investigate the effects of gas accretion on the surrounding matter reservoir in a physical manner.

We test our approach by running a set of simulations of a several-parsec-wide region with conditions similar to those at the centre of our Galaxy using the 3D hydrodynamical code Gadget-3 [5]. Each model consists of four main components: the central SMBH ($M_{\rm bh} = 4 \times 10^6\,{\rm M}_\odot$), the Circumnuclear Disc-like toroidal gas ring ($M_{\rm r} = 10^5\,{\rm M}_\odot$, $R_{\rm in} = 1.5\,{\rm pc}$, $R_{\rm out} = 4\,{\rm pc}$), an infalling molecular cloud ($M_{\rm mc} = 10^5\,{\rm M}_\odot$, $R_{\rm mc} = 3\,{\rm pc}$) and diffuse background gas ($M_{\rm bg} \approx 1.2 \times 10^3 {\rm M}_\odot$); $R_{\rm bg} = 25$ pc). A retrograde collision between the molecular cloud and the gas ring results in significant accretion, where the accretion disc is fed by the gas that crosses a sink boundary ($r_{\rm sink} = 0.01\,{\rm pc}$) in the hydrodynamical model. We show that feedback has a significant effect in regulating the growth of the SMBH (Fig. 1). The growth rate of the SMBH, $\dot{M}_{\rm BH}$, is reduced and spread more evenly over time as compared with the instantaneous accretion prescription. A significant amount of matter escapes via the outer boundary and may lead to star formation in the central parsec.

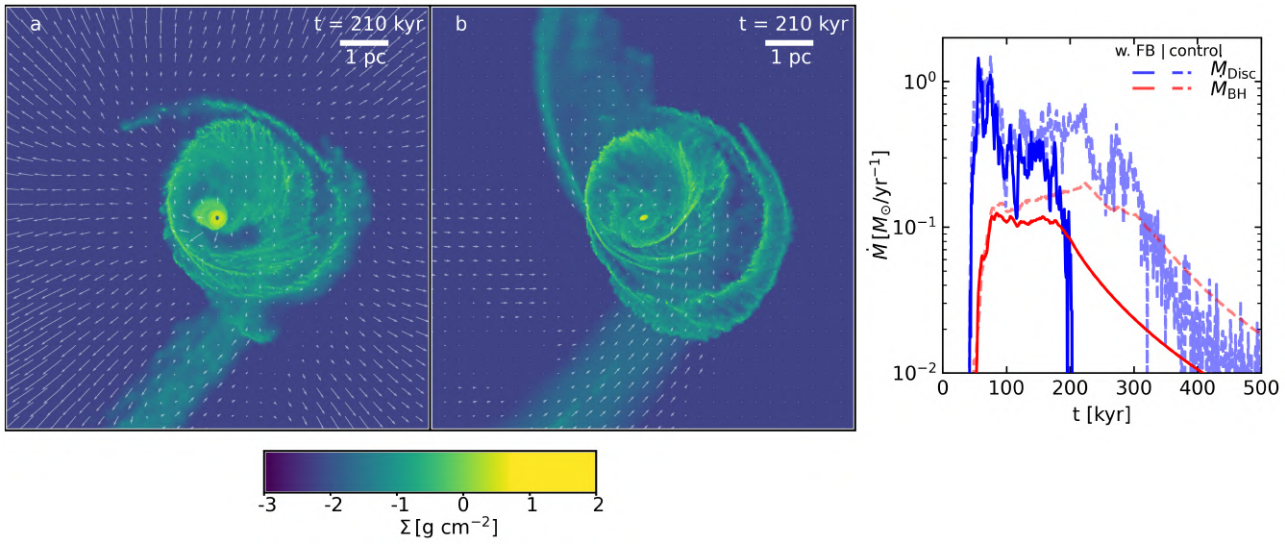


Fig. 1. Surface density maps of the resultant systems with (a) and without (b) feedback on the left and accretion rate graph on the right. AGN wind clears out a central ~ 0.1 pc region of gas stopping further accretion disc feeding at around $t = 200$ kyr, while the black hole continues to feed on matter already accumulated in the disc. In the absence of regulation by feedback, rapid accretion by the disc would continue for another ~ 100 kyr.

[1] M. Gaspari, F. Tombesi and M. Cappi, Linking macro-, meso- and microscales in multiphase AGN feeding and feedback, Nature Astronomy, 4:10–13 (2020)
[2] C. Power, S. Nayakshin and A. King, The accretion disc particle method for simulations of black hole feeding and feedback, Monthly Notices of the Royal Astronomical Society, 412(1):269–276 (2011)
[3] N. I. Shakura and R. A. Sunyaev. Black holes in binary systems. Observational appearance. Astronomy & Astrophysics, 24:337–355 (1973)
[4] B. Paczynsky and P. J. Wiita, Thick accretion disks and supercritical luminosities, Astronomy & Astrophysics, 500:203-211 (1980)
[5] V. Springel, The cosmological simulation code gadget-2, Monthly Notices of the Royal Astronomical Society, 364:1105–1134 (2005)

COSMOLOGICAL CONSTRAINTS FROM A TOMOGRAPHIC ANALYSIS OF THE SUBMILLIMETER GALAXY MAGNIFICATION BIAS

Marcos Muñiz Cueli[1], Laura Bonavera[1], Joaquín González-Nuevo[1], David Crespo[1], José Manuel Casas[1], Andrea Lapi[2], Tommaso Ronconi[2] and Marina Migliaccio[3]

[1]Departamento de Física, Universidad de Oviedo, C. Federico García Lorca 18, Oviedo, Spain
[2]Scuola Internazionale Superiore di Studi Avanzati (SISSA), Via Bonomea 265, Trieste, Italy
[3]Dipartimento di Fisica, Università di Roma Tor Vergata, Via della Ricerca Scientifica 1, Rome, Italy
mcueli@uniovi.es

Magnification bias is a weak lensing phenomenon which modifies the number counts of background sources due to the presence of mass in the foreground, thus revealing information about its distribution or physical composition. Although traditionally considered suboptimal with respect to the usual approach of shear, it has been recently shown [1, 2] to constitute an independent and robust cosmological probe when combined with a background sample of submillimeter galaxies, whose physical properties make it the perfect objects to use in this kind of study.

In this work [3], we have measured the angular cross-correlation function between a foreground sample of GAMA galaxies $(0.1 < z < 0.8)$ and a background sample of H-ATLAS submillimeter galaxies $(1.2 < z < 4.0)$, an unambiguous manifestation of the magnification bias phenomenom. In contrast to the preliminary work of [2], and as a step forward, we have performed a tomographic analysis, that is, we have divided up the foreground sample into four distinct redshift bins and estimated the cross-correlation between each of them and the full background sample, effectively having four independent observables. The theoretical estimate for the cross-correlation function between bin i and the background is given by

$$w^i(\theta) = 2(\beta - 1)\int_0^\infty \frac{dz}{\chi^2(z)} n_f^i(z) W^{lens}(z) \int_0^\infty \frac{dl}{2\pi}\, l\, P_{g-dm}\left(\frac{l}{\chi^2(z), z}\right) J_0(l\theta), \tag{1}$$

where β is the logarithmic slope of the background source number counts, $\chi(z)$ is the comoving distance up to redshift z, $n_f^i(z)$ is the unit-normalized foreground redshift distribution of bin i, $W^{lens}(z)$ is the so-called lensing kernel, J_0 is the zeroth-order Bessel function and P_{g-dm} is the galaxy-dark matter cross-power spectrum.

Given the clear dependence of these observables on cosmology, we have carried out a Markov chain Monte Carlo algorithm to derive posterior probability distributions for the main parameters describing three common cosmological models, namely ΛCDM, w_0CDM and w_0w_aCDM, the last of which characterize a time-evolving dark energy component. The results for Ω_m, σ_8 and h are shown in Fig. 1, where one can see a remarkable improvement in the uncertainty of Ω_m and σ_8 with respect to the non-tomographic work [2], whereas h seems to remain unconstrained. No significant differences are found among the three models.

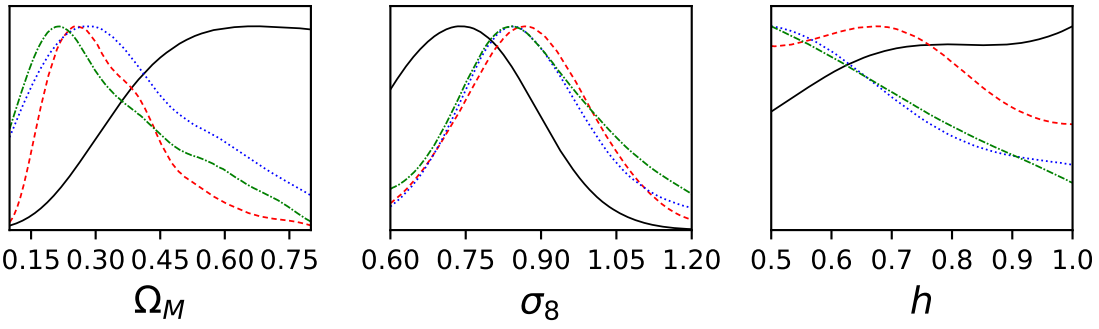


Fig. 1. Posterior probability distributions for the the matter density parameter (Ω_m; left panel), the variance of the filtered cosmic density field (σ_8; centrla panel) and the adimensional Hubble constant (h; right panel. Colored lines depict the results for the ΛCDM (red), w_0CDM (blue) and w_0w_aCDM (green) models, while the solid black line show the results from [2].

As for the dark energy parameters w_0 and w_a, the results from the w_0CDM and w_0w_aCDM models yield values which are in perfect agreement with a cosmological constant. Moreover, the uncertainties are comparable with non-combined results from other experiments.

[1] J. González-Nuevo, A. Lapi, L. Bonavera et al., H-ATLAS/GAMA: Magnification Bias Tomography. Astrophysical constraints above ∼ 1 arcmin, Journal of Cosmology and Astroparticle Physics, **024** (2017).
[2] L. Bonavera, J. González-Nuevo, M. M. Cueli et al., Cosmology with the submillimetre galaxies magnification bias: Proof of concept, Astronomy and Astrophysics, **639** (2020).
[3] L. Bonavera, M. M. Cueli, J. González-Nuevo et al., Cosmology with the submillimetre galaxies magnification bias. Tomographic analysis, Astronomy Astrophyisics, **656** (2021).

EVOLUTION OF MOLECULAR CLOUDS ABLATED BY AGN-DRIVEN OUTFLOWS: EFFECT OF TURBULENCE

Martynas Laužikas[1], Kastytis Zubovas[1,2]

[1]Astronomical Observatory, Vilnius University, Saulėtekio al. 3, Vilnius LT-10257, Lithuania
[2]Centre for Physical Sciences and Technology, Saulėtekio al. 3, Vilnius LT-10257, Lithuania
martynas.lauzikas@ftmc.lt

Galactic activity undoubtedly plays a major role in the evolution of galaxies. Energy released during activity episodes initiates galaxy-wide material transport - an outflow forms. Outflows are multiphase systems with a wide range of physical properties. Cooler, slower outflows are found within a few kpc of the galactic nucleus, have wide opening angles and affect the whole galactic disc. The galactic disc is rich with molecular clouds - dense, cool star forming regions. These cradles for stars are responsible for chemical evolution of the galaxy. Molecular clouds have been measured extensively and their properties obey Larson laws [1]. These laws describe size, mass and turbulent energy of clouds in quiescent galaxies.

Turbulence is undoubtedly one of the main factors that determine the distribution of matter in evolved molecular clouds. The turbulent velocity field results in formation of eddies and star formation occurs in the densest knots of these filaments. Turbulent flows are probably the last unsolved problem in classical mechanics. One of the major advances was statistical description of turbulence, where kinetic turbulent energy distribution in eddies obeys a power law. In Fourier domain it takes the form $E \sim k^{-n}$, where n describes the steepness of energy distribution in inverse wave number space. Turbulent vortexes can be split by types. These types are closely connected to basic fact of vector analysis: any continuous vector field (e.g. turbulent velocity) can be decomposed into orthogonal components

$$\mathbf{v} = -\nabla\Phi + \nabla \times \mathbf{A}. \tag{1}$$

These components are described as compressive and solenoidal, respectively. Compressive field works in the direction of the gravity well surrounding a dense clump. The solenoidal field, on the other hand, can be visualised as a vortex. In computer simulations turbulence is often initialised as a purely solenoidal field. However, this involves making several implicit assumptions - the gas is incompressible and the velocity field is homogeneous. But it is naive to expect for gas to be incompressible in molecular clouds. For realistic molecular clouds a compressive turbulent field component must be present. Therefore it is of particular interest to explore the effect of different types of turbulence, where the ratio of solenoidal to total turbulence τ is between 0-1.

We use the SPH code Gadget 4 [2] to model hydrodynamics and gravity; we include relevant cooling and heating processes via a cooling function. The model used in this work can be described as a virtual wind tunnel where a stationary molecular cloud with mass of 10^5 $M_\odot$ is ablated by outflows with velocities of 10 - 200 km/s and temperatures of $10^4, 10^5$ K. For each system we measure the fragmentation time, defined as the time when the mass of cool dense clumps reaches 2 % of initial cloud mass.

As expected, at speeds $\leq$100 km/s, compressive turbulence $\tau < 0.5$ works in hand with gravity and gas collapses much faster. For higher τ solenoidal velocity field produces less dense regions and they evolve slower. Kinematic outflow pressure has almost no effect for $\tau <$ 0.5. Above this value anti-correlation in outflow velocities and fragmentation time is observed. However outflows with velocity $\geq$180 km/s no longer induce gas collapse for $\tau < 0.5$, but lead to delayed fragmentation or even destruction of the cloud. Kinetic and thermal pressure of the outflow combined with compressional turbulent field accelerate cloud material, which overshoots local potential well and cloud disperses.

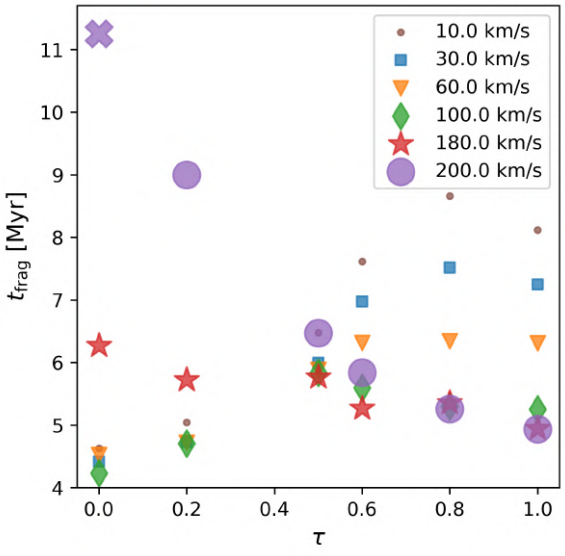


Fig. 1. Fragmentation times for 10^4 K outflows. τ is defined as ratio of solenoidal to total turbulence. Each symbol represents individual system with outflow velocity indicated in the legend. X shows a system where mass of fragmented gas did not reach 2 %.

[1] R. B. Larson, Turbulence and star formation in molecular clouds., MNRAS **194**, 809–826(1981).
[2] V. Springel, R. Pakmor, O. Zier, M. Reinecke, Simulating cosmic structure formation with the GADGET-4 code, MNRAS **506**(2), 2871–2949 (2021).

NEO OBSERVATIONS AND THEIR ROTATION PERIOD DETERMINATION

Kristers Nagainis[1], Ilgmārs Eglītis[1]

[1]Institute of Astronomy, University of Latvia, Latvia
kristers.nagainis@lu.lv

Since 2018 in Baldone Observatory around 50 new asteroids were discovered and for more than 6000 asteroids astrometric positions were published in MPC circulars. For many asteroids, there are physical properties that have not been analyzed and calculated yet, including one of the most important – the rotation period.

To get the rotation period, time-resolved photometry is needed for each of the asteroids, which can be used to acquire the light curve of the object. To get a precision of 0.03^m for measurments, the following was done: each sky region was observed at least from 3 to 5 nights. To process the images, flats, bias, and dark calibration images were taken each night. The program "MaxIm DL 5" was used to reduce and align the images. The flat-field images were taken against the twilight sky. The exposure time for dark images was the same as for respective light images – two or three minutes for all asteorids. Position measurements were made with the help of "Astrometrica", the new genesis of the program "CoLiTec" ("Lemur" [1]) and "Sky Sift" [2] programs. The brightness measurements were made with "MaxIm DL 5" or "Lemur". The program 'Lemur" was used to perform differential photometry on the reduced data. For each data set, more than five stars were used for brightness comparison to the asteroid. Aperture photometry using a differential photometry technique was done to determine the brightness of comparison stars and the asteroid in GAIA G(RP) passband.

A standardized methodology is used to process the luminosity curves to eliminate differences in observations over time. For example, data from all series of observations are reduced to a single epoch, usually to the first series of observations. For brightness, two adjustments are made – related to distance and phase - to change all measurements to the first series of observations.

After the data has been processed, a program made in Python is used to get the rotation period with Fourier series analysis. A simple version of rotation around a single axis is showed in Eq.(1):

$$V_r = A_0 + \sum_{i=1}^{n} B_n \sin\left(\frac{2\pi n\Theta}{P}\right) + \sum_{i=1}^{n} C_n \cos\left(\frac{2\pi n\Theta}{P}\right), \quad (1)$$

where V_r is the apperant magnitude, A_0, B_n, C_n are Fourier constants, P is the period and t is the time in Julian days. The algorithm works with itterating through intial guesses two times with different time steps for the period and searching for the best fit for the light curve. In the end the acquired period is visualized as in Fig. 1.

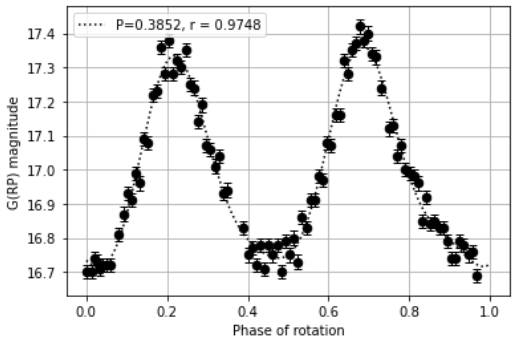


Fig. 1. Asteroid 9450=Akikoizumo=1998 BT1 best period $P = 0.39$ days

[1] A. V. Pohorelov, S. V. Khlamov, V. E. Savanevych, A. B. Briukhovetskyi and V. P. Vlasenko, "Virtual observatory and CoLiTec software: modules, features, methods," *Odessa Astronomical Publications*, vol. 29, pp. 136-140, 2016.
[2] Holvorcem P. http://sites.mpc.com.br/holvorcem/SkySift_presentation_Holvorcem_WSP2015.pdf

FUNDAMENTAL STELLAR PARAMETERS FOR 222 B-TYPE STARS FOR THE X-SHOOTER SPECTRAL LIBRARY

Cormac Larkin[1], Scott Trager[1], Kristiina Verro[1], Anaïs Gonneau[2]

[1]Kapteyn Astronomical Institute, University of Groningen, The Netherlands
[2]Institute of Astronomy, University of Cambridge, UK
larkin@astro.rug.nl

Stellar population models are building blocks for furthering our understanding of galaxies. With short lifetimes and high bolometric luminosities, B-type stars dominate the first few to tens of Myr of a stellar population, and strongly influence the chemical evolution of their environment via nucleosynthesis of metals and supernovae explosions. Currently, empirical spectral libraries such as the X-shooter Spectral Library (XSL) have a paucity of these stars compared to cooler stars, making it difficult to probe younger populations. We use the MIDE3700 code to find effective temperatures $T_{\rm eff}$ and surface gravities $\log g$ via the BCD method for 222 B-type stars in the XSL calibration archive in preparation for their inclusion as an extension to the XSL itself. We find agreement to within $\sim 0.1\sigma \log T_{\rm eff}$ and $\sim 0.25\sigma \log g$ between our results and a sample of literature stars. As can be seen in Figure 1, we populate a previously bare region of the XSL Hertzsprung-Russell diagram in the ranges $9000 \leq T_{\rm eff} \leq 23000$ and $2.8 \leq \log g \leq 4.0$, and extend the lower age limit for XSL stellar population models by up to a factor ~ 10 for [Fe/H] $= -1.2$, and a factor ~ 2 for Solar metallicity.

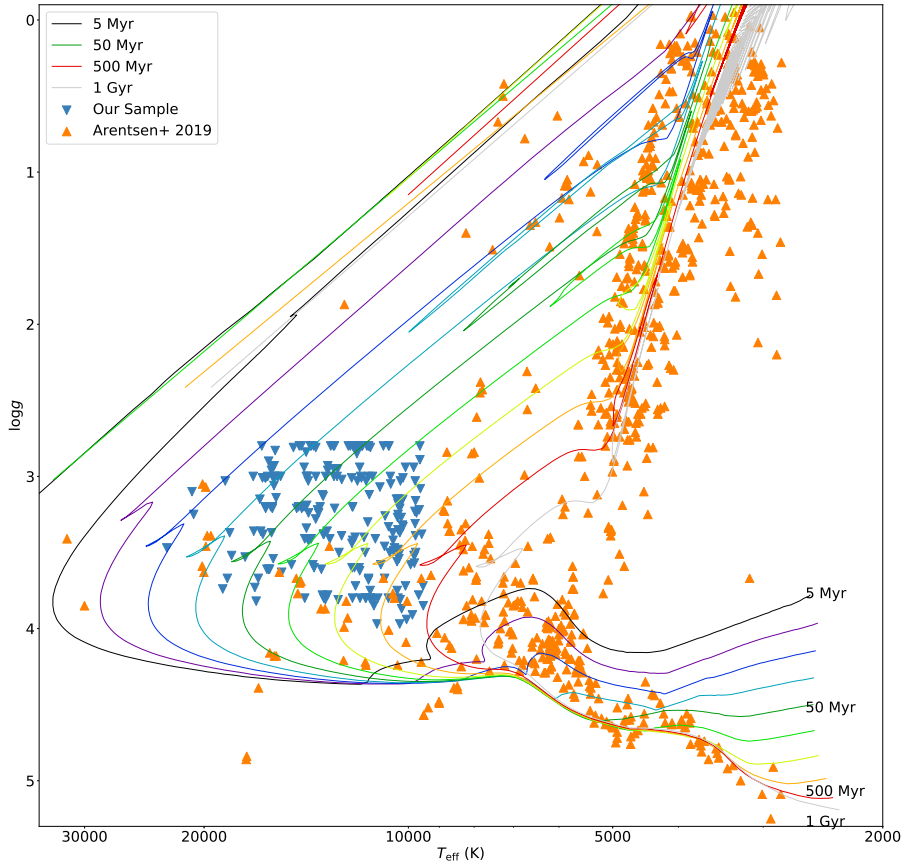


Fig. 1. Hertzsprung-Russell (HR) diagram for the XSL based on parameters found by Arentsen et al. (2019) [1] (orange), and in this work (light blue), with PARSEC/COLIBRI stellar isochrones at Solar metallicity overlaid. The new spectra analysed in this work are in a hotter, younger part of the HR diagram, and will allow for younger stellar population models to be generated using XSL data.

[1] A. Arentsen, P. Prugniel, A. Gonneau et al., Stellar atmospheric parameters for 754 spectra from the X-shooter Spectral Library, Astronomy & Astrophysics **627** (2019).

FABRICATION AND CHARACTERIZATION OF NANOPOROUS ANODIC ALUMINA MEMBRANE FOR NANOFILTRATION APPLIATION

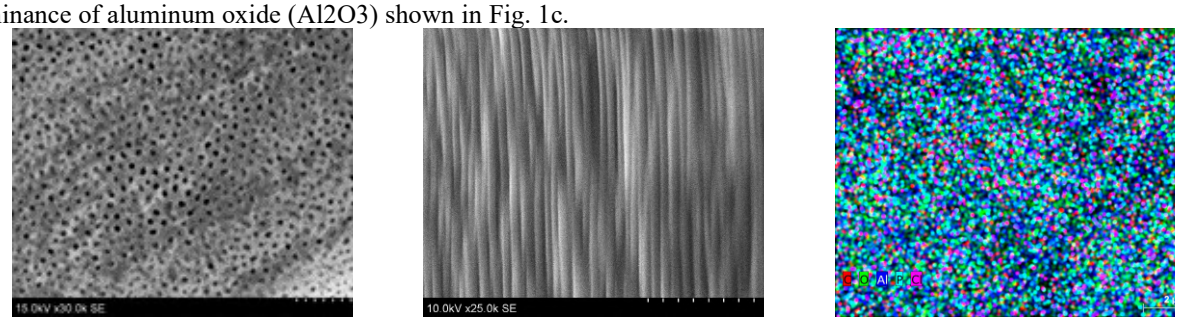
Yatinkumar Patel[1]*, Arvydas Palevicius[1], Giedrius Janusas[1]

[1] Department of Mechanical Engineering, Kaunas University of Technology, Lithuania
y.patel@ktu.lt

Nanomembranes are one of the most interesting groups of nanomaterials in nanotechnology [1]. Additionally, the application may be impacted by changes in the use of various materials throughout time, environmental changes, diverse studies, new technologies, requirements, or human needs. As a result, the materials used to manufacture nanomembranes have changed. Nanomembrane fabrication processes are included in one of the categories. Porosity, durability, permeability, chemical or thermal stability, and a variety of other factors should be considered while selecting a procedure for synthesizing nanomembranes [2]. Metal nanomembranes are made from a variety of metals and oxides. When it comes to metals such as gold or palladium, examples include Al_2O_3 and titanium dioxide (TiO_2). Because of its regular nanoporous hexagonal structure, pore regularity, and mechanical properties, nanoporous alumina has received the most attention for application in numerous fields of engineering and at the industrial level.

The most difficult mechanical issue in the filtration process is to avoid mechanical damage to the bioparticles as they pass through the micro pores in the aluminum oxide membrane. Bioparticles must be able to pass through the nano holes in the aluminum oxide membrane without being damaged by mechanical forces during the filtration process [3]. Surface acoustic waves modulation is the convenient method for manipulation of bioparticle and allows them to pass through the nanochannels without damaging the cells and reduce the friction from inside wall of nanochannels.

The aim of the research work is to fabricate the nanoporous anodic alumina from 99.5% pure aluminum sheet (0.5 mm) in 0.3M oxalic acid ($C_2H_2O_4$) using two step electrochemical anodization process [3]. Anodization process contains mild anodization (MA) and hard anodization (HA) for 90 min and 15 hours respectively followed by chemical etching for removal of backside aluminum later and to open other side of pores. After fabrication process Scanning electron microscopy (SEM) analysis confirms the pore diameter 80±10 nm, interpore distance 110±20 nm, and thickness of 95 µm using $C_2H_2O_4$ at constant DC 60V (Fig. 1a and 1b). To investigate the chemical properties of synthesized nanoporous alumina, energy-dispersive X-ray spectroscopy (EDS) research was performed, which verifies the dominance of aluminum oxide (Al2O3) shown in Fig. 1c.



a b c

Fig.1 SEM image of nanoporous alumina showing nanoporous (a), nanotubes (b), and elemental mapping (c)

A numerical simulation was performed to understand the pressure distribution inside the nanotube using piezoelectric actuation. The study was divided into two sections. Acoustic pressure distribution analysis was used in the first investigation to figure out the frequency where particles concentrate in the channel's central area, between 900 and 1100MHz, by using 10mHz steps between each frequency range. Also, transverse oscillations occurring at 900 MHz produce the lowest center-channel acoustic pressure. Increased frequency causes disorder in the acoustic pressure inside the nanochannel, resulting in increased friction between particles and the nanochannel wall as they pass through it. The second investigation determined the time required for nanoparticles to focus in the nanochannel's core. For this investigation, the time range was set to 0 seconds to 0.3 seconds in 0.0001 second increments. The findings of the analysis indicate that nanoparticles with a diameter of 22.65 nm and a density of 480 kg/m^3 focus in 0.27 s in the center of the nano channel. The result of numerical simulation shows that fabricated nanoporous alumina could be used for application for nanoparticle filtration and separation.

Acknowledgement: This research was funded by a Grant S-MIP-17-102 from the Research Council of Lithuania.

[1] Cha GD, Kang D, Lee J, Kim DH. Bioresorbable electronic implants: history, materials, fabrication, devices, and clinical applications. Adv Healthc Mater 8:1801660. (2019)

[2] U. Ciganė, A. Palevičius, & G. Janušas. Review of nanomembranes: materials, fabrications and applications in tissue engineering (bone and skin) and drug delivery systems. Journal of Materials Science 2021 56:24, 56(24), (2021), pp. 13479–13498.

[3] Y. Patel, G. Janusas, A. Palevicius, & A. Vilkauskas. Development of nanoporous AAO membrane for nano filtration using the acoustophoresis method. Sensors (Switzerland), 20(14), (2020), pp. 1–26.

SINGLE-PULSE FEMTOSECOND LASER FABRICATION OF CONICAL AND ANTENNA-LIKE STRUCTURES ON THIN GOLD FILM

Kernius Vilkevičius, Evaldas Stankevičius

Department of Laser Technologies, Center for Physical Sciences and Technology, Lithuania
Kernius.vilkevicius@ftmc.lt

A single-pulse shot of ultrashort laser irradiation enables the formation of complex microstructures on the surface of the thin gold film. The high elasticity of the metal allows to achieve both small and round-shaped, and high and narrow antenna-shaped structures. The driving force of the formation is the induced momentum normal to the surface at the heated or even molten layer of the noble metal and the fast solidification of it after structural change [1, 2].

This phenomenon achieved only by a single pulse leads to the formation of energy-dependent differently shaped microstructures [2]. Using energies at or a bit above the film modification threshold, the small hollow protrusions - microbumps are fabricated. The higher energies melt more material, and cone-like structures can be manufactured. Meanwhile, using energies a bit below the ablation threshold, the high and sub-wavelength width sharp nanoantennas are formed. The shape of microstructures depends not only on the energies used but also on the thickness of the layer. The bump structures remain quite similar, while the formation and shape of the antenna changes significantly. The produced microstructures are represented by a scanning electron microscope in Fig. 1.

It was investigated that the arrays of microbumps are exciting hybrid lattice plasmon polariton in VIS-NIR spectra with narrow resonant peak. Such polariton is excited due to interaction of diffracted from the grating light, which excites surface plasmon polariton, with surface lattice plasmons excited and amplified by interacting localized plasmons in periodic microstructures [3].

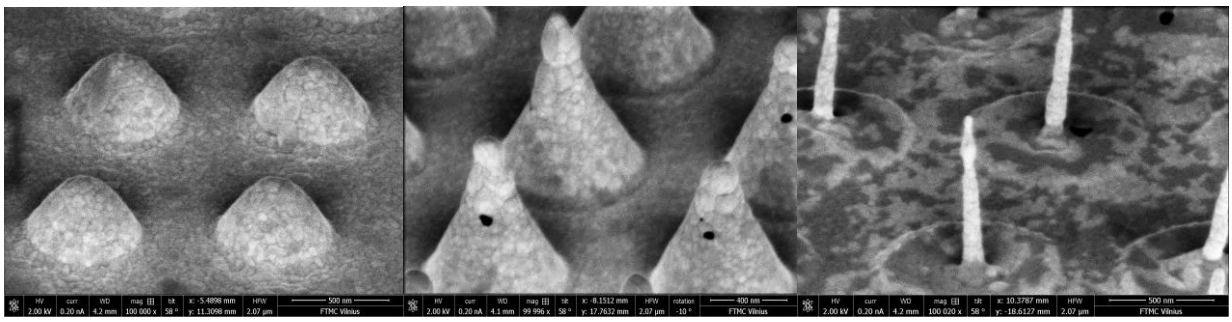


Fig. 1. SEM micrograph of microbumps (left), nanocones (middle) and nanoantennas (right) tilted at 45° angle.

The periodic 3x3 mm^2 arrays of such microstructures were fabricated using the direct laser writing method and the reflectance spectra were investigated with a spectrophotometer. All different structure arrays act as gratings exciting hybrid lattice plasmon polariton, only with a different response. The bumps show the best results, and the resonant peak is the deepest and narrowest. The resonance in the array of cones is wider and not so deep, while antennas have very shallow resonance spread in the spectra. While the response and place of the resonance are different for both orthogonal polarizations, the tendency of the results is the same for both of them.

The influence of the film thickness was also investigated, but only a slight difference in the resonance depth and width was observed.

[1] Y.P. Meshcheryakov, N.M. Bulgakova. Thermoelastic modeling of microbump and nanojet formation on nanosize gold films under femtosecond laser irradiation, Applied Physics A 82(2), 363–368 (2006).

[2] D. Pavlov, S. Syubaev, A. Kuchmizhak, S. Gurbatov, O. Vitrik, E. Modin, & M. Lapine. (2019). Direct laser printing of tunable IR resonant nanoantenna arrays. Applied Surface Science, 469, 514–520.

[3] E. Stankevičius, K. Vilkevičius, M. Gedvilas, E. Bužavaitė-Vertelienė, A. Selskis, & Z. Balevičius. (2021). Direct Laser Writing for the Formation of Large-Scale Gold Microbumps Arrays Generating Hybrid Lattice Plasmon Polaritons in Vis–NIR Range. Advanced Optical Materials, 9(12), 2100027.

EFFECT OF GRAPHENE ADDITION ON THE THERMAL AND PERSISTENT LUMINESCENCE PROPERTIES OF THE $Gd_{2.994}Ce_{0.006}Ga_3Al_2O_{12}$ AND $Gd_{2.964}Ce_{0.006}Dy_{0.03}Ga_3Al_2O_{12}$ CERAMICS

Daniela Kujawa[1,*], Daria Szewczyk[1], Vitalii Boiko[1], Damian Bęben[1,2], Paweł Głuchowski[1]

[1]Institute of Low Temperature and Structural Research PAS, PL-50422 Wroclaw, Poland
[2]Nanores, PL-51-317 Wroclaw, Poland
** e-mail: d.kujawa@intibs.pl*

Persistent luminescence is a phenomenon in which material is emitting light for a long time after ceasing the irradiation. The long-time luminescence fading is the effect of releasing the electrons from the deeper traps with the help of thermal energy [1]. The energy needed for releasing the traps is an important factor that has a big impact on the intensity and time of persistent luminescence. Therefore many experiments are made to prepare materials with the appropriate energy gap end electronic structure, where defects/traps are located close conduction band (CB) and energy of room temperature is sufficient to transfer the electron from the trap through CB to excited state of luminescent centre [2]. The work was focus on check if the addition of graphene flakes will have an influence on the thermal conductivity of the ceramics and in consequence on the persistent luminescence properties. It was checked whether the changed thermal conductivity has an impact on the release of electrons from shallow and deep traps. Better thermal conductivity should reduce the amount of energy needed to release carriers from energy traps and thus improve the properties of persistent luminescence. To verify this assumption, ceramics showing persistent luminescence and composites containing an admixture of graphene flakes were prepared and characterized. For all materials, their structure, morphology, thermal conductivity, thermoluminescence, and spectroscopic properties were examined. Based on the obtained results, the mechanism of persistent luminescence was constructed, taking into account the influence of the graphene flakes addition and its relationship with the thermal conductivity of composites.

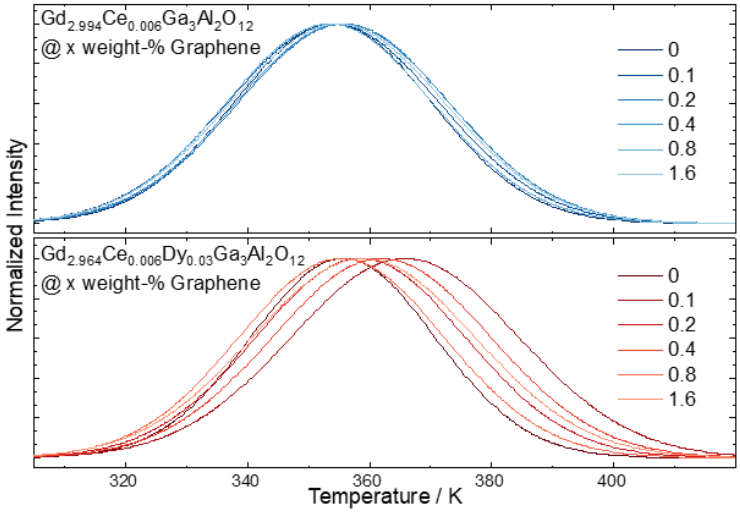


Fig. 1 Thermoluminescence (TL) glow curves registered for $Gd_{2.994}Ce_{0.006}Ga_3Al_2O_{12}$ and $Gd_{2.964}Ce_{0.006}Dy_{0.03}Ga_3Al_2O_{12}$ ceramics with different graphene content.

[1] J. Hölsä, „Persistent Luminescence Beats the Afterglow:400 Years of Persistent Luminescence", Electrochem. Soc. Interface, **4**, 18, 42 - 45, 2009.
[2] T. Aitasalo i in., „Persistent luminescence phenomena in materials doped with rare earth ions", J. Solid State Chem., **171**, 1–2,114–122, 2003, doi: 10.1016/S0022-4596(02)00194-9.

This work was supported by the National Science Centre, Poland under SONATA 13 project, grant number - 2017/26/D/ST5/00904

STEADY-STATE SPECTROSCOPIC PROPERTIES OF MAGNETIC NANODIAMONDS

Yaraslau Padrez[1], Lena Golubewa[1], Tatsiana Kulahava[1], Boris Zousman[2], Olga Levinson[2], Renata Karpicz[1], Yuri Svirko[3], Polina Kuzhir[3]

[1] Department of Molecular Compound Physics, Center for Physical Sciences and Technology, Lithuania
[2]Ray Techniques Ltd., Israel
[3]Department of Physics and Mathematics, Institute of Photonics, University of Eastern Finland, Finland
yaraslau.padrez@ftmc.lt

Carbon nanomaterials have unique properties that are attracting attention in various fields of research. Among the perspective nanomaterials are nanodiamonds (NDs). They possess exceptional mechanical, thermal, and optical properties that are inherited from a pure diamond. NDs are biocompatible, easily penetrate living cells and exhibit a low level of toxicity. This allows using them for biomedical purposes as fluorescent labels for bioimaging, or optical sensors on chemical reactions [1]. Despite numerous studies of optical properties of NDs, the data obtained evidence their difference for NDs produced by different methods.

In the present work, high-purity and high-homogeneity solutions of NDs (RayND-M, Ray Techniques Ltd) were investigated. These NDs were produced by laser synthesis [2] followed by an undisclosed surface modification process intended to impart them magnetic and fluorescent properties and colloidal stability. Water-based nanofluids were prepared by dispersing NDs in triple distilled water using ultrasound. These nanoparticles have a cubic diamond lattice in the core and chemically active hybrid graphene-like structures on their surface. The average size of NDs is about 5.0 nm. NDs were investigated by means of UV-vis, steady-state and time-resolved fluorescence spectroscopies.

The absorption spectra of NDs (Fig. 1a) have two maxima. The first absorption peak, at 276 nm, is probably related to the π–π* transition of sp2 carbon atoms on the ND surface and originates from the quantum confinement effect. The second one, less pronounced, around 390 nm, is more likely associated with the presence of oxygen functional groups (C=O/COOH) on hybrid graphene-like structures on the ND surface or related to lattice defects and impurities like in natural and synthetic diamonds [3].

There is a dominating contribution of Rayleigh scattering at high concentrations of NDs (0.01% – 0.04%) in absorption spectra which is proved by the correspondence of their shape to the λ^{-4} function. As the concentration decreases, the spectra shape becomes close to the λ^{-2} function which could be due to the absorption of light by the sp2 conducting layer on the surface of NDs [4].

Fluorescence in nanodiamonds is more often caused by the presence of impurities, defects, etc. either in the lattice or on the surface. The NDs are characterized by excitation-dependent fluorescence in the visible region (Fig. 1b). The dependence of fluorescence maxima position on the excitation wavelength is due to the different contributions of oxygen-containing groups (such as OH, ketone C═O, and ester C═O) on the surface of NDs in absorption.

Thus, investigated NDs are unique multifunctional nanoobjects, which combine magnetic and specific fluorescent properties and can be successfully applied for, e.g., image-guided magnetic separation of living cells [5].

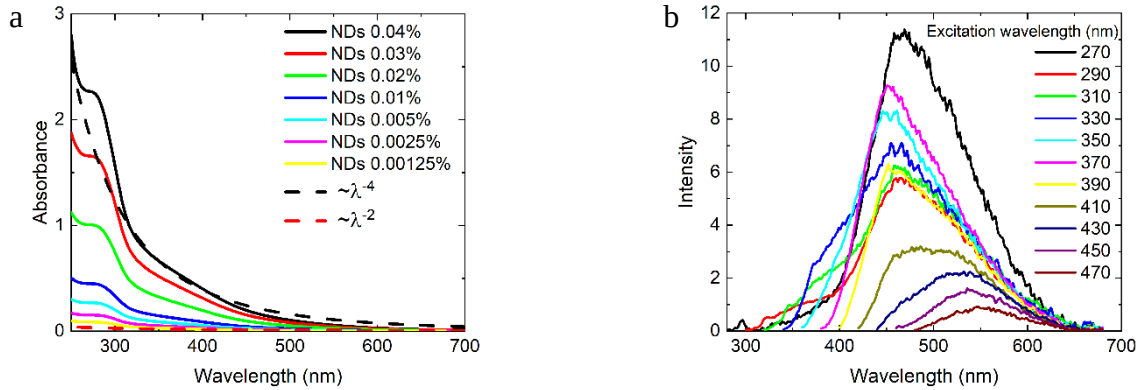


Fig. 1. a) The absorption spectra of ND solutions with different concentrations; b) The fluorescence spectra of 0.01% ND solution recorded with excitation wavelengths from 270 nm to 470 nm, in 20-nm increments.

[1] S. Prabha, D. D. Durgalakshmi, S. Rajendran et al., Plant-derived silica nanoparticles and composites for biosensors, bioimaging, drug delivery and supercapacitors: a review, Environ. Chem. Lett. **19**, 1667–1691 (2021).
[2] B. Zousman and O. Levinson, Pure nanodiamonds produced by laser-assisted technique, RSC Nanosci. Nanotechnol., **2014**, 112–127 (2014).
[3] A. E. Aleksenskii, A. Ya. Vul, S. V. Konyakhin et al., Optical properties of detonation nanodiamond hydrosols, Phys. Solid State **54**(3), 578–585 (2012).
[4] E. D. Eidelman, E. D., Siklitsky, V. I., Sharonova et al., A stable suspension of single ultrananocrystalline diamond particles, Diam. Relat. Mater. **14(**11), 1765–1769 (2005).
[5] S. Hou, S. H. Mahadevegowda, D. Lu et al., Metabolic Labeling Mediated Targeting and Thermal Killing of Gram-Positive Bacteria by Self-Reporting Janus Magnetic Nanoparticles, Small **17**(2) (2021).

THERMAL NANOCRYSTALLIZATION OF BISMUTH OXIDE GLASSES

Maciej Nowagiel[1], Tomasz K. Pietrzak[1], Tomasz Płociński[2], Julien Trébosc[3], Olivier Lafon[3], Marek Wasiucionek[1], Jerzy E. Garbarczyk[1]

[1] Faculty of Physics, Warsaw University of Technology, Poland
[2] Faculty of Materials Science and Engineering, Warsaw University of Technology, Poland
[3] Unité de Catalyse et Chimie du Solide, University of Lille, France
maciej.nowagiel.dokt@pw.edu.pl

Crystalline δ–Bi_2O_3 is the best known O^{2-} ion conductor, but it is stable in a relatively narrow temperature range 729–825 °C only. Its very high ionic conductivity (1 S/cm at 750 °C) has motivated many researchers to look for a method to stabilize this fluorite-type structure to lower temperature. So far the successful strategies to achieve the stabilization of the delta phase have included doping (e.g. by rare-earth elements [1]) or synthesis in form of thin layers [2].

Our approach to reach the same goal is significantly different from those two strategies. It consists of two steps: preparation of the Bi_2O_3 glass (pure or doped) and its nanocrystallization. Our experience with nanocrystallization has shown that by the appropriate heat-treatment one can achieve a gigantic (even by a factor of 10^9) and irreversible electrical conductivity enhancement in glassy analogs of some cathode materials for Li-ion batteries [3,4]. This effect is closely related to changes in the microstructure – namely to formation of nanoscale crystalline olivine grains, with dimensions going down even to a few nanometers, confined in the glassy matrix.

In this research, we first obtained Bi_2O_3 glasses at various synthesis conditions. Al and Si additives, originating from the crucibles, facilitated the glass formation upon quenching. Then we subjected them to an appropriate thermal treatment [5]. As a result, materials with various crystalline Bi_2O_3 phases were obtained: delta, beta and gamma – depending on the synthesis conditions. The phases (including delta) were found to be stable down to room temperature. The microstructure of samples was investigated by electron microscopy techniques (both SEM and HRTEM). The grains of δ–Bi_2O_3 phase were observed always as 10–40 nm nanocrystallites, confined in a residual glassy matrix (Fig. 1). On the contrary, the grains of beta and gamma phases were of micrometer sizes. The total electrical conductivity of nanocrystallized samples as a function of temperature has been determined in preliminary measurements by impedance spectroscopy.

MAS NMR was applied to determine the neighborhood of Al and Si, and to investigate their role in the stabilization of the Bi_2O_3 phases. From this experiment, one can conclude that Al and Si additives are rather unlikely to stabilize directly the delta-like phase, because they remain in amorphous matrix. On the contrary, they are believed to participate in formation of glass and induce the confinement effect of pure delta-Bi_2O_3 nanocrystallites.

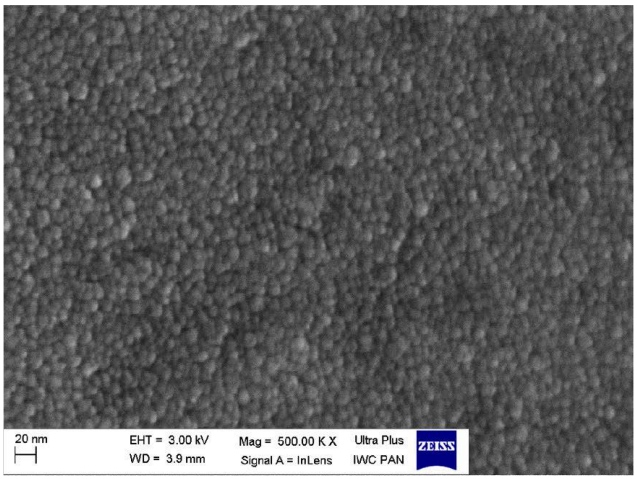


Fig.1. SEM image of a sample heat-treated up to 630°C. Microstructure consists mostly of 10-20 nm grains with δ-like Bi_2O_3 structure. [5]

This research was funded by POB TechMat of Warsaw University of Technology within the Excellence Initiative: Research University (IDUB) program. NMR experiments received funding from the European Union's Horizon 2020 research and innovation program under grant agreement No 731019 (EUSMI). M.N. and M.W. are grateful to the National Science Centre (NCN), Poland, for funding in frames of a grant Preludium BIS 2 no. 2020/39/O/ST5/00897.

[1] M. Leszczynska et al., J. Mater. Chem. A 2 (2014) 18624–18634.
[2] H.T. Fan et al., Thin Solid Films 513 (2006) 142–147.
[3] J.E. Garbarczyk et al., Solid State Ionics 272 (2015) 53–59.
[4] T.K. Pietrzak et al., Materials Science and Engineering B 213 (2016) 140–147.
[5] T.K. Pietrzak et al., Scientific Reports 11 (2021) 19145.

POLY (LACTIC ACID)/HYDROXYAPATITE (PLA/HAp) POROUS COMOSITE WITH INORGANIC NANOPARTICLES FOR BONE REGENERATION

Magdalena Bartolewska[1,3], Monika Biernat[3], Maciej Mazur[2] , Marcin Wasylewski[3]

[1] Faculty of Physics, University of Warsaw, Pasteura 5, 02-093 Warsaw, Poland
[2] Faculty of Chemistry, University of Warsaw, Pasteura 1, 02-093 Warsaw, Poland
[3] Łukasiewicz Research Network - Institute of Ceramics and Building Materials, Ceramic and Concrete Division in Warsaw, Postępu 9, 02-676 Warsaw, Poland
bartolewskamagdalena@gmail.com

Osteoporosis-related bone fractures are a major global problem, especially among the elderly. Despite significant advances in the treatment of osteoporosis over the past few decades, osteoporotic fractures remain a major clinical challenge in the elderly population due to impaired healing. One of the treatments is to generate a porous topographic implant, by mimicking the native extracellular matrix (ECM) to promote the regeneration of damaged bone tissues. Composites containing biodegradable matrix (PLA) and bioactive filler (hydroxyapatite) are the new hope in this research field. To improve the properties of such synthetic composites, in recent years, particular attention has been focused on the use of nanoparticles that can improve the growth of new bone. One of the interesting nanoparticles is nano-selenium which is known to regulate various physiological functions, such as cell differentiation and anti-inflammatory functions, and plays an important role in the regulation of ROS as an antioxidant revealing a huge potential for the development of new osteoporosis treatment strategies, yet, it has not been widely explored for osteoporosis applications.

For this research, selenium nanoparticles (SeNP) were adsorbed on a common orthopedic tissue engineering material, poly-l-lactic acid (PLLA) with hydroxyapatite (HAp). Selenium-coated PLLA-HAp materials have been examined with a range of physicochemical methods including dynamic light scattering, electron microscopy, and spectroscopic techniques. The research showed that the technique of coating composites with nanoparticles is effective. Suggesting they should be further studied to show promoting osteoblast functions. The composite appears to be new promising material for bone regeneration treatment.

The „Multifunctional composites biologically active for applications in regenerative medicine of bone system" project (POIR.04.04.00-00-16D7/18) is carried out within the TEAM - NET programme of the Foundation for Polish Science financed by the European Union under the European Regional Development Fund.

DARK MATTER IN THREE-HIGGS-DOUBLET MODELS WITH S_3 SYMMETRY

Wafaa Khater[1], Anton Kunčinas[2], Odd Magne Øgreid[3], Per Osland[4], Margarida Nesbitt Rebelo[2]

[1]Department of Physics, Birzeit University, Palestine
[2]Centro de Física Teórica de Partículas – CFTP and Dept de Física Instituto Superior Técnico – IST, Universidade de Lisboa, Av. Rovisco Pais, P-1049-001 Lisboa, Portugal
[3]Western Norway University of Applied Sciences, Postboks 7030, N-5020 Bergen, Norway
[4]Department of Physics and Technology, University of Bergen, Postboks 7803, N-5020 Bergen, Norway
anton.kuncinas@tecnico.ulisboa.pt

The Standard Model of particle physics has been extensively tested for a few decades and is the most successful description of nature. Nearly all theoretical Standard Model predictions have been experimentally verified and the last missing piece, the Higgs boson, was discovered in 2012 [2, 3]. This is undoubtedly a fascinating discovery in the field of particle physics and might be the final missing piece. Nevertheless, there is no experimental verification that it is the only Higgs boson, and it will be tested at the LHC and future colliders. While the Standard Model of particle physics keeps on triumphing, there is a vast amount of both theoretical and experimental phenomena that cannot be resolved within the Standard Model framework. Cosmological observations, based on the standard cosmological model, Λ_{CDM} , where CDM stands for cold dark matter, indicate that around a quarter of the total mass-energy density of the Universe is made up of dark matter [1]. However, there is no good dark matter candidate within the Standard Model framework. The multi-Higgs models could resolve some of the Standard Model issues and are commonly invoked when models beyond the Standard Model are constructed. Thus, we propose and are motivated that such extension could potentially solve several problems.

Models with two or more scalar doublets with discrete or global symmetries can have vacua with vanishing vacuum expectation values in the bases where symmetries are imposed. If a suitable symmetry stabilises such vacua, these models may lead to interesting dark matter candidates, provided that the symmetry prevents couplings among the dark matter candidates and the fermions. We analyse three-Higgs-doublet models with an underlying S_3 symmetry. These models have many distinct vacua with one or two vanishing vacuum expectation values [4] which can be stabilised by a remnant of the S_3 symmetry which survived spontaneous symmetry breaking. In our framework the stability of the dark matter sector results from a $\mathbb{Z}_2$ symmetry. We identify all possible dark matter models based on vacua in the context of S_3-symmetric three-Higgs-doublet models, allowing also for softly broken S_3.

We focus on a specific S_3-symmetric scalar model R-II-1a [5]. In the case we explore, one of the doublets provides the dark matter sector, while the other two are active. Therefore, the active sector behaves in many ways like a two-Higgs doublet model [6, 7]. The way the fermions couple to the scalar sector is constrained by the S_3 symmetry and is such that the flavour structure of the model is solely governed by the V_{CKM} matrix which, in our framework, is not constrained by the S_3 symmetry. In the model there is no CP violation in the scalar sector. The R-II-1a model is compatible with several constraints, both theoretical and experimental. After performing the numerical analysis we found a possible dark matter mass range [52.5, 89] GeV.

[1] N. Aghanim *et al.* [Planck], Astron. Astrophys. **641** (2020), A6 [erratum: Astron. Astrophys. **652** (2021), C4] doi:10.1051/0004-6361/201833910 [arXiv:1807.06209 [astro-ph.CO]].
[2] G. Aad *et al.* [ATLAS], "Observation of a new particle in the search for the Standard Model Higgs boson with the ATLAS detector at the LHC," Phys. Lett. B **716** (2012), 1-29 doi:10.1016/j.physletb.2012.08.020 [arXiv:1207.7214 [hep-ex]].
[3] S. Chatrchyan *et al.* [CMS], "Observation of a New Boson at a Mass of 125 GeV with the CMS Experiment at the LHC," Phys. Lett. B **716** (2012), 30-61 doi:10.1016/j.physletb.2012.08.021 [arXiv:1207.7235 [hep-ex]].
[4] D. Emmanuel-Costa, O. M. Ogreid, P. Osland and M. N. Rebelo, JHEP **02** (2016), 154 [erratum: JHEP **08** (2016), 169] doi:10.1007/JHEP08(2016)169 [arXiv:1601.04654 [hep-ph]].
[5] W. Khater, A. Kunčinas, O. M. Ogreid, P. Osland and M. N. Rebelo, [arXiv:2108.07026 [hep-ph]].
[6] J. F. Gunion, H. E. Haber, G. L. Kane and S. Dawson, Front. Phys. **80** (2000), 1-404 SCIPP-89/13.
[7] G. C. Branco, P. M. Ferreira, L. Lavoura, M. N. Rebelo, M. Sher and J. P. Silva, Phys. Rept. **516** (2012), 1-102 doi:10.1016/j.physrep.2012.02.002 [arXiv:1106.0034 [hep-ph]].

MOLECULAR DYNAMICS MODELLING OF INTERMOLECULAR STRUCTURE OF AQUEOUS MIXTURES OF 1-BUTYL-3-METHYLIMIDAZOLIUM NITRATE IONIC LIQUID

Einaras Sipavičius[1], Kęstutis Aidas[1]

[1]Institute of Chemical Physics, Faculty of Physics, Vilnius University, Lithuania
einaras.sipavicius@ff.stud.vu.lt

1-alkyl-3-methylimidazolium based ionic liquids (ILs) are widely investigated systems that are characterized by such peculiar properties as wide electrochemical potential window, amphiphilic character of cation [1] etc. These properties might be explained by developing understanding of intermolecular structure in ILs. In recent years a few related discoveries were made, including observation of nanoconfined water pockets in 1-butyl-3-methylimidazolium nitrate (Fig. 1) and other ILs mixtures with water. Water pockets were characterized using small angle X-ray scattering (SAXS) and neutron scattering (SANS) [2], nuclear magnetic resonance (NMR) techniques [3] although a few later published works [4, 5] question the formation of such structures – e.g., molecular dynamics (MD) modelling only predicts formation of water pockets in hydrophobic ILs, but not in hydrophilic ones [6]. MD modelling is an applicable method for structural investigation of ILs, but it is needed to carefully consider features like slow dynamics of ILs and the choice of suitable force field.

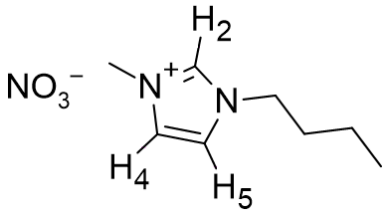


Fig. 1. [C_4mim^+][NO_3^-] structure with added explicit imidazole ring hydrogens, denoted H_2, H_4 and H_5.

The objective of this study: extracting information about intermolecular structure in pure 1-butyl-3-methylimidazolium nitrate [C_4mim^+][NO_3^-] and in its mixtures with water by performing MD simulations using two different force fields: one published by J. N. Canongia Lopes et al. [7] and one published by O. Acevedo et al. [8] Results of MD simulations may provide us information about important structural changes that happen when water molar fraction is increasing and how these changes are related with possible formation of water pockets.

MD simulations were performed using *Amber* package for four ensembles with water molar fractions 0% (pure IL), 20%, 50% and 80%. Pure IL was investigated at four different temperatures (313 K, 323 K, 333 K and 343 K) whereas mixtures were only simulated at 343 K temperature. Densities of pure IL were calculated and its relationship with temperature was compared with experimentally determined values and used to decide which of the two used force fields is more suitable for further analysis. Intermolecular structure was investigated by calculating radial distribution functions (RDFs) and coordination numbers of nitrate ions and water molecules around imidazole hydrogen atoms H_2, H_4 and H_5 (see Fig. 1). Besides that, NO_3^- and H_2O orientation around imidazole ring was analyzed using intermolecular distance-angle plots.

It was shown that force field published by O. Acevedo et al. is preferable for intermolecular structure investigation using density calculations. RDFs were used to deduce that both NO_3^- and H_2O coordinate around all imidazole ring hydrogen atoms: NO_3^- coordination number was highest at H_2 position, H_2O – at H_4 position when water molar fraction is 80%. Several noticeable structural changes were observed by analyzing distance-angle relationships: both NO_3^- and H_2O are more likely to be positioned above or below imidazole ring and less likely to be positioned in the imidazole ring plane between H_4 and H_5 atoms when water molar fraction increases. Also, orientational distribution of water molecules becomes more homogeneous at small distances when water molar fraction is higher.

These conclusions may be valuable for questioning the existence of water pockets and might be supported by our future studies, including theoretical ^{1}H BMR chemical shifts calculations and water cluster analysis.

We want to thank *"HPC Saulėtekis"* for providing us computational resources to perform MD simulations.

[1] E. Binetti et al., Spectroscopic Study on Imidazolium-Based Ionic Liquids: Effect of Alkyl Chain Length and Anion, J. Phys. Chem. B, **116**, 3512–3518 (2012).
[2] H. Abe et al., Direct Evidence of Confined Water in Room-Temperature Ionic Liquids by Complementary Use of Small-Angle X-ray and Neutron Scattering. J. Phys. Chem., **5**, 1175-1180 (2014).
[3] K. Saihara et al., Properties of Water Confined in Ionic Liquids, Sci Rep, **5**, 10619 (2015).
[4] S. S. Bystrov et al., Translational Diffusion in a Set of Imidazolium-Based Ionic Liquids [bmim]+A– and Their Mixtures with Water, J. Phys. Chem. B., **123**, 9187-9197 (2019).
[5] D. Lengvinaitė et al., Structural Features of the [C_4mim][Cl] Ionic Liquid and Its Mixtures with Water: Insight from a ^{1}H NMR Experimental and QM/MD Study, J. Phys. Chem. B., **125**, 13255-13266 (2021).
[6] A. Verma et al., Tuning Water Networks via Ionic Liquid/Water Mixtures, Int. J. Mol. Sci., **21**, 403 (2020).
[7] J. N. Canongia Lopes et al., Modeling Ionic Liquids Using a Systematic All-Atom Force Field, J. Phys. Chem. B, **108**, 2038-2047 (2004).
[8] B. Doherty et al., Revisiting OPLS Force Field Parameters for Ionic Liquid Simulations, J. Chem. Theory Comput, **13**, 6131-6145 (2017).

MAGNETIC PROPERTIES OF BULK AND THIN FILMS OF FEPT $L1_0$ PHASE FROM DENSITY FUNCTIONAL THEORY CALCULATIONS

Joanna Marciniak[1], Wojciech Marciniak[1,2], Mirosław Werwiński[1]

[1]Institute of Molecular Physics, Polish Academy of Sciences, M. Smoluchowskiego 17, 60-179 Poznań, Poland
[2]Institute of Physics, Poznan University of Technology, Piotrowo 3, 60-965 Poznań, Poland
joanna.marciniak@ifmpan.poznan.pl

The constantly developing computer technology requires an extensive search for materials to increase the data density. One of the factors influencing the applicability of a given material in magnetic recording media is strong magnetocrystalline anisotropy. This property is observed, for example, in the $L1_0$ FePt phase [1].

For this reason, its magnetic properties have been repeatedly analyzed using the density functional theory (DFT) [2]. We decided to perform further research, emphasizing the full potential methods, including the full-potential local-orbital (FPLO) scheme. We used disordered local moments theory and coherent potential approximation to obtain Curie temperatures of the bulk $L1_0$ FePt. We paid particular attention to the dependence of the magnetocrystalline anisotropy energy (MAE) on the value of the magnetic moment (m) of the system using the fully relativistic fixed spin moment (FSM) method for various exchange-correlation potentials. This dependency allowed us to explain the differences between the results obtained earlier using different exchange-correlation potentials and determine the potential ways of system modification to increase the MAE of the system. Interestingly, the determined dependencies of MAE(m) for different correlation-exchange potentials are almost identical near the equilibrium point [3]. We also determined the magnetocrystalline anisotropy constants K_1 and K_2, the magnetic moments and the Curie temperature.

The basic magnetic parameters [4] were studied further for a decreasing number of atomic layers, down to a single atomic bilayer of $L1_0$ FePt. A complete structural optimization preceded the calculations. We derived the dependence of the in-plane lattice parameter and the c/a ratio in a single unit cell on the multiatomic layer thickness. Furthermore, the dependence of the magnetic moment *versus* the distance to the interface was obtained.

We acknowledge the financial support of the National Science Centre Poland under DEC-2018/30/E/ST3/00267. The computations were in the main part performed on resources provided by the Poznan Supercomputing and Networking Center (PSNC). We thank Paweł Leśniak and Daniel Depcik for compiling the scientific software and administration of the computing cluster at the Institute of Molecular Physics, Polish Academy of Sciences.

[1] O. Gutfleisch, J. Lyubina, K.-H. Müller, L. Schultz, *FePt Hard Magnets*, Adv. Eng. Mater. **7** (2005) 208–212
[2] S. Ayaz Khan, P. Blaha, H. Ebert, J. Minár, O. Šipr, *Magnetocrystalline anisotropy of FePt: A detailed view*, Phys. Rev. B **94** (2016) 144436
[3] J. Marciniak, W. Marciniak, M. Werwiński, *DFT calculation of intrinsic properties of magnetically hard phase $L1_0$ FePt*, under review
[4] R. V. Chepulskii, W. H. Butler, *Ab initio magnetocrystalline anisotropy at nanoscale: The case of FePt*, Appl. Phys. Lett. **100** (2012) 142405

CLASSICAL AND QUANTUM EXCEPTIONAL POINTS IN NON-HERMITIAN BOSONIC SYSTEMS

Ewelina Lange[1], Grzegorz Chimczak[1], Anna Kowalewska-Kudłaszyk[1]

[1]Institute of Spintronics and Quantum Information, Faculty of Physics, Adam Mickiewicz University, ul. Uniwersytetu Poznańskiego 2, 61-614 Poznań, Poland
ewelan@st.amu.edu.pl

In recent years, there has been an increasing interest in investigating non-Hermitian physical systems. Spectral singularities displayed by non-Hermitian Hamiltonians, where two or more eigenvalues and their corresponding eigenvectors coalesce, are known as an exceptional points (EPs). EPs are extensively investigated in many fields of physics, but quantum optics is especially promising platform. There are numerous examples of novel features detected directly at and around EPs in atomic [1], optical [2], optomechanical [3], plasmonic [4], photonic crystalline [5], and many other physical systems.

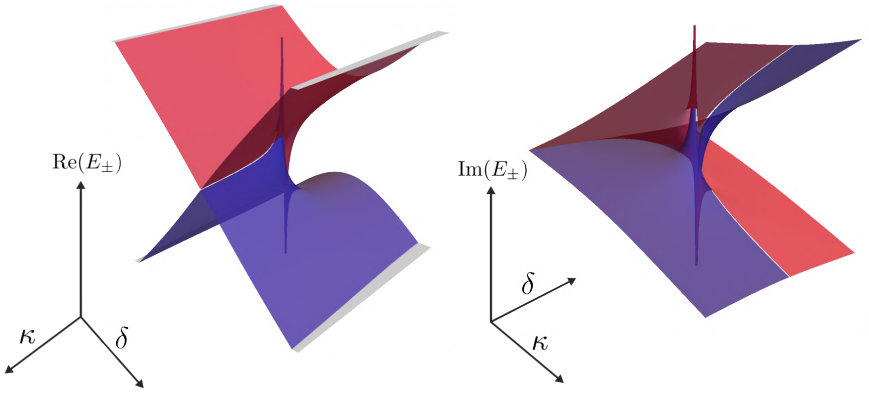


Fig. 1. Plots of real and imaginary part of eigenvalues of Hamiltonian. κ denotes gain/loss parameter, and δ - the detuning. These Riemann sheets show exceptional point [7].

EPs can be found both in classical and fully quantum systems. Recently, Minganti *et al.* [6] have pointed out that in quantum systems one has to take into account quantum jumps. We have investigated the effect of jumps on EP in a passive PT-symmetric bosonic system. We show that this effect is important when the reservoir is in a thermal state.

[1] Cartarius, H., Main, J. & Wunner, G. Exceptional points in atomic spectra. Phys. Rev. Lett. **99**, 173003 (2007)
[2] Miri, M.-A. & Alù, A. Exceptional points in optics and photonics. Science **363**, eaar7709 (2019)
[3] Jing, H., Özdemir, Ş.K., Lü, H. et al. High-order exceptional points in optomechanics. Sci Rep **7**, 3386 (2017).
[4] Alaeian, H. & Dionne, J. A. Parity-time-symmetric plasmonic metamaterials. Phys. Rev. A **89**, 033829 (2014)
[5] Cerjan, A., Raman, A. & Fan, S. Exceptional contours and band structure design in parity-time symmetric photoniccrystals. Phys. Rev. Lett. **116**, 203902 (2016)
[6] Minganti, F., Miranowicz, A., Chhajlany, R. W., & Nori, F. Quantum exceptional points of non-Hermitian Hamiltonians and Liouvillians: The effects of quantum jumps. Physical Review A, **100**, 062131 (2019)
[7] Lange, E., Chimczak, G., Kowalewska-Kudłaszyk, A. et al. Rotation-time symmetry in bosonic systems and the existence of exceptional points in the absence of PT symmetry. Sci Rep **10**, 19906 (2020)

SEMI-EMPIRICAL PREDICTIONS OF ENERGY LEVELS AND HYPERFINE STRUCTURE FOR THE ODD-PARITY CONFIGURATION SYSTEM OF HO II

Marcin Klempka[1], Sebastian Wilman[1], Magdalena Elantkowska[1], Jarosław Ruczkowski[2]

[1] Institute of Materials Research and Quantum Engineering, Faculty of Materials Engineering and Technical Physics, Poznan University of Technology, Piotrowo 3, 60-965 Poznan, Poland
[2] Institute of Robotics and Machine Intelligence, Faculty of Control, Robotics and Electrical Engineering, Poznan University of Technology, Piotrowo 3a, 60-965 Poznan, Poland
marcin.klempka@student.put.poznan.pl

The aim of the thesis is to present the results of a semi–empirical calculations of the Landé g_J factors, along with energy levels, fine (*fs*) and hyperfine structure (*hfs*) for the odd parity-level system of the holmium ion (Ho II). For this purpose we used our package of programs for semi-empirical analysis of energy levels structure of complex atoms. To obtain the results, all available experimental data were used.

Knowledge of holmium neutral and ionized spectra helps scientists to interpret the results of various experiments, observations in astrophysics or solve problems of quantum engineering. It's also essential in cosmology. The distribution of elements in Galaxy provides critical information about the process of nucleosynthesis in stars. It allows to get better understanding of the history of the Universe, which would be impossible without very detailed spectral data. Values of Landé g_J factors are essential in planning trapping and cooling atoms or ions experiments.

The considered configuration system consisted of 5 odd configurations: $4f^{11}6s+4f^{11}7s+4f^{11}5d+4f^{10}6s6p+4f^{10}5d6p$. The procedure of calculating the energy structure of a complex atom using semi-empirical methods begins with the determination of the fine structure. For this purpose our own fine structure parameterization method were used, taking into account all electromagnetic interactions in an atom up to the second-order perturbation theory. The eigenvector amplitudes determined by means of the fine-structure analysis were used next in the process of the hyperfine structure parameterization.

Basing upon precise experimental magnetic dipole and electric quadrupole hyperfine structure constants A and B presented by Gurell et all. [3], we have made an attempt to extract some attributes for the odd–parity configuration system of Ho II, such as predicted values of energy levels with their Landé g_J factor as well as and *hfs* constants. The correctness of the fine structure wave functions was verified by the simultaneous analysis of the hyperfine structure. Using 22 experimental hyperfine structure constants very good results of *hfs* parameterization were obtained. In the final fine structure least–square fit we achieved a mean error for the energy levels values of $\sigma(E) = 15$ cm^{-1} and the mean relative discrepancy amounting to 0.1%. The differences between experimental and calculated values of *hfs* constants are presented in Fig. 1. Therefore, we conclude that the obtained wave functions describe the real electronic states, and the predicted Landé g_J factors are properly determined for both the experimental energy values and the calculated energy values in the range up to 30000 cm^{-1}.

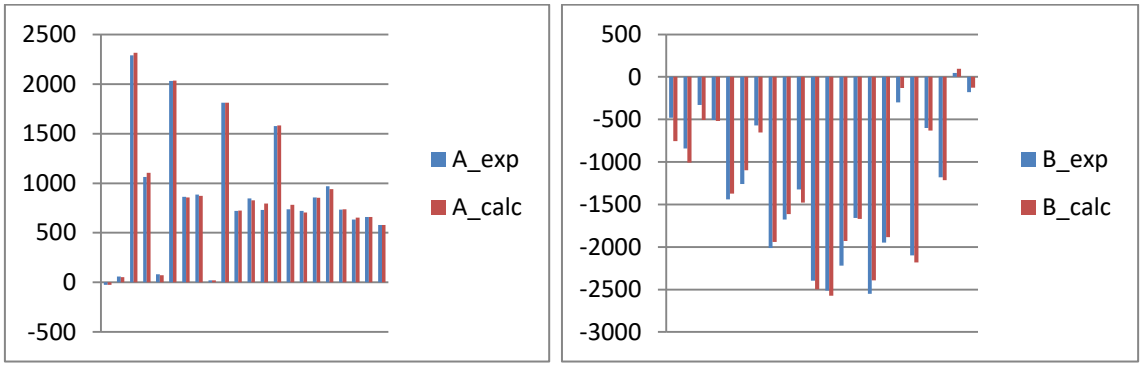


Fig. 1. Comparison of experimental and calculated values of *hfs* a) A and b) B constants.

We are hoping that the results of our calculations will be confirmed in near future by experimental studies.

[1] D. Stefanska, S. Werbowy, A. Krzykowski, B. Furmann, *Lande g_J factors for even-parity electronic levels in the holmium atom*, J Quant Spectrosc Radiat Transfer 210 (2018) 136–140. doi:10.1016/j.jqsrt.2018.02.015.
[2] M. Elantkowska, J. Ruczkowski, A. Sikorski, S. Wilman, *Fine- and hyperfine structure investigations of the odd-parity configuration system in atomic holmium*, J Quant Spectrosc Radiat Transfer 237 (2019) 106642. doi:10.1016/j.jqsrt.2019.106642.
[3] J. Gurell, G. Wahlgren, G. Nave, J.-F. Wyart, *Wavelengths, energy levels and hyperfine structure constants in Ho II*, Phys Scr 79 (2009) 035306. doi:10.1088/0031-8949/79/03/035306.

INVESTIGATION OF HIGH-PRESSURE EFFECTS ON STRUCTURAL AND MAGNETIC PROPERTIES OF MULTIFERROIC Sm DOPED $BiFeO_3$

Andrius Pakalniškis[1], Ramūnas Skaudžius[1], Dmitry Karpinsky[2], Gediminas Niaura[3], Aivaras Kareiva[1]

[1] Institute of Chemistry, Vilnius University, Naugarduko 24, LT-03225 Vilnius, Lithuania
[2]Scientific-Practical Materials Research Centre of NAS of Belarus, 220072 Minsk, Belarus
[3]Department of Organic Chemistry, Center for Physical Sciences and Technology (FTMC), Sauletekio Ave. 3, LT-10257, Vilnius, Lithuania
andrius.pakalniskis@chgf.vu.lt

The term morphotropic phase boundary (MPB) usually refers to a concertation region where different crystal structures with a low energy barrier can coexist. The most common and well understood MPB exists between the polar rhombohedral (R3m) and tetragonal (P4mm) structures in lead zirconate titanate (PZT) [1]. While currently dominant piezoelectric materials with MPB are extremely efficient they contain lead which is highly toxic. Due to this drawback and overall shift towards green and sustainable chemistry, which was partly induced by anti Pb legislations, a search for a greener alternative is ongoing. The search for a new type of materials led scientists to a discovery of the polar to non-polar transition containing MPB. This significantly improved the approach of new lead-free ferroelectric material design with properties similar to PZT [2].

$BiFeO_3$, a lead free multiferroic compound with perovskite type structure, was found to have a polar to non-polar morphotropic phase boundary. Chemical substitution of bismuth ions by rare-earth elements (La–Sm) causes the structural transition from the polar rhombohedral phase (described by the space group R3c) to the non-polar orthorhombic phase (Pnma space group) via stabilization of $PbZrO_3$-like anti-polar orthorhombic phase (Pbam space group) [3]. The concentration ranges of the structural stability of the rhombohedral and the anti-polar orthorhombic phases strongly depend on the type of rare-earth element and the reduction in the ionic radius of the dopant ions leads to a shrinkage of the mentioned ranges [3]. The concentration range attributed to the anti-polar orthorhombic phase reduces to 1% in the system $Bi_{1-x}Sm_xFeO_3$[4]. In the case of Sm-doping the concentration range ascribed to structural stability of the antipolar orthorhombic phase becomes extremely dependent on the preparation conditions and post synthesis treatment of the samples see Fig. 1. It should be noted that structural characterization of the MPB region performed based on microscopic measurements such as XRD, Raman or IR spectroscopy can give different results as compared to local measurements such as TEM or PFM, which poses a great problem for further scientific research [5].

In the present study, we report on the correlation between the type of structural distortions. Morphology of crystallites and an onset of remanent magnetization for Sm-doped $BiFeO_3$ compounds prepared by different methods. As well the effects of high pressure on the structural and magnetic properties.

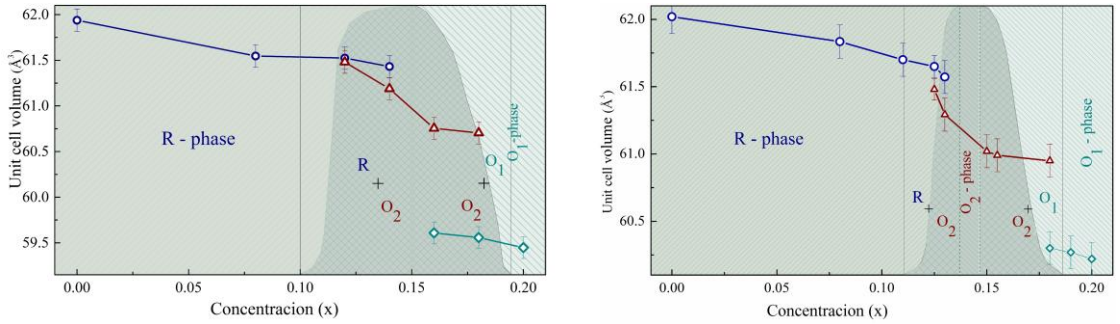


Fig. 1. Phase diagrams of the compounds $Bi_{1-x}Sm_xFeO_3$ prepared by sol-gel (left) and solid-state (right) reaction technique.

Acknowledgements. This work was supported by the European Union's Horizon 2020 research and innovation programme under the Marie Skłodowska-Curie grant agreement No. 778070.

[1] H. Zheng, I.M. Reaney, W.E. Lee, et al., Effects of strontium substitution in Nb-doped PZT ceramics, Journal of the European Ceramic Society **21,** 1371-1375 (2001).
[2] D. Damjanovic, A morphotropic phase boundary system based on polarization rotation and polarization extension, Applied Physics Letters, **97**, 062906 (2010).
[3] O. Troyanchuk, D.V. Karpinsky, M.V. Bushinsky, et al., Phase transitions, magnetic and piezoelectric properties of rare-earth-substituted $BiFeO_3$ ceramics, Journal of the American Ceramic Society, **94**, 4502-4506 (2011).
[4] S. Karimi, I.M. Reaney, Y. Han, et al., Crystal chemistry and domain structure of rare-earth doped $BiFeO_3$ ceramics, Journal of Materials Science, **44**, 5102-5112 (2009).
[5] K.A. Schönau, L.A. Schmitt, M. Knapp, et al., Nanodomain structure of $Pb[Zr_{1-x}Ti_x]O_3$ at its morphotropic phase boundary: Investigations from local to average structure, Physical Review B, **75**, 184117 (2007).

RAMAN SPECTROSCOPY INVESTIGATION OF MOLECULAR ROTORS WITH STEROIDAL STATORS, AND 1,4-DIETHYNYLPHENYLENE ROTATOR SUBSTITUTED WITH FLUORINE

Olszewska Karolina[1], Jastrzębska Izebella[2], Santillan Rosa[3], Runka Tomasz[1]

[1] Institute of Materials Research and Quantum Engineering, Poznan University of Technology, Poland
[2] Institute of Chemistry, University of Bialystok, Poland
[3] Departamento de Química, Centro de Investigación y de Estudios Avanzados del IPN, Mexico
karolina.j.olszewska@doctorate.put.poznan.pl

Molecular rotors are molecular assemblies constructed from sizeable stators surrounding a fast-moving inner component, called rotator, that is embedded on an axle of rotation. The role of stators is to provide a rigid frame and to shield the movement of the rotator. Due to their build molecular rotors are considered efficient building blocks for amphidynamic crystals.

The term amphidynamic crystals is a denomination for a broad group of molecular crystals that contain highly mobile components inside a rigid crystal frame. Such crystals, created from molecular rotors, can provide materials with tunable optical and electrical properties. The rotation of the rotators can be modulated by external stimuli or interaction with the environment (e.g., illumination, temperature, density, or viscosity of medium the crystal/rotor was placed into). Materials thus created can find application in numerous measurement techniques. It was shown that molecular rotors can find application as molecular sensors [1], viscosity sensors [2] and can provide tunable and switchable dielectrics [3,4].

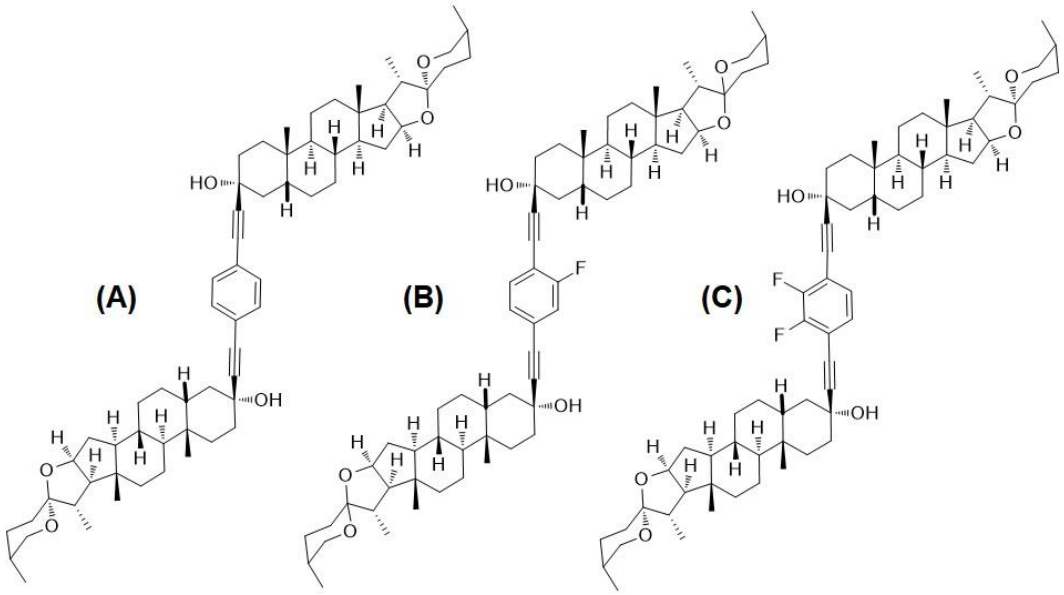


Fig. 1. Structures of rotor A, B and C.

In this paper we present three structures (Fig. 1) that are candidates for molecular rotors. They are composed of steroidal stators and have 1,4-diethynylphenylene rotator, in the case of rotor A. For rotors B and C, 1,4-diethynylphenylene group was substituted with one, and two atoms of fluorine respectively. Fluorine was used due to its high electronegativity. For rotors described Raman spectroscopy measurements, at room temperature, with excitation wavelength of 785 nm, were conducted. Behavior of bands assigned to stretching vibrations of C=C, and C≡C bonds, present in rotator and axle of rotation, was analyzed. Based on that analysis conclusions about difference in molecular dynamics have been drawn. Spectral measurement of the band intensity in function of the angle of rotation of the sample were conducted in order to confirm the crystallinity of the samples.

[1] Mu, X.; Liu, Y.; Liu, S.; Sun, Y.; Lu, N.; Lu, Y.; Li, W.; Zhou, X.; Liu, B.; Li, Z. A cyanine-derived near-infrared molecular rotor for ratiometric imaging of mitochondrial viscosity in cells. Sens. Actuators, B 2019, 298, 126831– 126839, DOI: 10.1016/j.snb.2019.126831
[2] Aguilar-Granda, A.; Pérez-Estrada, S.; Roa, A. E.; Rodríguez-Hernández, J.; Hernández-Ortega, S.; Rodriguez, M.; Rodríguez-Molina, B. Synthesis of a Carbazole-[pi]-carbazole Molecular Rotor with Fast Solid State Intramolecular Dynamics and Crystallization-Induced Emission. Cryst. Growth Des. 2016, 16, 3435– 3442, DOI: 10.1021/acs.cgd.6b00395
[3] Zhang, W.; Ye, H.-Y.; Graf, R.; Spiess, H. W.; Yao, Y.-F.; Zhu, R.-Q.; Xiong, R.-G. Tunable and Switchable Dielectric Constant in an Amphidynamic Crystal. J. Am. Chem. Soc. 2013, 135, 5230– 5233, DOI: 10.1021/ja3110335
[4] Kobr, L.; Zhao, K.; Shen, Y.; Shoemaker, R. K.; Rogers, C. T.; Michl, J. Tris-o-phenylenedioxycyclotriphosphazene (TPP) Inclusion Compounds Containing a Dipolar Molecular Rotor. Cryst. Growth Des. 2014, 14, 559– 568, DOI: 10.1021/cg4013608

SPECTROSCOPIC PROPERTIES OF Bi_3TeBO_9 MICROCRYSTALLINE POWDERS DOPED WITH RARE EARTH IONS

Taras Zhezhera[1], Pawel Gluchowski[2], Marek Nowicki[1,3], Maciej Chrunik[4], Andrzej Majchrowski[4] and Dobroslawa Kasprowicz[1]

[1]Faculty of Materials Engineering and Technical Physics, Poznan University of Technology, Poznan, Poland
[2]Institute of Low Temperature and Structure Research of Polish Academy of Sciences, Wroclaw, Poland
[3]Center for Advanced Technology, Adam Mickiewicz University, Poznan, Poland
[4]Institute of Applied Physics, Military University of Technology, Warsaw, Poland
taras.v.zhezhera@put.poznan.pl

Bifunctional microcrystalline powders Bi_3TeBO_9 activated with selected rare earth ions (RE^{3+}) exhibit the nonlinear optical (NLO) properties as well as efficient luminescence derived from RE^{3+} ions. Bi_3TeBO_9 microcrystals doped with RE^{3+} can provide an excellent alternative to Bi_3TeBO_9 monocrystals doped with RE^{3+} as may lead to further miniaturization of optoelectronic devices. The microcrystalline Bi_3TeBO_9: RE^{3+} powders were synthesized by means of the modified Pechini method [1]. XRD measurements of Bi_3TeBO_9 confirmed its hexagonal structure (fig.1), $P6_3$ space group (Z=2) [2-4]. Previous studies of pure Bi_3TeBO_9 powders have revealed its high efficiency of second (SHG) and third harmonic generation (THG), in fact the highest among borate materials. The intensity of SHG is by about 20 times greater when compared to the intensity of SHG generated in the well-known NLO KDP-crystal [2,3]. However, after doping the Bi_3TeBO_9 matrix with RE^{3+}, these materials show also efficient luminescent properties [4].

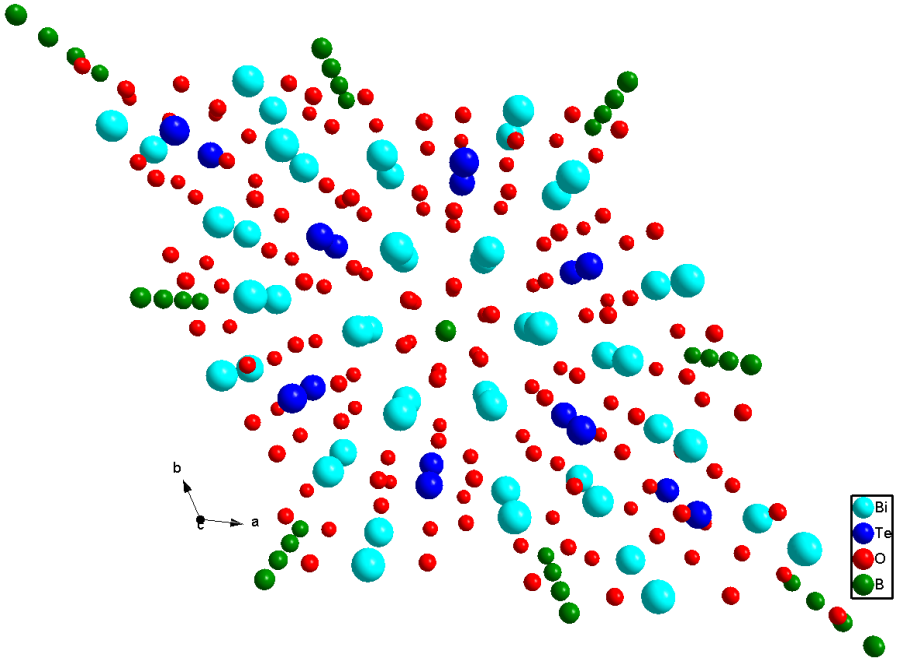


Fig. 1. Structure of Bi_3TeBO_9 crystal: view along the c axis [4].

In this work, we present the results of investigations of some structure, optical and spectroscopic properties of Bi_3TeBO_9:RE^{3+} powders studied by Raman spectroscopy and optical spectroscopy methods. Moreover, the characteristic emission of RE^{3+} ions were measured and analyzed.

Acknowledgement

This work was supported by the Research Project of the Polish Ministry of Sciences and Higher Education 0511/SBAD/2151.

[1] M. P. Pechini, Washington, DC: U.S. Patent and Trademark Office. U.S. Patent No. 3.330.697. (1967).
[2] M. Xia, X. Jiang, Z. Lin, R. Li, "All-Three-in-One": A New Bismuth−Tellurium−Borate Bi_3TeBO_9 Exhibiting Strong Second Harmonic Generation ResponseJ. Am. Chem. Soc. **138**, 14190–14193 (2016).
[3] D. Kasprowicz, T. Zhezhera, A. Łapiński, M. Chrunik, A. Majchrowski, A. V. Kityk, Ya. Shchur, Lattice dynamics of Bi_3TeBO_9 microcrystals: m-Raman/IR spectroscopic investigation and ab initio analysis, J. Alloys Comp. **782**, 488–495 (2019).
[4] T. Zhezhera, P. Gluchowski, M. Nowicki, M. Chrunik, A. Majchrowski, K. M. Kosyl and D. Kasprowicz1, Efficient near-infrared quantum cutting by cooperative energy transfer in Bi_3TeBO_9:Nd^{3+} phosphors, J Mater Sci. 57, 185–203 (2022).

OPTICAL PRINTING OF 3D MICROPOROUS SCAFFOLDS, THEIR BIOCOMPATIBILITY EVALUATION AND ENHANCEMENT IN VITRO

Jurga Jeršovaitė[1,*], Ugnė Šarachovaitė[2], Arnoldas Solovjovas[1],
Daiva Baltriukienė[2], Mangirdas Malinauskas[1]

[1]Laser Research Center, Faculty of Physics, Vilnius University, Vilnius LT-10223, Lithuania
[2]Institute of Biochemistry, Life Sciences Center, Vilnius University, Vilnius LT-10257, Lithuania
jurga.jersovaite@ff.stud.vu.lt

One of the first 3D printing technologies is stereolithography (SLA), which creates structures by selectively solidifying a liquid resin during photopolymerization reactions and has attracted considerable interest in electronics, biomedicine [1], and more over the past decade. In this work, the application of SLA printer in tissue engineering was investigated. It is an interdisciplinary branch of science that involves the use of complex scaffolds and cells to create functional tissues that would replace damaged tissue or missing organ. This treatment can overcome the obstacles of traditional methods, such as the lack of organ donors and the rejection of transplanted tissues. One of the main problems in printing scaffolds for tissue engineering is the selection of biocompatible materials, biomimicking geometries, and post-exposure processing[2].

The aim of this report is to present the fabrication of 3D micro-porous scaffolds from commercial resins and their application to cell growth. The study was performed using *Asiga PICO2* device, finding the optimal printing parameters for *Formlabs Clear* and *Formlabs Flexible* resins. The critical time T_k and the penetration depth h_a were calculated according to Beer-Lambert's law as proposed earlier [3]. Based on the obtained parameters, a study of printer evaluation to create samples of different geometries for two materials, was performed. The qualitative parameter (A) of repeatability of the printed structures was calculated on the basis of it samples with different thickness gaps and building blocks, different materials and geometry were compared. Quantitative biocompability MTT studies [4] supported by qualitative scanning electron microscope (SEM) and fluorescence microscope studies were performed after printed scaffolds were processed with different post-exposure methods to investigate biocompatibility and cell morphology.

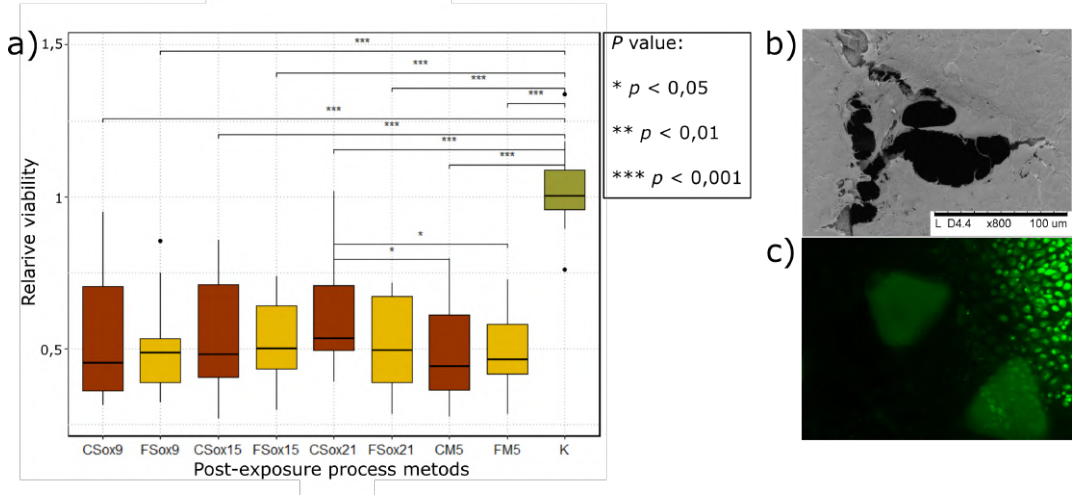


Fig. 1. Biocompatibility test results. a) MTT results given depend on the additional treatment methods used after additional exposure to UV (22 h): Sox9, Sox15, Sox21 – soaking in a Soxhlet extractor 9, 15, 21 h; M5 – soaking in methanol 5 h. F – *Formlabs Flexible*, C – *Formlabs Clear*, K – control. Qualitative biocompability test results (representative images) by b) scanning electron microscope (SEM) and c) fluorescence microscope studies

It was observed that it is more difficult to print rare geometry (fine strings and broad gaps) materials with *Formlabs Clear* resin than with *Formlabs Flexible*. The investigated repeatability parameter A shows that by changing the geometry of the structure (in order: rectangle, square, triangle), obtained values were decreasing. The assessed biocompatibility of differently treated scaffolds showed that none of methods completely removed the monomers but all were suitable for cell growth. The materials showed similar results with each other. A superior performance was observed in the sample soaked in methanol and the Soxhlet extractor using ethanol. Quantitative MTT biocompability results shown in Fig. 1. Also, validated by a qualitative biocompatibility study and depicted cell arrangement on 3D scaffold.

[1] Melchels, F. P., Feijen, J., Grijpma, D. W. A review on stereolithography and its applications in biomedical engineering. *Biomaterials*, **2010**, 31, 24, 6121-6130. https://doi.org/10.1016/j.biomaterials.2010.04.050
[2] Grigaleviciute, G.; Baltriukiene, D.; Bukelskiene, V.; Malinauskas, M. Biocompatibility Evaluation and Enhancement of Elastomeric Coatings Made Using Table-Top Optical 3D Printer. *Coatings* **2020**, 10, 254. https://doi.org/10.3390/coatings10030254
[3] Gong, H., Beauchamp, M., Perry, S., Woolley, A. T., Nordin, G. P. Optical approach to resin formulation for 3D printed microfluidics. *RSC advances*, **2015**, 5, 129, 106621-106632. DOI: 10.1039/C5RA23855B
[4] Kumar, P., Nagarajan, A., Uchil, P. D. Analysis of cell viability by the MTT assay. *Cold spring harbor protocols*, **2018** 2018.6: pdb-prot095505.

WO_3 PHOTOANODE FOR ADVANCED OXIDATION PROCESSES

Maliha Parvin, Milda Petrulevičienė, Irena Savickaja, Arnas Naujokaitis, Vidas Pakštas, Jurga Juodkazytė

Center for Physical Sciences and Technology, Saulėtekio av. 3, Vilnius 10257, Lithuania
maliha.parvin@ftmc.lt

Electrochemical advanced oxidation processes (EAOPs) have received great attention recently as a promising technology for utilization of renewable solar energy to produce strong oxidants, e.g. reactive chlorine species (RCS), persulfate, hydrogen peroxide, percarbonate, etc [1]. Tungsten (VI) oxide (WO_3) is an n-type semiconductor that has been widely investigated as a photoanode due to its relatively low cost, chemical stability, and ability to absorb visible light (bandgap is 2.5 - 2.8 eV) [2,3].

In this work, WO_3 layers with different morphology and thickness (0.4–10 μm) have been prepared by two different chemical solution deposition methods ("peroxotungstic acid route" and "tungstic acid route") and their performance in photoelectrochemical (PEC) generation of RCS and persulfate was tested. The crystalline structure and morphology of the coatings were analyzed by X-ray diffraction and scanning electron microscopy (SEM) techniques (Fig. 1). Photoelectrochemical behavior was investigated by cyclic voltammetry, electrochemical impedance spectroscopy and chronoamperometry. Iodometric and chromatometric titration methods were used to determine the amounts of photoelectrochemically produced RCS and $S_2O_8^{2-}$, respectively, to evaluate the faradaic efficiency (FE) of PEC processes.

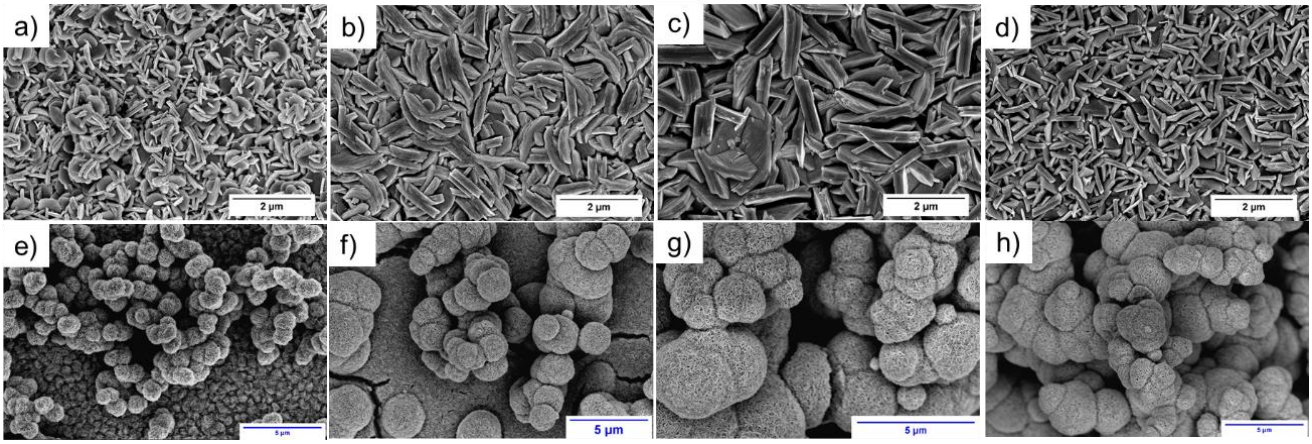


Fig. 1. SEM images of WO_3 films prepared by two different chemical solution deposition procedures: "peroxotungstic acid route" using (a) MeOH, (b) EtOH, (c) IsoPrOH, and (d) BuOH as reductants; (e) one-, (f) two-, (g) three-, and (h) four-layered coatings prepared via "tungstic acid route".

The morphology-dependent competition between possible photoanodic processes occurring on WO_3 surface in the solutions of 0.5 M NaCl and 0.5 M H_2SO_4 was analyzed considering the specific adsorption and electrostatic interactions between the reacting species at rough electrified interfaces. It was demonstrated that chloride ions tend to adsorb specifically on the surface of WO_3 electrodes, which provides them with a kinetic advantage over other solution species in the process of hole scavenging and leads to high Faradaic efficiencies (up to almost 100%) of PEC generation of reactive chlorine species (ClO^- + ClO_2^-). FE of $S_2O_8^{2-}$ formation ranged between 40 % and 80 % [4]. Hole-mediated formation of radical intermediates was suggested to explain the photoelectrochemical performance of prepared photoanodes.

The stability of WO_3 films during prolonged photoelectrolysis in 0.5 M NaCl and 0.5 M H_2SO_4 solutions was tested and antimicrobial effect of PEC generation of strong oxidants was demonstrated. The obtained results show that photoelectrochemical systems with WO_3 can find application in visible light-assisted advanced oxidation processes in the areas of water disinfection and organic pollutants degradation.

[1] F. C. Moreira, R. A. R. Boaventura, E. Brillas, and V. J. P. Vilar, Electrochemical advanced oxidation processes: A review on their application to synthetic and real wastewaters, Appl. Catal. B. **202**, 217–261, (2017).

[2] K. Sayama, Production of high-value-added chemicals on oxide semiconductor photoanodes under visible light for solar chemical-conversion processes, ACS Energy Lett. **3**,1093–1101, (2018).

[3] J. C. Hill and K. S. Choi, Effect of electrolytes on the selectivity and stability of n-type WO_3 photoelectrodes for use in solar water oxidation, J. Phys. Chem. C **116**, 7612–7620, (2012).

[4] M. Parvin, M. Petrulevičienė, I. Savickaja, B. Šebeka, R. Karpicz, A. Grigucevičienė, R. Ramanauskas, J. Juodkazytė, Influence of morphology on photoanodic behaviour of WO_3 films in chloride and sulphate electrolytes, Electrochim. Acta **403**,139710, (2022).

Acknowledgment: This research was funded by the M-ERA.NET project "Multiscale computer modelling, synthesis and rational design of photo(electro)catalysts for efficient visible-light-driven seawater splitting" (CatWatSplit), Ref. Number: project8168, under a grant agreement Nr. S-M-ERA.NET-21-3 with the Research Council of Lithuania(LMTLT).

FINE-TUNING THE SPIKE: ROLE OF THE NATURE AND TOPOLOGY OF THE GLYCAN SHIELD IN THE STRUCTURE AND DYNAMICS OF SARS-COV-2

Carl A. Fogarty[1], Aoife M. Harbison[1], Toan K. Phung[2],Akash Satheesan[1], Benjamin L. Schulz[2], Elisa Fadda[1]

[1]Department of Chemistry, Maynooth University, Ireland
[2]School of Chemistry, University of Queensland, Australia
carl.fogarty.2016@mumail.ie

The SARS-CoV-2 spike (S) is a type I fusion glycoprotein, responsible for initiating the infection leading to COVID19. As a feature unique of SARS-CoV-2, the thick glycan shield covering the S protein is not only essential for hiding the virus from immune detection, but it also plays multiple functional roles, stabilizing the S prefusion "open" conformation, which is competent for binding the ACE2 primary receptor, and gating the open-to-close transitions. This newly discovered functions of the glycan shield suggest the evolution of its sites of glycosylation is potentially intertwined with the evolution of the overall protein sequence to affect optimal activity. Furthermore, recent studies indicate that the occupancy and structures of SARS-CoV-2 S glycosylation depends not only on the host-cell, but also on the structural stability of the prefusion trimer; a point that raises important questions about the relative binding competence of different glycoforms. In this work we use multi-microsecond molecular dynamics simulations to characterize the structure and dynamics of different SARS-CoV-2 S models with different N-glycans at key functional sites, namely N234, N165 and N343. We also assessed the effect of a change in the SARS-CoV-2 S glycan shield's topology at N370, due to the recently acquired T372A mutation. Our results indicate that the structures of the N-glycans at N234, N165 and N343 affect the stability of the active (or open) S conformation, and thus its exposure and accessibility. Furthermore, while glycosylation at N370 stabilizes the open S conformation, we find that the N370 glycan binds the closed receptor binding domain (RBD) surface, essentially tying the closed protomers together. These results suggest that the loss of the N370 glycosylation site in SARS-CoV-2 may have increased the availability of the open S form, perhaps contributing to its higher infectivity relative to CoV1 and other variants carrying the sequon. Finally, we discuss these specific changes to the topology of the SARS-CoV-2 S glycan shield through ancestral sequence reconstruction of select SARS strains and discuss how they may have evolved to affect S activity.

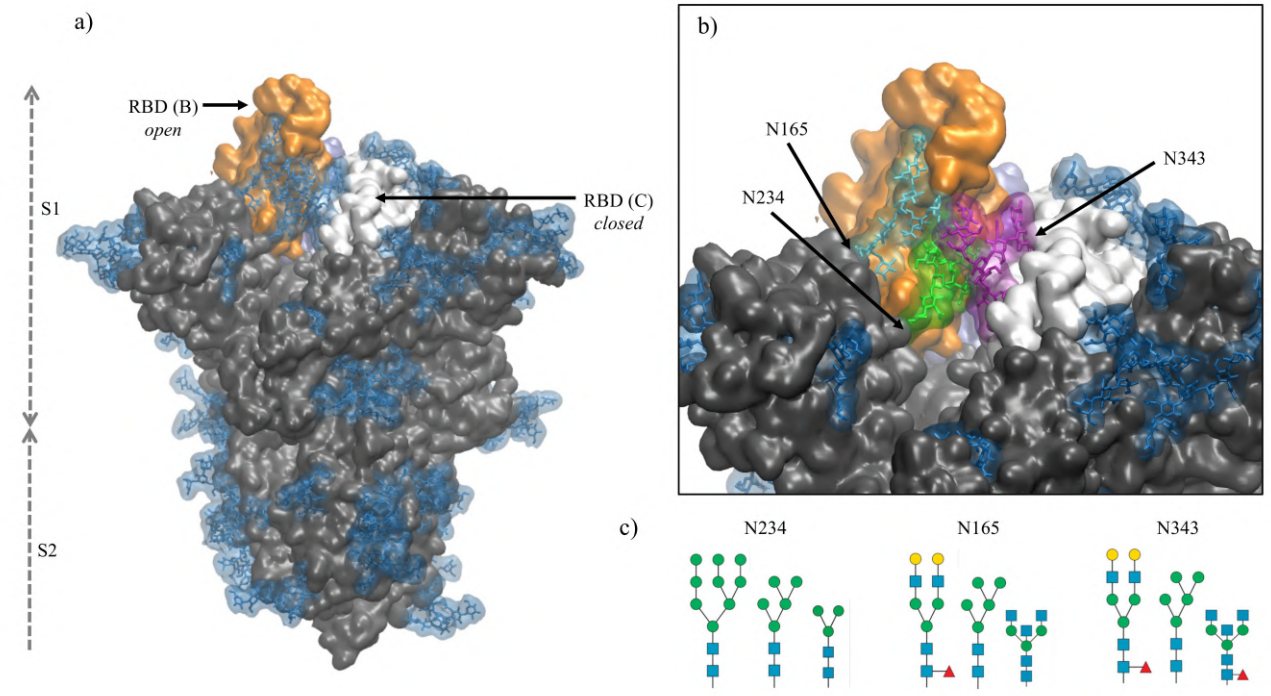


Fig. 1. Illustrates the S 1/2 units of the spike protein in the open conformation and panel c) shows the SNFG representation of the variations in the glycan shield explored in the paper.

EEG SIGNAL SEGMENTATION FOR HUMAN RESPONSE DETECTION

Marta Lotka[1]

[1] Department of Physics, Computer Science and Astronomy, Jagiellonian University, Poland
marta.lotka@student.uj.edu.pl

The non-stationarity of the human EEG signal has been well-established. It is of interest to find a method of dividing the EEG signal into quasi-stationary spells to determine its local properties. One proposed method to achieve this, which has been introduced and on other biological signals by [1], is using an algorithm utilizing the Kolmogorov-Smirnov test for comparing empirical distribution function between two samples.

This presentation will cover the performance of this segmentation algorithm (the KS segmentation) for artificial Gaussian series and for series that have been used as models of the EEG: 1/f-like noise and autoregressive series. To evaluate the performance, normalized mutual information and number of segments identified are used. It was found that the algorithm accurately segments Gaussian series in a wide range of parameters. For the 1/f-like and AR series oversegmentation occurs. This indicates a direction for possible improvement of the KS segmentation algorithm.

KS segmentation has been then applied to the EEG of subjects participating in the Eriksen Flanker Task – a task commonly used in psychology to study detection of a target in presence of distraction. The subjects in the task are presented a target arrow pointing either left or right, surrounded by other arrows (distractors) which either all point left or right. In each trial the subjects are asked to press a button indicating the direction of the target arrow. This task is known to elicit a specific pattern of event-related potentials – peaks in segments of EEG signal (epochs) surrounding the response, averaged over many trials.

In spite of the EEG signal having a non-Gaussian, heavy-tail distribution, when segmentation is performed on many epochs and its distribution density is calculated, the results appear to reproduce the pattern present in the event-related potentials (as shown in Fig. 2). This suggests that KS segmentation might offer an alternative to the prevalent event-related potential method which would allow for human response detection on a single-trial basis.

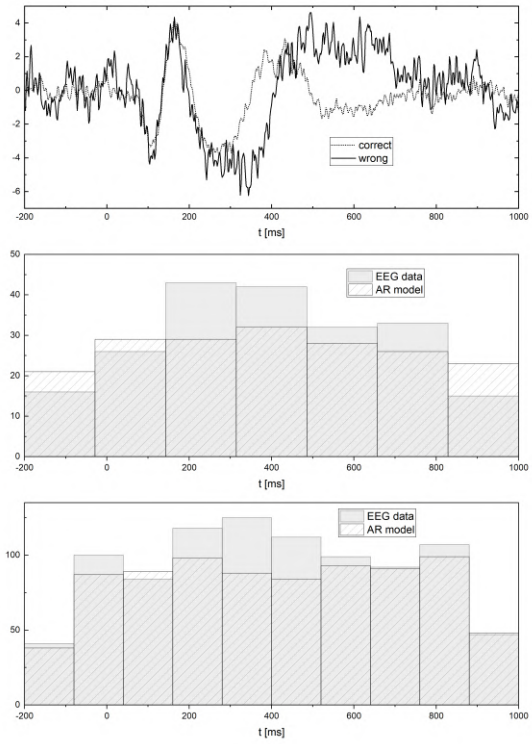


Fig. 1. Comparison of an event-related potentials with segmentation results for a single subject. Top panel: stimulus-locked event-related potentials for correct and incorrect answers in the flanker task. Middle panel: histogram of number of partitions found by the KS segmentation algorithm in the EEG epochs in the incorrect condition, compared to fitted AR series. Bottom panel: histogram of number of partitions found by the KS segmentation in the EEG epochs in the correct condition, compared to fitted AR series.

[1] S. Camargo, S. M. Duarte Queirós, and C. Anteneodo. Nonparametric segmentation of nonstationary time series, Phys. Rev. E 84, 046702 (2011)

THROUGHS THE CRYOPRESERVED SPERM PROTEOME: A BIOINFORMATIC APPROACH TO IDENTIFY RELEVANT DIFFERENTIALLY EXPRESSED PROTEINS

Pedro Oliveira Corda[1], Joana Vieira Silva[1,2,3], Sara Catarina Pereira[3], Alberto Barros[2,4,5], Marco Alves[3], Margarida Fardilha[1]

[1]Institute of Biomedicine (iBiMED), Department of Medical Sciences, University of Aveiro, 3810-193, Aveiro, Portugal

[2] QOPNA & LAQV, Department of Chemistry, University of Aveiro, Aveiro, Portugal.

[3]Unit for Multidisciplinary Research in Biomedicine (UMIB) & Department of Anatomy, Institute of Biomedical Sciences Abel Salazar (ICBAS), University of Porto, 4050-313, Porto, Portugal

[4]Centre for Reproductive Genetics A. Barros, 4100-012 Porto, Portugal

[5]Department of Genetics, Faculty of Medicine, University of Porto, Porto, Portugal

pedrocorda@ua.pt

Sperm cryopreservation is a crucial procedure in reproductive medicine worldwide. Nowadays, two conventional freezing techniques are used in sperm cryopreservation: (a) slow freezing (SF) and (b) rapid freezing (RF). Notwithstanding, the cryopreservation protocols are still not ideal inducing significant changes at spermatozoon structural and molecular levels that are poorly characterized. Proteomics emergence brought a new perspective on sperm physiology, allowing the evaluation of the protein profile in certain physiological/pathological contexts. The main objective of the present work was to unveil relevant differentially expressed proteins (DEPs) that can be used as potential quality markers or modulation targets for sperm cryopreservation.

A literature search was conducted to identify proteomic studies that compared fresh samples VS freeze-thawed human spermatozoa from normozoospermic donors. From the included studies, DEPs were collected into two groups: SF and RF groups. For each group, enrichment analyses (gene ontology and KEGG pathways) were, and protein-protein interactions were collected. Combining this data, integrative networks were built to identify key DEPS (proteins with higher degrees). For the identified DEPs, an additional search was performed to identify known associations with male infertility and/or poor sperm quality.

For SF and RF groups, 160 and 555 DEPs were collected, respectively. SF proteins were mainly associated with translation pathways, whereas RF proteins were strongly associated with the proteasomal pathway. Among the key DEPS, Arylsulfatase A (ARSA) was decreased in both freezing groups and low ARSA levels have been associated with poor sperm quality in literature. Thus, ARSA was selected for experimental investigation and its levels were assessed in cryopreserved samples (n=15) by western blot. ARSA levels were significantly decreased in RF and SF samples (~31.97% and ~39.28%, respectively).

The integration and analysis of the available proteomic data allowed the identification of key DEPs in freeze-thawed human spermatozoa. The bioinformatic analysis reduced the list of potential candidates and directed the investigation to one protein. ARSA has the potential to be used as a marker to assess sperm quality after cryopreservation.

STUDY OF SARS-COV-2 SPECIFIC MPRO PROTEASE AND INTERACTIONS OF ITS CATALYTIC CENTER WITH POTENTIAL INHIBITORS

Mariia Oleksiivna Yurchikova[1], Daria Sergiivna Ponomariova[2], Anatoliy Ivanovich Dragan[2*]

[1] Department of Molecular Biology and Bioinformatics, Institute of High Technologies, Ukraine
mariia.yurchikova1999@gmail.com

The main SARS-CoV-2 protease, Mpro, is a key enzyme in the life cycle of the coronavirus. Catalytic residues Cys145 and His41 in 3CL Mpro located in the cavity of the active site can be a potential target for molecular inhibitors. Proteins cleaved by Mpro are essential enzymes for viral replication. To inhibit Mpro and thereby stop the life cycle of the virus, it is necessary to find high-affinity ligands capable of binding in the catalytic region of its active site. [1]

Thus, the main task of this work is to search for candidates for further drug development among highly effective Mpro inhibitors. In accordance with the goal, the following tasks were set: 1. Analysis of the life cycle structure and properties of the SARS-CoV-2 coronavirus; 2. An overview of the many potential inhibitors in known publicly available libraries of chemicals; 3. Molecular docking of potential inhibitors; 4. Refinement of docking results by modeling the molecular dynamics of complexes of Mpro proteases with the best inhibitor candidates.

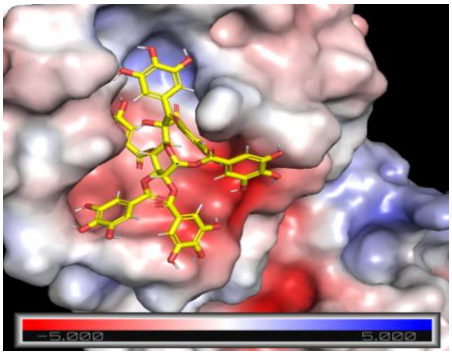


Fig. 1. Mpro catalytic center - ligand complex. Active site and catalytic center surface is filled in according to electrostatic potential.

In this study using the methods of virtual screening and molecular docking in the software package Schrödinger Suites 2018-1 free energy XP Gscore of 119 482 molecules PubChem and ZINC15 free access databases were tested and evaluated .XP Gscore, calculated by the XP method, was used for compound evaluation as it provides the most accurate predictions of molecular interactions. [2] As a result we obtained 42 compounds with free binding energy (ΔG) values in the range from -17 to -10 kcal / mol from the category of natural polyphenol Pentagaloylglucose analogues, investigated due to the high indicators of affinity to SARS-CoV-2 Mpro protease active site observed for compound Pentagaloylglucose in similar research. [3] Among the drugs approved by world jurisdictions are 18 drugs with ΔG from -13,5 to -9 kcal / mol and 37 substances with ΔG from -14,3 to -10,9 kcal / mol among human metabolites, substances found in food.

10 nsec molecular dynamics simulations were performed in Gromacs for Mpro complexes with different categories of ligands selected according to the docking results. We analyzed the stability of these complexes with Mpro, the level of fluctuations of amino acid residues and interaction energies based on the RMSF and RMSD values, as well as the binding energy values (average energy of the Coulomb interaction and Lennard-Jones energy) correlate with the data of free binding energies obtained from molecular docking.

A number of ligands capable of forming complexes with the catalytic center of Mpro SARS CoV 2 were discovered during the study. Selected candidates inhibit the protease by forming a variety of chemical bonds with the catalytic dyad as well as amino acids that form the active center:VAL20, THR21, CYS22, GLY23, THR24, THR25, THR26, LEU27, ASN28, PRO39, ARG40, HID41, VAL42, CYS44, THR45, SER46, ASP48, MET49, LEU50, PRO52, TYR54, TYR118, ASN119, ILE136 SER139, PHE140, LEU141, ASN142, GLY143, SER144, CYS145. All studied ligands are non-toxic, and the resulting complexes are of interest for further study. Currently, the in silico approaches presented in this work help in repurposing already known drugs, which can significantly save time and money in the development of drugs against COVID-19.

[1] Jin Z., Du X., Xu Y. et al. Structure of Mpro from COVID-19 virus and discovery of its inhibitors. Nature 582,289-293(2020).
[2] Salam, Noeris K.; Nuti, Roberto; Sherman, Woody (2009). Novel Method for Generating Structure-Based Pharmacophores Using Energetic Analysis. Journal of Chemical Information and Modeling, 49(10), 2356–2368. doi:10.1021/ci900212v.
[3] Chiou, W.-C., Chen, J.-C., Chen, Y.-T., Yang, J.-M., Hwang, L.-H., Lyu, Y.-S., Huang, C. (2021). The inhibitory effects of PGG and EGCG against the SARS-CoV-2 3C-like protease. Biochemical and Biophysical Research Communications. doi:10.1016/j.bbrc.2020.12.106.

AN INVESTIGATION INTO THE BIOCHEMICAL AND PHYSIOCHEMICAL FREQUENCIES DISTRIBUTIONS OF AMP FAMILIES

Michela Caprani [1], John Healy[2], Orla Slattery [2] and Joan O'Keeffe [2]

[1]Marine and Freshwater Research Centre (MFRC), Galway-Mayo Institute of Technology, Galway, Ireland
[2] Dept. of Computer Science & Applied Physics, Galway-Mayo Institute of Technology, Galway, Ireland
michela.caprani@research.gmit.ie

Currently one of the greatest challenges to human health is the growing emergence of antimicrobial resistance (AMR). Antimicrobial peptides (AMPs) are essential components in innate immunity and have recently gained considerable interest as novel antibiotics due to their potent antimicrobial activities against bacteria, viruses, and cancer [1]. AMPs are classified into families and subfamilies based on distinct physiochemical features such as amino acid composition and secondary structure. In recent years, the implementation of computational models has aided in the classification of AMPs prior to experimental designs. Such models, can aid in identifying key features that discriminate AMPs families from each other, assisting in the isolation and purification of novel AMPs.

In this study, we investigated the frequency distributions of amino acid residues and the key biochemical properties of the 21 most studied AMP families. While most studies to date have either focused on specific AMP families or properties common to all AMPs, this investigation analysed the frequency distributions and key properties of each AMP family and the aggregated frequencies of all families. We also benchmarked each of these frequency distributions against the full curated reference set of the UniProt database of 565,928 sequences. The results from this study, indicate that many of the commonly cited characteristics of AMPs are not universal. Properties such as, amino acid composition vary widely between the different families and some amino acids appear with far greater frequency in specific families than across the full spectrum of AMPs. The analysis also identified biochemical properties that have not been reported to date, including partition coefficients and the weight positions of secondary structures, such as alpha helix, beta sheet and coil.

[1] Zasloff, M.: Antimicrobial peptides of multicellular organisms. *Nature*, 415(6870), p.389, (2002)

STUDY OF SARS COV 2 M PRO DIMERIZATION SITE AND ITS INTERACTIONS WITH POTENTIAL INHIBITORS

Daria Ponomariova, Mariia Yurchikova, Anatoliy Dragan*

Department of Molecular Biology and Bioinformatics, Institute of High Technologies, Ukraine
Ponomariovads@gmail.com

COVID-19 is a highly contagious respiratory infection. An attractive therapeutic target for SARS-CoV-2 (severe acute respiratory syndrome 2, etiologic agent of COVID-19) is the main protease (Mpro), as this enzyme plays a major role in the processing of viral polyproteins. SARS-CoV-2 Mpro is a dimer formed by two monomers, each consisting of three domains. Since Mpro SARS-CoV-2 is active in dimeric form only, effective drug development strategies can include the search for inhibitors aimed at dimerization [1].

The aim of this study was to identify a number of ligands that are capable of inhibiting Mpro activity by interacting with the enzyme dimerization site. Drugs targeting Mpro SARS-CoV-2 can inhibit viral replication and, due to the highly conserved primary enzyme structure in different members of the coronavirus family, reduce the risk of mutation-mediated drug resistance while exhibiting broad-spectrum antiviral activity.

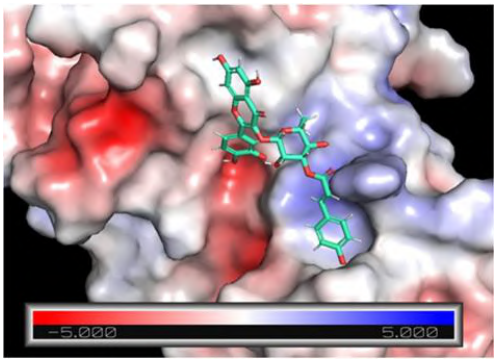


Fig. 1. Mpro dimerization site - ligand complex. Dimerization site surface is filled in according to electrostatic potential.

During the search for compounds capable of binding to the dimerization site of Mpro protease with the most favorable indicators of free binding energy 8,793 ligands approved for medical use by the FDA and other major jurisdictions, 111178 substances frequently detected in food products, and 8 million compounds that do not contain PAINS (pan assay interference compounds), were analyzed via Schrodinger Glide [2], a ligand docking program that uses an empirical scoring function (XP GScore) as a measure of the ligand free binding energy, which led to the identification of 8242 compounds with XP GScore values below - 5 kcal / mol.

Screening of substances approved for use as medication in the United States, the EU, Japan and China was carried out first and foremost. As a result, thirteen compounds with binding scores ranging from -5 to -9 kcal / mol were identified. From the “in man” subgroup of the ZINC15 database used as a source for structures of compounds frequently detected in food products, 41 compounds with XP GScore ranging from -10.9 to -8 kcal / mol were identified. In the ZINC subgroup anodyne, from which substances that do not contain interfering structures (PAINS) were obtained, we found 8188 compounds with XP G Score values less than -5.8 kcal / mol.

Ligands with best XP GScores were used for MD simulation studies with GROMACS [3]. To ensure the stability of ligand-protein complexes standard deviations, calculated by performing least squares approximations for the protein-ligand complexes were compared to the values obtained for the Mpro protease not bound to the ligand. Calculations showed sufficient stability of most Mpro-ligand complexes.

Our study introduces a number of ligands capable of forming complexes with the dimerization site of Mpro SARS CoV 2. These compounds work primarily via forming hydrogen bonds, salt bridges, and pi-cation interactions with amino acids vital for dimerization, for example LYS4; ARG5; TYR126; VAL125, GLU290, LYS137, PHE140; GLU166 and others. Several compounds that successfully underwent clinical trials and were approved by FDA for medical use were found to possess high binding affinity to dimerization site of Mpro SARS CoV 2, which opens the possibility for drug repurposing.

[1] M. Jin Z, Wang H, Duan Y, Yang H. The main protease and RNA-dependent RNA polymerase are two prime targets for SARS-CoV-2. Biochem Biophys Res Commun. 2021 Jan 29;538:63-71. doi: 10.1016/j.bbrc.2020.10.091. Epub 2020 Nov 21. PMID: 33288200; PMCID: PMC7680044.

[2] Friesner, R. A.; Murphy, R. B.; Repasky, M. P.; Frye, L. L.; Greenwood, J. R.; Halgren,T. A.; Sanschagrin, P. C.; Mainz, D. T., "Extra Precision Glide: Docking and Scoring Incorporating a Model of Hydrophobic Enclosure for Protein-Ligand Complexes," J. Med. Chem., 2006, 49, 6177–6196

[3] Maik Gotte. Free energy calculations of protein-ligand complexes with computational molecular dynamics. // Dissertation zur Erlangung des Doktorgrades der Mathematisch-Naturwissenschaftlichen Fakult¨aten der Georg-August-Universit¨at zu G¨ottingen

TRUE ZERO-BIAS THZ DETECTOR WITH GRAPHENE FIELD-EFFECT TRANSISTOR

Domantas Vizbaras[1], Kęstutis Ikamas[1,3], Andrey A. Generalov[2], Alvydas Lisauskas[1,4]

[1]Institute of Applied Electrodynamics and Telecommunications, Vilnius University, Vilnius, 10257, Lithuania
[2] VTT Technical Research Centre of Finland LTD, P.O. Box 1000, FI-02044 VTT, Finland
[3]General Jonas Žemaitis Military Academy of Lithuania, 10322 Vilnius, Lithuania
[4]CENTERA Laboratories, Institute of High Pressure Physics PAS, Warsaw, 01-142, Poland
domantas.vizbaras@ff.stud.vu.lt

Graphene is a two-dimensional allotrope of carbon consisting of a single layer of atoms. Because of its high charge carrier velocity and extraordinary saturation velocity, graphene field-effect transistors (GFET) have a chance to become serious contenders in the field of terahertz (0.1-10 THz range) electronics [1]. GFET technology is used primarily as THz radiation detectors and has potential applications, such as non-ionizing medical imaging or security screening [1].

GFET technology has seen great improvements during the last decade. The best results for a single transistor so far were published in 2017, reporting the maximum optical responsivity of $74\ \mathrm{V/W}$ and the noise equivalent power (NEP) of $130\ \mathrm{pW/\sqrt{Hz}}$ at 400 GHz [2]. Despite the achieved promising performance values, GFETs are still heavily outshined by silicon-based detectors [3].

The device used in this study was grown by Chemical Vapor Deposition (CVD) and processed at VTT (Finland). The graphene was transferred onto a SiO_2 wafer and formed the field-effect-transistor channel with a channel length of 2 µm. The source and drain contacts are evaporated using Ti/Au. The ALD grown Al_2O_3 is used as a gate dielectric, another evaporated layer of Ti/Au is used as a gate metal. The source, drain, and gate terminals form a bowtie antenna shown in Fig. 1 a).

The detector's static electrical characteristics were measured using a semiconductor analyzer Keysight B1500A. The frequency multiplier (Virginia Diodes Inc.) and low-noise voltage amplifier were used for the response measurements as a THz radiation source in the 250-380 GHz range. It was calibrated using a Thomas Keating broadband absolute power detector. The optical system employed two 4" parabolic mirrors in a 4-f configuration. A hyper-hemispheric silicon lens (12 mm diameter, 6.8 mm height) was used to focus the THz radiation onto the detector from the substrate side.

Measurements were performed at room temperature ($295\ \mathrm{K}$). Fig. 1a presents the measured spectra of optical responsivity. The maximum value of $14\ \mathrm{V/W}$ was obtained at $337\ \mathrm{GHz}$ frequency. The dependencies of voltage responsivity and NEP on the GFET gate voltage are depicted in Fig. 1b. Both characteristics show a slight hysteresis. It is common in GFET technology and can be suppressed by various methods [4]. More importantly, both the highest responsivity and the lowest NEP of $627\ \mathrm{pW/\sqrt{Hz}}$ were observed close to $0\ \mathrm{V}$ gate voltage. This means that the detector does not require additional bias and can be utilized as a true zero-bias detector.

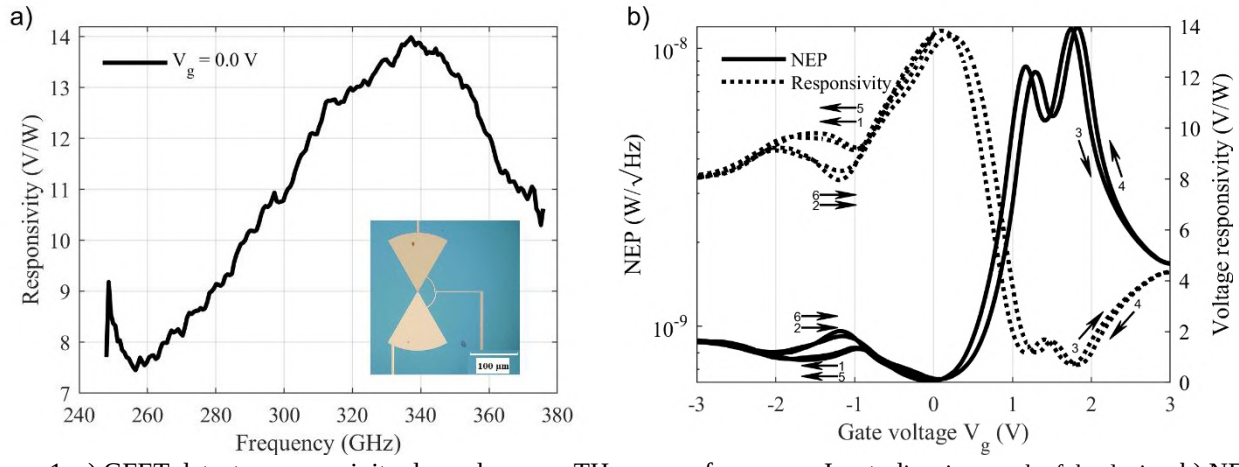


Figure 1. a) GFET detector responsivity dependency on THz source frequency. Inset: die micrograph of the device. b) NEP and responsivity dependency on transistor gate voltage at 337 GHz.

[1] G. Valušis, A. Lisauskas, H. Yuan, W. Knap, and H. G. Roskos, "Roadmap of Terahertz Imaging 2021," *Sensors*, vol. 21, no. 12, Art. no. 12, Jan. 2021, doi: 10.3390/s21124092.

[2] A. A. Generalov, M. A. Andersson, X. Yang, A. Vorobiev, and J. Stake, "A 400-GHz Graphene FET Detector," *IEEE Transactions on Terahertz Science and Technology*, vol. 7, no. 5, pp. 614–616, Sep. 2017, doi: 10.1109/TTHZ.2017.2722360.

[3] E. Javadi, D. B. But, K. Ikamas, J. Zdanevičius, W. Knap, and A. Lisauskas, "Sensitivity of Field-Effect Transistor-Based Terahertz Detectors," *Sensors*, vol. 21, no. 9, p. 2909, Apr. 2021, doi: 10.3390/s21092909.

[4] H. Wang, Y. Wu, C. Cong, J. Shang, and T. Yu, "Hysteresis of Electronic Transport in Graphene Transistors," *ACS Nano*, vol. 4, no. 12, pp. 7221–7228, Dec. 2010, doi: 10.1021/nn101950n.

MODIFIED DIKETOPYRROLOPYRROLE EMITTERS FOR TUNABLE NIR-TO-VISIBLE PHOTON UPCONVERSION

Lukas Naimovičius[1], Edvinas Radiunas[1], Barbara Chatinovska[2], Augustina Jozeliūnaitė[2], Edvinas Orentas[2], Karolis Kazlauskas[1]

[1]Institute of Photonics and Nanotechnology, Vilnius University, Lithuania
[2]Department of Organic Chemistry, Vilnius University, Lithuania
lukas.naimovicius@ff.stud.vu.lt

Triplet-triplet annihilation (TTA) mediated NIR-to-visible photon upconversion (UC) attained under incoherent and low power excitation is a rapidly advancing field of photonics with promising applications in photocatalysis, bio-imaging, photovoltaics, targeted drug delivery and night vision devices. [1-3] Generally, TTA-UC systems are comprised of a sensitizer and an emitter. The sensitizer is responsible for absorption of low energy photons and generation of triplet states via intersystem crossing, whereas the emitter accumulates those triplets and performs TTA resulting in upconverted emission of higher energy. Currently, there is a lack of efficient, stable, and tunable TTA emitters in the visible range preventing numerous possible applications. In this work, the modified diketopyrrolopyrrole (DPP) compounds are proposed as the tunable and stable alternatives [4] to widely used rubrene and perylene diimide emitters.

Five DPP compounds (DPP-eh, DPP-c, DPP-s, DPP-Ph, DPP-2Ph) functionalized with different moieties were investigated as the emitters for NIR-to-visible UC. Palladium-phthalocyanine (PdPc) served as a sensitizer in this study. Essentially, the DPP compounds exhibited high Φ_{FL} (64% - 74%) in the isolated form and a red shift of FL spectra with increasing the complexity of the moieties allowing to implement the tunable UC. DFT modelling was found to be in agreement with experiment and showed the same trend of singlet energy reduction. All DPP derivatives demonstrated the feasibility for TTA in a solution with moderate Φ_{UC} (0.4% - 2.3%) as compared to the widely used rubrene (Φ_{UC} = 5.6%). (Fig. 1) While most of the derivatives exhibited UC threshold in the range of 6 – 22 W/cm^2, the compound with large side moieties (DPP-2Ph) expressed a way higher threshold (>100 W/cm^2) making Φ_{UC} determination impossible. Furthermore, DPP compounds displayed significant aggregation in the solid state facilitating strong non-radiative decay, and thus, complete inhibition of UC emission.

The obtained results suggest that the DPP derivatives can be considered as potential TTA emitters for solution-based applications in NIR-to-vis UC.

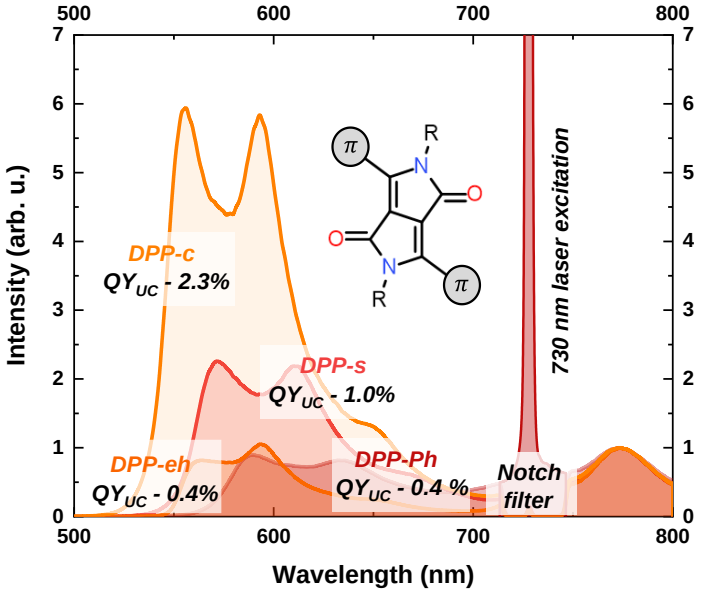


Fig. 1 UC emission spectra of DPP compounds in deoxygenated toluene solution. DPP and PdPc concentration, 8 mM and 30 μM, respectively. Φ_{UC}, indicated.

[1] M. Wu et al., Nat. Photonics, vol. 10, no. 1, pp. 31–34, (2016).
[2] Radiunas, E. et al., J. Mater. Chem. C 8, 5525–5534 (2020).
[3] Fallon, K. J. et al., J. Am. Chem. Soc. 142, 19917–19925 (2020).
[4] Andrew B. Pun et al., J. Am. Chem. Soc., 141, 3777-3781 (2019).

MOVPE OF GaN ON GRAPHENE-COVERED GaN/SAPPHIRE TEMPLATES

Kazimieras Badokas[1*], Dominykas Augulis[1], Arūnas Kadys[1], Jūras Mickevičius[1], Ilja Ignatjev[2], Benjaminas Šebeka[2], Martynas Skapas[2], Giedrius Juška[1] and Tadas Malinauskas[1]

[1] Vilnius University, Faculty of Physics, Sauletekio av. 3, Vilnius 10257, Lithuania
[2] Center for Physical Sciences and Technology, Sauletekio av. 3, Vilnius 10257, Lithuania
kazimieras.badokas@ff.vu.lt

Graphene turns epitaxial GaN substrate into a *copy machine* enabling the process known as remote epitaxy [1]. During metalorganic vapor phase deposition, growing crystalline layer bonds to van der Walls surface of graphene relatively weakly. Non-covalent interaction results in a facile membrane release. A seeding effect from the substrate beneath manifests in the formation of a high-quality membrane. Practical benefits of remote epitaxy include: cost savings due to the reusable substrate, novel designs of flexible devices due to exfoliated thin films; and dissimilar material integration by stacking freestanding membranes. However, the process of remote epitaxy is relatively unexplored and needs further refinement.

In this work, we investigated the main steps of remote epitaxy, including the transfer of multiple graphene layers, as it was previously shown for bilayer graphene to permit interaction between the seeding GaN layer beneath and the growing layer on top [2]. Both dry and wet transfers were implemented. Lower cost and better initial quality led to the adoption of the wet transfer process. The properties of transferred layers were investigated by Raman spectroscopy.

High temperature combined with reactive species in the MOVPE process atmosphere could be detrimental to graphene. Initial growth temperature effects on the quality of graphene were investigated. A two-step growth protocol, including nucleation at optimal 700 °C temperature, was developed to grow high-quality GaN membranes [3]. Fully coalesced crystalline films were investigated by atomic force microscopy, transmission electron microscopy, X-ray diffraction, and photoluminescence techniques. Successful exfoliation of GaN thin film was demonstrated.

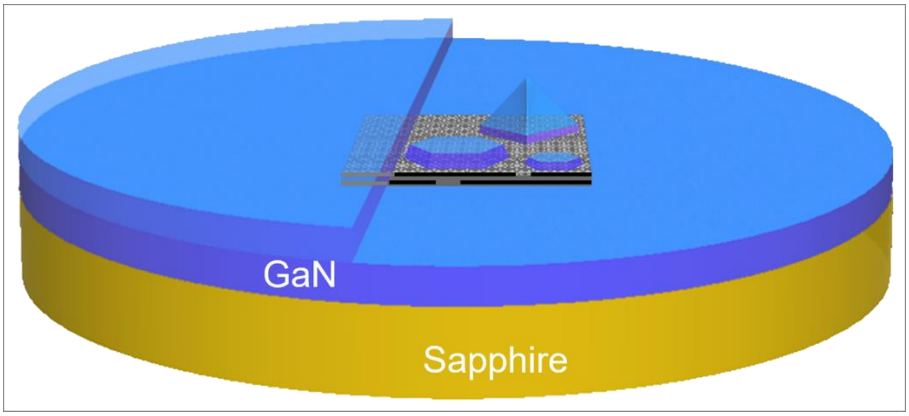


Fig. 1. Schematic representation of GaN remote epitaxy on our GaN/sapphire template covered with bilayer (aperture-free) graphene.

[1] Kim et al., Remote epitaxy through graphene enables two-dimensional material-based layer transfer, Nature **544**, 340-343 (2017)
[2] Hong et al., Polarity governs atomic interaction through two-dimensional materials, Nat. Mater. **17**, 999-1004 (2018)
[3] Badokas et al., Remote epitaxy of GaN via graphene on GaN/sapphire templates, J. Phys. D: Appl. Phys. **54**, 205103 (2021)

IN-SITU QUANTUM DOTS FORMATION IN MBE USING SEGREGATION PROCESS

Arnas Pukinskas[1], Nerijus Jurkūnas[2], Silvija Keraitytė[1,3], Algirdas Jasinskas[1], Andrea Zelioli[1], Simona Pūkienė[1], Andrius Bičiūnas[1], Bronislovas Čechavičius[1], Arnas Naujokaitis[1], Martynas Skapas[1], Monika Jokubauskaitė[1,3], Evelina Dudutienė[1], and Renata Butkutė[1,3]

[1] Department of Optoelectronics, Centre for Physical Sciences and Technology, Saulėtekio av. 3, Vilnius, Lithuania
[2]Optonas Ldt., Savanorių av. 235, Vilnius, Lithuania
[3]Institute of Photonics and Nanotechnology, Faculty of Physics, Vilnius University, Saulėtekio av. 3, Vilnius, Lithuania
arnas.pukinskas@ftmc.lt

The engineering of new materials exhibiting synergy of electro-optical properties in the near infrared (NIR) spectrum region has attracted a lot of attention of scientific community in the last decade. On the other hand, the scientists are focused into the reduction of the active media dimensions by proceeding to quantum nanostructures like quantum dots, quantum wells, quantum wires etc. Minimization of dimensions (optimization of the quantum well geometry) induces quantum effects, which opens the opportunity to technologically manipulate characteristic parameters of the device, while applying various technological protocols including growth interruptions for atom diffusion, pulse mode supply of components, carrying out *ex-situ* and *in-situ* annealing to smooth out boundaries of layers is possible to achieve the enhancement of fundamental properties. Moreover, scientists are exploring the modification of epitaxy methods for different formation effects of nanostructures, that would lead to flexible properties of functional materials.

Two decades ago, new AIII-BV-Bi compounds, called bismides, were discovered. Bismides are one of the most perspective compounds for the NIR applications because of their unique property – reduction of band gap energy replacing As by Bi atoms. Theoretically it is proven, that at least 1% of Bi can reduce the band gap energy up to 88 meV [1]. Using platform of GaAs ternary GaAsBi compound band gap energy can be changed from 1.42 eV to 0.75 eV [2], which corresponds to spectrum range from 875 nm to 1500 nm. Whereas bismide alloy has lower band gap energy dependance on temperature [3], NIR light sources based on bismide nanostructures (quantum well and quantum dots) could easily work at room temperature without additional cooling.

The main goal of this work was to explore new and different from usual Stranski-Krastanov Bi quantum dots formation mechanism employing *in-situ* bismuth segregation process in Molecular Beam Epitaxy (MBE) reactor via annealing for a short time at higher temperatures under arsenic overpressure conditions. This study would let us to analyze and understand complex quantum effects in AIII-BV-Bi quantum well containing Bi quantum dots and apply them in active media of NIR laser diodes or LEDs. The optimization of growth and *in-situ* annealing conditions was made in MBE for complex system: ternary GaAsBi and Bi compounds. Main attention in MBE optimization process was concentrated to the search of quantum barriers (which play Bi blocking layer role), GaAsBi well composition (Bi content) and geometry (well thickness and shape). Featured samples were characterized using high resolution transmission electron microscopy, meanwhile all grown quantum structures were examined by photoluminescence measurements.

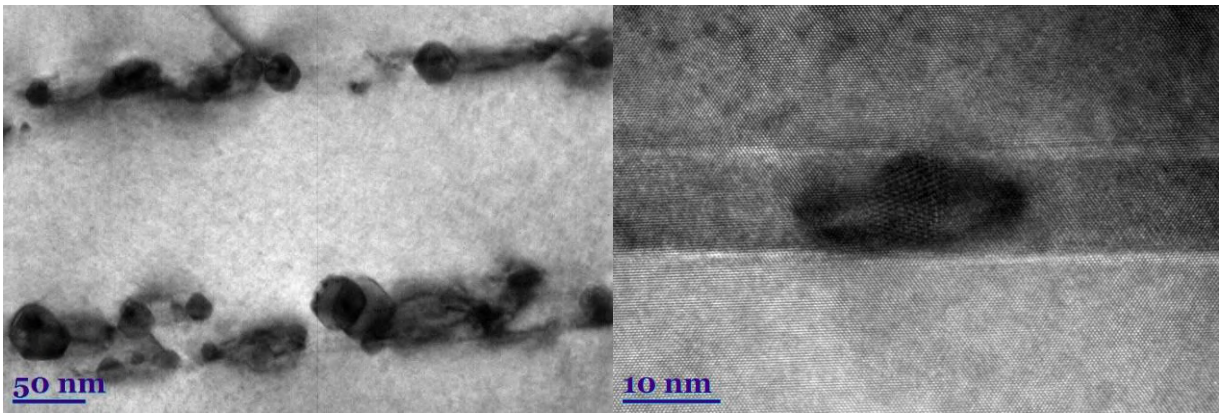


Fig. 1. HR-TEM pictures of randomly oriented and uncontrolled in sized Bi QDs (on the left) vs disc shaped Bi QDs squeezed between blocking AlAs barriers (on the right).

[1] Francoeur, S. et al. (2003). *Band gap of GaAs1−xBix*, Appl. Phys. Lett. 82, 3874.
[2] Ludewig, P. et al. (2013). *Electrical injection Ga(AsBi)/(AlGa)As single quantum well laser*. Applied Physics Letters, 102(24), 242115.
[3] Liu, J. et al. (2017). *Electrically injected GaAsBi/GaAs single quantum well laser diodes*. AIP Advances, 7(11), 115006.

THE COPPER INFLUENCE ON ZnO STRUCTURAL AND OPTICAL PROPERTIES

Ewelina Nowak[1], Alicja Stachowiak[2], Daria Piechowiak[3], Jan Raczyński[2], Edyta Chłopocka[1]

[1] Institute of Materials Research and Quantum Enginering, Faculty of Material Engineering and Technical Physics, Poznań University of Technology, Poznań, Poland
[2] Institute of Physics, Faculty of Material Engineering and Technical Physics, Poznań University of Technology, Poznań, Poland
[3] Institute of Material Engineering, Faculty of Material Engineering and Technical Physics, Poznań University of Technology, Poznań, Poland
ewelina.nowak@put.poznan.pl

ZnO is one of the most exhaustive investigated materials nowadays. This is because the material exhibits a wide energy gap (3.4 eV), piezoelectric properties, and large exciton binding energy at 60 meV. Thus, the semiconductor finds its usage in optoelectronics, gas sensors, or as a TCO film [1].

One of the essential features of ZnO is the possibility of tuning its electrical properties by controllable doping. In the case of controlling ZnO properties, one of the most considerable is group-Ib elements [2]. According to a similar shell structure, copper (Cu) is one of the most elemental impurities used in ZnO. When Cu atoms dope ZnO, Zn^{2+} ions are substituted by Cu^{1+} ions in the ZnO lattice. Considering the nearness of Cu+ and Zn2+ ion radii, the substitution of Cu^{2+} ions for Zn^{2+} ions must not result in a substantial change in the parameters of the ZnO lattice [3]. Hall coefficient measurements show that Cu doping at room temperature reduces the number of carriers since some of the n-type ZnO electrons occupy empty lower energy 3d Cu states leading to Cu^{1+} ions [4]. Cu-doped ZnO can improve ZnO's electrical, magnetic, and photocatalytic characteristics and gas sensing [5]. When used as a dopant, Cu has been known to cause ZnO emission in the light-blue range. Cu doping can change the conductivity because there is a visible luminescence connected to Cu [6]. It was shown that the maximum absorption shifts towards longer wavelengths with increasing copper content. Several studies into the photoluminescence (PL) properties of Cu-doped ZnO have been reported, but few have investigated PL centered between 2.4 and 2.5 eV (green range) [7, 8]. The Cu-doped ZnO exhibits half-metallic ferromagnetism [8].

This work's primary purpose is to investigate the copper doping effect on the properties of ZnO–layers fabricated with a sol-gel method. The main goal is to estimate the changing spectral and structural properties of Cu-doped ZnO layers and ZnO: Cu alloys and verify the quality of films synthesized with an easy and economical method. One of the main goals is to estimate the influence of Cu on ZnO native defects with the investigation of LVM in Raman spectroscopy. In addition, the copper impact on electrical properties was investigated with van der Pauw's Hall Measurements.

[1] Borysiewicz, M.A. ZnO as a functional material, a review. Crystals 2019
[2] Nowak, E.; Szybowicz, M.; Stachowiak, A.; Koczorowski, W.; Schulz, D.; Paprocki, K.; Fabisiak, K.; Los, S. A comprehensive study of structural and optical properties of ZnO bulk crystals and polycrystalline films grown by sol-gel method. Applied Physics A: Materials Science and Processing 2020, 126, 1–12
[3] Banu Bahşi Z. , Oral A.Y., Optical Materials 29, 2007, 672
[4] Sokovnin S. Y., Il'Ves V. G., Medvedev A.I, and Murzakaev A.M., Inorganic Materials: Applied Research 4, 2012, 410
[5] Torchynska, T. V., El Filali, B., Ballardo Rodríguez, I. C., & Shcherbyna, L. (2016). Defect related emission of ZnO and ZnO Cu nanocrystals prepared by electrochemical method. Physica Status Solidi (C) Current Topics in Solid State Physics, 13(7–9), 594–597
[6] Hausmann, B. Schallenberger, and R. Roll, Zeitschrift Für Physik B Condensed Matter 40, 1 (1980).
[7] Allabergenov, S.-H. Chung, S. M. Jeong, S. Kim, and B. Choi, Optical Materials Express 3, 1733 (2013).
[8] A. Janotti, C.G. Van De Walle, Native point defects in ZnO, 2007, 1–22
[9] Ye, L. H., Freeman, A. J., & Delley, B. (2006). Half-metallic ferromagnetism in Cu-doped ZnO: Density functional calculations. *Physical Review B - Condensed Matter and Materials Physics*, *73*(3), 73–76

TAMM PLASMONS AND CAVITY MODES FOR BIOSENSING APPLICATION IN A COMBINED SPECTROSCOPIC ELLIPSOMETRY AND QUARTZ CRYSTAL MICROBALANCE METHOD

Ernesta Bužavaitė-Vertelienė[1], Ieva Plikusienė[1,2], Vincentas Mačiulis[1], Audrius Valavičius[1], Almira Ramanavičienė[1,2] and Zigmas Balevičius[1]

[1] State Research Institute Center for Physical Sciences and Technology, Lithuania
[2] NanoTechnas – Center of Nanotechnology and Materials Science, Faculty of Chemistry and Geosciences, Vilnius University, Lithuania
ernesta.verteliene@ftmc.lt

In recent years, interest in combination of different sensing methods has emerged [1,2]. Being able to perform different measuring techniques at the same time on one platform allows to gain more information on the investigated object. One of such measuring techniques that merges two methods is the combination of spectroscopic ellipsometry (SE) and quartz crystal microbalance (QCM-D). Both methods are widely used for studies of thin films, thus the combination of the two allows to evaluate parameters of the investigated layers simultaneously.

Thin gold layers are widely employed in planar nanophotonic devices and plasmon based optical sensors. One of such sensing applications uses the surface plasmon polaritons (SPP). In order to generate the SPP, a prism coupler is usually used in order to achieve the total internal reflection (TIR) condition required for the excitation of such surface waves, which are p-polarized. Due to the high sensitivity of the SPPs they are widely used in biosensing applications by using the surface plasmon resonance (SPR) method. The sensitivity of the SPP can be enhanced by employing total internal reflection ellipsometry (TIRE) method [3] allowing the measurement of the phase difference between p- and s-polarization components, giving much higher sensitivity compared to the commercial SPR optical biosensors that measure only the p- intensity. However, the advantages given by SPP in TIR configuration cannot be employed for the combined SE and QCM-D method as it is not possible to use a prism as a coupler. One of the solutions that could be employed is the use of Tamm plasmon polaritons (TPP). The TPP is an optical state similar to the electron states proposed by I. Tamm [4]. TPPs that can be generated at the boundary of a 1D photonic crystal (PC) and a thin metal layer. The TPP is an optical state occurring in the photonic band gap (PBG) of a 1D PC. Due to the in-plane wave vector ($\boldsymbol{k_{TPP}}$) that is smaller than the wave vector of light in vacuum ($\boldsymbol{k}$), the TPPs can be excited directly without a coupler in contrast to the case of SPP. This advantage of the excitation configuration of the TPPs shows potential for their application to the combined SE and QCM-D method.

In this research, a plasmonic-nanophotonic structure supporting TPP and cavity (CM) modes that was obtained by modifying a commercial QCM-D sensor chip was used. A 1D PC consisting of 10 TiO_2/SiO_2 (60 nm/110 nm) bilayers was grown on top of a 200 nm thick gold layer of the QCM-D sensor chip. Further, a 40 nm gold layer was sputtered on top of the PC. The modified sensor chip was then inserted in a chamber designed for combined SE/QCM-D measurements in liquids. In order to determine the sensitivity of the TPP and CM modes, the chamber was filled with H_2O and ethanol. The experimental results of the commercial QCM-D and the modified QCM-D sensor chips were compared. The obtained sensitivity of ellipsometric parameters (Ψ and Δ) to the refractive index unit (RIU) were Ψ_{TPP}=126.78 RIU^{-1}, Δ_{TPP}=325 RIU^{-1} for the TPP and Ψ_{CM}=264 RIU^{-1}, Δ_{CM}=645 RIU^{-1} for the CM exhibiting 23 and 49 times higher sensitivity for refractive index, respectively, for TPP and CM when compared to the standard QCM-D sensor chip. Furthermore, modified QCM-D sensorchip was employed for optical biosensing. The results showed higher sensitivity for the TPP mode than for the CM. This can be explained by the origin of both modes as the TPP excitation is generated near the surface where proteins attach, while the cavity mode is generated in the cavity between the two gold surfaces.

[1] S. Patskovsky, V. Latendresse, A.-M. Dallaire, L. Doré-Mathieu, and M. Meunier, "Combined surface plasmon resonance and impedance spectroscopy systems for biosensing," Analyst **139**(3), 596–602 (2014).
[2] X. Kang, G. Cheng, and S. Dong, "A novel electrochemical SPR biosensor," Electrochemistry Communications **3**(9), 489–493 (2001).
[3] H. Arwin, "TIRE and SPR-Enhanced SE for Adsorption Processes," in *Ellipsometry of Functional Organic Surfaces and Films*, K. Hinrichs and K.-J. Eichhorn, eds. (Springer Berlin Heidelberg, 2014), **52**, pp. 249–264.
[4] I. Tamm, "Über eine mögliche Art der Elektronenbindung an Kristalloberflächen," Z. Physik **76**(11–12), 849–850 (1932).

NUMERICAL SIMULATIONS AND EXPERIMENTAL ANALYSIS OF SCANNING TECHNIQUES FOR LOW-ROUGHNESS SURFACES USING UV FEMTOSECOND PULSES

Evaldas Kažukauskas[1], Simas Butkus[1,2], Vytautas Jukna[1], Domas Paipulas[1] and Valdas Sirutkaitis[1]

[1] Laser Research Center, Faculty of Physics, Vilnius University, Saulėtekio Ave. 10, LT-10223 Vilnius, Lithuania
[2] Light Conversion, Keramikų 2b, LT-10233 Vilnius, Lithuania
evaldas.kazukauskas@ff.vu.lt

Surface roughness is an important parameter that has a great influence on various material properties. It determines the rate of corrosion, wettability, biocompatibility, as well as optical properties of different materials [1-3]. Low roughness (< 100 nm Ra) surfaces are difficult to achieve through an ablation-based process even with fs pulses, therefore investigation of the theoretical intricacies is of major interest when engraving transparent materials.

In our study we present an in-depth investigation of the scanning techniques and how they influence the final surface roughness. We numerically investigate the evolution of the surface roughness when it is scanned with UV femtosecond pulses multiple times (multiple layers) and compare the numerical results to the experimentally acquired values. We found that in the case of a single scan the dominant surface roughness determining factor is the overlap of modifications. We observed that parameters such as modification overlap, laser-scanner synchronization and initial beam profile strongly influence the resulting surface roughness in a non-linear manner. In the case of a multi-scanned surface we have determined that the resulting surface roughness can be minimized by introducing rotation of every following layer at a certain angle with respect to the previous one. The angle for minimized surface roughness highly depended on system configuration. The investigated theoretical model is in good relation to the experimentally acquired results and provides valuable information when optimizing the process for minimal-roughness micromachining when performing deep engraving of transparent materials.

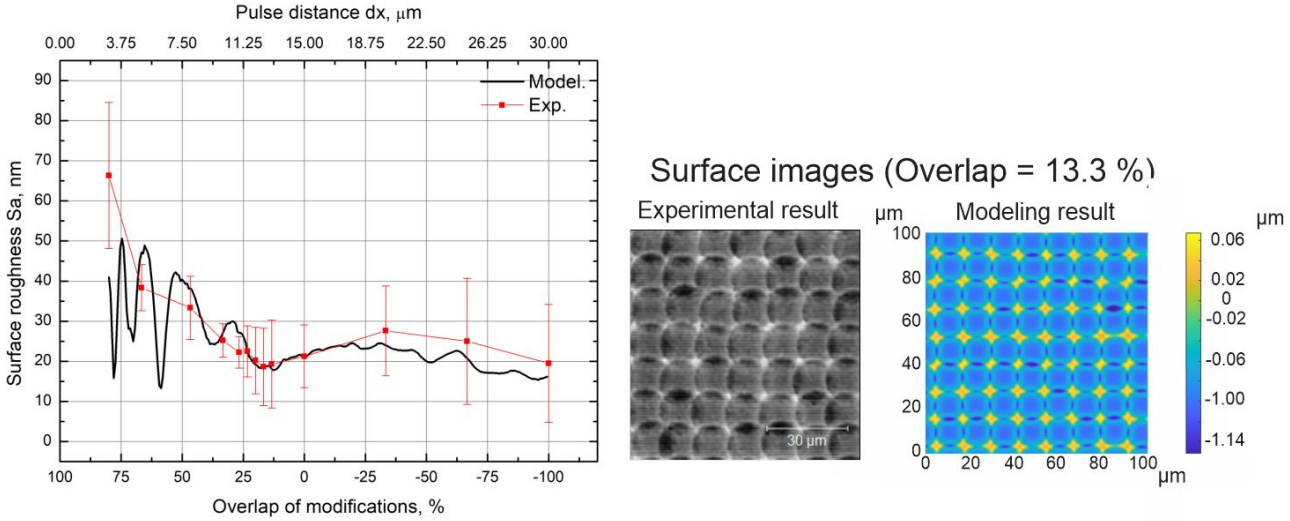


Fig. 1. Surface roughness dependence on the overlap of modifications after a single scan using UV femtosecond pulses (on the left). Surface images after laser micromachining (when modification overlap is 13.3 µm) achieved experimentally and via numerical modelling (on the right).

[1] D. Bergstrom, The Absorption of Laser Light by Rough Metal Surfaces, Material Science, (2008).
[2] A. S. Toloei, V. Stoilov, D. Northwood, The Relationship Between Surface Roughness and Corrosion, ASME 2013 International Mechanical Engineering Congress and Exposition, Proceedings (IMECE), vol. 2B, (2013).
[3] M. H. Hatamleh, X. Wu, A. Alnazzawi et al., Surface characteristics and biocompatibility of cranioplasty titanium implants following different surface treatments, Dent. Mater. **34**, 676-683 (2018).

FEMTOSECOND LASER-INDUCED PERIODIC SURFACE STRUCTURES ON FUSED SILICA WITH TUNABLE-WAVELENGTH PULSES

Marius Navickas[1], Robertas Grigutis[1], Gintaras Tamošauskas[1], Vytautas Jukna[1], Audrius Dubietis[1]

[1]Laser Research Center, Vilnius University, Saulėtekio av. 10, LT-10223, Vilnius, Lithuania
marius.navickas@ff.vu.lt

Irradiation of inorganic materials: dielectrics, semiconductors and metals with multiple femtosecond laser pulses at high repetition rate induces structural modifications resulting in formation of self-organized laser-induced periodic surface structures (LIPSS) [1]. According to the periodicity Λ and morphology, LIPSS are classified into three types: low-spatial frequency (LSFL) with $\Lambda = \lambda/n_0$ [2] (n_0 is a refractive index of material), high-spatial frequency (HSFL) with $\Lambda = \lambda/2n_0$ [3] and wavelength-independent periodic annular surface structures (LIPASS) [4]. Many studies of LIPSS predict the dependence of its surface spatial characteristics on various experimental parameters such as number of pulses and irradiation wavelength, in particular. The latter experiments were performed mostly by using fundamental wavelengths of standard lasers and its harmonics, so its not enough to fully establish the LIPSS properties in the short-wave infrared range. Therefore there are still unanswered questions how the periodicity and morphology changes within this spectral range under irradiation of multiple femtosecond pulses. In this work we present the experimental study of LIPSS morphology and its periodicity evolution at high repetition rate with broadly tunable (in the $1-3$ μm range) femtosecond laser pulses.

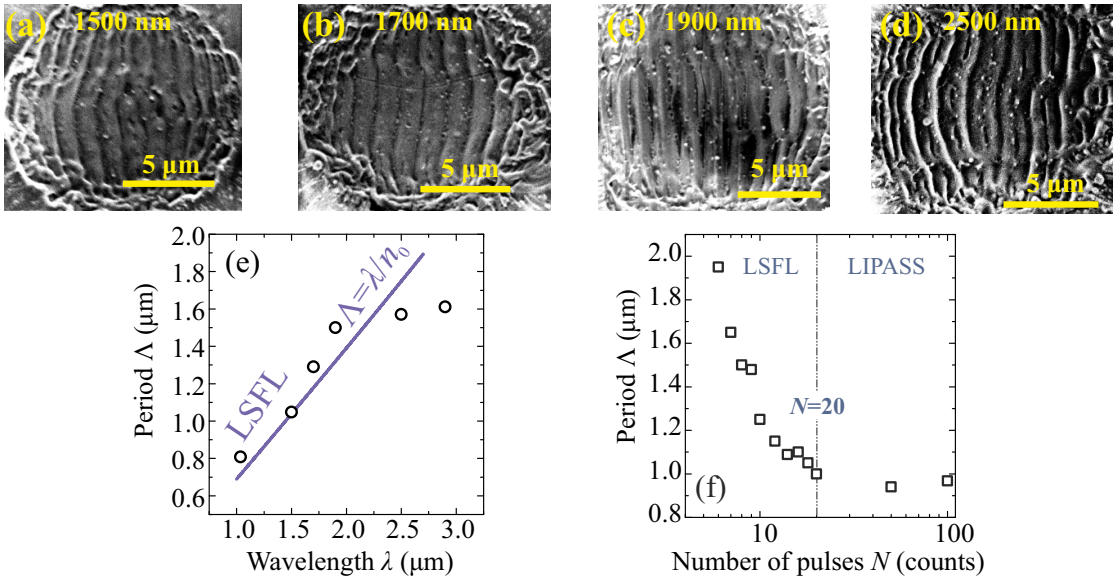


Fig. 1. SEM images of LSFL in fused silica, produced with (a) 1500 nm, (b) 1700 nm, (c) 1900 nm and (d) 2500 nm wavelength pulses. (e) and (f) represent their period dependence on wavelength and number of pulses, respectively.

The experiments were performed using a commercial optical parametric amplifier (Orpheus, Light Conversion Ltd), pumped by Yb:KGW laser pulses, where the pulse duration and repetition rate were 180 fs and 10 kHz, respectively. The main results are summarized in Fig. 1. Fig. 1. (a)–(d) represent SEM images of LSFL in fused silica, produced with different irradiation wavelengths pulses and Fig. 1. (e)–(f) show LSFL period evolution with increasing inscription wavelength and number of pulses. Experimental results revealed an increase of LSFL period with increasing the inscription laser wavelength (Fig. 1 (e)), which was also obtained previously for HSFL [5]. In this way, the results indicates the same dependence of period on wavelength for both structures despite different formation mechanisms. In addition, the period values, retrieved from 2D Fourier transform, are very close to λ/n_0, therefore the modifications can be assigned to LSFL. Interestingly, we observed that short exposure to laser pulses at 1900 nm (Fig. 1. (f)) results in a significant decrease of the period. Such a result is reliable due to decrease of radiation peak fluence caused by surface ablation and formation of a crater. After 20 laser pulses, there are no significant changes of LIPSS period due to LIPASS formation, whose periodicity is not sensitive for ablation effect.

[1] J. Bonse, J. Krüger, S. Höhm et. al., Femtosecond laser-induced periodic surface structures, Journal of laser applications **24**, 042006 (2012).
[2] J.-Wu Yao, C.-Yun Zhang, H.-Ying Liu et. al., High spatial frequency periodic structures induced on metal surface by femtosecond laser pulses, Optics express **20**, 905–911 (2012).
[3] Z. Fang, J. Shao, Femtosecond laser-induced periodic surface structure on fused silica surface, Optik **127**, 1171–1175 (2016).
[4] Y. Liu, Y. Brelet, Z. He, L. Yu et. al., Laser-induced periodic annular surface structures on fused silica surface, Applied physics letters **102**, 251103 (2013).
[5] S. Richter, M. Heinrich, S. Döring et. al., Nanogratings in fused silica: formation, control and applications, Journal of laser applications **24**, 042008 (2012).

NUMERICALLY PROCESSED INTERFEROMETRIC NONLINEAR REFRACTIVE INDEX MEASUREMENTS IN THE SPECTRAL RANGE FROM 1μm TO 3μm

Gaudenis Jansonas[1], Rimantas Budriūnas[1,2], Arūnas Varanavičius[1]

[1] Laser Research Center, Vilnius University, Lithuania
[2] Light Conversion, Vilnius, Lithuania
gaudenisjansonas@yahoo.com

Nonlinear refractive index (n_2) describes how the refractive index of a medium depends on the intensity of light. This parameter is responsible for many phenomena of nonlinear optics and in modeling such phenomena it is important to know the most precise value of n_2. Popular methods for measuring n_2, like Z-scan [1], are based on the assumption that the temporal and spatial intensity distributions of the laser radiation are in the form of a Gaussian function. In practice this is sometimes difficult to fulfill, especially in the mid-infrared (MIR) wavelength range between 2µm and 20µm, where there is a shortage of information about n_2. Therefore, n_2 measurements, with included real spatial and temporal intensity distributions, are of great importance.

In this work we chose to measure n_2 by using a Mach-Zehnder type interferometer to detect a total on-axis nonlinear phase shift B acquired in a sample and including measured spatial and temporal intensity distributions by numerically simulating the experiment. A simplified optical scheme of the measurement is shown in Fig. 1. For infrared light generation we used a label-free optical parametric amplifier (OPA), pumped by a femtosecond Yb:KGW laser (Pharos, Light Conversion). From the interference pattern we obtain a surface of spatial phase difference between two interfering waves (using Fourier transform method (FTM) [2]). To avoid the effects of linear wave front distortion and tilted pulse fronts we obtain a change of B (ΔB) from a change of two phase surfaces, corresponding to a different pulse energy. Here ΔB was found by fitting spatial intensity distribution (which can be in the form of any numerical function) of a beam at the sample to a phase difference surface.

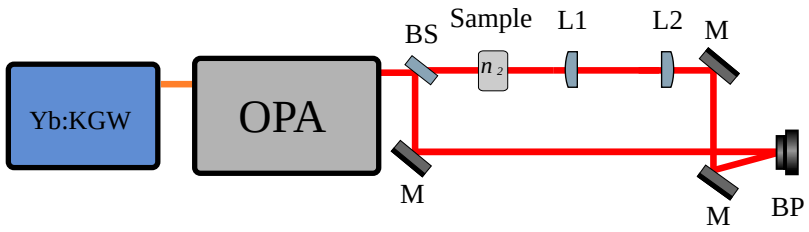


Fig. 1. Simplified optical scheme of a measurement. Here L1, L2 – converging lenses, denoting an imaging system, M – mirror, BP – beam profiler.

We measured the effective n_2 of some popular IR materials at different wavelengths λ and often using different polarization modes. The values of ΔB were measured at different pulse energy changes ΔE. Obtained ΔB values were corrected according to the measured pulse shape and the n_2 was found from linearly fitted experimental data with a intercept value fixed at zero. Final results, along with a full list of measured materials, are presented in table 1.

Table 1. Results. All n_2 values are in 10^{-14}cm^2/W$\pm$ ~17%, S – sample, o – ordinary wave, e – extraordinary wave.

S/λ, μm	GaSe	AGS(o)	AGS(e)	ZGP(o)	ZGP(e)	BGSe	SBN-61	KTA(o)	KTA(e)	LGS(o)	LGS(e)	Si	GaAs	ZnS	ZnTe	ZnSe	KRS-5	KRS-6	UVFS
1.03	-	-	-	-	-	-	0.69	0.21	0.19	0.52	0.47	-	-	0.78	-	2.59	-	-	0.025
2.2	2.14	1.95	2.29	5.99	7.1	1.96	0.87	0.22	0.13	-	0.57	7	-	0.74	3.01	1.59	2.6	1.21	-
3.2	0.73	1.99	1.37	4.4	1.02	0.95	0.56	0.22	0.22	0.56	0.48	4.54	8.56	0.6	1.32	1.22	2.14	1.2	-

In conclusion, we measured effective nonlinear refractive index of some popular infrared materials in the spectral range from 1μm to 3μm with included real temporal and spatial intensity distributions.

[1] M. Sheik-bahae, A. A. Said, and E. W. Van Stryland, "High-sensitivity, single-beam n2 measurements," Opt. Lett. **14**, 955-957 (1989).
[2] Mitsuo Takeda, Hideki Ina, and Seiji Kobayashi, "Fourier-transform method of fringe-pattern analysis for computer-based topography and interferometry," J. Opt. Soc. Am. **72**, 156-160 (1982).

THE IMPACT OF ELECTRON-DONATING/-WITHDRAWING GROUPS ON RED-FLUORESCENT BODIPY MOLECULAR ROTOR

Karolina Maleckaitė[1], Domantas Narkevičius[2], Rugilė Žilėnaitė[2], Jelena Dodonova-Vaitkūnienė[2], Stepas Toliautas[3], Sigitas Tumkevičius[2], Aurimas Vyšniauskas[1]

[1] Center of Physical Sciences and Technology, Saulėtekio av. 3, Vilnius, LT-10257, Lithuania.
[2] Institute of Chemistry, Faculty of Chemistry and Geosciences, Vilnius University, Naugarduko str. 24, Vilnius, LT-03225, Lithuania
[3] Institute of Chemical Physics, Faculty of Physics, Vilnius University, Saulėtekio av. 9-III, Vilnius, LT-10222 Lithuania
karolina.maleckaite@ftmc.lt

Fluorescent molecular probes are very useful for studying live cells and various organelles because they can indicate changes in environmental properties [1]. One of these properties—microviscosity—can be detected with viscosity–sensitive fluorophores called 'molecular rotors'. The mechanism of these derivatives is based on the competition between intramolecular rotation and fluorescence, which can be registered by time-resolved fluorescence spectroscopy. Molecular rotation alters the electronically excited state and causes a faster non-radiative relaxation, which consequently determines a longer fluorescence lifetime in a highly viscous medium [2].

Many microviscosity probes are based on dipyrromethene boron difluoride, commonly known as BODIPY. One of such molecular rotors is BODIPY-C_{10}, an excellent lifetime-based microviscosity sensor exceptional for data-simplifying monoexponential fluorescence decay. However, green absorbance and fluorescence spectra make BODIPY-C_{10} imperfect to use for microviscosity imaging in biological samples where light scattering is an issue. The extension of molecular conjugation length is a simple solution to red–shift absorbance and emission spectra. It should also be considered that a single BODIPY conjugate can be sensitive to all three environmental parameters: microviscosity, temperature and polarity. Recently, we investigated BODIPYs with extended molecular conjugation [3] and decided to explore how the sensory properties of these derivatives can be tuned by introducing different moieties.

To find out how electron-donating/withdrawing groups (EDG/EWG) can affect molecular rotor's properties of sensing viscosity, temperature and polarity, we compare the most popular green-fluorescent BODIPY-C_{10} and four *β*–phenyl–substituted BODIPYs (Fig. 1A): BP-PH as a red-emitting reference, methyl-substituted BP-PH-8M with suppressed rotation, as well as trifluoromethyl-substituted BP-PH-CF_3 and methoxy-substituted BP-PH-OMe to evaluate the effects of EWG and EDG, respectively. All *β*–phenyl–substituted conjugates, except BP-PH-8M, have an increased conjugation of the molecule, which helps to achieve the red spectral region required for the biological samples.

In this work [4], we present investigation of quantum chemical calculations, absorbance and fluorescence spectra, time-resolved fluorescence measurements and sensitivity to viscosity, temperature and polarity. DFT calculations showed that BP-PH-8M has the highest activation energy barrier (almost 0.3 eV) because the methyl groups prevent molecular rotation. In contrast, the other conjugates have twice as low barrier, resulting in faster non-radiative relaxation. Steady-state fluorescence measurements revealed that EWG blue-shifts the fluorescence spectrum, while EDG shifts it to the longer wavelengths (Fig. 1B). Finally, fluorescence decay kinetics demonstrated that BP-PH-CF_3 is a moderate temperature sensor, while BP-PH-OMe could be used as a lifetime–based polarity probe (Fig. 1C).

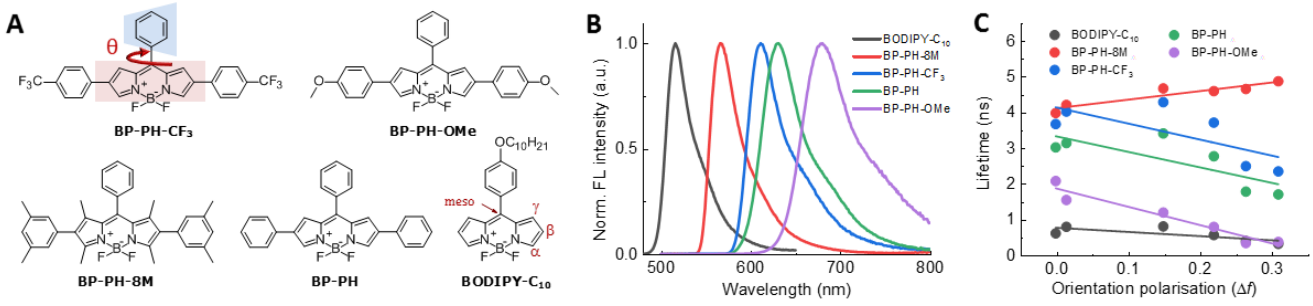


Fig. 1. (A) The structures of the molecular rotors used in this work, and the rotor mechanism showed on BP-PH-CF_3. Fluorescence spectra (B) and polarity-dependent fluorescence lifetimes (C) of BODIPY-C_{10} (grey), BP-PH-8M (red), BP-PH-CF_3 (blue), BP-PH (green) and BP-PH-OMe (purple).

[1] P. Sarder, D. Maji, and S. Achilefu, "Molecular probes for fluorescence lifetime imaging," Bioconjug. Chem., vol. 26, no. 6, pp. 963–974, 2015.
[2] M. K. Kuimova, "Mapping viscosity in cells using molecular rotors," Phys. Chem. Chem. Phys., vol. 14, no. 37, pp. 12671–12686, 2012.
[3] K. Maleckaitė et al., "Designing a red-emitting viscosity-sensitive BODIPY fluorophore for intracellular viscosity imaging," Chem. Eur. J., vol. 27, no. 67, pp. 16768–16775, 2021.
[4] K. Maleckaitė et al., "Give or take: Effects of electron-accepting/-withdrawing groups in red-fluorescent BODIPY molecular rotors," Molecules, vol. 27, no. 1, art. no. 23, 2021.

OPTICAL PROPERTIES IVESTIGATION OF $K_2Gd(PO_4)(WO_4)$:10% Yb^{3+} 20% Tb^{3+}, xEu^{3+} AS A FUNCTION OF Eu^{3+}

Julija Grigorjevaite[1], Arturas Katelnikovas[1]

[1] Institute of Chemistry, Department of Chemistry and Geosciences, Vilnius University, Lithuania
julija.grigorjevaite@chf.vu.lt

One of the most serious worldwide problems is counterfeiting of currency, goods, and important documents. These mentioned counterfeits are a huge problem for everyone, including government bodies or big companies. The modern achievements in science and technology create new ways to overcome this serious problem. One of the way to prevent counterfeiting is downconversion and upconversion security pigments, where inorganic luminescence materials are used as security markers and security labels. All of anti-counterfeiting techniques have their advantages and limitations. From this point of view, inorganic luminescent materials doped with rare earth elements improve the security pigments industry due to their unique optical properties.

In this research we represent new inorganic $K_2Gd(PO_4)(WO_4)$ matrix doped with three elements – Yb, Tb and Eu. These materials show unique emission spectra when samples were excited with 340 nm and 980 nm (laser) wavelength. Due to the energy transfer from Tb^{3+} to Eu^{3+} the most intense emission lines are observed in red spectral region (590 – 720 nm).

In order to investigate upconversion luminescence Gd^{3+} ions are replaced by 10% Yb^{3+} ions. The Yb^{3+} absorbs 980 nm laser radiation, transfers the energy to Tb^{3+}, which, in turn, transfer the energy to Eu^{3+}. As it was expected the intensity of the most intense Eu^{3+} $^5D_0 \rightarrow {}^7F_2$ transition at 614 nm increase with increasing Eu^{3+} concentration.

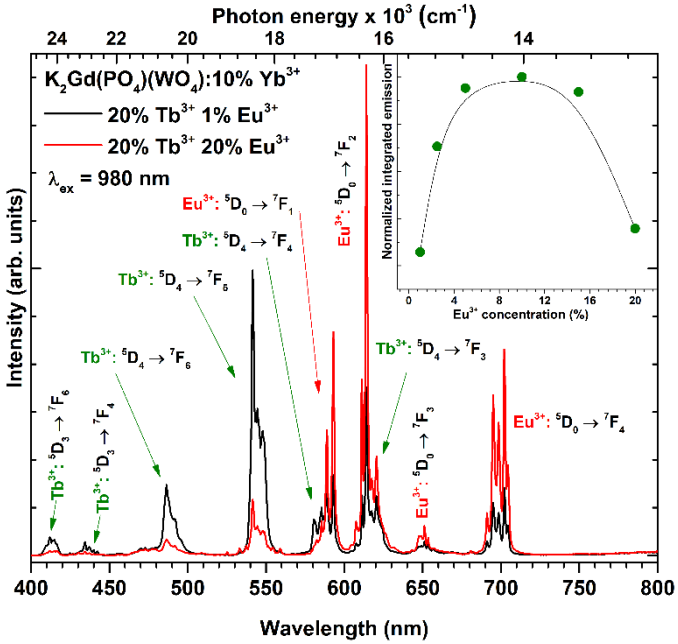


Fig. 1. Upconversion emission spectra of $K_2Gd(PO_4)(WO_4)$:10% Yb^{3+} doped with 20% Tb^{3+} and different Eu^{3+} concentrations under 980 nm excitation. The inset shows normalized integrated upconversion emission intensity as a function of Eu^{3+} concentration.

The upconversion emission spectra of the $K_2Gd(PO_4)(WO_4)$:20% Yb^{3+} doped with 1% and 20% Eu^{3+} were measured and depicted in Figure 1. The inset of the graph shows normalized integrated emission intensity of all synthesized samples as a function of Eu^{3+}. The normalized integrated emission intensity of the samples increases if samples are doped with up to 10% of Eu^{3+}. Increasing Eu^{3+} content further leads to decreasing of the intensity what could be attributed to energy transfer between Eu^{3+} and Tb^{3+} ions. The upconversion PL spectra for both phosphors doped with 1% and 20% of Eu^{3+} show typical emission lines which could be attributed to Tb^{3+} and Eu^{3+}.

Characterization and investigation of the optical properties of the synthesized compounds will be discussed during the presentation.

This research was funded by grant (No. D-2018-0703 “Controlling the up-conversion emission by tuning band gap of the host matrix”) from the Research Council of Lithuania.

[1] Bayart, A., Szczepanski, F., Blach, J. F., Rousseau, J., Katelnikovas, A., Saitzek, S., Upconversion luminescence properties and thermal quenching mechanisms in the layered perovskite $La_{1.9}Er_{0.1}Ti_2O_7$ toward an application as optical temperature sensor, Journal Alloys and Compounds, 744, 2018, 516-527.

CONTROL OF THE EUROPIUM OXIDATION STATES IN THE GLASS MATRIX AND ITS INFLUENCE ON THE PHOTOLUMINESCENCE SPECTRA

Agata Jarocka[1], Paweł Dębowski[1], Bartosz Fetliński[2], Tomasz Karol Pietrzak[1], Marek Wasiucionek[1]

[1] Faculty of Physics, Warsaw University of Technology, Warsaw, Poland
[2] The Institute of Microelectronics and Optoelectronics, Warsaw University of Technology, Warsaw, Poland
agata.jarocka.dokt@pw.edu.pl

It is well known that the photoluminescence (PL) of lanthanides centers in inorganic matrices depends on their oxidation states. Therefore, it is desirable to control that factor at the stage of synthesis of the PL materials which can be promising phosphors in many applications. The experience of our group with controlling the oxidation states of transition metals present in prospective glassy and nanostructured cathode materials for Li-ion and Na-ion [1], has helped us to use similar methods to take control of the oxidation states of lanthanides centers embedded in transparent glassy matrices. Lanthanides are widely used in today's technology and this is due to a large variety of their *4f* configurations of electrons in Ln atoms, which leads to a wide range of fluorescent states and wavelengths [2, 3].

Our recent work [4] proved that it is possible to synthesize Eu-doped glassy materials whose photoluminescence spectra can be tuned depending on synthesis conditions by using melt-quenching process. During that work, we found out that one can control the relative Eu^{3+}/Eu^{2+} ions concentrations. However, further studies are needed to improve this method of europium ion reduction and to specify the exact influence of melting time and temperature on the final properties of the samples.

In order to do that, a series of glassy matrices (10 samples in total) with nominal composition $Na_3Al_2(PO_4)_2F_3$ doped with 1 wt% of Eu_2O_3 were successfully synthesized by a melt-quenching process, using a double crucible method [5] – 9 samples, and 1 sample without reducing atmosphere. Samples synthesis condition differed, temperature was controlled in the range of 1000 °C, 1100 °C and 1200 °C and time was set as 5 min, 10 min or 15 min. Obtained glasses were carefully investigated using X-ray diffractometry (XRD), photoluminescence spectroscopy (PL) – Fig. 1, photoluminescence excitation (PLE) and absorption spectroscopy.

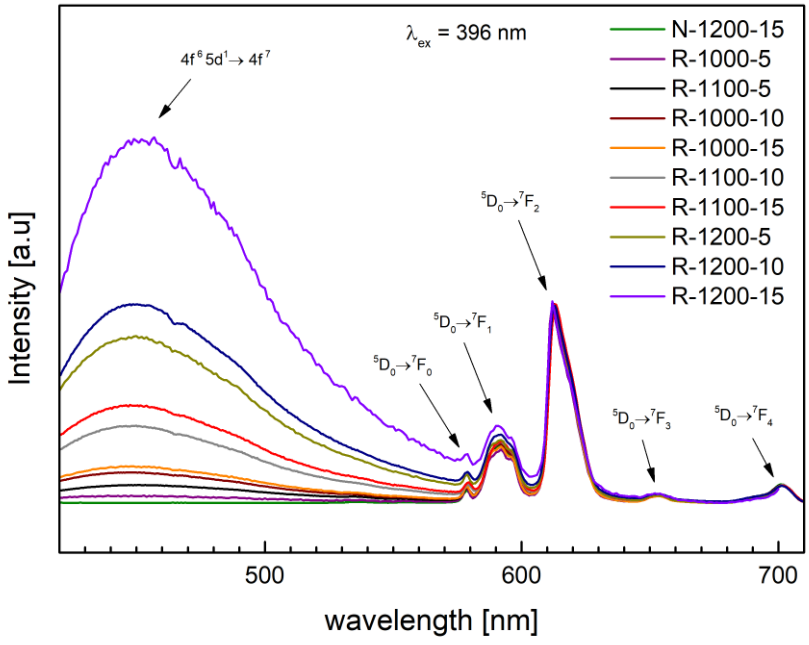


Fig. 1. Photoluminescence spectra for obtained samples.

[1] T.K. Pietrzak *et al.*, Materials Science and Engineering B 213 (2016) 140-147.
[2] M. C. Gonçalves *et al.*, Comptes Rendus Chimie, 5 (2002) 845–854.
[3] B. M. Walsh: *Advances in Spectroscopy for Lasers and Sensing. Judd-ofelt theory: principles and practices.* [red.] Baldassare Di Bartolo, Ottavio Forte. Erice Italy, Springer, 2005
[4] T.K. Pietrzak, A. Gołębiewska et al., Journal of Luminescence 208 (2019) 322–326.
[5] K. Hirose *et al.*, Solid State Ionics, 178 (2007) 801–807.

RESULTS ON ABLATION OF WIDE BAND-GAP MATERIALS WITH FEMTOSECOND UV LASER PULSES AT LINEAR ABSORPTION REGIME

Dominyka Stonytė[1], Vytautas Jukna[1], Domas Paipulas[1]

Laser Research Center, Faculty of Physics, Vilnius University, Saulėtekio av. 10, LT-10223 Vilnius, Lithuania
dominyka.stonyte@ff.vu.lt)

High quality and precision micro fabrication of transparent materials has been quite a challenge in the past. Fortunately, recent advancements in industrial-grade laser systems, delivering ultrashort high-intensity femtosecond pulses has made it possible to process even high bandgap materials. However, typical photon energies from solid-state laser's first or second harmonic are not sufficient to induce linear absorption in almost all transparent materials and therefore only a nonlinear absorption mechanism can excite materials electrons to a conduction band and sustain the ablation process. Yet, the smoothest ablation results with low heat affected zones (HAZ) are expected in the linear absorption regime. That is why UV lasers where the energy of photons is large enough for a linear absorption can lead to better results than using IR or visible spectrum [1]. Currently, most of the research in ablation with UV light is conducted usually with excimer lasers delivering longer nanosecond pulses [2, 3]. It is well known that shorter pulses have characteristic timescales much smaller than the material's atomic vibrations timescale and produce reduced HAZ which causes better ablation precision and quality if compared to longer pulses. For this reason, higher harmonics of solid-state femtosecond lasers could be a better choice if compared to excimer nanosecond lasers.

In this study, we present femtosecond laser (206 nm, 50 kHz, 210 fs) ablation results on Sapphire, BK7 and LiNbO3 crystal. Groove formation experiments were performed with Yb:KGW laser system (PHAROS, Light Conversion) with 5th harmonic generator, Aerotech ANT180 micro-positioning system, and calcium fluoride lenses for beam focusing. The parametrical analysis of ablation outcome versus processing parameters is presented which indicates that UV machining can produce high-quality grooves absent from HAZ without any additional post-processing. We demonstrate, that roughness values in the order of tens of nanometers and sometimes even less than 10 nanometers can be achieved and that is sufficient for fabrication of micro optical components.

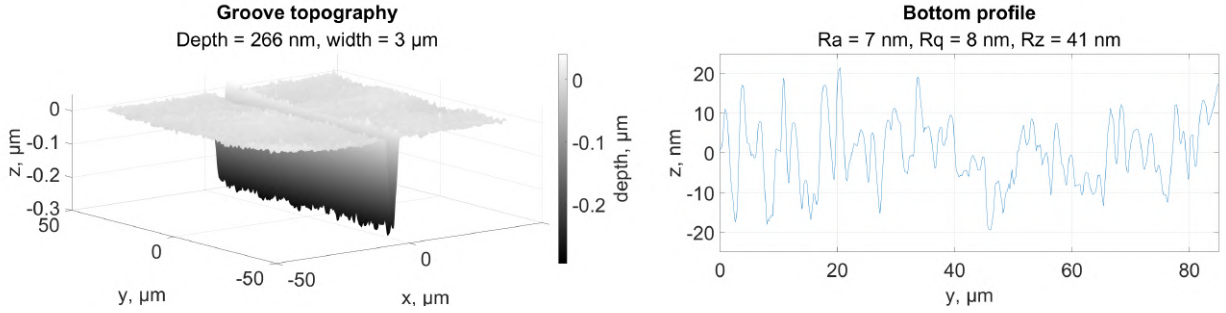


Fig. 1. Groove, fabricated on the surface of Sapphire at the linear absorption regime: a) topography of groove, where depth is calculated using mass center expression, width is calculated at half maximum and b) groove's bottom profile, where Ra is the arithmetical mean height, Rq - root mean square deviation (RMS), Rz - maximum height of profile.

[1] D. M. Karnakis, M. R. H. Knowles, K. T. Alty, M. Schlaf, H. V. Snelling, Comparison of glass processing using high-repetition femtosecond (800 nm) and UV (255 nm) nanosecond pulsed lasers, Proc. SPIE (January 2005)

[2] J. Shin and B. Nan, Groove Formation in Glass Substrate by a UV Nanosecond Laser, Applied Sciences **10(3)**, 987 (2020).

[3] M. E. Shaheen, J. E. Gagnon, B. J. Fryer, Studies on laser ablation of silicon using near IR picosecond and deep UV nanosecond lasers, Opt. Lasers Eng, **119**, 18-25 (2019)

LASER DIRECT WRITING FOR THE FORMATION OF LARGE-SCALE SILVER MICROBUMPS ARRAYS

Rodrigas Liudvinavičius, Evaldas Stankevičius

Department of Laser Technologies, Center for Physical Sciences and Technology, Lithuania
rodrigas.liudvinavičius@ftmc.lt

Many applications of metal nanoparticles are possible due to their interaction with light. Such interaction of the particles can be described as plasmonic effect (plasmonics) which holds huge interest in numerous investigations as the novel optical devices are based on such property, surface plasmon polaritons (SPPs) which are collective charge oscillations coupled to an external electromagnetic field that propagates along metal and a dielectric interface [1]. However, to successfully apply the advantages of it over lithography-based techniques, more investigations have to be done, especially with the material as silver.

In this investigation, SPPs effect is achieved with diffraction phenomena [2], where arranged nanoparticles of metal act as diffractive grating showing plasmonic resonances for incidence light. Here, when a plasmon is excited by a photon, the absence of photon results in a dip in reflected light at that specific angle for incident light. Such use of diffraction grating is based on theory as SPP waves cannot be excited by the incident light on a flat metal surface due to momentum mismatch as a free-space photon has less momentum (wavevector is smaller) than SPP.

During the investigation, periodic arrays of microbumps formation were produced on a thin 50 nm silver layer by laser direct writing technique (LDW) forming silver microbumps by a 1.1 nJ single laser pulse. Formed gratings were analyzed with a scanning electron microscope (SEM) and spectrophotometer.

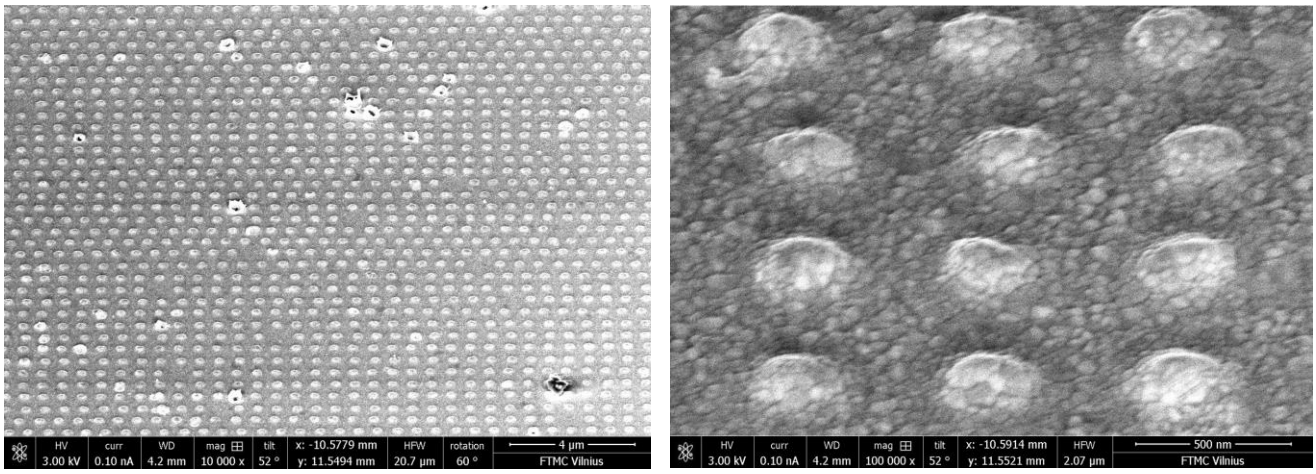


Fig. 1. SEM micrograph of fabricated silver bumps array in a thin silver film (50 nm). Micrographs were taken at a sample tilt angle of 52°. Each microbump was fabricated using a single laser pulse with 1.05 nJ energy.

The results show that SPRs depend on the period of the fabricated arrays, light polarization, incident angle of light, and the sample orientation as the deepest and narrowest peaks were achieved parallelly to the incident light orientated sample and s-polarization. Such experimental results are in good agreement with theoretical estimations. Investigation on periodicity of arrays shows a strong dependency on it as for SPP peaks smaller period of arrays is desired.

The influence of the oxidation effect was also investigated, where after a month, resonance depth decreased almost twice. However, a solution for the oxidation effect was suggested.

[1] S. T. Koev, A. Agrawal, H. J. Lezec, V. A. Aksyuk, An Efficient Large-Area Grating Coupler for Surface Plasmon Polaritons, Plasmonics, 7, 269-277, 2012.
[2] V. G. Kravets, F. Schedin, A. N. Grigorenko, Extremely Narrow Plasmon Resonances Based on Diffraction Coupling of Localized Plasmons in Arrays of Metallic Nanoparticles, Phys. Rev. Lett. 101, 087403, 2008.

PERFORMANCE INVESTIGATION OF OPTICAL PARAMETRIC GENERATOR BASED ON PERIODICALLY POLED LITHIUM NIOBATE CRYSTAL PUMPED BY SUBNANOSECOND MICRO-LASER PULSES

Jonas Banys[1], Ona Balachninaitė[1], Viktorija Tamulienė[1], Vygandas Jarutis[1], Justina Savickytė[1], Simona Armalytė[1], Julius Vengelis[1]

[1]Laser Research Center, Faculty of Physics, Vilnius University, Lithuania
jonas.banys@ff.vu.lt

Optical-parametric light generation is a unique way to obtain continuously tunable laser radiation in a wide spectral region. Relatively inexpensive and compact subnanosecond (100 ps - 1 ns) optical parametric generators (OPG) with broad wavelength tunability are needed for a variety of applications that do not require the high temporal resolution supplied by expensive and sophisticated ultrashort (<10 ps) laser systems, but nanosecond (>1 ns) time resolution is not sufficient. Such applications are spectroscopy, laser-induced fluorescence, detection of chemical materials, nonlinear microscopy and THz generation to name a few [1-3]. Development and the reduced cost of the micro-laser manufacturing technologies permits them to be used as a high energy pump source for subnanosecond OPGs. Such micro-laser pumped subnanosecond OPGs would allow the implementation of low-cost, compact, continuously tunable laser radiation sources suitable for the aforementioned applications, especially in near-infrared (NIR) and visible (VIS) spectral ranges where the demand is high. To date, no subnanosecond OPGs based on short (up to 2 cm in length) periodically poled (PP) crystals have been demonstrated that could also be continuously tunable over a wide spectral range. Extensive and detailed investigation of such OPGs is necessary in order to create a commercially attractive product.

In this paper we investigate optical parametric generator based on periodically poled lithium niobate (PPLN) crystal pumped by subnanosecond pulses from a micro-laser. Pump source was a passively Q-switched Nd:YAG micro-laser that generated 520ps (FWHM) pulses at 1 kHz repetition rate with pulse energy up to 1 mJ. Pump light was focused into a relatively short 2 cm in length PPLN crystal doped with MgO and poled in 8 gratings with periods ranging from 28.9 - 31.75 µm. Continuous tuning of signal wave wavelength in 1440 - 2128 nm spectral range was achieved by varying the grating period and the temperature of PPLN, whereas internal conversion efficiency for the signal wave reached up to ~33% and depended on the grating period (Fig. 1). Experimentally measured spatial, temporal and spectral characteristics of the generated light are presented. Moreover, optical parametric amplification scheme using injection seeding technique is shown and discussed. The experimentally measured data is supplemented by the numerical simulations based on the three-wave interaction in a dispersive medium model. Good agreement with the theoretical results is obtained.

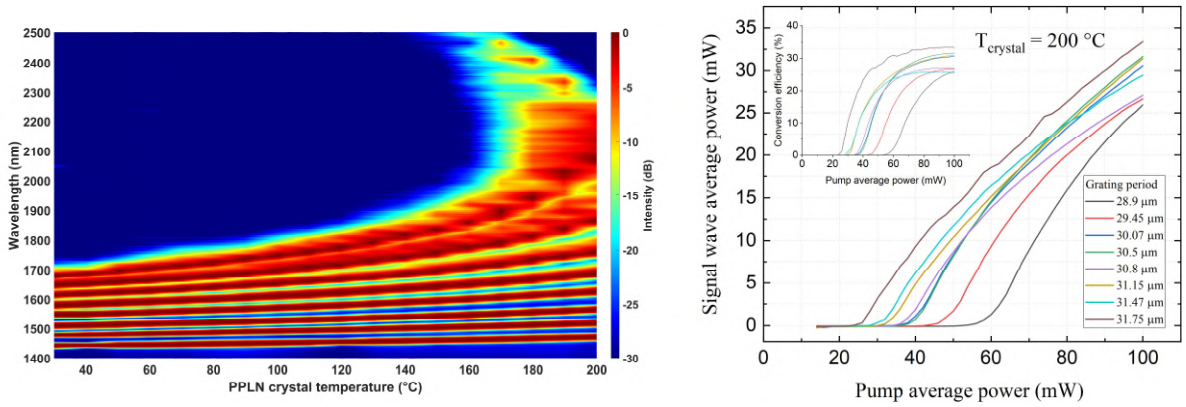


Fig. 1. On the left - signal wave spectral envelope evolution with increasing PPLN temperature for 8 gratings. On the right - signal wave output power and conversion efficiency dependance on pump power.

This work has received funding from European Regional Development Fund (project No. 01.2.2-LMT-K-718-03-0004) under grant agreement with the Research Council of Lithuania (LMTLT).

[1] S. I. Hayashi, K. Nawata, T. Taira, J. I. Shikata, K. Kawase and H. Minamide, Ultrabright continuously tunable terahertz-wave generation at room temperature, Sci. Rep. **4**(1), 1-5 (2014).
[2] M. Hori, H. Aghai-Khozani, A. Soter, A. Dax and D. Barna, Laser spectroscopy of pionic helium atoms, Nature **581**, 37-41 (2020).
[3] G. W. Baxter, M. A. Payne, B. D. W. Austin, C. A. Halloway, J. G. Haub, Y. He and B. J. Orr, Spectroscopic diagnostics of chemical processes: applications of tunable optical parametric oscillators, Appl. Phys. B **71**(5), 651-66 (2000).

CROSSTALK REDUCTION WITH A MULTIMODE FIBER IN FOURIER-DOMAIN FULL-FIELD OPTICAL COHERENCE TOMOGRAPHY

[1]Karolis Adomavičius, [1]Austėja Trečiokaitė, [2]Dawid Borycki,
[2]Slawomir Tomczewski, [2]Piotr Wegrzyn, [1]Ieva Žičkienė, [2]Maciej Wojtkowski,
[1,2]Egidijus Auksorius

[1] Center for Physical Sciences and Technology, Department of Optoelectronics, Vilnius, Lithuania
[2] Institute of Physical Chemistry, Polish Academy of Sciences, Warsaw, Poland
karolis.adomavicius@ftmc.lt

Optical coherence tomography (OCT) is an interferometric imaging method – widely used for retinal imaging – that can image deep in tissue. Full-field OCT (FF-OCT), compared to classical OCT systems, uses a CMOS camera instead of a single point detector, which eliminates the need to scan sample in both *x* and *y* directions, and achieves higher lateral resolution [1]. Moreover, if the fastest CMOS camera is employed and a Fourier-domain data acquisition method is used (by utilizing a tunable narrowband light source) FF-OCT becomes a powerful tool, suitable for high-speed eye imaging [2]. However, crosstalk formation in images has been limiting the technique's performance preventing from seeing choroid in the human retina.

Choroid is a crucial determinant in the pathogenesis of many ocular diseases of the posterior pole as its principle role is to supply oxygen to the outer retina [3]. Crosstalk noise appears due to the use of the wide-field detection and spatially coherent laser, which can compromise image quality effectively reducing its spatial resolution, especially deep in tissue. A spatially incoherent light source can be used to remove crosstalk, as it makes laterally scattered photons that are detected in other pixels average to uniformity. Therefore, we have previously solved the crosstalk problem by reducing spatial coherence of the laser by the help of an ultrafast deformable membrane [4]. We demonstrate that a multimode fiber with carefully chosen parameters [5] enables crosstalk-free imaging over long axial range and without significant artifacts. Specifically, we study here how depth of field (DOF) is extended because of the use of the multimode fiber. Finally, we show that it can be used to image the human retina and choroid *in vivo* with exceptional contrast, as shown in Fig. 1.

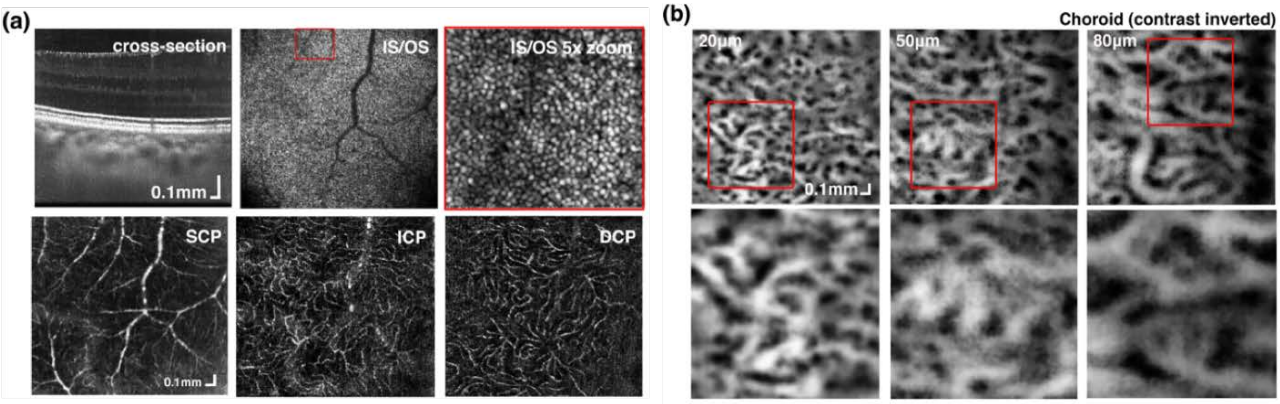


Fig. 1. FD-FF-OCT images of: (a) retina and (b) choroid of a healthy volunteer. Choroidal images are contrast-inverted to give a more realistic representation of the blood vessels. The distances shown in choroidal images are those with respect to the Bruch's membrane. SCP, ICP, DCP: superficial, intermediate and deep capillary plexus, respectively; IS/OS: inner/outer segment junction.

In conclusion, FD-FF-OCT as a tool for high-speed eye imaging has limitations due to crosstalk and coherence noise. However, we have demonstrated that carefully selected multimode fiber parameters and Fourier space filtering can produce crosstalk-free high-resolution images.

[1] E. Auksorius *et al.*, "Dual-modality fluorescence and full-field optical coherence microscopy for biomedical imaging applications," *Biomed. Opt. Express*, vol. 3, no. 3, pp. 661-666, 2012.
[2] D. Hillmann *et al.*, "Aberration-free volumetric high-speed imaging of in vivo retina," *Scientific Reports*, vol. 6, Oct 20 2016, Art no. 35209, doi: 10.1038/srep35209.
[3] H. Laviers and H. Zambarakji, "Enhanced depth imaging-OCT of the choroid: a review of the current literature," *Graefe's Archive for Clinical and Experimental Ophthalmology*, vol. 252, no. 12, pp. 1871-1883, 2014.
[4] E. Auksorius, D. Borycki, and M. Wojtkowski, "Crosstalk-free volumetric in vivo imaging of a human retina with Fourier-domain full-field optical coherence tomography," *Biomed. Opt. Express*, vol. 10, no. 12, pp. 6390-6407, 2019.
[5] E. Auksorius, D. Borycki, and M. Wojtkowski, "Multimode fiber enables control of spatial coherence in Fourier-domain full-field optical coherence tomography for in vivo corneal imaging," *Opt. Lett.*, vol. 46, no. 6, pp. 1413-1416, 2021/03/15 2021, doi: 10.1364/OL.417178.

10 mJ, 20 Hz SUB-PICOSECOND HYBRID LASER SYSTEM

Aivaras Kazakevičius[1,2], Raimundas Burokas[1,2], Audrius Zaukevičius[2], Rokas Danilevičius[2], Andrejus Michailovas[1,2]

[1] Fizinių ir technologijos mokslų centras, Savanorių pr. 231, LT-02300 Vilnius
[2] UAB Ekspla, Savanorių pr. 237, LT-02300 Vilnius
aivaras.kazakevicius@ftmc.lt

The ever increasing output energy of ultrafast lasers allows new advances in optical parametric broadband wavelength converter and amplifier system (OPCPA) development and high intensity fields physics experiments, such as high harmonic generation, THz radiation generation and acceleration of elementary particles.

One of the key features of ideal pump sources for high intensity OPCPA systems is high pulse energy. A classical approach to achieving high pulse energy is to use an Yb:KGW regenerative amplifier, which is limited to few mJ pulse energy. State of the art high energy lasers are usually constructed using thin disc or slab technologies based on amplification in ytterbium doped yttrium aluminum garnet (Yb:YAG). Recent advances on these technologies have shown that pulse energies as high as 0,7 J are achievable [1, 2]. Another promising new technology is coherent combination of laser pulses that has also allowed to reach few tens of mJ of energy [3]. However, these technologies rely on highly complex and expensive optical arrangements which are not always necessary when aiming for few tens of mJ energy [4].

Our approach to reaching pulse energies of about 10 mJ is by making use of hybrid laser technology, where we combine a fiber seed source and free space Yb:YAG amplifiers. This allows us to take advantage of reliability, scalability and compactness of fiber laser technology while retaining the ability to reach high pulse energies.

We demonstrate a 10 mJ laser system that is comprised of a high energy fiber seed source and two free space 2 pass Yb:YAG amplifier stages (fig. 1).

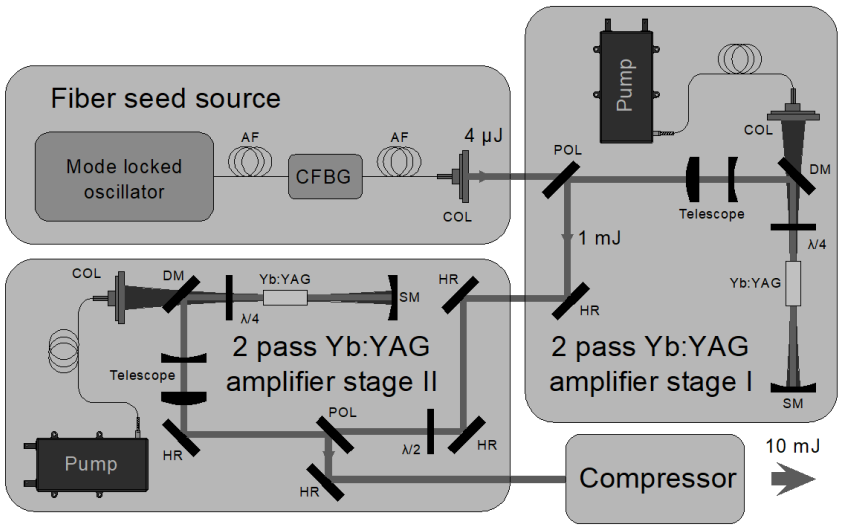


Fig. 1. Schematic representation of 10 mJ, 20 Hz laser system. AF – fiber amplifier, CFBG – chirped fiber Bragg grating, λ/4, λ/2 – quarter-wave and half-wave plates COL – beam collimator, POL – thin film polarizer, DM – dichroic mirror, SM – spherical mirror, HR – high reflectivity mirror.

Parameters of the seed for the first Yb:YAG stage were determined by an all-fiber source. It consisted of a SESAM mode-locked fiber oscillator, dispersion matched chirped fiber Bragg grating (CFBG) pulse stretcher and two fiber amplifiers. The initial laser pulses, generated in the mode locked fiber oscillator were pre-amplified to a sufficient energy to undergo the spectral broadening in a passive fiber and then were stretched with CFBG to 240 ps pulse duration. Afterwards pulses were amplified to 4 µJ in two fiber amplifiers with pulse repetition rate reduced to 10 kHz before the final fiber amplifier in order to achieve high energy. The pulse repetition rate was further reduced to 20 Hz by an external free-space pulse picker and then the beam was directed to the first solid-state amplifier stage. The seed radiation was then amplified in a 2-pass Yb:YAG amplifier up to 1 mJ energy. The chirped pulse duration was reduced to ≈ 100 ps due to relatively narrow amplification bandwidth of Yb:YAG. The beam quality was close to ideal ($M^2 \approx 1.03$) after the amplification and the Fourier transform-limited pulse duration was ≈ 700 fs. The laser beam was further amplified at the second 2-pass Yb:YAG amplifier up to > 10 mJ energy and compressed down to ~1 ps using a conventional diffraction grating compressor. The further system characterization results will be presented at the conference.

[1] C. Herkommer, P. Krötz, R. Jung et al., Ultrafast thin-disk multipass amplifier with 720 mJ operating at kilohertz repetition rate for applications in atmospheric research, Opt. Express **25**, 30164-30173 (2020).
[2] B. E. Schmidt, A. Hage, T. Mans et all, Highly stable, 54 mJ Yb-InnoSlab laser platform at 0,5 kW average power, Opt. Express, **25**, 17549 – 17555 (2017).
[3] H. Stark, J. Buldt, M. Muller et al., 23 mJ high-power fiber CPA system using electro-optically controlled divided-pulse amplification, Opt. Lett., **44**, 5529 – 5532 (2019).
[4] P. Mackonis, A. M. Rodin, Laser with 1.2 ps, 20 mJ pulses at 100 Hz besed on CPA with a low doping level Yb:YAG rods for seeding and pumping of OPCPA, Opt. Express, **28**, 1261 – 1268 (2020).

CANCER IMMUNOTHERAPY OF PANCREATIC ADENOCARCINOMA: EFFICACY, LIMITATIONS, AND SIDE EFFECTS

Radka Lencová[1], Andrea Frejlachová[1], Jan Ženka[1]

[1] Department of Medical Biology, Faculty of Science, University of South Bohemia, České Budějovice, Czech Republic
lencor00@prf.jcu.cz

Cancer remains an unsolved problem of current medicine, and its incidence rises every year [1]. The way to solve this problem could be cancer immunotherapy. Although the first attempts at modern history are attributed to doctor William Coley in 1893 [2], this therapeutic approach has not been fully developed until the last few decades. It could replace or supplement ineffective and dangerous chemotherapy and radiotherapy.

Tumour cells are mutated cells that have escaped the immune system's attention, usually eliminating such damaged cells. Tumour cells can effectively defend themselves against the cells of the immune system, are invisible to them, or the specific tumour microenvironment does not allow immune cells to enter the tumour. For immunotherapy to be successful, these mechanisms must be broken or bypassed [3].

To solve this problem, we successfully developed a therapeutical mixture consisting of several components: mannan-BAM (biocompatible anchor for cell membrane with covalently bounded mannan), Toll-like receptors (TLR) agonists R-848, poly (I:C), and lipoteichoic acid (LTA); and agonistic anti-CD40 antibody. This mixture was named MBTA [4, 5].

The primary mechanism of MBTA cancer immunotherapy is based on both innate and adaptive immunity. After the therapeutic mixture is applied directly into the tumour, mannan-BAM is anchored in the cell membrane of the tumour cells. The mannan-binding lectin recognises mannan and triggers the complement cascade via a lectin pathway that ends with the opsonisation of tumour cells by iC3b molecules. Opsonised cancer cells are recognised and killed by innate immune cells whose infiltration into the tumour is promoted by TLR agonists. Anti-CD40 antibody supports the maturation of dendritic cells, which travel to the lymph nodes where they present antigens of killed cancer cells to naïve T cells. Adaptive immunity is involved, establishing immune memory, and activated T lymphocytes travel back to the tumour or metastases and attack them [5].

MBTA immunotherapy is independent of tumour type, including cold tumours with low infiltration by immune cells. We achieved 80% cure of mice bearing advanced pancreatic adenocarcinoma tumours and 100% resistance to re-transplantation [4, 5]. After such positive results, it was decided to move to a more complicated model – a two-tumour pancreatic adenocarcinoma, with one of the tumours simulating a large metastasis. The presence of a second tumour has been found to reduce the effectiveness of MBTA treatment. When MBTA therapeutics were administered into only one of the two tumours, a growth slowdown of the distal tumour was observed. A certain positive effect was also observed when splitting the standard dose of MBTA between the two tumours. However, for better results, it was necessary to double the dose of MBTA, therefore the same amount was applied to each tumour as in the single-tumour models [4].

Nonetheless, increasing the therapeutic dose also increases the risk of side effects. Although the side effects of MBTA are relatively mild than other current therapeutic approaches, we decided to explore them to find ways to avoid them.

Wild-type mice show mild side effects, appearing primarily during the first application of MBTA, and may be attenuated by antihistamines. On the other hand, despite antihistamine administration, mice with genetically blocked adaptive immune cells respond rapidly and die after MBTA application for two or three consecutive days. This situation is avoidable by applying an MBTA with at least five-day gaps.

Due to the high efficacy, we see great potential in MBTA therapeutics in the field of cancer therapy. Therefore, we will continue to investigate its side effects and how to avoid them so that a possible shift from mice to human patients can occur as smoothly as possible.

[1] R. L. Siegel, Cancer Statistics, 2020. CA: A Cancer Journal for Clinicians, **70**, 7–30 (2020).
[2] W. B. Coley, The treatment of malignant tumors by repeated inoculations of erysipelas: With a report of ten original cases. The American Journal of the Medical Sciences, **1991**(262), 3-11 (1893).
[3] Y. A. Fouad and C. Aanei, Revisiting the hallmarks of cancer. American Journal of Cancer Research, **7**(5), 1016–1036 (2017).
[4] O. Uher, V. Caisova, L. Padoukova et al. Mannan-BAM, TLR ligands, and anti-CD40 immunotherapy in established murine pancreatic adenocarcinoma: understanding therapeutic potentials and limitations, **70**, 3303-3312 (2021).
[5] O. Uher, V. Caisová, P. Hansen et al., Coley's immunotherapy revived: Innate immunity as a link in priming cancer cells for an attack by adaptive immunity. Seminars in Oncology **46**(4-5), 385-392 (2019).

CHANGES IN PLANT DISTRIBUTION IN THE FACE OF CLIMATE CHANGE - THE CASE OF ORCHIDS

Ewa Michalska[1], Marta Kolanowska[1]

[1]Department of Geobotany and Plant Ecology, Faculty of Biology and Environmental Protection, University of Lodz, Poland
ewa.michalska@edu.uni.lodz.pl

According to the latest research, a third of all plant and animal species on our planet may become extinct due to global warming [1]. Orchid species are threatened globally mainly due to the complex relationships between plants, their habitats, pollinators and mycorrhizal communities. Orchids are completely dependent on their pollinators, and insect extinction may alter the geographic range of plants. Most vulnerable are species which are dependent on a single pollen vector.

In this presentation, the estimation of future distribution of suitable niches of Australian orchid *Leporella fimbriata* and its pollinator (*Myrmecia urens*) will be present. This sexually deceptive orchid is more fragile than plants with numerous pollen vectors. Our study shows that as a result of global warming, the overlap of orchid and its only pollen vector will most probably decrease. Climate changes will not reduce the currently available niches of the orchid - depending on modeling method (using three machine learning algorithms: MaxEnt, Random Forest and Boosted Regression Trees) - they will be larger or slightly reduced than currently observed. However, the ant will face a significant loss of suitable niches. The unavailability of pollen vector will lead to decreased reproductive success of studied orchid and as a result, it will be a great threat for *L. fimbriata* existence.

The topic will be discussed on the example of own research [2] and available literature.

[1] Román-Palacios C. & Wiens J. J. 2020. *Recent responses to climate change reveal the drivers of species extinction and survival*. Proceedings of the National Academy of Sciences 117(8): 4211-4217.

[2] Kolanowska M., Michalska E., & Konowalik K. 2021. *The impact of global warming on the niches and pollinator availability of sexually deceptive orchid with a single pollen vector*. Science of The Total Environment, 795, 148850.

TRYPANOSOMATIDS IN WILD-CAUGHT BITING MIDGES (*CULICOIDES*) FROM THE NESTS OF RAPTOR BIRDS

Margarita Kazak, Dovilė Bukauskaitė, Rimgaudas Treinys, Rasa Bernotienė

Nature Research Centre, Akademijos str. 2, Vilnius Lithuania
margarita.kazak@gamtc.lt

Trypanosomatids are protozoan parasites of animals. Based on their ecology Trypanosomatids are subdivided into two non-taxonomic groups: monoxenous parasites develop in invertebrate hosts, meanwhile dixenous parasites develop in two different hosts – vertebrates, such as mammals, birds or even fishes, and invertebrates, which serve as vectors [1]. Avian trypanosomes infect hundreds of bird species worldwide, however the biology and life cycles of most avian *Trypanosoma* species remain unknown. Although it is known that avian trypanosomes are transmitted mostly by bloodsucking dipterans, knowledge about particular species of insects capable transmitting different trypanosomes remains scarce. Only a few avian trypanosome vector species have been determined so far [2].

The main purpose of this study was to get new information on the prevalence of trypanosomatids in wild-caught biting midges (Ceratopogonidae, *Culicoides*) nearby the nests of raptor birds. We collected parous biting midge females using UV light traps located nearby nests of raptor birds in Utena district (Lithuania) in June and July 2021. DNA extraction, PCR and sequencing were applied to estimate the infections of biting midges by trypanosomatids.

In total 604 parous wild caught biting midge females were investigated. We have detected trypanosomatids in 22 (3,64 %) *Culicoides* females. Insect species were determined. The vast majority of infected biting midges were infected with dixenous parasite of birds *Trypanosoma everetti*. Five *T. everetti* haplotypes were identified with genetic distance between them being 1,07 %. Monoxenous parasite *Crithidia brevicula* was detected in several *Culicoides* females. This parasite is known to infect true bugs of families Nabidae, Gerridae and nonpredatory Miridae as well as Culicidae mosquitoes and flies of the families Calliphoridae, Muscidae, Heleomyzidae, Sepsidae and Antomyidae. This was the first time when *C. brevicula* was detected in biting midges. In this study 2 haplotypes of *C. brevicula* were identified in *Culicoides* midges. In previous studies conducted in Lithuania, other monoxenous parasites belonging to genera *Sergeia* and *Herpetomonas* were detected in *Culicoides* biting midges.

This research was funded by a grant (No. S-MIP-20-57) from the Research Council of Lithuania.

[1] Kostygov, A. Y., Karnkowska, A., Votýpka, J., Tashyreva, D., Maciszewski, K., Yurchenko, V. and Luke, J. *Euglenozoa: taxonomy, diversity and ecology, symbioses and viruses*. Open Biology.11200407200407 (2021).

[2] Bernotienė, R., Iezhova, T. A., Bukauskaitė, D., Chagas, C. R. F., Kazak, M., and Valkiūnas, G. *Development of Trypanosoma everetti in Culicoides biting midges*. Acta Tropica, 210 (April) (2020).

STARVATION MEDIATES PANCREATIC CANCER CELL SENSITIVITY TO FERROPTOSIS VIA ERK1/2, JNK AND CHANGES IN CELL MESENCHYMAL STATE

Eglė Žalytė[1,3], Jonas Cicėnas[1,2]

[1]Proteomics Centre, Institute of Biochemistry, Vilnius University Life Sciences Centre, Lithuania
[2]MAP Kinase Resource, Bioinformatics, Switzerland
[3]Institute of Biosciences, Vilnius University Life Sciences Centre, Lithuania
egle.zalyte@gf.vu.lt

Pancreatic cancer is one of the most aggressive cancers in the world. Due to a poor prognosis and the lack of specific biomarkers, 94% of pancreatic cancer cases lead to patient death [1]. Most of the time pancreatic cancer is diagnosed in an advanced stage. As surgical resection is then impossible, chemotherapy becomes the only hope for the patient. Gemcitabine is a classical pancreatic cancer chemotherapeutic, however, development of resistance is almost inevitable [2]. For this reason, new combination therapies are constantly under development.

In 2012, scientists discovered a new iron-dependent cell death form, ferroptosis [3], which is caused by an excessive membrane lipid peroxidation. Iron mediated Fenton reactions constantly generate lipid peroxides. Normally, to prevent oxidative damage, cells activate lipid antioxidant glutathione peroxidase 4 (GPX4). Ferroptosis inducers inhibit activity or expression of GPX4, which leads to accumulation of harmful lipid peroxides and eventual cell death. It was shown that cancer cells are especially sensitive to ferroptosis inducers, as they have more cytosolic iron in comparison to their normal counterparts. Thus, ferroptosis can be successfully targeted to different types of cancer cells, including pancreatic [4]. Another emerging anticancer strategy is starvation based therapy. It includes various methods: blocking angiogenesis, enhancing intratumoral nutrient catabolism and treatment with compounds that mimic starvation, such as inhibitors of growth factor receptors and mammalian target of rapamycin (mTOR) pathway [5].

In this study, we explored a novel anticancer approach: ferroptosis induction combined with cell starvation. In our experiments, we used pancreatic cancer cell lines Miapaca-2, Panc-1, Su.86.86, T3M4, as well as a unique cell line Capan-26, previously established in our laboratory [6]. We showed that in these pancreatic cancer cell lines sensitivity to ferroptosis is regulated by cell starvation-induced changes of ERK1/2 and JNK kinase activation. Also, in some of the lines used, growth factor starvation made cells alternate between epithelial and mesenchymal states. We found out that compounds targeting epithelial-to-mesenchymal transition (EMT)-related signaling pathways enhance ferroptotic cell death and therefore prove to be useful for pancreatic cancer treatment. In this way, our study elucidates new prospects of combination therapy using ferroptosis inducers and kinase inhibitors.

[1] H. Sung, J. Ferlay, R. L. Siegel et al., Global cancer statistics 2020: GLOBOCAN estimates of incidence and mortality worldwide for 36 cancers in 185 countries, CA: a cancer journal for clinicians 71, 209-249, (2021).
[2] M. Amrutkar, I. P. Gladhaug, Pancreatic cancer chemoresistance to gemcitabine, Cancers 9 (2017).
[3] S. J. Dixon, K. M. Lemberg, M. R. Lamprecht et al., Ferroptosis: an iron-dependent form of nonapoptotic cell death, Cell 149: 1060-1072 (2012).
[4] G. Chen, G. Guo, X. Zhou, H. Chen, Potential mechanism of ferroptosis in pancreatic cancer, Oncology letters 19(1):579-87 (2020).
[5] S. Yu, Z. Chen, X. Zeng, et al., Advances in nanomedicine for cancer starvation therapy, Theranostics 9: 8026-8047 (2019).
[6] E. Zalyte, V. Dedonyte, B. Kurlinkus et al., Establishment and characterization of a new pancreatic ductal adenocarcinoma cell line Capan-26. Anticancer research 41: 1401-1406 (2021).

HARVEST TIME EFFECT ON CANNABINOIDS PROFILE CHANGES IN *CANNABIS SATIVA* L. PLANTS

Kaolina Barčauskaitė[1*], Ieva Čalkaitė[1], Antony Szumny[2], Vita Tilvikienė[1]

[1] Lithuanian Research Centre for Agriculture and Forestry, Lithuania
[2] Department of Horticulture, Wrocław University of Environmental and Life Sciences, Poland
Karolina.Barcauskaite@lammc.lt

Hemp is a type of *Cannabis sativa* plant and becomes more and more attractive due to its wide application in several industries such as food, construction, pharmaceuticals, textile, paper [1,2]. Plants could adapt to various climates and broad soil types. Due to its deep and large root system hemp has a high potential for removing nutrients and water from the soil [3]. Maturated hemp presents around 10,000 various structures phenolic compounds, including flavonoids (flavones and flavonols), phenolic acids, stilbenes and lignans [4]. These compounds are called plants secondary metabolites which protect plant tissues from harmful effects of the environment [5]. However, the main valuable and main interesting compounds for scientists in hemp tissue are cannabinoids. The cannabis flower is comprised of over 100 different cannabinoids, the active compounds found within the cannabis plant [6]. The two most well-researched phytocannabinoids are delta-9 tetrahydrocannabinol (Δ9-THC) and cannabidiol (CBD). Δ9-THC is the primary psychoactive component of cannabis which is responsible for the "high" associated with cannabis use. Industrial hemp cultivated in Lithuania must contain Δ9-THC less than 0.2%. CBD has received a lot of attention for its potential therapeutic effects, antibacterial properties etc. In contrast, hemp contains minor cannabinoids which are found in low amounts or below detection limit using standard identification methods.

This study aimed to find out how harvest time influences the quality and quantity of seven cannabinoids.

The hemp monoecious cultivar, *Felina32* (French national hemp grower association) were cultivated at Lithuanian Research Centre for Agriculture and Forestry located in Central Lithuania (55˚24′ N, 23˚52′ E, 65 m asl) on an Endogleyic Endostagnic Endocalcaric Luvisol (Loamic) soil according to WRB. Hemp's inflorescences grown without any pesticides and fertilizers at two different densities (15 and 35 kg per ha) were chosen for this study. One part of the plants was harvested 140 days (1st harvest) after sowing and another after 173 days (2ed harvest). Collected samples were air-dried at ambient temperature, ground using a coffee bean mill (Bosch, Germany) packed in paper bags and stored at ambient temperature until use. The seven cannabinoids (CBD, CBC, Δ8-THC, Δ9-THC, CBG, CBD-A, CBG-A) content was determined using GCMS-QP2020 (Shimadzu Company, Kyoto, Japan) equipped with Zebron ZB-5MSi (30 m × 0.25 mm × 0.25 μm) column (Phenomenex, Torrance, CA, USA) after samples derivatization.

It was obtained that sowing density doesn't affect the amount of cannabinoids in hemp inflorescences. However, a higher ratio of CBD and Δ9-THC was found in plants harvested after 173 days. Likely it could be influenced by the reduced amount of CBD-A as it is known that decarboxylation of CBD-A directly increases CBD concentration. These and all other results step by step will be presented during the conference.

Acknowledgement. This research was funded by European Social Fund (No 09.3.3.-LMT-K-712-19-0132) under the grant agreement with the Research Council of Lithuania (LMTLT).

[1] Farinon, B.; Molinari, R.; Costantini, L.; Merendino, N. The Seed of Industrial Hemp (*Cannabis sativa* L.): Nutritional Quality and Potential Functionality for Human Health and Nutrition. Nutrients ***12***, 1935 (2020).

[2] Ji, A.; Jia, L.; Kumar, D.; Yoo, C.G. Recent Advancements in Biological Conversion of Industrial Hemp for Biofuel and Value-Added Products. Fermentation ***7***, 6 (2021).

[3] Angelini, L.G.; Tavarini, S.; Cestone, B.; Beni, C. Variation in mineral composition in three different plant organs of five fibre hemp (Cannabis sativa L.) cultivars. Agrochimica 58, 1–18 (2014).

[4] Andre, C.; Larondelle, Y.; Evers, D. Dietary Antioxidants and Oxidative Stress from a Human and Plant Perspective: A Review. Curr. Nutr. Food Sci. ***6***, 2–12 (2010).

[5] Auger, B.; Marnet, N.; Gautier, V.; Maia-Grondard, A.; Leprince, F.; Renard, M.; Guyot, S.; Nesi, N.; Routaboul, J.M. A detailed survey of seed coat flavonoids in developing seeds of brassica napus L. J. Agric. Food Chem. ***58***, 6246–6256 (2010).

[6] Babson, K.A.; Sottile, J.; Morabito, D. Cannabis, Cannabinoids, and Sleep: a Review of the Literature. Curr. Psychiatry Rep. ***19***, 1–12 (2017).

ANTIMICROBIAL ACTIVITY OF NANOCRYSTALLINE HYDROXYAPATITES DOPED AND CO-DOPED WITH Zn^{2+} AND Cu^{2+} IONS AGAINST GRAM-NEGATIVE BACTERIA

Justyna Rewak-Soroczynska[1], Paulina Sobierajska[1] and Rafal J. Wiglusz[1]

[1] Institute of Low Temperature and Structure Research, Polish Academy of Sciences, Okolna 2, 50-422 Wroclaw, Poland
j.rewak@intibs.pl

Nanotechnology is a multidisciplinary field of research that still gets a lot of interest. Nanomaterials show interesting chemical and physical properties different from those in the micro-sized scale so that they may be applied in various areas, among others in biology, chemistry and physics.

Hydroxyapatite ($Ca_{10}(PO_4)_6(OH)_2$ (HAp)) is a natural component of human body, especially teeth and bones. Its synthetic analogue can be synthesized and structurally modified in order to obtain apatite with desired properties. Nanocrystalline HAp is being used as bone cement as well as an implant coatings, dermal fillers and drug delivery systems due to its high biocompatibility (*in vitro* and *in vivo*) [1-3]. Moreover, the hydroxyapatite crystallizes with a hexagonal structure belonged to the $P6_3/m$ space group and is able to substitute different cations in the *4(f)* and *6(h)* crystallographic positions. Among various cations, Ag^+, Cu^{2+} or Zn^{2+} are well-known for their antimicrobial properties therefore the cations-doped hydroxyapatite could be used in a bacterial infection prevention, in particular as concerns implant insertion procedure.

The materials were synthesized using a co-precipitation method, where the concentrations of Zn^{2+} and Cu^{2+} ions were set on 5 mol% in a ratio to entire calcium ions molar content (see Table 1).

Table 1 Formulas of tested hydroxyapatites

Dopants	Hydroxyapatite formula
Pure HAp	$Ca_{10}(PO4)_6(OH)_2$
5 mol% Zn^{2+}	$Ca_{9,5}Zn_{0,5}(PO_4)_6(OH)_2$
5 mol% Cu^{2+}	$Ca_{9,5}Cu_{0,5}(PO_4)_6(OH)_2$
5 mol% Zn^{2+}, 5 mol% Cu^{2+}	$Ca_{9,0}Zn_{0,5}Cu_{0,5}(PO_4)_6(OH)_2$

The XRPD (X-ray powder diffraction) was performed in order to confirm the formation of pure hydroxyapatite structure. For the evaluation of antimicrobial activity of nanohydroxyapatites colloidal solutions, pressed disks and galactose-based hydrogels were prepared. Furthermore, the SEM (Scanning Electron Microscopy) images were taken to evaluate the morphology of tested materials. The antibacterial activity was checked against Gram-negative bacteria: *Pseudomonas aeruginosa* and *Escherichia coli* strains. The surveillance of tested strains in the presence of the tested nanomaterials (in a form of colloidal solutions) was assessed using colony counting method, confocal laser scanning microscopy (CLSM) with live/dead staining and the SEM images. Moreover, the biofilm formation on the surface of pellets (pressed materials) and hydrogels was compared using the CLSM with live/dead staining. The influence of surface topography on bacterial adhesion to pellets was also assessed with the CLSM.

The obtained results suggest that the studied materials, especially those doped and co-doped with Cu^{2+} ions, effectively decrease bacterial viability in the saline and limit bacterial growth in the culture medium. Additionally, changes in bacterial adhesion to hydrogels and pellets were visible and hydrogels were more prone to be colonized by both tested strains. The morphology of the biofilms on the surface of particular materials was also altered, especially by nHAp:Cu^{2+} and nHAp:Cu^{2+}-Zn^{2+} materials. The biofilms formed on the surface of hydrogels were scattered while the one formed on other materials were more clumped [4].

[1] T. Tite,. et al. Cationic substitutions in hydroxyapatite: Current status of the derived biofunctional effects and their in vitro interrogation methods, Materials. 11 (2018) 1–62.
[2] K. Yang et al. Antimicrobial hydrogels: Promising materials for medical application, International Journal of Nanomedicine. 13 (2018) 2217–2263.
[3] D. Arcos and M. Vallet-Regí, Substituted hydroxyapatite coatings of bone implants, Journal of Materials Chemistry B. 8 (2020) 1781–1800.
[4] P. Sobierajska et al. Investigation of topography effect on antibacterial properties and biocompatibility of nanohydroxyapatites activated with zinc and copper ions: In vitro study of colloids, hydrogel scaffolds and pellets. Materials Science and Engineering: C, 2021,112547.

Acknowledgements: The authors would like to acknowledge the National Science Centre in Poland (NSC Poland) for financial support within the Project ‘Preparation and investigation of multifunctional biomaterials based on nanoapatites for possible application in bone tumor treatment’ UMO-2017/27/N/ST5/02976.

STUDY OF POTENTIAL NEW DRUG COMBINATIONS FOR TREATMENT OF RESISTANT LEUKEMIA CASES

Sergej Charkavliuk, Veronika Borutinskaitė

Department of Molecular Cell Biology, Institute of Biochemistry, Life Science Center, Vilnius University, Lithuania
sergej.charkavliuk@gmc.stud.vu.lt

Acute Myeloid Leukemia (AML) is an aggressive hematologic malignancy of the myeloid bloodline. The risk of developing this tumor grows over the years, whereas the efficiency of the conventional treatment drastically drops. Patients over 20 years of age have a 68% chance of surviving within 5 years, compared with just 26% for patients over 20 years of age. The unacceptable rates of survival are the results of high adaptation rates to standard treatment. More than 60% of elderly patients failed to induce chemotherapy owing to recurrence, and over 85% of patients failed in treatment [1].

Like so, there is a need for the development of new strategies with new or already existing drugs and their combination for patients with chemoresistance cases.

All malignant tumors share the consistent characteristic – avoidance of an apoptotic mechanism. In a number of leukemia types, the anti-apoptotic protein MCL1 is significantly higher compared to other proteins of the corresponding class. As follows, the way to the novel treatment of the patients may lay through the inhibition of the MCL1 proteins. The merge of the S63845 inhibitor, a BH3 mimetic, allowed to target these proteins in the cytoplasm. Both in vivo and in vitro studies showed a potential anti-cancer effect of S63845 on the number of MCL1 dependent leukemias and lymphomas cells. It was shown that S63845 caused poly ADP-ribose polymerase (PARP) breakage, exposure with caspase-dependent phosphatidyl-serine, and release of the mitochondrial cytochrome C. This indicates that S63845 affects cancer cells by directly inhibiting MCL1 and activating the BAX/BAK-dependent mitochondrial apoptotic pathway [2]. Although, there are not enough evidence to suggest the potential use of the novel inhibitor in the treatment of real patients. The therapeutical mechanism and the clinical effects of the S63845 require more research, which is jet to be conducted.

The aim of our study was to investigate the anti-proliferative and apoptotic effect of MCL1 inhibitor S63845 alone or in combination with conventional chemotherapy (Cytarabine, Idarubicin) on leukemia cells. KG-1a, the stem-like AML cell line was chosen as a model system for our study. We demonstrated that the S65845 alone at 100 nM concentration had no impact on the proliferation and viability of the KG1a cells during 96-hour treatment. Although, the combination of S65845 with 8 nM of Idarubicin caused a double effect on the viability, rather the 8 nM of Idarubicin or S65845 alone after 96-hour of treatment but has no impact on the proliferation. The combination of the S65845 with conventional treatment (Cytarabine 30nM and Idarubicin 8 nM) inhibited the growth of cells (70%) and viability compared to control cells after the 96 h of treatment. Expression changes of anti-, pro-apoptotic, oncogenes were detected by real-time –PCR analysis. We observed up-regulation of anti-apoptotic genes like BCL2L1, BCL2, BCL2A1, after combined treatment (S65845, Idarubicin, Cytarabine) at 24h point. Moreover, pro-apoptotic gene (BAX, PT53, BAK, APAF1) expression was up-regulated after 24 hours of combined treatment, however, mightier changes were observed after 96 h treatment. Also, changes in the expression of genes responsible for drug resistance (ABCB1), oncogenes, genes critical in epigenetic regulation (HDAC, DNMT), and stemness (NOTCH1, Lin28A) were observed.

In conclusion, these results suggest the combination of MCL1 inhibitor S63845 with conventional chemotherapy leads to growth inhibition in KG1a cells.

[1] Zhang, J., Gu, Y. and Chen, B., 2019. Mechanisms of drug resistance in acute myeloid leukemia. *OncoTargets and Therapy*, [online] Volume 12, pp.1937-1945. Available at: <https://doi.org/10.2147/OTT.S191621> [Accessed 6 October 2020].

[2] Kotschy, A., 2016. The MCL1 inhibitor S63845 is tolerable and effective in diverse cancer models. *Nature*, 538(7626), pp.477–482.

DYNAMIC NUMERICAL MODELLING OF TUMOR TISSUE ELECTROPORATION

Veronika Malyško-Ptašinskė[1], Eivina Radzevičiūtė[1,2]

[1]Faculty of Electronics, Vilnius Gediminas Technical University, Vilnius, Lithuania
[2]State Research Institute Centre for Innovative Medicine, Department of Immunology, Vilnius, Lithuania
veronika.malyško-ptasinske@vilniustech.lt

Electroporation phenomenon nowadays is used in different spheres of application, covering cancer treatment. The method requires very precise designation of pulsing parameters and evaluation electric field distribution in tissue [1], where on of the most important parameters is tissue conductivity. From previous research it is known, that conductivity in tissue vary if electric field exceeds irreversible electroporation threshold [2]. Therefore, in this work conductivity dynamics were employed in numerical model. The results obtained from simulation creates a possibility of more accurate evaluation of electric field distribution and pre-treatment planning.

In this work the deep settled mice Lewis lung carcinoma (LLC1) three-dimensional tumor model was simulated in COMSOL Multiphysics (COMSOL, Stockholm, Sweden). Electric pulses were delivered through non-invasive plate electrodes placed with 3.8–4 mm distance between tumor tissue. In order to reduce inhomogeneity spaces between the electrodes and skin were partially covered with conductive gel [3] (conductivity of 1.1 S/m). Our purposed skin model involves an inhomogeneity of tissue structure considering skin multilayers such as stratum corneum with epidermis, dermis combination with fat, muscle and subcutaneous tumor, with corresponding parameters and thicknesses of mice skin layers [4] [5]. It has been already established that tissue conductivity is dependent on electric field strength, therefore, smoothed Heaviside function was employed in numerical modelling. In this function initial conductivity (0.003–0.5 S/m), reversible (150–400 V) and irreversible (800–1200 V) electroporation voltage values were defined for each layer [6][7][8]. The boundary conditions were characterized using Dirichlet`s and Neumann boundary conditions, hence, two plate electrodes represent ground (0 V) and terminal (1,3 kV/cm amplitude value for μsPEF and 3,5 kV/cm – for nsPEF) with insulated outer boundaries. The results were obtained using stationary analysis.

It was observed that electric field strength in top and the bottom parts of the tumor was lowest, while the stratum corneum which was in contact with the electrodes received the highest dose of PEF and, therefore, increased possibility of skin ablation. It was observed that the amplitude of the pulsed electric field within the tumor can be increased more than 30%. Although, this may trigger even larger are of the tissue ablation. Volume fraction versus electric field shows that for micro second treatment whole tumor is affected by 1000 V/cm electric field strength, then the volume with higher value of electric field decreases. There are very little areas of tumor covered by electric field up to 1500 kV/cm. For nanosecond PEF 100% of tumor is covered by 1600 V/cm, then the curve decreases exponentially while reaches 3750 kV/cm. Moreover, the numerical modeling simulation results showed negligible deviation between computed and measured data.

It was shown that dynamic numerical modelling including the changes in conductivity while applying electric pulses can serve more precise spatial distribution of electric field in tumor tissue. However, our proposed model can be improved including the thermal calculations, which also have an effect on conductivity dynamics.

The research was funded by Research Council of Lithuania, Grant Nr. S-LL-21-4

[1] Pavselj, N. and Miklavcic, D., 2008. Numerical models of skin electropermeabilization taking into account conductivity changes and the presence of local transport regions. IEEE Trans Plasma Sci, 36(4), pp.1650-1658.
[2] Zhao, Y., Bhonsle, S., Dong, S., Lv, Y., Liu, H., Safaai-Jazi, A., Davalos, R.V. and Yao, C., 2017. Characterization of conductivity changes during high-frequency irreversible electroporation for treatment planning. IEEE Transactions on Biomedical Engineering, 65(8), pp.1810-1819.
[3] Ivorra, A., Al-Sakere, B., Rubinsky, B. and Mir, L.M., 2008. Use of conductive gels for electric field homogenization increases the antitumor efficacy of electroporation therapies. Physics in Medicine & Biology, 53(22), p.6605.
[4] Wei, J.C., Edwards, G.A., Martin, D.J., Huang, H., Crichton, M.L. and Kendall, M.A., 2017. Allometric scaling of skin thickness, elasticity, viscoelasticity to mass for micro-medical device translation: from mice, rats, rabbits, pigs to humans. Scientific reports, 7(1), pp.1-16.
[5] Hew, J., Solon-Biet, S.M., McMahon, A.C., Ruohonen, K., Raubenheimer, D., Ballard, J.W.O., Le Couteur, D.G., Nicholls, C., Li, Z., Maitz, P.K. and Wang, Y., 2016. The effects of dietary macronutrient balance on skin structure in aging male and female mice. PloS one, 11(11), p.e0166175.
[6] Forjanič, T., Markelc, B., Marčan, M., Bellard, E., Couillaud, F., Golzio, M. and Miklavčič, D., 2019. Electroporation-induced stress response and its effect on gene electrotransfer efficacy: In vivo imaging and numerical modeling. IEEE Transactions on Biomedical Engineering, 66(9), pp.2671-2683.
[7] Pavselj, N. and Miklavcic, D., 2008. Numerical models of skin electropermeabilization taking into account conductivity changes and the presence of local transport regions. IEEE Trans Plasma Sci, 36(4), pp.1650-1658.
[8] Corovic, S., Lackovic, I., Sustaric, P., Sustar, T., Rodic, T. and Miklavcic, D., 2013. Modeling of electric field distribution in tissues during electroporation. Biomedical engineering online, 12(1), pp.1-27.

PURIFICATION AND THE IDENTIFICATION OF PHYSICAL AND CHEMICAL PROPERTIES OF *SACCHAROMYCES CEREVISIAE* K2 TOXIN

Monika Navickaitė[1], Ramunė Stanevičienė[2], Juliana Lukša[2], Elena Servienė[2], Jolanta Sereikaitė[1]

[1]Department of Chemistry and Bioengineering, Vilnius Gediminas Technical University, Saulėtekio av. 11, 10223, Vilnius, Lithuania

[2]Laboratory of Genetics, Nature Research Centre, Akademijos str. 2, LT-08412 Vilnius, Lithuania

monika.navickaite@stud.vilniustech.lt

Saccharomyces cerevisiae secreted K2 toxin has proven in the past to have antibacterial effects against bacteria, protozoa as well as fungi, which could be used in medicine, food industry and agriculture [1,2]. Yet not much is known about K2 protein's secretion mechanisms and structural properties. K2 toxin is secreted in insignificant quantities, making purification and analysis difficult. In this study, we attempt to purify the K2 toxin and analyze its properties using various analysis methods such as HPLC and gel electrophoresis.

The first step of our study is the purification of K2 toxin using liquid chromatography. To isolate the protein, the concentrate of cultivation media is loaded on the SP-Sepharose column, and the K2 toxin is eluted using a linear sodium chloride gradient. Collected fractions are tested by assessing their biocidal activity against a toxin sensitive strain *Saccharomyces cerevisiae* α'1. The active fractions are further purified using a second column filled with CM-Sephadex C50 sorbent. Approximately 0.05 mg of K2 toxin was obtained from three liters of yeast cultivation media.

The next step of our study is the characterization of the purified K2 toxin. Using HPLC and gel- electrophoresis, the molecular mass as well as subunit structure of the K2 toxin was determined. Referencing literature describing the genetic structure of K2 [2], we were able to better understand the post-translational modification mechanism of the K2 toxin.

This study helps to better understand the structure of K2 toxin and allows further application of target protein in food biopreservation technologies.

[1] Mannazzu I., Domizio P., Carboni G., Zara S., Zara G., Comitini F., Budroni M and Ciani M. Yeast killer toxins: from ecological significance to application. Critical Reviews in Biology **39**, 603-617 (2018).

[2] Dignard D., Whiteway M., Germain D., Tessier D. ir Thomas D. Y. Expression in yeast of a eDNA copy of the K2 killer toxin gene. Molecular Genetics and Genomics **227**, 127-136 (1991).

HOW DOES DEUTERATION OF THE PHOSPHOLIPID AFFECT ITS MONOLAYERS PROPERTIES?

Edvinas Navakauskas[1], Simona Strazdaitė[1]

[1]Center of Physical Sciences and Technology, Department of Organic Chemistry, Saulėtekis ave. 3, LT-10257 Vilnius
Edvinas.Navakauskas@ftmc.lt

The fragility of living cells and the particular complexity of their membranes make in situ spectroscopic investigation of the cell's membrane rarely feasible. To circumvent this problem, biomimetic membranes, limited to a few elements, are frequently used. Furthermore, to avoid overlapping of the vibrational bands in multi-compound systems, often one of the components must be isotopically labelled. In practice, an isotope labelling of membrane-forming phospholipids, where distinct lipid moieties can be deuterated, is the most commonly utilized (Fig. 1).

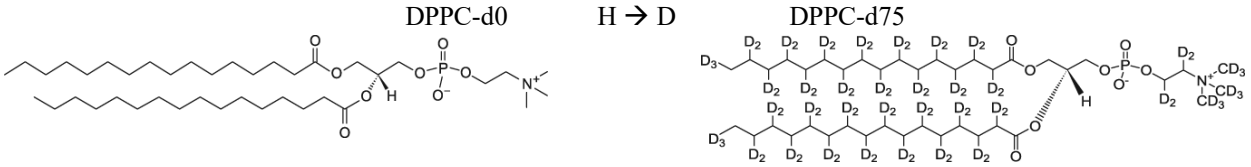


Fig. 1 The structure of 1,2-dipalmitoyl-*sn*-glycero-3-phosphocholine (DPPC) in its non-deuterated form (left; DPPC-d0) and in one of the deuterated forms, where majority of hydrogen atoms are replaced with deuterium (right; DPPC-d75).

Although lipid deuteration has been employed in numerous spectroscopic studies, it is still unclear how it affects the model system. Thus, to evaluate the properties of different deuteration lipid monolayers, we used the Langmuir-Blodgett layer formation technique combined with vibrational sum frequency generation (VSFG) spectrometry, which enabled the characterization of the monolayer structure at the molecular level (Fig. 2).

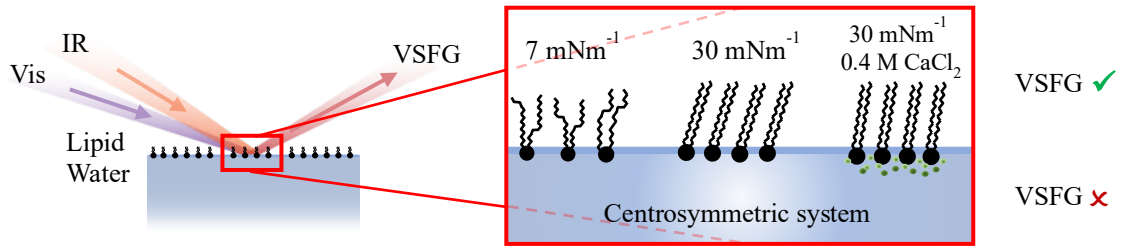


Fig. 2 The concept of VSFG measurement and the experimental design.

In our study, we have shown that deuteration of both the alkyl chain and the choline group affects the properties of the monolayers. Deuteration of the choline group changes the orientation of the lipid's headgroup, resulting in a more water open, but Ca+ ions blocking structure. Moreover, it affects the packing of the alkyl chains under tight lipid packing conditions (≥ 30 mNm^{-1}). These results were obtained by probing and analyzing vibrations of the alkyl chains and the phosphate group (Figure 3 and 4). Meanwhile, deuteration of the alkyl chains results in a more disordered alkyl chains at higher surface pressures (30 mNm^{-1}) compared to monolayers with non-deuterated alkyl chains.

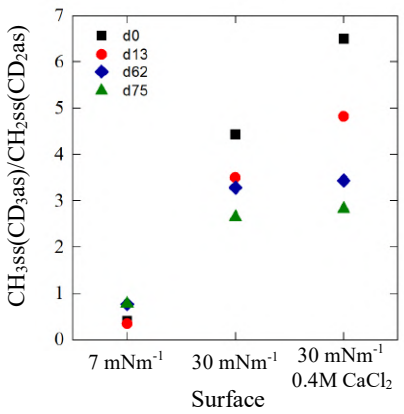


Fig. 3 The ratio of the symmetric CH_3ss/CH_2ss and antisymmetric CD_3as/CD_2as resonances for lipids with different deuterations as a function of the surface pressure.

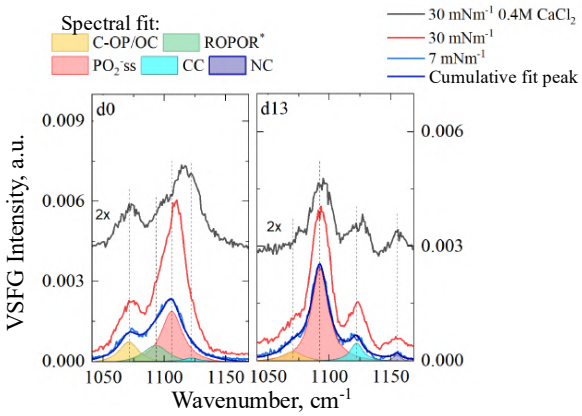


Fig. 4 VSFG spectra of lipid monolayers with non-deuterated (left) and deuterated (right) choline group in the phosphate group vibrational region.

BIO-POTPOURRI OF *SACCHAROMYCETALES* KILLER YEASTS

Kristupas Paulius, Aleksandras Konovalovas, Saulius Serva

Department of Biochemistry and Molecular Biology, Institute of Biosciences, Life Sciences Center, Vilnius University, Vilnius, Lithuania
kristupas.paulius@chgf.stud.vu.lt

Many members of the flora tend to co-exist with various other organisms, some of which drive plants' survival and biological prosperity. It is hardly astonishing that a wide spectrum of those symbiotic organisms are yeasts, however, their properties can be rather peculiar – they significantly diverge from a family point of view and can possess biocidic properties, regardless of their species. Our ambition was to disclose this magnitude of different yeasts with double-stranded RNA (dsRNA) killer viruses and identify their position in the *Saccharomycetales* family tree. Comprehending such biodiversity with linkage to yeasts' virulent capabilities may be fundamental for novel discernments of life.

We have inspected 384 unique yeast strains from a vast range of natural niches in different geographical zones of Lithuania. More than a tenth of them had some sort of killer phenotype – a phenomenon which was verified by combining methods of RNA gel electrophoresis and growth on a selective medium. Out of the biocidic yeasts we selected 12 unique strains with most palpable morphological disparities and performed parallel analyses of restriction fragment length polymorphism (RFLP) and internal transcribed spacer (ITS) sequencing. The outcome suggests that most yeast strains are of *Metschnikowia sp.* origin, yet several other species were also identified. This may imply that killer activity is much more moderately dispersed throughout a variety of *Saccharomycetales,* and new types of viruses with their unique capabilities are yet to be perceived.

TOWARDS THE SCALABLE TOTAL SYNTHESIS OF SARPAGINE FAMILY ALKALOIDS

Barbara Chatinovska[1], Edvinas Orentas[1]

[1] Department of Organic Chemistry, Faculty of Chemistry and Geosciences, Vilnius University, Lithuania
barbara.chatinovska@chgf.stud.vu.lt

The sarpagine family is a major class of structurally related monoterpenoid indole alkaloids (Fig. 1), naturally occuring in the dogbane *(Apocynaceae)* family of plants. Historically, the extracts of these plants have been used in traditional medicine to treat a variety of illnesses – for example, the Indian snakeroot *(Rauvolfia serpentina)* contains a wide variety of sarpagine, macroline and ajmaline alkaloids and has been used as a source of the phytochemical reserpine. Curiously, the extracts from this plant are used up until modern day in the treatment of systolic hypertension [1]. Unfortunately, natural occurrence of these compounds is scarce, therefore making sarpagine alkaloids an interesting and challenging synthetic target. To date, Cook et al. have synthesised a variety of these compounds elegantly employing Pictet-Spengler type chemistry [2], laying down the foundation to synthetic sarpagine research. Unfortunately, this pathway is almost impossible to scale due to the length of the total syntheses (up to 15 steps), making it extremely challenging to furthermore clinically analyze these compounds and find potential pharmaceutical applications.

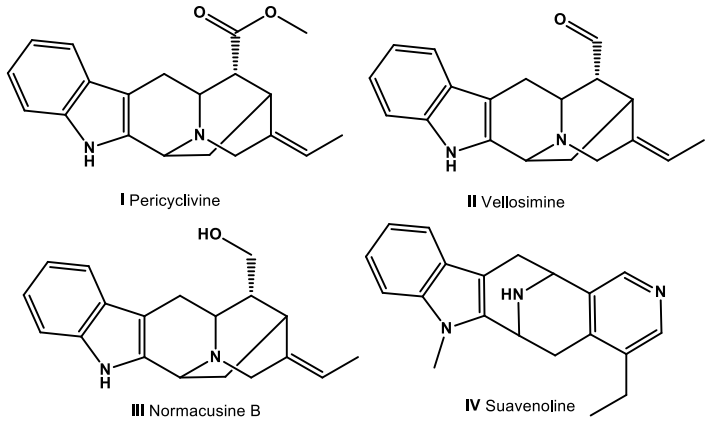


Fig. 1. Examples of the sarpagine family alkaloids.

We suggest a conceptually novel approach towards the total synthesis of these complex molecules employing azabicyclo[3.3.1]nonanes. Using these compounds would enable easily applicable large scale synthesis; furthermore, the length of the synthesis would drastically decrease (Fig. 2). Past efforts have shown an easy way to obtain enantiomerically pure bicyclic diol **1** using lipase from *Candida rugosa* [3].

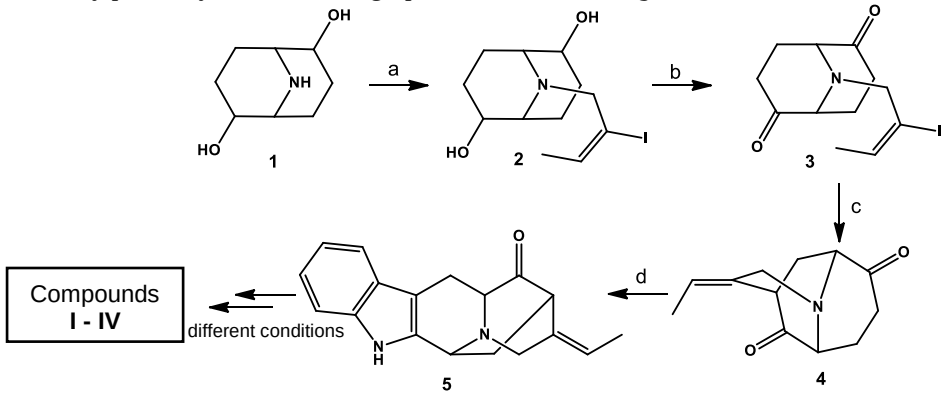


Fig. 2. Synthesis pathway. a - (Z)-1-bromo-2-iodo-2-butene, K_2CO_3, THF; b – $(COCl)_2$, TEA, DMSO, DCM; c – PhOH, ^{t}BuOK, $Pd(PPh_3)_4$, THF; d – $PhNHNH_2$, AcCl, 2,4 – dichlorobenzaldehyde, EtOH/MeOH/$CHCl_3$

.

To date, we have successfully synthesised and identified compounds **1**-**5**, establishing a promising pathway towards the final products, such as vellosimine, normacusine B, pericyclivine and other congenerates.

[1] Srivastava, A.; Tripathi, A. K.; Pandey, R.; Verma, R. K.; Gupta, M. M. (2006). "Quantitative determination of reserpine, ajmaline, and ajmalicine in Rauvolfia serpentina by reversed-phase high-performance liquid chromatography". Journal of Chromatographic Science. 44 (9): 557–60.
[2] C. R. Edwankar, R. V. Edwankar,O. A. Namjoshi, J. Deschamps, X. Liao, J. M. Cook, J. Org. Chem. 2013, 78, 6471 – 6487.
[3] V. Bieliūnas, D. Račkauskaitė, E. Orentas, S. Stončius (2013). "Synthesis, Enantiomer Separation, and Absolute Configuration of 2,6-Oxygenated 9-Azabicyclo[3.31]nonanes"

SYNTHESIS AND ANALYSIS OF $GdPO_4 \cdot H_2O$:Eu MODIFIED WOOD

Monika Baublytė[1], Denis Sokol[1], Ramūnas Skaudžius[1]

[1]Department of Inorganic Chemistry, Faculty of Chemistry, Vilnius University, Naugarduko st. 24, Vilnius,
monika.baublyte@mb.vu.lt

The use of luminescent lanthanide-doped materials is growing in all industries. Significant usage increase in technologies is associated with high thermal stability, refractive index and quantum yield, good photochemical stability, magnetic properties, low toxicity, and solubility in water [1]. Notable progress has been made in exploring the applications of luminescent lanthanide-doped materials in phosphors, lasers, optical devices, solar cells, catalysis, and bioimaging [2]. Nevertheless, lanthanide-doped materials have never been introduced as the potential wood dopants.

Due to high sustainability, thermal and electrical insulating properties, and aesthetics, wood is the most abundant building material used in residential and non-residential buildings, furniture constructions, and decoration. Thus, high weathering, biological and pyrolytic resistance of wood is essential [3, 4]. Mechanical, biological, thermal, and accelerated weathering behaviours of wood can be increased using various materials [5]. Therefore, this work proposes inorganic $GdPO_4 \cdot H_2O$:Eu compound produced by in situ hydrothermal syntheses as a new alternative method to increase wood chemical resistance and confer new optical properties.

After in situ synthesis, the characteristics of the samples were observed by scanning electron microscopy (SEM) and computed tomography (CT) (Fig.1); optical properties were determined by luminescence analysis. Thermogravimetric (TG) analysis was performed to attest the effects of $GdPO_4$ on the thermal degradation of wood.

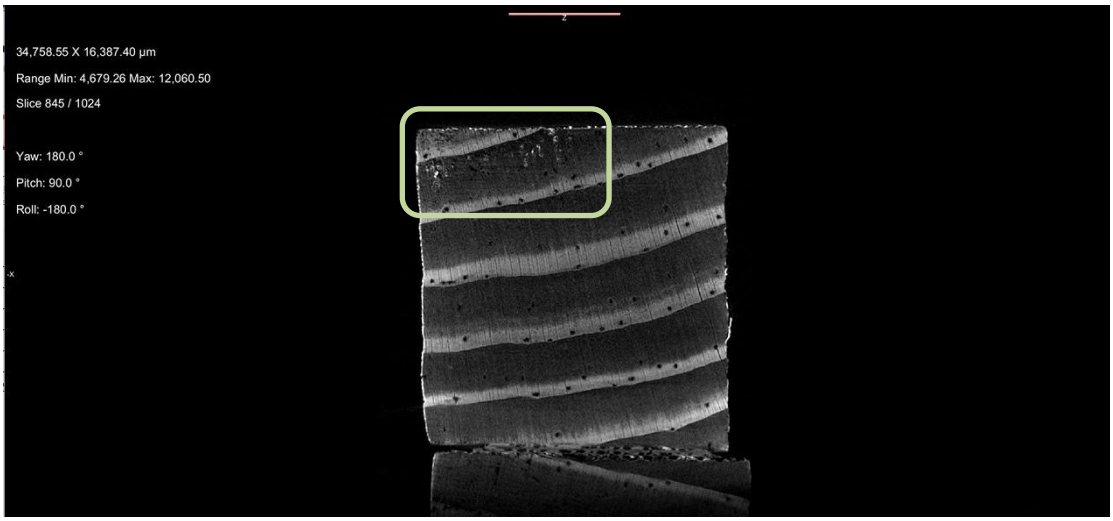


Fig. 1. CT image of wood – ceramic composite.

[1] S. Wu, J. Yin, H. Qu, A. Li, L. Liu, and Y. Shao, Photoluminescence properties of gadolinium phosphate nanoprisms doped with lanthanide ions for multicolor live cell imaging, J. Mater. Sci. Mater. Electron. **30**, 11336–11345 (2019).

[2] N. B. Amar, T. Kallel, T. Koubaa, M. A. Hassairi, M. Dammak, and E. Cavalli, Synthesis, characterization and optical spectroscopy of $GdPO_4:Er^{3+}$, Luminescence, **35** (7) 1056–1067 (2020).

[3] J. S. Fabiyi and A. G. McDonald, Effect of wood species on property and weathering performance of wood plastic composites, Compos. Part Appl. Sci. Manuf. **41**, 1434–1440 (2010).

[4] J. Chen, Z. Zhu, H. Zhang, S. Tian, and S. Fu, Wood-derived nanostructured hybrid for efficient flame retarding and electromagnetic shielding, Mater. Des. **204**, 109695 (2021).

[5] S. V. Levchik and E. D. Weil, Developments in phosphorus flame retardants, in Advances in Fire Retardant Materials, A. R. Horrocks and D. Price, Eds. Woodhead Publishing, 41–66 (2008).

THE EFFECT OF BORON DOPING ON LUMINESCENCE OF YAG AND LuAG POWDER, CERAMIC AND THIN FILMS

Greta Inkrataitė[1], Meldra Kemere[2], Anatolijs Sarakovskis[2], Ramūnas Skaudžius[1]

[1] Institute of Chemistry, Faculty of Chemistry and Geosciences, Vilnius University, Vilnius, Lithuania
[2] Institute of Solid State Physics, University of Latvia, 8 Kengaraga street, LV-1063, Riga, Latvia
greta.inkrataite@chgf.vu.lt

To convert high-energy radiation, such as gamma or X-rays, into visible light, a certain type of material is needed. Such compounds are usually referred to as scintillators. Over the years many different candidates to fit the required criteria were examined. Compounds with garnet structure have attracted a particularly large amount of attention as potential scintillators [1]. Cerium doped yttrium and lutetium aluminum garnets (YAG:Ce, LuAG:Ce), have high density, high thermal stability, a rather intensive emission/excitation and high quantum efficiency which are needed for a good scintillator. However, further optimization and improvement are still required, especially towards obtaining high luminescence intensity and even more so on the shortening of the decay time. One way to approach this problem is to alloy the aforementioned compounds with different elements, such as boron and magnesium [2,3]. By replacing one element with another in the crystal lattice it is possible to influence the properties of the materials. As such, by doping we could potentially be able to improve key aforementioned parameters: emission intensity (Fig. 1), quantum efficiency and decay times [2]. The form of the samples is also known to be and important factor for scintillators. Although the most common and easiest to work with form of the samples is powder, however coatings and ceramics are more applicable in practice. Therefore, when it comes to scintillators, it is important to consider this as well [4].

In the present work it is investigated the effect of boron doping on the various characteristic of the aforementioned garnets in a different form. This is especially important for ceramics and thin films as most of the scientific data is present only for compounds in powder form. In this research this doping was described as YAG and LuAG garnets in all three forms: powder, thin films and ceramics were synthesized and investigated. Garnets doped with different amounts of boron and/or magnesium were synthesized by the sol-gel method. The coatings were synthesized using the sol-gel spin and dip-coatings methods on different quartz and sapphire substrates and ceramics were obtained using hydrostatic pressure. Crystal structure of the samples was analyzed by means of X-ray diffraction (XRD). Morphology of the compounds was evaluated using scanning electron microscopy (SEM) and atomic force microscopy (AFM). Luminescence properties such as emission, excitation, decay time, quantum efficiency and temperature dependency of emission intensity have been investigated. Radioluminescence was also measured in order to determine the scintillation properties of the samples. The positive impact of boron addition into the garnet structure on the luminescence properties will be discussed in detail.

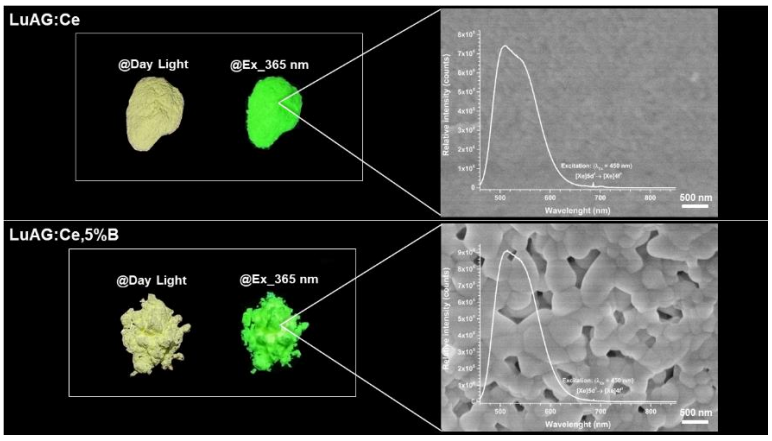


Fig. 1. Boron doping effect on particle size and emission intensity for LuAG samples [5].

ACKNOWLEDGEMENTS:
This research is funded by the European Social Fund under the No 09.3.3- LMT K-712 " Development of Competences of Scientists, other Researchers and Students through Practical Research Activities" measure.

[1] I.P. Machado, V.C. Teixeira, C.C.S. Pedroso, et. al., X-ray scintillator Gd2O2S:Tb3+ materials obtained by a rapid and cost-effective microwave-assisted solid-state synthesis, Journal of Alloys and Compounds **777**, 638 – 645 (2019).
[2] C. Foster, Y. Wu, M. Koschan, et. al., Boron Codoping of Czochralski Grown Lutetium Aluminum Garnet and the Effect on Scintillation Properties, Journal of Crystal Growth **486**, 126 – 129 (2018).
[3] M. Lucchini, O. Buganov, E. Auffray, et. al., Measurement of non-equilibrium carriers dynamics in Ce-doped YAG, LuAG and GAGG crystals with and without Mg-codoping, Journal of Luminescence **194**, 1 – 7 (2018).
[4] D. S. McGregor, Materials for Gamma-Ray Spectrometers: Inorganic Scintillators, Annual Review of Materials Research **48**, 254-277 (2018).
[5] G. Inkrataite, M. Kemere, A. Sarakovskis, R. Skaudzius, Influence of boron on the essential properties for new generation scintillators, Journal of Alloys and Compounds **875**, 160002 (2021).

STRUCTURAL, MORPHOLOGICAL, AND MAGNETIC INVESTIGATION OF VARIOUS PEROVSKITE-TYPE SOLID SOLUTIONS

Dovydas Karoblis[1], Aleksej Žarkov[1], Ramūnas Diliautas[1], Kęstutis Mažeika[2], Dalis Baltrūnas[2], Gediminas Niaura[3], Martynas Talaikis[4], Edita Garškaitė[5], Aldona Beganskienė[1], Aivaras Kareiva[1]

[1] Institute of Chemistry, Vilnius University, Lithuania
[2] Center of Physical Sciences and Technology, Vilnius, Lithuania
[3] Institute of Chemical Physics, Faculty of Physics, Vilnius University, Lithuania
[4] Department of Bioelectrochemistry and Biospectroscopy, Institute of Biochemistry, Life Sciences Center, Vilnius University, Lithuania
[5] Wood Science and Engineering, Department of Engineering Sciences and Mathematic, Luleå University of Technology, Sweden
dovydas.karoblis@chgf.stud.vu.lt

Perovskites are a large group of materials with the general formula ABX_3 (A and B – different size cations, X – anion). Various elements can occupy either A, B, or X sites, which can influence the structure and physical properties. The ideal structure of perovskite compounds is cubic lattice, but many oxides have slightly distorted ones with lower symmetry, like hexagonal, tetragonal, etc. Variety in both structures and chemical compositions leads to large variation in physical properties, like ferroelectricity, electrical conductivity, magnetism, catalytic properties, etc [1]. Multiferroicity is another extensively researched characteristic of perovskite-type materials [2]. Although many multiferroic perovskites are known, there still remain many challenges in this field: magnetism control via electric field with smaller voltages, the need for a wider array of compounds, which could exhibit magnetoelectric and multiferroic behavior at room temperature [3].

In this work, we investigated three different solid solutions series: $Y_xGd_{1-x}Mn_{0.97}Fe_{0.03}O_3$ [4], $Y_{1-x}Gd_xFeO_3$ [5], and $Bi_{1-x}Gd_xFe_{0.85}Mn_{0.15}O_3$. The sol-gel synthetic method was successfully employed for the preparation of the perovskite-type compounds. A combination of various characterization techniques, including X-Ray diffraction, FT-IR, Raman, and Mösbauer spectroscopies, revealed that structure depends on chemical composition. For $Y_xGd_{1-x}Mn_{0.97}Fe_{0.03}O_3$ samples, three separate structural regions (hexagonal, mixture of hexagonal and orthorhombic, and orthorhombic) can be seen, while $Y_{1-x}Gd_xFeO_3$ compounds have an orthorhombic structure with two different space groups. A trigonal, mixture of orthorhombic and trigonal, and orthorhombic unit cells was observed for $Bi_{1-x}Gd_xFe_{0.85}Mn_{0.15}O_3$ solid solutions. Surface morphology and particle size were evaluated by applying scanning electron microscopy (SEM). In most cases, samples consisted of uniform nanosized particles, which were necked to each other forming larger agglomerates. Generally, the formation of solid solution led to particle size increase and largest particles of 100-900 nm size interval were observed for $BiFe_{0.85}Mn_{0.15}O_3$ compound. Paramagnetism was observed for $Y_xGd_{1-x}Mn_{0.97}Fe_{0.03}O_3$ and $Bi_{1-x}Gd_xFe_{0.85}Mn_{0.15}O_3$ solid solutions, while $Y_{1-x}Gd_xFeO_3$ demonstrated ferromagnetic behavior at room temperature.

Acknowledgments. This work was supported by a Research grant BUNACOMP (No. S-MIP-19-9) from the Research Council of Lithuania.

[1] T. Ishihara, *Perovskite Oxide for Solid Oxide Fuel Cells, Fuel Cells and Hydrogen Energy*. (Springer Science & Business Media, 2009).
[2] M.V. Vopson, Fundamentals of multiferroic materials and their possible applications, Critical Reviews in Solid State and Materials Sciences **40 (4)**, 223-250 (2015).
[3] N. A. Spaldin, R. Ramesh, Advances in magnetoelectric multiferroics. Nature materials **18(3)**, 203-212 (2019).
[4] D. Karoblis, A. Zarkov, E. Garskaite et al., Study of gadolinium substitution effects in hexagonal yttrium manganite YMnO3, Scientific Reports **11(1)**, 1-14 (2021).
[5] D. Karoblis, A. Zarkov, K. Mazeika et al., YFeO3-GdFeO3 solid solutions: Sol-gel synthesis, structural and magnetic properties, Solid State Sciences **118**, 106632 (2021).

THREE-DIMENSIONAL Au(NiMo)/Ti CATALYSTS FOR EFFICIENT OXYGEN EVOLUTION

Sukomol Barua, Aldona Balčiūnaitė, Loreta Tamašauskaite-Tamašiūnaitė, Eugenijus Norkus

Department of Catalysis, Center for Physical Sciences and Technology,
Saulėtekio av. 3, LT-10257 Vilnius, Lithuania
sukomol.barua@ftmc.lt

Water splitting in the alkaline electrolytes is a promising technology for large-scale hydrogen production, although kinetically very sluggish due to the multi-electron transfer mechanism of oxygen evolution reaction (OER) and thermodynamics. Albeit the noble metals are capable to overcome those limitations and barriers by achieving much lower overpotential, but their scarcity proves them economically infeasible. Thus, developing and designing low-cost, highly active, and stable non-noble metal electrocatalysts is still a core issue but of great challenge.

Here, we report a catalyst constructed via widely used electrodeposition method by using Ni and Mo bimetallic system supported on Ti surface and decorated with very low Au-crystallites by galvanic displacement. It was found that the Au-loadings were 1.8, 2.3, and 3.9 $\mu g_{Au} cm^{-2}$ on the prepared Au(NiMo)/Ti catalysts. The prepared catalysts' morphology, structure, and composition were examined using Field Emission Scanning Electron Microscopy, Energy Dispersive X-ray Analysis, and Inductively Coupled Plasma Optical Emission Spectroscopy. The investigation of the electrocatalytic properties of the prepared catalysts was performed by recording linear sweep voltammograms in 1M NaOH solution at a potential scan rate of 10 mVs^{-1} at 25-75ºC temperature range. Obtained results revealed that the decoration of the Ni-Mo-based binary alloy with Au nanoparticles allows enhancing catalytic activity for the oxygen evolution from 1.2 up to 3.2 times in the range of 25-75ºC, compared with those of the bare Ni-Mo system.

Acknowledgment

This project has received funding from European Social Fund (project No 09.3.3-LMT-K-712-19-0138) under a grant agreement with the Research Council of Lithuania (LMTLT).

COMBINED RAMAN SPECTROSCOPY AND BROAD RANGE DENSITY FUNCTIONAL THEORY ANALYSIS OF INOSITOL PHOSPHATES AND THEIR CONFORMATIONS

Wojciech Marciniak[1,2], Joanna Marciniak[2], Jonasz Łasut-Balcerzak[1], Karolina Olszewska[3], Arkadiusz Ptak[1]

[1]Institute of Physics, Poznań University of Technology, Piotrowo 3, 61-139 Poznań, Poland
[2]Institute of Molecular Physics, Polish Academy of Sciences, Smoluchowskiego 17, 60-179 Poznań, Poland
[3]Institute of Materials Research and Quantum Engineering, Poznań University of Technology, Piotrowo 3, 61-139 Poznań, Poland
wojciech.robe.marciniak@doctorate.put.poznan.pl

There is a considerable amount of inositol phosphates in living cells. They fulfil regulatory purposes in general, with lower inositol phosphates constituting a part in the metabolic cycle of beans, grain, legumes, and other plants [1]. Myo-inositol hexakisphosphate along with myo-inositol trispyrophosphate are considered good candidates for allosteric effectors of hemoglobin, promising in treating hypoxia [2].

Despite their undeniable importance in living organisms, only a few recent studies discuss physical and chemical properties related to the evolution of their electronic structure, charge density, protonation state, and conformation relative to each other and in a changing environment. The goal of the presented research is to derive a robust model of inositol phosphates in different conformations and isomeric forms for MD analysis in order to resolve exact mechanisms of interaction with hemoglobin, suppressor protein PTEN [3] and their red blood cell membrane permeation, which is known to be highly selective [4].

In the presented study, all possible inositol phosphates conformations are studied using the density functional theory. Theoretical calculations of conformational space of varying protonation states in standard generalized gradient approximation methods (in the parametrization of Perdew, Burke, and Ernzerhof if applicable) are compared with Raman spectra of the molecules. In order to tailor parameters needed in MD models, the most important phosphate derivatives of inositol are reconsidered using combinations of mixed potentials - PBE and revPBE exchange with LMKLL and BLYP correlation parts utilizing *Siesta* code.

The models are utilized to obtain binding energies by a classical docking procedure using the Autodock package.

The work has been funded by Polish Ministry of Science and Higher Education under the grant DI2017/007947 in the Diamont Grant programme 2018 edition. We want to thank Marian W. Radny for valuable insights and suggestions.

[1] Frank, A. (2013). Chemistry of plant phosphorus compounds. Elsevier.

[2] Kieda C., Greferath R., Silva C.C.D., Fylaktakidou K.C., Lehn J.M. and Nicolau C. Suppression of hypoxia-induced HIF-1α and of angiogenesis in endothelial cells by myo-inositol trispyrophosphate-treated erythrocytes. PNAS, 103 (42) 15576 (2006). doi:10.1073/pnas.0607109103.

[3] Kieda C., Hafny-Rahbi B.E., Collet G., Lamerant-Fayel N., Grillon C., Guichard A., Dulak J., Jozkowicz, A., Kotlinowski J., Fylaktakidou K.C., Vidal A., Auzeloux P., Miot-Noirault E., Beloeil J.C., Lehn J.M. and Nicolau C. Stable tumor vessel normalization with pO2 increase and endothelial PTEN activation by inositol trispyrophosphate brings novel tumor treatment. Journal of Molecular Medicine, 91 (7) 883 (2013). doi:10.1007/s00109-013-0992-6.

[4] Fylaktakidou K.C., Lehn J.M., Greferath R. and Nicolau C. Inositol tripyrophosphate: a new membrane permeant allosteric effector of haemoglobin. Bioorganic & Medicinal Chemistry Letters, 15 (6) 1605 (2005). doi:10.1016/j.bmcl.2005.01.064.

THE BACTERIAL POPULATION IN DRAINAGE WATER FROM TAILINGS POND IN HODRUŠA-HÁMRE (SLOVAKIA)

Veronika Prepilková[1], Katarína Trnková[2], Juraj Poništ[1*]

[1] Department of Environmental Engineering, Technical University in Zvolen, Slovakia
[2] Department of Environmental Management, Matej Bel University, Slovakia
jurajponist1111@gmail.com

As a result of gold ore mining, a tailings pond was built in the Hodruša-Hámre village (central Slovakia) to store flotation waste. Drainage water from the tailings pond is a source of contamination of local stream not only with sulphates, but also with heavy metals, especially Mn, Zn and Pb [1].

Such water is often inhabited by unique groups of microorganisms. Due to their properties (resistance to heavy metals, bioaccumulation) they could be usable in biotechnologies e.g. for metal recovery or remediation. The aim of the work was to characterize the composition of the bacterial population of drainage water from the tailings pond.

Drainage water sample was collected directly from the water flowing out of tailings pond in Hodruša-Hámre. 100 ml of water was taken into sterile bottle. The water was transported under cold, dark conditions to the laboratory. 1 ml of drainage water was spread directly onto Petri dishes with nutrient agar and cultivated at 25 °C for 48 hours. By sequential isolation four morphologically different pure cultures were obtained.

A sample for extraction by MALDI-TOF mass spectrometry was prepared from the 24-hour pure culture. Samples were prepared according to the procedure of a MALDI Biotyper (Bruker Daltonik). The measured spectra were compared with the BDAL, Listeria spectral library.

Isolate 1 could not be reliably identified. The most similar was the genus *Aeromonas* sp. Isolate 2 was reliably identified only at the genus level as *Aeromonas* sp., at the species level probably as *Aeromonas hydrophila*. Isolate 3 was also reliably identified at the species level as *Lysinibacillus fusiformis*. Isolate 4 was reliably identified only at the genus level as *Bacillus* sp., probably *Bacillus cereus*. The results indicate that representatives of at least three different genera are present in the drainage water.

The use of some identified species in biotechnology has been documented. In study [2] a strain of *Aeromonas hydrophila* (isolated from industrial effluent) was capable of efficiently degrading triarylmethane dyes. Another research [3] examined potential of *Aeromonas hydrophila* to remove insecticide from the soil under various growing conditions.

Gupta et al. [4] observed the sequestration and volatilization of mercuric ions by *Lysinibacillus* sp. It was confirmed that *Lysinibacillus fusiformis* was able to tolerate 5 ppm concentration of all the heavy metals by showing visible growth on surfaces of nutrient agar Petri plates and possess the capacity to biosorption of Pb, Cr, Cd and Ni and can be developed as biosorption agent for these heavy metals [5]. It was reported ability of *Bacillus cereus* to biosorption of lead [6]. Hasan et al. [7] confirmed capability of *Bacillus cereus* to simultaneous biosorption of Pb and Mn.

There is a possibility of using bacteria in the drainage water for the tailings pond remediation and reducing its negative impact on surface water, at least in concentrations of Mn and Pb. This should be the subject for further research.

[1] P. Bajtoš, E. Mašlár, I. Mašlárová et al., Vplyv ťažby nerastov na životné prostredie Správa za rok 2020 (Spišská Nová Ves, 2020).
[2] CH. J. Ogugbue, T. Sawidis, Bioremediation and Detoxification of Synthetic Wastewater Containing Triarylmethane Dyes by Aeromonas hydrophila Isolated from Industrial Effluent, Biotechnology Research International 2011, 1-11 (2011).
[3] S. S. Mohammed, A. M. Fadhil, H. R. Kifah, Bioremediation of Chlorpyrifos Insecticide by using Aeromonas Hydrophila Bacteria, Indian Journal of Forensic Medicine and Toxicology 15 (2), 1299-1384 (2021).
[4] S. Gupta, R. Goyal, J. Nirwan et al., Biosequestration, Transformation, and Volatilization of Mercury by Lysinibacillus fusiformis Isolated from Industrial Effluent, Journal of Microbiology and Biotechnology 22 (5), 684-689 (2012).
[5] A. M. Jibrin, O. A. Oyewole, S. K. Okeke et al., Heavy metals biosoprtion by Lysinibacillus fusiformis 5B, Annual International Conference held at Institute of Agriculture and Training (I.A.R.& T) Moor Plantation, Apata Ibadan, Nigeria (2021).
[6] S. Murthy, G. Bali, S. K. Sarangi, Biosorption of Lead by Bacillus cereus Isolated from Industrial Effluents, Biotechnology Journal International 2 (2), 73-84 (2012).
[7] H. A. Hasan, S. R. S. Abdullah, N. T. Kofli et al., Interaction of environmental factors on simultaneous biosorption of lead and manganese ions by locally isolated Bacillus cereus, Journal of Industrial and Engineering Chemistry 37, 295-305 (2016).

ENHANCEMENT AND REVERSION OF IRREVERSIBLE ELECTROPORATION VIA OSMOTIC SHOCK TREATMENT

Greta Gančytė[1], Povilas Šimonis[1], Arūnas Stirkė[1]

[1] Laboratory of Bioelectrics, Center for Physical Sciences and Technology, Lithuania
greta.gancyte@gmail.com

Saccharomyces cerevisiae yeast adapted to employ HOG pathway to recover after dangerous shape modifications and intracellular water disbalance caused by environmental osmotic pressure changes [1]. Pulsed electric field (PEF) treatment is known to cause plasma membrane permeabilization, an effect known as electroporation, yet at the moment there is no information on whether HOG biochemical pathway has a role in yeast response to PEF treatment [2].

It was investigated if post-PEF osmotic pressure change of the media has any effect on yeast cells' viability and size and if HOG pathway is involved in recovery. Experiments were performed with wild type Y00000 yeast and a mutant strain derived from WT, Y02724, with no active *HOG1* gene. Cells were grown until 1OD, transferred to electroporation buffer (20 mM TRIS, 1 M sorbitol, pH = 7.4), yeast suspension was exposed to single electric field pulse with duration of 150 µs and field strength of up to 10 kV/cm. Electroporation buffer was used as a reference point to represent isoosmotic conditions. Swift osmotic pressure change is defined as osmotic shock. After PEF treatment cells were immediately transferred to hyperosmotic (1.5/2 M sorbitol), isoosmotic or hypoosmotic (0.1/0.5 M sorbitol) solution, incubated for 5 minutes and plated on solid YPD media. After two days of incubation in 30 °C CFU were counted. Cell size was calculated by measuring the turbidity of the solution after 10 seconds and 30 minutes of osmotic shock treatment [3].

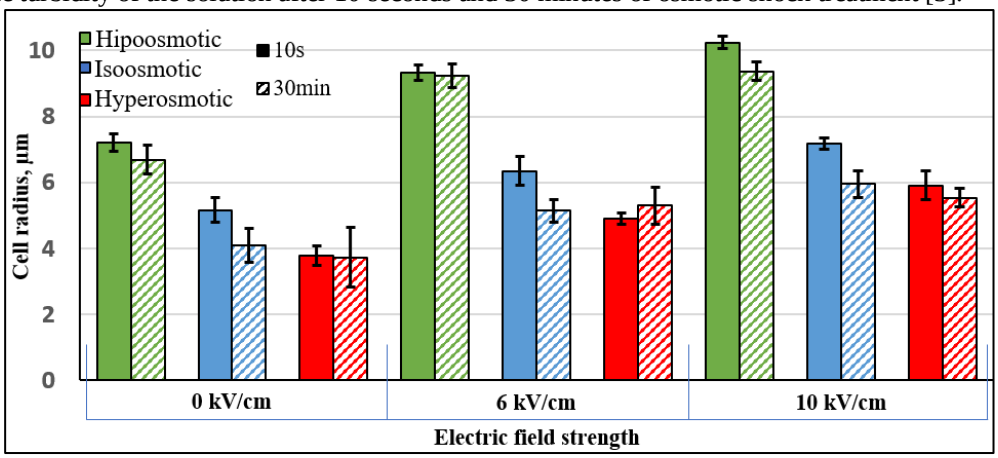


Fig. 1. WT yeast cell radius dependance on field strength and osmotic shock treatment after PEF. Measurements taken 10 s after treatment are depicted in solid fill; 30 min – striped fill. Hipoosmotic (0.1 M sorbitol), isoosmotic (1 M sorbitol) and hyperosmotic (2 M sorbitol) treatment is depicted in green, blue and red colours respectively.

It was shown that post-pulsed electric field treatment by sudden change of osmolarity of the media has a significant impact on the yeasts' viability, cell size and leakage of intacellular components into the media when compared to isoosmotic conditions. Thus we show that electroporation efficiency is not only dependent on electric field strength, duration and the number of impulses applied, but also on whether post-PEF treatment was applied. While it is known that electric fields of 8-10 kV/cm causes irreversible damage to membrane, after incubation in hyperosmotic conditions after PEF viability increased by ~20-30% and radius of the cell was reduced by as much as ~2 µm (Fig.1) After weaker field strengths of 2 and 4kV/cm PEF and hyperosmotic shock treatment viability of WT yeasts was restored to 100%, for Δ*hog* such result was achieved only after 2 kV/cm treatment. Hipoosmotic shock, evidently, caused the opposite effect: after 4 kV/cm viability decreased by 12% (WT) and 39% (Δ*hog*); after 6 kV/cm by 16% and 25%. The size of the cells increased almost two times, after 10 kV/cm field (Fig.1)

Protein and thiol group concentration evaluation revealed that amount of intracellular compounds in the media decreased after hyperosmotic shock and increased after hipoosmotic shock, supporting the hypothesis that mechanical cell shape alteration influences cells' reaction to PEF. Furthermore, Δ*hog* strain was more sensitive to beforementioned treatments suggesting that HOG pathway is of relevance to recovery after electroporation.

To summarise, yeast cell viability and size after exposure to PEF can be altered by subsequent change in osmolarity of media. HOG pathway involvement was linked to recovery after electroporation.

[1] S. Hohmann, "Control of high osmolarity signalling in the yeast Saccharomyces cerevisiae", FEBS Lett. 17;583(24):4025-9, (2009)
[2] A. Stirke, R. Celiesiute-Germaniene, A. Zimkus, N. Zurauskiene, P. Simonis, A. Dervinis, A. Ramanavicius, and S. Balevicius, "The link between yeast cell wall porosity and plasma membrane permeability after PEF treatment." Scientific reports vol. 9,1 14731, (2019)
[3] Melik, D. H., & Fogler, H. S. (1983). Turbidimetric determination of particle size distributions of colloidal systems. Journal of Colloid And Interface Science, 92(1), 161–180

HUMAN DERMAL MESENCHYMAL STEM CELLS AS NANOPARTICLES VEHICLES

Alėja Marija Daugėlaitė[1,2], Greta Jarockytė[1,2], Artiom Skripka[3], Vilius Poderys[1], Vitalijus Karabanovas[1,4], Fiorenzo Vetrone[3], Ričardas Rotomskis[1,5]

[1] Biomedical Physics Laboratory of National Cancer Institute, Vilnius, Lithuania
[2] Life Sciences Center, Vilnius University, Vilnius, Lithuania
[3] Centre Énergie, Matériaux et Télécommunications, Institut National de la Recherche Scientifique, Université du Québec, Varennes, QC, Canada
[4] Department of Chemistry and Bioengineering, Vilnius Gediminas Technical University, Vilnius, Lithuania
[5] Biophotonics group of Laser Research Centre, Vilnius University, Vilnius, Lithuania
aleja.daugelaite@nvi.lt

Oncological diseases remain a major problem worldwide. There is still no effective method for detecting cancer at an early stage, and the treatments currently on the market are non-specific and cause side effects. One solution is to use mesenchymal stem cells (MSCs) in combination with upconverting nanoparticles (UCNPs). UCNPs are small in size, have low toxicity and, due to their photoluminescent properties, could be used as fluorophores in cancer diagnostics and treatment [1]. However, only a small fraction of nanoparticles reaches cancer cells due to their low specificity and microenvironmental effects. MSCs have great potential in the field of medicine due to their regenerative properties, their anti-tumour efficacy and their migration towards inflammation and cancer due to chemokine stimulation. Because of these MSCs properties, they could be used as "Trojan horses" to deliver nanoparticles directly to the tumour. Therefore, combining stem cells with UCNPs could lead to an innovative approach to cancer theranostics – therapy combined with diagnostics [2].

The aim of the study was to investigate the *in vitro* properties and theranostic potential of upconverting nanoparticles and mesenchymal stem cells. In our study, we investigated upconverting nanoparticles with an embedded photosensitizer chlorin e_6 (Ce_6) (UCNPs-Ce_6). Along with that, we used chlorine-free UCNPs as controls. Different excitation wavelengths produce different effects – 980 nm excitation produces a therapeutic effect, while 793 nm excitation produces photoluminescence in the near-infrared part of the spectrum, which is suitable for diagnostics. The irradiation used to excite the UCNPs (λ_{ex} = 980 nm and λ_{ex} = 793 nm) falls within the optical tissue transparency window (650-1300 nm). This light is more penetrating in biological tissues, allowing it to reach deeper tissues without damaging them.

Intracellular accumulation of upconverting nanoparticles in MSCs and human breast cancer cell lines MCF-7, MDA-MB-231 was demonstrated using confocal microscopy. In addition, the cytotoxicity of the nanoparticles was assessed using the lactate dehydrogenase (LDH) cytotoxicity test. A wound healing assay was also used to demonstrate MSCs migration after incubation with UCNPs. Finally, the potential efficacy of photodynamic effect of UCNPs-Ce_6 was investigated. After irradiation with 980 nm laser light, the cells were stained with the fluorescent viability dyes calcein AM and propidium iodide.

Our results demonstrated that UCNPs and UCNPs-Ce_6 accumulate inside MSC, MCF-7, MDA-MB-231 cells and localize in endocytic vesicles, especially around the nucleus. This pattern of nanoparticles accumulation in cells is common for all endocytic pathways, including UCNPs [1]. Moreover, we showed that both UCNPs and UCNPs-Ce_6 are non-toxic for MSC, MCF-7, MDA-MB-231 cells when cells are incubated with nanoparticles in the dark for up to 24 h. A wound healing assay demonstrated that intracellular accumulation of UCNPs does not affect the migration of MSCs towards the scratch. Additionally, our results showed that UCNPs-Ce_6 accumulated in cells and irradiated with 980 nm laser excitation has a significant phototoxic effect on cells, while UCNPs alone are non-toxic.

Overall, MSCs combined with upconverting nanoparticles show great potential in cancer theranostics.

[1] E. Voronovic, A. Skripka, G. Jarockyte, et al., Uptake of Upconverting Nanoparticles by Breast Cancer Cells: Surface Coating versus the Protein Corona, ACS Appl. Mater. Interfaces 13, 39076–39087 (2021).
[2] D. Dapkute, M. Pleckaitis, D. Bulotiene, et al., Hitchhiking Nanoparticles: Mesenchymal Stem Cell-Mediated Delivery of Theranostic Nanoparticles, ACS Appl. Mater. Interfaces 13, 43937–43951 (2021).

BYSTANDER EFFECT TRIGGERED BY CALCIUM ELECTROPORATION, BLEOMYCIN ELECTROTRANSFER AND IRREVERSIBLE ELECTROPORATION

Neringa Barauskaitė[1], Paulius Ruzgys[1], Vitalij Novickij[2], Saulius Šatkauskas[1]

[1] Biophysical Research Group, Faculty of Natural Sciences, Vytautas Magnus University, Lithuania
[2] Institute of High Magnetic Fields, Vilnius Gediminas Technical University, Naugarduko st. 4103227, LT-10224 Vilnius, Lithuania
neringa.barauskaite@vdu.lt

Electroporation is a method used for local cancer therapy in a form of electrochemotherapy or electroablation [1]. The mechanism of electrochemotherapy is triggered by the process of reversible electroporation; when high intensity electric field increase transmembrane potential of affected cells to a critical value. This triggers the formation of hydrophilic pores in the cellular membrane and act as a bridge between cytosol and extracellular matrix for various hydrophilic substances such as calcium ions or anticancer drug bleomycin [2]. If the transmembrane potential is much higher than the electroporation threshold, then the process of irreversible electroporation occurs, hence triggering anticancer treatment of electroablation. The use of such treatment initiate affected cell death as a result of triggered irreversible changes in cell plasma membrane [3]. Both therapies share similarities with another method that has been applied in cancer therapy – radiotherapy. The main mechanism of those treatments is based on the generation of reactive oxygen species (ROS) in the targeted tissue, resulting in multiple genomic DNA breaks that may lead to cell death.

It is known that irradiated cells at lethal doses does secrete signaling molecules that affect adjacent unirradiated cells. This phenomenon is termed as the "Bystander effect" [4]. Although, the "Bystander effect" is well-known in radiotherapy, it has not been researched in the process of electrochemotherapy. According to our resent publication, intracellular electrotransfer of bleomycin into the targeted cells result in decrease of viability on the directly unaffected adjacent cells. Controversially, irreversible electroporation on the targeted cells has a positive impact to the viability of directly unaffected adjacent cells [5].

Further investigation of these inverse phenomena of Bystander effect after bleomycin electrotransfer and irreversible electroporation led to the combination of these processes. Therefore, the aim of this study is to evaluate the "Bystander effect" when combining $CaCl_2$ electrotransfer, irreversible electroporation and electrotransfer of anticancer drug bleomycin.

Mouse breast cancer cell line (4T1) was used for the presented experiments. Electric fields were generated with BTX T820 system. Stainless steel plate electrodes with 2 mm gap were used. Laboratory-made electroporation buffer (Na2HPO4 5.59 mM, NaH2PO4 3.00 mM, MgCl2 1.73 mM, sucrose 242.2 mM) at conductivity of 0.1 S/m was used. To obtain CaCl2 and bleomycin electrotransfer one 100 μs duration and 1400 V/cm amplitude pulse was applied. In the case of irreversible electroporation the amplitude was raised 2 times to 2800 V/cm. The cells after electroporation were incubated in a 24-well plate for 10 minutes, then a 0.2 ml RPMI growth medium was added and incubated for 48 hours. Afterwards the media was removed and put on untreated cells to measure the formation of colonies.

The results showed that bystander effect is present when media from effected cells is transferred on the unaffected cells. Bleomycin electrotransfer triggered Bystander effect diminished the growth of directly unaffected cells. Similar results were obtained after calcium electrotransfer. An inverse Bystander effect was obtained after application of irreversible electroporation. Nevertheless, the effect is medium dependent. When the media was diluted twice all of the Bystander effects were not present. However, the combination of two bystander effects by adding 50 % of media from cells after bleomycin electrotransfer and 50 % of media from cells after irreversible electroporation had a highly negative impact on cell viability. Similar trends are observed when combining bystander effect after bleomycin electroporation and calcium electroporation.

Funding: This work was supported by grant Nr. S-MIP-19-13 from the Research Council of Lithuania.

[1] Y. Peng, H. Tao, Y. Gao, Y. Yang and Chen, Z., Review and Prospect of Tissue-agnostic Targeted Strategies in Anticancer Therapies, Curr. Top. Med. Chem., **21**, 404–425, 2020.
[2] U. Probst, I. Fuhrmann, L. Beyer and P. Wiggermann, Electrochemotherapy as a new modality in interventional oncology: A review, Technol. Cancer Res. Treat, **17**, 2018.
[3] Melancon, M. P., Gupta, S., Shen, B., Peng, W. et al., Irreversible electroporation reverses resistance to immune checkpoint blockade in pancreatic cancer, Nat. Commun. **10**, 1–14, 2019.
[4] N. Jalal, S. Haq, N. Anwar, S. Nazeer and U. Saeed., Radiation induced bystander effect and DNA damage, J. Cancer Res. Ther., **10**, 819–833, 2014
[5] P. Ruzgys, N. Barauskaitė, V. Novickij, J. Novickij, S. Šatkauskas, The Evidence of the Bystander Effect after Bleomycin Electrotransfer and Irreversible Electroporation, Molecules. **26**, 19, 2021.

THE EFFECT OF STRUCTURE OF TERTIARY AMINE ON THE ACETOLYSIS OF 2-(CHLOROMETHYL)OXIRANE: AB INITIO AND EXPERIMENTAL STUDY

Kseniia Yutilova, Elena Shved

Faculty of Chemistry, Biology and Biotechnologies, Vasyl' Stus Donetsk National University, Ukraine
k.iutilova@donnu.edu.ua

The ring opening of asymmetric oxiranes is an essential class of reactions for obtaining epoxy polymers, biologically active compounds, heterocyclic substances. One of the most widely used asymmetric oxirane in organic synthesis is 2-(chloromethyl)oxirane (epichlorohydrin, ECH) [1]. The ring opening of ECH is performed with proton-donating nucleophiles such as carboxylic acids in the presence of catalysts (Fig. 1). The effective catalysts of ECH acidolysis are tertiary amines (R_3N). The opening of asymmetric ring of ECH leads to formation of two products, however, the major ("normal") products only are able for the further cyclization into the glycidyl esters, which are the monomers of epoxy resins. According to that, the selection of effective and regioselective catalysts for the reaction is a challenge of a great research and practical interest [2].

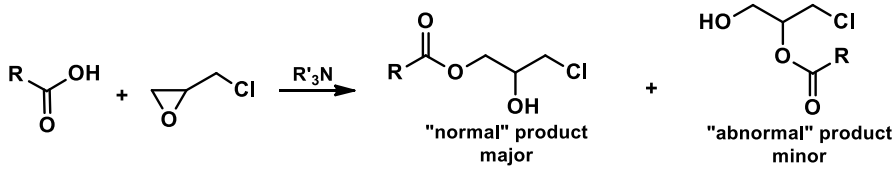


Fig. 1. Catalytic ring opening of 2-(chloromethyl)oxirane with carboxylic acids.

The objective of the study is to establish the effect of the substituents in the tertiary amine on the kinetic law and regioselectivity of the oxirane ring opening with acetic acid. To achieve this objective, the research was divided into two parts: theoretical, which includes quantum chemical modelling of the ECH ring opening with tertiary amines $Me_nEt_{3-n}N$ (Me_3N, Me_2EtN, $MeEt_2N$, Et_3N), and experimental, which consists of ECH reaction with acetic acid (AcOH) in the presence of R_3N (R_3 = Et_3, *n*-Bu_3, *n*-Oct_3, *n*-Oct_2Me). The computation was performed by the density functional theory (DFT) method with the B3LYP basic set in the gas phase. Acetolysis of ECH was conducted at 333 K under condition of the excess of ECH in a binary solvents ECH : tetrahydrofuran (THF) and ECH : nitrobenzene (NB) (50% vol. ECH).

The transition states of the reaction of ECH with $Me_nEt_{3-n}N$ were localized by quantum chemical modelling (Fig. 2). It was shown that the activation barriers increase with addition of more steric hindered substituents to the nitrogen atom, so the computed rate of interaction rises in the presence of less substituted amines (Et_3N < $MeEt_2N$ < < Me_2EtN < Me_3N).

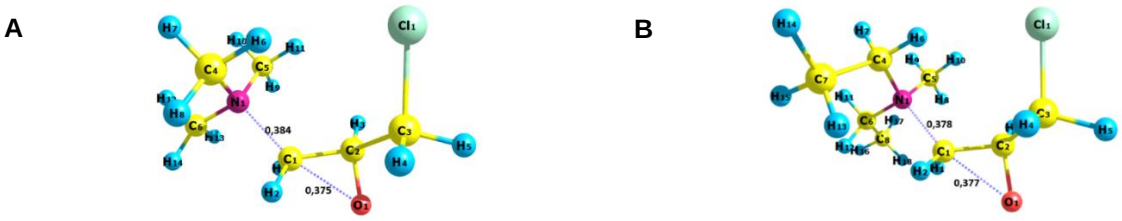


Fig. 2. Structures of the localized transition states on the reaction pathway of ECH with: A – Me_3N; B – $MeEt_2N$, DFT B3LYP/6-31+G**, gas phase, 298,15 K.

The kinetic law of the experimental reaction of acetolysis of ECH was investigated, the order of the reaction was established as zeroth by AcOH and first by R_3N. The catalytic activity of tertiary amines in the reaction of ECH with acetic acid grows in the rows: Oct_3N < Bu_3N < Et_3N < $MeOct_2N$ (binary solvent ECH : THF) and Oct_3N < Bu_3N < < $MeOct_2N$ ≈ Et_3N (binary solvent ECH : NB), that is in agreement with the results of the quantum chemical modelling. The correlation analysis of the effect of amine structure on the catalytic activity revealed that the reaction rate is most sensitive to the change of nucleophilicity of R_3N. It was established that the regioselectivity of the acetolysis of ECH in the presence of tertiary amines is weakly dependent on the structure of amine but slightly increases in more polar solvent (ECH : THF < ECH < ECH : NB). The obtained results of the complex studies allow to propose the mechanism of transfer of nucleophilic reagent anion by an ion pair for the oxirane ring opening by carboxylic acids.

[1] Yu. Bespalko, E. Shved, Experimental and theoretical study on the kinetics and mechanism of the amine-catalyzed reaction of oxiranes with carboxylic acids. Reaction Kinetics, Mechanisms and Catalysis **126**, 903–919 (2019).
[2] S. Bakhtin, Yu. Bespalko, E. Shved et al., Detailing the elementary stages in the oxirane ring opening reactions with carboxylic acids catalyzed by tertiary amines, J Phys Org Chem. **33**, e4071 (2020).

SYNTHESIS AND STRUCTURE OF {[Zn(HL)$_2$] × 4 DMF}$_n$ (H$_2$L = 2,2′-diaminobiphenyl-4,4′-dicarboxylic acid)

Milica G. Bogdanović[1], Nikola D. Radnović[1], Marko V. Rodić[1]

[1] University of Novi Sad, Faculty of Sciences, Department of Chemistry, Biochemistry and Environmental Protection, Trg Dositeja Obradovića 3, 21000 Novi Sad, Serbia.
dh.milica.bogdanovic@student.pmf.uns.ac.rs

A new coordination polymer, {[Zn(HL)$_2$] × 4 DMF}$_n$, has been synthesized under mild solvothermal conditions by the reaction of $ZnCl_2$ with ligand 2,2′-diaminobiphenyl-4,4′-dicarboxylic acid in presence of formic acid, in *N*,*N*-dimethylformamide (DMF) at 100 °C for 48 h. The colorless needle-shaped single crystals thus obtained were suitable for X-ray crystallographic measurements. The compound was additionally characterized by IR spectroscopy.

The asymmetric unit (Fig. 1) is composed of one Zn(II) atom, one ligand molecule and two uncoordinated DMF molecules. Ligand is coordinated in a monoanionic form as *ONN* tridentate, and acts as a bridging ligand linking two atoms of Zn(II). To one Zn(II) atom the ligand is coordinated through oxygen atom from deprotonated carboxylic group, while it binds second Zn(II) atom through both amino nitrogen atoms, thus forming a seven-membered chelating ring (Fig. 2). Each Zn(II) is coordinated by four nitrogen atoms that form the equatorial plane and two oxygen atoms that occupy the axial positions of the octahedrally shaped coordination polyhedron. The slightly distorted octahedral environment is indicated by different bond lengths as equatorial bonds Zn1–N1 [2.183(2) Å], and Zn1–N1′ [2.189(3) Å] are significantly longer than the axial Zn1–O2 [2.0817(19) Å] bond. Coordination polymer molecules extend along the *b*-axis direction and form layers parallel to the (−1 0 1) plane, while interleaved are layers filed with molecules of DMF (Fig. 3). Interlayer hydrogen bonds are observed between DMF and ligand molecules.

The data were collected on Gemini R Ultra (Oxford Diffraction) using Mo *Kα* radiation. The structure was solved using *SHELXT* [1] and refined by full matrix least square methods on F^2 using *SHELXL* [2] and *ShelXle* as a graphical user interface [3]. *Crystallographic data:* $C_{44}H_{58}N_8O_{12}Zn$, M_r = 956.36, monoclinic crystal system, space group $P2_1/n$, a = 11.3914 (13) Å, b = 8.8086 (6) Å, c = 22.691 (3) Å, β = 99.388 (11)°, V = 2246.3 (4) Å^3, Z = 2, R = 0.053, $wR(F^2)$ = 0.113, S = 1.04, for 303 parameters and 4574 reflections.

This research was supported by the Science Fund of the Republic of Serbia, PROMIS, #6066708, CASCH-MOF.

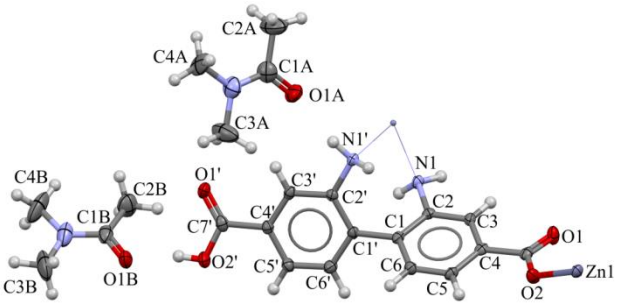


Fig. 1. The asymmetric unit of {[Zn(HL)$_2$] × 4 DMF}$_n$ complex.

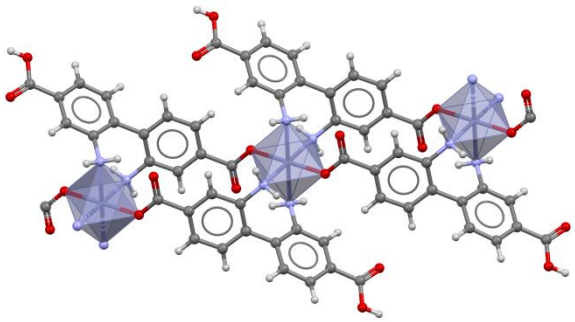


Fig. 2. Fragment of polymer structure [Zn(HL)$_2$]$_n$ shown from the perspective of one zinc atom.

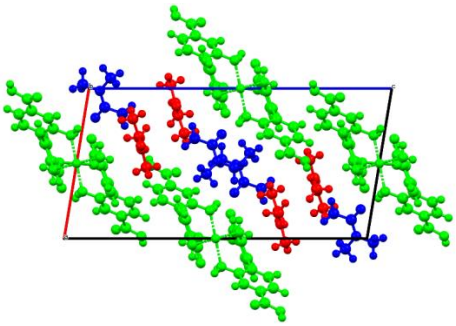


Fig. 3. Crystal packing of coordination polymers and DMF in layers.

[1] G. M., Sheldrick, SHELXT – Integrated space-group and crystal-structure determination, Acta Crystallographica Section A, **71**(1), 3–8 (2015).
[2] G. M., Sheldrick, Crystal structure refinement with SHELXL, Acta Crystallographica Section C, **71**(1), 3–8 (2015).
[3] C. B., Hübschle, G. M., Sheldrick, B., Dittrich, ShelXle: a Qt graphical user interface for SHELXL, Journal of Applied Crystallography, **44**(6), 1281–1284 (2011).

CORRELATION STUDY OF 5-YEARS SUBMICRON ORGANIC AEROSOLS WITH TEMPERATURE IN THE RURAL ENVIRONMENT

Touqeer Gill[1], Julija Pauraitė[1], Steigvilė Byčenkienė[1] and Kristina Plauškaitė[1]

[1] Center for Physical Sciences and Technology, Vilnius, Lithuania
touqeer.gill@ftmc.lt

Aerosol particles affect the climate directly modifying the global radiation budget by scattering and absorbing solar and terrestrial energy. Furthermore, they have negative impact on human health, reduce visibility, and act as a cloud condensation nucleus (CCNs). Therefore, it is crucial to understand the influence of temperature on aerosols chemical composition [1].

Correlation of organic and inorganic aerosol compounds with ambient temperature were analysed in Rūgšteliškis (Lithuania) rural environment. The analysis of 5 years (2013, 2014, 2016, 2018 and 2019) data series was performed for 3 seasons (spring, summer and autumn). Correlation coefficients between organics (Org) and daily averaged temperature in spring 2014, 2016, 2018 and 2019 are presented in Fig. 1 and in Table 1. The varied colors in Table 1 indicated the intensity of the correlation coefficient, such as red (strong correlation), green (moderate correlation), and blue (no correlation). It can be seen, that in spring and summer there is a strong positive correlation between Org and temperature but only a moderate correlation in the autumn. Furthermore, the correlation of Org with temperature in all the 3 seasons varies within different years, for instance, in 2018 correlation coefficient was r = 0.62 for spring, r = 0.71 for summer, and r = 0.80 for autumn respectively. This higher correlation during autumn 2018 could be associated with about 1.8 – 2.8 ˚C higher monthly averaged temperature than long-term statistical average for autumn in these latitudes.

Table. 1. Correlation coefficients organic and inorganic species with temperature.

	Seasons	2013	2014	2016	2018	2019
Org	Spring		0.94	0.66	0.62	0.60
	Summer	0.62	0.72	0.63	0.71	0.52
	Autumn	0.28	0.50	0.50	0.80	
$NO_{3(Org)}$	Spring		0.89	0.35	0.77	0.63
	Summer	0.55	0.62	0.45	0.64	0.41
	Autumn	0.00	0.30	0.37	0.71	
$NO_{3(Inorg)}$	Spring		0.05	0.22	-0.45	0.10
	Summer	0.40	0.44	0.28	0.11	-0.46
	Autumn	-0.07	0.16	0.42	-0.07	
SO_4	Spring		0.79	0.59	0.32	0.43
	Summer	0.47	0.63	0.63	0.59	0.30
	Autumn	0.30	0.01	0.37	0.78	
NH_4	Spring		0.83	0.14	-0.12	0.33
	Summer	0.59	0.71	0.45	0.63	0.41
	Autumn	0.28	0.06	0.36	0.72	

A strong correlation was observed between organic nitrates ($NO_{3(org)}$) and temperature over springs in 2014, 2018, and 2019 (Fig. 2). In addition, the higher values of correlation coefficients were observed over summers (Table 1). These results revealed that there is a strong positive link between $NO_{3(org)}$ and temperature during warmer seasons. Meanwhile, the same correlation showed different results during autumns: no correlation in 2013 (r = 0.00), weak correlation in 2014 and 2016 (r = 0.30 and r = 0.37, respectively) and quite strong correlation in 2018 (r = 0.71) (Fig. 2). The latter strong correlation could be likely associated with about 1.8 – 2.8˚C higher monthly averaged temperature comparing to long-term statistical average for autumn in these latitudes.

In addition, inorganic nitrates ($NO_{3(Inorg)}$), sulphates (SO_4), ammonium (NH_4), and chloride (Chl) correlation with temperature in 2013, 2014, 2016, 2018, and 2019 were calculated (Table 1). Obtained results indicated that $NO_{3(Inorg)}$, SO_4, NH_4, and Chl has no correlation with temperature in all the three seasons (spring, summer and autumn).

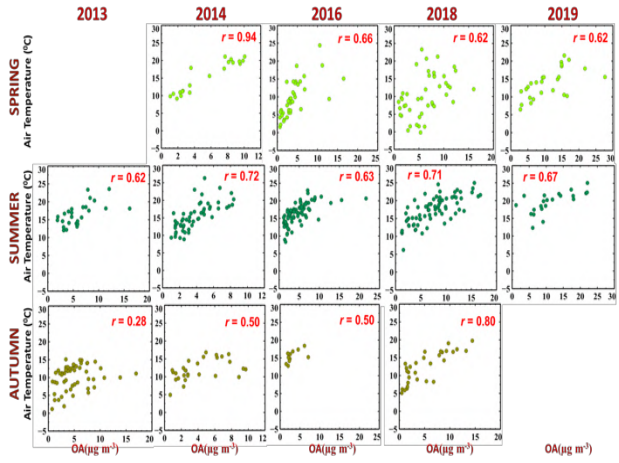


Fig. 1. Correlations of five years daily OA and temperature for 3 seasons (spring, summer and autumn).

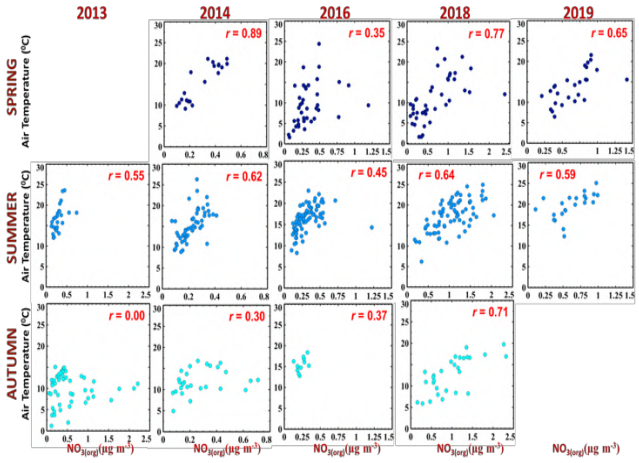


Fig. 2. Correlations of five years daily $NO_{3(org)}$ and temperature for 3 seasons (spring, summer and autumn).

[1] Y. Zhou, "The link between secondary organic aerosol and monoterpenes at a boreal forest site," no. 410, 2016.

EXIPLEX-FORMING COMPOUNDS CONTAINING 1H-1,2,3-TRIAZOLE AND CARBAZOLE MOIETIES FOR SOLUTION PROCESSED WHITE OLEDs

Mariia Stanitska[1,2], Malek Mahmoudi[1], Nazariy Pokhodylo[2], Roman Lytvyn[2], Dmytro Volyniuk[1], Ausra Tomkeviciene[1], Rasa Keruckiene[1], Mykola Obushak[2], Juozas Vidas Grazulevicius[1]

[1] Department of Polymer Chemistry and Technology, Kaunas University of Technology, Baršausko Str. 59, LT-52423, Kaunas, Lithuania

[2] Ivan Franko National University of Lviv, Kyryla i Mefodiya 6, Lviv, Ukraine

mariia.stanitska@ktu.lt

Our primary effort was to develop the way of molecular design and convenient synthesis of new compounds bearing 1H-1,2,3-triazoles as accepting fragments and exhibiting thermally activated delayed fluorescence (TADF). 4-Benzoyl-5-trifluoromethyl-1H-1,2,3-triazole was identified as suitable accepting unit for our goals. Decoration of triazole moiety with carbazole donors through ortho- and meta-positions (or both) of benzoyl fragment lead to donor-acceptor type compounds with through-space TADF effect. The developed synthetic pathway to such compounds was based on application of low-cost commercially available starting materials and simple synthetic protocols Synthesis of the target compounds was based on convenient Dimroth-type 1,2,3-triazole synthesis [1] and the following Ullmann-Goldberg C-N coupling [2].

Due to the exciplex formation between covalently bonded electron-donating carbazole and 1,2,3-triazole-based electron-accepting moieties with small singlet-triplet splitting (0.07-0.13 eV), the compounds exhibit intersystem crossing-assisted bluish-green TADF. The compounds were characterized by high triplet energy levels ranging from 2.93 to 2.98 eV. The most efficient exciplex-type TADF was observed for orto-substituted carbazole–benzoyl-1*H*-1,2,3-triazole which was selected as a host for efficient solution processed white light-emitting diodes [3]. The best device exhibited the maximum power efficiency of 10.7 lm/W, current efficiency of 18.4 cd/A, and quantum efficiency of 7.1%. This device also showed the highest brightness exceeding 10 thousand cd/m^2. Usage of the exciplex-forming host allowed to achieve low turn-on voltage of 3.6 V. High quality white electroluminescence was obtained with the close to nature white colour coordinates of (0.31, 0.34) and colour rendering index of 92.

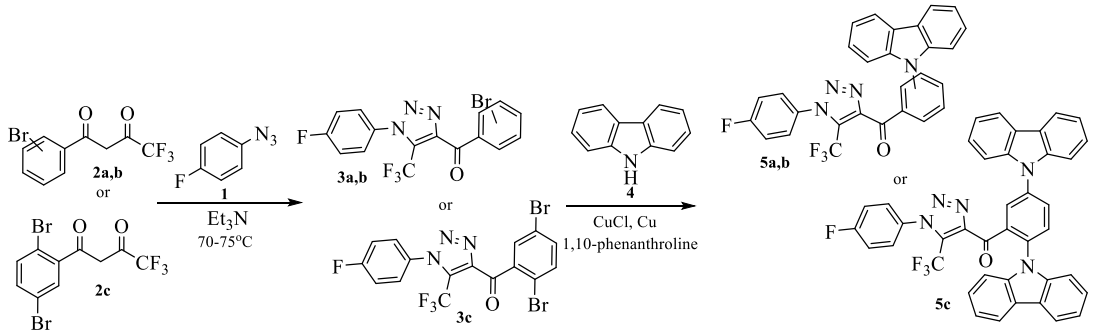


Fig. 1. General synthetic scheme of benzoyl-1*H*-1,2,3-triazole and carbazole derivatives.

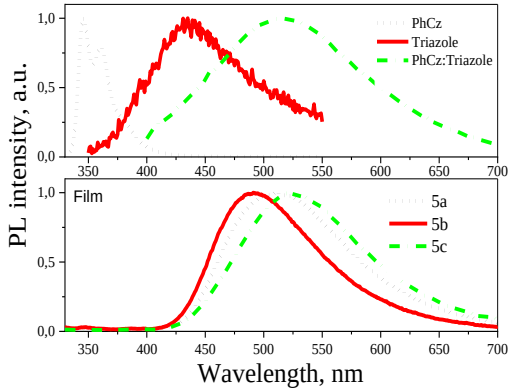


Fig. 2. PL spectra of solutions of phenylcarbazole (PhCz), triazole, exiplex and of the films of **5a, 5b, 5c**

[1] V. A Mamedov, N. A. Zhukova et al., The Dimroth Rearrangement in the Synthesis of Condensed Pyrimidines – Structural Analogs of Antiviral Compounds, *Chem. Heterocycl. Compd.*, *57* (4), 342–368, 2021.

[2] R Altman, S.L. Buchwald, Cu-Catalyzed Goldberg and Ullmann Reactions of Aryl Halides Using Chelating N- and O-Based Ligands, Nature 2(10), 2474–2478 (2007).

[3] B. Geffroy,P. le Roy, C. Prat, Organic Light-Emitting Diode (OLED) Technology: Materials, Devices and Display Technologies, *Polymer International*, John Wiley & Sons, 572–582 (2006).

CHIROPTICAL SPECTROSCOPY IN STUDIES OF PROTEIN AGGREGATION

Natalia Hachlica[1], Aleksandra Wajda[1], Klaudia Rachwał[1], Aleksandra Szymczyk[1], Agnieszka Kaczor[1]

[1]Faculty of Chemistry, Jagiellonian University, Poland
natalia.hachlica@doctoral.uj.edu.pl

Protein aggregation is a biological phenomenon in which intrinsically disordered or misfolded proteins aggregate and form so-called amyloid fibrils characterized by fibrillar morphology. In living organisms, misfolded protein aggregates are hallmarks of various amyloidosis [1]. Several common neurodegenerative diseases such as Alzheimer's, Parkinson's or Huntington's disease are induced by the formation of pathogenic amyloid fibrils in living tissues. An important agent in the formation of amyloid fibrils is the destabilization of the native conformation of the protein. This process can be caused *in vitro* by the change of certain parameters, including pH, temperature, centrifugation, salinity or seeding. However, many proteins are organized naturally in the form of fibrils, having different structures and regulatory functions. The morphological and structural plurality of the protein fibrils and their toxicity are ambiguous, so better understanding of the supramolecular organization of amyloid fibrils may help in the treatment of many diseases.

Chiroptical spectroscopies, such as VCD (Vibrational Circular Dichroism) and ECD (Electronic Circular Dichroism), which are sensitive to chiral biological systems, were used in this study to show variations in the structure of obtained amyloid fibrils at different levels of their hierarchy. Due to a regular long-range chiral organization of amyloid fibrils, it was possible to observe the enhanced VCD signal [2]. By the appropriate selection of the obtaining parameters, we were able to obtain fibrils with controlled reversal of supramolecular helical chirality.

Moreover, ECD information about the secondary structure changes during protein aggregation process. Additionally, to establish the morphology of amyloid fibrils, TEM (Transmission Electron Microscopy) was applied.

The results of VCD and ECD measurements of hen egg white lysozyme are presented in Figure 1. ECD spectra confirm aggregation process (fibrilization), as a transition of the α-helix into β-sheet secondary structure is observed. VCD spectra show negative bands originated from the normal fibrils and intense positive signal typical for reversed fibrils, obtained due to intensive agitation (1400 rpm). TEM images present different morphology of the normal and reversed fibrils. It can be noticed that there are visible differences between normal and reversed fibrils not only in their structure, but also in their morphology. To summarize, the research enabled us to obtain fibrils of tailored structures due to proper choice of fibrilization parameters and monitoring of the structures *via* chiroptical spectroscopies.

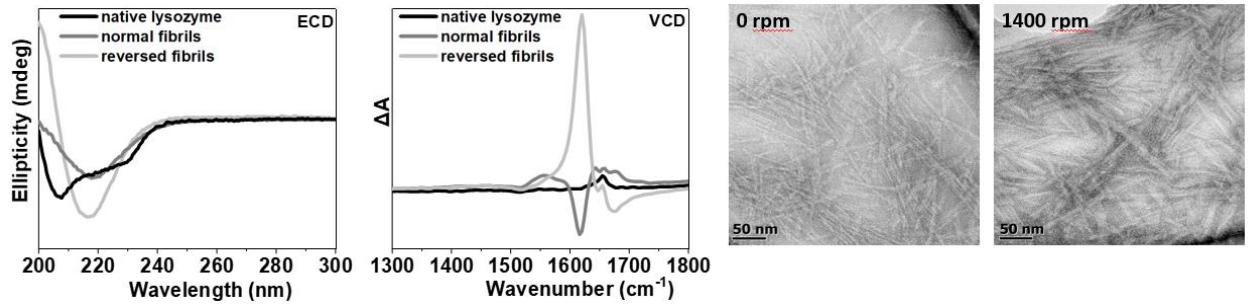


Fig. 1. VCD, ECD spectra and TEM images of hen egg white lysozyme (HEWL) incubated at pH 2 for four days at 60°C, with agitation rate of 1400 rpm and without agitation (0 rpm).

Acknowledgements: We thank dr Michał Pacia for performing TEM imaging.
This work was supported by the National Science Centre Poland (project no. 2020/37/B/ST4/01168 to A.K.).

[1] G. Merlini, V. Bellotti, A. Andreola, G. Palladini, L. Obici, S. Casarini, V. Perfetti, *Protein Aggregation*, Clin Chem Lab Med, **39**, 1065-1075 (2001).
[2] M. Pazderková, T. Pazderka, M. Shanmugasundaram, R. K. Dukor, I. K. Lednev, L. A. Nafie, *Origin of enhanced VCD in amyloid fibril spectra: Effect of deuteriation and pH*, Chirality, **29**, 469–475 (2017).

DETECTION of IgM ANTIBODIES AGAINST the SARS-CoV-2 VIRUS via COLLOIDAL GOLD - BASED ELECTROCHEMICAL ASSAY

Ainis Jarusaitis[1], Matas Matulevicius[1], Ali Jafarov[3], Alexandra Elsakova[3], Ieva Galdikaite[1], Arunas Ramanavicius[1,2], Ausra Baradoke[2]

[1] Faculty of Chemistry and Geosciences, Vilnius University, Naugarduko str. 24, 03225, Vilnius, Lithuania
[2] State Research Institute Center for Physical Sciences and Technology, Sauletekio ave. 3, 10007, Vilnius, Lithuania
[3]Institute of Technology, University of Tartu, Nooruse 1, 50411, Tartu, Estonia
ainis.jarusaitis@chgf.stud.vu.lt

Methods that allow the identification of protein biomarkers can potentially make a significant contribution to biomedical applications and individual health. In our work, several analytical methodologies using carbon based electrodes modified with various nanostructures were reported [1 - 4]. However, the sensing of biomarkers related to Coronavirus disease (COVID-19) is still in demand; the World Health Organization in 2020 has declared COVID-19 as a global pandemic. Because of the presence of asymptomatic carriers, nucleic acid testing for diagnosing of COVID-19, may result in false negatives and is difficult to apply for every suspected patient. Meanwhile, detecting specific antibodies in blood against the Severe acute respiratory syndrome coronavirus 2 (SARS-CoV-2) virus, such as the Immunoglobulin M (IgM) antibody, is another option for COVID-19 diagnosis (including different strains), as IgM is widely accepted as an important indicator during the acute infection period, and can be detected within 5-7 days since infection.

Through the indirect electrochemistry method, a colloidal gold nanoparticle-based novel assay was developed to achieve rapid diagnosis and on-site detection of the IgM antibody against the SARS-CoV-2 virus.

The aqueous synthesis of gold nanoparticles (AuNPs) was carried out using 'green and sustainable' reducing agents. The effect of various variables such as temperature and the presence of nontoxic capping agents on the reduction of auric chloride (Au (III)) salt and the growth of AuNPs was investigated using UltraViolet-Visible Spectroscopy (UV-VIS), Raman spectroscopy (RS), transmission electron microscopy (TEM).

Subsequently, the SARS-CoV-2 spike protein was conjugated with AuNPs for IgM capturing to form an electrochemical transducer for electrochemical sensing of IgM. Physiological concentrations of IgM were detected using screen printed carbon electrodes. For IgM detection, different electrochemistry methods were used, including differential pulse voltammetry (DPV), electrochemical impedance spectroscopy (EIS), and fast Fourier transform electrochemical impedance spectroscopy (FTT-EIS).

Additionally, blood serum samples were used to assess the performance of the AuNP assay, and the experimental results will be presented.

Acknowledgements: Dr Ausra Baradoke is grateful to the European Social Fund (No. 09.3.3-LMT-K-712-23-0159) under a grant agreement with the Research Council of Lithuania (LMTLT). Alexandra Elsakova and Ali Jafarov are thankful to the Erasmus+ funding program.

[1] A. Baradoke, R. Hein, X. Li, J.J. Davis. Reagentless Redox Capacitive Assaying of C-Reactive Protein at a Polyaniline Interface. Anal. Chem. **92**, 3508–351, 2020.

[2] A. Baradoke, I. Pastoriza-Santos, E. González-Romero. Screen-printed GPH electrode modified with Ru nanoplates and PoPD polymer film for NADH sensing: Design and characterization. Electrochim. Acta 300, 2019.

[3] A. Baradoke, B. Jose, R. Pauliukaite, R. J. Forster. Properties of Anti-CA125 antibody layers on screen-printed carbon electrodes modified by gold and platinum nanostructures. Electrochim. Acta **306**, 299–306, 2019.

[4] A. Baradoke, A. Santos, P. R. Bueno, J.J. Davis Introducing polymer conductance in diagnostically relevant transduction. Biosens. Bioelectron. 112705, 2020.

O16-6

DID NOT PARTICIPATE

.

APPLICATION OF POLY(FOLIC ACID) MODIFIED ELECTRODES FOR pH MONITORING

Vytautas Žutautas, Tadas Jelinskas, Rasa Pauliukaite

Department of Nanoengineering, Center for Physical Sciences and Technology (FTMC), Savanoriu Ave. 231, LT-02300 Vilnius, Lithuania
vytautas.zutautas@ftmc.lt

Since a majority of chemical and biological processes are pH-dependent, its monitoring is an important research subject. Glass electrodes are widely used for this purpose nowadays as they have already been known since Max Cremer reported potentiometric pH measurement using glass membrane more than a hundred years ago [1]. However, glass electrodes have limited application in flat and flexible minimized device systems, moreover, they need calibration. Owing to this, a new type of pH sensor is required.

According to the literature, electrochemical redox processes of conducting polymers are frequently pH-dependent and due to this reason, they can be used for pH monitoring in a certain pH range [2]. Folic acid (FA), known as vitamin B9, is an electrochemically active heterocyclic redox compound with biological activity. It has been shown that FA can be polymerized electrochemically forming a conducting polymer poly(folic acid) (PFA) [3,4]. The application of PFA in the development of electrochemical sensors already has been reported, in particular, it was used for glucose detection [5].

In this, work, we used PFA deposited on pyrolytic graphite electrode (PGE) for pH determination in the range from 6 to 9. To prolong the stability of PFA during an extended exposition to slightly alkaline solutions, it was deposited on chitosan (Chit) modified PGE, since Chit is an environmentally friendly hydrogel polymer [6]. Resulted sensor PFA/Chit/PGE was characterized electrochemically and microscopically, and its response to pH was registered using chronoamperometry and potentiometry. The obtained results will be presented and discussed.

Acknowledgments. This work was supported by Lithuanian Research Council Grant No. 01.2.2-LMT-K-718-03-0038.

[1] F. Scholz, From the Leiden jar to the discovery of the glass electrode by Max Cremer, J. Solid State Electrochem. **15**, 5-14 (2011).
[2] U. Lange, N.V. Roznyatovskaya, V.M. Mirsky, Conducting polymers in chemical sensors and arrays, Anal. Chim. Acta **614**, 1–26 (2008).
[3] R. Pauliukaite, Application of natural polymers for electrochemical sensing, In "Biophysics for Biomedical and Environmental Sciences", ed. M. Florescu, Transilvania University of Brasov Press, Brasov 185-210 (2016).
[4] R. Celiešiūtė, T. Venckus, Š. Vaitekonis, R. Pauliukaite, Electrosynthesis and characterization of poly(folic acid) films, Electrochim. Acta **138**, 62–68 (2014).
[5] T. Venckus, R. Celiešiūtė, A. Radzevič, T. Rakickas, Š. Vaitekonis, Ž. Ruelė, R. Pauliukaite, Application of polyfolates in the development of electrochemical glucose biosensors, Electroanalysis **26,** 2273–2282 (2014).
[6] R. Pauliukaite, M.E. Ghica, O. Fatibello-Filho, C.M.A. Brett, Comparative study of different cross-linking agents for the immobilization of functionalized carbon nanotubes within a chitosan film supported on a graphite-epoxy composite electrode, Anal. Chem. **81**, 5364–5372 (2009).

ELECTRON SPIN RESONANCE OF PARAMAGNETIC IMPURITIES IN CeO_2

Pija Gadonaitė[1*], Gediminas Usevičius[1], Vidmantas Kalendra[1], Jūras Banys[1], Mantas Šimėnas[1]

[1] Faculty of Physics, Vilnius University, Sauletekio 9, LT-10222 Vilnius, Lithuania
pija.gadonaite@ff.stud.vu.lt

Electron spin centers in solid state matrices provide one of the key platforms for various quantum technologies [1]. For most of the quantum applications, a long electron spin coherence time (T_2) is highly desirable, but difficult to achieve in practice due to the electron spin interaction with the environment, especially nuclear spin bath of the host material [2]. Recently, CeO_2 was proposed as a potential nuclear-spin-free host matrix with the expected T_2 time close to 50 ms [3]. However, the relaxation times of the paramagnetic centers in this material were never explored experimentally.

Here, we use X-band (9.5 GHz) continuous-wave (CW) and pulsed electron spin resonance (ESR) to study paramagnetic impurities in a commercially available CeO_2 single crystal. CW ESR experiments reveal presence of different paramagnetic metal centers including Yb^{3+}, which has electron spin S = ½ and attractive spin Hamiltonian parameters for quantum technology applications. Low temperature pulsed ESR experiments are used to probe the coherence properties of this and other impurities. We further discuss how the so called 'clock transitions' can be used to suppress the magnetic field noise and thus increase the measured electron spin coherence times in this system [3].

[1] J.M. Taylor et al., High-sensitivity diamond magnetometer with nanoscale resolution, Nature Physics **4**, 810 (2008)
[2] G. Wolfowicz et al., Atomic clock transitions in silicon-based spin qubits, Nature Nanotechnology 8, 561, (2013).
[3] S. Kanai et al., Generalized scaling of spin qubit coherence in over 12,000 host materials, arXiv:2102.02986 (2021).

ELECTROSPINNING NONWOVEN MATERIALS WITH ANTISEPTIC PROPERTIES

Daria Kuchynska, Olena Ishchenko, Viktoriia Plavan, Mariia Kuchynska, Irina Liashok

Department of applied ecology, technology of polymers and chemical fibers, Kyiv National University of Technologies and Design, Ukraine
e.ishchenko5@gmail.com

Nonwoven materials based on ultra-thin fibers are used to make bandages for burns, wounds of various origins and trophic ulcers from biocompatible and biodegradable polymers. The use of such materials demonstrates high air and vapor permeability and accelerates skin regeneration. The use of chitosan as a polymer carrier is due to the presence of reactive amino groups in protonated form [1, 2]. The introduction of chitosan into the composition of ultra-thin fibers of the obtained nonwoven materials makes it possible to expand their scope due to the possibility of interaction with other modifiers [3].

Experimental ratios of the composition of PVAc and PVA to chitosan dissolved in lactic acid are 1:1, 3:1 and 4:1. When the content of chitosan (1:1), (3:1) content takes place drop formation, which leads to impossible electrospinning.

The ratio of PVA with chitosan (3:2) led to insufficient electrospinning, the fibers were short, reducing the distance between the electrodes (ex. >7 cm). The solution in the ratio of PVAc and PVA with chitosan in the ratio (4:1) and the distance between the electrodes of 9 cm showed good results the electrospinning process. The nonwovens obtained from the PVAc / Chitosan and PVA / Chitosan compositions have fibers with a diameter in the range of 0.05-0.45 μm (Fig. 1). The use of a solution of chitosan in lactic acid improves the electrospinning.

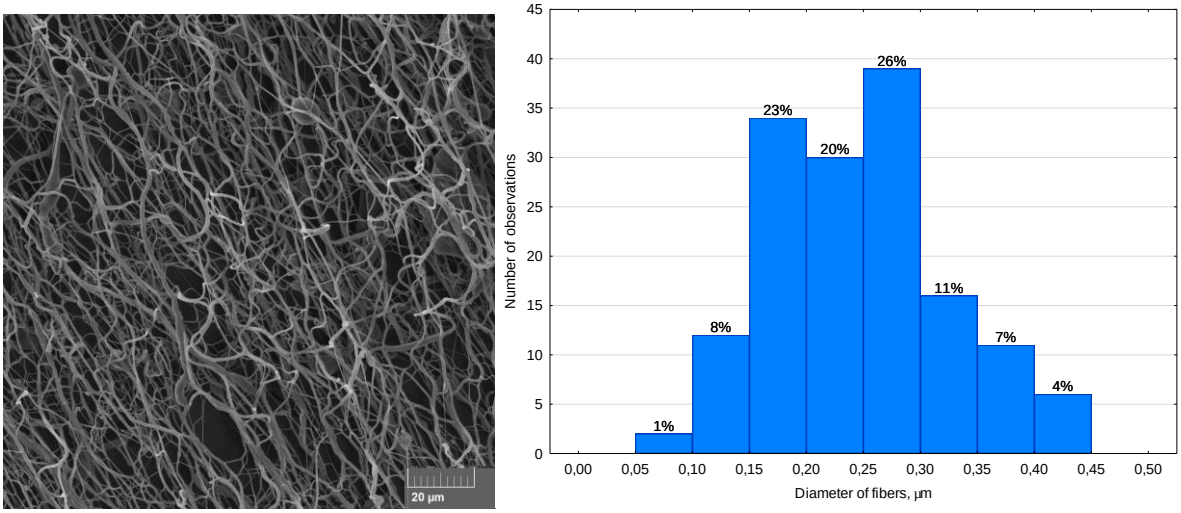


Fig. 1. Photomicrographs and histographs of the diameter distribution of PVA-based fibers with the addition of chitosan dissolved in lactic acid.

It is shown that the introduction of 2-ethoxy-6,9 diaminoacridinium-3-nitroanthranylate (antiseptic drug SG 112) to ultrathin fibers provides the formation of antiseptic properties for the obtained nonwovens. The use of SG 112 increases the fiber diameter to 0.4-0.75 μm, but reduces the width of the distribution of the formed fibers by diameter.

Studies of fungal resistance of nonwovens were performed in a nutrient medium Chapek-Dox. Nonwoven materials based on PVAc and PVA with the addition of solutions of chitosan in lactic acid and the antiseptic drug SG112 showed high air permeability (2.07-2.55 mg/cm^2·h), controlled solubility in water, and good antiseptic properties. A positive result was considered to be the absence of fungal growth on the surface of nonwoven fabrics.

It has been shown that the process of thermal stabilization of nonwoven materials based on ultrathin fibers for 1-3 hours can regulate water absorption from 350 to 780%.

[1] Haider A., Haider S., Kang I. K. A comprehensive review summarizing the effect of electrospinning parameters and potential applications of nanofibers in biomedical and biotechnology. *Arabian Journal of Chemistry* **11 (8)**, 1165 – 1188 (2018).

[2] Oliveira J. E., Mattoso L. H., Orts W. J., Medeiros E. S. Structural and morphological characterization of micro and nanofibers produced by electrospinning and solution blow spinning: a comparative study. *Advances in Materials Science and Engineering.* (2013).

[3] Koliada M., Ishchenko O., Plavan V., Bessarabov V. Characterisation of electrospun fibers made of PVA or PVAc and collagen derivative. *Vlakna a textil (Fibres and Textiles)*. № 2 (25), 48 – 52 (2018).

P1-4

DID NOT PARTICIPATE

.

THE BIOACTIVE PROPERTIES OF CHITOSAN AND GREEN COFFEE BEAN OR ARTICHOKE EXTRACT COMPLEXES

Deimante Rosliuk[1], Dovile Liudvinaviciute[1], Ramune Rutkaite[1], Anne Loron[2], Véronique Coma[2]

[1] Department of Polymer Chemistry and Technology, Kaunas University of Technology, Lithuania
[2] University of Bordeaux, UMR 5629, CNRS, LCPO, 16 Avenue Pey Berland, 33607 Pessac, France
deimante.rosliuk@ktu.lt, dovile.liudvinaviciute@ktu.lt

The caffeoylquinic acid (CQ) derivatives, esters of caffeic and quinic acids, are the main phenolic compounds in green coffee bean (GCBE) and artichoke (AE) extracts. These phenolic compounds are known to have numerous biological activities such as antifungal, antioxidant or antimicrobial. However, the application of CQ derivatives is limited by its low bioavailability, high vulnerability to oxygen or thermal processing. To overcome these disadvantages, water insoluble complexes have been formed between chitosan (ChS) and CQ derivatives present in AE and GCBE by the equilibrium adsorption method.

In the present study, the bioactive properties such as antioxidant and antifungal activities of water insoluble complexes of ChS and phenolic compounds such as CQ, present in GCBE and AE, have been investigated.

The antioxidant activity of AE/ChS and GCBE/ChS was evaluated by the $ABTS^{\bullet+}$ method, and expressed as time dependent $ABTS^{\bullet+}$ radical scavenging activity (RSA, %) (Fig. 1). The antioxidant activity of phenolic compounds attached to ChS is higher in comparison with antioxidant activity of AE and GCBE. Moreover, AE/ChS and GCBE/ChS powders exhibited the prolonged radical scavenging. It should be noted that chitosan itself possesses good antioxidant activity due to its unique properties and this also effects activity of the complexes.

Antifungal activity of AE/ChS and GCBE/ChS was evaluated by growth inhibition bioassay against two fungi i.e. *F. graminearum* and *B. cinerea* (Fig. 2). ChS was used for comparison. The growth of both fungi was reduced by using AE/ChS and GCBE/ChS complexes, however calculated inhibition of growth values were lower than those determined for ChS powder. This could indicate that CQ derivatives adsorbed on ChS may increase the growth of both fungi to some extent.

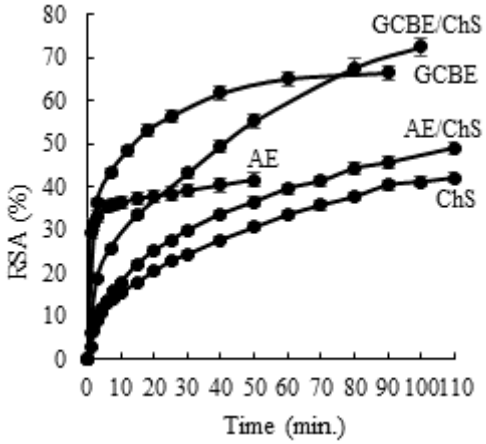


Fig. 1. $ABTS^{\bullet+}$ radical scavenging activity (*RSA*) depending on time. Concentration of extract alone or added with AE/ChS or GCBE/ChS in $ABTS^{\bullet+}$ solution was 0.0038 g/l.

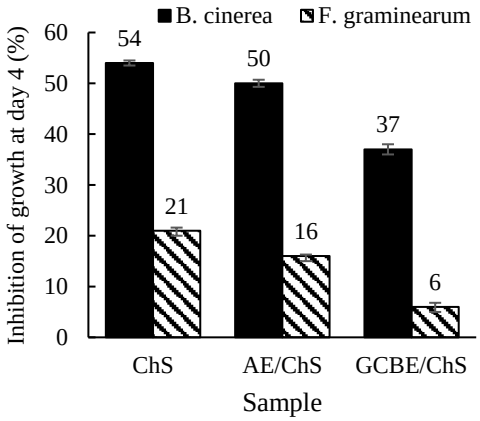


Fig. 2. Inhibition of growth of *F. graminearum* and *B. cinerea* on PDA medium with ChS, AE/ChS and GCBE/ChS particles after 4 days of inoculation at 25°C

Acknowledgment. The financial support of the Research Council of Lithuania and Campus France for the Lithuanian-French programme "Gilibert" project No. S-LZ-19-6 is highly acknowledged. The research was performed in the frame of the COST Action CA19124.

IMMOBILIZATION OF ESSENTIAL OILS IN MODIFIED STARCH FOR ACTIVE PACKAGING APPLICATIONS

Vesta Navikaite-Snipaitiene[1], Simona Sukackaite[1], Dovile Liudvinaviciute[1], Ramune Rutkaite[1]

[1] Department of Polymer Chemistry and Technology, Kaunas University of Technology, Kaunas, Lithuania
vesta.navikaite@ktu.lt

Antioxidant packaging releasing antioxidants to prevent food oxidation is one of the main packaging technologies. Compared to synthetic antioxidants, natural antioxidants such as herbs and spices are of great interest because of their safety and health characteristics [1]. Our previous work has shown that incorporation of essential oils in biopolymers can secure their high antioxidant properties, and such active materials potentially could be applied in food packaging [2].

In this study, eugenol (EU) and thyme essential (TH) oils were immobilized in hydrophobically modified starch (HS) and their potential as antioxidant packaging materials was investigated. Emulsions containing 20 % of HS and 5, 10 or 15 % of essential oil were prepared, and droplet size, zeta potential, viscosity and antioxidant activity characteristics were determined (see Table 1 and Fig. 1).

Table 1. Characteristics of emulsions containing eugenol or thyme essential oil

Emulsion	Particle size of emulsion droplets (nm)	Zeta potential (mV)	Viscosity (mPa·s)
HS-EU(5%)	326 ± 4	-10.5 ± 0.5	32.3 ± 1.6
HS-EU(10%)	1049 ± 31	-10.6 ± 0.3	41.9 ± 2.1
HS-EU(15%)	1307 ± 24	-4.6 ± 1.3	49.4 ± 2.5
HS-TH(5%)	1040 ± 18	-13.6 ± 1.2	30.1 ± 1.5
HS-TH(10%)	1320 ± 24	-7.2 ± 1.0	33.8 ± 1.7
HS-TH(15%)	1333 ± 2	-5.7 ± 0.9	50.1 ± 2.5

It was determined, that the particle size of emulsion droplets depended on the type of essential oil and its amount in composition. The particle size was increasing with increasing concentration of essential oil in both types of emulsion. The emulsions with smallest droplets of about 362 nm diameter were obtained when using 5 % of eugenol. Moreover, particles were negatively charged. It was found that the viscosity of both types of emulsion was increasing with increasing amount of essential oil in the composition. The antioxidant activity (AA) of emulsions containing eugenol was higher (88-94 %) compared to emulsions with thyme essential oil (25-43 %). In addition, the stability of the emulsions and demulsification process were assessed when keeping the samples for up to 10 days at 20 °C and 5 °C temperature. It was determined that 5°C temperature was more favorable for storing of emulsions.

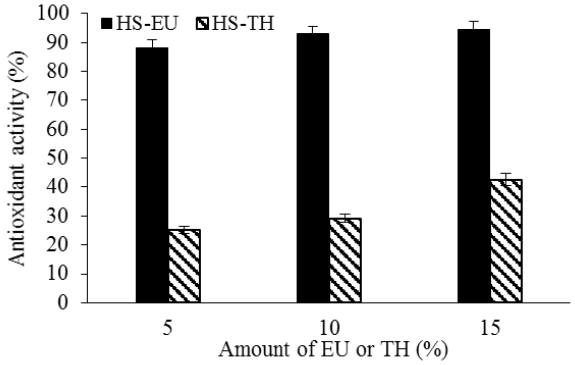


Fig. 1. The antioxidant activity (AA) of HS-EU and HS-TH depending on amount of EU or TH in emulsion.

For active coatings preparations HS-EU(15 %) and HS-TH(15%) emulsions were cast on paper by using a coating equipment. It was found that the coating containing eugenol had the significant higher AA (90 %) comparing to coating with thyme essential oil (AA=40 %). Consequently, hydrophobically modified starch can be successfully used as a matrix for immobilization of natural antioxidants such as eugenol and thyme essential oils and these compositions have potential to be used in antioxidant packaging application.

Acknowledgment. The research was performed in the frame of the COST Action CA19124.

[1] R. P. P Fernandes et al., Evaluation of antioxidant capacity of 13 plant extracts by three different methods: Cluster analyses applied for selection of the natural extracts with higher antioxidant capacity to replace synthetic antioxidant in lamb burgers, Journal of Food Science and Technology **53**, 451-460 (2016).

[2] V. Navikaite-Snipaitiene et al., Development of antioxidant food packaging materials containing eugenol for extending display life of fresh beef, Meat Science **145**, 9-15 (2018).

FERROELECTRIC PROPERTIES OF BARIUM CALCIUM TITANATE DOPED WITH RARE EARTH METALS

Patricija Lapienytė[1], Šarūnas Svirskas[1], Lucjan Kozielski[2], Juras Banys[1]

[1] Faculty of Physics, Vilnius university, Saulėtekio al. 3, 10257 Vilnius, Lithuania
[2] Faculty of Science and Technology, University of Silesia, 1A 75 Pułku Piechoty St., 41-500 Chorzów, Poland
patricija.lapienyte@ff.stud.vu.lt

Recently, considerable amount of research has been dedicated to ferroelectric oxides because of their application in various electronic devices. Ferroelectric oxides epitomize excellent dielectric and piezoelectric properties. Barium titanate (BTO) is one of the widely used materials in electronics. BTO can be doped with various different ions to modify its electrical properties for different application needs. Calcium is attractive dopant to modify the temperature stability and reliability of the dielectric properties of barium titanate [1]. BCT solid solutions can be implemented in various other applications like: dielectric filters, antennas, resonators, duplexers, phase shifters and piezoelectric actuators [2].

This research focuses on barium calcium titanate (BCT) doped with 0.1 % of different rare earth metals (specifically neodymium and praseodymium). The investigated ceramics were prepared using Pechini method. This method is a variation of the sol-gel technique dedicated to simple titanates and niobates of lead and alkali metals, mainly using nitrates and alcoholates as reagents [3]. The polarization and strain response was recorded by applying a high voltage signal using AixACCT TF 2000 equipped with a single-beam laser interferometer.

Fig. 1 shows polarization hysteresis loops of BCT doped with different rare earth metals measured at 25 °C. The figure suggests that at a room temperature examined materials are ferroelectrics. Further details on piezoelectric and ferrroelectric properties will be presented and discussed.

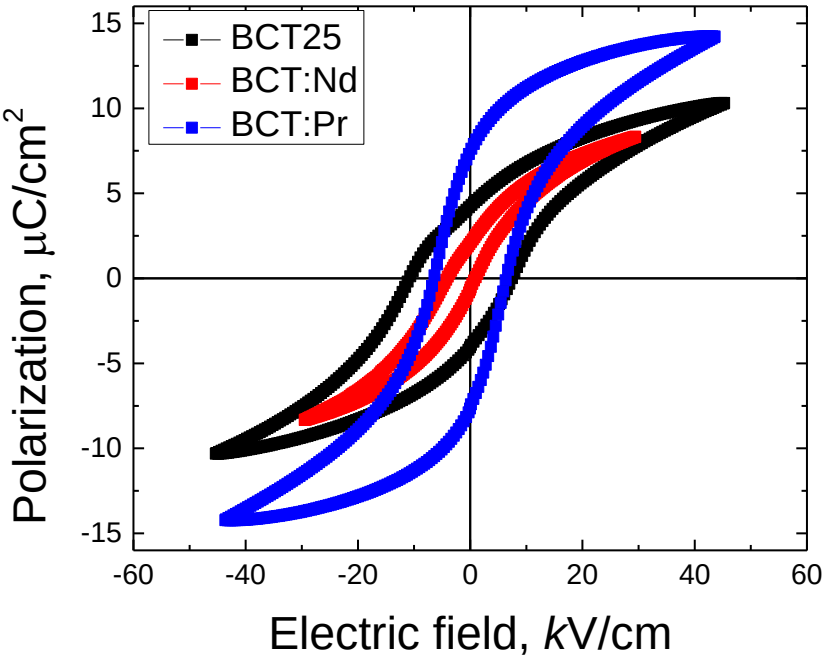


Fig. 1. Comparison of polarization hysteresis of BCT doped with different rare earth metals measured at 25°C.

[1] Xiaowen Z, Ying W, Longtu L. Study of defect chemistry of Ca doped $BaTiO_3$ ceramics. Ferroelectrics1990;101:61 ± 74.
[2] Liang-Yu Li, Xin-Gui Tang, Mater. Chem. Phys. 115 (2009) 507–511.
[3] Pechini, M.P. Method of Preparing Lead and Alkaline Earth Titanated and Niobates and Coating MethodsUsing the Same to Form A Capacitor. U.S. Patent US3330967 A, 11 July 1967.

DIELECTRIC SPECTROSCOPY OF TIN DOPED BARIUM TITANATE

Eglė Šlinkšytė[1], Šarūnas Svirskas[1], Eriks Birks[2], Stanislav Kamba[3], Jūras Banys[1]

[1]Faculty of Physics, Vilnius University, Saulėtekio 9/3, LT-10222, Vilnius, Lithuania
[2]Institute of Solid State Physics, University of Latvia, Kengaraga 8, LV-1063, Latvia
[3]Institute of Physics, Czech academy of sciences, Na Slovance 2, Prague 8, Prague, Czech Republic
egle.slinksyte@ff.stud.vu.lt

Since the discovery of ferroelectricity (which could be described as electrically switchable spontaneous polarization [1]) in the first half of the 20th century, ferroelectric materials were extensively studied due to their potential application in the areas of pyroelectric detection and imaging, optical memory, electro-optic modulators [2] and large piezoelectricity. Nowadays $BaTiO_3$ (barium titanate - the first inorganic piezoelectric transducer ceramic ever developed) is still widely researched. Very often properties of ceramic material can be improved when substituted with another chemical elements in the lattice [1]. Barium titanate is rarely studied in an original chemical form.

In this work the tin substituted barium titanate ($BaTi_{1-x}Sn_xO_3$) will be presented. The main goal of this research was to determine the change of dielectric permittivity by altering the concentration of tin, which varied from $x = 0.15$ to $x = 0.30$. The research was carried out in the temperature range of 10 – 500 K and 10 Hz – 1 THz frequency region. The majority of experiments focused on dielectric spectroscopy – six methods were used to determine the scalar and complex permeability and refraction coefficients in different frequency ranges. The results were calculated, and the change of dielectric permittivity was analyzed. Additionally, piezoelectric and ferroelectric properties were researched with the use of a commercial AixaCCT TF2000 analyzer. Fig. 1 compares hysteresis loops of barium titanate samples with different concentrations of tin at the temperature of 200 K. The electric field dependence of strain and polarization shown in the figure suggest that $BaTi_{0.85}Sn_{0.15}O_3$ and $BaTi_{0.80}Sn_{0.20}O_3$ have ferroelectric properties, which barium titanate with tin concentrations of 25 and 30 percent lack of. The poster presentation will demonstrate detailed investigation of ferroelectric and dielectric properties of tin doped barium titanate.

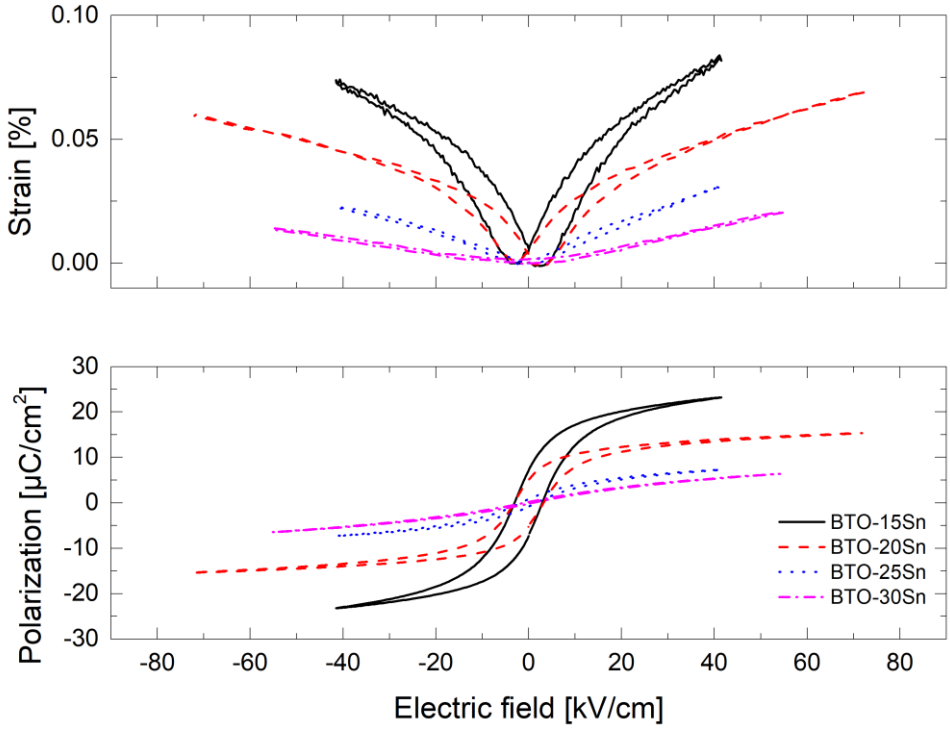


Fig. 1. Electric field dependence of strain and polarization at 200 K.

[1] G. H. Haertling, Ferroelectric Ceramics: History and Technology, J. Am. Ceram. Soc., 82 [4] 797–818 (1999).
[2] M. E. Lines, A. M. Glass, *Principles and Applications of Ferroelectrics and Related Materials* (Clarendon Press, 1977).

ENCAPSULATION OF *VACCINIUM MYRTILLUS L.* ANTHOCYANINS INTO LIPOSOMES

Zygimantas Augys[1], Vesta Navikaite-Snipaitiene[1], Ramune Rutkaite[1]

[1] Department of Polymer Chemistry and Technology, Kaunas University of Technology, Kaunas, Lithuania
zygimantas.augys@ktu.edu

Nowadays, bilberries have received considerable interest as a functional food or nutraceuticals for health improvement. These berries contain biologically active compounds – anthocyanins, known as natural antioxidants, which are able to bind free radicals in the human body and inhibit the ageing processes. In addition, research confirmed that anthocyanins are effective in improving vision, treating cardiovascular diseases, cancer and diabetes [1]. However, the main disadvantage of anthocyanins is their instability due to various external factors such as pH, light, temperature and etc. [2].

The aim of this study was to study the encapsulation of *Vaccinium Myrtillus L*. anthocyanins (ATC) into liposomes formulated from soy lecithin. First of all, the antioxidant activity of anthocyanins (ATC) from bilberry extract was determined by using ABTS (2,2'-azino-bis(3-ethylbenzothiazoline-6-sulfonic acid) method. The antioxidant efficiency of ATC varied from 2.8 to 92.7 % depending on the concentration of active compounds in the reaction mixture (see Fig. 1). In addition, the stability of ATC was evaluated by storing the samples for up to 28 days at different temperatures. It was found that the antioxidant efficiency of ATC decreased from 93 % to 60 % and 55 % when the samples were kept at 5 °C and 20 °C, respectively.

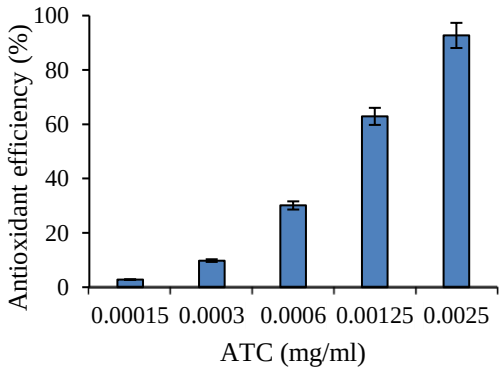


Fig. 1. Dependence of antioxidant efficiency of anthocyanins on their concentration in the reaction mixture

ATC from *Vaccinium Myrtillus L*. were encapsulated into liposomes from soy lecithin (LE). Six formulations containing various amounts of anthocyanins and lecithin were prepared in water or acetate buffer (pH=3.5) medium by using high shear homogenizer (see Table 1).

Table 1. The main parameters of liposomal system consisting of LE and ATC

Sample	Composition (%)		Medium	Particle size (nm)	PI	ζ-potential (mV)	pH
	LE	ATC					
1-LE-ATC	5.0	0.06	Distilled water	205 ± 2	0.287	-68.42	5.83
2-LE-ATC			Acetate buffer solution	128 ± 2	0.250	-55.75	4.16
3-LE-ATC	2.5	0.09	Distilled water	271 ± 8	0.291	-66.44	5.43
4-LE-ATC			Acetate buffer solution	160 ± 4	0.259	-52.30	4.19
5-LE-ATC	1.0	0.11	Distilled water	217 ± 1	0.282	-64.27	5.00
6-LE-ATC			Acetate buffer solution	200 ± 7	0.297	-37.02	4.26

It was revealed that smaller particles were formed when acetate buffer solution was used as a medium. In this case, the particle size varied from 128 to 200 nm depending on lecithin and anthocyanin amount in the formulation. When distilled water was used in the system the liposomes with particle size varying from 205 to 271 nm were obtained. The polydispersity index (PI) of all samples was lower than 0.3 indicating that those systems were quite homogenous and had particle size distribution within a narrow range. Measurements of the zeta potential showed that all formulations exhibited high negative surface charge, indicating that all liposomal systems were relatively stable.

Acknowledgment. This research was funded by the European Social Fund under the measure No 09.3.3-LMT-K-712 "Development of Competences of Scientists, other Researchers and Students through Practical Research Activities".

[1] N. Tena, J. Martín, A.G Asuero, State of the Art of Anthocyanins: Antioxidant Activity, Sources, Bioavailability, and Therapeutic Effect in Human Health, Antioxidants **9(5)**, 451 (2020).

[2] P. Yang et al, Stability of anthocyanins and their degradation products from cabernet sauvignon red wine under gastrointestinal pH and temperature conditions, Molecules **23(2)**, 354 (2018).

P1-10

DID NOT PARTICIPATE

.

FORMATION OF COMPLEXES BETWEEN ANTHOCYANINS AND CROSS-LINKED PECTIN

Rugile Grabauskaite, Dovile Liudvinaviciute, Vesta Navikaite-Snipaitiene, Ramune Rutkaite, Joana Bendoraitiene

Department of Polymer Chemistry and Technology, Kaunas University of Technology, Lithuania
dovile.liudvinaviciute@ktu.lt

Anthocyanins (ANC), classified as flavonoids, possess some bioactive properties, such as antioxidant activity [1], though these compounds have low stability at elevated temperatures, varying pH and exposure to light, which limits their application. ANC are cationic compounds and could form complexes with biopolymers having oppositely charged groups, such as pectin (PEC). The stability of ANC could be improved through formation of water insoluble complexes e.g. by exploiting adsorption process. Since PEC is soluble in water, before adsorption process it has to be modified to reduce solubility. Cross-linking is one of the ways to obtain insoluble polymers and for this purpose cross-linkers such as epichlorohydrin can be used [2].

The aim of the present work was to investigate the formation of insoluble complexes between ANC present in aqueous wild bilberry extract and cross-linked PEC by evaluating kinetic and equilibrium adsorption of ANC on $PEC_{0.05}$ powder.

Since PEC is soluble in water, it was cross-linked with epichlorohydrin in alkaline medium, to obtain insoluble PEC with a low cross-linking degree. The degree of cross-linking was expressed as the molar ratio of epichlorohydrin to PEC being equal to 0.05:1. Obtained cross-linked PEC was denoted as $PEC_{0.05}$.

For the kinetic studies aqueous ANC extract was added to the flask with $PEC_{0.05}$ powder and shaken at a constant rate and temperature of 30 °C. Residual concentration of ANC was determined after certain time intervals and the amount of adsorbed ANC was calculated (q_e (mmol/g)). The obtained kinetic data were fitted by using the pseudo-second order kinetic model. Kinetic curves showed that adsorption of ANC on $PEC_{0.05}$ powder proceeded quickly during the first 10 min and reached equilibrium after 2 hours.

Equilibrium adsorption of ANC on $PEC_{0.05}$ powder was studied at temperatures of 20 °C, 30 °C and 40 °C keeping the samples for 120 min. The Dubinin-Radushkevich, Freundlich and Langmuir adsorption models were used to describe obtained adsorption isotherms. Obtained adsorption isotherms showed (see Fig.1) that with an increase in the adsorption temperature the amount of ANC adsorbed onto $PEC_{0.05}$ powder decreased. Based on the values of linear regression coefficient R^2, Dubinin-Radushkevich adsorption model fitted experimental data the best. It was demonstrated, that adsorption takes place due to electrostatic interactions between the flavylium cation of ANC and the ionized carboxyl groups of $PEC_{0.05}$.

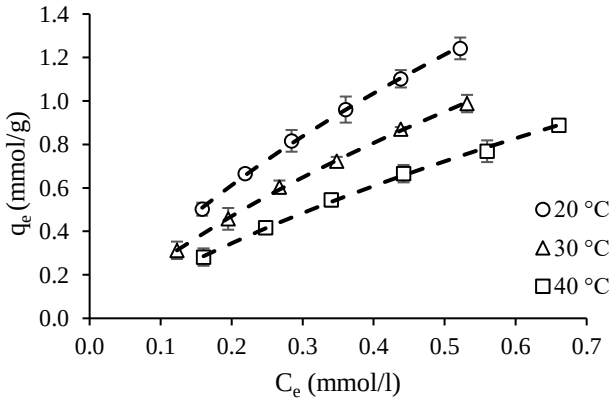


Fig. 1. Isotherms of ANC adsorption on $PEC_{0.05}$ powder at different temperatures. Symbols represent experimental data and dashed lines represent fitted curves of the Dubinin-Radushkevich adsorption model

Acknowledgment. The research was performed in the frame of the COST Action CA19124.

[1] M. G. Miguel. Anthocyanins: Antioxidant and/or anti-inflammatory activities, Journal of Applied Pharmaceutical Science, **1(6)**, 07-15 (2011).

[2] R. Semdé, A. Moës, M. J. Devleeschouwer et al. Synthesis and Enzymatic Degradation of Epichlorohydrin Cross-Linked Pectins, Drug Development and Industrial Pharmacy **29(2)**, 203–213, (2003).

DIELECTRIC PROPERTIES OF $Ba_{0.9}Ca_{0.1}Zr_xTi_{1-x}O_3$ CERAMICS

Domantas Čiapas[1], Šarūnas Svirskas[1], Lucjan Kozielski[2], Jūras Banys[1]

[1]Faculty of Physics, Vilnius University, Saulėtekio 9/3, LT10222 Vilnius, Lithuania
[2]Faculty of Science and Technology, University of Silesia, 1A 75 Pułku Piechoty St., 41-500 Chorzów, Poland
domantas.ciapas.2@ff.stud.vu.lt

Barium titanate-based materials has very attractive properties such as high dielectric constant, low dielectric loss and ferroelectric behavior. It is an essential electroceramic that is being used in multilayer capacitors, thermistors, and electro-optic devices [1],[2],[3]. Lead free barium zirconate and barium calcium titanate are getting more attention because it is environmentally friendly and pertains high dielectric permittivity while the ferroelectric phase transitions are suppressed. This onsets a relaxor behavior that is observed below room temperature. Some compositions are very attractive for applications because it has frequency independent dielectric permittivity at least up to 300 MHz.

In this presentation dielectric properties of barium zirconate titanate/barium calcium-titanate ceramics (samples with different concentrations of zirconium) will be presented. For $Ba_{0.9}Ca_{0.1}Zr_xTi_{1-x}O_3$ (x=1, 0.3, 0.1, 0.2, 0,8) ceramics, the temperature dependence of dielectric constant was measured in the 20Hz-1MHz frequency range HP 4284A precision LCR meter and Closed-cycle Helium cryostate with Lakeshore 331 (6-300 K).

Figure 1 represents the temperature dependence of real part of dielectric permittivity at 100 kHz frequency. The increase of zirconium concentration reduces the maximum value of permittivity while shifting relaxor anomaly to lowest temperatures. No structural phase transition is evidenced in all temperature range. The detailed discussion about the dielectric relaxation will be presented in this work.

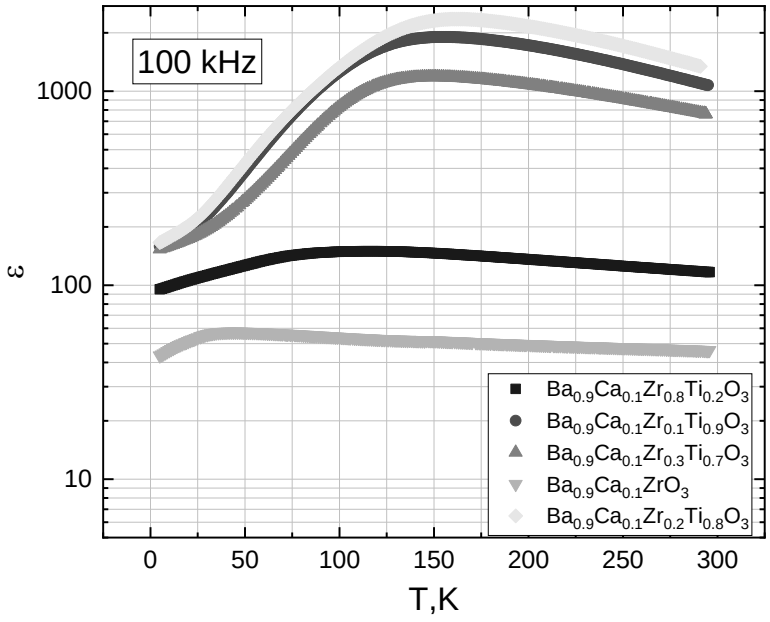


Fig. 1 Temperature dependence of dielectric constant for $Ba_{0.9}Ca_{0.1}Zr_xTi_{1-x}O_3$ (x=1, 0.3, 0.1, 0.2, 0,8) ceramics at 100 kHz frequency.

[1] J. F. Scott, "Applications of Modern Ferroelectrics," Science., vol. 315, no. 5814, pp. 954–959, Feb. 2007.
[2] J. G. Bell, T. Graule, and M. Stuer "Barium titanate-based thermistors: Past achievements, state of the art, and future perspectives," Appl. Phys. Rev., vol. 8, no. 3, p. Sep. 2021.
[3] S. Abel et al., "Electro-Optical Active Barium Titanate Thin Films in Silicon Photonics Devices," Adv. Photonics 2013

P1-13

DID NOT PARTICIPATE

.

SYNTHESIS OF CHITOSAN AND N-ISOPROPYLACRYLAMIDE GRAFT COPOLYMERS

Migle Babelyte[1], Ramune Rutkaite[1], Volodymyr Samaryk[2]

[1] Department of Polymer Chemistry and Technology, Kaunas University of Technology, Lithuania
[2] Department of Organic Chemistry, Lviv Polytechnic National University, Ukraine
migle.babelyte@ktu.edu

Chitosan (CS) is well known as biodegradable and biocompatible polymer also having antimicrobial activity. This biopolymer is nontoxic, renewable and also its behavior is pH-sensitive [1]. Because of these properties, chitosan is an interesting natural polymer which can be further modified *via* grafting reactions. One of the most attractive compounds which can be used for grafting of chitosan is N-isopropylacrylamide (NIPAAm). Poly(N-isopropylacrylamide) (PNIPAAm) is highly thermo-sensitive polymer and shows sharp solubility changes in water around a specific temperature which is known as lower critical solution temperature (LCST) [2]. Beyond 32 ºC PNIPAAm turns into precipitate and could be dissolved again by lowering the solution temperature. Therefore, the graft copolymers with CS in the backbone and NIPAAm in the side chains could have dual stimuli responsive behavior and may be interesting in terms of drug delivery system.

In this study, chitosan-graft-N-isopropylacrylamide (CS-g-NIPAAm) copolymers were synthesized by free-radical polymerization of chitosan and NIPAAm using potassium persulfate (PPS) as an initiator. The reaction conditions and feed molar ratio of the compositions are presented in the Table 1. The copolymers were prepared by dissolving CS and NIPAAm in 1 % acetic acid aqueous solution, stirring the mixture at room temperature for 30 minutes under a nitrogen atmosphere, then adding PPS and elevating reaction temperature to 60 ºC. The polymerization was allowed to process for 6 hours. After the reaction, the products were precipitated into ethanol and filtrated to separate the polymeric products. To remove the homopolymer of NIPAAm, the products were followed by Soxhlet extraction with methanol for 48 hours.

Table 1. Feed composition and reaction conditions

Copolymer sample	**Molar ratio**			**Molar ratio CS / NIPAAm**	**Reaction temperature, °C**	**Reaction time, h**
	CS	**NIPAAm**	**PPS**			
CS-g-NIPAAm-1	1	1	0.16	1:1	60	6
CS-g-NIPAAm-2	1	5	0.16	1:5		
CS-g-NIPAAm-3	1	10	0.16	1:10		

By changing the amounts of the grafting reagents copolymers with different grafting ratio were prepared by free radical mechanism. The obtained CS-g-NIPAAm copolymers were characterized by NMR, FTIR spectroscopy and other techniques. The properties of aqueous solutions of synthesized copolymers were also assessed.

Acknowledgment. The financial support of the Research Council of Lithuania for the project No. S-LU-22-11 in the frame of Lithuanian–Ukrainian Cooperation Programme in the Fields of Research and Technologies is highly acknowledged.

[1] Xi. Jin, J. Wang, J. Bai. Synthesis and antimicrobial activity of the Schiff base from chitosan and citral, Carbohydrate Research **344,** 825-829 (2009).
[2] H. Bao, L. Li, W. Ch. Leong and L. H. Gan. Thermo-Responsive Association of Chitosan-graft-Poly(N-isopropylacrylamide) in Aqueous Solutions, J. Phys. Chem. B **114**, 10666–10673 (2010).

POLYLACTIC ACID MODIFICATIONS WITH FULLERENES FOR BIOFILM TREATMENT WITH PHOTODYNAMIC THERAPY

Gabrielė Saulėnienė[1], Monika Kirsnytė[1], Wanessa De Cassia Martins Antunes De Melo[1], Arūnas Stirkė[1]

[1] Department Functional Materials and Electronics, Center for Physical Sciences and Technology, Lithuania
gabriele.sauleniene@stud.vilniustech.lt

Microbial biofilms cause up to 80% of all human bacterial and fungal infections [1]. Pathogens producing biofilm are particularly resistant to antibiotic treatment, so there is a need to look for new treatments and prevention methods. Antimicrobial photodynamic therapy (aPDT) can be applied for the treatment of infectious diseases. The aPDT uses non-toxic dyes, also called photosensitizers (PS), which are excited by harmless visible light and can form reactive oxygen species that attack adjacent targets, including proteins, lipids, and nucleic acids, in the biofilm matrix, on the cell surface, and inside microbial cells. Damage to non-specific targets destroys both planktonic cells and biofilms [2]. Fullerenes have received considerable attention due to their good quantum yields [3]. The aim of this study is to attach fullerenes on polylactic acid surface for aPDT use.

Polylactic acid surface was modified 3 different ways before reaction with fullerene: with ethylenediamine (EDA), phosphorus pentachloride (PCl_5), and phosphorus pentachloride and EDA.

XPS analysis was used to obtain information on the chemical states and surface composition of the elements. After reactions with EDA atomic nitrogen increased and a new peak at 398.6 eV in the N1 spectrum was observed, which indicates a new bond formation. In reactions with phosphorus pentachloride the measured amount of atomic chlorine increased. After the reaction with fullerene, an atomic carbon content increased and a new peak appeared at 289 eV, which corresponds with π-π bonds deriving out of fullerene.

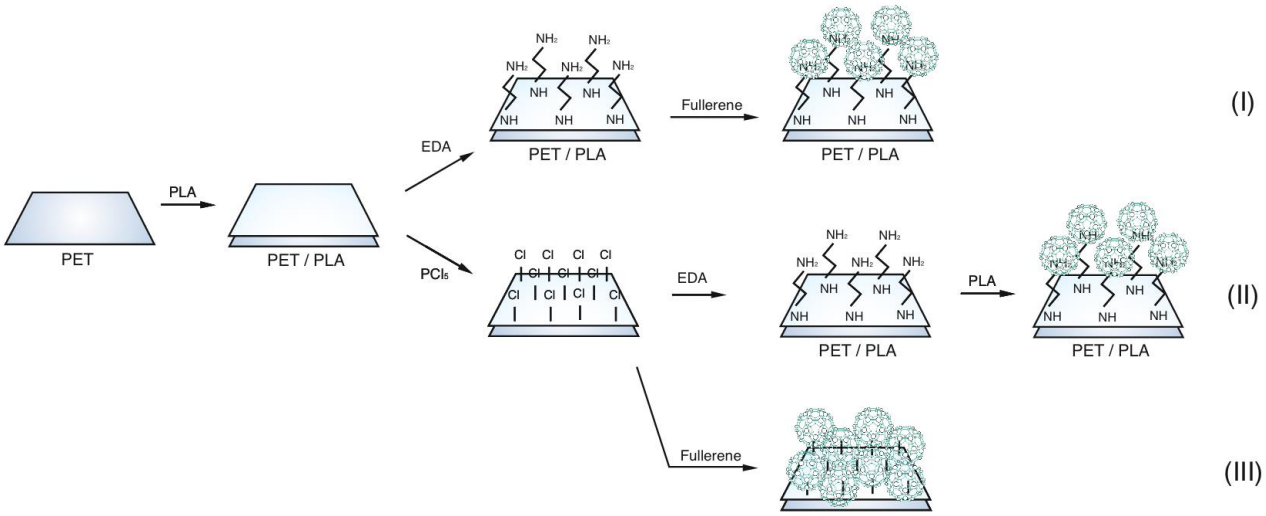


Fig. 1. General scheme for polylactic acid modifications.

In conclusion, fullerene precipitation on modified PLA surface was evaluated by XPS analysis as an increase of carbon content. In Fig. 1 after (I) synthesis carbon content increased 12.6%, in (II) synthesis – 6.9%, and the highest carbon increase was observed in (III) synthesis - 22.8%. To conclude, polylactic acid modified with fullerene could later be used in aPDT. Nevertheless, antimicrobial polymer could potentially be applied in different fields, for example, health care and medical devices.

[1] M. A. BIEL, "Photodynamic therapy of bacterial and fungal biofilm infections," Methods Mol. Biol., vol. 635, pp. 175–194, 2010, doi: 10.1007/978-1-60761-697-9_13.

[2] X. HU, Y. Y. HUANG, Y. WANG, X. WANG, and M. R. HAMBLIN, "Antimicrobial photodynamic therapy to control clinically relevant biofilm infections," Frontiers in Microbiology, vol. 9, no. JUN. Frontiers Media S.A., p. 1299, Jun. 27, 2018, doi: 10.3389/fmicb.2018.01299.

[3] P. MROZ, G. P. TEGOS, H. GALI, T. WHARTON, T. SARNA, and M. R. HAMBLIN, "Photodynamic therapy with fullerenes," Photochemical and Photobiological Sciences, vol. 6, no. 11. Royal Society of Chemistry, pp. 1139–1149, 2007, doi: 10.1039/b711141j.

P1-16

DID NOT PARTICIPATE

.

P1-17

DID NOT PARTICIPATE

.

HYDROPHOBIC AND THERMAL PROPERTIES OF ACETYLATED STARCH OCTENYL SUCCINATES

Laura Peciulyte[1], Ugne Naruseviciute[1], Ramune Rutkaite[1]

[1] Department of Polymer Chemistry and Technology, Kaunas University of Technology, Lithuania
laura.peciulyte@ktu.lt

Biodegradable polymers represent a solution to the problems of contamination caused by conventional synthetic polymers. For this reason, starch is considered be one of the most promising substances due to its biodegradability, low cost and abundant availability. The starch application areas remain limited due to its poor resistance to water and no plastic behaviour under heating. Chemical modification of starch is one of the most attractive methods to reduce the number of hydrogen bonds and increase the hydrophobicity of starch.

The aim of this study was to synthesize thermoplastic starch esters with controllable properties by using organic anhydrides of different chemical composition and varying the degree of substitution (DS). Potato starch was modified with acetic (Ac) or/and octenyl succinic (OSA) anhydrides and characterized by Fourier-transform infrared spectroscopy and scanning electron microscopy. The hydrophobicity of starch acetate octenyl succinate was assessed by measuring water contact angle. The thermal properties of the modified starches were evaluated using thermogravimetry and differential scanning calorimetry.

For OSA starch with DS_{OSA}=0.06 and starch acetate at low degree of substitution, DS_{Ac} being up to 0.62, the glass transition (T_g) temperature was not observed and the destruction temperature (T_d) was decreasing with increasing of DS_{Ac} (Table 1). Starch acetate with high DS_{Ac}≥0.8 had T_g which is in the interval of 162-167 °C and T_d was increasing with increasing DS_{Ac}. Starch modified with both Ac and OSA showed T_g even at low DS_{Ac} values, and glass transition temperature was increasing with increasing of DS_{Ac}. When the DS_{Ac} was higher than 1.06 the T_g dependence was not observed for dual modified samples.

Table 1. The effect of DS on hydrophobicity and thermal properties of starch derivatives

No	DS_{Ac}	DS_{OSA}	T_d, °C	T_g, °C	Contact angle, °
1	0	0	291	-	38
2	0.43	0	267	-	46
3	0.62	0	240	-	65
4	0.8	0	249	162	66
5	1.07	0	267	166	66
6	1.67	0	278	167	68
7	0	0.06	272	-	76
8	0.03	0.06	287	162	44
9	0.43	0.06	279	163	56
10	0.53	0.06	302	164	64
11	1.06	0.06	318	175	74
12	1.23	0.06	316	171	78
13	1.58	0.06	315	167	84
14	1.68	0.06	312	171	88

The hydrophobicity of starch acetate was gradually increasing with increasing DS_{Ac} (Table 1), as reflected by increasing water contact angle. Moreover, the modification of starch with octenyl succinic anhydride dramatically changed the hydrophobicity of starch i.e., the water contact angle of starch octenyl succinate with DS 0.06 was twice higher compared to that of native starch. Meanwhile, dual modified starch at low DS_{Ac} had lower contact angle than that of OSA starch. However, contact angle values increased with increment of DS_{Ac} reaching 88º for acetylated starch octenyl succinate with DS_{Ac}=1.68 and DS_{OSA}=0.06.

INSIGHTS INTO STRUCTURE OF SEDIMENTARY SUCCESSION OF WESTERN LITHUANIA BASED ON INTERPRETATION OF NEW SEISMIC DATA

Milda Grendaitė[1], Dainius Michelevičius[1,2], Sigitas Radzevičius[1]

[1] Faculty of Chemistry and Geosciences, Vilnius University, Lithuania
[2] UAB Geobaltic, Lithuania
milda.grendaite@chgf.vu.lt

A detailed investigation of the geological structure of sedimentary cover of Western Lithuania had been conducted since 1960's as part of the state-sponsored hydrocarbon exploration programme by means of geophysical methods, among them – the two-dimensional (2D) seismic (single channel seismic reflection method, 2D common mid-point reflection method). The obtained information had been presented in exploration reports that are now available at the Lithuanian Geological Survey (LGS). Reports were aided with graphical appendices, among them – structural maps of main seismic horizons. In addition, a few suites of the maps of main seismic horizons were compiled for Western Lithuania or the entire Lithuania [1, 2, 3, 4].

After the break-up of USSR, the exploration activity shifted to private interest, and years from 1995 to 2015 were the most active for the industry of hydrocarbon exploration and production in Lithuania – hundreds of square kilometers of 3D seismic and thousands of kilometers of 2D seismic data were acquired, mainly in Western Lithuania. Despite lots of newly acquired 3D and 2D seismic data, none of this new information was included in the post-2000 maps produced by LGS [3, 4]. Publications, that consider the interpretation of these new seismic data, are scarce [5].

In our work, these relatively recently acquired 3D and 2D seismic data have been incorporated into a single seismic interpretation. Depth maps for the main seismic reflection horizons as well as a new presentation of fault traces have been made for the area which spans more than 50 km x 50 km and includes the so-called Gargždai Elevation. This elevation contains some of the Lithuanian hydrocarbon fields and is limited by the so-called Gargždai Fault to the east and south. The new maps are derived from the detailed 3D seismic and dense 2D seismic profile network, therefore, compared to the old maps, they are superior in the fine details and reveal new features as well. Though the change in structural pattern (horizon structure, re-mapping of faults) is an expected outcome when 2D-based interpretation is replaced with 3D-based interpretation, the new interpretation can demonstrate that the Gargždai Fault is not a single, continuous fault, rather, it is a system of faults which does not reach nor terminate at another regional fault in the north (the Telšiai Fault).

[1] Baltijos jūros pietrytinės dalies ordoviko atspindinčio horizonto struktūrinis žemėlapis M 1:500000, Lietuvos geologijos tarnyba (1975).
[2] Atraminio atspindinčio horizonto O3 – S1ln1 paviršiaus struktūrinis žemėlapis M1:200000, Lietuvos geologijos tarnyba (1996).
[3] Ordoviko kraigo struktūrinis žemėlapis M 1:500000, Lietuvos geologijos tarnyba (2003).
[4] Kambro sistemos kraigo struktūrinis žemėlapis M1:200000, Lietuvos geologijos tarnyba (2006).
[5] I. Šeštokas, 3D seismic exploration in Lithuania, Geologijos akiračiai (Journal of the Geological Society of Lithuania), **44**, 14-20 (2001).

DEVELOPMENT OF CFD-SUITABLE ANN MODEL OF LAMINAR BURNING VELOCITY

Andrius Ambrutis[1]

[1] Laboratory of Nuclear Installation Safety, Lithuanian Energy Institute, Lithuania
Andrius.ambrutis@lei.lt

Nowadays, as humanity faces a problem of climate friendly and powerful fuel, research in this field becomes more important than ever before. While electrical engines are one of the options, in many cases the amount of power produced by them is insufficient. Another good option is hydrogen based fuel. Combined with oxygen it burns, producing energy while leaving water as a product of this reaction. However, scientific understanding and predictive capabilities required for safe and efficient exploitation of hydrogen for fuel is still lacking.

To perform application-relevant simulations of complex turbulent hydrogen combustion, various simplifications are employed. One of them is omitting detailed chemistry modelling and approximating required data using other methods. In our CFD simulations we substitute chemistry model with parametric estimation of laminar burning velocity (LBV). Up to now, we have been using internationally established correlations of LBV as a function of mixture equivalence ratio, temperature and pressure. However, these correlations lack accuracy in the whole domain of required conditions, therefore, in this paper we investigate the behavior of hydrogen flame in dry air by using various machine learning algorithms in order to predict LBV. Our aim is to produce an experimental data (from literature) based LBV model which is both more accurate than established correlations and sufficiently fast to be of use for CFD simulations. Created model will be implemented in our turbulent combustion CFD solver flameFoam [1], where it will be available as an option to estimate LBV required for the simulations.

In one previous work [2] we created an artificial neural network (ANN) which managed to explain approximately 98 % of data points, however that model was too slow to be used in CFD calculations. To achieve faster estimation speeds, large variety of algorithms were tested. This led to a new ANN model with reduced number of weights with a prediction speed faster by around 30 times than original ANN model, with a mean absolute error equal to 6.094699 cm/s and R-Squared value of 0.997.

Other estimation methods were also tested for comparison - support vector machines (SVM), random forest (RF), k-nearest neighbor (kNN) and multivariate adaptive regression splines (MARS). The ANN model clearly showed better results (Fig. 1.) than other tested models of this study. Most likely in 2nd place would be Support Vector Machines (SVM), which after extra transformation to turn negative predictions to 0 gives a mean absolute error equal to 23.37 cm/s.

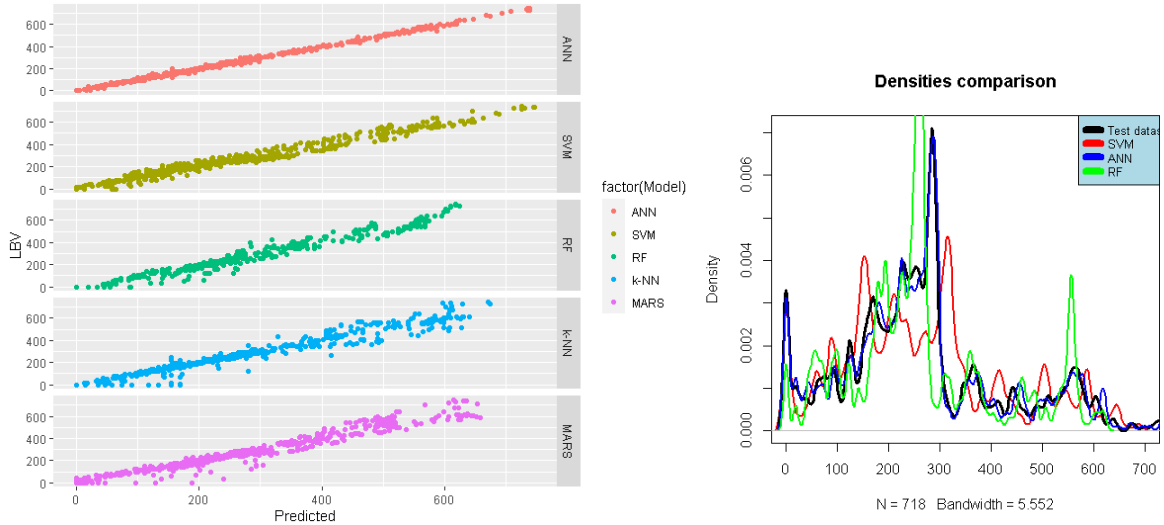


Fig. 1. Predicted and real values comparison of used models.

Overall, all models worked well compared with models founded in literature. This could be possible most likely for a few reasons:

1. Training data was prepared with most of the noise removed to make models more reliable.
2. Training was done using large amount of data (over 2000 data points), collected from literature.

A faster and accurate ANN model of hydrogen LBV was created for dry air and varying values of mixture equivalence ratio, temperature and pressure. Its accuracy is shown to be better than other tested methods. The work is being continued by implementing developed model into flameFoam CFD solver for validation simulations.

[1] M. Povilaitis, J. Jaseliūnaitė, flameFoam: An open source CFD solver for turbulent premixed combustion, Nuclear Engineering and Design, Volume 383, (2021), 111361, ISSN 0029-5493.

[2] M. Povilaitis, A. Ambrutis, Laminar burning velocity estimation using deep neural network, CYSENI 2021. Proceedings of annual conference of young scientists on energy issues, 393- 402, (2021).

SCALING OF EMPIRICAL COMPARTMENTAL DISTRIBUTIONS

Justas Kvedaravicius[1], Aleksejus Kononovicius[2]

[1]Faculty of Physics, Vilnius University, Lithuania
[2]Institute of Theoretical Physics and Astronomy, Faculty of Physics, Vilnius University, Lithuania
justas.kvedaravicius@ff.stud.vu.lt

Opinion dynamics is a focal topic in sociophysics. Yet some authors note that there's a lack of comparison between voter model's theoretical results and empirical (experimental) data [1]. To overcome this issue some authors have suggested to include space (geography) in modelling opinion dynamics [1, 2]. To understand the implications of space to opinion dynamics, it's worth studying how empirical data can entail structures of opinion or such indicators.

This research analyzes changes in empirical compartmental distributions by changing the scale of empirical data. For this purpose empirical data from United Kingdom 2011 census have been chosen. Different demographic indicators of this data exhibit narrowing distributions as scale becomes less detailed. Yet it is unclear whether distributions stem from existing socio-demographic structures in United Kingdom or are of spatial nature.

A randomized spatial model is proposed to discover the nature of observed distributions. It takes compartments (distinct territorial units) from the most detailed scale of empirical data and joins them to replicate the number of compartments of a less detailed scale. Thus the compartments of the new scale are not consistent with geography but rather randomized. The said procedure is repeated for all non-first data scales. Then two diversity quantities are chosen for which relative changes in their value are calculated. These quantities are, namely, standard deviation and Theil index. Changes of these quantities for randomized spatial model are compared to the ones produced by empirical data. Overall, the procedure used in this model resemble what is well-known in statistics as null-hypothesis testing.

Results of randomized spatial model with the ones produced by empirical data are shown in Fig. 1. It is shown that relative changes of diversity indices in random model decline more rapidly than the ones of empirical data. Furthermore, we show that changes of proposed model follow the $N^{-1/2}$ power-law for standard deviation whilst for Theil index these correspond to N^{-1}. These results also demonstrate that the changes in selected demographic indicators are not of stochastic (random) nature as they decay noticeably slower.

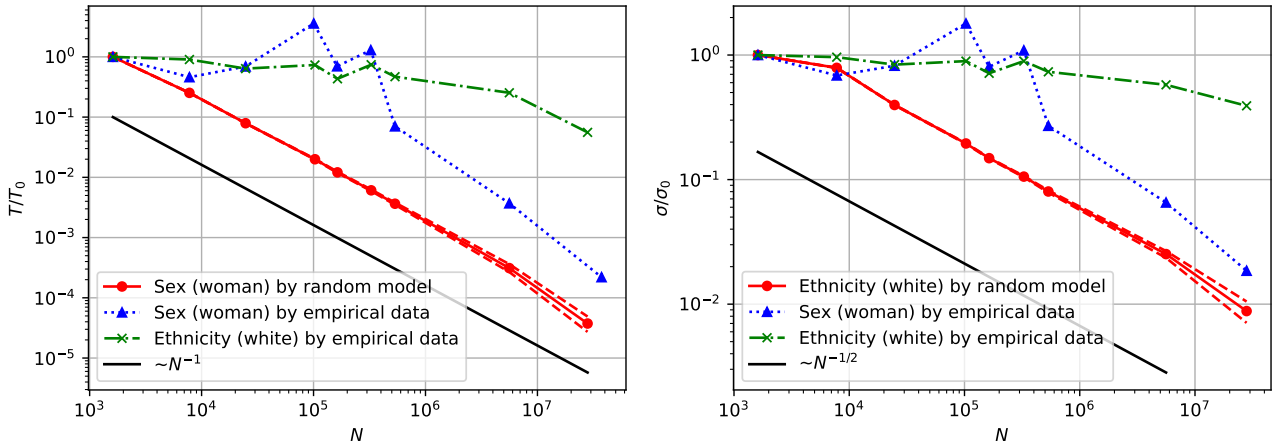


Fig. 1. Changes in relative measures of Theil index (left) and relative standard deviation (right). N (on the horizontal axis) represents the mean population in compartment at different scales of empirical data.

Among other results, it has also been noted that chosen diversity indices describe changes in different quality. Other two quantities (range and Gini coefficient) have also been tested for results with empirical data. Their relative changes are somewhat similar to the previously mentioned ones: range to Theil index and Gini coefficient to standard deviation.

In conclusion, the proposed randomized spatial model provides researchers with easy yet delicate measure to assess whether or not empirical data (or data generated by spatial models) is of stochastic nature. Different diversity and inequality quantities may be chosen for data evaluation as they are bound only to calculability via compartments. Lastly, the model is rather flexible so further adaptations can prove beneficial in testing other hypothesis.

[1] J. Fernandez-Gracia, K. Suchecki, J. J. Ramasco, M. Miguel, V. Eguiluz, *Is the voter model a model for voters?*, Physical Review Letters 112, 158701 (2014)
[2] A. Kononovicius, *Compartmental voter model*, Journal of Statistical Mechanics: Theory and Experiment 2019, 103402 (2019).

THE UNSCENTED KALMAN FILTER IMPLEMENTATION FOR THE SENSORLESS SPEED CONTROL OF A PERMANENT MAGNET SYNCHRONOUS MOTOR

Justas Dilys[1]

[1]State Research Institute Center for Physical Sciences and Technology
justas.dilys@ftmc.com

This paper addresses the implementation and optimization of an Unscented Kalman Filter (**UKF**) for the Permanent Magnet Synchronous Motor (**PMSM**) sensorless control using an ARM Cortex-M3 microcontroller. A various optimization levels based on arithmetic calculation reduction was implemented in ARM Cortex-M3 microcontroller. The execution time of UKF estimator was up to 90µs without loss of accuracy.

The unscented Kalman filter is mainly based on unscented transformation (**UT**). Unscented transformation is similar in its concept with Monte Carlo simulation which randomly picks sample, but this method makes a delicate selection of weighting for each sample. This significantly reduces the number of samples required compared to Monte Carlo simulation [1].

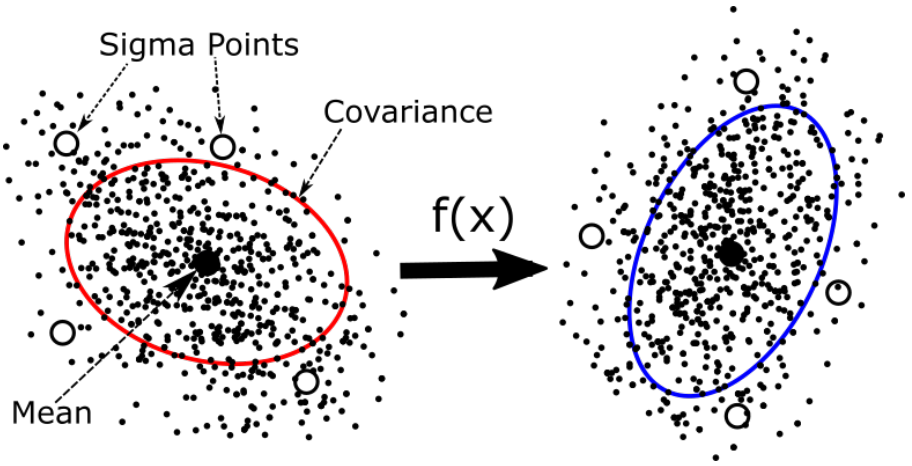


Fig. 2. Mean and covariance propagation through non-linear system

These sample points completely capture the true mean and covariance of the Gaussian random variable, and when propagated through the true non-linear system [2].

The complete UKF algorithm for position and speed estimation:

$$
\begin{aligned}
[\chi, \mathbf{W}] &= \text{SigmaPoints}(\hat{\mathbf{x}}_{k-1}, \hat{\mathbf{P}}_{k-1}, \kappa) \\
\mathbf{f}\chi &= \text{StatePrediction}(\chi, \mathbf{u}) \\
[\hat{\mathbf{x}}_k^-, \mathbf{P}_k^-] &= \text{UT}(\mathbf{f}\chi, \mathbf{W}, \mathbf{Q}) \\
\mathbf{h}\chi &= \mathbf{H}\mathbf{f}\chi \\
[\hat{\mathbf{y}}_k, \mathbf{P}_y] &= \text{UT}(\mathbf{h}\chi, \mathbf{W}, \mathbf{R}) \\
\mathbf{P}_{xy} &= \sum_{i=1}^{2n+1} W_i \{\mathbf{f}\chi_i - \hat{\mathbf{x}}_k^-\}\{\mathbf{h}\chi_i - \hat{\mathbf{y}}_k\}^T \\
\mathbf{K}_k &= \mathbf{P}_{xy}\mathbf{P}_y^{-1} \\
\hat{\mathbf{x}}_k &= \hat{\mathbf{x}}_k^- + \mathbf{K}_k(\mathbf{y}_k - \hat{\mathbf{y}}_k) \\
\mathbf{P}_k &= \mathbf{P}_k^- - \mathbf{K}_k\mathbf{P}_y\mathbf{K}_k^T
\end{aligned}
\tag{1}
$$

[1] Kim P., Huh L., "Kalman Filter for Beginners with MATLAB Examples", A-JIN, 2010.
[2] E. A. Wan and R. Van Der Merwe, "The unscented Kalman filter for nonlinear estimation, " Proceedings of the IEEE 2000 Adaptive Systems for Signal Processing, Communications, and Control Symposium (Cat. No.00EX373), 2000, pp. 153-158, doi: 10.1109/ASSPCC.2000.882463.

P1-23

DID NOT PARTICIPATE

.

RENORMALIZATION FLOW OF THE GRIMUS-NEUFELD MODEL AT ONE LOOP LEVEL

Rokas Garbačauskas[1], Thomas Gajdosik[1]

[1]Vilnius university, institute of theoretical physics and astronomy, Lithuania
rokas.garbacauskas@ff.stud.vu.lt

The Standard Model (SM) of particle physics is a very succesful theory. Taking as an input 19 (or 26 if one includes neutrino masses and their mixing angles) input parameters it produces a lot of testable predictions which up to now have withstood the experimental tests almost flawlessly. In fact some of the theoretical groundwork helped to make interesting discoveries, latest of which is the discovery of the Higgs boson.

On the other hand, the current widely accepted formulation of the SM is incomplete. For example the mechanism generating the aforementioned neutrino masses is still an open question. It has been experimentally verified in many independent experiments [1] that neutrinos can change their gauge eigenstates. This phenomenon is called neutrino oscillation. The mathematical apparatus that describes this requires that neutrinos have a mass. Many different SM additions have been proposed to accomplish this and are waiting for more experimental data to narrow down the parameter space. One such model is the Grimus-Neuefeld model (GNM) [2] which attempts to describe the two measured neutrino mass differences by an addition of an extra Higgs doublet and a sterile Majorana neutrino which via radiative mass corrections at 1 loop and the seesaw mechanism respectively do just that.

In our study we were searching for analytical expressions of the beta functions

$$\beta_\alpha = \mu \frac{d}{d\mu}\alpha. \tag{1}$$

which describe the change of the given parameters with respect to scale. Calculations involved corrections up to one loop level for some parameters essential for GNM, namely the gauge couplings of U(1) and SU(2), Yukawa couplings and the mass of the Majorana neutrino.

Achieving this required writing down the Lagrangian densities ($\mathscr{L}$) of these sectors in D dimensions in a consistent way. That is in order for the action ($S = \int d^D x \mathscr{L}$) to be dimensionless all terms of $\mathscr{L}$ have to be of mass dimension D, i. e. $[\mathscr{L}] = D$ (as usual in particle physics $\hbar = c = 1$). It is then conventional to rescale the couplings of the theory with a parameter μ ($[\mu] = 1$) in a way that the coupling itself remains a dimensionless number. For examle, in QCD $e \to \mu^{\frac{4-D}{2}} e$.

Feynman formalism was then used to write down amplitudes for events described by the parameters of interest. These amplitudes suffer from one of the issues that slowed down the advance of the mathematical apparatus behind the SM - Quantum Field Theory (QFT) - in mid XXth century: infinities emerging when evaluating integrals of some loop level corrections. The integrals generally have the form of

$$T^N_{\mu_1 \dots \mu_P}(p_1, \dots, p_{N-1}, m_0, \dots, m_{N-1}) = \frac{(2\pi\mu)^{4-D}}{i\pi^2} \int d^D q \frac{q_{\mu 1} \cdots q_{\mu P}}{D_0 D_1 \cdots D_{N-1}}, \tag{2}$$

where D is the dimension number, N is the number of propagator factors, P is the number of the integration momenta in the numerator and

$$D_i = (q + p_i)^2 - m_i^2 + i\varepsilon,\ p_0 = 0 \text{ and } i = 1, \dots, N-1.$$

In general these integrals diverge for $D \geq 4$ [3].

These divergences spurred the development of an entire new branch of mathematics called regularization. There are many regularization schemes but we used the most popular one - dimensional regularization - as it preserves Lorentz invariance. This approach lets the dimensionality of the problem stray from 4 by a small amount ε: $D = 4 - \varepsilon$. This allows to get analytical expression for the given integral. The divergent part is easily isolated and is written down in a counterterm Δ_α along with some constants depending on the convention and the dependance on the scale parameter. The couplings responsible for this specific interaction or field values are shifted by this counterterm. This allows to get finite values for measurable quantities as the diverging parts simply cancel out so ε can be safely sent to 0 at the end of the calculations. This also introduces the notion of running couplings as the new renormalized couplings are scale dependent. And details of this dependance are described by the beta functions eq. (1).

[1] M. G. Aartsen, M. Ackermann, J. Adams, et al., Search for nonstandard neutrino interactions with icecube deepcore, Phys. Rev. D, Apr 2018, 97, 072009

[2] Draukšas, Simonas & Dūdėnas, Vytautas & Gajdosik, Thomas & Juodagalvis, Andrius & Juodsnukis, Paulius & Jurčiukonis, Darius. (2019). The Grimus–Neufeld Model with FlexibleSUSY at One-Loop. Symmetry. 11. 1418. 10.3390/sym11111418.

[3] A. Denner, Techniques for the calculation of electroweak radiative corrections at the one-loop level and results for w-physics at lep200, 2007.

P1-25

DID NOT PARTICIPATE

.

P1-26

DID NOT PARTICIPATE

.

P1-27

DID NOT PARTICIPATE

.

DRELL-YAN PROCESS BACKGROUND ESTIMATION USING EM METHOD

Nomeda Tvaskaitė, Marijus Ambrozas

Institute of Theoretical Physics and Astronomy, Faculty of Physics, Vilnius University, Lithuania
nomeda.tvaskaite@ff.stud.vu.lt

Using the Large Hadron Collider (LHC) at CERN, scientists perform high-energy proton-proton collisions, which allow them to test predictions of different particle physics theories. Colliders like LHC reach a much higher center-of-mass energy than fixed target setups. Energy of proton-proton collisions at LHC reaches 13 TeV, which is the highest man-made collision energy ever achieved. A lot of new particles are produced during such collisions. Some of them are very heavy and decay almost instantly.

The Compact Muon Solenoid (CMS) is one of the four large particle detectors at the LHC. It is a general-purpose detector, used to study the Standard Model, search for extra dimensions and particles that possibly could make up dark matter. CMS has systems designed to measure the energy of electrons, photons, and other collision products. It uses a triggering system that allows it to register the rarest events that are later stored to be analyzed by physicists.

The Drell-Yan process occurs in high energy hadron-hadron collisions when a quark and an antiquark annihilate and create a lepton-antilepton pair. This process is interesting to scientists because its measurement results help them to test theoretical calculations of perturbative Quantum Chromodynamics (QCD), provides constraints on the evaluation of parton distribution functions (PDFs), which describe the inner structure of the proton. Drell-Yan also allows physicists to refine hadronization models, descriptions of the proton collision process and so on. However, it is very important to have the highest possible measurement accuracy to be able to refine the theory as much as possible.

Drell-Yan process cross section depends on several different parameters, and those different dependencies are measured by different scientific groups. The measured distributions always contain some percentage of background that needs to be estimated in order to measure the correct cross section. The easiest way to estimate background is to use Monte Carlo (MC) simulation, but it has its own uncertainties, such as imperfect modeling of detector response. To get rid of those uncertainties, scientists choose to estimate the background events using data-driven methods. Background processes that may produce two leptons of the same or different flavors are predicted using the eμ method, which will be presented in more detail during the conference.

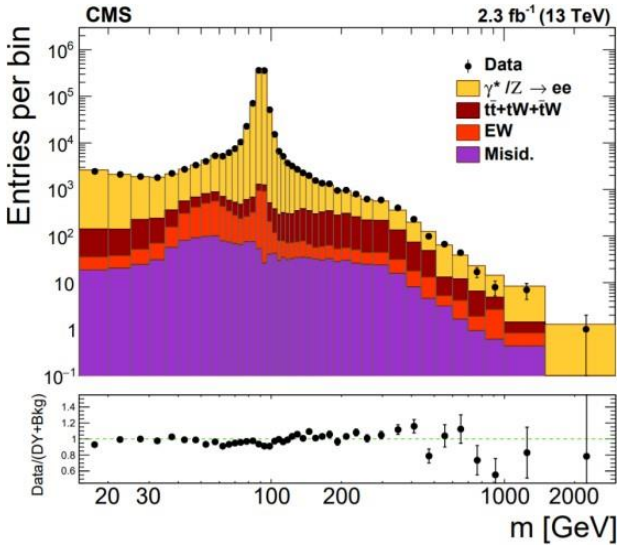


Fig. 1. Dielectron invariant mass spectrum at the proton-proton collision energy of 13 TeV [1]. The black dots represent the number of events measured with the CMS detector. The colors represent contribution of different processes. Yellow color marks the signal – the Drell-Yan process events. "EW" denotes diboson and DY → ττ processes. "Misid." corresponds to W+Jets and QCD processes.

[1] CMS Collaboration, Measurement of the differential Drell-Yan cross section in proton-proton collisions at √s=13 Tev, JHEP 12 059 (2019).

THE GRIMUS-LAVOURA APPROXIMATION FOR A LOW SEESAW SCALE

Simas Jankauskas[1], Thomas Gajdosik[1]

[1]Institute of Theoretical Physics and Astronomy, Vilnius University, Lithuania
simas.jankauskas@ff.stud.vu.lt

The Grimus-Neufeld model (GNM) [1] is an extension of the Standard Model (SM) of particle physics which can explain neutrinos having such a small mass. The model combines two principles: the seesaw mechanism and radiative masses, which allows Higgs mechanism to generate masses for the left-handed leptons. However, radiative one-loop corrections can generally be gauge-dependant and/or divergent. The Grimus-Lavoura approximation (GLA) [2] allows us to analytically calculate those masses at one-loop level, showing that right-handed neutrino and Dirac mass terms are subdominant and leaving us with only one massless neutrino. The final result depends on the ratios between right-handed neutrino and boson masses. The original paper [1] had the seesaw scale taken to be bigger than any mass in the standard model. In this work we try to find a way to show whether these approximation formulas also work in a regime where $M_R < M_Z < M_{S_b}$.

[1] W. Grimus and H. Neufeld, Radiative neutrino masses in an SU(2) × U(1) model, Nuclear Physics, section B **325**, 18–32 (1989).
[2] W. Grimus and L. Lavoura, One-loop corrections to the seesaw mechanism in the multi-Higgs-doublet Standard model, Physics Letters, section B **546**, 86–95 (2002).

RIGOROUS MODELLING OF DIFFRACTION GRATING DIFFRACTION EFFICIENCY UNDER MULTIPLE ANGLE ILLUMINATION

Tomas Klinavičius[1], Tomas Tamulevičius[1,2]

[1] Institute of Materials Science, Kaunas University of Technology, Lithuania
[2] Department of Physics, Kaunas University of Technology, Lithuania
tomas.klinavicius@ktu.edu

In recent decades the diffraction grating has become an essential component of many optical systems and devices, for example, spectrometers [1]. What is more, their manufacturing technologies such as different replication methods including nanoimprinting and soft lithography are widespread [2], thus opening up the possibilities for their mass production. However, diffraction efficiency of diffraction gratings depends on many factors, such as grating period, height, filling factor, materials used and other parameters [3]. Moreover, grating geometry can be optimized for best performance under defined spectral illumination conditions [4]. Numerical methods, like those based on finite differences or Fourier expansion [5] are frequently used as powerful tools for rigorous diffraction efficiency estimation of gratings at the pre-production stage. An example of the idealized grating structure unit cell visualization used for Finite-Difference Frequency-Domain (FDFD) is depicted figure 1

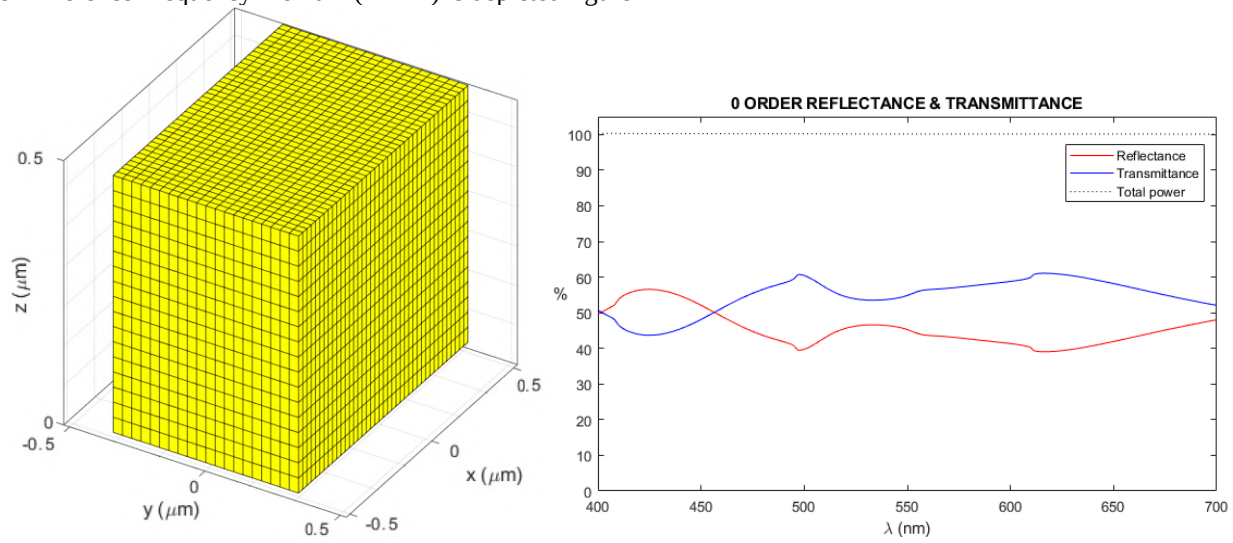


Fig. 1. Visualization of the one-dimensional 0.5 μm pitch, 0.5 μm trench depth, and 0.7 filing factor SiO_2 diffraction grating discretization in the FDFD numerical method (left) and its spectral response for TE polarization at 80º incidence (right)

In this work, the dependence of relative diffraction efficiency on diffraction grating height, period, and filing factor is determined employing numerical methods implemented in MATLAB. Diffraction efficiency is estimated for different light polarizations and angles of incidence as well as wavelengths in the visible range (400 nm – 700 nm). FDFD formulation of the Slice Absorption Method was used to compute diffraction efficiency [6]. The optimized grating structures are going to be used for realization of dot matrix holograms.

[1] E. Popov, Gratings: Theory and Numeric Applications, Presses universitaires de Provence, ISBN 978-2-8539-9860-4
[2] C. Palmer, Diffraction Grating Handbook 6th edition, Newport Corporation
[3] E. Sokolova, Optimization Techniques for Diffraction Spectrometers, SPIE, ISBN 978-1-6284-1673-2
[4] R. Aylwin, et al. Optimization methods for achieving high diffraction efficiency with perfect electric conducting gratings, Journal of the Optical Society of America A **37** (2020)
[5] T. Tamulevičius, et al. Numerical and experimental analysis of optical response of sub-wavelength period structure in carbonaceous film for refractive index sensing, Optics Express **22** (2014).
[6] R. Rumpf, et al. Rigorous electromagnetic analysis of volumetrically complex media using the slice absorption method, Journal of the Optical Society of America A **24** (2007)

P1-31

DID NOT PARTICIPATE

.

THEORETICAL INVESTIGATION OF OPTICAL PARAMETRIC GENERATOR AND AMPLIFIER BASED ON PERIODICALLY POLED LITHIUM NIOBATE PUMPED BY SUBNANOSECOND LASER PULSES

Simona Armalytė[1], Viktorija Tamulienė[1]

[1] Laser Research Center, Vilnius University, Saulėtekio 10, Vilnius LT-10223, Lithuania
simona.armalyte@ff.stud.vu.lt

Optical parametric generation (OPG) of subnanosecond pulses is a challenge due to the following restrictions: 1) the laser induced damage threshold is close to the generation threshold; 2) the synchronous pump configuration cannot be applied in the case of low repetition rate of the order of 1 kHz.

In the present work we present the results of the numerical simulations of the OPG and optical parametric amplification (OPA) in periodically poled lithium niobate (PPLN) crystal pumped by a subnanosecond laser pulses. The simulation parameters are based on the performed experiments with a 2 cm long crystal that will be presented elsewhere. The duration of a Gaussian pump pulse was 470 ps, the input energy was varied from 10 to 100 μJ, beam diameter was 160 μm.

Signal spectra for 8 different grating periods were calculated from phase-matching condition using temperature-dependent Sellmeier equation [1]. For OPG, output signal spectrum and output signal power were calculated according to formalism developed in [2]. The resulting spectra at T = 60 °C are presented in figure 1 (solid lines). As we can see, the spectra become broader with increase of signal wavelength.

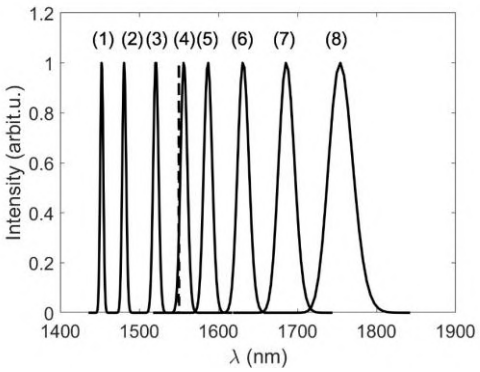


Fig. 1. OPG output signal spectra at 8 different grating periods (solid lines) and OPA output spectrum for the seed laser diode operating at 1550 nm wavelength and 4th grating (dashed line). Temperature T = 60 °C and pump energy E_3 = 40 μJ. Grating periods Λ (in μm): (1) 28,9, (2) 29,45, (3) 30,07, (4) 30,5, (5) 30,8, (6) 31,15, (7) 31,47, (8) 31,75. Laser diode power P_1 = 1 mW.

Temperature tuning was achieved for all 8 gratings. The simulations showed that conversion efficiency is larger at larger grating period and effective generation starts at pump energy of about 30 μJ for longer grating period and at around 40 μJ for shorter gratings.

For OPA, three-wave interaction model including dispersion terms was implemented. As in experiment, the seed of a laser diode operating in a continuous wave (cw) mode at 1550 nm wavelength was used. In contrast to OPA, in OPG the signal generation starts from the quantum noise. In OPA, the presence of the coherent light as a seed reduces the observed generation threshold. The spectrum width reduces, too, see figure 1, dashed line.

[1] Q. Paul, A. Quosing, T. Bauer, M. Nittmann, J.Bartschke, G. Anstett, J. A. L'Huillier, Temperature-dependent Sellmeier equation in the MIR for the extraordinary refractive index of 5% MgO doped congruent LiNbO3, Appl. Phys. B. **86**, 111-115 (2007).
[2] S. Acco, P. Blau, A. Arie, Output power and spectrum of optical parametric generator in the superfluorescent regime, Optics Letters **33**, 1264-1266 (2008).

CONSTRUCTION AND INVESTIGATION OF BBO SUBNANOSECOND OPTICAL PARAMETRIC AMPLIFIER

Gabrielė Stanionytė, Viktorija Tamulienė, Julius Vengelis, Rimantas Grigonis

Laser Research Center, Faculty of Physics, Vilnius University, Lithuania
gabriele.stanionyte@ff.stud.vu.lt

The wavelength of laser radiation is usually constant and changing it is extremely hard, which is why, in practice, parametric light generators are used, which allow to continuously change radiation wavelength in a wide spectral range. Currently, the parametric generators are created with ultrashort (less than 100 ps) and long (more than 1 ns) pulse durations, however subnanosecond pulse (less than 1 ns and more than 100 ps) generators have not yet been invented, this is due to certain physical limitations [1-3].

The goal of this research was to construct and investigate an optical parametric amplifier (OPA), which uses 15 mm beta barium borate (BBO) crystal as a nonlinear medium and Nd:YAG MOPA laser as a pump source. Here, fundamental harmonic (1064 nm) was used as pump source for seed radiation, and 3rd harmonic of laser (355 nm) – as pump radiation for the OPA. The seed was supercontinuum generated in a 1 m long solid-core highly nonlinear photonic crystal fiber (PCF).

The supercontinuum radiation extended from 720 nm to 1600 nm at maximum pump pulse energy. The maximum seed energy was measured to be 5.7 mW over the entire spectrum. We achieved signal wave generation via optical parametric amplification of idler wave. Further on, we measured spectral and energy characteristics of OPA. Signal wave tuning range was from 470 nm to 660 nm and was limited by idler wave tuning range which depends on seed radiation spectrum extension (idler wavelength tuning range was from 768 nm to 1450 nm). Generated signal wave power was low (of the order of microwatts) over the whole wavelength tuning range due to the fact that seed radiation spectral power density was low, pump intensity was also relatively low and limited by the laser induced damage threshold (LIDT) in the BBO crystal. Moreover, strong spatial walk-off effect between pump and signal/idler waves in the BBO crystal also limited parametric amplification efficiency. The experiment data was consistent with numerical simulation of the BBO OPA.

The results of this work will be used for further development of more effective subnanosecond OPA systems.

This research is founded by the European Regional Development Fund according to the supported activity 'Research Projects Implemented by World-class Researcher Groups' under Measure No. 01.2.2-LMT-K-718. Grant No. 01.2.2-LMT-K-718-03-0004.

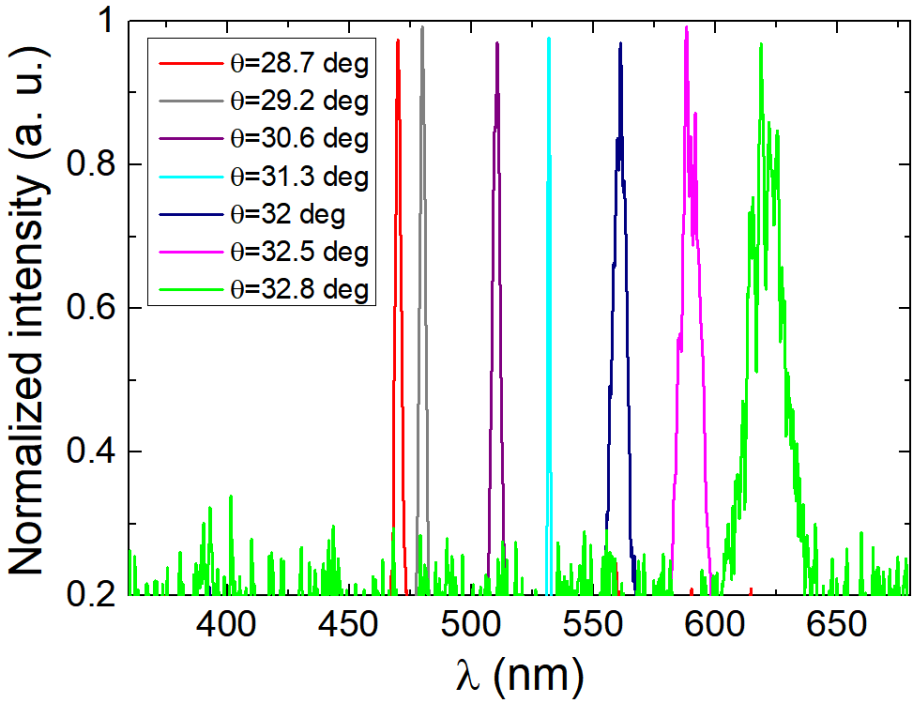


Fig. 1. Spectra of signal wave at different BBO crystal rotation angles.

[1] M. H. Dunn and M. Ebrahimzadeh, Parametric Generation of Tunable Light from Continuous-Wave to Femtosecond Pulses, Science 286, 1513–1518 (1999).
[2] R. W. Boyd, *Nonlinear Optics* ed. 3 (Academic press, New York 2008).
[3] A. Dubietis, *Netiesinė optika*, (Publisher Vilnius University, Vilnius 2011).

MEASUREMENT OF NONLINEAR REFRACTIVE INDEX AND ITS DISPERSION IN PHOTONIC CRYSTAL FIBER

Jokūbas Pimpė[1], Julius Vengelis[1], Vygandas Jarutis[1], Miglė Kuliešaitė[1]

[1] Laser Research Center, Faculty of Physics, Vilnius University, Lithuania
jokubas.pimpe@ff.vu.lt

Photonic crystal fibers (PCFs) are a unique type of optical fibers, completely different from conventional optical fibers, due to their periodic microstructure geometry of air holes running along the entire length of the PCF and surrounding the fiber's solid core. The engineering ability to alter various geometry parameters (air hole size and position) enabled various unique features that are not accessible for a common optical fiber. Due to their exceptional properties, solid-core PCFs are considered to be a perfect nonlinear medium for enhancing nonlinear effects, related to the third order nonlinear susceptibility $\chi^{(3)}$ or nonlinear refractive index n_2. Processes related with nonlinear refractive index, also known as optical Kerr effect, are self-phase modulation (SPM), cross-phase modulation (XPM), four-wave mixing (FWM) and even stimulated Raman scattering. Combined nonlinear processes can lead to different temporal and spatial pulse modulations, e. g., supercontinuum generation [1-4]. Therefore, it is necessary to properly evaluate the fiber's nonlinear refractive index and its dispersion. Although traditional nonlinear refractive index measurements methods, such as Z-scan, are practical and simple for bulk medium, this method is unsuitable when dealing with fibers, due to the waveguiding effect. Other methods based on FWM, or other nonlinear processes are also not applicable when ultrashort femtosecond pulses are used [5-6].

In this work we present a new method to measure nonlinear refractive index in optical fibers. It combines cross-correlation frequency-resolved optical gating (XFROG) measurement of controlled chirp femtosecond pulse spectrum broadening inside PCF together with theoretical modeling to determine the photonic crystal fiber's nonlinear refractive index and its dispersion values. Photonic crystal fiber nonlinear refractive index measurement was performed using Yb:KGW "Flint" oscillator generating 110 fs duration pulses with 75.2 MHz repetition rate and with a central wavelength of 1028 nm. A transform-limited pulse was obtained by evaluating and compensating pulse chirp values after passing all optical elements and additionally considering the dispersion caused by the focusing microscope objective. Pulse broadening measurements were performed by implementing XFROG technique and XFROG traces were measured at different pump power values. Then numerical simulations of pulse broadening at different pump power values were performed. The result is obtained (correct nonlinear refractive index value determined), when numerical simulation and experiment results are in good agreement.

Comparison between measured results and theorical modeling (Fig. 1) allowed to determine the nonlinear refractive index of a polarization maintaining SC-5.0-1040-PM photonic crystal fiber (mode field diameter is 4.3 μm ± 0.2 μm and ZDW is at 1040 nm ± 15 nm), which was equal to $1.8 \cdot 10^{-20}$ m^2/W and its dispersion $n_2' = 6.5 \cdot 10^{-20}$ m^2·fs/W. Furthermore, this approach also allowed to evaluate another important parameter describing the pulse propagation in PCF: pulse intensity modulation nonlinear coefficient, which in our case was equal to $\Delta n_2' = -1.3 \cdot 10^{-19}$ m^2 ·fs/W.

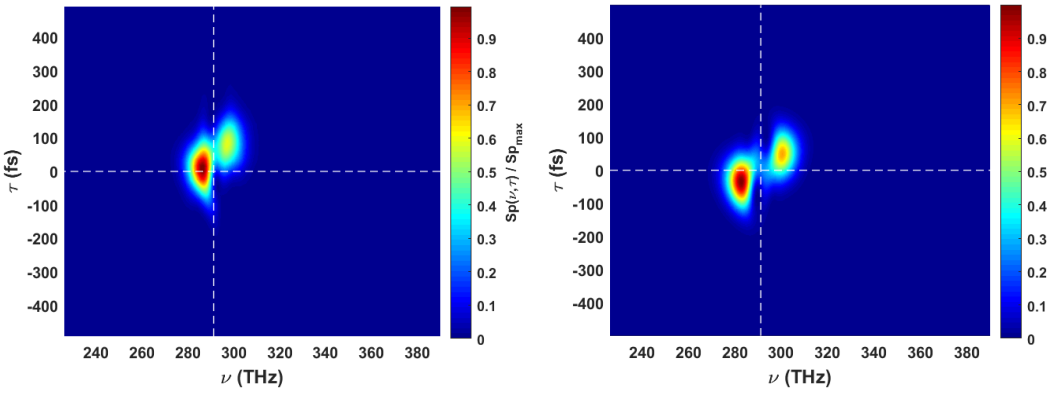


Fig. 1. Left: experiment results at 200 mW pump power. Right: theoretical model results at 200 mW pump power. The dashed lines indicate the initial pump 291 THz (1028 nm) pulse position.

[1] R. Buczynski, Photonic crystal fibers, Acta Physica Polonica Series A **106**(2), 141–168 (2004).
[2] P. Russell, Photonic crystal fibers, science **299**(5605), 358–362 (2003).
[3] A. Dubietis, *Netiesinė optika* (Vilniaus universiteto leidykla, 2011).
[4] R. W. Boyd, *Nonlinear Optics*, *Third Edition* (Academic Press, Inc., USA, 2008), 3rd edition.
[5] L. P´alfalvi, B. Tóth, G. Alm´asi, J. Fülöp, J. Hebling, A general z-scan theory, Applied Physics B **97**(3), 679–685 (2009).
[6] M. Artiglia, R. Caponi, F. Cisternino, C. Naddeo, D. Roccato, A new method for the measurement of the nonlinear refractive index of optical fiber, Optical Fiber Technology **2**(1), 75–79 (1996).

SELF-FOCUSING IN NONLINEAR PHOTONIC CRYSTALS

Tomas Montvydas[1], Vytautas Jukna[1] and Audrius Dubietis[1]

[1] Laser Research Center, Vilnius University, Saulėtekio Ave. 10, Vilnius LT-10223, Lithuania
tomas.montvydas@ff.stud.vu.lt

Femtosecond light filamentation is a common process that occurs during laser beam propagation through a nonlinear material. During this process, light self-focusses in to a very long, but small diameter zone, that exhibits crystal degradation due to plasma generation and color centers formation. In order to avoid these unwanted effects it is often beneficial to partially or even completely suppress the effect of self-focusing. It is demonstrated that for this purpose we can use light manipulating devices – photonic crystals [1]. Suppression of filamentation can be very beneficial for supercontinuum (SC) generation in bulk materials, as it could stop crystal degradation and prolong the SC lifetime.

In this work, we numerically model nonlinear laser beam propagation through modified spatial dispersion materials – photonic crystals. It is demonstrated that, beam propagation is dependent on the shape and radius of spatial dispersion curves. A few distinct modes of beam propagation can be distinguished: diffraction, antidiffraction and self-collimation (as shown in Fig. 1). Filamentation usually occurs in photonic crystals that exhibit positive spatial dispersion (diffractive materials). Complete suppression of filamentation can be seen in negative spatial dispersion photonic crystals (antidiffractive materials). We demonstrate that a crystal exhibiting flat spatial dispersion, can be used to suppress filamentation, but still maintain a partially collimated light beam propagation. Calculated total on axis nonlinear shift (also known as B integral) shows us that suppressed filamentation maintains a very similar amount of nonlinear phase shift when compared to beam propagation with filamentation. This result indicates that in photonic crystals that exhibit flat spatial dispersion we can expect a very similar amount of self-phase modulation, which could lead to a similar spectral broadening. At the same time largest achievable laser light intensity (at beam waist) is almost an order of magnitude lower.

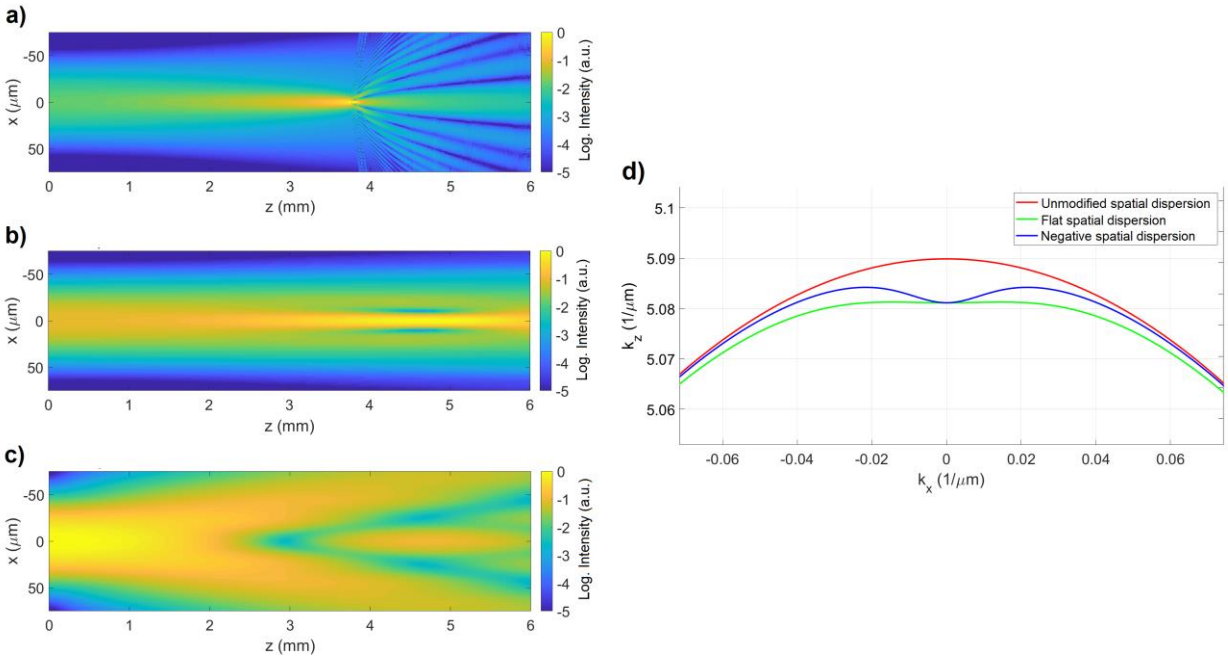


Fig. 1. Numerically modeled light beam propagation through: a) unmodified diffractive material (positive spatial dispersion), b) photonic crystal that exhibits self-focusing effect (flat spatial dispersion), c) photonic crystal that exhibits antidiffraction (negative spatial dispersion). Part d) shows corresponding spatial dispersion curves.

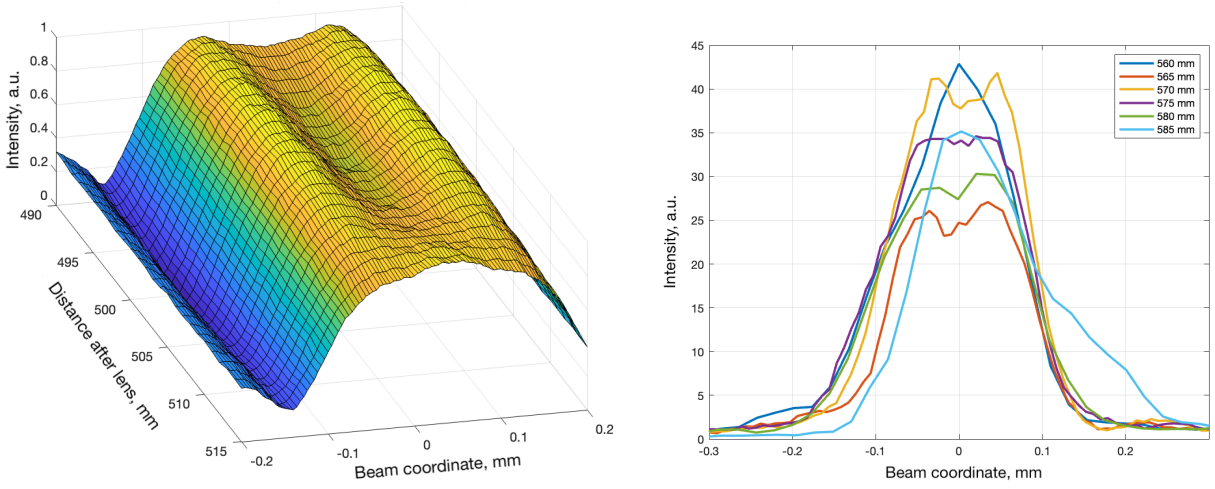
[1] K. Staliunas, R. Herrero, Nondiffractive propagation of light in photonic crystals, Physical Review E, 73(1), 016601 (2006).

SIMULATION AND DESIGN OF FLAT-TOP INTENSITY DISTRIBUTION GENERATING PHASE MASKS

Aivaras Labžentis, Simas Butkus, Vytautas Jukna, Valdas Sirutkaitis

Laser Research Center, Faculty of Physics, Vilnius University, Saulėtekio av. 10, Vilnius, Lithuania
aivaras.labzentis@ff.stud.vu.lt

Conventional material processing methods are being replaced by modern laser micromachining, as lasers are great tools when working with micro/nano scale objects, exhibits excellent machining and edge quality applicable in industry such as making miniature watch internal parts or nozzles in ink jets [1]. Most lasers emit beams having a Gaussian intensity distribution [2], though the peak of the distribution may initiate strong ablation of the material, the periphery of the beam may not be sufficient for material ablation, and the material may undergo heating and the micromachining quality decreases [3]. In addition, due to a non-zero gradient of the Gaussian beam the depth of the ablated channels tends to saturate and the profiles are not cylindrical and resemble a a V-shape. The peripheral damage may be reduced if a non-Gaussian intensity distribution is used [5]. Using a different beam intensity distribution such as a top-hat beam may be beneficial as it is reported that it reduces the heat affected zone and improves micromachining quality [6]. Top-hat beam can be shaped by using various optical designs such as πShaper from AdlOptica [7] or top hat beam shaping lens from Eksma [8]. Commercially available top-hat shapers usually are not easy to use, i.e. require careful tuning, work in a narrow wavelength and beam diameter range, are costly in range of thousands euros. Therefore, simpler solutions on how to transform a Gaussian beam into a beam resembling a top-hat distribution are on the search.



(a) Theoretical top-hat beam shape intensity propogation after f = 500 mm lens.

(b) Experimental data

Fig. 1. Beam propagation along the z axis after introducing a binary phase mask in its path.

A possible solution might be using binary phase plates, which would cost several EUR/piece and would require little to no adjustments prior to use. In this research a binary phase plate was designed and fabricated from BK glass and was examined both theoretically and experimentally. It was discovered that it is possible to form quasi top-hat beam using a binary phase plate with a square aperture, which introduces a $\lambda/2$ phase shift at certain parts of the Gaussian beam the quasi top-hat beam distribution is maintained along the propagation direction of approximately 0.3 parts of the Raileygh range. The acquired experimental results were comparable with the theoretical data by using diffraction theory.

[1] R. S. Taylor, C. Hnatovsky, E. Simova, D. M. Rayner, V. R. Bhardwaj, P. B. Corkum, Femtosecond laser fabrication of nanostructures in silica glass, Optics Letters 28(12), 1043 (2003)
[2] H. Le, P. Penchev, A. Henrottin, D. Bruneel, V. Nasrollahi, J. A. R. de Campos, S. Dimov, Effects of top-hat laser beam processing and scanning strategies in laser micro-structuring, Micromachines 11(2), 221 (2020)
[3] A. Horn, U. Klug, J. Düsing, J. G. Moreno, V. Schütz, O. Suttmann, L. Overmeyer, A. Lenk, B. Wojakowski, Micromachining, in Springer Series in Optical Sciences (Springer International Publishing, 2015), 155–173
[4] G. Kamlage, T. Bauer, A. Ostendorf, B. Chichkov, Deep drilling of metals by femtose- cond laser pulses, Applied Physics A 77(2), 307–310 (2003)
[5] C. Bischoff, E. Jäger, U. Umhofer, Beam shaping optics for process acceleration, La- ser Technik Journal 12(3), 53–57 (2015)
[6] O. Homburg, F. Toennissen, T. Mitra, V. Lissotschenko, Laser direct micro-machining with top-hat-converted single mode lasers, in W. Pfleging, Y. Lu, K. Washio, W. Hoving, J. Amako (eds.), Laser-based Micro- and Nanopackaging and Assembly II (SPIE, 2008)
[7] http://pishaper.com/k.html Last checked 2022-01-20
[8] https://eksmaoptics.com/optical-systems/top-hat-beam-shaping-lenses. Last checked 2022-01-20

THE FORMATION OF OPTICAL COATINGS ON HYBRID POLYMER SZ2080 USING ATOMIC LAYER DEPOSITION TECHNOLOGY

Darija Astrauskytė[1], Mantas Drazdys[1], Ramutis Drazdys[1], Darius Gailevičius[2], Lina Grinevičiūtė[1]

[1] Center for Physical Sciences and Technology, Savanorių av. 231, LT-02300, Vilnius, Lithuania
[2] Laser Research Center, Vilnius University, Saulėtekio av. 10, LT-10223, Vilnius, Lithuania
darija.astrauskyte@ftmc.lt

Hybrid organic-inorganic polymers are widely used for the fabrication of photonic crystals, metamaterials or micro-optical components using two-photon polymerization and deep UV lithography techniques [1]. The demand for deposit coatings on 3D structures is growing and it is necessary to find alternatives to conventional physical vapor deposition technologies that are not capable to fabricate conformal coatings on 3D components [2]. Atomic layer deposition (ALD) is a promising thin film deposition technique because of strict control of the growth rate and the opportunity to fabricate coating on complex structure substrates. The principle of ALD is the formation of an atomic layer per one ALD cycle during self-limiting surface exchange reactions [3].

Hybrid polymer SZ2080™ is used for the fabrication of micro-optical components using the two-photon polymerization technique [4]. SZ2080 is synthesized mainly from methacryloxypropyl trimethoxysilane (MAPTMS) and zirconium propoxide (ZPO) precursors. In this work we present thin films grown on SZ2080 surface using the atomic layer deposition technique. Growth dynamics of the aluminium oxide on SZ2080 were investigated using quartz crystal microbalance. Linear growth begins after 10 cycles.

Trimethylaluminum and tetrakis(dimethylamino)titanium were used as precursors and oxygen plasma was used as a reactant. Aluminium oxide and titanium oxide singlelayer coatings were synthesized at 60 ºC. The refractive indices and optical losses of the manufactured Al_2O_3 and TiO_2 films were evaluated from the transmittance spectra of thin single layers and used for the numerical design of the anti-reflective (AR) optical coating.

To achieve a low reflectance R < 0,1 % at the wavelength of 1064 nm, TiO_2 was used as the high refractive index material while Al_2O_3 was used as the low refractive index material. The final structure was fabricated and analyzed. Experimental measurements are in good agreement with theoretical simulations (see Fig. 1). The coating decreases the reflection from 3,3 % to 0,1 % at the wavelength of 1064 nm for one surface of SZ2080 layer without any visible cracks or destructive deformations. In perspective, this is the first step toward technologically viable applications.

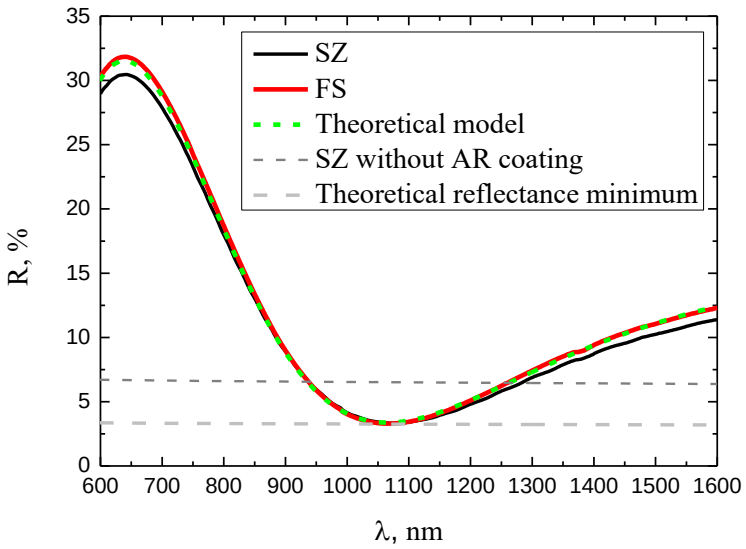


Fig. 1. Reflectance spectra of anti-reflective coating, synthesized on fused-silica and SZ2080 surfaces.

[1] Emons, Moritz, et al. Two-photon polymerization technique with sub-50 nm resolution by sub-10 fs laser pulses, Optical Materials Express 2.7 (2012).
[2] Žukauskas, Albertas, Mangirdas Malinauskas, and Etienne Brasselet, Monolithic generators of pseudo-nondiffracting optical vortex beams at the microscale, Applied Physics Letters 103.18 (2013).
[3] M. Ritala, J. Niinisto, Chemical Vapour Deposition, Royal Society of Chemistry, 9–11, (2009).
[4] Ovsianikov, Aleksandr, et al. "Ultra-low shrinkage hybrid photosensitive material for two-photon polymerization microfabrication." *ACS nano* 2.11 (2008).

LASER INDUCED DAMAGE STUDY OF SCULPTURED THIN FILM BASED ALL-SILICA MIRRORS EXPOSED TO VARIOUS ENVIRONMENTS

Gustė Dolmantaitė, Lukas Ramalis, Rytis Buzelis, Tomas Tolenis

Center for Physical Sciences and Technology, Savanoriu Ave. 231, LT-02300 Vilnius, Lithuania
guste.dolmantaite@ftmc.lt

Optical resistance to laser radiation is a significant parameter of the coatings. Conventional approach for dielectric mirror formation is to utilize high and low refractive index dielectric materials which are deposited using various physical vapor deposition methods. However, such coatings are limited by a high refractive index material (low band-gap) in terms of Laser Induced Damage Threshold (LIDT) value. An innovative materials engineering technique, Glancing Angle Deposition (GLAD), may be used as a promising technology to avoid low band-gap material usage.

Over the past few years GLAD method has shown its potential for all-silica highly resistant optical coatings [1, 2]. This method allows to manipulate the refractive index of the layer by depositing the same material at oblique angle. The porosity of the material and, correspondingly, the refractive index can be altered by changing the deposition angle between the substrate normal and the incident vapor flux. Therefore, Bragg mirror is formed by combining porous silica layers, considered as low refractive index layer, and dense silica as high refractive index films. Such mirrors are deposited with very low mechanical intrinsic stress value, which is crucial in nanosecond regime.

However, water and other harmful particles from the environment can be absorbed by the coating. Therefore, all-silica mirrors held in different environments are investigated by using high laser radiation.

In this work four highly reflective all-silica Bragg mirrors were produced using GLAD technique. Their design was modeled to reflect >99% at normal angle of the incidence light at the wavelength of 355nm. One sample was placed in desiccator and three samples were placed separately in polyethylene terephthalate glycol (PET-G) boxes with different gas environments: oxygen, argon, and nitrogen. The boxes were sealed with Kapton tape. After one week 1-on-1 LIDT measurements were performed to the coatings, stored in different environments, to investigate the optical resistance of mirrors and to analyze how environment affects the samples. Laser induced damage after one week for a sample stored in argon gas is presented in Fig. 1. The same measurements were repeated after two weeks of storage.

Presented results in Fig. 2 show that the most stable mirror persists stored in argon environment (LIDT 91.2 J/cm^2) and one week after the first measurements LIDT value decreased by 10%. Similar LIDT was achieved after one week storage in nitrogen environment (90 J/cm^2). Even though porous silica coatings tend to absorb water and other harmful particles from the environment, this study has shown that it is feasible to preserve optical parameters and to achieve high LIDT values.

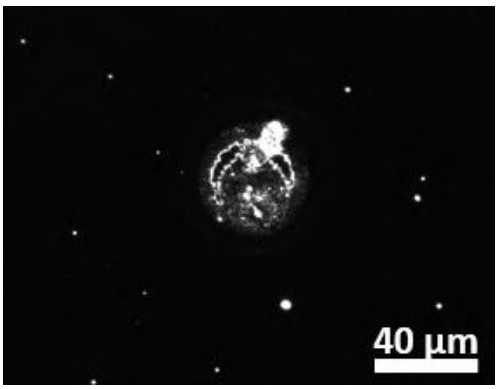


Fig. 1. Laser induced damage (energy flux at 118.6J/cm^2).

Ambient: argon gas.

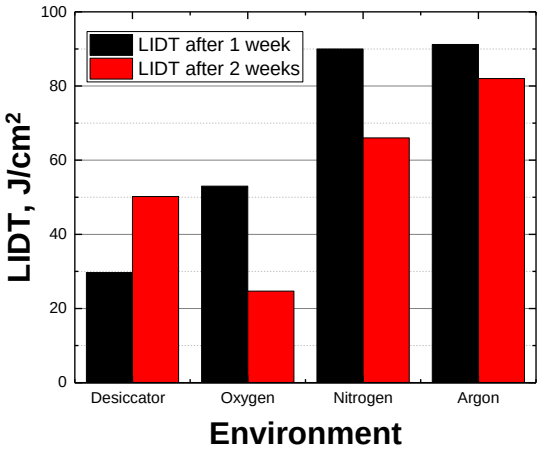


Fig. 2. LIDT results after 1 and 2 weeks storage in different environments.

[1] T. Tolenis et al., Next generation highly resistant mirrors featuring all-silica layers, Sci. Reports **7**, 1–9, (2017).
[2] C. Smith, J. Foster, J. Spaulding, et al., Glancing-angle-deposited silica films for ultraviolet wave plates, Appl. Opt. **59**, A155–A161, (2020).

ABLATION OF MICROCHANNELS IN GLASS USING 206 NM – 1030 NM WAVELENGTH FEMTOSECOND PULSES

Bernadeta Labžentienė[1], Simas Butkus[1], Domas Paipulas[1] and Valdas Sirutkaitis[1]

[1] Laser Research Center, Faculty of Physics, Vilnius University, Saulėtekio Ave. 10, LT-10223 Vilnius, Lithuania
bernadeta.labzentiene@ff.vu.lt

Conventional material processing methods cannot meet the demands of high precision requirements for products with micro – scale dimensions [1]. For this reason, laser material processing has attracted more attention because of its accuracy and wide range of potential industrial application, such as micromachining [2]. Working with femtosecond pulses exhibits high microchannel micromachining accuracy and great quality in comparison to longer laser pulses, thus its' use is increasing in various industrial applications [3].

Although femtosecond lasers are great for micromachining applications, there are difficulties working on microchannel formation in glass. First of all, it is complicated to control the depth and shape of the channel a s it tends to taper [4]. Secondly, laser induced channel width and depth ratio control is not trivial as it depends on laser power, pulse frequency and number of passes [5], as well it depends on laser pulse wavelength, because for infrared pulses multi-phonon absorption dominates due to low photon energy, however, for ultraviolet (UV) pulses direct absorption dominates because of high photon energy. Since direct absorption leads of a smaller skin-depth, it is expected that UV wavelengths would yield better results in terms of microchannel form.

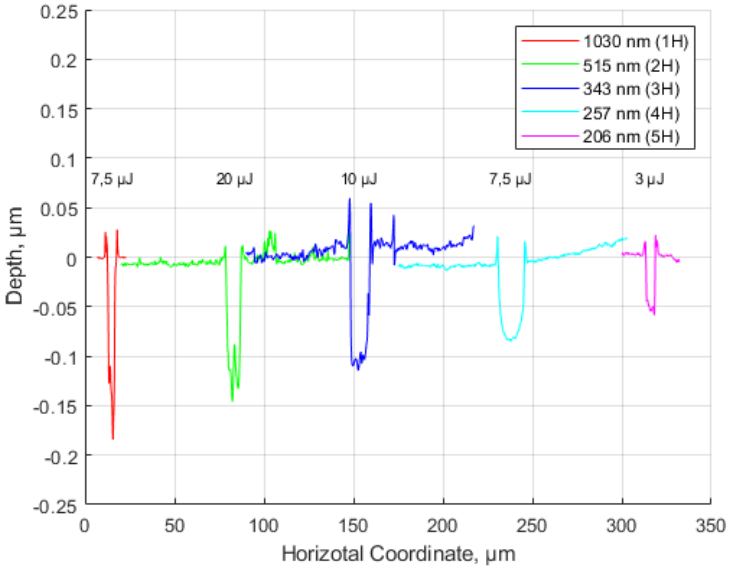


Fig. 1 Profiles of microchannels after one laser pulse.

The aim of this study is to observe the properties of ablation of microchannels in glass using various wavelength femtosecond pulses (laser "Pharos"). During the experiment, microchannels were formed on the surface of soda – lime glass using different pulse energies, pulse count and wavelengths. The sample was moved using a positioning table "Aerotech ABL1500WB". The shape of the microchannels, their depth dependence on fluence was examined using a laser scanning microscope "OLYMPUS OLS5000" and optical profilometer "SensoFar PLµ2300". Fig. 1 shows the profiles of microchannels ablated with different wavelengths ranging from infrared to ultraviolet after one laser pulse. It was seen, that a higher depth of the microchannels was achieved using the 1st harmonic compared to the 4th and 5th ones because of different absorption mechanisms.

[1] I. John, *Laser processing of engineering materials: principles, procedure and industrial application* (Elsevier, 2005)
[2] M. C. Gower, Industrial applications of laser micromachining, Opt. Express **7**, 56-67 (2000)
[3] D. N. García and G. O'Connor, *Advances in Microfluidics*, New Applications in Biology, Energy, and Materials Sciences. (InTechOpen, 2016).
[4] H. Huang, L.-M. Yang, J. Liu, Micro-hole drilling and cutting using femtosecond fiber laser, Optical Engineering **53**(5) (2014)
[5] S. Darvishi, T. Cubaud, J. P. Longtin, Ultrafast laser machining of tapered microchannels in glass and PDMS, Optics and Lasers in Engineering **50**(2) 210-214 (2012)

CONTROLLED GENERATION OF AIRY BEAMS USING PHASE ELEMENTS

Karolis Mundrys[1,2], Sergejus Orlovas[2], Paulius Šlevas[2]

[1] Department of Physics, Vilnius University, Lithuania
[2] Center for Physical Sciences and Technology, Lithuania
Karolis.mundrys@ff.stud.vu.lt

Unconventional laser beams have an increasing demand in laser micro-processing of transparent material. One of such unconventional laser beams is an Airy beam. The main advantage of the Airy beam is that its intensity distribution can be controlled both in the direction of the propagation axis and in the cross-section. This feature allows for the generation of an Airy beam with desired parameters.

The solution of the Schrödinger equation for a free particle may be mathematically defined using the Airy function [1]. The Fourier transform of this wave packet gives the following expression for the spatial spectra $\tilde{\varphi}$ [2]:

$$\tilde{\varphi}(k_x, k_y) = A_0 \mathrm{e}^{-a\left(k_x^2+k_y^2\right)} \exp\left(i\frac{k_x^3+k_y^3}{3}\right), \quad (1)$$

where A_0 is the normalization constant and k_x, k_y are spatial frequencies for x and y coordinates. Thus, in order to obtain an Airy beam, it is only necessary to modulate the Gaussian beam with a cubic phase and perform a Fourier transform. By adding a linear term to the cubic phase mask, the position of the central maxima of the Airy beam can be flexibly positioned in a transverse plane. The expression for the phase mask is as follows:

$$T = \mathrm{e}^{-i[a(x^3+y^3)+b(x+y)]}, \quad (2)$$

where a is a constant denoting the period of the cubic phase and b is a constant denoting the slope of the linear phase. The Airy beam can be flexibly adjusted by changing the value of b, see Fig. 1

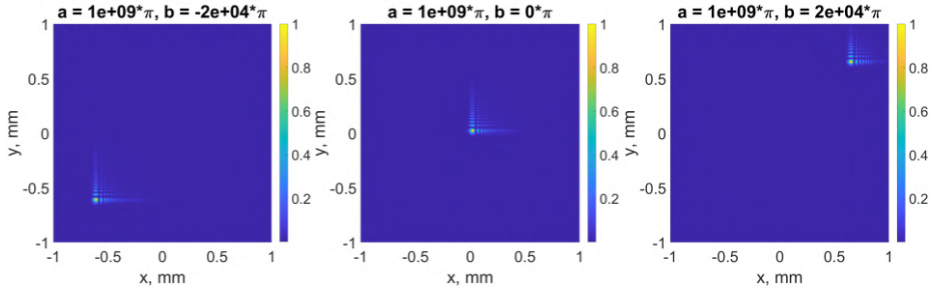


Fig. 1. Influence of $b(x+y)$ term in the phase mask on the resulting intensity distribution of the Airy beam. The results are shown in the XY plane. Used parameters: $a = 10^9$ π, $b = -2\times10^4$ π; $a = 10^9$ π, $b = 0$; $a = 10^9$ π, $b = 2\times10^4$ π.

The Airy beam can also be flexibly positioned with respect to the direction of propagation by adding a parabolic term to the cubic phase mask. The expression of the phase mask is described as follows:

$$T = \mathrm{e}^{-i[a(x^3+y^3)+c(x^2+y^2)]}, \quad (3)$$

Here c is a constant describing the slope of the phase delay. The Airy beam can be controlled by varying the value of the coefficient c, see Fig. 2

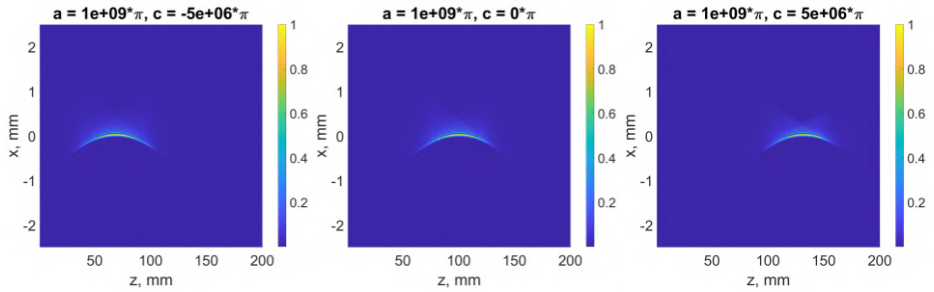


Fig. 2. Influence of $c(x^2+y^2)$ term in the phase mask on the resulting intensity distribution of the Airy beam. The results are presented in the XZ plane. Used parameters: $a = 10^9$ π, $c = -5\times10^6$ π; $a = 10^9$ π, $c = 0$; $a = 10^9$ π, $c = 5\times10^6$ π.

These approaches help to generate a non-diffractive Airy beam with flexibly adjusted properties of the central intensity lobe.

[1] Berry, M. V., & Balazs, N. L. Nonspreading wave packets. American Journal of Physics, 47 (3), 264-267 (1979).
[2] Wei, Bing-Yan, et al. Polarization-controllable Airy beams generated via a photoaligned directorvariant liquid crystal mask. Scientific reports, 5.1: 1-8. (2015).

MICROSTRUCTURING OF TRANSPARENT SURFACES FOR EFFICIENT DIFFRACTIVE OPTICAL ELEMENTS

Evelina Stonytė[1],* Dominyka Stonytė[1], Domas Paipulas[1]

[1] Laser Research Center, Faculty of Physics, Vilnius University, Saulėtekio av. 10, LT-10223 Vilnius, Lithuania
evelina.stonyte@ff.vu.lt

Recent technological miniaturization trends show a growing need for an improvement in the quality of microprocessing technologies. Currently available solid state laser systems deliver ultrashort, high-intensity pulses and are a common choice when there is a need for high precision in microfabrication. However, the beam of these systems has a gaussian intensity distribution, and material ablation corresponding to one pulse is also gaussian – the oval pit is left on the surface. Unfortunately, gaussian intensity distribution is no longer sufficient for maintaining extremely low roughness in polishing applications. That is where diffractive optical elements (DOE) play an important role in the improvement of accuracy and processing speed in various micromachining methods. By manipulating the incident beam‘s phase, these microstructured elements are able to obtain a desired beam intensity distribution. One of the commonly used elements is a flat-top beam shaper, which forms a square shaped beam with a homogeneous intensity distribution [1]. After interacting with the material, a laser pulse shaped like this would leave a squared pit with a smooth bottom. Since the micro-structuring resolution of these elements is a key point in achieving a great beam conversion efficiency, they are mostly manufactured by using lithographic methods, as these techniques are associated with an ability to achieve small feature sizes in the order of tens of nanometers [2, 3]. However, these methods are quite expensive and robust if compared to the direct laser ablation technique.

In this study, we present modelling results of a phase mask, adapted for manufacturing with our experimental setup, which consists of Yb:KGW laser system (PHAROS, Light Conversion) with 5th harmonic generator, Aerotech ANT180 micro-positioning system, and calcium fluoride lenses for beam focusing. The phase mask, producing a flat top intensity distribution at the far field, was generated by the LightTrans company's software package "VirtualLab" which uses the iterative Fourier transformation algorithm [4]. Geometrical microstructuring parameter optimization was conducted and an optimal parameter set was found (10 μm x 10 μm pixel size and 5 phase levels), resulting in the highest experimentally obtainable conversion efficiency of 85 percent. It was also noticed that by increasing the number of phase levels up to 7, conversion efficiency increases and saturates above that value.

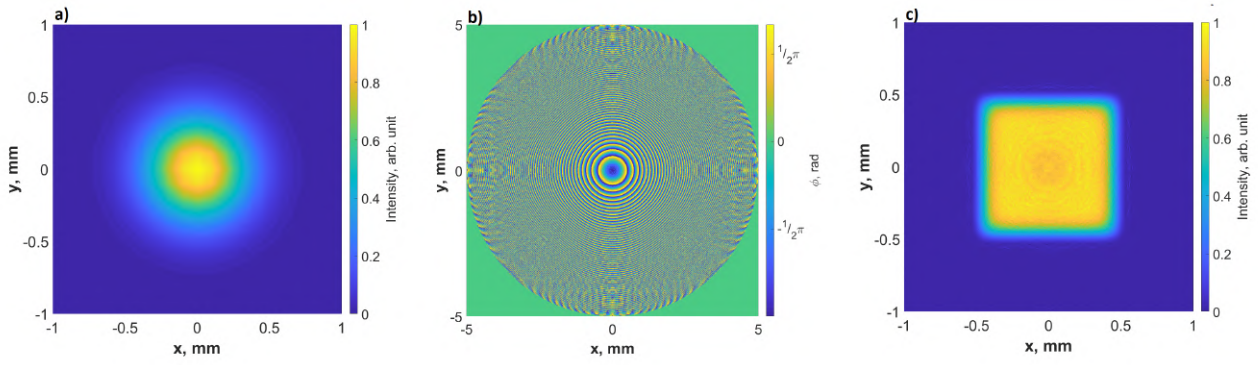


Fig. 1. Flat top beam shaper modelling results: a) input beam, b) optimal phase mask, c) resulting output field.

[1] S. Katz, *Using Diffrac tive Optical Elements* (Optik & Photonik, Israel, 2018).
[2] T. Wildi, *Diamond Diffractive Beam Shapers* (Optica Publishing Group, Switzerland, 2019).
[3] Y. Sun, *Design of beam shaping and focusing metasurface device based on GS algorithm* (Elsevier, China, 2020).
[4] P. Birch, *A comparison of the iterative Fourier transform method and evolutionary algorithms for the design of diffractive optical elements* (Elsevier, UK, 2000).

IMPLEMENTING THE GERCHBERG-SAXTON ALGORITHM IN DIGITAL SIGNAL PROCESSORS

Varis Karitans[1]

[1] Institute of Soid State Physics, University of Latvia, Latvia
[2] Department of Optometry and Vision Science, University of Latvia, Latvia
Varis.Karitans@cfi.lu.lv

In computational optics, phase retrieval is a widely studied field. Phase retrieval seeks to solve the phase problem, i.e., to retrieve the missing information about the phase of an object from intensity measurements. Over years, many phase retrieval algorithms have been developed. The first successful algorithm was the Gerchberg-Saxton algorithm based on alternating projections [1]. Here, we describe implementation of the Gerchberg-Saxton algorithm in digital signal processors to be used in embedded systems for phase retrieval of transparent phase objects.

First, software is written in MPLAB IDE environment for a digital signal processor dsPIC30F6014A. In simulations, a cross-section of tertiary spherical aberration is used as the test object. Distribution of light intensity is calculated in the central plane and planes equally spaced on both sides of the central plane. The plane of unknown phase is propagated forth and back, and the phase is continuously updated while the intensity after the propagation is replaced by the actual intensity. The true phase is approached iteratively and compared to the actual phase.

Figure below shows the results of simulations – the original object is shown on the left while its reconstruction is shown on the right. Similarity between the original object and the reconstruction can be seen clearly. The noise present in the reconstructed object may be due to an insufficient number of iterations and/or inappropriate initial guess of the phase.

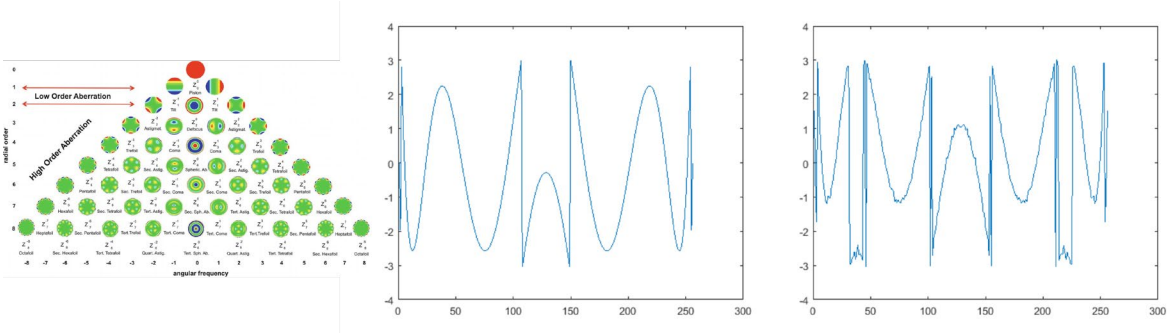


Fig. 1. Zernike pyramid (left); the cross-section of tertiary spherical aberration (middle); the retrieved object (right).

Next, we plan to implement the digital signal processor in an embedded system where it will receive real data from an imaging sensor. It is intended to study two-dimensional objects by optically splitting them into parallel vectors each of which will be retrieved by the algorithm implemented in the embedded system. Next, all the vectors will be merged based on the method of least squares. In this way, the time required to retrieve two-dimensional objects could be significantly reduced compared to the time required to retrieve these objects from two-dimensional diffraction patterns (see Figure 2).

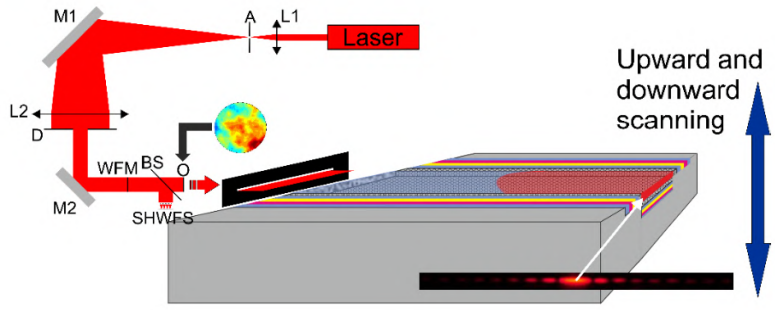


Fig. 2. The intended optical system for retrieving the phase of a two-dimensional object using the Gerchberg-Saxton algorithm implemented into an embedded system.

The study is supported by the UL Foundation and company “MikroTik” (project “Implementing phase retrieval algorithms in embedded systems”; project code 2257).

[1] Y. Shechtman, Y. C. Eldar, O. Cohen et al., Phase retrieval with application to optical imaging, IEEE Signal Processing Magazine **32**, 87-109 (2015).

LEAKY MODES OF MODULATED WAVEGUIDES FOR SPATIAL FILTERING

Ignas Lukošiūnas[1], Darius Gailevičius [1], Kestutis Staliūnas [1,2,3]

[1] Vilnius University, Faculty of Physics, Laser Research Center, Saulėtekio Ave. 10, Vilnius, Lithuania
[2] ICREA, Passeig Lluís Companys 23, 08010, Barcelona, Spain
[3] UPC, Dep. de Fisica, Rambla Sant Nebridi 22, 08222, Terrassa (Barcelona) Spain
ignas.lukosiunas@ff.vu.lt

One of the ways to improve the beam's spatial quality is by applying a spatial filtering mechanism onto the resonator system. Classical laser systems use a confocal arrangement of lenses and a membrane stationed between them to filter the beam. Such a system is extremely necessary if the pump power is highly increased. However, small compact micro-laser, as well as semiconductor devices, acquire new means of filtering for improvement of the beam's spatial quality, which is realized through implementing sub-wavelength periodic waveguide or photonic crystal systems either as low-pass transmitting filters or as reflectors [1].

Photonic crystals possess unique abilities to guide, transmit and reflect light, which entirely depends on the periodicity and aperiodicity of the device's geometrical layout (i.e. its lattice) as well as its modulation of refractive index. Various numerical models of such devices are being made and analyzed, especially the speedy Rigorous Coupled Wave Analysis (RCWA) [2], which is a semi-analytical method that numerically solves Maxwell's equations via Fourier expansion of the electric, magnetic fields, as well as the dielectric permittivity itself. It is used to primarily calculate transmittance and reflection of periodic waveguides that consist of arbitrary geometry. With the implementation of a global optimization algorithm, the geometrical parameters, as well as the distribution of refractive index in the system of periodic waveguides, can be optimized to achieve desired filtering effect.

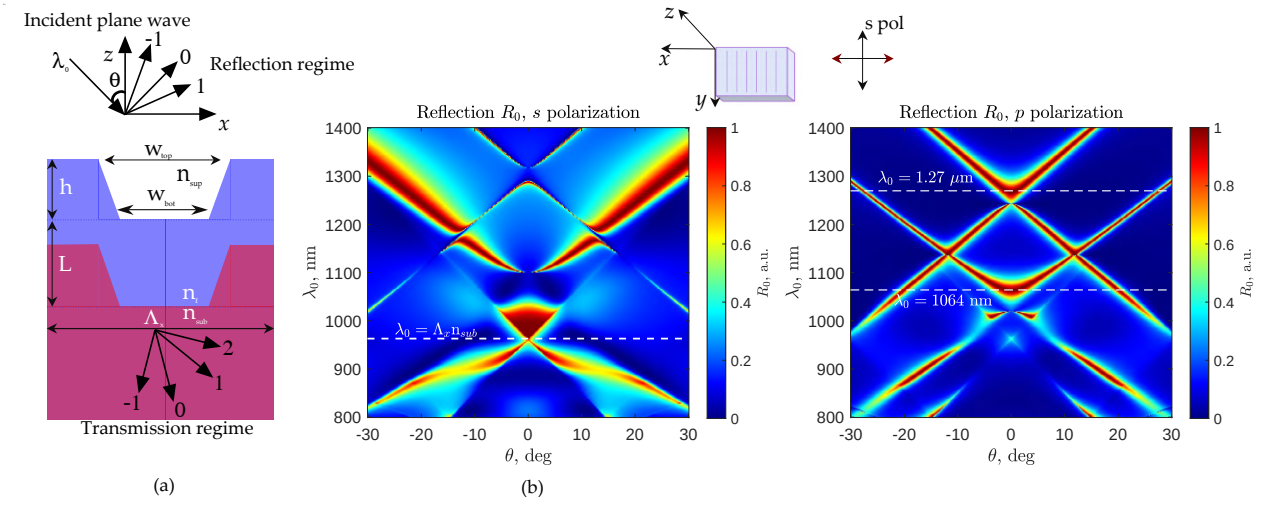


Fig. 1. Periodic waveguide in one period (a) and its angular reflection spectra for incident plane waves of angle θ for s (a) and p (b) polarizations. Waveguide parameters: $\Lambda_x = 638$ nm, $h = 230$ nm, $L = 580$ nm, $w_{bot} = 195$ nm and $w_{top} = 375$ nm , $n_f = 2.25$, $n_{sub} = 1.5$, $n_{sup} = 1$.

This work is dedicated to exploiting bound edge field modes within the device for spatial filtering. Such modes are leaky towards the substrate of the modulated waveguide. In the angular domain, a sharp transition from the zeroth-order reflection to the first transmission order is observed at the particular wavelength. Such an effect is allocated in the wavelength domain where the Rayleigh anomaly occurs [3], which can be interpreted as the energy redistribution between the diffraction orders when one of them becomes evanescent. By realizing this effect, filtering via reflection is obtained for a continuous range of wavelengths instead of a single one. In this work the theoretical concept is proposed. In the following, resonant reflections take place because of their localization within the film (inside a waveguide) or outside of it because of different arrangements of field modes in respect to energy within the asymmetrical quantum potential well.

[1] L. Grinevičiūtė, C. Babayigit, D. Gailevicius, M. Peckus, M. Turduev, T. Tolenis, M. Vengris, H. Kurt and K. Staliunas. (2021). Nanostructured Multilayer Coatings for Spatial Filtering. Advanced Optical Materials. 10.1002/adom.202001730.
[2] M. G. Moharam, Drew A. Pommet, Eric B. Grann, and T. K. Gaylord, "Stable implementation of the rigorous coupled-wave analysis for surface-relief gratings: enhanced transmittance matrix approach," J. Opt. Soc. Am. A 12, 1077-1086 (1995)
[3] R. Magnusson, "Flat-top resonant reflectors with sharply delimited angular spectra: an application of the Rayleigh anomaly," Opt. Lett. 38, 989-991 (2013)

MODELLING OF PLASMON – EXCITON STRONG COUPLING IN SILVER/GOLD FILM WITH RHODAMINE 6G DYE IN POLYMETHYL METHACRYLATE LAYER

Justina Anulytė[1], Ernesta Bužavaitė-Vertelienė[1], Zigmas Balevičius[1]

[1] Plasmonics and nanophotonics lab., Department of Laser Technologies, State research Institute Center for Physical Sciences and Technology,
Saulėtekio ave. 3, LT-10257, Vilnius, Lithuania
justina.anulyte@ftmc.lt

In reasent years a lot of attention has been paid for coupling in plasmon-exciton sytems [1] Due to strong light-matter interaction lower losses in such systems can be achieve. Strong coupling is an extreme form of light-matter interaction in which molecules exchange energy with an electromagnetic mode, often the mode is that of an optical cavity. For strong coupling to occur the exchange rate has to be faster than the rate of any competing dissipative process [2]. Strong coupling between plasmons and excitons are important for plasmonic laser application, biosensing, chemical reaction rate, integrated photonics devices [3-4]. In this study the plasmon-exciton polariton formation under strong coupling regime was investigated. The structure from silver-gold metal thin film and PMMA (polymethyl methacrylate) with Rhodamine R6 (R6G) dye layer were modelled in the Kretschmann configuration. The optical model was consists from BK7 glass prism, metal layer (Ag(35nm)-Au(9nm)) 44 nm in thickness and various thicknesses of the PMMA/R6G from 5 to 70 nm. In order to study coupling strength versus the R6G dye concentration in the PMMA matrix the refractive index dispersion of PMMA/R6G layer were tuned by changing strength of absorption lines of R6G dye. In the case of plasmon-exciton polariton hybrid mode the strong coupling was realized only in p-polarized light. For detail analysis of simulated optical response of the planar nanostructure the changes of state of light polarization were used upon total internal reflection, a so called total internal reflection ellipsometry. The changes in the polarization were expressed in the ellipsometric parameters Ψ and Δ and further presented through the reflection intensity of p- and s-polarizations. The Rabi splitting at the anti-crossing point which determined the coupling strength was evaluated from the optical dispersions maps of the p-polarized reflectance. Such numerical simulations gives possibilities to optimize strong coupling supported plasmonic-nanophotonic structures in order to fabricate them.

[1] Shaimaa I. Azzam et. al., Ten years of spasers and plasmonic nanolasers, Light: Science & Applications 2047-7538 (2020).
[2] G. Khitrova et. al,. Vacuum Rabi splitting in semiconductors, Nature Physics **2**, 81–90 (2006).
[3] E. Buzavaite-Vertaliene, et. al,. The experimental evidence of a strong coupling regime in the hybrid Tamm plasmon-surface plasmon polariton mode, Nanophotonics; **10**(5): 1565–1571 (2021).
[4] E. Buzavaite et. al,. Hybrid Tamm-surface plasmon polariton mode for highly sensitive detection of protein interactions, Optics Express **28**(20), (2020).

DOWNSCALLING IGNALINA NUCLEAR POWER PLANT TO CENTIMETERS AND MICRO-METERS BY USING 3D PRINTING TECHNOLOGIES

Arnoldas Solovjovas[1], Marius Navickas[1], Gabriele Gudaitiene[2], Mindaugas Masaitis[2], Mangirdas Malinauskas[1]

[1] Laser Research Center, Faculty of Physics, Vilnius University, Lithuania
[2] The National Museum of Lithuania, Lithuania
arnoldas.solovjovas@ff.stud.vu.lt

The history of 3D printing starts back in the 1920s when the fundamental perception of polymers was understood. Then the golden age of polymers started. Many scientists tried various ways for synthesizing polymers commercially [1]. DuPont company was a pioneer in synthesizing first photosensitive materials (photopolymers). The invention of light-emitting diodes (LED) was a boost for creating the first commercial 3D printer. The first 3D printing technology worked based on layer-by-layer fabrication technology. Nowadays we count various 3D printing methods [2].

In this work we present the results of printed Ignalina Nuclear Power Plant (IAE) model. Below in Fig. 1 a) part we see a picture of a real IAE which is then digitalized in Fig. 1 b) part. We depict results from our experiments using desktop digital light processing stereolithography (DLP-SLA) 3D printer (Fig. 1 c) part) and direct laser writing (DLW) system (Fig. 1 d) part). The DLP-SLA printing technology consists of a UV light source in our case laser diode with a 405 nm wavelength and a semiconductor digital micro-mirror device (DMD) [3]. DLP-SLA printing technology possess a fixed matrix of pixels on a building area. The IAE model was printed with *Asiga Pico 2* DLP-SLA printer with an ability to reach approximately 40 µm feature size. This is perfect for printing objects in cm/mm dimensions (used in dental implants), but to reach µm we need to move from a single photon absorption (SPA) to two photon absorption (TPA). TPA mechanism consists of simultaneously absorbing two photons and initiating the transit of molecules to a higher energy level. The cross section of TPA mechanisms is smaller compared with SPA and the result we see in Fig. 1 d) part: our printed object's dimensions are [300×300×200] μm^3 [4].

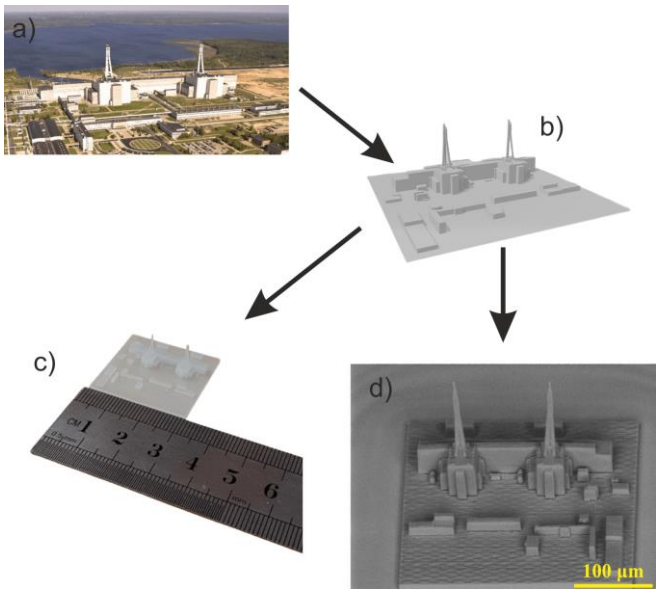


Fig. 1. IAE versions: a) real, b) digital model, c) printed with DLP-SLA 3D printer, d) printed with DLW system

Experiments showed that DLP-SLA printer allows us to print 3D objects in centimeters and DLW system in micro-meter dimensions. Photon absorption is a probability. For DLW system the probability to absorb two photons is very low. This is the reason why polymerization starts only in laser focused place.

[1] D. Feldman, (January 2008). "Polymer History". Designed Monomers and Polymers. 11 (1): 1–15. 10.1163/156855508X292383. ISSN 1568-5551. S2CID 219539020.
[2] N. Shahrubudin, T. C. Lee, and R. Ramlan, "An Overview on 3D Printing Technology: Technological, Materials, and Applications," Procedia Manuf.,. 35. 1286–1296, 2019, 10.1016/j.promfg.2019.06.089.
[3] M. Pagac and others., „A Review of Vat Photopolymerization Technology: Materials, Applications, Challenges, and Future Trends of 3D Printing", Polymers, 13, 4, 598, Feb. 2021, 10.3390/polym13040598.
[4] X. Zhou, Y. Hou, and J. Lin, "A review on the processing accuracy of two-photon polymerization," AIP Adv., 5, 3, 030701, Mar. 2015, 10.1063/1.4916886.

GRAPHENE CAPACITOR FOR FABRY-PEROT RESONANCE CONTROL

Andrius Kamarauskas[1], Laurynas Staišiūnas[1], Gediminas Šlekas[1], Dalius Seliuta[1], Žilvinas Kancleris[1]

[1] Department of Physical Technologies, Center for Physical Sciences and Technology, Lithuania
andrius.kamarauskas@ftmc.lt

Fabry-Perot (FP) resonance is a well-known phenomenon occurring in various fields of physics [1]. It is linked to wave propagation through a transparent material, in this case, dielectric. Due to multiple internal reflections inside the material, propagating waves experience constructive and destructive interference. Those phenomena depend on dielectric thickness and wavelength (frequency). Observing transmission spectra, peak transmittance (constructive interference) occurs at frequencies when inside dielectric slab fits integer number of half-waves. Transmission spectra minimums (destructive interference) happen at frequencies when an odd number of quarter wavelengths match inside the dielectric slab.

Various techniques are proposed to control FP resonance. One of the most popular is using a laser beam to change surface conductivity of substrate to achieve near 95% suppression of resonance [2]. This setup requires the adjustment of the THz beam perpendicularly to the sample together with the laser beam, falling at some angle to it, both having to be focused to the same spot of the sample simultaneously.

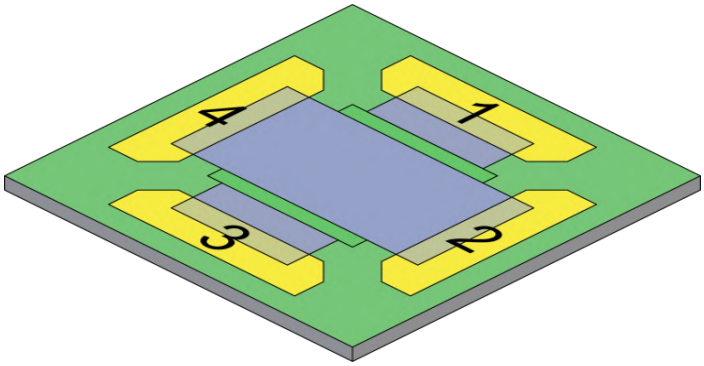


Fig. 1. Fabry-Pero modulator made of graphene sheets on Si insulating substrate ε =11.9 substrates (grey). Graphene sheets (blue), separated by hafnium oxide (green) ε =30. Gold contact pads (yellow), The THz beam spot is aimed at overlapping graphene sheets perpendicularly to the surface.

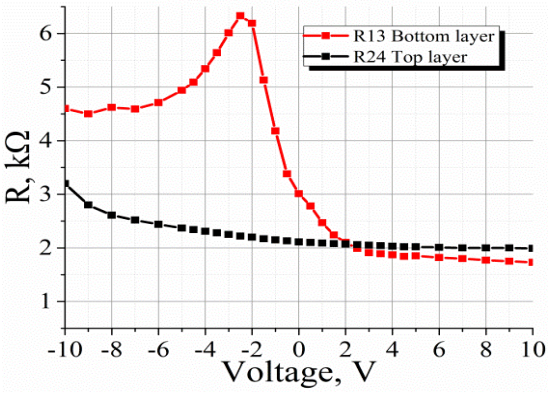


Fig. 2. Dependences of resistance of graphene layers on DC voltage applied to the graphene capacitor. The voltage polarity in the graph is determined by the potential being connected to the top layer.

Our work in progress offers a novel way for controlling FP resonance using dielectric substrate covered by graphene capacitor. Its arrangement is shown in Fig. 1. Using atomic layer deposition technology, 60 nm thick HfO2 layer (green) is deposited on a surface of isolating silicon substrate (grey). Image reversal photolithography is applied to form areas for gold contact pads (1-4). Easy transfer graphene layer from Graphenea is placed between contact pads 1-3, later on, Poly(methyl methacrylate) (PMMA) layer covering graphene is removed. Then additional HfO_2 layer is placed on the first layer intersection with the second layer (green). Finally, top layer graphene with PMMA is put between pads 2-4.

Applying the voltage to the graphene capacitor, the DC measurements are performed by measuring the resistance of each layer. The potential of the top layer determines the voltage polarity in the dependences shown in Fig. 2. One can see that the resistance of the bottom layer demonstrates a sharp resistance spike at -2.5 V that can be attributed to the Dirac point. On the contrary, when the negative voltage is applied to the top layer, it displays a monotonous increase of resistance. The observed difference might be caused by the fact that different layers cover lower and upper graphene sheets. The lower graphene sheet is inserted between HfO_2 layers, whereas the upper part of the top sheet is covered by the PMMA layer.

At a voltage corresponding to the Dirac point, the overall conductivity of graphene sheets is the lowest, which suppose the highest transmittance of THz radiation through the silicon plate covered with graphene capacitor. Changing the applied voltage, the conductivity of graphene increases, and in this way, we have demonstrated the modulation of THz radiation.

Since the bottom graphene layer is controlled only, our further research is focused on removing PMMA from the top layer of graphene and changing it with HFO_2. We believe that in this way, we shall be able to control the resistance of both layers of the capacitor and increase the efficiency of modulation.

[1] Ž. Kancleris, A. Laurinavičius, T. Anbineris. *Sensitivity of homogeneity mapping of dielectric wafer using millimeter waves*, International Journal of Infrared and Millimeter Waves. 25(7):1099-1108 (2004).

[2] G. Šlekas, D. Seliuta, J. Devenson, A.Urbanovič, Ž.Kancleris. *Modulation of terahertz radiation using optical control of Fabry-Perot resonances*, Electronics letters. 51(23): 1908 – 1909 (2015).

RADIALLY SPLIT AXICON PHASE OPTIMISATION FOR ELONGATED BESSEL BEAM PEAK GENERATION FOR TRANSPARENT MATERIAL DICING

Laura Tauraitė[1], Ernestas Nacius[1,2], Orestas Ulčinas[1,2], Sergej Orlov[1], Vytautas Jukna[1,3]

[1] Center for Physical Sciences and Technology, Coherent Optics laboratory, Saulėtekio Ave. 3, Vilnius, Lithuania
[2] Workshop of Photonics, Mokslininkų str. 6A, Vilnius, Lithuania
[3] Laser Research Center, Vilnius University, Saulėtekio Ave. 10, Vilnius, Lithuania
laura.tauraite@ff.stud.vu.lt

Laser micro-fabrication of transparent media with ultrafast laser pulses has seen substantial interest in scientific and industrial communities, as the demand for rapid cutting, dicing, ablation is skyrocketing. The Bessel-Gaussian beam is becoming increasingly popular in this field due to its elongated focal zone that reduced the processing complexity by eliminating the need to translate Gaussian beam over the full depth of the material. The use of Bessel-Gaussian beam in transparent material cutting does not compromise surface quality, while the processing speed is increased dramatically. It is shown that it is possible to cut various glasses of up to a few millimetres thickness [1].

The most common Bessel-Gaussian beam shaping element is an axicon – a glass cone with a sharp tip. However, any deviations from the perfect shape of the element - any irregularities of its surface and especially a rounded tip greatly reduces the quality of the generated beam by inducing unwanted axial intensity modulations along the focal zone [2]. Alternative beam shaping elements are used to generate more complex beam patterns or to improve overall beam quality: diffractive optical elements, spatial light modulators, complex sub-wavelength metasurfaces [3,4,5]. Using these alternative options, it is possible to generate beams that have been modified for higher efficiency micro-fabrication while still exhibiting Bessel-Gaussian beam propagation characteristics.

In our research we use beam shaping elements that are created by inscribing birefringent nanogratings in bulk fused silica [6]. With direct laser written nanogratings we can control retardance and orientation of them over the full width of the element enabling manufacture of custom flat optical elements, known as geometric phase elements (GPEs). GPEs can be used for many purposes, as their damage threshold is very high, close to the material damage threshold they are made of. In our scope of the research, we know that it is possible to form new Bessel-Gaussian beam intensity distribution, for example, a beam with an elliptical central peak (Fig. 1, b) [7]. The elongation of the beam central peak can be used to initiate controllable and oriented microfractures in transparent material, i.e. stealth dicing.

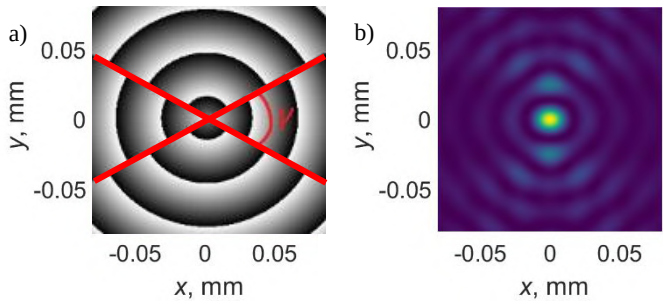


Fig. 1. a) Modified axicon phase distribution and b) generated Bessel-Gaussian beam intensity distribution with an elliptical central peak.

In this work we use numerical simulation to investigate Bessel-Gaussian beam intensity distribution. We divide the axicon phase and induce a phase shift between them which in turn can form a necessary modification to Bessel beam intensity distribution (Fig. 1, a). We scan the parameter space to find optimal modified axicon phase to generate elongated peak with relatively good contrast. This phase distribution will be used to manufacture GPE and after confirmation of the beam transformation quality, the element will be used for transparent material dicing.

[1] R.Meyer, M.Jacquot, R.Giust, J.Safioui, L.Rapp, L.Furfaro, P.-A. Lacourt. J.Dudley and F.Courvoisier „Single shot ultrafast laser processing of high-aspect ratio nanochannels using elliptical Bessel beams“, Optics Letters, **42,** 21 (2017)
[2] O.Brzobohaty, T.Čižmar and P.Zemanek „High quality quasi-Bessel beam generated by round-tip axicon“, Opt.Express, **16**, 12688-12700 (2008)
[3] J.Baltrukonis, O.Ulčinas, S.Orlov, and V.Jukna „Void and micro-crack generation in transparent materials with high-energy first order vector Bessel beam“, J.Opt.Soc.Am., **B37**, 2121-2127 (2020)
[4] A.Vasara, J.Turunen and A.T.Friberg „Realization of general nondiffracting beams with computer-generated holograms“, J.Opt.Soc.Am **A6**, 1748-1754 (1989)
[5] D.Lin, P.Han, E.Hasman and M.Brongersma „Dielectric gradient metasurface optical elements“, Science,**345**, 298-302 (2014)
[6] Y.Shimotsuma, P.G. Kazansky, J.Qiu and K.Hirao „Self-organized nanogratings in glass irradiated by ultrashort light pulses“, Phys.Rev.Lett. **91**, 247405 (2003)
[7] Ernestas Nacius, Pavel Gotovski, Orestas Ulčinas, Sergej Orlov, Antanas Urbas, and Vytautas Jukna, "Spatially displaced and superposed Bessel beams for transparent material laser microprocessing," J. Opt. Soc. Am. B **38**, 3886-3895 (2021)

SUPERCONTINUUM GENERATION WITH BURSTS OF FEMTOSECOND LASER PULSES

Vaida Marčiulionytė, Vytautas Jukna, Gintaras Tamošauskas, Audrius Dubietis

Laser Research Center, Vilnius University, Lithuania
vaida.marciulionyte@ff.stud.vu.lt

Supercontinuum (SC) generation is an effect produced by filamentation of ultrashort laser pulses in transparent dielectric media and resulting in broad spectra with high spatial and temporal coherence [1]. Traditionally, SC is generated and characterized under single pulse laser exposure. Two or more laser pulses, that are equally temporally separated are called bursts of laser pulses. Material processing by bursts of laser is advantageous for various micromachining areas such as ablation, laser welding, fabrication of Bragg grating waveguides, glass scribing and cleaving [2–4]. It has been demonstrated, that SC generation can also be achieved using bursts of laser pulses in photonic crystal fiber [5]. However, to the best of our knowledge SC generation in bulk materials has not been studied.

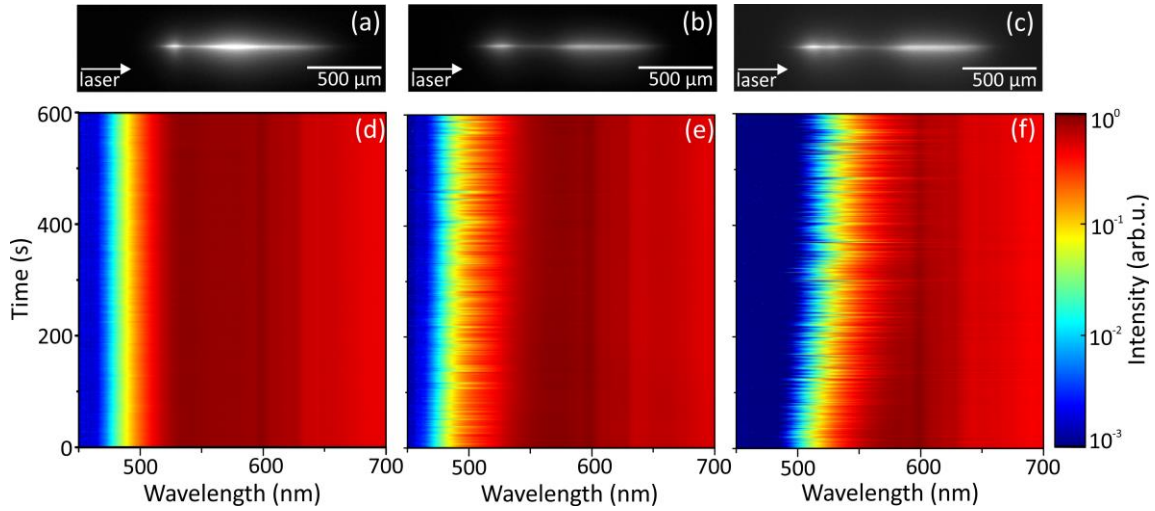


Fig. 1. Filament-induced luminescence traces (first row) and time evolutions of supercontinuum spectrum (second row), in YAG crystal generated at 500 kHz repetition rate using single laser pulse (a, d) and bursts of laser pulses with 16 ns (b,e) and 400 ps (c, f) separation times.

In this study, we investigate SC generation using single pulses and burst of laser pulses temporally separated by 400 ps and 16 ns provided by amplified Yb:KGW laser (Carbide Light Conversion Ltd.) laser having a pulse duration of 210 fs and a central wavelength of 1030 nm.

We examined SC generation in 5 mm sapphire and YAG crystals using single and 2 pulses burst with 400 ps and 16 ns time separation between the pulses with the 500 kHz repetition rate. Sapphire crystal degrades rapidly using even a single pulse and no stable SC generation was observed with both types of bursts. In contrast, stable SC generation in YAG crystal was observed with single pulse and standard deviation of spectral intensity fluctuations (≈ 0.6 %) were measured for 550 nm wavelength (Fig. 1). Fairly stable SC generation was achieved with 16 ns bursts (for 550 nm spectral intensity fluctuations ≈ 1 %) although with slight shrinking of SC spectrum, while rapid narrowing of SC spectrum and highest spectral intensity fluctuations ≈ 9 % for 550 nm wavelength were measured using 400 ps bursts indicating rapid optical degradation of the crystal.

[1] A. Dubietis, G. Tamošauskas, R. Šuminas, V. Jukna, and A. Couarion, Ultrafast supercontinuum generation in bulk condensed media, Lith. J. Phys. 57, 133-157 (2017).
[2] C. Kerse, H. Kalaycıoğlu, P. Elahi, B. Çetin, D.K. Kesim, Ö. Akçaalan, S. Yavaş, M.D. Aşık, B. Öktem, H. Hoogland, R. Holzwarth, F.Ö. Ilday, Ablation-cooled material removal with ultrafast bursts of pulses, Nature, 537, 84-88 (2016).
[3] S. Rezaei, J. Li and P.R. Herman, Burst train generator of high energy femtosecond laser pulses for driving heat accumulation effect during micromachining, Opt. Lett., 40, 2064-2067 (2015).
[4] J. Li, E. Ertorer and P.R. Herman, Ultrafast laser burst-train filamentation for non-contact scribing of optical glasses, Opt. Express, 27, 25078 (2019).
[5] J. Vengelis, M. Kuliešaitė, V. Jukna, V. Jarutis and V. Sirutkaitis, Investigation of supercontinuum generation in photonic crystal fiber using bursts of femtosecond pulses, Opt. Commun., 496, 127132 (2021).

SUBNANOSECOND OPTICAL PARAMETRIC GENERATOR BASED ON PERIODICALLY POLED LITHIUM NIOBATE CRYSTAL

Justina Savickytė[1], Jonas Banys[1], Ona Balachninaitė[1], Viktorija Tamulienė[1], Julius Vengelis[1]

[1]Laser Research Center, Faculty of Physics, Vilnius University, Lithuania
justina.savickyte@ff.stud.vu.lt

Subnanosecond (from 100 ps to 1 ns) optical parametric generators (OPGs) are continuously tunable in a wide spectral region and can be applied in spectroscopy, gas detection, biochemical research where high temporal resolution is not necessary but nanosecond time resolution is not sufficient enough. Such tunable coherent light sources are commercially attractive because of their quite simple configuration, compactness and relatively low-cost. Although there is demand, but only a few subnanosecond OPGs have been obtained because of damage threshold of nonlinear media for subnanosecond pulses being very near the threshold of optical parametric generation [1-3].

In this research we investigated an OPG based on a 1 cm in length periodically poled 5 % magnesium-oxide-doped lithium niobate (MgO:PPLN) crystal pumped by Nd:YAG MOPA microlaser that produces up to 1 W power of 473 ps 1064nm wavelenght pulses with 1 kHz repetition rate. The use of a short crystal can further reduce the cost of such a tunable broadband coherent light source. The crystal has 8 gratings varying from 28.28 µm to 31.59 µm in period. When using grating tuning (Fig.1) and temperature tuning from 60ºC up to 200ºC we obtained signal wave tuning from 1439 nm to 2120 nm and respectively calculated idler wave tuning from 2769 nm to 4166 nm. Energy characteristics were measured as well. Dependency of optical parametric generation output power on pump power at different crystal temperatures is shown in Fig.2. Calculated signal wave frequency conversion efficiencies for different gratings vary from 2.8 % up to 17.5 % when crystal was heated to 200ºC temperature. For the development of a more effective OPG longer crystals will be investigated.

This work has received funding from European Regional Development Fund (project No. 01.2.2-LMT-K-718-03-0004) under grant agreement with the Research Council of Lithuania (LMTLT).

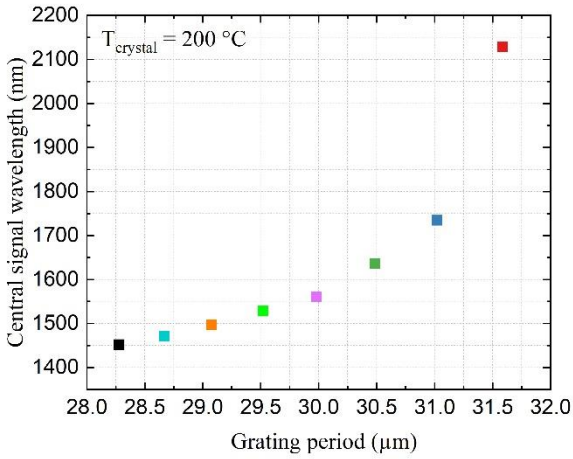


Fig.1. Dependency of signal wavelenght on grating period.

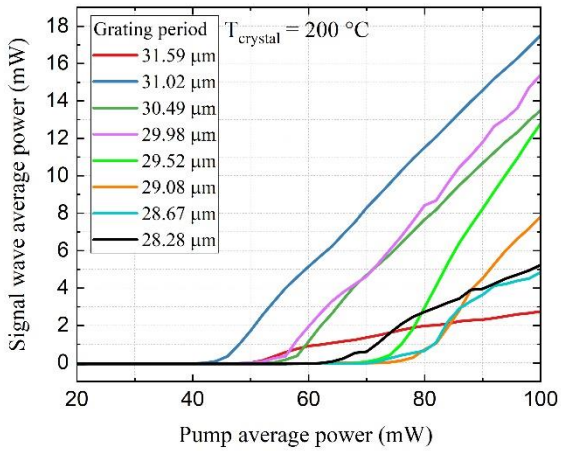


Fig.2. Dependency of OPG signal output power on pump power at 200ºC crystal temperature.

[1] M. H. Dunn and M. Ebrahimzadeh, Parametric Generation of Tunable Light from Continuous-Wave to Femtosecond Pulses, Science 286, 1513-1517 (1999).
[2] F. Duarte, *Tunable laser applications* (CRC Press, 2016).
[3] R.W. Boyd, *Nonlinear Optics, Third edition* (Academic Press, Inc., USA, 2008).

P2-1

DID NOT PARTICIPATE

.

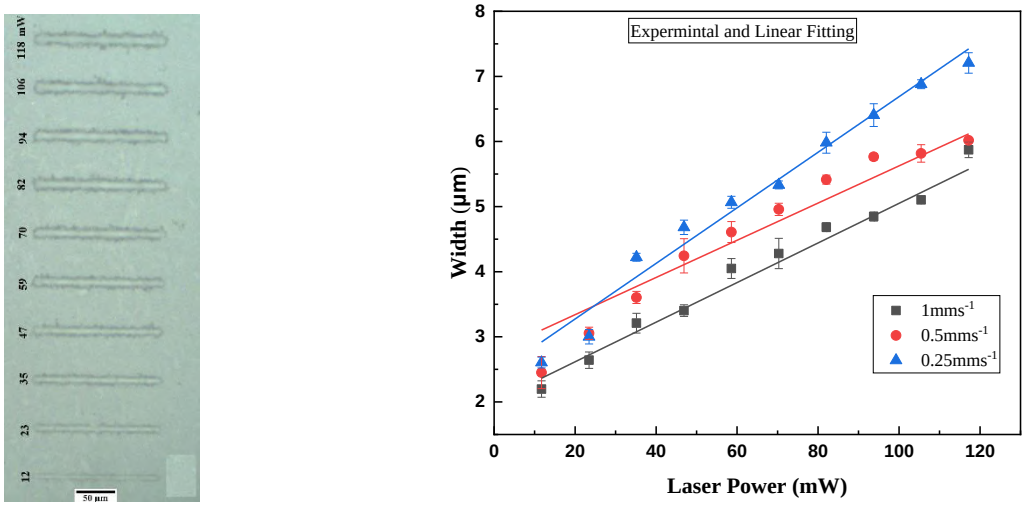
DIRECT FEMTOSECOND LASER ABLATION OF NITROCELLULOSE MEMBRANES

Gazy Khatmi Rodowan[1], Mohamed Ahmed Baba[2], Martynas Simanavičius[3], Laimis Silimavičius[3], Agnė Barkauskienė[3], Gintautas Gylys[3], Tomas Tamulevičius[1,2,4]

[1] Department of Physics, Kaunas University of Technology, Lithuania
[2] Institute of Materials Science, Kaunas University of Technology, Lithuania
[3] UAB Sanpharm, Lithuania
[4] UAB Nanoversa, Lithuania
gazy.khatmi@ktu.edu

Nitrocellulose membranes are widely used in lateral-flow immunoassays (LFA) for different purpose diagnostic tests where the fluid sample added to the membrane flows through the LFA by capillary forces, interacting with detection antibody-labeled gold nanoparticles [1]. The need for better spatial and temporal liquid flow control requires local modifications of surface wettability. LFAs are one of the kinds of so-called paper-based microfluidic devices [2]. Ultrashort lasers enable cold ablation of porous materials and were already applied for imposing surface structures and wettability handling aiming for bio sensing applications [3-5].

In this work, we are demonstrating a technique for the fabrication of hydrophilic channels in nitrocellulose membranes using a femtosecond laser micromachining system. Nitrocellulose membranes (pore size 0.2 µm, ROTI®NC, Carl Roth GmbH) were structured employing a second harmonic of the femtosecond Yb:KGW laser (Light Conversion) employing XYZ translation stage based workstation (Altechna R&D). A set of parallel channels were imposed from the series of ablation experiments carried out under different average femtosecond laser power ranging from 12 to 118 mW focused with a micro objective laser beam and stage translation speeds of 0.25, 0.5, and 1 mm/s. Laser micromachined nitrocellulose membranes were studied under an optical microscope (Optika, Fig. 1 a). The obtained results indicated that the width of the hydrophilic microchannels increased from 2.19 to 7.20 µm with the increased average laser power and reduces with the sample translation speed. A typical example of a positive correlation between the width of the microchannels under different average laser power with different scanning speeds is depicted in Fig. 1 b.



a b

Fig. 1. Femtosecond laser micromachining of nitrocellulose membrane at 200 kHz laser pulse repetition rate, 515 nm wavelength, different laser average power, and stage translation speed: (a) optical microscope micrograph of parallel lines; (b) line width dependence on laser average power and stage translation speed.

This work was supported by the Agency for Science, Innovation and Technology, Grant No. Biotech-02-014.

[1] Zhan, Li, et al. Development and optimization of thermal contrast amplification lateral flow immunoassays for ultrasensitive HIV p24 protein detection." *Microsystems & Nanoengineering* **6** (1) 1-11 (2020).
[2] Cate, David Met al. Recent developments in paper-based microfluidic devices. *Analytical Chemistry* **87** (1) 19-41 (2015).
[3] Müller, Daniel Wyn, et al. Applying ultrashort pulsed direct laser interference patterning for functional surfaces. *Scientific Reports* **10** (1) 1-14 (2020).
[4] Wu, Junrui et al. Laser fabrication of bioinspired gradient surfaces for wettability applications. *Advanced Materials Interfaces* **8** (5) 2001610 (2021).
[5] Chatzipetrou, Marianneza, et al. Digital Printing and Functionalization of Surfaces for Biosensing Applications. *IEEE Sensors Journal* **21** (20) 22182-22189 (2021).

SUPERCONTINUUM GENERATION IN DIFFERENT LENGTH PHOTONIC CRYSTAL FIBERS

Miglė Kuliešaitė, Julius Vengelis, Vygandas Jarutis

Laser Research Center, Faculty of Physics, Vilnius University, Lithuania
migle.kuliesaite@ff.vu.lt

Photonic crystal fibers (PCFs) are different from conventional optical fibers, because PCFs have a periodic microstructure region inside where light is propagating. Solid core PCFs are perfect nonlinear media, in which nonlinear processes can occur due third-order nonlinearity, which results in the generation of the supercontinuum [1]. It is one of the most important and widely analyzed nonlinear optics phenomena, in which pump pulse spectrum broadens hundreds or thousands of times [2]. This phenomena has many important applications, in areas such as spectroscopy, frequency metrology, and optical coherence tomography [3]. Although a wide variety of supercontinuum generation in PCFs research has been done, research in which the length of a short PCF is changed in small steps has not been performed.

In this study, we present the experimental and theoretical model results of femtosecond supercontinuum generation in different length photonic crystal fiber. The pump source for supercontinuum generation was an Yb:KGW "Flint" oscillator generating 1028 nm wavelength with a repetition rate of 75.2 MHz and 110 fs duration pulses. For supercontinuum generation, we used a highly nonlinear polarization-maintaining solid-core PCF in which the core diameter and the pitch were 4.8 µm and 3.25 µm, respectively. The zero-dispersion wavelength of this PCF, was at 1087.4 nm nm±10 nm (very similar for both polarization modes). During the experiment, we performed the spectra measurements at PCF output by changing average power of the pump pulses.

Experiment results show, that by changing the length of PCF we observed different spectral features in spectra at PCF output. When using shortest PCF lengths the extreme spectrum broadening was not visible, but we observed three separate nonlinear processes: self-phase modulation of the pump pulse; generation of the third harmonic (TH) (342,7 nm) and partially coherent UV-VIS light generation within 375 - 500 nm wavelength range. At longer PCF length spectra we observed new spectral components. In this case, more nonlinear processes occur which results in supercontinuum generation. UV-VIS light is visible in all cases: this can be explained by the formation of self-trapped excitons (STE), which are trapped by their interaction with lattice distortions. Free excitons are created along the PCF due to multi-photon absorption, and then decay due to STE by emitting UV-VIS light [4]. Numerical simulation was also performed and had a good agreement with experiment results.

This work has received funding from European Regional Development Fund (project No. 01.2.2-LMT-K-718-03-0004) under grant agreement with the Research Council of Lithuania (LMTLT).

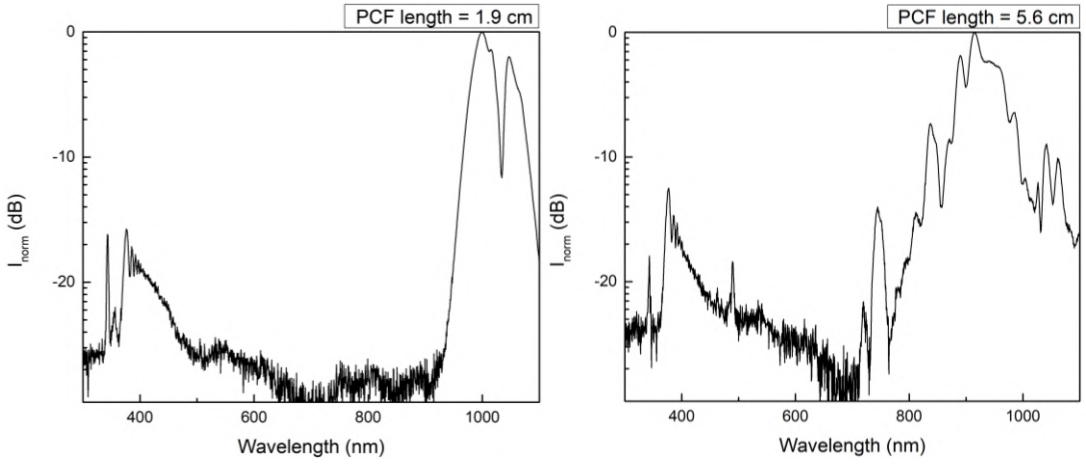


Fig. 1. Measured spectra at PCF output using CZC7 and CZC17 filters. Left: spectrum obtained when PCF length was 1.9 cm, right: spectrum obtained when PCF length was 5.6 cm.

[1] P. St. J. Russell, Photonic-crystal fibers, J. Light. Technol. **24**(12), 4729-4749 (2006).
[2] J. M. Dudley, G. Genty, S. Coen, Supercontinuum generation in photonic crystal fiber, Rev. Mod. Phys. **78**, 1135-1184 (2006).
[3] J. Vengelis, V. Jarutis, V. Sirutkaitis, Extension of supercontinuum spectrum, generated in polarization-maintaining photonic crystal fiber, using chirped femtosecond pulses, Opt. Eng. **57**(1), 1-10 (2018).
[4] M. Kuliešaitė, V. Jarutis, J. Pimpė, J. Vengelis, Partially coherent UV-VIS light generation in photonic crystal fiber using femtosecond pulses, Results Phys. **31,** 1-5 (2021).

PHOTOLUMINESCENCE DYNAMICS OF MAPI PEROVSKITE FILMS INDUCED BY LATERAL ELECTRIC FIELD

Simonas Driukas[1], Vidmantas Gulbinas[1], Danielis Rutkauskas[1]

[1] Center of Physical Sciences and Technology, Department of Molecular compound physics, Photoelectronics laboratory, Lithuania
simonas.driukas@ftmc.lt

Over the last decade hybrid metal-halide perovskites have attracted huge interest in the semiconductor and optoelectronics science community. A combination of easy and cheap synthesis from solution and excellent optoelectronic properties makes these materials excellent for devices like solar cells, LED's, photodetectors, transistors and many more [1]. However, many uncertainties concerning the stability of perovskite devices under working conditions remain.

In our work we seek to measure and identify processes causing perovskite device instability under applied electric field. Using florescence microscopy, we report photoluminescence (PL) properties of CH3NH3PbI3 (MAPI) thin films deposited on interdigitated electrodes under the applied electric field. Additionally, for electric-field mapping inside the perovskite film an electric field-induced second harmonic (EFISH) microscopy technique was performed.

Three main PL dynamic steps were observed: a dark PL front moving from the positive electrode side throughout the perovskite film at the start of voltage stressing, a change of homogenous PL distribution to many bright blinking spots in a dark background and finally, after the voltage is turned off an increase of PL near the negative electrode.

Combining these results with EFISH microscopy we propose a model explaining such PL dynamics. We suggest that two types of PL quenching defects become active under applied electric field. The first one is caused by negatively charged ionic interstitials drifting throughout the perovskite film and causing a polarity-dependant PL quenching which is seen at the start of voltage stressing and after voltage termination. The second quenchers are immobile shallow ionic traps that form deep lying PL quenching states after interaction with injected holes.

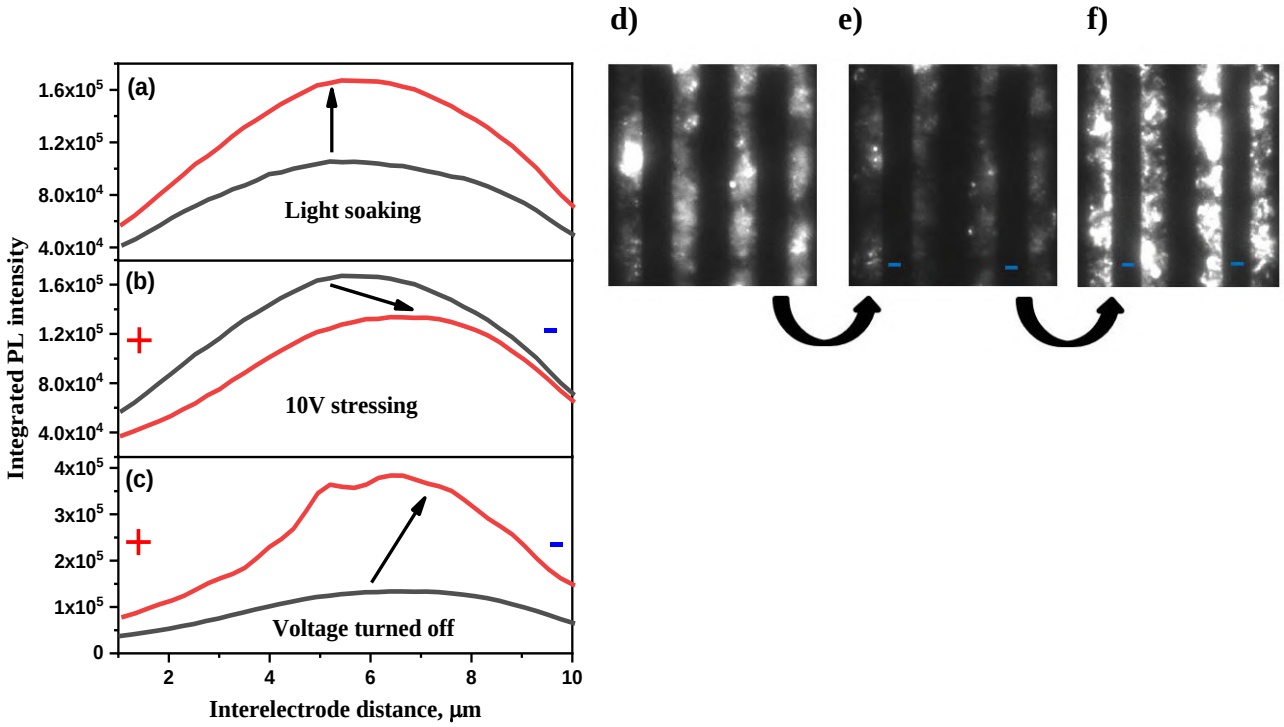


Figure 1. Integrated PL intensity of different measurement steps. **a)** homogenous PL increase during light-soaking. **b)** PL quenching near the positive electrode after voltage application. **c)** PL increase near the negative electrode after stressing. Different perovskite areas are summed up. **(d-f)** Corresponding microscopic PL images **d)** before stressing, **e)** immediately after voltage application and **f)** after stressing.

[1] Li, J., Duan, J., Yang, X., Duan, Y., Yang, P., & Tang, Q. (2020). Review on Recent Progress of Lead-Free Halide Perovskites in Optoelectronic Applications. Nano Energy, 105526.doi:10.1016/j.nanoen.2020.105526.

ATOMIC FORCE MICROSCOPY AS VERSATILE TOOL TO DISCERN THE PHYSICO-CHEMICAL PROPERTIES OF PROTEINS AT THE NANOSCALE

Carlos Marcuello[1,2], Anabel Lostao[1,2,3]

[1] Instituto de Nanociencia y Materiales de Aragón (INMA), CSIC-Universidad de Zaragoza, 50009 Zaragoza. Spain.
[2] Laboratorio de Microscopias Avanzadas (LMA), Universidad de Zaragoza, 50018 Zaragoza. Spain.
[3] Fundación ARAID, 50018 Zaragoza. Spain
cmarcuel@unizar.es

Atomic force microscopy (AFM) emerged as promising technique to address multitude of biological system properties at the single molecule level. This tool provides high-resolution imaging by scanning the surface of almost any type of sample with ultra-sharp tips. Moreover, AFM allows to acquire data under liquid environment mimicking the intracellular conditions inner the living cell or bacteria. This aspect becomes AFM more appealing in comparison with other scanning probe (SPMs) or electron microscopies (TEM) when the study is focused on biomolecular systems. Here, we overview the potential applications of AFM and their operational modes by real examples that our group has been deeply studied in the last decade. First, we present AFM as suitable technique to gather topography information with sub-nanometer resolution in aqueous media. Several examples are showed: I) The analysis of the FAD synthetase from *Corynebacterium ammoniagenes* upon ligand binding and catalysis [1] and II) The conformational study of the novel family of Ferredoxin-dependent Flavin Thioredoxin Reductases [2], both through imaging. Then, the methodology to immobilize in an oriented manner the Ferredoxin $NADP^+$ Reductase (FNR) flavoenzyme on a substrate towards its redox partners Ferredoxin (Fd) and Flavodoxin (Fld) [3] and use this strategy for molecular recognition imaging (MRI) and do force spectroscopy (FS). MRI enabled us to identify biomolecules on mixtures immobilized on surfaces by unbinding force mapping. This approach reaches to quantitatively discriminate FNR molecules on a sample through the rupture of the aforementioned FNR:Fd complexes using Fd- functionalized tips (Fig. 1, a-d) [3]. Finally, the study of the intermolecular forces and energy landscapes through dissociation of complexes under force using dynamic FS between immobilized FNR and Fd and Fld molecules covalently linked onto the AFM tip [4]. The results indicated that the FNR:Fd complex is more specific, mechanically stronger and more durable than FNR:Fld. In addition, Fd dissociates from FNR through a single barrier while Fld followed two energy barriers (Fig. 1 e).

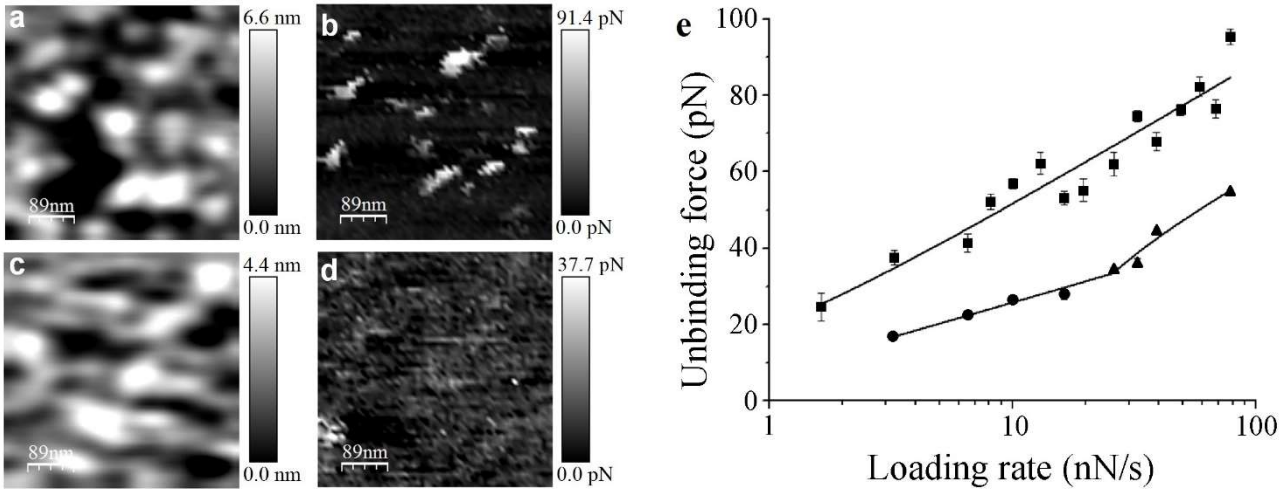


Fig. 1. Molecular recognition imaging of FNR sample scanned using Fd-tips. (a) topography and (b) force adhesion map rendered by oriented immobilized FNR, while (c) topography and (d) force adhesion map depicted by the blocking experiment with free Fld molecules in solution. (e) Loading-rate dependence of the most probable unbinding forces for the FNR:Fd complex (squares) and the FNR:Fld complex (circle and triangles).

[1] C. Marcuello et al. Detection of a quaternary organization into dimer of trimers of Corynebacterium ammoniagenes FAD synthetase at the single-molecule level and at the in cell level. Biochimica et Biophysica Acta (BBA)-Proteins and Proteomics **1834**, 665-676 (2013).
[2] C. Marcuello et al. Atomic force microscopy to elicit conformational transitions of ferredoxin-dependent flavin thioredoxin reductases. Antioxidants **10**, 1497 (2021).
[3] C. Marcuello et al. An efficient method for enzyme immobilization evidenced by atomic force microscopy. Protein Engineering, Design & Selection **25**, 715-723 (2012).
[4] C. Marcuello et al. Mechanostability of the Single-Electron-Transfer Complexes of Anabaena Ferredoxin-$NADP^+$ Reductase. ChemPhysChem **16**, 3161-3169 (2015).

COULD SeNPs REVERT SIDE EFFECTS OF CISPLATIN CHEMOTHERAPY? INSIGHTS FROM MASS SPECTROMETRY AND CHROMATOGRAPHY ANALYSIS

Alejandro Iglesias Jiménez[1], Gema Artiaga[1], Estefanía Moreno[1], Milagros Gómez[1]

[1]Department of Analytical Chemistry, Faculty of Chemical Sciences, Complutense University of Madrid, Avenida Complutense s/n, 28040, Madrid, Spain
alejandroiglesias@ucm.es

Cisplatin is one of the most widely used antitumor drugs in the world, but its clinical use is limited by the side effects that it could produce in patients, such as nephrotoxicity [1]. This has motivated, for decades, an extensive search for renoprotective strategies that allow improving the effectiveness of the drug, which is still irreplaceable in many cases [2].

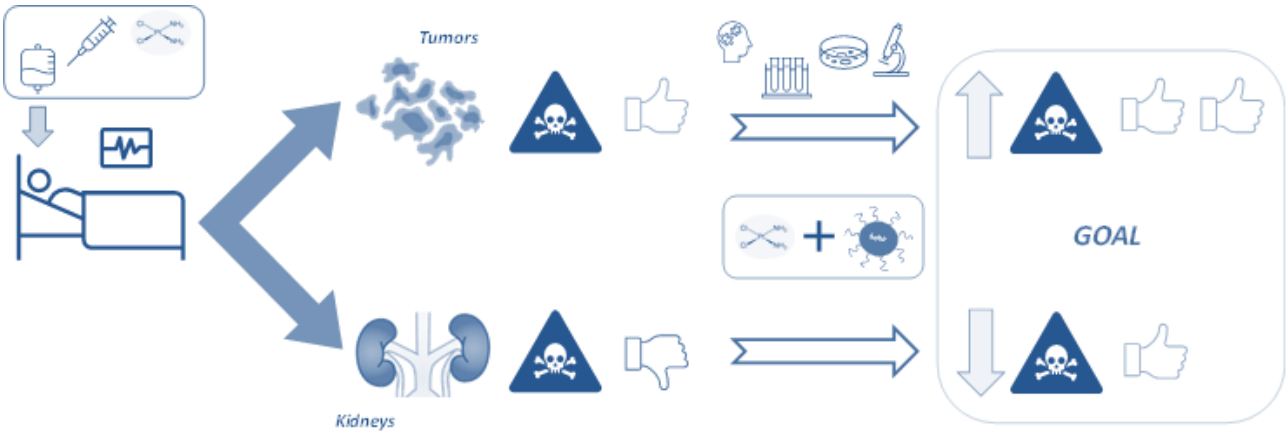
One possibility is the use of selenium nanoparticles (SeNPs), the object of research for various current biomedical applications [3]. Therefore, in this work we tested the feasibility of SeNPs as a potential nephroprotective agent in treatments with cisplatin, due to the intrinsic antioxidant properties of selenium, which could reduce oxidative damage in kidney cells.

To consider a possible nephroprotective capacity of the SeNPs, they should not only protect renal cells against the cytotoxicity of cisplatin, but at the same time it would be essential that they do not interfere with the anticancer action. Hence, as a first approach to this purpose, in the present work HeLa cells (from cervical cancer) were cultured at different incubation times with cisplatin and/or with chitosan-stabilized SeNPs (Ch-SeNPs).

Cell viability was determined by the MTT assay ((3-(4,5-dimethylthiazol-2-yl)-2,5-diphenyltetrazolium bromide) tetrazolium reduction assay) for all cultures. The morphology and size of the Ch-SeNPs, as well as their cellular internalization, were studied using TEM-XEDS (Transmission Electron Microscopy coupled to Energy-Dispersive X-ray Spectroscopy). The intracellular content of Se and Pt was quantified by ICP-MS (Inductively Coupled Plasma Mass Spectrometry) analysis, after acid digestion of the cell pellets, and also the amount of Pt bound to DNA, which is the final target of the drug. Furthermore, Se and Pt speciation studies were carried out at the cellular cytosolic level, using liquid chromatography (LC) coupled to ICP-MS or UV/VIS.

The results showed that cells could assimilate these SeNPs, which were found in different subcellular locations, but their coadministration with cisplatin had no influence on the cellular drug uptake or the quantity of DNA-bound platinum, two factors traditionally related to Pt-drug cytotoxicity. However, in terms of cell viability, HeLa suffered more damage when cisplatin was mixed with SeNPs than in the case it was administered alone, suggesting a possible synergistic effect, which could be interesting in order to try to decrease cisplatin clinical dose and also the risk of nephrotoxicity.

Although this work is preliminary and it should be extended to kidney cells, the above results are promising enough for further study of the applications of SeNPs against renal toxicity in antitumor treatments with cisplatin.



[1] R.P. Miller et al., Mechanisms of Cisplatin Nephrotoxicity, Toxins **2**, 2490-2518 (2010).

[2] N. A. Dos Santos et al., Cisplatin-induced nephrotoxicity and targets of nephroprotection: an update, Arch Toxicol **86** (8), 1233-1250 (2012).

[3] S. Chaudhary et al., Surface functionalized selenium nanoparticles for biomedical applications, J Biomed Nanotechnol **10** (10), 3004-3042 (2014).

INTERCALATION OF HISTIDINE INTO MOLYBDENUM DISULFIDE FILMS FOR EFFICIENT HYDROGEN EVOLUTION REACTION

Paulius Gaigalas[1], Arūnas Jagminas[1]

[1] State Research Institute Center for Physical Sciences and Technology, Saulėtekio ave. 3, LT-10257, Vilnius, Lithuania
paulius.gaigalas@ftmc.lt

With the ever increasing demand of clean and renewable energy, hydrogen gas, which could be produced via catalytic water splitting, has been attracting great interest in recent years. Currently, platinum and its alloys are best performing electrocatalysts, although their practical usage is hindered by the scarcity and cost of Pt noble metal [1]. Therefore, cheaper alternatives are sought after and two dimensional layered materials, such as molybdenum disulfide, are showing promising hydrogen evolution reaction activity, thus garnering the attention of researchers [2].

In this study, we report the effect of histidine amino acid for the synthesis of more efficient and stable MoS_2-based catalyst, fabricated via hydrothermal processing directly onto the conductive Ti/TiO_2 substrate. From the SEM images (Fig.1a,b), the thickness of TiO_2 film was approximately 0,56 μm, and the thickness of nanoplatelet-shaped MoS_2 film varied from 0,9 to 1,2 μm. The catalytic activity of fabricated electrocatalysts was investigated by cyclic voltammetry in 0,5 M H_2SO_4 solution using a three-electrode setup. From the cyclic voltammograms (Fig. 1c) it can be seen that MoS_2-his films are initially more active in comparison with MoS_2 films without histidine, displaying insignificant current density decrease after 1000 potential cycles, indicating high working stability during prolonged hydrogen evolution reaction processing.

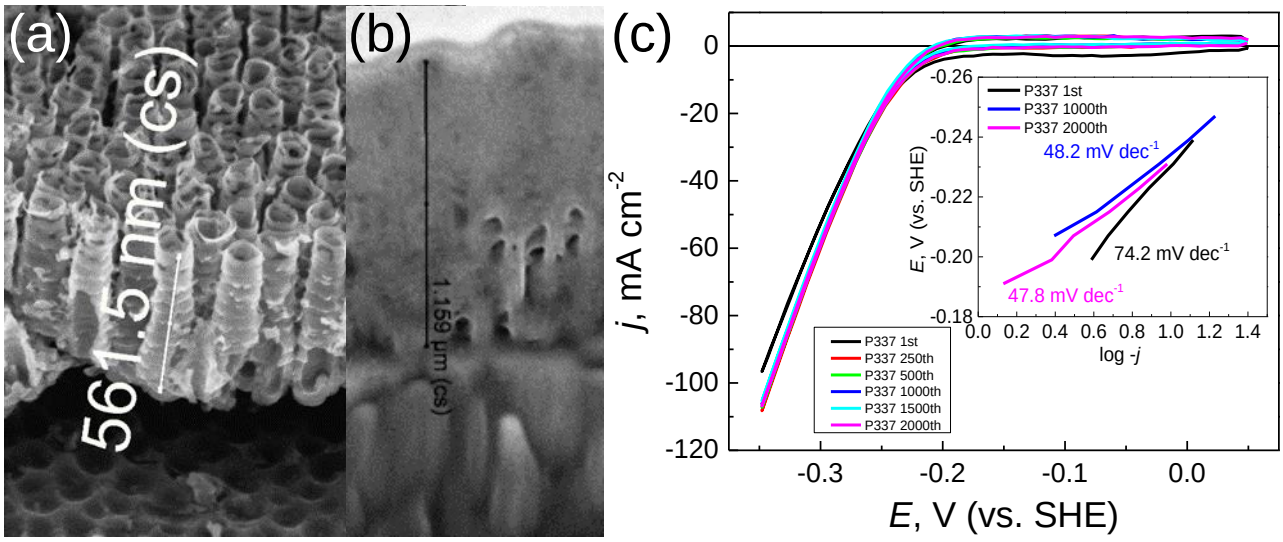


Fig. 1. Ti/TiO_2 substrate (a) and fabricated MoS_2-his (b) electrocatalyst SEM images (a,b) and cyclic voltammogram (c) of MoS_2-his.

Tafel slopes (Fig. 1c. Inset) were found to be around 48 mV/dec after 2000 potential cycles, confirming the activity and stability of fabricated electrocatalysts during prolonged hydrogen evolution reaction processing. We demonstrated that increased stability of MoS_2-his hybrid electrocatalyst could be attributed to the formation of 1T-MoS_2 and 2H-MoS_2 mixture during the hydrothermal synthesis. Further research into the influence of amino acids on MoS_2 electrocatalyst synthesis should provide a better understanding of the conditions needed to fabricate efficient MoS_2-based electrocatalysts.

[1] Li, W., Liu, G. et al., Hydrogen evolution reaction mechanism on 2H-MoS_2 electrocatalyst, Applied Surface Science **498**, 143869 (2019).
[2] Murthy, A.P., Theerthagiri, J. et al., Highly active MoS_2/carbon electrocatalysts for the hydrogen evolution reaction – insight into the effect of the internal resistance and roughness factor on the Tafel slope, *Phys. Chem. Chen. Phys.* 19, 1988 (2017).

DEVELOPMENT OF AN ELECTROCHEMICAL REACTOR FOR THE FABRICATION OF NANOPOROUS AAO MEMBRANES

Urte Cigane[1], Arvydas Palevicius[1]

[1] Department of Mechanical Engineering, Faculty of Mechanical Engineering and Design, Kaunas University of Technology, Lithuania
urte.cigane@ktu.lt

This article is intended for the research and development of innovative functional nanoporous membranes manufacturing technology. To produce better quality nanoporous membranes with controlled pore areas, a novel electrochemical reactor was designed. The reactor is composed of corps of the reactor, cover of the reactor, aluminum sheet, mixing device, Peltier element, gasket, M3 nuts, and M3x50 screws. 3D model of the electrochemical reactor for the fabrication of nanoporous AAO membranes is presented in Figure 1. In order to maintain a low and uniform temperature inside the reactor during the anodization process, a mixing device and Peltier element were installed. Mixing simulations were developed and performed in the new reactor by using ANSYS 17 software. Theoretical mixing results compared to experimental ones. Furthermore, experiments on temperature changes inside the reactor were also performed. The result of the temperature changes experiment is shown in Figure 2.

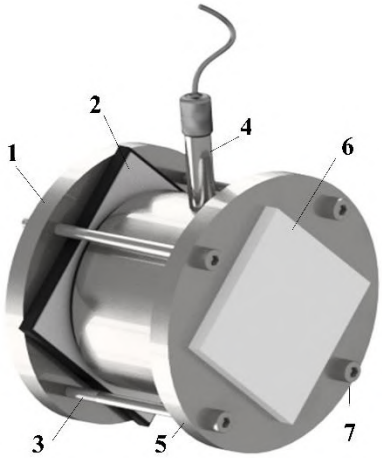


Fig. 1. 3D model of the electrochemical reactor for the fabrication of nanoporous AAO membranes: 1) cover of the reactor; 2) aluminum sheet; 3) screw M3x50; 4) mixing device; 5) corps of the reactor; 6) Peltier element; 7) nut M3.

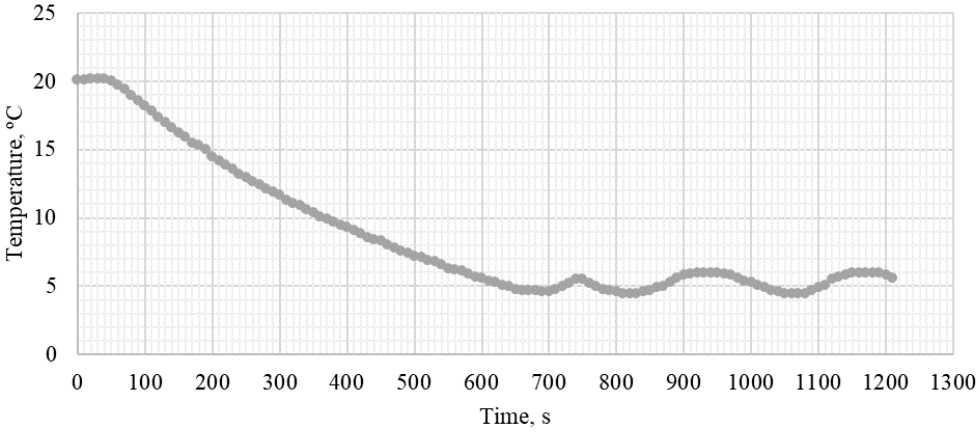


Fig. 2. Temperature changes inside the reactor.

The results of the mixing and temperature analysis confirmed that the design of the electrochemical reactor met the requirements that are important during the two-step anodization process. The observed results will be useful in the further development of the electrochemical reactor that is designed for the fabrication of nanoporous AAO membranes.

SYNTHESIS AND CHARACTERISATION OF THERMALLY REDUCED GRAPHENE OXIDE AND ITS APPLICATION AS A NOVEL ELECTRODE MATERIAL FOR DOPAMINE DETECTION

Rūta Aukštakojytė[1], Justina Gaidukevič[1, 2], Rasa Pauliukaitė[2], Jurgis Barkauskas[1]

[1] Institute of Chemistry, Faculty of Chemistry and Geosciences, Vilnius University, Lithuania
[2] Department of Nanoengineering, Center for Physical Sciences and Technology, Lithuania
ruta.aukstakojyte@chgf.vu.lt

Thermal reduction of graphene oxide (GO) is considered as a prospective technique for the simple, rapid, low-cost, and high yield preparation of graphene-based materials. However, this synthesis method has certain limitations, such as a high release of energy and the formation of structural disorders occurring during the reduction process [1]. Therefore, the thermal decomposition could be more precisely controlled and π-conjugated aromatic system may be effectively repaired by using additives. The reaction between malonic acid and phosphorus pentoxide at 150 ºC temperature gives unstable carbon suboxide (C_3O_2) that decomposes into elemental carbon and carbon monoxide [2,3]. Thermal reduction of GO in the presence of C_3O_2 additive could be an effective method to tailor electronic properties, manipulate surface chemistry, and produce local changes to the elemental composition of the reduced GO (rGO) final material. The improved physicochemical characteristics could also positively influence the electrochemical performance of rGO in the detection of biomolecules. The sensitive and precise determination is extremely essential to detect low concentrations of dopamine (DA) in the human body since its abnormal levels can potentially lead to neurodegenerative disorders such as senile dementia, depression, Parkinson's and Alzheimer's diseases [4].

This study proposes the novel synthesis, characterisation and successful application of rGO as an electrochemical sensor for effective DA detection. Two GO samples have been prepared using modified Hummer's methods, including the pre-oxidation of natural graphite powder by mixtures of $K_2S_2O_8/P_2O_5/H_2SO_4$ and $H_2SO_4/H_3BO_3/CrO_3$ [5, 6]. Thermal reduction of GO samples has been carried out in the presence of malonic acid and phosphorus pentoxide additives under Ar gas atmosphere for 1 h at 800 ºC temperature. Structural changes of rGO products obtained have been characterised by XRD, FTIR, XPS, and Raman spectroscopy techniques. The surface morphology of graphene-based samples has been studied using scanning electron and transmission electron microscopies. Electrical behaviour has also been determined by measuring the dependence between electrical conductivity and bulk density. The electrochemical measurements, including cyclic voltammetry (CV) and differential pulse voltammetry (DPV), have been performed to evaluate the sensitivity of rGO products (rGO_1_10 and rGO_2_10) towards DA detection.

The results obtained have shown that the thermal GO treatment using malonic acid and phosphorus pentoxide results in an efficient restoration of the π-conjugated system of graphene layers and an effect of P-doping. It indicates that the additive used in the thermal GO reduction plays a significant role in healing structural defects and increasing electrical conductivity in the rGO products. The CV studies have revealed that rGO_1_10 and rGO_2_10 samples exhibit prospective electrocatalytic activity towards the DA redox peak. The DPV studies have determined that the proposed sensor based on rGO_2_10 demonstrate relatively high sensitivity (28.64 μA μM^{-1} cm^{-2}) and low limit of detection (105 nM), showing that it is a promising electrode material for the sensitive DA detection.

Acknowledgments
This project has received funding from European Social Fund (project No 09.3.3-LMT-K-712-19-0050) under grant agreement with the Research Council of Lithuania (LMTLT).

[1] Y. Qiu, F. Guo, R. Hurt, I. Külaots, Explosive thermal reduction of graphene oxide-based materials: Mechanism and safety implications, Carbon, **72**, 215–223 (2014).
[2] O. Bortolini, L. Pandolfo, C. Tomaselli, P. Traldi, Ion-molecule chemistry of carbon suboxide in an ion-trap mass spectrometer, Int. J. Mass Spectrom, **190–191**, 171–179 (1999).
[3] M. Allen, Carbon suboxide in Halley, Nature **354**, 272 (1991).
[4] R. Franco, I. Reyes-Resina, G. Navarro, Dopamine in Health and Disease: Much More Than a Neurotransmitter, Biomedicines, **9**,109 (2021).
[5] X. Yan, J. Chen, J. Yang, Q. Xue, P. Miele, Fabrication of free-standing, electrochemically active, and biocompatible graphene oxide-polyaniline and graphene-polyaniline hybrid papers, ACS Appl. Mater. Interfaces, **2**, 2521–2529 (2010).
[6] J. Gaidukevic, R. Aukstakojyte, T. Navickas, R. Pauliukaite, J. Barkauskas, A novel approach to prepare highly oxidized graphene oxide: structural and electrochemical investigations, Appl. Surf. Sci., **567**, 150883 (2021).

SODIUM BOROHYDRIDE OXIDATION AT GOLD SILVER NANOPARTICLES ON REDUCED GRAPHENE OXIDE

Jadranka Milikić[1,*], Kristina Radinović[1], and Biljana Šljukić[1]

[1] University of Belgrade, Faculty of Physical Chemistry, Studentski trg 12-16, 11158 Belgrade, Serbia
*jadrankamilikic87@gmail.com

The world's energy crisis led to the investigation and improvement of renewable energy sources. Sodium borohydride ($NaBH_4$) is the main anodic fuel in the direct borohydride fuel cells (DBFCs). These electrochemical devices operate with alkaline anolyte and catholyte with oxygen (O_2) as the oxidant. Borohydride oxidation reaction (BOR) occurs by the next **equation (1)** where eight electrons are released per mol of BH_4^- [1–3]:

$$BH_4^- + 8\ OH^- \rightarrow BO_2^- + 6H_2O + 8\ e^- \qquad E^0 = -1.24\ V\ vs.\ SHE \qquad (1)$$

In this study, the nanosized gold silver particles supported on reduced graphene oxide (AuAg/rGO) were prepared by the modified recipe given in ref [4]. In the first step, reduced graphene oxide was prepared by adapting Hummer's method and then was mixed with silver and gold salts [4]. The final product was obtained by adding reducing agent L-AA with $NaBH_4$ [4].

Transmission electron microscopy (TEM) and scanning electron microscope with integrated energy-dispersive X-ray spectroscopy (SEM-EDS) were used for the determination morphology and metal content of AuAg/rGO electrode. Nanosized metal sphere particles were noticed at the gray surface of rGO by both SEM and TEM analysis. Particle size distribution obtained by TEM analysis showed low average diameters of the AuAg/rGO particles up to 2 nm. Au and Ag content of 25 and 52 mass %, respectively, were determined by EDS analysis in AuAg/rGO.

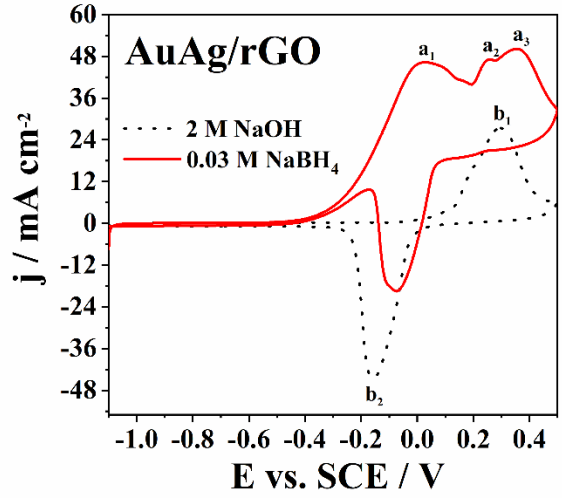


Fig. 1. Cyclic voltammograms of AuAg/rGO in 0.03 M $NaBH_4$ + 2 M NaOH solution at scan rate of 0.05 V s^{-1} at 25 °C.

Then, AuAg/rGO was examined in 2 M NaOH and 0.03 M $NaBH_4$ + 2 M NaOH (**Fig. 1**) by cyclic voltammetry (CV). b_1 and b_2 peaks of AuAg/rGO were seen at 0.3 and -0.2 V in 2 M NaOH correspond to Ag_2O formation and reduction, respectively [5]. Additional well-defined a_1, a_2, and a_3 anodic peaks were noticed at 0.02, 0.2, and 0.4 V, respectively, in the $NaBH_4$ solution. These peaks clearly showed that AuAg/rGO electrode is active for direct BOR (peak a_3) as well as for oxidation of BH_4^- hydrolysis products, eg. BH_3OH^- ion (peaks a_1 and a_2) [1–3]. Namely, BH_4^- hydrolysis often proceeds simultaneously with its direct oxidation, thus reducing fuel utilization.

This appearance and high current densities of three anodic peaks (especially peak a_1) suggest the high catalytic activity of AuAg/rGO electrode for BOR.

Acknowledgments

The authors would like to thank the Ministry of Education, Science and Technological Development of the Republic of Serbia (contract no. 451-03-9/2021-14/200146).

[1] J. Milikić, R.C.P. Oliveira, A. Tapia, D.M.F. Santos, N. Zdolšek, T. Trtić-Petrović, M. Vraneš, B. Šljukić, Ionic Liquid-Derived Carbon-Supported Metal Electrocatalysts, Catalysts. **11**, 632 (2021).

[2] J. Milikić, U. Stamenović, V. Vodnik, S.P. Ahrenkiel, B. Šljukić, Gold nanorod-polyaniline composites: Synthesis and evaluation as anode electrocatalysts for direct borohydride fuel cells, Electrochim. Acta. **328** (2019) 135115.

[3] J. Milikić, R.C.P. Oliveira, I. Stoševski, J. Krstić, R. Hercigonja, Š. Miljanić, D.M.F. Santos, B. Šljukić, Evaluation of silver-incorporating zeolites as bifunctional electrocatalysts for direct borohydride fuel cells, New J. Chem. **43**, 14270–14280 (2019).

[4] R. Krishna, D.M. Fernandes, C. Dias, J. Ventura, E. Venkata Ramana, C. Freire, E. Titus, Novel synthesis of Ag@Co/RGO nanocomposite and its high catalytic activity towards hydrogenation of 4-nitrophenol to 4-aminophenol, Int. J. Hydrogen Energy. **40**, 4996–5005 (2015).

[5] I. Stoševski, J. Krstić, J. Milikić, B. Šljukić, Z. Kačarević-Popović, S. Mentus, Š. Miljanić, Radiolitically synthesized nano Ag/C catalysts for oxygen reduction and borohydride oxidation reactions in alkaline media, for potential applications in fuel cells, Energy. **101**, 79–90 (2016).

EFFICIENT COBALT SILVER ELECTROCATALYST FOR OXYGEN REDUCTION REACTION IN ALKALINE MEDIA

Ana Nastasić[1*], Jadranka Milikić[1], Sara Knežević[2] and Biljana Šljukić[1]

[1]University of Belgrade, Faculty of Physical Chemistry, Studentski trg 12-16, 11158 Belgrade, Serbia
[2] University of Belgrade, Faculty of Chemistry, Studentski trg 12–16, 11158 Belgrade, Serbia.
*ana.nastasic8@gmail.com

Alkaline fuel cells (AFCs) convert chemical energy into electricity in a clean and highly efficient way with a low impact on the environment. The oxygen reduction reaction (ORR) is one of the most important reactions in fuel cells because most alternative cathode reactions are not practical [1]. The ORR as the cathodic reaction in alkaline media follows either four-electron (**eq. 1**) or the alternative two-electron mechanism (**eq. 2**) which is followed by further reduction of generated hydrogen peroxide (**eq. 3a**) or by its decomposition (**eq. 3b**) [1]:

$O_2 + 2H_2O + 4e^- \rightarrow 4OH^-$ $E^0 = +0.401$ V vs. SHE (1)

$O_2 + H_2O + 2e^- \rightarrow HO^-_2 + OH^-$ $E^0 = +0.065$ V vs. SHE (2)

$HO^-_2 + H_2O + 2e^- \rightarrow 3OH^-$ $E^0 = +0.867$ V vs. SHE (3a)

$2HO^-_2 \rightarrow 2OH^- + O_2$ (3b)

ORR is kinetically sluggish, so efforts have been made to improve the efficiency of this reaction in alkaline media, and thus the performance of AFCs. Some research is focused on non-platinum electrocatalysts due to their low cost and high abundance [1]. In this study, Raman spectroscopy was used for characterization of the reduced graphene oxide and transmission electron microscopy (TEM) for examining the morphology and microstructure of the CoAg/rGO electrode. Two characteristic peaks of graphene oxide known as D and G bands were observed at Raman spectra [2]. TEM image shows diameters of nanoparticles of CoAg/rGO electrocatalyst to be up to about 9 nm.

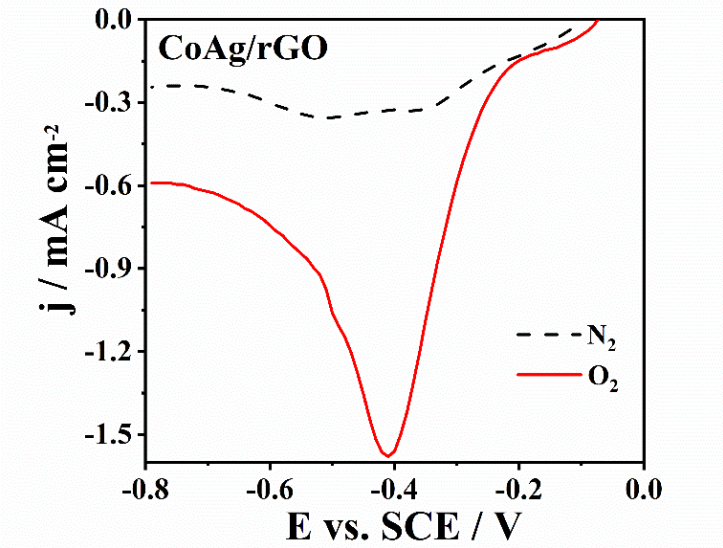


Fig. 1. Polarisation curves of CoAg/rGO electrocatalyst recorded in N_2- and O_2-saturated 0.1 M KOH solution at a scan rate of 0.02 V s^{-1}.

CoAg/rGO was examined in N_2- and O_2- saturated 0.1 M KOH solution (**Fig. 1**) by linear sweep voltammetry (LSV). ORR peak current density of -1.58 mA cm^{-2} of CoAg/rGO was obtained at -0.41 V in O_2- saturated 0.1 M KOH solution. Increasing current density of 1.3 mA cm^{-2} at -0.4 V in O_2- saturated solution compared with current density obtained in N_2- saturated solution clearly showed that CoAg/rGO electrocatalyst is active for ORR [3]. This CoAg/rGO nanosize ORR electrocatalyst could be a good replacement for costly Pt electrocatalysts because of its fast, easy, and low-cost synthesis.

Acknowledgments

The authors would like to thank the Ministry of Education, Science and Technological Development of the Republic of Serbia (contract no. 451-03-9/2021-14/200146).

[1] Y. Xie, Y. Yang, D.A. Muller, H.D. Abrunã, N. Dimitrov, J. Fang, Enhanced ORR Kinetics on Au-Doped Pt-Cu Porous Films in Alkaline Media, ACS Catal. **10**, 9967–9976 (2020).
[2] S.N. Alam, N. Sharma, L. Kumar, Synthesis of Graphene Oxide (GO) by Modified Hummers Method and Its Thermal Reduction to Obtain Reduced Graphene Oxide (rGO)*, Graphene. **06**, 1–18 (2017).
[3] J. Milikić, R.C.P. Oliveira, I. Stoševski, J. Krstić, R. Hercigonja, Š. Miljanić, D.M.F. Santos, B. Šljukić, Evaluation of silver-incorporating zeolites as bifunctional electrocatalysts for direct borohydride fuel cells, New J. Chem. **43**, 14270–14280 (2019).

FUNCTIONALIZATION OF SILVER NANOPARTICLES WITH 4-MERCAPTOBENZOIC ACID FOR IRON (II) DETECTION

Edita Daublytė[1], Tatjana Charkova[2]

[1] Life Sciences Center, Vilnius University, Lithuania
[2] Department of Organic Chemistry, Center for Physical Sciences and Technology, Lithuania
editadaublyte@gmail.com

Iron is an essential nutrient that helps the body perform many daily functions. One of the main functions of iron is to carry oxygen through the blood. Iron deficiency is the most prevalent cause of anemia. On the other hand, excess iron can harm human health by increasing free radicals, leading to renal failure, liver damage, or even death [1].

Iron ions naturally exist in all types of rocks, soil, and water. Because the iron salts can be washed away, the water is typically rich in iron, which not only influences the entry of iron ions into the human body but also changes the flavor of the water. Therefore, it is very important to develop a simple, sensitive, and reliable method for binding iron ions [2].

Many methods have been developed to detect different ions in water (atomic absorption spectrometry, inductively coupled plasma mass spectroscopy, electrochemical methods), but they often require complex sample preparation and advanced instruments. Due to its low cost and ease of management, the colorimetric method has received considerable attention in recent years [3].

Synthesized by chemical reduction silver nanoparticles (AgNPs) were subsequently functionalized with 4-mercaptobenzoic acid (MBA) and used for Fe^{2+} detection. Modified nanoparticles (Ag-MBA) aggregate in the presence of Fe^{2+}. The binding of ions to aggregates can be monitored by different methods. We combine UV-Vis and SERS techniques. The formation of the aggregated complex (Ag-MBA-Fe) was detected by visible color exchange (from greenish-gray to brownish-gray) and UV-Vis absorption spectra (Fig. 1). We also succeeded in recording the SERS spectrum of the Ag-MBA-Fe complex (Fig. 2). The concentration of iron ions in water used in our work was 10^{-3} M, but we have reason to believe that the detection limits may be lower.

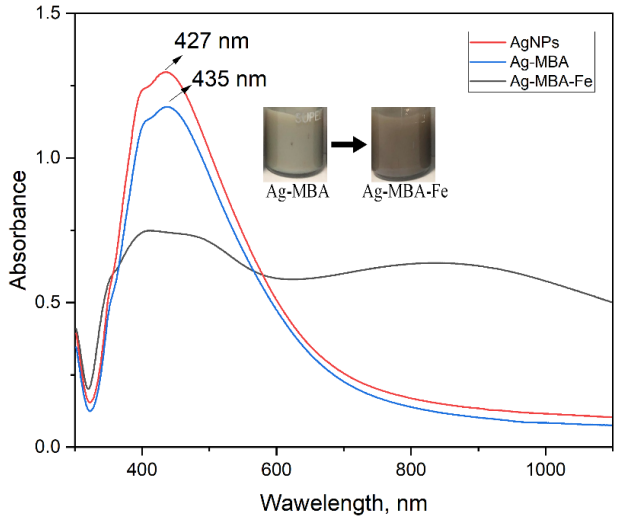


Fig. 1. UV-Vis spectra of AgNPs, Ag-MBA and Ag-MBA-Fe complex.

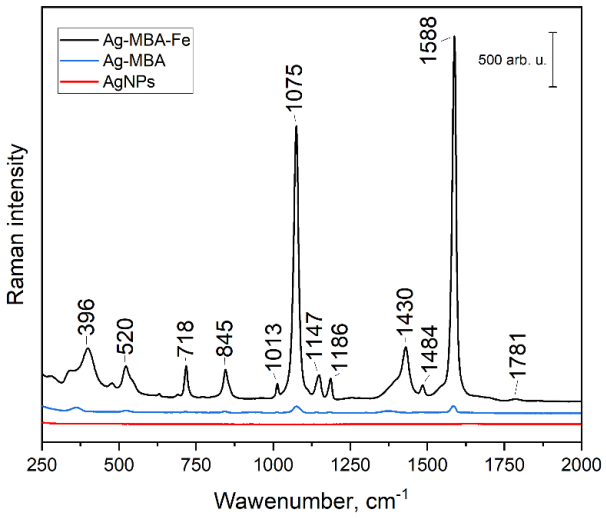


Fig. 2. Raman spectrum of AgNPs, SERS of Ag-MBA and Ag-MBA-Fe complex.

[1] M. Nordberg, G. F. Nordberg, Toxicology and biological monitoring of metals, Gen. Appl. & Sys. Toxicol. 20-21 (2009).
[2] W. F. McDonough, S. S. Sun, The composition of the Earth, Chem. Geol. **120**, 223-253 (1995).
[3] Z. Li, M. Ti, K. Yang, X. Li, L. Wu, Y. He, Colorimetric detection of iron (II) using 4-mercaptobenzoic acid and 3, 3′, 5, 5′-tetramethylbenzidine modified silver nanoparticles, Microchem. J. **151**, 104254 (2019).

CATALYST-LESS AND TRANSFER-LESS SYNTHESIS OF GRAPHENE ON Si(100) USING DIRECT MICROWAVE PLASMA ENHANCED CHEMICAL VAPOR DEPOSITION AND PROTECTIVE ENCLOSURES

Šarūnas Jankauskas[1], Rimantas Gudaitis[1], Algirdas Lazauskas[1], Šarūnas Meškinis[1]

[1] Institute of Materials Science of Kaunas University of Technology, K. Baršausko st. 59, LT-51423, Kaunas, Lithuania
sarunas.jankauskas@ktu.lt

Graphene, 2D nanomaterial with hexagonally shaped carbon atoms is one of the most researched exotic materials due to its many peerless properties, which are believed to pave the way for future high-speed electronics, solar cell technologies and many more [1]. Even though graphene has a lot of potential, its applications in various technologies are rather limited by a very complex transfer process, which prevents graphene's large-scale synthesis. To overcome that, microwave plasma enhanced chemical vapor deposition (MW-PECVD) is used as a viable method for production of graphene on various dielectric and semiconductor substrates [2]. However, etching is one of the most prominent mechanisms that prevents graphene growth in PECVD related systems, thus protective enclosures are usually used to suppress it [3]. As monocrystalline Si(100) is still the most often used substrate for the fabrication of microelectronic devices, solar cells, and different photodiodes, catalyst-less and transfer-less graphene synthesis on Si(100) using a direct microwave plasma system was considered in the present study.

In this work, graphene was grown on the Si(100) substrates by using MW-PECVD system (IPLAS Innovative Plasma Systems GmbH) and four different protective steel enclosures. 1st - 3nd enclosures are circular with different hole diameters and arrangements on top (3.5 mm, 2 mm and 3.5 mm with no holes at the top respectively) with a 4th enclosure having a simple open ended rectangular configuration. The characterization of samples was carried out using Raman scattering spectroscopy (Renishaw inVia, 532 nm) by evaluating I_{2D}/I_G and I_D/I_G, peak intensity ratios.

Altogether, it is clear, that the most detrimental parameter in graphene synthesis, using our system, is the CH_4/H_2 flow ratio. Based on Raman spectra findings, CH_4/H_2 ratio as low as 0.11 produces no graphene, while increasing it to 0.33 gives a clear graphene fingerprint (I_{2D}/I_G for 1st, 2nd and 3rd enclosure is 0.81, 0.7 and 0.92 respectively). Further increase of methane flow compared to hydrogen flow increases the number of layers as evident from the decrease of I_{2D}/I_G (for 1st, 2nd and 3rd enclosure, I_{2D}/I_G ratio is 0.62, 0.52 and 0.3 respectively).

No top-hole size effects were found, when studying enclosure designs. The absence of top holes in the middle of the enclosure (3rd) reduced the plasma effect on the growing graphene and decreased defect density. The graphene was also successfully synthesized using just a rectangular steel sheet folded in two places as a simplified protective enclosure (4th).

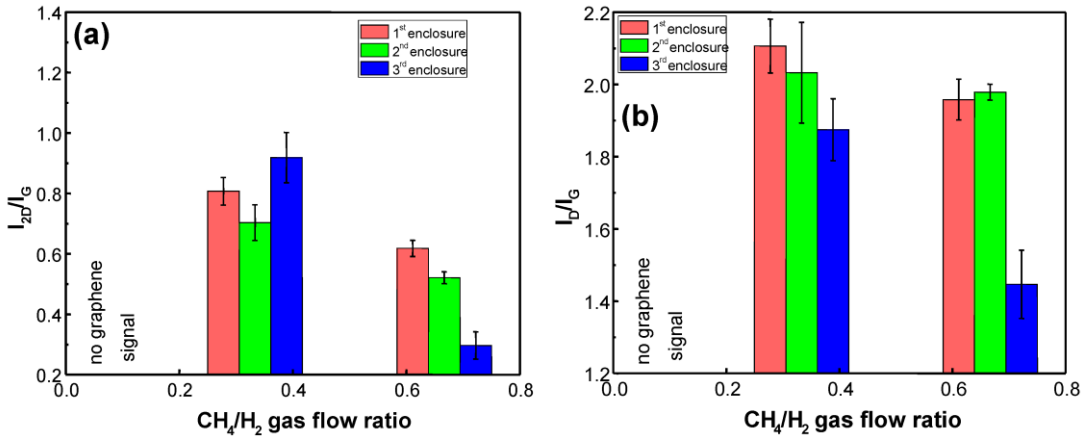


Fig. 1. I_{2D}/I_G (a) and I_D/I_G (b) ratios of graphene synthesized using different flow ratio (0.11, 0.33, 0.67) CH_4/H_2 mixture of gas and enclosures. In all cases, every other process parameter is kept constant (power 1.2 kW, pressure 30 mBar, temperature 900 °C, time 30 min).

[1] E. P. Randviir, D. A. C. Brownson et al., A decade of graphene research: production, applications and outlook, Materials Today **17(9)**, 426–432 (2014).

[2] A. Khan, S. Islam et al., Direct CVD Growth of Graphene on Technologically Important Dielectric and Semiconducting Substrates, Advanced Science **5(11)**, 1800050 (2018).

[3] S. Zheng, G. Zhong et al., Metal-catalyst-free growth of graphene on insulating substrates by ammonia-assisted microwave plasma-enhanced chemical vapor deposition, RSC Advances **7(53)**, 33185–33193 (2017).

DETECTION OF NITROBENZENE DERIVATIVES USING SILVER COPPER ELECTRODE ON REDUCED GRAPHENE OXIDE IN NEUTRAL MEDIA

Aleksandar M. Đorđević[1,2,*], Jadranka Milikić[3], and Biljana Šljukić[3]

[1]University of Belgrade, Institute of General and Physical Chemistry, Studentski trg 12/V, 11158 Belgrade, Serbia
[2]University of Belgrade, Faculty of Chemistry, Studentski trg 12–16, 11158 Belgrade, Serbia
[3]University of Belgrade, Faculty of Physical Chemistry, Studentski trg 12-16, 11158 Belgrade, Serbia
*alek2102@gmail.com

In recent years, environmental pollution caused by the disposal of industrial waste has been a serious problem. Aromatic nitro compounds stand out among the pollutants that are very harmful to human health. They are organic pollutants in wastewater from various industrial processes such as the paint and varnish industry, explosives, perfumes, plastics, pesticides, and the pharmaceutical industry [1-3]. They are classified as highly toxic and carcinogenic, showing carcinogenic activity even at trace levels, especially nitrobenzene (NB) and its derivatives [2-5]. Therefore, detection of NB is vital for the protection of human health and the environment [5]. Within the present study, novel electrode materials were developed for application in the electrochemical sensor for the detection of NB in neutral media.

Herein silver copper supported on reduced graphene oxide (AgCu/rGO) was characterized by transmission electron microscopy (TEM) and scanning electron microscopy (SEM) where nanosized spherical metal particles distributed on a grey surface of rGO were seen.

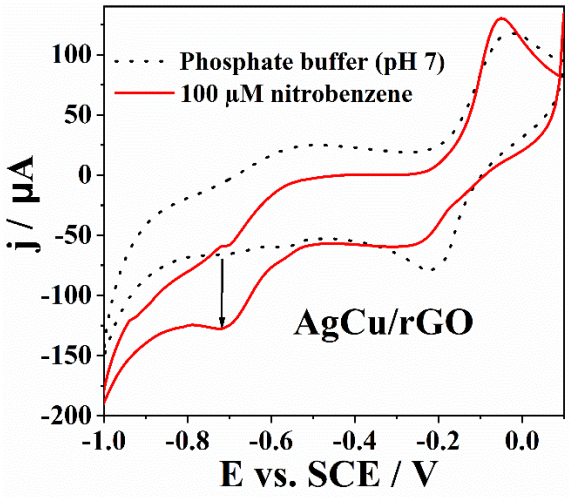


Fig. 1. Cyclic voltammograms of AgCu/rGO recorded in the absence (•••) and presence (—) of 100 µM nitrobenzene in 0.1 M phosphate buffer (pH 7) saturated with N_2 at a scan rate of 10 mV s^{-1}.

The electrochemical behavior of AgCu/rGO nanocomposites in NB solution was studied by cyclic voltammetry (CV). **Fig. 1** shows that the control cyclic voltammogram of AgCu/rGO electrode recorded in 0.1 M phosphate buffer doesn't show peaks in the potential range where the NB reduction reaction is expected, while the cyclic voltammogram recorded in 100 µM NB shows a reduction peak of NB at a potential of about - 0.7 V. A similar response to the presence of NB in a neutral medium was shown by silver nanoparticles (Ag NPs) deposited on spheres of modified silica (SiO_2) [4]. The results showed electrodes' good sensitivity to the presence of NB. AgCu/rGO electrode could be a promising sensor for NB detection in neutral media because of its low cost and fast synthesis.

Acknowledgments

The authors would like to thank the Ministry of Education, Science and Technological Development of the Republic of Serbia (contract no. 451-03-9/2021-14/200146; 451-03-9/2021-14/ 200051 and 451-03-9/2021-14/200168).

[1] S.-S. Li, J.-H. Fang, L. Li et al., An ultra-sensitive electrochemical sensor of Ni/Fe-LDH toward nitrobenzene with the assistance of surface functionalization engineering, Talanta **225,** 122087 (2021).
[2 J. Liu, R. Ye, J. Shi, et al.,Construction of Cu nanoparticles embedded nitrogen–doped carbon derived from biomass for highly boosting the nitrobenzene reduction: An experimental and theoretical understanding, Chemical Engineering Journal **419**, 129640 (2021).
[3] A. Nematollahzadeh, A. Babapoor, S. M. Mousavi, et al., Nitrobenzene adsorption from aqueous solution onto polythiophene-modified magnetite nanoparticles, Materials Chemistry and Physics **262**, 124266 (2021).
[4] P. Rameshkumar, R. Ramaraj, Electroanalysis of nitrobenzene derivatives and nitrite ions using silver nanoparticles deposited silica spheres modified electrode, Journal of Electroanalytical Chemistry **731**,72-77 (2014).
[5] C. Karuppiah, K. Muthupandi, S.-M. Chen, et al., Green synthesized silver nanoparticles decorated on reduced graphene oxide for enhanced electrochemical sensing of nitrobenzene in waste water samples, RSC Advances **5,** 31139-31146 (2015).

COMPARATIVE STUDY OF WSe_2 THIN FILMS SYNTHESIZED VIA PRE-DEPOSITED WO_3 AND W PRECURSOR MATERIAL SELENIZATION

Kevon Kadiwala, Edgars Butanovs, Andrejs Ogurcovs, Martins Zubkins, Boris Polyakov

Institute of Solid State Physics, University of Latvia, Kengaraga street 8, Riga, Latvia, LV-1063
kevon.kadiwala@cfi.lu.lv

Layered two-dimensional (2D) materials, such as p-type WSe_2, are potential key materials in manufacturing of the next generation electronic devices. One of the remaining main challenges is the large area growth of high-quality 2D films. A potential large-scale 2D WSe_2 synthesis method is conversion (selenization) of a pre-deposited sacrificial precursor coating, however, its use is still limited mainly due to lack of understanding of the growth mechanisms involved. Here, we have studied and compared properties of thin crystalline WSe_2 films, prepared via selenization of sputter-deposited sacrificial WO_3 and W films. Surface morphology of the as-grown films was studied using scanning electron microscope complemented with atomic force microscope. Structural and chemical composition was confirmed by X-ray diffraction and micro-Raman spectroscopy, respectively. On-chip photoconductive devices were made using standard photolithography process and their photoresponse was investigated for 405 nm wavelength light. The obtained results give insight into the growth of crystalline WSe_2 via sacrificial film selenization.

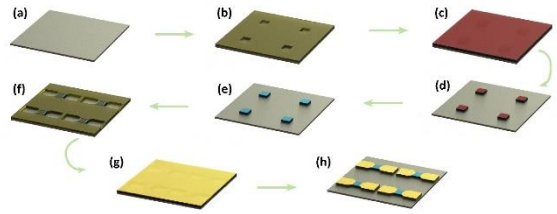


Fig. 1. Schematic of the process of on-chip device fabrication: first SiO_2/Si substrate is cleaned using acetone and isopropanol (a), then using standard photolithography process the first mask is made (b) on which precursor material is deposited (c). After first mask lift-off, precursor material film is in desired pattern (d), which is subsequently selenized (e). Afterwards, the second photoresist mask is deposited (f) for the deposition of contact material (Cr ~ 5nm, Ag ~ 95nm, Al ~ 50nm) using thermal evaporation method (g), followed by lift-off to obtain photoconductor device array on chip (h).

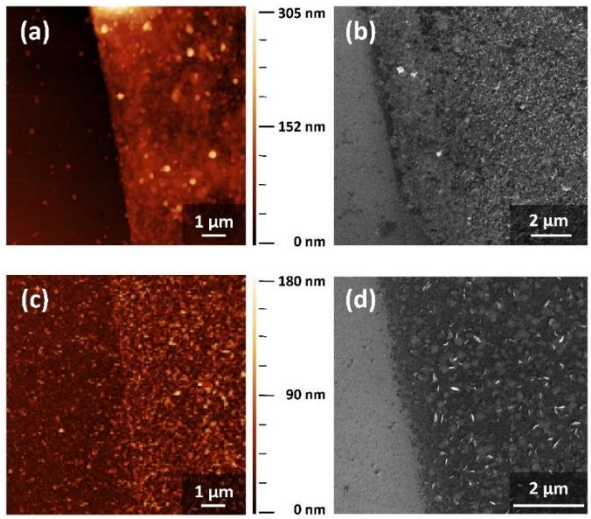


Fig. 2. Atomic force microscope (AFM) Z-drive images of WSe_2 films, made from WO_3 precursor (a) and from metal W precursor (c) showing the difference between film surfaces, further complimented by SEM images of the same samples in respective order of (b) and (d).

The study is financially supported by the Institute of Solid State Physics of the University of Latvia under Student and Young Scientists project.

FEMTOSECOND LASER ABLATED SILVER NANOPARTICLE MORPHOLOGY DEPENDENCE ON THE APPLIED LIQUID

Jaunius Mykolaitis[1], Tomas Tamulevičius[1, 2, 3], Asta Tamulevičienė[1, 2, 3]

[1] Department of Physics, Kaunas University of Technology, Studentų St. 50, LT-51368 Kaunas, Lithuania
[2]Institute of Materials Science, Kaunas University of Technology, K. Baršausko St. 59, LT-51423 Kaunas, Lithuania
[3]JSC "Nanoversa", K. Baršausko St. 59, LT-51423 Kaunas, Lithuania
jaunius.mykolaitis@ktu.edu

For the last few years, the attention and interest in metal nanoparticles, their applications, and possible synthesis methods is noticeably increasing faster than ever before. This is mainly because of the specific and unique nanoparticle's chemical, optical, electric properties, compared with their bulk counterparts. Additionally, nanoparticles can be used for numerous practical applications, like catalysis, medicine, biotechnology, and so on [1]. Different synthesis methods of nanoparticles exist, but laser ablation in liquid (LAL) method seems to be one of the most favorable because the system itself is simple and it allows to produce nanoparticles of small size range deviation, varies their morphology, and produced nanoparticles are contamination-free when no additional surfactants are used in the process [1].

The purpose of this work was to produce silver nanoparticles using LAL of a silver target (99.9%, JSC Lithuanian Mint). The influence of the ablation media (ultrapure type 1 water, chloride, and iodide salt solutions) was related to the size and shape of the resulting nanoparticles. The laser ablation was carried out employing a first harmonic of 1030 nm of a 270-fs pulse length Yb:KGW femtosecond laser (Pharos, Light Conversion) operating at a 200 kHz repetition rate. A galvoscanner and a telecentric f-Theta lens equipped in a laser micromachining workstation (FemtoLab, Altechna R&D) were used. The analysis of the shape and size of produced silver nanoparticles was performed using scanning electron microscopy (SEM, Quanta 200 FEG, FEI) and software Ilastik whereas the optical properties were evaluated using UV – vis spectroscopy (AvaSpec 2048, Avantes).

The successful formation of the silver colloidal solutions was confirmed by their unique distinguished yellow color. Absorption spectra of silver colloidal solutions synthesized in different environments are depicted in figure 1, a. The absorption peak corresponds to localized surface plasmon resonance of silver nanostructures [2] and varies from 398 nm to 408 nm depending on the ablation media.

Even though, using different media for target immersion the optical spectra did not change considerably, the SEM analysis revealed that it had an expressed effect on the shape and size of nanoparticles as is seen in Figure 1, b-d. From the results, it was observed that halogen etching and photo-irradiation using laser beam leads to the conversion of silver nanoparticles morphology to more complex geometries than spheres observed in the case of water [2]. The diameter of spherical silver nanoparticles produced in ultrapure water was in the range of 15 – 25 nm. On the other hand, nanoparticles produced in chlorides and iodides solutions demonstrate nanotriangles, nanocubes, and nanorods morphologies. Length of the edges of such nanostructures vary from 100 nm to 400 nm. Obtained results show that changing the immersion liquid LAL synthesis of metal nanoparticles can be effectively used to produce silver nanoparticles of different morphology.

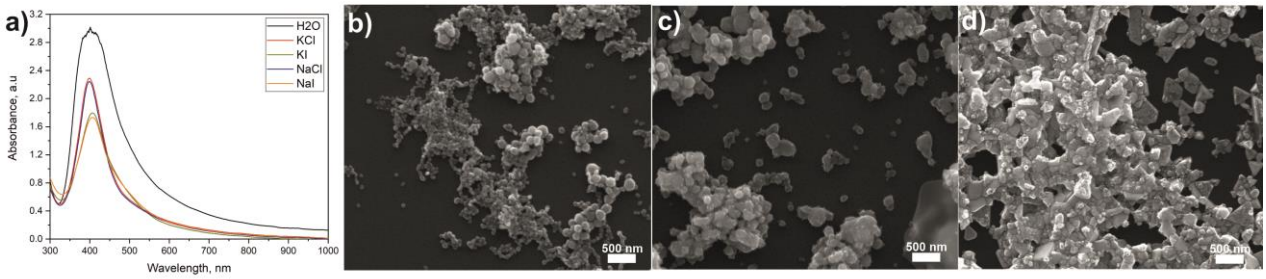


Figure 1. Absorbance spectra of colloidal solutions formed in different media (a) and SEM images of nanoparticles formed in water (b), sodium chloride (c) and sodium iodide (d)

[1] Tarasenko, N. V. et al., (2006). Synthesis of nanosized particles during laser ablation of gold in water. Applied Surface Science, 252(13), 4439–4444. doi: 10.1016/j.apsusc.2005.07.150

[2] Tsuji, T., Okazaki, Y., & Tsuji, M. (2008). Photo-induced morphological conversions of silver nanoparticles prepared using laser ablation in water—Enhanced morphological conversions using halogen etching. Journal of Photochemistry and Photobiology A: Chemistry, 194(2-3), 247–253. doi: 10.1016/j.jphotochem.2007.08

ASSESSMENT OF ZnO NANOWIRES APPLICATION FOR THE COVALENT PROTEINS IMMOBILIZATION BY TOTAL INTERNAL REFLECTION ELLIPSOMETRY

Vincentas Mačiulis[1], Ieva Plikusienė[1,2], Silvija Juciutė[2], Justina Liesytė[2], Saulius Balevičius[1], Arūnas Ramanavičius[1,2], Vilius Vertelis[1], Almira Ramanavičienė[2]

[1]Center for Physical Sciences and Technology, Vilnius, Lithuania
[2] Department of Physical Chemistry, Faculty of Chemistry and Geosciences, Vilnius University, Lithuania
vincentas.maciulis@ftmc.lt

Zinc oxide (ZnO) is a versatile material with a variety of properties suited for high-technology such as light-emitting diodes, photodetectors, energy harvesting devices and biosensors. ZnO also has a great diversity in structural morphology and nanostructures in both structural and properties point of view. Thus, ZnO has received much attention from scientists. Wide morphological diversity of nanostructures can be produced using this metal oxide such as nanolaminates, nanowires, nanorods, nanotubes, nanobelts, and other complex morphologies. ZnO thin layers and nanostructures are attractive for biosensing as the surface can be easily modified using functional groups for various biomolecules immobilization [1].

ZnO nanowires (NWs) are one-dimensional structures, that have received great interest due to wide application potential in the field of chemical sensors and biosensors. ZnO nanowires can be synthesized by various means; thus a large number of articles dedicated to synthesis, characterization, and growth mechanisms has been published [2].

In this study, the optical method of total internal reflection ellipsometry (TIRE) was used for the real-time investigation of proteins immobilization on functional groups modified ZnO NWs. This non-destructive, label-free, and highly sensitive optical method has been applied for the characterization of various thin films, as well as for the real-time interaction [3].

In this work, we present the formation of ZnO NW formation using electrodeposition on an ITO glass substrate, functionalization of NWs with amine groups using 3-aminopropyltriethoxysilane (APTES), and investigation of covalent immobilization of bovine serum albumin (BSA) in ZnO NWs. It was obtained that calculated diffusion constant of BSA molecule into ZnO NW matrix in PBS along the length of ZnO NWs was 6 orders lower, than conventional BSA molecule diffusion in PBS buffer. Investigation of immobilization kinetics and diffusion coefficient calculation could be applied to evaluate biomolecule sizes.

[1] Z. Balevicius *et al.*, "Towards the application of Al2O3/ZnO nanolaminates in immunosensors: total internal reflection spectroscopic ellipsometry based evaluation of BSA immobilization," *J. Mater. Chem. C*, vol. 6, no. 32, pp. 8778–8783, 2018, doi: 10.1039/c8tc03091j.
[2] I. Plikusiene *et al.*, "Total internal reflection ellipsometry for kinetics-based assessment of bovine serum albumin immobilization on ZnO nanowires," *J. Mater. Chem. C*, vol. 9, no. 4, pp. 1345–1352, 2021, doi: 10.1039/d0tc05193d.
[3] I. Plikusiene *et al.*, "Evaluation of kinetics and thermodynamics of interaction between immobilized SARS-CoV-2 nucleoprotein and specific antibodies by total internal reflection ellipsometry," *J. Colloid Interface Sci.*, vol. 594, pp. 195–203, 2021, doi: 10.1016/j.jcis.2021.02.100.

INVESTIGATION OF CORRELATION BETWEEN PHOTOLUMINESCENCE INTENSITY AND WAVELENGTH IN InGaN MQWs ON SUB-MICROMETER SCALE

Gytis Babaitis[1], Darius Dobrovolskas[1]

[1]Institute of Photonics and Nanotechnology, Faculty of Physics, Vilnius University, Lithuania
gytis.babaitis@ff.stud.vu.lt

Indium gallium nitride (InGaN) is a III-V direct band gap semiconductor made with a mix of InN and GaN materials. First InGaN materials were grown back in 1993 by Nakamura. Since then InGaN LEDs have attracted a lot of attention because of possibility to develop optoelectronic devices emitting from ultraviolet to red region of the electromagnetic spectrum. However, a sharp efficiency drop as indium content is increased still remains a massive issue when trying to manufacture green or red light emitting devices. In fact it is quite surprising that InGaN LEDs are working at all despite their high density of defects. Local indium segregation is responsible for localizing of carriers from defects. In this work the spatial distribution of photoluminescence (PL) is investigated using confocal microscope.

During the research three groups containing different InGaN samples emitting in a wide spectral range were investigated. They either had varying quantum well (QW) thickness (1 – 4 nm) or varying In content (9 – 25 %). Samples were excited with a 405 nm wavelength laser diode through a high numerical aperture (NA = 0.9). PL distributions in 10x10 μm^2 (100x100 points) areas in each sample were measured.

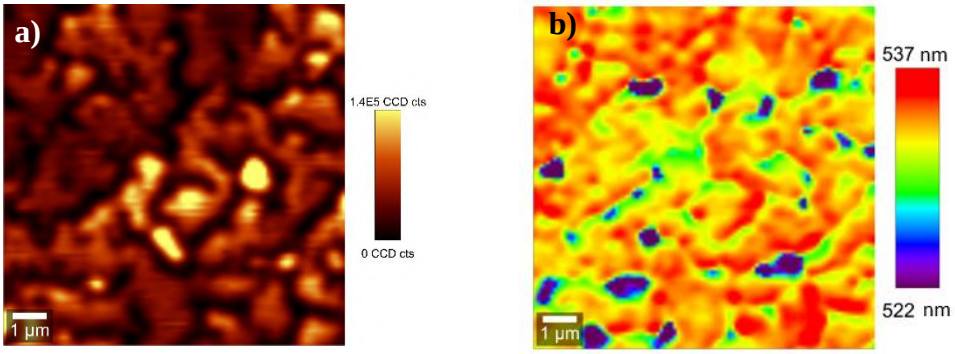


Fig. 1 a) PL intensity and b) peak position images of one of the measured samples

Highly inhomogeneous spatial distributions of PL intensity and peak position typical for InGaN samples were observed and was attributed to localization in the indium rich areas, which isolate carriers from the nonradiative recombination. A redshift of samples PL peak position was observed with increasing indium content due to decreased bandgap. A redshift also was observed in sample group where indium content stayed constant but the quantum well width was changing.

To better characterize samples, correlation coefficient between PL intensity and peak position were calculated (Fig. 2). For samples emitting at shorter wavelengths than ~500 nm, correlation coefficient is positive indicating that higher PL intensity is observed in areas emitting at longer wavelengths. This is in line with localization model. However, for samples with average PL peak wavelength larger than 500 nm correlation coefficient decreases and shifts from positive to negative. Negative values are unexpected and does not agree with localization model. In this work different explanations for this transition were overviewed and discussed, including larger amount of dislocation densities at higher In content regions along with stronger quantum confined Stark effect.

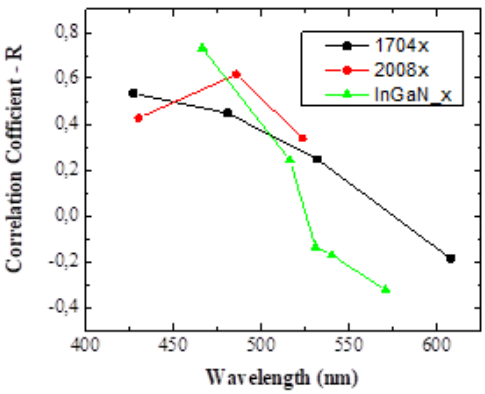


Fig. 2 Correlation coefficients between the PL intensity and peak position of the measured samples

SYNTHESIS OF HYBRID GOLD-SILVER NANOPARTICLES FROM THIN BIMETALLIC COATINGS USING LASER ABLATION

Vita Petrikaitė[1], Evaldas Stankevičius[1]

[1] Department of Laser Technologies, Center of Physical Sciences and Technology, Lithuania
vita.petrikaite@ftmc.lt

Precious metals gold and silver nanoparticles have become the focus of nanotechnology due to the wide absorption band in the electromagnetic spectrum. They have a high area-to-volume ratio, electrical conductivity, chemical stability, catalytic functions and good biocompatibility [1, 2]. The optical properties of metal nanoparticles depend on the localized surface plasmon resonance (LSPR). LSPR is the frequency caused by conductive electron oscillations generated by the interaction with an electromagnetic wave [3]. This quantum phenomenon can be manipulated by altering the size, dispersion, shape, composition, and other physical and chemical characteristics of nanoparticles [4]. To do this, different synthesis methods and parameters are used, which determine the morphology, stability and physicochemical properties.

Nanoparticles generated by laser ablation in water from bulk material tend to aggregate. To avoid aggregation, a method was tested by synthesizing nanoparticles from thin coatings on a glass substrate in water and KCl salt solution. Salt was introduced into the experiment as an additional stabilizer.

The absorption of gold and silver nanoparticles occurs in different areas of the visible electromagnetic spectrum. Hybrid gold-silver and silver-gold nanoparticles are used to extend the resonant wavelength range. The scheme for the synthesis of hybrid nanoparticles is shown in Figure 1 (a). The target is immersed in the selected solution and exposed to a laser. In one laser scan, the entire glass substrate is cleaned and the coating is broken down into fragments - nanoparticles that spread through the liquid and form a colloidal solution. A TEM image of the hybrid nanoparticles is shown in Figure 1 (b).

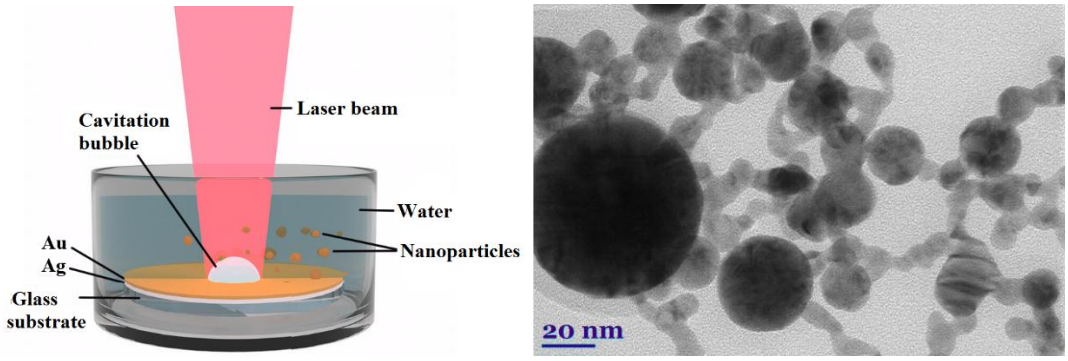


Fig. 1. a) Laser ablation scheme for bimetallic coatings; b) TEM image of the formed (Ag 50 nm - Au 50 nm) hybrid nanoparticles.

A method for generating hybrid gold-silver nanoparticles from thin coatings on glass substrate in a liquid by nanosecond laser ablation and investigation of the plasmonic properties and stability of the formed particles will be presented.

[1] Y. C. Yeh, B. Creran, V. M. Rotello, Gold nanoparticles: preparation, properties, and applications in bionanotechnology, Nanoscale 4(6), 1871–1880 (2012).
[2] E. Stankevičius, M. Garliauskas, L. Laurinavičius, R. Trusovas, N. Tarasenko, R. Pauliukaitė, Engineering electrochemical sensors using nanosecond laser treatment of thin gold film on ITO glass, Electrochimica Acta (297) 511-522, (2019).
[3] E. Petryayeva, U. J. Krull, Localized surface plasmon resonance: Nanostructures, bioassays and biosensing-A review, Analytica Chimica Acta, 706(1), 8–24, (2011).
[4] K. A. Willets, R. P. Van Duyne, Localized surface plasmon resonance spectroscopy and sensing, Annual Review of Physical Chemistry, 58, 267–297, (2007).

P2-20

DID NOT PARTICIPATE

.

SODIUM-ION BATTERIES: HIGHLY-CONDUCTING NANOCRYSTALLIZED GLASS-CERAMIC CATHODE MATERIALS

Maciej Nowagiel[1], Mateusz J. Samsel[1], Aldona Zalewska[2], Tomasz K. Pietrzak[1]

[1] Faculty of Physics, Warsaw University of Technology, Poland
[2] Faculty of Chemistry, Warsaw University of Technology, Poland
maciej.nowagiel.dokt@pw.edu.pl

Application of renewable power sources (e.g. wind and solar power plants) carries new challenges concerning energy storage. One of the remedies to stabilize their output is the utilization of battery storage stations. In this field, sodium-ion batteries (NIBs) are expected to be a sustainable and cheap alternative to lithium ones [1].

Materials called alluaudites, first described by Fisher in 1955 [2], are among prospective cathode materials for NIBs, with the theoretical gravimetric capacity close to 170 mAh/g [3]. In our research, we studied materials with nominal composition of $Na_2M_3(PO_4)_3$ (M = Fe, V, Mn). Another interesting compound is $Na_3M_2(PO_4)_2F_3$ (M = V, Ti, Fe) with the NASICON structure (theoretical capacity reaching ca. 192 mAh/g) [4-5]. Poor electrical conductivity is one of the main obstacles to their implementation.

Thermal treatment of glassy samples led to nanocrystallization of alluaudite or NASICON phase [6-7]. Previous studies on amorphous analogues of cathode materials for Li-ion batteries show a significant increase of electrical conductivity as a result of their thermal nanocrystallization, due to the occurrence of the preferable conditions for polaron hopping mechanism of conduction [8]. We have shown that a similar procedure can be successfully applied to sodium compounds as well. We observed a significant (5 orders of magnitude) and irreversible increase of conductivity, which resulted in nanomaterials with $\sigma(25°C) \approx 1$ mS/cm. We also elaborated optimal syntheses conditions to obtain alluaudite-like nanomaterials with maximum possible phase purity.

Optimization of nanocrystallization process allowed us to assemble and test our materials as cathodes in prototype sodium-ion cells. They were tested at various current rates. Practical capacities generally did not exceed 60 mAh/g and cells often suffered from modest cycle life and limited rate performance. There is, however, place for improvements and presented results can be a good basis for further research.

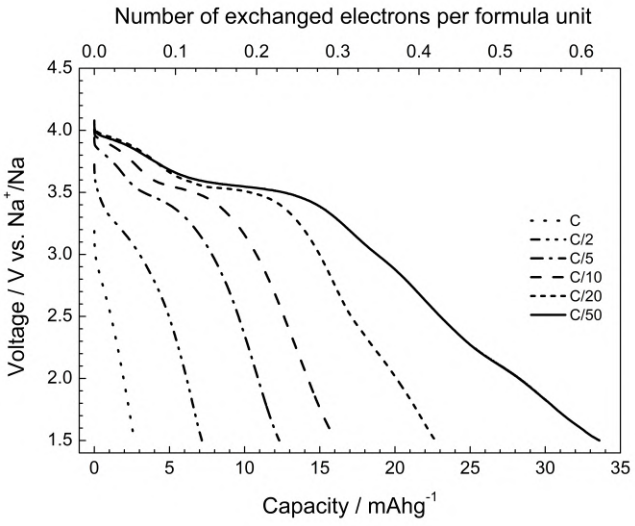


Fig. 1. Discharge curves at various current (C) rates for $Na_3V_2(PO_4)_2F_3$ nanocrystallized NASICON cathode.

This research was funded by POB "Energy" of Warsaw University of Technology within the Excellence Initiative: Research University (IDUB) programme (2020-2021).

[1] V. Palomares et al., Energy & Environmental Science 5 (2012), 5884–5901.
[2] D.J. Fisher, American Mineralogist 40 (1955), 1100–1109.
[3] K. Trad et al., Chemistry of Materials 22 (2010), 5554–5562.
[4] I. Matts et al., Chemistry of Materials 27 (2015), 6008–6015.
[5] I. Matts, PhD Thesis, MIT 2016.
[6] M. Nowagiel et al., Materials 14(17) (2021), 4997.
[7] T.K. Pietrzak et al., International Journal of Applied Glass Science 11 (2020), 87–96.
[8] T.K. Pietrzak et al., Materials Science and Engineering B 213 (2016), 140–147.

MULTICOLOR COLORIMETRIC ASSAY FOR CYANIDE DETECTION

Viktorija Lisyte, Eimantas Bucmys, Anton Popov, Almira Ramanaviciene

NanoTechnas – Center of Nanotechnology and Materials Science, Faculty of Chemistry and Geosciences, Vilnius University, Vilnius, Lithuania
viktorija.lisyte@chgf.vu.lt

Nowadays nanomaterials are one of the most interesting and developing areas of science [1]. Among them, gold nanoparticles (AuNPs) are highly remarkable [2]. AuNPs can be used for fabrication of various sensors due to their unique optical properties coming from localized surface plasmon resonance (LSPR) [3]. Changes in nanostructures size, shape or environmental refractive due to molecules absorbed on the surface have a significant effected on the properties of LSPR. As a result, these nanostructures can be used in high-sensitivity optical systems without the use of variety of markers that typically require for reaching low limit of detection of proteins [4]. One of the most attracted AuNPs is gold nanorods (AuNRs) which have garnered a great deal of scientific interest because of their unique optical properties and they have the potential to greatly impact many areas of science and technology [5]. By changing their ratio of diameter to length, colloidal solutions of these structures can acquire various colors. These can be used in AuNR optical systems based on varying the length or diameter of these structures at different amounts of analyte. Due to the intense color changes, AuNRs optical systems can be used to detect a variety of materials with the naked eye without the use of diagnostic equipment, making them suitable for a variety of medical care points or locations where testing with sophisticated equipment is not available. One of the most interesting AuNRs optical analytical systems is based on the directional etching of nanorods, resulting a reduction in length and interconnected changes in absorption spectra. A major advantage of this method is that only substances with sufficiently strong oxidative properties is required for the analysis. System of horseradish peroxidase (HRP), H2O2 and 3,3′,5,5′ tetramethylbenzidine (TMB) is suitable for AuNRs etching. Therefore, concentration of various HRP inhibitors such as an extremely poisonous substance cyanide (CN^-) possible can be measured based on this system. About 1.4 tons of cyanide are produced each year and used in various industries, such as gold and silver mining, metal plating, petrochemical plants, steels mills and plastic factories. The increasing production of cyanide has a negative effect for underground water, animals, food, the environment and humans [6].

The main goal of this work was applying of AuNRs etching to create optical method for the determination of cyanide ions. The synthesized AuNRs were characterized using UV/Vis spectroscopy, SEM and DLS methods. Optimization of parameters, such as solution pH, TMB concentration and H_2SO_4 concentration, on which depends HRP enzymatic reaction was performed. The impact of reaction time on AuNRs was evaluated. HRP inhibition reaction was applying for detection of cyanide ions concentration. Investigated optical analytical system could be used for detection of cyanide by naked eye.

Acknowledgments

This work is part of a project that has received funding from the European Union's Horizon 2020 research and innovation programme under grant agreement No. 778157 CanBioSe

[1] Brasiunas B. et al. Gold nanoparticle based colorimetric sensing strategy for the determination of reducing sugars. *Food Chemistry*, 2021, 351: 129238.

[2] Elahi N., Kamali M., Baghersad M. H. Recent biomedical applications of gold nanoparticles: A review. *Talanta*, 2018, 184: 537-556.

[3] Ungureanu C., Rayavarapu R. G., Manoha, S., & van Leeuwen, T. G. (2009). Discrete dipole approximation simulations of gold nanorod optical properties: Choice of input parameters and comparison with experiment. *Journal of Applied Physics*, *105*(10), 102032.

[4] Pissuwan D., Valenzuela S. M., Cortie M. B. (2008). Prospects for Gold Nanorod Particles in Diagnostic and Therapeutic Applications. *Biotechnology and Genetic Engineering Reviews*, *25*(1), 93–112.

[5] Burrows N. D., et al. Surface chemistry of gold nanorods. *Langmuir*, 2016, 32.39: 9905-9921.

[6] Lee, S., et al. Highly sensitive photometric determination of cyanide based on selective etching of gold nanorods. *Microchimica Acta*, 2016, 183.11: 3035-3041.

MICROWAVE-ASSISTED SYNTHESIS OF 3D METAL OXIDE MAGNETO-PLASMONIC NANOPARTICLES

Greta Olimpija Remeikytė[1,2*], Zenonas Kuodis[2], Olegas Eicher-Lorka[2]

[1]Faculty of Chemistry and Geosciences, Vilnius University, Lithuania
[2]Department of Organic Chemistry, Center for Physical sciences and technology, Lithuania
greta.remeikytė@gmail.com

Magneto-plasmonic (MP) particles composed of several elements where plasmonic materials are mainly Au, Ag, and Cu, and magnetic materials are 3d metals and their oxides. Magneto-plasmonic multicomponent nanoparticles has properties of their components and unique properties. Due to their distinctiveness and multifunctional properties, they show promising application in biotechnology and medicine. The particles are used for drug transport in organisms, as contrast agents in MRT studies and to enhancing SERS spectra [1].

As the world moves towards sustainability scientists are searching for the new ways to shorten and facilitate routes of the synthesis. Our experiments simplify the polyol synthesis pathway of Fe_3O_4, $NiFe_2O_4$, $CoFe_2O_4$ to the one pot synthesis without the use of any other additives except tetraethylene glycol (TEG). TEG is used as a reaction medium and as a reducing agent. The reaction is performed in a microwave reactor at 260 ºC. Resulting ferrites were ~8–10 nm. Like other authors observed ferrites tends to form nearly uniformly sized spherical ~120 nm aggregates Fig. 1 [2].

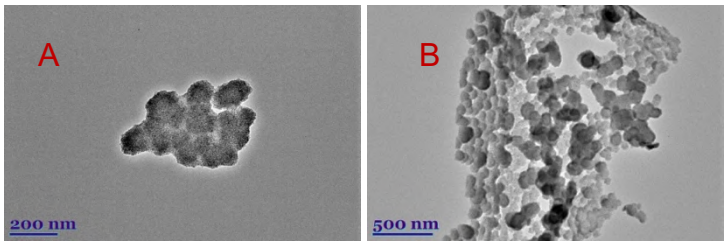


Fig. 1. A and B TEM images of $CoFe_2O_4$ nanoparticles.

In the second stage of the synthesis $HAuCl_4$ was added to the cooled ferrite reaction mixture and heated in a microwave reactor at 120 ºC. The obtained Au nanoparticles ~ 50 nm were coated with a thin 2-3 nm shell of $CoFe_2O_4$ Fig. 2. These nanoparticles show plasmonic and ferromagnetic properties. Enhancement of SERS was tested with the mercaptohexylpyridinium chloride (MHP) Fig. 3.

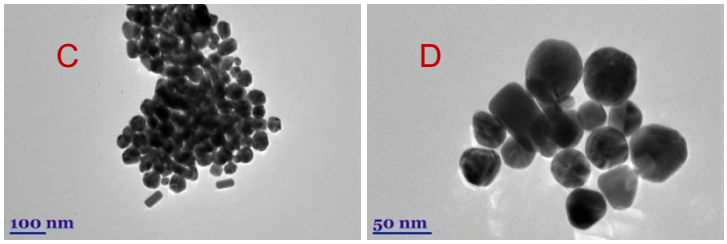


Fig. 2. C and D TEM images of $Au/CoFe_2O_4$ nanoparticles.

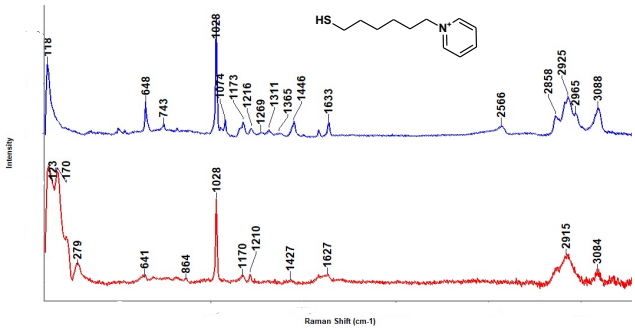


Fig. 3. SERS enhancement. Blue line- Raman spectra of MHP crystals. Red line- SERS spectra of $Au/CoFe_2O_4$ nanoparticles coated with a monolayer of MHP.

[1] César de Julián Fernández and Francesco Pineider. Magneto-Plasmonic Nanoparticles. D. Peddis et al. (eds.), New Trends in Nanoparticle Magnetism, Springer Series in Materials Science 308. (2021).
[2] Wei Wang, Zui Ding, Xiruo Zhao, Sizhu Wu, Feng Li, Ming Yue, and J. Ping Liu. Microstructure and magnetic properties of MFe2O4 (M = Co, Ni, and Mn) ferrite nanocrystals prepared using colloid mill and hydrothermal method. Journal of Applied Physics 117, 17A328 (2015).

GOLD NANOPARTICLES FOR SENSITIVE HEPARIN DETECTION BY OPTICAL AND ACOUSTIC SIGNAL REGISTRATION METHODS

Ernesta Lubinaite[1]*, Vincentas Maciulis[1], Ieva Plikusiene[1], Kristina Sobol[1], Almira Ramanaviciene[1]

NanoTechnas – Center of Nanotechnology and Materials Science, Institute of Chemistry, Faculty of Chemistry and Geosciences, Naugarduko str. 24, Vilnius, Lithuania
ernesta.lubinaite@chgf.stud.vu.lt

Heparin is a highly sulfated linear glycosaminoglycan which is widely used as an anticoagulant in medicine for the formation of blood clots. Excessive levels of heparin in the body can lead to severe circulatory diseases [1]. For this reason, it is very important to monitor the level of this drug in the blood during surgery and its regular use. From the structural point of view, it is a highly sulfated and negatively charged linear polysaccharide [2]. This property can be successfully applied for the development of an analytical systems for sensitive heparin determination [3].

Methods that are currently used for clinical heparin detection are not specific for heparin and there are loads of analytical interferences. These drawbacks led to a need for a new analytical system that is specific for heparin. Some of the techniques that are adapted for detection and analysis of heparins are nuclear magnetic resonance, mass spectrometry, electrophoresis, high-performance liquid chromatography and size exclusion chromatography. In addition to these methods, some of the new techniques can be adapted for heparin detection. The examples of those include fluorescent probes and gold nanomaterial labelled sensors. In this work, we presented two new methods for negatively charged heparin determination in the presence of negatively charged colloidal gold nanoparticle (GNP) solution [4].

First analytical system relies on the aggregation of negatively charged colloidal GNP solution in the presence of positively charged polymer poly-L-lysine (PLL). Stable GNP solution is red color and the local surface plasmon resonance (LSPR) maximum is registered at a wavelength of 520 nm. Visible color changing to blue color and LSPR peak shifting to a wavelength of 650 nm can be observed after the PLL induced aggregation of GNP solution. Heparin as a negative molecule interacts with positive PLL and stabilizes the GNP solution.

Second analytical system for the heparin detection relies on the application of Quartz Crystal Microbalance with Dissipation (QCM-D) where real-time interactions of heparin or GNP with premodified sensor disk were registered. The first part of the layer consists of primarily immobilized positively charged PLL. After that, a mixture of heparin and GNP solution is added. Since heparin more likely interacts with PLL than GNP, the layer itself can be easily characterized by the difference in heparin concentration.

[1] L. Tian, H. Zhao, Z. Zhao, J. Zhai, and Z. Zhang, "A facile voltammetric method for detection of heparin in plasma based on the polyethylenimine modified electrode," *Anal. Methods*, vol. 11, no. 10, pp. 1324–1330, 2019, doi: 10.1039/c8ay02722f.

[2] M. A. Smythe, J. Priziola, P. P. Dobesh, D. Wirth, A. Cuker, and A. K. Wittkowsky, "Guidance for the practical management of the heparin anticoagulants in the treatment of venous thromboembolism," *J. Thromb. Thrombolysis*, vol. 41, no. 1, pp. 165–186, 2016, doi: 10.1007/s11239-015-1315-2.

[3] X. Ma, X. Kou, Y. Xu, D. Yang, and P. Miao, "Colorimetric sensing strategy for heparin assay based on PDDA-induced aggregation of gold nanoparticles," *Nanoscale Adv.*, vol. 1, no. 2, pp. 486–489, 2019, doi: 10.1039/c8na00162f.

[4] B. Li, H. Zhao, and M. Yu, "Techniques for Detection of Clinical Used Heparins," *Int. J. Anal. Chem.*, vol. 2021, 2021, doi: 10.1155/2021/5543460.

P2-25

DID NOT PARTICIPATE

.

P2-26

DID NOT PARTICIPATE

.

THE ROLE OF TREE FOLIAGE ON BLACK CARBON DEPOSITION AN URBAN BACKGROUND IN VILNIUS

Daria Pashneva[1], Steigvilė Byčenkienė[1], Ieva Uogintė[1], Julija Pauraitė[1], Agnė Minderytė[1], Lina Davulienė[1], Kristina Plauškaitė[1], Martynas Skapas[1], Vadimas Dudoitis[1], Jelena Andriejauskiene[1], Vidmantas Ulevicius[1], Dalia Jasinevičienė[1], Valda Araminienė[2], Eugenija Farida Dzenajavičienė[3], Pierre Sicard[4], Valda Gudynaitė-Franckevičienė[2], Iveta Varnagirytė-Kabašinskienė[2], Nerijus Pedišius[3], Egidijus Lemanas[3], Tomas Vonžodas[3]

[1] Department of Environmental Research, SRI Center for Physical Sciences and Technology (FTMC), Lithuania;
[2] Lithuanian Research Centre for Agriculture and Forestry, Lithuania;
[3]Lithuanian Energy Institute, Lithuania;
[4]ARGANS, France.
daria.pashneva@ftmc.lt

In recent years green strategies trend may lead to a redistribution of BC sources, as the contribution of BC from wood burning would increase [1]. Urban trees can offer great potential to remove PM and other air pollutants, especially nearby sources, by absorbing gaseous air pollutants through their stomata and trapping PM on the leaf surface [2][3]. Thus, reducing BC emissions could provide climatic and human health benefits in the coming decades[4].The purpose of the study is to consider the role of urban trees on the removal of BC by common spruce and birch, as well as on the formation of BC, mass concentration and distribution of sources.

Measurements were performed during July-October 2020at an urban background station in Vilnius (capital of Lithuania).The aethalometer (A Magee Scientific Company Aethalometer model AE31) provided continuous real-time measurements of BC mass concentration.Transmission electron microscopy (Tecnai G2 F20 X-TWIN, resolution 0.25-0.102 nm) in combination with energy scattering X-ray spectroscopy (EDX) was used to characterize and obtain detailed information on the morphology, size, and elemental composition of individual aerosol particles deposited on leaf of silver birch (Betula pendula Roth) and needle of Scots pine (Pinus sylvestris L.). BC aerosol particles were found in all samples of leaves and needles as a result of the deposition .The largest agglomerate of the detected BC particles had a length of 288.5 nm and a width of 220.4nm. The diameter of primary particles ranged from 24.2to 30.0 nm on leaves of silver birch, and from 32.45 to 44.13 nm on spruce needles (Fig.1). Larger agglomerates were found on the needles of conifers than on deciduous trees, as they form a thicker epicuticular waxy layer and accumulate BC more efficiently.This study showed a significant contribution of transport (54%) and combustion of firewood and agrobiomass to BC emissions during the warm season in the urban background zone from June to October 2020.

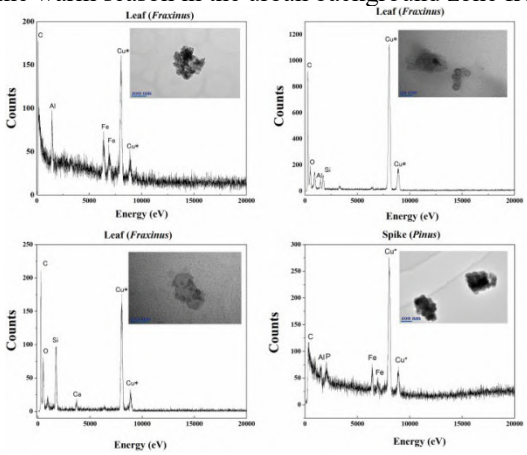


Fig. 1. TEM images and EDX spectra of black carbon containing particles found on leaves and needles.

This work was carried out in the framework of the project "Investigation of aerosol black carbon emissions from biomass incineration units and deposition on tree foliage" (RTO Lithuania).

[1] S. Saarikoski, J. V Niemi, M. Aurela, L. Pirjola, and A. Kousa, “Sources of black carbon at residential and traffic environments,” no. April, pp. 1–27, 2021.
[2] J. Muvuna *et al.*, “Information Integration in a Smart City System — A Case Study on Air Pollution Removal by Green Infrastructure through a Vehicle Smart Routing System.”
[3] Y. Barwise, “Designing vegetation barriers for urban air pollution abatement : a practical review for appropriate plant species selection,” *npj Clim. Atmos. Sci.*, pp. 1–19, 2014, doi: 10.1038/s41612-020-0115-3.
[4] A. Helin *et al.*, “Characteristics and source apportionment of black carbon in the Helsinki metropolitan area, Finland,” *Atmos. Environ.*, vol. 190, no. January, pp. 87–98, 2018, doi: 10.1016/j.atmosenv.2018.07.022.

ATR IR SPECTROSCOPY APPLICATION FOR THE IDENTIFICATION OF PATHOGENIC BACTERIA AND FUNGI

Gerda Anužienė[1], Rimantė Bandzevičiūtė[1], Eglė Lastauskienė[2], Justinas Čeponkus[1]

[1]Chemical Physics Institute, Faculty of Physics, Vilnius University, Saulėtekio Av. 3, LT-10257 Vilnius, Lithuania
[2]Institute of Biosciences, Life Sciences Center, Vilnius University, Saulėtekio Av. 7, LT-10257 Vilnius, Lithuania
gerda.anuziene@ff.stud.vu.lt

Pathogenic microorganisms can cause infectious diseases and complication of these diseases endangered humans' life. For a long time, it was believed that fungi do not affect infections which are caused by bacteria, but with the development of diagnostic equipment and more research, it has been observed that interaction between bacteria and fungi may worsen patient's condition. Antibiotics are used for the treatment of bacterial infections and antifungals for the yeast caused infections. It is known that bacteria can develop antibiotic resistance while fungi are not sensitive for the treatment by antibiotics and vice versa. In mixed infections, only one domain of pathogenic microorganism (eukaryote or procaryote) can be killed while allowing another to spread even faster. Methods which are used nowadays for pathogenic microorganisms' identification requires sample preparation and/or cultivation and takes a long time until the identification results are obtained, especially in the case of eukaryotic microorganisms. ATR IR spectroscopy is a non-destructive method and often does not require sample preparation. The collection of the ATR IR absorption spectrum takes several minutes therefore the identification of pathogenic microorganisms can be accomplished faster [1-3].

In this work, the method of an attenuated total reflection of infrared radiation (ATR IR) spectroscopy was applied for the analysis. ATR IR absorption spectra of 150 samples of different bacteria (57 samples, 8 different species) and fungi (93 samples, 3 different species) were analyzed.

The main differences between bacteria and fungi ATR IR absorption spectra were observed in the 1800 cm^{-1} – 750 cm^{-1} spectral region which is associated with carbohydrates in bacterial and fungal cells. Also, a change in the contour of the spectra is observed in the 1360 cm^{-1} – 1280 cm^{-1} spectral region. Fig. 1 shows ATR IR absorption spectra of different species of bacteria and fungi.

In this work hierarchical cluster analysis (HCA) and principal component analysis (PCA) were applied to determine how accurately bacteria and fungi ATR IR absorption spectra can be identified. HCA showed that the ATR IR absorption spectra of bacteria can be identified with 89,9 % accuracy and the ATR IR absorption spectra of fungi can be identified with 100 % accuracy. Six *Arthrobacter* sp. ATR IR spectra were assigned to the incorrect group. PCA showed that the ATR IR absorption spectra of bacteria can be identified with 91,2 % accuracy and the ATR IR absorption spectra of fungi can be identified with 100 % accuracy. PCA diagram showed that five *Arthrobacter* sp. ATR IR spectra were assigned to the incorrect group.

All in all, ATR IR spectroscopy is a suitable method for the identification of different pathogenic microorganisms. In order to apply the method for clinical diagnostics it is important to carry out studies with larger sample number and to continue to use both methods of statistical analysis.

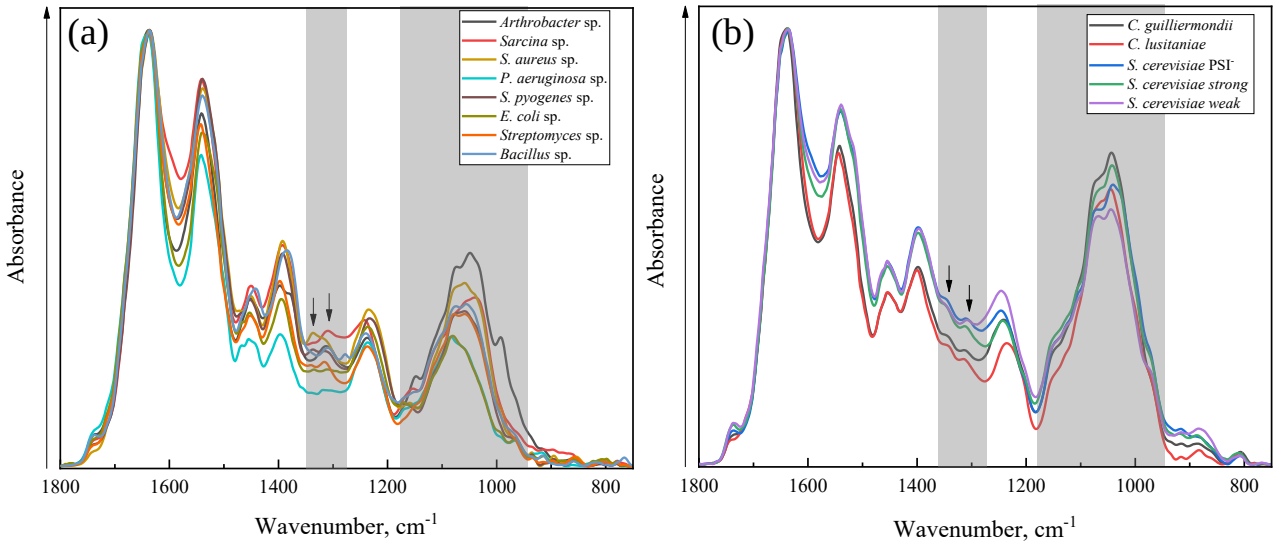


Fig. 1. ATR IR absorption spectra of different (a) bacteria and (b) fungi species

[1] M. Pigłowski, Int. J. Environ. Res. Public Health **16**, 477 (2019)
[2] M. Harz, P. Rösch, J. Popp, Cytometry **75A**, 104-113 (2009)
[3] B. Buszewski, A. Rogowska, P. Pomastowski, M. Złoch, V. Railean-Plugaru, J. AOAC Int **100**, 1607-1623 (2017)

ATR-SEIRAS PROBES DIELECTRIC ENVIRONMENT OF THE SUBMEMBRANE LAYER OF THE TETHERED BILAYER LIPID MEMBRANES (tBLMs)

Vaidas Pudzaitis[1], Martynas Talaikis[2] and Gediminas Niaura[1]

[1]Department of Organic chemistry, Center for Physical Sciences and Technology, Lithuania
[2] Institute of Biochemistry, Life Sciences Center, Vilnius University
vaidas.pudzaitis@ftmc.lt

tBLMs that mimic biological cell membranes have become broadly used in studying lipid-protein interactions and the construction of biosensors for toxin detection. It is quite often used in synergy with vibrational spectroscopy techniques such as surface-enhanced Raman or infrared absorption spectroscopy *in-situ* (SERS and SEIRAS accordingly). Such systems can generate copious amounts of data providing information and complexity at the very same time. The incorporation of molecular markers can help to identify various physical and structural properties of the different domains in the system.

In this work, we used the **MHP** (N-(6-mercapto) hexylpyridinium, [1]), lipid-like molecule **WC14** (20-tetradecyloxy-3,6,9,12,15,18,22-heptaoxahexatricontane-1-thiol), and **βME-D4** (deuterated 2-mercaptoethanol) to form tBLM anchoring self-assembled monolayer (SAM). The MHP, spectral marker molecule, allowed us to probe the dielectric environment of the submembrane layer of tBLM. SAM formed on ~25 nm SEIRAS potentiometrically activated gold layer on silicon ATR prism [2] was monitored by FTIR spectrometer (Bruker, Germany). Spectral marker at 3062 cm^{-1} assigned to stretching =C–H vibrations of pyridinium ring monitored within a series of different ratio D_2O/Isopropanol solutions from 0 to 100% (Fig. 1, A). Water addition to the solution has an impact showing absorption band shift by δ = 6.4 cm^{-1} towards higher wavenumbers. A similar experiment of MHP in solution with double wavenumber shift (13.3 cm^{-1}) (Fig. 1, B) indicates lowered dielectric constant of the environment in the SAM layer. Which is explained by a less hydrophilic environment as MHP is surrounded by WC14 and βME-D4. Additionally, we determined an unchanged peak position value after the formation of tBLM membrane on SAM. It seems logical, that the additional membrane layer does not change the environment of MHP because lipids are located further from the surface.

Overall, MHP as a marker can be used to indicate the dielectric constant of the local environment. However, changes in the pyridinium ring stretching C–H vibrations become rather small after 20–30% D_2O concentration has been reached. Additionally, the potential of MHP as a hydrophobicity marker of the gold-SAM interface has been revealed, which needs additional study.

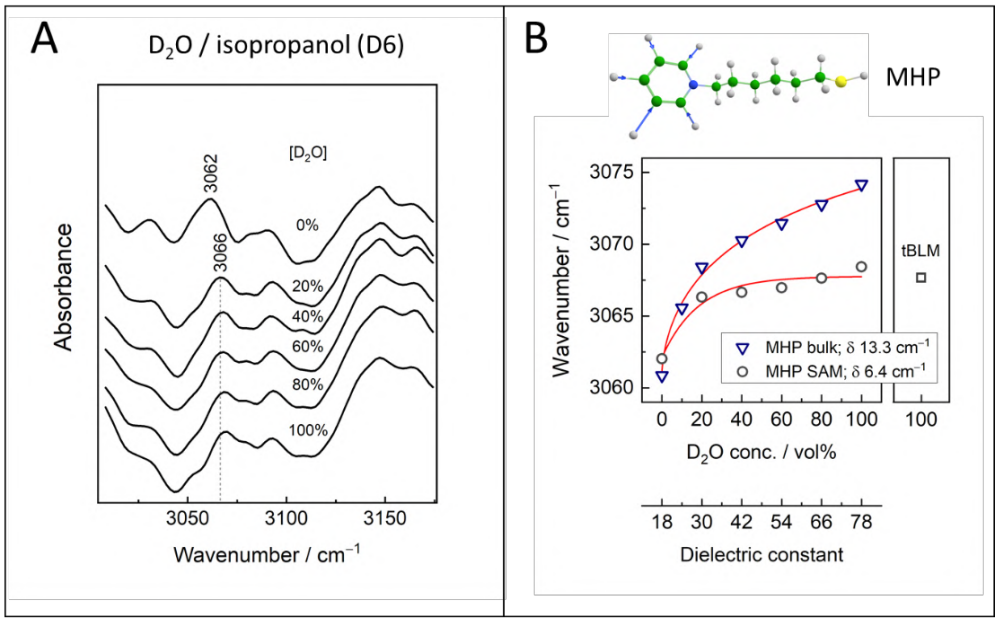


Fig. 1. ATR-SEIRAS spectra of gold-adsorbed SAM measured in different D_2O/Isopropanol solutions. The reference was 100% isopropanol without SAM. The 3060 cm^{-1} corresponds to stretching C–H vibrations of MHP (A). The dependency of bands frequency on D_2O concentration in the SAM environment (circles), tBLM (square), and MHP in solution (triangles) (B).

[1] I. Matulaitiene, Z. Kuodis, A. Matijoška et al., *SERS of the Positive Charge Bearing Pyridinium Ring Terminated Self-Assembled Monolayers: Structure and Bonding Spectral Markers*, J. Phys. Chem. C 2015, **119**, 47, 26481–26492

[2] J. M. Delgado, J. M. Orts, J. M. Pe´rez et al., *Sputtered thin-film gold electrodes for in situ ATR-SEIRAS and SERS studies*, The Journal of Physical Chemistry C 2015 **119** (47), 26481-26492

CONFORMATIONAL STUDY OF 1-METHYL-GERMACYCLOHEXANE BY MEANS OF VIBRATIONAL SPECTROSCOPY

Jogilė Mačytė[1], Rasa Platakyte[1], Justinas Čeponkus[1], Gamil A.Guirgis[2], Valdas Šablinskas[1]

[1] Institute of Chemical Physics, Vilnius University, Saulėtekio av. 3, 10257 Vilnius, Lithuania
[2] Department of Chemistry and Biochemistry, College of Charleston, Charleston, SC 29424, USA
jogile.macyte@ff.stud.vu.lt

Organosilicon and organogermanium compounds are rather attractive in the field of surface science. Cyclic hydrocarbon films have good surface adhesion properties which are mostly related to a π electron orbitals[1]. Substituting one carbon atom in the ring with a silicon or germanium enhances adhesion since it acts as hydrolytically sensitive center that can react with inorganic substrates such as glass to form stable covalent bonds[2]. 1-methyl-germacyclohexane is a newly synthesized cyclic organic compound with unknown structural parameters and conformational diversity.

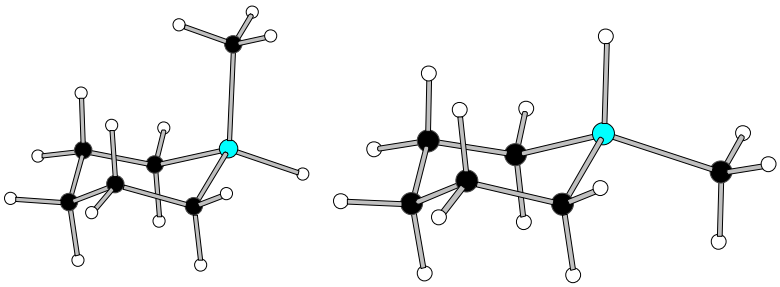


Fig. 1. Theoretically predicted axial and equatorial conformers of 1-methyl-germacyclohexane

Various methods of vibrational spectroscopy were employed to analyze the properties of this molecule. Infrared and Raman spectra were recorded for the liquid samples. Additionally, IR absorption spectra were registered in gas phase. DFT calculations were performed utilizing B3LYP functional and augmented Dunning correlation-consistent valence double zeta basis set. The calculations reveal that 1-methyl-germacyclohexane has two stable conformations out of which the axial conformation has the lowest energy.

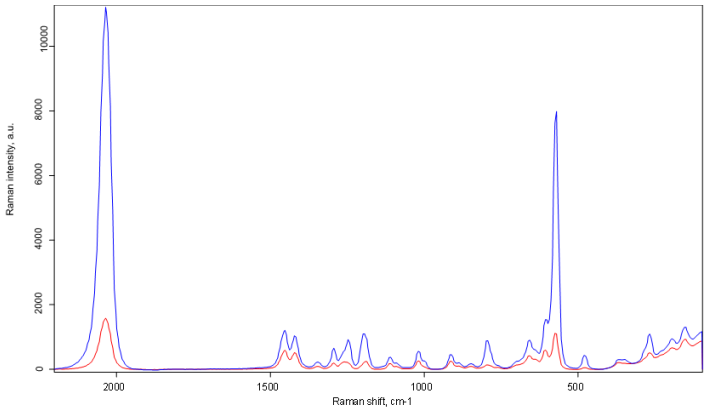


Fig. 2. Raman spectrum of 1-methyl-germacyclohexane in vertical (red) and horizontal (blue) polarization.

According to the calculations, both conformers - axial and equatorial (see fig.1) differ in potential energy just by $\Delta E = 1.4$ kJ/mol. Calculations show that most of the vibrational spectral bands overlap. Experimental Raman spectra (see fig. 2) of horizontal and vertical polarizations confirmed our assignment of non-overlapped Raman bands of both conformers. The band of equatorial conformer at 693 cm^{-1} is assigned as out of plane C-Ge-C deformation, while the band of axial conformer at 632 cm^{-1} is assigned to Ge-C stretching vibration. Experiments will be continued using matrix isolation FTIR spectroscopy, which should result in narrow spectral bands with better separation of the bands arising from both conformers.

[1] H. Butt, K. Graf, M. Kappl, *Physics and Chemistry of Interfaces* (Wiley, 2003)
[2] J. Ceponkus, V. Sablinskas, V. Aleksa, M. Pucetaite, R. Platakyte, C.W. Reed, C.Cotter, G. Guirgis, *Vibrational Spectroscopy* (81, 136-143. 2015)

COMPARISON OF METHODS FOR DETERMINATION OF OLEIC ACID IN SUNFLOWER SEEDS

Inna Hutsalo[1], Svitlana Litvynchuk[1], Antonina Boiko[1], Lyubov Zakidysheva[2]

[1]Department of Physics, National University of Food Technologies,Kyiv,Ukraine
[2]Engineering and Education Faculty of the National Pedagogical Drahomanov University, Kyiv,Ukraine
hutsaloiv@ukr.net

Currently, the importance of maintaining healthy human health is the consumption of high quality healthy foods that normalize nutritional status through the intake of essential proteins, fats and carbohydrates. One of the main elements in the structure of the population's diet is vegetable oils, and the most important oil crop is undoubtedly sunflower. And for Ukraine, which is one of the largest producers of sunflower seeds, sunflower oil is traditional.

There are many varieties and hybrids of sunflower seeds in the world with a high mass fraction of oleic acid. In terms of fatty acid composition, high-oleic sunflower oil is close to olive oil, and in price it is much cheaper than the latter. In addition, this oil has a number of technological properties, which, favorably, distinguishes it from traditional sunflower oil.

Oleic acid is one of the main fatty acids in sunflower seeds. The mass fraction of oleic acid in sunflower seed oil of different varieties and hybrids ranges from 10-30% (traditional varieties) to 80-92% (high oleic hybrid varieties). The register of plant varieties of Ukraine already includes about 300 names of sunflower, and about 58 hybrids are marked as high oleic. The high mass fraction of oleic acid in the oil significantly improves its consumer properties.

The mass fraction of oleic acid in sunflower seed oil is due to the genetic characteristics of plants and growing conditions. Production of high-quality oil is possible on the basis of strict compliance with technical and technological regulations, recipes, sanitary and hygienic norms and rules and the implementation of multi-parameter monitoring of quality indicators of raw materials and finished products.

Among producers and suppliers, the issue of controlling the content of mass fraction of oleic acid in sunflower oil is relevant. Such control is expedient at all stages of its production: quality control of seed material, harvesting, storage and processing at the enterprises.

Until recently, two methods were known for determining the mass fraction of oleic acid in sunflower seed oil: the method of gas-liquid chromatography (GC) and the refractometric method. But the authors of this work at the National University of Food Technology also developed another method. This is an express method based on the measurement of infrared spectra of diffuse reflection of sunflower seeds in the near region (NIR).

All these methods differ in the range of determination of oleic acid in sunflower seeds. It should be noted that the maximum range for determining the mass fraction of oleic acid in sunflower seed oil is provided by the chromatographic method, but it is quite expensive. The refractometric measurement range (58-84%) is explained by the fact that it was developed for enterprises engaged in the selection of high-oleic sunflower seeds (and during its implementation this range was sufficient) [1].

It should be noted that these two methods use oil extracted and filtered from the analyzed seed sample to determine the mass fraction of oleic acid, while the method developed by the authors is non-destructive, which is especially important for breeders. In addition, the GC method requires additional sample preparation using toxic chemical reagents (methyl alcohol), consumables and highly qualified staff [2].

When performing chromatographic analyzes, the ambient temperature (sample) may be in the range from 15 to 30°C, while when using the refractometric method, the temperature significantly affects the results of the analysis and should be (20.0 ± 0.2)°C.

The express method based on the method of NIR spectroscopy was developed as an estimate to reduce the number of analyzes performed by the arbitration method, due to its complexity and duration [3]. That is, the application of the developed method for determining the mass fraction of oleic acid in sunflower seed oil based on the method of NIR spectroscopy allows to reduce the number of analyzes and, accordingly, to avoid additional time.

Therefore, the developed method for determining the mass fraction of oleic acid in sunflower seed oil has the following advantages: non-destructive (does not require extraction of oil from seeds), does not require special sample preparation, eliminates the use of toxic chemicals, analysis time is 2 minutes, provides high sample visibility, and the simplicity and automation of the analysis process reduces the qualification requirements of laboratory personnel. In addition, it should be noted that the determination of the mass fraction of oleic acid in sunflower seed oil can be carried out simultaneously with the determination of oil content and moisture.

[1] Высокоолеиновый подсолнечник и современные методы контроля содержания олеиновой кислоты / О. С. Агафонов [и др.]//Минск: Пищевая промышленность: наука и технология. №4(22).- 2015.- С. 91-94.
[2] Lee M. M.; Lin S. S. (2000). Dietary fat and breast cancer. Annual Review of Nutrition, 221-248. doi:10.1146/annurev.nutr.20.1.221.
[3] Roggo, Y., et al. (2007), A review of near infrared spectroscopy and chemometric sinpharmaceutical technologies, Journal of pharmaceutical and biomedical analysis, 44(3),pp. 683-700.

DIELECTRIC SPECTROSCOPY OF $x(Bi(Zn_{2/3}Nb_{1/3})O_3)$-$(1-x)BaTiO_3$ CERAMICS

Eidvidas Šatkauskas[1], Sergejus Balčiūnas[1], Jūras Banys[1]

[1] Faculty of Physics, Vilnius University, Lithuania
eidvidas.satkauskas@ff.stud.vu.lt

Relaxor ferroelectrics can be used in diverse applications, for example, energy storage [1]. Relaxor additives are added to ferroelectric solid solutions to alter its characteristics. However, commonly used lead titanate is allowed to be utilized only in limited applications due to health concerns raised by the European Parliament and the Council on RoHS [2]. Because of these legislative enforcements, demand for lead-free analogues appeared and they were heavily studied in previous decade. One of these materials, $x(Bi(Zn_{2/3}Nb_{1/3})O_3)$-$(1-x)BaTiO_3$ has received interest as a high-capacity relaxor dielectric material. These ceramics have different composition regimes depending on x concentration, such as: $BaTiO_3$-like ferroelectric ($0 < x < 3.0\%$), relaxor ferroelectric ($4.0\% < x < 5.0\%$), low loss relaxor dielectric ($x > 10.0\%$) [3].

In the present work the dielectric properties of four $x(Bi(Zn_{2/3}Nb_{1/3})O_3)$-$(1-x)BaTiO_3$ ceramics in 129Hz-1GHz frequency range and 150-500K temperature range are analyzed. Conductive silver paste electrodes were applied on and gradually annealed up to 773K. The measurements of dielectric permittivity were performed during cooling cycle at close to 1K/min temperature decline rate. Fig. 1 shows frequency and temperature dependency of real and complex parts of dielectric permittivity. The peak of real part of dielectric permittivity (at around $T \approx 361$K) corresponds to the temperature where polar clusters become so large that they stop following the applied field [4]. Whereas, the peak of the complex part at temperature $T \approx 356$K indicates that dielectric dispersion reached its maximum.

Fig. 1. shows discussed dependency in 129Hz-1MHz frequency range. However, presented results will be up to 1GHz frequency.

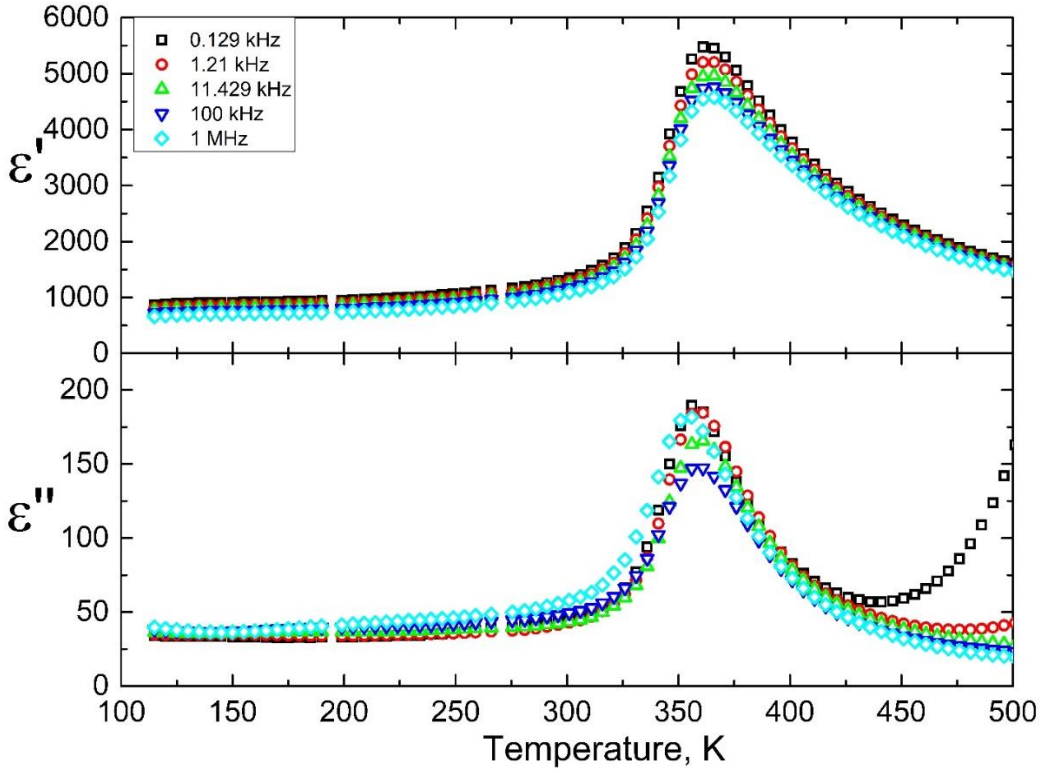


Fig. 1. Frequency and temperature dependency of real and complex parts of dielectric permittivity of $0.02(Bi(Zn_{2/3}Nb_{1/3})O_3)$-$0.98BaTiO_3$ ceramics.

[1] Brown, E., Ma, C., Acharya, J., Ma, B., Wu, J., Li, J., *Controlling dielectric and Relaxor-ferroelectric properties for energy storage by tuning PB0.92la0.08Zr0.52Ti0.48O3 film thickness* (ACS Applied Materials and Interfaces, United States, 2014).

[2] EU-Directive 2011/65/EU: *Restriction of the use of certain hazardous substances in electrical and electronic equipment* (Official Journal of the European Union L174 p. 88–110, 2011).

[3] Marshall, J., Walker, D., Thomas, P., *Bismuth zinc niobate: BZN-Bt, a new lead-free BATIO3-based ferroelectric relaxor?* (Journal of Advanced Dielectrics, United Kindom, 2020).

[4] Lu, Z. G., Calvarin, G., *Frequency dependence of the complex dielectric permittivity of Ferroelectric relaxors* (Physical Review B, France, 1995).

A COMPARISON OF THE SPECTRAL PROPERTIES IN THE UV REGION OF ARSENIC HIGH FREQUENCY ELECTRODELESS LAMPS AND HOLLOW CATHODE LAMPS

Kristiāna Rancāne[1], Anda Ābola[1]

[1]Institute of Atomic Physics and Spectroscopy, University of Latvia
kristianarancane@lu.lv

To ensure precise measurements and low detection limits, the light sources used for the atomic absorption spectroscopy must meet certain criteria – the spectral lines used in the analysis must be narrow, stable in time and have no self-absorption. It is also preferable for the light sources themselves to have long lifetimes.

In this work we compare some spectral properties of high-frequency electrodeless lamps (HFEDL) and hollow cathode lamps (HCL) with arsenic filling. We measured relative and absolute intensities of several spectral lines in the UV region as a function of power, and afterwards compared the radiation intensities for both types of the light sources in the relative and absolute units. The registration of the spectra was done by the spectrometer Jobin Yvon SPEX 1000M. An identification of spectra was performed, along with the observation of the behavior of the spectral lines, when the generator voltage or the current was changed.

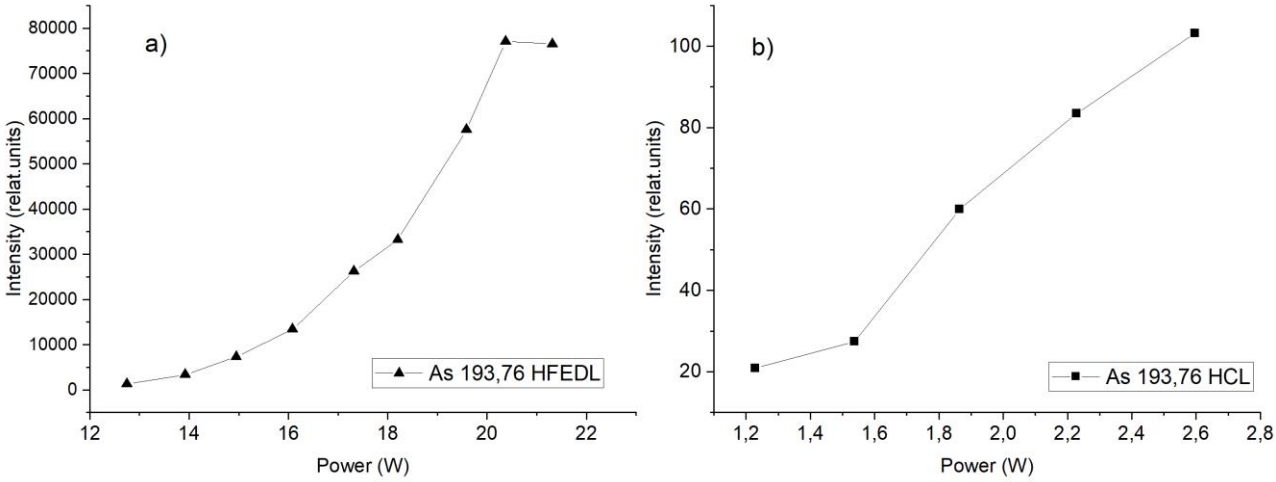


Fig. 1. The dependance of the relative intensity of As 193,76 nm spectral line on the generator operating power in a) HFEDL and b) HCL.

In Fig. 1 an example of the relative intensity values depending on the operating power for the As 193,76 nm atomic spectral line in both of the light sources is shown. Graph a) shows that the relative intensity of the chosen spectral line in the high-frequency electrodeless lamp increases exponentially with the increasing power. For the HCL (graph b), the increase of the intensity is linear.

The operating power value range of the HFEDLs and the HCLs is influenced by the physical properties of the light sources, and is limited on both ends by the lamp and excitation generator properties. In our case the difference is about 10 times – as the HFEDLs are operated at approximately 10 times higher power values than the HCLs. While we are not able to compare the spectral line intensity at the same power values, the results clearly indicate that for the respective power regions the relative intensities of the arsenic spectral lines are significantly higher for the HFEDLs. Similar results are expected when comparing the absolute intensities.

Acknowledgements
Authors acknowledge the Latvian Council of Science grant No. lzp-2020/1-0005.

INFRARED SPECTROSCOPY OF URINARY DEPOSITS

Morta Stadulytė[1], Rimantė Bandzevičiūtė[1], Justinas Čeponkus[1], Marius Snicorius[2], Arūnas Želvys[2], Valdas Šablinskas[1]

[1] Institute of Chemical Physics, Faculty of Physics, Vilnius University, Saulėtekio Av. 3, LT-10257 Vilnius, Lithuania
[2] Institute of Clinical Medicine, Faculty of Medicine, Vilnius University, Santariškių Str. 2, LT-08661, Vilnius, Lithuania
morta.stadulyte@ff.stud.vu.lt

Urolithiasis is a disease of stone formation in urinary tract. Most commonly occurring stones are calcium oxalate stones, other types of stones such as uric acid, struvite, calcium phosphate and cystine are found in urinary tract but less frequently than the calcium oxalate ones.

It is widely accepted that infrared (IR) spectroscopy is well suited for the identification of chemical composition of urinary stones, and some libraries of IR absorption and IR ATR (attenuated total reflection) spectra are available. The urinary sediments also can be analyzed by means of infrared spectroscopy, but this research field is still underdeveloped due to the sampling problems related to extremally small size of the sediments (deposits). The main task of this study is to extend capabilities of the IR spectroscopy to early diagnostics using urine samples.

Infrared spectroscopic study of deposits of patient urine could be a simple and non-invasive way to detect urinary stone formation and determine its composition. This could help in early detection of the stone formation of certain type for patient with suspected stone disease. Knowledge about chemical composition of the stone allows to prescribe specific medicines or diet to prevent further formation of stones. We have performed pilot studies of the set of samples removed from various patients. The set consists of three parts – urine before medical surgery (A), during the surgery (B) and removed urinary stone (C). Urine samples were first centrifuged to get urinary deposits, then deposits were measured using an ATR FTIR spectrometer. IR absorption spectra of the removed urinary stones were also measured.

From 26 patients, in 11 cases sample A only had organic compounds, no characteristic chemical components of the stones were detected. Among the remaining 15 cases, 13 IR spectra of A samples well correlated (86.7 %) with the spectra of the removed stones. Our spectroscopic pilot study leads to conclusion that IR absorption spectra of urine deposits (small crystals) allows us to diagnose urolithiasis and to determine chemical composition of the stones with accuracy up to 86.7 % .

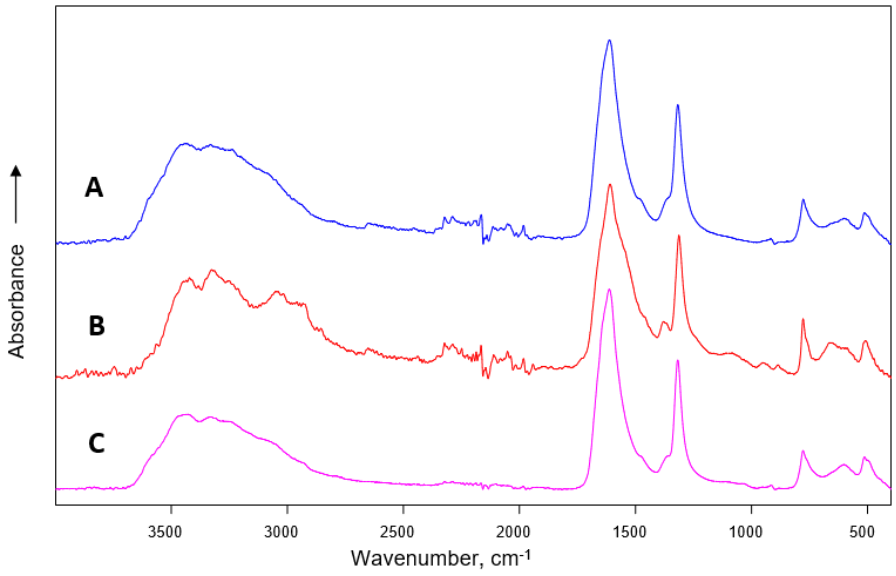


Fig. 1. Patient sample IR absorption spectra of: A – urine deposits of the urine taken before the surgery, B – urine deposits of the urine taken during surgery, C – removed stone. All three samples contain calcium oxalate monohydrate. This is an ideal case, where both urine tests formed stone deposits and they coincide with each other as well as with removed stone.

From 26 patients, 3 samples B had no characteristic chemical components of the stones, only organic compounds were deposited. Among the remaining 23 cases, 22 B samples the IR spectra correlated with removed stones spectra with accuracy of 95.7 %. Such correlation could be helpful since endoscopic surgeries without complete removal of the stones became widely used. In such circumstances measuring the IR spectra of deposits of patient urine could be useful to determine composition of the stones and help patients prevent further formation of the stones by recommending specific diet and medication.

APPLICATION OF FIBER ATR IR SPECTROSCOPY FOR TUMOROUS LIVER TISSUE IDENTIFICATION

Rimantė Bandzevičiūtė[1], Katja Liedel[2], Christian Teske[2], Carina Riediger-Schweipert[2], Justinas Čeponkus[1], Valdas Šablinskas[1], Gerald Steiner[3]

[1] Chemical Physics Institute, Faculty of Physics, Vilnius University, Saulėtekio Av. 3, LT-10257 Vilnius, Lithuania
[2] Department of Visceral, Thoracic and Vascular Surgery, University Hospital Carl Gustav Carus Dresden, Dresden University of Technology, Fetscherstr. 74, 01037 Dresden, Germany
[3]Clinical Sensoring and Monitoring, Faculty of Medicine Carl Gustav Carus, Dresden University of Technology, Fetscherstr. 13, 01307 Dresden, Germany
rimante.bandzeviciute@ff.vu.lt

Liver cancer is one of the most frequently diagnosed malignancies and is one of the leading causes of cancer related deaths worldwide [1]. Malignant neoplasms in liver could form as primary liver tumors or as metastasis from other organs. In both cases, partial hepatectomy is the standard treatment for liver tumors. During the surgery, the tumor and a small amount of the surrounding normal tissue are removed to ensure the complete resection. The success of the treatment depends on the ability to determine the exact border between normal and malignant tissues. All the malignant tissue should be removed in order to prevent the recurrence of the tumor. On the other hand, it is important to preserve as much as possible of normal tissue to maintain functions of the organ. Therefore, a method that could be used directly in the operating room during the surgery and could give a reliable and fast diagnostic result, is needed.

In recent decades, a variety of methods of vibrational spectroscopy are applied for the examination of biological tissues [2]. Using ATR (attenuated total reflection) technique, samples can be examined without any specific preparation. In this study, the fiber ATR IR probe was applied for the spectroscopic measurements that allows to investigate samples *ex vivo* under native conditions what is important during the surgery.

In this study, 25 cases of patients with liver tumors were investigated. Measurements were performed for two types of samples: (I) the tissue immediately after the surgical removal (13 patients) and (II) frozen tissue (12 patients) samples. In both cases normal and tumorous tissues for each patient were investigated. Samples of freshly resected tumorous tissue included primary tumors of liver (hepatocellular carcinoma (HCC), cholangiocarcinoma (CCC)) and metastasis from other organs (colorectal carcinoma (CRC), pancreatic adenocarcinoma (PDAC) and oesophagogastric junctional adenocarcinoma (EGJA)). Samples of frozen tumorous tissue included primary liver tumors (HCC and CCC). The spectra of normal, HCC and CCC liver tissue are represented in fig. 1. Spectral bands of higher intensity located at 1028, 1082 and 1155 cm^{-1} can be attributed to glycogen and they are observed in spectra of normal (1) and HCC (2) liver tissue. Such findings can be explained considering liver function accumulating glycogen in hepatocytes. Intensity of the glycogen spectral bands decreases in the spectrum of the CCC tissue. Whereas CCC tumors form out of epithelial cells of the biliary tract, level of glycogen in CCC tumorous tissue is reduced compared to normal liver spectra. Besides the decreased intensity of the glycogen spectral bands, increased intensity of collagen spectral bands located at 1207, 1283 and 1338 cm^{-1} is clearly visible. The increased intensity of these spectral bands indicates higher amount of collagen in the tissue. Increased level of collagen is related to desmoplastic stroma of the tumor that is rich in connective tissue containing collagen and is characteristic for CCC tumors. In case of HCC tumor, spectral differences between normal and tumorous tissue spectra are not clearly visible. Despite of this fact, after application of hierarchical cluster analysis (HCA), spectra of normal tissue can be classified with 88 % accuracy while spectra of tumorous tissue (including HCC tumors) - with 80 % accuracy.

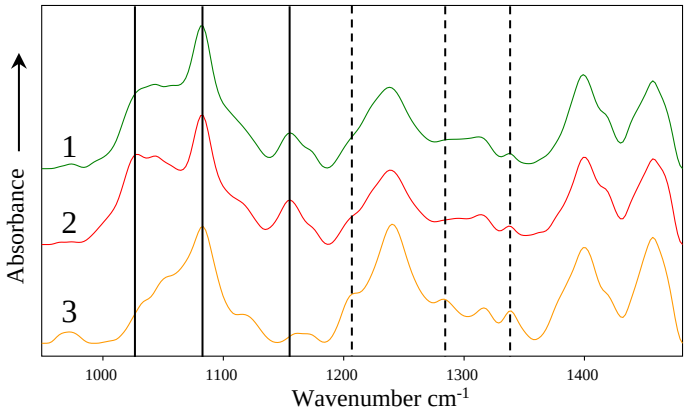


Fig. 1. Fiber ATR IR absorption spectra of freshly resected normal (1) and cancerous (hepatocellular carcinoma (HCC) (2) and cholangiocarcinoma (CCC) (3)) human liver tissue. Solid lines indicate spectral bands assigned to glycogen, dashed lines – to collagen.

[1] H. Sung et al, CA CANCER J CLIN 71 (3) (2021)
[2] G. Bellisola, C. Sorio, Am J Cancer Res 2 (1) (2012).

CYTOTOXICITY OF BORON NITRIDE QUANTUM DOTS ON RED BLOOD CELLS

Rugilė Lukaševičiūtė[1,2], Lena Golubewa[2,3], Tatsiana Kulahava[3], Renata Karpicz[2]

[1] Department of Physics, Vilnius University, Lithuania
[2] Department of Molecular Compounds Physics, Center for Physical Sciences and Technology, Lithuania
[3]Institute for Nuclear Problems, Belarusian State University, Belarus
rugile.lukaseviciute@gmail.com

There is a great interest in the search of the drug nanocarrier that would accelerate the delivery of the anticancer drugs to the target. Quantum dots (QDs) exhibit extraordinary optical and physical properties, and, thus, have proven themselves in various fields of research including bio-imaging, biological labeling, drug delivery, photocatalyst, electrical devices and sensors [1]. One of the most promising types of QDs are boron nitride quantum dots (BNQDs), as they exhibit the unique physical and chemical properties [2], including excellent mechanical strength, high thermal stability, luminescent properties, large surface area, superb oxidation resistance, which provide extremely high drug-loading capacity, making them good candidates for various bio-medical applications. Therefore, significant attention has been paid recently towards the synthesis and fabrication of stable non-toxic BNQDs with controllable and scalable properties.

In this work BNQDs were synthesized via hydrothermal treatment of the mixture of boric acid and ammonia solution at 200°C for 12 h. Erythrocytes were isolated from preserved donor blood by washing three times in PBS buffer using centrifugation at 3500 rpm for 5 minutes.

The purpose of this study was to evaluate the cytotoxicity of boron nitride quantum dots on erythrocytes. Structural parameters of the cells were determined by analysis of scanning electron microscopy (SEM) images. The amount of released hemoglobin and its transformations were analyzed by UV-Vis absorption spectroscopy. The experiments were carried out at two values of the ambient temperature of 4ºC (typical storage conditions for erythrocytes) and 20ºC. BNQDs were added to the erythrocyte suspension to final concentration of 50 μg/ml. After the end of the incubation, the cells were pelleted by centrifugation and resuspended in fresh medium, and the supernatant was collected to determine the release of hemoglobin from the cells.

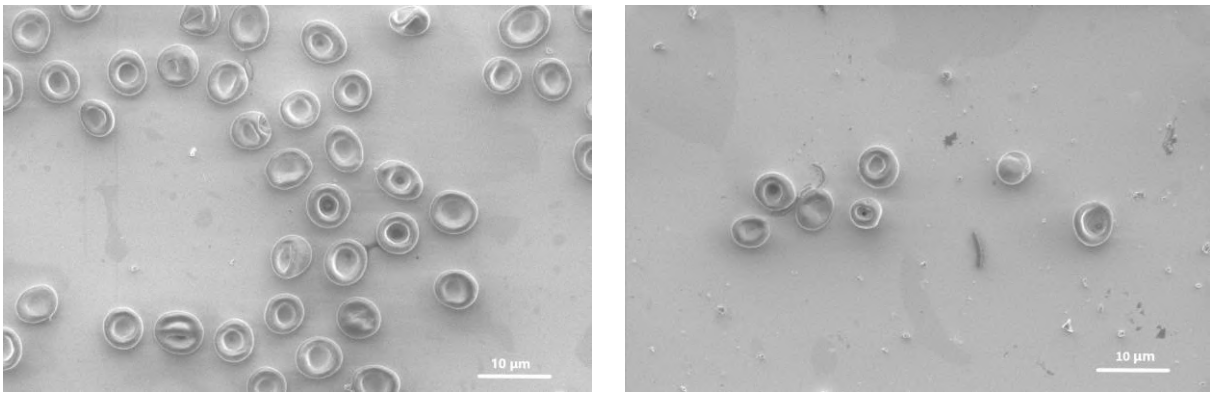


Fig. 1. SEM images of erythrocytes in the control (on the left) and treated with BNQDs samples (on the right) at 4ºC.

BNQDs affected the concentration of erythrocytes by destroying some of the cells. From the absorption spectra of hemoglobin, the absorption intensity slightly increases after incubation with quantum dots. The shape of the peaks remains those of oxidated hemoglobin which indicates that the formation of methemoglobin did not occur.

[1] R. Jerome, Ashok K. Sundramoorthy, Hydrothermal Synthesis of Boron Nitride Quantum Dots/Poly(Luminol) Nanocomposite for Selective Detection of Ascorbic Acid, J. Electrochem. Soc. **166**, B3017 (2019).
[2] C.R. Dean, A.F. Young, I. Meric, C. Lee et al., Boron nitride substrates for high-quality graphene electronics, Nat. Nanotechnol. **5**, 722-726 (2010).

P2-37

DID NOT PARTICIPATE

.

IR SPECTROSCOPY OF FOOD MIXTURES CONTAINING BEE POLLEN

Volodymyr Vyshniak, Svitlana Litvynchuk, Kateryna Boatri

National University of Food Technologies
vladimir_kiev@i.ua

Materials and methods. Infrared spectra [1, 2] of diffuse reflection of dry powdered food products were obtained on the spectrometer "Infrapid-61" in the wavelength range from 1330 to 2370 nm.

Several samples of dry food powdered products were selected as the studied objects: bee pollen in natural form; crushed bee pollen; a mixture of bee pollen and powdered sugar. In the general case, depending on the botanical origin of the bee pollen, the infrared spectra of diffuse reflection will undergo some transformations. Bee pollen, based on its functional properties, can be recommended as a natural food ingredient in healthy food preparation [3].

In Fig. 1 presents a typical spectrum of a mixture of powdered sugar and crushed bee pollen, taken in equal proportions (by volume). It should be noted that this spectrum has absorbed the characteristic features of the spectra of crushed bee pollen and powdered sugar. In the spectrum of the mixture of pollen and powdered sugar there is a peculiarity *c*, which is absent in the spectrum of bee pollen; the spectral maximum *s*, which is characteristic of pollen, also appeared.

The spectral feature *h*, characteristic only for powdered sugar, was also manifested in the spectrum of a mixture of powdered sugar and bee pollen. Peculiarity *r*, present in the spectra of bee pollen and a mixture of powdered sugar with bee pollen, is absent in the spectrum of powdered sugar.

Infrared spectra of all four samples (Fig. 1) differ significantly in the intensity of spectral lines. The most intense spectral maximum corresponds to a wavelength of 1855 nm (feature *j*). Spectral maxima at the given wavelength are placed in the following sequence (from higher to lower intensity): powdered sugar, a mixture of crushed bee pollen and powdered sugar, bee pollen. In this case, the spectral maxima corresponding to the bee pollination are significantly lower in intensity than other studied samples (Fig. 1).

Conclusions. It is established that the change in the dispersion of the powders does not affect the position of the maxima of the spectral lines. Reducing the particle size of food powder samples by mechanical grinding leads to changes in the infrared reflection spectrum: the maxima of the spectral lines become more pronounced and increase their intensity. Infrared reflection spectra of food mixtures reflect in their structure the characteristic features of the spectra of the powder's constituent components. The intensity of the spectral lines of the ingredients correlates with the component's concentration in the food mixture. The spectra of samples of different chemical nature differ significantly in structure, position of the maxima of spectral lines and intensity. The obtained results can be can be practically applied in the creation and implementation of portable devices that can be used for preliminary qualitative analysis of food products.

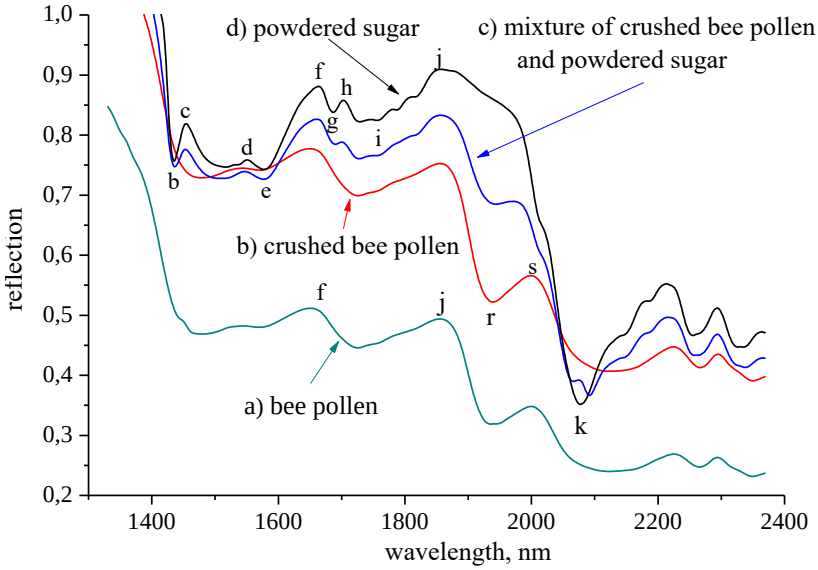


Fig.1. Infrared spectra: a) bee pollen; b) crushed bee pollen; c) mixture of crushed bee pollen and powdered sugar; d) powdered sugar

[1] Magdalena W., Roman S. et. al., Determination of nutritional parameters of bee pollen by Raman and infrared spectroscopy, Talanta,15 May, 2020, 120790. https://doi.org/10.1016/j.talanta.2020.120790

[2] Wang X. 7 - Near-infrared spectroscopy for food quality evaluation. Evaluation Technologies for Food Quality, Woodhead Publishing Series in Food Science, Technology and Nutrition. 2019. 105-118. https://doi.org/10.1016/B978-0-12-814217-2.00007-X

[3] Sevgi K., Merve K., Chapter 7 - Natural bee products and their apitherapeutic applications, Studies in Natural Products Chemistry, 66, 2020, P.175-196. https://doi.org/10.1016/B978-0-12-817907-9.00007-6

EMISSION ENHANCEMENT BY ENERGY TRANSFER IN $YP_{0.5}V_{0.5}O_4$: Bi^{3+}, Eu^{3+}

Marta Wujczyk[1], Sara Targonska[1], Philippe Boutinaud[2], Adam Watras[1] and Rafal J. Wiglusz[1]

[1] Institute of Low Temperature and Structure Research, PAS, Poland
[2] Université Clermont Auvergne, SIGMA Clermont, Institut de Chimie de Clermont-Ferrand, France
m.wujczyk@intibs.pl

Yttrium orthophosphate and orthovanadate are attractive host lattices that found applications as sensors, fluorescent labels, optical devices, solar cells, and laser materials when doped with luminescent activators like trivalent lanthanides [1-4]. The addition of Bi^{3+} in these systems has further been demonstrated as a relevant strategy to sensitize the emission of cations like Eu^{3+}, Sm^{3+} and Dy^{3+} by means of energy transfer [5-7].

YPO_4 and YVO_4 crystallize in the tetragonal zircon system with $I4_1/amd$ space group [8,9]. Therefore, form continuous solid-state solution with the general formula $YV_xP_{1-x}O_4$ ($0 \leq x \leq 1$). The optical behaviour of Eu^{3+} in this solid solution has been investigated in detail by G. Pan et al. [10] and that of Bi^{3+} in E. Cavalli et al. [11]. In the present work, we focus on the luminescence properties of these two dopants incorporated in the $YV_{0.5}P_{0.5}O_4$ obtained via the wet chemistry - co-precipitation method. This specific composition is structurally disordered by the random distribution of the (PO_4) and the 8% larger (VO_4) units within the crystal lattice. Our purpose is to investigate to which extent this structural disorder affects the efficiency of the Bi^{3+}-to-Eu^{3+} energy transfer.

Acknowledgements

The authors would like to acknowledge the National Science Centre in Poland (NCN − Narodowe Centrum Nauki) for the financial support within the Project „Preparation and modulation of spectroscopic properties of $YXZO_4$, where X and Z-P^{5+}, V^{5+}, As^{5+}, doped with 's^2-like'ions and co-doped with rare earth ions" (No. UMO-2019/33/B/ST5/02247).

[1] U. Rambabu, S. Do Han, Broad band down conversion from ultra violet light to near infrared emission in YVO_4:Bi^{3+}, Yb^{3+} as spectral conversion phosphor for c-Si solar cells, Ceram. Int. **39,** 1603–1612, 2013.
[2] D. Wang, S. Tie, X. Wan, White light emitting from YVO_4/Y_2O_3:Eu^{3+},Bi^{3+} composite phosphors for UV light-emitting diodes, Ceram. Int. **41**, 7766–7772, 2015.
[3] Y. Pu, K. Tang, D.-C. Zhu et al., Synthesis and Luminescence Properties of (Y, Gd)(P, V)O_4:Eu^{3+}, Bi^{3+} Red Nano-phosphors with Enhanced Photoluminescence by Bi^{3+}, Gd^{3+} Doping, Nano-Micro Lett. **5**, 117–123, 2013.
[4] Y. Zheng, F. Li, Y. Wang et al., High-stability single-frequency green laser with a wedge Nd:YVO_4 as a polarizing beam splitter, Opt. Commun. **283**, 309–312, 2010.
[5] D. Chen, Y. Yu et al., Color-tunable luminescence for Bi^{3+}/Ln^{3+}: YVO_4 (Ln = Eu, Sm, Dy, Ho) nanophosphors excitable by near-ultraviolet light, Phys. Chem. Chem. Phys. **12**, 7775–7778, 2010.
[6] X.Y. Huang, J.X. Wang et al., Spectral conversion for solar cell efficiency enhancement using YVO_4:Bi^{3+},Ln^{3+} (Ln Dy, Er, Ho, Eu, Sm, and Yb) phosphors, J. Appl. Phys. **109**, 113526, 2011.
[7] E. Cavalli, F. Angiuli, A. Belletti, P. Boutinaud, Luminescence spectroscopy of YVO_4:Ln^{3+}, Bi^{3+} (Ln^{3+} = Eu^{3+}, Sm^{3+}, Dy^{3+}) phosphors, Opt. Mater. **36**,1642-1648, 2014.
[8] W.O. Milligan, D.F. Mullica, Structural Investigations of YPO_4, $ScPO_4$, and $LuPO_4$, Inorganica Chem. Acta. **60**, 39–43, 1982.
[9] B.C. Chakoumakos, M.M. Abraham, L.A. Boatner, Crystal Structure Refinements of Zircon-Type MVO_4 (M = Sc, Y, Ce, Pr, Nd, Tb, Ho, Er, Tm, Yb, Lu), J. Solid State Chem. **109**, 197–202, 1994.
[10] G. Pan, H. Song, Q. Dai, X. Bai, B. Dong, L. Fan, F. Wang, Microstructure and optical properties of Eu^{3+} activated $YV_{1-x}P_xO_4$ phosphors, J. Appl. Phys. **104**, 084910, 2008
[11] E. Cavalli, F. Angiuli, F. Mezzadri, M. Trevisani, M. Bettinelli, P. Boutinaud, M. G. Brik, Tunable luminescence of Bi^{3+}-doped $YP_xV_{1-x}O_4$ ($0 \leq x \leq 1$), J. Phys.: Condens. Matter **26**, 385503, 2014.

MODELING MOLECULAR AGGREGATES USING DIRAC-FRENKEL VARIATIONAL METHOD

Mantas Jakučionis[1], Darius Abramavičius[1]

[1]Institute of Chemical Physics, Vilnius University, Sauletekio Ave. 9-III, LT-10222 Vilnius, Lithuania
mantas.jakucionis@ff.vu.lt

The linear absorption spectrum of H and J molecular aggregates, where both the electronic and vibrational molecular degrees of freedom are considered. It is made up of a collection of molecules (*sites*) coupled via an electrostatic dipole-dipole interaction. Intramolecular vibrational modes are modeled as harmonic oscillators. Molecular aggregate excitation dynamics and spectra can be computed using the wavefunction based time-dependent Dirac-Frenkel variational principle by postulating an Ansatz wavefunction, which ought to be complex enough to represent all the necesary electron-vibrational quantum states of the aggregate.

Vibronic states can be represented using the multi-Davydov D_2 (mD_2) Ansatz [1], given by

$$|\Psi_{\mathrm{mD}_2}(t)\rangle = \sum_m^M \sum_n \alpha_{i,n}(t)\,|n\rangle \otimes |\boldsymbol{\lambda}_m(t)\rangle, \tag{1}$$

where $|n\rangle = |1_n\rangle \bigotimes_{m\neq n} |0_m\rangle$ is an electronic state with amplitude $\alpha_n(t)$, which define a singly excited nth site. Intramolecular vibrational mode state is represented in terms of the multidimensional time-dependent coherent states $|\boldsymbol{\lambda}_m(t)\rangle = \bigotimes_{k,q} |\lambda_{m,kq}(t)\rangle$, where $|\lambda_{m,kq}(t)\rangle$ is an mth coherent state multiple of a qth mode coupled to the kth site. By consider a sufficient number of multiples M, Dirac-Frenkel variational method with mD_2 Ansatz can match accuracy of the *Hierarchical Equations of Motion* and *Multi Configuration Time Dependent Hartree* methods [2].

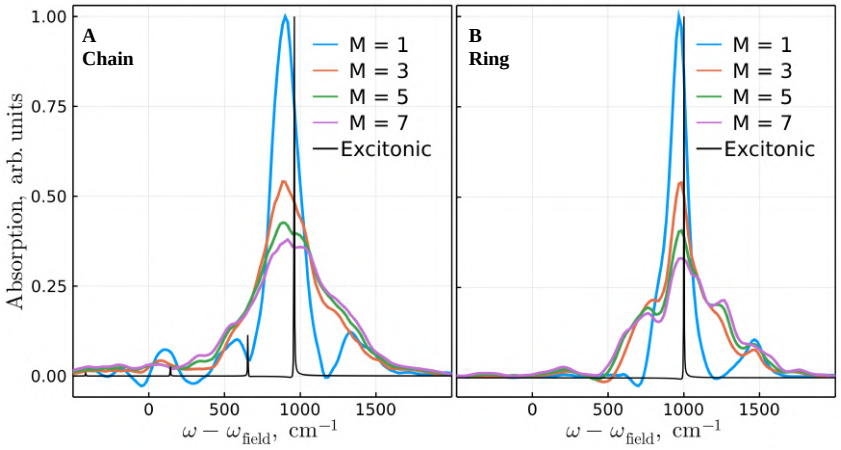


Fig. 1. Absorption spectrum of the model H aggregate in (A) chain and (B) ring configuration, computed with an increasing number of Davydov D_2 multiples M considered. Purely excitonic spectrum is also shown.

By inspecting and comparing absorption spectra of both the ring and chain aggregates over a range of electrostatic nearest neighbor coupling and temperature values, we find the mD_2 Ansatz with multiplicity of $M = 7$ is required to obtain accurate aggregate absorption spectrum, while the regular D_2 Ansatz (Eq. (1) with $M = 1$) is not sufficient. For H aggregates, see Fig. (1), multiplicity is required to obtain absorption lineshape positivity and correct peak intensities. For J aggregates, increasing the number of multiples considered, mostly just redshifts whole absorption spectrum, keeping the overall lineshape qualitatively the same, especially in ring aggregate. Due to vibronic energy level structure of an aggregate, vibrational mode coordinate and momentum variances exhibit out-of-phase oscillatory behaviour and an overall wavepacket broadening, which again is not captured by the non-multiple D_2 Ansatz.

[1] Zhou, Nengji, Chen, Lipeng, Huang, Zhongkai, Sun, Kewei, Tanimura, Yoshitaka, and Zhao, Yang, Fast, Accurate Simulation of Polaron Dynamics and Multidimensional Spectroscopy by Multiple Davydov Trial States, J. Phys. Chem. A **120**, 9 (2016), pp. 1562--1576.

[2] Zhao, Y, Sun, K, Chen, L, Gelin, M. The hierarchy of Davydov's Ansätze and its applications. WIREs Comput Mol Sci. 2021; e1589

DIFFUSE LARGE B-CELL LYMPHOMA (DLBCL) SUBTYPES DISTINGUISHED USING RAMAN IMAGING

Patrycja Dawiec[1], Patrycja Leszczenko[1], Anna M. Nowakowska[1], Paulina Laskowska[2], Aleksandra Borek-Dorosz[1,3], Adriana Adamczyk[1], Justyna Jakubowska[4], Marta Ząbczyńska[4], Agata Pastorczak[4], Kinga Ostrowska[4], Maciej Szydłowski[2], Piotr Mrówka[2,5], Małgorzata Barańska[1,3], Katarzyna Majzner[1,3]

[1] Faculty of Chemistry, Jagiellonian University, Poland
[2]Department of Experimental Hematology, Institute of Hematology and Transfusion Medicine, Poland
[3]Jagiellonian Centre for Experimental Therapeutics (JCET), Jagiellonian University, Poland
[4] Department of Pediatrics, Oncology and Hematology, Medical University of Lodz, Poland;
[5]Department of Biophysics, Physiology and Pathophysiology, Medical University of Warsaw, Poland
patrycja.dawiec@student.uj.edu.pl

Diffuse large B-cell lymphoma (DLBCL) is a genetically heterogeneous group of aggressive malignancies. It is the most common type of non-Hodgkin's lymphoma in adults. These lymphomas exhibit highly diverse clinical features and a complex molecular basis. The precursors of DLBCL cells are antigen-exposed normal B lymphocytes undergoing neoplastic transformation. There are two subtypes of DLBCL, i.e., non-OxPhos, where B-cell receptor signaling is crucial, and OxPhos, characterized by increased oxidative phosphorylation. DLBCL is a rapidly progressing cancer, so the disease must be diagnosed quickly, thus increasing the chances of a complete recovery.

Raman spectroscopy is a promising diagnostic tool that provides unique information on the biochemical composition of cells and allows the differentiation of acute lymphoblastic leukemia (ALL) subtypes in clinical samples [1] and the detection of DLBCL and chronic lymphocytic leukemia (CLL) [2]. The research aims to characterize DLBCL lymphoma cells and their subtypes by identifying biochemical, spectroscopic markers using Raman imaging.

In the study, four DLBCL lymphoma cell lines (OCI-Ly1, OCI-Ly7, Pfeiffer, and Toledo) were used as *in vitro* models of the disease. Normal B lymphocytes, were isolated from the peripheral blood of healthy donors. Cell Raman imaging was performed using a WITec Alpha 300 confocal Raman microscope with a 532 nm laser as an excitation source. The obtained spectra were pre-processed using Project Five 5.1 Plus software. Then, K-means cluster analysis (KMCA) was performed. In the next step, principal component analysis (PCA) was done using the Unscrambler X software. Chemometric analyses revealed subtle differences in the Raman spectra of investigated cells.

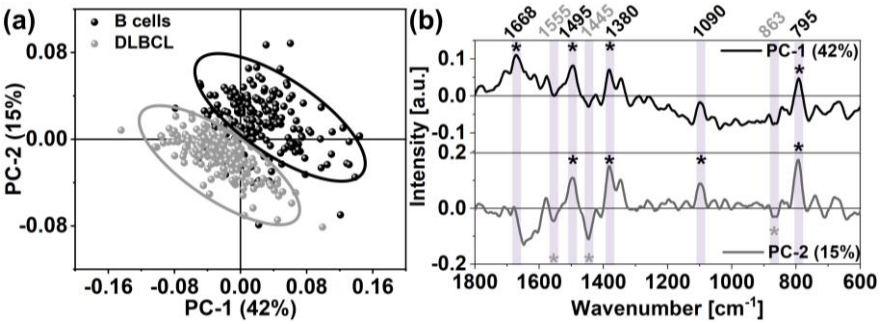


Fig. 1. The score plot (a) and loadings (b) of PCA analysis for B cells and DLBCL lymphoma cells.

PCA analysis performed on the spectra of normal B lymphocytes and tumor cells clearly showed that both groups differ significantly (Fig. 1a). B lymphocytes were mainly characterized by the bands derived from nucleic acids, while cancer cells had a larger share of proteins and lipids (Fig. 1b). Analyzes performed within the studied cell lines also revealed biochemical differences between non-OxPhos and OxPhos DLBCL subtypes. Spectra from cells of non-OxPhos subtype (OCI-Ly1, OCI-Ly7) are separating from the OxPhos subtype (Pfeiffer, Toledo) in PCA score plots. No grouping was observed in the set consisting of OCI-Ly1 and OCI-Ly7 cell lines. In the case of the Pfeiffer cell line, each time, it was characterized by the bands derived from hemeproteins.

Raman spectroscopy has proven to be an efficient tool in order to characterize biochemical composition on lymphoma cells. Moreover, this method allowed to discover the metabolic differences of the studied DLBCL subtypes and identify their characteristic spectroscopic markers.

The „Label-free and rapid optical imaging, detection and sorting of leukemia cells" project is carried out within the Team-Net programme of the Foundation for Polish Science co-financed by the EU.

[1] Leszczenko, P. *et al.* Towards Raman-Based Screening of Acute Lymphoblastic Leukemia-Type B (B-ALL) Subtypes. *Cancers.* **13**, 5483 (2021).
[2] Bai, Y. *et al.* Raman spectroscopy-based biomarker screening by studying the fingerprint characteristics of chronic lymphocytic leukemia and diffuse large B-cell lymphoma. *J. Pharm. Biomed. Anal.* **190**, 113514 (2020).

REGOLITH AS RADIATION PROTECTIVE MATERIAL FOR ASTRONAUTS ON MARS

Dionysios Gakis[1,2]

[1]Department of Physics, University of Patras, Patras, 26504, Greece
[2]Blue Marble Space Institute of Science, Seattle, WA, 98154, USA
dgakis5@gmail.com

Radiation ranks as one of the main issues space agencies have to address when planning and executing a crewed mission, including the proposed human missions to Mars. Because of the many health issues ionizing radiation can cause (e.g. [1]), it is inevitable to seek for ways to sufficiently protect astronauts from the hazardous cosmic rays. One these techniques is the so-called passive shielding, which takes advantage of a particle's energy loss when it travels through the mass of a shielding material. In this work, we specifically examine how effective Martian regolith is against low-energy cosmic radiation. Regolith has been proposed as a shielding material on Mars [2], as it can easily be found there.

For that purpose, we employed the computational program Geant4, a Monte-Carlo numerical model that simulates particle propagation. The Martian environment is represented as a series of absorbing layers, ranging from the top of its atmosphere up until its surface, where a habitat is supposed to be located. An 1-m water slab stands for the body of an astronaut, and before reaching that, radiation passes through a layer of protective material. Astrophysical radiation coming from the Sun and other galactic sources mainly consists of protons. That is why, we test the behavior of regolith as a shielding material against protons. We consider low-energy particles (energies below 1 GeV), at which radiation-matter interactions are mostly electromagnetic. In our simulations, we calculate the energy deposited in the water slab per depth, a quantity known as linear energy transfer (LET).

Based on their shielding abilities, materials are characterized by their stopping power $-\mathrm{d}E/\mathrm{d}x$, which is given by the Bethe-Bloch equation [3]:

$$-\frac{\mathrm{d}E}{\mathrm{d}x} = 0.1535\frac{\mathrm{MeV}\cdot\mathrm{cm}^2}{\mathrm{g}}\rho\frac{Z}{A}\frac{z^2}{\beta^2}\left[\ln\left(\frac{2\mathrm{m_e}\upsilon^2 W_{max}}{I(1-\beta^2)}\right) - 2\beta^2 - \delta - 2\frac{\mathrm{C}}{Z}\right] \tag{1}$$

where ρ, Z and A are the density, atomic number and weight of the material, whereas z and $\beta = \upsilon/c$ are the projectile's charge and normalized velocity.

Fig. 1 shows the LET within the water slab dependent on the regolith thickness (Bragg curve). We also show for comparison the behavior of two other materials commonly used in aerospace, aluminum and ploy ethylene, against radiation (Fig. 2).

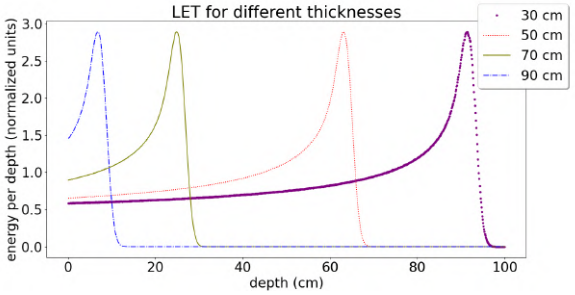


Fig. 1. LET by 600 MeV protons within the water slab for various regolith thicknesses.

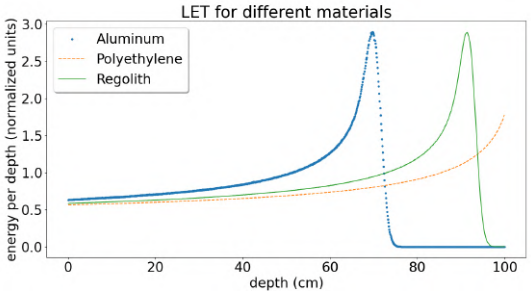


Fig. 2. LET by 600 MeV protons within the water slab for aluminum, polyethylene and regolith.

We observe that the Bragg peak shifts to shallower depths when the thickness of the regolith rises. Also, polyethylene seems to respond better against the incoming radiation. This is of course expcted by Eq. (1), since low atomic number and high density materials attenuate radiation more effectively. We conclude that regolith is not a really effective material against radiation, considering its intermediate performance.

Acknowledgements. This work was done under the Blue Marble Space Young Scientist Program. The author would like to thank his advisor, Dr. Dimitra Atri (New York University Abu Dhabi), for his guidance.

[1] A. R. Kennedy, "Biological effects of space radiation and development of effective countermeasures,"Life sciences in space research, vol. 1, pp. 10–43 (2014).
[2] L. C. Simonsen, J. E. Nealy, L. W. Townsend, J. W. Wilson, Martian regolith as space radiation shielding. Journal of Spacecraft and Rockets, 28(1), 7–8 (1991).
[3] W. R. Leo, Techniques for nuclear and particle physics experiments: a how-to approach. Springer Science & Business Media (2012).

NACO ADAPTIVE OPTICS: THE KEY EXPLORATION OF BLACK HOLE LENSES

Algita Stankevičiūtė[1], Joachim Borowicz[1], Łukasz Wyrzykowski[1]

[1] Astronomical Observatory, Faculty of Physics, University of Warsaw, Poland
algita@astrouw.edu.pl, atigla@gmail.com

In modern ground-based optical astronomy, Adaptive Optics (AO) plays an important role minimising strong effects (e.g. wind influence [1], temperature fluctuations [2], light interaction with particles [3] and etc.) that comes from the atmosphere. Nowadays, all largest ground-based optical telescopes are equipped with single or multiple AO systems that corrects perturbed photon wavefront coming from desired astronomical object to an almost ideal diffraction pattern with a clear visible Airy disk [4]. This makes a good job for astronomers to obtain high-resolution images and detect faint objects or not clearly resolvable parameters.

For the time being, exploration of Black Holes (BHs) is a hot topic among astronomers. It is believed that dozens of stellar mass BHs are found in the binary systems [5] but isolated BHs are far beyond the detection limits. Detecting isolated BHs will help scientists to perform theoretical predictions and modelling of stellar evolution [6].

For this purpose, Gravitational Microlensing Phenomenon [7] comes to hand because it is very powerful method on detecting isolated BHs. It was first described by Albert Einstein relying on the General Relativity Theory. By a reson of a massive object (a lensing star), which is passing in front of the background star, the coming light wavefront is bend and the magnification is observed [8]. After many years, lens and a star move away and can be observed separately [9]. This means that not detecting a luminous lens, we can still investigate constrains on the black holes nature [10].

In this research, we analyse two images of target star OGLE3-ULENS-PAR-2 that are showed in red circles at (Fig. 1). Images at J and K-bands were taken by NaCo AO system ((NAOS CONICA) Nasmyth Adaptive Optics System Near-Infrared Imager and Spectrograph instrument) which was mounted on 8.2 m Very Large Telescope (VLT) observatory.

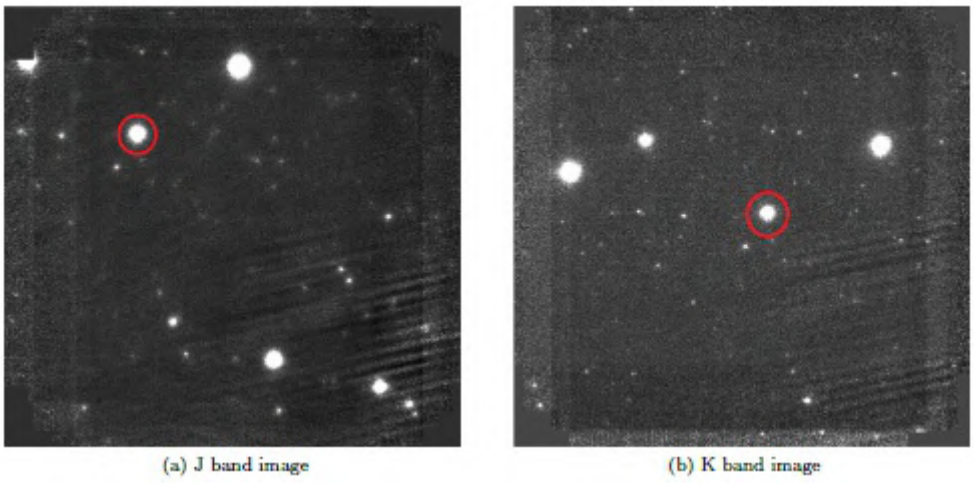


Fig. 1. NaCo images with target star OGLE3-ULENS-PAR-2 (red circles)

In conclusion, by analysing the Point Spread Function of the target star in junction with the reference stars, we detect no additional light. This means that lens can be dark or relative proper motion is very small.

[1] M. Campbell. *Atmospheric Turbulence and its Influence on Adaptive Optics.* (2009): 10.
[2] R. Stuik, et al. Characterization of deformable mirrors for high-order adaptive optics systems. In: Advancements in Adaptive Optics. International Society for Optics and Photonics, 1572-1578 (2004).
[3] F. Pinto. Adaptive optics actuation by means of van der Waals forces: a novel nanotechnology strategy to steer light by light. In: Optomechatronic Technologies 2008. International Society for Optics and Photonics, 726616 (2008).
[4] G. Rousset., et al. First diffraction-limited astronomical images with adaptive optics. Astronomy and Astrophysics, 230: L29-L32 (1990).
[5] J. R. Lu, et al. A search for stellar-mass black holes via astrometric microlensing. The Astrophysical Journal, 830.1: 41 (2016).
[6] Ł. Wyrzykowski, et al. Black hole, neutron star and white dwarf candidates from microlensing with OGLE-III. Monthly Notices of the Royal Astronomical Society, 458.3: 3012-3026 (2016).
[7] B. Paczyński. Gravitational microlensing in the local group. Annual Review of Astronomy and Astrophysics, 34.1: 419-459 (1996).
[8] F. Delplancke, K. M. Górski and A. Richichi. Resolving gravitational microlensing events with long-baseline optical interferometry-Prospects for the ESO Very Large Telescope Interferometer. Astronomy Astrophysics 375.2: 701-710 (2001).
[9] Ł. Wyrzykowski and I. Mandel. Constraining the masses of microlensing black holes and the mass gap with Gaia DR2. Astronomy Astrophysics 636: A20 (2020).
[10] J. P. Luminet. An illustrated history of black hole imaging: Personal recollections (1972-2002). arXiv preprint arXiv:1902.11196 (2019).

VARIABLE STARS IN BINARY SYSTEMS

Rūta Urbonavičiūtė[1], Erika Pakštienė [1]

[1]Institute of Theoretical Physics and Astronomy, Vilnius University, Lithuania
ruta.urbonaviciute@ff.vu.lt

Binary stars are crucial for understanding the evolution of stars and their influence on the formation of clusters, galaxies and their structure. The brightness of eclipsing binary system changes due to the relative movement of two stars. From the observers perspective, as they move, the stars obscure each others light, leading to significant brightness changes. Photometric and spectrometric observations of eclipsing binary stars and analyses of them allow us to more accurately determine the parameters of the stars. Studies of binary stars provide an opportunity to find out not only the parameters such as luminosity, size and temperature, but also masses of the components. While determining individual star mass is a difficult task, gravitational interaction of stars in binary or multiple systems with each other makes this task easier.

Variable stars can be found over the entire HR diagram and new variable stars are still being discovered to this day. Variable stars are studied by a branch of astronomy called asteroseismology which aims to understand the structure and evolution of stars by examining their oscillations [1]. Asteroseismology became more popular, as more and more space telescopes were launched and could produce continuous and more detailed lightcurves than ground based telescopes.

In 2018, a TESS (Transiting Exoplanet Survey Satellite) [2] space telescope was launched. TESS originally was designed to search for exoplanets, but it is a perfect tool for observations of eclipsing binary stars too. Therefore, we decided to analyse all known Algol type eclipsing binary stars observed with TESS and create a catalogue of eclipsing binary stars that contain variable stars. We obtained a list of known eclipsing binary stars from AAVSO International Variable Star Index VSX catalogue [3]. Among known 95893 Algol binary systems, we found that 13045 are binary stars with periods longer than 4 days. 10318 of them were observed with TESS. We downloaded their light curves observed with 2 min and 30 min cadences. Using binary stars modeling tool Phoebe [4], we removed eclipses and analysed remaining light curves. We calculated their Lomb-Scargle periodograms (LSP) to test variabilities of their components. If the condition $S/N > 4$ is met in LSP, then we assume that variability is significant, and we conclude that binary system contains a variable component.

A great advantage of analysing and modeling of binary stars with variable component is that components of a binary system share similar evolutionary history. By combining asteroseismic analysis and the results obtained from observations of eclipses, we can more accurately determine parameters of stars, their evolution and internal structure.

[1] John R. Percy, Understanding variable stars (Cambridge University Press, 2007)

[2] This paper includes data collected by the TESS mission. Funding for the TESS mission is provided by the NASA's Science Mission Directorate.

[3] C. L. Watson, A. A. Henden, A. Price, *The International Variable Star Index (VSX)* (In Society for Astronomical Sciences Annual Symposium Vol. 25, p. 47, 2006).

[4] A. Prsa, G. Matijevic, O. Latkovic, F. Vilardell, P. Wils, *PHOEBE: PHysics Of Eclipsing BinariEs* (Astrophysics Source Code Library, ascl-1106, 2011).

VARSTAR DETECT, A PYTHON LIBRARY DEDICATED TO THE SEMI-AUTOMATIC DETECTION OF STELLAR VARIABILITY

Jorge Perez Gonzalez[1], Nicolas Carrizosa Arias [2], Andres Cadenas Blanco[3]

[1]Department of Physics and Astronomy, University College London, Gower Street, WC1E 6BT London, UK
[2]Facultad de Ciencias, University of Oviedo, C. Federico García Lorca, 18, 33007 Oviedo, Spain
[3]Escuela de Ingeniería Informática, University of Oviedo, Calle Valdés Salas, 11, 33007 Oviedo, Spain
jorper.gonzalez@gmail.com, nicocarrizosaarias@gmail.com

At the time of writing, over 2 000 000 variable stars are catalogued in the Variable Star Index (VSX), which is currently ran by the American Association of Variable Stars Observers [1]. Due to the expensive cost of spectroscopic studies, these catalog submission studies adopt phenomenological approaches rather than physical ones. These analysis, classify stars by parameters such as its period P, initial epoch T_0 and magnitude range $m_{\max} - m_{\min}$. Variability type classification is performed manually by visual inspection of the light curve or phase plot, where the variability cycles are displayed with higher resolution.

In addition, the amateur community can easily contribute to variable star detection since said community obtains several CCD images for a variety of purposes (astrophotography, comet tracking, etc.). In this work we present `VarStar Detect`, a Python library dedicated to the semi-automatic detection of stellar variability. This library is thought to be the basis code of the `VarStar Detect` program (with implemented GUI) which remains to be written. This program will perform aperture photometry of all targets in the FOV automatically and present possible stellar variable candidates for later visual inspection by the astronomer. Through such program usage, the effort and time consumed in mining variability in the astronomer's images will be significantly reduced, encouraging astronomers to look for variability in their data for VSX submission. This presentation describes the functionality and assessment of the `VarStar Detect` package available on PyPI[2] for installation.

For variable star detection `VarStar Detect` must accomplish four tasks:

1. Fit a trigonometric polynomial of degree s (P_s) to the light curve [1] (using the weighted least squares method) and calculate its corresponding reduced χ^2 parameter (χ^2_r).

$$P_s(t) = C_0 + \sum_{i=1}^{s} (C_{i,1} \cdot \cos(i\omega(t - T_0)) + C_{i,2} \cdot \sin(i\omega(t - T_0))) \tag{1}$$

$$\chi^2_r = \frac{\sum_{j=1}^{n} \left(\frac{y_j - P_s(t_j)}{\sigma(y_j)} \right)^2}{n - 2s - 1} \tag{2}$$

2. Choose the trigonometric polynomial fit which satisfies $\chi^2_r \to 1$.

3. Calculate the amplitude of the polynomial fit.

$$Amp = \texttt{max}(P_s(t)) - \texttt{min}(P_s(t)) \qquad \text{where t} \in [0, 30] \tag{3}$$

4. Determine if star is variable using the amplitude test.

The purpose of the amplitude test is to decide if the star in question is a potential variable candidate that deserves to be visually inspected. In essence, it nominates all stars which have an amplitude greater or equal than the threshold amplitude as potential variables. The question comes when selecting the threshold amplitude, which will depend on the equipment used and quality of the night sky. The threshold measures the smallest amplitude detected before the equipment measures just noise. Our work does not go into explaining the physical meaning of this threshold; we encourage further investigations to do so. In testing of the code, an empirical approach was used to determine the value of threshold for the data used.

Finally, to test the program's functionality, the program as a whole was tested on Sector 1 TESS PDCSAP data, downloaded with the `data_download` function designed and available in the python repository. The program was proved to be 96.45 % efficient, detecting a total of 163 variable stars inside the imported sector 1 database.

[1] Andronov I. L. 2012, Astrophysics, 55, 4

[1]Obtained from `https://www.aavso.org/vsx/index.php`

[2]To access the package (version 1.1.0 described here) see `https://pypi.org/project/varstardetect/` for installation instructions or type `pip install varstardetect` in your command line. Full documentation of available functions and tutorials are available on the VarStar Detect github repository: `https://github.com/VarStarDetect/varstardetect`

CENN: A FULLY CONVOLUTIONAL NEURAL NETWORK FOR CMB RECOVERY IN REALISTIC MICROWAVE SKY SIMULATIONS

José Manuel Casas González[1,2], Laura Bonavera[1,2], Joaquín González-Nuevo González[1,2]

[1]Departamento de Física, Universidad de Oviedo, España
[2]Instituto de Ciencias y Tecnologías Espaciales de Asturias (ICTEA)
casasjm@uniovi.es

Component separation was one of the central objectives of the Planck mission. Develop more accurate and reliable methods to extract the cosmic microwave background (CMB) signal in regions with high Galactic contamination and at small scales is relevant for future experiments such as the Simons Observatory, the CMB-S4 or LiteBIRD.

In our approach, we present the CMB Extraction Neural Network (CENN), a fully convolutional neural network trained with realistic simulations of the microwave sky in total intensity to extract the CMB signal. Our work is based on the competitive results obtained using this type of architectures for point source detection in single-frequency (PoSeIDoN, [1]) and multifrequency (MultiPoSeIDoN, [2]) approaches.

To train the neural network, we use random patches of size 256×256 pixels formed by realistic simulations of the 143, 217 and 353 GHz Planck channels with the CMB signal and foregrounds such as the thermal dust and cosmic infrared background, the Sunyaev-Zel'dovich effect and point source contributions and instrumental noise. To evaluate the performance of the neural network, we use validation datasets built with simulations different from the training one. Firstly, a validation dataset formed by patches at all sky is used. Secondly, three more datasets at different sky latitudes are generated: $0^\circ<|\mathrm{lat}|<5^\circ$, $5^\circ<|\mathrm{lat}|<30^\circ$ and $30^\circ<|\mathrm{lat}|<90^\circ$.

We obtain a CMB power spectrum at all sky with a relative error lower than $50\pm120\ \mu K^2$ for multipoles up to $l\sim4.000$. We compute the residuals as the difference between the input and output mean patch, obtaining values at all sky between 0 and $10\ \mu K^2$ for $l\leq1.000$ and $5\pm12\ \mu K^2$ for $l\leq4.000$. For each latitude interval, we get residuals of $7\pm25\ \mu K^2$ for $0^\circ<|\mathrm{lat}|<5^\circ$, $2\pm10\ \mu K^2$ for $5^\circ<|\mathrm{lat}|<30^\circ$ and $2\pm3\ \mu K^2$ for $30^\circ<|\mathrm{lat}|<90^\circ$. We validate the neural network also in a patch with high contamination at small scales, obtaining a relative error of $50\pm120\ \mu K^2$ and residuals of $40\pm10\ \mu K^2$. All these results are presented without the use of any Galactic and point source masks.

In conclusion, based on our results, CENN is a promising new method to extract the CMB signal in future experiments.

[1] L. Bonavera, S.L. Suárez-Gómez, J. González-Nuevo et al., Point source detection with fully convolutional networks. Performance in realistic microwave sky simulations, Astronomy & Astrophysics **648**, A50 (2021).

[2] J. M. Casas, J. González-Nuevo, L. Bonavera et al., Multi-frequency point source detection with fully convolutional networks: Performance in realistic microwave sky simulations, Astronomy & Astrophysics Forthcoming article.

P2-27

DID NOT PARTICIPATE

.

TESTS OF HIERARCHICAL FORMATION IN THE VIRGO CLUSTER

Aikaterini-Niovi Triantafyllaki[1], Alessia Longobardi[2]

[1]Department of Physics, Aix-Marseille University, France
[2]Department of Physics, University of Milan, Italy
aikaterini-niovi.triantafyllaki@etu.univ-amu.fr

Large concentrations of mass are now understood to be the products of a Hubble time's worth of merging and accretion. This history is preserved in distribution of stars, although it is traced at a surface brightness much fainter than the sky. Planetary nebulae (PNe) can solve this observational challenges: because of their strong [OIII] emission line— they are easily detected— PNe offer a unique tool to investigate the regions in space where fossil records of structure evolution are preserved.

Here, we are going to explore the difficulties faced by today's observations when it comes to the very faint universe and how we overcome this difficulty. Analysis on the deep [OIII]-band survey of the Virgo cluster, the nearest large concentration of mass, provided the necessary base to study the physical properties of its PN population. In particular, I produced 2D maps of the PN specific frequency, or α-parameter, which links the number of PNe associated with a stellar population to its bolometric luminosity which correlate to the physical properties of the system.

[1] Longobardi, A., Arnaboldi, M., Gerhard, O., et al. 2013, AAP, 558, A42.
[2] Mihos, J. C., Harding, P., Feldmeier, J., et al. 2005, ApJ, 631, L41.
[3] Mihos, J. C., Harding, P., Feldmeier, J. J., et al. 2017, ApJ, 834, 16.

INVESTIGATION OF AMORPHIZATION RINGS GENERATED ON SILICON SURFACE VIA ULTRASHORT LASER PULSES

Carlos Vytautas Diamond Manikas[1*], Vygandas Jarutis[1], Domas Paipulas[1], Simas Butkus[1], Vytautas Jukna[1]

[1] Laser Research Center, Vilnius University, Saulėtekio Ave. 10, LT-10223 Vilnius, Lithuania
carlos.diamond@ff.vu.lt

The laser assisted manufacturing of flat surfaces is a hot topic in the laser community. The ability to change the properties of the surface just by applying high energy pulses is fascinating. After the laser treatment materials can obtain new colors due to recrystallisation, heat assisted chemical reactions, or even surface nanograting formation. Materials can also get other property changes such as wetting or hardness. The interesting ring-shaped features appear after a single shot on the silicon surface heats the scientific community[1,2,3]. It was found that the higher reflectivity ring can be attributed to the silicon chaotic recrystallization and the change of the state of matter induces higher reflectivity[2]. However, the reasoning of the formation is still unclear. We have experimentally and numerically investigated this ring formation induced by intense ultrashort laser pulses.

We focus Pharos (Light Conversion Ltd.) laser beam, having 300fs FWHM pulse duration with central wavelength of 1032nm, to a Silicon surface with a long focal length lens (100mm). The beam diameter at the focus is 14.5 μm FWHM. We observe the energy threshold of the recrystallisation which manifests in formation of the higher reflectivity circle, while the increase of pulse energy forms the ring. We track the inner and outer ring radius with the increase of the pulse energy. The position of the sample can be shifted with the respect of the lens focus, which enables us to easily change the impinging to the surface beam diameter. Therefore, we experimentally obtained data of the ring energy threshold, inner and outer beam diameter change with the change of laser beam diameter and energy.

To explain this phenomenon, we devise a semi analytical expression where linear and two photon absorption is accounted for in the laser energy deposition estimation. We define the absorbed energy threshold to the energy needed to melt the Silicon. This threshold will also serve as the outer ring radius, while the inner ring radius is connected to the energy needed for Silicon to boil. We found that these two above mentioned laser energy absorption mechanisms are not enough to fit the experimental data. To get a better match we had to set the linear absorption coefficient to depend on laser beam fluence. The analytical and experimental points are plotted in Fig. 1 A. For better description of the energy deposition, we developed a numerical code which accounts not only for linear and two photon absorption, but also electron impact absorption which leads to avalanche. After parametric study of the material parameters we observe that indeed the impact absorption is contributing greatly to the laser absorption. Please see Fig. 1 B dotted line representing results of the numerical model with the inclusion of impact ionisation for 25.4μm beam FWHM diameter.

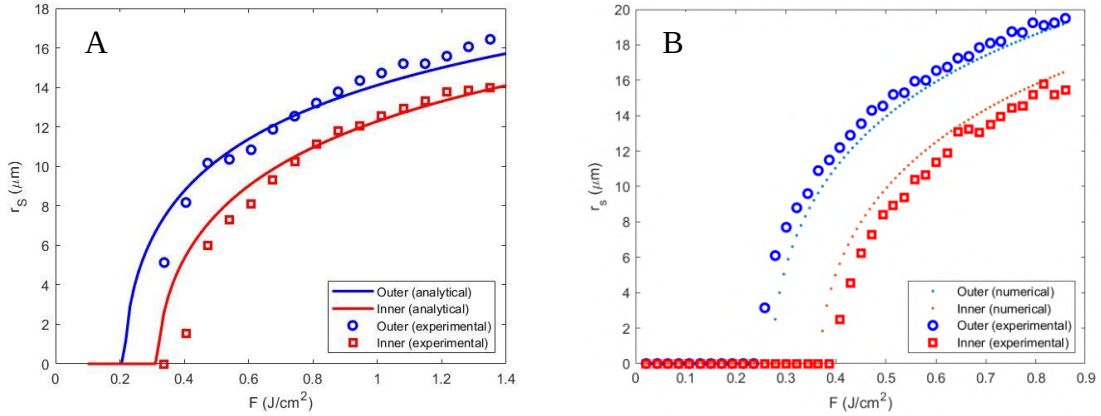


Fig. 1. Inner (red colored) and outer ring (blue colored) radius dependence on maximum beam fluence. Circles, solid lines and dotted lines represent experimental, analytical and numerical results respectively. A represents 14.5 μm diameter beam and B represents 25.4μm beam FWHM diameter.

With this experimental and numerical investigation, we can estimate nonlinear absorption coefficients with relatively high precision. We found that the two-photon absorption is $1.98 \cdot 10^{10}$ m/W, and cross-section of bremstrahlung of $1.56 \cdot 10^{-22}$ m^2, which are close to the material parameters found in the literature. In the future work we will combine the thermal diffusion model to see whether the heat transfer has an impact on the results.

[1] R. Moser, M. Domkes, J. Winter et al. Single pulse femtosecond laser ablation of silicon – a comparison between experimental and simulated two-dimensional ablation profiles, Advanced Optical Technologies, **7,** 255-264 (2018).

[2] J. Bonse, S. Baudach, J. Krüger et al. Femtosecond laser ablation of silicon–modification thresholds and morphology. Appl Phys A **74,** 19–25, (2002).

[3] C. Florian, D. Fischer, K. Freiberg et al. Single Femtosecond Laser-Pulse-Induced Superficial Amorphization and Re-Crystallization of Silicon. Materials **14**, 1651 (2021).

AEROSOL FILTRATION EFFICIENCY OF HOUSEHOLD MATERIALS WITH ANTIMICROBIAL HYDROPHOBIC COATING

Kamilė Kandrotaitė[1,2], Steigvilė Byčenkienė[2], Vadimas Dudoitis[2], Ieva Uogintė[2], Kristina Plauškaitė Šukienė[2], Francis Pope[3], Peter Strizak[4]

[1]Faculty of Physics, Vilnius University, Lithuania
[2]Department of Environmental Research, Center for Physical Sciences and Technology, Lithuania
[3]The University of Birmingham, UK
[4]L.V. Pisarzhevskii Institute of physical chemistry of NAS of Ukraine, Ukraine
kamile.kandrotaite@ff.stud.vu.lt

The global spread of Severe Acute Respiratory Syndrome Coronavirus 2 (SARS-CoV-2) proved to be a challenge of a public health. It has limited the supply of medical masks and filtering facepiece respirators (e.g., FFP2), so it has been recommended that their use be restricted to healthcare settings. For this reason, the World Health Organization has suggested the use of non-medical face masks in a public places to reduce airborne spread of SARS-CoV-2. The quality of public masks can be assured by evaluating two main filtering masks properties: filtration efficiency (FE) and pressure drop (ΔP). Both of these quantities are not widely studied for non-medical facemasks. Moreover, many studies have shown that silver nanoparticles have antiviral, anti-inflammatory and antibacterial properties [1]. Thus it may prove beneficial in prolonging wearing time of masks.

This study was based on the recommendations of CWA 17553: 2020 standard, which sets minimum safety requirements for the use of community face masks. An experimental stand consisting of aerosol generation, transport, dilution and material testing units was constructed to evaluate the FE of the fabric masks. Particle size distribution and numerical concentration were measured with an aerodynamic particle spectrometer (APS, TSI model 3321). Aerosol particles were generated using 2 % NaCl solution.

The study found that after coating the material with a solution containing silver nanostructures, the filtration efficiency in the 2,50 - 3,50 μm particle size range (which is suggested by the CWA standard) decreased (Fig. 1). Materials with a predominance of cotton (80 - 100 %) had a decrease in FE ranging from 5 % to 7 %, while materials with a predominance of polyester (78 - 100 %) had a FE reduction of 17 - 20 %. Comparing the obtained FE values with those provided by the CWA standard ($FE > 70$ %) it can be stated that the coating of cotton material with a solution containing silver nanostructures has a minimal effect on the filtration efficiency. Thus it meets the standard of non-medical masks.

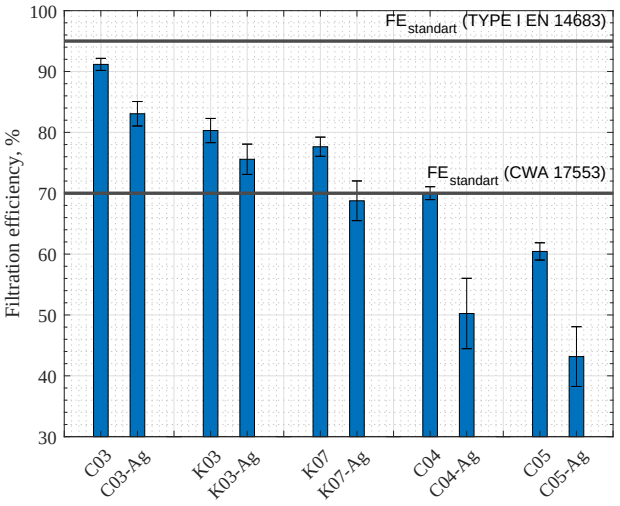


Fig. 1. Filtration efficiency before and after coating materials with silver nanostructures. Also, FE standards for medical and non-medical masks (CWA). The composition of materials: C03 - 100 % cotton, K03 - 80 % cotton, K07, C04 - 78 % polyester, C05 - 100 % polyester.

In conclusion, it should be noted that textile masks do not guarantee better protection than medical masks and respirators. Also, if additional coating does not decrease filtration efficiency, it can be a great solution for expanding masks wear time.

Acknowledgments: Joint UK-Lithuania-Ukraine aerosol tiny particles COVID-19 transmission study was supported by the UK Embassy in Lithuania.

[1] Eremenko, Anna Petrik, I. Smirnova, N. Rudenko, AV Marikvas, YS. Antibacterial and Antimycotic Activity of Cotton Fabrics, Impregnated with Silver and Binary Silver/Copper Nanoparticles. Nanoscale Research Letters **11**, (2016).
[2] H. Gong, and B. Ozgen, Engineering of High-Performance Textiles, The Textile Institute Book Series, 107-131 (2018).

ZnO NANOTETRAPODS FOR ROOM TEMPERATURE UV SENSORS

Mindaugas Ilickas[1,2], Simas Račkauskas[1,2]

[1] Department of Physics, Kaunas University of Technology, Lithuania
[2]Institute of Materials Science, Kaunas University of Technology, Lithuania
mindaugas.ilickas@ktu.edu

Among all the semiconductors, zinc oxide (ZnO) is broadly and tremendously attracted material due to its multifunctional characteristics including a huge band gap of ~ 3.37 eV and an excessive exciton binding energy ~60 meV at room temperature, moreover it is an environmentally friendly, low visible absorption and low-cost material. Therefore, ZnO is a promising material for ultraviolet (UV) photodetector and sensor applications [1]. The potential of ZnO to absorb ultraviolet light (10-400 nm) is implemented in the manufacturing of solar cells coatings and ultraviolet sensors [2]. ZnO is an inorganic compound observed in the form of a white powder, nearly insoluble in water. ZnO is an incredibly soft material with a Mohs hardness of ~ 4.5 [3]. Single nanowire (NW) UV sensors exhibit very high ON/OFF ratios between photoresponse currents and dark currents due to their large surface area to volume ratio and high-quality crystal structure. Practical applications require large-scale, low-cost integration, compatibility with flexible electronics, and sufficiently high photoresponse currents to be detected without high-precision measurement systems [4]. By illuminating the surface of the ZnO coating with ultraviolet light, it is able to create free vacancies of the oxygen atom, which adjusts the internal properties of the material, along with growing the n-type conductivity and wetting the material. Such properties have also great potential in room temperature UV and humidity sensing.

In this work we investigated our ZnO nanotetrapod (ZnO-T) sensors and compared with commercially available kadox. Tetrapods were obtained by continuous combustion synthesis [5], and further separated into lower dimension fractions using centrifugation (1000 and 3000 rpm) of initial ZnO-T powders. UV photodetection (λ =365 nm) were measured with an electrometer in ambient air with a controlled relative humidity of 40%. The UV response was described as the ratio of current in the dark (I_{dark}) to current under UV illumination (I_{UV}). It was found that even at low UV power density (0.31 mW/cm^2) ZnO-T sensors show much better results compared to their commercial nanoparticle sensor counterparts. Commercial ZnO nanoparticles have the lowest I_{UV}/I_{dark} ratio (1020 %) compared to the highest of ZnO-T @1000 (307350 %). Other ZnO-T ratio was 105200 % (ZnO-T before centrifugation) and ZnO-T @3000 7470 %.

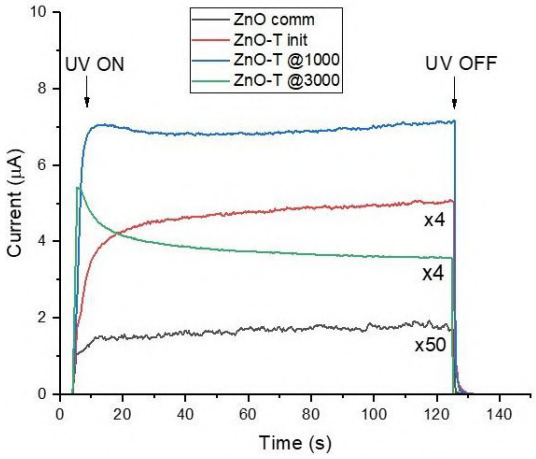


Fig. 1. UV Response rate: commercial ZnO kadox (black), initial ZnO-T (red) obtained by continuous synthesis and centrifugated ZnO-T powders ZnO-T @1000 (blue) and ZnO-T @3000 (green).

This research is funded by the European Regional Development Fund according to the supported activity "Multifunctional coatings based on ZnO nanowires for selective sensing and efficient solar harvesting (MultiFun)", project No. 01.2.2-LMT-K-718-02-0011.

[1] Shobhnath P. Gupta, et al. Superior humidity sensor and photodetector of mesoporous ZnO nanosheets at room temperature. *Sensors and Actuators B: Chemical, (293)*, 83-92, 2019.
[2] Jacobs, Christopher B et al. UV-activated ZnO films on a flexible substrate for room temperature O_2 and H_2O sensing. *Scientific Reports*, **7(1)**, 6053, 2017.
[3] A. Hernández Battez et al. CuO, ZrO2 and ZnO nanoparticles as antiwear additive in oil lubricants. Elsevier, **265(3-4)**, 422–428, 2008.
[4] Suo Bai et al. High-Performance Integrated ZnO Nanowire UV Sensors on Rigid and Flexible Substrates. *Advanced functional materials*, **21(23)**, 4464–4469, 2011.
[5] S. Rackauskas, et al. A Novel Method for Continuous Synthesis of ZnO Tetrapods. *The Journal of Physical Chemistry C*, **119(28)**, 16366–16373, 2015.

DEVELOPMENT OF MCNP MODEL AND PRELIMINARY SIMULATION OF LIEBE PROTON TARGET

Benjaminas Togobickij[1], Mantas Povilaitis[1], Gediminas Stankūnas[1]

[1]Laboratory of Nuclear Installation Safety, Lithuanian Energy Institute, Lithuania
benjaminas.togobickij@lei.lt

In order to increase the primary beam intensity in next generation of radioactive ion beam installations, the production of targets capable of dissipating high beam power, especially for molten targets, is a major challenge. In that context, a direct molten loop concept was proposed for short-lived isotopes by EURISOL. To validate this concept a target prototype was designed and assembled, called LIEBE, in the ISOLDE operation environment [1].

The aim of this work was to develop a MCNP model of liquid lead LIEBE target and perform preliminary simulations of proton beam impact. To achieve this a detailed CAD model of the target was converted to an MCNP readable format using SALOME software McCAD module. The CAD model needed to be manually decomposed before the conversion, since the geometry of the LIEBE target was complex and detailed. For this reason, many elements of the model needed to be manually modified as well.

Developed model was used for the MCNP simulation of incident proton beam. The proton flux distribution after the impact was evaluated and maps were produced (Fig. 1). FENDL-3.1 cross-section data library has been used.

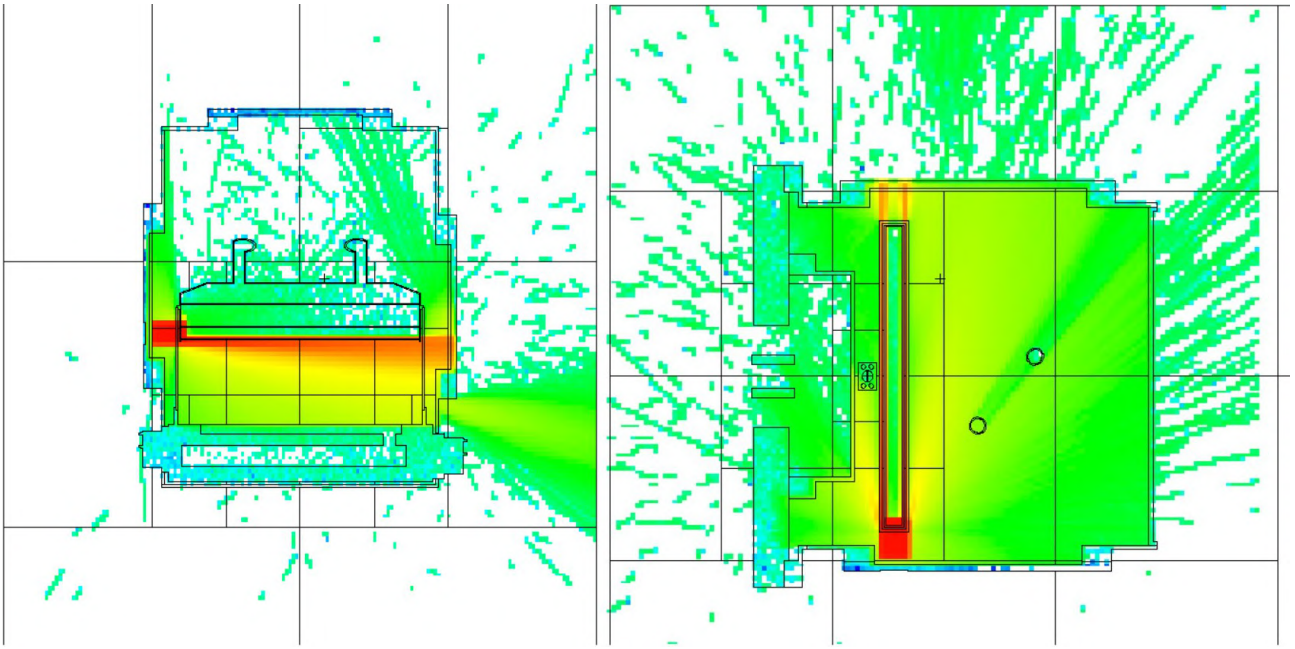


Fig. 1. Monoenergetic (70 MeV) proton beam distribution cross sections in the LIEBE target, $[\#/\mathrm{cm}^2/s]$.

Preliminary results revealed that the proton beam window's should be revised in CAD and MCNP models, in order more protons hit the target at the required position. From the produced proton flux maps it can be seen that part of the beam penetrates under the LIEBE target construction. Therefore, from a radiation safety perspective, certain biological safety measures will be evaluated in the future under this study.

[1] F. Boix Pamies, T. Stora, E. Barbero et al., The LIEBE high-power target: Offline commissioning results and prospects for the production of ^{100}Sn ISOL beams at HIE-ISOLDE, Nuclear Instruments and Methods in Physics Research Section B: Beam Interactions with Materials and Atoms **463**, 128-133 (2020).

VANILLIN ACRYLATE-BASED SHAPE MEMORY POLYMERS

Aukse Navaruckiene[1], Egidija Rainosalo[2], Jolita Ostrauskaite[1]

[1] Department of Polymer Chemistry and Technology, Kaunas University of Technology, Lithuania
[2] Centria University of Applied Sciences, Kokkola, Finland
aukse.navaruckiene@ktu.lt

Shape memory polymers have a unique ability to obtain temporary shapes and return to their permanent shape in response to stimuli. This unique ability greatly increased the area of application of such polymers [1]. Dual curing is one of the possible ways to obtain shape memory materials. It allows us to create materials with unique properties by combining two different polymerization reactions [2].

In this study, cross-linked polymers were obtained by dual curing of vanillin diacrylate, vanillin dimethacrylate and vanillin hydroxypropane dimethacrylate with 1 or 0.5 mol.% of 1.3-benzenedithiol, using ethyl(2,4,6-trimethylbenzoyl)phenylphosphinate as photoinitiator. Two different reactions, free-radical and thiol-acrylate photopolymerisation, were tuned by varying the ratio of thiol to acrylate.Photorheometry was used to monitor the evolution of the photocross-linking process. The UV/Vis real-time photorheometry curing tests were performed on a MCR302 rheometer from Anton Paar equipped with the plate/plate measuring system. It was determined that the increase in the amount of thiol in the resins reduced the photocuring rate and the rigidity of the resulting polymers.

To show shape memory properties of vanillin-based polymers, we heated the polymer samples above their glass transition temperature (T_g) and then deformed them to the desired temporary shape. The glass stick was used to form polymer samples. When the temporary shape was obtained, it was fixed by cooling the polymer sample below its T_g. Polymer samples were able to maintain their temporary shape in the temperature below their T_g. All polymer samples were able to return to their permanent shape in a short period of time after heating above their T_g. The scheme of heating-cooling-heating cycles is presented in Fig. 1.

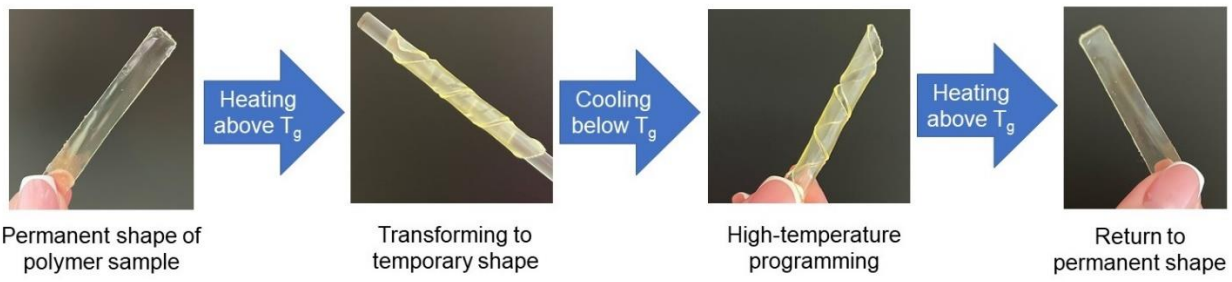


Fig. 1. The scheme of shape memory behaviour of polymer sample

The tensile test was performed to investigate the mechanical properties of vanillin-based polymers. The reduction in thiol content was determined to improve the mechanical performance of polymers as Young's modulus increased from 1.4 - 3.5 MPa to 3952.3 – 11339.4 MPa [3].

Acknowledgement. This research was funded by the Research Council of Lithuania (project No. S-MIP-20-17) and the EU ERDF, through the INTERREG BSR Programme (ECOLABNET project #R077).

[1] K. Yang, J. Du, Z. Zhang, T. Ren, A facile strategy to fabricate robust triple-shape memory polymer. Materials Letters, **257**, 126753 (2019).
[2] C. Aymes-Chodur, H. Salmi-Mani, D. Dragoe et al., Optimization of microwave plasma treatment conditions on polydimethylsiloxane films for further surface functionalization. European Polymer Journal, **150**, 110416 (2021).
[3] A. Navaruckiene, D. Bridziuviene, V. Raudoniene et al., Vanillin acrylate-based thermo-responsive shape memory antimicrobial photopolymers. Express Polymer Letters, **16**, 279-295 (2022).

HYDROXYAPATITE FORMATION BY SOLVOTHERMAL TREATMENT OF ALPHA-TRICALCIUM PHOSPHATE WITH WATER-ALCOHOL SOLUTION

Rasa Karalkeviciene[1], Eva Raudonyte-Svirbutavičiene [1,2], Aleksej Zarkov[1], Aivaras Kareiva[1]

[1] Institute of Chemistry, Faculty of Chemistry and Geosciences, Vilnius University, Naugarduko St. 24, LT-03225 Vilnius, Lithuania
[2] Institute of Geology and Geography, Nature Research Centre, Akademijos Str. 2, LT-08412, Vilnius, Lithuania
rasa.karalkeviciene@chgf.vu.lt

The most widely used bioceramics material for bone grafting in humans is hydroxyapatite (HA) [1], which has a chemical composition and crystalline structure similar to those of bone [2]. HA and some other calcium-based ceramic materials can be regarded as bioactive materials since they have been reported to support bone ingrowth [3-5]. HA, a calcium phosphate biomaterial, is a very promising candidate for the treatment of air, water and soil pollution. It can be extremely useful in the field of environmental management due to its specific structure and attractive properties, such as great adsorption capacities, acid-base adjustability, ion-exchange capability, and good thermal stability [6]. The protein adsorption characteristics of HA crystals depend on their morphology, with different crystal faces having different characteristics [7, 8].

In the present work, we expect that the solvothermal treatment of alpha-tricalcium phosphate (a-TCP) in water-alcohol solution will enable the control of HA formation. The mixed water-alcohol solvent system should retard the reaction and cause slower crystal growth of HA. In this study, the effects of the alcohol fraction in solution on the formation of HA via solvothermal treatment of α-TCP were investigated. α-TCP was synthesized by wet precipitation method and the hydrolysis reaction was performed in water-alcohol solutions with different ratios of alcohol to water under hydrothermal conditions at 120 °C for 3 hour. Hydrothermal reactions were performed with water-ethylene glycol, water-methyl alcohol, water- butyl alcohol, water-isopropyl alcohol and water-ethyl alcohol. The ratio of water to alcohol was chosen as follows: 20:80, 40:60 and 60:40. The changes in crystal phase, size, morphology, and composition of the product as a function of the water-alcohol fraction were examined. The obtained synthesis products were characterized by X-ray powder diffraction (XRD) analysis and scanning electron microscopy (SEM).

Formation of HA phase was completed when higher concentration of water (40, 60 %) was introduced to the reaction solution. Increasing concentration of alcohol (80 %) induced formation of some β-TCP in addition to HA. It was found to affect the morphology of the final product: samples synthesized using larger concentrations of water (Fig. 1) contained not only plate-like, but also rod-like crystals. This implies that morphology of HA could be controlled by applying water-alcohol mixtures with different ratios during the hydrothermal treatment of α-TCP.

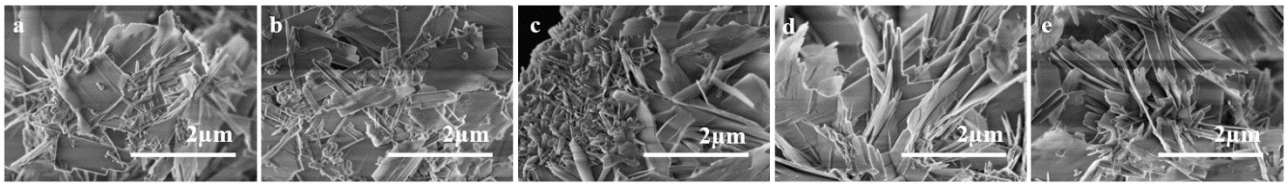


Fig. 1. SEM images of the samples. The ratio of water to alcohol 60:40: a) water-ethylene glycol; b) water-methyl alcohol; c) water-butyl alcohol; d) water-isopropyl alcohol; e) water-ethyl alcohol.

Acknowledgements: This work has received funding from the European Social Fund (project No 09.3.3-LMT-K-712-23-0070) under grant agreement with the Research Council of Lithuania (LMTLT).

[1] Supova M. Problem of hydroxyapatite dispersion in polymer matrices: a review. J. Mater. Sci. Mater. Med. 2009;20:1201–1213.
[2] Ana I.D., Matsuya S., Ishikawa K. Engineering of carbonate apatite bone substitute based on composition-transformation of gypsum and calcium hydroxide. Engineering. 2010;2(05):344–349.
[3] Martinetti R., Dolcini L., Mangano C. Physical and chemical aspects of a new porous hydroxyapatite. Anal. Bioanal. Chem. 2005;381:634–638.
[4] Nascimento C., Issa J.P.M., Oliviera R.R., Iyosoma M.M., Siessere S., Regalo S.C.H. Biomaterials applied to the bone healing process. Int. J. Morphol. 2007;25(4):839–846.
[5] Heilmann F., Standard O.C., Möller F.A., Hoffman M. Development of graded hydroxyapatite/$CaCO_3$ composite structures for bone ingrowth. J. Mater. Sci. Mater. Med. 2007;18:1817–1824.
[6] M. Ibrahim, M. Labaki, J.M. Giraudon, J.F. Lamonier, Hydroxyapatite, a multifunctional material for air, water and soil pollution control: A review, Journal of hazardous materials 383, 121139 (2020).
[7] T. Kawasaki, S. Takahashi, K. Ikeda, Hydroxyapatite high-performance liquid chromatography: column performance for proteins, Eur. J. Biochem. 152 (1985) 361–371.
[8] T. Kawasaki, K. Ikeda, S. Takahashi, Y. Kuboki, Further study of hydroxyapatite high-performance liquid chromatography using both proteins and nucleic acids, and a new technique to increase chromatographic efficiency, Eur. J. Biochem. 155 (1986) 249–257.

UV-CURABLE RESINS FROM RENEWABLE RESOURCES FOR SYNTHESIS OF VITRIMERS

Sigita Grauželienė, Brigita Kazlauskaitė, Jolita Ostrauskaitė

Department of Polymer Chemistry and Technology, Kaunas University of Technology, Lithuania
sigita.grauzeliene@ktu.lt

The worldwide manufacturing of thermosets has been expanding in later years initiating fast usage of fossil-based feedstocks which contributes to the rise of plastic waste in the environment, particularly since they can not be effectively reprocessed or recycled at the end of their lifetime [1]. To solve this issue, scientists have been introducing dynamic cross-links which were capable of exchange reactions enabling rearrangement of the network, scratch repairing, self-healing, and reprocessability [2]. One class of such new dynamic materials discovered by French researcher Ludwik Leibler is vitrimers and they were termed since they flow like a vitreous silica (quartz glass) following the Arrhenius law [3]. At operating temperatures, they behave as permanently cross-linked polymers, however at elevated temperatures, the exchange reactions within their network speed up, making flow possible, while maintaining a constant number of chemical bonds and cross-links [4, 5]. Due to this behavior, vitrimers can be reshaped (shape memory polymers), repaired, and reprocessed by injection, extrusion or 3D printing [6]. Plenty structural and fast acting devices such as actuators for soft robotics which even could be repaired or reprocessed can be manufactured leading for sustainable development and environmental protection [7, 8].

The aim of this work was to combine renewable resources, UV curing, and repairability as environmental friendly strategy for the synthesis of vitrimers. Therefore, two bio-based functionalized monomers obtained from vegetable oil and from glycerol, as a by-product of biodiesel, were chosen for preparation of UV-curable resins. Vitrimers were synthesized by mixing the monomers at different ratios with photoinitiator and transesterification catalyst and applying irradation under solvent-free condition. After UV curing, the dynamic networks were able to rapidly undergo thermo-activated rearrangements of their network topology as stress relaxation experiments performed on a MCR302 rheometer from Anton Paar showed. To verify repairability the scratch repairing tests were performed by scrathing the UV-cured vitrimer sample by a razor blade and curing at 200 °C for 1 h and monitoring by optical microscope Olympus BX41. All vitrimer samples showed a self-healing efficiency of more than 45 % (Fig. 1) due to the sufficient hydroxyl and ester groups. The designed resins from renewable resources are potential candidates for synthesis of vitrimers by UV curing.

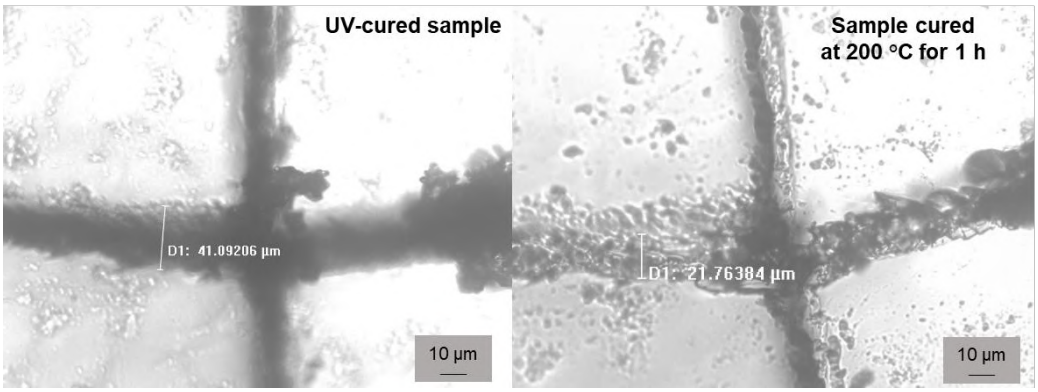


Fig. 1. Scratch-repairing images of vitrimers synthesized from renewable resources.

Acknowledgement. This project has received funding from European Social Fund (project No. 09.9.9-LMT-K-712-23-0088) under grant agreement with the Research Council of Lithuania (LMTLT).

[1] A. Rahimi, J.M. García, Chemical recycling of waste plastics for new materials production, Nat. Rev. Chem. **1**, 0046 (2017).
[2] W. Post, A. Susa, R. Blaauw et al., A Review on the Potential and Limitations of Recyclable Thermosets for Structural Applications, Polym. Rev. **60**, 359-388 (2019).
[3] D. Montarnal, M. Capelot, F. Tournilhac et al., Silica-Like Malleable Materials from Permanent Organic Networks, Science **334**, 965-968 (2011).
[4] J. Tellers, R. Pinalli, M. Soliman et al., Reprocessable vinylogous urethane cross-linked polyethylene via reactive extrusion, Polym. Chem. **10**, 5534-5542 (2019).
[5] A. Zych, J. Tellers, L. Bertolacci et al., Biobased, Biodegradable, Self-Healing Boronic Ester Vitrimers from Epoxidized Soybean Oil Acrylate, ACS Appl. Polym. Mater. **3**, 1135-1144 (2021).
[6] B. Zhang, K. Kowsari, A. Serjouei et al., Reprocessable thermosets for sustainable three-dimensional printing, Nat. Commun. **9**, 1831, (2018).
[7] M. D. Hager, S. Bode, C. Weber et al., Shape memory polymers: Past, present and future developments, Prog. Polym. Sci. **49-50**, 3-33 (2015).
[8] E. Rossegger, R. Höller, D. Reisinger et al., Digital light processing 3D printing with thiol–acrylate vitrimers, Polym. Chem. **12**, 639-644 (2021).

PRISM COUPLING TECHNIQUE FOR PLANAR GaN WAVEGUIDES

Gustas Petrusevičius[1], Marek Kolenda[1]

[1] Institute of Photonics and Nanotechnology, Vilnius University, Sauletekio ave. 3, LT-10257 Vilnius, Lithuania
gustas.petrusevicius@ff.stud.vu.lt

Waveguide - a structure that confines electromagnetic waves within the material and guides them with minimal loss of energy due to restricted transmission of energy in one direction. The well-known ones are optical fibers, but nowadays as new materials come into play, and having sophisticated fabrication methods waveguides are transferred into a micro-world dimension. One of the new materials is GaN with its' unique properties that make it particularly attractive for the use in waveguiding. GaN excels with its' properties that include wide direct band gap, large transparency window, and high second order nonlinearity (10 pm/V) [1]. GaN waveguides can be used in low loss photonics [2], generation of second harmonic [1], can be fabricated into microrings [2] and microdisks [3]. Latter photonic structures can improve SHG in GaN waveguides as they provide greater power densities [1].

In this work, guiding of 633 nm and 1064 nm wavelength light through planar GaN waveguide grown on a sapphire substrate by metalorganic chemical vapor deposition (MOCVD) using prism coupling technique is investigated.

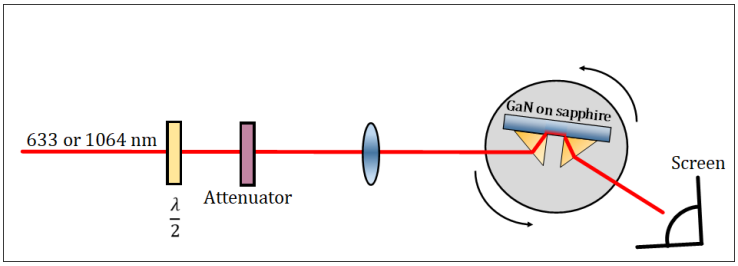


Figure. 1. Scheme of prism coupled waveguiding through GaN.

Optical scheme used for waveguiding is depicted in Figure 1. 633 or 1064 nm light is passed through a half-wave plate to control light polarization between transverse electric (TE) and transverse magnetic (TM). Attenuator is placed to lower the energy of 1064 nm pulses. Convex lens is placed that its' focal length is greater than the distance to the prism to avoid potential damage to the prism. Two prisms are made of TiO_2 (rutile) and are mounted on a goniometer with custom designed holders. Measurements are performed by selecting single polarization of the light and measuring coupling angles when distinct modes are being guided through GaN. This coupling angle is used in the calculations of effective refractive index of all waveguide modes. The latter is calculated using the following equation:

$$n_e = n_p sin\left[A + sin^{-1}\left(\frac{\sin\,\theta_i(m)}{n_p}\right)\right], \quad (1)$$

where n_p is prism refractive index, A - prism angle, $\theta_i(m)$ – measured coupling angle for a distinct mode. Thickness of GaN layer was numerically calculated using MATLAB according to the following equation:

$$\frac{2\pi d\left(n_2^2 - n_e^2\right)^{\frac{1}{2}}}{\lambda_0} = m\pi + \Phi_1 + \Phi_3, \quad (2)$$

where n_2 is refractive index of GaN, n_e – calculated effective index, d – thickness of GaN, Φ_n – evanescent field phase shifts. Figure 2 shows the calculation results of equation (2). The GaN thickness is obtained from the intersection of the curves.

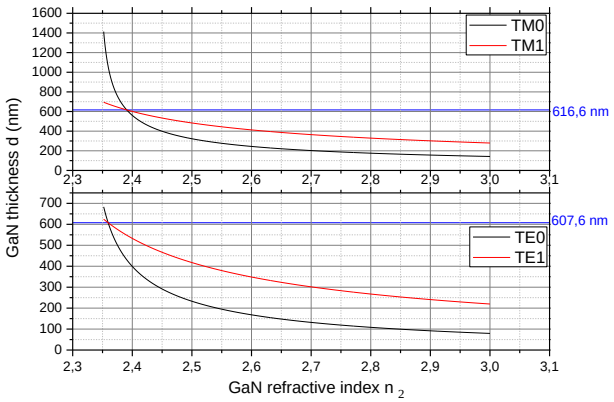


Figure. 2. Numerical calculation of GaN thickness using experimentally obtained effective refractive index.

[1] M. Gromovyi *et al.*, *Opt. Express*, 2017, doi: 10.1364/oe.25.023035.
[2] A. W. Bruch, *et al.*, *Appl. Phys. Lett.*, 2015, doi: 10.1063/1.4933093.
[3] I. Roland *et al.*, *Opt. Express*, 2016, doi: 10.1364/oe.24.009602.

CRUSHED PERLITE AS A MICROSTRUCTURAL FILLER FOR SUPERHYDROPHOBIC COATINGS

Denys Baklan[1], Oleksiy Myronyuk[1], Jia Zilong[1]

[1] Department of Chemical Technology of Composite Materials, Faculty of Chemical Technology, National Technical University of Ukraine "Igor Sikorsky Kyiv Polytechnic Institute", Kyiv, Ukraine
d.baklan@kpi.ua

Superhydrophobic coatings are not widely used due to high cost, difficulties in scaling and low mechanical resistance. The way to solve these problems is to use the conventional application methods that are used for organic paints (brush, roller or airspray coating) to facilitate scalability and the use of components that can reduce the cost [1]. This approach involves the use of fillers - materials in the form of particles with the desired particle shape, or it can be materials treated to obtain water-repellent properties. Nanoparticles are good candidates, but they have low mechanical resistance, so they can be combined with microtextured particles [2]. Lamellar particles can minimize the contact area of a water droplet with a substrate. Such particles can be mica, talc, or ground expanded perlite [3].

Expanded Aragats perlite was used in the work. For surface treatment of crushed perlite was found that the most effective agent is polymethylhydrogensiloxane. Styrene-acrylate copolymer was used as a polymeric binder. For the water contact angle is the ratio of polymer and filler: when the polymer content is more than 50 wt. % and more than 40 wt. % for untreated and treated perlite, respectively, the Cassie steady state is achieved. More than 140 degrees water contact angle has been achieved. When crushed, expanded perlite has a large internal volume that acts as an air gap to maintain Cassie's condition. The mechanical wear resistance of the coatings was determined by sand test (average particle size 350 μm) and results shown on Fig.1. The value of the contact angle with water does not depend on the thickness and does not drop significantly during the test due to the high wear resistance of the siloxane layer on the surface of the particles.

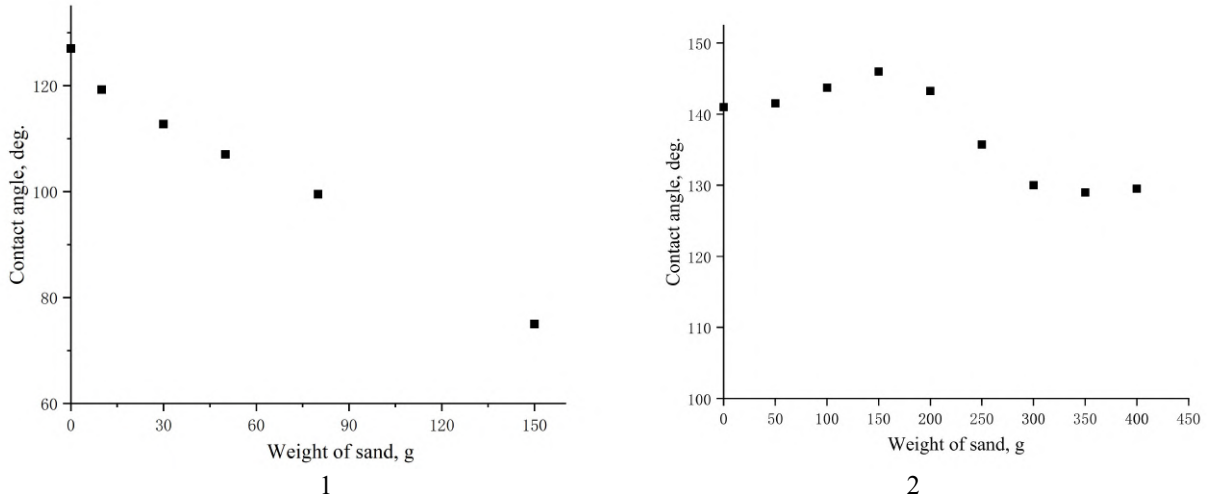


Fig. 1. Contact angles after wear resistance testing: 1 – Initial crushed perlite; 2 – polymethylhydrogensiloxane treated crushed perlite.

After grinding and treatment with polymethylhydrogensiloxane, expanded perlite can be used as a filler for superhydrophobic coatings due to various particle shapes from flat to irregular. As a result, the coatings have porosity, which as a result provides high values of water contact angle after mechanical wearing. These coatings can be considered as a base layer for creating hierarchical superhydrophobic coatings.

[1] Shadmani, S., Khodaei, M., Chen, X., & Li, H. (2020). Superhydrophobicity through coatings prepared by chemical methods. Superhydrophobic Surfaces - Fabrications to Practical Applications. https://doi.org/10.5772/intechopen.92626

[2] Hu, W.-H., Yang, D.-Q., & Sacher, E. (2018). Improving the mechanical durability of superhydrophobic coating by deposition onto a mesh structure. Materials Research Express, 5(6), 065521. https://doi.org/10.1088/2053-1591/aacc7b

[3] Assessment of using secondary raw materials from sunflower oil production as a compound of elastomeric compositions. (2019). Voprosy Khimii i Khimicheskoi Tekhnologii, (2), 99–105. https://doi.org/10.32434/0321-4095-2019-123-2-99-105

THE LUMINISCENT PROPERTIES OF ZnS:Mn THIN FILMS

Agnese Spustaka[1*], Ernests Einbergs[1], Donāts Millers[1], Edgars Vanags[1]

[1] Institute of Solid State Physics, Univeristy of Latvia, Latvia
agnese.spustaka@cfi.lu.lv

The thin films are promising for sensors development. The development of sensors for mechanical stress monitoring is an actual topi. Possible solution is the appropriate luminescent sensor based on thin films. Several materials are showing luminescence changes under mechanical interaction, this phenomenon is known as mechanoluminescence (ML). Within known set of ML materials the $SrAl_2O_4$:Eu,Dy [1] and ZnS:Mn [2] attract attention due to relatively intensive and stable ML. Therefore the ZnS:Mn films on metal substrates were prepared via magnetron sputtering process. The luminescence centres in ML and photoluminescence as well in radioluminescence are the same, however the mechanisms of the luminescence centres excited states creation are different. Thus, the data obtained in the study of prepared thin films luminescence, structure and morphology is a good base for estimation of film applicability for sensor.

Investigation of sputtering parameters influence on thin films radioluminescence and photoluminescence properties as well as on structure and morphology was carried out. The results obtained were compared with those for targets used for sputtering. It was found the structure and luminescent properties of films are almost independent on the power of magnetron as well as on time for film fabrication. The comparison of ZnS:Mn films photoluminescence and radioluminescence spectra reveals difference. The photoluminescence was excited by 266 nm photons, which are in the range of ZnS fundamental absorption. Therefore, the thin surface layers of films are excited and luminescence spectra were strongly affected by surface states. The difference between radioluminescence and photoluminescence spectra indicated the surfaces of films are defect rich. The intensities of films luminescence were significantly reduced in comparison with that from powders. The origin of luminescence intensity reduction could be structure of sputtered films – it is close to amorphous, the additional information was obtained from SEM data – well resolved crystallites were not find. The polycrystalline or even single crystalline films could show more intense luminescence and could be more appropriate for mechanical stress sensors. The study of polycrystalline thin films obtainment is in progress.

[1] P. Jha, A. Khare, $SrAl_2O_4$:Eu,Dy mechanoluminescent flexible film for impact sensors, Journal of Alloys and Compounds **847**, 156428 (2020).
[2] Y. Deng, J. Wei et al., Enhancing the mechanoluminescence of traditional ZnS:Mn phosphors via Li^+ Co-doping, Journal of Luminescence, **225**, 117364 (2020).

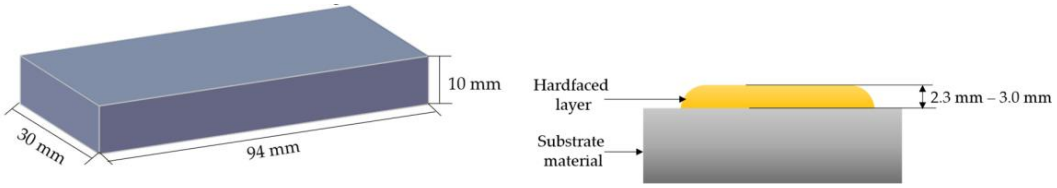
HARDFACING OF MILD STEEL WITH WEAR-RESISTANT NI-BASED POWDERS CONTAINING WC PARTICLES USING PPTAW TECHNOLOGY

Augustine Nana Sekyi Appiah[1*], Oktawian Bialas[1], Marcelina Jedrzejczyk[2], Natalia Ciemamala[2], Lucja Wantuch[2], Marcin Zuk[3], Artur Czuprynski[3], Marcin Adamiak[1]

[1] Laboratory of Materials Research, Faculty of Mechanical Engineering, Silesian University of Technology, Gliwice, Poland
[2] Student of the Faculty of Mechanical Engineering, Silesian University of Technology, Gliwice, Poland
[3] Chair of Welding, Faculty of Mechanical Engineering, Silesian University of Technology, Gliwice, Poland
augustine.appiah@polsl.pl

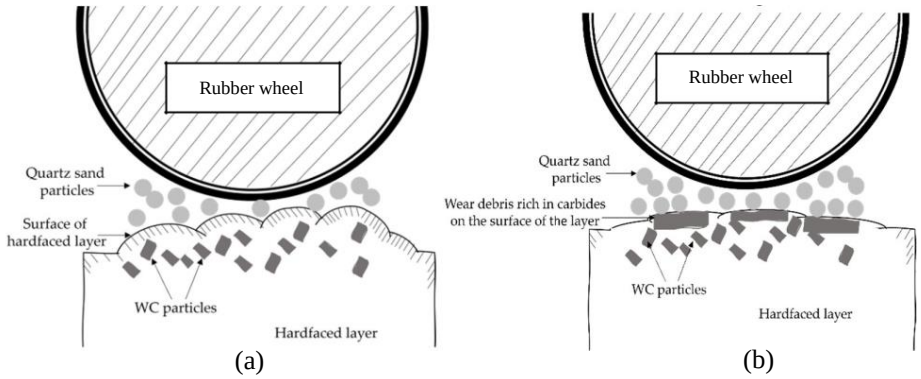
In this study, the technology of powder plasma transferred arc welding (PPTAW) was used to improve upon the wear resistance and hardness of mild steel, by deposition of hardfaced layers composed of Ni-based powders reinforced with tungsten carbide (WC) particles. Two Ni-based metal matrix composite (MMC) powders were used; PG, with a composition of NiSiB + 60wt% WC, and PE, with a composition of NiCrSiB + 45wt%WC. PPTAW process parameters - plasma gas flow rate (PGFR) and plasma transferred arc (PTA) current were varied in the preparation of the hardfaced layers onto the surface of the substrate mild steel, with eight (8) samples prepared. Schematic diagrams of the prepared samples with dimensions are shown in Fig. 1. The surface hardness of the prepared hardfaced layers was estimated to be in the range of 46.3 – 48 HRC for PG powder samples, and 52.7 – 58.3 HRC for PE powder samples. Microhardness of the Ni-based matrix was in the range of 573.3 – 893.0 HV, and the WC reinforcement had microhardness in the range of 2128.7 – 2436.3 HV. The relative abrasive wear resistance of the as-deposited layers was investigated against the performance of abrasive wear resistant steel, Hardox 400, which has an approximate nominal hardness of 400 HV.

It was concluded from this study that the use of Cr as an alloying element enhanced the hardness and wear resistance. Increasing the PGFR increased the hardness and wear resistance of the layers, alongside an increase in the number of surface cracks. Increasing the PTA current reduced the wear resistance, but improved the hardness, alongside a reduction in the number of surface cracks. The wear mechanism is illustrated in Fig. 2.



(a) (b)

Fig. 1. Schematic illustration of experimental samples (a) dimensions of the prepared mild steel plate to be used as a substrate material (b) cross-section of the final material after deposition of the hardfaced layer onto the substrate material, showing the range of thicknesses of the hardfaced layers for the various samples.



(a) (b)

Fig. 2. Abrasive-wear mechanism of hardfaced layers (a) onset of wear, rubber wheel and quartz sand in contact with the surface of hardfaced layers. Immediate surface is free of WC particles (b) final stage of wear, rubber wheel and quartz sand have worn off WC particle-free surface and now in contact with wear debris rich in carbides, reducing wear. [1].

[1] A. Bansal, S. Zafar, and A. K. Sharma, Microstructure and abrasive wear performance of Ni-WC composite microwave clad, J. Mater. Eng. Perform.**24**, 3708–3716 (2015).

HOT STAMPING AND VIBRATION BASED INNOVATIVE MICROSTRUCTURE FORMATION TECHNOLOGY

Justas Ciganas[1], Giedrius Janušas[1]

[1] Department of Mechanical Engineering, Kaunas University of Technology, Lithuania
justas.ciganas@ktu.lt

Traditionally, the formation of microstructures is divided into stamping, photolithography, material removal, and deposition [1]. Combining different technologies can create an innovative and better-performing production method. The aim of this work is to improve hot stamping technology by using vibration. Vibration should improve hot stamping shape reproduction and high geometry filling at lower loads and temperatures [2].

Magnetostrictor actuator is the main device used in this application. Vibrations are generated by using the variable magnetic field and the magnetostrictive material [3]. The forming tool is heated by a ferromagnetic shunt and Eddy current. Vibration and heating can be controlled by three main parameters: frequency, voltage and current. In addition, the intensity of the deformations will be adjustable with an additional magnetization coil. Due to localized heating, it was decided to use a coolant to protect the magnetic coils. The results obtained from the simulations can be seen in Figure 1.

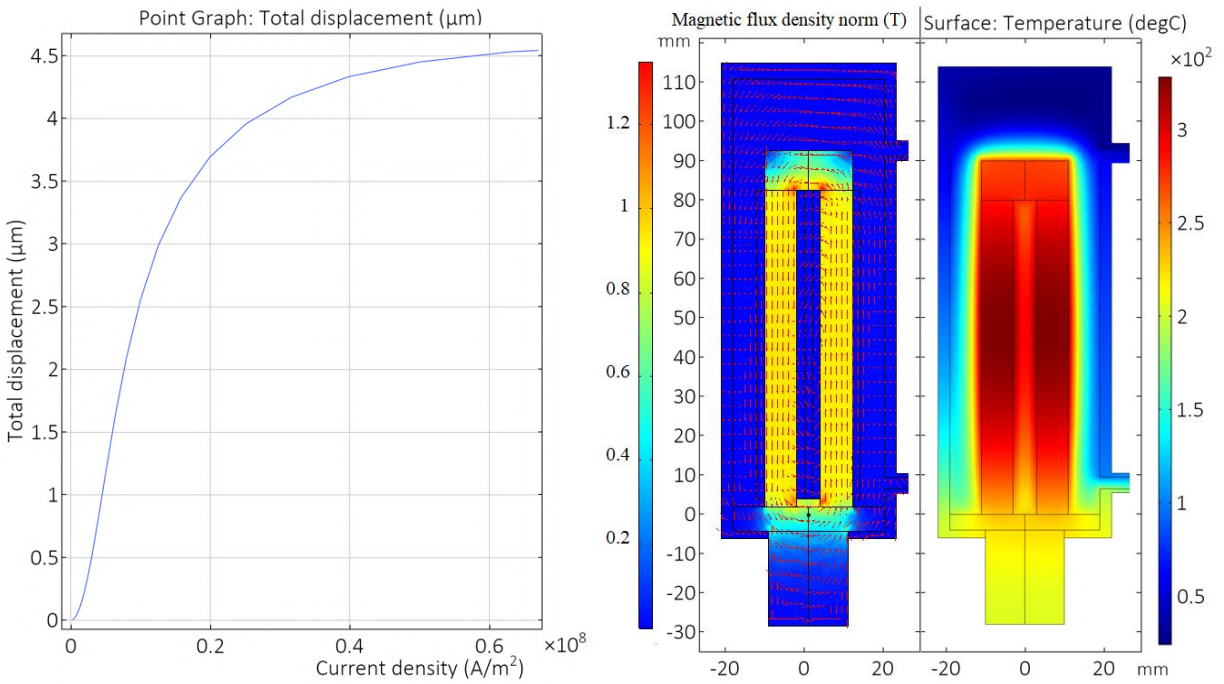


Fig. 1. Magnetostrictive deformations of the drive, the intensity of the magnetic field and the temperature curve.

Simulations show that at 1 tesla magnetic intensity, we can expect a temperature of about 200° C and a deformation of 4.5 μm. In Figure 1, it can be seen that the magnetostrictive material heats up even more, but due to intensive cooling its temperature does not rise above 320° C. The obtained results will be useful for further development of the technology and will be compared with experimental results.

Acknowledgements

This research was funded by a grant No. 0.1.2.2-CPVA-K-703-03-0015 “Development of new technology for the formation of microstructures in functional materials” from the European Regional Development Fund.

[1] Yu ChangKimab and Joo H.Kanga, Microfluidic biomechanical device for compressive cell stimulation and lysis, Sensors and Actuators B: Chemical **128**, 108-116, (2007)
[2] Gracious Ngaile and Cristina Bunget, Influence of ultrasonic vibration on microforming,, Materials Science, (2008)
[3] Zhihua Wang and odher, Dynamics Compensation and Rapid Resonance Identification in Ultrasonic-Vibration-Assisted Microforming Syste Using Magnetostrictive Actuator, IEEE/ASME Transactions on Mechatronics, 16, 489-497, (2011)

BIMETALLIC STRUCTURE FORMATION BY LASER ADDITIVE MANUFACTURING

Ada Steponavičiūtė, Aušra Selskienė, Ričardas Petkus, Karolis Stravinskas

Department of Laser Technologies, Center for Physical Sciences and Technology, Lithuania
ada.steponaviciute@ftmc.lt

Bimetallic structures are an excellent solution for a lot of engineering applications which require varying properties at different locations of the same object. Implementation of such structures into engineering fields can lead to easier maintenance, economical and space savings and can also open wider application possibilities [1].

In recent years, production of bimetallic structures has been made possible with help of additive manufacturing (AM) technologies. Using laser powder-bed fusion AM, bimetallic structures can be created by depositing different materials in a layer-by layer fashion.

In this work, two materials in powder form were used for bimetallic structure formation – 17-4 PH stainless-steel and CoCr. According to SEM-EDS results, the two materials consist of 73.8 at. % Fe, 16.0 at. % Cr, 4.6 at. % Ni, 4.2 at. % Cu and 61.8 at. % Co, 29.4 at. % Cr, 6.9 at. % Mo accordingly. Particle size distribution is similar for both materials and is in the range of 10-80 μm.

The bimetallic structure (Fig. 1) was successfully produced by using the direct metal laser sintering (DMLS) technology applied in EOSINT M280 machine.

In-depth analysis of the 17-4 PH SS and CoCr materials and microstructural properties of the produced bimetallic sample were investigated and will be presented in this work.

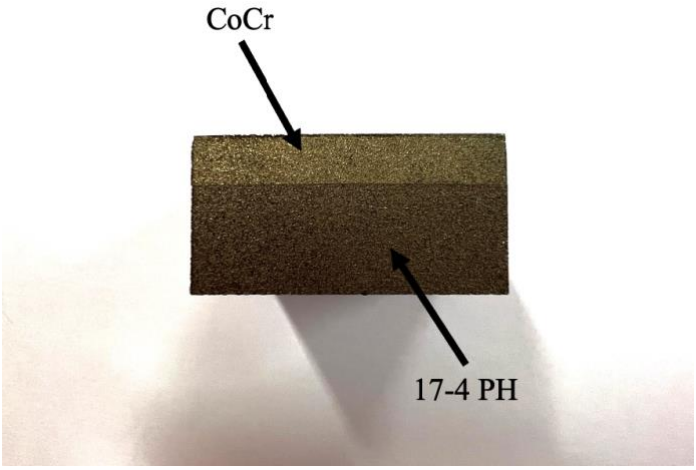


Fig. 1. Bimetallic CoCr and 17-4 PH SS structure.

[1] H. Sahasrabudhe, R. Harrison, C. Carpenter, A. Bandyopadhyay, Stainless steel to titanium bimetallic structure using LENS™, Additive Manufacturing 5, 1-8 (2015).

INVESTIGATION OF POWDER FLOW FOR METAL DEPOSITION NOZZLE

Romuald Petkevič[1], Giedrius Jočbalis[2], Sergejus Borodinas[2], Genrik Mordas[1]

[1] Department of Laser Technologies, Center for Physical Sciences and Technology, Vilnius, Lithuania
[2]Faculty of Civil Engineering, Vilnius Gediminas Technical University, Vilnius, Lithuania
romuald.petkevic@ftmc.lt

Metal additive manufacturing has been at the top of attention for the past few decades, and it offers a variety of technologies for three-dimensional object production. One of such technologies, allowing large-sized object production, is laser-assisted metal deposition, the limits of which are determined by the capabilities of the positioning system. The already existing nozzles have either a relatively low build rate or a poor resolution [1,2].

The goal of this work is to develop a centered particle beam at high velocity for the laser-assisted new nozzle with metal additive manufacturing technologies. Scientific challenges are addressed at the fluid dynamics of two nozzles based on the de Laval geometry with Witoszynski and Bicubic curves [3,4] of convergence zone, the particle-substrate contact and tracking of the thermodynamic state during contact.

De Laval nozzles consist of four parts, namely the straight part, the convergent part, the throat and the spread part (Figure 1). The flow of compressed gas has a high degree of turbulence, which is not conducive to gas shrinkage in the convergent section of the nozzle. Therefore, a straight section is established in front of the convergent part of the nozzle to ensure an even distribution of the flow inlet velocity.

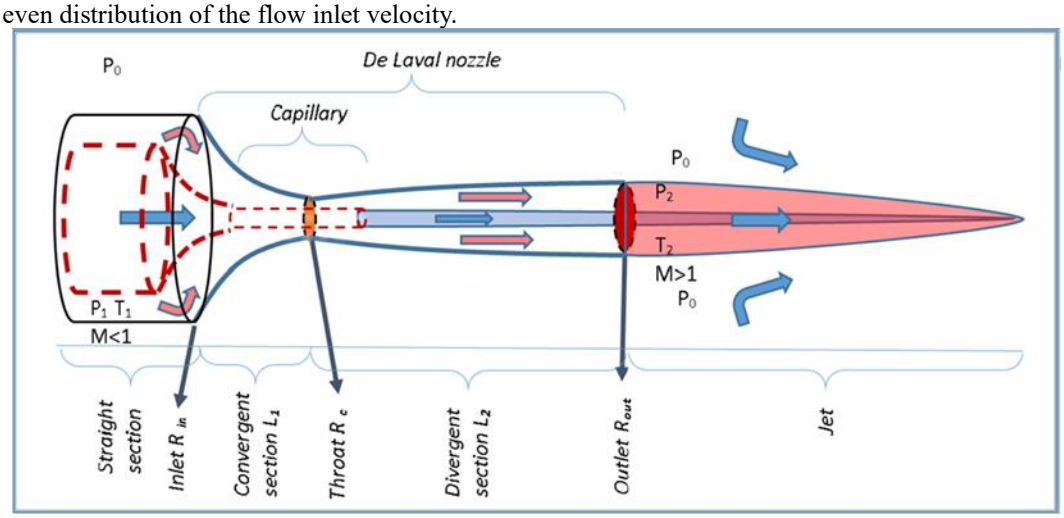


Fig. 1 Measurement setup of the metal powder nozzle.

Fluid dynamics investigation results showed average flow velocity in Bicubic outlet curve nozzle is around 615 m/s and in Witoszynski - 435 m/s. Studies of particle beam formation for the Bicubic curve geometry revealed that small particles have the highest velocity and the lowest total force at the nozzle outlet. Fine particles have a shorter response time, and therefore a smaller dispersion area.

The elasto-plastic particle-surface contact showed that particles of diameter limited up to 3 μm are able to reach experimentally obtained critical velocity without additional heating. Wherein, for particle sizes above 10 μm additional heating is needed for deposition. The maximum coefficient of restitution is achieved with a particle size of 30 μm, smaller particles are characterized by the values of coefficient of restitution which are lower due to a relatively high velocity. Particles larger than 30 μm are scalable, characterized by a small change in velocity and a rise in temperature as their mass in-creases.

The numerical simulation results showed that the suggested a centered particle beam at high velocity based on Bicubic curve geometry of metal deposition nozzle has potential abilities of effective particle deposition.

[1] Huang, Y.; Khamesee, M. B.; Toyserkani, E. A Comprehensive Analytical Model for Laser Powder-Fed Additive Manufacturing. Additive Manufacturing 2016, 12, 90–99. https://doi.org/10.1016/J.ADDMA.2016.07.001.
[2] He, Y.; Wei, J.; Liu, J.; Wang, X.; Wang, Y.; He, L. Experimental Study on the Fabrication Profile and Mechanical Properties by Substrate-Inclined Angle Using Laser Melting Deposition (LMD) Integrating with the Substrate of Stainless Steel. Optics & Laser Technology 2020, 125, 106038. https://doi.org/10.1016/J.OPTLASTEC.2019.106038.
[3] Chen, J.; Jiang, W.; Han, C.; Liu, Y. Numerical Study on the Influence of Supersonic Nozzle Structure on the Swirling Condensation Characteristics of CO2. Journal of Natural Gas Science and Engineering 2021, 88. https://doi.org/10.1016/J.JNGSE.2020.103753.
[4] Liu, Y.; Zhang, J.; Wei, J.; Liu, X. Optimum Structure of a Laval Nozzle for an Abrasive Air Jet Based on Nozzle Pressure Ratio. Powder Technology 2020, 364, 343–362. https://doi.org/10.1016/J.POWTEC.2020.01.086.

FEATURES INFLUENCE OF THE PHYSICAL fIELDS ON THE STRUCTURE AND PHYSICAL PROPERTIES OF POLYMER MATERIALS WITH METAL OXIDES

Yuliia Bardadym[1], Edward Sporyagin[2]

[1] Department of polymer modification, Institute of Macromolecular Chemistry of the NAS of Ukraine, Ukraine
[2] Department of Chemical Technology of Macromolecular Compounds, Oles Honchar Dnipro National University, Ukraine
yuliia.bardadym@gmail.com

Epoxy resins are an important thermoset class, as well as a popular matrix in advanced composites. They have a wide application field, e.g. in composites for the aviation industry, or in electronics as encapsulation or coating materials, or as glues. Of key importance for the mentioned applications are the epoxies good thermal, mechanical and dielectric properties, their resistance to corrosion and low shrinkage upon cure. Their properties can be further improved by incorporation of co-monomers or additives, which enhance the epoxies thermal stability, adhesion to various surfaces, toughness, flexibility, corrosion resistance or which introduce new properties like flame retardancy or electrical conductivity [1].

Polymer modifications are intended to impute different, typically desired properties to the new modified material properties such as enhanced thermal stability, strength, ductility, compatibility or degradability, flexibility, rigidity, melting and glass-transition temperatures etc. Physical modification is a directed change in the physical properties of polymers carried out by the transformation of their supramolecular structure under the influence of physical influences. Physical modification is a simpler and more economical method of obtaining new materials than the synthesis of new polymers. Physical modification of polymers arises under the influence of various force fields (mechanical, electrical, magnetic, etc.).

The present work aims to explore the influence of the external permanent magnetic or electric fields on the structure, thermophysical, dielectric properties of epoxy polymers and their composites with metal oxide.

Samples of nanocomposites were formed from epoxy resin ED-20 and triethylenetetramine. Stoichiometric ratio was 1 mole of epoxy resin to 0,18 mole triethylenetetramine. Powder CdO, PbO, Cr_2O_3 and polyaniline (PAn) were used as fillers. The content of metal oxide was 3 vol. %. Samples of nanocomposites were subjected to curing with different conditions. The influence of constant magnetic field was $2 \cdot 10^5$ A/m. All curing processes were done at 293 – 297 K for 24 hours. Then all polymeric samples were carried out temperature stabilization at 333 ± 2 K for 24 hours. Studies of the structure, thermophysical, thermomechanical and dielectric properties of composites filled with diamagnetic or paramagnetic metal oxides formed under the influence of external constant physical field were carried.

Studies of the specific heat capacity of epoxy polymers and their composites depending on the composition and curing conditions have been carried out. In this case, the introduction of fillers into the composition of the epoxy composite contributes to a decrease in the specific heat and an increase in the glass transition temperature for the studied composites. This is explained by an increase in the packing density macrochains and free volume of epoxy polymer (EP). The glass transition temperature increases by 5 K for samples containing CdO, PbO and Cr_2O_3 and PAn, and decreases by 15 K for samples filled with cadmium oxide and by 7 K for samples containing CdO and PAn.

The introduction of fillers causes an increase in dynamic modulus of elasticity, but a slight decline after the influence of constant physical fields. As a result of the use of external physical fields allows to change the relative deformation of the studied filled epoxy composite materials from 5% to 15%.

For samples of EP – CdO, which was formed under the action of external constant physical fields, are decrease in the destruction temperature by 50 K, the total amount of gaseous products recorded in the mass spectrum to 87 units and 18% of the total ion current. However, EP – PbO is characterized by an increase in the temperature of decomposition maxima and up to 13.8% of the total ion current. The impact of physical fields on the EC - Cr_2O_3 provokes a decrease in the total ion current by 25%, the specific intensity of ion fragments up to 20%. The introduction of polyaniline into the composition of the filler leads to a significant decrease in the temperature of the maximum release of volatile components [2].

[1] B. Mossety-Leszczak, B. Strachota et al., The orientation-enhancing effect of diphenyl aluminum phosphate nanorods in a liquid-crystalline epoxy matrix ordered by magnetic field, European Polymer Journal 72, 238 – 255 (2015).

[2] Y. Bardadym, E. Sporyagin, The Influence of the Physical Fields on the Structure and Physical Properties Nanocomposites, 2018 IEEE 8th International Conference Nanomaterials: Application & Properties (NAP), ISSN 978-1-5386-5334-0, Zatoka, Ukraine, 1-5 (2018).

CALIBRATION OF PIXEL DETECTOR PROTOTYPES FOR THE PHASE-2 CMS INNER TRACKER UPGRADE

Marijus Ambrozas[1], Stefano Mersi[2]

[1] Faculty of Physics, Vilnius University, Lithuania
[2]CERN, Switzerland
marijus.ambrozas@ff.stud.vu.lt

The Large Hadron Collider (LHC) at CERN will undergo a massive upgrade in the years 2025-2027 and will change its name to High Luminosity LHC (HL-LHC). The goal of the upgrade is to increase the luminosity ten times compared to the nominal luminosity of the LHC. This is done in order to increase the discovery potential by producing more collisions that may allow physicists to observe extremely rare events.

The HL-LHC upgrade comes with significant challenges for detector builders. The increase in luminosity means much higher radiation damage to the detector material. The number of simultaneous proton collisions during the crossing of the proton bunches will also increase tenfold, to an average pile-up of 200 [1], which means that the current detector granularity would not be enough to separate all the tracks emerging from collision points. The Phase-2 upgrade of the CMS detector, which will be carried out at the same time as the HL-LHC upgrade, will aim to cope with these difficulties.

A completely new tracker (the innermost layer of CMS) is getting prepared for the CMS Phase-2 upgrade. It will consist of two main parts: the Inner and the Outer Tracker. The Inner Tracker, consisting of silicon pixel detectors, will have 6 times smaller pixels than the current one, and the number of its forward disks will grow to 12 in place of the current 3, which will bring the total number of pixels to about 2 billion. It will feature a radiation-hard frontend chip, the RD53, which is being developed in collaboration between CMS and ATLAS experiments and will be able to handle such data transmission rates. On top of that, a new, dedicated data acquisition system is being developed for use with both Inner and Outer Tracker [2].

The preparation for the Phase-2 upgrade of the CMS Inner Tracker is well underway and functional prototypes are already being tested and optimized. Some of the ongoing prototype testing activities and their results will be presented during the talk.

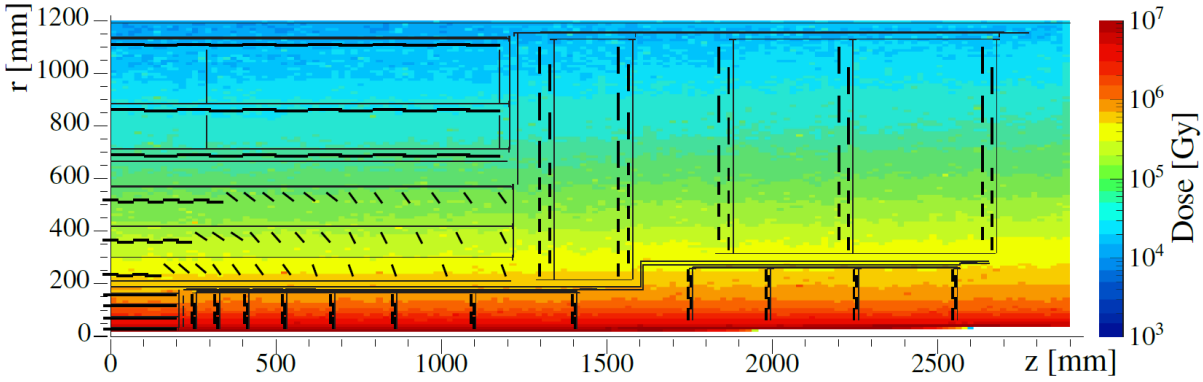


Fig. 1. Expected total ionizing dose for the Phase-2 CMS tracker, expressed in Gy. The simulated estimate corresponds to the integrated luminosity of 3000 fb^{-1} of proton-proton collisions at 14 TeV center-of-mass energy [2].

[1] O. Aberle, I. Béjar Alonso, O. Brüning et al., High-Luminosity Large Hadron Collider (HL-LHC): Technical design report, CERN-2020-010 (2020).
[2] CMS Collaboration, The Phase-2 Upgrade of the CMS Tracker, CMS-TDR-014 (2017).

MODELING AND DEPOSITION OF ANTIREFLECTIVE COATINGS FOR III-V MULTI-JUNCTION SOLAR CELLS USING ATOMIC LAYER DEPOSITION

Mantas Drazdys[1], Darija Astrauskytė[1], Ramutis Drazdys[1], Tadas Paulauskas[2]

[1]Microoptical Components Laboratory, Center for Physical Sciences and Technology, Lithuania
[2]Optoelectronics Technology Laboratory, Center for Physical Sciences and Technology, Lithuania
mantas.drazdys@ftmc.lt

Multi-junction solar cells composed of group III-V semiconductor alloys are widely employed in space and concentrated-sun photovoltaic applications. For the devices to achieve high power conversion efficiency, the reflection losses must be minimized over a wide 400 – 1600 nm spectral range in which they typically operate. Therefore, the design and deposition techniques of antireflection coatings (ARC) play an important role.

Atomic layer deposition (ALD) is a branch of chemical vapour deposition (CVD) techniques and is a promising chemical coating technology. In ALD, when depositing dielectric films, substrates are cyclically exposed to gaseous precursors which react in a self-limiting manner. This cyclic process prevents precursors from reacting in the gas phase and limits the reaction to the surface. The surface-limited ALD reactions allow for controlling of film thickness within a sub-nanometer range. Due to these characteristics, deposited coatings are highly conformal and have been extensively used for the protection of electronic devices in open atmospheric conditions [1].

The optical design of an ARC typically uses a sequence of layers with high and low refractive indices. For a low refractive index material, Al_2O_3 can be used since ALD thermal deposition of Al_2O_3 is well known and does not require a complex reactor design [2]. Silicon dioxide (SiO_2) may also be employed as a low refractive index material and can be advantageous in a triple layer ARC design to minimize reflection losses over a wide spectral range. However, due to the nature of silicon precursors, the deposition of SiO_2 using a thermal process, where oxidant is water, is not sufficient [3]. In this case, a combination of thermal and plasma enhanced ALD may be necessary to deposit SiO_2.

In this work, two different antireflective coatings were deposited on GaAs and AlGaAs subcells and a fused silica (FS) glass. The first coating was deposited using exclusively thermal ALD and consisted of two layers – TiO_2 and Al_2O_3. The second coating was deposited using a combination of thermal and plasma enhanced ALD and consisted of three layers: Al_2O_3 (thermal), HfO_2 (thermal), and SiO_2 (plasma enhanced). Here, we present optical coating modelling and deposition results, including reflection spectra, surface morphology, and photovoltaic characteristics comparison of the cells with different coatings.

[1] S. M. George, Atomic Layer Deposition: An Overview, Chem. Rev. **110**, 111-131 (2010).
[2] D. Riihelä et al., Introduction atomic layer epitaxy for the deposition of optical thin films, Thin Solid Films **289**, 250-255 (1996).
[3] B. B. Burton et al., SiO_2 Atomic Layer Deposition Using Tris(dimethylamino)silane and Hydrogen Peroxide Studied by in Situ Transmission FTIR Spectroscopy, J. Phys. Chem. **113**, 8249-8257 (2009).

PASSIVATION OF THE HYDROGEN-TERMINATED DIAMOND SURFACE WITH ORGANIC MATERIALS

Tomas Grigaitis, Karolis Bacevičius

Institute of Chemical Physics, Vilnius University, Lithuania
tomas.grigaitis@ff.vu.lt

Focus of the researchers on diamond electronics has been intensified, when it was demonstrated that C-H bonds are formed on diamond surface after treatment with hydrogen plasma. This treatment creates conductive surface known as H-terminated surface. H-terminated surface creates two dimensional hole gas (2DHG) with carriers mobility of 30 - 200 (cm2/V·s) and carrier density of the order of 1013 (cm^{-2}) [1]. A number of devices, based on this principle, already have been produced. However, the 2DHG surface is not stable chemically and conductivity depends on the environment.

When diamond is terminated by hydrogen, C–H bond at the terminated surface creates a dipole layer that induces a negative electron affinity χ. The transfer of electrons from the diamond valence band into the accepting state of an appropriate adsorbate layer on the diamond surface gives rise to subsurface hole accumulation and p‑type surface conductivity [2]. This phenomena is also known as "surface transfer doping" and it is not limited to just atmospheric adsorbate molecules.

We demonstrate the influence of newly synthesized organic materials on electrical properties of H-terminated diamond surface. The charge transfer from diamond to organic acceptor layer is ensured by the selection of organic materials with as low as -3.52 eV and -4.48 eV LUMO (lowest unoccupied molecular orbit) energetic levels (Fig. 1).

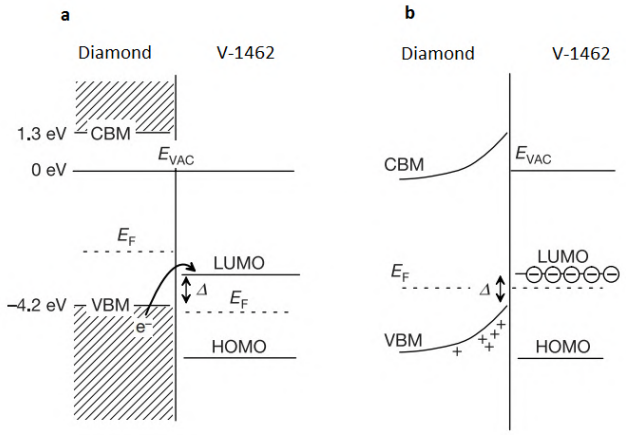


Fig. 1. Schematic representation of the surface transfer doping of intrinsic diamond by V-1462 organic material. a, Level scheme before electron transfer from the diamond. b, Band bending in chemical equilibrium

[1] J. H. C. Wort, R. S. Balmer, Diamond as an electronic material, Materials Today, Vol. 11, Issues 1–2, 22-28 (2008).
[2] M. I. Landstrass, Hydrogen passivation of electrically active defects in diamond, Appl. Phys. Lett. **55**, 1391-1393 (1989).

EYE TRACKER CALIBRATION FOR THE ASSESSMENT OF MULTI-PLANE DISPLAY'S USER EXPERIENCE

Linda Krauze, Tatjana Pladere, Vita Konosonoka, Gunta Krumina

Department of Optometry and Vision Science, Faculty of Physics, Mathematics and Optometry, University of Latvia, Latvia
linda.krauze@lu.lv

The objective assessment of user experience for innovative three-dimensional (3D) visualization systems, such as multi-plane volumetric displays [1], requires the adoption of the methods that were previously used only for flat-panel monitors. Eye tracking has been widely used in user experience research as it allows to elucidate which parts of images attract visual attention. It should be noted that the accuracy of analysis of eye movements depends on the accuracy of eye tracker calibration. Therefore, to make a calibration software for the multi-plane display, the factors that may significantly affect the accuracy of obtained data should be assessed.

Optimization of the calibration process is an essential part of the study, especially when 3D images are displayed on several planes of the screen. Calibration for one display plane takes about 20 to 30 seconds. As the multi-plane display contains 20 planes and calibration is performed for each of them, the total calibration time can reach 7-10 minutes. If the calibration fails, the process must be repeated. It can lead to subject's fatigue and decrease of motivation. Therefore, it is important to elucidate whether there is a possibility to calibrate eye tracker for one plane, and to obtain sufficiently accurate data for planes which are located closer or further away from the calibration plane.

The aim of the study was to evaluate the effect of calibration stimulus and viewing distance on gaze parameters using the EyeLink 1000 Plus eye tracker. The task of subjects was to follow the stimulus that appeared at different positions on the flat-panel display in two calibration conditions: 1) the distances of calibration planes and the ones of stimulus planes coincided, 2) the calibration was performed at a distance of 70 cm, but the stimuli were shown per 1 cm closer or farther away from the calibration plane. Motivated by [2], four types of stimuli were demonstrated at five positions on the screen.

As a result, no considerable effect of stimulus geometrical shape on the accuracy of eye tracker calibration was revealed. The gaze parameters changed significantly depending on the location of calibration plane only for some positions on the screen. The research results are important to be taken into consideration when making the calibration software for the novel 3D image displays with several depth planes. The study has shown that by calibrating the eye tracker for one depth plane, eye movements may be assessed with a certain accuracy for the depth planes which are 1 cm closer or further away from the calibration plane.

The authors acknowledge the support from the Latvian Council of Science project "Development of guidelines for evaluating the visual effectiveness and ergonomics of innovative 3D displays" (No. lzp-2021/1-0399).

---

[1] Osmanis, K., Valters, G., Zabels, R., Gertners, U., Osmanis, I., Kalnins, L., Kandere, U., Ozols, A., Advanced multiplanar volumetric 3d display. *Proceedings of SPIE*, 10555, Article No. 1055510, 1-13 (2018).
[2] Thaler, L., Schütz, A.C., Goodale, M.A., & Gegenfurtner, K.R., What is the best fixation target? The effect of target shape on stability of fixational eye movements. *Vision Research*, 76, 31-42 (2013).

PHOTORHEOMETRICAL STUDY OF VANILLIN ACRYLATE-BASED PHOTORESINS

Justinas Jaras[1], Aukse Navaruckiene[1], Jolita Ostrauskaite[1]

[1] Department of Polymer Chemistry and Technology, Kaunas University of Technology, Lithuania
justinas.jaras@ktu.edu

Vanillin can be extracted from vanilla orchids or obtained by chemical modification of lignin. Vanillin produced by chemical modification of lignin is considered natural vanillin and is 250 times cheaper than synthetic vanillin. Due to the aromatic structure, it could be able to replace widely used petroleum-based aromatic monomers [1]. Recently, vanillin and its derivatives have attracted a great deal of attention as renewable building blocks for high-performance polymers mainly due to their rigid aromatic structures [2].

In this study, commercially available vanillin derivatives were used in photoresins to find efficient photocurable systems for the production of cross-linked polymers with excellent mechanical properties. Real-time photorheometry was used to monitor the evolution of the photocross-linking process. As an example, the dependencies of the storage modulus G ‘, the loss modulus G’, loss factor tanδ, and the complex viscosity η* of the vanillin-based resin on the irradiation time are presented in Figure 1. When resin irradiation started, the values of storage modulus G', loss modulus G’, and complex viscosity η* started to increase, indicating the beginning of the cross-linking process. The onset of the gelation process is described as the gel point (t_{gel}), that is, the point at which the G' and G" modulus curves intersect is defined as [3]. As the resin irradiation of the resin proceeded with time, the values of G', G" modulus, and η* continued to increase due to gel aging and settled down in a steady state, indicating the end of the cross-linking process. All vanillin-based resins investigated in this study showed similar behavior. The dependence of the addition of various comonomers and their concentration in the photoresin composition on the photocuring kinetics and rheological characteristics was investigated.

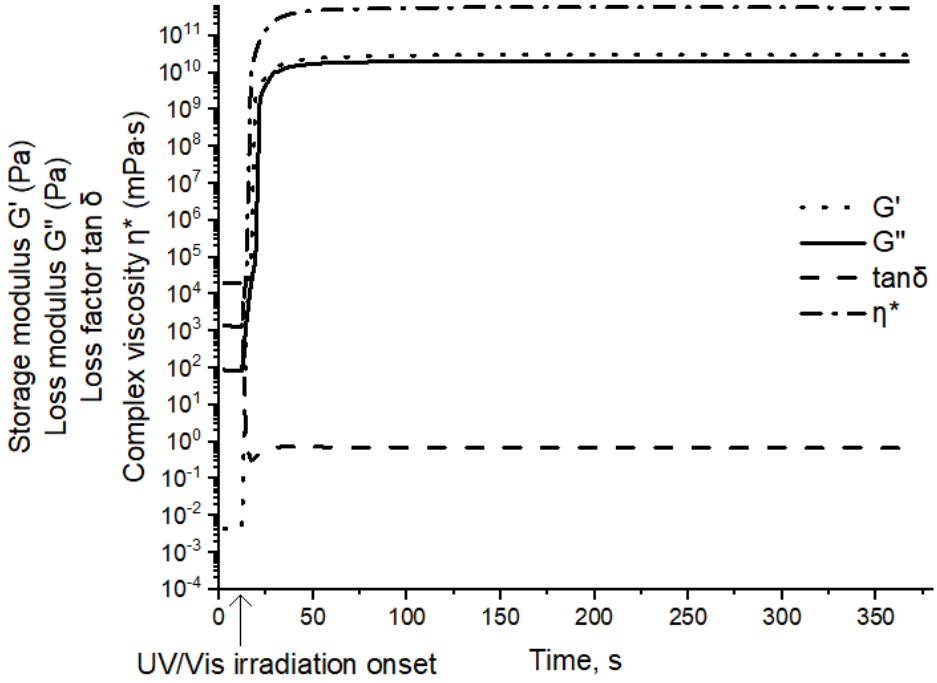


Fig. 1. Dependencies of storage modulus G', loss modulus G", loss factor tan δ, and complex viscosity η* of the vanillin-based resin on irradiation time.

Acknowledgement. This research was funded by the Research Council of Lithuania (project No. S-MIP-20-17).

[1] R. Ciriminna, A. Fidalgo, F. Meneguzz, F. Parrino, L.M. Ilharco, M. Pagliaro, Vanillin: the case for greener production driven by sustainability megatrend. ChemistryOpen, **8**, 660–667 (2019).
[2] J.F. Stanzione, J.P. Sadler, J.J La Scala, K.H. Reno, R.P. Wool, Vanillin-based resin for use in composite applications. Green Chemistry, **14**, 2346-2352 (2012).
[3] T. G. Mezger, The Rheology Handbook, 3rd ed. (Vincentz Network, Hanover, 2011)

EXFOLIATION OF GAN THIN FILMS GROWN BY MOVPE VIA GRAPHENE

Dominykas Augulis[1], Kazimieras Badokas[1], Arūnas Kadys[1], Benjaminas Šebeka[2], Ilja Ignatjev[1,2], Jūras Mickevičius[1] and Tadas Malinauskas[1]

[1] Institute of Photonics and Nanotechnology, Vilnius University, Vilnius LT-10257, Lithuania
[2] Center for Physical Sciences and Technology, Vilnius LT-10257, Lithuania
dominykas.augulis@ff.stud.vu.lt

Group III nitride technology has been investigated extensively during the last decades, especially after the creation of the first blue LED. Nitrides have exceptional photonic and electronic properties. For example, gallium nitride (GaN) has a direct band gap which is equal to approximately 3.4 eV [1]. Thus, it can be used as a detector and emitter in the blue region of the visible light spectrum and as a key element in high power transistors. Also, GaN has a more niche application in the biosensing sphere due to outstanding chemical stability and transparency for specific radiation, which enables easy optical readout [2]. For practical application, GaN has to have superb quality and the ability to chemically bond with foreign substrates.

Nitrides are usually grown epitaxially on foreign substrates such as sapphire. The problem of the growth process on foreign substrates is that it deteriorates crystalline quality due to induced stress in the grown material. The stress appears because of the lattice constant and thermal expansion differences between substrate and epilayer. Nearly stress-free GaN can be grown on native substrates or by remote epitaxy via two-dimensional material. In the latter epitaxy, GaN epilayer is formed by its interaction with the GaN substrate through a two-dimensional material such as graphene. The seeding effect of the substrate enables high quality GaN growth through interlayer, while the weak van der Waals interaction facilitates subsequent layer release, reduces grown layer strain and enables the reuse of an expensive substrate [3]. Important aspect of this technology is flexibility of inorganic released layers from graphene due to relatively small thicknesses.

In this work, we investigate the lift-off process of GaN that was grown by remote epitaxy. Before the lift-off process, GaN growth on graphene by MOVPE was studied and afterwards GaN exfoliation was performed by an electrochemically deposited Ni stressor. To enhance adhesion between Ni and the GaN epilayer, Ti and Au metal films were coated by two techniques: electron-beam evaporation or magnetron sputtering. We managed to exfoliate GaN from the growth substrate, on which Ti and Au were deposited by electron beam evaporation. X-ray energy dispersive spectroscopy (EDX) results showed that the GaN film was exfoliated together with stressor metal layers (Fig. 1). After the lift-off procedure, XRD and Raman shift measurements of the exfoliated membrane were conducted. The strain of the released GaN membrane was calculated. Results showed that GaN experienced tensile stress in a direction and compressive stress in c direction.

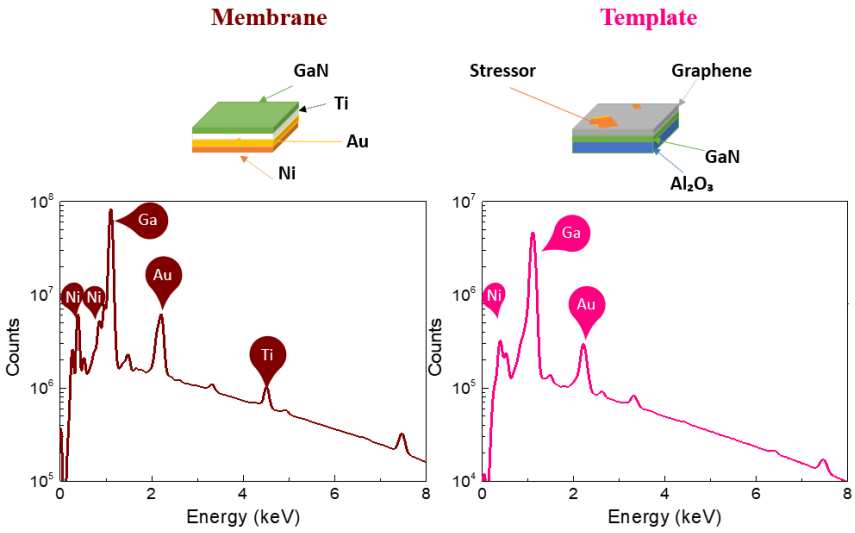


Fig. 1. EDX spectra of released GaN membrane and growth substrate.

[1] C. Koughia, S. Kasap, P. Capper, Springer Handbook of Electronic and Photonic Materials (Springer-Verlag, Berlin, Heidelberg, 2007).

[2] C. Gergely, Nitride devices and their biofunctionalization for biosensing applications, III Nitride Semiconductors and their Modern Devices 505–518 (2014).

[3] K. Badokas, A. Kadys, J. Mickevicius, I. Ignatjev, M. Skapas, S. Stanionytė, E. Radiunas, G. Juška, T. Malinauskas, Remote epitaxy of GaN via graphene on GaN/sapphire templates, Journal of Physics D: Applied Physics 54 (2021).

INVESTIGATION OF LEDS AND THEIR MODULATION CIRCUIT FOR VISUAL LIGHT COMMUNICATIONS

Paulius Sakalauskas, Pranciškus Vitta

Vilnius university, Faculty of Physics, Institute of Photonics and Nanotechnology,
Saulėtekio av. 3, LT-10257, Vilnius
paulius.sakalauskas@ff.stud.vu.lt

Visual Light Communication (VLC) is a promising and emerging technology employing visible light modulation for high-speed data transfer. Although visual light communications dates back to the end of 19th century, this technology received more attention in last 20 years in particular after invention of high-power Light-Emitting Diodes (LEDs). This communication is immune to electromagnetic interference, safe to use and environment-friendly. Considering the fact that VLC technology has no electromagnetic pollution, it can be applied to medical appliances, aircrafts, industrial control and other radio frequency sensitive areas. While lasers are used for a long-distance communication, the data transfer rates up to several Gbit/s at short distances could be achieved by LEDs.

Here we present a short study of simple LED modulation circuit based on high-speed and high-power operational amplifier (LM7171). Modulation frequency throughput of the circuitry and sample LEDs was measured as the most important parameter for high-speed data transfer. In addition, electrical and optical properties of the LEDs were investigated separately.

We conclude that high brightness LEDs can be modulated at tenths of MHz with such a simple circuitry and could be applied for the data transfer at tenths of Mbit/s rate. On the other hand, high-power LEDs exhibited much lower modulation cut-off frequencies.

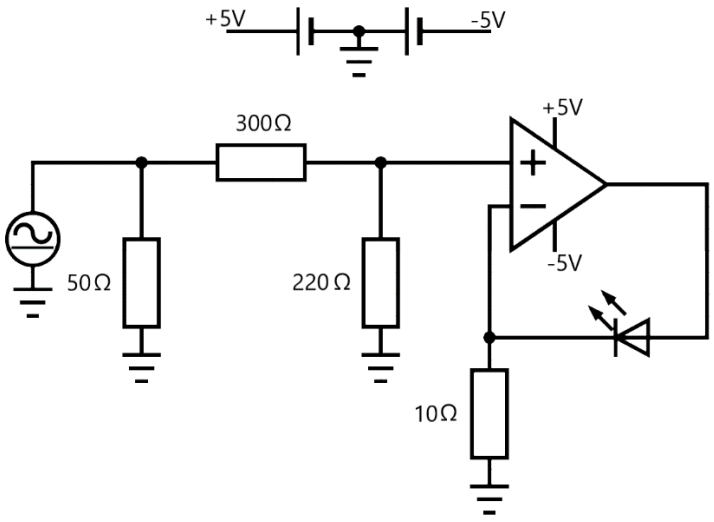


Fig 1. Circuit diagram of LED modulator.

Keywords: VLC, LED.

THE PROBLEM OF WATER LOSS OF ALGINATE HYDROGELS: A LITERATURE REVIEW AND AN INTRODUCTION TO OWN RESEARCH

Maria J. Skrodzka[1], Magdalena B. Łabowska[1]

[1] Department of Mechanics, Materials and Biomedical Engineering, Faculty of Mechanical Engineering, Wroclaw University of Science and Technology, Poland
marysiaskrodzka@gmail.com

The presentation is aimed at discussing the problem of water loss of alginate hydrogels. The current state of knowledge on hydrogel drying, as well as future, prospective research directions are indicated.

Alginate hydrogels consist of a three-dimensional network of polymer chains and water filling the space between the macromolecules. A characteristic feature of hydrogels is the ability to swell and retain a significant amount of water in their structure. Because of their biocompatibility, alginate hydrogels are used in the biomedical industry as bioinks in additive technologies, drug carriers, and tissue engineering [1-2].

Due to the high water content of hydrogels, they are exposed to water loss e.g., during storage or during the manufacturing elements in additive technologies. The loss of water affects the properties of hydrogels, which may result in limiting their potential applications.

Ongoing research is focusing mainly on analyzing the effects of alginate hydrogel additives such as other polymers to limit the effects of water loss [3-4].

The plan of own research includes the investigation of the influence of material additives (such as: gelatin and methylcellulose) and the conditions of storage of alginate hydrogels (increased humidity and reduced temperature) on the drying kinetics and mechanical properties of rehydrated after drying hydrogels. The mechanical properties of the specimens will be determined by a uniaxial tensile test.

Preliminary studies included a qualitative assessment of alginate hydrogel shrinkage after 24 hours of storage at 4°C (results shown in Figure 1). The first group of alginate hydrogel was prepared by cross-linking sodium alginate with 0.5 M calcium chloride and the second included addition of hydroxymethylcellulose solution and was cross-linked in the same conditions.

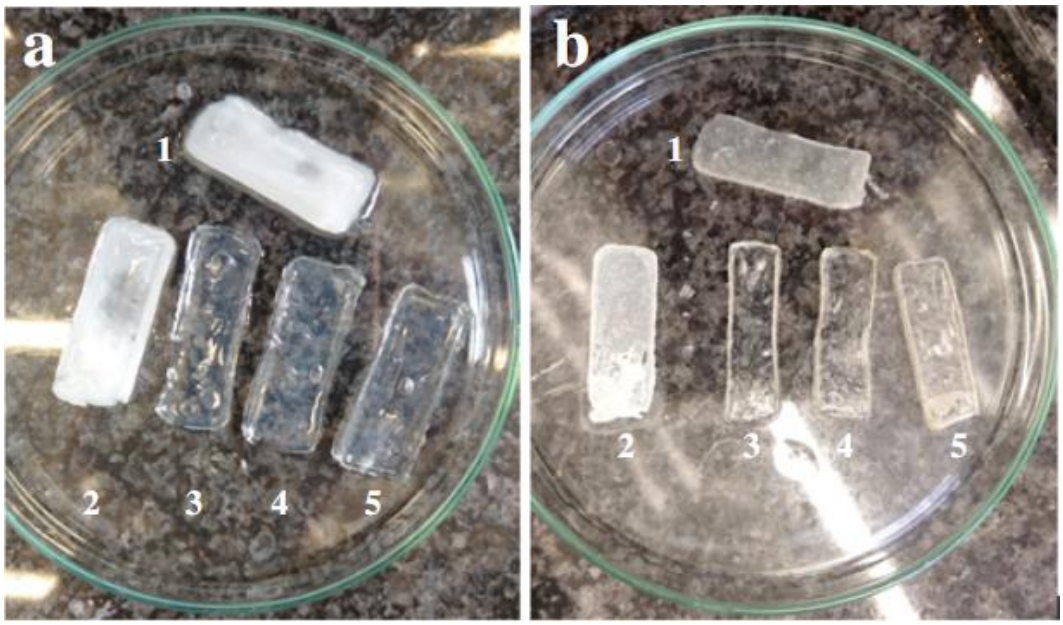


Fig. 1 Alginate (3-5) and hydroxymethylcellulose-alginate (1-2) hydrogels: a) before drying b) after 24h drying

[1] Ahmed, E. M. (2015). Hydrogel: Preparation, characterization, and applications: A review. *Journal of advanced research*, *6*(2), 105-121.
[2] Malda, J., Visser, J., Melchels, F. P., Jüngst, T., Hennink, W. E., Dhert, W. J., ... & Hutmacher, D. W. (2013). 25th anniversary article: engineering hydrogels for biofabrication. *Advanced materials*, *25*(36), 5011-5028.
[3] Naghieh, S., Sarker, M. D., Sharma, N. K., Barhoumi, Z., & Chen, X. (2020). Printability of 3D printed hydrogel scaffolds: Influence of hydrogel composition and printing parameters. *Applied Sciences*, *10*(1), 292.
[4] Fang, Y., Li, L., Vreeker, R., Yao, X., Wang, J., Ma, Q., ... & Phillips, G. O. (2011). Rehydration of dried alginate gel beads: Effect of the presence of gelatin and gum arabic. *Carbohydrate polymers*, *86*(3), 1145-1150.

P3-23

DID NOT PARTICIPATE

.

RADIO FREQUENCY ENERGY HARVESTER

Justina Žemgulytė[1], Paulius Ragulis[1], Gediminas Šlekas[1], Romualdas Trusovas[2], Karolis Ratautas[2], Rimantas Simniškis[1], Žilvinas Kancleris[1], Gediminas Račiukaitis[2]

[1] Department of Physical Technologies, Center for Physical Sciences and Technology, Lithuania
[2] Department of Laser Technologies, Center for Physical Sciences and Technology, Lithuania
justina.zemgulyte@ftmc.lt

Improper disposal of heavy metals and chemicals used in the battery manufacturing process highly contributes to the pollution of the environment, solution to that could be ambient energy harvesters. For a long time, our ability to harvest energy from natural sources on a small scale was limited due to inefficient electronic components and lack of power storing options, but nowadays availability of ultra-low barrier radio frequency (RF) diodes, and specialized chipsets enables us to develop highly efficient harvesters.

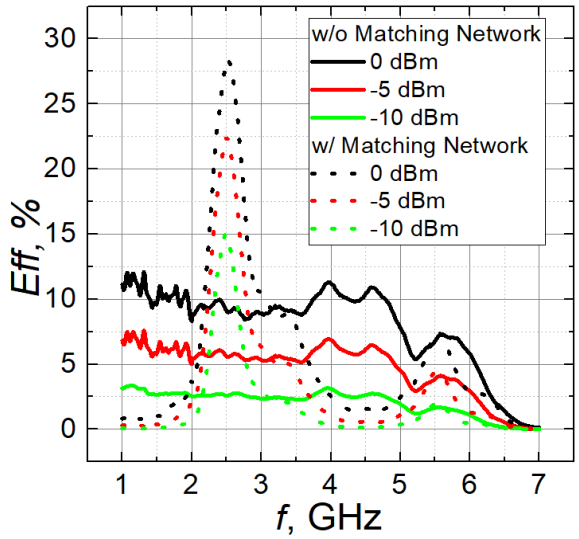


Fig. 1. Full-wave rectifier efficiency when input power is 0 dBm, -5 dBm and -10 dBm, with matching network (dashed line) and without matching network (solid line)

In this paper, we are investigating RF energy harvesting in Wi-Fi band to power one sensor wireless network without using batteries. The energy harvesting system consists of an RF power source, antenna, matching network, rectifier, and power managing system. Due to the growing number of wireless signals like Wi-Fi networks and mobile phones, RF energy is widely available. However, it suffers from low energy density due to free space path loss. To reach higher efficiency multiple antenna arrays could be used.

We chose to use a dual-band (2.45 GHz and 5.1 GHz) patch antenna for this project due to its low directivity and relatively simple manufacturing process. At first, we modeled it using finite-difference time-domain (FDTD) method, then etched the pattern of the antenna on a plate of Rogers RT5880 with a laser cutting machine.

The rectifier transforms the power collected by antenna into DC current. We're considering a few rectifier topologies (Cockcroft, half-wave rectifier, full-wave rectifier) to find the most optimal variant between efficiency and power conversion. To ensure maximum power transfer, the impedance of antenna and rectifier is matched using an impedance matching network. Using RF generator, full-wave rectifier efficiency was measured when input power is 0 dBm, -5 dBm, and -10 dBm (Fig. 1). According to our results full-wave rectifier with matching network has efficiency of 14.4% at 2.4 GHz when input power is -10 dBm, which is low. Due to poor matching and losses in diodes efficiency at 5.5 GHz is even lower (0.19 %).

We think, that half-wave rectifier (Fig. 2) is a better solution for low power, because diodes are the major source of power loss and this topology uses only one. Half-wave rectifier will be investigated in our further work.

For power managing, we use the BQ25570 evaluation board. It can harvest microwatts of power from high impedance sources using the MPPT algorithm and has a regulated output to power a microcontroller. To store harvested power, we use a 1 F supercapacitor. In preliminary testing with a full-wave rectifier, we measure that our system can fully charge a supercapacitor (from 0 to 4 V) in 10 hours when the antenna is positioned 1 meter from the source and is fed by 20 dBm of power.

One day harvesting energy from the ambient sources will replace the need for batteries in low-power electronic devices. For now, our job is to find a way to make RF harvesting system more efficient and able to periodically power one sensor network.

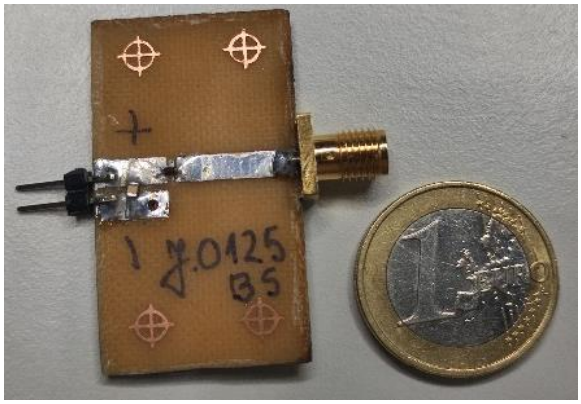


Fig. 2. Half-wave rectifier without matching network

[1] Tran, LG., Cha, HK. & Park, WT. RF power harvesting: a review on designing methodologies and applications. Micro and Nano Syst Lett 5, 14 (2017). https://doi.org/10.1186/s40486-017-0051-0

FLUORESCENCE DYNAMICS OF TRANS-STILBENE DUE TO THE PRESENCE OF AGGREGATES

Gabrielė Kareivaitė[1], Renata Karpič[1], Martynas Skapas[2], Mindaugas Mačernis[2], Darius Abramavičius[2], Leonas Valkūnas[1,2]

[1]Center for Physical Sciences and Technology, Saulėtekio al. 3, Vilnius, Lithuania
[2] Institute of Chemical Physics, Faculty of Physics, Vilnius University, Saulėtekio al. 3, Vilnius, Lithuania
gabriele.kareivaite@ff.stud.vu.lt

Stilbene is a diarylethene group compound, that has aromatic groups bonded to the carbon – carbon double bond. This group compounds are known due to their sensitivity, therefore they are suitable for molecular switches or sensors [1]. Because of this property, stilbenes are already applied for ionized radiation detectors [2]. However, the main characteristic of stilbene is reversible *cis – trans* isomerisation. That makes stilbene a great model for molecular rotary motors [3]. During isomerisation, there is a twisting of phenyl rings around single carbon – carbon bond in stilbene molecule. The potential energy dependence on the twisting angle between two phenyl rings indicates the potential minimum at 90° twist. Moreover, it shows that isomerisation from the trans to cis form is more complicated due to the existing barrier in first excited state [1].

In this study, we determined fluorescence spectra of heterostructured *trans*-stilbene and its films in polystyrene matrix with different concentrations. The samples were made by using a spin-coating technique. Steady – state photoluminescence spectra and its decay kinetics were measured using a time-correlated single photon counting spectrophotometer. For sample excitation picosecond pulsed laser diode EPLED – 300 was used.

Although there is no isomerisation of *trans*–stilbene in polystyrene matrix, by varying the concentration, aggregates may cause the changes of spectroscopic properties. The increase of *trans*–stilbene concentration resulted in the red shift and broadening of fluorescence spectral bands (Fig.1). At low concentrations, spectral bands are narrow due to the excitation of separated molecules. The increase of concentration results in the creation of dimers and leads to shorter relaxation times.

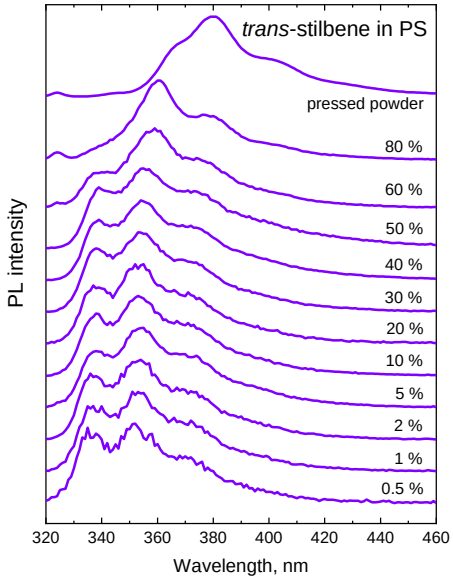


Fig. 1. Photoluminescence spectra of *trans*–stilbene films in PS matrix with different concentrations.

[1] D. H. Waldeck, Chem. Rev., 1991, 91, 415-436
[2] S. K. Lee, Prog. Nuclear Sci. Techn., 2011, 292-295.
[3] F. Liu, J. Am. Chem. Soc. 2012, 134, 10, 4864–4876

P3-26

DID NOT PARTICIPATE

.

$Na_4FeV(PO_4)_3$ –ALTERNATIVE CATHODE FOR AQUEOUS SODIUM ION BATTERIES

Gintarė Gečė[1], Jurgis Pilipavičius[1], Jurga Juodkazytė[1], Linas Vilčiauskas[1]

[1] Center for Physical Sciences and Technology (FTMC), Saulėtekio al. 3, LT-10257 Vilnius, Lithuania
gintare.pleckaityte@ftmc.lt

Aqueous sodium-ion battery (NIB) technology is one of the alternatives to the lithium batteries due to the low cost, abundance of sodium and environmental friendliness. Exploration and development of suitable positive and negative electrode materials are critically important for high-performance of NIBs. Among all polyanionic compounds, phosphates particularly gained a great deal of interest, because of their excellent structural stability due to the strong P-O chemical bond, while compared to sulfates which have low thermal decomposition and high moisture reactivity [1]. The NASICON (Na Super Ionic Conductor) family of phosphates has been extensively studied. Thanks to the excellent tunability of the NASICON type structure, it can accommodate a wide selection of transition metals, e.g. Fe^{3+}, Ti^{3+}, Zr^{3+}, V^{3+} and Mn^{3+}. Indeed several mixed-metal materials have been reported such as $Na_3MnTi(PO_4)_3$ [2], $Na_3MnZr(PO_4)_3$ [3] and $Na_4MnV(PO_4)_3$ [4]. One of alternatives for NIBs cathodes is novel $Na_4FeV(PO_4)_3$ material which has active Fe^{2+}/Fe^{3+} and V^{3+}/V^{4+} redox couples[1,5] and could possibly work not only as cathode but also as symmetrical cathode/anode battery.

In this investigation, we prepared pure phase $Na_4FeV(PO_4)_3$ via solid-state synthesis method using Na_2CO_3, V_2O_3, $FeC_2O_4{\cdot}2H_2O$ and $NH_4H_2PO_4$ precursors. The structure and morphology of prepared materials were characterized by X-ray diffraction, scanning electron microscopy and thermogravimetric analysis. The electrochemical properties of prepared electrodes were investigated by cyclic voltammetry (Fig. 1) and charge/discharge galvanostatic cycling using different aqueous electrolytes.

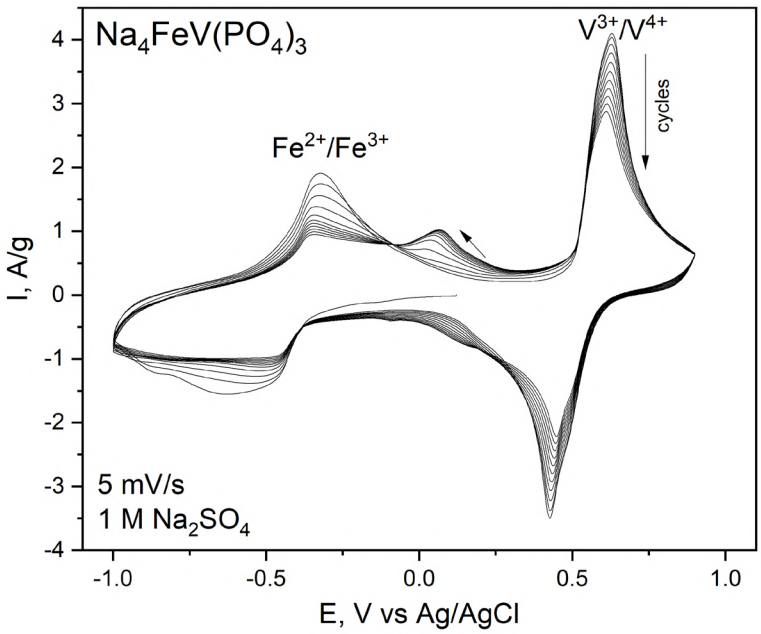


Fig. 1. Cyclic voltammogram of $Na_4FeV(PO_4)_3$ electrode.

Acknowledgements:
This project has received funding from the European Regional Development Fund (Project No. 01.2.2-LMT-K-718-02-0005) under grant agreement with the Research Council of Lithuania (LMTLT).

[1] M. Hadouchi et. al., Fast sodium intercalation in $Na_{3.41}£_{0.59}FeV(PO_4)_3$: A novel sodium-deficient NASICON cathode for sodium-ion batteries, Energy Storage Mater. 35, 192-202 (2021)
[2] G. Snarskis et. al., Peculiarities of Phase Formation in Mn-Based Na SuperIonic Conductor (NaSICon) Systems: The Case of $Na_{1+2x}Mn_xTi_{2-x}(PO_4)_3$ ($0.0 \leq x \leq 1.5$), Chem. Mater. 33, 21, 8394-8403 (2021)
[3] H. Gao et. al., $Na_3MnZr(PO_4)_3$: A High-Voltage Cathode for Sodium Batteries, J. Am. Chem. Soc., 140, 51, 18192-18199 (2018)
[4] W. Zhou et. al., $Na_xMV(PO_4)_3$ (M = Mn, Fe, Ni) Structure and Properties for Sodium Extraction, Nano. Lett.16, 7836-7841 (2016)
[5] S.Park et al., Crystal Structures and Local Environments of NASICON-Type $Na_3FeV(PO_4)_3$ and $Na_4FeV(PO_4)_3$ Positive Electrode Materials for Na-Ion Batteries, Chem. Mater. 33, 5355-5367 (2021)

DEVELOPMENT OF A COMPUTERISED METHODOLOGY FOR THE TREATMENT OF AMBLYOPIA

Kristine Kalnica–Dorosenko[1,2,3], Dzmitry Viarenich[3], Andrei Karol[3], Aliaksei Haraks[3], Artsem Makarau[3], Aliaksandr Katolik[3], Aiga Svede[1]

[1] Department of Optometry and Vision Science, University of Latvia, Latvia
[2] Eye Diseases Clinic, Children's Clinical University Hospital, Latvia
[3]Gameblyo Team, Latvia, Poland, Belarus, The United States of America
kristinekalnica@gmail.com

Amblyopia, or "lazy eye", is reduced vision in one or both eyes that cannot be corrected with glasses, contact lenses, or by surgery [1]. One of the main treatments for amblyopia is to cover the better–seeing eye for a certain period [2], however, this does not contribute to the recovery and development of the binocular functions. New methods are therefore being developed to involve both eyes in the visual process and to stimulate their cooperation. In recent years, computer–based treatments have been developed and introduced, which include video and computer games where the patient's eyes are steadily exercised during the game so that they learn to work together and therefore participate in the visual processes (if possible). New studies have shown that the use of a specialised computer games is an effective method of treating amblyopia, which is more or equally effective than occlusion. Treatment with specialised computer games has been shown to rapidly improve visual acuity and results are stable even after treatment is stopped, as well as improving binocular cooperation, stereovision, contrast sensitivity, eye–hand cooperation, etc. [3, 4, 5].

However, the lack of clarity in the choice of methodology and the parameters of the specialised game/stimulus hampers both the understanding of theoretical knowledge and the design of tests. Amblyopia is the most common cause of visual impairment in childhood. If amblyopia is not successfully treated in childhood, it can cause permanent visual impairment throughout life [6]. The data on the prevalence of amblyopia are alarmingly high and indicate the relevance of the problem not only at the scientific level but also at the societal level (healthcare). The aim of the study was to develop a specialised computer game methodology for amblyopia that describes the effects of different stimuli and their parameters on the visual system in amblyopia.

A game with different difficulty levels was developed as a specialised binocular mobile game for amblyopia. By creating different levels of difficulty to keep the patient's attention, the patient was forced to pay more attention, was motivated to play every day, and thus improved his visual function. Successful use of the specialised mobile game required red–blue glasses, which were given to all participants to take home immediately after the vision test and trial. During the game, the red–blue glasses separated the individual elements of the game – each eye was shown its own stimulus. The game could only be played successfully if the information from both eyes was fused.

The new improved and developed specialised mobile game can improve visual function as effectively as the existing specialised computer games available. In addition, developing new methodologies and improving treatment options for amblyopia is an integral part of public health prevention.

[1] M. W. Rouse, J. S., Cooper, S. A. Cooter et al., *Care of the patient with amblyopia* (American Optometric Association, 2004).
[2] S. E. Loudon, H. J. Simonsz, The history of the treatment of amblyopia, Strabismus **13(2)**, 93–106 (2005).
[3] S. L. Li, R. M. Jost, S. E. Morale et al., A binocular iPad treatment for amblyopic children, Eye **28(10)**, 1246–1253 (2014).
[4] K. R. Kelly, R. M. Jost, L. Dao et al., Binocular iPad game vs patching for treatment of amblyopia in children, JAMA Ophthalmology **134(12)**, 1402–1408 (2016).
[5] P. Žiak, A. Holm, J. Halička et al., Amblyopia treatment of adults with dichoptic training using the virtual reality oculus rift head mounted display preliminary results, BMC Ophthalmology **17(105)**, 1–8 (2017).
[6] M. M. Parks, *Treatment of the sensorial adaptations and amblyopia* (In: Duane TD, editor. Clinical ophthalmology 1(11), 1989).

THE SIGNATURES OF ACHROMATIC RETARDANCE IN MULTILAYER ANISOTROPIC COATINGS

Mantas Slipkauskas[1*], Emanuelis Lazauskas[2], Tomas Tolenis[2,3], Lina Grinevičiūtė[2]

[1] Faculty of Physics, Vilnius University, Lithuania
[2] Center for Physical Sciences and Technology, Savanorių ave. 231, LT-02300, Vilnius, Lithuania
[3] ELI Beamlines, Institute of Physics, The Czech Academy of Sciences, Za Radnicí 835, Dolní Brežany, Czech Republic
[*]mantas.slipkauskas@ff.stud.vu.lt

Waveplates (also known as retarders) are used to manipulate the polarization state of transmitting light without attenuating, deviating, or displacing the beam. They work by using the birefringent property of certain materials to manipulate the polarization state of the transmitted light.

Waveplates can be manufactured in various ways. One of the most popular method is to use birefringent crystal. Such waveplates are popular due to its longevity and possibility to make high quality retarders with exact desired retardance. However, such type of waveplates is difficult to produce and production process is relatively expensive. Furthermore, waveplates can also be manufactured using polymers. However, one of the main drawbacks is that such waveplates are sensitive to temperature changes and it has low laser-induced damage threshold (LIDT), which greatly affects its longevity. Also, polymer waveplates usually have lower retardance accuracy and both types of retarders are usually manufactured for just one particular wavelength [1, 2]. However, in a variety of applications, involving polarized laser light, an achromatic waveplate with particular retardation across a large wavelength range is required. To achieve such achromatism, various strategies to merge numerous crystal waveplates have been employed [3].

Most of these drawbacks can be avoided by forming waveplates using thin film evaporation technologies. Layers formed using glancing angle deposition technique are optically anisotropic, meaning that refractive index depends on the polarization and propagation direction of light which enables manufacturing of thin film waveplates with multiple advantages: elements with diameters exceeding few centimeters can be formed, high variety of materials, such as metal oxides or fluorides, can be chosen for manufacturing [4]. Furthermore, formation of achromatic waveplates on simple fused silica glass was made possible using this technique. One of the main advantage of such retarders is that it can be made by combining not multiple separate crystal waveplates but by precisely selecting anisotropic thin films and aligning their optical axis at optimal angles.

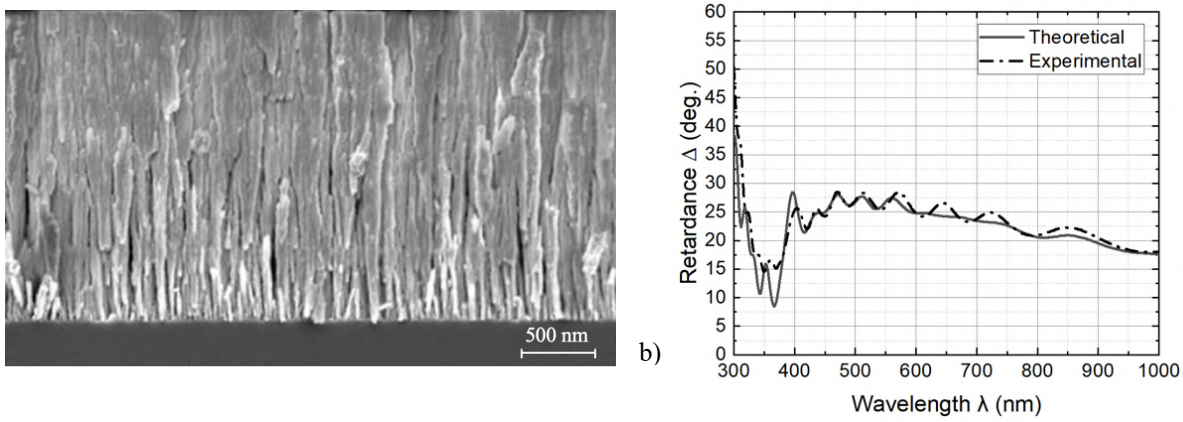


Fig. 1. a) Cross-section SEM image of Ta_2O_5 and HfO_2 λ/4 waveplate and b) the phase retardance dispersion of fabricated Ta_2O_5 and HfO_2 nanostructured coating.

In this work, the set of experiments were conducted to determine the highest anisotropy of Ta_2O_5 layer. The refractive indices of different polarizations were determined for three deposition angles - 65, 70 and 75 degrees. It was found that the highest anisotropy can be reached by depositing Ta_2O_5 layers at 70 degrees. Furthermore, by combining anisotropic and dense layers the theoretical design of achromatic waveplate were achieved and experimentally fabricated. The SEM image was taken (Fig. 1 (a).) and phase retardance dependency on wavelength (Fig. 1(b).) was measured. The initial results where we demonstrate the achromatic properties in the 500 – 700 nm wavelength range was achieved, although further research and development is still needed in order to completely fabricate λ/2 or λ/4 waveplate.

[1] C.K. Ullal, M. Maldovan, E.L. Thomas, G. Chen, Y.-J. Han, S. Yang, "Photonic crystals through holographic lithography: simple cubic, diamond like, and gyroid-like structures", Appl. Phys. Lett. 84 (26) 5434–5436, (2004).
[2] S. Wilbrandt, O. Stenzel, N. Kaiser, "Experimental determination of the refractive index profile of rugate filters based on in situ measurements of transmission spectra",J. Phys. D. Appl. Phys. 40 (5), 1435–1441, (2007)
[3] A. Saha, K. Bhattacharya, A. K. Chakraborty, "Achromatic quarter-wave plate using crystalline quartz", Appl. Opt. 51, 1976-1980, (2012).
[4] T. Motohiro, Y. Taga, "Thin film retardation plate by oblique deposition", Appl. Opt. 13, p. 2466, (1989).

SURFACE MODIFICATION OF POLYTETRAFLUOROETHYLENE (PTFE) POLYMER BY ULTRASHORT PULSE LASER RADIATION TO IMPROVE THE SURFACE ADHESION OF CHEMICALLY DEPOSITED COPPER

Šarūnas Mickus[1], Vytautas Vosylius[1], Evaldas Kvietkauskas[1], Viktorija Vrubliauskaitė[1], Karolis Ratautas[1]

[1]3D Technologies and Robotics Laboratory, Department of Laser Technologies, State research institute Center for Physical Sciences and Technology, Savanorių ave. 231, Vilnius LT-02300, Lithuania.
sarunas.mickus@ff.stud.vu.lt

Our daily lives are packed with number of integrated, functional, and miniaturized devices. The amount of these devices is still increasing therefore high demand for fast and cheap manufacturing methods arise. One of the newer method for molded interconnect devices (MID) [1] production is Selective Surface Activation Induced by Laser (SSAIL) [2,3]. Technology copes with complex 3D surfaces and allows different materials metallization by electroless metal plating. However, several challenges related to selection of optimal surface modification parameters for different surfaces and copper adhesion strength are yet to overcome.

The work is focused on SSAIL process application on high-performance polytetrafluoroethylene (PTFE) [4] polymer as well as its impact on PTFE surface properties. Various surface roughness properties including root mean square height (Sq) and core void volume (Vvc) parameters were thoroughly researched. Sq parameter exhibited no correlation with selective copper deposition on samples whereas Vvc parameter showed a potential connection of surface texture parameter and metallization quality. The successful selective metallization window appeared on the sample areas with Vvc values between 4.75 and 7.85 µm3/µm2 (Fig. 1).

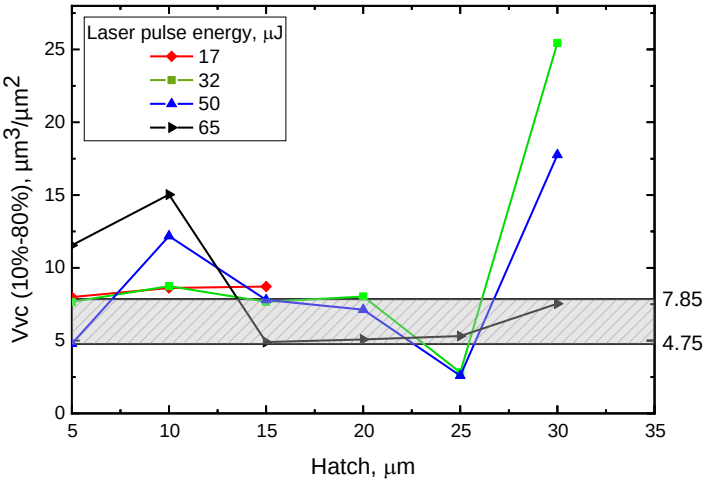


Fig. 1. Core Void Volume (Vvc) dependance on hatch for different laser pulse energies for chemically untreated sample. Shaded area depicts expected Vvc values for good selectiveness. Repetition rate 400 kHz.

The SSAIL method is successfully applicable on PTFE surface. The surface texture parameters correlation with selective copper deposition shows great potential for quick and easy determination of material compatibility with SSAIL process but requires further investigation.

[1] Islam, A., Hansen, H. N. & Giannekas, N. Quality investigation of miniaturized Moulded Interconnect Devices (MIDs) for hearing aid applications. CIRP Ann. 64, 539–544 (2015).
[2] Ratautas, K. et al. Laser-induced selective electroless plating on pc/abs polymer: Minimisation of thermal effects for supreme processing speed. Polymers (Basel). 12, 1–16 (2020).
[3] Ratautas, K., Jagminienė, A., Stankevičienė, I., Norkus, E. & Račiukaitis, G. Laser assisted fabrication of copper traces on dielectrics by electroless plating. Procedia CIRP 74, 367–370 (2018).
[4] Dhanumalayan, E. & Joshi, G. M. Performance properties and applications of polytetrafluoroethylene (PTFE)—a review. Adv. Compos. Hybrid Mater. 1, 247–268 (2018).

THE STUDY OF EMISSION SPECTRUM OF VOLTAGE-CONTROLLED OSCILLATORS

Ieva Morkūnaitė[1], Kęstutis Ikamas[1,3], Dmytro B. But[2], Alvydas Lisauskas[1,2]

[1]Institute of Applied Electrodynamics and Telecommunications, Vilnius University, Vilnius, 10257, Lithuania
[2]CENTERA Laboratories, Institute of High Pressure Physics PAS, Warsaw, 01-142, Poland
[3]General Jonas Žemaitis Military Academy of Lithuania, LT-10322, Vilnius, Lithuania
ieva.morkunaite@ff.stud.vu.lt

Terahertz (THz) frequency electronics is one of the most developing fields of electronics. Terahertz waves fill the frequency range from the loosely defined beginning at 100 GHz up to 10 THz. The expansion of electronics into the THz frequency range is highly regarded nowadays due to the faster data communication and the perspective applicability in many other areas [1]. For example, this frequency range of electromagnetic radiation can be used in security systems - in airports to search for explosives, in medicine to detect cancer cells [1]. Both the good penetration through various dielectric materials as well as non-ionizing energies of THz photons make the radiation in the THz frequency range safe for medical applications [2].

There are different approaches to generate THz radiation using the concepts of the electronic. For example, nonlinearity in the electric circuit can be exploited for frequency multiplication, or the amplifier with positive feedback can be used to create the oscillator. Depending on the nature of amplification and the peculiarities of implementation, various oscillators exist. Whereas the methods of integrated electronics allow the implementation of many different types of oscillators, one architecture – a so-called Colpitts oscillator, gained high popularity for the fabrication of voltage-controlled oscillators for the THz frequency range. The Colpitts oscillator scheme can be transformed into a differential scheme consisting of two transistors and an LC resonant circuit [3]. The differential circuit implementation has several advantages: without increasing the size of the transistors, it allows to add on the power of two oscillators; and it provides a virtual ground along the symmetry axis, which can be used to bias the oscillators [3]. Furthermore, the intrinsic nonlinearity of the employed transistor (either field-effect or a bipolar) allows the efficient frequency multiplication and generation at higher harmonics. This work is therefore devoted to investigations of those higher harmonics.

The device in this study has been implemented in a 130 nm BiCMOS technology with Si/Ge bipolar transistors using a Colpitts architecture (Fig. 1a and 1b). It delivers the maximum power of 500 µW at the first harmonic at 200 GHz. The spectral content of the emission was investigated with a Michelson-type interferometer with a broad-band detector (Golay cell). Fig. 1c (curve 0x Atten.) presents the direct analysis (the amplitude of Fourier transformed autocorrelation signal) of the emitted spectrum with many higher harmonics. The majority of these higher-harmonics are believed to be caused by the reflections in the interferometer, i.e., they are the numerical artifacts of the analysis due to the influence of the back-reflected radiation on the emission strength of the source. Therefore, we employed attenuators that decrease the emitted power as well as minimize the back-coupling by reflections. The results obtained with one and two additional attenuators presented in Fig. 1c support the abovementioned hypothesis. Yet, even two attenuators did not completely suppress the harmonics, leaving the second and third at 396 GHz and 597 GHz. However, to be certain about the origin of spectral peaks at higher harmonics, it is necessary to carry out an additional experiment with resonant detectors.

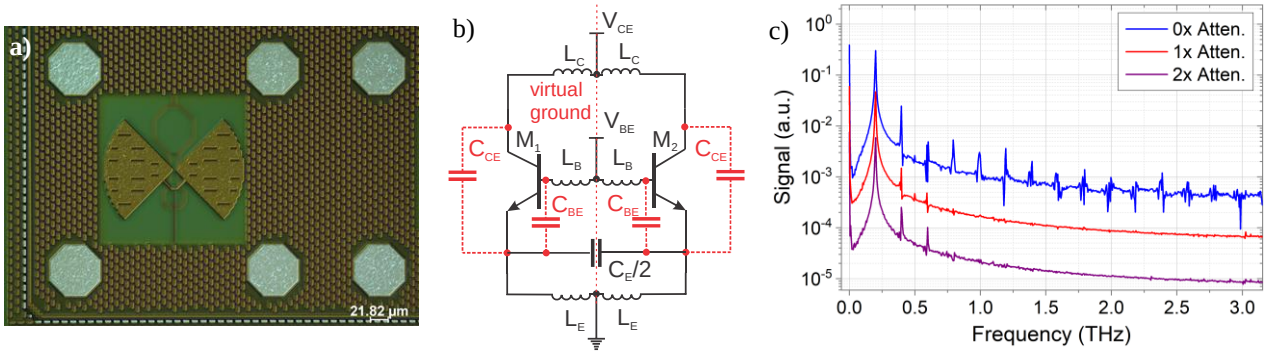


Fig. 1. a) The micrograph of the 130 nm Si/Ge BiCMOS source. b) The proposed VCO is based on the differential configuration of the Colpitts oscillator. c) The measured spectra of the oscillator.

[1] P. U. Jepsen, D. G. Cooke, M. Koch, Terahertz spectroscopy and imaging - Modern techniques and applications. Laser & Photonics Reviews, vol. 5, pp. 124–166, 2011.
[2] U. R. Pfeiffer et al., "Ex Vivo Breast Tumor Identification: Advances Toward a Silicon-Based Terahertz Near-Field Imaging Sensor," IEEE Microwave, vol. 20, no. 9, pp. 32–46, Sep. 2019.
[3]] B. Khamaisi and E. Socher, "A 209–233 ghz frequency source in 90 nm CMOS technology," *IEEE Microwave and Wireless Components Letters*, vol. 22, no. 5, pp. 260–262, 2012.

CALLAGEN BASED SCAFFOLD WITH HYDROXYAPATITE DOPED WITH RUBIDIUM IONS ENHANCES VIABILITY AND FORMING OF CELLULAR NETWORK OF DENTAL PULP STEM CELLS

Nicole Nowak[1,2], Tomasz Gebarowski[2] and Rafal Jakub Wiglusz[1]

[1] Institute of Low Temperature and Structure Research, Polish Academy of Sciences, Okolona St. 2, PL 50-422 Wroclaw, Poland

[2] Department of Department of Biostructure and Animal Physiology, Wroclaw University of Environmental and Life Sciences, Norwida St. 31 PL 50-375 Wroclaw, Poland

n.nowak@intibs.pl

Tissue engineering is a scientific field which binds together biological, chemical and physical sciences. There becomes possible to create new solutions in the treatment and better regeneration of bone, dental, cartilage or even nervous tissue due to the combination of factors such stem cells, biopolymers, ceramics or composite materials The grate biocompatible and bioactive properties but also highly developed specific surface of well-known hydroxyapatite compound gives opportunity to develop apatite based scaffolds for cell anchorage material and improve regeneration of bone tissue[1].

Many research confirmed that rubidium(I) ions have many biological advantages such anti-canter properties, anti-depressant activity [2,3]. In the trace amounts Rb^+ ions are also known to be essential for human bone development [4]. A specific dopant like biological active element such Rb^+ ions can additionally improve biocompatibility of hydroxyapatite based scaffolds and enhance osteoinductive properties towards osteoblasts or dental stem cells. Collagen, the most plentiful protein in extracellular matrix, maintains biological and structural integrity of tissues. Its porous arrangement, low immunogenicity, biocompatible and biodegradable properties but also by its regulation of cell adhesion, proliferation, differentiation seems to be promising biopolymer for scaffold in tissue regeneration processes [5].

In our research the structural and morphological properties of the obtained nanosized hydroxyapatite doped with Rb^+ ions were determined by using XRD (X-ray powder diffraction) and SEM (scanning electron microscopy) techniques. Moreover, it was evaluated biocompatibility toward ram's red blood cells to exclude potential cytotoxic features of our compounds. Experimental *in vitro* bioactive properties of nanocrystalline hydroxyapatite doped with Rb^+ ions by using dental pulp stem cell, were established. To confirm biocompatible features of rubidium ions there was evaluated its best biologically active concentration via viability assay toward dental pulp stem cells. Furthermore, the collagen based scaffold combined with hydroxyapatite doped with 1 mol% Rb^+ ions and dental pulp stem cells was obtained. It was evaluated and observed the proliferation rate and forming of cellular network of dental pulp stem cells in collagen-hydroxyapatite-Rb^+ scaffold. At the end it was discussed in detail a novel approach of obtained biomaterial in the tissue engineering field.

[1] K Szcześ, A., Hołysz, L., & Chibowski, E. (2017). Synthesis of hydroxyapatite for biomedical applications. Advances in Colloid and Interface Science, 249(April), 321–330. https://doi.org/10.1016/j.cis.2017.04.007

[2] Kordjazy, N., Haj-Mirzaian, A., Amiri, S., Ostadhadi, S., Kordjazy, M., Sharifzadeh, M., & Dehpour, A. R. (2015). Elevated level of nitric oxide mediates the anti-depressant effect of rubidium chloride in mice. European Journal of Pharmacology, 762, 411–418. https://doi.org/10.1016/j.ejphar.2015.06.030

[3] Su, Y., Chen, L. J., He, J. R., Yuan, X. J., Cen, Y. L., Su, F. X., Tang, L. Y., Zhang, A. H., Chen, W. Q., Lin, Y., Wang, S. M., & Ren, Z. F. (2011). Urinary rubidium in breast cancers. Clinica Chimica Acta, 412(23–24), 2305–2309. https://doi.org/10.1016/j.cca.2011.08.035

[4] Ouyang, Z., Huang, Q., Liu, B., Wu, H., Liu, T., & Liu, Y. (2019). Rubidium chloride targets JNK/p38-mediated NF-κB activation to attenuate osteoclastogenesis and facilitate osteoblastogenesis. Frontiers in Pharmacology, 10(MAY), 1–12. https://doi.org/10.3389/fphar.2019.00584

[5] Dong C, Lv Y. Application of Collagen Scaffold in Tissue Engineering: Recent Advances and New Perspectives, Polymers (Basel). 2016;8(2):42. Published 2016 Feb 4. doi:10.3390/polym8020042

DETAILED INVESTIGATIONS FROM NANOSCALE TO BULK OF SILVER FILM GROWTH

Ignas Bitinaitis[1], Anna Sytchkova[2], Naglis Kyžas[1], Rimantas Simniškis[1], Ramutis Drazdys[1], Alexandr Belosludtsev[1]

[1]Center for Physical Sciences and Technology, Savanoriu ave. 231, Vilnius,
[2]Optical Coatings Group, ENEA Casaccia, via Anguillarese 301, Rome 00123, Italy
Ignas.Bitinaitis@ftmc.lt

In recent study [1], we compare in-situ transmittance and plasma emission spectra with ex-situ resistance and ellipsometric measurements performed on ultrathin silver films with thicknesses varying from 3 nm through 40 nm and on relatively thick layers up to 100 nm.

We show that the transmittance broadband monitoring (BBM) of the growing silver layer allows for in-situ reliable estimation of the minimum thickness when the film becomes continuous. Moreover, a proper selection of the monitoring wavelength(s) renders the coalescence and percolation stages of the film growth clearly distinguishable.

For our films deposited by magnetron sputtering on fused silica substrates, the minimum thickness when a film becomes continuous was found to be approximately 12 nm. The percolation threshold was determined as approximately 6 nm. The method of selective-wavelength transmittance BBM is practical, intuitive and hence may represent a useful tool enabling high-precision growth of ultrathin silver layers.

Furthermore, we show here for the first time that ellipsometry is sensitive to the metal coalescence development. In particular, the ellipsometric analysis suggests that the percolation of silver sputtered films begins at the top of the growing layer and hence propagates towards the film bottom.

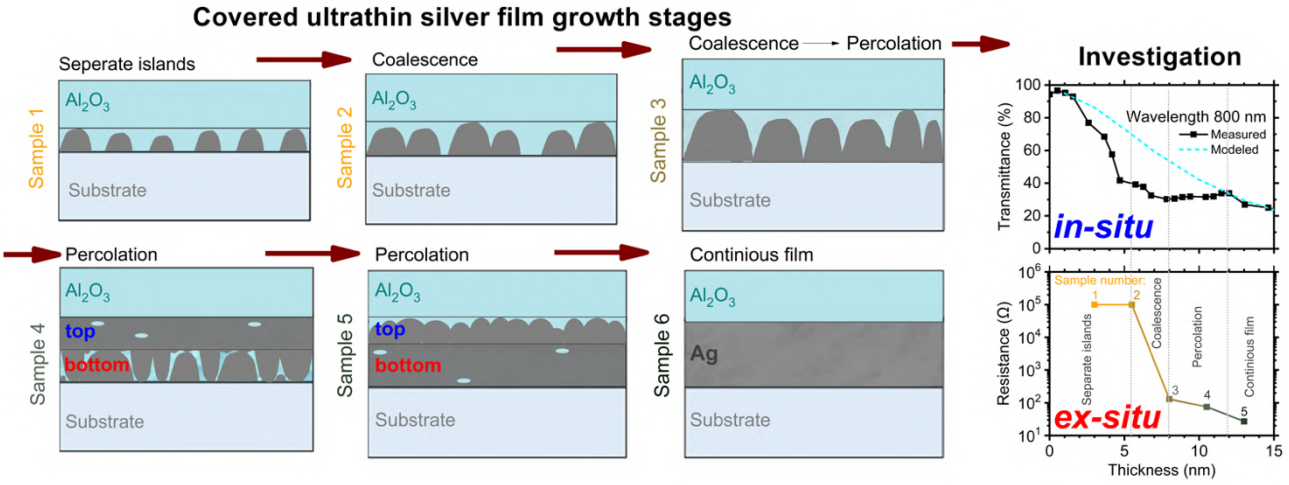


Fig. 1. Schematic of the coating model. Sample 1 – initial seeds; Samples 2 and 3 merging of seeds into bigger particles. Sample 4 – initial percolation as formation of a denser top sub-layer; Sample 5 - percolation proceeds as densification of the bottom sub-layer. The bilayer describing silver film in samples 4 and 5 consists of two effective media. Sample 6 - formation of a continuous silver film, the coating may be considered as a bilayer of flat dense silver and alumina.

Acknowledgement

This work was supported by the European Social Fund (project No 09.3.3.-LMT-K-712-21-0102) under a grant agreement with the Research Council of Lithuania (LMTLT).

[1] A. Belosludtsev, A. Sytchkova, N. Kyžas, I. Bitinaitis, R. Simniškis, R. Drazdys, Vacuum 110669 (2021). doi.org/10.1016/j.vacuum.2021.110669

PHOTOLUMINESCENCE INTENSITY BOOST IN GaAsBi PARABOLIC QUANTUM WELLS

Monika Jokubauskaitė[1], Arnas Pukinskas[1], Evelina Dudutienė[1], Bronislovas Čechavičius[1], Nerijus Jurkūnas[3], Arnas Naujokaitis[2], Martynas Skapas[2], Renata Butkutė[1]

[1] Department of Optoelectronics, Center for Physical Sciences and Technology, Lithuania
[2] Department of Characterisation of Materials Structure, Center for Physical Sciences and Technology, Lithuania
[3]Optonas UAB, Lithuania
monika.jokubauskaite@ftmc.lt

Only few percent of bismuth incorporated in GaAs lattice sufficiently reduces the band gap of the material. Large bowing and energy band gap, less sensitive to temperature, makes bismides an attractive material for the applications of optoelectronic devices in infrared range such as light-emitting diodes [1], photodetectors [2], solar cells [3] etc. However, for the optimization of the devices more efficient quantum structure designs should be obtained. Widely used technique to characterize semiconductor structures and track the progress is photoluminescence (PL) measurements.

One of the recently by our group [4] developed quantum structure designs is GaAsBi quantum wells with parabolic AlGaAs barriers (PQW). It was demonstrated that by using this design PL intensity at room temperature was increased by more than 50 times in comparison with conventional rectangular quantum wells. This outcome is related to more efficient carrier trapping into the GaAsBi quantum wells (QW) and carrier localization. It is worth mentioning, that the reproducibility of QW exhibiting enhanced PL using this design is significantly increased.

To establish the relationship between technological conditions and optical properties more detailed study of GaAsBi PQW grown by molecular beam epitaxy (MBE) was continued. The latest results will be presented in this work. To explore optical properties temperature-dependent PL measurements were carried out in a temperature range of 3 – 300 K. Moreover, to understand deeper and explain carrier recombination processes excitation-dependent PL experiments were done. The measured spectra revealed the influence of various quantum structure designs to luminescent properties. First, growth parameters (substrate temperature, bismuth content) were varied to increase PL intensity. Then the influence of GaAsBi QW number was investigated by comparing PL spectra of one or two QW with parabolic barrier (1PQW or 2PQW) and three QWs in one parabolic AlGaAs barrier (3in1PQW). The room temperature PL results are presented in Fig. 1 (a). It was demonstrated that thermal annealing, which is traditional way to improve the quality of MBE grown quantum structures, could cause the structural changes as well. The room temperature PL spectra of in situ annealed 2PQW structure is redshifted (see Fig. 1 (a) red line). Moreover, the cross-section transmission electron microscopy images evidenced the formation of Bi nanocrystals during annealing, and increased distortion of the GaAsBi QW layer. Consequently, the PL band of annealed 2PQW structure was assigned to emission from Bi nanocrystals rather than to GaAsBi QW. Wide temperature-dependent PL spectra of annealed 2PQW (Fig. 1 (b)) support that presumption (*FWHM* = 113 meV at 3 K).

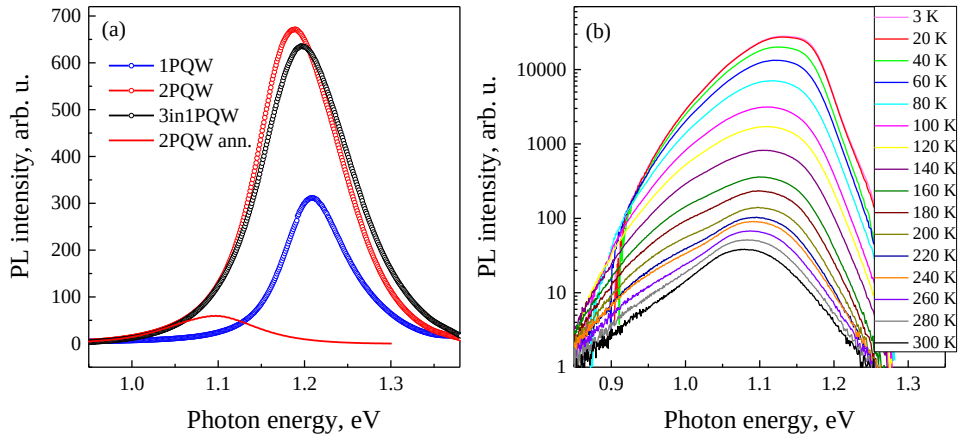


Fig. 1. (a) Room temperature PL spectra of investigated GaAsBi PQW structure of different designs: 1PQW – one QW with parabolic barrier (sample VGA145), 2PQW – two QWs with parabolic barriers (sample VGA0888) and 3in1PQW – three rectangular QWs surrounded by outer parabolic AlGaAs barriers (sample VGA0898). (b) Temperature-dependent PL spectra of annealed 2PQW structure (sample VGA0638).

[1] P.K. Patil, E. Luna, T. Matsuda, K. Yamada, K. Kamiya, F. Ishikawa, and S. Shimomura, GaAsBi/GaAs multi-quantum well LED grown by molecular beam epitaxy using a two-substrate-temperature technique, *Nanotechnology* **28**, 105702 (2017).
[2] C. J. Hunter, F. Bastiman, A. R. Mohmad, R. Richards, J. S. Ng, S. J. Sweeney, and J. P. R. David, Absorption characteristics of $GaAs_{1-x}Bi_x$/GaAs diodes in the near-infrared, *IEEE Photonics Technol. Lett.* **24**, 2191–2194 (2012).
[3] R. N. Kini, L. Bhusal, A. J. Ptak, R. France, and A. Mascarenhas, Electron Hall mobility in GaAsBi, *J. Appl. Phys.* **106**, 043705 (2009).
[4] S. Pūkienė, M. Karaliūnas, A. Jasinskas, E. Dudutienė, B. Čechavičius, J. Devenson, R. Butkutė, A. Udal, and G. Valušis, Enhancement of photoluminescence of GaAsBi quantum wells by parabolic design of AlGaAs barriers, *Nanotechnology* **30**, (2019).

BEHAVIOR OF FULLERENE C_{60} MOLECULES IN A SOLVENT SYSTEM

Urol Makhmanov[1,2], Abdulmutallib Kokhkharov[1], Shaxboz Esanov[1], Ulugbek Turdaliev[3]

[1] Institute of Ion-Plasma and Laser Technologies, Uzbekistan Academy of Sciences, Uzbekistan
[2] National University of Uzbekistan named after Mirzo Ulugbek, Uzbekistan
[3] Namangan State University, Uzbekistan
urol_m@mail.ru

In recent years, solutions of carbon nanoparticles have attracted more and more attention of physicists and chemists as a natural model of a self-organizing system. By controlling the type of solvent used, the concentration of solutes and external conditions (temperature of the medium, the method of preparation of the solution, etc.), it will be possible to control self-organizing systems [1-2].

The aim of this work is to experimentally study the refractive, dimensional and structural properties of fullerene C_{60} (purity ≥99.8%, SES Research, USA) in binary mixtures of solvents "toluene+hexane" at room temperature. Experiments on measuring the exact values of the refractive indices (n) of the toluene/hexane and C_{60}/toluene/hexane systems at various solvent concentrations (~0÷1.0 mole fraction) were carried out at the wavelength of the D_1 line of the sodium atom (~589.3 nm). It was found that with an increase in the concentration of fullerene C_{60} and the volume fraction of toluene in a solution of C_{60}/toluene/hexane, the values of the refractive index of the solution increase. This is due to the fact that an increase in the number of bonds formed between the molecules "C_{60}-C_{60}" and "C_{60}-solvents" causes more interactions with photons and leads to an increase in the refractive index of the medium. In addition, the main features of intermolecular interactions of fullerene C_{60} in binary mixtures of solvents "hexane+toluene" at various concentrations of the components were studied by UV-visible spectroscopy, electron microscopy, and dynamic light scattering (DLS).

The experimental data presented in this work are of key importance for the controlled synthesis of various C_{60} nanostructures in binary solvents, as well as for assessing the composition of the colloidal system.

---

[1] J. Antonio Tamayo-Ramos, S. Martel, Rocío Barros et al., On the behavior of quercetin + organic solvent solutions and their role for C_{60} fullerene solubilization, Journal of Molecular Liquids **345,** 1177143 (2022).

[2] U.K. Makhmanov, A.M. Kokhkharov et al., The formation of self-assembled structures of C_{60} in solution and in the volume of an evaporating drop of a colloidal solution, Lithuanian Journal of Physics **60**, 194–204 (2020).

EXCESS CONDUCTIVITY AND PSEUDOGAP IN SINGLE CRYSTALS UNDER PRESSURE UP TO 1.7 GPA

Liudmyla Omelchenko[1], Eugene Petrenko[1], Andrei Solovjov[1], Ruslan Vovk[2]

[1]B.Verkin Institute for Low Temperature Physics and Engineering of NAS of Ukraine,
Nauky Ave., 47, Kharkiv 61103, Ukraine
[2]Physics Department, V. Karazin National University, 4 Svoboda Sq., 61077 Kharkiv, Ukraine
omelchenko@ilt.kharkov.ua

The pseudogap (PG) state, which is realized in high-temperature superconductors (HTSCs) at the characteristic temperature T*»Tc with the doping less than optimal, is one of the most mysterious properties of HTSC cuprates [1]. Understanding the physics of the PG would answer the question about the mechanism of superconducting pairing in HTSCs, which is also not fully clarified yet [2]. One of the most promising materials for studying the PG is the $YBa_2Cu_3O_{7-\delta}$ (YBCO) family. It is so due to the possibility of variation in its composition by substitution of yttrium (Y) with the isovalent analogues, or changing the degree of oxygen nonstoichiometry. The compounds $Y_{1-x}Pr_xBa_2Cu_3O_{7-\delta}$ (YPrBCO) with partial substitution of Y by praseodymium (Pr) atoms are of particular interest in that respect. The replacement of Y with other rare-earth elements in this compound does not lead to a significant change in its resistive characteristics [1]. The only exception is the replacement of Y with Pr (also known as the "praseodymium anomaly"), which leads to a noticeable increase in the resistivity ρ and a decrease in the critical temperature Tc of the superconducting (SC) transition [2]. Doping of the $Y_{1-x}Pr_xBa_2Cu_3O_{7-\delta}$ with Pr on the one hand leads to a gradual suppression of superconductivity with increasing of the concentration x, and on the other, it allows to preserve almost constant both the lattice parameters and the oxygen content (7-δ) of the sample under investigation [1]. It should also be stressed that Pr^{+3} atoms have an intrinsic magnetic moment of $\mu_{Pr} \approx 3.58\mu_B$,which is $m_{eff} \approx 2\mu_B$ in the PrBCO compound. That is why the study of the effect of Pr impurity on the properties of YPrBaCuO single crystals is considered very promising for revealing the mechanisms of the interplay of the superconductivity and magnetism in HTSC, which is important for the final clarification of the physical nature of both the PG and high-temperature superconductivity ingeneral.

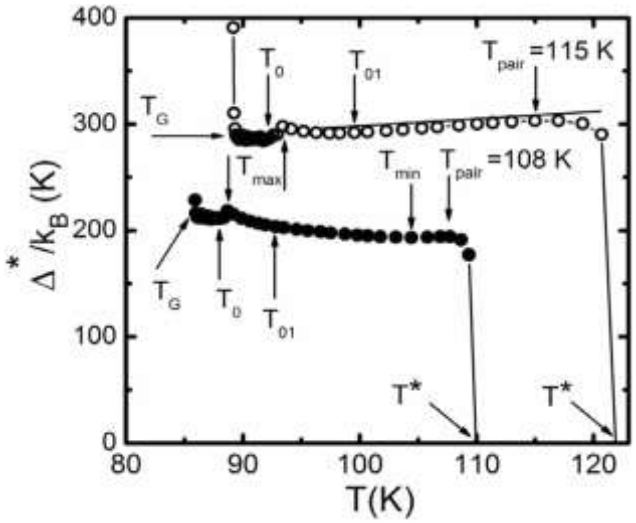


Fig. 1. Temperature dependences of the pseudogap Δ*(T) of $Y_{0.95}Pr_{0.05}Ba_2Cu_3O_{7-\delta}$ single crystal at P = 0 (points) P = 1.7 GPa (circles).

The effect of hydrostatic pressure up to P = 1.7 GPa on the fluctuation conductivity σ′(T) and pseudogap Δ*(T) in $Y_{0.95}Pr_{0.05}Ba_2Cu_3O_{7-\delta}$ single crystal with critical temperature Tc = 85.2 K (at P = 0) was investigated. The application of pressure leads to the increase in Tc with dTc/dP = +1.82 K·GPa^{-1} while the resistance decreases as dlnρ(100 K)/dP = −(10.5 ± 0.2) %·GPa^{-1}. Regardless of the pressure, in the temperature interval from Tc to T_0 (~88 K at P=0) the behaviour of σ′(T) is well described by the Aslamazov – Larkin (AL–3D) fluctuation theory, and above the T_0 by the Lawrence – Doniach theory (LD). The Maki-Thompson (MT–2D) fluctuation contribution is not observed. This indicates the presence of structural defects in the sample induced by Pr. Here it is determined for the first time that when the pressure is applied to the $Y_{1-x}Pr_xBa_2Cu_3O_{7-\delta}$ single crystal, the pseudogap increases as dlnΔ*/dP=0.17 GPa^{-1}.

[1] R. V. Vovk, A. L. Solovjov, Electric transport and pseudogap in high-temperature superconducting compounds of system 1-2-3 under conditions of all-round compression. Low Temp. Phys. **44**, 111–153 (2018).
[2] A. L. Solovjov et. al, Pseudogap and fluctuation conductivity in Y1−*x*Pr*x*Ba2Cu3O7−δ single crystals with different concentrations of praseodymium. Low Temp. Phys. **43**, 841 (2017).

MAGNETOCONDUCTIVITY STUDY IN YBCO MONOLAYERS

Eugene Petrenko[1], Lyudmila Omelchenko[1], Andrei Solovjov[1]

[1] B. I. Verkin Institute for Low Temperature Physics and Engineering of National Academy of Science of Ukraine, 47 Nauki ave., 61103 Kharkov, Ukraine
petrenko@ilt.kharkov.ua

It is believed that understanding the mechanism of electron pairing in high-temperature superconductors (HTSC) will indicate the direction of synthesis of superconductors with a desired high T_c. For this, it is necessary to study the properties of HTSCs in the normal state, where the pseudogap is opened at $T^*>>T_c$. Applying of an external magnetic field is one of the excellent methods to study superconducting fluctuations in HTSCs in the vicinity of critical temperature T_c.

From the literature, it is known that the orbital motion of the superconducting carriers is strongly suppressed when $\boldsymbol{H}\perp$c axis is applied. For this reason, only the Zeeman terms contribute to the fluctuation conductivity.

In our work, we have studied a high quality 100 nm-thick YBCO film with T_c = 88.7 K. The resistive measurements have been performed up to 8 T in $\boldsymbol{H}$||ab configuration in order to extract the pure Zeeman contributions to magnetoconductivity $\Delta\sigma_H$.

According to Aronov *et al*. [1], the contribution of the Zeeman effect on the Aslamazov-Larkin (ALZ) and Maki-Thompson (MTZ) terms reads as following:

$$\Delta\sigma_{ALZ} = -0.526\frac{e^2}{\hbar d\varepsilon^2}\frac{1+\alpha}{(1+2\alpha)^{3/2}}\left[\frac{\omega_s}{4\pi k_B T_c}\right]^2 \quad (1)$$

and

$$\Delta\sigma_{MTZ} = -\frac{e^2}{16\hbar d\varepsilon}\left[\frac{1+\delta}{(1+2\delta)^{3/2}} - \frac{1+\delta+\delta/\alpha}{\left[(1+\delta/\alpha)(1+2\delta+\delta/\alpha)\right]^{3/2}}\right]\left[\frac{\omega_s\tau_\varphi}{\hbar}\right]^2 \quad (2)$$

where $\omega_s = g\mu_B H$ is the Zeeman energy, g is the Lande g factor, μ_B is the Bohr magneton, τ_φ is the phase relaxation time, k_B is the Boltzman constant, $\hbar$ is the reduced Planck's constant, d is the length of the unit cell along the c-axis, α and δ are pairing and pair-breaking parameters, respectively, and ε is the reduced temperature.

It was shown that the found $\Delta\sigma_H$ is well described within the ALZ and MTZ approaches in magnetic fields starting only from 3 T. The clear crossover, observed at 91.7 K, retains up to 6 T, up to which the 2D-MTZ contribution still persists. With further increase of magnetic field, the magneto-conductivity shows exclusively ALZ behavior.

An additional analysis of the upper critical field within the Werthamer–Helfand–Hohenberg (WHH) theory [2] allowed us to determine corresponding coherence lengths in the ab-plane (ξ_{ab} = 10.1 Å) and along the c-axis (ξ_c = 3.3 Å) in a good agreement with the literature data [3].

[1] A.G Aronov, S. Hikami and A.I. Larkin, Phys. Rev. Lett. **62**, 965 (1989).
[2] N.R. Werthamer, E. Helfand, and P.C. Hohenberg. Phys Rev. **147**, 295 (1966).
[3] J. Sugawara, H. Iwasaki, N. Kobayashi, H. Yamane, and T. Hirai, Phys Rev.B **46**, 22 (1992).

HOT CARRIERS IN PHOTORESPONSE FORMATION ACROSS GaAs P-N JUNCTION

Oleksandr Masalskyi[1], Jonas Gradauskas[1,2], Steponas Ašmontas[2], Algirdas Sužiedėlis[2], Aldis Šilėnas[2], Aurimas Čerškus[1,2], Ihor Zharchenko[2]

[1] Department of Physics, Vilnius Gediminas Technical University, Lithuania
[2] Lab of Electronic Processes, Center for Physical sciences and Technology, Lithuania
oleksandr.masalskyi@vilniustech.lt

The Shockley–Queisser (SQ) limit determines the maximum theoretically possible efficiency of a single junction solar cell [1]. Under normal conditions, this limit is about 30% for conventional solar cells. According to the SQ theory, only photons with energy equal or higher than the band gap of the semiconductor can participate in the formation of an electron-hole pair. Photons with energy less than the band gap do not contribute to the photoresponse of the solar cells at all. The theory can be applied for the solar cells under illumination of one Sun with an AM 1.5G (1000 W/m^2) spectrum standard.

We propose an idea that the photons with energies less than the semiconductor band gap as well as those of large energy should be accounted via the hot carrier phenomenon (Fig.1) before the thermalisation process.

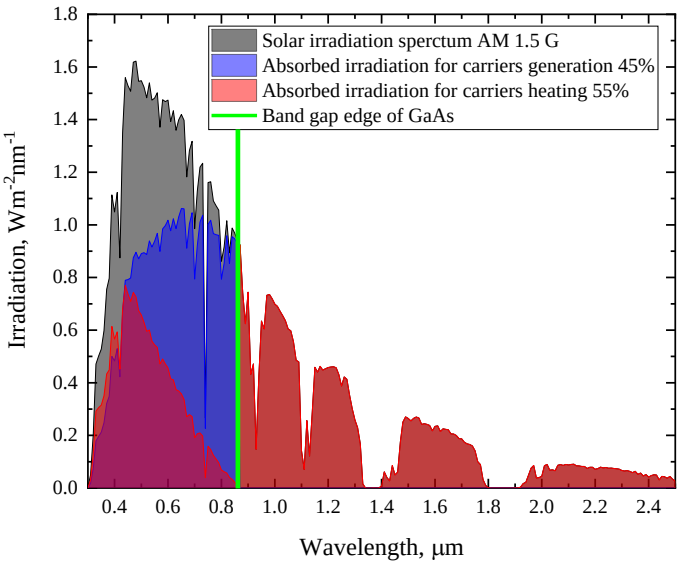


Fig.1 Absorption of solar spectrum AM 1.5 G by a GaAs solar cell.

The object of investigation was GaAs p-n junction as known for its relatively expressed two-photon absorption [2]. The sample was illuminated by a laser light with wavelength 1.06 μm, pulse duration 25 ns, and maximum intensity 10 MW/cm^2. The laser photon energy is less than the bang gap of GaAs, 1.16 eV and 1.42 eV respectively. In this case, the process of electron-hole pair generation occurs only though two-photon absorption, and carrier heating process happens due to the intraband absorption.

Additionally, we provide a model describing a solar cell's photoresponse signal via three its components initiated by generation, lattice heating and hot carrier phenomena. The model is based on the assumption that the p-n-junction is a first-order linear time-invariant system. The finding opens the way to estimate conditions determining contribution of each component into the net photovoltage [3].

As for application, the negative effect of hot carriers should be reduced to boost the efficiency of solar cells. This can be achieved by way of harvesting the energy of hot carriers before they cool or by developing solar cell structures preventing free carrier heating.

[1] W. Shockley, H Queisser, Detailed balance limit of efficiency of p–n junction solar cells, J. Appl. Phys. **32**, 510–519 (1961).
[2] W. Hurlbut, Y. Lee, et al., Multiphoton absorption and nonlinear refraction of GaAs in the mid-infrared, Opt. Lett. **32**, 668–670 (2007).
[3] J. Gradauskas, A. Steponas, et al., Influence of hot carrier and thermal components on photovoltage formation across the p–n junction, Appl. Sci. **10**, 7483(1–8) (2020).

EXPLORING POTENTIAL SPIN QUBITS OF GROUP-VI DONORS IN SILICON

Justinas Turčak[1*], Gediminas Usevičius[1], Jūras Banys[1], Mantas Šimėnas[1]

[1] Faculty of Physics, Vilnius University, Sauletekio 9, LT-10222 Vilnius, Lithuania
justinas.turcak@ff.stud.vu.lt

Donors in silicon offer a promising platform for spin-based quantum technologies [1]. The effects of group-V dopants such as Bi have been widely studied [2], revealing electron spin coherence times of several seconds at the so-called 'clock-transitions' of the spin system. In contrast, there has been relatively little work done on group-VI chalcogen donors [3].

Here, we explore feasibility of group-VI donors (S, Se, Te) in Si for electron spin-based quantum technologies. We use EasySpin tool [4] to simulate the electron spin resonance (ESR) transitions of these donors. This allows us to examine the first order magnetic field dependence on the transition frequencies and to determine the 'clock transitions' in these systems. We also discuss the experimental difficulties in achieving these transitions.

[1] B.E. Kane, A silicon-based nuclear spin quantum computer, Nature **393**, 6681 (1998).
[2] G. Wolfowicz et al., Atomic clock transitions in silicon-based spin qubits, Nature Nanotechnology **8**, 561, (2013).
[3] R.L. Nardo et al., Spin relaxation and donor-acceptor recombination of Se^+ in 28-silicon, Physical Review B **92**, 165201 (2015).
[4] S. Stoll, A. Schweiger, a Comprehensive Software Package for Spectral Simulation and Analysis in EPR, J. Magn. Reson. **178**, 42 (2006).

PHOTOLUMINESCENCE STUDY OF InGaN/GaN QUANTUM WELLS WITH A SUPERLATTICE UNDERLAYER

Aleksandra Širvinskytė[1], Jūras Mickevičius[1]

[1] Institute of Photonics and Nanotechnology, Vilnius University, Vilnius, Lithuania
aleksandra.sirvinskyte@ff.stud.vu.lt

Development of InGaN-based photonic devices enabled the commercialization of efficient blue light-emitting diodes (LEDs) and laser diodes (LDs), white light sources. The main challenge in development of long-wavelength InGaN LEDs is the decrease of radiative efficiency, which is usually attributed to higher strain and increased defect density. One of the approaches to solve this problem is based on a low-indium-content InGaN underlayer or superlattice (SPSL) below the active region multiple quantum wells (MQWs), which leads to higher efficiency values. However, the origin of such efficiency increase is still not clear: several groups have contributed this effect to the strain relaxation between GaN and InGaN/GaN MQW layers [1], while recent studies link the inclusion of SPSL to lower defect density in the active region [2,3].

In this study, eight InGaN/GaN MQWs samples were studied. Samples were grown on sapphire substrate by metalorganic chemical vapor deposition (MOCVD), and were composed of *n*-GaN buffer layer on top of which SPSL or InGaN/GaN MQWs or both of these structures were grown. The samples differed in the number of SPSL periods and SPSL growth temperature. Optical properties of the samples were studied by using photoluminescence (PL) spectroscopy. PL measurements were performed in a wide range of temperatures from 8 to 300 K. The CW semiconductor laser (405 nm) was used to excite the samples.

The room-temperature PL spectra of the studied samples showed that MQWs-related PL band is stronger by almost two orders of magnitude compared to the SPSL-related PL band (see Fig. 1.). The inclusion of SPSL structure below the active region resulted in the redshift of PL band and its broadening. Strong carrier localization was evidenced by the large PL band widths as well as the characteristic S-shaped peak position temperature dependence. Obtained PL efficiency values revealed that introduction of SPSL below the MQWs led to an efficiency improvement from 3% (for the sample containing only MQWs) to 6% and 11% (for the samples containing both SPSL and MQWs). However, it was accompanied by the slight reduction of In content in the active region MQWs.

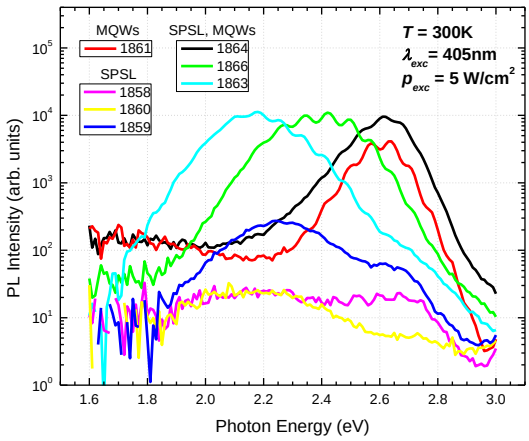


Fig. 1. PL spectra of studied samples excited using a semiconductor laser.

[1] Leem, S. J. et al., *J. Cryst. Growth* **311**, 103–106 (2008)
[2] Armstrong, A. M. et al., *J. Appl. Phys.* **117**, 134501 (2015)
[3] Chen, Y. et al., *Appl. Phys. Lett.* **118**, 111102 (2021)

PLUSES AND MINUSES OF DIFFERENTLY SUBSTITUTED INDOLOCARBAZOLE ISOMERS USED IN NON-DOPED ORGANIC LIGHT EMITTING DIODES

Malek Mahmoudi, Ervinas Urbonas, Dalius Gudeika, Dmytro Volyniuk, Juozas V. Grazulevicius

Department of Polymer Chemistry and Technology, Kaunas University of Technology, Radvilenu pl. 19, LT-50254, Kaunas, Lithuania;
malek.mahmoudi@ktu.edu

Thanks to the molecular design of compound exhibiting thermally activated delayed fluorescence (TADF), their lowest excited singlet and triplet states lie very close energetically. Their charge donating and accepting moieties are spatially separated [1]. This feature of these compounds can lead to the thermally activated upconversion from the latter to the former state through reverse intersystem crossing which is the inverse transition processes of phosphorescence [2]. In this work, four indolocarbazole-based compounds (abbreviated as **1IndCz**, **2IndCz**, **3IndCz** and **4IndCz**) were synthesized in high yields and studied as TADF emitters for non-doped organic light emitting diodes (OLEDs). Photophysical, photoelectrical, charge-transporting, and electrochemical properties of the compound have been examined. In addition, the temperatures of thermal transitions of four compounds were measured by thermogravimetric analysis and differential scanning calorimetry. Aggregation-induced emission enhancement for the studied compounds was proved by studying photophysical properties of their dispersions in THF/water mixtures [3,4]. The compounds exhibited efficient emission in solid state with the wavelengths of fluorescence intensity maxima ranging from 483 to 521 nm and photoluminescence quantum yields ranging from 6 to 58%. Time-of-flight measurements showed that small differences in the molecular architecture can considerably change charge-transporting properties of the compounds. Compounds **1IndCz** and **3IndCz** were only capable of transporting holes, **4IndCz** could transport both holes and electrons and maximum hole mobility reached 10^{-4} cm^2/Vs at high electric fields. The optical band gaps of the solid samples were found to be in the range of 2.59-2.92 eV. Electrochemical properties of the derivatives were examined by cyclic voltammetry (CV) and according to the oxidation potentials using equation: $IP_{CV} = (E_{onset}^{ox} + 4.8)$ (eV), the ionization potential (IP_{CV}) values of **1IndCz, 2IndCz, 3IndCz** and **4IndCz** were found to be 5.62, 5.79, 5.55 and 5.52 eV, respectively. Additionally, photoelectron emission spectroscopy was used for the measurements of ionization potentials of the solid samples of the compounds in air. The values of IP in a relatively close range of 5.78-5.99 eV were observed. Multiple non-doped OLEDs were fabricated and electroluminescent characteristics of the compounds were studied using them as TADF emitters. The fabricated devices with non-doped light-emitting layers of **1IndCz, 2IndCz, 3IndCz** or **4IndCz** were characterized by blue/sky-blue electroluminescence with CIE1931 coordinates of (0.25,0.47), (0.24,0.47), (0.19, 0.3) and (0.23, 0.4), respectively. The highest external quantum efficiency (EQE_{max}) of 4.8% was obtained for **2IndCz**-based device. This value clearly exceeds the theoretical limit of EQE_{max} of 2.9 % assuming only conventional fluorescence with a photoluminescence quantum efficiency of 58 % from neat films of **2IndCz**. Maximum current efficiency of 12.5 cd/A, maximum power efficiency of 8.8 lm/W and maximum brightness of 24807 cd/m^2 were observed for **2IndCz**-based device. Efficient injection of charge carriers from electrodes and the following transport to emitting layer was evidenced by relatively low turn-on voltages of all fabricated OLEDs. Turn-on voltage of devices were in the range of 4.1 to 5.1 V. **2IndCz**-based device demonstrated the lowest turn-on voltage of 4.1 V.

Acknowledgements

This research was carried out with the support of the Research Council of Lithuania (Project "ELOS" No S-MIP-21-30).

[1] F.B. Dias, *et al*, Photophysics of thermally activated delayed fluorescence molecules, Methods Appl. Fluoresc. 5 (2017).
[2] T.J. Penfold, On Predicting the Excited-State Properties of Thermally Activated Delayed Fluorescence Emitters, J. Phys. Chem. C. 119, 13535–13544, (2015).
[3] H Nie *et al*, Aggregation-Induced Emission Luminogens (AIEgens) for Non-Doped Organic Light-Emitting Diodes, Materials and Applications 2, 173-198, (2016).
[4] Y. Hong *et al*, Aggregation-induced emission, *Chem. Soc. Rev*.,40, 5361–5388, (2011).

THEORETICAL MODELING OF LUMINESCENCE LINESHAPE IN SILICON DUE TO A CARBON-CARBON PAIR COMPLEX

Rokas Silkinis[1], Lukas Razinkovas[1], Audrius Alkauskas[1]

[1]Department of Fundamental Research, Center for Physical Sciences and Technology (FTMC), Lithuania
rokas.silkinis@ftmc.lt

In recent years quantum technologies have been at the forefront of scientific interest due to a vast array of possible applications in sensing, communications, and computing. Given its history of commercial and practical success as an essential part of solid-state devices, silicon seems to be a rational choice as a host material for future quantum technologies. Of particular interest are optically-active single point defects which could be used for long-distance exchange of information [1]. The so called G-center, thought to be composed of an interstitial-substitutional carbon pair (C_iC_s) in silicon, is one of such defects [2, 3, 4]. It emits light at telecom wavelengths of 1280 nm (0.97 eV) and is thus a suitable candidate for a telecom-range single-photon source [5].

In this work, we present a theoretical analysis of the luminescence lineshape of the C_iC_s defect in silicon. We performed first principles density functional theory (DFT) calculations with a semilocal functional based on the generalized gradient approximation (GGA), in particular the Perdew–Burke–Ernzerhof (PBE) variant. Our results indicate a zero-phonon line (ZPL) energy of 0.82 eV, which is comparable to the experimental value of 0.97 eV. The Debye–Waller factor w_{ZPL} (the weight of the ZPL) and the Huang–Rhys factor S (the average number of phonons emitted during an optical transition) are calculated to be 12 % and 2.08, respectively. The calculated lineshape agrees with the experimental results for the G-center closely. This reinforces the conclusion that the G-center is the C_iC_s pair.

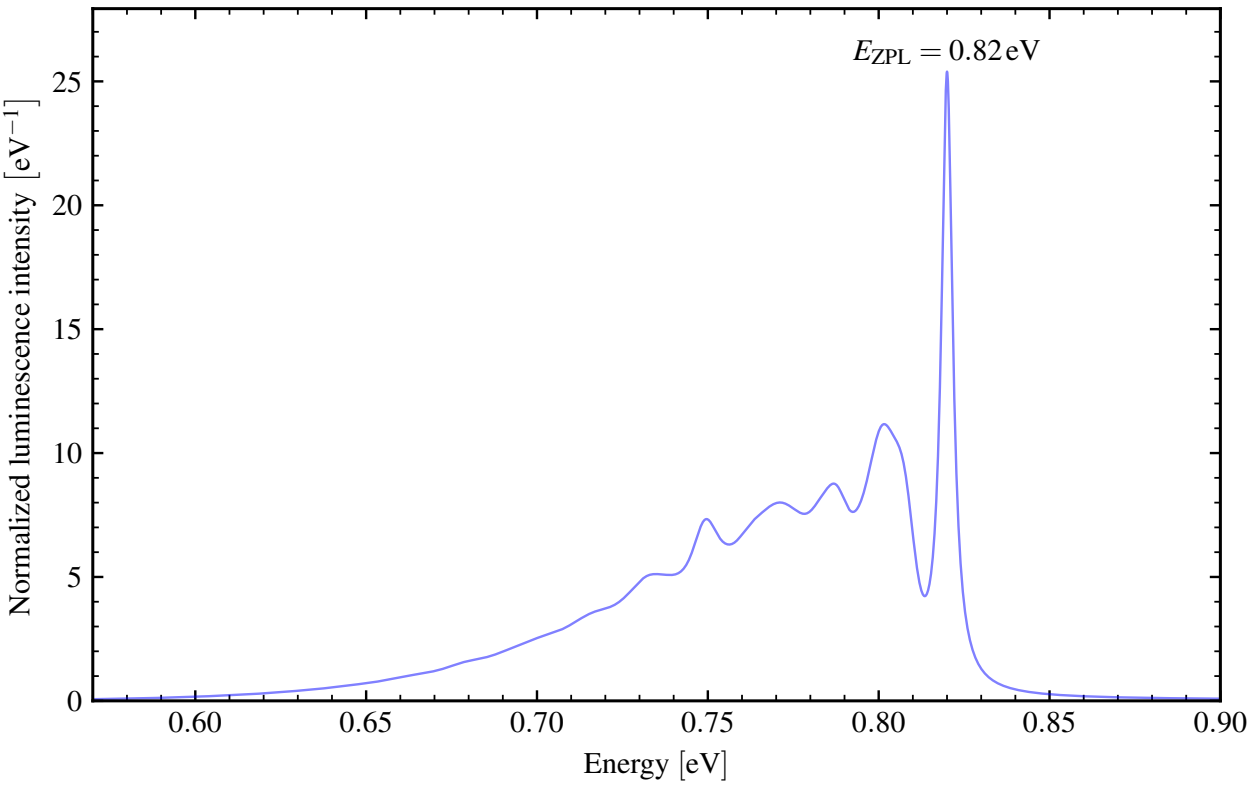


Fig. 1. Normalized luminescence intensity function of a C_iC_s defect in silicon. E_{ZPL} is the calculated zero-phonon line energy.

[1] W. Redjem, A. Durand, T. Herzig et al., Single artificial atoms in silicon emitting at telecom wavelengths, Nature Electronics **3**, 738–743 (2020).
[2] K. Thonke, H. Klemisch, J. Weber, and R. Sauer, New model of the irradiation-induced 0.97-eV (G) line in silicon: A C_S-Si* complex, Physical Review B **24**, 5874 (1981).
[3] R. B. Capaz, A. Dal Pino, and J. D. Joannopoulos, Theory of carbon-carbon pairs in silicon, Physical Review B **58**, 9845 (1998).
[4] P. Udvarhelyi, B. Somogyi, G. Thiering, and A. Gali, Identification of a Telecom Wavelength Single Photon Emitter in Silicon, Physical Review Letters **127**, 196402 (2021).
[5] C. Chartrand, L. Bergeron, K. J. Morse et al., Highly enriched ^{28}Si reveals remarkable optical linewidths and fine structure for well-known damage centers, Physical Review B **98**, 195201 (2018).

QUANTUM WELL INFRARED PHOTODETECTOR OPERATING AT ROOM TEMPERATURE

Karolis Redeckas[1], Ignas Grigelionis[1], Vladislovas Čižas[1], Vytautas Jakštas[2], Renata Butkutė[1], Andrius Bičiūnas[1], Linas Minkevičius[1]

[1] Department of Optoelectronics, Center for Physical Sciences and Technology, Saulėtekio al. 3, Vilnius, Lithuania
[2] Department of Physical Technologies, Center for Physical Sciences and Technology, Saulėtekio al. 3, Vilnius, Lithuania
karolis.redeckas@ftmc.lt

In today's quickly technologically emerging world infrared frequency range sensing systems are becoming more and more attractive for versatile applications like security, healthcare, agricultural industry etc. [1, 2]. Quantum well infrared photodetectors (QWIP) first demonstrated in early 90-ies, quickly became one of the most popular detector types for such sensing systems due to its economic efficiency and relatively simple manufacturing process [3]. Up to now the majority of applications, require cryogenic QWIP cooling in order to cancel out the room temperature background and obtain reasonable sensitivity and response time [4]. In the current study less cooling-dependent QWIP of the 7-12 μm wavelength range (atmospheric window) were developed to respond to the high demand of infrared detectors for specific gas sensing [5].

In this work, the properties of GaAs/AlGaAs QWIP detectors designed and built using the FTMC facilities for 8-9 μm wavelength detection range are investigated. To couple the radiation impinging the detector at normal angle to its surface efficiently, metallic gratings, optimized for specific wavelength, were put on the top of the structure in order to overcome quantum selection rule (check the left panel in Fig 1. for one of the gratings and typical QWIP structure used in the current study). Characterization at room temperature as well as at the temperatures below 100 K was performed by measuring electrical properties and acquiring spectra in order to estimate signal to noise ratio and spectral responsivity.

Spectra were obtained using conventional infrared Fourier spectroscopy. The collimated radiation emanating from the spectrometer was focused by a parabolic mirror (f = 5 cm) onto a surface of the QWIP. It was placed on the cold finger in the cryostat and biased with the DC voltage. Photo response was measured by using the Lock`in technique, mechanically chopping output radiation at 211 Hz. Spectra obtained with QWIPS having different grating couplers on top are presented in Fig. 1 (right). Each spectrum is smoothed and shifted by constant value in horizontal axis for easier comparison.

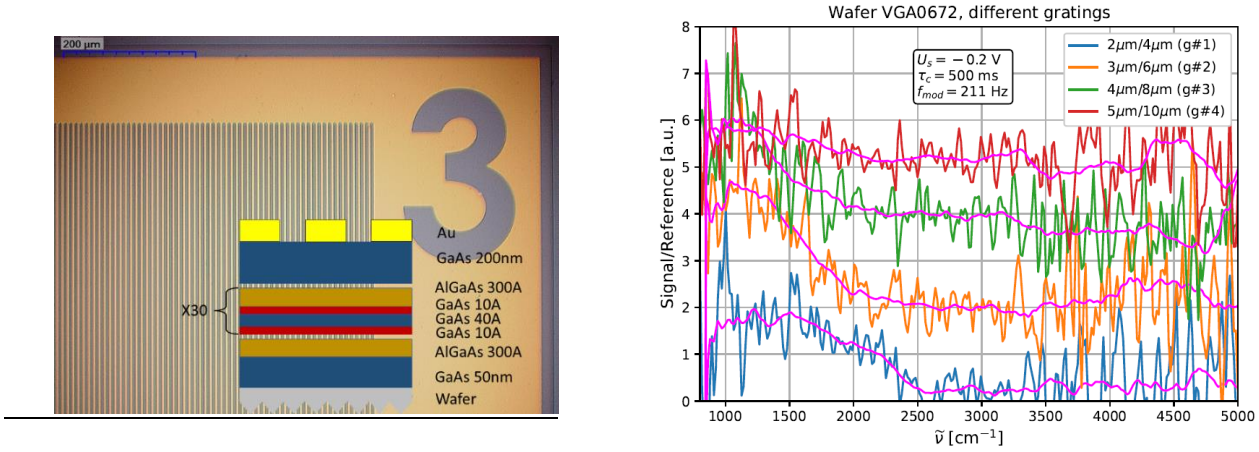


Fig. 1. The photo of the part of QWIP detector and its schematic cross section (left). Spectra obtained at room temperature (right).

The obtained results give an opportunity for the development of less cooling-dependent QWIP which in turn opens possibilities for compact and light-weight sensing systems to be developed and used in wide amount of practical applications.

[1] D. Tyagi, H. Wang, W. Huang et al., Recent advances in two-dimensional-material-based sensing technology toward health and environmental monitoring applications, Nanoscale **12**, 3535-3559 (2020).
[2] L. Karthikeyan, I. Chawla, A. K. Mishra, A review of remote sensing applications in agriculture for food security: Crop growth and yield, irrigation, and crop losses, Journal of Hydrology **586**, 124905 (2020).
[3 R.Dudek, A. Shenet al., QWIPs beyond FPAs: high-speed room-temperature detectors, Proc. SPIE Infrared Technology and Applications XXVII **4369**, (2001).
[4] G. P. Wang, J. H. Cai , N. Li et al., *Cryocoolers 14*, 2007, (Springer, USA, 2004).
[5] A. Agarwal et al., On-chip mid-infrared gas detection using chalcogenide glass waveguide, Appl. Phys. Lett. **108**, 141106 (2016).

A COMPUTATIONAL QM/MD NMR STUDY OF MOLECULAR ASSOCIATION IN BINARY MIXTURES OF ACETIC ACID AND DIMETHYL SULFOXIDE

Žyginta Einorytė[1], Greta Majauskaitė[1], Kęstutis Aidas[1]

[1]Institute of Chemical Physics, Faculty of Physics, Vilnius University, Lithuania
zyginta.einoryte@ff.stud.vu.lt

Neat acetic acid (AA) and its binary mixtures are a frequent object of studies because of various and often unexpected hydrogen bonded aggregates forming in them. These aggregates determine different physical properties of the system and in liquid phase exist in a dynamic equilibrium. Dimethyl sulfoxide (DMSO) is known for being highly polar and prone to forming hydrogen bonds, so AA and DMSO systems are greatly suitable for investigating such intermolecular interactions.

The motivation of present study originates from the recorded ^{1}H NMR spectra in binary systems of acetic acid and dimethyl sulfoxide [1]. A curious non-monotonic evolution of the NMR chemical shift of AA acidic proton with the changing composition of the binary AA/DMSO mixture was observed. When the molar fraction of acetic acid in the AA/DMSO system increases from 0 to ~0.7, the chemical shift of the acidic hydrogen drops by around 0.5 ppm (from 11.9 ppm to 11.4 ppm), then starts to rise, eventually reaching around 11.7 ppm in pure AA. This phenomenon is caused by the shifting equilibrium between various molecular aggregates formed between acetic acid molecules themselves as well as between acetic acid and DMSO, when the composition of the binary mixture changes. It is virtually impossible to dissect the nature of these molecular aggregates, in particular their population, experimentally, however, these problems can be effectively dealt with by using advanced molecular modelling techniques such as molecular dynamics (MD) simulations and combined quantum mechanics/molecular mechanics (QM/MM) approaches. These techniques have also been very recently applied to study molecular aggregation in glacial acetic acid [2].

The main objective of this study is to carry out a qualitative and quantitative analysis of molecular aggregates forming in AA/DMSO systems and to compute the NMR isotropic shielding constants of the acidic hydrogen of the AA molecules in various molecular aggregates. Comparison between computational and experimental NMR results allows for a detailed understanding of the equilibrium between various AA and DMSO molecular aggregates forming at different compositions of the binary AA/DMSO mixture.

We have considered AA:DMSO mixtures at molar ratios of 1:3, 1:1 and 3:1, as well as pure AA. MD simulations were executed using an all-atom OPLS force field and standard Coulomb plus 12-6 type Lennard-Jones potential. System's equilibrium was achieved by allowing system's density to converge in NPT simulations, then switching to NVT ensemble, running another equilibration run and completing with 2ns long production run. Atomic point charges were calculated for pure AA and DMSO, according to the CHelpG scheme, and then averaged considering mole fractions of components in each system. NMR shielding constants were calculated for all three AA/DMSO systems using QM/MM calculations. These calculations were performed for a set of molecular configurations captured during MD simulations of a given system. The analysis of hydrogen bonds in different AA/DMSO systems was based on geometric definition of a hydrogen bond which allowed identifying different types of molecular aggregates that form in these systems.

The analysis of molecular trajectories recorded during the MD simulations shows that the chemical equilibrium in the binary AA/DMSO mixtures is mainly dominated by three types of aggregates: the ones forming between AA and DMSO molecules, AA open dimers and AA cyclic aggregates (dimers or trimers). Based on the structural analysis alone we may conclude that experimentally observed decrease of the NMR chemical shift of the acidic proton up to ~0.7 molar fraction of the AA is due to increasing population of open acetic acid dimers in the mixture. The further rise of proton NMR chemical shift is due to increasing relative population of cyclic AA self-aggregates, as the acidic proton is the most deshielded in this type of aggregates [2].

Surprisingly, the calculated NMR shielding constants of the AA acidic proton in their aggregates with DMSO are slightly larger than those in AA open dimers. This computational result is inconsistent with the experimentally observed evolution described above, and we believe is a consequence of the imperfections of the OPLS force field used to describe intermolecular interactions in our MD simulations. Additional MD simulations were carried out, where a modified potential for DMSO molecules was used, which led to shorter hydrogen bonds between AA and DMSO molecules. The QM/MM calculations performed for the newly obtained trajectories lead to significantly smaller shielding constants in AA-DMSO aggregates as compared to those in open dimers of AA molecules. This result is in line with the experimental observation. Consequently, the experimentally observed evolution of the NMR signal of the acidic proton is due to subtle change of chemical equilibrium between AA-DMSO aggregates, AA open dimers and AA cyclic dimer/trimers.

Acknowledgement: Computations were performed on resources provided by the High Performance Computing Center "HPC Saulėtekis" at Vilnius University, Lithuania

[1] H. Fujiwara, Studies of hydrogen bonding in carboxylic acid-dimethyl sulfoxide systems by nuclear magnetic resonance dilution shifts, J. Phys. Chem. 78 (1974) 1662–1666. https://doi.org/10.1021/j100609a013.

[2] D. Lengvinaite, K. Aidas, L. Kimtys, Molecular aggregation in liquid acetic acid: Insight from molecular dynamics/quantum mechanics modelling of structural and NMR properties, Phys. Chem. Chem. Phys. 21 (2019) 14811–14820. https://doi.org/10.1039/c9cp01892a.

INVESTIGATION OF REAR SIDE GLASS MILLING USING NANOSECOND LASER PULSES

Miglė Mackevičiūtė , Juozas Dudutis, Paulius Gečys

Center for Physical Sciences and Technology, 231 Savanoriu avenue, LT-02300, Vilnius, Lithuania
migle.mackeviciute@ftmc.lt

Laser machining allows to achieve relatively high processing speeds and high quality when it comes to glass processing. The two major laser milling techniques are direct ablation and laser rear side ablation (Fig. 1). The milling efficiency of direct ablation is limited due to plasma shielding [1]. Additionally, the milled sidewalls has a taper angle of 8 – 10 degrees [2]. Therefore, direct ablation is only convenient for the relatively thin (<1 mm) glass milling. For thicker glass (>1 mm) rear side milling is more suitable. During the rear side milling process the laser beam is focused onto the bottom surface of the sample. This small difference allows us to achieve higher efficiency and taper-less walls. Studies show that high milling efficiencies can be achieved when nanosecond pulses are used [3-4].

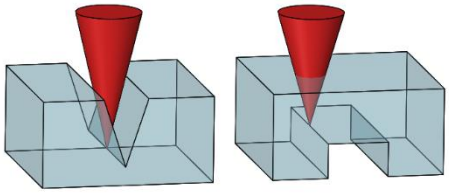


Fig. 1. Illustrations of direct ablation (on the left) and rear side ablation (on the right).

In this study, laser rear side milling of fused silica using 1064 nm, 60 µJ, 50 kHz and 5 ns pulses was investigated. At first, no stable milling could be achieved – the machined surface had high roughness and large cracks (Fig. 2, left). To achieve stable milling, higher absorption of the laser beam was needed. This was done by coating the rear surface of the sample with black dye. This additional coating allowed us to achieve the stable milling (Fig. 2, right). The idea was similar to the laser induced backside dry etching (LIBDE) method, where metal films are coated on transparent samples to increase the absorption of the laser energy [5].

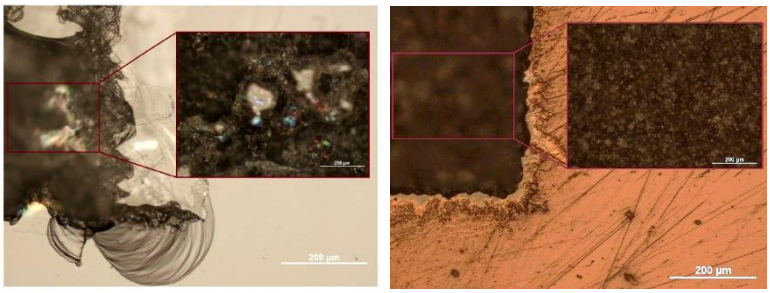


Fig. 2. Optical microscope pictures of a machined surface. The left picture corresponds to unstable laser milling with no additional film on the sample. On the right the sample is coated with black dye.

The investigation of the milling was done by changing the distance between the subsequent pulses (pitch) and the distance by subsequent scanning lines (spacing). It was found out, that the optimal pitch and spacing values and milling efficiency depends on the loops scanning number. The increment of the loops number leads to higher optimal pitch and spacing values and more efficient milling.

[1] G. Račiukaitis, M. Brikas, P. Gečys, B. Voisiat, and M. Gedvilas, „Use of high repetition rate and high power lasers in microfabrication: How to keep the efficiency high?“, *J. Laser Micro Nanoeng.*, **4**, 186–191 (2009).
[2] K. L. Wlodarczyk, A. Brunton, P. Rumsby, and D. P. Hand, „Picosecond laser cutting and drilling of thin flex glass“, *Opt. Lasers Eng.*, **78**, 64–74 (2016).
[3] P. Gečys, J. Dudutis, ir G. Račiukaitis, „Nanosecond laser processing of soda-lime glass“, *J. Laser Micro Nanoeng.*, **10**, 254–258 (2015).
[4] V. Tomkus, V. Girdauskas, J. Dudutis, P. Gečys, V. Stankevič, and G. Račiukaitis, „High-density gas capillary nozzles manufactured by hybrid 3D laser machining technique from fused silica“, *Opt. Express*, **26**, 27965 (2018).
[5] B. Hopp, C. Vass, T. Smausz, and Z. Bor, „Production of submicrometre fused silica gratings using laser-induced backside dry etching technique“, *J. Phys. D. Appl. Phys.*, **39**, 4843–4847 (2006).

SYNTHESIS AND MAGNETIC PROPERTIES OF CYCLODEXTRINS-FERROCENE INCLUSION COMPLEXES

Aida Kamarauskienė[1], Vygailė Dudkaitė[2], Jorūnas Dobilas[1], Edvinas Orentas[3], Gintautas Bagdžiūnas[*1,2]

[1] Department of Functional Materials and Electronics, Center for Physical Sciences and Technology, Saulėtekio av. 3, LT-10257, Vilnius, Lithuania
[2] Group of Supramolecular Analysis, Institute of Biochemistry, Life Sciences Centre, Vilnius University, Saulėtekio av. 7, LT-10257, Vilnius, Lithuania
[3] Department of Organic Chemistry, Vilnius University, Naugarduko 24, LT-03225 Vilnius, Lithuania
aida.kamarauskiene@ftmc.lt

The fundamental structure of modern computers and information storage technologies will be aided by the development of materials showing strongly coupled magnetic and electronic properties. This technology of spin-based electronics can show the way to a new generation of electronic devices with spin-dependent effects that arise from the quantum magnetic interactions in molecular level [1]. On the one hand, characterization and modelling of the magnetic properties of molecular-based compounds are a major challenge for these technologies. On the other hand, supramolecular chemistry can solve this problem because it can offer ways to stabilize the molecules of a suitable spin [2].

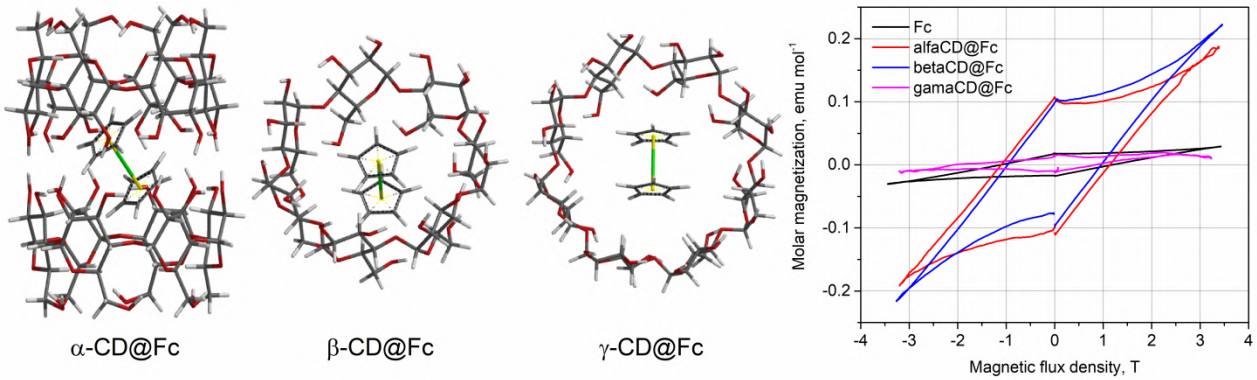


Fig. 1. Optimized structures of the α-, β-, and γ-cyclodextrins and ferrocene inclusion complexes and their molar magnetization.

In this work, the supramolecular complexes based on ferrocene (Fc) as a guest and α-, β-, and γ-cyclodextrins (CD) as the hosts with chiral cavities were synthesized to achieve this goal. These inclusion complexes were characterized using nuclear magnetic resonance, vibration, and chiroptical spectroscopy methods to confirm their structures. Moreover, density functional theory was used to optimize and compare the possible structures of these inclusion complexes and analyse the Fc orientation in the cavities (Fig. 1). We found that the orientation of Fc in α- and β-CD is considered to be nearly parallel to the molecular axis of CDs while that of Fc appears to be close to normal to the molecular axis of the γ-CD. Based on molar magnetization of these supramolecular materials, ten times better molar magnetization for the α- and β-CD@Fc complexes than for starting Fc and γ-CD@Fc was observed (Fig. 1). This effect correlates with Fc orientation in the CD cavities and this makes it possible to stabilize the higher spin structures at applied magnetic field.

Acknowledgements
This work was supported by the Research Council of Lithuania (grant number: S-MIP-20-45).

[1] E. Coronado. Molecular magnetism: from chemical design to spin control in molecules, materials and devices. Nature Reviews Materials **5**, 87–104 (2020)
[2] A. M. Garcia, G. Martínez, A. Ruiz-Carretero. The Importance of Spin State in Chiral Supramolecular Electronics. Front. Chem. **9**, 722727 (2021)

COUPLING OF MICROWAVES TO A PLANAR EPR MICRORESONATOR VIA A 3D CAVITY

Paulina Verbaitytė[1*], Gediminas Usevičius[1], Vidmantas Kalendra[1], Jūras Banys[1], Mantas Šimėnas[1]

[1] Faculty of Physics, Vilnius University, Sauletekio 9, LT-10222 Vilnius, Lithuania
paulina.verbaityte@ff.stud.vu.lt

Electron Paramagnetic Resonance (EPR) is a broadly used technique to study and manipulate electron spins across different disciplines covering quantum information, material science, physics and biology. However, in conventional EPR spectroscopy, sensitivity often limits the range and type of systems that can be studied. Recently, major advances in EPR sensitivity were achieved using planar superconducting microresonators [1,2]. However, these applications were limited to very low temperatures and spins in substrates of the resonators severely limiting the applicability of such resonators for conventional EPR samples. Thus, the full potential and compatibility of such microresonators to study a more general spin systems remains to be shown, which requires solving of several problems such as a convenient coupling to the driving microwave field.

Here, we explore the feasibility of microwave coupling to a planar EPR microresonator using a standard 3D cavity. First, we use CST Microwave Studio computational electromagnetics tool to simulate frequency response of a Bruker MD-5 dielectric ring resonator (Fig. 1). Our simulations successfully reproduce the resonance frequency of about 9.75 GHz of the $TE_{01\delta}$ mode of the resonator, which is revealed in the calculated frequency response of the S_{11} scattering parameter (Fig. 1). Then we use this model as a basis to simulate microwave coupling to a planar microresonator placed into an EPR tube, which is then inserted into the dielectric ring resonator. We compare our simulation results with the experimental observations and further discuss the best coupling geometry.

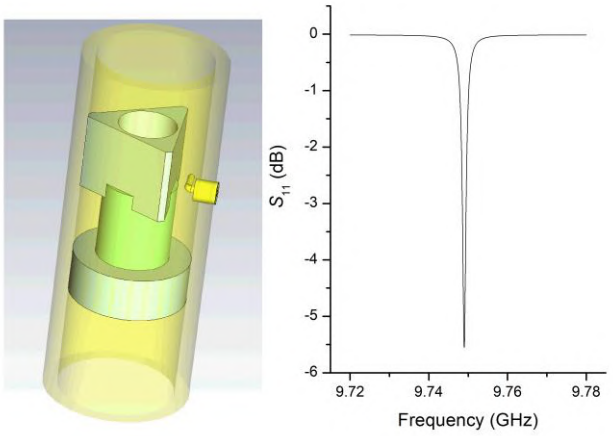


Fig. 1. Model of a Bruker MD-5 dielectric resonator (left) and simulation of its microwave response at X-band (right).

[1] A. Bienfait, et al., Reaching the quantum limit of sensitivity in electron spin resonance, Nature Nanotechnology **11**, 253-257 (2016).
[2] J.J.L. Morton, P. Bertet, Storing quantum information in spins and high-sensitivity ESR, Journal of Magnetic Resonance **287**, 128-139 (2018).

ENCAPSULATION EFFICIENCY OF NISIN LOADED FUCOIDAN PARTICLES

Aiste Galinskaite[1*], Ruta Gruskiene[1], Jolita Pachaleva[2], Edita Kodyte[3], Jolanta Sereikaite[1]

[1]Department of Chemistry and Bioengineering, Vilnius Gediminas Technical University, Vilnius, Lithuania
[2]State Research Institute Centre for Innovative Medicine, Vilnius, Lithuania
[3]Faculty of Medicine, Vilnius University, Vilnius, Lithuania
aiste.galinskaite2@gmail.com

Natural antimicrobial agents are used for food preservation. These agents can interact with food components and their efficiency could be reduced. To overcome this problem, antimicrobial agents can be encapsulated using various materials such as lipids, proteins, and carbohydrates.

Nisin is the most popular antimicrobial peptide which has been used in the food industry against Gram-positive bacteria. It is a cationic 3510 Da peptide and is used in dairy, meat, juice, and vegetable products. Sensitivity to environmental stresses, susceptibility to proteolysis, and undesirable interactions with food components can decrease the biological activity of nisin in food products. The encapsulation of nisin into nanoparticles has many advantages such as sustained release, prevention of undesirable interactions, high stability, and efficient antimicrobial activity during food storage [1]. In this work, for the synthesis of particles fucoidan was used.

Fucoidan is an anionic, sulfated polysaccharide found in brown seaweed (e.g., *Fucus vesiculosus, Macrocystis pyrifera*, *Laminaria japonica*). This polysaccharide also has antivirus, antitumor, antithrombotic, anticoagulant, anti-inflammatory, and antioxidant activity. Also, fucoidan itself could eliminate cancer cells by inducing apoptosis [2].

In this study, nisin-fucoidan particles were synthesized by the simple and cost-efficient complexation method at different pH values ranged from 4.0 to 7.0. Nisin concentration in a sample ranged from 0 to 1 mg/mL and fucoidan concentration was 0.4 mg/mL. Nisin encapsulation efficiency was determined by measuring unencapsulated nisin using bicinchoninic acid protein assay. Encapsulation efficiency was found to be close to 100% when nisin concentration was up to 0.6 mg/mL at all pH values. At the nisin concentration of 1.0 mg/mL, the encapsulation efficiency close to 100% was achieved only at pH 7.0.

The stability of nisin-fucoidan particles over time was also investigated. Nisin encapsulation efficiency was monitored for 4 weeks. It was found that the encapsulation efficiency does not change significantly and nisin remains protected.

Acknowledgments: This research was funded by the European Social Fund under the No 09.3.3-LMT-K-712. "Development of Competences of Scientists, Other Researchers and Students through Practical Research Activities" measure. Grant No 09.3.3-LMT-K-712-25-0056.

[1] A. Bahrami, R. Delshadi, S. M. Jafari et al., Nanoencapsulated nisin: An engineered natural antimicrobial system for the food industry, Trends in Food Science & Technology **94**, 20-31 (2019).
[2] J. Venkatesan, S. Anil, S. K. Kim, M. S. Shim. Seaweed polysaccharide-based nanoparticles: Preparation and Applications for Drug Delivery, Polymers **8** (2016).

β-CYCLODEXTRIN ASSISTED EXTRACTION OF DAIDZEIN AND GENISTEIN FROM *TRIFOLIUM PRATENSE* L.

Jurga Andrėja Kazlauskaitė[1,2], Jurga Bernatonienė[1,2]

[1] Department of Drug Technology and Social Pharmacy, Lithuanian University of Health Sciences, Lithuania
[2] Institute of Pharmaceutical Technologies, Medical Academy, Lithuanian University of Health Sciences, Lithuania.
jurga.andreja.kazlauskaite@lsmu.lt

Isoflavones contained almost exclusively in leguminous plants, with soya, red clover and its processed products as the major source of these compounds, which contain main molecules (genistein, daidzein) that occur as aglycones or more often as glucose-conjugated forms [1]. Isoflavonoids have demonstrated usefulness in the treatment of various diseases - diabetes, some allergies, inflammation, bacterial and viral infections [2]. Traditional extraction methods are not effective in extracting large amounts of isoflavones aglycones, so new methods are being used and one of them may be the use of excipients such as cyclodextrins.

The aim of this study was to enhance the yield of isoflavones genistein and daidzein using *β*-cyclodextrin as excipient in the extraction of *Trifolium pratense* L. blossoms.

β-cyclodextrin-assisted extraction was performed using 1.0 ± 0.001 g of dried and milled flower heads and 30 mL of solvent (water or 50 % ethanol). Excipient quantity in the samples varied from 1 to 5% (v/w). The excipient amount was based on solvent quantity. The extraction was done in a 250 mL round bottom flask and refluxed in the sand bath at 100 °C for 1 hour [3]. Control sample was prepared using the same conditions without excipient. Extraction samples for identification and quantification of aglycones genistein and daidzein were investigated using HPLC.

Highest genistein yield was detected in aqueous sample prepared with 1% of excipient and refluxed for 1 hour (258.67 ± 10.34 µg/g). Using 5 % of *β*-cyclodextrin in aqueous extraction media yielded highest amount of daidzein (417.1 ± 16.68 µg/g). The results were statistically significant compared with aqueous control samples. Changing solvents from water to 50 % of ethanol the amount of extracted daidzein significantly increased to 442.10 ± 22.11 µg/g.

The results indicated that the use of excipient during the extractions of isoflavones increased significantly. The use of purified water with *β*-cyclodextrin enhanced isoflavones yields compared with samples without excipients. Using purified water as a solvent and increasing cyclodextrin in the extraction media from 1 to 5 % daidzein increased on average by 1.4 times ($p<0.05$). Genistein decreased increasing *β*-cyclodextrin concentration.

Acknowledgements

The authors would like to thank Open Access Centre for the Advanced Pharmaceutical and Health Technologies (Lithuanian university of Health Sciences) and for the opportunity to use modern infrastructure and perform this research. The authors declare no conflicts of interest.

This work was supported by the Research council of Lithuania (grant no. 09.3.3-ESFA-V-711-01-0001).

[1] M. L. Pérez-Chabela and A. M. Hernández-Alcántara, "Agroindustrial Coproducts as Sources of Novel Functional Ingredients," in *Food Processing for Increased Quality and Consumption*, Elsevier, 2018, pp. 219–250.

[2] T. Blicharski and A. Oniszczuk, "Extraction Methods for the Isolation of Isoflavonoids from Plant Material," *Open Chem.*, vol. 15, no. 1, pp. 34–45, Mar. 2017, doi: 10.1515/chem-2017-0005.

[3] J. A. Kazlauskaite, L. Ivanauskas, and J. Benatoniene, "Cyclodextrin-Assisted Extraction Method as a Green Alternative to Increase the Isoflavone Yield from," *Pharmaceutics*, vol. 13, no. 5, pp. 1–14, 2021, doi: https://doi.org/10.3390/pharmaceutics13050620.

P4-3

DID NOT PARTICIPATE

.

INVESTIGATION OF KLUYVEROMYCES MARXIANUS AS A HOST FOR THE EXPRESSION OF THE HETEROLOGOUS GENES FOR THE BIOCATALYSTS PRODUCTION

Aušra Kondrataitė[1], Inga Matijošytė[1], Rimantas Šiekštelė[1]

[1] Sector of Applied Biocatalysis, Institute of Biotechnology, Life Sciences Center, Vilnius University, Lithuania
ausra.kondrataite@gmc.stud.vu.lt

Unlike chemical catalysis, biocatalysis is considered to be an effective and environmentally friendly process where enzymes perform variety of chemical reactions. It is extremely relevant in industry due to properties, such as stereo-, chemo-, regioselectivity as well as high catalytic activity and mild operational conditions [1]. Biocatalytic processes have been applied in a number of fields including bioremediation, pharmaceutical, food, textile industries and polymer synthesis, *etc.*

The key step for the production of biocatalysts is the development of an efficient protein expression system. Since the expression of genes in their native organisms is usually too low, it becomes crucial to design protein expression systems that would be capable of producing high yields of the target proteins. A very common problem related to the development of such biological system is protein insolubility that in turn leads to protein aggregation. In order to overcome this obstacle, target genes can be fused to highly soluble proteins, so-called chaperones or fusion partners [2]. Besides this, expression vectors must include other essential parts, such as origin of replication, promoter, terminator, selection markers, affinity tags. Each of these parts have to be selected according to the gene of interest. The choice of expression host is another important aspect to be considered and, to this date, the most widely used organisms are bacteria and yeasts [3].

In this study we aim to develop yeast expression system for the synthesis of several industrially important bacterial enzymes – laccase (Lacc) and β-carbonic anhydrase (β-CA). *Kluyveromyces marxianus* yeasts serve as a host for the expression of the mentioned enzymes since it is known as thermotolerant and fast-growing organism, having a GRAS (generally recognized as safe) status as well as an ability to metabolize wide variety of carbon sources [4]. To ensure high expression and solubility of Lacc and β-CA, three proteins – maltose-binding protein, endo-polygalacturonase and triose-phosphate isomerase – were investigated as fusion partners.

[1] A. Dev, A. K. Srivastava, S. Karmakar, New generarion hybrid Nnnobiocatalysts. Elsevier, 217-231 (2018).
[2] M-R. Ki, S. P. Pack. Fusion tags to enhance heterologous protein expression. Applied Microbiology and Biotechnology **104** (6), 2411-2425 (2020)
[3] P. F. Stanbury, A. Whitaker, S. J. Hall. The production of heterologous proteins. Elsevier, 725-775 (2017).
[4] A. K. Gombert, J. V. Madeira, M-E. Cerdán, M-I. González-Siso. Kluyveromyces marxianus as a host for heterologous protein synthesis. Applied Microbiology and Biotechnology **100** (14), 6193-6208 (2016).

STABILITY AND TOXICITY INVESTIGATION OF A NOVEL AROMATIC AMINE FOR LACCASE ACTIVITY SCREENING ON HIGH-THROUGHPUT AGAR PLATES

Justinas Babinskas[1], Jerica Sabotič[2], Inga Matijošytė[1]

[1] Sector of Applied Biocatalysis, Institute of Biotechnology, Life Sciences Center, Vilnius University, Lithuania
[2]Department of Biotechnology, Jožef Stefan Institute, Slovenia
justinas.babinskas@gmc.vu.lt

Laccases are multi-copper oxidases (EC 1.10.3.2), containing T1, T2 and T3 copper sites. Thought the years of investigating various laccases, a lot of information has already been accumulated: catalytic mechanism, redox potentials, enzyme sources, reorganization energies. These enzymes catalyze a unique oxidation of phenols, aromatic amines and thiols by using oxygen as a co-substrate and produce water as a by-product.[1] This process has an enormous potential for food, textile, paper, biofuel, cosmetics, paints, furniture industries and organic synthesis, nanobiotechnology and bioremediation.[2] By employing laccase-mediator systems, and thus expanding their substrate spectrum they could replace hydrogen peroxide and other chemical oxidators at industrial scale. However, tangible application of laccases is hindered by the unresolved drawbacks such as poor stability, commercial unavailability, lack of efficient expression systems, low immobilization yields, etc.

One of the shortcomings for discovering laccases with new and/or novel features is a lack of substrates suitable for high-throughput screening and functional analysis. Currently, the most common compounds used for laccase functional analysis are 2,2'-azino-bis(3-ethylbenzothiazoline-6-sulphonic acid) under the trivial name ABTS and 4-[[2-[(3,5-dimethoxy-4-oxocyclohexa-2,5-dien-1-ylidene)methyl]hydrazinyl]methylidene]-2,6-dimethoxycyclohexa-2,5-dien-1-one known as syringaldazine.[3,4] Spectrophotometric activity assays with these substrates give acceptable results, but these compounds have poor stability, low specificity and are rather expensive. Their use for high-throughput screening on agar plates is very hindered due to their thermal and pH instabilities.

By our investigation, we present a new substrate named Ferbamine for laccase activity screening on high-throughput agar-plates. Its thermal and pH stability in aqueous buffer solutions were studied. The latter substrate toxicity for *Kluyveromyces marxianus*, *Kluyveromyces lactis*, *Saccharomyces cerevisiae* and *Pichia pastoris* strains were investigated. Furthermore, Ferbamanine was tested on substrate-agar plates with commercially available laccase Novozym 51003 from *Aspergillus oryzea* and with the collection of wild fungi protein extracts provided by Jožef Stefan Institute (Fig. 1) [5].

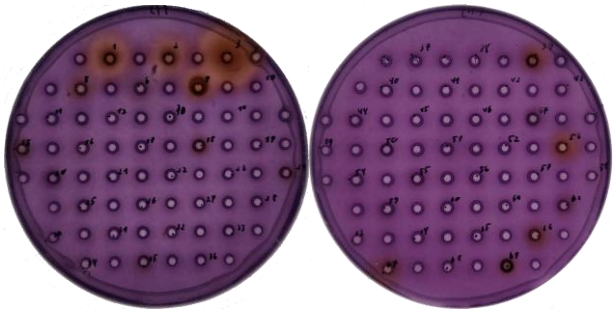


Fig. 1. The results of screening for laccase activity with the collection of wild fungi protein extracts on agar plates with 830 μM Ferbamine.

Ackowledgment. This study is based on collaboration work from COST Action CA18238 (Ocean4Biotech), supported by COST (European Cooperation in Science and Technology) program.

[1] S. M. Jones, E. I Solomon; Cellular and Molecular Life Sciences, 2014, 72, 869-883.
[2] D. M. Mate, M. Alcalde; Microbial Biotechnology, 2016, 10, 1457-1467.
[3] H. P. Call, I. Mücke; Journal of Biotechnology, 1997, 53, 163-202.
[4] M. F. Lucas et al.; Journal of Chemical Theory and Computation, 2017, 13, 1462-1467.
[5] J. Babinskas et al.; Manuscript in preparation.

ANALYSIS OF ANTIMICROBIAL PROPERTIES OF MEDICAL PLANTS *Levandula* L. AND *Helichrysum* L.

Karolina Lankaitė, Rūta Mickienė, Vilma Kaškonienė, Audrius Sigitas Maruška

Faculty of Natural Sciences, Instrumental Analysis Open Access Centre, Vytautas Magnus University, Vileikos str. 8, LT44404, Kaunas, Lithuania
karolina80808@gmail.com

Lavender (*Lavandula angustifolia*) essential oil is one of the most popular and can be considered one of the best-selling essential oils for anxiety, stress and depression. International organizations such as the World Health Organization (WHO), the European Scientific Cooperative for Phytotherapy (ESCOP) or the European Medicines Agency (EMA) validate the properties of this medicinal plant, such as anxiety and stress relief [1]. Also, interest in *Helichrysum italicum* essential oil is growing rapidly. *Helichrysum italicum* essential oil has been shown to have anti-inflammatory properties in recent decades. In addition, several studies have shown that secondary metabolites of *Helichrysum italicum* act as a free radical scavenger that can restore cellular redox balance and slow tumor cell growth and can be used in cancer therapy [3].

Helichrysum L. and *Lavandula* L. essential oils are widely used all over the world (in cosmetics, aromatherapy, perfumery, pharmacy, etc.), so the composition and antimicrobial properties of these natural products are very important. Synthetic antimicrobials and antibiotics have long been used against a variety of infectious diseases in humans and animals. The main disadvantage of antimicrobial chemotherapy is the increasing resistance to antimicrobials, which makes treatment less effective. Recent research has therefore highlighted the use of alternative natural products, especially those derived from plants.

Plants and plant extracts have been used as traditional medicine for many centuries. Volatile plant extract compounds, especially essential oils, are known as secondary plant metabolites that have been used primarily in aromatherapy, cosmetics, and medical purposes. Various essential oils of various plants have been observed to have strong antimicrobial properties [2].

Essential oils and their components play a key role in antimicrobial activity. Due to their hydrophobic nature, essential oils are able to move bacteria through the lipids of cell membranes, disrupting cell wall structures and making them permeable. This change in membrane permeability results in the leakage of ions and other cellular materials, leading to cell death. Essentially, essential oils are more active against gram-positive bacteria due to the peptidoglycan layer behind the outer membrane. In gram-negative bacteria, the outer membrane consists of a double layer of phospholipids that lipopolysaccharides bind to the inner membrane. Also, the properties of the major compounds present in essential oils and volatile compounds and their interactions may enhance the antibacterial effect [1].

Levandula angustifolia and *Helichrysum italicum* essential oils were tested against 2 bacteria and 2 fungi. The antimicrobial activity of these essential oils was tested using two agar diffusion methods using sterile 8 mm filter paper discs and 8 mm wells. The antimicrobial activity of the essential oils was also tested using two methods of inoculating bacteria and fungi on an agar plate: inoculation with Drigalskipatel aus Glas and inoculation with media (LB and ME). The DEN-1B densitometer used to measure the turbidity of the solution from 0.3 to 5.0 McFarland units. Bacterial suspensions were standardized to 150 x 10^6 cells / ml (0.5 Mac Farland), respectively. 100 µL suspensions were spread on broth agar (LB). Mushroom suspensions were standardized to 5 x 10^6 cells / ml (0.5 Mac Farland), respectively. 100 µL suspensions were spread on malt agar (ME). Filter paper discs were precipitated at equal distances on the surface of the agar LB and ME and 10 µL of crude essential oil and diluted essential oil (75%, 50% and 25% concentration) were added. 10 µL of crude essential oil and diluted essential oil (75%, 50% and 25% concentration) were added to the prepared wells in petri dishes. Dilutions of essential oils were performed with liquid media (LB and ME VWR CHEMICALS, Belgium). Inhibition diameter was measured after 24 hours at 37 ° C for bacteria and after 28 days at 28 ° C for fungi.

Assessing the antimicrobial properties of *Levandula* L. and *Helichrysum* L., it can be concluded that lavender oil was effective in inhibiting the growth of *Azotobacter vinelandii* and *Bacillus subtilis* at essential oil concentrations of 100% and 75%, respectively. When the concentration of the essential oil was 50%, the growth inhibition was lower and the concentration of 25% of the essential oil did not inhibit the growth of *Azotobacter vinelandii* and *Bacillus subtilis*. The fungal strain *Ulocladium chartarumbuva* was more sensitive to lavender essential oil at concentrations of 100% and 75% than *Cryptococcus neoformans* (Sanfelice). The results show that the essential oil of *Helichrysum italicum* had an inhibitory effect on the bacteria *Azotobacter vinelandii* and *Bacillus subtilis* at a concentration of 100% of the essential oil. The strains of the fungi *Ulocladium chartarum* and *Cryptococcus neoformans* (Sanfelice) were the least sensitive to the essential oil of *Helichrysum italicum*.

[1] Bhavaniramya S., Vishnupriya S., SalehAl-Aboodyb M., Vijayakumar R., Baskaran D., (2019). Role of essential oils in food safety: Antimicrobial and antioxidant applications. Volume 2, Issue 2, June 2019, Pages 49-55.

[2] Hossain S., Heo H., B.C.J. De Silva, S.H.M.P. Wimalasena, H.N.K.S. Pathirana, and Gang-Joon Heocorresponding (2017). Antibacterial activity of essential oil from lavender (Lavandula angustifolia) against pet turtle-borne pathogenic bacteria. Pages 195–201.

[3] Gismondi a., Marco G., Canini A., (2020). Helichrysum italicum (Roth) G. Don essential oil: Composition and potential antineoplastic effect. South African Journal of Botany Volume 133, Pages 222-226.

SINGLE ENZYME BIOFUEL CELL POWERED BY GLUCOSE

Algimantas Kaminskas[1*], Asta Kausaite-Minkstimiene[1]

[1] NanoTechnas–Center of Nanotechnology and Materials Science, Faculty of Chemistry and Geosciences, Vilnius University, Lithuania
algimantas.kaminskas@chgf.stud.vu.lt

Due to abundance in nature, availability in all organic tissues, low volatility, nontoxicity, inexpensiveness and relatively high energy density, glucose has been widely studied and considered to be an ideal renewable fuel source for biofuel cells (BFCs) [1]. For glucose oxidation, redox enzymes are most commonly used. High enzyme selectivity to analyte provides the possibility to construct particularly small membrane-less BFCs, which in the future may be adapted in the field of implantable medical devices [2]. However, despite all the advantages and scientific progress, glucose-powered BFCs (GBFCs) are still not efficient enough to be long-lived and applied practically. To increase efficiency, BFCs that used enzymatic reactions on both electrodes have also been researched and published over the past decade [3,4].

During this work, BFC powered by glucose, with both anode and cathode electrodes modified with the same enzyme was constructed and it operation was investigated. The anode was made of gold nanoparticles (AuNPs), 1,10-phenanthroline-5,6-dione (PD) and pyrrole-2-carboxylic acid (PCA) and glucose oxidase (GOx). Polymerization of PD and PCA polymeric layers with encapsulated AuNPs was performed by cyclic voltammetry (CV). Formed polymers improved electron transfer and provided a stable matrix for enzyme immobilization while AuNDs increased electron transfer efficiency. GOx was immobilized by a strong covalent bond and catalysed a reaction between glucose and dissolved oxygen, producing an electrical current.

The cathode was constructed of Prussian blue (PB) nanoparticles encapsulated in poly(pyrrole-2-carboxylic acid) (PPCA) layer also by CV. To improve cathode durability and increase the amount of immobilized enzyme, second PPCA layer was formed on the top of the first layer. Finally, the GOx was covalently linked to the carboxyl groups of the second PPCA layer. PB could reduce H_2O_2, which was produced during the enzymatic glucose oxidation reaction.

The single enzyme GBFC was constructed using the anode and cathode described above. Both the anode and cathode surface morphology and electrical properties were investigated as well as electrochemical performance of constructed GBFC. Obtained data indicates that this GBFC can generate electricity using glucose as the main fuel source.

Acknowledgment
This project was funded by the European Union (project No 09.3.3-LMT-K712-25-0013) under the agreement with the Research Council of Lithuania (LMTLT).

[1] G. Slaughter, T. Kulkarni, Enzymatic Glucose Biofuel Cell and its Application, J. Biochips Tissue Chips. 05 (2015).
[2] J.L. Zhang, Y.H. Wang, K. Huang, K.J. Huang, H. Jiang, X.M. Wang, Enzyme-based biofuel cells for biosensors and in vivo power supply, Nano Energy. 84 (2021) 105853.
[3] A. Koushanpour, M. Gamella, N. Guz, E. Katz, A Biofuel Cell Based on Biocatalytic Reactions of Glucose on Both Anode and Cathode Electrodes, Electroanalysis. 29 (2017) 950–954.
[4] A. Kausaite-Minkstimiene, A. Kaminskas, A. Popov, A. Ramanavicius, A. Ramanaviciene, Development of a new biocathode for a single enzyme biofuel cell fuelled by glucose, Sci. Rep. 11 (2021) 1–11.

SOLUBLE AND LIPOSOMAL DOXORUBICIN UPTAKE IN CANCER CELLS AFTER SHORT TERM EXPOSURE

Lavija Žibutytė[1,2], Gintaras Zaleskis[1]

[1] Laboratory of Immunology, National Cancer Institute, Lithuania
[2] Insititute of Chemistry, Faculty of Chemistry and Geosciences, Vilnius University, Lithuania
zibutyte.lavija@gmail.com

Doxorubicin (DOX) and liposomal doxorubicin (L-DOX) are part of the anthracycline drug class, which kills cancer cells by intercalating with DNA, inhibiting topoisomerase II activity and generating reactive oxygen species. Despite being introduced more than 50 years ago, these drugs are still mainly used for treatment of solid tumors. However, doxorubicin has one key disadvantage – it possesses poor selectivity for tumor cells, which can lead to severe cardiotoxicity [1]. In order to increase selectivity of tumor cells and avoid potentially lethal side effects, researchers have incapsulated anthracycline into liposomes with polyethylene glycol (PEG) coating, thus creating liposomal doxorubicin. The size of the liposome allows greater extravasation into the tumor through vessels, meaning that L-DOX possesses greater selectivity for tumor cells than its soluble form. But the drug still has its own dose-limiting effect through palmar–plantar erythrodysesthesia. Researchers have hypothesized that the liposome of L-DOX slowly degrades and expresses its anti-tumor activity through releasing doxorubicin into the extracellular space [2]. Our working hypothesis follows this by suggesting that short term exposure to the liposomal drug may not always show high cellular uptake comparing to DOX, because of its inability to quickly accumulate in cells and release the soluble form of the drug.

In this study, we set out to compare cellular uptake of live and permeabilized tumor cells after short exposure to fresh and degraded forms of DOX and L-DOX. The degradation of drugs in tissues was simulated through keeping the drugs for several months in 37°C and protection from light. Live and permeabilized mice lymphoma SL2 cells were subjected to 10 μg/ml concentration of both drugs for 30 minutes, then washed and analyzed by flow cytometry. Results show that in both live and permeabilized cells the uptake of DOX between fresh and degraded drug does not significantly change - concentration only decreases by 1.1 times and 1.4 times, respectively, with degraded DOX. However, with L-DOX, the change in concentration is more significant – we have detected an increase of 13.3 times in live and 3.5 times in permeabilized cells, comparing the degraded drug with fresh L-DOX. Comparing the difference between uptake of DOX and L-DOX, the uptake of fresh DOX was measured 10.2 times higher in live cells and 8.6 times higher in permeabilized cells, than after incubating cells with L-DOX. With degraded drugs, uptake was 1.5 times lower and 1.8 times higher in live and permeabilized SL2 cells, respectively.

These results show that initial cellular uptake of L-DOX is significantly lower than DOX, even in permeabilized cells, which also show limited internalization of the drug. Results also suggest that while, over a short term, soluble DOX may be significantly more effective than its liposomal form, over a longer term, with liposomal degradation and slow drug release into tumor cells, L-DOX might look promising in prolonged or locoregional cancer treatment. However, this speculation still needs further study to demonstrate.

[1] J.V. McGowan, R. Chung, A. Maulik, I. Piotrowska, J. M. Walker, and D. M. Yellon, Anthracycline Chemotherapy and Cardiotoxicity, Cardiovascular Drugs and Therapy, vol. 31, 63–75, (2017).
[2] A.A. Gabizon, Y. Patil, and N.M. La-Beck, New insights and evolving role of pegylated liposomal doxorubicin in cancer therapy, Drug Resistance Updates, vol. 29, 90–106(2016)

SCREENING AND CHARACTERIZATION OF AMINOTRANSFERASES FOR ASYMMETRIC SYNTHESIS OF CHIRAL AMINES

Rokas Statkevičius[1], Justas Vaitekūnas[1], Renata Gasparavičiūtė[1], Jonita Stankevičiūtė[1], Rolandas Meškys[1]

[1]Department of Molecular Microbiology and Biotechnology, Vilnius University, Lithuania
rokas.statkevicius@gmc.vu.lt

Chiral amine compounds are widely used as active pharmaceutical ingredients, agricultural chemicals, and other biologically active compounds [1]. Aminotransferases (AT) are enzymes that mediate the transfer of an amino group to a ketone acceptor. ATs have been already proven to be a promising catalyst in the synthesis of chiral amine compounds. The catalysis by ATs is performed under mild conditions, without the use of toxic metals and solvents, and has a higher stereo- and regio-selectivity compared to the organic synthesis [2]. However, the broad application of such enzymes is restricted by a limited number of the identified ATs.

In this study, we searched for aminotransferases in the metagenomic DNA libraries using indol-3-ylmethylamine as a prochromogenic amino donor. We found and recombinantly expressed 18 different ATs. The experimental analysis revealed that the tested aminotransferases were active towards a wide variety of aromatic and aliphatic keto compounds and were capable of using isopropylamine as an amino donor (Fig. 1). In small-scale amination experiments, we were able to achieve a conversion of 95% for 2-acetylpyridine and 2-indanone using AT as a biocatalyst. Furthermore, some ATs showed activity towards monosaccharides and, therefore, could be employed for the synthesis of different aminopolyols – a class of products that are of particular interest as carbohydrate mimetics.

In summary, we successfully identified ATs active towards a wide scope of keto compounds. We showed ATs to be promising biocatalysts for chiral amine production.

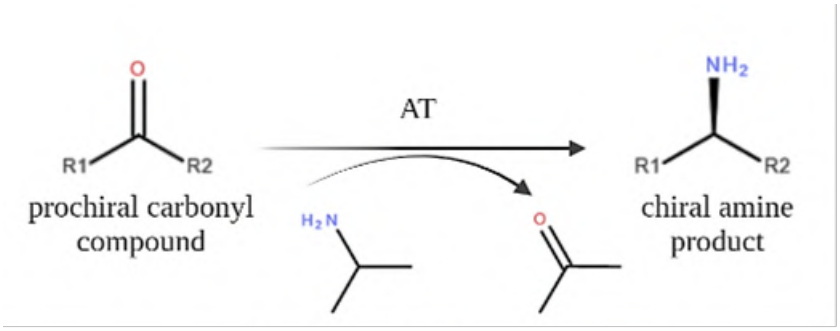


Fig. 1 Asymmetric synthesis using ATs.

[1] L.-J. Guan et al., "A new target region for changing the substrate specificity of amine transaminases," Sci. Reports 2015 51, vol. 5, no. 1, pp. 1–11, Jun. 2015, doi: 10.1038/srep10753.
[2] F. Guo and P. Berglund, "Transaminase biocatalysis: Optimization and application," Green Chem., vol. 19, no. 2, pp. 333–360, 2017, doi: 10.1039/c6gc02328b.

SYNTHESIS OF BIOLOGICALLY ACTIVE 1,2,4-TRIAZOLE-3-THIOL DERIVATIVES BEARING HYDRAZONE MOIETY

Aida Šermukšnytė[1*], Ilona Jonuškienė[1], Kristina Kantminienė[2], Ingrida Tumosienė[1]

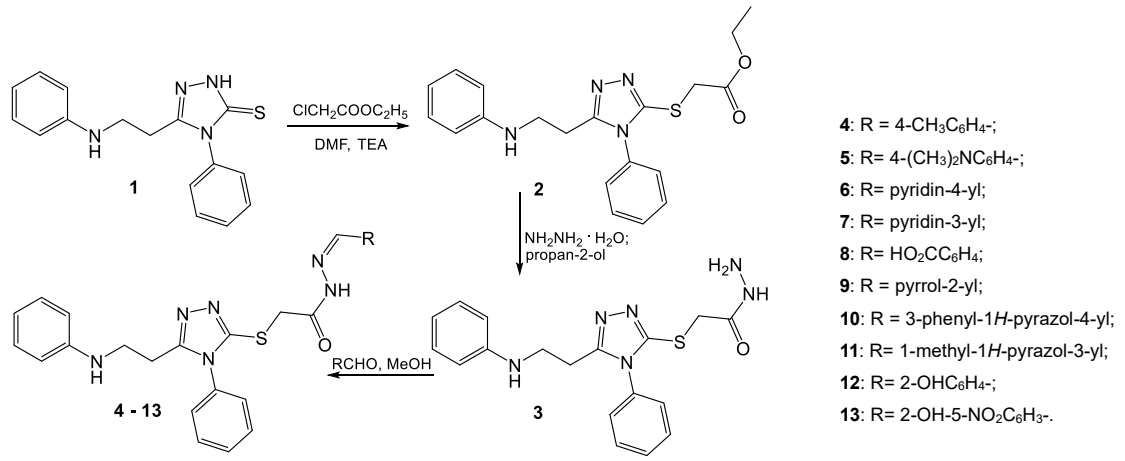
[1] Department of Organic Chemistry, Kaunas University of Technology, Lithuania
[2] Department of Physical and Inorganic Chemistry, Kaunas University of Technology, Lithuania
aida.sermuksnyte@ktu.edu

The emergence and spread of drug-resistant pathogens that have acquired new resistance mechanisms, leading to antimicrobial resistance, limit the therapeutic options for treatment of common infections Therefore, new antibacterial agents are urgently needed [1].

1,2,4-Triazoles are important heterocyclic compounds that are widely found in molecular architectures with medicinal and pharmaceutical properties. Triazole heterocycles which incorporate sulphur in a form of mercapto and thione substitution show more potency compared to parent derivatives. 1,2,4-Triazole-3-thione derivatives are attractive scaffolds in medicinal chemistry for their broad biological activity, e.g. antibacterial, antioxidant, anticonvulsant, antidepresant, anti-inflammatory, etc. [2,3].

Hydrazone derivatives, which biological activity is associated with the presence of the active azomethine -NH-N=CH- pharmacophore, constitute another significant class of biologically active compounds in medicinal and pharmaceutical chemistry. These compounds, in combination with various heterocyclic scaffolds, possess diverse biological activity, including antimicrobial, antiviral, antimycobacterial, antimalarial, anticancer, etc. [4].

With the aim to synthesize potentially biologically active compounds bearing these two pharmacophores along with other aromatic and heterocyclic moieties, compounds **2-13** were synthesized (Scheme 1). Reaction of 4-phenyl-3-[2-(phenylamino)ethyl]-1*H*-1,2,4-triazole-5(4*H*)-thione (**1**) with ethyl chloroacetate in DMF in the presence of triethylamine provided ethyl 2-[[4-phenyl-5-[(phenylamino)ethyl]-4*H*-1,2,4-triazol-3-yl]thio]acetate (**2**), which subsequent reaction with hydrazine hydrate in propan-2-ol gave 1,2,4-triazol-3-ylthioacetohydrazide **3**. The target hydrazones **4-13** bearing various aromatic and heterocyclic moieties were synthesized from **3** and corresponding aldehydes in methanol in good yield yield. [5,6].



Scheme 1. Synthesis of 1,2,4-triazole-3-thiol derivatives **2–13**

Screening of the antibacterial activity of the synthesized compounds **4-13** by agar diffusion method has revealed that compound **6** possesses the highest antibacterial activity against *Escherichia coli*, *Rhizobium radiobacter*, and *Xanthomonas campestris* bacteria. Among the tested compounds **4-13**, compound **4** has been shown to possess the highest DPPH radical scavenging activity and **7** has been identified as the one exhibiting the strongest reducing activity by the reducing power assay.

Acknowledgement. Part of the research leading to these results has received a funding from European Social Fund (project No 09.3.3-LMT-K-712-22-0083) under grant agreement with the Research Council of Lithuania (LMTLT).

[1] Antimicrobial resistance, Fact Sheets, World Health Organization: Geneva, Switzerland, 17 November 2021; Available online: https://www.who.int/news-room/fact-sheets/detail/antimicrobial-resistance (accessed on 10 January 2022).
[2] A. Abdelli, S. Azzouni, et al., Recent advances in the chemistry of 1,2,4-triazoles: Synthesis, reactivity and biological activities, Tetrahedron Letters **86**, 153518 (2021).
[3] R.M. Shaker, The chemistry of mercapto- and thione-substituted 1,2,4-triazoles and their utility in heterocyclic synthesis, Arkivoc **9**, 59-112 (2006).
[4] J.O.C. Brum, T.C.C. França, et al., Synthesis and Biological Activity of Hydrazones and Derivatives: A Review, Mini-Reviews in Medicinal Chemistry **20**, 342-368 (2020).
[5] I. Tumosienė, K. Kantminienė, et al., Synthesis of 1-(5-Chloro-2-hydroxyphenyl)-5-oxopyrrolidine-3-carboxylic Acid Derivatives and Their Antioxidant Activity, Molecules **24**, 971-985 (2019).
[6] I. Tumosienė, K. Kantminienė, et al., Synthesis of Azole Derivatives from 3-Phenylaminopropanhydrazide and Evaluation of Their Antimicrobial Efficacy, Heterocycles **78**, 59–70 (2009).

IN SILICO INTERACTION OF ONOSMONE AND TRUXILLIC ACID AGAINST THE MAIN PROTEASE OF SARS-COV-2

Tarik Corbo[1], Abdurahim Kalajdzic[1], Naris Pojskic[1]

[1] Institute for Genetic Engineering and Biotechnology, University of Sarajevo, Bosnia and Herzegovina
tarik.corbo@ingeb.unsa.ba; tarik.corbo@gmail.com

Main protease (*Mpro*), also known as 3CL protease, is a cysteine protease that plays a key role in the maturation of functional polypeptides involved in the replication-transcription mechanism assembly. Furthermore, *Mpro* has no human homologue and is highly conserved in all coronaviruses, making it a great antiviral target. A variety of plant compounds have been investigated for their natural antiviral properties and a review of the literature revealed that the phytochemicals onosmone and truxilic acid, which are found in the Indian medicinal plants *Onosma echioides* and *Erythroxylum coca*, had a weighted quantitative estimate of drug-likeness (QEDw) score ≥0.9 and were categorized as the most druggable phytochemicals by Mohanraj et al. (2018) [1]. The objective of this research was to simulate and predict structural interactions of onosmone and truxillic acid against the SARS-CoV-2 main protease and determine their potential antiviral activity. The three-dimensional crystal structure of *Mpro* (PDB ID: 6Y84) was retrieved from Protein Data Bank in PDB format and the preparation was performed using AutoDock Tools 1.5.6 [2], where the target protein was converted from PDB to PDBQT format. Also, using AutoDock Tools 1.5.6 we defined a gridbox with which we tried to capture the oxyanion hole (Cys145, Gly143 and Ser144) and the catalytic dyad (Cys145 - His41), which is a highly conserved area that serves as an active site. The three-dimensional structures of the two selected compounds, onosmone (CID: 102212116) and truxillic acid (CID: 78213), and positive controls were retrieved from PubChem in the SDF format and then converted to the PDBQT format using OpenBabel 3.1.1 [3]. As positive controls of binding affinity we used rutin (CID: 5280805) and remdesivir (CID: 121304016) due to their proven antiviral activity in previous studies. Molecular docking was performed using AutoDock Vina 1.1.2 [4], while the results were visualized using Pymol 2.5.2 [5]. After analyzing the structural interactions of onosmone and truxillic acid against *Mpro*, it was shown that both compounds interact with *Mpro* in its active site. Onosmone reacted with Thr25, Thr26, Cys44, Ser46, Asn142 and Gly143, forming two good (yellow) hydrogen bonds with Gly143 (2.7 Å and 3.3 Å) (Fig. 1A), with a binding affinity for *Mpro* at −7.1 kcal/mol, while truxillic acid reacted with His41, Cys44, Thr45, Ser46, Asn 142 and His164, forming three good (yellow) hydrogen bonds with His41 (2.4 Å), Cys44 (3.0 Å) and His164 (2.2 Å) (Fig. 1B), with a binding affinity at −6.7 kcal/mol. These findings indicate that these two compounds could be potentially antiviral and utilized as a treatment for COVID-19, although more *in vitro* and *in vivo* research is required.

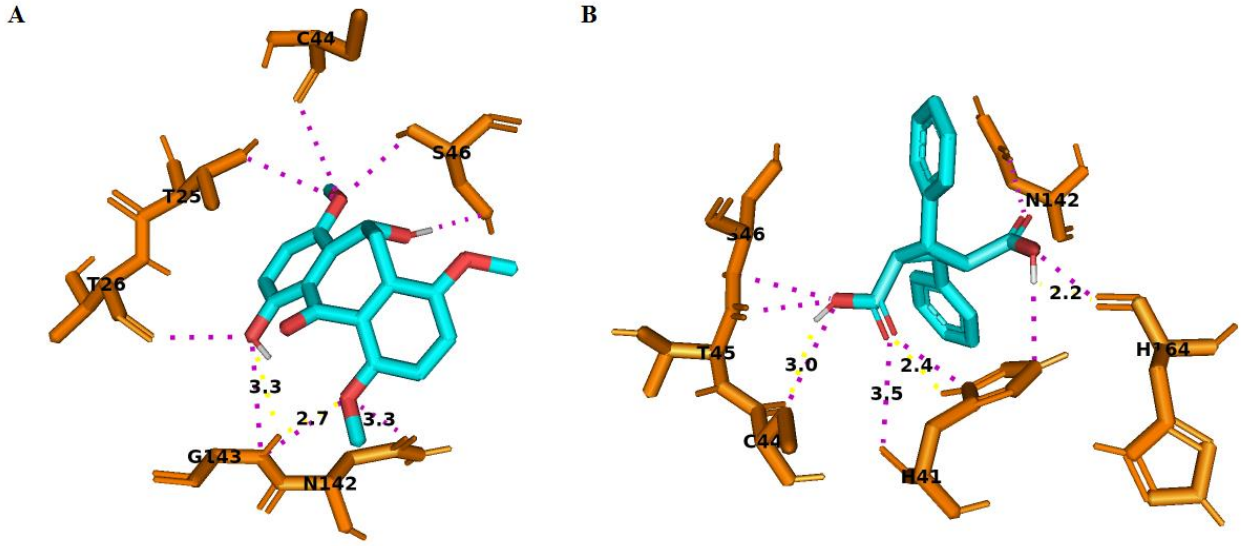


Fig. 1. A Interaction of onosmone with *Mpro* residues; B Interaction of truxillic acid with *Mpro* residues.

[1] K. Mohanraj, B. S. Karthikeyan, R. P. Vivek-Ananth, R. Chand, S. R. Aparna, P. Mangalapandi, A. Samal, IMPPAT: A curated database of Indian Medicinal Plants, Phytochemistry And Therapeutics, Scientific reports, 8(1), 4329 (2018).
[2] G. Morris, R. Huey, W. Lindstrom, M. Sanner, R. Belew, D. Goodsell, and A. Olson, Autodock4 and AutoDockTools4: automated docking with selective receptor flexibility, Journal of Computational Chemistry, 30(16), 2785-91 (2009).
[3] N. M. O'Boyle, M. Banck, C. A. James, C. Morley, T. Vandermeersch, G. R. Hutchison, Open Babel: An open chemical toolbox, Journal of Cheminformatics, 3, 33 (2011).
[4] O. Trott, A. J. Olson, AutoDock Vina: improving the speed and accuracy of docking with a new scoring function, efficient optimization, and multithreading, Journal of Computational Chemistry, 31(2), 455–461 (2010).
[5] The PyMOL Molecular Graphics System, Version 2.5.2, Schrödinger, LLC.

OPTIMISATION OF BEE POLLEN FERMENTATION TIME BY FERMENTING WITH TIBICO AND KOMBUCHA CULTURES.

Lukas Asanavičius, Vilma Kaškonienė, Nicola Tiso, Audrius Sigitas Maruška

Instrumental Analysis Open Access Center, Vytautas Magnus University, Lithuania
lukas.asanavicius@stud.vdu.lt

Bee pollen is pollen collected from various plants by bees and stuck together by nectar and enzymes, such as amylase and catalase, and then formed into granules. Bee pollen is rich in a plethora of nutrients such as phenolic compounds, minerals, and vitamins which can improve the health of humans [1]. Great things never come cheap, the same is with bee pollen. The main flaw of bee pollen is that they have a wall named exine which is made from sporopollenin, this kind of wall is extremely elastic, sturdy, and resilient to chemicals. Due to the exine wall resilience, humans only digest only about 10-15% of bee pollen [2].

Fermentation is recommended to increase the bioavailability of bee pollen. In this project, bee pollen was fermented using symbiotic cultures of bacteria and yeast which are naturally present in tibico and kombucha cultures. Prepared tibico and kombucha drinks were used to ferment bee pollen. One random sample from Lithuania was selected in order to optimize the ratio of bee pollen and tibico/kombucha drink and the fermentation time required to extract the highest amount of phenolic compounds and flavonoids. Spontaneous fermentation without the addition of tibico or kombucha drink was performed for comparison. After 3 or 8 days of fermentation, methanolic extracts from fermented pollen mass were prepared and tested for the total amount of phenolic compounds and flavonoids. Results are presented in the Fig. 1.

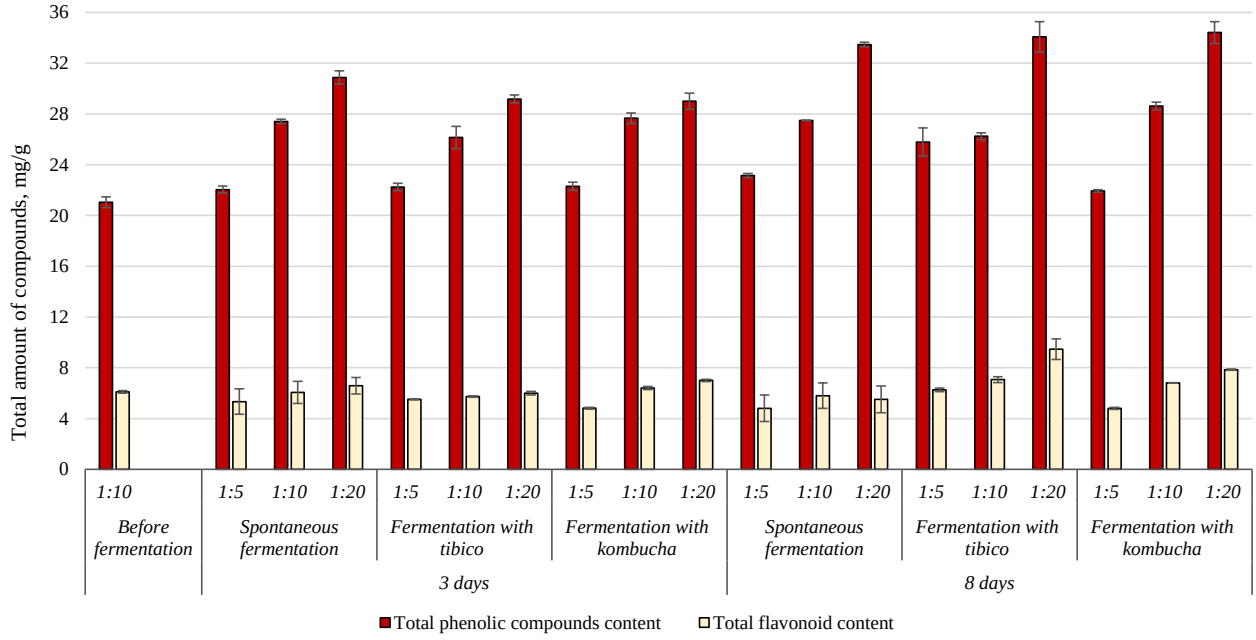


Fig. 1. Total amount of phenolic compounds and flavonoids extracted from bee pollen after fermentation using different ratios of bee pollen and tibico/kombucha drink and using different fermentation time (expresses in mg/g rutin equivalents)

As it can be seen, both spontaneous fermentation and fermentation with tibico or kombucha cultures had a positive effect, mainly on the total content of phenolic compounds. However spontaneous fermentation showed similar results to tibico/kombucha, but in the samples of spontaneous fermentation the growth of molds is evident after 2-3 days and due to that they became unusable for consumption. The highest amount of phenolic compounds were extracted after 8 days of fermentation both with tibico and kombucha cultures at the 1:20 ratio 34.1±1.2 mg/g and 34.4±0.9 mg/g, respectively. The highest amount of flavonoids was also extracted after 8 days of fermentation at the 1:20 ratio: 9.5±0.8 mg/g and 7.9±0.1 mg/g using tibico and kombucha cultures, respectively.

The performed study showed, that the highest amount of phenolic compounds and flavonoids is achieved after 8 days of fermentation at room temperature using a 1:20 ratio (1 gram of bee pollen and 20 ml of the fermented drink).

Acknowledgements: Financial support from Research Council of Lithuania project No. 09.3.3-LMT-K-712-25-0193 is acknowledged.

[1] B. Denisow ir M. Denisow-Pietrzyk., Biological and therapeutic properties of bee pollen: a review, Journal of the Science of Food and Agriculture **96**, 4303-4309 (2016).
[2] J. Brooks ir G. Shaw, Sporopollenin: A review of its chemistry, palaeochemistry and geochemistry, Grana **17**, 91-97 (1978)

VALUABLE COMPOUNDS EXTRACTION FROM MICROALGAE CULTIVATED IN AQUACULTURE WASTEWATER USING COLD PLASMA AND PULSED ELECTRIC FIELDS

Gintarė Dalmantaitė[1,2], Kamilė Jonynaitė[2]

[1]Life Sciences Center, Vilnius university, Lithuania
[2] Laboratory of Bioelectrics, Center for Physical Sciences and Technology, Lithuania
gintare.dalmantaite@gmc.stud.vu.lt

As aquaculture industry grows, microalgae could be used for the bioremediation of its wastewater. This is in accordance with principals of circular economy, since these microalgae clean wastewater and synthesize highly valuable compounds at the same time. One of the most effective methods to extract these compounds is high-pressure homogenization technology. However, different fractions of algae compounds are mixed during this process, thus there is a need for an additional purification step. Therefore, other effective extraction methods are investigated [1].

Pulsed electric fields (PEF) is an intensively researched extraction method. It is based on usage of short (μs-ms) and strong (5-80 kV/cm) electric pulses, which cause an increase of cell membrane permeability. Advantages of this method are selectiveness and purity of extracted substances [2]. Nevertheless, extraction with PEF isn't effective enough, hence researchers are trying to improve it. Cold plasma treatment could possibly be a solution. During the treatment, generated radicals may cause lipid oxidation, leading to membrane weakening and pore formation [3]. A combination of these techniques could be useful strategy to increase extraction yields of valuable compounds from microalgae. Moreover, they could be adapted to an industrial scale.

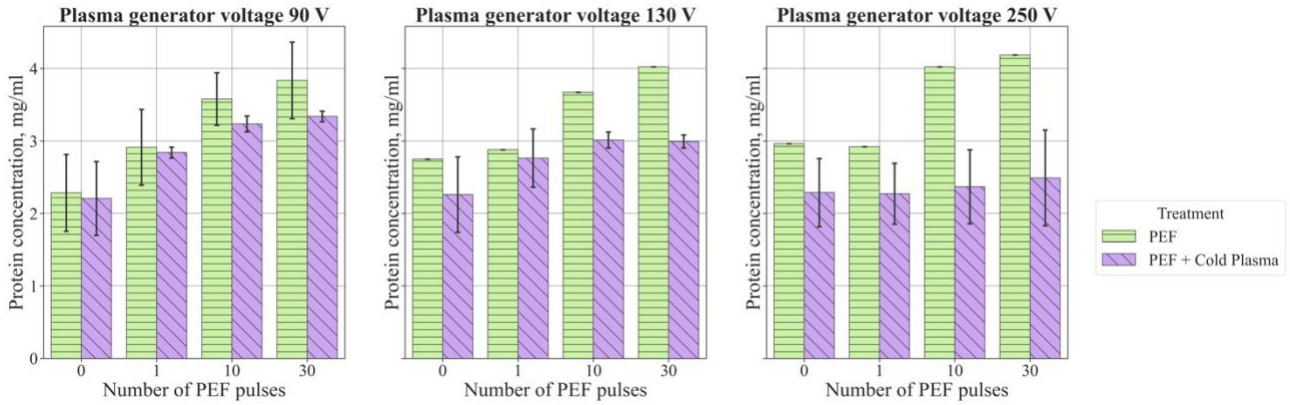


Fig. 1. Protein concentration extracted from *C. vulgaris* (cultivated in wastewater) after cold plasma and/or PEF treatments.

For protein extraction experiments, suspension of *Chlorella vulgaris* microalgae was washed once and concentrated up to 100 g/L wet biomass with BG-11 medium (σ = 1,96 mS/cm). Then they were treated with cold plasma or PEF only, or firstly by cold plasma and then by PEF. Cold plasma treatment lasted for 5 minutes, and plasma generator voltages were 90 - 250 V. PEF parameters were U = 3,5 kV, t = 10 μs, f = 1 Hz, n = 1;10;30, d = 0,1 cm. Conductivity of the suspensions was measured after cold plasma treatment. Further, after selected treatment, samples were incubated for 2h at room temperature. Finally, protein concentration in the supernatant was determined with Bradford method.

Firstly, conductivity changes were observed after cold plasma treatment – there was an increase of it in microalgae suspensions. For instance, after treatment with plasma generator voltage of 250 V, suspension's conductivity has risen by 52 %. This indicates that cells' membranes were permeabilized. Additionally, when samples were treated with a combination of cold plasma and PEF (plasma generator voltage 90 V, n (PEF) = 1; 10; 30), protein extraction has increased, compared to only plasma treatment control. However, the results (Fig. 1) have shown that PEF alone is more efficient for protein extraction than combination of PEF and cold plasma. For example, obtained protein concentrations after PEF (n = 10) and cold plasma + PEF (plasma generator voltage 90 V, PEF n =10) treatments were respectively 3,58 ± 0,51 mg/ml and 3,24 ± 0,15 mg/ml. After PEF (n = 10) and cold plasma + PEF (plasma generator voltage 250 V, n (PEF) =10), the results were accordingly 4,02 mg/ml and 2,37 ± 0,72 mg/ml. Therefore, further investigation on how cold plasma and PEF together affect microalgae cells is needed.

[1] Han, P., Lu, Q., Fan, L., & Zhou, W. (2019). A Review on the Use of Microalgae for Sustainable Aquaculture. *Applied Sciences*, *9*(11), 2377.
[2] Zocher, K., Banaschik, R., Schulze, C., Schulz, T., Kredl, J., Miron, C., Schmidt, M., Mundt, S., Frey, W., & Kolb, J. F. (2016). Comparison of Extraction of Valuable Compounds from Microalgae by Atmospheric Pressure Plasmas and Pulsed Electric Fields. *Plasma Medicine*, *6*(3–4), 273–302.
[3] Gururani, P., Bhatnagar, P., Bisht, B., Kumar, V., Joshi, N. C., Tomar, M. S., & Pathak, B. (2021). Cold plasma technology: Advanced and sustainable approach for wastewater treatment. *Environmental Science and Pollution Research International*, 1–21

PRODUCTION OF RECOMBINANT MOUSE CARBONIC ANHYDRASES PROTEINS

Agnė Mikelevičiūtė[1], Tautvydas Kojis[1], Aurelija Mickevičiūtė[1], Lina Baranauskienė[1]

[1]Department of Biothermodynamics and Drug Design, Institute of Biotechnology, Life Sciences Center, Vilnius University, Vilnius, Lithuania
agne.mikeleviciute@gmc.vu.lt

Carbonic anhydrases (CA) responsible for reversible carbon dioxide's hydration in recent years have become one of the emerging therapeutic targets. However, carbonic anhydrases are linked to many diseases and disorders because of their importance in many physiological processes such as pH regulation, ion transport, or metabolic reactions, where bicarbonate is used as a substrate [1]. For example, CA I is associated with anemia; CA II and CA IV with glaucoma; and CA IX with cancer [2].

Several CA inhibitors are used to control glaucoma, epilepsy, edema, etc. Moreover, one of the important discoveries in recent years was carbonic anhydrase isozyme, specifically CA IX, connection to cancer. Some of the inhibitors for CA IX have already entered preclinical or clinical trials [2]. In the preclinical research step, new drug testing is performed on animals. House mouse (*Mus musculus*) is the most often used model organism for preclinical drug testing. While orthologous proteins are highly similar, sometimes even small structural differences result in significant affinity variations towards small molecule inhibitors. By producing murine carbonic anhydrases (Car), we will be able to test whether human CA inhibitors that were selected using *in vitro* methods have comparable affinity and selectivity to murine Car, and thus we could expect more accurate results in the preclinical testing.

Previously we produced several recombinant mouse carbonic anhydrases [3] [4]. Now we were able to produce most of the active mouse carbonic anhydrases. Most of them were expressed in different *Escherichia coli* strains and purified by chromatographic methods. Their expression and purity have been confirmed using SDS-PAGE (Fig. 1).

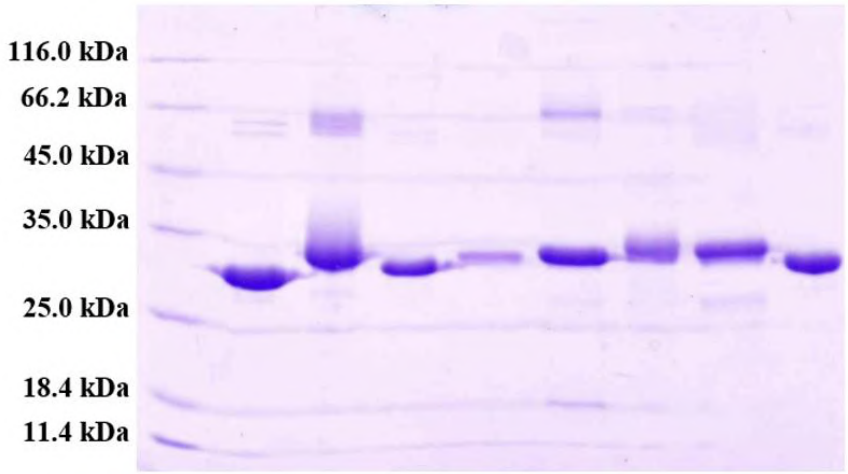


Fig. 1. SDS-PAGE of carbonic anhydrases (from left to right protein marker, Car I, Car II, Car III, Car IV, Car VA, Car VI, Car VII, Car XIII).

[1] Chegwidden W.R. (2021) The Carbonic Anhydrases in Health and Disease. In: Chegwidden W.R., Carter N.D. (eds) The Carbonic Anhydrases: Current and Emerging Therapeutic Targets. Progress in Drug Research, vol 75. Springer, Cham. https://doi.org/10.1007/978-3-030-79511-5_1.

[2] Matulis, D. (Ed.). (2019). *Carbonic Anhydrase as Drug Target.* doi:10.1007/978-3-030-12780-0.

[3] E. Timoščenka, Production of recombinant mouse carbonic anhydrases Car I, Car II, Car III, Car VII, Car XIII, 64th international conference for students of physics and natural sciences, Open Readings 2021.

[4] T. Kojis, Production of recombinant mouse carbonic anhydrase Car XIV protein, 64th international conference for students of physics and natural sciences, Open Readings 2021.

APPLICATION OF FLUORESCENCE SPECTROSCOPY FOR INVESTIGATION OF pH BANDING IN *NITELLOPSIS OBTUSA*

Aušrinė Navickaitė[1], Vilmantas Pupkis[1], Saulius Bagdonas[2]

[1] Department of Neurobiology and Biophysics, Vilnius University, Vilnius, Lithuania
[2] Laser Research Center, Vilnius University, Vilnius, Lithuania
ausrine.navickaite@gmc.stud.vu.lt

Due to the development of a deeper understanding of the relationship between photosynthesis and fluorescence parameters, chlorophyll fluorescence measurements are frequently used to monitor photosynthetic performance. The processes of photochemistry and emission are in direct competition for excitation energy. Therefore, if the rate of one process increases, the rate of the other one decreases [1]. Characean algae represent a unique model to study photosynthesis. Upon irradiation with actinic light characean internodes develop alternating pH bands along their surface [2]. This phenomenon is known to be beneficial for photosynthesis, as increased photosynthetic efficiency is observed at the acid zones [3]. However, whilst emission parameters can be easily acquired, many different factors can affect fluorescence in a similar way. Thus, further evaluation of changes in fluorescence parameters is needed to understand complex physiological patterns.

An optical fiber system paired with controlled stepper motor enabled registration of chlorophyll fluorescence signals along *Nitellopsis obtusa* internodes in 1 mm intervals. A low intensity (< 1 mW) LED light source emitting at 405 nm was used for excitation. Two types of experiments were carried out to determine fluorescence parameters best suited to monitor photosynthetic activity - signals were registered in dark-adapted internodes and in cells that underwent no dark adaptation.

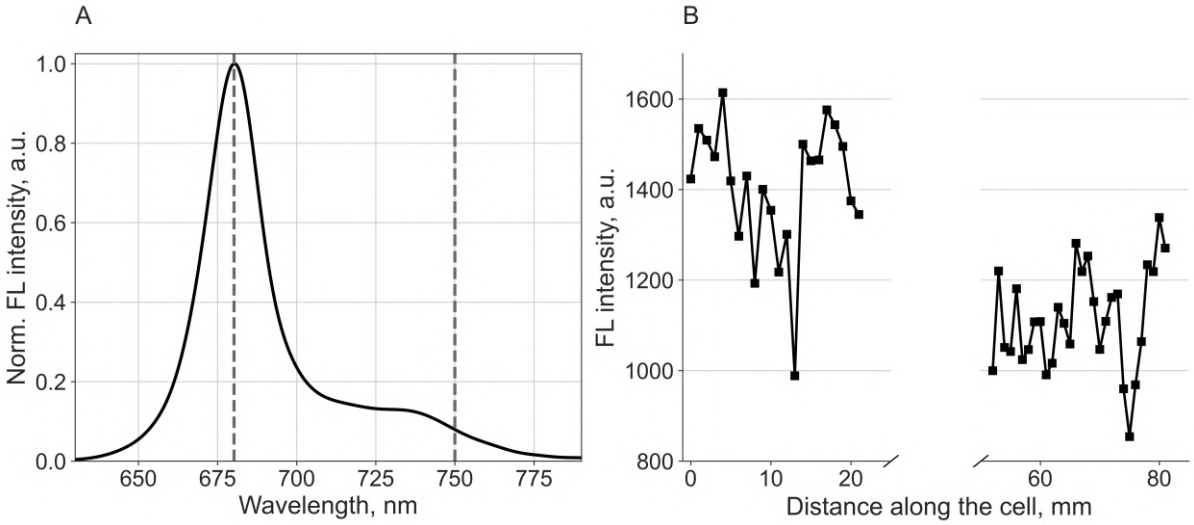


Fig. 1. Typical chlorophyll fluorescence (FL) spectrum (A) and variation of peak fluorescence intensity at around 680 nm (B).

Algae exhibited a chlorophyll fluorescence spectrum with two peaks around 680 nm and 739 nm (Fig. 1A). Fluorescence intensity values registered at the first peak displayed variations along the cell (Fig. 1B) in accordance with changes of fluorescence intensity ratio between 680 nm and 750 nm (F680/F750). Patterns of alterations of maximum fluorescence intensity remained similar regardless of illumination, however, variation of the F680/F750 ratio was significantly lower in dark-adapted cells compared to internodes that underwent no dark adaptation. This result could be related to the disappearance of pH banding in the dark as this phenomenon causes changes of photosynthetic performance, yet is only observed after constant illumination.

Hence, the F680/F750 fluorescence ratio is a more suitable parameter to draw conclusions about physiological changes in algae cells than the peak fluorescence intensity value as it is less affected by non-physiological factors.

[1] N. R. Baker, Chlorophyll Fluorescence: A Probe of Photosynthesis In Vivo, Annual Review of Plant Biology 59(1), 89-113 (2008).
[2] A. A. Bulychev, A. A. Polezhaev, S. V. Zykov, et al., Light-Triggered pH Banding Profile in Chara Cells Revealed with a Scanning pH Microprobe and Its Relation to Self-Organization Phenomena, Journal of Theoretical Biology 212(3), 275-294 (2001).
[3] N. A. Krupenina, A. A. Bulychev, M. R. G. Roelfsema, U. Schreiber, Action Potential in Chara Cells Intensifies Spatial Patterns of Photosynthetic Electron Flow and Non-Photochemical Quenching in Parallel with Inhibition of pH Banding, Photochem. Photobiol. Sci. 7(6), 681-688 (2008).

EVALUATION OF THE IMPACT OF OAK (*QUERCUS* SPP.) ACORNS TREATMENT ON PHENOLIC COMPOUNDS AND FLAVONOIDS

Aurelija Kondratavičiūtė, Vilma Kaškonienė, Rūta Mickienė, Audrius Maruška

Instrumental Analysis Open Access Centre, Faculty of Natural Sciences, Vytautas Magnus University, Lithuania
aurelija.kondrataviciute@stud.vdu.lt

Oaks (*Quercus* spp.) are perennial, widespread throughout the Northern Hemisphere trees of whose certain parts can have a positive impact on human life. Knowing that the common oak (*Quercus rubra* L.) is a naturally growing oak in Lithuania, its fruits were selected for research. Acorns are the fruit of the oak, also known as oak nuts. Acorns are a natural food that has been used in the diet of people for thousands of years. However, research shows a wider use of acorns due to the antioxidant and antibacterial potential of phytochemical compounds in the acorns.

Acorns are known to have antioxidant activity [1]. However, it is known that antioxidant activity depends both on the sample preparation technique and geographic origin of the natural object. Different treatments of acorns can affect their phytochemical compounds. Fermentation, soaking, germination and enzymatic treatment are methods used to reduce toxic compound presence in acorns - phytic acid, in order to increase an application of acorns in food industry [2]. Moreover, heat-treated acorns have lower levels of tannins but higher levels of phenolic compounds [3]. Due to the lack of data on the acorns' biological activity of oaks growing in Lithuania, the aim of this study was to evaluate the impact of acorns' treatment on their antioxidant activity. Acorns were collected in 5 different Lithuanian regions (Kaunas, Šilutė, Jonava, Kretinga, Kėdainiai). Three treatment methods were applied, i.e. soaking in water at 45 ºC degrees for 18 hours, drying at 37 ºC for three days, and drying at 200 ºC for 15 minutes. After treatment, methanolic extracts were prepared and tested using spectrophotometric tests for evaluation of the total content of phenolic compounds and flavonoids.

The study showed that the antioxidant properties of acorns were depended on the collection region and sample treatment method (Fig. 1). The highest content of phenolic compounds was found in the Kretinga region (57.6 mg/g) after the treatment of acorn at 200 ºC, while similar results (57.5 mg/g) were determined in Jonava after the treatment of acorn at 37 ºC. Additionally, it is noticeable that the lowest amount of flavonoids was found in the extracts from Kaunas acorns despite the treatment. Total flavonoid content varied in the range from 1.4 to 2.8 mg/g, depending on the acorns collection region and the treatment.

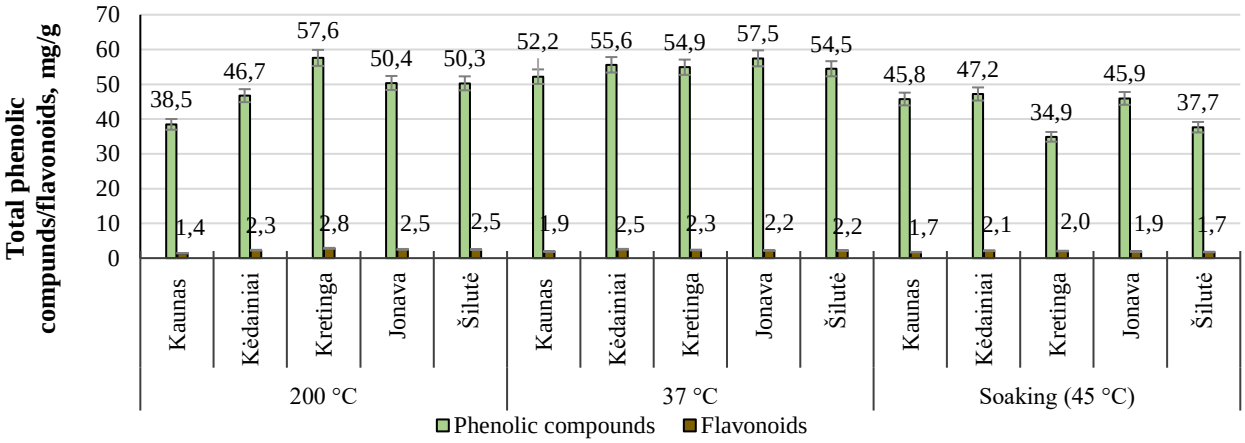


Fig. 1. Total amount of phenolic compounds and flavonoids extracted from *Q. rubra* acorns using different heat treatments.

There is no clear tendency from the current data on the dependence of total phenolic compounds and flavonoids on the acorns' treatment method. The amount of biologically active compounds depends not only on the method of treatment but also on the acorns' collected region. It is obvious that the treatment of the acorns affects the total amount of phenolic compounds extracted from acorns as the differences between the individual methods are as high as 50 percent.

Acknowledgements: This project was financed by Research Council of Lithuania, grant No. 09.3.3-LMT-K-712-25-0192.

[1] E. Burlacu, A. Nisca & C. Tanase. Acomprehensive review of phytochemistry and biological activities of Quercus species, Forests **11(9)**, 904 (2020).
[2] R.K. Gupta, S.S Gangoliya, & N.K. Singh, Reduction of phytic acid and enhancement of bioavailable micronutrients in food grains, Journal of Food Science and Technology **52(2)**, 676–684 (2013).
[3] S. Rakić, S. Petrović, J. Kukić et. al., Influence of thermal treatment on phenolic compounds and antioxidant properties of oak acorns from Serbia, Food Chemistry **104(2)**, 830–834 (2007).

INACTIVATION OF *ACINETOBACTER BAUMANNII* BIOFILMS BY ANTIMICROBIAL PHOTODYNAMIC THERAPY

Enrika Vyčaitė [1], Edita Sužiedėlienė[1], Saulius Bagdonas[2], Irina Buchovec[3]

[1]Institute of Biosciences, Department of Biochemistry and Molecular Biology, Life Sciences Center, Vilnius University, Lithuania
[2]Laser Research Center, Faculty of Physics, Vilnius University, Lithuania
[3]Institute of Photonics and Nanotechnology, Faculty of Physics, Vilnius University, Lithuania
enrika.vycaite@chgf.stud.vu.lt

Acinetobacter baumannii is known as a multidrug-resistant (MDR) opportunistic Gram-negative nosocomial pathogen dangerous for patients with critical illness [1]. One of the most important traits responsible for *A. baumannii* survival in clinical settings is pathogen's ability to form biofilms, which are 10–1000 times more resistant to antibiotic treatment than the planktonic cells [2]. A promising approach to fight MDR planktonic and biofilm bacteria is the antimicrobial photodynamic therapy (aPDT). aPDT is a biophotonic technology based on the interactions of a non-toxic photosensitizer (PS), molecular oxygen and light [3]. After photoexcitation, PS interacts with molecular oxygen and generates reactive oxygen species that initiate cellular damage, thus destroying the bacterial cells. The main goal of the present study was to investigate inactivation of *A. baumannii* planktonic and biofilm cells by applying riboflavin-based (RF-aPDT) and chlorophyllin-based aPDT (Chl-aPDT).

The LED-based light source for the experiment was constructed at the Institute of Photonics and Nanotechnology (Vilnius University). The 402 nm and 440 nm LEDs were chosen as optimal for Chl and RF photoactivation, respectively. For the inactivation of *A. baumannii* clinical isolate Ab52, 200 µl of the prepared samples were placed into sterile flat-bottom wells and exposed to the LED light for different periods. The illumination dose (J/cm^2) was calculated as irradiance (mW/cm^2) multiplied by irradiation time (sec.). The surviving cell populations were counted, the average values were calculated and expressed as $\log_{10}$ (CFU/ml).

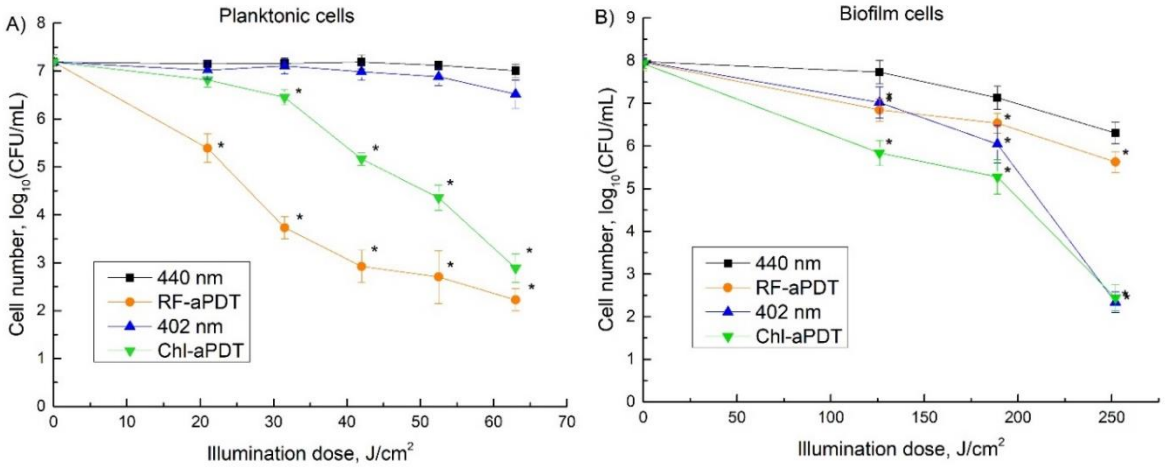


Fig.1 Inactivation of *A. baumannii* planktonic (A) and biofilm (B) cells by aPDT as a function of illumination doses (irradiance 35 mW/cm^2). 440 nm and 402 nm – bacteria in 0.01 M PBS without PS; RF-aPDT – bacteria with 0.011 mM RF; Chl-aPDT – bacteria with 0.015 mM Chl. Every point is the average of 3-6 experiments, error bars indicate standard deviation. * indicates statistical significance compared to control culture, $p < 0.05$.

aPDT results showed that *A. baumannii* planktonic cells were more sensitive to RF-aPDT when the illumination dose varied from 20 J/cm^2 to 50 J/cm^2 compared to Chl-aPDT. The increase of illumination dose to 63 J/cm^2 led to similar sensitivity, where the viability of bacteria after RF-aPDT and Chl-aPDT were diminished by 4.8 $\log_{10}$ and 4.2 $\log_{10}$, respectively (Fig. 1A). On the contrary, the biofilm cells were more efficiently inactivated by Chl-aPDT (reduction by 5.5 $\log_{10}$) than RF-aPDT (inactivation by 2.35 $\log_{10}$) when the illumination dose was 252 J/cm^2 (Fig. 1B). However, 402 nm LED light without PS (252 J/cm^2) dramatically reduced viability of biofilm cells, *A. baumannii* CFU number decreased by 5.6 $\log_{10}$. In summary, RF-aPDT and Chl-aPDT can be used as a potential means for *A. baumannii* inactivation, both planktonic and biofilm cells.

Acknowledgement: This research was funded by the European Social Fund under the No 09.3.3-LMT-K-712 "Development of Competences of Scientists, other Researchers and Students through Practical Research Activities" measure.

[1] Howard A, O'Donoghue M, Feeney A, Sleator RD. Acinetobacter baumannii: an emerging opportunistic pathogen. Virulence. 2012 May 1;3(3):243-50. doi: 10.4161/viru.19700. Epub 2012 May 1. PMID: 22546906; PMCID: PMC3442836.
[2] Sharma D, Misba L, Khan AU. Antibiotics versus biofilm: an emerging battleground in microbial communities. Antimicrob Resist Infect Control. 2019;8:76. Published 2019 May 16. doi:10.1186/s13756-019-0533-3
[3] Buchovec, I.; Gricajeva, A.; Kalėdienė, L.; Vitta, P. Antimicrobial Photoinactivation Approach Based on Natural Agents for Control of Bacteria Biofilms in Spacecraft. Int. J. Mol. Sci. 2020, 21, 6932. https://doi.org/10.3390/ijms21186932

INTERPLAY BETWEEN EPIGALLOCATECHIN-3-GALLATE AND IONIC STRENGTH DURING AMYLOID AGGREGATION

Kamile Mikalauskaite, Mantas Ziaunys, Andrius Sakalauskas, Vytautas Smirnovas

Institute of Biotechnology, Life Sciences Center, Vilnius University, Vilnius, Lithuania
kamile.mikalauskaite@bti.stud.vu.lt

Amyloid fibrils formed during the aggregation of amyloidogenic proteins are a hallmark of neurodegenerative diseases such as Alzheimer's or Parkinson's [1]. Although scientists around the world have been searching for drugs or treatments for these diseases for many years, few have been discovered, and the field of research analyzing the mechanisms of protein aggregation and what factors may change them is still unclear. Studies show that various environmental factors such as temperature, pH, or protein concentration can affect not only the rate of aggregation but also the structure and morphology of the fibrils formed [2,3]. For this reason, analyzing the efficacy of inhibitory compounds under different environmental conditions may give incorrect results. This work investigated how the ionic strength of a solution changes the inhibitory effect of an anti-amyloid compound epigallocatechin-3-gallate (EGCG), using three amyloid proteins.

To elucidate the influence of ionic strength, the aggregation kinetic parameters of three proteins with different amino acid sequences at different NaCl concentrations in the sample were first analyzed. Two proteins / peptides associated with neurodegenerative diseases, amyloid β (Alzheimer's disease) and α-synuclein (Parkinson's disease), and one model protein - recombinant human insulin, were selected for the study. Further, Fourier-transform infrared spectroscopy (FTIR) was used to verify that different structures of amyloid fibrils formed in the reaction mixture with EGCG during the aggregation under different ionic strength conditions.

In the study, it was observed that each amyloid protein has its own characteristic ionic strength value in the solution at which the EGCG inhibition efficiency is highest. In the case of insulin and α-synuclein, it was observed that the inhibition efficiency is higher at lower NaCl concentration and increasing the ionic strength of the solution, the efficiency is significantly reduced. In the case of amyloid β, the inhibition remained similar with increasing NaCl concentrations from 100 mM. Additionally, the analysis of the FTIR spectra of fibrils shows that the ionic strength of the solution affects not only the aggregation kinetic parameters but also the structure of the resulting fibrils.

[1] Chiti F, Dobson CM. 2017. Protein misfolding, amyloid formation, and human disease: a summary of progress over the last decade. Annual Review of Biochemistry 86(1):27–68. DOI 10.1146/annurev-biochem-061516-045115.
[2] Sneideris T, Darguzis D, Botyriute A, Grigaliunas M, Winter R, Smirnovas V. 2015. pH-Driven polymorphism of insulin amyloid-like fibrils. PLOS ONE 10(8):e0136602. DOI 10.1371/journal.pone.0136602.
[3] Sakalauskas A, Ziaunys M, Smirnovas V. 2019. Concentration-dependent polymorphism of insulin amyloid fibrils. PeerJ 7(13):e8208. DOI 10.7717/peerj.8208.

P4-19

DID NOT PARTICIPATE

.

DESIGN OF AN ANESTHETIC MEDICINE PROLONGED ACTION BASED ON NOVOCAINE

Karyna Savchenko, Vadym Lisovyi, Dmytro Oliinyk, Daryna Taran,
Galyna Kuzmina, Volodymyr Bessarabov

Department of Industrial Pharmacy, Kyiv National University of Technology and Design, Ukraine
k.savchenko@kyivpharma.eu

Pain is a peculiar psychophysiological state of a human, which arises due to the influence of excessive stimuli, which cause organic or functional disorders in the body. Effective treatment of pain eliminates physical suffering, stress, facilitates the work of the heart and lungs, reduces the risk of venous thrombosis and helps to normalize digestion [1].

Despite the achievements of modern local anesthesia, novocaine remains the standard analgesic in clinical practice. Being a weak base, it blocks Na^+ channels, prevents the generation of impulses in the endings of sensitive nerves and the conduction of impulses through nerve fibers. It changes the potential of action in the membranes of nerve cells without a pronounced effect on the resting potential, suppresses the conduction of pain and mechanical impulses. When absorbed and entering the bloodstream, it reduces the excitability of peripheral cholinergic systems, reduces the formation and release of acetylcholine from the preganglionic extremities (has some ganglioblocking action), eliminates spasm of smooth muscles [2] and reduces excitability.

When administered parenterally, novocaine is well absorbed and rapidly hydrolyzed in the bloodstream under the action of two types of cholinesterases: acetylcholinesterase and butyrylcholinesterase to paraaminobenzoic acid and diethylaminoethanol. Cholinesterase inhibitors were added to the analgesic drug to prolong the action of novocaine. Polyphenolic compounds from the group of flavonoids, which are known to have antioprotective, antioxidant, anti-inflammatory and immunomodulatory properties, were considered inhibitors. As potential analgesics, flavonoids suppress inflammatory processes, oncological diseases, progress of neuropathic conditions. As a result, silibinin was chosen due to its high bioavailability and low toxicity.

The following methods were used during the study: bibliometric, empirical, mathematical. Kinetic studies were performed using the spectrophotometric method using a UV spectrophotometer SPECORD 200 (Analytic Jena, Germany).

When silibinin is introduced into the reaction mixture, the rate of hydrolysis of novocaine by butyrylcholinesterase is reduced. The rate constant of the first order when adding 100 μm of silibinin to the system decreased from $1.26\pm0.07\times10^{-3}$ c^{-1} to $0.76\pm0.07\times10^{-3}$ c^{-1}, which confirms the inhibitory properties of flavonoids. At concentrations of silibinin in the system of 25, 50 μm, the rate constant decreases by 1.2 and 1.4 times, respectively.

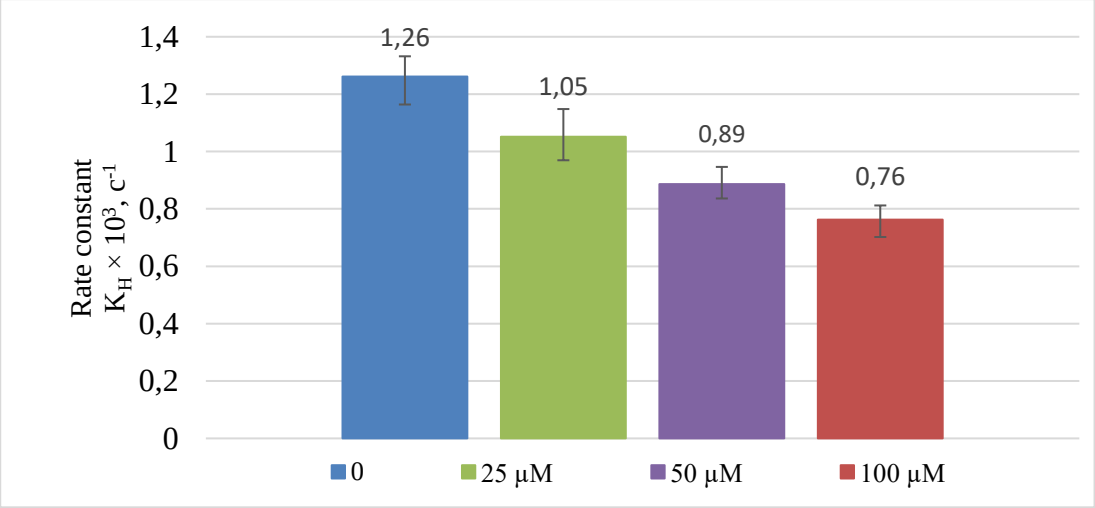


Fig. 1. Dependence of the rate constant of the first order of hydrolysis of novocaine without inhibitor and in the presence of silibin

The study found that silibinin effectively inhibits human serum butyrylcholinesterase. Thus, the development of a prolonged-release analgesic drug based on novocaine with the addition of silibinin to prolong the analgesic effect is promising.

[1] Joseph M Neal 1, Anne Gravel Sullivan, Richard W Rosenquist, Dan J Kopacz (2017). Regional Anesthesia and Pain Medicine: US Anesthesiology Resident Training-The Year 2015, 42(4):437-441. doi: 10.1097/AAP.0000000000000623.
[2] Ombregt L. (2013). Procaine: Principles of treatment. A System of Orthopaedic Medicine. Science Direct, 83–115 e.5 https://doi.org/10.1016/B978-0-7020-3145-8.00005-3.

CONCENTRATION QUENCHING OF CHLOROPHYLL A AND ZINC PHTHALOCYANINE IN THIN POLYSTYRENE FILMS

Justė Tamošiūnaitė[1,2], Simona Streckaitė[2], Jevgenij Chmeliov[2,3], Andrius Gelžinis[2,3], Leonas Valkūnas[2,3]

[1] Life Sciences Centre, Vilnius University, Vilnius, Lithuania
[2] Department of Molecular Compound Physics, Centre for Physical Sciences and Technology, Vilnius, Lithuania
[3] Institute of Chemical Physics, Faculty of Physics, Vilnius, Lithuania
juste.tamosiunaite@gmc.stud.vu.lt

Increasing fluorophore concentration often leads to diminished fluorescence quantum yield, a process that is denoted as concentration quenching, or aggregation-induced quenching [1]. This phenomenon is encountered in many systems from optoelectronics [2] to biology [3]. One example of *in vitro* quenching appears in chlorophyll solutions, which has been studied since the previous century [3,4].

This work demonstrates experiments regarding concentration quenching of Chlorophyll a (Chl a) and Zinc 2,9,16,23-tetra-tert-butyl-29H,31H-phthalocyanine (TB-ZnPC) in thin films. While phthalocyanine molecules show interesting characteristics [5], their resemblance to chlorophyll makes them a potential model system. In Fig. 1a we show normalized fluorescence spectra and fluorescence decay kinetics of Chl a thin films made with toluene and polystyrene (0.288 M) for different concentrations. Redshifting and broadening of emission spectra occurred in the Q_y band within increasing Chl a concentration. The fluorescence kinetics were observed to be faster for increased concentration. In Fig. 1b the normalized fluorescence spectra and fluorescence decay kinetics of TB-ZnPC thin films made with toluene and polystyrene (0.288 M) for some concentrations are displayed. Here broadening of the spectra band at higher TB-ZnPC concentration thin films appeared, while the fluorescence decay kinetics demonstrate faster quenching in higher concentration films. This suggests that further examination of these molecules in different environment is needed.

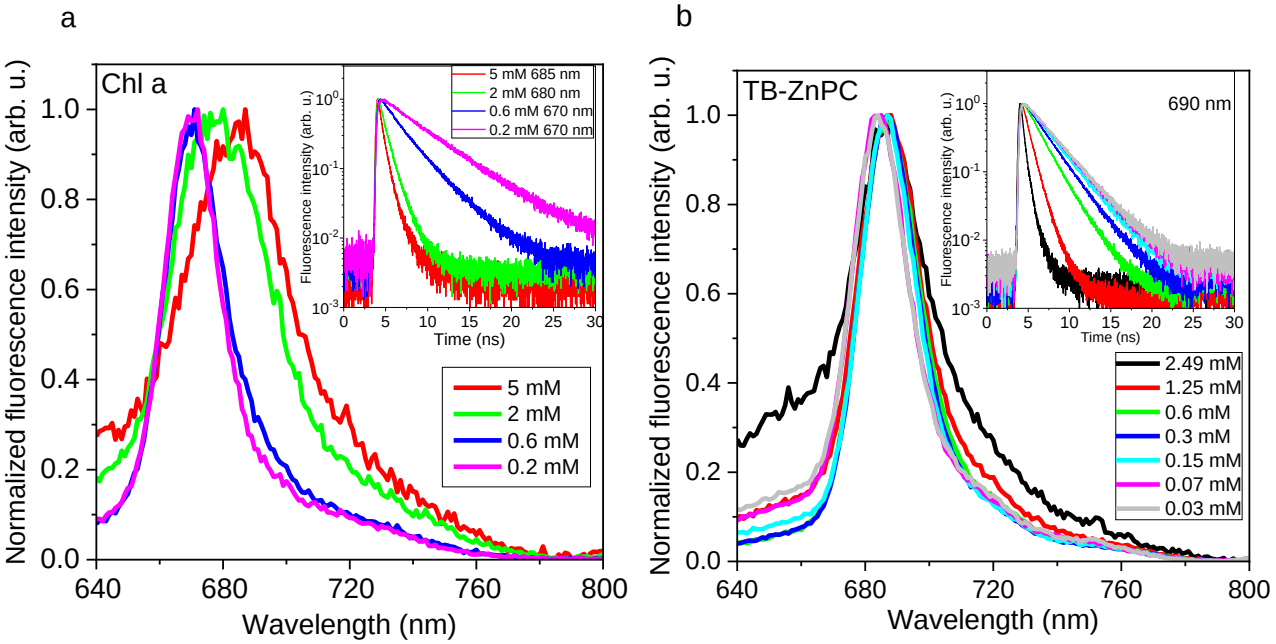


Fig. 1. Normalized fluorescence spectra and fluorescence decay kinetics at emission maximum of a) Chlorophyll a, and b) Zinc 2,9,16,23-tetra-tert-butyl-29H,31H-phthalocyanine thin films.

[1] Burshtein A. I., Concentration of noncoherent excitation in solutions, Sov. Phys. Usp. 27,579-606, 1984.
[2] Chen, C.-T. Evolution of Red Organic Light-Emitting Diodes: Materials and Devices. Chem. Mater., 16, 23, 4389–4400, 2004.
[3] Watson, W. F., & Livingston, R. Self-Quenching and Sensitization of Fluorescence of Chlorophyll Solutions. J. Chem. Phys., *18*(6), 802–809, 1954.
[4] Beddard, G. S., & Porter, G. Concentration quenching in chlorophyll. Nature, *260*, 366–367, 1976.
[5] Mack J., & Kobayashi N., Low Symmetry Phthalocyanines and Their Analagoues, Chem. Rev. 111, 281-321, 2011.

ANALYSIS OF SITE-DIRECTED MUTANT (ASP94ALA) OF *STREPTOMYCES SCABIEI* 87.22 CUTINASE

Aurimas Greičius, Agnė Savickaitė, Renata Gudiukaitė

Department of Microbiology and Biotechnology, Institute of Biosciences, Life Sciences Center, Vilnius University
aurimas.greicius@gmc.stud.vu.lt

Cutinases, belonging to the α/β-hydrolase superfamily, have recently been shown to be able to degrade one major component of today's plastic industry – PET (polyethylene terephthalate) [1,2,3]. PET has a variety of properties that make it attractive for everyday use including it being clear, lightweight and strong. However, PET and other plastics have one major issue surrounding them – waste management. An effective eco-friendly management practice for plastic waste is still absent. For this reason, it is critical to fill the gap of fundamental knowledge surrounding these enzymes and be able to advance current research on effective and eco-friendly ways to manage and dispose of unwanted plastic goods.

This study investigates the influence of the Asp94Ala mutation on thermostability and activity of the *S. scabiei* 87.22 cutinase. The Asp94Ala mutant of *S. scabiei* 87.22 cutinase was created using the overlap extension method. Mutated gene was cloned into pET-21c(+) vector, expressed in *E. coli* BL21 (DE3) cells and purified using immobilized metal affinity chromatography (IMAC). Activity and physiochemical characterization was carried out using synthetic *p*-NP esters as substrates.

Acquired results suggested that the Asp94Ala mutation increases optimal temperature of target cutinase. Thermostability and activity are the most desirable characteristics of target cutinases when developing effective biocatalysts for plastic degradation.

[1] Furukawa, M., Kawakami, N., Tomizawa, A. et al. Efficient Degradation of Poly(ethylene terephthalate) with Thermobifida fusca Cutinase Exhibiting Improved Catalytic Activity Generated using Mutagenesis and Additive-based Approaches. Sci Rep 9, 16038 (2019). https://doi.org/10.1038/s41598-019-52379-z.

[2] Oda, Masayuki, et al. "Enzymatic Hydrolysis of PET: Functional Roles of Three Ca2+ Ions Bound to a Cutinase-like Enzyme, Cut190*, and Its Engineering for Improved Activity." Applied Microbiology and Biotechnology, vol. 102, no. 23, 2018, pp. 10067–77. Crossref, https://doi.org/10.1007/s00253-018-9374-x.

[3] Ronkvist, Åsa M., et al. "Cutinase-Catalyzed Hydrolysis of Poly(Ethylene Terephthalate)." Macromolecules, vol. 42, no. 14, 2009, pp. 5128–38. Crossref, https://doi.org/10.1021/ma9005318.

IDENTIFICATION AND ANTIMICROBIAL PHOTODYNAMIC INACTIVATION OF MOLDS ISOLATED FROM STRAWBERRIES

Gabriele Sejonaite[1], Alisa Gricajeva[1]

[1]Department of Microbiology and Biotechnology, Institute of Biosciences, Life Sciences Center, Vilnius University, Lithuania
gabriele.sejonaite@gmail.com

With the current worldwide challenge to reduce food waste, while ensuring consumer safety, the protection of fruits and other foods from spoilage molds is becoming an increasingly important topic. Diseases of strawberry (and other fruits), for instance, gray mold (*Botrytis cinerea*), anthracnose (*Colletotrichum acutatum*), powdery mildew (*Podosphaera aphanis*), *Cladosporium* sp., *Alternaria* sp., and others can cause severe losses by reducing yield and causing fruit decay during production and after harvest [1]. One of the solutions to inactivate molds associated with food spoilage is photodynamic therapy (PDT) which has emerged as an effective treatment modality for various malignant tumors [2]. Since then, PDT or antimicrobial inactivation (API) has been studied and developed more as an anti-cancer therapy, and less as antimicrobial therapy [3].

This research aims to evaluate the efficiency of using natural photosensitizers (PSs) in combination with 405 and 450 nm light against molds (their spores) commonly found on strawberries. Natural PSs such as riboflavin (RF) and chlorophyllin (Chl) that are generally regarded as safe (GRAS) and do not cause any harm to human health were used in this work. For the analysis, strawberries from the greenhouse of "Audriaus Juškos ūkis" farm (Anykščiai, Lithuania) were used for the isolation of the fungi. 20 morphologically different isolates were obtained using PDA (Potato Dextrose Agar) and MEA (Malt Extract Agar) media. Macromorphological and microscopic structures revealed that isolated fungi could belong to different *Cladosporium, Penicillium, Rhizopus,* and *Aspergillus* species. Molecular barcoding of isolated fungi and more accurate identification of the fungi using PCR amplification and sequencing of the internal transcribed region (ITS) region, actin (ACT), elongation factor-α, β-tubulin (benA), Calmodulin (CaM), RNA polymerase II second largest subunit (RPB2-1) and other, was done. Further, regarding API, this study focused on *Cladosporium* spp. since it is reported as one of the most prevalent pathogens of the strawberries and, yet only a little or no research on *Cladosporium* sp. inactivation has been done. Some primary results of RF and Chl-based API of *Cladosporium* sp. are presented in this work.

[1] Janisiewicz, Wojciech J. et al., Dark Period Following UV-C Treatment Enhances Killing of Botrytis Cinerea Conidia and Controls Gray Mold of Strawberries, Phytopathology® 106, 386–394 (2016).

[2] Ahmed El-Hussein et al., A Review of Chemotherapy and Photodynamic Therapy for Lung Cancer Treatment, Anti-Cancer Agents in Medicinal Chemistry 21, 149–161 (2020).

[3] Moan J. and Q. Peng, An outline of the hundred-year history of PDT, Anticancer Res. 23, 3591–3600 (2003).

THE COMPARISON OF GLUCOSE BIOSENSORS MODIFIED BY ENZYME-ASSISTED POLYANILINE NANOCOMPOSITES WITHOUT AND WITH GOLD DERIVATIVES

Rugile Chmieliauskaite[1], Natalija German[2]

[1] Department of Chemistry and Bioengineering, Faculty of Fundamental Sciences, Vilnius Gediminas Technical University Vilnius Tech, Sauletekio ave.11, LT-10223, Vilnius, Lithuania
[2] Division of Immunology, State Research Institute Center for Innovative Medicine, Santariskių g. 5, LT-08406, Vilnius, Lithuania
rugile.chmieliauskaite@stud.vgtu.lt

The design and wide application of electrochemical biosensors in nanoscience, nanotechnology, medicine, pharmaceutics industry, environmental and food monitoring significantly increased during the past decade [1,2]. The research community is working to develop effective tools for diabetes management and diagnosis, because diagnosed for seven million people every year diabetes mellitus is considered a worldwide public health problem (the risk of heart disease, kidney failure, blindness, postoperative and wound infections) [2,3]. Last time such π-π conjugated polymers as polyaniline (PANI), polypyrrole are becoming an integral part of biomolecules immobilization strategies and electrochemical sensor platforms [1,4]. During the enzyme-assisted formation of π-π conjugated polymers, the monomer is attacked by a radical cation induced by H_2O_2 [5]. Combined with electroactive gold nanoparticles (AuNPs) and enzyme polyaniline is suitable for the development of biosensors dedicated for the monitoring of glucose due their positive effect on the sensitivity and selectivity [1,6].

The main aim of this research was to compare analytical characteristics of glucose biosensors modified by enzyme-assisted polymeric nanocomposites (PNC) with embedded enzyme enzyme (glucose oxidase (GOx)) without/with 6 nm of gold nanoparticles. Firstly, polyaniline nanocomposites with GOx (PANI-GOx) without and with AuNPs (PANI-GOx-AuNPs) were synthesized by enzyme-assisted polymerization, washed, separated and dispersed in the solution of sodium acetate (SA) buffer (Fig. 1). Then, graphite rod (GR) electrode was immobilized by described above kind of polyaniline nanocomposites with following addition of GOx. Electrochemical investigations were performed by cyclic voltammetry (CV) and chronoamperometry (ChA) in the presence of red-ox mediator phenazine methosulfate (PMS). The reversibility of electrochemical reaction was evaluated by CV, the analytical characteristics, stability and selectivity – by ChA. It was investigated that the biosensor based on GR/PANI-GOx-AuNPs/GOx has been found more efficient than an analogous electrode coated with PANI-GOx nanocomposites. Developed glucose biosensors based on GR/PANI-GOx/GOx and GR/PANI-GOx-AuNPs/GOx electrodes were characterized by high sensitivity (52.0 and 65.4 μA mM^{-1} cm^{-2}), low detection limit (0.084 or 0.070 mmol/L), wide linear concentration range (till 16.5 mmol/L), good correlation coefficient (0.9936 or 0.9968) and repeatability (6.10 and 4.67 %), appropriate stability (17 and 22 days). Biosensor based on GR/PANI-GOx-AuNPs/GOx electrode presented the excellent anti-interference ability to ascorbic and uric acids, successful practical application for glucose determination in serum.

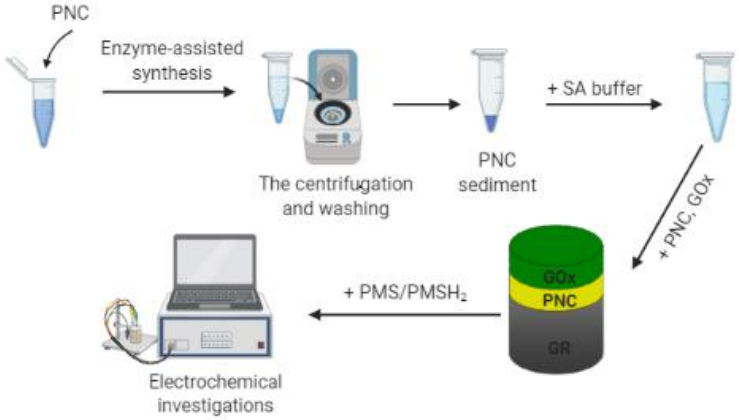


Fig.1. Schematic representation of PNC enzyme-assisted synthesis and electrochemical investigation.

[1] R. Batool, A. Rhouati, M.H. Nawaz, A. Hayat, J.L. Marty, A review of the construction of nano-hybrids for electrochemical biosensing of glucose, Biosensors **9**, 1–19 (2019).
[2] H.C. Wang, A.R. Lee, Recent developments in blood glucose sensors, Journal of Food and Drug Analysis **23**, 191–200, (2015)
[3] E-H. Yoo, S.-Y. Lee, Glucose biosensors: An overview of use in clinical practice, Sensors **10**, 4558-4576 (2010).
[4] N. German, A. Ramanaviciene, A. Ramanavicius, Formation and electrochemical evaluation of polyaniline and polypyrrole nanocomposites based on glucose oxidase and gold-nanostructures, Polymers **12**, 3026 (2020).
[5] N. German, A. Popov, A. Ramanaviciene, A. Ramanavicius, Evaluation of enzymatic formation of polyaniline nanoparticles, Polymer **115**, 211–216 (2017).
[6] B. Haghighi, M.A. Tabrizi, Direct electron transfer from glucose oxidase immobilized on an overoxidized polypyrrole film decorated with Au nanoparticles, Colloids Surfaces B Biointerfaces **103**, 566–571 (2013).

EVALUATION OF ELECTROPORATION EFFICIENCY, PORE RESEALING AND CELL VIABILITY USING TITANIUM VS STAINLESS-STEEL ELECTRODES

Dominyka Gabulaitė[1], Baltramiejus Jakštys[1], Saulius Šatkauskas[1]

[1] Faculty of Natural Sciences, Vytautas Magnus University, Kaunas, Lithuania
dominyka.gabulaite@vdu.lt

Electroporation (EP) exploits short electrical pulses to controllably elevate cell plasma membrane permittivity to exogenous and endogenous molecules [1]. Control of the process, low joule heating and simplicity of the method resulted in electroporation to be widely implied in food processing, pasteurization, biotechnology and medicine. Such broad application of electroporation requires constant research to improve design and material composition for electroporation chambers or electrodes in order to make the process as reliable and cost efficient as possible. Many of electrode compositions as aluminum, copper, stainless steel, gold, platinum either carbon was investigated, where literature of the use of titanium electrodes for electroporation is scarce [2; 3]. The golden standard electrodes for electroporation are made of stainless steel. Electrodes of other alloys and materials are less popular mainly due to remarkably high metal ion release (i.e. aluminum, copper) or high material price (gold, platinum, carbon fibers). However, the most substantial criteria for proper electrodes is inertia longer lasting of the electrodes and reduces contamination of the sample material with metal ions. During our investigation we intended to evaluate whether the use of titanium electrodes for electroporation would substantially improve viability of electroporated cells without sacrificing the efficiency of electrotransfer of extracellular molecules into the cells.

Experiments were performed using Chinese hamster ovarian (CHO) cells. We used stainless steel (AISI 304: 18.1% chromium, 8.3% nickel) and titanium (BT-20: 5.5-7% aluminum, 0.5-2% molybdenum, 0.8-2.5% vanadium, 1.5-2.5% zirconium) electrodes separated by 2 mm gap for placement of the cells. Cells were electroporated in low conductivity electroporation medium (0.1 S/m, 270 mOsmol, 7.2 pH) in order to reduce current but maintain pH and osmolality. Cells were treated with 1 or 9 high voltage (HV) pulses of 100 µs duration repeating at 1 Hz frequency while pulse intensity was gradually changed from 0.6 kV/cm to 2.2 kV/cm. Cell electropermeabilization efficiency and level of irreversibly permeabilized cells was assessed by measuring intracellular Propidium iodide (PI) fluorescence intensity and number of PI positive cells (PI^+) by flow cytometry. Viability of cells was determined using MTS assay 24 and 48 hours after treatment and colony formation assay (CFA) 6 days post treatment.

The results revealed that electrotransfer of extracellular PI into cells was identical comparing stainless steel vs titanium electrodes, where the number of PI^+ cells and fluorescence intensity of the cells increased with amplification of electric field intensity. Interestingly, cell viability results demonstrated that cell viability of the cells electroporated between stainless steel or titanium electrodes remained similar under all conditions except 1.8 kV/cm 1 HV (55±4 % vs 31±12 % stainless steel vs titan) and 0.8 kV/cm 9HV (43±25 % vs 25±10 % stainless steel vs titan) when assayed with MTS 48 h after EP. After measuring the amount of irreversibly permeabilized cells we determined that the impact of titan electrodes on cell viability was not related to pore resealing. Results showed that a part of electroporated cells were electroporated irreversibly under all conditions, but this measure did not exceed 30 % of cells per sample.

Summing everything up, the use of titanium electrodes had nearly the same impact on cell membrane permeabilization and pore resealing after electroporation compared to stainless steel electrodes, while at particular pulse parameters cell viability was lower using titan electrodes. However, this effect was not related to pore resealing. In conclusion, the choice for which electrodes to use for cell electroporation remain solely under user's decision while titanium electrodes demonstrated nearly the same outcome of electroporated cells.

[1] Jakstys B., Jakutaviciute M., Uzdavinyte D., Satkauskiene I., Satkauskas S., Correlation between the loss of intracellular molecules and cell viability after cell electroporation, Bioelectrochemistry **135** 107550 (2020).

[2] Rodaitė RR., Saulė, R., Snitka, V., Saulis, G., Release of Iron Ions from the Stainless-Steel Anode Occurring During High-Voltage Pulses and Its Consequences for Cell Electroporation Technology, IEEE Transactions on Plasma Science **42** 249-254 (2014).

[3] Vižintin A., Vidmar J., Ščančar J., Miklavčič D., Effect of interphase and interpulse delay in high-frequency irreversible electroporation pulses on cell survival, membrane permeabilization and electrode material release, Bioelectrochemistry **134** 107523 (2020).

AUTOMATIC SUBSTRATE FEEDING SYSTEM FOR NON-GROWTH-LIMITING FED-BATCH CULTIVATION PROCESSES OF RECOMBINANT *E. COLI* IN INDUSTRIAL BIOTECHNOLOGY

Mindaugas Matukaitis[1*], Lukas Zlatkus[1], Deividas Masaitis[1]

[1] Department of Automation, Kaunas University of Technology, Lithuania
*mindaugas.matukaitis@ktu.lt

Escherichia coli cell strain is a typical choice of microorganism to produce heterologous proteins in pharmaceutical industries due to its fast growth time, high cell densities, high product yield, and relatively easy cultivation scale-up process [1,2].

Controllability of the glucose concentration in a cultivation medium secures bioprocess productivity in fed-batch cultures [2]. Insufficient glucose concentration in the medium limits the growth rate and productivity of E. coli; however, excess glucose in the bioreactor also inhibits the growth of biomass and products by synthesizing metabolic by-products. [1-3].

This work presents a simulation of a real bioreactor based on a mathematical model with its substrate feeding control system. The recombinant *E. coli* non-growth-limiting fed-batch cultivation process was simulated. The substrate feeding control system maintained stable glucose concentration in the cultivation medium and ensured high biomass growth and overall efficiency of the bioprocess. The approach for the controllability of substrate concentration [4] is based on the maximal glucose consumption rate of the cells (σ_{max}) and mass balance equations for biomass concentration, X [g/kg] and glucose concentration, S [g/kg], Eq. (1-2):

$$\frac{dX}{dt} = \mu * X - \frac{F}{W} * X \tag{1}$$

$$\frac{dS}{dt} = -\sigma * X - \frac{F}{W} * S + \frac{F_S}{W} * S_F \tag{2}$$

Where μ – specific biomass growth rate [g/L], σ- glucose specific consumption rate [1/L], F- total mass flow to the bioreactor [g/h], W – culture medium weight [kg], S_f – substrate concentration in feeding solution [g/kg]. Glucose concentration (S) is a feedback signal for an adaptive PI regulator that controls [5,6] the flow rate to the bioreactor (F). Adaptation of the control systems parameters ensures a smooth transition from biomass growth to recombinant protein production during cultivation.

The proposed control feeding system ensured stable glucose concentration level in bioreactor during non-growth-limiting E. coli growth cultivation bioprocess, resulting in higher biomass and faster cell growth than the limited E. coli growth cultivation bioprocess.

The technique estimates glucose concentrations in bioreactors and can be applied to creating feeding profiles for fed-batch cultivation bioprocesses.

Funding: This project received funding from the European Regional Development Fund (project no. 01.2.2-LMT-K-718-03-0039) under a grant agreement with the Research Council of Lithuania (LMTLT).

[1] S. Schaepe, A. Kuprijanov, R. Simutis, A. Lubbert, Avoiding overfeeding in high cell density fed-batch cultures of E. coli during the production of heterologous proteins, Journal of Biotechnology. 192 (2014) 146–153. https://doi.org/10.1016/j.jbiotec.2014.09.002

[2] V. Galvanauskas, R. Simutis, D. Levisauskas, R. Urniezius, T. Tekorius, V. Vaitkus, Design and Adaptation of Robust Feeding Profiles for Recombinant E. coli Fed-batch Cultivation Processes, in: 2021 29th Mediterranean Conference on Control and Automation (MED), IEEE, PUGLIA, Italy, 2021: pp. 532–537. https://doi.org/10.1109/MED51440.2021.9480282

[3] V. Galvanauskas, R. Simutis, D. Levisauskas, M. Butkus, R. Urniezius. Development and Investigation of Efficient Substrate Feeding and Dissolved Oxygen Control Algorithms for Design of Recombinant E. coli Cultivation Process, in: 2018 IEEE 14th International Conference on Automation Science and Engineering (CASE), IEEE, Munich, Germany, 2018: pp. 657–660. https://doi.org/10.1109/COASE.2018.8560495

[4] V. Galvanauskas, R. Simutis, D. Levisauskas, R. Urniezius, V.Vaitkus, T. Tekorius, M. Butkus, A. Survyla. Patent LT6861B. Method for design and adaptation of feeding profiles for recombinant E.coli fed-batch cultivation processes. Published 2021b-11-10. [Accessed 2022-01-28] https://patents.google.com/patent/LT6861B

[5] R. Urniezius, V. Galvanauskas, A. Survyla, R. Simutis, D. Levisauskas, From Physics to Bioengineering: Microbial Cultivation Process Design and Feeding Rate Control Based on Relative Entropy Using Nuisance Time, Entropy. 20 (2018) 779. https://doi.org/10.3390/e20100779

[6] D. Levisauskas, R. Simutis, V. Galvanauskas, R. Urniezius, Simple Control Systems for Set-point Control of Dissolved Oxygen Concentration in Batch Fermentation Processes, Chemical Engineering Transactions. 74 (2019) 127–132. https://doi.org/10.3303/CET1974022

THE PHOTOSTABILITY OF CuInS/ZnS-COOH QUANTUM DOTS IN BIOLOGICAL MEDIA

Emilija Januškaitė[1], Agnė Kalnaitytė[1,2], Saulius Bagdonas[1,2]

[1]Biophotonics Group, Laser Research Center, Vilnius University, Saulėtekio 9, bld. 3, LT – 10222, Vilnius, Lithuania
[2]Institute of Ecology, Nature of Research Centre, Akademijos str. 2, LT – 08412, Vilnius, Lithuania
emilija.januskaite@gmc.stud.vu.lt

Quantum dots (QDs) are nanoscale semiconductors, usually consisting of a crystalline core surrounded by a protective shell [1]. QDs are currently used in various fields of science, especially in biomedical applications such as drug delivery, gene therapy, bioimaging, etc. [2]. The core of conventional QDs contains potentially toxic substances (eg., Cd, Te), so less harmful elements, such as Cu, can be used as an alternative [3]. Many core-shell combinations and unique properties provide the plethora of QDs, so it is important to study them under natural environmental conditions, such as prolonged exposure to light, and media with various ions and biomolecules, to obtain information about their fate, after QDs are released into the environment.

In this work, we monitored the photostability of hydrophilic CuInS/ZnS-COOH QDs (Nanooptical materials, USA) in various biological media by measuring changes in optical density (OD) and photoluminescence (PL) spectra. After preparation of QDs samples (the main concentration was 4 nM), both OD and a peak PL intensity at 548 nm were similar in deionized water and in MWC algae growth medium. The peak position of the PL spectrum of QDs in deep well water remained the same, but the initial PL intensity was lower, and scattering was recorded in the spectrum of OD. During the first week, the spectral properties of QDs stored in the dark at room temperature (18 ℃) practically did not change, regardless of the medium.

Some QDs samples were also stored at room temperature, but under continuous white light illumination (Osram Dulux Star, 11W/827). For another part of the samples kept in the Shrimp Set Smart aquarium (Aquael, Poland) at about +22 ℃, an 8h/16h light/dark cycle was applied using a LED lamp (6 W) designed forgrowing aquatic plants. Regardless of the medium, both the OD and the PL intensity decreased in the illuminated samples, but this decrease was dose-dependent: samples that were under continuous white light illumination ceased to produce measurable fluorescence signals within three days, while samples exposed to light/dark cyclic illumination – after five days.

During the irradiation experiment, the QDs samples were prepared in a 12-well plate, and the collimated violet LED light (404 nm, 30 mW/cm^2) was directed from below the plate from a distance of 8 cm. The fractionated exposures were delivered for 20 minutes to obtain the partial cumulative dose up to 36 J/cm^2 (in intervals of 1.8 J/cm^2 and 3.6 J/cm^2) in all media, and from 36 J/cm^2 to the total dose up to apparent decrease in the PL intensity (in intervals of 3.6 J/cm^2 and 9 J/cm^2) according to the samples. Initially, the PL intensity decreased in all media (in deep well water faster than in other), but after reaching approximately 21.6 J/cm^2 (in deep well water) and 28.8 J/cm^2 (in deionized water and MWC algae growth medium) the decline slowed down (Fig. 1). The spectral properties of CuInS/ZnS-COOH QDs can be considered so photo-unstable that the effect of the medium is negligible compared to light, despite the initial spectral differences.

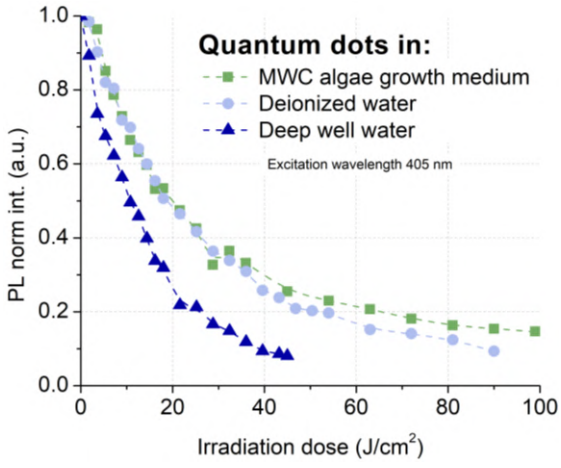


Fig. 1. The decrease in the PL intensity of a spectral peak (at about 550 nm, excitation at 405 nm) of CuInS/ZnS-COOH QDs in different media with increasing dose of irradiation.

[1] L.A. Bentolila, Photoluminescent quantum dots in imaging, diagnostics and therapy, Applications of Nanoscience in Photomedicine, 77-104 (2015).
[2] V.G. Reshma, P.V. Mohanan, Quantum dots: Applications and safety consequences, Journal of Luminescence (205), 287-298 (2019).
[3] L. Li, T.J. Daou, I. Texier, T.T.K. Chi, N.Q. Liem, P. Reiss, Luminescent $CuInS_2$/ZnS Core/Shell Nanocrystals: Cadmium-Free Quantum Dots for in Vivo Imaging, Chem. Mater (21), 2422-2429 (2009).

P4-28

DID NOT PARTICIPATE

.

THE INFLUENCE OF GLYCEROL ON CHEWABLE GEL TABLETS PROPERTIES

Inga Matulytė [1,2*], Jurga Bernatonienė [1,2]

[1] Department of Drug Technology and Social Pharmacy, Lithuanian University of Health Sciences, Kaunas, Lithuania
[2] Institute of Pharmaceutical Technologies, Lithuanian University of Health Sciences, Kaunas, Lithuania
inga.matulyte@lsmu.lt

Chewable gel tablets are similar to gummies, they have a gel base - usually gelatin, pectin or agar agar. This pharmaceutical form is prepared by using silicones, plastic or metal forms, and is not compressed by tablet machine punches as simple tablets [1–3]. Sweeteners (cane or beet sugar, glucose syrup, maltitol) are usually used [4,5]. Tablets, which have a lower sugar content, lose their texture properties quicker, so excipients are needed to solve this problem. One of them is glycerol, it protects tablets from sugar crystallization on their top and saves their physical properties. It does not let the gel tablets to harden and lose their elasticity [6]. The aim of this study was to manufacture chewable gel tablets and evaluate their properties.

Chewable gel tablets were prepared using by silicone forms, and their variation of mass, firmness, hardness, stickiness and springiness were evaluated by a texture analyzer. The two samples of gel tablets' composition were manufactured (the optimal composition of the gel tablets was selected from previous studies). Chewable gel tablets base was made from gelatin and water (1:2) or gelatin, water and glycerol (1:1:1). The amount of base was 27%, it was melted, and thyme-sugar syrup (68.5%) and thyme extract (2.5%) were added. A citric acid solution (2%) as a preservative was added.

The same silicone form was used to prepare gel tablets but the mass was different – tablets with glycerol were 3.65±0.11 g and without glycerol – 3.57±0.05 g (p>0.05). After one month (tablets were kept at room temperature), the mass variation was statistically significant: tablets with glycerol were 3.51±0.12 g, without – 2.61±0.03 g. A chewable gel tablets example is presented in Figure 1, and clear changes in texture are visible. Tablet A contains no glycerol, and sugar crystals are seen on the top, moreover, this tablet has cracks.

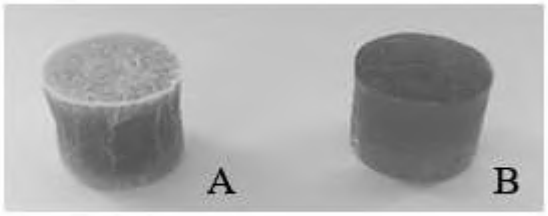


Fig. 1. Chewable gel tablet without glycerol in composition (A), and with glycerol (B).

Comparing other parameters, the differences between different composition of freshly made tablets were not detected, but after one-month the differences were significant. Tablets without glycerol had over 3 times higher firmness and 4 times hardness, their springiness was 39% lower and they were not sticky.

The study found an important effect of glycerol on gel tablets. It helps to maintain the proper properties of chewable gel tablets when they contain a reduced amount of sugar and are kept in an open box at room temperature.

[1] R. Taranum and S. Mittapally, "Soft Chewable Drug Delivery System: Oral Medicated Jelly and Soft Chew," *J. Drug Deliv. Ther.*, vol. 8, no. 4, pp. 65–72, 2018.
[2] European Pharmacopoeia, "Tablets Compressi," *European Pharmacopoeia*, no. 10.3, pp. 937–939, 2018.
[3] L. L. DeMars and G. R. Ziegler, "Texture and structure of gelatin/pectin-based gummy confections," *Food Hydrocoll.*, vol. 15, no. 4–6, pp. 643–653, 2001.
[4] L. Cai, J. Feng, J. Regenstein, Y. Lv, and J. Li, "Confectionery gels: Effects of low calorie sweeteners on the rheological properties and microstructure of fish gelatin," *Food Hydrocoll.*, vol. 67, pp. 157–165, 2017.
[5] O. G. Bhusnure, F. E. Shaikh, B. K. Sugave, B. S. Kavale, R. A. Sayyed, and B. S. Hucche, "Formulation strategies for taste-masking of chewable tablets," *Indo Am. J. Pharm. Res.*, vol. 5, no. 12, pp. 3836–3849, 2015.
[6] I. Matulyte, A. Mataraite, S. Velziene, and J. Bernatoniene, "The Effect of Myristica fragrans on Texture Properties and Shelf-Life of Innovative Chewable Gel Tablets," *Pharmaceutics*, vol. 13, no. 2, p. 238, 2021.

DEVELOPMENT AND APPLICATION OF GELS FOR CHIRAL CAPILLARY ELECTROCHROMATOGRAPHY

Ernesta Lisauskaitė[1], Audrius Sigitas Maruška[1], Mantas Stankevičius[1], Kristina Bimbiraitė-Survilienė[1]

[1] Instrumental Analysis Open Access Center, Faculty of Natural Sciences, Vytautas Magnus University, Kaunas, Lithuania
ernesta.lisauskaite@stud.vdu.lt

The development and application of chiral capillary electrochromatography gels is directly related to public health research, the development of new smart, selective materials, and this is in line with the priorities of Lithuanian smart specialization research and experimental development and EU research priorities. Several enantiomerically recognizable chiral capillary electrochromatography gels suitable for the separation of chiral drugs and other enantiomeric compounds using new polymeric stationary phases in a capillary format have been developed. This new method of analysis differs from conventional capillary electrophoresis methods in that the working buffer does not require the addition of an expensive chiral selector of high purity. This saves expensive pure chiral compounds used in capillary chiral electrophoresis. As new chiral phases suitable for capillary separation are developed, the study is also in line with research priorities in the development of environmentally friendly technologies, as the objectives of miniaturized analysis are achieved using 500-1000 times less reagents, analytes and solvents than the conventional analytical form. Several gel chiral phases have been developed that are capable of generating sufficient electroosmic flow, are suitable for the elution of neutral enantiomeric compounds in a capillary column, and have enantiomeric selectivity for neutral and charged compounds.

Capillary electrochromatography is a separation technique developed less than 30 years ago with high efficiency and high selectivity for many compounds. These two properties are the result of the best combination of high performance liquid chromatography and capillary electrophoresis properties. In practice, capillary electrochromatography is an high performance liquid chromatography method, but the mobile phase and analytes are transferred to the capillary column not by a pressure-driven flow but by a strong electroosmotic flow [1].

Medicinal products and naturally occurring biologically active compounds have chiral forms that depend on their biological activity, which can be dual, one that provides a therapeutic effect, another that can be inactive, toxic, or a source of side effects [2]. Various methods are used to determine the chiral composition, mainly chromatographic and electrophoretic. A new method, capillary chiral gel-electrochromatography, was developed during the research. The sorbents in the method are homogeneous because of the gel structures.

Gelatin was used in different concentrations. Gelatin is a polymer that has an orderly and entirely homogeneous structure at the macromolecular level, which eliminates vortex diffusion and is therefore expected to be more efficient. The capillary was filled with molten gelatin gel of different concentrations. An electroosmotic flow was obtained by inducing an electrical field across the capillry. It was measured using a 1% dimethyl sulfoxide solution, as electroosmotic marker. The enantiomers were then separated. The results of the work will be presented during the conference. Such method is used for the enantioseparation for the first time.

The grant from the Lithuanian Science Council for this research is acknowledged (No. 09.3.3-LMT-K-712-25-0194).

[1] Rocco, A. et al. Chapter 21 – Capillary Electrochromatography: A Look at Its Features and Potential in Separation Science. *Liquid Chromatography: Fundamentals and Instrumentation*, 469–492 ISSN 978-0-12-415807-8 (2013).

[2] Hu, M., Yuan, Y., Wang, W., Li, D., Zhang, H., Wu, B., Liu, M., Zheng, Y. Chiral recognition, and enantiomer excess determination based on emission wavelength change of AIEgen rotor. *Nature communications*, 1-10 (2020)

EVALUATION OF ELECTROPORATION AND YEAST CELL DEATH BY AMPEROMETRY

Sabina Pavliukovič[1], Povilas Šimonis[1], Greta Gančytė[1], Rasa Garjonytė[2] , Arūnas Stirkė[1]

[1] Laboratory of Bioelectrics, [2] Laboratory of Spectroelectrochemistry,
State Research Institute, Center for Physical Sciences and Technology,
Saulėtekio al. 3, Vilnius, Lithuania
sabina.pavliukovic@gmc.stud.vu.lt

Nowadays the Pulsed Electric Field (PEF) is often used method to increase the permeability of various cells and tissues, to facilitate the introduction of extracellular compounds, or cause the outflow of intracellular components [1]. The development of new, simple, fast, and reliable methods for the investigation of electroporation effects is essential to understand the mechanism of electroporation and to investigate the process of cell death after exposure to PEF.

This work was aimed to evaluate the efficiency of electroporation by amperometry using non-immobilized wild *Saccharomyces cerevisiae* cells. Amperometry was carried out with a BAS-Epsilon Bioanalytical system and a three-electrode cell arranged with a magnetic stirrer. Measurements were performed in 2 ml of 20 mM TRIS buffer containing 0.4 mg/ml of yeast cells (non-electroporated or exposed to single square-shaped electric field pulse with a duration of 300 µs to various electric field strengths). After the addition of two well-known mediators in bioelectrochemistry menadione and potassium ferricyanide (final concentrations, respectively, 50 µM, 0.25 mM) or both, the oxidation currents originating from menadione and potassium ferricyanide interaction with yeast cells were registered [2]. The results are summarized in Fig. 1.

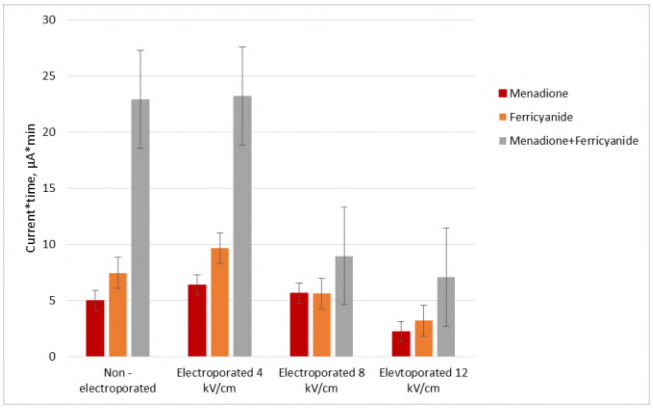


Fig. 1. Evaluation of menadione- and potassium ferricyanide-generated currents (by trapezoidal method).

Menadione is a lipophilic mediator that penetrates inside the cell and is reduced to menadiol by several enzymes catalyzing electron transfer from NAD(P)H to a quinone. In the cases of non-electroporated cells and cells affected with 4 or 8 kV/cm, menadione-generated currents are similar suggesting that the cell membrane was not essentially damaged by electric field or electroporation was reversible. After exposure to 12 kV/cm, the 1.7-fold decrease of the currents was observed indicating possible leakage of NAD(P)H through an injured membrane. The mechanism of hydrophilic ferricyanide interaction with yeast cells is not elucidated yet. The double mediator system consisting of menadione and ferricyanide served for signal amplification. After exposure to 12 kV/cm, the ferricyanide- and both mediator-generated currents dropped as well possibly due to decreased amount of menadiol.

Conclusions: amperometry using non-immobilized yeast cells showed the difference among non-affected and electroporated cells; therefore, it was suitable to investigate the effect of electroporation of the cells; the electric fields up to 8 kV/cm practically did not have a harmful effect on yeast cells, thus, could be used for further experiments with penetration of various compounds; the decrease of menadione-generated currents could indicate the beginning of cell death after subjection to a higher electric field.

[1] Chen, R., "Permeability issues in whole-cell bioprocesses and cellular membrane engineering" Applied Microbiology and Biotechnology 74, 730-738 (2007).
[2] R. Garjonyte, V. Melvydas, and A. Malinauskas, "Mediated amperometry reveals different modes of yeast responses to sugars", Bioelectrochemistry 107, 45–49 (2016).

A SPECTROSCOPIC STUDY ON PORPHYRINS' COMPOSITION IN 5-AMINOLEVULINIC ACID INDUCED *ACINETOBACTER BAUMANNII* AND *STENOTROPHOMONAS MALTOPHILIA*

Brygida Serebriakova[1], Edita Sužiedėlienė[1], Saulius Bagdonas[2], Irina Buchovec[3]

[1] Institute of Biosciences, Department of Biochemistry and Molecular Biology, Life Sciences Center, Vilnius University, Lithuania
[2] Laser Research Center, Faculty of Physics, Vilnius University, Lithuania
[3] Institute of Photonics and Nanotechnology, Faculty of Physics, Vilnius University, Lithuania
brygida.serebriakova@gmc.stud.vu.lt

Acinetobacter baumannii and *Stenotrophomonas maltophilia* are multidrug resistant opportunistic pathogens, with most virulent strains found in hospitals, and are among the main causes of nosocomial outbreaks.[1][2] New preventative measures against these bacteria are needed because of their ability to quickly gain antibiotic resistance through horizontal gene transfer or spontaneous mutations. One of the perspective methods is antimicrobial photodynamic therapy (aPDT) – a biophotonic technology, where a photosensitizer is excited at an appropriate wavelength and inactivates microorganisms by creating reactive oxygen species in the presence of molecular oxygen.[3]

5-aminolevulinic acid (ALA) is a porphyrin precursor in the heme biosynthesis pathway. An excess of exogenously added ALA in bacterial cells leads to accumulation of endogenous porphyrins, such as coproporphyrin, uroporphyrin and protoporphyrin IX, which can act as photosensitizers for aPDT when excited within the Soret band spectral range.[4] The aim of this study is to find out whether *A. baumannii* and *S. maltophilia* are capable of producing endogenous porphyrins when incubated with 1 mM ALA and to assess their arrangement in intracellular and extracellular environments.

We evaluated the synthesis of porphyrins in bacteria (~1×10^7 colony forming units per milliliter) at different incubation periods (0 – 24 h) with 1 mM ALA by measuring fluorescence intensity at excitation wavelengths within the Soret band (390 nm and 405 nm). Extracellular porphyrin fluorescence spectra were recorded after filtrating the solution through 0.22 µm filter. Fluorescence excitation and emission spectra were recorded by means of a LS55 fluorescence spectrophotometer (PerkinElmer, USA). Excitation and emission slits were set to 5 and 10 nm, respectively.

The results indicate that the amount of porphyrins increases over time in both bacteria incubated with ALA as seen from the fluorescecne intensity being monitored at excitation wavelength 390 nm (not shown) and 405 nm (Fig. 1). Compared to *A. baumannii*, *S. maltophilia* generates a greater amount of porphyrins at $\lambda_{ex.}$= 390 nm (not shown). At excitation wavelength of 405 nm, fluorescence bands of ALA-induced porphyrins synthesized by *A. baumannii* shift towards 618 nm, which is characteristic of uroporhyrin (Fig. 1 A). In contrast, the emission spectra of *S. maltophilia* shift towards 612 nm, which corresponds to coproporphyrin (Fig. 1 B).

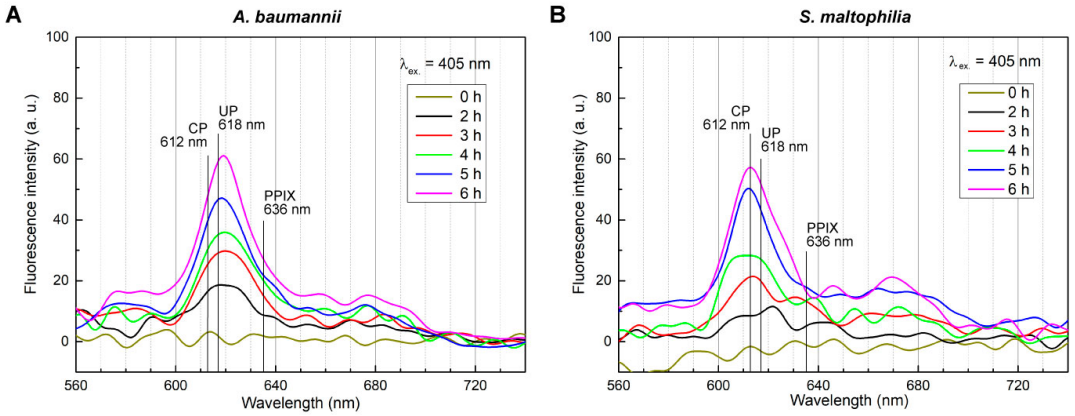


Fig. 1 Fluorescence emission spectra of porphyrins produced by *A. baumannii* (A) and *S. maltophilia* (B) after incubation with 1 mM ALA at different time intervals and at 405 nm excitation. CP – coproporphyrins, UP – uroporphyrins, PPIX – protoporphyrins IX.

In conclusion, both *A. baumannii* and *S. maltophilia* are capable of synthesizing porphyrins when incubated with externally added ALA. Part of them bacteria excrete to extracellular environment, while the rest stays in intracellular environment (data not shown) which makes them suitable for aPDT.

Acknowledgments: This research was funded by the European Social Fund under the No 09.3.3-LMT-K-712 "Development of Competences of Scientists, other Researchers and Students through Practical Research Activities" measure.

[1] Nocera, F. P., *et al.*, 2021. *Acinetobacter baumannii*: Its Significance in Human and Veterinaty Medicine. *Pathogens 10*, 127.
[2] Lira, F, *et al.*,2017. Double-Face Meets the Bacterial World: The Opportunistic Pathogen *Stenotrophomonas maltophilia. Frontiers Microbiology 8*.
[3] Harris, F., *et al.*, 2011. Photodynamic Therapy Based on 5-Aminolevulinic Acid and Its Use as an Antimicrobial Agent. *Medicinal Research Reviews*.
[4] Polmickaite-Smirnova, E., Bagdonas, S., & Anusevičius, Ž. (2019). Sensitization of: Salmonella enterica with 5-aminolevulinic acid-induced endogenous porphyrins: A spectroscopic study. *Photochemical and Photobiological Sciences*, *18*(11), 2730–2739.

TECHNOLOGICAL PROPERTIES OF ENZYMATICALLY HYDROLYSED APPLE POMACE AND THEIR IMPACT ON WHEAT BREAD PROPERTIES

Jolita Jagelavičiūtė, Gustė Staniulytė, Dalia Čižeikiene, Loreta Bašinskienė

Department of Food Science and Technology, Kaunas University of Technology, Lithuania
jolita.jagelaviciute@ktu.lt

Apple pomace is the solid remain after juice processing and is the major by-product of apple juice industry, representing approximately 25% of the fruit weight. Apple pomace is a good source of dietary fibre and the antioxidants [1]. By-product that contains high amounts of dietary fibre can be used for the improvement of nutritional value of bread. Apple pomace has been used in the bread not only for enrichment with dietary fibre but also for sensory properties improvement [2, 3]. However, high content of dietary fibre has negative impact on taste, texture and colour of the bread [4]. Enzymatically hydrolysed dietary fibres of pomace can change technological properties of pomace and improve bread characteristics. This study aimed to evaluate the technological properties of enzymatically hydrolysed apple pomace and their impact on wheat bread properties.

The apple pomace (protein 3.8 g/100g; fat 1.27 g/100g; ash 2.23 g/100g; soluble dietary fibre 9.26 g/100g; insoluble dietary fibre 25.92 g/100g; other carbohydrates 49.48 g/100g; moisture 8.46 g/100g) was hydrolysed with commercially available Novozyme A/S enzymes (Viscozyme® L, Pectinex® Ultra Tropical, Celluclast® 1.5L) for 1 h at 50 °C. The technological properties (oil and water retention capacity, solubility) of apple pomace were determined. Dietary fibre content was determined using the Megazyme kit (AOAC 991.43 and AACC 32-07.01 methods), while reducing saccharide content was determined by 3,5-dinitros-alicylic acid (DNS) colorimetric method. Wheat bread (control I) and wheat bread with apple pomace (5% of wheat flour was replaced with apple pomace (control II) or enzymatically treated apple pomace) were produced and the technological properties were evaluated.

Apple pomace after enzymatic treatment show reduced oil retention capacity, in most cases. The water retention capacity was decreased in sample treated with Pectinex® Ultra Tropical, while enzymatic hydrolysis with other enzymes did not affect the water retention capacity. The dietary fibre ratio was significantly changed after enzymatic hydrolysis and content of reducing saccharide was increased in all enzymatically hydrolysed samples. The addition of apple pomace to wheat bread dough decreased specific volume, pH value and increased total titratable acidity. Porosity in most cases also was decreased after the addition of apple pomace. The lowest porosity was obtained using apple pomace previously enzymatically hydrolysed with Viscozyme® L, while apple pomace enzymatically hydrolysed with Celluclast® 1.5L increased the bread porosity. Apple pomace significantly affected the texture properties of the bread. Hardness of the bread was increased in most cases after the addition of apple pomace, while apple pomace enzymatically hydrolysed with Celluclast® 1.5L did not increase the hardness. Overall acceptability of bread was higher of enzymatically hydrolysed apple pomace with Pectinex® Ultra Tropical comparing with other bread samples. In summary, enzymatic hydrolysis changed apple pomace technological properties. The addition of apple pomace enzymatically hydrolysed with Celluclast® 1.5L improved the technological properties of wheat bread and had not a negative impact on sensory properties.

[1] M. L. Sudha *Apple Pomace (By-Product of Fruit Juice Industry) as a Flour Fortification Strategy* (Agricultural and Biological Sciences 2011)
[2] Masoodi, F.A. & Chauhan, G.S.. Use of apple pomace as a source of dietary fiber in wheat bread. Journal of Food Processing and Preservation, 22, 255–263 (1998).
[3] Ktenioudaki, A., O'Shea, N. & Gallagher, E.. Rheological properties of wheat dough supplemented with functional by-products of food processing: Brewer's spent grain and apple pomace. Journal of Food Engineering, 116, 362–368 (2013).
[4] McKee, L.H. & Latner, T.A.. Underutilized sources of dietary fiber: a review. Plant Foods for Human Nutrition, 55, 285–304 (2000).

3D STRUCTURE MODELING OF HUMAN TELOMERASE REVERSE TRANSCRIPTASE

Varun P. Talati[1], Virupaksha A. Bastikar[1*]

1*Amity Institute of Biotechnology,Amity University Mumbai, Panvel, Maharashtra, Indc.ia.
varun.talati@student.amity.edu

Human telomerase activity has been observed in 90% of cancers, thus validating it as a significant therapeutic target. [1] However, a scarce number of drug candidates have reached clinical trials. One of the reasons for this anomaly is the limited knowledge of telomerase complete protein/enzyme 3D structure, more importantly that of its catalytic subunit – the telomerase reverse transcriptase (hTERT) [2]. Computational modeling has vastly supported the structure based drug discovery projects in last decade. With a poor template homolog from the Protein Data Bank, in the present work we have modeled the whole length of 1132 amino-acid sequence of hTERT using I-TASSER (Iterative Threading ASSEmbly Refinement). 5 distinct 3D structures of hTERT protein were generated with a c-score range from -1.55 to -2.73. Model-1 with highest c-score of -1.55 was considered for further evaluation. The model-1 from ITASSER exhibited a ProSA score of -9.05 and Ramchandran plot analysis reported with 72% most favored regions, 22.3% additionally allowed regions, 2.7% generously allowed regions and 3.0% disallowed regions. The energy minimization was carried out using YASARA force field minimization server and reported Initial Energy to be -507554.7 kJ/mol and Final Energy to be -680715.9 kJ/mol. Further, the current modeled structure would be studied under MD simulation to understand its dynamic behavior in an appropriate solvent system and conditions and can be subjected to in silico based molecular interaction studies for detail drug designing mechanism.

[1] Hanna Holysz NL, Paszel-Jaworska A, Rubis B. Telomerase as a useful target in cancer fighting—the breast cancer case. Tumour Biology; 2013. p. 1371-1380.

[2] Hernandez-Sanchez W, Xu M, Taylor DJ. Telomere Maintenance and Genome Stability. In Kovalchuk I, Kovalchuk O, editors. Genome Stability. Lethbridge: Academic Press; 2016. p. 353-371.

SYNERGISTIC EFFECT OF aPDT & ELECTROPORATION AGAINST *CANDIDA ALBICANS* BIOFILM

Viktorija Juščenko[1], Arūnas Stirkė[2] and Wanessa de Cássia Martins Antunes de Melo[2]

[1] Faculty of Chemistry and Geosciences, Vilnius University, Lithuania
[2]State research institute Center for Physical Sciences and Technology (FTMC), Lithuania
viktorija.juscenko@chgf.stud.vu.lt

Candida species have been reported as the fourth most frequent microorganism that cause bloodstream infections in clinical settings and are the predominant fungi isolated from medical device infections. The ability of this pathogen to form biofilm is the mainly virulence factor which contributes for the persistence of Candida infections associated with high mortality rates (~ 50%) [1, 2]. Thus, several approaches/therapies are being studied to overcome the *C. albicans* biofilm. However, some of them are still in preclinical stages of development and others shows disadvantage such as: specificity for one microbial species, intrinsic mutagenesis and damage to host cell [1].

Antimicrobial photodynamic therapy (aPDT) appears to be an interesting alternative once presents multiple targets process (no development of microbial resistance) and selective killing of microbial cells with minimal damage to the host tissues [3]. aPDT involves the synergistic combination of a photosensitizer (PS), molecular oxygen and visible light of appropriate wavelength in order to produce highly reactive oxygen species (ROS), which leads to the oxidation of several cellular components and to rapid cell inactivation [3]. Despite aPDT advantages, the EPS 'trapping' decreases the PS accumulation into the biofilms and hampers the PS access to the biofilm bottom layers. The electroporation technique (PEF) may be an attractive technique to overcome that and enhance the aPDT effectiveness.

Thus, this study aimed to investigate the synergism between aPDT and electroporation to overcome *C. albicans* biofilms. A mature biofilm of *C. albicans* was performed on cellulose membrane (48 hours – 37°C) and exposed to aPDT (1mg mL^{-1} of methylene blue, light dose 40 Jcm^{-2} - 630 nm), following electroporation (50 µs duration, 1 Hz frequency, 1000 Vcm^{-1}). The results showed the beneficial effects aPDT/PEF once inhibited about 30% and 80% more microbial cells compared to aPDT and PEF alone, respectively. In addition, the Light (only light) and Dark (methylene blue only) controls did not promoted a substantial effect against *C. albicans* biofilm. . Based on these results we suggest that PEF can potentiate the aPDT effect.

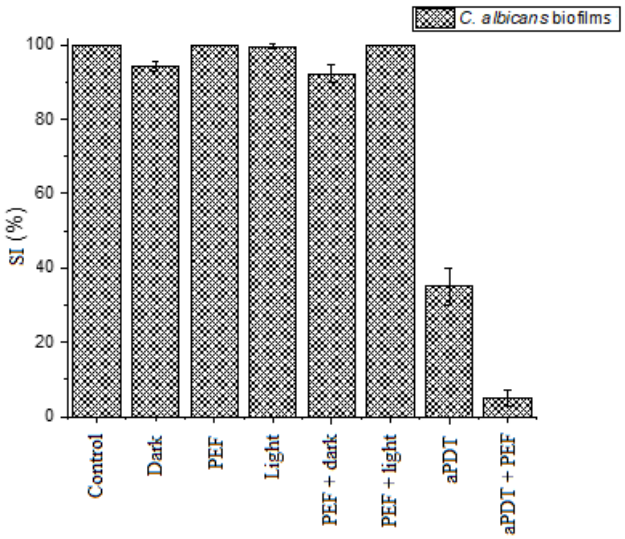


Fig. 1. Synergism of electroporation and aPDT mediated by methylene blue against *C. albicans* biofilm.
* Dark - methylene blue; PEF - electroporation, Light - application of 630 nm light, PEF + dark - application of electroporation and methylene blue, PEF + light - application of electroporation and 630 nm light, aPDT - antimicrobial photodynamic therapy, aPDT + PEF - application of antimicrobial photodynamic therapy in combination with electroporation.

[1] M. Gulati, C. J Nobile, Candida albicans biofilms: development, regulation, and molecular mechanisms, Microbes and Infection **18**, 310-321 (2016).
[2] C.C. Jordão, T. Viana de Sousa, Antimicrobial photodynamic therapy reduces gene expression of Candida albicans in biofilms, Photodiagnosis and Photodynamic Therapy **101825** (2020).
[3] M. R Hamblin, Antimicrobial photodynamic inactivation: a bright new technique to kill resistant microbes, Current Opinion in Microbiology **33**, 67-73 (2016).

OPTIMIZATION OF RECOMBINANT L-BC GAG PROTEIN SYNTHESIS IN *S. CEREVISIAE*

Indrė Krastinaitė[1], Enrika Celitan[1], Saulius Serva[1]

[1] Vilnius University, Life Sciences Center, Vilnius, Lithuania
indre.krastinaite@gmc.stud.vu.lt

During the past decade, virus-like particles (VLPs) were widely employed as vaccine platforms and nanodelivery systems. These nanoparticles are formed of self-assembling viral proteins so they can be functionalized and used for various purposes. Since VLPs are free of replicating viral genetic material, they are considered as safe [1]. Main steps in production of VLPs are: a) viral gene cloning into vector, b) synthesis of VLPs in selected expression system, c) purification of VLPs, d) identification and characterization of the particles [2]. One of the most limiting factor in successful VLP production is solubility of synthesized viral protein. In order to overcome this limitation, it is important to select suitable expression system and optimize conditions for soluble recombinant protein synthesis. Also, renaturation of insoluble proteins can be applied to obtain proteins that would self-assemble into VLPs [3].

The aim of this study was to synthesize the soluble *S. cerevisiae* dsRNA virus L-BC Gag protein that would self-assemble into VLPs to be used for further experiments. L-BC virus gag gene was cloned into expression vector which contains galactose-inducible promoter. The synthesis of the recombinant L-BC Gag protein was launched by induction for 18 hours in different *S. cerevisiae* strains. Our initial studies showed that protein expression was successful while most of the protein is in the insoluble form. Since for formation of VLPs it is essential to obtain the soluble protein, optimization of synthesis and protein purification conditions was performed. We tested different induction times of protein synthesis and cell disruption buffers with different concentrations of salt and detergents. Since all of the results indicated that the L-BC Gag protein is synthesized in rather insoluble form, we decided to perform additional refolding using urea, guanidine hydrochloride and arginine solutions. Unfortunately, the protein did not dissolve in any of the solutions, so further optimization for solubilization of L-BC Gag protein is required.

[1] C. Ludwig and R. Wagner, Virus-like particles—universal molecular toolboxes, Current Opinion in Biotechnology **18**(6), 537-545 (2007).
[2] A. Zeltins, Construction and characterization of virus-like particles: A review, Molecular Biotechnology, **53**(1), 92–107 (2013).
[3] Z. Shirbaghaee, and A. Bolhassani, Different applications of virus-like particles in biology and medicine: Vaccination and delivery systems, Biopolymers, **105**(3), 113–132, (2015).

STUDY OF THE INTERACTION BETWEEN BIOMIMETIC LIPID BILAYER AND AMYLOID-β PEPTIDE

Evelina Jankaitytė[1], Andrius Sakalauskas[2], Vytautas Smirnovas[2], Rima Budvytytė[1], Gintaras Valinčius[1]

[1] Institute of Biochemistry, Life Sciences Center, Vilnius University, Vilnius, Lithuania
[2] Institute of Biotechnology, Life Sciences Center, Vilnius University, Vilnius, Lithuania
evelina.jankaityte@bchi.stud.vu.lt

A common sign in neurodegenerative diseases is the misfolding, aggregation, and accumulation of proteins, leading to cellular dysfunction, loss of synaptic connections, and brain damage. Proteins can undergo misfolding from their native state to form intermolecular β-sheet rich structures, ranging from small oligomers to large fibrillar aggregates, in the diseased brain. Amyloid β that confers neurotoxicity has been central to the amyloid hypothesis of Alzheimer's disease pathology [1]. Intermediate structures of aggregation process are transient and heterogeneous and the mechanism by which amyloid β can be neurotoxic has not been fully elucidated. One prevailing hypothesis suggests that amyloid β can be toxic through a membrane disruption mechanism, which leads to loss of synaptic efficiency, neuronal dysfunction, and degeneration [2].

Biomimetic lipid bilayer systems are a useful tool for modelling specific properties of cellular membranes to get more knowledge about their structure and functions. In this study, as simplified membrane model, we are using large unilamellar liposomes. The aim of our work is to find out whether composition of lipids is an important factor for amyloid β and membrane interaction. By incorporating lipids, such as sphingomyelin, we can mimic membrane microdomains, also known as lipid rafts. Lipid rafts appear to be involved in the development of Alzheimer's disease by affecting the aggregation of the amyloid β peptide at neuronal membranes thereby forming toxic oligomeric species [3]. Additionally, in this work we study what extent of damage is caused by amyloid β at different stages of the aggregation process (small oligomers and fibrils). To study interaction between amyloid β and unilamellar liposomes we are using fluorescence spectroscopy. Fluorescent dye Thioflavin T allows us to monitor fibrils formation and calcein leakage essay helps to evaluate liposomes integrity changes. Our results show that small oligomers of amyloid β disrupt the liposomes at much higher level, compared to large fibrils.

[1] LI, M., Chen, L., Lee, D. H. S., Yu, L. C., Zhang, Y. (2007). The role of intracellular amyloid beta in Alzheimer's disease. Progress in Neurobiology, 83(3), 131-139.
[2] Kotler, S. A., Walsh, P., Brender, J. R., Ramamoorthy, A. (2014). Differences between amyloid-β aggregation in solution and on the membrane: Insights towards elucidation of the mechanistic details of Alzheimer's disease. Chemical Society Reviews, 43(19), 6692-6700.
[3] Staneva G., Watanabe, C., Puff, N., Yordanova, V., Seigneuret, M., Angelova, M. I.et al. (2021). Amyloid-β Interactions with Lipid Rafts in Biomimetic Systems: A Review of Laboratory Methods. Methods in Molecular Biology, 2187, 47-86.

THE INVESTIGATION OF BYSTANDER EFFECT AFTER BLEOMYCIN ELECTROTRANSFER OR IRREVERSIBLE ELECTROPORATION IN BETWEEN CELL LINES

Ugnė Borinskytė[1], Neringa Barauskaitė[1], Paulius Ruzgys[1], Vitalij Novickij[2], Saulius Šatkauskas[1]

[1] Biophysical Research Group, Faculty of Natural Sciences, Vytautas Magnus University, Lithuania
[2] Institute of High Magnetic Fields, Vilnius Gediminas Technical University, Naugarduko st. 4103227, LT-10224 Vilnius, Lithuania
ugne.borinskyte@vdu.lt

Cancer is a major public health problem worldwide and the second leading cause of death in the United States [1]. Therefore, currently cancer treatment research is a leading topic worldwide. Hence alternative anticancer treatments are being applied as a substitute to conventional ones. One of most promising novel anticancer therapies are electrochemotherapy and electroablation [2]. Both methods are based on the phenomenon of electroporation, that is dependent on the formation of the electropores in the affected cell membranes. Such process occurs as a result of electric field triggered transmembrane potential increase [3]. Pore formation is initiated when transmembrane potential surpasses the electroporation threshold. Reversible electroporation is triggered if transmembrane potential does not deviate far from the electroporation threshold. In other case of scenario transmembrane potential greatly exceed the electroporation threshold, hence irreversible electroporation is induced.

The phenomenon of reversible electroporation is used in clinics as a cellular membrane permeabilization method for various hydrophilic molecules, such as anticancer drug bleomycin, to be transferred into the malignant cell cytosol. Such combination of both treatments is termed as electrochemotherapy. Similarly, irreversible electroporation induces another anticancer treatment termed as electroablation.

Both of the mentioned methods are local, thus are comparable to radiotherapy, as it is also a local conventional cancer treatment method. It is known that cell affected by ionizing radiation can trigger the bystander effect on the adjacent cells. Recently, few publications had shown that the bystander effect is present after both electroporation driven cancer treatment methods, namely electrochemotherapy and electroablation [4]. However, there is still a lack of research that could respectively describe the phenomenon of bystander effect after both electroporation triggered cancer treatment methods. Moreover, none of the studies to date evaluate the bystander effect dependance on cell lines. Even more, it is still not known whether the bystander effect could be initiated in between the different cell lines.

The bystander effect triggered by irreversible electroporation or bleomycin electrotransfer was carried out in vitro. Chinese hamster ovary cells (CHO-K1) and human adenocarcinoma alveolar basal epithelial cell (A549) lines are used for experiments. The electrotransfer of the anticancer drug BLM (20 nM) was performed with one electrical pulse at (1400 V/cm) for the duration of 100 µs. Irreversible electroporation was performed also with a single electrical pulse at (2800 V/cm) for the duration of 100 µs. After electroporation, cells were incubated for 10 min, then 1 ml of RPMI growth media was applied on top and incubated for 72 hours in a 6-well plate. After incubation, the medium is collected and centrifuged twice. Then the collected media was applied on 400 cells in the 4 cm petri dish. Cell colony formation assay was performed form those cells.

The results presented here indicate that the bystander effect triggered by bleomycin electrotransfer is significantly decreasing CHO and A-549 cell viability. Furthermore, the bystander effect has similar effect on different cell lines i.e., bleomycin electrotransfer was performed on CHO cells and the media was transferred on A-549 cells or vice versa. However irreversible electroporation did not trigger positive bystander effect as with CHO cell lines.

[1] R. L. Siegel, K. D. Miller and Jemal, A., Cancer statistics, 2020. CA: A Cancer Journal for Clinicians. 70, 7–30, 2020.
[2] Y. Peng, H. Tao, Y. Gao, Y. Yang and Chen, Z., Review and Prospect of Tissue-agnostic Targeted Strategies in Anticancer Therapies, Curr. Top. Med. Chem., **21**, 404–425, 2020.
[3] B. Geboers, H. J. Scheffer, P. M. Graybill, A. H. Ruarus, S. Nieuwenhuizen, R. S. Puijk, P. M. van den Tol, R. V. Davalos, B. Rubinsky, T. D. De Gruijl, D. Miklavčič and Meijerink, M. R., High-Voltage Electrical Pulses in Oncology: Irreversible Electroporation, Electrochemotherapy, Gene Electrotransfer, Electrofusion, and Electroimmunotherapy. Radiology. **295**, 254–272, 2020.
[4] P. Ruzgys, N. Barauskaitė, V. Novickij, J. Novickij and Šatkauskas, S., The Evidence of the Bystander Effect after Bleomycin Electrotransfer and Irreversible Electroporation. Molecules. **26**, 6001, 2021.

TECHNOLOGY AND PROPERTIES OF HYDROGEL LAB-ON-CHIP PLATFORM FOR BIOMEDICAL POTENTIAL APPLICATIONS CONCERNING MAGNETIC FIELD EFFECTS ON CANCER CELL LINES

Eliza Hartel[1], Adrianna Cieślak[2], Magdalena B. Łabowska[2], Agnieszka Podwin[1], Jerzy Detyna[2]

[1] Department of Microsystems, Faculty of Electronics, Photonics and Microsystems, Wrocław University of Science and Technology, Wrocław, Poland.
[2] Department of Mechanics, Materials and Biomedical Engineering, Faculty of Mechanical Engineering, Wrocław University of Science and Technology, Wrocław, Poland.
elizahartel@gmail.com, adrianna.cieslak01@gmail.com

In the paper, the preliminary results on the microfluidic platform fabrication equipped with hydrogel matrix are shown. A 3D printing technique was used to provide a “sandwiched” type structure including two different microfluidic substrates. A special attention was paid herein to achieve uniformly bio-printed hydrogel layers of the unique composition and to cross-linking process as well, which properties were then verified by mechanical durability tests. Further investigation concerning the biomedical application of the LOC platform will be done shortly. For instance, the structure will be biologically validated and the magnetic field effects on the selected cancer cell lines will be studied in the context of cells viability and proliferation.

Lab-on-chip devices are so called, miniature laboratories enabling diverse microbiological research to be provided within a single microfluidic chip [1]. They are characterized by substantial reagents minimization, possible automation and high biocompatibility, especially when hydrogel layers are applied. Potential application of LOCs assisted by hydrogel matrix can open the way towards novel anti-cancer therapies and their validation. Planned research includes analysis of the effects of magnetic fields on cancer cells, because there is no clear pattern of cell behavior after exposure to the magnetic field, as reported in studies [2], [3].

For the microfluidic chip fabrication, the 3D printed substrates (Asiga FusionGRAY V2) were used as a base and a cover of the hydrogel layers. Two different types of hydrogel were manufactured (4% sodium alginate, 2% agar, 1% methylcellulose and 4% sodium alginate, 2% gum arabic, 1% methylcellulose) and applied. The process of bio-print was optimized and deposited layers were in a close relation to the model geometries. Our "sandwich structure" (Fig. 1) was then tested for mechanical durability and results were obtained for parameters, such as Young's modulus, for both hydrogels used. The Young's modulus results for the hydrogels are in the range of 50-60 MPa. These values are similar to the Young's modulus of biological structures (e.g. cornea 3MPa, skin 30MPa) [4].

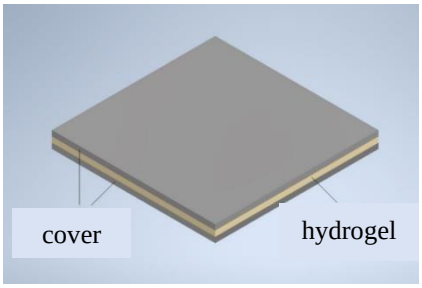


Fig. 1 Lab-on-chip - "sandwich structure"

There are lots of research about impact of the magnetic field on the cancer cells e.g. [2], [3], but it is not connected with LOCs. That is way our future studies are significant. The influence of the static magnetic field on the cancer cells will be identified directly on the cells cultured on LOC and the biological and physical effects (cells viability, proliferation and morphology) will be evaluated in cooperation with Wroclaw Medical University.

[1] Podwin, A. and all, Lab-on-Chip Platform for Culturing and Dynamic Evaluation of Cells Development. Micromachines 2020, 11 (2), 196. https://doi.org/10.3390/mi11020196
[2] Varshney A., Kumar G., Effects of magnetic field on cancer cell line. Journal of Experimental Biology and Agricultural Sciences, ISSN no. 2320 – 8694, India, 2013.
[3] Zafari J.et all, Anticancer Effects of Moderate Static Magnetic Field on Cancer Cells In Vitro. Molecular Medicine, 2017. http://dx.doi.org/10.18502/rmm.v6i3.4610
[4] McKee C. T. and all, Indentation versus tensile measurements of Young's modulus for soft biological tissues. Tissue Eng Part B Rev. 2011 Jun;17(3):155-64. https://doi.org/10.1089/ten.teb.2010.0520

RESEARCH OF ANTI-INFLAMMATORY PROPERTIES CICHORIUM INTYBUS EXTRACT

Karyna Savchenko[1], Vadym Lisovyi[1], Nazar Zderko[1], Volodymyr Bessarabov[1], Galyna Kuzmina[1], Nadia Matvieieva[2], Hanna Kharytonenko[1]

[1]Department of Industrial Pharmacy, Kyiv National University of Technology and Design, Ukraine
[2]Institute of Cell Biology and Genetic Engineering National Academy of Sciences of Ukraine, Ukraine
k.savchenko@kyivpharma.eu

Inflammation is a local response of the body to damage, aimed at destroying and removing the pathogenic agent, as well as eliminating the consequences of its action. Chronic inflammation occurs as a result of oxidative stress, which progress due to the formation of metabolites of the peroxidation reaction of polyunsaturated fatty acids under the catalytic action of 15-lipoxygenase (15-LOX) and other Redox enzymes in cells. Pharmacological inhibition of oxygenases reduces the symptoms of inflammation and pain.

Therefore, the study of compounds capable of inhibiting 15-LOX activity is potentially interesting. Although many compounds have been found and biologically studied that can affect the activity of this enzyme, there are still a small number of drugs on the pharmaceutical market that contain lipoxygenase inhibitors. Registered drugs do not have a specific effect, so it is important to isolate and study substances and natural biological mixtures that can affect on 15-lipoxygenase. It is known that flavonoids have an appropriate effect and are low-toxic. Therefore, an extract from Cichorium intybus, which is rich in these compounds, selected for this study to model a new anti-inflammatory drug.

UV-Vis spectrophotometry was used to study the ex vivo kinetic patterns and mechanisms of 15-lipoxygenase inhibition; for the development of the composition of anti-inflammatory drugs in the form of suppositories – mathematical planning of a complete factorial experiment.

The study of anti-inflammatory properties of Cichorium intybus extract is based on the determination of 15-LOX activity in the enzymatic oxidation reaction of linoleic acid as a substrate. Measurements were performed using the spectrophotometric method, recording the increase in the absorbance of the conjugated diene chromophore in the molecule of linoleic acid hydroperoxide over time at a wavelength of $\lambda = 235$ nm [1]. To determine the most acceptable kinetic model and the according type of inhibition, a series of calculations were performed under different conditions, ranking the results by the criterion of the correlation coefficient R^2. The calculation of kinetic parameters was performed in accordance with standard methods and kinetic models in the software package SigmaPlot 12.5. When ranking kinetic models by the criterion of the value of the correlation coefficient, it was found that the most suitable kinetic model is Mixed (Partial), inhibition of 15-LOX ($R^2 = 0{,}9608$). The concentration of semi-maximal inhibition is $IC_{50} = 84.13 \pm 7.22$ μM. The kinetic constants calculated according to the selected model have the following values: $K_i = 23.29 \pm 5.42$ μM, $K_m = 57.44 \pm 7.52$ μM.

Cichorium intybus extract is an effective inhibitor of 15-LOX by a mixed (partial) mechanism of inhibition, it means that the inhibitor binds both in the active site of the enzyme and externally, and the enzyme-substrate complex retains partial activity compared to the native enzyme. The obtained results suggest that the extract of Cichorium intybus can potentially be used as an API of drugs with anti-inflammatory properties, as it is highly effective as a 15-LOX inhibitor.

[1] Kharytonenko, H. I., Skaterna, T. D., Mel'nyk, A. K., Babiĭ, L. V., & Kharchenko, O. V. (2008). *Ukrains'kyi biokhimichnyi zhurnal (1999), 80*(3), 31–39.

INVESTIGATION OF NANOSECOND PULSED ELECTRIC FIELD TREATMENT EFFECTS ON YEAST CELLS

Gabrielė Vasiliauskaitė[1], Povilas Šimonis[1], Arūnas Stirkė[1]

[1] Laboratory of Bioelectrics,
State Research Institute, Center for Physical Sciences and Technology, Lithuania
gabriele.vasiliauskaite@gmc.stud.vu.lt

Budding yeast *Saccharomyces cerevisiae* are very important for the food industry, they are used to produce fermented food and drinks. Yeast cells are also often used as a model eukaryotic organism to investigate cellular responses to abiotic conditions [1]. One of the prospective abiotic treatments suggesting a wide range of applications and effects which depend on pulse duration and its strength is the pulsed electric field (PEF). When compared to electric field pulses with microsecond duration, nanosecond pulsed electric field (nsPEF) has a greater impact on intracellular structures and cells` functions [2]. nsPEF changes cells intracellular environment by damaging organelles and membranes, still, it is not clear how the cell reacts to occurred changes and what mechanisms are activated [3]. Besides lethal effects, sub-lethal injuries can occur, which lead to a loss of ability to grow on selective media [4]. This study aims to investigate nsPEF effects on yeast cells viability, occurred sub-lethal injuries caused by different pulse strength and a number of pulses.

Cells were collected in the early exponential phase at 0.9 – 1.1 OD^{600}, washed twice with electroporation buffer (EPB) and suspended in 1 mL EPB. Cells were exposured to 1, 3 and 5 impulses of 90 ns, with strengths of up to 250 kV/cm. The viability of cells was evaluated by counting colony-forming units on YPD and selective medium (YPD + 2% NaCl) (Fig. 1. A). Also, programmed cells death, dependent on metacaspase activation was evaluated using caspase detective FITC-VAD-FMK marker. Caspase detection assay was performed according to the producer protocols and YCA1+ metacaspase was evaluated using flow cytometer (Fig.1. B).

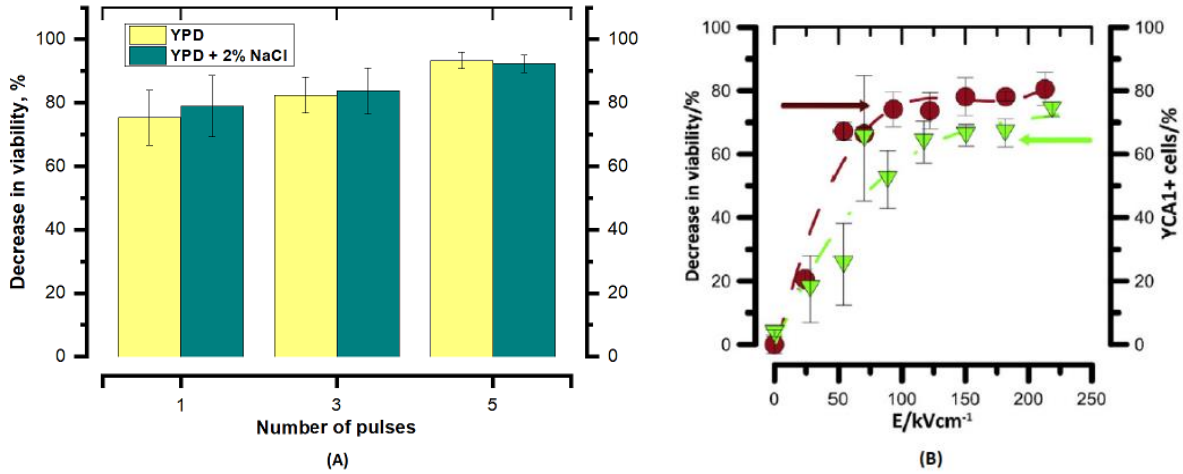


Fig. 1. Decrease in viability on YPD, YPD + 2% NaCl media after exposure to 1, 3, 5 pulses of nsPEF (A); changes in viability and YCA1+ activity after exposure to 5 pulses of nsPEF (B).

This study showed that cell viability is dependent on number of nanosecond pulsed electric field pulses and field strength, which cause lethal or sub-lethal injuries. We think, that cell viability decrease on selective media the same as on non-selective media, because nsPEF has a greater impact on intracellular environment than on cells' membrane. We also see that after nsPEF treatment metacaspase activity increase and result in metacaspase/dependent programmed cells death [5]. We assume that because of these intracellular changes after treatment with nsPEF yeast cells can not repair damaged organelles and membranes become permeable.

The prospect of this research is analyze how nsPEF damages cell organeles, such as mitochondria, how sub-lethal injuries affect death patterns and what reparation mechanisms work depending on type of induced damage.

[1] G. G. Stewart , *Encyclopedia of Food Microbiology*, Elsevier, . 309–315, 2014.
[2] T. Ning, *et al.*, *Stem Cell Res. Ther.*, 10, 45, 2019.
[3] Q. Yang, *et al.*, *J. Phys. Chem. B*, 25, 38, 10692–10700, 2021.
[4] V. Kethireddy, *et al.*, *Int. J. Food Microbiol.*, 233, 73–80, 2016.
[5] P. Simonis, *et al.* , *Bioelectrochemistry*, 115, 19–25, 2017.

LEVELS OF FGF-2 IN BLOOD PLASMA OF PATIENTS SUFFERED FROM COVID-19

Antonina Rachkovska, Daryna Krenytska, Olexiy Savchuk

Educational and Scientific Centre "Institute of Biology and Medicine" Taras Shevchenko National University of Kyiv
tonia01128@gmail.com

Background. Widespread of the virus SARS-CoV-2 has caused development of the pandemic as called COVID-19 around the world. Clinical information shows that SARS-CoV-2 induces acute respiratory distress syndrome (ARDS), however underlying reasons for starting are unclear. Inflammatory reaction and angiogenesis are interdependent processes in a number of pathogenic desearses. Activated lymphocytes could express factor grows fibroblast-2 (FGF-2) that is able to induce angiogenesis during development of the ARDS. Besides, nitrogen oxide (NO) is produced by vascular endothelium during stimulation cytokines at the time of response against pathogenic actions SARS-CoV-2. Simultaneously, synthesis of the nitrogen oxide causes to produce and activate FGF-2 [1,2]. Our research is aimed to study the potential role of FGF-2 in pathological condition of patients suffered from COVID-19.

Methods. Plasma of the blood 60 patients was used for measurement of concentration FGF-2. 40 patients have suffered from COVID-19 including 20 patients with titer of anti-SARS-CoV-2 IgG - 5 ± 3 Index (S/C) and 20 patients with titer of anti-SARS-CoV-2 IgG – 175 ± 5 Index (S/C), in particular 20 patients without anti-SARS-CoV-2 IgG in plasma were such as control group of donors. Quantitative analysis concentration of FGF-2 was performed with the ELISA technique.

Results. Statistical analysis has revealed that concentrations of FGF-2 differed between studied groups. Thus, in patients with anti-SARS-CoV-2 IgG levels of FGF-2 were higher than in group of patients without anti-SARS-CoV-2 IgG. Nevertheless, in patients with anti-SARS-CoV-2 - 175 ± 5 Index (S/C) the mean rank of concentration FGF-2 was higher than in patients with anti-SARS-CoV-2 – 5 ± 3 Index (S/C) and the difference was significant (H=10,14, p=0,0063). Elevated levels of FGF2 have been caused inflammatory and hypoxia and would been implicated FGF2-induced angiogenesis during infection of SARS-CoV-2.

Conclusion. Today we don't know whether elevated FGF-2 is adaptive and beneficial characteristic for clinical situations in pathogenesis COVID-19. Further researches of dynamic changes levels of FGF-2 in patients suffered from COVID-19 can help to improve existing and to create new approaches for diagnostics of possible complications. FGF-2 could be promising target for therapia COVID-19.

---

[1] Pedro Cuevas, Antonio Manquillo, Pedro Guillen, Guillermo GImínez-Gallego, Fibroblast growth factor: A target for COVID-19 infection, *International Journal of Medical Reviews and Case Reports* 4(5), 122-125 (2020).

[2] Presta M, Andres G, Leali D, Dell'Era P, Ronca R. Inflammatory cells and chemokines sustain FGF2-induced angiogenesis. *European Cytokine Network* 20(2), 39-50 (2009).

P4-43

DID NOT PARTICIPATE

.

PROSPECTIVE METHODS OF PREVENTING POISONING BY PHOSPHORORGANIC COMPOUNDS USING COMPOUNDS OF NATURAL ORIGIN

Viktoriia Lyzhniuk, Vadym Lisovyi, Roman Smishko, Volodymyr Bessarabov, Galyna Kuzmina

Department of Industrial Pharmacy, Kyiv National University of Technology and Design, Ukraine
v.lyzhniuk@kyivpharma.eu

Today, the topic of organophosphorus (OP) poisoning is becoming more relevant due to their easy availability and large-scale use not only in agriculture, but also in the chemical and pharmaceutical industries. Poisoning by these compounds actually ranks first among other exogenous poisonings not only in frequency but also in severity [1].

The main pathogenetic mechanism of action of organophosphorus compounds based on the inhibition of cholinesterase enzyme, which hydrolyzes acetylcholine and plays an important role in the process of synaptic transmission of nerve impulses in cholinergic formations [2]. As a result, in the case of organophosphorus poisoning, there is a significant decrease in serum butyrylcholinesterase (BCHE) activity and accumulation of acetylcholine in cholinergic synapses with excessive stimulation of cholinergic receptors, which in turn leads to "cholinergic syndrome" [3]. All this makes the task of finding a new way to treat or prevent poisoning very important.

A promising method of preventing OP poisoning is the use of flavonoids, compounds of natural origin that have a broad therapeutic effect and are also low-toxic. In this paper, a biologically active substance of flavonoid nature diosmin considered as a preventive against OP poisoning.

Evaluation of the premedical properties of diosmin were performed by determining the activity of butyrylcholinesterase in human serum, using a modified Ellman method. This method based on the ability of thiocholine, the reaction product, to reduce potassium hexacyanoferrate (III), which has a yellow color, to transparent potassium hexacyanoferrate (II). The use of potassium hexacyanoferrate (III) allows the analysis of serum butyrylcholinesterase in a wide linear range without prior dilution of samples. The advantage of the method is that it is possible to use liquid reagents that are quite stable over a long period of storage.

The study was performed spectrophotometrically. Kinetics was studied at $\lambda = 405$ nm. The rate of decrease in the absorbance of the reaction solution is directly proportional to the activity of BCHE serum. Ouragan-Forte, in which glyphosate, diluted to 10 mM, was the active ingredient, was selected as the model organophosphorus pesticide. At this concentration, glyphosate can inhibit the activity of the enzyme BCHE 1.7 times. Instead, pre-addition of diosmin to the reaction mixture reduced the negative effect of glyphosate on human serum BHE activity.

It has been found that diosmin at a concentration of 200 μM is able to reduce the inhibition of BCHE by glyphosate by approximately 15-20%. The results of the study show that the higher the concentration of diosmin, the more pronounced the effect of preventing the inhibition of BCHE by glyphosate. Diosmin acts as a reversible inhibitor - it binds to the active site of the enzyme without leaving spot for glyphosate. After a period of time, diosmin leaves the active site of the BCHE, as a result of which the activity of the enzyme is restored.

It concluded that diosmin can be a promising substance to prevent intoxication with organophosphorus compounds and can be used as an active pharmaceutical ingredient in the development of drugs to prevent OP poisoning.

[1] Ageev, V.O., Kachanova, T.L., Fomin, B.F. (2015). Natural classification of acute organophosphorus poisoning. Izvestiya SPbGETU "LETI".

[2] Hulse, E.J., Haslam, J.D., Emmett, S.R., Woolley, T. (2019) Organophosphorus nerve agent poisoning: managing the poisoned patient. British Journal of Anesthesia, 123 (4), 457-463. doi: 10.1016 / j.bja.2019.04.061.

[3] Costa L. G. (2018) Organophosphorus Compounds at 80: Some Old and New Issues. Toxicological sciences: an official journal of the Society of Toxicology. No. 162 (1). P.24-35.

CENTRIFUGAL FORMATION OF FIBERS OF SOLID DISPERSED SYSTEM OF POLYMER WITH HESPERIDINE

Vadym Lisovyi, Artem Kharchenko, Nazar Zderko, Olga Kovalevska, Volodymyr Bessarabov

Department of Industrial Pharmacy, Kyiv National University of Technology and Design, Ukraine
v.lisovyi@kyivpharma.eu

Hesperidin is a biologically active substance, a plant polyphenol that belongs to the class of flavonoids. Bioflavonoids have anti-inflammatory, antioxidant, immunomodulatory, antithrombotic, antiallergic, vasodilating effects [1]. The problem with their use is poor solubility in water, which means low bioavailability. That is why it is important to increase the solubility of hesperidin to expand the possibilities of application.

Method: to increase the solubility used centrifugal formation of a solid dispersed system (SDS) from a polymer melt (method of formation of "cotton candy"). To do this, we used a machine for making cotton candy "Cotton candy maker". The essence of the method is to melt the powder mass in the disk, which rotates with the subsequent force of the melt due to centrifugal force in the holes on this disk and solidification of the mass in the air in the form of thin fibers. As a pharmaceutically acceptable polymer used polyvinylpyrrolidone K-17 (PVP K-17), which is slower to form cotton wool, which allows the formation of an alloy with hesperidin.

To determine the coefficient of solubility increase, a method for studying the concentration of hesperidin in solution was developed. Usually, hesperidin in solution is determined by spectrophotometric method, because flavonoids have an absorption peak in the yellow region of the spectrum (284 nm). But during remelting, sugar and polyvinylpyrrolidone turn yellow, which interferes with the determination of hesperidin. That is why a method for determining the concentration of hesperidin in solution was developed and validated, the essence of which is the interaction of phenolic groups of hesperidin with ferric chloride (III) with the formation of a dark green compound with an absorption peak at 602 nm.

To check the solubility of the formed SDS in the form of cotton wool, it was weighed and dissolved in 1 ml of purified water. Then stirred for 30 minutes at 25 °C on a thermoshaker and centrifuged for 20 minutes. The supernatant formed was separated and 1 ml of 0.3 N ferric chloride solution (III) was added, left for 20 min and checked spectrophotometrically with 0.3 N ferric chloride (III) solution taken as reference.

Several samples were made with different ratios of polyvinylpyrrolidone to hesperidin 99:1, 95:5 and 90:10. According to the results of the solubility test, it was found that at a mass ratio of hesperidin to polyvinylpyrrolidone 90: 10, the coefficient of increase of the solubility of flavonoids increased 157 times. As the content of hesperidin in the SDS decreases, the coefficient of increase of solubility increases from 157 to 188 times. Also, with increasing content of hesperidin slightly decreases the final yield: at the lowest amount of hesperidin the yield is ~ 30%, about increased content of hesperidin to 5% yield is 27.5%, at 10% hesperidin - 26%.

To increase the yield, sugar was added, which in a mixture with polyvinylpyrrolidone allows to increase the final yield of cotton wool [2]. Samples were made in the ratios of hesperidin: sugar: polyvinylpyrrolidone 10:05:85, 10:10:80, 10:20:70, 10:30:60, 10:40:50, 10:50:40. When the amount of sucrose increases to 20%, the yield of the product increases, it is possible to increase the yield of cotton wool from 26% to 40%. However, when the sucrose content is more than 10%, the coefficient of increasing of solubility of hesperidin decreases by approximately 15%. The optimal content of components for the preparation of polymeric SDS by the method of "cotton candy" is the ratio of PVP K-17 and sucrose 80:10.

Infrared spectroscopic study of the components of SDS and complexes of polyvinylpyrrolidone K-17 and hesperidin suggests the formation of complexes mainly due to hydrogen bonds. The complexes formed are characterized by an increase in the number of hydrogen bonds by more than a third.

Therefore, a method for obtaining SDS by "cotton candy" technology has been developed, the essence of which is to alloy hesperidin with a polymer with subsequent centrifugal formation of "cotton candy" fibers. A method for detecting hesperidin based on the reaction with ferric chloride (III) was developed for the analysis of cotton wool. When testing the solubility of cotton wool, it was proved that this method increases the coefficient of solubility of hesperidin in 188 times. Also, there was a study of the effect on the solubility of the addition to the mixture of polymer and hesperidin sugar, which was able to increase the final yield to 40%.

[1] Effects of flavonoids on the release of reactive oxygen species by stimulated human neutrophils. Biochem Pharmacol. 1993. № 46. P. 1257– 1271.
[2] Nasir, Sidra, et al. “Improved Bioavailability of Oxcarbazepine, a BCS Class II Drug by Centrifugal Melt Spinning: In-Vitro and in-Vivo Implications.” International Journal of Pharmaceutics, vol. 604, 2021, p. 120775., https://doi.org/10.1016/j.ijpharm.2021.120775.

ARTEMISIA TILESII LEDEB EXTRACT INHIBITS 15-LIPOXYGENASE ENZYME

Iryna Pashchenko[1], Vadym Lisovyi[1], Viktor Kostyuk[1], Nadia Matvieieva[2], Volodymyr Bessarabov[1]

[1]Department of Industrial Pharmacy, Kyiv National University of Technology and Design, Ukraine
[2]Institute of Cell Biology and Genetic Engineering National Academy of Sciences of Ukraine, Ukraine
i.pashchenko@kyivpharma.eu

Inflammation is the cause of many chronic diseases of various human body systems. According to the modern understanding, inflammation on the one hand is a necessary protective and adaptive reaction of the organism to the influence of pathogenic factors, on the other hand - a pathological process that in chronic course leads to atherosclerosis, cancer, neurodegenerative diseases, etc. [1, 2].

Neurodegenerative disorders, including Alzheimer's disease, which directly linked to inflammation, are one of the leading causes of disability in Europe [1, 2].

Enzymatic and non-enzymatic ways of formation of lipid peroxidation metabolites play a significant role in the formation and progress of inflammatory processes, initiating oxidative stress and provoking secondary alteration as a mediator of inflammation. One of the key enzymes of lipid metabolism is lipoxygenase. Thus, the search for compounds capable of inhibiting 15-lipoxygenase activity and the development of a drug with anti-inflammatory action using inhibitors of this enzyme is relevant [3].

There is information in the literature on the use of plants that contain substances that inhibit enzymes that play a role in the progress of inflammatory processes, such as 15-lipoxygenase. Such plants include *Artemisia tilesii* Ledeb [3].

Artemisia tilesii Ledeb is a little-known plant with a very narrow range that grows in Japan and North America. This plant belongs to the class *Magnoliopsida*, a division of the *Magnoliophyta* family *Asteraceae* [4]. There are practically no publications on the biological activity of these plants. We only know that the indigenous population uses them to treat various diseases [4].

An extract from *Artemisia tilesii* Ledeb, which contains a large amount of flavonoids, selected for the study. It is promising and expedient to conduct research on the use of *Artemisia tilesii* extract as an inhibitor of the enzyme 15-lipoxygenase, which will allow us to evaluate the possibility of its use as a potential active pharmaceutical ingredient for development an effective anti-inflammatory drug for the treatment of neurodegenerative diseases.

The study of the extract from Artemisia tilesii Ledeb using FTIR spectroscopy revealed that the main part of the extract substances has an aromatic nature, a small amount of substances contains aliphatic groups with a branched structure. In comparison with rutin, this water-ethanol extract (30:70%) *Artemisia tilesii* Ledeb, contains about 34% flavonoids. It was also proved that this extract effectively inhibits the enzyme 15-lipoxygenase (IC50 = 17.94 ± 1.20 μm), because this effect is manifested in the studied concentration range for rutin 25-100 μm. Probable mechanism of inhibition of 15-lipoxygenase extract from *Artemisia tilesii* Ledeb – mixed (partial). Mixed (partial) inhibition occurs when the inhibitor binds both in the active site of the enzyme and externally, and the enzyme substrate complex retains partial activity compared to the native enzyme. The mechanism of inhibition established in this study fully accord to the essence of the extract composition as a mixture of different biologically active and inert substances. Thus, it can be argued about the potential anti-inflammatory properties of the extract of Artemisia tilesii Ledeb in vitro.

The results indicate that the extract of *Artemisia tilesii* Ledeb can be used in the development of new anti-inflammatory drugs for the treatment of neurodegenerative diseases.

[1] S. López-Ortiz, J. Pinto-Fraga, P. L. Valenzuela, et.al. Physical Exercise and Alzheimer's Disease: Effects on Pathophysiological Molecular Pathways of the Disease. Int J Mol Sci. **22(6)**, 2897. doi:10.3390/ijms22062897.

[2] Bajwa Ekta, Pointer Caitlin B, Klegeris Andis. Modifiable risk factors of Alzheimer's disease and neuroinflammation: what are the links? Future Neurol., **11(4)**, 237–244 (2016). DOI: 10.2217/fnl-2016-0020.

[3] N.A Matvieieva, A.M. Shakhovsky, V.B. Belokurova, K.O. Drobot. *Artemisia tilesii* Ledeb hairy roots establishment using *Agrobacterium rhizogenes* mediated transformation. *Prep Biochem Biotechnol.*, **46(4)**, 342-345 (2016). DOI: 10.1080/10826068.2015.1031393.

[4] N.A. Matvieieva, B.V .Morgun, O.R. Lakhneko, et.al. *Agrobacterium rhizogenes*-mediated transformation enhances the antioxidant potential of *Artemisia tilesii* Ledeb. *Plant Physiology and Biochemistry*, **152,** 177-183. (2020). doi:10.1016/j.plaphy.2020.04.020.

DID NOT PARTICIPATE

.

MONITORING OF SOLUBLE FIBRIN MONOMER COMPLEXES AND VITAMIN K-DEPENDENT PROTEINS IN PATIENTS WITH CORONARY ARTERY DISEASE

Tetiana Marynenko, Tetiana Halenova, Olexii Savchuk, Ludmyla Ostapchenko

Department of Biochemistry, ESC "Institute of Biology and Medicine",
Taras Shevchenko National University of Kyiv, Ukraine
galenovatanya@gmail.com

Coronary artery disease (CAD) is a major public health problem all over the world. Therefore, the search for new biomarkers, which could detect early stages of CAD and improve survival, is of highest priority. In the present study, we investigated the association between content as well as composition of both soluble fibrin monomer complexes (SFMCs) and vitamin K-dependent proteins (VKDPs) with adverse cardiovascular events.

A total of 88 subjects with CAD, as well as 20 individuals free from cardiovascular disease were studied. Patients were classified into 4 groups: group I – patients with stable angina (n=25), group II – patients with unstable angina pectoris of new onset (n=17), group III – patients with progressive unstable angina (n=28), and group IV – patients with myocardial infarction (n=18). Concentrations of fibrinogen and SFMCs in blood plasma were measured by using commercial kits (Renam, Rassia). ELISA technique was used to determine plasma prothrombin. Isolation of SFMCs and VKDPs from blood plasma was performed according to the procedures described previously [1, 2]. Size-exclusion chromatography on Superdex 200 pg column (HiLoad 16/60, Healthcare Life Sciences) was used to identify and characterize separate fractions present in total pool of SFMCs and VKDPs. The appearance of corresponding peaks (protein fractions with particular molecular weight) was monitored by means of UV detector of BioLogic LP chromatographer (BioRad, USA). The peak areas were calculated using OriginLab (v 9.1).

According to the results obtained, there were no significant differences between fibrinogen concentrations in plasma of patients with angina pectoris, and control subjects. However, patients suffering from myocardial infarction have been shown to have increased fibrinogen values. Our findings revealed that prothrombin levels were similar in plasma of all groups of patients with CAD, and were significantly decreased compared to control subjects. Our results showed that plasma SFMC concentrations were increased 12-fold in both groups of patients with unstable angina as well as patients with myocardial infarction, compared to healthy volunteers. It should be note that concentration of SFMC in plasms of patients suffering from stable angina was remarkably lower compared to other CAD groups but still significantly higher than in control subjects. Additionally, the development of CAD was accompanied by the changes in both quantity and quality of SFMC composition, compared to that of healthy subjects. Thus, SFMCs with higher molecular weight (approximately 670-690 kDa) were identified in plasma of patients of all CAD groups, in contrast to control group. Our results also demonstrated that 80% of total VKDPs pool in plasma of healthy subjects was represented by protein fraction with molecular weight of 55-70 kDa, while in CAD patients the content of this particular fraction was decreased. Simultaneously, the level of VKDPs with molecular weight of 145-150 kDa were elevated in all CAD groups. Furthermore, the level of these high molecular weight complexes appears to corelate with more severe form of CAD.

Overall, our results indicate that both SFMCs and VKDPs have a potential role in CAD development and progression. Clearly, more studies are needed to evaluate the relationship between circulating SFMCs as well as VKDPs, and severity of cardiovascular events in the CAD patients.

[1]. T. Katrii, N. Shabanova, S. Ostapchuk et al., The characterization of the soluble fibrin monomer complex in patients with acute and one year post acute ischemic stroke, Bulletin of Taras Shevchenko National University of Kyiv: Series "Problems of Physiological Functions Regulation" **1**, 58-61 (2017).
[2] T.B. Katrii, T.B. Vovk, T.I Halenova et al., Difference in coagulation markers in acute and one year post acute ischemic stroke, Period biol; **119**, 189-98 (2017).

CHANGES IN MICROBIOTA AND PH VALUES OF CREOSOTE-TREATED WOOD DURING MYCOREMEDIATION

Guoda Kolkatovaitė, Rūta Mickienė, Vilma Kaškonienė, Audrius Sigitas Maruška

Instrumental Analysis Open Access Centre, Faculty of Natural Sciences, Vytautas Magnus University, Lithuania
guoda.kolkatovaite@stud.vdu.lt

Creosote oil is a thick liquid obtained by the fractional distillation of crude coal tars. The color of this compound varies from yellow to amber and it was used as the main preservative for wood structures like railway sleepers to protect the wood from microorganisms, fungi, and bacteria [1, 2].

Coal tar contains several hundreds of organic compounds therefore creosote is a mixture of more than 200 organic compounds [2]. Its composition differs depending on origin of coal and manufacturing processes but in general, creosote consists of approximately 85% of polycyclic aromatic hydrocarbons (PAH) and 10% of phenolic compounds [1]. PAH cause negative effects to humans and the environment due to their recalcitrant character and their carcinogenic and mutagenic properties. Therefore, the combustion of creosote-treated wood is allowed only in highly protected plants. This way of handling pollutants is costly and complicated. Potentially, mycoremediation could be a less expensive and more environmentally friendly approach [3]. In order to achieve highly effective bioremediation, it is important to analyze the changes of pH and the total count of microbiota during the biodegradation [1]. To our knowledge, there are no studies related to PAH biodegradation using white-rot fungi by optimizing pH and the total count of microbiota of the media.

This study was performed in the transparent buckets using white-rot fungus, namely *Pleurotus ostreatus*, *Pleurotus eryngii* and *Irpex lacteus*. Creosote-treated wood was chopped into smaller pieces (6.0±0.1) cm. Wheat straw was sterilized in order to prevent the contamination of inoculant in early growth stage. Creosote-treated wood, wheat straw and inoculant were layered in 3 different ways in order to analyze samples obtained under different conditions. Initial pH of wood was 4.97. On the 60th day of the experiment, the highest 7.01 pH was reached with *P. ostreatus* inoculum pH 6.92 was measured with *I. lacteus* inoculum, and pH 6.83 with *P. eryngii*. The smallest pH value was observed in control sample, where pH 5.4 was obtained.

The total count of bacteria and the total count of yeasts and molds together were determined using commercial selective Compact Dry^{TM} media for bacteria (TC), and for yeasts and molds (YM). In the beginning of experiment, $5.1 \cdot 10^3$ CFU/ml of bacteria and $2.3 \cdot 10^3$ CFU/ml of yeasts and molds together were calculated in the samples. Total count of microbiota increased after biodegradation. Samples with *P. ostreatus* inoculum contained the highest amount of microorganisms ($2.4 \cdot 10^4$ CFU/ml bacteria, $6.1 \cdot 10^3$ CFU/ml yeasts and molds), while the lowest values were observed in samples with *Irpex lacteus* inoculum ($1.9 \cdot 10^4$ CFU/ml bacteria, $5.2 \cdot 10^3$ CFU/ml yeast and mold).

White-rot fungi *Pleurotus ostreatus, Pleurotus eryngii* and *Irpex lacteus* change pH values in PAH biodegradation process from 4.97 to 7.01 and change total count of microbiota from $7.4 \cdot 10^3$ CFU/ml to $3.0 \cdot 10^4$ CFU/ml.

Acknowledgements: The study was financed by the Research Council of Lithuania (project No. 09.3.3-LMT-K-712-25-0195).

[1] JÚLIO, Aline Daniela Lopes, et al. Metataxonomic analyses reveal differences in aquifer bacterial community as a function of creosote contamination and its potential for contaminant remediation, Scientific reports **9.1**, 1-14 (2019).

[2] LEE, Hwanhwi, et al. Bioremediation of polycyclic aromatic hydrocarbons in creosote-contaminated soil by Peniophora incarnata KUC8836, Bioremediation Journal **19.1**, 1-8 (2015).

[3] POLCARO, C. M., et al. Fungal bioremediation of creosote-treated wood: a laboratory scale study on creosote components degradation by *Pleurotus ostreatus* mycelium, Bulletin of environmental contamination and toxicology **81.2**, 180-184 (2008).

P4-50

DID NOT PARTICIPATE

.

INACTIVATION OF ANTIBIOTIC RESISTANT OPPORTUNISTIC PATHOGENS *STENOTROPHOMONAS MALTOPHILIA* BY ANTIMICROBIAL PHOTODYNAMIC THERAPY

Inga Garšvaitė[1], Edita Sužiedėlienė[1], Saulius Bagdonas[2], Irina Buchovec[3]

[1] Institute of Biosciences, Department of Biochemistry and Molecular Biology, Life Sciences Center, Vilnius University, Lithuania
[2] Laser Research Center, Faculty of Physics, Vilnius University, Lithuania
[3] Institute of Photonics and Nanotechnology, Faculty of Physics, Vilnius University, Lithuania
inga.garsvaite@chgf.stud.vu.lt

The emergence of multidrug resistance amongst nosocomial infection agents is one of the most pressing worldwide health issues. One of the ways to combat biofilm-associated bacterial infections is antimicrobial photodynamic therapy (aPDT). aPDT is based on the interaction of a photosensitizer, the appropriate wavelength of light and oxygen. After light excitation, the triplet-state photosensitizer interacts with molecular oxygen, electron donors or acceptors and can produce reactive oxygen species, thereby triggering photo-oxidative reactions that initiate various cellular damages and destroy the bacterial cells. [1]

Stenotrophomonas maltophilia is an emerging global multidrug-resistant opportunistic pathogen, which resistance to antibiotics is associated with a biofilm formation [2]. There is no published data about the aPDT caused inactivation of *S. maltophilia* pathogen. The main goal of the present study was to investigate the inactivation of *S. maltophilia* by riboflavin-based (RF-aPDT) and chlorophyllin-based aPDT (Chl-aPDT). The LEDs were chosen as optimal for the selected PSs (402 nm and 440 nm for Chl and RF, respectively) Two multidrug-resistant biofilms forming clinical *S. maltophilia* isolates (SM3 and SM21) were used for aPDT [3]. Bacterial cultures (~1×10^7 CFU/mL) were suspended with 0.011 mM RF or 0.015 mM Chl in the dark. For the photoinactivation, 200 µl of the samples were exposed to light for different periods. The antibacterial effects of aPDT were evaluated by the microdilution method. The surviving cell populations were counted and the results were expressed as $\log_{10}$ of CFU/mL.

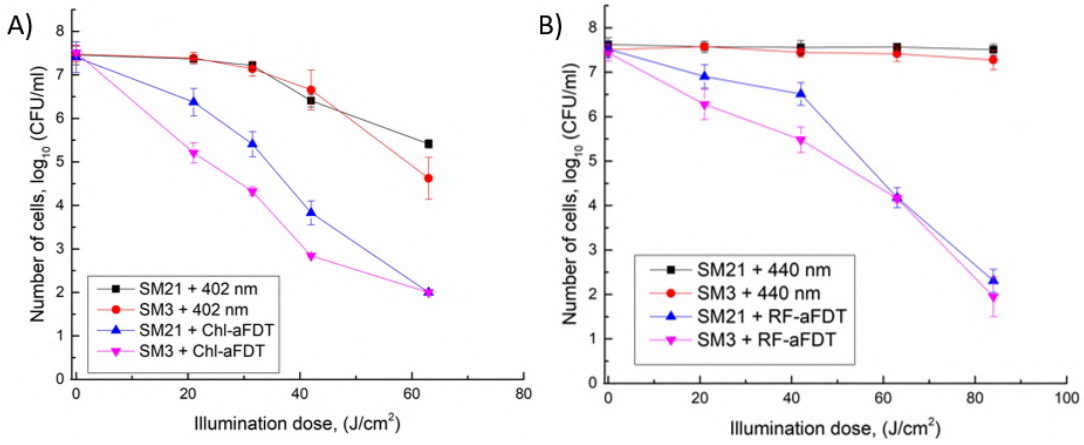


Fig. 1. Photodynamic inactivation of *S. maltophilia* by RF-aPDT (A) and Chl-aPDT (B) as function of illumination doses (irradiance 35 mW/cm^2): 440 nm and 402 nm – bacteria in 0.01 M PBS without RF and Chl; RF-aPDT- bacteria in 0.01 M PBS with 0.011 mM RF; Chl-aPDT - bacteria in 0.01 M PBS with 0.015 mM Chl. Every point is the average of 3-6 experiments, error bars indicate standard deviation.

The experiment results showed that *S. maltophilia* SM3 isolate was more sensitive to RF-aPDT when the illumination doses were 21 J/cm^2 and 42 J/cm^2 compared to SM21. The increase of illumination dose to 84 J/cm^2 led to similar sensitivity, where the viability of SM3 and SM21 after RF-aPDT were diminished by 5.5 $\log_{10}$ and 5.1 $\log_{10}$, respectively (Fig. 1A). The SM3 isolate was more susceptible to Chl-aPDT (reduction by 4.6 $\log_{10}$) than SM21 (reduction by 3.4 $\log_{10}$) when the illumination dose was 42 J/cm^2 (Fig. 1B). Nevertheless, 402 nm LED light without PS (63 J/cm^2) reduced survival of SM3 and SM21, CFU number decreased by 100 and 800 times respectively, whereas 450 nm light had no impact on both isolates. When illumination dose is 63 J/cm^2, Chl-aPDT more sufficiently damages *S. maltophilia* cells than RF-aPDT. In summary, RF-aPDT and Chl-aPDT can be used as a potential means for *S. maltophilia* inactivation.

Acknowledgement: This research was funded by the European Social Fund under the No 09.3.3-LMT-K-712 "Development of Competences of Scientists, other Researchers and Students through Practical Research Activities" measure.

[1] Qingyan Jia, Rejuvenated Photodynamic Therapy for Bacterial Infections (Adv Healthc Mater, 2019)
[2] Joanna S Brooke, Stenotrophomonas maltophilia: an emerging global opportunistic pathogen (Clin Microbiol Rev 2012)
[3] Klimkaite, The Toxin-Antitoxin Systems of the Opportunistic Pathogen Stenotrophomonas maltophilia (2020)

ANTIOXIDANT PROPERTIES OF *TAGETES PATULA IN VIVO* AND *IN VITRO* EXTRACTS

Justė Narmontaitė[1], Ilona Jonuškienė[2], Rima Stankevičienė[2], Neringa Petrašauskienė[1]

[1]Department of Physical and Inorganic Chemistry, Kaunas University of Technology, Lithuania
[2]Department of Organic Chemistry, Kaunas University of Technology, Lithuania

juste.narmontaite@ktu.edu

Tagetes patula natural extracts are widely used in pharmaceutical industry because of their antioxidant and antibacterial activities. In traditional and homeopathic medicine it has been used for wounds and burns, skin complaints, conjunctivitis and poor eyesight, varicose veins, menstrual irregularities, hemorrhoids, etc. *Tagetes patula* grows as common garden plant throughout North America and Europe. The flowers of these plants are bright-yellow or brownish-yellow or golden-orange and are used as spice, tea and medicine. They may be used as fresh or dried, and can be made into tea, tinctures, ointments and creams. *Tagetes patula* is a popular plant found in the *Asteraceae* family and it is widely cultivated for the extraction of carotenoids, as well as for its decorative properties. It has been used to treat a wide variety of diseases and conditions in traditional medicine since ancient times. The pharmacological activity of *Tagetes patula* is related to the content of several classes of secondary metabolites such as flavonoids, essential oils, sterols, tannins, carotenoids, saponins, polysaccharides, triterpene alcohols, a bitter principle, mucilage, and resin. *Tagetes patula* flowers contain rutin, isoquercitrin, isorhamnetin-3-O-rutinosylrhamnoside, quercetin-3-O-rutinosylrhamnoside, isorhamnetin-3-O-glucoside and isorhamnetin-3-O-glucosylglucoside.

According to the fact that *Tagetes patula* contains polyphenols, the assessment of its antioxidant properties is of great interest in the understanding of positive effect of these compounds.

Plant cell and tissue culture was developed in order to study the biochemistry of plants without the complication of the whole plant. Plant callus cultures *in vitro* were found to accumulate of the compounds characteristic of the original plant.

The current research has been designed to access antioxidant properties of *Tagetes patula* plant *in vivo* and *Tagetes patula* plant callus cultures *in vitro* using 2,2-diphenyl-1-picrylhydrazyl radical scavenging assay (DPPH) and reducing antioxidant power assay methods [1, 2].

Extracts of the leaves, flowers and stems in *vivo* of *Tagetes patula* and callus cultures in *vitro* were used for the study.

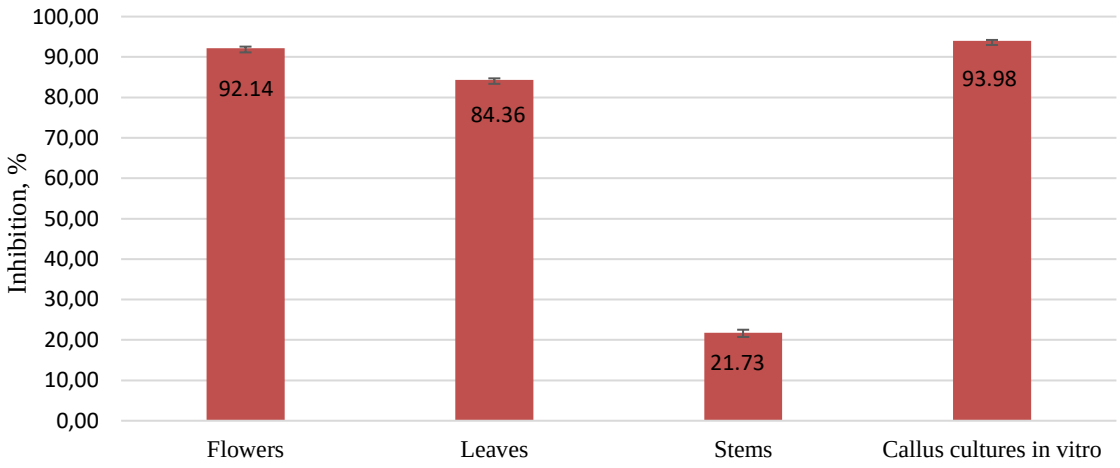


Fig. 1. Antioxidant activity according to DPPH method of analysed plant extracts.

Study analysis showed (Figure 1), that highest antioxidant activities (93.98 % and 92.14 %) according to DPPH method of *Tagetes patula* plant extracts was in analysed plant callus cultures, which were formed in Murashige and Skoog medium with TDZ (0.5 mg/l) and IAA (0.1 mg/l), and in *Tagetes patula* flowers. The lowest antioxidant activity of the extracts was in stems *of Tagetes patula in vivo.*

The present study could be helpful to reveal new sources of antioxidant and antibacterial phytochemicals for potential biotechnological studies of *Tagetes patula* callus cultures *in vitro*.

[1] I. Tumosienė, K. Kantminienė, A. Klevinskas, V. Petrikaitė, I. Jonuškienė, V. Mickevičius, Antioxidant and anticancer activity of novel derivatives of 3-[(4-methoxyphenyl)amino]propanehydrazide, Molecules **25**, 2980-2300 (2020).
[2] G.S. Cetkovic, S.M. Djilas, J.M. Canadanovic-Brunet, V.T. Tumbas, Antioxidant Properties of Marigold Extracts, Food Res. Int. **37(7),** 643-650, (2004).

S100A9 PROTEIN INTERACTION WITH BIOMIMETIC LIPID MEMBRANES

Rimgailė Tamulytė[1], Evelina Jankaitytė[1], Zigmantas Toleikis[2], Marija Jankunec[1]

[1]Institute of Biochemistry, Life Sciences Center, Vilnius University, Vilnius, Lithuania
[2]Institute of Biotechnology, Life Sciences Center, Vilnius University, Vilnius, Lithuania
rimgaile.tamulyte@bchi.stud.vu.lt

Pro-inflammatory, calcium-binding protein S100A9 is localized in the cytoplasm of a wide range of cells and regulates several intracellular and extracellular processes [1]. One of them is the participation in the inflammation associated with the pathogenesis of Alzheimer's disease (AD) [2]. The number of studies on the impact of S100A9 in co-aggregation processes with amyloid-like proteins is increasing. However, the interest in the interaction mechanism of protein S100A9 with biological membranes is still limited. In this work various biomimetic membrane models, as lipid vesicles in solution and tethered lipid bilayers (tBLMs), were used to examine the binding and interaction between protein and the membrane surface. For this purpose we employed atomic force microscopy and fluorescence spectroscopy techniques. Our results indicate that the initial binding and accumulation of S100A9 protein on the lipid membrane surface is lipid phase-sensitive (Fig. 1). The most significant loss of integrity is observed in lipid bilayers composed of lipid mixture (total brain lipid extract). These results might broader the understanding of S100A9 interactions with lipid membrane and potentially affect the development of new diagnostic and therapeutic approaches for AD or other related diseases.

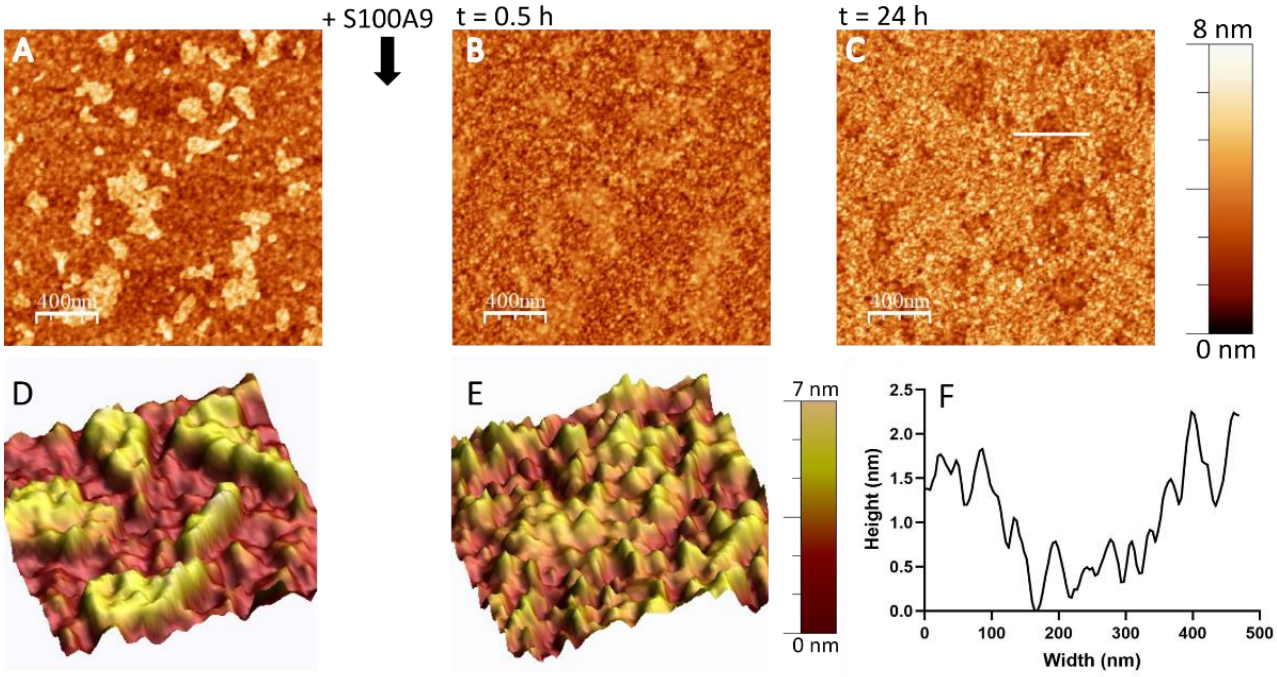


Fig. 1. AFM observation of phase-specific S100A9 interaction with tBLM. (A) AFM topographic image of two-phase tBLM. S100A9 (5 uM) induced disruption of liquid-ordered phase after 0.5 (B) and 24 (C) hours. 3D images of non-disrupted (D) and S100A9 disrupted (E) tBLM. (F) Cross-section along the highlighted line (white line in the insert C).

[1] C. Wang, I.A. Iashchishyn, J. Pansieri et al., S100A9-Driven Amyloid-Neuroinflammatory Cascade in Traumatic Brain Injury as a Precursor State for Alzheimer's Disease. *Sci Rep* **8**, 12836 (2018).
[2] T.Y. Ha, K.A. Chang, J.A. Kim et al., S100a9 knockdown decreases the memory impairment and the neuropathology in Tg2576 mice, AD animal model. *PloS one* **5**, e8840 (2010).

IDENTIFICATION AND CHARACTERIZATION OF *P*-COUMARATE AND FERULATE-INDUCIBLE SYSTEMS FOR TRANSCRIPTION FACTOR-BASED BIOSENSORS DEVELOPMENT

Ernesta Augustiniene[1], Ingrida Kutraite[1], Naglis Malys[1]

[1] Bioprocess Research Centre, Faculty of Chemical Technology, Kaunas University of Technology, Radvilėnų pl. 19, Kaunas LT-50254, Lithuania
ernesta.augustiniene@ktu.lt

Phenolic acids comprise a class of phytochemical compounds that are well known for their anti-inflammatory, anti-oxidative, and anti-viral properties. Naturally occurring phenolic acids are found in plants and fungi and are utilized by various industries, including food, pharmaceutical, cosmetics, and chemical [1]. *p*-Coumarate (*p*-hydroxycinnamate) and ferulate (4-hydroxy-3-methoxycinnamate) are the most abundant hydroxycinnamates covalently bound to lignin and polysaccharides in the cell wall of plants. These phenolic acids are usually synthesized chemically or extracted from plant biomass using physicochemical methods. However, these approaches have disadvantages, including the requirement of large amounts of solvent, the low recovery yield, and the consequent high cost that limits widespread use [2, 3].

There is a particular global socioeconomic interest in the industrial use of phenolic acids obtained by bacterial lignin valorization. However, the utilization of lignin for phenolic acids production is restricted due to high cost and limited efficiency of enzymes required for the valorization of lignin. The application of cell-based strategies for improving enzyme and metabolic pathway characteristics provides multiple advantages and contributes to the robustness of the valorization. One of the most powerful tools for the development and screening of cell-based systems is transcription factor-based whole cell biosensor [4, 5]. Previous studies have shown that this type of biosensors is adaptable to the design–build–test–learn cycle and have been successfully applied for high-throughput systems screening, dynamic pathway control, and adaptive laboratory evolution [5, 6, 7].

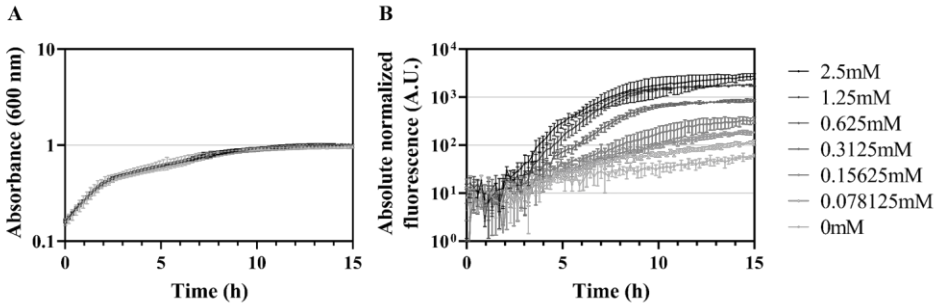


Fig. 1. (A) Absorbance and (B) absolute normalized fluorescence of the *p*-coumarate inducible system from *P. putida* in response to different concentrations of *p*-coumarate added at time zero. Error bars represent standard deviations of three biological replicates.

In this study, we identified and characterized *p*-coumarate and ferulate-inducible systems that can potentially be used for developing transcription factor-based biosensors. Our data show that inducible system from *Pseudomonas putida* KT2440 regulated by MarR transcription factor is specific to the *p*-coumarate and can be used to achieve up to 53-fold induction of gene expression using inducer concentration range from 0.078 to 2.5 mM (Fig. 1). Whereas the system from *Acinetobacter baylyi*, which is also regulated by MarR transcription factor, along with the systems from *Bacillus* sp. (*B. megaterium, B. pumilus,* and *B. subtilis* subsp. *subtilis*), which are regulated by PadR transcription factor, are non-specific and all are induced by *p*-coumarate and ferulate.

Acknowledgments
This work was supported by the European Regional Development Fund [Project No. 01.2.2-LMT-K-718-02-0023] under grant agreement with the Research Council of Lithuania (LMTLT).

[1] Valanciene, E. et al., Advances and prospects of phenolic acids production, biorefinery and analysis, Biomolecules **10**(6), 874 (2020).
[2] Li, M. et al., Enhancing isolation of *p*-coumaric and ferulic acids from sugarcane bagasse by sequential hydrolysis, Chemical Papers **74**, 499–507 (2020).
[3] Zavala-López, M. & García-Lara, S., An improved microscale method for extraction of phenolic acids from maize, Plant Methods **13**, 81 (2017).
[4] Alvarez-Gonzalez, G. D. N., Genetically encoded biosensors for lignocellulose valorization, Biotechnology for Biofuels **12**, 246 (2019).
[5] Lee, S. et al., Bacterial valorization of lignin: strains, enzymes, conversion pathways, biosensors, and perspectives, Frontiers in Bioengineering and Biotechnology, **7**, 209 (2019).
[6] Hossain, G. S. et al., Genetic biosensor design for natural product biosynthesis in microorganisms, Trends in Biotechnology, **38**(7), 797-810 (2020).
[7] Mitchler, M. M., Garcia, J. M., Montero, N. E. & Williams, G. J., Transcription factor-based biosensors: a molecular-guided approach for natural product engineering, Current Opinion in Biotechnology, **69**, 172-181 (2021).

COBALT AND NICKEL COATINGS WITH MANGANESE AND MOLYBDENUM AS EFFICIENT CATALYSTS FOR HYDROGEN GENERATION

Povilas Petras Stepanenko[1], Zita Sukackienė[2], Arnas Naujokaitis[2], Loreta Tamašauskaitė-Tamašiūnaitė[2], Eugenijus Norkus[2]

[1] Faculty of Environmental Engineering, Vilnius Gediminas Technical University, Vilnius, Lithuania
[2] Department of Catalysis, Center for Physical Sciences and Technology, Vilnius, Lithuania.
povilas-petras.stepanenko@stud.vilniustech.lt

In today's world, scientists' task is to create new metal coatings with near the same properties as noble metals like gold, palladium, platinum, and others for a fraction of a price. Noble metals effectively catalyze the catalytic hydrolysis of sodium borohydride ($NaBH_4$). However, such catalysts are very expensive, and their application is not viable. This study presents low-cost and promising catalysts: cobalt (Co) and nickel (Ni) coatings with transition metals such as manganese (Mn) and molybdenum (Mo) for efficient hydrogen generation via hydrolysis reaction of $NaBH_4$. NiMo, NiCoMo, NiCoMn, and NiCoMoMn coatings have been deposited on the copper (Cu) surface with a geometric area of 2 cm^2. The deposition of coatings has been performed from a freshly prepared solution at a temperature of 50 and 60 ºC. The plating solution pH was in the range of 6-7.

The surface morphology and composition of the catalysts have been characterized using Scanning Electron Microscopy (SEM) and Energy Dispersive X-Ray Analysis (EDX) (Table 1). The catalytic activity of the different catalysts towards the hydrolysis of $NaBH_4$ in an alkaline medium has been investigated under various conditions by measuring the amount of hydrogen generated. In order to make a comparison of the activity of the catalysts, the activation energy of the hydrolysis reaction of $NaBH_4$ has been determined using the Arrhenius equation.

It has been found that all prepared catalysts show promising catalytic activities for hydrogen generation from the $NaBH_4$ solution.

Table. 1. Element composition of prepared coatings deposited on copper surface analyzed by EDX.

Catalyst	**Element, wt%**			
	Ni	**Mo**	**Co**	**Mn**
NiMo/Cu	98	2	-	-
NiCoMo/Cu	18	8	76	-
NiCoMn/Cu	7	-	92	1
NiCoMoMn/Cu	9	5	85	1

THE INVESTIGATION OF SPECIFIC ANTIBODIES INTERACTION WITH CD44 PROTEIN

Anton Popov[1,2], Gabija Agasarjanaite[2], Neda Zenkeviciute[2], Viktorija Lisyte[2], Asta Kausaite-Minkstimiene[1,2], Almira Ramanaviciene[1,2]

[1] Department of Immunology, Centre for Innovative Medicine, Vilnius, Lithuania
[2] NanoTechnas – Center of Nanotechnology and Materials Science, Faculty of Chemistry and Geosciences, Vilnius University, Vilnius, Lithuania
anton.popov@imcentras.lt

The World Health Organization (WHO) estimated that in 2019 cancer was the 1st or 2nd leading cause of death under the age of 70 years in 112 of 183 countries. Furthermore, in 2020, more than 19 million new cancer cases were diagnosed and almost 10 million cancer deaths were recorded [1]. Diagnosing cancer in the early stages increases the likelihood of effective treatment and prolongation of the patient's life [2]. Transmembrane glycoprotein - CD44 (P-glycoprotein 1) is a cell surface adhesion receptor, which is highly expressed in many cancers. CD44 also controls metastasis by the expression to the cell surface [3]. Moreover, due to clinicopathological impacts and its isoforms in promoting tumorigenesis CD44 can be considered as a possible molecular target for cancer therapy [4]. The concentrations of cancer biomarkers in the human body in the early stages are quite low. Moreover, matrix effects caused by various species, which are present in body fluids, complicates the detection of biomarkers and normally requires sample dilution prior to testing [5]. Therefore, every opportunity should be taken to increase the sensitivity of immunosensors. One way of doing this is to select antibody that are best suited for immunosensors fabrication. Surface plasmon resonance (SPR) method is traditionally used for evaluation antibody-antigen interaction. Moreover, the calculation of immunoreaction kinetic parameters can be performed by analyzing of SPR results.

The main aim of this work was to investigate the interaction of CD44 protein with specific antibodies. The optimization of interaction conditions was performed. Moreover, the regeneration solution needed for multiple use of SPR sensor was chosen. Few types of specific antibodies against CD44 protein were selected for this work. The kinetics of antibody-antigen interaction were evaluated. Finally, the most suitable for fabrication of immunosensor specific antibodies against CD44 protein was chosen.

Acknowledgments

This project has received funding from European Social Fund (project no. 09.3.3-LMT-K-712-19-0170) under grant agreement with the Research Council of Lithuania (LMTLT).

[1] H. Sung, J. Ferlay, R. L. Siegel et al., Global cancer statistics 2020: GLOBOCAN estimates of incidence and mortality worldwide for 36 cancers in 185 countries, CA Cancer J Clin **71(3)**, 209-249 (2021).
[2] K. Whitaker, Earlier diagnosis: the importance of cancer symptoms, Lancet Oncol. **21**, 6–8 (2020).
[3] L. T. Senbanjo, M. A. Chellaiah, CD44: A multifunctional cell surface adhesion receptor is a regulator of progression and metastasis of cancer cells, Front. Cell Dev. Biol. **5**, (2017).
[4] C. Chen, S. Zhao, A. Karnad et al., The biology and role of CD44 in cancer progression: therapeutic implications, J Hematol Oncol **11,** 64 (2018).
[5] A. Ramanaviciene, A. Popov, E. Baliunaite et al., Magneto-immunoassay for the detection and quantification of human growth hormone. Biosens. **12**, 65 (2022).

P5-7

DID NOT PARTICIPATE

.

INVESTIGATION OF CELL POPULATIONS ON BREAST CANCER CELL MODELS

Yuliia Khmelnytska[1,2,3], Olena Perepelytsina[2,3], Anna Prokopchuk[2,3], Mykhailo Sydorenko[3]

[1] Educational and Scientific Centre „Institute of Biology and Medicine“. Taras Shevchenko National University of Kyiv, Ukraine
[2] National Children's Specialized Hospital "OHMATDYT", Kyiv, Ukraine
[3] Department of Biotechnical Problems of Diagnostics, Institute for Problems of Cryobiology and Cryomedicine, National Academy of Science of Ukraine, Kyiv, Ukraine.
iuliakhmelnitska@gmail.com

Background. Cancer stem cells (CSC) play a key role in tumor recurrence after therapy. It’s important to find new test systems for screening drugs that will affect cancer stem cells.

Methods. The cells MCF-7 were cultured in standard conditions. Multicellular tumor spheroids (MCTS) were cultured with 2% carboxymethyl cellulose (Sigma, USA) and incubated on an orbital shaker (PSU-10i, Biosan, Latvia) at 80 rpm for 3–5 hours at non-adhesive conditions. Enriched MCTS, cancer stem cells (eMCTS) were cultured with the addition of growth factors (fibroblast growth factor, epidermal growth factor, insulin, and hydrocortisone) but without the serum. Detection of markers was performed using flow cytometry (BD FACS Aria III) with antibodies Anti-EpCam (EBA-1) («BD Pharmingen», USA), CD133 clone W6B3C1 («BD Pharmingen», USA), Mouse Anti-Nestin, clone 25/nestin («BD Pharmingen», USA) in 2D cell culture, MCTS, and eMCTS.

Results. Flow cytometry results demonstrated that the highest expression of EpCam was found in 95% of 2D culture cells. The lowest level of EpCam expression was in eMCTS - 62.9% (Fig.1). Thus, the cells in eMCTS were less differentiated and had the lowest phenotypic expression of the tumor of epithelial origin. Also, the results of flow cytometry showed that the marker of CSC - nestin was the highest in 2D culture. However, the level of nestin in eMCTS was 1.5 times higher than in MCTS. The expression level of CD133 in 2D culture - 5.8%, in MCTS - 16.5% and in MCTS, enriched with CSC 2.1%. The decrease of the expression of CD133 may indicate increased proliferative activity and a lower degree of cell differentiation.

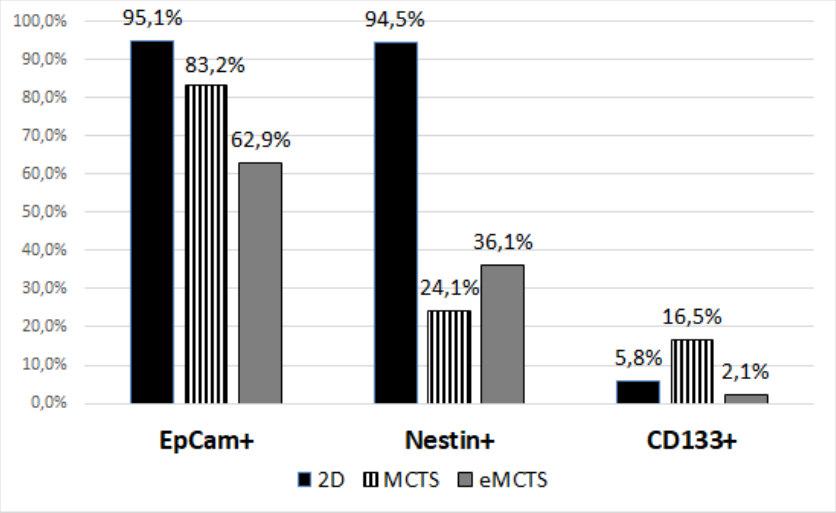


Fig.1. Comparison of expression of epithelial cell adhesion molecule markers - EpCam, CSC markers - CD133, Nestin in 2D culture, MCTS and eMCTS, flow cytometry, 585/42 filter with emission wavelength at 575 nm.

Conclusion. Our results demonstrate that the eMCTS population is enriched in cells with CSC characteristics. We have demonstrated that eMCTS express markers CD133, nestin and EpCam. Increased expression of CSC characteristic markers of breast cancer (CD133, nestin) was detected in MCTS and eMCTS, in comparison with the adhesive culture of MCF cells.

DELAYED MORTALITY AND SUBLETHAL EFFECTS OF COLD STRESS IN *DROSOPHILA MELANOGASTER*

Vladimír Koštál[1], Robert Grgac[2], Jaroslava Korbelová[1]

[1] Biology Centre CAS, Institute of Entomology, Czech Republic
[2] Faculty of Science, University of South Bohemia, Czech Republic
robert.grgac@entu.cas.cz

Analysis of sublethal responses in cold-stressed insects can provide important information about fitness costs and a better understanding of the physiological mechanisms used to prevent and/or to cope with cold injury. Yet, such responses are understudied and often neglected in the literature. Here, we analyzed the effects of cold stress applied to larvae on the mortality/survival and fitness parameters of survivor adults of the vinegar fly, *Drosophila melanogaster*.

Third instar larvae (either cold-sensitive or cold-acclimated) were exposed to either supercooling or freezing stress, both at −5 °C. A whole array of sublethal effects were observed, from mortality that occurs with some delay after cold stress, through delayed development to the pupal stage, to shortened life-span of the adult, and decreased female fecundity.

Taking the sublethal effects into account improves the ecological meaningfulness of cold hardiness assay outcomes. For instance, we observed that although more than 80% of cold-acclimated larvae survive freezing to −5 °C, less than 10% survive until adulthood, and survivor females exhibit more than 50% reduction in their fecundity relative to controls. Female fecundity was positively correlated with dry mass and negatively correlated with total protein and glycogen stores. Hence, these parameters may serve as good predictors of survivor adult female fecundity. Further, we provide the concept of a two-component defense system, which (based on analysis of sublethal effects on fitness parameters) distinguishes between physiological mechanisms that help insects to resist (reduce or avoid) or tolerate (survive or repair) injuries linked to cold stress.

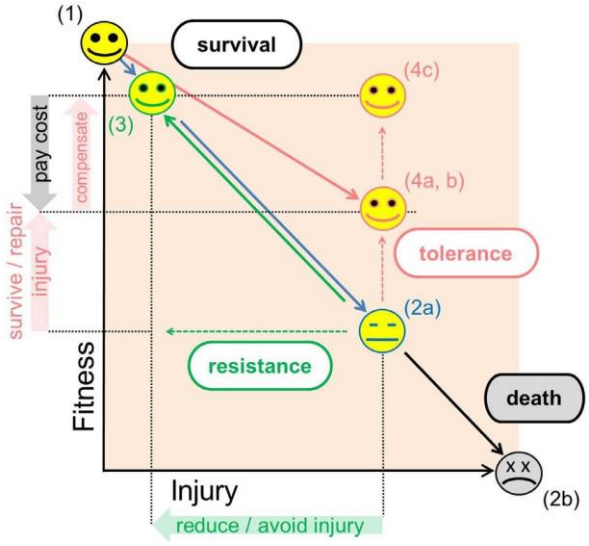


Fig. 1. Concept of a two-component defense system to cope with cold stress injuries. (1) control animal (not exposed to cold stress) shows maximum survival and maximum fitness (upper left corner of diagram); (2) having no mechanisms of cold hardiness available/activated, the animal exposed to cold stress would suffer from cold injury, which would severely decrease its fitness (2a, blue arrow) or, ultimately, would result in lethality (2b, black arrow); (3) the resistance mechanisms (green arrows) help to reduce (or avoid) injury at a given dose of cold stress (combination of temperature, time, supercooling/freezing), which means that the animal survives and maintains high (3) (or even max) fitness without any need to pay costs after the cold stress (of course, recruitment of resistance mechanisms prior to cold stress – during acclimation, may need allocation of energy resources); (4) the tolerance mechanisms (pink arrows) help to cope with the injury that incurred during a given dose of cold stress, which means that the animal survives, but its fitness may be significantly impaired due to: (4a) deleterious consequences of un-repaired injury; (4b) cost of energy expenditure at the expense of larval resources required to repair the injury. Alternatively, (4c) fitness is not reduced because the cost of repair is either small or compensated from external energy resources. This concept has been adapted from Råberg et al., 2007 [1] and Schneider and Ayres, 2008 [2].

[1] L. Råberg, D. Sim, A.F. Read, Disentangling genetic variation for resistance and tolerance to infectious diseases in animals, Science **318**, 812–814 (2007).

[2] D.S. Schneider, J.S. Ayres, Two ways to survive infection: what resistance and tolerance can teach us about treating infectious diseases, Nature Reviews Immunology **8**, 889–895 (2008).

DIABETES RELATED MIRNA ANALYSIS IN BLOOD OF PREGNANT WOMEN DIAGNOSED WITH GESTATIONAL DIABETES

Gabrielė Dzimitravičiūtė[1], Gintarė Naskauskienė[2], Žydrūnė Visockienė[2], Kristina Daniūnaitė[1]

[1]Institute of Biosciences, Life Sciences Center, Vilnius University, Vilnius, Lithuania;
[2]Centre of Endocrinology, Clinic of Family Medicine, Internal Diseases and Oncology, Institute of Clinical Medicine, Faculty of Medicine, Vilnius University, Vilnius, Lithuania;
gabriele.dzimitraviciute@gmc.vu.lt

Gestational diabetes mellitus (GD) is described as a chronic hyperglycemia diagnosed during the 2nd trimester of pregnancy and tends to disappear after delivery. This disease causes a higher risk of type 2 diabetes (T2D) for both the mother and her child, which determines its impact on global diabetes epidemic [1]. Therefore, investigation of potential molecular biomarkers for the early risk assessment of both GD and T2D development is important. Epigenetic alterations, such as expression differences of small regulatory RNAs, are among the most promising liquid–biopsy biomarkers in the context of diabetes [2].

The present study was aimed at the analysis of four miRNAs (miR-17-5p, miR-29a-3p, miR-195-5p and miR-499a-5p), which have been previously associated with particular cellular processes related to the development of diabetes [3], in a unique cohort of serial samples from women diagnosed with GD.

In total, 76 women were included in the study, of which 64 were pregnant women with GD, 7 – healthy pregnant and 5 – healthy non–pregnant women. Peripheral blood samples of the GD group (129 in total) were collected at 24–28 weeks of gestation (n = 59), from the umbilical artery (n = 21) and vein (n = 21) during the delivery, and at 6–12 weeks after delivery (n = 28). Total RNA fraction was extracted from 200 µl of whole blood and target miRNAs were quantified by means of probe-based real–time PCR.

In the GD group, higher levels of miR-17-5p and miR-195-5p were detected in blood samples collected after delivery as compared to the 2nd trimester of pregnancy (all $p < 0.05$, Fig. 1). Moreover, amounts of miR-17-5p, miR-29a-3p and miR-499a-5p after delivery were higher than in healthy non–pregnant women (all $p < 0.05$, Fig. 1). Also, miR-29a-3p level was higher in the GD group during pregnancy as compared to healthy non–pregnant women, while miR-195-5p showed the opposite difference when compared to the healthy pregnant women (both $p < 0.05$). Even though the majority of tested miRNAs did not show significant differences in blood from umbilical artery and vein, the level of miR-195-5p in umbilical artery in the GD group was significantly lower as compared to the group of healthy pregnant women ($p = 0.04$).

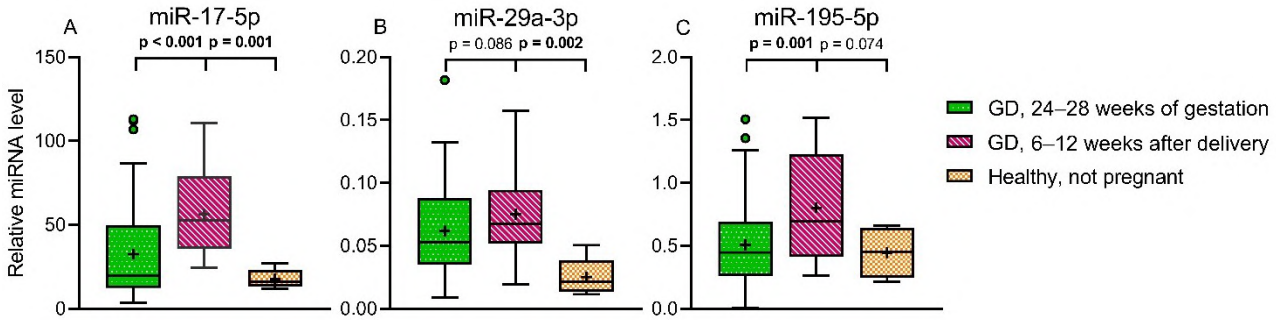


Fig. 1. Comparison of whole-blood miRNA levels among the study groups.
GD – gestational diabetes. Significant p-values are marked in bold.

A few associations between the tested miRNAs and clinical parameters were determined. The levels of miR-17-5p and miR-29a-3p during pregnancy correlated with body mass index (both $p < 0.05$). Also, amounts miR-195-5p in umbilical artery and vein were associated with women's age, while the level of miR-29a-3p correlated with high– and low–density lipoproteins, respectively (all $p < 0.05$). Finally, the quantities of miR-17-5p and miR-499a-5p in blood from umbilical vein were associated with plasma glucose levels (both $p < 0.05$).

The present study revealed the differences of the tested miRNAs among the GD women and control groups as well as their associations with clinical and biochemical parameters, suggesting these miRNAs as potential biomarkers for GD. Despite that, larger independent studies would be necessary to validate these miRNAs for potential clinical applications.

[1] Dias et al. Molecular Biomarkers for Gestational Diabetes Mellitus. International Journal of Molecular Sciences, 26, 2926-2953 (2018).
[2] Collares et al. Identifying Common and Specific microRNAs Expressed in Peripheral Blood Mononuclear Cell of Type 1, Type 2, and Gestational Diabetes Mellitus Patients. BMC Research Notes. 6, 491-506 (2013).
[3] Hromadnikova et al. Diabetes Mellitus and Cardiovascular Risk Assessment in Mothers with a History of Gestational Diabetes Mellitus Based on Postpartal Expression Profile of MicroRNAs Associated with Diabetes Mellitus and Cardiovascular and Cerebrovascular Diseases. International Journal of Molecular Sciences, 21, 2437-2483 (2020).

EFFECTS OF ELECTROCHEMOTHERAPY ON MURINE LEWIS LUNG CARCINOMA CELL LINE

Eivina Radzevičiūtė[1], Veronika Malyško-Ptašinskė[2], Irutė Girkontaitė[1], Vitalij Novickij[2]

[1]State Research Institute Centre for Innovative Medicine, Department of Immunology, Vilnius, Lithuania
[2]Faculty of Electronics, Vilnius Gediminas Technical University, Vilnius, Lithuania
eivina.radzeviciute@imcentras.lt

Chemotherapy is the most often used way to treat cancer patients worldwide despite drug resistance, low efficiency, and many adverse side effects on patients [1]. Therefore, this encourages to search for novel cancer treatment methods. Electrochemotherapy (ECT) is the application of pulsed electric fields (PEF) to introduce chemotherapeutic drugs through membrane pores into target cells for cancer treatment. For decades used standard microsecond ECT procedure (µsECT, ESOPE*) induces side effects while nanosecond electrochemotherapy (nsECT) causes lower tumor cell viability, better drug delivery, and less tumor-surrounding tissue necrosis [2].

In this work, we analyzed the effects of different conditions of nsECT with bleomycin (BLEO) and doxorubicin (DOX) on murine Lewis lung carcinoma (LLC1) cell line. nsECT conditions differ from each other by pulse duration (100–500 ns), electric field strength (5–10 kV/cm), and frequency (10 kHz, 100 kHz, 1 MHz). Electric pulses were applied using 0–3 kV, 100 ns–1 ms square wave high voltage and high up to 1 MHz frequency pulse generator [3]. Cell permeabilization was evaluated by using Yo-Pro1. The cells were mixed with a stain for the final concentration of 1 µM and treated with different nsECT protocols. Afterwards, the samples were analyzed by flow cytometry. Moreover, we evaluated optimal chemotherapeutics concentration (BLEO 0,8 – 100 µg/ml; DOX 0,2 – 5,8 µg/ml) using standard microsecond electroporation. Using determined drugs concentrations, different conditions of nsECT effect on carcinoma cells viability were assessed. The LLC1 cells (25 µl) were mixed with drugs (25 µl) where 50 µl samples were placed between the electrodes and treated by PEF, transferred to 96-well plate followed by 20 min incubation on ice. Afterward, 150 µ of growth media was added to the well and the sample left for incubation period. Subsequently, cells viability was evaluated after 24, 48, and 72 hours using Alamar blue reagent.

This study showed that the permeabilization rate of LLC1 cells was increasing, while increasing pulse duration and electric field from 5 up to 10 kV/cm. However, it was observed that 5 kV/cm electric field strength was less effective in comparison with the results obtained with different electric pulse strength, frequency and duration. Consequently, was no longer used in nsECT viability experiments. For further viability experiments, bleomycin and doxorubicin concentrations were selected depending on the largest viability difference between LLC1 + drug and LLC1 + nsECT groups to ensure low drug toxicity itself. The most significant difference in cell viability was observed following 72 h incubation after µsECT with bleomycin and 48 h with doxorubicin. Results after 24 hours showed high cell viability and, therefore, weak treatment outcome. For nsECT it was noticed that while increasing pulse duration cells viability declines gradually. It was observed, that the best cells response was reached applying pulses from 300 to 500 ns duration, while 100 and 200 ns pulses had little to no effect on cell viability. Moreover, as it was expected, higher electric field strength initiated lower cell viability, though, the notable treatment outcome is detected with 8 – 10 kV/cm, when viability goes under 50 %. Nevertheless, the most significant results were obtained with 1 MHz frequency protocols, where even 6 kV/cm triggered cell response to electrochemotherapy (below 30 % viability after 48 h) with both drugs.

Our study shows that high frequency nsECT with bleomycin and doxorubicin could be as effective as standard microsecond treatment procedures. Collected nsECT results confirmed cell permeabilization results – nanosecond electroporation permeabilized cells create pores that ensure better antineoplastic drugs delivery to the cancer cells. Although, further *in vivo* studies need to be performed.

Acknowledgement: The research was funded by Research Council of Lithuania within the DAINA framework, Grant Nr. S-LL-21-4

[1] Bukowski K, Kciuk M, Kontek R. Mechanisms of Multidrug Resistance in Cancer Chemotherapy. Int J Mol Sci. 2020;21(9):3233.
[2] Novickij et al. Electrochemotherapy using doxorubicin and nanosecond electric field pulses: A pilot in vivo study. Molecules, 25(20), 2020.
[3] V. Novickij et al., High-frequency submicrosecond electroporator. Biotechnol. Biotechnol. Equip., vol. 30, no. 3, pp. 607–613, May 2016.
*ESOPE - European standard operating procedures for electrochemotherapy. 1.3 kV/cm x 100 µs x 8 /1 Hz

RAB11 AND RAB35 REGULATED CYTOKINESIS EVENT THAT AFFECTS PHENOTYPE OF CANCER CELLS

Paulius Gibieža, Emilija Ratkevičiūtė, Girstautė Dabkevičiūtė, Vilma Petrikaitė

Laboratoraty of Drug Targets Histopathology, Lithuanian University of Health Sciences, Lithuania
paulius.gibieza@lsmuni.lt

Intracellular membrane transport is a key factor of controlling cellular metabolism and survival. Vesicular delivery of membranes and various proteins to the specific cell sites and organs at different stages of the cell cycle and during the performance of different cell functions is essential for the maintenance of normal cell homeostasis. In this regard, Rab GTPases are one of the most important regulators of endocytic membrane transport in eukaryotic cells during cell division. Both activating and inactivating mutations in Rab genes have been associated with human diseases such as neurological disorders and cancer, while altered Rab expression has been associated with disease progression. Significant research is still needed to understand tumor gene expression, mutations, and drug susceptibility.

Rab proteins form the largest family of small GTPases and control different stages of intracellular membrane transport. These proteins have already been shown to control cell apoptosis, adhesion, division, survival, and migration by regulating various intracellular signaling pathways. Regulation of these processes usually occurs by the recruitment of Rab protein effectors and other regulatory proteins that control the interaction of Rab proteins with endocytic membranes and determine the activity of these organs in cells. Therefore, changes or disorders in the regulation of Rab proteins and their effectors are often associated with many human diseases, including neurodegeneration, immune diseases, infections, Parkinson's disease, and cancer. Although the mediation of Rab proteins in the maintenance and regulation of vital functions important to the cell is a highly relevant scientific topic, the functions of all Rab proteins have not yet been thoroughly investigated. It is important to emphasize that knowledge of altered intracellular dynamics of Rab GTPases and intercellular transport disorders at the molecular level may contribute to the development of new cancer therapy strategies.

According to recent research, the proteins Rab11 and Rab35, which belong to the Rab GTPase family, have been recognized as oncogenes [1, 2]. Also, due to the association of these proteins with the regulation of many important cellular functions, including cell division, proliferation, invasiveness, and migration, Rab proteins are a targeted object of study in cancer cell models. Despite studies on the regulation of Rab11 and Rab35 endosomes, it is not clear whether these proteins can function synergistically. Based on the recommendations from other scientific groups studying these regulators [3], it is important to identify interactions and compensatory mechanisms between these proteins in regulating cell-important processes, such as cell division, proliferation, migration, and invasiveness, the dysregulation of which, may influence cancer and promote tumorigenicity. Therefore, the aim of this study was to investigate the functions of Rab11 and Rab35 in regulating the last stage of cell division, - cytokinesis, which upon dysregulation, might influence phenotypic alterations of cancer cells. As well as to complement previous studies, while getting more insights of alternating cellular functions upon Rab11 and Rab35 genes downregulation.

[1] Villagomez F.R, et. al. The role of the oncogenic Rab35 in cancer invasion, metastasis, and immune evasion, especially in leukemia. *Small GTPases*. 2020, 11(5): 334-345.
[2] Ferro E, et. al. Rab11-Mediated Trafficking and Human Cancers: An Updated Review. *Biology*. 2021, 10(1):26.
[3] Fremont S, Echard A. Membrane Traffic in the Late Steps of Cytokinesis. *Current Biology*. 2018, R458-R470.

INVESTIGATION OF MOTHER-TO-CHILD TRANSMISSION OF HUMAN ANELLOVIRUSES

Aurelija Cicilionytė[1], Joanna Kaczorowska[1], Lia van der Hoek[1*]

[1]Department of Medical Microbiology, Laboratory of Experimental Virology, Amsterdam UMC, The Netherlands
a.cicilionyte@amsterdamumc.nl

Anelloviruses (AVs) are relatively recently discovered small, highly abundant, eukaryotic viruses. Family *Anelloviridae* consists of 14 genera (namely from *Alphatorquevirus* to *Zetatorquevirus*) and 76 species according to the 2019 release of Taxonomy by International Committee on Taxonomy of Viruses (ICTV), and is known to infect various vertebrate hosts, including humans. The first member of this diverse family, Torque Teno Virus (TTV), was identified in 1997, in an individual with a post-transfusion nonviral hepatitis, although there no disease association [1]. Other human anelloviruses include Torque Teno Midi Virus (TTMDV) and Torque Teno Mini Virus (TTMV), which differ from TTV in the size of genome. In human population, individuals become infected during the first year of life, which suggests a vertical transmission route of AVs.

In this work we aimed to investigate a possible mother to child transmission of three human-infecting AV genera: TTV, TTMV and TTMDV, in longitudinally collected serum samples of five HIV-1 positive mothers and their infants. Using Illumina next generation sequencing (NGS) data, we identified 449 unique AV genomes across the analyzed five pairs. The level of AV richness was different in each subject, which emphasized that anellovirus virome (anellome) is person-specific. Based on the analysis of longitudinally collected samples we observed that children were mainly infected with TTMVs, while most of the genomes found in mothers were TTV. Most importantly, we identified 35 genomes which were shared between mother and her child (Figure 1). The genomes were identical or nearly identical, showing ≥91% whole genome sequence identity on the nucleic acid level. We could confirm the NGS data by specific qPCR for three selected shared genomes. Additionally, a different set of children samples was analyzed to evaluate which AV genus is the most prevalent in the first months of life. We hypothesized that TTMV and TTMDV could be the early-infecting human AVs and performed a second analysis using 25 cross sectional serum samples obtained at ages between 0 and 65 months. We show here for the first time that TTMV and TTMDV are the first AVs colonizing a child. In conclusion, our in-depth analysis supports a possible transmission of AVs from mother to child via air or the oral-fecal route, with early colonization by the shortest AVs.

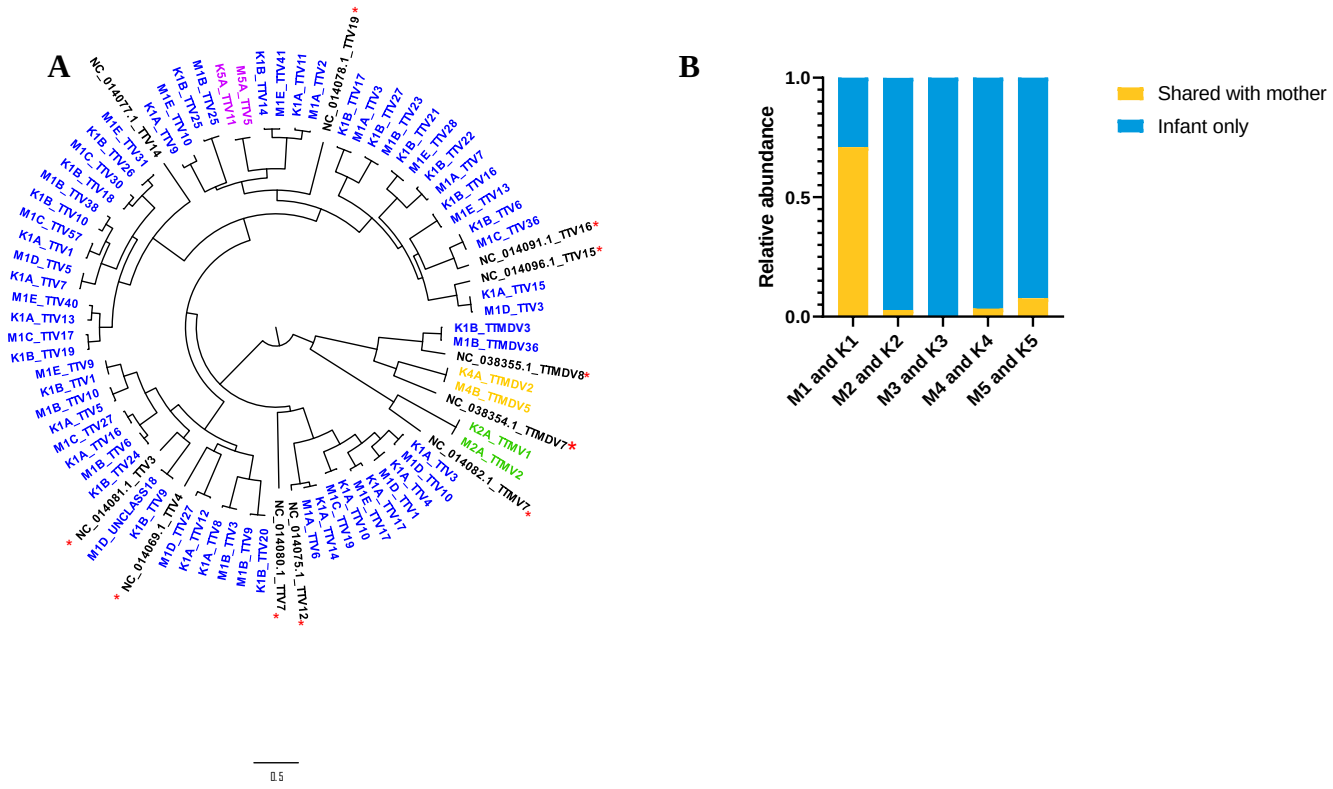


Figure 1. Cluster analysis of shared genomes between mothers and corresponding children. (A) A consensus phylogenetic tree representing anellovirus genomes shared between mothers and their children. The tree was generated using IQ-TREE web server. Different colors correspond to different pairs (pair 1 – blue; pair 2 – green; pair 4 – yellow and pair 5 – purple). Sequences starting with "M" refer to mothers-derived AVs, while the sequences starting with "K" refer to the ones identified in children samples. Reference sequences (obtained from NCBI database) are labelled with a star. (B) Relative abundance of the infant anellovirus virome that is shared with mother. The relative abundance corresponds to the number of clustered genomes to the total amount of infant genomes per pair.

[1] Nishizawa, T., Okamoto, H., Konishi, K., Yoshizawa, H., Miyakawa, Y., and Mayumi, M. (1997). A Novel DNA Virus (TTV) Associated with Elevated Transaminase Levels in Posttransfusion Hepatitis of Unknown Etiology. Biochemical and Biophysical Research Communications 241, 92–97.

NOTCH AND WNT GENE EXPRESSION SIGNATURE IN HIGH GRADE SEROUS OVARIAN CANCER

Ieva Vaicekauskaitė[1,2], Diana Žilovič[1,2], Rūta Čiurlienė[1], Juozas Rimantas Lazutka[2], Rasa Sabaliauskaitė[1], Sonata Jarmalaitė[1]

[1] National Cancer Institute, Vilnius, Lithuania
[2] Institute of Biosciences, Vilnius University, Vilnius, Lithuania
ieva.vaicekauskaite@nvi.lt

Introduction. High grade serous ovarian cancer (HGSOC) is the deadliest gynecologic malignancy in the world [1]. The HGSOC 5-year survival rate is only 3-19% [2]. The high mortality rates are attributed to a lack of specific symptoms and biomarkers used for HGSOC screening, which leads to late disease diagnosis and early chemoresistance. Moreover, CA125, the only biomarker used in HGSOC patient care is not specific for ovarian cancer and is only recommended for disease monitoring [3]. Thus, HGSOC and other oncogynecolgic diseases are in great need of diagnostic, prognostic, and predictive markers which would help earlier disease detection and aid in choosing the correct treatment.

NOTCH and WNT signaling pathways are both involved in ovary development and are necessary for normal female reproductive organ function. Both pathways interact to govern ovarian angiogenesis and are crucial for ovarian cell survival. The inactivation of the NOTCH and WNT ligand-receptor systems leads to stunted ovarian cell migration and proliferation as well as increased apoptosis [4]. Canonical WNT signaling genes *CTNNB1* and *FBXW7* are amongst the most commonly mutated sequences in gynecologic malignancies [5], while changes in *NOTCH* gene expression were previously detected in endometrial cancer [6]. Both NOTCH and WNT signaling pathways are important in HGSOC development, progression and chemoresistance, thus they could be useful as HGSOC biomarkers and targets for treatment.

The aim of this study was to analyze *NOTCH* receptor and *WNT* pathway gene expression in tissues from patients with HGSOC and other gynecologic diseases in order to determine gene expression correlations with the disease type and clinical features.

Methods. Tissue samples from 51 patients with ether HGSOC (n=32), non-serous ovarian or endometrial carcinoma (n=10) or benign gynecologic pathologies (n=9) were collected during 2018-2021 at National Cancer Institute. Tissues were used for RNA extraction and subsequent RT-qPCR analysis of *NOTCH1-4*, *CTNNB1*, *FBXW7* and *ARID1A* mRNA expression.

Results. *NOTCH1*, *NOTCH2,* and *NOTCH4* as well as *CTNNB1* and *FBXW7* expression were significantly altered in HGSOC samples when compared with samples of other gynecologic malignancies and benign pathologies. All HGSOC samples were in the same stage and grade, thus no gene expression correlations with HGSOC clinical features could be made. However, *NOTCH4* and *CTNNB1* expression were significantly related to CA125 serum concentration.

In conclusion, *NOTCH* and *WNT* pathway gene expression are potential diagnostic and prognostic biomarkers for HGSOC. More research is needed in order to determine whether the changes in *NOTCH* and *WNT* gene expression are detectable in non-invasively collected samples.

[1] F. Bray, J. Ferlay, I. Soerjomataram et al., Global cancer statistics 2018: GLOBOCAN estimates of incidence and mortality worldwide for 36 cancers in 185 countries, CA. Cancer J. Clin. 68, 394-424 (2018).
[2] H. J. Whitwell, J . Worthington, O. Blyuss et al., Improved early detection of ovarian cancer using longitudinal multimarker models, Br. J. Cancer 122, 847-856 (2020).
[3] Colombo, N. et al., ESMO-ESGO consensus conference recommendations on ovarian cancer: Pathology and molecular biology, early and advanced stages, borderline tumours and recurrent disease, Ann. Oncol. 30, 672–705 (2019).
[4] Bocchicchio, S., Tesone, M. and Irusta, G., Convergence of Wnt and Notch signaling controls ovarian cancer cell survival, J. Cell. Physiol. 234, 22130–22143 (2019).
[5] Cancer Genome Atlas Research Network, Integrated genomic analyses of ovarian carcinoma, Nature. 474, 609–615 (2011).
[6] Orzechowska, M., Anusewicz, D. and Bednarek, A. K., Functional Gene Expression Differentiation of the Notch Signaling Pathway in Female Reproductive Tract Tissues—A Comprehensive Review With Analysis, Cell. Dev. Biol. 8, 1–34 (2020).

DETECTION OF BABESIA SP. (APICOMPLEXA, PIROPLASMIDA, BABESIIDAE) IN TICKS AND DOGS: COMPARISON OF MOLECULAR AND MORPHOLOGICAL METHODS

Gintarė Mockevičienė[1], Jurga Turčinavičienė[1], Asta Križanauskienė[1], Jekaterina Havelka[1], Mantas Adomaitis[1]

[1]Vilnius University, Life Sciences Centre, 7 Saulėtekio Ave, Vilnius, LT- 10257, Lithuania
E-mail: mockeviciene.gintare@gmail.com / gintare.mockeviciene@gmc.stud.vu.lt

Babesia is the causative agent of babesiosis, a tick-borne zoonosis. The studies on tick's seasonal activity and use of molecular methods for detection of Babesia sp. are important for prevention, epidemiology, effective treatment and control of tick-borne diseases in Lithuania. The aim of present study was to investigate *Ixodes ricinus* seasonal activity and *Babesia* sp. prevalence in Verkiai regional park and to compare light microscopy and molecular methods for diagnosis of canine babesiosis. Main research tasks were: to conduct *I. ricinus* abundance and seasonal activity in Verkiai regional park; to identify level of tick infection of *Babesia* sp.; to compare light microscopy and molecular methods for detection of *Babesia* sp. in dogs; to evaluate the changes of hematological parameters of dogs with babesiosis. Collection of ticks was carried out from early spring of 2016 in Verkiai regional park once in week using flagging method. Ticks were investigated for the presence of *Babesia* sp. by microscopic examination of midgut and salivary glands smears and polymerase chain reaction with specific for *Babesia* primers. Changes of hematological parameters of dogs were evaluated as well. Seasonal activity peaks of ticks were observed in May and August in 2016. The largest number of ticks was registered in May, the lowest in July. In total 309 ticks were investigated, the overall prevalence of *Babesia* sp. infection was detected to be 4.2 % (13/309). Intraerythrocytic parasites were detected in 21 (80,76 %) out of 26 dogs. By PCR with specific primers detected *Babesia* sp. detected in all 26 dogs (100 %). These findings show the necessity to apply the molecular analysis for precise diagnosis of canine babesiosis in Lithuania. This study also shows that babesiosis can be characterized by marked anemia, hemoglobinemia, thrombocytopenia, leukopenia and the specificity of these parameters is useful for diagnosis of parasitosis.

PHENOTYPIC AND MOLECULAR CHARACTERIZATION OF *ACINETOBACTER BAUMANNII* ISOLATES FROM LITHUANIAN NATIONAL CANCER INSTITUTE HOSPITAL (2013-2019)

Anastasija Borisova[1], Danutė Labeikytė[1], Julija Armalytė[1]

[1]Department of Biochemistry and Molecular Biology, Institute of Biosciences, Life Science Centre, Vilnius University, Lithuania
anastasija.borisova@gmc.stud.vu.lt

Multidrug-resistant *Acinetobacter baumannii* (MDR-AB) presents a critical challenge to human health. In 2017, the World Health Organization identified carbapenem-resistant *A. baumannii* as a 'Critical' pathogen that urgently requires novel treatment options [1]. Despite their nephrotoxicity, polymyxins are stated as a last-line therapeutic against MDR-AB outbreaks. Due to the rapid emergence of resistance during antibiotic monotherapy, synergistic combinations of polymyxin with some other antibiotics are recommended for the treatment of MDR-AB infections [2]. One of antibiotic complexes that can resist MDR-AB is the combination of polymyxins with trimethoprim-sulfamethoxazole. However, this combination of antibiotics, like most other combination therapies, is mostly empirical, so research is needed to understand the mechanism of synergistic antibacterial action. The objective of this study was to determine the distribution of multidrug resistance phenotypes of *A. baumannii* in 61 clinical isolates collected in 2013-2019 from hospital of Lithuanian National Cancer Institute.

Isolates were identified as *A. baumannii* by conventional microbiological methods and confirmed by species-specific PCR for the $bla_{\text{OXA-51-like}}$ and rRNR genes. Following that, minimum inhibitory concentrations (MICs) for meropenem (carbapenem), gentamicin (aminoglycoside), ciprofloxacin (fluoroquinolone) and trimethoprim-sulfamethoxazole were determined according to EUCAST guidelines [3].

Our preliminary results showed that 83% of *A. baumannii* clinical isolates are resistant to meropenem (MIC > 8mg/L), 88% - to gentamicin (MIC > 4mg/L), 88% - to ciprofloxacin (MIC > 1mg/L). Interestingly, we stated that only 39% of *A. baumannii* isolates are resistant to trimethoprim-sulfamethoxazole treatment (MIC> 4mg/L). Our preliminary results indicate that 8,7% of isolates are extensively-drug resistant (XDR) and 78,3% are multidrug-resistant (MDR).

Resistance to sulfamethoxazole was studied further by PCR of dihydropteroate synthetase inhibitor genes (*sul1, sul2, sul3)*. Out of isolates possessing *sul1* gene, 87% were resistant to trimethoprim-sulfamethoxazole. 100% of isolates found to have *sul2* were resistant, and *sul3* was not found in the collection.

Cell permeability barrier is considered an important mechanism of resistance for antibiotic treatment. Therefore we attempted to detect *ade* genes as a sign of active efflux systems. The presence of *adeA, adeB, adeJ* was investigated by PCR. *adeA* was found in 90% of isolates, *adeB* in 84% of isolates, *adeJ* in 98% of all isolates, however no clear correlation was observed with resistance to individual antibiotics.

In Lithuania, 78,5% of studied *A. baumannii* isolates have been shown to be multidrug-resistant [4]. Our results confirmed that *A. baumannii* antibiotic resistance is a serious problem in Lithuanian National Cancer Institute hospital (MDR phenotype - 78,3%). Therefore hospitals should strengthen the surveillance of this opportunistic pathogen in hospital environments. Additionally, further examination of mechanisms for effective MDR-AB killing are needed to prevent infections.

[1] World Health Organization, electronic resource, accessed 13 January 2022, https://www.who.int/news/item/27-02-2017-who-publishes-list-of-bacteria-for-which-new-antibiotics-are-urgently-needed.

[2] M. H. Rigatto, F. J. Vieira, L. C. Antochevis, T. F. Behle, N. T. Lopes, A. P. Zavascki, *Polymyxin B in Combination with Antimicrobials Lacking In Vitro Activity versus Polymyxin B in Monotherapy in Critically Ill Patients with Acinetobacter baumannii or Pseudomonas aeruginosa Infections*, Antimicrobial agents and chemotherapy, 59(10), 6575–6580 (2015).

[3] The European Committee on Antimicrobial Susceptibility Testing. Breakpoint tables for interpretation of MICs and zone diameters, version 12.0, 2022 https://eucast.org/clinical_breakpoints/

[4] European Centre for Disease Prevention and Control. Antimicrobial resistance in the EU/EEA (EARS-Net) - Annual Epidemiological Report 2019. Stockholm: ECDC; 2020.

STAT3 SIGNALING PATHWAY AS A POTENTIAL THERAPEUTIC TARGET IN TRIPLE NEGATIVE BREAST CANCER

Aistė Gerulaitytė[1,2], Justina Gaizevska[1,2], Monika Drobnienė[1], Rasa Sabaliauskaitė[1], Sonata Jarmalaitė[1]

[1] National Cancer Institute, Vilnius, Lithuania
[2] Vilnius University, Lithuania
aiste.gerulaityte@nvi.lt

Triple-negative breast cancer (TNBC) is the most aggressive form of breast cancer and accounts for much higher recurrence and metastasis rates. TNBCs are a specific subtype of epithelial breast tumours that are immunohistochemically negative for the protein expression of the estrogen receptor, the progesterone receptor, and lack of overexpression/gene amplification of human epidermal growth factor receptor 2 [1]. TNBC is the most lethal subtype of breast cancer owing to its high heterogeneity, aggressive nature, and lack of treatment options. This aggressive metastatic cancer contributes to the overall shortened survival of patients diagnosed with TNBC [2].

Currently, chemotherapy remains the standard of care for TNBC treatment due to the absence of molecular targets, but unfortunately, patients frequently develop resistance which underscores the need for developing novel therapeutic and preventive approaches for this disease [3]. It has become evident that the development of TNBC chemoresistance is multifaceted and based on the elaborate interplay of the tumor microenvironment, drug efflux, and cancer stem cells. Alterations of multiple signaling pathways govern these interactions [2]. Recent evidence from clinical trials and preclinical studies have demonstrated a pivotal role of the STAT3 (signal transducer and activator of transcription 3) signaling pathway in the initiation, progression, and metastasis of TNBC [3].

The aim of this study is to investigate the expression of *STAT3*, *ALDH1A1*, *NFIB* genes, compare it with samples before and after treatment and discuss their potential as biomarkers for therapeutic purposes.

In this study, we used quantitative PCR to determine *STAT3*, *ALDH1A1*, *NFIB* expression in 22 blood plasma samples of TNBC patients before treatment and 22 samples after treatment. The results revealed statistically significant differences in gene expression of *STAT3* ($p=0.0067$) between samples before and after treatment. Furthermore, using logistic regression we determined that these three genetic biomarkers have potential to distinguish clinically significant samples before treatment from after treatment, however, more samples need to be tested to confirm the validity of the model.

In conclusion, the studied genes, especially the *STAT3* oncogene, are promising targets, which may be used for further TNBC research, prevention, and therapy.

[1] E. A. O'Reilly *et al.*, "The fate of chemoresistance in triple negative breast cancer (TNBC)," *BBA Clin.*, vol. 3, pp. 257–275, Jun. 2015, doi: 10.1016/J.BBACLI.2015.03.003.

[2] M. Nedeljković and A. Damjanović, "Mechanisms of Chemotherapy Resistance in Triple-Negative Breast Cancer-How We Can Rise to the Challenge," *Cells*, vol. 8, no. 9, Aug. 2019, doi: 10.3390/CELLS8090957.

[3] J. J. Qin, L. Yan, J. Zhang, and W. D. Zhang, "STAT3 as a potential therapeutic target in triple negative breast cancer: a systematic review," *J. Exp. Clin. Cancer Res. 2019 381*, vol. 38, no. 1, pp. 1–16, May 2019, doi: 10.1186/S13046-019-1206-Z.

INVESTIGATION OF SYNERGISTIC NEUROTOXIC EFFECT OF AMYLOIDOGENIC PROTEINS ON PRIMARY BRAIN CELL CULTURES

Jovita Gružaitė[1], Katryna Pampuščenko[1], Vytautas Smirnovas[2], Ramunė Morkūnienė[1]

[1] Biochemistry laboratory, Neuroscience Institute, Medical Academy, Lithuanian University of Health Sciences, Lithuania
[2] Institute of Biotechnology, Life Sciences Center, Vilnius University, Lithuania
jovita.gruzaite@gmail.com, jovita.gruzaite@stud.lsmu.lt

Aggregation of α-synuclein (α-Syn) leading to dopaminergic neuronal death and chronic neuroinflammation has been identified as the main hallmark of Parkinson's disease (PD). Recently, another proinflammatory and highly amyloidogenic protein S100A9 has been indicated to be involved in PD pathogenesis, as both proteins were found co-localized and co-aggregated in Lewy bodies in PD patients [1]. Although a few studies suggest that S100A9 changes the aggregation kinetics of α-Syn [1,2] and stabilizes certain amyloid fibril structures [2], the exact mechanisms of co-aggregation, cytotoxicity and synergistic effects remain yet to be discovered.

α-Syn monomers might produce aggregates in a dose- and time-dependent manner *in vitro* and formed oligomers can vary in molecular weight, structure, size, and therefore might have a different impact on cells [3]. Here, we aimed to investigate whether extracellular recombinant α-Syn and S100A9 in various aggregated forms induce neurotoxicity and have synergistic effect on primary cultures of rat brain neurons and glial cells.

Neuronal-glial cell cultures (NGC) were prepared from the cerebellum of 5-7 days old Wistar rat pups and incubated for 7 days *in vitro*. Subsequently, cells were exposed to different concentrations (0.5, 1.5 and 2.5 μM) and various pre-incubation times (30 min, 6 and 24 h at room temperature (RT)) of α-Syn and S100A9 proteins separately or together for 48 h. Cell number and viability were assessed using light and fluorescence microscopy. All quantifications were performed using ImageJ program. Additionally, the ELISA method was used to evaluate the concentration of the pro-inflammatory cytokine TNF-α released in the culture growth medium after exposing cells to α-Syn and S100A9 mixtures for 48 h. Human recombinant proteins α-Syn and S100A9 were produced at Vilnius University.

Interestingly, we found that S100A9 aggregates were more toxic to neurons than those of α-Syn and induced death of neurons at micromolar concentration after 48 h. While studying the synergistic effect of α-Syn and S100A9, we revealed that mixture of both proteins pre-incubated together for 30 min at RT, resulted in microglia proliferation but did not affect neuronal viability nor the number of neurons in NGC after 48 h. By contrast, mixtures of α-Syn and S100A9 pre-incubated for 6 h at RT strongly decreased neuronal viability in a dose-dependent manner (Fig. 1). Finally, pre-incubation of mixtures of both proteins for 24 h at RT had no effect on cell viability and number after 48 h. However, solution of α-Syn + S100A9 induced a considerable increase of TNF-α concentration in cell growth medium.

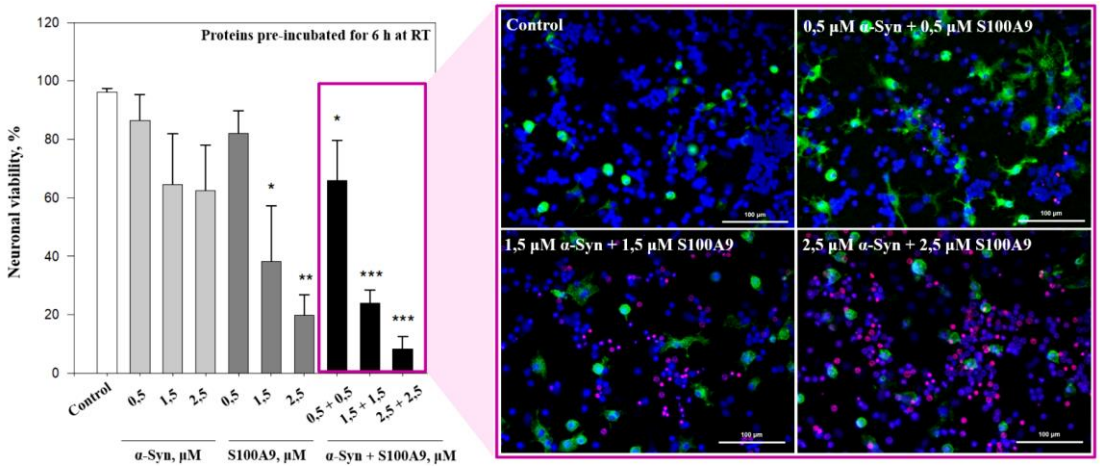


Fig. 1. The effects of α-Syn, S100A9 and mixtures of both proteins on neuronal viability in NGC after 48 h. * – $p < 0,05$; ** – $p < 0,01$; *** – $p < 0,001$, compared to control.

In conclusion, our results show that α-Syn and S100A9 act synergistically, and the impact on NGC depends on protein preincubation time and concentration. Further research of α-synuclein and S100A9 neurotoxicity mechanism is needed to gain more insight into PD pathology, and eventually to develop effective therapeutics.

[1] Horvath I, Iashchishyn IA, Moskalenko RA, Wang C, Wärmländer SKTS, Wallin C, et al. Co-aggregation of pro-inflammatory S100A9 with α-synuclein in Parkinson's disease: Ex vivo and in vitro studies. J Neuroinflammation. 2018;15(1):1–16.
[2] Toleikis Z, Ziaunys M, Baranauskiene L, Petrauskas V, Jaudzems K, Smirnovas V. S100a9 alters the pathway of alpha-synuclein amyloid aggregation. Int J Mol Sci. 2021;22(15).
[3] Du XY, Xie XX, Liu RT. The role of α-synuclein oligomers in parkinson's disease. Int J Mol Sci. 2020;21(22):1–17.

TRANSPOSITION FREQUENCY IN YEAST *SACCHAROMYCES CEREVISIAE*: ROLE OF SCV-LA VIRUS

Gerda Skinderytė[1], Saulius Serva[1], Aleksandras Konovalovas[1]

[1]Department of Biochemistry and Molecular Biology, Vilnius University, Lithuania
gerda.skinderyte@gmail.com

Yeast *Saccharomyces cerevisiae* is one of the best understood eukaryotic model organisms. It is used for research of various biological processes like gene expression, cell cycle, and metabolism, as well as for virus research [1,2]. ScV-LA is a dsRNA yeast virus belonging to *Totiviridae* family. The extracellular phase of this virus is unknown and virus does not interfere with cell growth, though it is capable in maintenance of another dsRNA yeast virus – M satellite [3]. The yeast also possess endogenous mobile genetic elements – transposons. Six families of transposons (Ty1-Ty5 and Ty3p) belonging to LTR-retrotransposons are found in yeast [4,5]. Transposons can impact the integrity of the genome, alter the expression of adjacent genes, or even cause gross chromosomal rearrangements [6]. Basing on observations stemming from transcriptomic and proteomic data, the hypothesis was raised that ScV-LA virus may influence transposition efficiency. In order to assess the influence of ScV-LA on the transposition rate, we constructed a new fluorescence-based transposition rate assay based on the classical transposition test [7].

In this study, auxotrophic selective marker in the reporter plasmid was replaced by a marker conferring resistance to the cells. It allowed the application of fluorescence-based transposition rate assay within the wild-type strains, as well as the cultivation of laboratory strains in rich medium prior to the transposition assay due to the lack of auxotrophic markers. Furthermore, the influence of carbon source on the overall intensity of fluorescence was tested. It was established that the intensity of fluorescence is lower when galactose is a carbon source, compared to that when glucose is used for BY4741 and DBY4975 strains. It was also shown that M-1 virus has no effect on the intensity of fluorescence in DBY4975 strain. Finally, the new non-auxotrophic fluorescence-based transposition assay was used to test the influence of ScV-LA virus to transposition in *S. cerevisiae*. It was found that elimination of M-1 virus incurs no effect on the transposition rate in DBY4975 strain. Meanwhile, elimination of M-2 virus results in almost two-fold drop of transposition rate, whereas elimination of both LA-lus and M-2 viruses results in transposition not being detected with our transposition assay in wild M437 strains. Non-auxotrophic transposition assay will be further used to test various wild and laboratory strains to study the interplay between ScV-LA virus system and transposition in *S. cerevisiae*.

[1] D. Petranovic, K. Tyo, G.N. Vemuri, J. Nielsen, Prospects of yeast systems biology for human health: integrating lipid, protein and energy metabolism, FEMS Yeast Research. 10 (2010) 1046–1059.
[2] R.Y. Zhao, Yeast for virus research, Microb Cell. 4 (2017) 311–330.
[3] R.B. Wickner, T. Fujimura, R. Esteban, Viruses and prions of Saccharomyces cerevisiae, Adv Virus Res. 86 (2013) 1–36.
[4] J.M. Kim, S. Vanguri, J.D. Boeke, A. Gabriel, D.F. Voytas, Transposable Elements and Genome Organization: A Comprehensive Survey of Retrotransposons Revealed by the Complete Saccharomyces cerevisiae Genome Sequence, Genome Res. 8 (1998) 464–478.
[5] M. Carr, D. Bensasson, C.M. Bergman, Evolutionary Genomics of Transposable Elements in Saccharomyces cerevisiae, PLoS One. 7 (2012).
[6] G. Bourque, K.H. Burns, M. Gehring, V. Gorbunova, A. Seluanov, M. Hammell, M. Imbeault, Z. Izsvák, H.L. Levin, T.S. Macfarlan, D.L. Mager, C. Feschotte, Ten things you should know about transposable elements, Genome Biol. 19 (2018).
[7] M.J. Curcio, D.J. Garfinkel, Single-step selection for Ty1 element retrotransposition, PNAS. 88 (1991) 936–940.

ANTICANCER ACTIVITY OF SUNITINIB ANALOGUES IN BRAIN CANCER MODELS

Girstautė Dabkevičiūtė[1], Elias Maccioni[2], Vilma Petrikaitė[1*]

[1]Department of Drug Targets Histopathology, Institute of Cardiology, Lithuanian University of Health Sciences, Lithuania

[2] Department of Life and Environmental Sciences, Cagliari University, Italy

girstaute.dabkeviciute@lsmu.lt

Glioblastoma (GBM) is the most aggressive type of brain cancer. Median survival time for GBM patients is about 12.1 to 14.6 month [1], and there are still extremely limited opportunities of conventional therapy. Tyrosine kinase inhibitors currently are considered as perspective targeted therapy for GBM. There are numerous studies linking changes in kinase activity to carcinogenesis and tumour progression. Tyrosine kinase inhibitors generally target the active site of the kinase and thereby prevent the phosphorylation resulting in inhibition of migration and apoptosis of cancer cells [2]. One of them is sunitinib, a multi-targeted agent, approved for the treatment of kidney cancer and gastrointestinal stromal tumours [3]. Moreover, the new chemical compounds are suggested as more effective sunitinib analogues [4]. The aim of our study was to evaluate the effect of new sunitinib analogues on human brain cancer cell viability and migration.

The two human GBM cell lines, U87-MG and A172, and non-malignant cell line – human fibroblasts were used to investigate cytotoxic effect of 16 sunitinib analogues in vitro. The effect of kinase inhibitors on cell viability was evaluated by MTT assay after 72 hours of incubation, and the most active kinase inhibitors that reduced cell viability up to 5% or less were selected. Then the EC_{50} values of the most active compounds were established and compared to the sunitinib activity. Single cell migration assay was performed to examine the effect of selected compounds on U87-MG and A172 cell migration. Cells were seeded in the dishes with numbered grids. Photos were taken of cells every hour up to 8 hours. Then coordinates of each cell were calculated. The single cell distance travelled per hour was determined and defined as cell velocity. The data are presented as average cell velocity ± standard deviation

The results of MTT assay have shown that compounds 1, 6 and 7 were the most active ones. All three tested compounds more efficiently reduced brain cancer cell viability of A172 cell line than U87-MG cell line, also non-malignant cell viability. It should be noted that compound 6 was the only one that had stronger cytotoxic effect on both cancer cell lines in comparison with non-malignant cells. However, compound 1 had the greatest effect on cell viability (EC_{50} values on U87-MG, A172 and HF were 82 ± 6 nM, 72 ± 6 nM and 82 ± 6 nM, respectively). Compounds 6 and 7 reduced 50% of cell viability at range of concentrations from 112 to 397 nM. All tested sunitinib analogues were more active than sunitinib. Regarding migration assay in U87-MG cell line, compound 1 was 16% more effective than sunitinib and decreased average cell velocity by 2.5 times compared to the control. Compounds 6 and 7 decreased average cell velocity by 55% and 48%, respectively, compared to the control. In A172 cell line, compounds 6 and 7 had the greatest effect on cell migration as cell velocity was reduced by 51% and 60%, respectively, compared to the control.

To conclude, compound 6 may be worthy of further studies as it had U87-MG and A172 cancer cell specific cytotoxicity as well as was effective kinase inhibitor in both cell lines.

[1] Bahadur, S., Sahu, A. K., Baghel, P. & Saha, S. *Oncol Rev.* **13**, (2019).

[2] Pottier C, Fresnais M, Gilon M, et al. Cancers. 2020 Mar;12(3):731.

[3] Le Tourneau C, Raymond E, Faivre S. Sunitinib: a novel tyrosine kinase inhibitor. A brief review of its therapeutic potential in the treatment of renal carcinoma and gastrointestinal stromal tumors (GIST). Ther Clin Risk Manag. 2007 Jun;3(2):341–8.

[4] Meleddu R, Petrikaite V, Distinto S, Arridu A, Angius R, Serusi L, et al. Investigating the Anticancer Activity of Isatin/Dihydropyrazole Hybrids. ACS Med Chem Lett. 2019 Apr 11;10(4):571–6.

ISOLATION OF OPPORTUNISTIC PATHOGEN STENOTROPHOMONAS MALTOPHILIA FROM ENVIRONMENTAL SOURCES

Karolis Krinickis, Laurita Klimkaitė, Julija Armalytė, Edita Sužiedėlienė

Institute of Biosciences, Life Sciences Center, Vilnius University, Vilnius, Lithuania
karolis.krinickis@gmc.stud.vu.lt

Stenotrophomonas maltophilia is a gram-negative, aerobic, motile bacterium known as an opportunistic pathogen causing nosocomial infections with high mortality rates. Multidrug resistance phenotype, biofilm formation on various clinical surfaces and immunity to disinfectants are the main traits determining its survival in clinical settings [1, 2]. S. maltophilia is also ubiquitously found in the natural environment e. g. plant rhizosphere, river water, fish, snakes, deep sea invertebrates [1, 3], therefore it is important to assess the potential pathogenicity of environmental strains. The aim of this study was to isolate S. maltophilia from a diverse spectrum of natural sources and analyse isolated bacteria virulence associated traits.

In order to isolate the bacteria of genus Stenotrophomonas environmental samples from soil (gardens, forests, plains), various water sources were collected and incubated on selective medium that contains vancomycin, imipenem and amphotericin B as selective agents with mannitol/bromothymol-blue system [4]. To select bacteria from genus Stenotrophomonas polymerase chain reaction (PCR) with genus specific primers was performed [5]. Random amplified polymorphic DNA PCR was used to identify bacteria with distinct genetic profiles. Bacterial species were confirmed by 16S rRNA gene sequencing analysis. After Stenotrophomonas maltophilia species identification biofilm formation ability, swarming and twitching motility of isolated environmental isolates were evaluated.

38 samples from various environmental sources were collected during 2021 in different parts of Lithuania. The selective medium system was sufficient to isolate 190 colonies out of which 138 colonies were identified belonging to the genus Stenotrophomonas. 42 isolates with distinct genetic profiles were selected, of which 26 isolates were identified as S. maltophilia by 16S rRNA gene sequencing. All isolates belonging to species S. maltophilia originated from samples collected in forests, parks and plains, while no colonies of this opportunistic pathogen were isolated from lakes and seaside regions (beaches, sandy shores).

[1] Brooke JS. Stenotrophomonas maltophilia: an emerging global opportunistic pathogen. Clin Microbiol Rev. 2012;25(1):2-41.doi:10.1128/CMR.00019-11

[2] Insuwanno W, Kiratisin P, Jitmuang A. Stenotrophomonas maltophilia Infections: Clinical Characteristics and Factors Associated with Mortality of Hospitalized Patients. Infect Drug Resist. 2020;13:1559-1566 https://doi.org/10.2147/IDR.S253949

[3] Berg G, Roskot N, Smalla K. Genotypic and phenotypic relationships between clinical and environmental isolates of Stenotrophomonas maltophilia. J Clin Microbiol. 1999;37(11):3594-3600. doi:10.1128/JCM.37.11.3594-3600.1999

[4] Kett KG, Denton M, Todd N, Corps CM, Kumari P, Hawkey PM. A new selective differential medium for isolation of Stenotrophomonas maltophilia. Eur J Clin Microbiol Infect Dis. 1996 Jul;15(7):607-10. doi:10.1007/BF01709373. PMID: 8874082

[5] Whitby PW, Carter KB, Burns JL, Royall JA, LiPuma JJ, Stull TL. Identification and detection of Stenotrophomonas maltophilia by rRNA-directed PCR. J Clin Microbiol. 2000;38(12):4305-4309. doi:10.1128/JCM.38.12.4305-4309.2000

MULTIGENE TESTING FOR PROSTATE CANCER RISK ASSESSMENT AND DIAGNOSIS

Justina Gaizevska[1,2], Rasa Sabaliauskaite[1], Augustinas Matulevicius[3], Albertas Ulys[2], Feliksas Jankevicius[3,4], Sonata Jarmalaite[1,2]

[1] Laboratory of Genetic Diagnostic, National Cancer Institute, Vilnius, Lithuania
[2] Insitute of Biosciences, Vilnius University Life Sciences Center, Vilnius, Lithuania
[3]Urology Centre, Vilnius University Hospital Santaros klinikos, Vilnius, Lithuania
[4]Institute of Clinical Medicine, Faculty of Medicine, Vilnius University, Vilnius, Lithuania
justina.gaizevska@nvi.lt

Recently, prostate cancer (PCa) diagnosis and disease monitoring have improved significantly. However, in Lithuania, approximately 2,000 men are diagnosed with PCa yearly. Prostate-specific antigen (PSA) is one of the most common diagnostic tools used for PCa in everyday clinical practice. This biomarker is specific for prostate tissue, but not for the disease; therefore, PSA diagnostic sensitivity is high, but specificity remains extremely low. However, genetic testing in conjunction with other screening tools can improve diagnostic efficiency and risk assessment of PCa.

A total of 30 PCa patients from National Cancer Institute were included in this study. Thirty-seven genes were selected for multigene testing based on their significance for disease development and interface with an increased risk of developing the disease (e.g. DNA damage response genes (DDR)). Next generation sequencing (NGS) technology was applied for genomic profile analysis of selected PCa cases. All identified mutations were validated by reviewing the results with Integrative Genomics Viewer (IGV). All identified genetic changes were classified as pathological, non-pathological, and risk factors. Though ClinVar is the major database used in clinical practice, detected variants were additionally checked in other databases (COSMIC, VarSome).

Pathological mutations, such as c.1813delA and c.470T>C were detected respectively in *BRCA2* and *CHEK2* genes. SNP associated with potential increased PCa risk accounted for 10.4% of all detected missense changes. Among them, risk-related single nucleotide variants in *MSMB* and *RNASEL* genes were the most common. At least one PCa risk-related SNP was observed for each patient. Furthermore, elderly patients with clinically significant PCa (Gleason 4+3 and 4+4) had a significantly higher number of risk-related PCa SNPs ($p=0.03$).

In conclusion, this genetic profiling revealed that pathological genetic alterations in PCa patients are predominantly observed in DDR genes, such as *BRCA* and *CHEK2*. We also noticed quite a high prevalence of SNPs related to a higher risk of the disease. Thus, the multigene diagnostic system in conjunction with clinical data has the potential to allow the accurate assessment of particularly heterogeneous PCa, proper prediction of disease risk, tumour aggressiveness, and reduce overdiagnosis of clinically insignificant cancer.

RESEARCH OF THE EFFECT OF SILICON DIOXIDE AND POLYSTYRENE NANOPARTICLES IN *ALLIUM CEPA* ROOT CELLS BY CYTOGENETIC AND MOLECULAR METHODS

Gabija Monˇciūtė, Asta Stapulionytė

Institute of Biosciences, Life Sciences Center, Vilnius University, Lithuania
gabija.monciute@gmc.stud.vu.lt

Nanotechnology is one of the technology fields working at a very small scale. The wide use of nanoparticles (NP) is due to their unique physical and chemical properties, such as easy-to-modify surface, strong mechanical properties, and easy synthesis, thus NP have great potential in many areas, from construction to healthcare. With the increasing use of nanoparticles, there is a growing concern about their harmful effects on the environment and living organisms. Being of extremely small size, NP can enter the cells easily and cause damage, which can later turn into mutations affecting the entire organism. We selected to study effects of silicon dioxide nanoparticles for their widespread use in manufactured products of everyday life, and in the medical field for their biodegradability and compatibility in the cellular environment [1], whilst polystyrene nanoparticles interest us because of environmental concerns.

Previous studies of silicon dioxide nanoparticles showed lethal effects on development and growth when genotoxicity occured through reactive oxygen species (ROS) [1]. Other studies revealed polystyrene nanoparticles can also cause oxidative stress in plants. NP can affect root germination when particles adhere to the peripheral root tissues and interfere with water absorption or might be absorbed and stored in various compartments of the cell [2]. For these reasons, it is important to determine the lowest concentration required to cause effects in cells.

We applied cytogenetic and molecular methods to assess the detriment of nanoparticles, either silicon dioxide or polystyrene, in onion root cells using Allium and RAPD-PCR assays. We tested various concentrations of nanoparticle solutions consisting of 10–20 nm silicon dioxide or 50–100 nm polystyrene on onion bulbs (*Allium cepa* var *Sturon*). Root growth, mitotic index and frequency of chromosome aberration in onion root cells were determined. RAPD method was applied to evaluate if nanoparticles can induce DNA polymorphism in onion. Initially, DNA was purified by three methods: CTAB and commercial Plant gDNA Purification Kits K0512 and K0791 (ThermoFisher Scientific) to determine the most suitable. End-point PCR was performed with random sequence RAPD primers and further visual analysis of PCR products was performed to conduct statistical analysis for polymorphism evaluation and differential analysis.

In summary, the observed cytotoxicity and genotoxicity results of silicon dioxide and polystyrene nanoparticles indicate what kind of damage can be caused when these nanoparticles are absorbed through plant roots and enter the cell.

[1] Liman R, Acikbas Y, Ciğerci İH, Ali MM, Kars MD. Cytotoxic and Genotoxic Assessment of Silicon Dioxide Nanoparticles by Allium and Comet Tests. Bull Environ Contam Toxicol. 2020 Feb;104(2):215-221. doi: 10.1007/s00128-020-02783-3.

[2] Giorgetti L, Spanò C, Muccifora S, Bottega S, Barbieri F, Bellani L, Ruffini Castiglione M. Exploring the interaction between polystyrene nanoplastics and *Allium cepa* during germination: Internalization in root cells, induction of toxicity and oxidative stress. Plant Physiol Biochem. 2020 Apr;149:170-177. doi: 10.1016/j.plaphy.2020.02.014.

OPTIMIZATION OF CULTIVATION, DNA PURIFICATION AND PCR-RAPD CONDITIONS FOR *PUCCINIA* SP.

Tatjana Ščavlinskaja, Asta Stapulionytė, Ingrida Prigodina-Lukošienė, Eglė Lastauskienė

Institute of Biosciences, Life Sciences Center, Vilnius University, Lithuania
tatjana.scavlinskaja@gmc.stud.vu.lt

Pucciniales are parasitic rust fungi with a wide range of host plants. Genus *Puccinia* consists of more than 4000 different species all of which are plant pathogens [1]. *Puccinia* is macrocyclic with five spore stages: urediniospores, teliospores, basidiospores, pycniospores, and aeciospores (Fig. 1) that vary depending on the host plant.

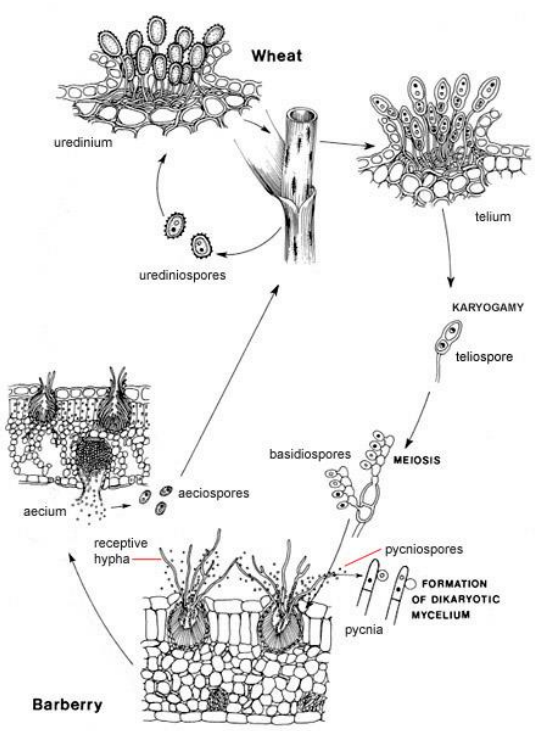


Fig. 1. *Puccinia graminis* life cycle on a primary host (wheat) and alternate host (barberry) plants [2].

Species like *P. coronata* Corda, *P. graminis* Pers, *P. recondita* Roberge ex Desm, and *P. striiformis* Western threaten cereal crops in Lithuania and worldwide [3]. Our research aim is to compare the genetic variation of old herbarium *Puccinia* specimens with the corresponding ones naturally occurring nowadays. It is like looking 30–100 years back to see if, or how much *Puccinia* sp. changed over the last century compared with the current species.

We received herbarium specimens of *Puccinia* sp. from Vilnius University herbarium (WI), and the corresponding rust species were collected in a field during the 2021 season. We selected the potato dextrose agar (PDA) medium that is commonly used for growing yeast and mould for the cultivation of rust fungus species in our research. Later, we extracted fungi DNA from spores and mycelium harvested on Petri dishes to avoid cross-contamination with the host plant DNA. This step was essential, as RAPD primers are not species or taxon-specific, so they could easily anneal to plant DNA. The DNA was purified using the CTAB method or GeneJET Genomic DNA Purification Kit K0721 (ThermoFisher Scientific, Lithuania) with some modifications. After purification, the RAPD was performed to determine the polymorphism level in the DNA sequence between modern and herbarium rust specimens.

Not all the herbarium species and those collected in summer 2021 succeeded to outgrow on PDA medium. Field species that sprouted well on the medium were *P. graminis*, pear rust and one undefined species, while revived herbarium specimens were mostly *P. graminis*. The yield of extracted DNA was greater with the conventional CTAB method compared to commercial kit. However, A260/280 ratio was insignificantly variable among all samples. Eight RAPD primers (OPA-02, OPA-03, OPB-08, OPB-15, OPB-17, OPC-08, and OPG-02) were selected for further downstream genetic diversity investigation.

[1] Kirk PM, Cannon PF, Minter DW, Stalpers JA (2008). *Dictionary of the Fungi (10th ed.)*. Wallingford, UK: CAB International. p. 576. ISBN 978-0-85199-826-8.
[2] Schumann, G.L. and K.J. Leonard. 2000. Stem rust of wheat (black rust). *The Plant Health Instructor*. DOI: 10.1094/PHI-I-2000-0721-01
[3] Minkevičius, Antanas, Milda Ignatavičiūtė, *Lietuvos grybai. V, Rūdiečiai (Uredinales) / 2, Gentis Puccinia* (Mokslo ir enciklopedijų leidykla, 1993).

MODELING OF LOCAL ANTICANCER THERAPIES USING DU-145 PROSTATE CANCER CELLS AND MONOCLONAL ANTIBODY ATEZOLIZUMAB

Žilvinas Survila[1], Gintaras Zaleskis[2]

[1] Institute of Bioscience, Life Science Center, Vilnius University, Vilnius, Lithuania
[2] Laboratory of Immunology, National Cancer Institute, Vilnius, Lithuania
zilvinas.survila@gmc.stud.vu.lt

Pembrolizumab and atezolizumab are monoclonal antibodies approved for cancer immunotherapy targeting immunosuppressive PD-1 and PD-L1 axis used by cancer cells to avoid the host immune system [1]. Despite their efficacy in some types of cancer, they show limited capabilities in the treatment of prostate cancer. However, a combination of monoclonal antibodies with other medications was found to elicit stronger responses. The exact mechanism of such an outcome is unknown [2].

One of the possible factors which may determine treatment effectiveness is the expression of PD-L1 on cancer cells. Herein we assess the expression of PD-L1 in human prostate cell line DU-145 and evaluate atezolizumab binding efficiency to membranous PD-L1 by using flow cytometry approach. Our results show that around 70 % of DU-145 cells are PD-L1 positive and atezolizumab *in vitro* completely saturates membranous PD-L1 at concentrations higher than 0.5 μg/ml indicating that immunotherapy directed towards PD-L1 and PD-1 axis could be effective in prostate cancer.

[1] Y. Wang et al., Advancing to the era of cancer immunotherapy, Cancer communications (London, England), 41(9), 803-829 (2021).
[2] A. Rizzo, V. Mollica, A. Cimadamore et al., Is There a Role for Immunotherapy in Prostate Cancer?, Cells; 9(9), 2051 (2020).

CELL SUSPENSION CULTIVATION OF TRANSGENIC NICOTIANA TABACUM L. FOR BIOMASS PRODUCTION

Rugilė Pranskūnaitė[1], Rytis Rugienius[2], Danas Baniulis[2]

[1] Department of Biology, Vytautas Magnus University, Lithuania
[2] Department of Horticulture, Lithuanian Research Centre for Agriculture and Forestry, Lithuania
rugile.pranskunaite@vdu.lt

Plant genetic engineering not only helps to improve yields, health, and resistance of plants, but also could be used to produce recombinant proteins, vaccines, and biofuels [1]. Methods for plant cultivation under closed environment conditions (in vitro) provide effective solution for the use of genetically modified plants. Application of the technology of molecular farming for production of biological raw materials - provides cost and product quality-effective alternatives as compared to traditional sources, and it could be easily adapted for the large-scale industrial production [2, 3]. Our aim is to develop the technology for plant tissue cultivation under in vitro conditions that is dedicated for production of specific peptides mimicking the functional domains of extracellular matrix proteins (PMEM), collagen-mimetic peptide (CMP) in particularly. Specific challenges that are addressed in this work - to selection of tissue type and growing conditions that ensure production cost and peptide function-efficient plant raw material preparation.

Transformation of tobacco leaf explants were achieved using *Agrobacterium tumefaciens*. Using green fluorescence of the GFP marker under ultraviolet light at 530 nm was used to select three transgenic lines (N1, N2 and N3) of tobacco callus which were further used to initiate cell suspensions. Tobacco callus clones were grown on agarized Murashige and Skoog medium with 3% sucrose and different combinations of growing regulators: 1 mg/l BAP, 0.1 mg/l NAA (RM1), 0.25 mg/l BAP, 2.0 mg/l NAA (TK1) and 0.1 KIN, 1.0 mg/l NAA (TKSIM). Callus clones and cell suspensions were grown at 24, 27 and 31 C° temperatures under 16-hour photo period and transplanted regularly every two weeks. Cell suspensions were stirred at 100 rpm on a shaker in liquid medium. Control (untransformed tobacco callus and cell suspensions) were grown under the same conditions. After two weeks cell suspensions were centrifuged for 15 minutes at 2000 rpm. The supernatant obtained was filtered off with suction and the mass was weighed. The increase in biomass compared to the initial weight is calculated. Statistical analysis was performed using the ANOVA test of the MS Excel package.

The results obtained show that the largest yield of transgenic tobacco calluses obtained in agarized RM1 medium at 27 °C, with an initial mean weight of one callus 400,0 ± 0,4 mg. The maximal biomass increases of the transgenic tobacco cell suspensions compared to the initial mass obtained by culturing them in liquid TKSIM medium at 24 °C temperature (Fig. 1). The control (untransformed) tobacco showed different biomass accumulation properties as compared to the transformants, as the control tobacco calluses had the highest mass increase in the agarized TKSIM medium and the cell suspensions in the liquid RM1 medium at 27 °C temperature. The results of the study suggest that the transformed N2 tobacco callus clone and the cell suspension initiated from it had the largest increase in biomass under the optimal conditions. The weight of the N2 callus clone increased as much as 5,057 ± 0,241 times, and the cell suspension - 11,017 ± 0,384 times comparing with initial weight.

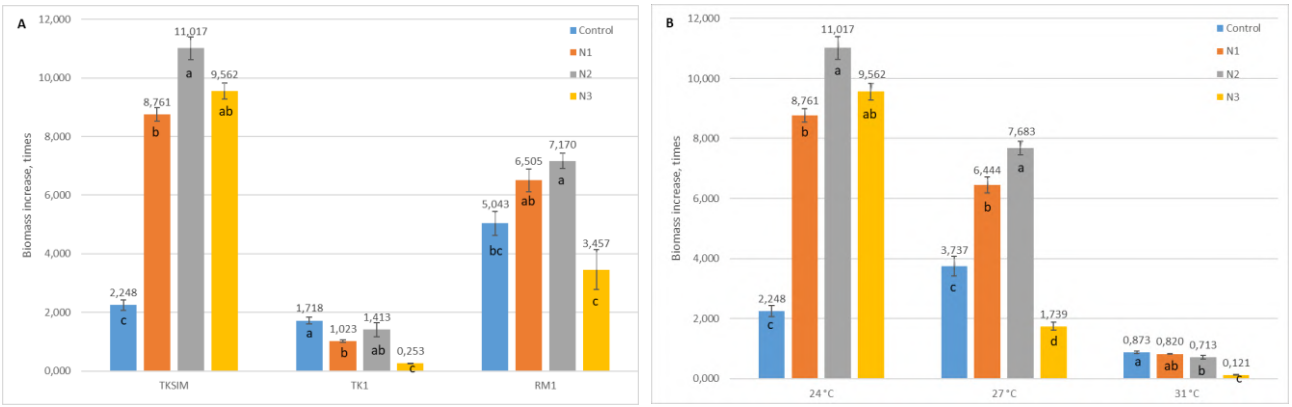


Fig. 1. Increase times in biomass of tobacco cell suspensions, compared with initial weight of control (untransformed) and CMP transformed tobacco clones N1, N2 and N3, depending on medium composition (A) and cultivation temperature (B). Means indicated by the different letters are significantly different, P≤0,05.

[1] L. Low et al., Transgenic plants: gene constructs, vector and transformation method, new visions in plant science, Rijeka:IntechOpen (2018).
[2] H. Jee et al., Development of collagen-based 3D matrix for gastrointestinal tract-derived organoid culture, Stem Cells International **4**, 1-15 (2019).
[3] Z. Poborilova et al., Transient protein expression in tobacco BY-2 plant cell packs using single and multi-cassette replicating vectors. Plant Cell Reports **39**, 1115-1127 (2020).

VARIATION OF ESSENTIAL OIL FROM *ARTEMISIA VULGARIS* (L.) DURING DIFFERENT VEGETATION STAGES

Sandra Saunoriūtė[1,2], Ona Ragažinskienė[2], Liudas Ivanauskas[3], Mindaugas Marksa[3]

[1] Vytautas Magnus University, Faculty of Natural Science, Vileikos str. 8, LT-44404 Kaunas, Lithuania
[2]Vytautas Magnus University, Botanical Garden, Ž. E. Žilibero str. 6, LT-46324 Kaunas, Lithuania
[3]Lithuanian University of Health Science, Faculty of Pharmacy, Sukilėlių str. 13, LT-50162 Kaunas, Lithuania
sandra.saunoriute@vdu.lt

During the past years a number of studies have been carried out concerning the application of biologically active compounds from *Artemisia* (L.) genus [2]. Various pharmacological activities of *Artemisia* (L.) essential oil have been reported such as antibacterial, antihelminthic, antioxidant, diuretic, tonic, anticancer, antidepressant and other effects [1]. As different studies showed, the constituents and yield of *Artemisia* essential oils are highly depends on geografical loacation and vegetation period [2,4,5]. The object of investigation was *Artemisia vulgaris* (L.) a perennial medicinal, aromatic plant of *Asteraceae* (Bercht. & J. Presl) family.

The aim of our study was to determine the qualitative and quantitative composition of the essential oils obtained from *Artemisia vulgaris* (L.) raw material during different vegetation stages.

The raw material of *Artemisia vulgaris* (L.) were colected during different vegetation stages in collection of Spice-Milliferous Plants, Scientific Sector of Medicinal and Aromatic Plants, Scientific Department of Botanical Garden at Vytautas Magnus University in 2019. The essential oils have been extracted by hydrodistillation method and analysed by the chromatographic techniques in the gas phase and chromatography in gas phase coupled with mass spectrometry (GC/MS) so as to determine their chemical composition and identify their chemotype. Qualitative analysis was based on a comparison of retention times, indexes and mass spectra with the corresponding data in the literature [3] and computer mass spectra libraries.

A total of 40 different compounds were found in *Artemisia vulgaris* (L.) essential oils. The highest content and diversity of compounds have been obtained from *A. vulgaris* essential oil during the flower bud development stage. In this vegetation stage we detected thirty-seven constituents of essential oil, representing 89.1% of identified compounds. The principal compounds were found to be camphor (18.96%) and 1,8-cineole (14.76%). As results shown, caryophylene oxide, spathulenol, copaene have been found as the first principal components in all vegetation stages.

The chemical composition of essential oils of *Artemisia vulgaris* (L.) was investigated in 2019-2020. The highest content and diversity of compounds were determined during flower bud development stage. Thirty-seven constituents of the oil were identified in this vegetation stage of which camphor (18.96%) and 1,8-cineole (14.76%) were major components.

[1] M. J. Abad, L. M. Bedoya, L. Apaza, P. Bermejo. The *Artemisia* L. genus: A review of bioactive essential oils. Molecules, **17** (2), 2542-2566 (2012).
[2] R. Abiri, A. L. M. Silva, L. S. S. Mesquita, J. W. C. Mesquita, N. Atabaki, E. B. Almeira, Jr E. B. Almeira, N. A. Shaharuddin, S. Malik.Towards a better understanding of *Artemisia vulgaris*: Botany, phytochemistry, pharmacological and biotechnological potencial. Food Research International, **109**, 403-415 (2018).
[3] R. P. Adams. Identification of Essential Oil Components by GC/MS, Allured Publishing Corp., Carol Stream, IL (1995).
[4] B. Koul, P. Taak, A. Kumar, T. Khatri, I. Sanyal. The *Artemisia* Genus: A Review on Traditional Uses, Phytochemical Constituents, Pharmacological Properties and Germplasm Conservation. Journal of Glycomics and Lipidomics, **7** (1), 2-7 (2017).
[5] S. Saunoriūtė, O. Ragažinskienė, L. Ivanauskas, M. Marksa. Essential oil composition of *Artemisia abrotanum* L. during different vegetation stages. Chemija, **31**(1), 52-56 (2020).

SYNTHESIS OF NOVEL RODENT POLYOMAVIRUSES VIRUS-LIKE PARTICLES IN YEAST

Rūta Kiseliūnaitė, Emilija Vasiliūnaitė[1], Alma Gedvilaitė[1]

[1] Department of Eukaryete Gene Engineering, Institute of Biotechnology, Life Science Center, Vilnius University, Lithuania
ruta.kiseliunaite@gmc.stud.vu.lt

Polyomaviruses (PyVs) are small (40 – 45 nm diameter) nonenveloped circular DNA viruses, widespread in nature - various mammals, including humans, birds and fish are known to be infected. Due to their small genome, compact virion size, low pathogenicity to humans and ability to transform cells both *in vitro* and *in vivo*, *Polyomaviridae* family members (e.g. *Simian virus 40*, SV40) have been repeatedly used as models in studies related to the detection of DNA superspiralisation, cancer research and others. Furthermore, the major structural capsid protein VP1 of polyomaviruses can assemble into virus-like particles (VLPs) [1]. VLPs mimic the native virus and retain its immunogenicity and can transfer DNA. These properties are very important in studying viral mechanisms and is attractive in gene therapy and vaccine creation. While human polyomaviruses are relatively well studied, the information on other mammalian polyomaviruses is still lacking. Only 16 out of 117 species of polyomaviruses are currently known to infect rodents. Given that rodents are the largest group of mammals, this is a relatively small number of viruses found.

In this study, the VLPs of novel *Rattus rattus polyomavirus 1* (RratPyV1) and *Microtus arvalis polyomavirus* 2 (MarPyV2) were synthesized in yeasts *Saccharomyces cerevisiae*. Both these viruses were discovered in our laboratory in 2020 while screening *Microtus arvalis* and *Rattus rattus* rodent samples for polyomaviruses. Recombinant VP1 plasmids with galactose-inducing promoter (pFX7-RratPyV1-VP1 and pFX7-MarPyV2-VP1) were transformed into *S. cerevisiae* and protein synthesis was induced by galactose. VLPs were purified from yeast cell biomass through ultracentrifugation in saccharose and CsCl density gradients. SDS-PAGE analysis showed RratPyV1 and MarPyV2 VP1 proteins are ~ 45 kDa. Purified particles were analysed by Electron Microscopy imaging and it revealed the possible size of the capsid (MarPyV2 ~ 53 nm; RratPyV1 ~ 51 nm). VP1 VLPs of RratPyV1 were tested as antigen in ELISA and reacted positively with rat blood serums. Thus, these particles will be a useful resource for further research on rodent polyomaviruses and their seroprevalence.

[1] Salunke, D. M., Caspar, D. L. D., & Garcea, R. L. (1986). Self-assembly of purified polyomavirus capsid protein VP1. *Cell*, *46*(6), 895–904. https://doi.org/10.1016/0092-8674(86)90071-1

SEARCH FOR PYRETHROIDS-DEGRADING MICROORGANISMS

Ugnė Rickevičiūtė[1], Alisa Gricajeva[1]

[1]Department of Microbiology and Biotechnology, Institute of Biosciences, Life Sciences Center, Vilnius University, Sauletekio av. 7, Vilnius, Lithuania
ugne.rickeviciute@gmc.stud.vu.lt

Pyrethroids are pesticides with high insecticidal potential, however, they do not degrade immediately after spraying and their persistent use can affect non-target organisms and contaminate environment [1]. The biggest pollution is caused by the agricultural sector since it uses pyrethroids on a regular basis and it in turn pollutes terrestrial and aquatic environments. [2]. Pyrethroid residues such as permethrin, cypermethrin, deltamethrin and allethrin are detected in the soil, so the pyrethroid-contaminated environment needs to be remedied urgently. One of the potential solutions of cleaning pesticide-contaminated soil could be the use of microorganisms for the bioremediation. Microorganisms such as *Bacillus* sp., *Catellibacterium* sp., *Serratia marcescens* and *Acidomonas* sp. are reported to have the ability to break down ester-bond having pyrethroid pesticides residues such as cypermethrin, deltamethrin and allethrin [1,3], however, to date there is still a lack of research made in the area of effective microbiological decontamination of our environment from pyrethroids and their residues.

In this study we aimed to perform primary search, identification and analysis of microorganism and their enzymes that could have a potential to break down pyrethroids. To achieve the set goal, we performed screening of microorganisms isolated from the substrate used for the cultivation of agricultural products in some Lithuanian farms. Primary screening of microorganisms was performed on agar plates enriched with fatty substrates having ester-bond (tributyrin and rhodamine B with olive oil agar plates) (Fig. 1). Microbial isolates (bacteria, yeast and fungi) having high activity towards mentioned fatty substrates were subsequently selected to be identified by 16S rDNA analysis and for further analysis of the ability to break-down pyrethroids.

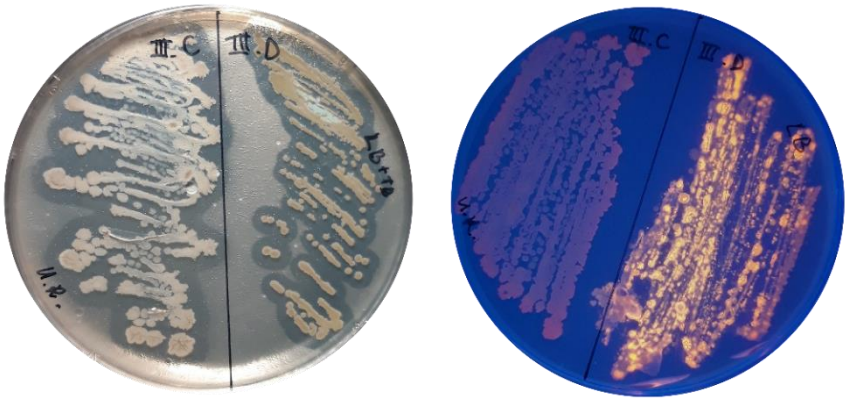


Figure 1. Potentially pyrethroid-degrading isolates of microorganisms on trybutirin and rhodamine B and olive oil agar plates.

[1] Cycoń M, Piotrowska-Seget Z. Pyrethroid-Degrading Microorganisms and Their Potential for the Bioremediation of Contaminated Soils: A Review. *Frontiers in Microbiology*. 2016;7.
[2] Huang Y, Lin Z, Zhang W, et al. New Insights into the Microbial Degradation of D-Cyphenothrin in Contaminated Water/Soil Environments. *Microorganisms*. 2020;8(4).
[3] Bhatt P, Huang Y, Zhan H, Chen S. Insight Into Microbial Applications for the Biodegradation of Pyrethroid Insecticides. *Frontiers in Microbiology*. 2019;10.

GOTTA CATCH 'EM ALL: DESIGNING UNIVERSAL PRIMERS FOR POLYOMAVIRUS DETECTION

Emilija Vasiliūnaitė[1], Albertas Timinskas[2], Alma Gedvilaitė[1]

[1] Department of Eukaryote Gene Engineering, Institute of Biotechnology, Life Sciences Center, Vilnius University, Lithuania
[2] Department of Bioinformatics, Institute of Biotechnology, Life Sciences Center, Vilnius University, Lithuania
emilija.vasiliunaite@gmc.vu.lt

Polyomaviruses (PyVs) are widespread, small (~5 kb) double-stranded DNA viruses that infect mammals, birds, and fish. PyVs are associated with various human diseases, including cancer, progressive multifocal leukoencephalopathy, nephropathy, skin, and respiratory tract diseases, however, pathogenesis normally occurs only in immunocompromised patients. Since their discovery in the 1950s, polyomaviruses have been a model for research of important cellular processes, such as oncogenesis and replication [1]. Recently, pathogenesis, evolution, and zoonotic abilities of PyVs are being extensively studied. SARS-CoV-2 pandemic emphasized the importance of virus evolution, emergence and host-change studies and lack of reliable viral models for such research. Despite few known zoonoses (Simian virus 40 is known to infect humans; *Sorex araneus polyomavirus 1*, formerly known as *Human polyomavirus 12*, was first identified in human hosts, later – in shrews), polyomaviruses are thought to co-evolve with, rather than change their hosts, however, host change and recombination events were an important part of PyV evolution. Rodents, the largest group of mammals, is one of the biggest reservoirs of zoonotic diseases. Rodents have been relatively little investigated for PyVs (rodent PyVs make up only 10% of all known mammalian PyVs, while rodents cover 40% of all mammalian diversity), making them a good target to search for new polyomaviruses. Furthermore, closely related rodent species and their PyVs are a suitable model for the analysis of virus-host coevolution.

To detect novel polyomaviruses in rodent samples, we decided to create PyV-universal nested PCR primers. 1966 polyomavirus complete genome sequences were downloaded and filtered using CD-HIT [2] to 90% identity level. The resulting clusters were reduced to a final dataset of 174 sequences representing distinct PyVs. For these PyVs, nucleotide and amino acid (aa) sequences of most conserved genome parts - large T antigen (LTag) and structural protein VP1 - were extracted. Multiple alignments for aa sequences of both proteins were created using MAFFT and aa residues in the alignment were replaced with nucleotides of the corresponding sequences. Conserved alignment regions were analyzed and 4 possible primer targets of 16-17 nucleotides were selected in LTag coding sequence. VP1 sequence was omitted from further analysis due to lack of conservative targets. Degenerated nucleotides were incorporated in 3-4 sites of each primer. Conducted DegePrime [3] analysis gave corresponding results, thus primers amplifying 1700-2200 bp and 150 bp length LTag DNA fragments were selected. Novel primers were tested with previously PyV-positive rodent samples of *Microtus arvalis polyomavirus 2*, as well as with rodent samples of *Cricetus cricetus*, not yet screened for PyVs. In both cases, a nested PCR DNA band of 150 bp was observed.

[1] Jandrig B, Krause H, Zimmermann W, Vasiliunaite E, Gedvilaite A, Ulrich RG. Hamster Polyomavirus Research: Past, Present, and Future. Viruses. 2021;13(5):907. Published 2021 May 13. doi:10.3390/v13050907.
[2] Li W, Godzik A. Cd-hit: a fast program for clustering and comparing large sets of protein or nucleotide sequences. Bioinformatics. 2006 Jul 1;22(13):1658-9. doi: 10.1093/bioinformatics/btl158. Epub 2006 May 26. PMID: 16731699.
[3] Hugerth LW, Wefer HA, Lundin S, et al. DegePrime, a program for degenerate primer design for broad-taxonomic-range PCR in microbial ecology studies. Appl Environ Microbiol. 2014;80(16):5116-5123. doi:10.1128/AEM.01403-14

ANALYSIS OF *IN VITRO* GENOTOXICITY OF DIFFERENTLY SIZED COBALT OXIDE NANOPARTICLES IN HUMAN LYMPHOCYTES

Milda Babonaitė[1], Veronika Dedonytė[1], Juozas Rimantas Lazutka[1]

[1] Institute of Biosciences, Vilnius University, Vilnius, Lithuania
milda.babonaite@gmc.vu.lt

Cobalt (II, III) oxide nanoparticles (Co_3O_4-NPs) can be potentially used in different technological and medical applications, including drug delivery or as possible anticancer therapeutic tool [1][2].

In this study, we report genotoxicity of 10-30 nm and <50 nm cobalt oxide nanoparticles to human lymphocyte cultures *in vitro.* The genotoxicity tests used in this study were Comet assay, cytokinesis-block micronucleus (CBMN) assay and analysis of sister-chromatid exchange (SCE). Human lymphocytes obtained from 5 donors were treated with Co_3O_4-NPs at concentrations of 20-80 μg/ml in comet assay and no clear dose-response relationship was found. However, individual donor sensitivity was observed. Lymphocytes from three donors were sensitive to DNA damaging action of Co_3O_4–NPs, lymphocytes of two donors were insensitive. In CBMN assay, lymphocytes from three donors showed dose-dependent increase (up to 40 μg/ml) in the frequency of micronucleated cells, treated with 10-30 and <50 nm size Co_3O_4-NPs. In SCE analysis, lymphocytes from two out of three donors showed dose-dependent increase of DNA damage, treated with 10-30 nm size of Co_3O_4-NPs. No correlation between SCE and concentration of <50 nm size Co_3O_4-NPs was observed. What is more, in most cases, <50 nm NPs induced more DNA damage, compared to 10-30 nm NPs.

Taken together all results of our study, it could be concluded that Co_3O_4-NPs are genotoxic in human lymphocytes *in vitro*, at least for some donors and in some assays. This raises concern about safety of use of Co_3O_4-NPs and requires thorough genotoxicity analysis of Co_3O_4-NPs in different cell cultures.

[1] O.I. Medvedeva, S.S. Kambulova, O.V. Bondar, et al., Magnetic Cobalt and Cobalt Oxide Nanoparticles in Hyperbranched Polyester Polyol Matrix, Journal of Nanotechnology, vol. 2017, Article ID7607658 (2017).

[2] H. Huang, J. Wang, J. Zhang et al., Inspirations of Cobalt Oxide Nanoparticle Based Anticancer Therapeutics, Pharmaceutics **13**, 1599 (2021)

DYNAMICS OF CULTIVABLE MICROORGANISMS IN COMMERCIALLY REARED BLACK SOLDIER FLY LARVAE

Guoda Varnelytė[1,2], Bazilė Ravoitytė[1], Stanislavas Tracevičius[3], Elena Servienė[1]

[1]Institute of Botany, Nature Research Centre, Akademijos 2, 08412 Vilnius, Lithuania
[2]Institute of Biosciences, Life Sciences Center, Vilnius University, Sauletekio 7, 10257 Vilnius, Lithuania
[3]UAB „Insectum“, P. Zadeikos 20, 06321, Vilnius, Lithuania
guoda.varnelyte@gmc.stud.vu.lt

Insects have been consumed by the ancient communities and are currently eaten in 58% of the world countries [1,2]. Insects are attractive because of the high quality and balanced amounts of proteins, fats and even minerals. Cultivation of insects requires less resources and feed, in contrast to animal farming [1], thus insect rearing is a promising alternative to meet the increasing need of high-quality proteins for animals and humans. Besides advantages of consumption of insects, safety questions must be addressed. Microbial hazards are among the main safety concerns that must be monitored during the production of high-quality insects and their products.

Black soldier fly (*Hermetia illucens*) is among the most consumed insects [3]. Black soldier fly larvae (BSFL) can convert organic waste into valuable products such as proteins and fats. The residues left after BSFL rearing, called frass, can be returned to the food chain and to fertilize plants, thereby making this process even more sustainable.

We have investigated the extent of cultivable microorganisms at different stages of industrial BSFL rearing process (second and fourth instars), heat and cold treated larvae, and frass after BSFL harvesting. We have registered and compared total viable counts of microorganisms in each sample. Morphologically distinct colonies have been inspected by molecular methods and several species of bacteria have been identified. The obtained results are important for creating optimization strategies of the production process as well as for the evaluation of microbial safety.

[1] K. Papastavropoulou, A. Koupa, E. Kritikou, M. Kostakis, C. Proestos, Edible insects: Benefits and potential risk for consumers and the food industry, Biointerface Research in Applied Chemistry **12**, 5131 – 5149 (2022).
[2] J. Tao, Y.O. Li, Edible insects as a means to address global malnutrition and food insecurity issues. Food Quality and Safety **2**, 17-26 (2018).
[3] J.C. Ortiz et al., Insect mass production technologies. Insects as sustainable food ingredients. Academic Press 153-201 (2016).

ACTIVITY OF NEW SUNITINIB ANALOGUES ON HUMAN BREAST CANCER CELL MIGRATION IN NORMOXIA AND HYPOXIA

Paulina Jonutė[1], Elias Maccioni[2], Vilma Petrikaitė[1]*

[1] Laboratory of Drug Targets Histopathology, Institute of Cardiology, Lithuanian University of Health Sciences, Lithuania

[2]Department of Life and Environmental Sciences, University of Cagliari, Italy

vilmapetrikaite@gmail.com

The search for new anticancer drugs has increased in the last decades since currently used chemotherapeutic drugs show many adverse effects. Previous studies show that kinase inhibitors exhibit antitumor activity [1,2]. According to studies, protein kinase dysfunctions have been associated with the development of various types and subtypes of human cancers [1]. Over 25 kinase inhibitors are approved as anticancer drugs [3]. One of them is sunitinib, which is used to treat kidney cancer and gastrointestinal stromal tumors [4]. A common feature of most tumors is a low level of oxygen, called hypoxia. This hypoxic stress creates an adaptive mechanism on cancer cells survival, proliferation, and plays a vital role in migration and invasiveness in cancer cells [5], thus there is a need to study compounds activity in hypoxia conditions.

The aim of our study was to evaluate the effect of new sunitinib analogues on migration of triple negative breast cancer cell line MDA-MB-231 in normoxia and hypoxia.

Materials and methods. Experiments were performed on human cancer cell line MDA-MB-231. Kinase inhibitors, which are sunitinib analogues, have been synthesized at the University of Cagliari, Italy, and their synthesis and characterization was published [6]. Compound effect on breast cancer cell ability to migrate was examined using single cell tracking assay. This experiment was performed on a special imaging dish with a grid. Cells were seeded at a low concentration, to get 50-70 cells in total on a grid area. Cells were allowed to attach overnight, and then the compound solutions were added. Images of the migrating cells were taken at one-hour intervals for 8 hours by using an inverted microscope. Single cells were tracked and the cell migration distance was measured by ImageJ software. Then the average cell migration velocity was calculated. Also, wound healing assay was used to evaluate compound effect on cell migration. The wound was created in a cell monolayer. Images were taken at the beginning and at regular 24 hours intervals. All compounds were used at 50% of their established EC_{50} values. Hypoxia was induced using cobalt chloride.

Results. Single cell experiment results showed that in normoxia conditions kinase inhibitors 1,6 and 8 reduced cell migration compared to the control. In hypoxia, only compound 6 inhibited breast cancer cells migration. However, sunitinib was from 1,4 to 2,5 times more active compared to analogues. Wound healing assay results showed that compounds 1,6 and 17 had the greatest effect on the migration of the MDA-MB-231 cell line. In hypoxia, compounds inhibitory effect was statistically significantly stronger.

Conclusions. Tested kinase inhibitors possess anticancer activity on triple-negative breast cancer cell line. They inhibit migration of cells, and may be worthy for further studies.

[1] J. Cicenas, E. Zalyte, A. Bairoch et al., Kinases and Cancer, Cancers, 10(3), 63 (2018).

[2] KS. Bhullar, NO. Lagaron, EM. McGowan et al., Kinase-targeted cancer therapies: progress, challenges and future directions, Mol Cancer 17: 48 (2018)

[3] S. Gross, R. Rahal, N. Stransky et al., Targeting cancer with kinase inhibitors, J Clin Invest., 125(5):1780–9 (2015).

[4] Z. Hao, I. Sadek, Sunitinib: the antiangiogenic effects and beyond, OncoTargets Ther. 9:5495–505 (2016).

[5] C. Paneerselvam. S.Ganapasam. β-Escin alleviates cobalt chloride-induced hypoxia-mediated apoptotic resistance and invasion via ROS-dependent HIF-1α/TGF-β/MMPs in A549 cells, Toxical Res 9(3):191–201 (2016).

[6] R. Meleddu, V. Petrikaite, S. Distinto et al., Investigating the Anticancer Activity of Isatin/Dihydropyrazole Hybrids, ACS Medicinal Chemistry Letters, 10, 4, 571–576 (2019).

.

URINARY MIRNA ASOSCIATION WITH TREATMENT RESISTANCE IN TRIPLE-NEGATIVE BREAST CANCER

Kornelija Rauduvytė[1], Agnė Šeštokaitė[1,2], Monika Drobnienė[1,2,] Rasa Sabaliauskaitė[2], Sonata Jarmalaitė[1,2]

[1]Institute of Biosciences, Life Sciences Center, Vilnius University, Vilnius, Lithuania
[2]National Cancer Institute, Vilnius, Lithuania
kornelija.rauduvyte@gmc.stud.vu.lt

Triple-negative breast cancer (TNBC) is the most aggressive breast cancer subtype. The main features of TNBC are lack of estrogen receptors (ER), progesterone receptors (PR) and human epidermal growth factor 2 receptors (HER2) [1]. Chemotherapy is the main treatment strategy for TNBC patients. However, severe side effects and unpredictable treatment efficacy remain the main concern of chemotherapy [2]. In recent years it has been shown that many different microRNAs (miRNAs) are frequently dysregulated and can be secreted into the circulatory system. For the following reasons, miRNAs in urine could serve as a promising tool for identifying non-invasive biomarkers for TNBC [3].

The aim of this research was to identify dysregulated miRNAs which are associated with chemoresistance in TNBC and could help to predict the response to treatment.

To evaluate miRNAs abundance differences in serial urine specimens, we used quantitative reverse transcription PCR (RT-qPCR). In our going research, in more than 50 serial TNBC samples 4 miRNAs expression was examined (miR-200a, miR-210, miR-125a, miR-454). The samples were collected before and 6 months after the treatment of paclitaxel combined with carboplatin, or 4 cycles of doxorubicin combined with cyclophosphamide. Comparative analysis showed that all miRNAs were upregulated, however, not all of them showed significant differences comparing before and after treatment groups. This suggests our analyzed miRNAs involvement in response to chemotherapy treatment and that urine could be used as a completely non-invasive tool for TNBC treatment monitoring.

Overall, miRNA-200a, miRNA-210, miRNA-125a and miRNA-454 are involved in resistance to chemotherapy mechanisms. Identification of these miRNAs level differences in TNBC patients' urine specimens could be used as a completely non-invasive method which would help to predict the efficacy of treatment.

[1] Pareja, F., Geyer, F. C., Marchiò, C., Burke, K. A., Weigelt, B., & Reis-Filho, J. S. (2016). Triple-negative breast cancer: The importance of molecular and histologic subtyping, and recognition of low-grade variants. *Npj Breast Cancer*, *2*(1), 1–11.
[2] Nedeljković, M., & Damjanović, A. (2019). Mechanisms of Chemotherapy Resistance in Triple-Negative Breast Cancer—How We Can Rise to the Challenge. *Cells*, *8*(9).
[3] Shin, V. Y., Siu, J. M., Cheuk, I., Ng, E. K. O., & Kwong, A. (2015). Circulating cell-free miRNAs as biomarker for triple-negative breast cancer. *British Journal of Cancer*, *112*(11), 1751–1759.

CUMULATIVE EXPOSURE FROM COMPUTED TOMOGRAPHY SCANS. ASSESSMENT OF RECURRENT EXAMINATION

Daira Paškevičiūtė[1], Birutė Gricienė[2]

[1] Faculty of Medicine, Vilnius University, Lithuania
[2] Department of Radiology, Nuclear Medicine and Medical Physics, Faculty of Medicine, Vilnius University, Lithuania
daira.paskeviciute@mf.stud.vu.lt

Computed tomography (CT) is an indispensable imaging technique used in everyday medical practice. While main drawback of CT has always been ionizing radiation, until the last few decades it was a manageable problem with infrequent imaging and single scans. Nowadays, CT makes up only 9,6% of all radiology procedures, but up to 61,6% of all effective doses (ED) received [1], as more and more patients get large cumulative effective doses (CED) of 100 mSv and more, in short periods of time (1-5 years) [2]. The currently accepted risk model about radiation induced cancer is linear non-threshold (LNT), which states that even the smallest doses can increase the risk of cancer [3]. Taking LNT into consideration, the large CED being received by increasing amounts of patients getting CTs are very concerning [4].

The aim of this study was to analyze current literature about health risks posed by cumulative exposure and available methods of minimizing high doses without losing diagnostic value of the images, as well as to retrospectively evaluate cumulative exposure of a group of patients from a hospital in Lithuania.

From January, 2019 to December, 2021, CT imaging data of 30,313 patients from a single hospital was collected. 5,060 (16,7% of all) patients who have received multiple (varying between 2 and 18) CT procedures were selected for this study. The majority of patients received 2 scans (9,3% of all), while only 0,83% received 7 or more scans. Lowest cumulative doses were of those having received 2 scans (average 2731,6 mGy*cm; max 21948 mGy*cm), the highest of those having received 13 scans (average 11620,4 mGy*cm; max 42533 mGy*cm). On average, it was estimated that recurrent scans of 3 and more had an average ED above 50 mSv. Information from recent literature and research provides strong evidence for higher cancer risks in patients who have received above 100 mSv ED, and good evidence for doses above 50 mSv [4].

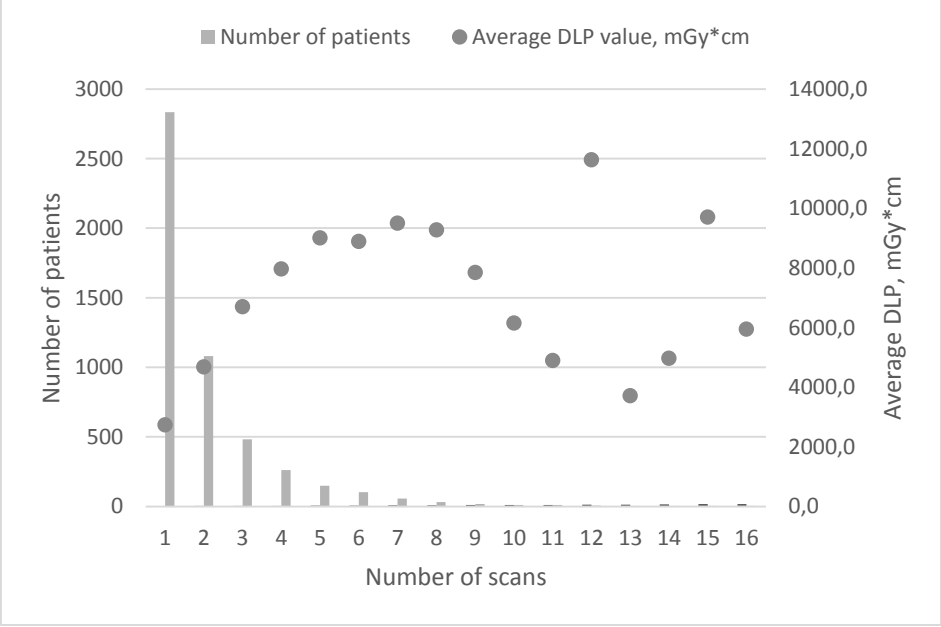


Fig. 1 Number of patients and the average DLP values by numbers of scans received

[1] Report of the United Nations Scientific Committee on the Effects of Atomic Radiation, 2021. . United Nations Scientific Committee on the Effects of Atomic Radiation, New York.
[2] Rehani, M.M., 2013. Challenges in Radiation Protection of Patients for the 21st Century. American Journal of Roentgenology 200, 762–764. https://doi.org/10.2214/AJR.12.10244
[3] Health Risks from Exposure to Low Levels of Ionizing Radiation: BEIR VII Phase 2, 2006. . National Academies Press, Washington, D.C. https://doi.org/10.17226/11340
[4] Brambilla, M., Vassileva, J., Kuchcinska, A., Rehani, M.M., 2020. Multinational data on cumulative radiation exposure of patients from recurrent radiological procedures: call for action. Eur Radiol 30, 2493–2501. https://doi.org/10.1007/s00330-019-06528-7

TOXICITY EVALUATION OF POLYSTYRENE NANOPLASTICS IN SALMONID EMBRYOS

Emilija Dešč[1,2], Gintarė Sauliutė[1], Arvydas Markuckas[2]

[1] Nature Research Centre, Akademijos St. 2, LT-08412 Vilnius, Lithuania
[2]Vilnius University, Life Sciences Center, Saulėtekio av. 7, 10223 Vilnius, Lithuania
emilija.desc@gmc.stud.vu.lt.

Polystyrene is a mass produced polimer. Most of polystyrene containing products are single-use items such as cutlery, plates, caps for takeaway cups, as well as food storage containers. Polystyrene is also widely used for thermal insulation purposes as extruded polystyrene foam (XPS). Mass production of polystyrene and multiple possibilities for applications means rapid growth of its waste. Unfortunately, polystyrene cannot biodegrade in the environment. However, there is scientific evidence showing an existence of plastic fragmentation processes[1]. The latter is of great concern knowing that plastic fragments can become as small as nanosized particles[2]. Recent findings suggest that polystyrene is capable of fragmentation and can exist as nanoplastic[3]. Polystyrene nanoplastics (PS-NPs) hold similar physicochemical properties as engineered nanoparticles, therefore have the ability to pass through biological barriers and accumulate in living organisms[4]. Salmonid fish embryos and larvae are of particular interest because exposure to PS-NPs during early developmental stages show long-term damage and may cause serious consequences such as morphological abnormalities, changes in behaviour and locomotor activity[5]. These harmful effects occur due to the physiological state disturbances on the cellular and molecular level. It was found that exposure to 20 nm PS-NPs can induce oxidative stress in zebrafish (*Danio rerio*) embryos[6].

The aim of this study was to evaluate the level of toxicity in *Oncorhynchus mykiss* embryos exposed to 25 nm sized PS-NPs. Fish embryos were exposed to 10 µg/L and 1000 µg/L PS-NPs concentrations for 4- and 12 days. As aformentioned, oxidative stress may occur during exposure to PS-NPs, therefore an antioxidant anzyme catalase (CAT) was chosen as biomarker.

Results obtained during our experiments showed significantly decreased CAT activity in 4 day embryos exposed to 10 µg/L PS-NPs and non-significantly decreased CAT activity with 1000 µg/L PS-NPs compared to control group. Moreover, no significant changes were detected in 12 day embryos for both 10 µg/L and 1000 µg/L PS-NPs concentrations, however the overall CAT activity was higher in 12 day embryos exposed to both PS-NPs concentrations than in 4 day embryos.These data suggest that 25 nm PS-NPs may induce oxidative stress as early as 4 days in *O.mykiss* embryos due to noticible changes in CAT activity after exposure to 10 µg/L. However, slight CAT activity changes in 4 day *O.mykiss* embryos exposed to 1000 µg/L PS-NPs show a potential „shutdown" of antioxidant anzyme system due to cellular damage caused by reactive oxygen species (ROS)[7]. On the contrary, after 12 day exposure to both PS-NPs concentrations *O.mykiss* embryos showed low response from antioxidant enzyme system, meaning that the used concentrations are not similarly toxic for more aged embryos. It is worth mentioning that response to oxidative stress is carried out by more that one antioxidant anzyme, therefore further experiments should draw attention to a wider spectra of molecules, responding to oxidative stress, induced by various concentrations and sizes of PS-NPs.

Aknowledgments

This research was funded by the Research Council of Lithuania, Project No. S-MIP-21-10, MULTIS.

[1] Gerritse, J., Leslie, H.A., de Tender, C.A., Devriese, L.I., Vethaak, A.D. Fragmentation of plastic objects in a laboratory seawater microcosm. Sci Rep 10, 10945 (2020).
[2] Gigault, J., Pedrono, B., Maxit, B. & Ter Halle, A. Marine plastic litter: the unanalyzed nano-fraction. Environ. Sci.: Nano 3, 346–350 (2016).
[3] Lambert S, Wagner M., Characterisation of nanoplastics during the degradation of polystyrene. Chemosphere, 145:265-8 (2016).
[4] Brandts, I. et al., Polystyrene nanoplastics accumulate in ZFL cell lysosomes and in zebrafish larvae after acute exposure, inducing a synergistic immune response in vitro without affecting larval survival in vivo. Environ. Sci.: Nano, 7, 2410-2422 (2020).
[5] Mattsson K, Ekvall MT, Hansson LA, Linse S, Malmendal A, Cedervall T., Altered behavior, physiology, and metabolism in fish exposed to polystyrene nanoparticles. Environ. Sci.: Technol. 49(1):553-561 (2015).
[6] Sökmen TÖ, Sulukan E, Türkoğlu M, Baran A, Özkaraca M, Ceyhun SB. Polystyrene nanoplastics (20 nm) are able to bioaccumulate and cause oxidative DNA damages in the brain tissue of zebrafish embryo (Danio rerio). Neurotoxicology, 77:51-59 (2020).
[7] Pitt JA, Trevisan R, Massarsky A, Kozal JS, Levin ED, Di Giulio RT. Maternal transfer of nanoplastics to offspring in zebrafish (Danio rerio): A case study with nanopolystyrene. Sci Total Environ.1;643:324-334 (2018).

INHIBITION OF MIRNA TO TREAT PERIODONTITIS

Ema Lomsargyte[1], Kristina Snipaitiene[1], Benita Buragaite-Staponkiene[1], Adomas Rovas[2], Egle Punceviciene[3], Raminta Vaiciuleviciute[4], Eiva Bernotiene[4], Irena Butrimiene[3], Alina Puriene[2], Sonata Jarmalaite[1]

[1]Human Genome Research Group, Life Science Center, Vilnius University, Vilnius, Lithuania
[2]Vilnius University Hospital Zalgiris Clinic, Vilnius, Lithuania
[3]Vilnius University Hospital Santaros Clinics, Vilnius, Lithuania
[4]Innovative Medicine Center, Vilnius, Lithuania
ema.lomsargyte@gmc.stud.vu.lt

Periodontitis (PD) is an inflammation of the periodontium (tissues that surround and support the teeth) caused by an aggressive immune response to an increased number of pathogenic microorganisms in the oral cavity. This disease affects around 40% of human population and can lead to tooth loss. A few risk factors are associated with PD, including smoking, systemic diseases (rheumatoid arthritis, diabetes, cardiovascular diseases), poor dental hygiene, etc. The early stages of periodontitis are usually asymptomatic, resulting in delayed diagnosis of PD [1, 2]. In addition, PD complicates the endurance of dental implants. Overall, it is crucial to detect periodontitis before its progression and invent a highly specific method of treatment. Cells, involved in the immune response to an inflammatory disease, such as PD, can be regulated by miRNAs –short non–coding RNA's that can control expression of genes. The goal of the present study is to assess the potential of miRNA blocking as a therapy method for PD.

Healthy (PD–) and affected (PD+) gingival crevicular fluid (GCF, N=40) specimens were tested in order to determine the expression changes four miRNA (miR-140-3p, miR-145-5p, miR-146a-5p, miR-190-5p). *In vitro* experiments were also carried out for selected miRNAs expression evaluation. Untreated control (CT) cells were compared with three types of cell treatment: with inflammatory mediator IL-1β (IL-1β), miRNA inhibitors (INH), and both (IL+INH). Variation of miRNA expression was assessed by quantitative reverse transcription PCR (RT-qPCR).

Significant differences in miRNA levels between PD– and PD+ groups were not detected ($P>0.05$), while the amount of miR-146a-5p was significantly higher in the control/mild group than in moderate/severe PD group ($P=0.0277$). MiRNA changes were also associated with clinical-pathological parameter – bone loss (BL), as GCF samples from BL ≥ 20% cases compared to BL < 20% had a higher amount of miRNA-145-5p and lower amount of miRNA-146a-5p ($P=0.0398$ and $P=0.0150$, respectively). Statistically significant increase in miRNA-146a-5p expression after cells were treated with IL-1β ($P<0.0001$) and a decrease in miRNA-145-5p expression after exposure to miRNA inhibitors ($P=0.0010$) was disclosed by *in vitro* experiments.

The current study showed that there is a link between miR-146a-5p amount changes in GCF and PD severity. *In vitro* results suggest that after more experiments directed to miRNA blocking, it could be a future treatment option for periodontitis treatment.

[1] Neville BW, Damm DD, Allen CM, Chi AC. Periodontal Pathology. In: Color Atlas of Oral and Maxillofacial Diseases. Elsevier; 2019. p. 93–107.
[2] Xu W, Zhou W, Wang H, Liang S. Roles of Porphyromonas gingivalis and its virulence factors in periodontitis. *Adv Protein Chem Struct Biol*. 2020;120:45-84. doi:10.1016/bs.apcsb.2019.12.001

COMBINED ANTIBIOTIC THERAPY CARRIED IN COLLAGEN MATRIX FOR OPPORTUNISTIC PATHOGENS TREATMENT

Liudmyla Lastovetska[1], Valeriia Maslak[1], Olga Iungin[1, 2*]

[1] Department of Biotechnology, Leather and Fur, KNUTD, Ukraine
[2] Biofilm study group, Institute of Molecular Biology and Genetics, Ukraine
olgaungin@gmail.com

The optimal deployment of antibiotics is a key treatment for wounds complicated with oportunistic infections. The most common infectious agents in such cases are *Staphylococcus*, *Escherichia*, *Klebsiella, Pseudomonas*, *Enterococcus* species. The pathogenesis of many orthopedic infections is associated with biofilms which are more resistant to antimicrobials compare to planktonic cells [1]. Collagen is a fibrillar protein used in drug delivery systems to treat burns and wounds, in gel compositions in combination with antibiotics and other antimicrobials [2].

The aim of the study was to determine the effectiveness of antibiotics chloramphenicol (CAP) and azithromycin (AZM) in collagen matrix against opportunistic pathogens. The effect of phenolic antibiotic chloramphenicol (CAP) and macrolide antibiotic azithromycin (AZM) on both gram-negative (*Pseudomonas*, *Klebsiella* sp.) and gram-positive (*Staphylococcus* sp.) species. was studied.

Methods. Collagen was extracted from leather production wastes as described [3], washed in deionized water and filtered with 0,22 μm syringe filter. The 96-well microtiter plate assay was used. The overnight cultures (NB, HiMedia Ltd.) of laboratory strains *P.aeruginosa*, *K. pneumoniae*, *S. aureus* were inoculated (1:10 ratio) in plates contained collagen matrices with CAP ethanol solution (1-30 μg/ml) and AZM water solution (1-30 μg/ml). And 70% ethanol was used as positive control. The strains were cultivated 24 hours at 37°C. The OD_{600} was measured and the crystal violet assay was applied.

Results. 30 μg/ml of AZM completly inhibited planktonic cultures of *S. aureus* laboratory strains and hospital isolates (non methicillin-resistant). The synergystic effect of joint antibitics use was observed in biofilm inhibition. Thus, CAP in combination with AZM successfully reduced bacterial cells surface attachment and biofilm formation. The most effective combination of AZM+CAP in equal concentrations (30+30 μg/ml) was chosen for further development of wound topical.

[1] Ciofu, O., Rojo- Molinero, E., Macià, M. D., & Oliver, A. *Antibiotic treatment of biofilm infections*. Apmis, 125(4), 304-319 (2017).
[2] Zhu, S., Yuan, Q., Yin, T., You, J., Gu, Z., Xiong, S., Hu, Y. *Self-assembly of collagen-based biomaterials: preparation, characterizations and biomedical applications.* Journal of Materials Chemistry B, 6 (18), 2650-2676 (2018).
[3] Maistrenko, L., Iungin, O., Savchuk, O., Okhmat, O. *Collagen matrices from leather industry wastes for biomedical application*, ICAMS Proceedings of the International Conference on Advanced Materials and Systems, 195-200 (2020).

MOLECULAR CHARACTERIZATION OF *LAELAPS AGILIS* MITES (MESOSTIGMATA: LAELAPIDAE) FROM SMALL RODENTS

Evelina Kaminskienė, Justina Snegiriovaitė

Department of Biology, Vytautas Magnus University, Lithuania
evelina.kaminskiene@vdu.lt

Laelaps agilis is the dominant species of mite parasitizing small rodents in Europe. Species determination of laelapid mites, including *L. agilis*, based on their morphological characteristics is difficult due to their high levels of morphological variability and small size of these mites. In recent years, DNA-based methods have been used to identify Mesostigmata mite species where morphological differentiation is problematic. In Europe, *Laelaps agilis* was reported by morphological identification. However, there is no study on molecular chracterisation of this species.

In this study, *L. agilis* mites parasitizing small rodents, for the first time, identified and genetically characterized by the comparison of nucleotide sequences of the cytochrome c oxidase subunit I (*COI*) gene region. *L. agilis* specimens were obtained from five different small rodent hosts collected in Lithuania, Slovakia and Czech Republic. Eight *COI* haplotypes (h = 8) between *L. agilis* sequences were identified (Hd = 0.910, Π = 0.03157 and S = 66). Correlation between *L. agilis COI* haplotypes and geographic location was detected. Some of *L. agilis* haplotypes were specific to *A. sylvaticus, M. glareolus* and *M. oeconomus* rodents.

This study provides new information on an identification and genetic diversity of *L. agilis* mites.

TREATMENT OF ADVANCED MURINE PANCREATIC ADENOCARCINOMA BY THE COMBINATION OF MBTA IMMUNOTHERAPY WITH A GLUTAMINE ANTAGONIST

Andrea Frejlachova[1], Radka Lencova[1], Anna Venhauerova[1], Marketa Skalickova[1], Jan Zenka[1]

[1] Department of Medical Biology, Faculty of Science, University of South Bohemia, Ceske Budejovice, Czech Republic
frejla00@prf.jcu.cz

Pancreatic adenocarcinoma is a disease with a very poor prognosis and its treatment is extremely challenging. Our immunotherapeutic approach, called MBTA therapy, is based on a combination of Toll-like receptor (TLR) agonists, phagocytosis-stimulating ligand (mannan), and agonistic antibody anti-CD40. TLR agonists have a signalling effect which leads to an inflammatory response and granulocytic infiltration. Mannan is anchored to tumor cells via a biocompatible anchor for cell membrane (BAM) and labels the tumor cells for phagocytes recognition. In the case of a single tumor murine model, this mixture cured 80% of mice with pancreatic adenocarcinoma Panc02 [1] and 62.5% of mice with pheochromocytoma PHEO [2]. It was shown that early MBTA therapy initiation positively correlated with higher efficacy of MBTA therapy. In the case of large tumors or in the presence of metastases, the effect of MBTA immunotherapy is significantly reduced. For these reasons, we studied the possibility of combining our immunotherapy with the simultaneous inhibition of glutamine metabolism. Glutamine is very important for the growth and proliferation of tumor cells, and its deficiency leads to apoptosis. Combining an intratumoral application of MBTA therapy with systemic intraperitoneal application of glutamine antagonist 6-diazo-5-oxo-L-norleucine (DON) (immunometabolic therapy) resulted in a complete elimination of advanced (140.8 ± 46.8 mm^3) Panc02 tumor in 50% of mice. In the case of the bilateral Panc02 model, growth reduction of both tumors and prolonged survival rate was observed. MBTA vaccination (subcutaneously applied dead Panc02 cell suspended in MBTA solution) combined with intraperitoneal application of DON improve the efficacy of treatment of distal tumors. Appropriate timing of immunometabolic therapy was also studied and the best results were obtained with intraperitoneal application of DON once a week. More frequent application was too aggressive which led to several side effects and eventually resulted in the death of mice.

[1] V. Caisova, O. Uher, P. Nedbalova et al., Effective cancer immunotherapy based on combination of TLR agonists with stimulation of phagocytosis, International Immunopharmacology **59**, 86-96 (2018).

[2] V. Caisova, L. Li, G. Gupta et al. The Significant Reduction or Complete Eradication of Subcutaneous and Metastatic Lesions in a Pheochromocytoma Mouse Model after Immunotherapy Using Mannan-BAM, TLR Ligands, and Anti-CD40, *Cancers* **11**, 654 (2019).

FRACTIONATION OF CHOKEBERRY POMACE LIPIDS BY SUPERCRITICAL CARBON DIOXIDE EXTRACTION

Laura Tamkutė, Audrius Pukalskas, Petras Rimantas Venskutonis

Department of Food Science and Technology, Kaunas University of Technology, Lithuania
laura.tamkute@gmail.com

Black chokeberries have a strong mouth-drying effect, for this reason, most of times these berries are used to make jams, juices, purées, jellies, syrups, teas or wines [1]. Pressing juices of these berries generates large amounts of pomace, which usually is discarded or used very inefficiently. For this reason, is very urgent to find a way how to recover high added value bioactives. It is well known that chokeberries are characterized by strong antioxidant properties due to high content of polyphenolic compounds, whereas its pomace is also rich in bioactives, especially anthocyanins, procyanidins, flavonols and phenolic acids; although these pomaces are a good source of lipophilic compounds such as fatty acids, triacylglycerols, tocopherols etc [2]. The aim of this study was to evaluate the possibilities of fractionation of the chokeberry pomace lipophilic fraction during supercritical fluid extraction with carbon dioxide (SFE-CO_2) with or without co-solvent ethanol (5%) in two post-extraction separators by changing the temperature in the range of subcritical CO_2 level at a constant pressure and to characterize the composition of the obtained fractions. SFE with pure CO_2 gave a 14% lower yield, while the addition of 5% co-solvent EtOH increased the yield. In the case of SFE with pure supercritical CO_2 the highest amount of the total extract was collected in first separator (1S), the remaining in second separator (2S). In the case of SFE with supercritical CO_2 and 5% EtOH, the effects of separation were not so negligible; although almost in all cases higher yields were detected in second separator. The antioxidant capacity of extracts and fractions was measured by using an L-ORAC assay which measures the peroxyl radical scavenging capacity of antioxidants which may donate a hydrogen atom. First of all, it may be noted that the ORAC values of lipophilic extracts obtained in first separator by pure supercritical CO_2 and 5% co-solvent EtOH were 2 folds higher than those of extracts obtained by supercritical CO_2. While in second separator antioxidant capacity was quite similar in both cases. Highly unsaturated TAGs were majorly found in the extracts and fractions. The LLLn constituted 23.26–24.18%, OLnL 20.35–22.10%, LLnLn 13.20–15.10% and OLL 10.02–12.06%. Four tocopherols (sometimes also called E-vitamers) and 4 phytosterols were preliminarily quantified by their peak areas in the extracts and fractions. It may be observed that, in the case of pure supercritical CO_2, the concentration of tocopherols was higher in second separator, while the content of phytosterols was slightly higher in first. The addition of co-solvent 5% EtOH increased the concentration of these compounds in second separator. It might be concluded that, by modifying the supercritical extraction solvent and changing the parameters of the system separators, it is possible to produce fractions of lipophilic substances of various compositions

[1] V. Kitryte, V. Kraujaliene, V. Sulniute, A. Pukalskas, P.R. Venskutonis, Chokeberry pomace valorization into food ingredients by enzyme-assisted extraction: Process optimization and product characterization. Food and Bioproducts Processing **105**, 36-50 (2017).

[2] A. Sidor and A. Gramza-Michałowska, Black chokeberry *Aronia Melanocarpa* L.—A qualitative composition, phenolic profile and antioxidant potential, Molecules **24(20)**, 3710 (2019).

UNSUPERVISED NAMING OF CHEMICAL COMPOUNDS

Miglė Urbonaitė[1], Andrius Merkys[2]

[1] Department of Mathematical Computer Science, Vilnius University, Lithuania
[2] Institute of Biotechnology, Life Sciences Center, Vilnius University, Lithuania
migle.urbonaite@mif.stud.vu.lt

The chemical diversity that already exists in the world is surprisingly extensive, and over time it is only expanding. Today, according to the CAS registry, almost 200 million chemicals and chemical compounds are registered for production and use. The natural problem that occurs is the identification of all these chemical compounds. Without unique names, the ability to unambiguously describe chemicals in literature, databases, and spoken language is lost.

However, identification by numbers or other index-based synthetic codes, although always unique, is not always convenient because without the index it says nothing about the compound or its properties [1]. In the chemical world, this problem is solved by nomenclatures. They describe the rules by which molecules are unambiguously named and the original molecules can be unambiguously reconstructed from these names [2]. One of the most popular and widely used is the IUPAC nomenclature. When using the nomenclature, it is very important that the name formed is unique and has an unambiguous relationship with the compound, as the chemical compounds may be very similar but have completely opposite properties (a well-known example is the stereochemistry of drug Thalidomide that caused birth defects). Thus, it is very important for the name to reflect each and every property of the compound. This is one of the research subjects of the field of cheminformatics [3]. Using chemical molecular graphs and graph theory algorithms, software packages, which can cover a large set of nomenclature rules and create unambiguous and correct names for chemical compounds, are created.

Here we report the development of ChemOnomatopist [4], a free and open source software package to name chemical compounds according to the IUPAC nomenclature. Our method employs graph algorithms to implement IUPAC nomenclature rules, as opposed to database or machine-learned model-based tools like STOUT [5]. ChemOnomatopist is able to read SMILES linear notation and output IUPAC names without supervision, opening a possibility to process large volumes of chemical data.

[1] J.-L. Faulon, D. P. Visco Jr and D. Roe, Enumerating molecules. Reviews in Computational Chemistry **21**, 209-286 (2005).
[2] A. J. Williams and A. Yerin, Automated systematic nomenclature generation for organic compounds, Wiley Interdisciplinary Reviews: Computational Molecular Science **3.2**, 150-160 (2013).
[3] T. Engel, Basic overview of chemoinformatics, Journal of chemical information and modeling **46.6**, 2267-2277 (2006).
[4] A. Merkys. https://github.com/merkys/ChemOnomatopist
[5] K. Rajan, A. Zielesny and C. Steinbeck, STOUT: SMILES to IUPAC names using neural machine translation, Journal of Cheminformatics **13**, 34 (2021). https://doi.org/10.1186/s13321-021-00512-4

X AND Y TYPE ZEOLITES IN ZINC FORM AS CARIERS FOR 6 - MERCAPTOPURINE

Marcel Jakubowski, Mariusz Sandomierski, Adam Voelkel

Institute of Chemical Technology and Engineering, Poznan University of Technology, Poland
marcel.jakubowski@student.put.poznan.pl

6-Mercaptopurine (6MP) is a drug with a different spectrum of activity. In small doses it has an anti-inflammatory effect, in higher doses it is immunosuppressive, and in the largest doses it is cytotoxic [1, 2]. This drug is used mainly in the treatment of blood cancers especially Acute Lymphoblastic Leukemia, but also in diseases such as rheumatoid arthritis, Crohn's disease, inflammatory bowel disease, systemic lupus erythematosus [3, 4, 5, 6].

The main limiting reason for the use of this drug is its poor bioavailability, which is ranges from 10% to 50%, averaging around 16%. This is because 6MP is characterized by poor water solubility (0.170 μg / ml) and a short half-life in the body. The short half-life is due to the rapid renal clearance of the compound. [1, 2, 7, 8]

One way to overcome drug delivery problems is to use carriers that release the drug in a controlled manner. Creating such carriers is a pioneering direction of science that requires a multidisciplinary approach. Current 6MP carriers are based on the creation of a disulfide bond between the carrier and the drug that is released by glutathione (GSH), sufficient amounts of which must be present in the cell to release the drug [9, 10]. Therefore, a 6MP carrier should be created, which will release the drug under the influence of body fluids. It should also release the drug gradually and be biocompatible.

In our work, for the first time, we have developed a mercaptopurine delivery system using two types of zinc zeolites.

The prepared materials were characterized by a number of research techniques. All techniques confirmed the effective ion exchange in zeolites, as well as the sorption of the drug on the surface of the prepared carriers. Drug sorption studies have shown that zeolite Y retains more drug than zeolite X. Release studies performed in simulated body fluid (SBF), suggested that the drug was retained on the surface of the carriers by coordination bonds. Such bonds can be formed because 6MP has nitrogen and sulfur atoms in its structure, which have lone electron pairs capable of this type of bonds [11]. This is indicated by a gradual release of 6MP with no visible initial burst release. During the first 10 hours, both carriers released approximately 30% of retained drug. After this time, the release from the zeolite Y accelerated. This may be due to clogging of the pores in zeolite X, which are smaller than in zeolite Y. Both zeolites X and Y released large amount of drug. In our opinion this material can be used as an effective carrier for 6-mercaptopurine.

[1] M. Zacchigna, F. Cateni, G. Di Luca, S. Drioli, A simple method for the preparation of PEG-6-mercaptopurine for oral administration, Bioorganic & Medicinal Chemistry Letters, 17(23) (2007) 6607-6609.
[2] JE. Polifka, JM. Friedman, Teratogen update: azathioprine and 6-mercaptopurine, Teratology, 65(5) (2002) 240-261.
[3] J. P.M. Bökkerink, E. H. Stet, R. A. De Abreu, F. J.M. Damen, T. W. Hulscher, M. A.H. Bakker, J. A. Van Baal, 6-Mercaptopurine: Cytotoxicity and biochemical pharmacology in human malignant T-lymphoblasts, Biochemical Pharmacology, 45(7) (1993) 1455-1463.
[4] S. Bhatia, W. Landier, M. Shangguan, L. Hageman, A.N. Schaible, A.R. Carter, C.L. Hanby, W. Leisenring, Y. Yasui, N.M. Kornegay, L. Mascarenhas, A.K. Ritchey, J.N. Casillas, D.S. Dickens, J. Meza, W.L. Carroll, M.V. Relling, F.L. Wong, Nonadherence to oral mercaptopurine and risk of relapse in Hispanic and non-Hispanic white children with acute lymphoblastic leukemia: a report from the children's oncology group, Journal of clinical oncology , 30(17) (2012) 2094–2101.
[5] O. H. Nielsen,B. Vainer,J. Rask-Madsen, The treatment of inflammatory bowel disease with 6-mercaptopurine or azathioprine, Alimentary Pharmacology & Therapeutics, 15 (2001) 1699-1708.
[6]S. Sahasranaman, D. Howard, S. Roy, Clinical pharmacology and pharmacogenetics of thiopurines, Eur J Clin Pharmacol 64 (2008) 753–767.
[7] J.-R. Wang, X. Yu, C. Zhou, Y. Lin, C. Chen, G.Pan, X. Mei, Improving the dissolution and bioavailability of 6-mercaptopurine via co-crystallization with isonicotinamide, Bioorganic & Medicinal Chemistry Letters, 25(5) (2015) 1036-1039.
[8] P. Podsiadlo, V. A. Sinani, J. H. Bahng, N. W. S. Kam, J. Lee, N. A. Kotov, Gold Nanoparticles Enhance the Anti-Leukemia Action of a 6-Mercaptopurine Chemotherapeutic Agent, Langmuir 24(2) (2008) 568–574.
[9] M. Prabaharan, J. F. Mano, Chitosan-Based Particles as Controlled Drug Delivery Systems, Drug Delivery, 12(1) (2004) 41-57.
[10] M.Gong, J. Yang, Y. Li , J. Gu, Glutathione-responsive nanoscale MOFs for effective intracellular delivery of the anticancer drug 6-mercaptopurine, Chem. Commun., 56 (2020) 6448-6451.
[11] A. A. Sharfalddin, A-H. Emwas, M. Jaremko, M. A. Hussien, Transition metal complexes of 6-mercaptopurine: Characterization, Theoretical calculation, DNA-Binding, molecular docking, and anticancer activity, Appl Organomet Chem, 35 (2021) 6041.

SYNTHESIS AND ANALYSIS OF GRAPHITE INTERCALATION COMPOUND GRAPHITE BISULFATE

Gintarė Rimkutė[1], Mantvydas Gudaitis[1], Jurgis Barkauskas[1], Justina Gaidukevič[1], Gediminas Niaura[2]

[1] Faculty of Chemistry and Geosciences, Vilnius University, Lithuania
[2] Center for Physical Sciences and Technology (FTMC), Lithuania
gintare.rimkute@chgf.vu.lt

A special group of compounds known as graphite intercalation compounds (GICs) is formed when different atomic, molecular, or ionic species interpose between the layers in a graphite material. Of the various intercalation compounds, GICs have gained particular interest due to their comparatively high degree of structural order [1]. This structural order in GICs leads to a staging phenomenon that is described by intercalate layers that are periodically arranged in a graphite structure. Depending on the number of graphite layers between the intercalate layers, GICs are thus classified by a stage index. Hence, stage 1 GIC has one graphene layer in the midst of two layers of intercalant, stage 2 GIC has two graphene layers between the two layers of intercalant and so on [2].

Because of their unique properties, GICs have a wide range of applications. These compounds can be used as superconducting and anode materials, heterogeneous catalysts, in pyrophoric stabilization of reactants and in production of graphite-based dual-ion batteries – an environmentally friendly alternative for energy storage [1, 3]. Another relevant area, where GICs play a key role, is the production of graphene and graphene oxide. GIC known as graphite bisulfate (GBS), forms as an intermediate in the process of the preparation of graphene oxide, which is widely used for the further production of graphene [4]. However, chemical synthesis of graphene, starting with the intercalation of graphite, usually leads to a ruptured carbon lattice and defective final product. In order to improve the quality of the synthesized graphene, a more detailed understanding of the synthesis mechanism is needed. Thereby, one of the key factors for obtaining high quality graphene is the proper formation of GBS intermediate product [5]. The GBS stage number and kinetics of its formation strongly depends on graphite precursor, experimental conditions and especially the type of oxidizing agent used in the reaction mixture, therefore it is important to investigate as many different synthesis variations as possible [6].

The purpose of this work was to characterize and compare GBS compounds obtained using three different oxidizers. In particular, ammonium persulfate, potassium persulfate and chromium trioxide were used in the chemical synthesis as the oxidizing agents. The procedure of GBS synthesis was repeated with all three oxidizing agents additionally adding phosphorus pentoxide as water binding agent. Moreover, all GICs were heat treated at 800 °C. Obtained samples were characterized using optical microscopy, Raman spectroscopy, X-ray powder diffraction (XRD) and scanning electron microscopy (SEM).

The process of GBS formation was observed using all three oxidizing agents. However, highest intercalation degree was reached using ammonium persulfate and potassium persulfate oxidizers. Meantime, using chromium trioxide resulted in much higher concentration of defects, largest interplanar distances (0.337 nm) and smallest crystallite sizes (7.34 nm). After annealing, structure of the samples mostly returned to the graphite structure. Our study has shown that GBS compounds obtained using all three oxidizing agents can be successfully used for the production of graphene oxide and graphene.

[1] K. Tasaki, Density functional theory study on structural and energetic characteristics of graphite intercalation compounds, Journal of Physical Chemistry C **118**, 1443–1450 (2014).
[2] M.S. Dresselhaus, G. Dresselhaus, Intercalation compounds of graphite, Advances in Physics **51**, 1–186 (2002).
[3] W. Zhou, P.H.L. Sit, First-Principles Understanding of the Staging Properties of the Graphite Intercalation Compounds towards Dual-Ion Battery Applications, ACS Omega **5**, 18289–18300 (2020).
[4] C. Li, Y. Shi, X. Chen, D. He, L. Shen, N. Bao, Controlled synthesis of graphite oxide: Formation process, oxidation kinetics, and optimized conditions, Chemical Engineering Science **176**, 319–328 (2018).
[5] S. Seiler, C.E. Halbig, F. Grote, P. Rietsch, F. Börrnert, U. Kaiser, B. Meyer, S. Eigler, Effect of friction on oxidative graphite intercalation and high-quality graphene formation, Nature Communications **9**, 1–9 (2018).
[6] M. Salvatore, G. Carotenuto, S. de Nicola, C. Camerlingo, V. Ambrogi, C. Carfagna, Synthesis and Characterization of Highly Intercalated Graphite Bisulfate, Nanoscale Research Letters **12** (2017).

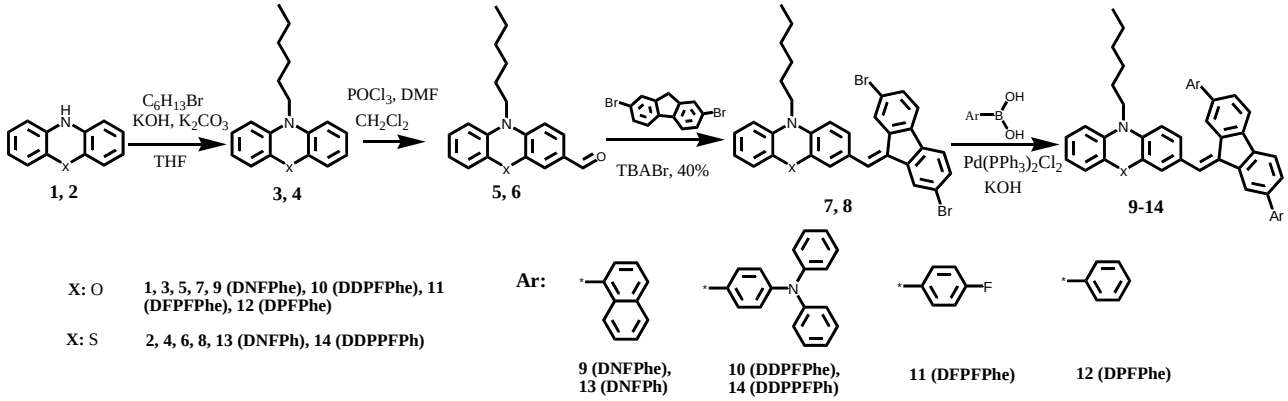
NEW PHENOTHIAZINE AND PHENOXAZINE SUBSTITUED FLUORENE CORED HOLE TRANSPORTING MATERIALS FOR HIGH-EFFICIENCY OLEDS

Raminta Beresneviciute[1], Mangey Ram Nagar[2], Abhijeet Choudhury[2], Daiva Tavgeniene[1], Dovydas Blazevicius[1], Vygintas Jankauskas[3], Krishar Kumar[4], Subrata Banik[5], Subrata Ghosh[4], Greta Jacunskaite[1], Saulius Grigalevicius[1], Jwo-Huei Jou[2]

[1] Department of Polymer Chemistry and Technology, Kaunas University of Technology, Lithuania
[2] Department of Materials Science and Engineering, National Tsing Hua University, Taiwan
[3]Institute of Chemical Physics, Vilnius University, Lithuania
[4]School of Basic Sciences, Indian Institute of Technology Mandi, India
[5]Department of Chemistry, School of Chemical and Biotechnology, SASTRA Deemed University, India
raminta.beresneviciute@ktu.edu

Organic light-emitting diode (OLED) technology has become the backbone of display technology after undergoing rapid adoption by major technological companies such as Apple, Samsung and Google [1]. It is expected to be the mainstay technology of the display industry until at least the next decade [2]. OLED technology is also increasing its presence in the lighting industry with applications in a diverse field from lighting panels to being used as high-end automotive taillights [3].

Nanotextured small molecule hole-transporting materials (HTMs) with high hole-mobility and effective triplet-energy are crucial to realize low-cost manufacturing of high-efficiency and large-area organic light emitting diodes for next-generation lightings and displays. In this study, a novel series of phenothiazine and phenoxazine substituted fluorene core-based hole transporting materials were synthesized and characterized. The synthesis of electroactive compounds (**9-14**) is shown in Scheme 1.



Scheme 1. Synthesis of electroactive compounds **9-14**.

All synthesized compounds were incorporated in solution-processed phosphorescent and thermally activated delayed fluorescence (TADF) OLEDs. Materials exhibit superior solubility in organic solvents and display nanotextured surface morphologies. These HTMs possess high hole-mobilities as compared to inventional hole transporting material NPB. By incorporating phosphorescent PO-01 yellow emitter, we demonstrate an improvement maximum power efficiency (PE_{max}) from 41,6 to 45,4 lm/W, current efficiency (CE_{max}) from 39,8 to 50,6 cd/A, external-quantum efficiency (EQE_{max}) from 12,9 to 19,6 %, maximum brightness (L_{max}) from 15200 to 19400 cdm^{-2}, and a lifetime (LT_{50}) from 151 to 465 hr at 1000 cdm^{-2} initial luminance of phosphorent OLED by substituting the conventional HTM, NPB with the compound **14**. Additionally, 4CzIPN green TADF emitter-based OLED displays the enhancement in PE_{max} from 42,5 to 69,1 lm/W, CE_{max} from 54,1 to 78,0 cd/A, EQE_{max} from 20,1 to 27,2 %, L_{max} from 12900 to 44200 cdm^{-2} and LT50 from 195 to 590 hr at initial brightness of 1000 cdm^{-2} by replacing NPB with the compound **14**. Based on these findings, the reported solution-processable HTMs appear to be promising candidates for high-efficiency OLEDs.

[1] G. Hong, X. Can, C. Leonhardt, Z. Zhang, J. Seibert, J. M. Busch and S. Bräse. A Brief History of OLEDs – Emitter Development and Industry Milestones. Adv. Mater., 2021, 33, 2005630.
[2] L. Zeng, E. Sun, J. Huang, Z. Wang and S. Liu. Developing High-Performance OLED Materials with Diverse Properties for Various Display Makers. SID Symp. Dig. Tech. Pap., 2021, 52, 652-654.
[3] J.-H. Jou, C,-Y. Hsiesh, J.-R. Tseng, S.-H. Peng, Y.-C. Jou, J. H. Hong, S.-M. Shen, M.-C. Tang, P.-C. Chen and C.-H. Lin. Candle Light-Style Organic Light-Emitting Diodes. Adv. Funct. Mater., 2013,23, 2750-2757.

THE EFFECT OF ANNEALING CONDITIONS ON Ca/P RATIO AND PHASE TRANSFORMATIONS IN BULK CALCIUM PHOSPHATES

Diana Griesiute[1,*], Erlandas Kabasinskas[1], Eva Raudonyte-Svirbutaviciene[1,2], Gabriele Klydziute[1], Aivaras Kareiva[1], Aleksej Zarkov[1]

[1] Institute of Chemistry, Vilnius University, Naugarduko 24, LT-03225 Vilnius, Lithuania
[2] Institute of Geology and Geography, SRI Nature Research Centre, Akademijos Str. 2, LT6 08412 Vilnius, Lithuania
[*]diana.griesiute@chgf.vu.lt

Calcium phosphates (CPs) are inorganic materials widely used in bone regeneration due to their structural and compositional similarity to natural bone [1]. Compositional and structural variety of CPs leads to their different physicochemical, mechanical and biological properties, which allows to apply these materials in medicine in various forms from cements to ceramics and coatings. One of the parameters, based on which CPs can be classified, is Ca/P ratio in these materials. Some CPs phases can be prepared using precipitation reactions from aqueous solutions, but some of them can be prepared only employing a thermal treatment [2]. The present work is inspired by the recent study by Döbelin et al. [3] who demonstrated the change of surface phase composition of different CPs pellets after annealing. The authors showed that thermal treatment leads to the selective evaporation of phosphates from the surface layer and the formation of secondary CPs phases with higher Ca-to-P ratio and even CaO. The thickness and composition of the phosphate-depleted surface layer was found to be dependent on the annealing parameters, but the aforementioned work studied the effects of annealing in air atmosphere only. The main aim of our study was to expand these results and to investigate the influence of different annealing conditions on phase transformations and composition of bulk materials.

In the present work, synthetic brushite ($CaHPO_4 \cdot 2H_2O$) with Ca-to-P ratio 1:1 was taken as a starting material and annealed at 1200 °C for different periods of time under three different conditions: in a static air atmosphere, in nitrogen flow and in vacuum. The purity and phase composition of powders were evaluated by powder X-ray diffraction (XRD) and Fourier-transform infrared spectroscopy (FTIR). Phase quantities were determined by Rietveld refinement using the FullProf suite. Scanning electron microscopy (SEM) was used for the characterization of morphological features of synthesized products.

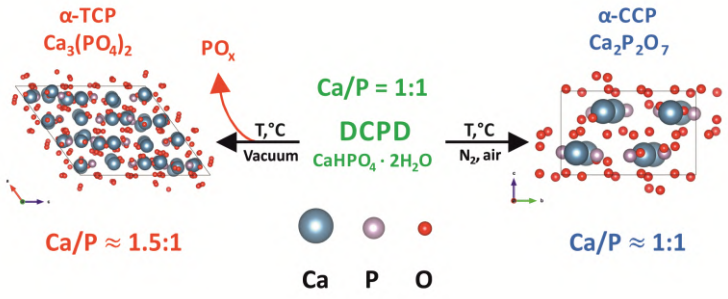


Fig. 1. Scheme summarizing results.

It was demonstrated that the phase composition and Ca/P ratio in the final product highly depend on the annealing conditions due to the evaporation of phosphate species. Annealing in air did not result in significant changes in Ca/P ratio, α-$Ca_2P_2O_7$ was obtained as a major phase with a minor α-$Ca_3(PO_4)_2$ phase. Similar phase composition was obtained after the heat treatment in nitrogen flow. The most drastic changes in stoichiometry and phase composition were obtained after annealing in vacuum. The resulting powders consisted mostly of α-$Ca_3(PO_4)_2$ with a negligible amount of α-$Ca_2P_2O_7$ as a secondary phase, which suggests a remarkable change in Ca/P ratio up to approximately 1.5:1. The evaporation of phosphate species from the bulk powders occurred exclusively from α-$Ca_2P_2O_7$, no obvious degradation of α-$Ca_3(PO_4)_2$ was observed under the selected conditions.

[1] Habraken, W., et al., *Calcium phosphates in biomedical applications: materials for the future?* Materials Today, 2016. **19**(2): p. 69-87.
[2] Dorozhkin, S.V. and M. Epple, *Biological and medical significance of calcium phosphates.* Angewandte Chemie International Edition, 2002. **41**(17): p. 3130-3146.
[3] Döbelin, N., et al., *A thermodynamic approach to surface modification of calcium phosphate implants by phosphate evaporation and condensation.* Journal of the European Ceramic Society, 2020. **40**(15): p. 6095-6106.

ADSORPTION MECHANISM OF CAESIUM AND COBALT ON MUSCOVITE MICA CLAY-GRAPHENE OXIDE-γ-Fe_2O_3/Fe_3O_4 COMPOSITE

Raman Novikau[1], Galina Lujanienė[1*]

[1] Department of Environmental Research, State research institute Center for Physical Sciences and Technology, Lithuania
raman.novikau@ftmc.lt

Technogenic disasters and the accidental release of radioactive waste are sources of radionuclide contamination, and the issue of radionuclide remediation remains open to this day [1–4]. Among the numerous technologies for radionuclide removal, adsorption and ion exchange technologies have proven to be the most effective and cost-efficient in environmental applications [5]. Clays and their minerals, as well as their modifications and treated forms, are among the best adsorbents due to their high efficiency, availability, and low toxicity, and are economically feasible [6, 7].

The clay-graphene oxide-γ-Fe_2O_3/Fe_3O_4 composite was prepared by ultrasonic treatment and subsequent mixing of the components in an argon flow at 60 ºC. The components of the composite were prepared in advance. Graphene oxide was obtained by the improved Hummers' method and γ-Fe_2O_3/Fe_3O_4 by a co-precipitation reaction of ferrous and ferric ions. Muscovite mica clay was obtained from industrial exploitation site Šaltiškiai, North Lithuania. The adsorption tests included the determination of the dependence of adsorption on the concentration of caesium and cobalt ions, the mass of adsorbent, pH, time and temperature. Based on the obtained experimental data, adsorption isotherms (Langmuir, Freundlich, Temkin and Dubinin-Radushkevich), pseudo-first, pseudo-second order kinetic models, and the Weber-Morris model of intraparticle diffusion, as well as thermodynamic parameters (Gibbs free energy (ΔG), enthalpy (ΔH) and entropy (ΔS)), were calculated. The data obtained from the calculations of the above isotherms, kinetic models and thermodynamic parameters allow us to talk about the features of the adsorption behaviour of caesium and cobalt on this composite.

Thus, adsorption occurred spontaneously, endothermically and favourably on a heterogeneous surface with minimal interaction between adsorbed atoms and was controlled by film diffusion in the case of caesium and by a mixed type – intraparticle and film diffusion in the case of cobalt. The mechanism of adsorption is physical in terms of the parameters E (kJ/mol) and ΔH (kJ/mol). However, according to the values of the parameters $1/n$ (The Freundlich constant, which refers to the heterogeneity of the adsorption surface) and BT (j/mol) and according to the pseudo-second order kinetic model, it is chemical adsorption. We assume that the adsorption of caesium and cobalt on clay-graphene oxide-γ-Fe_2O_3/Fe_3O_4 has a mixed mechanism involving both physical and chemical interactions, due to the complexity of the composite matrix.

[1] IAEA (International Atomic Energy Agency), 2006. Environmental Consequences of the Chernobyl Accident and Their Remediation: Twenty Years of Experience. Report of the Chernobyl Forum Expert Group 'Environment'. International Atomic Energy Agency Vienna, Austria.

[2] Sahoo, S.K., Kavasi, N., Sorimachi, A., Arae, H., Tokonami, S., Mietelski, J.W., Lokas, E., Yoshida, S. Strontium-90 activity concentration in soil samples from the exclusion zone of the Fukushima daiichi nuclear power plant. Sci. Rep. **6**, 1–10 (2016).

[3] Maksoud, M. A., Sami, N. M., Hassan, H. S., Bekhit, M., & Ashour, A. H. Novel adsorbent based on carbon-modified zirconia/spinel ferrite nanostructures: evaluation for the removal of cobalt and europium radionuclides from aqueous solutions. Journal of Colloid and Interface Science, **607**, 111-124 (2022).

[4] Ibrahim, A. B., Abass, M. R., El-Masry, E. H., & Abou-Mesalam, M. M. Gamma radiation-induced polymerization of polyacrylic acid-dolomite composite and applications for removal of cesium, cobalt, and zirconium from aqueous solutions. Applied Radiation and Isotopes, **178**, 109956 (2021).

[5] S. Yang, N. Okada, M. Nagatsu The highly effective removal of Cs^+ by low turbidity chitosan-grafted magnetic bentonite J. Hazard. Mater, **301**, 8-16 (2016).

[6] Luo, W., Huang, Q., Antwi, P., Guo, B., & Sasaki, K. Synergistic effect of ClO_4^- and Sr^{2+} adsorption on alginate-encapsulated organo-montmorillonite beads: Implication for radionuclide immobilization. Journal of colloid and interface science, **560**, 338-348 (2020).

[7] Jang, J., & Lee, D. S. Magnetite nanoparticles supported on organically modified montmorillonite for adsorptive removal of iodide from aqueous solution: Optimization using response surface methodology. Science of the Total Environment, **615**, 549-557 (2018).

SYNTHESIS AND PROPERTIES OF QUINOXALINE-BASED COMPOUNDS FOR OPTOELECTRONIC APPLICATIONS

Lukas Dvylys, Rasa Keruckiene, Juozas Vidas Grazulevicius

Department of Polymer Chemistry and Technology, Kaunas University of Technology, Lithuania
lukas.dvylys@ktu.edu

Organic light emitting diodes (OLEDs) based on thermally activated delayed fluorescence (TADF) materials without any noble metals are raising ever-increasing interest due to their potential in achieving 100% internal quantum efficiency (IQE) in theory via efficient up-conversion from non-radiative triplet (T1) to radiative singlet (S1) [1]. Efficient blue and green TADF emitters have been developed and the resulting OLEDs have achieved an external quantum efficiency (EQE) of over 20%. However, it is inherently difficult to design efficient long-wavelength TADF emitters, such as red or near-infrared (NIR) emitters, due to the contradiction between small singlet–triplet energy splitting and a high fluorescence radiative rate (k_{Sr}) [2]. Another reason is that the overlap of vibration coupling between ground state and excited state will increase with decreasing of energy gap and thereby decreases the photoluminescence quantum yields (PLQYs) of the emitters according to the energy gap law [1]. To obtain NIR emission and to narrow the optical bandgap two kinds of molecular design strategies are generally employed. One is to extend the π-conjugation of chromophores, but it ultimately converges to a limited redshift for NIR emission, as well as the increased difficulty of synthesis, purification, and device fabrication. The other way is to construct NIR chromophores using donor-acceptor (D–A) molecular architecture, which is a class of promising NIR materials for NIR OLED applications, due to very wide band gap tunable range of the emissive state with charge transfer characteristics, along with ambipolar charge transport and easy device fabrication by vacuum evaporation [3].

During recent years, there has been an increasing interest in quinoxaline and its derivatives implemented as building blocks of π-conjugated compounds for use in multiple optoelectronic and photovoltaic applications. This is mainly due to its unique properties for efficient light emission and absorption, high charge carrier mobility and broad possibilities for color-tuning. These properties can be modified by selecting the appropriate structure of the π-conjugated system and by introducing different side substituents including alkyl chains, aromatic rings and other functional groups. Quinoxaline itself is commonly used as an electron acceptor unit (A), which, being combined with different electron donor blocks (D), makes up for D-A type systems [4]. Quinoxaline has a weak electron withdrawing character. However, by fusing two weak electron-withdrawing units into one molecule, a strong π-accepting unit can be made to strengthen the acceptor capacity [1].

Frequently used electron donors are phenothiazine, phenoxazine, acridine, carbazole and their derivatives [5]. Phenothiazine and phenoxazine are strong electron donors, which give red emission [6]. Meanwhile acridine and carbazole are weaker donors and usually give blue emission, but their properties can be heavily modified by introducing various side alkyl- chains [5].

In this work, four D-A type compounds were synthesized, which consists of two electron withdrawing groups (quinoxaline and cyano) and various electron donors, such as phenothiazine, phenoxazine, dimethyldihydroacridine, and carbazole derivatives. Their thermal, electrochemical, and photophysical properties will be reported.

[1] LIANG, J., et al. Rational Design of Efficient Orange-Red to Red Thermally Activated Delayed Fluorescence Emitters for OLEDs with External Quantum Efficiency up to 26.0% and Reduced Efficiency Roll-off. J. Mater. Chem. C, 2020,8, 1614-1622.

[2] YU, L., et al. Achieving a balance between small singlet–triplet energy splitting and high fluorescence radiative rate in a quinoxaline-based orange-red thermally activated delayed fluorescence emitter. Chem. Commun., 2016, 52, 11012.

[3] WANG, C., et. al. Efficient Near-Infrared (NIR) Organic Light-Emitting Diodes Based on Donor–Acceptor Architecture: An Improved Emissive State from Mixing to Hybridization. Adv. Optical Mater. 2017, 5, 1700441.

[4] LEDWON, P., et. al. The effect of molecular structure on the properties of quinoxaline-based molecules for OLED applications. Dyes and Pigments, 173 (2020) 108008.

[5] DIAS, F. B., PENFOLD, T. J., and MONKMAN, A. P. Photophysics of thermally activated delayed fluorescence molecules. Methods and Applications in Fluorescence, IOPsience, 2017, vol. 5(1), 012001.

[6] GANESAN, P., et al. Methoxy Substituents Activated Carbazole-Based Boron Dimesityl TADF Emitters. Journal of Materials Chemistry C, Royal Society of Chemistry, 2020, vol. 8, 4780-4788.

CONCENTRATIONS OF AIRBORNE PM_{10} AND LEAD IN MAJOR BUS TERMINALS OF LAHORE AND PESHAWAR, PAKISTAN

Abdullah Khan[1], Muhammad Afzaal[2], Steigvilė Byčenkienė[1], Touqeer Gill[1], and Muhammad Bilal[3]

[1] Center for Physical Sciences and Technology, Vilnius 10257, Lithuania
[2]Sustainable Development Study Centre, Government College University, Lahore 54000, Pakistan
[3]Department of Environmental Sciences, University of Peshawar, Peshawar 25120 Pakistan
abdullah.khan@ftmc.lt

Air pollution is caused by various anthropogenic activities, i.e., industrial emergence, urbanization, forest burning, and vehicular exhausts, posing a serious threat to human health and the environment [1]. This research project is composed of the basic research analysis related to the air pollution in the specific bus terminals in the study areas of Peshawar and Lahore (Pakistan). Particulate matter (PM) is one of the major air pollutants, whose concentration is exceeding the World Health Organization (WHO) guidelines values and National Environmental Quality Standards (NEQs) values throughout the major cities of Pakistan [2]. A high-volume Reference Ambient Air Sampler (F&J) based on 24-h duration was used to collect the PM_{10} samples (n=96) on glass fiber filter paper. Furthermore, the collected samples were analyzed for the concentrations of lead (Pb) bound to the PM_{10} (PM with a diameter of 10 microns or less). For this purpose, the analysis was conducted via an Atomic absorption spectrometer (Perkin Elmer, AAS-PEA-700). The sampling period was divided into two seasons, i.e., summer from June to August (2019) and winter season from November to January (2019-20), respectively. The mean concentrations of PM_{10} in the Peshawar section of Haji camp bus terminal and Kohat bus terminal were 413 $\mu g/m^3$ and 396.3 $\mu g/m^3$ in summer whereas, in the winter season concentration were 492.5 $\mu g/m^3$ and 468.5 $\mu g/m^3$.Similarly, the mean PM_{10} concentrations for the Section Lahore, Niazi bus terminal, and Badami Bagh bus terminal were 478.2 $\mu g/m^3$ and 531.8 $\mu g/m^3$ in summer whereas, in the winter season concentrations were 708 $\mu g/m^3$ and 784 $\mu g/m^3$, respectively. The mean concentrations of Pb in the Peshawar section study area were 532.2 ng/m^3 in Haji camp bus terminal and 489.1 ng/m^3 were in the Kohat bus terminal in the summer season, whereas, for the winter season the mean concentrations were 732.7 ng/m^3 and 692.9 ng/m^3, respectively. The mean concentration of Pb in the Lahore section of the study area were 624.9 ng/m^3 in the Niazi bus terminal and 674.9 ng/m^3 in the Badami Bagh bus terminal in the summerseason, whereas, in the winter season the mean concentrations were 837.6 ng/m^3 and 910.5 ng/m^3, respectively.

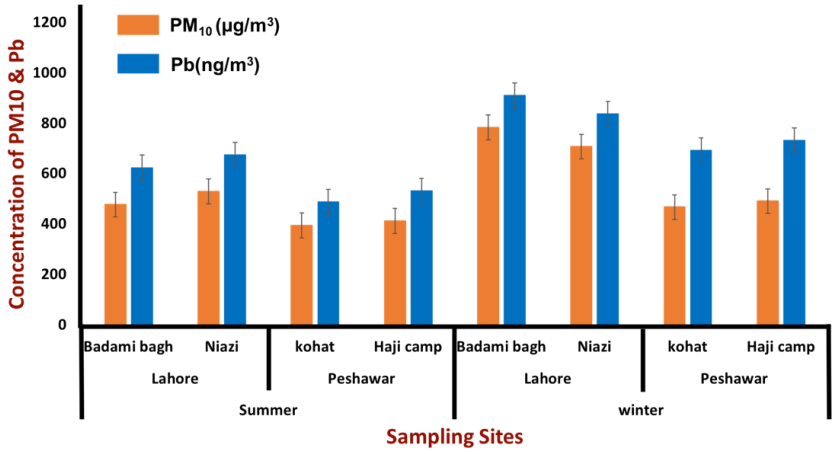


Fig. 1. Comparison of PM_{10} and Pb levels during the summer and winter season in Lahore and Peshawar.

Fig.1 indicated that the PM_{10} and Pb concentration in both the terminals of Peshawar (Haji camp terminal and Kohat terminal) and Lahore (Badami bagh terminal and Niazi Bus terminal) was lower in the summer as compared to the winter season. The analysis of correlations showed that the concentrations of PM_{10} collected at all sampling sites are positively correlated to the concentration of Pb and traffic intensity. The correlation value ranged from 0.35 to 0.96 whereas the values of correlation in the Peshawar section of the study area are a bit less positive as compared to Lahore. Furthermore, the results of Lahore as compared to Peshawar show a more positive correlation in both the summer and winter seasons. The statistical analysis of ANOVA showed a significant (0.05) difference in all the four selected study sites in both the summer and winter seasons.

[1] Popescu, F., & Ionel, I. (2010). Anthropogenic air pollution sources. *Air quality*, 1-22.
[2] Anjum, M. S., Ali, S. M., Subhani, M. A., Anwar, M. N., Nizami, A. S., Ashraf, U., & Khokhar, M. F. (2021). An emerged challenge of air pollution and ever-increasing particulate matter in Pakistan; a critical review. *Journal of Hazardous Materials*, *402*, 123943.

SYNTHESIS AND INVESTIGATION OF SELECTIVE SOLID PHASE MICROEXTRACTION SORBENT

Gerardas Laurinavičius[1], Vilius Poškus[1]

[1] Department of Analytical Chemistry, Faculty of Chemistry and Geosciences, Vilnius University, Lithuania
gerardas.laurinavicius@chgf.stud.vu.lt

Unsaturated aromatic compounds such as benzene and its derivatives and especially some unsaturated polycyclic aromatic hydrocarbons (PAHs) are known to be cancerogenic, mutagenic and genotoxic for humans and therefore are considered environmental and food contaminants. It is important to note that PAHs by themselves are not considered toxic, but their metabolites – are. The main ways that PAHs are presented in the environment are two: natural (forest fires, volcanos, oil seepage and carbonization) and anthropogenic (the combustion of fossil fuels and direct release of oil and its products). Determination of PAHs in natural waters and food is very important for public safety and usually done by either liquid chromatography (LC) or gas chromatography (GC), sometimes in combination with solid phase microextraction (SPME) [1].

In this study we decided to replicate an Ag nanoparticles (AgNP) modified silica LC column that was used for separation of benzene and various PAHs [2] with an idea that the final product could be used as a SPME sorbent in headspace extraction mode. It is well known that the AgNP modified sorbents exceeds the tendency to separate the unsaturated compounds by the number of unsaturated bonds/rings and their position. These properties is believed to be the result of AgNP tendency to form complexes with double bonds or aromatic systems [2].

A SPME sorbent was synthesized according to procedure provided in [2] with some modifications: the quartz capillary was much smaller in size and Ag reduction was performed in a formaldehyde solution for 24h. In order to have good capillary wall – sorbent bond, especially after calcination procedure, two surface activation methods E1 and E3 (provided in article [3]), in parallel with no activation were tested. In general, E1 and E3 methods are done by firstly washing capillary with NaOH solution (1 M in E1, 0.2 M in E3) for 30 min., then, washing capillary with HCl solution (0.1 M in E1, 0.2 M in E3) for 30 min., and lastly washing with stream of distilled water and acetone. Our results showed that the E1 method and no activation provided bad results with sorbent detaching from capillary walls. E3, however, provided a very good results (no sorbent flaking from capillary walls) and was chosen as main activation method for future synthesis. Synthesized SPME sorbent with capillary casing were glued on surgical needle with polyimide sealing resin to form a SPME sorbent holder and tested in headspace extraction setup with water-based solutions of various analytes: 4-methyl styrene, toluene, naphthalene and anthracene (standards were made in acetone). After extraction, sorbent was placed in an injector port of gas chromatograph coupled with mass spectrometric detector (GC – MS) and desorption was carried out for one minute. Analysis results showed that the toluene was not adsorbed by SPME sorbent – probably, because of small aromatic system it could not form a sufficient complex with AgNP that resulted no peak in a chromatogram. On the other hand, a 4-methyl styrene, which has a little bigger aromatic system than a toluene (benzene ring with a conjugated double bond) was visible in the chromatogram. Other aromatic compounds, such as naphthalene and anthracene, were also successfully extracted with SPME sorbent via headspace setup. To conclude our work, we can state that our synthesized silica SPME sorbent modified with AgNP can be used in a headspace mode to selectively extract aromatic compounds. Despite the decreasing volatility with an increasing size of aromatic system, bigger aromatic compounds, like anthracene, interact with sorbent more effectively and can be properly extracted from the headspace.

[1] G. Purcaro, S. Moret, L.S. Conte, Overview on polycyclic aromatic hydrocarbons: Occurrence, legislation and innovative determination in foods, Talanta 105, 292–305 (2013).
[2] Y. Zhu, K. Morisato, W. Li, K. Kanamori, K. Nakanishi, Synthesis of silver nanoparticles confined in hierarchically porous monolithic silica: A new function in aromatic hydrocarbon separations, ACS Appl. Mater. Interfaces 5, 2118–2125 (2013).
[3] J. Courtois, M. Szumski, E. Byström, A. Iwasiewicz, A. Shchukarev, K. Irgum, A study of surface modification and anchoring techniques used in the preparation of monolithic microcolumns in fused silica capillaries, J. Sep. Sci. 29, 14–24 (2016).

QUANTUM TUNNELING OF METHYL GROUPS IN Co^{2+}-DOPED DIMETHYLAMMONIUM ZINC FORMATE USING PULSED EPR

Gediminas Usevičius[1], Vidmantas Kalendra[1], Jūras Banys[1], Andreas Pöppl[2], Mantas Šimėnas[1]

[1] Faculty of Physics, Vilnius University, Lithuania
[2] Faculty of Physics and Earth Sciences, Leipzig University, Germany
gediminas.usevicius@ff.vu.lt

Methyl group is one of the simplest functional groups in chemistry, making it an abundant motif of organic and hybrid materials. At low temperature, methyl group acts as a quantum rotor, which exhibits quantum tunneling. Recently, for the first time, a quantum tunneling of methyl group was observed using pulsed Electron Paramagnetic Resonance (EPR) spectroscopy in Mn^{2+}-doped $[(CH_3)_2NH_2][Zn(HCOO)_3]$ (DMAZn:Mn) hybrid perovskite [1]. Despite this study, many unsolved problems remain regarding the applicability of pulsed EPR spectroscopy in observation and description of methyl group tunneling in hybrid and other materials.

In this work, we study the methyl group tunneling in Co^{2+}-doped $[(CH_3)_2NH_2][Zn(HCOO)_3$ (DMAZn:Co) hybrid perovskite by using pulsed Electron Spin Echo Envelope Modulation (ESEEM) spectroscopy. By comparing our results with DMAZn:Mn, we investigate how different paramagnetic dopants affect the rotation barrier and thus the methyl group tunneling.

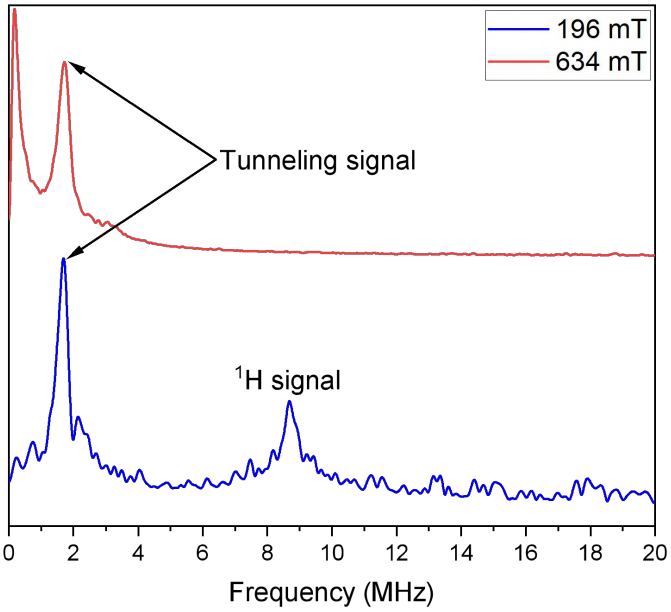


Fig. 1. Three-pulse ESEEM spectra of DMAZn:Co obtained at 193 and 634 mT at 5K. We observe a field-independent signal at 1.7 MHz, which originates from methyl group tunneling of the DMA cation.

[1] M. Šimėnas, D. Klose, M. Ptak, K. Aidas, M. Mączka, J. Banys, A. Pöppl, G. Jeschke, Magnetic excitation and readout of methyl group tunnel coherence. *Sci. Adv.* **6**, eaba1517 (2020).

RATIOMETRIC PH-RESPONSIVE ^{19}F MRI CONTRAST AGENTS BASED ON HYDRAZONE SWITCHES

Dawid Janasik[1], Krzysztof Jasiński[2], Władysław Węglarz[2], Ivan Nemec[3,4], Paweł Jewuła[3], and Tomasz Krawczyk[1]

[1] Department of Chemical Organic Technology and Petrochemistry, Silesian University of Technology, Poland
[2] Institute of Nuclear Physics Polish Academy of Sciences, Poland
[3] Central European Institute of Technology Brno University of Technology, Czech Republic
[4] Department of Inorganic Chemistry, Faculty of Science, Czech Republic
dawid.janasik@polsl.pl

MRI is a non-invasive diagnostic tool for soft tissues that uses the magnetic properties of the ^{1}H nucleus. It is one of the most widely used imaging procedures in medicine. It offers excellent spatial resolution, unlimited penetration depth and provides knowledge that cannot be accessed by other means. In order to improve the quality of the images ^{19}F MRI is extensively investigated as a complementary modality allowing so called hot spot imaging. Since ^{19}F atoms are not present in soft tissues, the modality allows for accurate representation of the targeted organ without background signals but require the introduction of an appropriate contrast agent containing ^{19}F nuclei into the organism.

Regarding the ^{19}F NMR or MRI as an aid in pH measurements several molecular probes were developed. The oldest reports concerned fluorinated aniline derivatives. The mechanism of action was based on protonation of aniline nitrogen, which changed the chemical shift of the fluorine. Other concepts utilized PEGylated nanogels containing perfluorocarbons, C_6F_6 loaded Au-fluorescent mesoporous silica nanoparticles, or copolymers. In those cases the mechanism of pH-depended signal changes was either based on the reversible volume phase transition of the nanogel structure, which releases the ^{19}F NMR signal, or the irreversible decomposition of the capsule under the influence of pH and the release of fluoroorganic groups respectively. In each case single ^{19}F signal of pH-dependent chemical shift was observed. More convenient for diagnostic purposes would be a probe displaying two separate signals of pH-dependent integrals ratio allowing internal reference and ratiometric measurements.

It occurred to us that in such role hydrazone-based molecular switches could be used. Molecular switches are usually defined as molecules that can reversibly transform between two (or more) thermodynamically stable states. It is a class of compounds sensitive to an external stimuli such as light, pH, or electric current and include classes like photochromic switches, host-guest switches, and rotaxanes. Here, we demonstrated for the first time the possibility of applying ratiometric reversible hydrazone-based molecular switches as ^{19}F NMR/MRI pH-responsive compounds that use chemical shift changes.

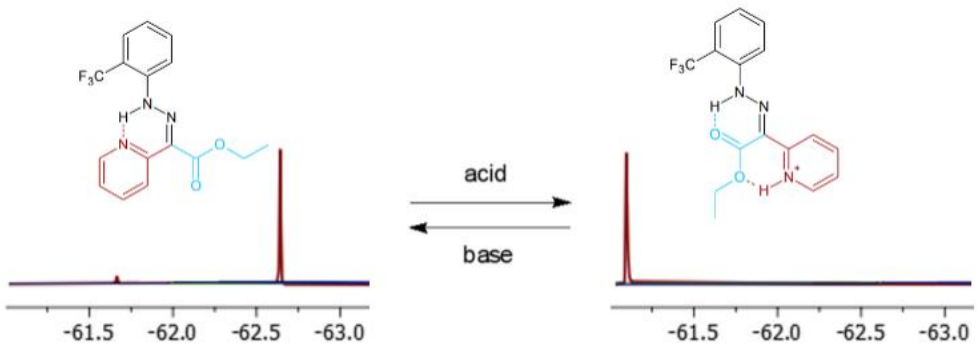


Fig. 1. Mechanism of acid-base switching.

[1] D. Janasik, T. Krawczyk, 19F MRI Probes for Multimodal Imaging, *Chem. – A Eur. J.*(2021).

ACRIDINE ORANGE DERIVATIVES TO PROMOTE MEMBRANE FUSION: MECHANISM BENEATH THE PROCESS

Víctor Galileo Almendro Vedia[1,2,3,], Marcin Makowski[2,3], Castor Salgado Soneira[5], José Osio Barcina[5], Manuel N. Melo[4] and Iván López Montero[2,3]

[1] Sección Departamental Farmacia Galénica y Tecnología Alimentaria,
Universidad Complutense de Madrid, Avda. Complutense s/n 28040 Madrid, Spain,
[2] Departamento Química Física, Universidad Complutense de Madrid, Avda. Complutense s/n 28040 Madrid, Spain,
[3] Instituto de Investigación Hospital Doce de Octubre (imas12), Avenida de Córdoba s/n, 28041 Madrid, Spain.
[4] Instituto de Tecnologia Química e Biológica António Xavier,
Universidade Nova de Lisboa, Av. da República, 2780-157 Oeiras, Portugal.
[5] Departamento Química Orgánica, Universidad Complutense de Madrid, Avda. Complutense s/n 28040 Madrid, Spain.
vgavedia@ucm.es

Nonyl acridine orange (*NAO*) is a fluorescent molecule that has traditionally been used for mitochondrial staining due to its affinity for cardiolipin lipid. Recent studies have shown that, at certain concentrations, it has the ability to stack forming *H-aggregates* in an antiparallel configuration, promoting events related to membrane remodelling [1]. In this work, we report fusion events on giant unilamellar vesicles (*GUVs*) containing *DOPE* lipid promoted by *NAO*. To enlight the underlying mechanism on these fusion events we have also synthesized derivatives of the molecule making modifications over its structure: removing its tertiary amine arms and decreasing its hydrocarbonated tail length or increasing it showing that the absence of sided amines and short tail chains avoid the process. To understand this relationship within the molecular structure, we approached the system by *coarse-grained* molecular simulations under Martini3 framework [2]. Results revealed a *lipid-hook* mechanism that triggers the process by displacing acridine derivatives molecules out of its equilibrium position. This remodelling enables the contact between lipids from different bilayers yielding to a hemifusion state of the system that would evolve into full fusion as seen on experiments.

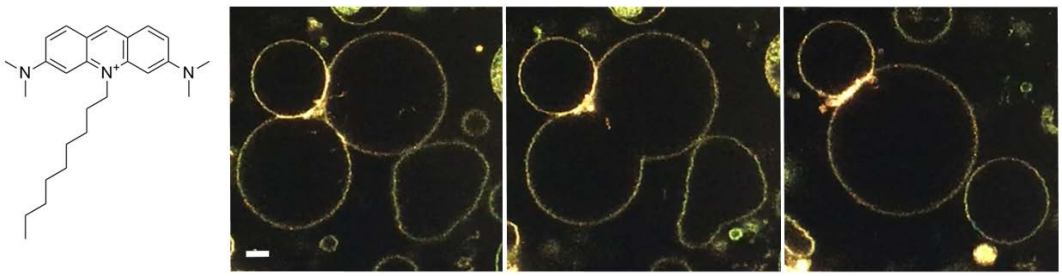


Fig. 1. Acridine orange molecule (left) and fusion process involving giant unilamellar vesicles.

[1] S. González Rubio, N. Montero Pastor et al. *Frontiers in Oncology*, **2018**, *8-514*, 1-8
[2] PCT. Souza, R. Alessandri, J. Barnoud et al. *Nature Methods*, **2021**, *18*, 382-388

GREEN CHEMISTRY INSPIRED CARBAZOLE-FLANKED CYCLOBUTANES AS HOLE SELECTIVE MATERIALS FOR SOLAR CELLS AND MODULES

Šarūnė Daškevičiūtė-Gegužienė[1], Yi Zhang[2], Kasparas Rakštys[1], Marytė Daškevičienė[1], Vygintas Jankauskas[3], Mohammad Khaja Nazeeruddin[2], Vytautas Getautis[1]

[1] Department of Organic Chemistry, Kaunas University of Technology, Kaunas, Lithuania
[2] Institute of Chemical Sciences and Engineering, École Polytechnique Fédérale de Lausanne, Sion, Switzerland
[3] Vilnius University, Vilnius, Lithuania
sarune.daskeviciute@ktu.lt

Over the recent years, organic-inorganic hybrid perovskite solar cells (PSCs) have been attracting a massive worldwide attention due to their low cost and facile fabrication. HTM is one of the quintessential components required for the efficient and stable PSC devices. The hunt is now on for new organic semiconductors that are prepared by simple, cost-effective, and green chemistry without sacrificing the efficiency [1].

Is known that photodimerized carbazole is an attractive building block due to the simple, elegant and green synthesis [2]. Herein, we disclose the development of novel HTMs, which comprises cyclobutane as a new structural core element for HTMs. Novel cyclobutane-based HTMs have been successfully applied in PSCs showing PCE up to 21%. Most importantly, to obtain novel HTMs we have applied protocols inspired by green chemistry, for the first time presenting that HTMs for PSCs could be synthesized eliminating the use of hazardous substances in order to reduce the adverse environmental impact without sacrificing the efficiency.

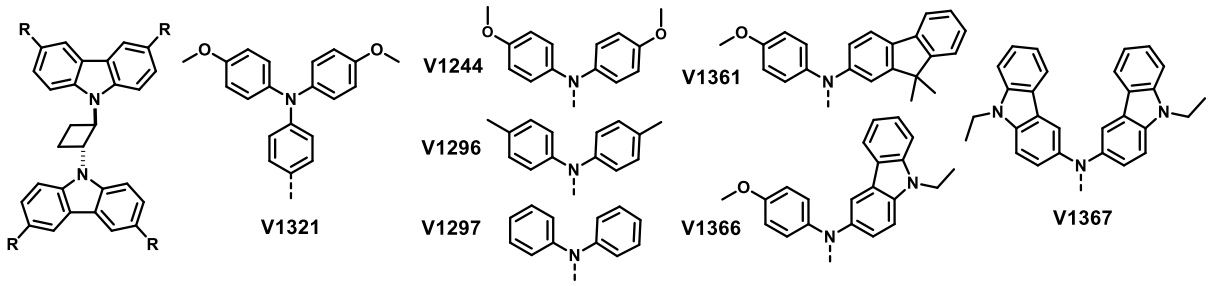
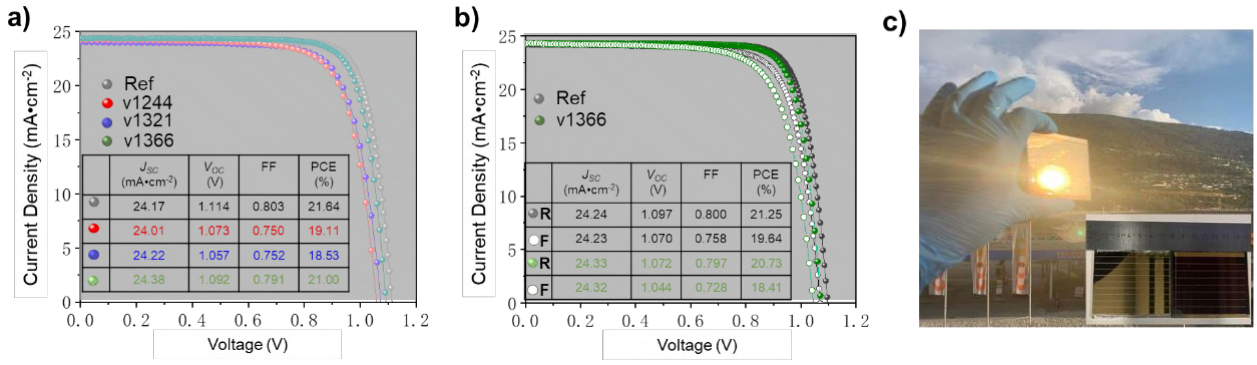


Fig. 1. Structures of novel hole transporting materials.



	J_{SC} (mA•cm^{-2})	V_{OC} (V)	FF	PCE (%)
Ref	24.17	1.114	0.803	21.64
v1244	24.01	1.073	0.750	19.11
v1321	24.22	1.057	0.752	18.53
v1366	24.38	1.092	0.791	21.00

	J_{SC} (mA•cm^{-2})	V_{OC} (V)	FF	PCE (%)
R	24.24	1.097	0.800	21.25
F	24.23	1.070	0.758	19.64
R	24.33	1.072	0.797	20.73
F	24.32	1.044	0.728	18.41

Fig. 2. a) *J-V* curves (reverse-scan) of the PSCs based on **V1244**, **V1321**, and **V1366** as HTMs and spiro-OMeTAD as the reference. b) *J-V* hysteresis of the spiro-OMeTAD and **V1366**. d) Photograph of the unsealed 6.5 × 7 cm solar module.

And another issue of importance to commercialization is their large-scale production. Modules based on V1366 at a size of 6.5 cm × 7 cm were fabricated. The performance of module with high PCEs of 19.06%, as far as we know, this is the highest non Spiro-OMeTAD system PSC modules photoelectric conversion efficiency.

[1] M. L. Petrus, A. Music, A. C. Closs, J. C. Bijleveld, M. T. Sirtl, Y. Hu, T. J. Dingemans, T. Bein and P. Docampo, J. Mater. Chem. A, **5** (2017) 25200–25210.
[2] Sun and J. Zhang, Curr. Org. Chem., **16** (2012) 2014–2025.

SYNTHESIS AND THERMAL, PHOTOPHYSICAL, ELECTROCHEMICAL PROPERTIES OF 3,3-DI[3-ARYLCARBAZOL-9-YLMETHYL]OXETANE DERIVATIVES

Tavgeniene Daiva[1], Korzec Mateusz[2], Samuel Nizy Sara[2], Krucaite Gintare[1], Pająk Agnieszka Katarzyna[2], Kotowicz Sonia[2], Vasylieva Marharyta[3], Gnida Paweł[3], Malecki Jan Grzegorz[2], Grigalevicius Saulius[1], Schab-Balcerzak Ewa[2,3]

[1] Department of Polymer Chemistry and Technology, Kaunas University of Technology, Lithuania
[2] Department Institute of Chemistry, University of Silesia, Poland
[3] Centre of Polymer and Carbon Materials, Poland
daiva.tavgeniene@ktu.lt

As a renewable energy source, solar energy is a very important way to solve environmental pollution and deficiency of current energy. Investigations into and development of efficient and cheap solar cells is a technological area where traditional silicon-based solar cells have been successfully commercialized regardless of some disadvantages. At this time, perovskite solar cells (PSCs) are regarded as one of the best alternatives to siliconbased photovoltaic (PV) devices. The intense heat required to purify silicon, the high amount of CO_2 emitted during this process, as well as difficultly in deposition on flexible substrates can be listed as drawbacks of silicon PV. PSCs possess strong light absorption, high bipolar charge transporting possibility, long carrier diffusion length and lifetime as well as low exciton binding energy [1]. PSCs can be made with a low-temperature screen-printing process that is not only less energy-intensive but also less expensive. Moreover, it is believed that PSCs have lower carbon footprints and shorter energy payback periods than silicon [2].

In this work, the carbazole functionalized oxetanes substituted with the 1-naphthyl, 9-ethylcarbazolyl and 4-(diphenylamino)phenyl units were synthesized and investigated. The new 3,3-di[3-(6-arylcarbazol-9-ylmethyl]oxetanes (4–6) were synthesized in the three synthesis steps as shown in Figure 1.

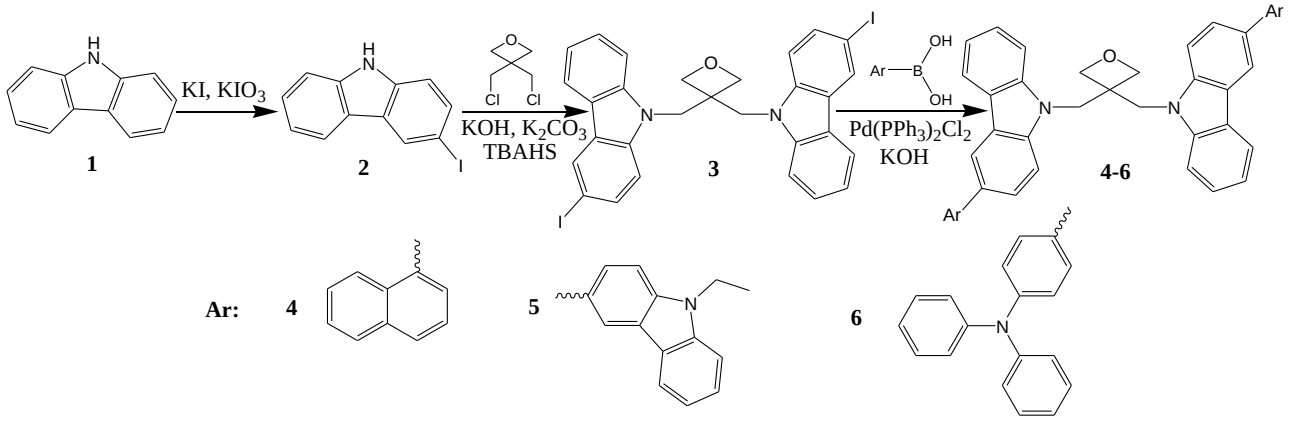


Fig. 1. Synthesis of the carbazole-functionalized oxetane derivatives (**4**–**6**).

The oxetanyl group containing molecules can form hydrogen bonds in solid state and the materials demonstrate high melting temperature (T_m) or high glass transition temperature (T_g) as well as formation of stable and homogeneous thin films due to intermolecular interactions, which can be promising for applications in organic optoelectronics including photovoltaics. They were tested as HTM in PSCs. The presented systematical studies are focused on finding the effect of some structural elements on crucial properties of the synthesized compounds. In design of new efficient HTMs, the role of systematical photophysical and optoelectronic investigations, which can help understand how to optimize the charge extraction and recombination processes by fine-tuning of the molecular structures, is essential to develop PV devices with improved performance. The obtained results should allow modeling of the chemical structure to obtain a material with specific characteristics for PV application. Some of the derivatives demonstrated improved amorphous film-forming properties, and, applied as HTM, lead to improvement of PV device parameters when compared with a reference cell without HTM font.

[1] M.K. Rao, D.N. Sangeetha, M. Selvakumar et al., Review on persistent challenges of perovskite solar cells'stability Sol. Energy **218**, 469–491 (2021).
[2] R. Vidal, J.-A. Alberola-Borràs, N. Sánchez-Pantoja et al., Comparison of Perovskite Solar Cells with other Photovoltaics Technologies from the Point of View of Life Cycle Assessment, Adv. Energy Sustain. Res. **2**, 2000088 (2021).

CARCINOEMBRYONIC ANTIGEN-SPECIFIC APTASENSOR BASED ON A REDUCED GRAPHENE OXIDE/GOLD NANOPARTICLE MODIFIED ELECTRODE

Anabel Villalonga[1], Borja Vegas[1], Gonzalo Paniagua[1], Marcos Eguílaz[2], Beatriz Mayol[1], Concepción Parrado[1], Gustavo Rivas[2], Paula Díez[1], Reynaldo Villalonga[1]

[1] Department of Analytical Chemistry Faculty of Chemistry, Complutense University of Madrid, Spain
[2] Department of Physical Chemistry Faculty of Chemical Sciences, National University of Córdoba, Argentina
anabelvi@ucm.es

Cancer remains as one of the major health concerns due to its high incidence, mortality and morbidity, being the second cause of mortality in the world and accounting for 25% of all deaths in developed countries [1]. The incidence of this disease is rapidly growing, with over 18 million new cases globally reported each year [2]. For these reasons, considerable efforts are currently devoted to increase the quality of life and survival expectancy for patients by improving prevention, diagnosis and treatment for cancer diseases.

This work describes the construction of a novel amperometric aptasensor for the highly specific detection of carcinoembryonic antigen (CEA) (Fig. 1). The sensing interface was assembled by electrodeposition of reduced graphene oxide and gold nanoparticles on a carbon screen-printed electrode, and further functionalization with a biotin and thiol-modified anti-CEA DNA hairpin aptamer. The sensing approach relies on the specific recognition of CEA by the folded aptamer, causing unfolding of the DNA hairpin structure and unmasking the biotin residues at the aptamer chain. Further incubation with a sptreptavidin-peroxidase conjugate (Strp-HRP) allows the amperometric detection of the cancer biomarker. This aptasensor was able to detect CEA in the broad range from 20 pg mL^{-1} to 2 µg mL^{-1} (112 fM–11 µM) with a detection limit of 16 pg mL^{-1} (90 fM). The aptasensor also showed high reproducibility, specificity and stability, and was successfully validated in diluted human serum samples.

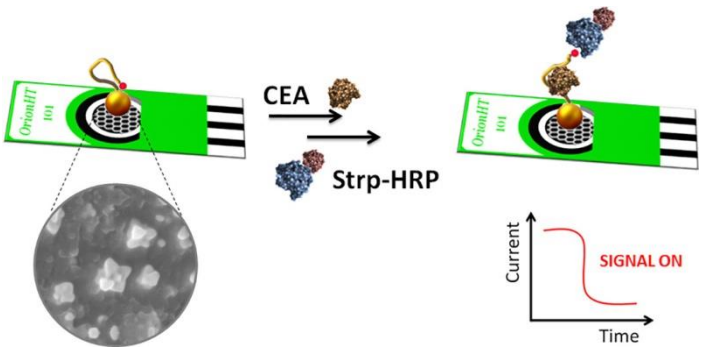


Fig. 1. Schematic representation of the specific amperometric aptasensor for CEA.

[1] R. L. Siegel, K. D. Miller, A. Jemal, Cancer statistics, 2016, CA: A Cancer Journal for Clinicians **66**, 7-30 (2016).
[2] F. Bray, J. Ferlay, I. Soerjomataram et al., Global cancer statistics 2018: GLOBOCAN estimates of incidence and mortality worldwide for 36 cancers in 185 countries, CA: a cancer journal for clinicians **68**, 394-424 (2018).

TOWARDS ELECTROCHEMICAL POLYMERIZATION OF POLYPYRROLE/POLY(METHYLENE BLUE) LAYER DOPED BY POLYSACCHARIDES

Raimonda Boguzaite[1], Vilma Ratautaite[1,2], Ernestas Brazys[2], Almira Ramanaviciene[3], Arunas Ramanavicius[1,2]

[1] Department of Functional Materials and Electronics, Center for Physical Sciences and Technology, Sauletekio av. 3, Vilnius LT-10257, Lithuania
[2] Department of Physical Chemistry, Institute of Chemistry, Faculty of Chemistry and Geosciences, Vilnius University, Naugarduko str. 24, Vilnius LT-03225, Lithuania
[3] NanoTechnas – Center of Nanotechnology and Materials Science, Faculty of Chemistry and Geosciences, Institute of Chemistry, Vilnius University, Naugarduko Str. 24, LT-03225 Vilnius, Lithuania
raimonda.boguzaite@ftmc.lt

Polypyrrole (Ppy) and methylene blue are electroactive compounds that can be polymerized by electrochemical polymerization methods [1]. Ppy is one of the most analyzed conducting polymers used for the development of various types of sensors. Meanwhile, methylene blue (MB) is a phenothiazine derivative, which in analytical chemistry is used as a redox mediator that undergoes color changes from bright blue to colorless when the oxidized form becomes reduced. In recent years several studies describing the combination of Ppy and PMB have been published [2,3].

The conductivity of Ppy can be effectively tuned by a careful selection of dopants [4,5]. In most cases, small ions of strong acids are used as dopants, for instance, chloride, sulfate, and others [5,6]. Among the various dopants, saccharides are special substances [4,7].

In this study the aim was to compare the effect of the saccharides (Lactose, Sucrose, and Heparin) on the Ppy-PMB layer. The electrochemical deposition was carried out from a solution containing of 50 mM of pyrrole, 10 mM of methylene blue, and one of the doping materials: 0.1 M Lactose, 0.1 M Sucrose, or 0.01 g/L Heparin. Polymerization was performed at a room temperature during 25 potential cycles in the range from –0.5 V to +1.2 V vs. Ag/AgCl, at the sweep rate of 50 mV/s and step potential of 2.44 mV.

The obtained layers were investigated, and their properties evaluated. The morphology of the layers was analyzed by the AFM method. From these images, it was concluded that the saccharides used in this study have a moderate effect on the surface morphology.

The Ppy-PMB layer doped with heparin was selected for the further experiment and it was applied in the design of electrochromic sensors.

[1] Plausinaitis, D.; Sinkevicius, L.; Samukaite-Bubniene, U.; Ratautaite, V.; Ramanavicius, A. Evaluation of Electrochemical Quartz Crystal Microbalance Based Sensor Modified by Uric Acid-imprinted Polypyrrole. Talanta, 220, 121414 (2020).
[2] Godwin, J.M.; Evitts, R.W.; Kennell, G.F. Microbial fuel cell with a polypyrrole/poly(methylene blue) composite electrode. Rep. Electrochem., 2, 3–11 (2012).
[3] Boguzaite, R.; Ratautaite, V.; Mikoliunaite, L.; Pudzaitis, V.; Ramanaviciene, A.; Ramanavicius, A. Towards analytical application of electrochromic polypyrrole layers modified by phenothiazine derivatives. J. Electroanal. Chem., 886, 115132 (2021).
[4] Serra Moreno, J.; Panero, S.; Materazzi, S.; Martinelli, A.; Sabbieti, M.G.; Agas, D.; Materazzi, G. Polypyrrole-polysaccharide thin films characteristics: Electrosynthesis and biological properties. J. Biomed. Mater. Res. A, 88A, 832–840 (2009).
[5] V. Ratautaite, R. Boguzaite, M.B. Mickeviciute, L. Mikoliunaite, U. Samukaite-Bubniene, A. Ramanavicius, A. Ramanaviciene, Evaluation of Electrochromic Properties of Polypyrrole/Poly(Methylene Blue) Layer Doped by Polysaccharides, Sensors, 22, 232 (2022).
[6] V. Ratautaite, G. Bagdziunas, A. Ramanavicius, A. Ramanaviciene, An Application of Conducting Polymer Polypyrrole for the Design of Electrochromic pH and CO2 Sensors, J. Electrochem. Soc., 166, B297-B303 (2019).
[7] Alizadeh, N.; Tavoli, F. Enhancing electrochromic contrast and redox stability of nanostructure polypyrrole film doped by heparin as polyanion in different solvents. J. Polym. Sci. A Polym. Chem., 52, 3365–3371 (2014).

COBALT (III) OXIDE AND MIXED COBALT(III) OXIDE - TIN OXIDE FOR OXYGEN EVOLUTION REACTION IN ALKALINE MEDIA

Tatjana Stanković[1,*], Jadranka Milikić[1], Sara Knežević[2], Miloš Ognjanović[3], Dalibor Stanković[2,3], and Biljana Šljukić[1]

[1] University of Belgrade, Faculty of Physical Chemistry, Studentski trg 12-16, 11158 Belgrade, Serbia
[2] University of Belgrade, Faculty of Chemistry, Studentski trg 12–16, 11158 Belgrade, Serbia
[3] University of Belgrade,"VINČA" Institute of Nuclear Sciences – National Institute of the Republic of Serbia, Mike Petrovića Alasa 12-14, 11000 Belgrade, Serbia
*tatjanastankovicffh@gmail.com

Electrochemical water dissociation involves two reactions: the hydrogen evolution reaction (HER) and the oxygen evolution reaction (OER), at the cathode and anode, respectively [1].

Water electrolysis could be sustainable and clean production of hydrogen as fuel, but HER and OER rates need to be improved for industrial applications. The OER involves the transport of four electrons which requires a high overvoltage to reach a satisfactory current density [1].

$$\text{OER:} \quad 4OH^- \rightarrow 2H_2O + O_2 + 4e^-$$

Numerous studies have been focused on synthesizing high-performance and low-cost anode materials [2]. Metal oxides and metal chalcogenides are recognized as promising electrocatalysts for OER [3]. They can be synthesized using various methods with a wide range of precursors.

Herein cobalt (III) oxide (Co_3O_4) and cobalt (III) oxide combined with tin oxide (Co_3O_4/SnO_2) were examined for OER in alkaline media by linear sweep voltammetry (LSV). A three-electrode system was used for electrochemical examination where saturated calomel electrode (SCE) and graphite rod were set as reference and counter electrodes, while Co_3O_4 and Co_3O_4/SnO_2 were used as the working electrodes. All potentials in this paper were given versus reversible hydrogen electrode (RHE).

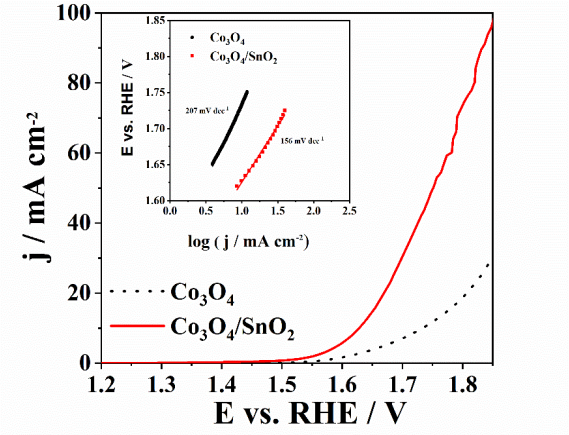


Fig. 1. The OER polarization curves of Co_3O_4 and Co_3O_4/SnO_2 (IR-corrected) recorded in 1 M KOH solution at 0.005 V s^{-1} with the corresponding Tafel plots in the inset.

Fig. 1 shows OER polarization curves of Co_3O_4 and Co_3O_4/SnO_2 electrocatalysts in alkaline media where both electrocatalysts showed high OER activity. Still, Co_3O_4/SnO_2 gave an almost three times higher OER current density of 98 mA cm^{-2} than Co_3O_4 electrocatalyst (30 mA cm^{-2}) at 1.85 V. Tafel slopes were found to be 207 and 156 mV dec^{-1} for Co_3O_4 and Co_3O_4/SnO_2 electrocatalysts, respectively. A lower slope means that less overpotential is required to get a high current. In this case, Co_3O_4/SnO_2 has a lower Tafel's slope which indicates synergetic effect of coupling two metal oxides when it comes to electro-oxidation of oxygen in alkaline media [1]. The iridium (IV) and ruthenium (IV) oxides (IrO_2 and RuO_2) as the best OER electrocatalysts but with low OER durability and high cost [1] could potentially be replaced with here tested Co_3O_4 and Co_3O_4/SnO_2 electrocatalysts because of their low-cost synthesis, and high OER activity in alkaline media.

Acknowledgments

The authors would like to thank the Ministry of Education, Science and Technological Development of the Republic of Serbia (contract no. 451-03-9/2021-14/200146).

[1] V.A. Tran, H.H. Do, V.T. Le, Y. Vasseghian, V. Vo, S.H. Ahn, S.Y. Kim, S.W. Lee, Metal-organic-framework-derived metals and metal compounds as electrocatalysts for oxygen evolution reaction: A review, Int. J. Hydrogen Energy. 1–19 (2021).
[2] J. Milikić, A. Balčiūnaitė, Z. Sukackienė, D. Mladenović, D.M.F. Santos, L. Tamašauskaitė-Tamašiūnaitė, B. Šljukić, Bimetallic Co-based (CoM, M = Mo, Fe, Mn) coatings for high-efficiency water splitting, Materials (Basel). **14**, 92 (2021)
[3] F. Buchner, M. Eckardt, T. Böhler, J. Kim, J. Gerlach, J. Schnaidt, R.J. Behm, Oxygen Reduction and Evolution on Ni-modified Co_3O_4(111) Cathodes for Zn–Air Batteries: A Combined Surface Science and Electrochemical Model Study, ChemSusChem. **13**, 3199–3211 (2020).

REAL TIME MONITORING AND MATHEMATICAL MODELLING OF SARS-COV-2 SPIKE PROTEIN AND SPECIFIC ANTIBODY INTERACTION KINETICS BY TOTAL INTERNAL REFLECTION ELLIPSOMETRY

Silvija Juciute[1], Ieva Plikusiene[1,2], Vincentas Maciulis[1,2], Saulius Balevicius[2], Rimantas Slibinskas[3], Arunas Ramanavicius[1,2], Almira Ramanaviciene[1]

[1] Nanotechnas, -Nantechnology and Materials Sciences Center, Faculty of Chemistry and Geosciences, Vilnius University, Naugarduko 24, Vilnius, Lithuania;
[2]State Research Institute Centre for Physical Sciences and Technology, Sauletekio Avenue. 3, Vilnius, Lithuania
[3]Life Sciences Center, Vilnius University, Sauletekio Avenue 7, Vilnius, Lithuania
silvija.juciute@chgf.stud.vu.lt

Two years after outbreak severe acute respiratory syndrome coronavirus 2 (SARS-CoV-2) is still a threat for people's health around the world. Although vaccines were created investigations about SARS-CoV-2 proteins need to be continued. The main protein, that is responsible for the virus attachment to the cell receptor is SARS-CoV-2 spike (S) protein. Spike protein (S) binds to the ACE2 receptor in the human body and allows the virus to spread further [1]. It is of great importance that human immune system could produce antibodies against SARS-CoV-2 S protein to block it and neutralize the virus. S protein is main target of immune system and in the development of vaccines. That is why it is very important to know how the S protein forms immune complex with specific antibodies.

The affinity of a specific antibody to S protein can show how effective is the interaction. For this reason, real-time monitoring of interaction kinetics between covalently immobilized S protein and specific monoclonal antibody is of high importance. For the interaction kinetics measurements, a sensitive, noncontact, nondestructive, and label-free method of total internal reflection ellipsometry (TIRE) was used.

Total internal reflection ellipsometry (TIRE) is an optical method and powerful tool for the investigation of proteins interactions [2]. This method is sensitive to even small changes in refractive index caused by immune complex formation on the sensing surface. A TIRE based evaluation of the interaction between the SARS-CoV-2 S protein and monoclonal antibodies against this protein was performed and the affinity of such complex formation was evaluated. Using mathematical modeling, the association and dissociation rate constants were calculated for the formed immune complex between S protein and specific antibody.

Acknowledgement
This work has received funding from European Regional Development Fund (project No. 01.2.2- LMT-K-718-05-0038) under grant agreement with the Research Council of Lithuania (LMTLT). Funded as European Union's measure in response to Cov-19 pandemic.



[1] Ramanathan, Muthukumar et al. "SARS-CoV-2 B.1.1.7 and B.1.351 spike variants bind human ACE2 with increased affinity," *Lancet Infect. Dis.*, vol. 21, no. 8, p. 1070, 2021.

[2] I. Plikusiene, V. Maciulis, A. Ramanaviciene, Z. Balevicius, A. Zvirbliene, and A. Ramanavicius, "Evaluation of kinetics and thermodynamics of interaction between immobilized SARS-CoV-2 nucleoprotein and specific antibodies by total internal reflection ellipsometry," *J. Colloid Interface Sci.*, vol. 594, pp. 195–203, 2021.

ELECTROCHEMICAL AND SPECTROELECTROCHEMICAL PROPERTIES OF 10H-PYRROLO[1,2-A]PERIMIDIN-10-ONE

Patryk Janasik[1*], Malgorzata Czichy[1], Mieczyslaw Lapkowski[1]

[1] Department of Physical Chemistry and Technology of Polymers, Silesian University of Technology, Poland
patryk.janasik@polsl.pl

Conductive polymers play an important role in several key technologies, such as printed electronics. For many potential applications, the properties of these materials do not meet the requirements due to the lack of long-range ordering. In the course of research on π-conjugated polymers characterized by ordered structure and high charge mobility, we wanted to investigate the perimidine as a polymerizable unit to obtain organic supramolecular layers which have efficient multi-dimensional electronic delocalization.

We have already shown in previous publications that the perimidine unit can be electrooxidized to form electroactive products on the electrode surface [1-4]. Going further, we want to show the electrochemical behavior of a missing member from the perinone dyes family. This missing member is compound **B0** (Fig. 1), the product formed during condensation reaction of maleic anhydride with 1,8-diaminonaphthale.

The compound we synthesized has been tested electrochemically. It was possible to obtain conductive layers during electrochemical oxidation. Along with computational research, we proposed a mechanism for electropolymerization or dimerization of perimidine units. The obtained layers showed a small bandgap and high stability in a wide range of polarization.

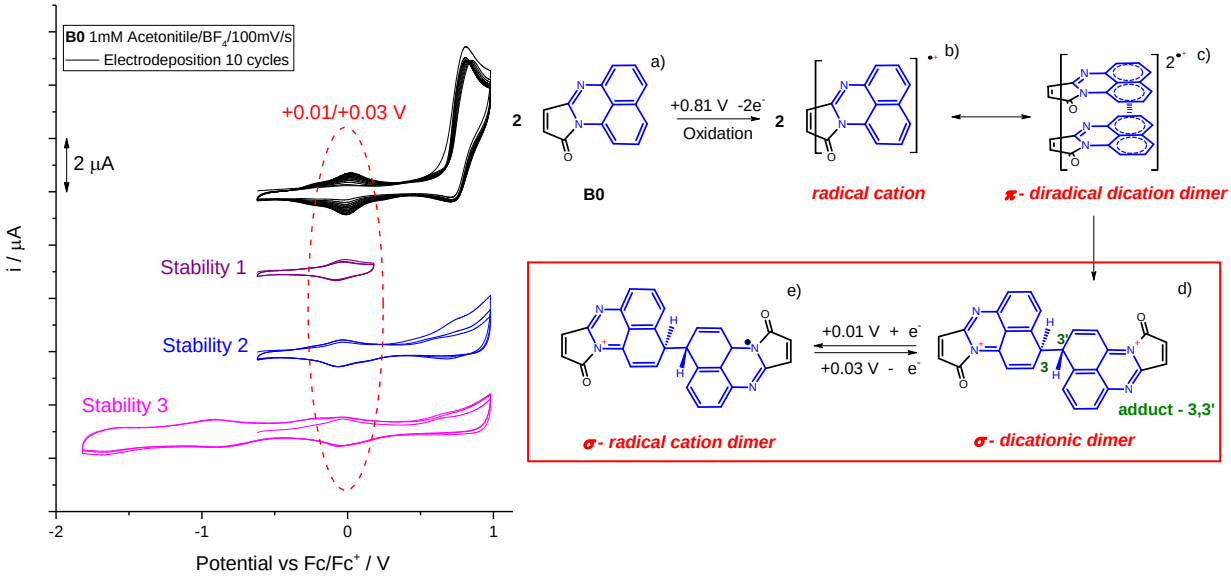


Fig. 1. Electrodeposition cyclicvolamogram of **B0** (left); Mechanism of **B0** electro-oxidation (right) with stable redoks system d)/e).

Acknowledgments: The work was financially supported by the Silesian University of Technology, grant for young scientists number 04/040/BKM21/0161(BKM-529/RCH4/2021).

[1] M. Czichy, H. Zhylitskaya, P. Zassowski, M. Navakouski, P. Chulkin, P. Janasik, M. Lapkowski, M. Stepien, Electrochemical Polymerization of Pyrrole–Perimidine Hybrids: Low-Band-Gap Materials with High n-Doping Activity, J. Phys. Chem. C **124**, 14350–14362 (2020).

[2] M. Czichy, P. Janasik, R. Motyka, P. Zassowski, E. Grabiec, A. Wolinska-Grabczyk, M. Lapkowski, Influence of isomeric phthaloperinone monomers on the formation of π-dimers and σ-bonded segments in electrochemically-crosslinked products, Electrochim. Acta, 137669 (2021).

[3] M. Czichy, R. Motyka, P. Zassowski, E. Grabiec, P. Janasik, A. Brzeczek-Szafran, K. Laba, A. Wolinska-Grabczyk, M. Lapkowski, Effects of solution-phase ordering on the spectroscopic properties and electrooxidative reactivity of isomeric mixtures and isolated isomers of synthesized amidine derivatives, Dye. Pigment. **178**, 108309 (2020).

[4] M. Czichy, P. Janasik, P. Wagner, D. L. Officer, M. Lapkowski, Electrochemical and Spectroelectrochemical Studies on the Reactivity of Perimidine–Carbazole–Thiophene Monomers towards the Formation of Multidimensional Macromolecules versus Stable π-Dimeric States, Materials **14**, 2167 (2021).

SYNTHESIS AND CHARACTERISTICS OF ORGANIC SEMICONDUCTORS WITH *N*-CARBAZOLYL-BASED CHROMOPHORES LINKED VIA ALIPHATIC CHAIN

Povilas Luizys[1], Vytautas Getautis[1], Kasparas Rakstys[1], Vygintas Jankauskas[2], Egidijus Kamarauskas[2]

[1] Department of Organic Chemistry, Kaunas University of Technology, Lithuania
[2] Institute of Chemical Physics, Vilnius University, Lithuania
povilas.luizys@ktu.lt

Global warming caused by burning of fossil fuels is increasing world's attention to renewable energy sources and solar energy is of the most promising sources, which could theoretically satisfy energy needs of mankind. Therefore, development of technologies utilizing solar energy is stimulated in various ways. Currently, silicon solar cells are the mostly used on the market, however, due to their high production costs, intensive research of alternative technologies is underway. One of them is perovskite solar cells, which have rapidly become the hottest topic in photovoltaics due to their unique optical and electrical properties. Since 2009 power conversion efficiency of perovskite solar cells devices has increased dramatically and currently exceeds 25% [1]. These solar cells are characterized by simplicity of construction and inexpensive raw materials. Although perovskite solar cells have achieved high efficiency, there are still several challenges limiting their commercialization. One of them is long-term stability. The perovskite layer is prone to rapid degradation when the device is exposed to high temperature [2], humidity [3], oxygen [4]. Therefore, the development of new materials for perovskite solar cells construction remains highly relevant.

In this work, organic semiconductors with two *N*-carbazolyl chromophores linked together by different length aliphatic chains have been developed to function as hole transporting materials in perovskite solar cells.

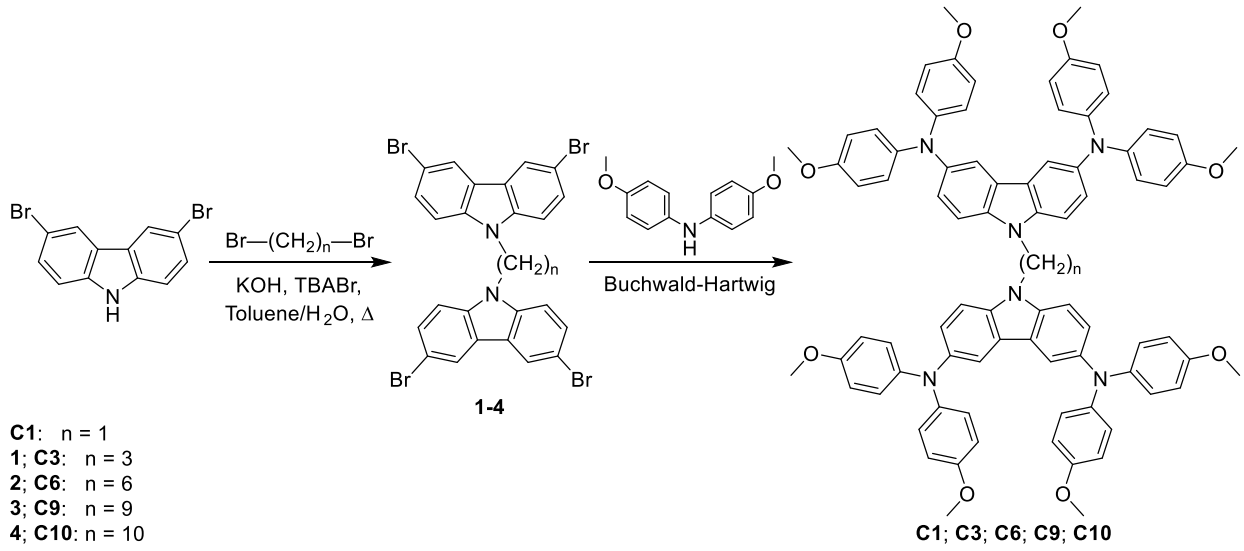


Fig. 1. Synthesis route to compounds **C1**, **C3**, **C6**, **C9** and **C10**.

Organic materials were obtained via two-step synthesis (Fig. 1). The structures of the newly synthesized hole transporting materials was confirmed by ^{1}H NMR and ^{13}C NMR spectroscopy. Thermal properties of target compounds proved that they are molecular glasses and are thermally stable at relatively high temperatures. Photoelectron spectroscopy in air method was used to measure ionization potentials of the investigated compounds. Obtained *Ip* values (5.06–5.11 eV) indicate that the HOMO energy level of the synthesized organic semiconductors optimally offsets with the perovskite valence band energy (~5.5 eV), therefore, effective hole transport from the photoactive perovskite to the electrode should be achieved. Charge transport properties were measured using xerographic time-of-flight technique. At high electric fields, hole transporting materials reach the hole drift mobility up to $\mu = 1.5 \cdot 10^{-3}$ cm^2/V·s. Therefore, compounds **C1**, **C3**, **C6**, **C9** and **C10** could potentially be used in construction of solar cells.

[1] Best Research-Cell Efficiency Chart, Photovoltaic Research, NREL. 2021.
[2] G. Divitini, S. Cacovich, F. Matteocci et al., In situ observation of heat-induced degradation of perovskite solar cells, Nature Energy **1**, 15012 (2016).
[3] N. Aristidou, I. Sanchez-Molina, T. Chotchuangchutchaval et al., Degradation observations of encapsulated planar $CH_3NH_3PbI_3$ perovskite solar cells at high temperatures and humidity, Journal of Materials Chemistry A **3**, 8139–8147 (2015).
[4] N. Aristidou, I. Sanchez-Molina, T. Chotchuangchutchaval et al., The Role of Oxygen in the Degradation of Methylammonium Lead Trihalide Perovskite Photoactive Layers, Angewandte Chemie International Edition, **54**, 8208–8212 (2015).

P6-19

DID NOT PARTICIPATE

.

HYDROTHERMAL SYNTHESIS OF HYDROXYAPATITE FROM α-TCP USING DIVALENT CATIONS AS MORPHOLOGY-CONTROLLING AGENTS

Gabrielė Klydžiūtė[1], Eva Raudonytė-Svirbutavičienė[1,2], Laura Lukavičiūtė[1], Aldona Beganskienė[1], Aleksej Žarkov[1], Aivaras Kareiva[1]

[1] Institute of Chemistry, Faculty of Chemistry and Geosciences, Vilnius University, Naugarduko 24, LT-03225 Vilnius, Lithuania

[2] Institute of Geology and Geography, Nature Research Centre, Akademijos Str. 2, LT-08412, Vilnius, Lithuania

gabriele.klydziute@chgf.stud.vu.lt

Calcium hydroxyapatite (Ca-HAp) is mostly seen as a synthetic material for biomedical applications due to its bioactivity and biocompatibility [1]. Ca-HAp ion exchange ability against various cations makes it highly biocompatible with inherent bioactivity properties [2]. Because of the flexibility in the structure of Ca-HAp, various cations, such as zinc or copper can substitute Ca^{2+} in Ca-HAp in order to improve the desirable properties [3]. Biomaterials having antibacterial activity within their structures could be applied not only for bone defects and implant's coating in orthopedic surgery but also for the treatment of skin infections, for microbiologically polluted water, as well as polymer additive and for general use [4]. To prepare biomaterials with desirable properties, it is essential to develop cost-effective and efficient synthesis methods which would at the same time provide the possibility to control morphology of the products.

This study investigates the properties of zinc-substituted and copper-substituted hydroxyapatites. For this purpose, α-TCP was synthesized by wet precipitation method and the hydrolysis reaction was performed in aqueous solutions of divalent cations (Zn^{2+} and Cu^{2+}) under hydrothermal conditions at 200 °C. Concentration of the metal ions in the reaction solution corresponded to Ca-HAp substitution levels of 0.1; 0.5; 1; 5, and 10 mol %. The phase purity and morphology of hydrolysis products was investigated with XRD and SEM, respectively.

The lowest concentration (0.1 mol %) of the foreign cation did not affect phase purity of the final product, single-phase HAp was obtained both using Zn^{2+} and Cu^{2+}. Increased concentration of Zn^{2+} (0.5; 1 mol %) induced formation of β-TCP. Formation of HAp phase was completely inhibited when higher concentration of Zn^{2+} (5 mol %) was introduced to the reaction solution. When Zn^{2+} concentration was 10 mol %, the phase composition of the precipitate was almost composed of Scholzite. Cu^{2+} had a similar effect on phase transformation: increased concentration of Cu^{2+} (0.5; 1 mol %) had also induced formation of β-TCP. At the higher concentrations of Cu^{2+}, hydrolysis of α-TCP was slightly hindered, and some remaining α-TCP was left after the hydrothermal treatment. Zn^{2+} and Cu^{2+} had impact on the morphology of the final product: increasing concentrations of these cations correlated with an increasing fraction of rod-like crystals (Fig. 1). The results of this study show that foreign ions could be applied as HAp morphology-controlling additives during the hydrothermal synthesis.

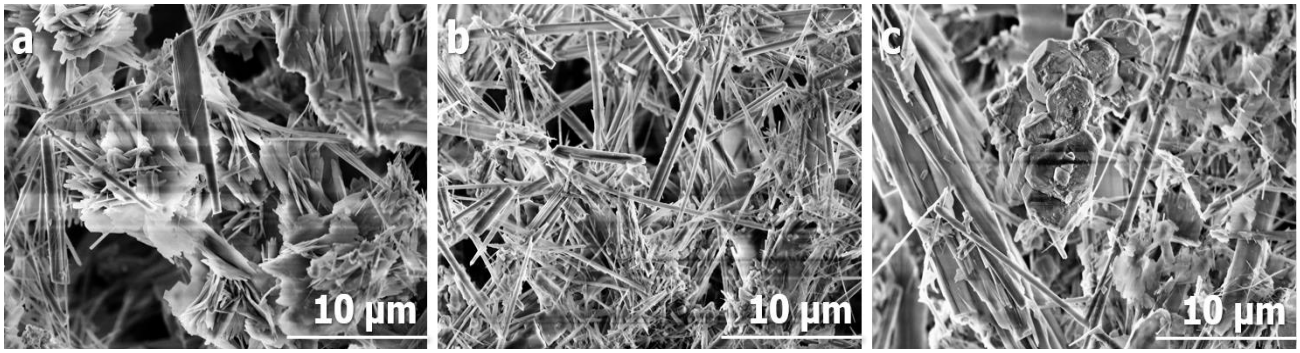


Fig. 1. SEM images of samples doped with different amount of Zn^{2+}: 0.5 mol % (a); 1 mol % (b); and with 1 mol % Cu^{2+} (c).

Acknowledgements: This work has received funding from the European Social Fund (project No 09.3.3-LMT-K-712-23-0070) under grant agreement with the Research Council of Lithuania (LMTLT).

[1] E. S. Thian, T. Konishi, Y. Kawanobe, et al., Zinc-substituted hydroxyapatite: a biomaterial with enhanced bioactivity and antibacterial properties, J Mater Sci: Mater Med **24**, 437-445 (2013).

[2] E. A. Ofudje, A. I. Adeogun, et al., Synthesis and characterization of Zn-Doped hydroxyapatite: scaffold application, antibacterial and bioactivity studies, Heliyon **5** e01716 (2019).

[3] S. Shanmugam, B. Gopal, Copper substituted hydroxyapatite and fluorapatite: Synthesis, characterization and antimicrobial properties, Ceramics International **40**, 15655-15662 (2014).

[4] V. Stanic, S. Dimitrijevic, J. Antic-Stankovic, et al., Synthesis, characterization and antimicrobial activity of copper and zinc-doped hydroxyapatite nanopowders, Applied Surface Science, **256**, 6083-6089 (2010).

PRUSSIAN BLUE-BASED ELECTROCHEMICAL BIOSENSOR FOR Hg^{2+} IONS

Povilas Virbickas[1], Gerda Žižiūnaitė[1], Aušra Valiūnienė[1]

[1] Faculty of Chemistry and Geosciences, Vilnius University, Lithuania
povilas.virbickas@chgf.vu.lt

Mercury and its derivates can be founded in water, air and soil as elemental mercury, organic mercury compounds and inorganic mercury compounds [1-2]. Moreover, mercury in all these forms can cause adverse effects on living organisms e.g. disturbance of the haemin synthesis [1]. In addition, mercury also tends to accumulate in living organisms in a form of organomercury derivatives [1-2], making mercury hardly degradable in environment. Therefore, mercury pollution is an important public health and environmental issue that has garnered lots of interest from the global regulatory community and policy makers [3].

Various analytical techniques can be applied to determine concentration of mercury and its compounds, including inductively coupled plasma mass spectrometry [4], fluorescent and colorimetric techniques [5] and electrochemical techniques [6, 7]. In comparison to other techniques, electrochemical methods of mercury determination are considered to be advantageous due to their simplicity of operation and high sensitivity [6]. However, electrochemical techniques often require expensive materials (e.g. Pt) to be used and/or an application of high potential during analysis [6, 7], which can reduce the sensitivity and reliability of the measurement due to the occurrence of side electrochemical reactions of other electrochemically active compounds in the sample [8, 9]. Therefore, investigations of Hg^{2+} ions biosensors which operates at low potentials and do not require a usage of expensive materials for their development have a great importance.

Prussian blue (PB) is an inorganic pigment widely used in the development of biosensors due to its catalytic activity in electrochemical reduction of hydrogen peroxide [8, 9]. When PB is combined with enzyme glucose oxidase (GOx) catalytic activity of GOx could be monitored by registering H_2O_2 reduction current, whereas H_2O_2 is a product of GOx-catalyzed oxidation of glucose [9]. In addition, PB enables to register reduction current of H_2O_2 at very low potentials (~ 0 V *vs* Ag|AgCl, KCl_{sat}) and its increases the reliability of the analysis [8, 9].

In this research PB was applied in the development of an electrochemical Hg^{2+} biosensor. The amperometric Hg^{2+} ions biosensor was formed by modifying a fluorine doped tin oxide coated glass slide with a layer of PB and immobilizing GOx. The operating principle of the Hg^{2+} biosensor developed in this research is based on measuring Hg^{2+} ions-caused changes in reduction current of H_2O_2. The Hg^{2+} ions biosensor developed in this research was able to measure concentration of Hg^{2+} ions concentration at low potential (~ 0.2 V *vs* Ag|AgCl, KCl_{sat}) of the working electrode, thus minimizing the probability of interferences caused by other electrochemically active species in the sample. Furthermore, the PB-based Hg^{2+} biosensor exhibited sensitivity to Hg^{2+} ion in micromolar range of Hg^{2+} concentrations.

[1] B. Elsebai, M. E. Ghica, M. N. Abbas, C. M. A. Brett, Catalase based hydrogen peroxide biosensor for mercury determination by inhibition measurements, Journal of Hazardous Materials **340**, 344-350 (2017).
[2] B. Gworek, W. Dmuchowski, A. H. Baczewska‐Dąbrowska, Mercury in the terrestrial environment: a review, Environmental Sciences Europe **32**, 128 (2020).
[3] M. S. Bank, The mercury science-policy interface: history, evolution and progress of the Minamata Conventio, Science of The Total Environment **722**, 137832 (2020).
[4] R. Clough, S. T. Belt, E. H. Evans, B. Fairman, T. Catterick, Investigation of equilibration and uncertainty contributions for the determination of inorganic mercury and methylmercury by isotope dilution inductively coupled plasma mass spectrometry, Analytica Chimica Acta **500**, 155-170 (2003).
[5] P. S. R. Devi, S. Suvarna, M. Ghosh, G. K. Kumar, R. Verma, A. V. R. Reddy, Preconcentration of mercury on polyaniline expands the horizon for energy dispersive X-ray fluorescence determination, X-Ray Spectrometry **45**, 162-168 (2016).
[6] A. M. Ashrafi, M. Sýs, E. Sedlackova, A. S. Farag, V. Adam, J. Pribyl, L. Richtera, Application of the Enzymatic Electrochemical Biosensors for Monitoring Non-Competitive Inhibition of Enzyme Activity by Heavy Metals, Sensors **19**, 2939 (2019).
[7] M. B. Gumpu, U. M. Krishnan, J. B. B. Rayappan, Design and development of amperometric biosensor for the detection of lead and mercury ions in water matrix—a permeability approach, Analytical and Bioanalytical Chemistry **409**, 4257-4266 (2017).
[8] A. A. Karyakin, Prussian Blue and Its Analogues: Electrochemistry and Analytical Applications, Electroanalysis **13**, 813-819 (2001).
[9] A. Valiūnienė, P. Virbickas, A. Rekertaitė, A. Ramanavičius, Amperometric Glucose Biosensor Based on Titanium Electrode Modified with Prussian Blue Layer and Immobilized Glucose Oxidase, Journal of The Electrochemical Society **164**, B781-B784 (2017).

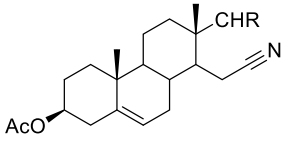
SYNTHESIS AND *IN SILICO* ADMET PREDICTION OF NEW 17-HYDRAZINYLIDENE-16,17-SECOANDROST-5-ENE DERIVATIVES

Branislava Tenjović, Dušan Živković, Tijana Jakica, Dušan Škorić, Andrea Nikolić

Department of Chemistry, Biochemistry and Environmental Protection, Faculty of Sciences University of Novi Sad
dh.dusan.zivkovic1@student.pmf.uns.ac.rs

Steroidal compounds have attracted the attention of pharmacologists, chemists, and biochemists because of widely used for the treatment of various diseases such as inflammation, allergic reaction, heart disease, cancer, and metabolic disease. The development of novel steroidal compounds with pharmacological efficacy is an attractive choice for scientists in recent years. Steroidal compounds can be transformed into potent forms by modifications of the basic steroid skeleton.

Searching for new molecules in the field of steroids, we have synthesized new 17-hydrazinylidene derivatives **1**-**3** starting from 3β-acetoxy-17-oxo-16,17-secoandrost-5-ene-16-nitrile. Characterization of compounds was accomplished through the analysis of IR and NMR spectroscopic data.



1 R = hydrazinylidene
2 R = benzylidenehydrazinylidene
3 R = 2-hydroxybenzylidenehydrazinylidene

In silico ADMET properties were tested for synthesized compounds using SwissADME and ProTox-II web tools. Drug-likeness profile was evaluated through *in silico* calculated physicochemical properties of synthesized compounds and it was detected that synthesized compounds fulfill the requirements of Lipinski's rule of five. The pharmacokinetic parameters like gastrointestinal absorption, passive brain permeation, skin permeation, and interaction of molecules with cytochrome P450 (CYP) enzymes were predicted. Virtual screening was also performed for selected compounds in order to determine the proteins (receptors or enzymes) for which the synthesized compounds will potentially bind, and thus predict their biological activities.

Compound **3** has a better safety profile than **1** and **2**. A low risk of being mutagenic, carcinogenic and hepatotoxic was found for compound **3**, while carcinogenicity was predicted for compounds **1** and **2**.

P6-23

DID NOT PARTICIPATE

.

MOLECULARLY IMPRINTED POLYPYRROLE BASED SENSOR FOR THE DETECTION OF SARS-COV-2 SPIKE GLYCOPROTEIN

Ernestas Brazys[1], Vilma Ratautaitė[2], Raimonda Bogužaitė[2], Arūnas Ramanavičius[1,2]

[1] Department of Physical Chemistry, Institute of Chemistry, Faculty of Chemistry and Geosciences, Vilnius University, Naugarduko str. 24, Vilnius LT-03225, Lithuania
[2] Laboratory of Nanotechnology, Department of Functional Materials and Electronics, Center for Physical Sciences and Technology, Sauletekio av. 3, Vilnius LT-10257, Lithuania
ernestasbrazys@gmail.com

Severe acute respiratory syndrome coronavirus 2 (SARS-CoV-2) is a virus that causes COVID-19 disease. The COVID-19 pandemic began in late 2019 and is still ongoing. SARS-CoV-2 virus contains four structural proteins: spike, nucleocapsid, envelope and membrane [1]. In this study SARS-CoV-2 spike glycoprotein was chosen as a target for the developed sensor system. Described research is dedicated to the design of electrochemical SARS-CoV-2 virus protein detection systems based on the application of molecular imprinting technique.

The typical molecular imprinting procedure consists of chemical or electrochemical polymerization from a mixture containing functional monomers and template molecules. Following template removal by washing in a selected solvent, the polymer binding sites are left in the structure of polymer, which are specific or complementary to the template molecules [2]. This characteristic can be applied in the design of both biological and chemical molecule sensor systems [3].

In this research, SARS-CoV-2 spike glycoprotein imprinted polypyrrole-based (MIP-Ppy) sensor was developed [4]. The polymeric mixture consisted of 0.5 M pyrrole as a monomer and 50 µg/mL of SARS-CoV-2 spike glycoprotein as a template in PBS solution, pH 7.4. The polymeric layer was formed electrochemically onto the surface of a platinum electrode by a sequence of potential pulses. After the polymerization template molecules were extracted by washing the polymeric film in 0.05 M H_2SO_4 for 10 min. The characteristics of the electrode modified by the imprinted polypyrrole films were evaluated by pulsed amperometric detection. In comparison an electrode was modified with non-imprinted polypyrrole film (NIP-Ppy).

Obtained results indicate that the sensor based on MIP-Ppy has a higher sensitivity toward SARS-CoV-2 glycoprotein than the electrode modified by NIP-Ppy film.

Acknowledgement: This project has received funding from the Research Council of Lithuania (LMTLT), GILIBERT 2021 program agreement No S-LZ- 21–4 and co-founded by Campus France grant No. 46593RA (PHC GILIBERT 2021).

[1] R. Lu, X. Zhao, J. Li, P. Niu, B. Yang, H. Wu, W. Wang, H. Song, B. Huang, N. Zhu, Y. Bi, X. Ma, F. Zhan, L. Wang, T. Hu, H. Zhou, Z. Hu, W. Zhou, L. Zhao, J. Chen, Y. Meng, J. Wang, Y. Lin, J. Yuan, Z. Xie, J. Ma, W.J. Liu, D. Wang, W. Xu, E.C. Holmes, G.F. Gao, G. Wu, W. Chen, W. Shi, W. Tan. Genomic Characterization and Epidemiology of 2019 Novel Coronavirus: Implications for Virus Origins and Receptor Binding. *The Lancet*, **395**(10224), 565-574 (2020).

[2] S. A. Piletsky, A. P. F. Turner. Electrochemical Sensors based on Molecularly Imprinted Polymers. *Electroanalysis*, **14**(5), 317–323 (2002).

[3] G. Vasapollo, R. D. Sole, L. Mergola, M. R. Lazzoi, A. Scardino, S. Scorrano, G. Mele. Molecularly Imprinted Polymers: Present and Future Prospective. *International Journal of Molecular Sciences*, **12**(9), 5908–5945 (2011).

[4] V. Ratautaite, R. Boguzaite, E. Brazys, A. Ramanaviciene, E. Ciplys, M. Juozapaitis, R. Slibinskas, M. Bechelany, A. Ramanavicius. Molecularly Imprinted Polypyrrole Based Sensor for the Detection of SARS-CoV-2 Spike Glycoprotein. *Electrochimica Acta*, **403** (2022).

MODELING OF CONCENTRATION QUENCHING IN 2D AND 3D CHLOROPHYLL SYSTEMS

Sandra Barysaitė[1,2], Andrius Gelzinis[1,2], Jevgenij Chmeliov[1,2], Leonas Valkunas[1,2]

[1] Faculty of Physics, Vilnius University, Vilnius, Lithuania
[2] Department of Molecular Compound Physics, Centre for Physical Sciences and Technology, Vilnius, Lithuania
sandra.barysaite@ff.stud.vu.lt

Concentration quenching occurs when fluorescence quantum yield decreases upon increasing concentration of fluorophores in solution. This has been investigated throughout the last century, however, its origin is not fully understood to this day. An example of such occurrence has been observed in chlorophyll solutions: at higher concentrations the relative fluorescence intensity becomes dependent on the concentration and starts decreasing [1]. It is important to note that in artificial systems the fluorescence is usually significantly quenched at fluorophore concentrations typical to that of unquenched *in vivo* photosynthetic systems.

In this work, concentration quenching was simulated using approach similar to Ref. [2]. In the two-dimensional model molecules, each 1 nm in diameter, were scattered in a 10000 nm^2 area using a uniform distribution. Different concentrations were obtained by changing the number of molecules. When two or more molecules were closer to each other than a certain distance (R_{trap}), they formed a trap; excitation, after reaching a trap, could not escape. At the initial time moment, excitation was distributed equally among all non-trap molecules. Time dependence of the total excitation probability was calculated by solving the system of kinetic equations with energy transfer rates between the molecules being proportional to the inverse sixth power of the distance between the molecules, following the Förster level of description. The same principle was used in the three-dimensional model, where molecules were scattered uniformly in an 8000 nm^3 box. However, the trap formation condition was modified: nearby molecules formed an aggregate which, depending on its type, could become a trap.

The two-dimensional model was used to fit the measured fluorescence lifetimes of chlorophylls in monolayers at the nitrogen-water interface [3], results are shown in Fig. 1. Fitting was performed by finding the minimal squared deviation between experimental data points and calculated excitation lifetime values in the same concentrations. The three-dimensional model was used to fit the measured chlorophyll fluorescence lifetimes in lipid liposomes [4], however, the current model cannot explain the data sufficiently well, and a more sophisticated model will be presented in the conference.

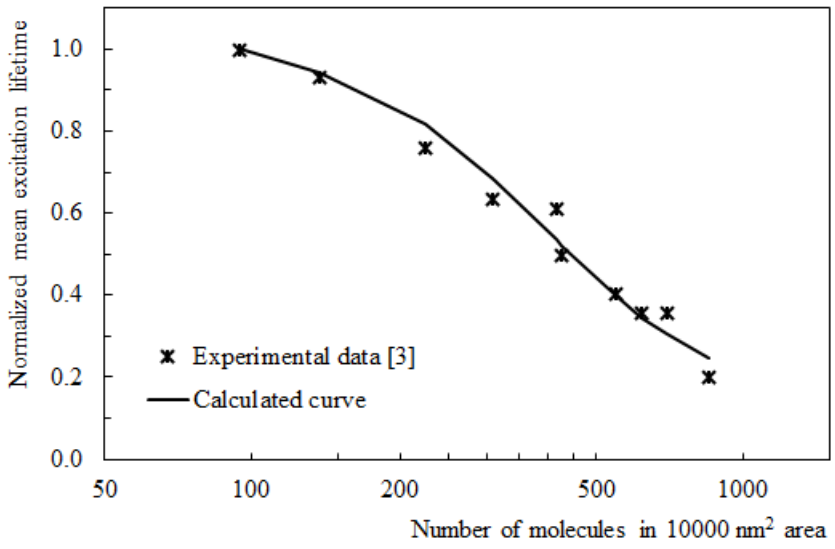


Fig. 1. Fitting of experimental data from Ref. [3].

[1] G. S. Beddard, G. Porter, *Nature* **260**, 366-367 (1976).
[2] W.-J. Shi, J. Barber, Y. Zhao, *The Journal of Physical Chemistry B* **117** (15), 3976-3982 (2013).
[3] M. L. Agrawal, J.-P. Chauvet, L.K. Patterson, *The Journal of Physical Chemistry* **89** (14), 2979-2982 (1985).
[4] G. S. Beddard, S. E. Carlin, G. Porter, *Chemical Physics Letters* **43** (1), 27-32 (1976).

SYNTHESIS OF NOVEL CALCIUM PHOSPHATES WITH WHITLOCKITE STRUCTURE VIA DISSOLUTION-PRECIPITATION PROCESS

Agne Kizalaite, Erlandas Kabasinskas, Diana Griesiute, Hanna Klipan, Gabriele Klydziute, Aleksej Zarkov

Institute of Chemistry, Vilnius University, Lithuania
agne.kizalaite@chgf.vu.lt

Trauma, various diseases such as osteoporosis, and other degenerative processes can weaken the human bone tissue. Moreover, with steadily increasing average population age this problem affects more and more people. Therefore, finding of new biomaterials with enhanced biological properties is very important for biomedicine of today.

One of the promising compounds in this area is whitlockite. Magnesium whitlockite ($Ca_{18}Mg_2H_2(PO_4)_{14}$) is the second most abundant mineral in human body and one of the main components of the human hard tissue, constituting to approximately 20–35 wt% [1]. Due to its excellent biocompatibility and osteogenic capability this compound attracted a lot of attention in recent years in the fields of bone regeneration and tissue engineering [2]. To further improve biological properties of whitlockite and achieve additional properties for specific clinical applications other bioactive ions instead of Mg can be introduced into the structure of the material.

This study presents simple and reliable way to synthesize metal ion substituted whitlockite compounds by dissolution-precipitation process using hydrothermal conditions. Pure phase whitlockite compounds containing Zn, Cu, and Mn were successfully synthesized. Synthesis conditions such as temperature, time, pH, and concentration were carefully studied and optimized for each compound individually. The amount of Zn, Cu, Mn ions in the crystalline structure was varied by varying their ratio with calcium in the reaction mixture. The effect of synthesis conditions on particle size and morphology was also investigated.

Synthesized compounds were analyzed by X-ray diffraction (XRD), Fourier-transform infrared spectroscopy (FTIR), scanning electron microscopy (SEM), inductively coupled plasma optical emission spectroscopy (ICP-OES) and Raman spectroscopy. Rietveld analysis was employed to calculate the structural parameters of the materials.

Acknowledgements

This research was funded by the European Social Fund under the No. 09.3.3-LMT-K-712 “Development of Competences of Scientists, other Researchers and Students through Practical Research Activities” measure (grant No. 09.3.3.-LMT-K-712-25-0012).

[1] H. Cheng, R. Chabok et al. Synergistic interplay between the two major bone minerals, hydroxyapatite and whitlockite nanoparticles, for osteogenic differentiation of mesenchymal stem cells, Acta Biomaterialia **69**, 342-351 (2018).

[2] H. L. Jang, G. Bin Zheng et al. s, In Vitro and In Vivo Evaluation of Whitlockite Biocompatibility: Comparative Study with Hydroxyapatite and β-Tricalcium Phosphate, Advanced Healthcare Material **5**, 128–136 (2015).

MOLECULAR ENGINEERING OF THE FLUORENE-BASED HOLE TRANSPORTING MATERIALS FOR EFFICIENT PEROVSKITE SOLAR CELLS

Aistė Jegorovė[1], Cristina Momblona[2], Marytė Daškevičienė[1], Artiom Magomedov[1], Rimgailė Degutytė[3], Abdullah M. Asiri[4], Vygintas Jankauskas[5], Albertus Adrian Sutanto[2], Mohammad Khaja Nazeeruddin,[2] Vytautas Getautis[1]

[1] Department of Organic Chemistry, Kaunas University of Technology, Lithuania.
[2] Group for Molecular Engineering of Functional Material, Institute of Chemical Sciences and Engineering, École Polytechnique Fédérale de Lausanne, Switzerland.
[3] Department of Food Science and Technology, Kaunas University of Technology, Lithuania.
[4] Center of Excellence for Advanced Materials Research (CEAMR), King Abdulaziz University, Saudi Arabia.
[5] Institute of Chemical Physics, Vilnius University, Lithuania.
aisilc@ktu.lt

Nowadays, people cannot imagine their life without everyday appliances. Most of these devices require electricity to operate. One of the most popular ways to extract energy is from non-renewable energy sources. But these energy sources have drawbacks, such as its residual products are generally non-biodegradable and can cause damage to environment. Consequently, scientists have been looking for alternative ways to generate energy from renewable sources, such as wind energy, solar energy, hydropower etc. The Sun is known to be the most powerful source of energy. Solar cells are devices that convert absorbed light into electricity and silicon solar cells are currently the most commonly used technology to do that. However, it has its own drawbacks and other high efficiency solar cell technologies have been developed. Perovskite solar cells (PSCs) have recently emerged as a promising technology for the further cost reduction of the energy production from the sunlight. Perovskite solar cells are among the most efficient third-generation cells however, there are several obstacles that need to be addressed for it to see a widespread use. One of them is the use of expensive charge-transporting semiconductors such as Spiro-OMeTAD or fullerene derivatives to obtain efficient devices [1]. Therefore, there is a vigorous search for cheaper and simpler methods for the synthesis of organic semiconductors. According to literature carbazole and fluorene chromophores are among the most popular structural building blocks, used for the construction of organic hole-transporting materials (HTMs) [2–4].

In this work we synthesized Spiro-OMeTAD analogues and simpler „half" structures, containing carbazolyl- and methoxyphenyl-chromophores, that have been obtained by a simple synthetic method. Thermal and photoelectrical properties were investigated and compared with Spiro-OMeTAD.

Molecular engineering of new hole transporting materials was realized under Hartwig-Buchwald amination conditions using commercially available starting materials. New compounds bear alkylated/arylated fluorene and spirobifluorene fragments as molecule-core, while 9-ethyl-*N*-(4-metoxyphenyl)-9*H*-carbazol-3-amine and bis(9-ethyl-9*H*-carbazol-3-yl)amine were used to build side chromophores. All synthesized HTMs exhibit good thermal stability, which depends on alkyl chain length and the number of carbazolyl moieties, at up to 400 °C. Almost all new HTMs showed T_g significantly exceeding 100 °C. According to DSC data the polymerization temperatures can be observed for materials **V1241** and **V1274**. These materials have vinyl group at central moiety. Polymers exhibit much better film-forming ability, than small-molecular organic HTM's and high hydrophobicity [5]. Unfortunately, these materials are not suitable for production of solar cells with an n-i-p structure due to their high polymerization temperatures (above 300 °C). Nevertheless, other compounds have amorphous state, which is important for homogenous films forming. The ionization potential (I_p) of target materials is in range of 4.85–5.28 eV which is suitable for use target materials in perovskite solar cells. From obtained data it is evident that all of materials are suitable for use in perovskite solar cells except for **V1241** and **V1274**. The PCE of the most efficient n-i-p PSCs perovskite device containing carbazolyl-terminated Spiro-OMeTAD analogue **V1267** have reached 18.3 %. The devices fabricated using the other HTMs reached lower efficiency: **V1269** (18.1 %), **V1258** (17.8 %), **V1240** (17.6 %), **V1257** (17.21 %), **V1238** (16.1 %), **V1226** (15.7 %), **V1222** (15.7 %). Furthermore, "half" structures with methoxyphenyl/carbazolyl fragments show good long-term stability and outperform Spiro-OMeTAD.

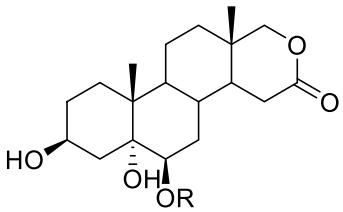
[1] T. P. I. Saragi, T.Spehr, A. Siebert, T. Fuhrmann-Lieker, J. Salbeck. *Chem. Rev*. **107**, 1011- 1065 (2007).
[2] X. Liu, S. Ma, M. Mateen, P. Shi, C. Liu, Y. Ding, M. Cai, M. Guli, M. K. Nazeeruddin, S. Dai, *Sustainable Energy Fuels*, **4**, 1875 (2020).
[3] D. Y. Lee, G. Sivakumar, Manju, R. Misra, S. I. Seok**,** *ACS Appl. Mater. Interfaces*, **12**, 28246 (2020).
[4] S. Daskeviciute, C. Momblona, K. Rakstys, A. A. Sutanto, M. Daskeviciene, V. Jankauskas, A. Gruodis, G. Bubniene, V. Getautis, M. K. Nazeeruddin, *J. Mater. Chem. A*, **9**, 301 (2021).
[5] X. Sun, X. Yu, Z. Li**.** *ACS Appl. Energy Mater*. **3**, 11, 10282–10302 (2020).

DETERMINING THE SUITABILITY OF *in silico* TOXICOLOGY PREDICTION TOOLS FOR APPLICATION ON STEROIDAL DRUG CANDIDATES

Milica Ilić[1], Marija Sakač[1], Ivana Kuzminac[1]

[1] 1 University of Novi Sad, Faculty of Sciences, Department of Chemistry, Biochemistry and Environmental Protection, Trg Dositeja Obradovića 3, Novi Sad, Serbia
milica.ilic@dh.uns.ac.rs

Assessing the toxicity of newly synthesized compounds is crucial for drug development. It is a well-known fact that determining toxic doses in animals is a common method of preclinical evaluation. A number of *in silico* tools are developed in the last decade with the purpose to facilitate and reduce costs of preclinical and clinical trials. *In silico* web tools for predicting the toxicity of compounds are rapid and diverse, and we have chosen five free-of-charge tools in order to compare their efficacy and to determine the most convenient one according to the data it provides. Since structurally modified steroids have proven to be good anticancer agents, many were synthesized and tested for their antiproliferative activity in our laboratories. We selected two D-homo lactone derivatives that have shown good activity, 3β,5α,6β-trihydroxy **1** and 3β,5α-dihydroxy-6β-methoxy derivative **2** and used them as samples in the *in silico* tools (Figure 1)[1]. Compound **1** has shown strong cytotoxicity toward lung cancer cells (A549 IC_{50} 0.99), and compound **2** toward estrogen negative breast cancer cells (MDA-MB-231 IC_{50} 3.38). We have compared the values obtained using five different *in silico* web tools for toxicity prediction: StopTox [2], ProTox II [3], Sintelly [4], admetSAR [5], and pkCSM [6]. Apart from that, the time required for calculation, the amount, and the form in which data were obtained, were also considered in order to determine the most convenient *in silico* web tool.



1 R_1=H A549 0.99
2 R_2=Me MDA-MB-231 3.38

Fig. 1. Stucture of selected steroidal D-homo lactones

[1] I. Z. Kuzminac, D. S. Jakimov et al., Synthesis and anticancer potential of novel 5,6-oxygenated and/or halogenated steroidal D-homo lactones, Bioorg. Med. Chem. **30**, 115935 (2021).
[2] https://stoptox.mml.unc.edu/ accessed: 14.01.2022.
[3] https://tox-new.charite.de/protox_II/ accessed: 14.01.2022.
[4] https://app.syntelly.com/ accessed: 14.01.2022.
[5] H. Yang, C. Lou, et al., admetSAR 2.0: web-service for prediction and optimization of chemical ADMET properties, *Bioinformatics* **35**, 1067–1069 (2019).
[6] D. E. V. Pires, T. L. Blundell, D. B. Ascher, pkCSM: predicting small-molecule pharmacokinetic and toxicity properties using graph-based signatures, *J. Med. Chem.* **58**, 4066–4072 (2015).

SYNTHESIS AND *IN SILICO* ADMET PROPERTIS OF B-RING-MODIFIED HYODEOXYHOLIC ACID

Ivana Zorić[1], Ksenija Pavlović[1]

[1] Department of Chemistry, Biochemistry and Environmental Protection, Faculty of Sciences, University of Novi Sad, Trg Dositeja Obradovića 3, 21000 Novi Sad, Serbia
izoric.b178.17@one.pmf.uns.ac.rs

Bile acids are a class of steroid molecules that are biosynthesized in the human liver from cholesterol. These molecules possess a rigid steroid nucleus and a short aliphatic side chain terminating in a carboxyl group. Their most important function is to promote the absorption of lipids from the intestine. However, the discovery that bile acids are natural ligands of the farnesoid X receptor (FXR), that they are signaling molecules for various endocrine and paracrine functions, indicated that these compounds possess a wide range of biological activities[1,2].

The introduction of heteroatom or replacement of carbon atoms in steroidal molecule of bile acids lead to changes in the chemical properties of the steroidal molecule and results in alterations of its biological activities [3].

In this paper, we report the synthesis of hyodeoxycholic acid derivatives with modifications on steroid skeleton. Modifications were included the introduction of oxyimino and lactam group in B-ring. New compounds **3** and **4** were obtained according to established synthetic procedures (Fig. 1.) and confirmed by NMR spectral data. In addition, the physicochemical properties of these compounds were predicted using SwissADME and ProTox-II web tools.

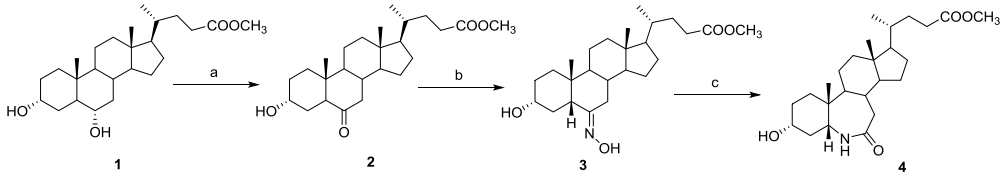


Fig. 1. Synthesis of new hyodeoxycholic acid laktam.

A suitable synthesis of new lactam derivative (**4**) was performed in three steps, starting from the hyodeoxycholic acid methyl ester (**1**). *In silico* ADMET analysis showed that synthesized oxyimino and lactam derivatives **3** and **4** possess desirable drug-like properties which are required for Lipinski, Veber, Egan, Ghose and Muegge criteria. The bioavailability radars indicated that compounds are in the optimal range for lipophilicity, polarity, solubility, saturation and flexibility and thus to possess appropriate biological potential. Prediction of pharmacokinetic behavior showed that compound **3** could be absorbable by the intestines but couldn't penetrate the brain and compound **4** could be absorbed cross the blood-brain barrier and by the human intestine. Toxicity prediction results showed that tested compounds do not possess mutagenic, carcinogenic and cytotoxic potential.

[1] R. Sharma, A. Long, J. F. Gilmer, Curr. Med. Chem. 18 (2011) 4029–4052
[2] S.M. Houten, M. Watanabe, J. Auwerx, EMBO J. 25 (2006) 1419-1425
[3] Y. Huanga, S. Chenb, J. Cui, C. Gan, Z. Liu, Y. Wei, H. Song, Steroids 76 (2011) 690–694

REACTION OF 1-(4-(PHENYLAMINO)PHENYL)-5-OXOPYRROLIDINE-3-CARBOHYDRAZIDE WITH AROMATIC ALDEHYDES

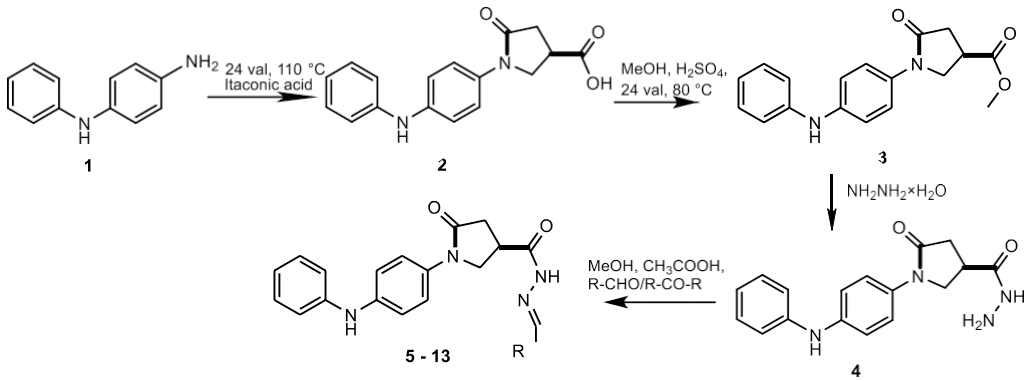
Irma Sanvaitytė[1*], Kristina Kantminienė[2], Ingrida Tumosienė[1]

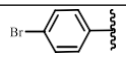
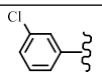
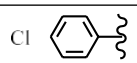
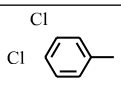
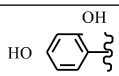
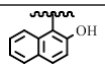
[1] Department of Organic Chemistry, Kaunas University of Technology, Lithuania
[2] Department of Physical and Inorganic Chemistry, Kaunas University of Technology, Lithuania
irma.sanvaityte@ktu.edu

Hydrazones constitute an important class of biologically active drug molecules which has attracted the attention of medicinal chemists due to their wide range of pharmacological properties. These compounds are synthesized as pharmaceutical agents in order to combat diseases with minimal toxicity and maximal effects [1]. Hydrazones, whose biological activity is associated with the presence of the active azomethine pharmacophore, are of wide interest because of their diverse biological activities, such as antimicrobial, antimycobacterial, antimalarial, antiviral, anti-HIV, anti-inflammatory, anticancer, anticonvulsant, antidepressant, analgesic, antiplatelet, anthelmintic, antidiabetic, etc. [2-4].

Diphenylamine is a naturally occurring compound present in coriander, onions, tea leaves and peel of citrus fruits. Diclofenac, a diphenylamine derivative, is a nonsteroidal anti-inflammatory drug with anti-inflammatory, analgesic, and antipyretic properties. Other important diphenylamine-based non-steroidal anti-inflammatory drugs are painkillers tolfenamic acid and mefenamic acid. Due to the secondary amine function diphenylamine derivatives have been studied as antioxidants. Other important biological activities of diphenylamine-based compounds include antimicrobial, antimycobacterial, analgesic, anti-inflammatory, anticonvulsant and anticancer [5].

With the aim to synthesize compounds bearing several moieties with pharmacological activity as potential hybrid drug candidates, compounds **5-13** were synthesized in good yield (Scheme 1).



No	5	6	7	8	9	10	11	12	13
R									

Scheme 1. Synthetic route towards hydrazones **5-13**

Reaction of the starting compound 4-aminodiphenylamine (**1**) with itaconic acid at reflux temperature provided carboxylic acid **2**, which was transformed to ester **3** by a classical esterification reaction in methanol in the presence of sulfuric acid. Reaction of **3** with an excess of hydrazine hydrate gave hydrazide 1-(4-(phenylamino)phenyl)-5-oxopyrrolidine-3-carbohydrazide (**4**). Target hydrazones **5-13** were synthesized by the reaction of **4** with various aldehydes in methanol [6,7]. Structures of all target compounds were confirmed by ^{1}H and ^{13}C NMR as well as mass spectrometry data.

[1] M. Asif, A. Husain, Analgesic, Anti-Inflammatory, and Antiplatelet Profile of Hydrazones Containing Synthetic Molecules, Journal of Applied Chemistry, Article ID 247203 (2013).
[2] S. Rollas, S.G. Küçükgüzel, Biological Activities of Hydrazone Derivatives, Molecules **12**, 1910-1939 (2007).
[3] G. Verma, A. Marella, et al. A review exploring biological activities of hydrazones, Journal of pharmacy & bioallied sciences **6**, 69-80 (2014).
[4] V. Kumar, Hydrazone: A promising pharmacophore in medicinal chemistry, Journal of Pharmacognosy and Phytochemistry **7**, 40-43 (2018).
[5] A. Kumar, A. K. Mishra, Pharmacological applications of diphenylamine and its derivatives as potent bioactive compounds: a review, Current Bioactive Compounds **14**, 217-233 (2018).
[6] I. Tumosienė, K. Kantminienė, et al., Antioxidant and Anticancer Activity of Novel Derivatives of 3-[(4-Methoxyphenyl)amino]propanehydrazide, Molecules **25**, 2980 (2020).
[7] I. Tumosienė, I. Jonuškienė, et al., Novel *N*-Substituted Amino Acid Hydrazone-Isatin Derivatives: Synthesis, Antioxidant Activity, and Anticancer Activity in 2D and 3D Models *In Vitro*, International Journal of Molecular Sciences **22**, 7799 (2021).

SYNTHESIS AND PROPERTIES OF FLUORENE DERIVATIVES AS HOLES AND ELECTRONS TRANSPORTING MATERIALS

Julius Petrulevičius[1], Marytė Daškevičienė[1], Egidijus Kamarauskas[2], Vygintas Jankauskas[2], Vytautas Getautis[1]

[1] Department of Organic Chemistry, Kaunas University of Technology, Lithuania
[2] Institute of Chemical Physics, Vilnius University, Lithuania
Julius.petrulevicius@ktu.edu

Solar energy is an inexhaustible and the most important source of renewable energy. Solar cells (SC) are used to extract this energy. Currently, Silicon based solar cells are the most common commercial product. However, production of these solar cells is complicated and expensive. A viable alternative to it is perovskite solar cells (PSC), which era began in 2009 with a power conversion efficiency of 3.8% [1]. Recently, the record power conversion efficiency (29.15%) has been achieved with the monolithic perovskite / silicon tandem [2].

Holes transporting material (HTM) is one of the main constituents of PSC, determining the cost, energy conversion efficiency and longevity of the device [3]. The main disadvantage of majority of organic HTMs is the low mobility of the holes. To overcome this shortcoming, HTM additives, which reduce the stability of the PSC are often used. Therefore, organic semiconductors that do not require additives have been receiving increasing attention. One of such organic semiconductors is bipolar organic semiconductors [4].

The aim of this work was to synthesize fluorene derivatives with hole- and electron--transporting ability and to investigate the properties of these compounds.

During the Buchwald reaction diphenylamine moieties were added to 2,7-dibromofluorenone or 2,8-dibromindeno [2,1-*b*] fluorene-6,12-dione [5] resulting in formation of intermediate HTMs **V1374** and **V1383**. During the Knoevenagel condensation reaction [6], the fluorenone carbonyl group was replaced with CN groups using malononitrile to provide HTMs **V1384** and **V1416**.

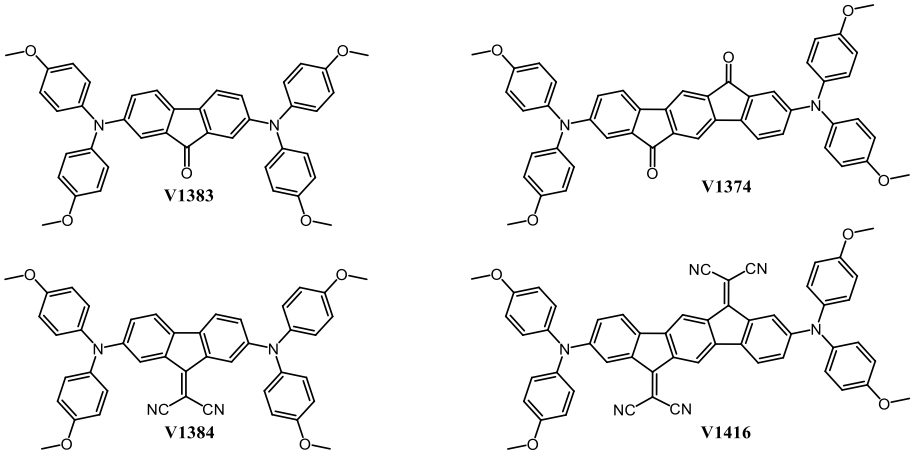


Fig. 1. Bipolar fluorene derivatives

The structure of the synthesized new compounds **V1374**, **V1383**, **V1384** and **V1416** was confirmed resonance ^{1}H and ^{13}C NMR, IR spectroscopy, and elemental analysis data. The measured drift charge mobility of the new organic semiconductors **V1374**, **V1383** and **V1384** has confirmed that these compounds can transport both positive ($\mu^{d} = 1.2 \cdot 10^{-6}$-$6.3 \cdot 10^{-6}$ cm^2/Vs) and negative ($\mu^{d} = 5.0 \cdot 10^{-5}$-$7.0 \cdot 10^{-4}$ cm^2/Vs) charge carriers. Their ionization potentials values (I_p = 5.28-5.33 eV) prove their suitability for application in perovskite solar cells.

[1] A. Kojima, K. Teshima, Y. Shirai, et al., Organometal Halide Perovskites as Visible-Light Sensitizers for Photovoltaic Cells, Journal of the American Chemical Society **131**, 6050-6051 (2009).
[2] A. Al-Ashouri, E. Köhnen, A. Magomedov et al., Monolithic Perovskite/Silicon Tandem Solar Cell with >29% Efficiency by Enhanced Hole Extraction, Science **370**, 1300-1309 (2020).
[3] H. D. Pham, T. C. Yang, S. M. Jain, et al. Development of Dopant-Free Organic Hole Transporting Materials for Perovskite Solar Cells, Advanced Energy Materials **10**, 1903326 (2020).
[4] K. Rakštys, C. Igcia, M. K. Nazeeruddin, Efficiency vs. stability: dopant-free hole transporting materials towards stabilized perovskite solar cells, Chemical Science **10**, 6748-6769 (2020).
[5] S.D. Surry, L.S. Buchwald, Dialkylbiaryl Phosphines in Pd-Catalyzed Amination: A User's Guide, Chemical Scienc. **2**, 27-50 (2011).
[6] C. Chakraborty, M. K. Bera, U. Rana et al., Vice versa donor acceptor fluorene–ferrocene alternate copolymer: a twisted ribbon for electrical switching, Chemical Communications **51**, 13123-13126, (2015).

SYNTHESIS OF 1,2,4-TRIAZOLE-3-THIONE DERIVATIVES BEARING 2-AMINOPYRIDINE MOIETY

Iveta Žukaitė[1*], Ingrida Tumosienė[1], Kristina Kantminienė[2], Zigmuntas Jonas Beresnevičius[1]

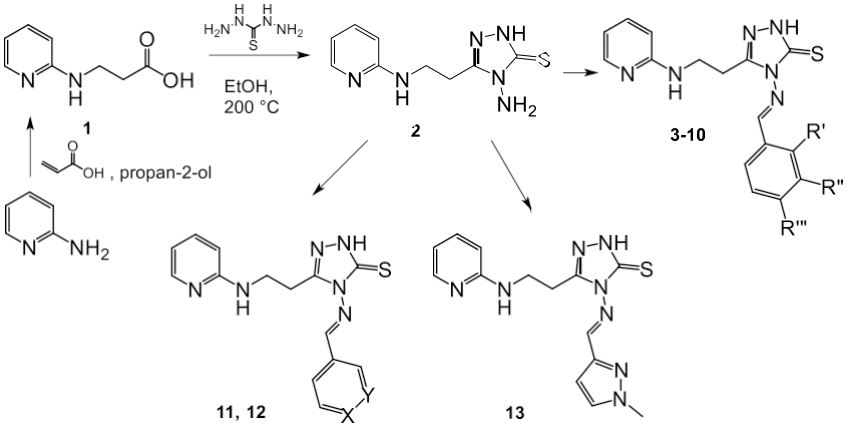
[1] Department of Organic Chemistry, Kaunas University of Technology, Lithuania
[2] Department of Physical and Inorganic Chemistry, Kaunas University of Technology, Lithuania
iveta.zukaite@ktu.edu

Throughout the history of medicinal chemistry, heterocyclic compounds have been attracting a particular attention of medicinal and organic chemists. Heterocyclic moieties constitute a structural core of many natural and synthetic medicinal substances. Nowadays, approximately 75% of modern low molecular mass pharmaceutical agents used in medicine contain heterocyclic fragments.

The pyridine ring is present in the structure of vitamins (vitamins B3 and B6), coenzymes (nicotinamide adenine dinucleotide (NAD)) and alkaloids (trigonelin and papaverine) [1]. Pyridine became an interesting target in 1930 with the importance of niacin for the treatment of dermatitis and dementia [2]. Today, pyridine is the second most common nitrogen-containing heterocycle found in many drugs, such as isoniazid, etionamide, torasemide, pyridostigmine, crizotinib, vismodegib and gefitinib, baricitinib, ticagrelor, etc. [3, 4]. Pyridine derivatives have been shown to possess antimicrobial, antioxidant, antiviral, anticancer, anti-malarial, anti-inflammatory, etc. activity [5].

1,2,4-Triazole-3-thione derivatives form another very important class of heterocyclic compounds and are being studied in medicinal chemistry for their broad biological activity, e.g. antibacterial, antioxidant, anticonvulsant, antidepresant, anti-inflammatory, etc. [6].

The aim of this work is synthesis of biologically active compounds bearing 2-aminopyridine and 1,2,4-triazole-3-thione moieties (Scheme 1).



No	R’	R”	R’”	No	R’	R”	R’”
3	H	H	H	**8**	OCH_3	OCH_3	H
4	H	H	CH_3	**9**	OCH_3	H	H
5	NO_2	H	H	**10**	OH	H	H
6	H	H	$N(CH_3)_2$	**11**		X = N; Y = H	
7	H	H	COOH	**12**		X = H; Y = N	

Scheme 1. Synthesis of compounds **2–13**

The starting compound 4-amino-3-(2-(pyridin-2-ylamino)ethyl)-*1H*-1,2,4-triazole-5(*4H*)-thione (**2**) was synthesized by melting carboxylic acid **1** with thiocarbohydrazide [4]. The subsequent reaction of **2** with various aldehydes provided novel 1,2,4-triazole derivatives **3–13** in 20-64% yield.

[1] Y. Hamada, Role of pyridines in medicinal chemistry and design of BACE1 inhibitors possessing a pyridine scaffold, in Pyridine, Ed. P.P. Pandey (London, IntechOpen, 2018).
[2] G.D. Henry, De Novo, Synthesis of Substituted Pyridines, Tetrahedron **60**, 6043-6061 (2004).
[3] M. A. Chiacchio, D. Iannazzo, et al. Pyridine and Pyrimidine Derivatives as Privileged Scaffolds in Biologically Active Agents. Current Medicinal Chemistry **26**, 7166-7195 (2019).
[4] S. Wang, X.-H. Yuan, et al. FDA-approved pyrimidine-fused bicyclic heterocycles for cancer therapy: Synthesis and clinical application, European Journal of Medicinal Chemistry **214**, 113218 (2021).
[5] A. A. Altaf, A. Shahzad, et al. A Review on the Medicinal Importance of Pyridine Derivatives. Journal of Drug Design and Medicinal Chemistry **1**, 1-11 (2015).
[6] Ş.G. Küçükgüzel, P. Çıkla-Süzgün, Recent advances bioactive 1,2,4-triazole-3-thiones, European Journal of Medicinal Chemistry **97**, 830-870 (2015).
[7] I. Tumosiene, Z. I. Beresnevicius, Synthesis of azoles from 3-[(3-hydrazino-3-oxopropyl)anilino]- and 3-[(3-hydrazino-3-oxopropyl)-4-methylanilino]propane hydrazides, Chemistry of Heterocyclic Compounds **43**, 1148-1153, (2007).

STRONTIUM SUBSTITUTION EFFECT ON THE STRUCTURE, SURFACE MORPHOLOGY AND THERMOANALYTICAL PROPERTIES OF $La_2Mo_2O_9$ SYSTEM

Giedrė Gaidamavičienė, Artūras Žalga

Faculty of Chemistry and Geosciences, Institute of Chemistry, Vilnius University, Naugarduko str. 24, LT-03225 Vilnius, Lithuania
giedre.prievelyte@chf.vu.lt

Due to the increasing ecological requirements for power sources, oxide-ion conductors have garnered various researchers' attention due to their potential applications in solid oxide fuel cells (SOFCs) as a next generation of the green energy system. One of the most widely used and investigated electrolytes is yttria-stabilized zirconia (YSC) which has excellent ionic conductivity at high temperatures (1000 °C). However, high working temperature results in electrolyte performance degradation and shortens the lifetime of SOFCs systems. Therefore, low-temperature alternative electrolytes with enhanced ionic conductivities are being investigated [1].

Since the first report by Lacorre et al. [2] that the LAMOX family of oxides based on $La_2Mo_2O_9$ can be a potential candidate for oxide-ion conduction a new window of materials in the field of oxide-ion conductors has been opened up [3]. This compound crystallizes into two different crystallographic modifications: low-temperature monoclinic α-phase and high-temperature cubic β-phase. It was found that the ionic conductivity of this material is strongly associated with the phase transition from monoclinic α-phase to cubic β-phase which occurs at 580 °C temperature. The main reason for the much higher ionic conductivity in the β-$La_2Mo_2O_9$ crystal phase is related to the higher oxygen vacancies concentration in its structure, which creates additional paths for oxygen ions diffusion. Thus, the increase in the conductivity of oxygen ions has a close connection with the enhanced concentration of vacancies in the electrolyte structure.

The stabilization of high-temperature cubic phase by substituting of La sites with alkaline earth (Ca, Sr, Ba) metals remains a great challenge because of the enhanced suppression of β-phase, however, the introduction of extra oxygen vacancies leads to higher anionic conductivity of corresponding ceramic mixture [4, 5]. Gao clearly showed that a suitable amount of Sr doping in $La_2Mo_2O_9$ not only can completely suppress the structural phase transition, resulting in high-temperature phase stabilization at room temperature but also can effectively increase oxide-ion conductivity of samples at higher temperatures [6].

The use of a conventional solid-state reaction method for the synthesis of $La_2Mo_2O_9$ ceramic is most common because of the simplicity and high availability of this technique. Despite these advantages, the control of the mixing stage of starting materials remains the main drawback for solid-state synthesis which usually leads to impurities, higher porosity, and lower connectivity between grains in final ceramic. This side effect could be successfully eliminated by using so-called wet chemical techniques, which enable the enhancement of the mixing stage at the molecular level and improve the properties of final ceramics. Moreover, it is possible to control final ceramic molar composition, particle size, morphology, purity, homogeneity, and other properties by changing synthesis parameters like temperature, nature of the starting materials and complexing agent, concentration, pH, solvent, reaction time, etc.

In this study, the homogenous oxide-system for $La_{2-x}Sr_xMo_2O_{9-\delta}$ (x=0.01–0.2) was prepared using an aqueous sol-gel synthesis method. This method is mainly based on the use of tartaric acid as a complexing agent that reduces interactions between the individual components avoiding the formation of precipitates during the evaporation stage from the reaction mixture. The thermal decomposition of La–Sr–Mo–O tartrate gel precursor and phase transition of $La_{2-x}Sr_xMo_2O_{9-\delta}$ crystalline system was investigated by thermogravimetric analysis and differential scanning calorimetry (TGA-DSC). The obtained results clearly showed that the substitution effect stabilizes cubic β-phase for $La_2Mo_2O_9$ at room temperature. Besides, no phase transition for the $La_{2-x}Sr_xMo_2O_{9-\delta}$ samples from meta-stable cubic to monoclinic phase was observed. X-ray diffraction (XRD) analysis was performed in order to determine the crystal structure of the heat-treated ceramic materials. The microstructure and surface morphology of the ceramics heat-treated at 1200 °C of temperature were analyzed by scanning electron microscopy (SEM).

[1] C. Tian, L. Shao, et al., Synthesis and characterization of tungsten and barium co-doped $La_2Mo_2O_9$ by sol-gel process for solid oxide fuel cells, Journal of Rare Earths, **37**, 984-988 (2019).
[2] P. Lacorre, F. Goutenoire, et al., Designing fast oxide-ion conductors based on $La_2Mo_2O_9$, Nature, **404**, 856-858 (2000).
[3] S. Basu, P. Sujatha Devi, et al., Synthesis, thermal and electrical analysis of alkaline earth doped lanthanum molybdate, Solid State Ionics, **231**, 87-93 (2013).
[4] C. Tealdi, G. Chiodelli, et al., Effect of alkaline-doping on the properties of $La_2Mo_2O_9$ fast oxygen ion conductor, Journal of Materials Chemistry, **14**, 3553-3557 (2004).
[5] D. Zhang, Z. Zhuang, et al., Electrical properties and microstructure of nanocrystalline $La_{2-x}A_xMo_2O_{9-\delta}$ (A = Ca, Sr, Ba, K) films, **181**, 1510-1515 (2010).
[6] X. Gao, T. He, et al., Structures, electrical and thermal expansion properties of Sr-doped $La_2Mo_2O_9$ oxide-ion conductors, Journal of Alloys and Compounds, **464**, 461-466 (2008).

MECHANOCHEMICAL PREPARATION OF DIFFERENT CRYSTAL FORMS OF PHARMACEUTICAL SUBSTANCES

Zane Čerpakovska[1], Artis Kons[1], Agris Bērziņš[1*]

[1] Faculty of Chemistry, University of Latvia, Jelgavas iela 1, Riga, Latvia
zc13011@edu.lu.lv

Drugs may exhibit different solid forms, and this diversity often modifies their physicochemical and bioabsorption properties. Pharmaceuticals can exist either as single component phases with the different crystal structures (polymorphs), and also as multicomponent phases such as solvates, co-crystals, and salts. Moreover, each of these multicomponent phases can form different polymorphs. It is reported that approximately 80% of all drug molecules exhibit polymorphism [1].

The most common method used to control polymorphism is crystallization. An alternative to the most commonly used solvent crystallization is the mechanochemical treatment of a crystalline substance or mixture of more than one substance. Mechanochemistry is defined as chemical synthesis induced by external mechanical energy, such as grinding two solids using a mortar-and-pestle, ball-mill, or shaker [2]. Such reactions are classified as Green Chemistry synthesis, prioritizing high yields, mild conditions and low to no use of solvents [3].

To date, three polymorphic forms of 3-hydroxybenzoic acid (3OHBA, Figure 1.a) have been described [4]. Similarly, crystal structures of three polymorphs have been found for co-crystal formed between urea (Figure 1.b) and barbituric acid (BA, Figure 1.c) [5].

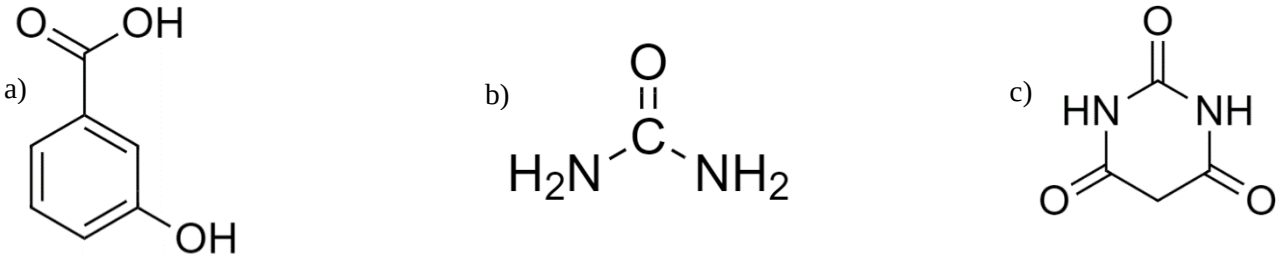


Fig. 1. a) Molecular structure of 3OHBA, b) Molecular structure of urea, c) Molecular structure of BA

In research of solid form landscape of 3-hydroxybenzoic acid two solvates and one salt not previously described in the literature were obtained mechanochemically. These phases were also obtained by a common evaporative crystallization method.

Polymorphic forms of urea-barbituric acid co-crystal can be obtained not only by the most commonly used crystallization methods from non-aqueous solvents as described in the literature, but also mechanochemically by grinding in presence of a few drops of water. This preparation procedure corresponds to the direction of green chemistry, and further research has the potential to identify an industrially useful and cost-effective preparation procedure.

[1] M. Solares-Briones, G. Coyote-Dotor, J. C. Páez-Franco, M. R. Zermeño-Ortega, C. M. de la O Contreras, D. Canseco-González, J. M. Germán-Acacio, Mechanochemistry: A Green Approach in the Preparation of Pharmaceutical Cocrystals, Pharmaceutics **13(6)**, 790 (2021).
[2] J. Stojakovic, L. R. MacGillivray, Cocrystals and Templates to Control Solid-State [2+2] Photodimerizations, Comprehensive Supramolecular Chemistry II **7**, 73–87 (2017).
[3] R. S. Varma, Greener and Sustainable Trends in Synthesis of Organics and Nanomaterials, ACS Sustainable Chemistry & Engineering **4(11)**, 5866–5878 (2016).
[4] D. E. Braun, The trimorphism of 3-hydroxybenzoic acid: an experimental and computational study, CrystEngComm **23(13)**, 2513–2519 (2021).
[5] M. Gryl, A. Krawczuk & K. Stadnicka, Polymorphism of urea–barbituric acid co-crystals, Acta Crystallographica Section B Structural Science **64(5)**, 623–632 (2008).

MOLECULAR DYNAMICS STUDY OF CATION DYNAMICS IN THE $[(CH_3)_2NH_2][Zn(HCOO)_3]$ HYBRID PEROVSKITE FRAMEWORK

Nojus Radzevičius[1], Linas Vilčiauskas[1,2]

[1]Institute of Chemistry, Faculty of Chemistry and Geosciences, Vilnius University, Lithuania
[2]Center for Physical Sciences and Technology (FTMC), Saulėtekio al. 3, LT-10257, Lithuania
nojus.radzevicius@chgf.stud.vu.lt

Dimethylammonium metal-formate frameworks $[(CH_3)_2NH_2][M(HCOO)_3]$ (DMAM, where M = Mn, Fe, Co, Ni, Zn, or Mg) are currently some of the most studied hybrid perovskite materials due to their magnetic, ferroelectric and multiferroic properties[1, 2]. Such materials have a typical perovskite structure (ABX_3), where the metal and formate ions form a framework with cavities that are filled with $(CH_3)_2NH_2^+$ (DMA^+) cations. The mechanical, magnetic and electric properties of such materials are determined by the hydrogen bonds that are formed by DMA^+ cations with the rest of the framework. Most DMAM materials exhibit phase transitions, in which the DMA^+ cations cooperatively form highly ordered structures and thus deform the metal-formate framework, leading to changes in magnetic and dieelectric properties[2, 3],

Many experimental methods have been used to study these frameworks and the cation dynamics within them [1, 2, 3]. However, none of these methods allow for elucidation of detailed, atom-level cation dynamics and their relation to the magnetic properties of the materials. Molecular dynamics simulations allow for detailed analysis of particle motion, calculated via Newton's equations using empirical sets of effective interatomic potentials.

In this study, the calculations of DMA^+ cation dynamics in DMAZn were performed using the *General AMBER Force Field* (GAFF) [4] and the *Universal Force Field for Metal–Organic Frameworks* (UFF4MOF) [5]. Cation dynamics and magnetic properties were analyzed at different phases and temperatures by calculating autocorrelation function of cation vector orientation and the moving average of total dipole moment of the system (Fig. 1). Physical properties, such as density and its dependence on temperature (Fig. 2) were compared with experimental data. The results show poor agreement between experimental results and GAFF simulations, but much better agreement in the case of UFF4MOF simulations, suggesting that more specialized force fields are needed for accurate results from molecular dynamics simulations.

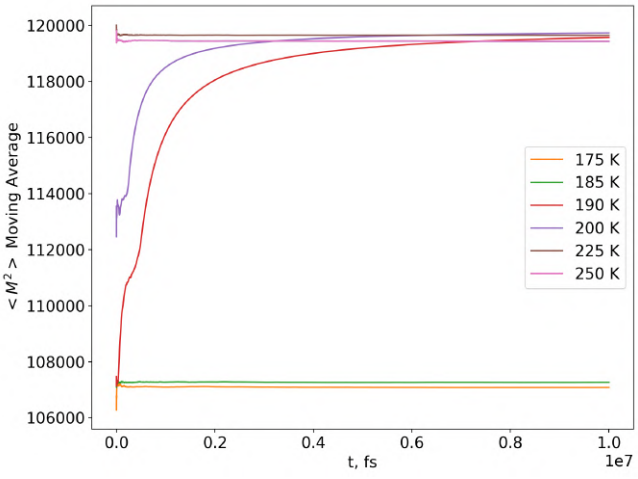


Fig. 1. Moving average of total dipole moment $< |M^2| >$ in UFF4MOF simulations

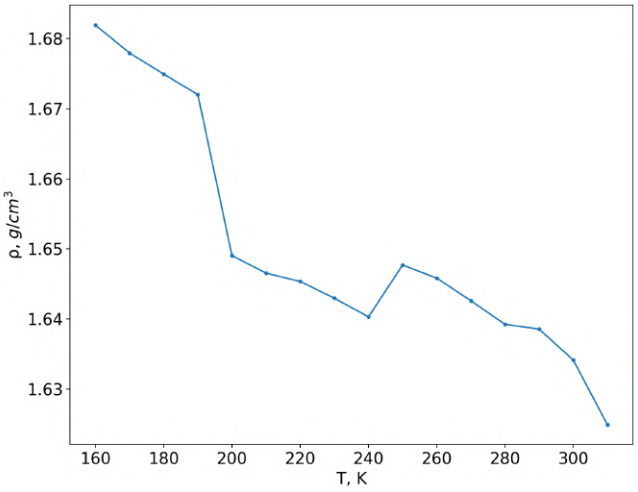


Fig. 2. Dependence of density on temperature in UFF4MOF simulations

[1] Besara, T. et al. (2011). *Mechanism of the order-disorder phase transition, and glassy behavior in the metal-organic framework* $[(CH_3)_2NH_2][Zn(HCOO)_3]$. Proceedings of the National Academy of Sciences, 108(17), 6828–6832.
[2] Jain, P. et al. (2008). *Order-Disorder Antiferroelectric Phase Transition in a Hybrid Inorganic-Organic Framework with the Perovskite Architecture.* Journal of the American Chemical Society, 130(32), 10450–10451.
[3] Jain, P. et al. (2009). *Multiferroic Behavior Associated with an Order-Disorder Hydrogen Bonding Transition in Metal-Organic Frameworks (MOFs) with the Perovskite* ABX_3 *Architecture.* Journal of the American Chemical Society, 131(38), 13625–13627.
[4] Wang, J. et al. (2004). *Development and testing of a general amber force field.* Journal of Computational Chemistry, 25(9), 1157–1174.
[5] Coupry, D. E. et al. (2016). *Extension of the Universal Force Field for Metal–Organic Frameworks.* Journal of Chemical Theory and Computation, 12(10), 5215–5225.

USING NEURAL NETWORKS TO DESCRIBE THE DYNAMICS OF ELECTRONIC EXCITATION IN TWO-DIMENSIONAL SYSTEMS

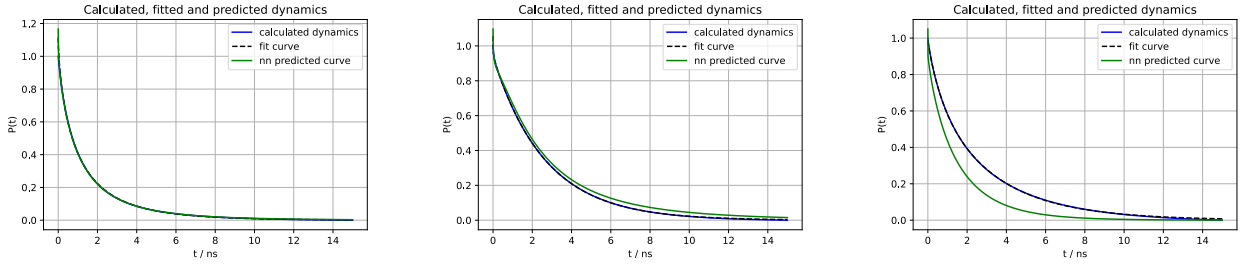
Pranas Juknevičius[1,2], Andrius Gelžinis[1,2], Jevegenij Chmeliov[1,2]

[1]Faculty of Physics, Vilnius University, Lithuania
[2]Center for Physical Sciences and Technology, Lithuania
pranas.juknevicius@ff.stud.vu.lt

Neural network is a machine learning algorithm, that has been successfully applied to tackle a wide range of physics related problems. In our work we try to describe the dynamics of electronic excitation in two-dimensional systems by using a neural netwok. These dynamics could also be described using a two-dimensional square lattice model. This type of lattice model can represent the arrangement of photosynthetic complexes in *in vitro* aggregates or in thylakoids membranes [1]. We assumed that each site of the lattice can be in either a fluorescing or a quenched state. Many different systems could be described by the considered lattice model, depending on the exact values of the parameters. Neural network should be able to predict a variety of such systems. Thus, we consider many different sets of parameter values. The values ranges are similar to previous modeling of real-life processes taking place in light-harvesting complexes at room temperature [1].

Real life light-harvesting systems can be described by an ensemble of such lattices, because light-harvesting complex can undergo conformational changes on a milisecond timescale. So we average through different lattice arrangements and exact number of dark complexes with the same model parameters.We assume that the initial excitation is distributed homogeneously across the whole lattice. Using the Pauli Master equations we calculated the averaged kinetics of the system. This type of description was successfully used to model assemblies of light-harvesting complexes [2].

The objective for the neural network is to predict the averaged fluorescing population kinetics from the lattice model parameters. It is convenient to fit the averaged kinetics with a function. The average mean squared error difference (MSE) between the fitted function and the averaged kinetics was $1.7697 \cdot 10^{-5}$. Thus, we only need to predict the fitting coefficients instead of the averaged kinetics. For this we use a fully connected sequantial neural network. We used a standart MSE loss function between the fitted coefficients and neural network predictions. With this loss function we got an average $1.8504 \cdot 10^{-2}$ MSE difference between the neural network predicted kinetics and the averaged kinetics. The averaged MSE difference between neural network predicted kinetics and the fitted averaged kinetics was $1.8447 \cdot 10^{-2}$. Then we redefined the loss as the MSE difference between the predicted curve and fitted/calculated curve and got an average MSE of $5.505 \cdot 10^{-5}$ between the neural network predicted kinetics and the fitted averaged kinetics. The average MSE between the neural network predicted kinetics and the averaged kinetics was $8.340 \cdot 10^{-5}$(see Fig.1 to get a sense of different MSE values).



(a) Predicted kinetics vs fitted kinetics MSE: 7.03e-06, predicted kinetics vs calculated kinetics MSE: 1.75e-05.

(b) Predicted kinetics vs fitted kinetics MSE: 4.73e-04, predicted kinetics vs calculated kinetics MSE: 5.01e-04.

(c) Predicted kinetics vs fitted kinetics MSE: 7.38e-03, predicted kinetics vs calculated kinetics MSE: 7.37e-03.

Fig. 1. Different MSE visualised.

The MSE difference between neural network predicted kinetics and the averaged kinetics, which were calculated using the squared lattice model, is of the same order of magnitude as the fitting MSE difference with the averaged kinetics. So we can say that using neural networks we are able to describe the dynamics of electron excitation in two-dimensional systems.

Computations were performed using the resources of the High Performance Computing Center “HPC Sauletekis” at Faculty of Physics, Vilnius University.

[1] J. Chmeliov, A. Gelzinis, E. Songaila, R. Augulis, C. D. Duffy, A. V. Ruban, and L. Valkunas, The nature of self-regulation in photosynthetic light-harvesting antenna, *Nature Plants*, 5 2016, **2**, 16045.

[2] J. Chmeliov, G. Trinkunas, H. V. Amerongen, and L. Valkunas, Light harvesting in a fluctuating antenna, *Journal of the American Chemical Society*, 6 2014, **136**, 8963–8972.

INVESTIGATION OF GOLD-CATALYZED NUCLEOPHILIC CYCLIZATION OF DIFFERENT ALKYNYL 2-THIOIMIDAZOLES

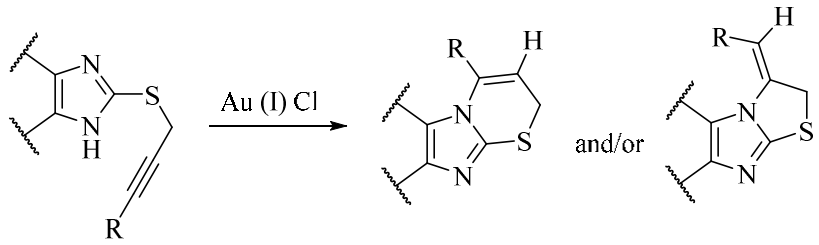
Indrė Misiūnaitė, Raminta Bajarūnaitė, Ieva Žutautė, Algirdas Brukštus[1]

[1] Faculty of Chemistry and Geosciences, Vilnius University, Naugarduko g. 24, LT-03225, Vilnius Lithuania
Indre.Misiunaite@gmail.com

Heterocyclic ring formation is fundamental reaction in organic chemistry. One of the best ways to obtain heterocycles from alkynes is via cyclization reactions using transition metals as catalysts, for example palladium, platinum, gold, copper, titanium, tungsten and organolanthanides [1]. In the last decade, metal-catalyzed cyclization reactions have been increasingly replaced by elekctrophile-initiated cyclization [2]. For this reason we have investigated halogen-initiated cyclization reactions of various alkynyl 2-thioimidazoles to form imidazo[2,1-b][1,3]thiazine fragments. Unfortunately, halogen-initiated cyclization with 2-propynylthioimidazoles was ambiguous with side reactions, therefore metal-catalyzed reactions were tried. There are some examples of silver-catalyzed cyclization reactions of fused benzimidazoles in literature [3] where starting materials generate 6-exo-dig or 7-endo-dig ringclosure products. Therefore, our investigation of 2-propynylthiobenzoimidazoles for a catalyst started with various silver salts. Other group IB metal salts were also investigated and the best results were obtained with gold (I) chloride. Further investigation of cyclization reaction scope with various alkynyl 2-thioimidazoles was carried out using 10 mol% of Au(I)Cl in dichloromethane.

Firstly, 2-propynylthiobenzoimidazoles were selected as model compounds in gold (I) – promoted nucleophilic closure to obtain new heterocyclic systems. It was hypothesized that alkynyl 2-thiobenzoimidazoles could form either five-membered or six-membered heterocyclic frameworks. It was detected that cyclization went throw 5-exo-dig and 6-endo-dig path, depending on the group R. Secondly, reactions with 2-propynylthioimidazoles and 4,5-dimethyl-2-propynylthioimidazoles were selective and gave desired imidazo[2,1-b][1,3]thiazine fragments.

More details about selectivity, scope and limitations of the gold (I) – promoted nucleophilic closure reactions will be discussed in presentation.



R= C_6H_5, p-Me-C_6H_4, p-OMe-C_6H_4, p-NO_2-C_6H_4, Et, H

Fig. 1. General scheme of reactions.

[1] (a), Y. Yamamoto, I.D. Gridnev, N.T. Patil, T. Jin, Alkyne activation with Brønsted acids, iodine, or gold complexes, and its fate leading to synthetic application, Chem. Commun. 5075-5087 (2009). (b), I. Nakamura, Y. Yamamoto, Transition-Metal-Catalyzed Reactions in Heterocyclic Synthesis, Chem. Rev. 104, 2127-2198 (2004).

[2] B. Godoi, R.F. Schumacher, G. Zeni, Synthesis of Heterocycles via Electrophilic Cyclization of Alkynes Containing Heteroatom, Chem. Rev. 111, 2937-2980 (2011).

[3] JX. Zhang, Y. Zhou, H. Wang, D. Guo, D. Ye, Y. Xu, H. Jiangb, H. Liu, Silver-catalyzed intramolecular hydroamination of alkynes in aqueous media: efficient and regioselective synthesis for fused benzimidazoles, Green Chem., 13, 397–405 (2011).

ELECTROACTIVE POLYMERS CONTAINING ELECTRONICALLY ISOLATED 4,7-DIARYLFLUORENE FRAGMENTS FOR OLEDS

Gintare Krucaite[1], Daiva Tavgeniene[1], Dovydas Blazevicius 1, Baohua Zhang[2], Aivars Vembris[3], Saulius Grigalevicius[1], Raminta Beresneviciute[1]

[1] Department of Polymer Chemistry and Technology, Kaunas University of Technology, Kaunas, Lithuania
[2]Center for Advanced Analytical Science, c/o School of Chemistry and Chemical Engineering, Guangzhou University, China
[3]Laboratory of Organic materials, Institute of Solid State Physics, University of Latvia, Kengaraga, Latvia
gintare.krucaite@ktu.lt

The advantages that organic light emitting diode (OLED) based technologies offer in terms of brightness, viewing angle, contrast ratio, production cost, opportunity for flexible displays, etc. are not rivaled by liquid crystal-based displays [1]. It is well established that multilayer devices comprising hole transport layer (HTL), electron transport layer and emissive layer are necessary for efficient light emission [2-4].

Solution processed derivatives containing substituted carbazole fragments are among the most studied materials for organic electronics due to their good chemical and environmental stability as well as high positive charge mobility in their layers. In addition, derivatives containing electronically isolated carbazole chromophores have high triplet energies and are widely used as host materials for electro-phosphorescent devices [5].

New electro-active polymers having 4,7-diarylfluorene chromophores were prepared by cationic polymerization of the corresponding oxetane-based monomers. The structures of polymers **7-9** containing the electroactive 2,7-diarylfluorenyl chromophores are shown in Figure 1.

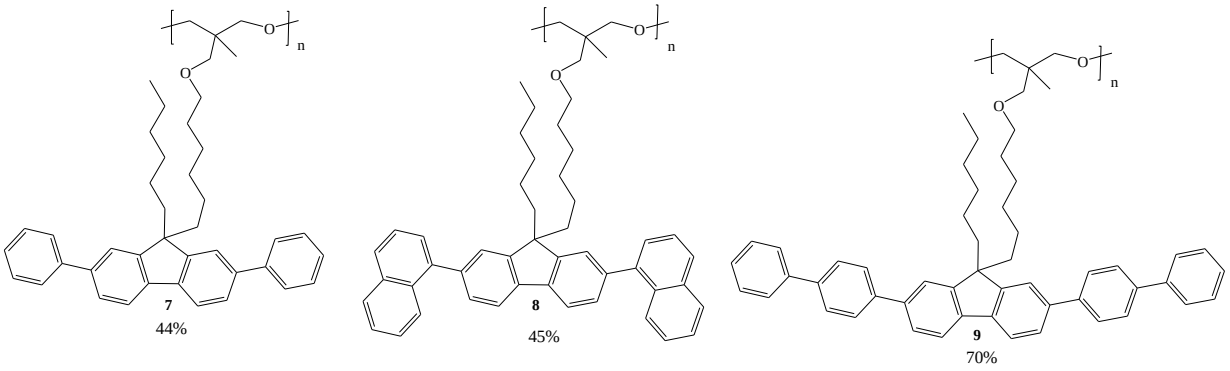


Fig 1. Structures of polymers **7-9**.

The newly synthesized derivatives were identified by mass spectrometry (for low-molar-mass compounds), IR and ^{1}H NMR spectroscopy as well as by elemental analysis. The data were found to be in good agreement with the proposed structures. The polymers **7 - 9** were soluble in common organic solvents at room temperature. Amorphous thin films of these materials could be prepared by using cheap spin coating technique.

The amorphous materials demonstrated very high thermal stability (392-397 °C) and glass transition temperatures in a range of 28-63 °C. Electron photoemission spectra of thin films of the polymers confirmed that ionization potentials of the materials are depending on their chromophores and are in a range from 5.8 eV to 6.0 eV. The polymers have been tested as positive charges transporting layers in bilayer organic light emitting diodes with tris(quinolin-8-olato)aluminium as an emitter as well as electron transporting layer. An OLED device with polymer having electro-active 2,7-di(4-biphenyl)fluorine chromophores exhibited the best overall performance with low turn on voltage of 3 V, maximum brightness exceeding 200 cd/m^2 and current efficiency of 1.7 cd/A.

[1] S. Jhulki, J. N. Moorthy, Small molecular hole-transporting materials (HTMs) in organic light-emitting diodes (OLEDs): structural diversity and classification, Journal of Materials Chemistry C **6**, 8280- 8325 (2018).
[2] S.S. Swayamprabha, M. R. Nagar, R. A. K. Yadav, et al., Hole-transporting materials for organic light-emitting diodes: an overview, Journal of Materials Chemistry C **7**, 7144-7158 (2019).
[3] X. Yang, X. Xu, G. Zhou, Recent advances of the emitters for high performance deep-blue organic light-emitting diodes, Journal of Materials Chemistry C 3, 913-944 (2015).
[4] Y. Tao, C. Yang, J. Qin, Organic host materials for phosphorescent organic light-emitting diodes, Chemical Society Reviews **40**, 2943-2970 (2011).
[5] D. Chen, S.-J. Su, Y. Cao, Nitrogen heterocycle-containing materials for highly efficient phosphorescent OLEDs with low operating voltage, Journal of Materials Chemistry C **2**, 9565-9578 (2014).

COMPARISON OF SILYLATING REAGENTS IN DERIVATIZATION REACTIONS OF SEDATIVE-HYPNOTIC DRUGS PRIOR TO FAST GAS CHROMATOGRAPHY-MASS SPECTROMETRY

Nerijus Karlonas

The State Forensic Medicine Service, Toxicology Laboratory, Didlaukio 86E, LT-08303 Vilnius, Lithuania
nerijuskarlonas@yahoo.com

Although sedative-hypnotic drugs (e.g. barbiturates, benzodiazepines, tricyclic antidepressants, and new generation Z-drugs) – the analytes can be determined by gas chromatography-mass spectrometry (GC-MS) without derivatization, however, several problems are usually encountered for the trace level analysis. Losses of the analytes and peak tailing due to adsorption in the GC inlet device and/or an interaction of the analytes with active sites on the walls of the capillary column can be observed [1-4]. The GC-MS analysis is not sensitive enough for the determination of sedative-hypnotic drugs without derivatization [3-7]. Because the analytes are lipophilic compounds, they should be converted into volatile derivatives prior to GC analysis.

Consequently, for most GC-MS methods derivatization of sedative-hypnotic drugs improves spectral determination/definition and reduces thermal degradation on-column [1,3,4]. Thus, derivatization by different reagents: mixtures of N-methyl-N-(trimethylsilyl)trifluoroacetamide (MSTFA), N,O-bis(trimethylsilyl)trifluoroacetamide (BSTFA) with 1 % trimethylchlorosilane (TMCS), N-tert-butyldimethylsilyl-N-methyltrifluoroacetamide (MTBSTFA) in acetonitrile and ethyl acetate were investigated. The derivatization procedure was optimized to obtain the highest sensitivity and repeatability of the derivatives and to avoid interferences from the sample matrix. The greatest peak areas of derivatized analytes were achieved by silylation using 100 µL of a mixture of MTBSTFA, acetonitrile, and ethyl acetate (at 20:40:40 v/v/v). A slightly lower sensitivity was observed after silylation by MSTFA if compared with BSTFA with 1 % TMCS. The peak areas of derivatized analytes using these reagents were smaller in comparison with MTBSTFA. Moreover, during silylation by MSTFA or BSTFA with 1 % TMCS many problems arose at the derivatization step because both reagents are very sensitive to humidity [2,4]. Subsequently, insufficient repeatability of MSTFA and BSTFA derivatives was observed.

After silylation by MTBSTFA, sedative-hypnotic drugs were readily converted to their corresponding tert-butyldimethylsilyl-derivatives (TBDMS), via an S_N2 substitution reaction, which yielded a single derivative for each sedative-hypnotic drugs compound. In addition, TBDMS derivatives of the analytes are hydrolytically stable and less sensitive to humidity.

In the next step of research, the derivatization time and temperature were optimized. The derivatization conditions including temperature, which was fixed at 60, 70, 80, **85**, 90, and 100 °C, and the duration of the reaction, which was defined at 20, 25, **30**, 35, and 40 min were tested. The optimal conditions are presented in bold. During the optimization of the derivatization temperature, the peak areas of silylated analytes-TBDMS kept increasing with the increase of temperature until the maximum peak area was reached at 85 °C. After this point, an increase in temperature resulted in the decrease of the peak areas of some analytes.

The silylation efficiency of the analytes was tested as a function of time. The highest peak areas were achieved when the reaction was carried out for 30 min, and after that increasing reaction time resulted in a decrease in the peak areas of some analytes. An increase in reaction time from 25 to 30 min did not affect the peak areas of the most silylated analytes. Therefore, the derivatization time and temperature for a mixture of MTBSTFA, acetonitrile, and ethyl acetate (at 20:40:40 v/v/v) at 85 °C for 30 min were chosen for further optimization studies.

The fast chromatographic conditions were tested at: 220, 230, 240, **250**, and 300 °C for injector temperature; 280, 290, **300** and 310 °C for detector temperature; 150, 170, **180** and 250 °C for initial column temperature; 290, 310, **325** and 340 °C for final column temperature; as well as 30, 40, **50** and 60 °C min^{-1} for the column temperature elevation rate. The optimal conditions are presented in bold and have been chosen based on the peak areas of the analytes derivatized with MTBSTFA and not derivatized, as well as on their resolution.

In conclusion, the derivatization reagent MTBSTFA, the derivatization time of 30 min, and the derivatization temperature at 85 °C were selected as the optimal derivatization condition for quantification of sedative-hypnotic drugs by GC-MS. This method will be used in my further investigations for the determination of the analytes in biological samples.

For more information on my research

This study was published in my doctoral dissertation (Solid-phase extraction and fast gas chromatography for a residue analysis of sedative-hypnotic drugs in biological samples), license agreement no. VU-ETD-4 (10-04-2015).

The author has declared no conflict of interest

[1] A. Kabir, K. G. Furton. Gas Chromatography (Second Edition), Handbooks in Separation Science **2**, 745-791 (2021).
[2] M. Caban, P. Stepnowski, M. Kwiatkowski, N. Migowska, J. Kumirska. Journal of Chromatography A **1218**, 8110-8122 (2011).
[3] I. A. Freire, P. Brunetti, P. C. Fernandez, A. F. Liste, M. J. T. Duque, et al. Journal of Pharmaceutical and Biomedical Analysis **159**, 45-52 (2018).
[4] N. Karlonas, A. Padarauskas, A. Ramanavicius, A. Ramanaviciene. Journal of Separation Science **36**, 1437-1445 (2013).
[5] N. Karlonas, A. Ramanavicius, A. Ramanaviciene. Journal of Separation Science **37**, 551-557 (2014).
[6] N. Karlonas, A. Padarauskas, A. Ramanavicius, Z. Minkuviene, A. Ramanaviciene. Chemija **23**, 91-99 (2012).
[7] I. A. Freire, T. M. Rodriguez, A. M. B. Barrera, P. C. Fernandez, M. J. T. Duque. Microchemical Journal **160,** 105715 (2021).

SYNTHESIS OF NEW 1,2,4-TRIAZOLE DERIVATIVES CONTAINING 1,2,4-OXADIAZOLE FRAGMENT

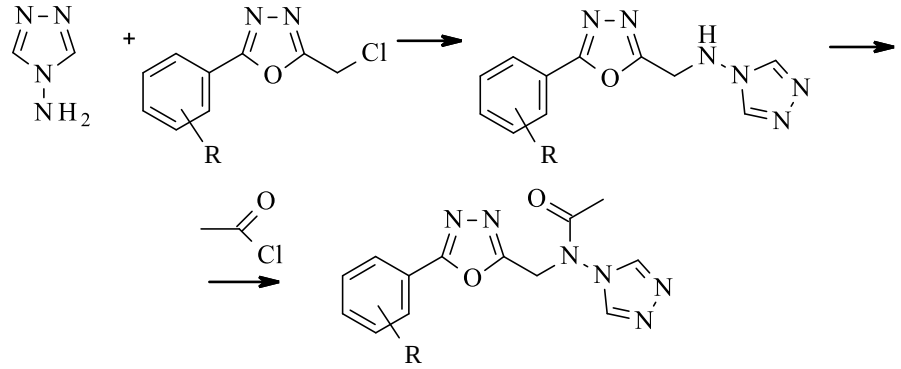
Michael Haletskyi, Nataliia Simurova[2]

[1] Department of Biotechnology, National university of food technologies, Ukraine
[2] Department of Food Chemistry, National university of food technologies, Ukraine
margunka123@gmail.com

The five-membered 1,2,4-triazole ring is an important building block in medical chemistry. Among the compounds containing this heterocyclic fragment, substances with high biological activity (antiviral, antibacterial, analgesic, antitumor, etc.) have been found. In particular, the antiviral drugs Ribavirin and Doravirin, based on 1,2,4-triazole derivatives, are already widely used in modern medical practice. At the same time it is relevant to design the compounds which, along with the triazole ring, contain other groups that can affect the biological properties of the molecule.

The aim of our study was to find new synthetic approaches to compounds that contain 1,3,4-oxadiazole and 1,2,4-triazole rings and an amide group at the same time, the combination of several pharmacophore blocks in the molecule is promising. In addition, both heterocyclic moieties can be considered as bioisosteres of carboxylic acids, amides and esters [1].

We have developed a convenient method of obtaining N-[(5-aryl-1,3,4-oxadiazol-2-yl)methyl]-N-(1,2,4-triazol-4-yl)acetamides **3**, which is based on the sequential substitution of nitrogen atoms in the amino group of 4-amino-1,2,4-aminotriazole 1 (Fig. 1.):



R=H, CH_3, Hal, NO_2

Fig. 1. General scheme of N-[(5-aryl-1,3,4-oxadiazol-2-yl)methyl]-N-(1,2,4-triazol-4-yl)acetamide synthesis

2-Aryl-5-chloromethyl-1,3,4-oxathiazoles **2** we synthesized according to the method [2]. The obtained products were identified by 1H NMR spectroscopy and mass spectrometry. The results of these study can be used in synthetic work and the synthesized compounds - for further study of biological activity.

[1] I. Mohammed, I.R. Kummetha, I. R. et al., 1,2,3-Triazoles as Amide Bioisosteres: Discovery of a New Class of Potent HIV-1 Vif Antagonists, J. Med. Chem. **59**, 7677- 7682 (2016).

[2] N.V. Simurova, O.I. Maiboroda et al., Synthesis of N-alkyl-N-[5-furyl/thienyl-1,3,4-oxadiazolyl]-2-pentenamides, Issues of Chemistry and Chemical Technology, **3**, 183-188 (2020).

THE DETECTION OF ANTIBODIES AGAINST SARS-COV-2 BY ELECTROCHEMICAL METHODS

Maryia Drobysh[1], Viktorija Liustrovaite[2], Alma Rucinskiene[3], Ausra Baradoke[1], Almira Ramanaviciene[2], Ieva Plikusiene[1,2], Urte Samukaite-Bubniene[1,2], Roman Viter[4], Chien-Fu Chen[5], Arunas Ramanavicius[1,2*]

[1]Department of Functional Materials and Electronics, State Research Institute Center for Physical Sciences and Technology, Lithuania
[2]Department of Physical Chemistry, Faculty of Chemistry and Geosciences, Vilnius University, Lithuania
[3]Department of Electrochemical Materials Science, State Research Institute Center for Physical Sciences and Technology, Lithuania
[4]Institute of Atomic Physics and Spectroscopy, University of Latvia, Latvia
[5]Institute of Applied Mechanics, National Taiwan University, Taiwan
maryia.drobysh@ftmc.lt

The entry of the severe acute respiratory syndrome coronavirus 2 (SARS-CoV-2) into an organism is accompanied by a humoral immune response, namely, the expression of antigen-specific antibodies. The SARS-CoV-2 genome encodes four structural proteins, one of which, the spike protein, is commonly used as an antigen for specific antibody binding. Biosensors for detecting antigen-antibody interactions are widely used to diagnose coronavirus disease 2019 (COVID-19). Because of their low cost and simplicity without losing sensitivity and accuracy, electrochemical biosensors are one of the leading types of biosensors [1].

Our research aimed to model an electrochemical-based biosensor for the detection of antibodies against SARS-CoV-2 (anti-rS). In the biosensor, the recombinant SARS-CoV-2 spike protein (rS) was employed as a sensitive element. Electrochemical impedance spectroscopy (EIS) was chosen as the initial electrochemical approach since it is a non-destructive method for studying the phenomena occurring on modified working surfaces [2,3]. The next step was to adapt and apply the approach for other electrochemical methods, namely, cyclic voltammetry (CV). CV is used to obtain data on the redox potential and other electrochemical characteristics of analyte solutions, as well as to monitor the processes occurring on the working surface [4].

For EIS based experiments anti-rS were detected by the gold electrode modified with a self-assembled monolayer (SAM), namely, 11-mercaptoundecanoic acid (11-MUA), followed by the covalent immobilisation of rS [5]. Following each stage, EIS measurements indicated correlations between impedimetric signals and working surface modification. On the crucial step of the anti-rS coupling, we observed a considerable increase in electron-transfer resistance. Nevertheless, when it came to CV, this immobilisation approach has been proved to be ineffective. CV showed that the SAM was densely packed and blocked the gold surface, which significantly hindered the transfer of electrons and, therefore, made it practically impossible to detect the signal at the subsequent stages of rS immobilisation and anti-rS coupling. We adjusted the immobilisation method by lowering SAM density through the use of mixed 11-MUA and 6-mercapto-1-hexanol as a spacer (SAMmix) [6]. The improved immobilisation technique allowed performing CV based experiments and the resulting cyclic voltammograms revealed the decrease of current density after the electrode modification with SAMmix and continuing sequential working surface insulation after rS immobilisation and anti-rS coupling.

Thus, it can be concluded that the modified technique makes it possible to adapt the experiment for other electrochemical methods, such as differential pulse voltammetry, chrono pulse amperometry, etc.

Acknowledgements: This research was conducted under Lithuanian-Latvian-Taiwan project and it has received funding according to agreement No S-LLT-21-3 with Research Council of Lithuania (LMTLT).

[1] M. Drobysh, A. Ramanaviciene, R. Viter et al., Biosensors for the Determination of SARS-CoV-2 Virus and Diagnosis of COVID-19 Infection, International Journal of Molecular Sciences **23(2)**, 666 (2022).
[2] A. Ramanavicius, A. Finkelsteinas, H. Cesiulis et al., Electrochemical impedance spectroscopy of polypyrrole based electrochemical immunosensor, Bioelectrochemistry **79(1)**, 11-16 (2010).
[3] V Liustrovaite, A. Valiuniene, G. Valincius et al., Electrochemical Impedance Spectroscopy Based Evaluation of Chlorophyll a Reconstitution within Tethered Bilayer Lipid Membrane, Journal of The Electrochemical Society **168(6)**, 066506 (2021).
[4] V. Ganesh, S.K. Pal, S. Kumar et al., Self-assembled monolayers (SAMs) of alkoxycyanobiphenyl thiols on gold - A study of electron transfer reaction using cyclic voltammetry and electrochemical impedance spectroscopy, Journal of Colloid and Interface Science **296**, 195–203 (2006).
[5] A. Ramanaviciene, A. Kausaite-Minkstimiene, A. Ramanavicius et.al., Comparative study of random and oriented antibody immobilization techniques on the binding capacity of immunosensor, Analytical Chemistry **82(15)**, 6401-6408 (2010).
[6] V. Sharma, V.K. Tanwar, S. K. Mishra et al., Electrochemical impedance immunosensor for the detection of cardiac biomarker Myogobin (Mb) in aqueous solution, Thin Solid Films **519(3)**, 1167-1170 (2010).

SYNTHESIS AND STUDY OF PROPERTIES OF COMBINED ALGINATE/GELATIN HYDROGELS

Olha Maikovych, Natalya Nosova, Natalya Bukartyk, Zoriana Nadashkevych, Serhii Varvarenko

Department of Organic Chemistry, Lviv Polytechnic National University, Ukraine
maikovych.olha@gmail.com

Recently the issue of new means for the treatment and protection of various wounds has attracted much attention. Along with traditional gauze, a variety of wound dressings are increasingly used. A large number of these dressings are obtained using biocompatible natural and synthetic polymers [1]. A wide range of requirements is set for polymeric materials used in medicine to obtain wound dressings, and the first selection criteria are the absence of cytotoxicity, biocompatibility, biodegradability [2,3]. To effectively treat wounds, dressings should possess high sorption activity, the ability to effectively remove excess wound exudate and its toxic components; be permeable to air and water vapor; prevent dehydration of the wound surface; prevent wound infection; to be modeled on wound surfaces with a difficult relief, and possess sufficient mechanical strength. In general, the wound dressing should provide the optimal microenvironment for wound healing in the absence of local irritants and allergic effects.

The paper presents a study of the synthesis of hydrogel material based on natural biopolymers (sodium alginate and gelatin) for medical applications. Sodium alginate and gelatin are biocompatible, non-toxic, biodegradable polymers and renewable raw materials. Gelatin is a direct functional analogue of collagen in amino acid composition. It is widely used in pharmaceuticals and medicine due to its biocompatibility, ability to biodegrade and accelerate tissue regeneration and wound healing. Alginate is known for its antibacterial properties and ability to stimulate epithelialization and development of granulation tissue in the treatment of wounds. Thus, the development of combined alginate-gelatin hydrogels is an urgent task.

In our work, combined alginate gelatin hydrogels are formed due to the formation of a hydrogel network by simultaneous cross-linking of calcium ions of sodium alginate macromolecules, gelatin, and macrochains of rarely crosslinked polyacrylic acid. The optimal synthesis conditions (reagent concentrations, the molar ratio of calcium ions to the number of carboxyl groups $Ca^{2+}/COOH^{-}$) of the combined hydrogels with satisfactory physicochemical and mechanical properties are determined.

Obtained combined hydrogels have mechanical strength 15-20 kPa depending on the hydrogel composition. Upon contact of the hydrogel with the wound, the wound fluid enters the hydrogel matrix, leading to the changes in the conformation of the polymer network and the stress of polymer chains; it can ultimately cause a decrease in strength and even the loss of structural integrity of the hydrogel. Therefore, studies of the mechanical performance of the hydrogel at uniaxial loading were performed according to the method of determining the maximum of hydrogel samples with different degrees of swelling. The obtained results suggest that alginate-gelatin hydrogels retain integrity even at maximum degrees of swelling withstanding the load only 2 times less than their initial maximum load.

The dependences of the mechanical properties of alginate-gelatin hydrogels on the degree of swelling indicate a wide range of their satisfactory performance characteristics.

An important characteristic of hydrogels as therapeutic materials is their ability to absorb wound fluid. It should be noted that too rapid absorption of wound fluid is not an advantage and, conversely, it should be avoided to prevent overdrying of the wound, as this may adversely affect the healing of wounds with the moderate release of fluids [4].

It should be noted that the amount of absorbed model exudate is in the range of 30-35 grams per 1 gram of gelforming polymers or 1900 grams per m^2 of the absorption area. According to the classification given in [5], the absorption in the range of 2000–2500 g/ m^2 for the period of application on the wound up to 24 hours is considered perfect for effective wound healing. Therefore, it can be assumed that the obtained alginate-gelatin hydrogel can be the basis of an effective therapeutic dressing capable of maintaining water balance by preventing both excessive dehydration of the wound and the accumulation of exudate.

The studies on sorption and release of analgesics (lidocaine and novocaine) showed long-term release of drugs and allow to predict the possibility of their prolonged delivery. In vitro cytotoxicity analysis proved the absence of a toxic effect on living cells. These results suggest that the obtained combined alginate-gelatin hydrogels are a promising material for producing hydrogel dressings for wound care.

[1] S. Schreml, R. Szeimies, L. Prantl et al., Wound healing in the 21 st century, J. Am. Acad. Dermatol., 63(5), 866–881 (2021).
[2] J.G. Powers, L.M. Morton, T.J. Phillips, Dressings for chronic wounds, Dermatol. Ther., 26(3), 197–206 (2013).
[3] F. Abasalizadeh, S. V. Moghaddam, E. Alizadeh et al., Alginate-based hydrogels as drug delivery vehicles in cancer treatment and their applications in wound dressing and 3D bioprinting, J. Bio. Eng., 14(8), (2020)
[4] Z. Peles, M. Zilberman, Novel soy protein wound dressings with controlled antibiotic release: mechanical and physical properties, Acta Biomater., 8(1), 209–217 (2012).
[5] K. Nagaraja, K. M. Rao, K. S. Rao, Alginate-based hydrogels, Plant and Algal Hydrogels for Drug Delivery and Regenerative Medicine, 11, 357-393 (2021).

THE EFFICIENCY OF POLYETHYLENE TEREPHTALATE GLYCOLYSIS REACTION USING MAYENITE AS A CATALYST

Diana Masiulionytė, Kotryna Laučiškytė, Monika Čekavičiūtė, Laura Pečiulytė, Joana Bendoraitienė, Karolina Almonaitytė

Department of Polymer Chemistry and Technology, Kaunas University of Technology, Lithuania
diana.masiulionyte@ktu.edu

Polyethylene terephthalate (PET) is one of the most used plastic in the world. It has properties such as high resistance of tensile and impact, high chemical resistance, transparency, easy machinability and high thermal stability [1, 2]. Due to these properties, PET is widely used in food and beverages packaging. Large consumption of PET is increasing the number of wastes in the world; therefore, nowadays there is very big problem of recycling.

There are known two PET recycling ways: mechanical and chemical [1]. During mechanical process, recycled PET (rPET) received, but quality of rPET is not as good as it could be [1]. Chemically recycling PET, there are known methods such as methanolysis, hydrolysis, aminolysis and glycolysis [1, 2]. The most popular method of PET recycling is glycolysis. Glycolysis recycling can be described as a depolymerization of PET polymer in ethylene glycol (EG) using different types of catalysts obtaining bis-2-hydroxyethylene terephthalate (BHET) monomer [1]. As the conditions and depolymerization process are not difficult, the other problem is the selection of metal catalysts to get the highest yield of BHET.

In this work, reaction was carried out in three-neck round bottom flask. Catalyst was added to EG solvent, heated until reflux (196 °C), then added PET and mixture was refluxed for 2.5 hours. Mayenite ($Ca_{12}Al_{14}O_{33}$) was used as the catalyst for PET depolymerization. We used three types of mayenite with different calcination temperatures: 350, 550 and 900 °C. After 2.5 hours, the mixture was cooled in ice-bath, added boiling water and heated until 100 °C. To obtain BHET, the hot mixture was filtered. The filtrate was reheated until its clear, and then it was cooled to 5 °C and left for 16 h. The obtained crystals were dried at 60 °C. The reaction yield was calculated. The BHET structure was proved by FTIR analysis.

Tendencies were observed. The smaller amount of mayenite was added to reaction mixture the higher BHET yield was obtained, but mayenite concentration can not exceed 600 molls. The highest BHET yield was received using 600 molls of mayenite, which was calcinated in 900 °C. This mayenite has largest surface area and highest crystallinity.

Table 1. Reaction efficiency of PET glycolysis by using mayenite as the catalyst

No.	Catalyst	PET/catalyst		Yield, %
		mol/mol	g/g	
1	$Ca_{12}Al_{14}O_{33}$ (900 °C)	800	112.5	65.7
2		600	84.4	69.2
3		400	56.2	64.4
4		200	28.2	50.6
5		100	13.9	46.6
6	$Ca_{12}Al_{14}O_{33}$ (550 °C)	800	108.7	48.2
7		600	79.0	59.5
8		400	53.9	56.8
9		200	27.2	46.1
10		100	14.0	22.4
11	$Ca_{12}Al_{14}O_{33}$ (350 °C)	800	105.6	55.0
12		600	83.4	55.8
13		400	54.7	56.1
14		200	28.4	45.3
15		100	14.1	30.6

Acknowledgment: This research was funded by the European Social Fund (Project No. 09.3.3-LMT-K-712-25-0034).

[1] J. Xin, Q. Zhang, J. Huang, R. Huang, Q. Zahra Jaffery, D. Yan, Q. Zhou, J. Xu, X. Lu. Progress in the catalytic glycolysis of polyethylene terephthalate, Journal of Environmental Management **296**, 1-10 (2021).

[2] Z. Laldinpuii, S. Lalhmangaihzuala, Z. Pachuau, K. Vanlaldinpuia. Depolymerization of poly(ethylene terephthalate) waste with biomass-waste derived recyclable heterogeneous catalyst, Waste Journal **126**, 1-10 (2021).

STABILITY AND PHOTOCHEMICAL FATE OF NADOLOL IN WATER

Andrijana Vukojević[1], Sanja J. Armaković[1]

[1] Faculty of Sciences, Department of Chemistry, Biochemistry and Environmental Protection, University of Novi Sad, Trg D. Obradovića 3, Novi Sad 21000, Serbia
andrijanavukojevic@gmail.com

β-blockers are pharmaceuticals prescribed for cardiovascular diseases and treating various disorders such as hypertension (high blood pressure), angina, and arrhythmias [1]. Nadolol is a commonly used β-blockers whose percentage excreted in urine is 24.6% [2]. Due to its ubiquitous occurrence and toxicity to aquatic organisms, it is crucial to determine its photochemical fate and stability in water.

For each pollutant, abiotic processes in surface waters include hydrolysis and photolysis. The nadolol hydrolysis was investigated in ultrapure water at 25 ± 1 °C in the dark. Also, direct and indirect photolysis of nadolol was investigated under different irradiation (Fig. 1, under simulated solar (SS), UV-LED and UV irradiations).

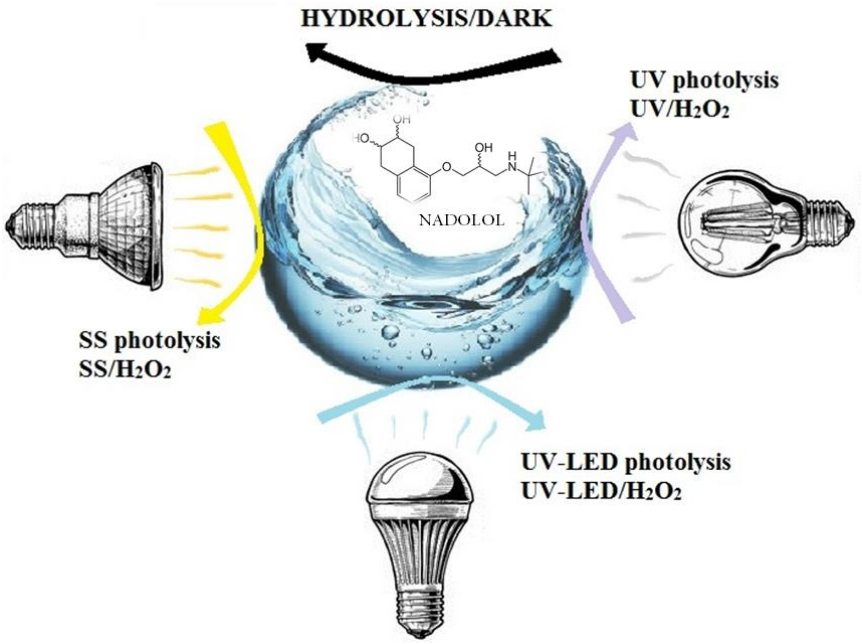


Fig. 1. Illustration of applied procedure for Nadolol degradation

Hydrolysis didn't significantly remove nadolol from aqueous solutions at 8.5 pH value. The stability of nadolol in water is a primary reason why it is detected in environmental waters [3]. For efficient direct photolysis to occur, there must be an appropriate overlap between the absorption spectrum of the nadolol and the spectrum of the corresponding radiation source. The UV spectrum of nadolol shows that it absorbs only radiation in the UVC area, which explains why degradation in water by simulated solar irradiation and LED isn't efficient. In this study, the efficiency of direct photolysis is improved by adding an oxidant whose photolytic dissociation yields •OH-radicals, H_2O_2. The most efficient process was the degradation of nadolol under UV irradiation with 3 mM H_2O_2.

[1] M. Maurer, B.I. Escher, P. Richle, C. Schaffner, A.C. Alder, Elimination of *β*-blockers in sewage treatment plants, Water Research **41**, 1614-1622 (2007).

[2] M. Yi, Q. Sheng, Q. Sui, H. Lu, β-blockers in the environment: Distribution, transformation, and ecotoxicity, Environmental Pollution **266**, 1152692 (2020).

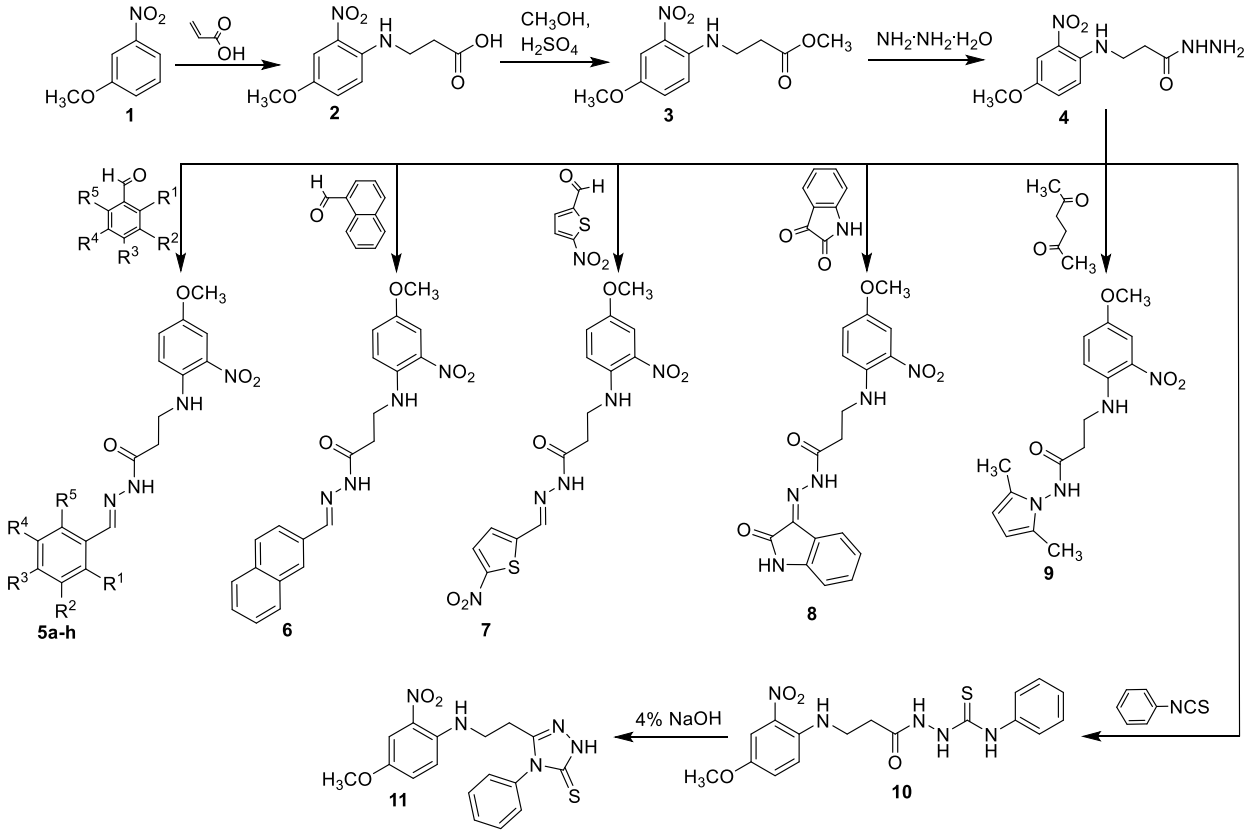
[3] R. López-Serna, A. Juradot, E.Vázquez-Suñé, et al., Occurrence of 95 pharmaceuticals and transformation products in urban groundwaters underlying the metropolis of Barcelona, Spain, Environmental Pollution **174**, 305-315, (2013).

SYNTHESIS OF NEW *N*-(4-METHOXY-2-NITRO)-*β*-ALANINE DERIVATIVES

Roberta Gelminauskaitė[1], Birutė Grybaitė[1]

[1] Department of Organic Chemistry, Kaunas University of Technology, Kaunas, Lithuania
roberta.gelminauskaite@ktu.edu

β-amino acids are components of a variety of natural products, occur in peptides, different heterocycle and in antibiotics. They show impressive pharmacological properties, such as in free form, or as their cyclized (*β*-lactam) derivatives. Besides their own pharmacological importance, the alicyclic *β*-amino acids can be used as building blocks for the preparation of modified analogues of occurring pharmacologically active peptide. It can be encouraging candidates for drug development due to benign properties, including high structural diversity, wide scope of functional groups, good solubility in aqueous media, and good binding affinity. [1-4]



5a = R^1, R^2, R^4, R^5 = H, R^3 = Cl; **5b** = R^1, R^2, R^4, R^5 = H, R^3 = Br; **5c** = R^1, R^2, R^4, R^5 = H, R^3 = NO_2; **5d** = R^1, R^2, R^4, R^5 = H, R^3 = $N(CH_3)_2$; **5e** = R^1, R^2, R^4, R^5 = H, R^3 = OCH_3; **5f** = R^1 = Cl, R^4 = NO_2, R^2, R^3, R^5 = H; **5g** = R^1, R^3, R^5 = OCH_3, R^2, R^4 = 4; **5h** = R^2, R^3, R^4 = OCH_3, R^1, R^5 = H.

Fig. 1. Synthesis of *β*-amino acids derivatives 3-11

3-[(4-methoxy-2-nitrophenyl)amino]propanoic acid was obtained by the reaction of 4-methoxy-2-nitroaniline and acrylic acid in the water. Acid **2** was esterified with methanol in the presence of a catalytic amount of sulfuric acid in the reaction mixture. The obtained methyl ester **3** reacted with hydrazine monohydrate in 2-propanol, and the corresponding hydrazide **4** was synthesized.

By the reaction of hydrazide **4** and heterocyclic or aromatic aldehydes in 2-propanol were prepared hydrazones **5-7**. Compound **8** was synthesized by the hydrazide **4** reaction with isatin reagent. Pyrrole derivative **9** was obtained by the hydrazide **4** condensation reaction with 2,5-hexanedione. The interaction of hydrazide **4** with phenyl isothiocyanate in methanol at reflux gave thiosemicarbazide **10.** The last step of the study was ring closure reaction when the thiosemicarbazide **10** were heated at reflux in aqueous sodium hydroxide solution.

[1] Fulop, F. (2000). Alicyclic b-amino acids: useful synthons in drug research. *Il Farmaco*, 181-183.
[2] Jianlin Han, Hiroyuki Konno, Tatsunori Sato, Vadim A. Soloshonok, Kunisuke Izawa. (2021). Tailor-made amino acids in the design of small-molecule blockbuster. *European Journal of Medicinal Chemistry*, 1-49.
[3] Lorand Kiss, Eniko Forró, and Ferenc Fulop. (2010). Synthesis of Carbocyclic b-Amino Acids. In *Amino Acids, Peptides and Proteins in Organic Chemistry* (pp. 367-409). Wiley-VCH.
[4] Víctor Manuel Gutiérrez-García, Gloria Reyes-Rangel, Omar Muñoz-Muñiz and Eusebio Juaristi. (2001). *Journal of the Brazilian Chemical Society*, 652-660.

ENCAPSULATION AS A WAY TO DELIVER APOLAR ACTIVE COMPOUNDS TO ADIPOCYTES

Aleksandra Orlef[1], Aleksandra Wajda[1], Ewa Stanek[2], Krzysztof Czamara[2], Agnieszka Kaczor[1,2]

[1]Faculty of Chemistry, Jagiellonian University in Krakow, Poland
[2] Jagiellonian Centre for Experimental Therapeutics (JCET), Jagiellonian University in Krakow, Poland
aleksandra.orlef@student.uj.edu.pl

Nowadays, the most common ways of administering drugs are orally, e.g. in the form of tablets or directly into the blood through injections or drips. Despite the many advantages of the oral administration, one of the problems is the first pass effect also known as first-pass metabolism, that causes a reduction of the drug concentration before it reaches the systemic circulation. First-pass metabolism may occur in the liver or in the gut.[1] Another problem is poor solubility of some active compounds in water.

Solutions to these problems, may be, firstly, the administration of the drug directly to the target site, and second, encapsulation. This method is based on the confinement of an active compound inside the cavity of a larger structure. In our research, we use polymer micelles to encapsulate active compounds (Fig. 1A), for example astaxanthin, for their successful administration to adipocytes. We used poloxamers, a triblock copolymer consisting of hydrophilic poly(ethylene oxide) (PEO) blocks and hydrophobic poly(propylene oxide) (PPO) blocks [2], that forms micelles quickly, simply and effectively in the aqueous solution. Due to its amphiphilic structure, it has surfactant properties, thanks to which it is widely used in industry, pharmacy and cosmetics.

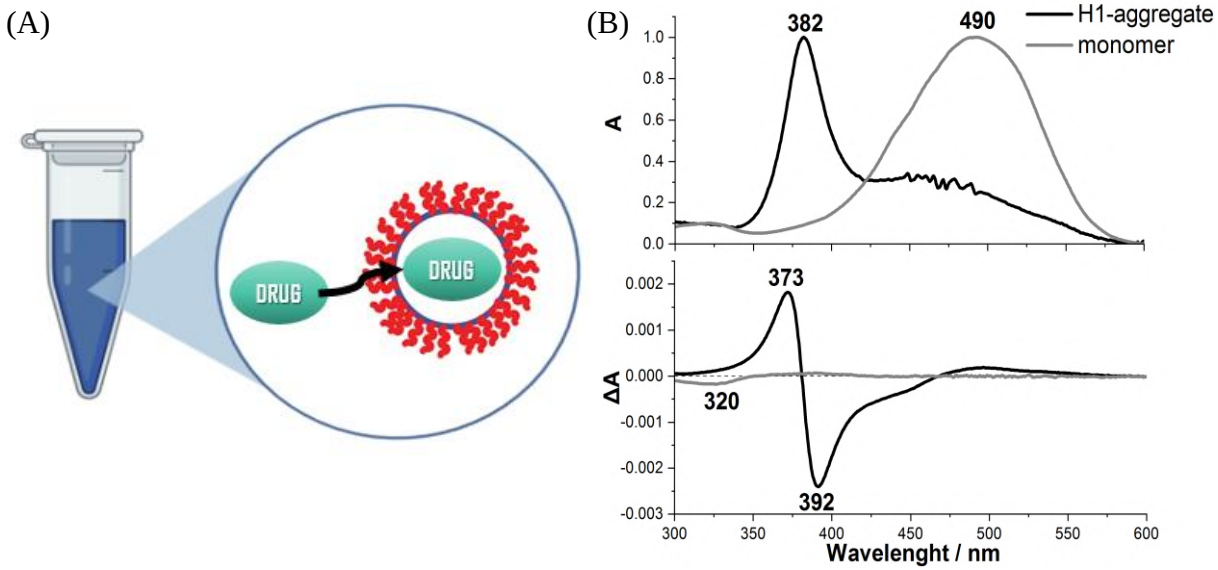


Fig. 1. A schematic diagram of the encapsulation process (A), Electronic absorption (top) and ECD (bottom) spectra of 3S,3'S-astaxanthin encapsulated in micelles (black line) and dissolved in DMSO (grey line) (astaxanthin concentration in the solutions equals to 10 uM) (B).

Chiroptical spectroscopies, in particular Electronic Circular Dichroism (ECD), supported by Vibrational Circular Dichroism (VCD) and Raman Optical Activity (ROA) were used to study the encapsulation process. Transmission electron microscope (TEM) was used to check the shape and size of formed micelles. Raman microscopy was applied technique to visualize the delivery of the active compounds from the micelles to adipocytes and the active compound distribution in the cells.

Among studied compounds, we investigated encapsulation of carotenoids that are practically insoluble in water. Carotenoids in mixed solvents and in the protein environment can form aggregates.[3-5] Our results demonstrate that astaxanthin forms stable *H*-aggregates in micelles (Fig. 1B) and in the encapsulated form can be successfully delivered to primary adipocytes isolated from mice.

[1] S. M. Pond, T. N. Tozer, First-pass elimination. Basic concepts and clinical consequences, Clin Pharmacokinetic 9,1-25 (1984).
[2] A. M. Bodratti, P. Alexandridis, Formulation of Poloxamers for Drug Delivery, J. Funct. Biomater 9, (2018).
[3] G. Zając, A. Kaczor et al., Aggregation-Induced Resonance Raman Optical Activity (AIRROA): A New Mechanism for Chirality Enhancement, J. Phys. Che. B, 120, 17,4028-4033, (2016).
[4] M. Dudek, E. Machalska et al., Chiral Amplification in Nature: Studying Cell-Extracted Chiral Carotenoid Microcrystals via the Resonance Raman Optical Activity of Model Systems, Angew. Chem. Int. Ed., 58, 8383, (2019).
[5] H. Ishikita, Bernhard Loll et al., Function of two β-carotenes near the D1 and D2 proteins in photosystem II dimers, Biochimica et Biophysica Acta-Bioenergetics, 1767(1), 79-97, (2007).

EXCITATION ANNIHILATION IN MOLECULAR AGGREGATES

Gabrielė Rankelytė[1,2], Jevgenij Chmeliov[1,2]

[1]Institute of Chemical Physics, Faculty of Physics, Vilnius University, Lithuania
[2]Department of Molecular Compound Physics, Centre for Physical Sciences and Technology, Vilnius, Lithuania
gabriele.rankelyte@ff.stud.vu.lt

Excitation annihilation is a common phenomenon in molecular structures. It is often difficult to ensure experimental conditions that could prevent annihilation; therefore, it might often be necessary to account for annihilation while analyzing data.

Simple annihilation model can be described by rate equation Eq. 1:

$$\frac{\mathrm{d}n}{\mathrm{d}t} = -\gamma n^2, \tag{1}$$

here $n(t)$ is the mean number of remaining excitations in the system at time t and γ is the rate constant for annihilation. In this model, the size of molecular aggregate, excitation transfer rate across the aggregate, and initial population of excitations are considered to be very large. In order to include finite transfer rate, γ must be considered as a function of time, which for one-dimensional systems at longer times can be approximated by a power law [1]. More precise statistical model accounts for the discrete number of excitations, but still considers the whole aggregate as a supermolecule, resulting in the system of Pauli Master equations [2].

To account for both finite transfer rate and discrete number of excitations in annihilation model, we have chosen to use Monte Carlo method. The model is based on continuous time random walk. After sufficient number of lattices have been generated, the average kinetics of specific initial number of exitations is calculated. The average kinetics is later recalculated considering that initial distribution of excitations obeys a Poisson distribution.

The Monte Carlo kinetics were approximated using two different approaches: the statistical approach and the kinetic equation. For both approaches the same seven annihilation rate time dependences were used. We show that statistical approach works well for excitation dynamics, whereas the kinetic equation fails for most cases. While using the annihilation rate function that works the best with the statistical approach, we approximate the Monte Carlo kinetics (Fig. 1) and determine the universal set of annihilation rate parameters.

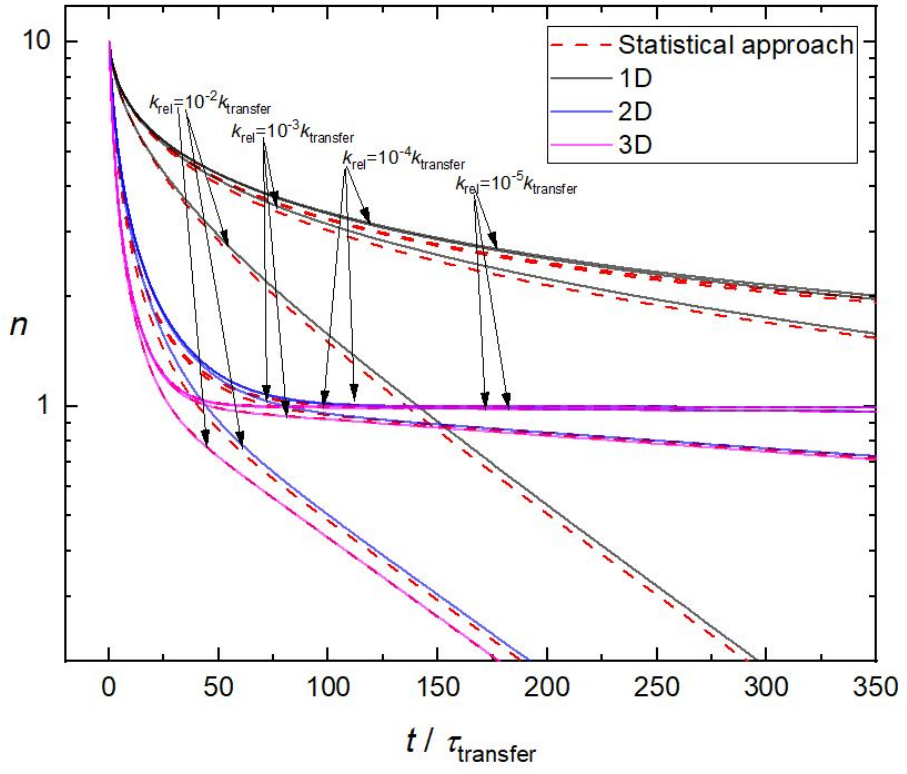


Fig. 1. Fitting of the Monte Carlo kinetics using the statistcal approach. The size of the aggregate is $N = 100$ nodes. k_{rel} stands for the relaxation rate, k_{transfer} and τ_{transfer} stand for the transfer rate and time, respectively.

[1] H. van Amerongen, L. Valkunas, R. van Grondelle. Photosynthetic Excitons. World Scientific, Singapore, 2000.
[2] V. Barzda, V. Gulbinas, R. Kananavicius, V. Cervinskas, H. van Amerongen, R. van Grondelle, L Valkunas, Singlet-Singlet Annihilation Kinetics in Aggregates and Trimers of LHCII, Biophys. J. 80 (2001) 2409–2421.

INVESTIGATION OF DIFFERENT METHODS OF CADMIUM SELENIDE THIN FILM DEPOSITION ON FTO/ZnO SUBSTRATE FROM AQUEOUS SOLUTIONS

Gediminas Jakubauskas, Neringa Petrašauskienė, Edita Paluckienė, Eglė Ūsovienė

Department of Physical and Inorganic Chemistry, Kaunas University of Technology, Lithuania
gediminas.jakubauskas@ktu.edu

Cadmium selenide (CdSe) is a semiconductive material with bulk optical bang gap energy of 1.74 eV, which means it can be excited by low energy, longer wavelength ($\lambda \approx 696$ nm) electromagnetic radiation. These properties make it a good candidate material for solar cell applications, as well as high efficiency thin film transistors, photo detectors, light emitting diodes and other optoelectronic devices [1]. Zinc oxide (ZnO) is a semiconductive material with bulk band gap energy of 3.37 eV, good mechanical and thermal stability, optical transparency. Combining the properties offered by CdSe with the properties of ZnO, a functional layer for light energy conversion to electrical energy should be produced, where electrons excited by low energy radiation would be injected into the more electrically conductive ZnO layer and through it – into the outer circuit, reducing the chances of electron and hole recombination [2]. The functional layers were deposited on conductive fluorine doped tin oxide (FTO) coated glass substrates.

The FTO substrates were ultrasonically cleaned in soap solution, distilled water, and ethanol, to remove any impurities from the surface. The ZnO layer was deposited from a suspension of ZnO nanoparticles in ethanol using the spin-coating method. To produce a sufficiently thick layer of ZnO nanoparticles, 10 spin coating operations were performed per substrate, with annealing after each deposition. CdSe layers were deposited using two methods: successive ionic layer adsorption and reaction (SILAR) method, chemical bath deposition (CBD) method and combinations of the two.

For the SILAR method, cadmium acetate ($Cd(CH_3COO)_2$) solution was used as the cation source and sodium selenosulfate (Na_2SeSO_3) as the anion source. The CdSe thin film was formed by performing 30 SILAR cycles with annealing after every 5th cycle. For the CBD method, the substrates were treated in diluted reaction mixture of $Cd(CH_3COO)_2$, Na_2SeSO_3 and a chelating agent for reaction rate control for 30 minutes. The CdSe thin film is formed by performing 4 CBD reactions, with annealing after each one. Two variations of combining CBD and SILAR methods were also investigated: one variation had CdSe thin film deposited with 15 SILAR cycles first and 2 CBD reactions second, the other variation had the thin film deposited with 2 CBD reactions first and 15 SILAR cycles second.

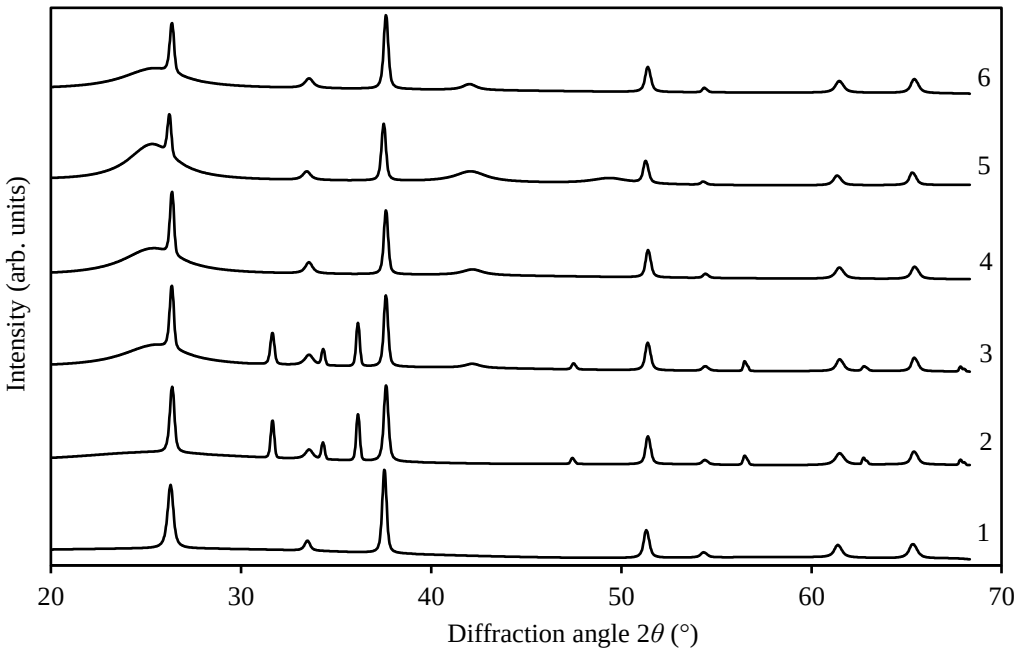


Fig. 1. X-ray diffraction patterns of samples:
1) FTO substrate; 2) FTO/ZnO substrate; 3) SILAR; 4) SILAR/CBD; 5) CBD/SILAR; 6) CBD

The X-ray diffraction patterns show that diffraction peaks that appeared with the deposition of ZnO nanoparticles disappear in every CdSe sample, where CBD method was used, but remain in the sample where only SILAR was used.

[1] Sahu, P. K. & Das, R. Influence of trivalent bismuth doping on optoelectronic and microstructural properties of hydrophilic nanocrystalline cadmium selenide thin films. *Thin Solid Films* **693**, 137675 (2020).
[2] Vinoth Pandi, D., Muthukumarasamy, N., Agilan, S. & Velauthapillai, D. CdSe quantum dots sensitized ZnO nanorods for solar cell application. *Mater. Lett.* **223**, 227–230 (2018).

FORMATION OF CdS LAYERS ON ZnO/FTO SUBSTRATES AND UV/VIS INVESTIGATION

Eglė Ūsovienė, Edita Paluckienė, Neringa Petrašauskienė, Gediminas Jakubauskas

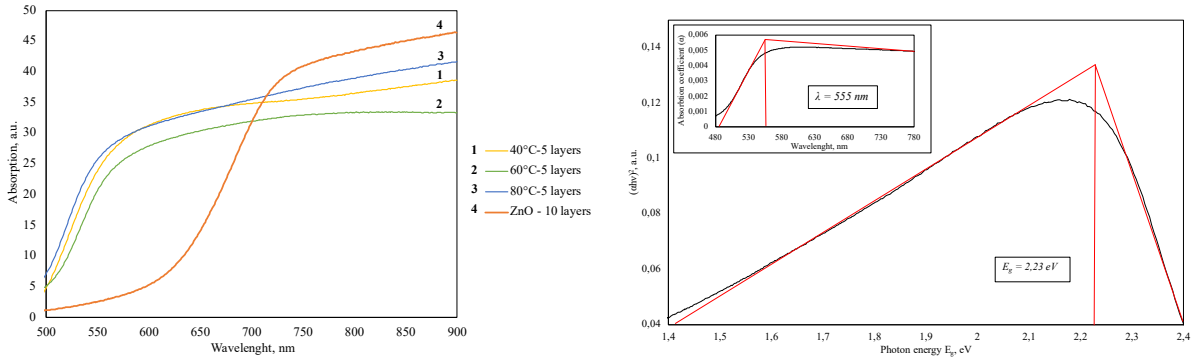
Department of Physical and Inorganic Chemistry, Kaunas University of Technology,
Radvilėnų pl. 19, LT-50254 Kaunas, Lithuania
egle.usoviene@ktu.lt

Zinc oxide (ZnO) and its properties have gone extensive research since the shortage of short-wavelength optoelectronic devices, transparent electrodes, and materials needed for screen and solar module production [1]. In materials science, it's classified as a semiconductor. When the surface of materials is coated with a ZnO nanoparticle layer, electron transfer improves. This means that ZnO nanostructures have a high surface-to-volume ratio which increases the number of photogenerated charge carriers [2].

Cadmium sulfide (CdS) is a chemical compound profound in its unique size and structure, which can affect its optical and electronic properties. This material can be formed on surfaces using a broad range of methods: vacuum evaporation, spray pyrolysis, or chemical bath deposition (CBD) [3].

In the present work, the deposition of CdS using the chemical bath deposition method on FTO/ZnO was investigated. Thin films were formed on FTO (TEC 10) glass substrates with ZnO nanoparticle layer deposited using the Spin-coating method. Thin films were formed using $CdCl_2$ as a cadmium source, thiourea as a sulfur source, NH_4Cl and NH_4OH as a complexing agent, and pH control.

UV/Vis analysis was carried out for all samples using ultraviolet light absorption. This analysis was achieved using cleaned FTO glass substrates as standard. Analysis results can be examined in the figure listed below (Fig. 1).



a *b*

Fig. 1. Absorption spectra of various samples (*a*) and calculated bandgap value of CdS sample treated at 80°C with 5 formed layers (*b*)

The absorption of various samples can be examined in Fig. 1 (a). ZnO nanoparticles on FTO glass substrates have the best absorption spectra. Samples with CdS had the best absorption when formed at 80°C. Sample with the lowest absorption is when CdS layer is formed at 60°C.

After recording UV/Vis spectra bandgap calculations were carried out, Fig (1, b). This calculation describes electrical properties of materials. bandgap values were calculated using Tauc's relation formula, Eq. (1):

$$\alpha h\nu = A(h_\nu - E_g)^n \quad (1)$$

The calculated bandgap value of the CdS sample treated at 80°C is E_g = 2,23 eV. The samples absorption starts at 555 nm.

[1] A. Kolodziejczak-Radzimska, T. Jesionowski, *Zinc Oxide - From Synthesis to Application: A Review*, Materials, vol.7, 2833-2881, (2014).
[2] A. D. Mauro, M. E. Fragala, V. Privitera, G. Impellizzeri, *ZnO for application in photocatalysis: From thin films to nanostructures*, Materials Science in Semiconductor Processing, 69, 44-51, (2017).
[3] J. Lee, *Comparison of CdS films deposited by different techniques: Effects on CdTe solar cell*, Applied Surface Science, vol. 252, 1398–1403, (2005).

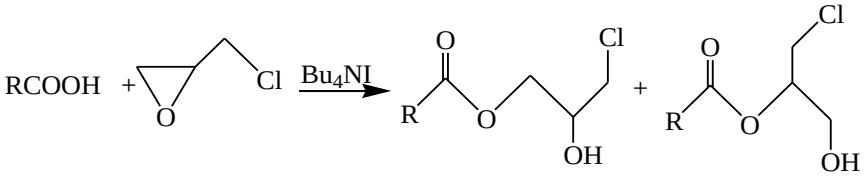
EFFECT OF STRUCTURE OF BENZOIC ACIDS ON CATALYTIC ACIDOLYSIS OF 2-(CHLOROMETHYL) OXYRANE

Evgeniia Bakhalova, Elena Shved, Anna Mishchenko, Liliia Lisova

Department of Chemistry, Biology and Biotechnologies, Vasyl' Stus Donetsk National University, Vinnytsia, Ukraine
je.bahalova@donnu.edu.ua

Reactions of oxiranes (epoxides) with proton-donating nucleophiles (carboxylic acids, phenols, alcohols, etc.) are widely used in the synthesis of epoxy resins, composite materials, plasticizers, and pharmaceutical substances. Asymmetric oxiranes, which are synthons in the aimed synthesis of various products, are of the greatest practical interest. In the practice of organic synthesis, the reaction of 2-chloromethyloxirane (ECH) with carboxylic acids, in particular aromatic acids, which give composites higher thermal and heat stability, is widely used.

The aim of the present work is the investigation of structure's effect of benzoic acids in the reaction series "2-chloromethyloxirane – benzoic acids – tetrabutylammonium iodide". The reaction proceeds according to the scheme:



R = C_6H_5, 3-$CH_3C_6H_4$, 2-$CH_3C_6H_4$

It has been selected benzoic acids (benzoic, 3-methylbenzoic, 2-methylbenzoic acids) as the proton-donating nucleophilic reagent, tetrabutylammonium iodide as the catalyst of reaction. ECH is taken in significant excess and is both a substrate and a solvent at the same time. The study was carried out at 60 °C in a binary solvent epichlorohydrin: tetrahydrofuran (1:1, vol.%). Tetrahydrofuran is inert to the reactant system and reduces the polarity of the solvent. The progress of the reactions was monitored by measuring the concentration of carboxylic acid by potentiometric acid-base titration. The purity of the reagents and the structure of the products were determined by IR and ^{1}H NMR spectroscopy. The order of reaction for acid was determined experimentally and by mathematical modeling. Processing of experimental data was carried out by methods of mathematical statistics and correlation analysis.

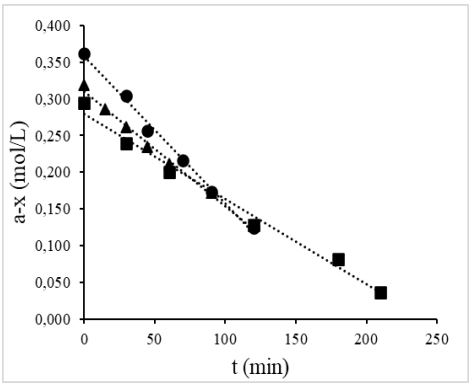


Fig. Time dependence of the concentration of benzoic acid (a – x) (mol / L) (RC_6H_4COOH, R: ● – 2-CH_3, ▲ – H, ■ – 3-CH_3.) for its reaction with 2-(chloromethyl)oxirane catalyzed by tetrabutylammonium iodide (b = 0.005 mol / L) at 60° C

The order of reaction with respect to the acid reagent was determined from the plots of benzoic acid concentration (a − x) versus time (t) (fig.). It was found that acid reagent consumption is linear, which corresponds to a zeroth order of reaction with respect to benzoic acid. This made it possible to calculate the observed rate constants (table). Using the KINET program, the calculated reaction rate constants ($k_{obs\ opt}$) corresponding to the first order of the reaction and the zeroth order of the reaction with respect to acid were estimated by mathematical modeling of the reaction order (table). The difference between the optimized and observed rate constants is insignificant.

Comparative evaluation of the reactivity of benzoic acids with 2-chloromethyloxirane in the presence of tetrabutylammonium iodide was carried out according to the Brønsted equation (1) based on the acidic (pKa) properties of the reagent and according to the Hammett equation (2) based on the influence of the substituent (σ).

Table. The rate constants of catalyzed reactions of benzoic acids with 2-chloromethyloxirane in the presence of tetrabutylammonium iodide (mol / L) at 60° C

R в R-C_6H_4COOH	pK_a	σ	$k_{obs} \cdot 10^6$, s^{-1}	$k_{obs\ opt} \cdot 10^6$, s^{-1}
3-CH_3	4,27	-0,069	3,75±0,31	3,28
H	4,18	0	4,76±0,22	4,34
2-CH_3	3,92	-0,17	5,45±0,19	5,34

$$lgk_{cat} = (2{,}9\pm0{,}7) + (-0{,}5\pm0{,}5)pKa \quad (1)$$

(r=0,947; N=3)

$lgk_{cat} = lgk_o + \rho\ \sigma$ –unsatisfactory correlation (2)

Comparison of the obtained data and the results of previous studies allowed to prove that benzoic acids with the highest steric factor have the highest reactivity, although the reaction has a rather low sensitivity to the acid structure. The increase in the acidic properties of the reagent is a favorable factor for the path of the reaction.

DEVELOPMENT AND TESTING OF CRYOFOCUSING ADD-ON FOR GAS CHROMATOGRAPHY

Audrius Sadaunykas, Audrius Zolumskis, Evaldas Naujalis

Metrology Department, State Research Institute Center for Physical Sciences and Technology
Lukiškių str. 9, LT-01108 Vilnius, Lithuania
audrius.sadaunykas@ftmc.lt

Gas chromatography (GC) is one of the most popular analytical method used around the world. This method is applied for various volatile compound analysis. Basics of gas chromatography is compound separation, performed on a chromatographic GC column. Analytes are pushed forward along the column (a thin silica capillary tube, covered in stationary phase) using inert gas flow and because of chemical forces and bonds between analytes and stationary phase of the column, analytes are retained and elute from the column at different rates [1]. GC requires a very precise temperature control to influence analyte separation and make analysis more efficient. Lack of sensitivity and not enough separation are the main problems researchers face while using gas chromatography. There are different ways to improve sensitivity and separation: changes in detector, column or injection system [2]. In our laboratory we are building an add-on, which could be used with existing GC systems, without any modification to existing parts.

Our prototype scheme showed in Figure 1 is based on cooling down part of the column to -60 ºC. Unit outside the GC houses cylindrical aluminum block, which is cooled down using external chiller. On top of the block there is a smaller disk-shaped part, that houses the GC column and resistive heaters. This part can be lifted up from the block heated to 100 ºC and then, lowered down to cool down quickly. By having part of the column at -60 ºC allows us to trap the analyte traveling from the injector and contain it there. Multiple injections could be made and analyte peak area enriched. After number of injections, disk is raised and heater is turned on. Temperature in the disk reaches 100 ºC and analyte is eluted quickly. Number of injections corelate with increase in peak area of the analyte. This process greatly increases the sensitivity of the system.

To test the accuracy and reproducibility of our add-on paired with GC system, we decided to measure nonane (1 µl) dissolved in pentane (1 ml) at different enrichment levels. This produced a curve (Figure 2) with R^2 of 0,9999. This indicates, that all injections are consistent and no loss of analyte is present.

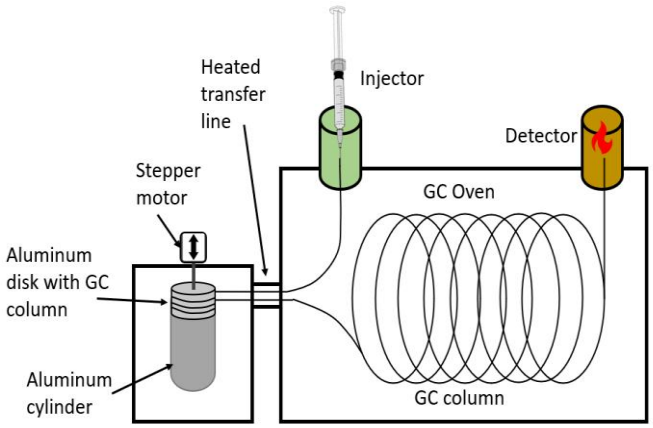


Fig. 1. Gas chromatography system with cryofocusing add-on

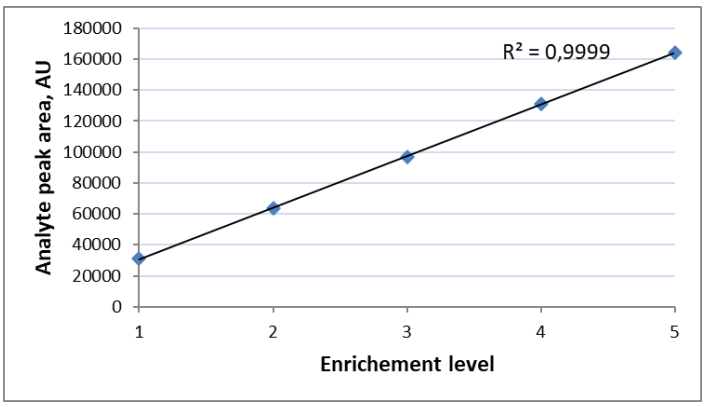


Fig. 2. Peak areas at different enrichment levels

These results are just the beginning of our work on this topic and we will continue with improvement of the prototype.

[1] Skoog, Douglas A.; West, Donald M.; James Holler, F.; Crouch, Stanley R., Fundamentals of analytical chemistry, (Ninth ed.). Belmont, CA, (2013) ISBN-13: 978-0495558286
[2] Schomburg G., Practical Limitations of Capillary Gas Chromatography, Journal of High Resolution Chromatography, 2(7), 461-474, (1979).
[3] Sadaunykas A., On-column cryofocusing and analyte enrichment device for gas chromatography systems, Chemija, Vol 31, Issue 4, 284-289, (2020)

PRUSSIAN BLUE AS REDOX MEDIATOR IN YEAST-BASED BIOFUEL CELL

Gabija Kavaliauskaitė[1], Povilas Virbickas[1], Aušra Valiūnienė[1]

[1] Department of Physical Chemistry, Faculty of Chemistry and Geosciences, Vilnius University, Lithuania
gabija.kavaliauskaite@chgf.stud.vu.lt.

Prussian Blue ($Fe_4[Fe(CN)_6]_3$) (PB) is a pigment, known for its electrochromic and electrocatalytic properties [1,2]. This compound is widely used in formation of electrochemical sensors and biosensors [3,4,5]. PB is often used as a redox mediator and signal transducer in biosensors, for example urea and glucose biosensors [6,7].

Saccharomyces cerecisiae, also known as Baker's yeast, are one of the most available and cost-effective unicellular eukaryotic cells to be used in a construction of biofuel cell [8]. Although yeast cells are popular in formation of biofuel cells, the charge transfer is limited by the yeast cell wall conductivity [9]. For this reason, mediators are needed to ensure the efficient operation of yeast-based biofuel cell. According to the literature, mediators, used in construction of already known yeast-based biofuel cells, are harmful to viability of *Saccharomyces cerecisiae* cells [10].

In this research work Baker's yeast (*Saccharomyces cerecisiae*) cells were modified with $FeCl_3$ and $K_3[Fe(CN)_6]$ salts to form PB. After the formation of PB, the increase of conductivity of yeast cells walls was measured by using cyclic voltammetry. Also, charge transfer of the biofuel cell based on PB-modified yeast cells was examined. The effect of yeast cells modification with PB on yeast cell viability was examined by optical microscope and gravimetric method.

[1] A. A. Karyakin, Prussian Blue and Its Analogues: Electrochemistry and Analytical Applications, Electroanalysis, No. **10**, 13 (2001).
[2] K. Itaya, N. Shoji, I. Uchida, Catalysis of the Reduction of Molecular Oxygen to Water at Prussian Blue Modified Electrodes, Journal of American Chemistry Society, **106**, 3423-3429 (1984)
[3] H. Dussel, A. Dostal, F. Scholz, Hexacyanoferrate-based composite ion-sensitive electrodes for voltammetry, Fresenius Journal of Analytical Chemistry, **355**, 21-28 (1996)
[4] N. Matei, S. Dobrinas, G. L. Radu, Spectrophotometric determination of ascorbic acid in grapes with the Prussian Blue reaction, Ovidius University Annals of Chemistry, **23**, No. 1, 174-179 (2012)
[5] F. Ricci, G. Palleschi, Sensor and biosensor preparation, optimisation and applications od Prussian Blue modified electrodes, Biosensors and Bioelectronics, **21**, issue 3, 389-407 (2005)
[6] P. Virbickas, A. Valiuniene, G. Kavaliauskaite, A. Ramanavicius, Prussian White-Based Optical Glucose Biosensor, Journal of The Electrochemical Society, **166** (12), B927- B932 (2019)
[7] A. Valiuniene, G. Kavaliauskaite, P. Virbickas, A. Ramanavicius, Prussian Blue based impedimetric biosensor, Journal of Electroanalaytical Chemistry, **895**, (2021)
[8] G.Reed, H.J.Peppler, Yeast Technologie, The Avi Publishing Company, Wesport, USA (1973)
[9] D. Prasad, S. Arun, M. Murugesan, S. Padmanaban, R.S. Satyanarayanan, S.Berchmans, V. Yegnaraman, Direct electron transfer with yeast cells and construction of a mediatorless microbial fuel cell, Biosensors and Bioelectronics, **22**, 2604 – 2610 (2007)
[10] S. Babanova, Y. Hubenova, M. Mitov, Influence of artificial mediators on yeast-based fuel cell performance, Journal of Bioscience and Bioengineering, **112**, No.4, 379-387 (2011)

THE SYNTHESIS OF L-HOMOCYSTINE DERIVATIVES AS PRECURSORS TO MODIFIED *S*-ADENOSYL-L-METHIONINE ANALOGUES

Edvin Parafjanovič, Martynas Malikėnas, Viktoras Masevičius

Faculty of Chemistry and Geosciences, Vilnius University, Lithuania
edvin.parafjanovic@chgf.stud.vu.lt

DNA methylation is a predominant epigenetic modification that regulates gene expression without altering the original DNA sequence [1]. The reaction occurs via methyltransferase (MTase) catalyzed S_N2 transfer of an activated sulfonium-bound methyl group from the cofactor *S*-adenosyl-L-methionine (SAM) to targeted DNA bases, *S*-adenosyl-L-homocystine (SAH) serving as a leaving group [1][2]. However, methylation itself has a limited practical utility. To find new tools for manipulating DNA in a selective and unique way various SAM analogues were synthesized [2][3]. Current cofactor alternatives (known as double-activated SAM analogues) involve a replacement of the methyl group with substituents containing allylic or propargylic systems next to the reactive carbon [1][3]. Unfortunately, these synthetic cofactors suffer from short lifetimes in physiological buffers, competing methylation by endogenous SAM and lower acceptance by MTases compared to SAM [1][4]. Selectivity and affinity problems can be solved by engineering MTases toward new cofactors, while excluding the natural cofactor [4]. One of the possible ways to improve the stability of SAM analogues and enhance selectivity towards engineered MTase variants is via modification of other important SAM binding sites [4].

The aim of this work is to modify the carboxyl group positioned in homocysteine moiety of the double activated SAM analogue. Herein we report the synthesis pathway (Fig. 1) of *N*-di-*tret*-butoxycarbonyl-L-homocystinol (**IV**) from starting compound L-methionine (**I**). *N*-di-*tret*-butoxycarbonyl-L-homocystinol (**IV**) can be a precursor to various L-homocystine derivatives and be used in preparation of SAM analogues (**VI**) with extended transferable groups suitable for methyltransferase-directed labeling of DNA and RNA. The products **V** and **VI** are yet to be synthesized.

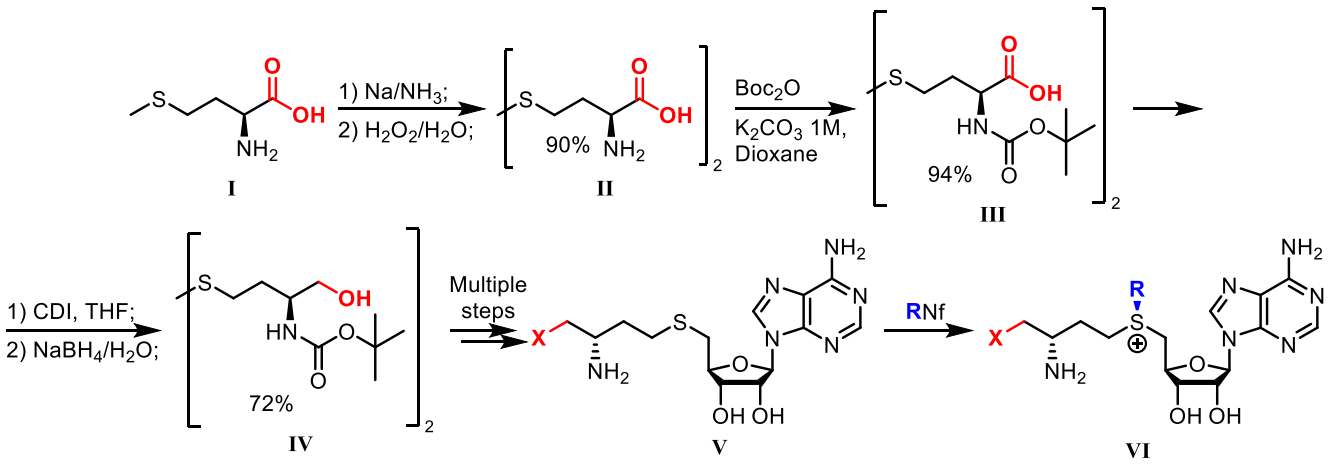


Fig. 1. The synthesis pathway of *N*-di-*tret*-butoxycarbonyl-L-homocystinol.

[1] S. Klimašauskas and E. Weinhold, "A new tool for biotechnology: AdoMet-dependent methyltransferases," *Trends Biotechnol.*, vol. 25, no. 3, pp. 99–104, 2007, doi: 10.1016/j.tibtech.2007.01.006.

[2] G. Lukinavičius, M. Tomkuvienė, V. Masevičius, and S. Klimašauskas, "Enhanced chemical stability of AdoMet analogues for improved methyltransferase-directed labeling of DNA," *ACS Chem. Biol.*, vol. 8, no. 6, pp. 1134–1139, 2013, doi: 10.1021/cb300669x.

[3] V. Masevičius, M. Nainytė, and S. Klimašauskas, "Synthesis of S-adenosyl-L-methionine analogs with extended transferable groups for methyltransferase-directed labeling of DNA and RNA," *Curr. Protoc. Nucleic Acid Chem.*, vol. 2016, no. March, pp. 1.36.1-1.36.13, 2016, doi: 10.1002/0471142700.nc0136s64.

[4] A. Jeltsch and R. Z. J. Editors, *Methyltransferases – Role and Function*.

SYNTHESIS OF 1,5-DISUBSTITUTED IMIDAZOLES AS POTENTIAL HSP90 INHIBITORS

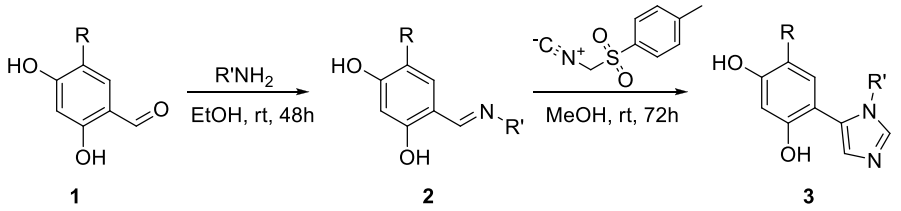
Paulina Kaziukonytė[1], Kamilė Venskūnaitė[1], Tomas Venslauskas[2], Algirdas Brukštus[1]

[1] Faculty of Chemistry and Geosciences, Vilnius University, Lithuania
[2] Faculty of Medicine, Vilnius University, Lithuania
paulina.kaziukonyte@chgf.vu.lt

Hsp90 (Heat shock protein) – chaperone protein, responsible for folding, stabilization and activation of client proteins. Despite Hsp90 playing an important role in normal cell regulation cycles, chaperone also aids several known cancerogenic proteins. [1] Therefore, it is postulated that inhibition of Hsp90 could lead to efficacious cancer treatment, with some inhibitors already going through clinical trials. [2]

One major class under investigation are compounds containing 1,3-benzenediol moiety, based on the natural product Radicicol. Active structures consistently include aromatic substitutes linked by a 5-membered heterocyclic ring. [3] As there is little information on imidazole ring impact on the effectiveness of inhibition, in our study, we designed an efficient synthetic way to obtain molecules containing 1,3-benzenediol and imidazole fragments.

2,4-dihydroxy-5-substituted benzaldehydes (**1**) and primary amines stirred in ethanol at room temperature for 48 hours gave respective imines (**2**). Latter compounds were used in a reaction with 1-(isocyanomethanesulfonyl)-4-methylbenzene and stirred at room temperature in methanol for 72 hours to give a series of imidazole compounds **3**.



Scheme 1. Synthetic pathway to 4-isopropyl-6-(1-substituted-1*H*-imidazol-5-yl)benzene-1,3-diols

Inhibition activity of 4-substituted 6-(1-substituted 1*H*-imidazol-5-yl)benzene-1,3-diols (**3**) is yet to be determined.

[1] Y. Miyata, H. Nakamoto, L. Neckers, The Therapeutic Target Hsp90 and Cancer Hallmarks, Curr Pharm Des. **19 (3)**, 347-365 (2013).
[2] A. Yuno, M. Lee, S. Lee, et al, Clinical Evaluation and Biomarker Profiling of Hsp90 Inhibitors, Methods Mol Biol. **1709**, 423-441 (2018).
[3]A. Khandelwal, V. M. Crowley, B. S. J. Blagg, Natural Product Inspired Hsp90 N-Terminal Inhibitors for the Treatment of Cancer: From Bench to Bedside, Med Res Rev. **36 (1)**, 92-118 (2016).

INFLUENCE OF PHOSPHATE GROUP INTRODUCTION ON PROPERTIES OF PSEUDO-POLY(AMINO ACID)S OF POLYESTER TYPE

Anna Stasiuk, Volodymyr Lyakh, Nataliia Fihurka, Iryna Dron, Volodymyr Samaryk

Department of Organic Chemistry, Lviv Polytechnic National University, Ukraine
anna.v.stasiuk@lpnu.ua

Pseudo-poly(amino acid)s (PPAA) of polyester type are considered promising materials for biomedical applications due to a number of properties - biodegradability, biocompatibility. Researchers pay special attention to preparing polyester-based dispersed delivery systems for therapeutic agents. However, polyesters based on dicarboxylic acids and diols do not include in their structure functional groups or active centers capable of chemisorption of biological substances and drugs, which significantly limits their use. Therefore, the synthesis of functionalized polyesters still remains an urgent problem. Solving this issue will allow preparing new forms to deliver various biologically active compounds. The introduction of phosphate groups into the polymer chain is particularly promising for this purpose as the pentavalent phosphorus atom is an excellent option for further modification or binding to low molecular weight therapeutic drugs or proteins.

Synthetic approaches for a number of pseudo-poly(amino acid) based on N-derivatives of glutamic acid and PEG/PPG diols using the Steglich reaction have been developed [1]. These techniques allow regulating the structure and composition of the final copolyester by introducing blocks and monomers of different nature and molecular weight. This, in turn, is an effective way to regulate the hydrophilic-lipophilic balance, and hence the colloidal properties of the obtained polyesters. The developed synthetic approach to the pseudo-poly(amino acid) of the polyester type allows the use of diols of different nature. It seems appropriate to functionalize this class of molecules by introducing a phosphate group into the structure of the diol.

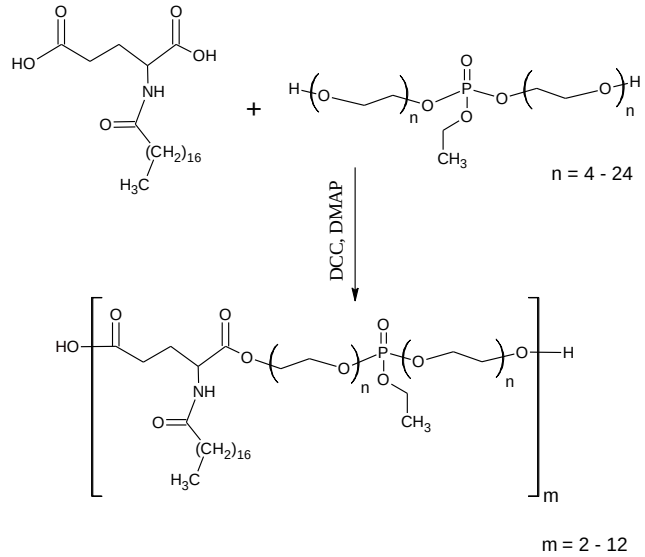


Fig. 1. Synthesis of pseudo-poly(amino acid) with ethylphosphate group (PPE).

To be suitable for drug delivery systems, polymers should possess surface-active properties. Studies of the obtained pseudo-poly(amino acid) with ethylphosphate group (PPE) revealed that the introduction of ethylphosphate group into the polyoxyethylene fragment to some extent affects surface-active properties. The surface tension curves of PPE obtained in comparison with PPAA confirm that the synthesized PPE have similar surfactant properties; the values of this activity show that PPEs are even more surface-active compared to PPAA with a similar structure. Accordingly, PPEs have the ability to form self-stabilized dispersions with a nanometric dispersed phase in aqueous media. This confirms the particle size distribution of the dispersed phase obtained by the dynamic light scattering method.

Studies show that aqueous dispersions of the obtained polymers are able to solubilize significant amounts of water-insoluble organic compounds and are non-toxic. The introduction of the phosphate group into the structure of the polyoxyethylene fragment leads to an increase in the absorption and solubilization properties of aqueous dispersions. Based on the described experimental data, it can be concluded that the developed method of polyphosphoesters and a set of properties makes them promising for use as polymer disperse delivery systems for therapeutic agents.

[1] Varvarenko, S., et al., Synthesis and Colloidal Properties of Polyesters Based on Glutamic Acids and Glycols of Different Nature, Chemistry and Chemical Technology, vol. **7**, no. **2**, 161-168 (2013).

CONDUCTING POLYMERS IN THE DESIGN OF BIOSENSORS

Greta Pilvenytė[1], Raimonda Bogužaitė[1], Vilma Ratautaitė[1,2], Aušra Baradokė[1], Arūnas Ramanavičius[1,2]

[1] Laboratory of Nanotechnology, Department of Functional Materials and Electronics, State Research Institute Center for Physical Sciences and Technology, Sauletekio av. 3, Vilnius LT-10257, Lithuania.
[2] Department of Physical Chemistry, Institute of Chemistry, Faculty of Chemistry and Geosciences, Vilnius University, Naugarduko str. 24, Vilnius LT-03225 Lithuania
greta.pilvenyte@ftmc.lt

Electrochemical biosensor is a type of sensing devices that utilises a transducer and recognition element to determine the presence of an analyte. As an electrochemical transducer, conducting polymers have been widely used in biomedical applications [1,2,3]. Mainly because conducting polymers offer a variety of technological solutions required for the development of electrochemical sensors and biosensors [1]. As a recognition element, to obtain the required selectivity of an electrochemical sensor, biological receptors (e.g. antibodies, antigens, etc.) or artificially synthesized materials as receptors (e.g. molecularly imprinted polymers) to mimic the molecular recognition process of biological macromolecules such as substrate-enzyme or antigen-antibody may be used [4,5,6].

Recently, molecularly imprinted polymers (MIPs) attracted a lot of attention, as specific molecular recognition sites – binding cavities with controlled size, shape as well as functionalities can be formed for specific recognition of the target analyte. Sensors with a molecularly imprinted conducting polymer are in tremendous interest, because they are mainly based on the electrochemically deposited polymeric matrix enabling us to design sensing films that are having various physical properties [1,7]. Up to now polyaniline, polypyrrole, polythiophene, and poly(3,4-ethylenedioxythiophene) are frequently used conducting polymers in the design of sensors and biosensors [1,2]. Polypyrrole has attracted special interest in development of economic and sensitive biosensors due to high conductivity, easy synthesis from water-based solutions, stability and good mechanical properties [2,7]. Electrochemical activity, electrical conductivity, mechanical elasticity, biocompatibility, and environmental stability of conducting polymers are mostly desired properties required for the advancement of sensing performance of analytical and bioanalytical systems. These properties of the films are easily controlled by changing electrochemical polymerisation conditions such as electrode potential, current density or solvent type [2,3].

Wide range of analytes can be analysed by using such electrochemical sensors and biosensors. The electrochemical sensor can be designed for selective detection by molecular imprinting with large molecules such as C-reactive protein [3] and SARS-CoV-2-S spike glycoprotein [4], as well as small analytes like uric acid [5,6] or methylene blue. In this presentation some here mentioned properties of conducting polymers will be overviewed/discussed and bioanalytical application of conducting polymer based structures will be presented.

[1] S. Ramanavicius, A. Ramanavicius. Conducting Polymers in the Design of Biosensors and Biofuel Cells, Polymers 13, 49 (2021) doi: https://doi.org/10.3390/polym13010049.
[2] A. Baradoke, A. Santos, P. R. Bueno, J.J. Davis Introducing polymer conductance in diagnostically relevant transduction. Biosens. Bioelectron. 112705, (2020). doi: https://doi.org/10.1016/j.bios.2020.112705.
[3] A. Baradoke, R. Hein, X. Li, J.J. Davis. Reagentless Redox Capacitive Assaying of C-Reactive Protein at a Polyaniline Interface. Anal. Chem. 92, 3508–351, (2020). doi: https://doi.org/10.1021/acs.analchem.9b05633.
[4] V. Ratautaite, R. Boguzaite, E. Brazys, A. Ramanaviciene, E. Ciplys, M. Juozapaitis, R. Slibinskas, M. Bechelany and A. Ramanavicius, Molecularly imprinted polypyrrole based sensor for the detection of SARS-CoV-2 spike glycoprotein. Electrochimica acta 403, 139581 (2022). https://doi.org/10.1016/j.electacta.2021.139581.
[5] V. Ratautaite, U. Samukaite-Bubniene, D. Plausinaitis, R. Boguzaite, D. Balciunas, A. Ramanaviciene, G. Neunert and A. Ramanavicius, Molecular imprinting technology for determination of uric acid. International Journal of Molecular Sciences 22, 5032 (2021). https://doi.org/10.3390/ijms22095032.
[6] D. Plausinaitis, L. Sinkevicius, U. Samukaite-Bubniene, V. Ratautaite and A. Ramanavicius, Evaluation of Electrochemical Quartz Crystal Microbalance Based Sensor Modified by Uric Acid-imprinted Polypyrrole Talanta, 220, 121414 (2020). Doi: https://doi.org/10.1016/j.talanta.2020.121414.
[7] S. Ramanavicius, A. Jagminas, A. Ramanavicius. Advances in Molecularly Imprinted Polymers Based Affinity Sensors (Review). Polymers 13, 974 (2021). doi: https://doi.org/10.3390/polym13060974.

SYNTHESIS AND CRYSTAL STRUCTURES OF $Na_9[Eu(W_5O_{18})_2]\cdot 35H_2O$ WITH PLATE-LIKE MORPHOLOGY

Oleksandra Yu. Mariichak[1,2], Anna O. Zaharchuk[2], Olena Yu. Popovska[2], Georgii M. Rozantsev[1], Serhii V. Radio[2]

[1] Faculty of Chemistry, Biology and Biotechnologies; Vasyl' Stus Donetsk National University, Ukraine
[2] Department for Research, Research Laboratory "Chemistry of Polyoxometalates and Complex Oxide Systems", Vasyl' Stus Donetsk National University, Ukraine
o.marijchak@donnu.edu.ua

The conditions for the synthesis of crystalline sodium heteropoly decatungstoeuropate(III) $Na_9[Eu(W_5O_{18})_2]\cdot 35H_2O$ with plate-like morphology were elaborated (Fig. 1).

X-ray single crystal analysis for $Na_9[Eu(W_5O_{18})_2]\cdot 35H_2O$ single crystal was performed and fundamental data for the crystal structure were obtained: a = 12,928, b = 13,064, c = 21,427 Å, α = 101,04, β = 103,43, γ = 103,030 deg., V = 3 313,8 Å^3, Z = 2, triclinic syngony, space group $P\bar{1}$) (Fig. 2).

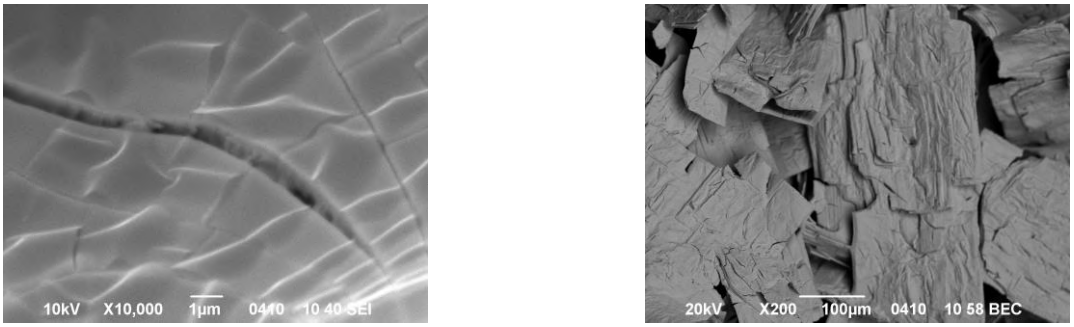


Fig. 1. SEM image of the of $Na_9[Eu(W_5O_{18})_2]\cdot 35H_2O$ in the SEI mode (*left*) and in the BEC mode (*right*)

It was shown that the polyhedron of the Eu(III) heteroatom is a square anti-prism formed by two tetradentate lacunar isopoly tungstate anions $[W_5O_{18}]^{6-}$.

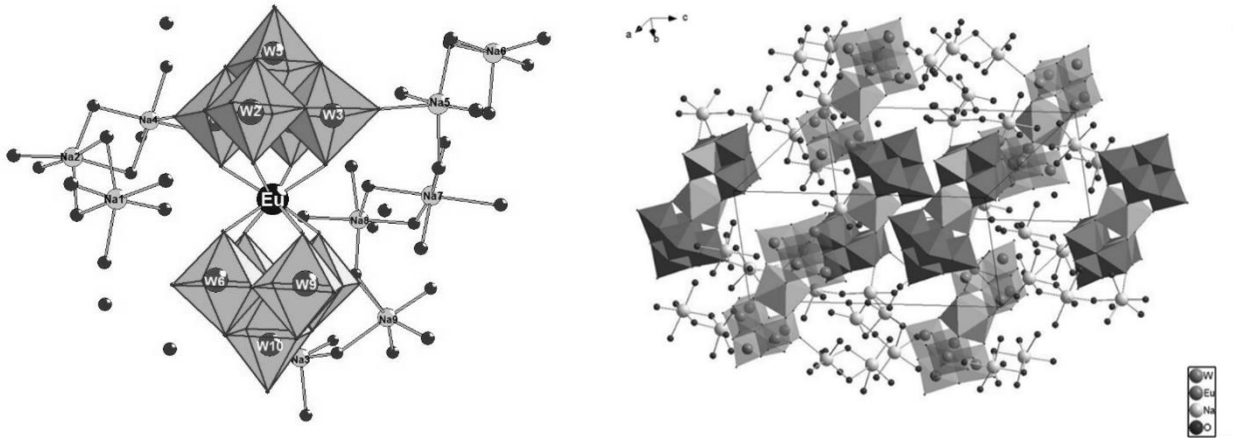


Fig. 2. *Left* – Image of the main structural unit in $Na_9[Eu(W_5O_{18})_2]\cdot 35H_2O$, *right* – crystal packing of $Na_9[Eu(W_5O_{18})_2]\cdot 35H_2O$ (cationic sub-lattice is presented in a "ball-and-stick" format)

The set of oscillations characteristic for the heteropoly tungstate anion with the Peacock–Weakley type of structure was established by the methods of FT-IR and FT-Raman spectroscopy. It is shown that changes in the composition of the cationic sub-lattice and the presence of different numbers of H_2O molecules in the structure do not affect the values of bond lengths and valence of angles in the heteropoly anion $[Eu(W_5O_{18})_2]^{9-}$. By the method of spectrophotometry in UV and visible range was shown that the formation of heteropoly anion $[Eu(W_5O_{18})_2]^{9-}$ occurs immediately after the addition of reactants in a stoichiometric amount in the temperature range 10–60^{0}C. By the method of scanning electron microscopy was shown that the grain size of $Na_9[Eu(W_5O_{18})_2]\cdot 35H_2O$ powder is up to 500 nm. The single-phase of salt was confirmed by the uniform surface contrast in the BEI mode and by the uniform distribution of Eu, Na, W, and O during the scanning of the surface in the characteristic X-ray radiation.

The study was carried out within the Fundamental Research Programme funded by the Ministry of Education and Science of Ukraine (grants ID 0120U102059, 0122U000762).

MOLECULAR DYNAMICS ANALYSIS FOR POTENTIAL ENERGY SURFACES OF BACTERIORHODOPSIN ACTIVE CENTER

Ligitas Vinciūnas[1], Mindaugas Mačernis[1]

[1]Institute of Chemical Physics, Faculty of Physics, Vilnius University, Saulėtekio av. 3, LT-10257 Vilnius, Lithuania
ligitas.vinciunas@ff.stud.vu.lt

Bacteriorhodopsin is a protein responsible for ion transfer across cell membrane.[1,2] To move ions light energy is required.[1,2] The active center of the bacteriorhodopsin is retinal.[1] When retinal absorbs light energy, its configuration changes from *all-trans* to *13-cis, 15-anti*.[1] These changes initiates proton transfer process.[1] After some time, retinal configuration returns to its initial state, and proton transfer process may be repeated.[1] This process is called bacteriorhodopsin photocycle.[1,2]

It is known that retinal's *13-cis, 15-anti* configuration duration is in the order of ps, μs, but *ab-initio* molecular dynamics (MD) calculations show that retinal's *13-cis, 15-anti* configuration duration is in the order of fs.[2,3] Our main objective is to evaluate stability of retinal's *13-cis, 15-anti* configuration.

In this work, we used Gaussian16 package. Calculation parameters: functional *B3LYP*, and basis set *cc-pVDZ*. For *ab-initio* molecular dynamics we used ADMP method. A lot of studies use these methods for bacteriorhodopsin modeling, because they describe bacteriorhodopsin protein quite well.[4]

We took 2 bacteriorhodopsin structures from pdb bank: 1C3W (ground state bacteriorhodopsin), and 2NTW (L state bacteriorhodopsin). From both structures, we cut out retinal, added hydrogen to retinal, and run structure optimization. Then we examined how environment affects *13-cis, 15-anti* configuration stability by adding residues: Trp86, Trp182, Tyr185, and Thr90 to L state system, optimizing active center, and running MD calculations. After that we investigated which part of retinal's Schiff base, and Lys216 rotates when configuration changes occur, by rotating specific parts of Schiff base, and Lys216, and observing energy changes. Then we monitored how additional structures affects *13-cis, 15-anti* configuration stability by adding more residues: Phe219, Leu93, Val20, and Met20 to our L state system, optimizing active center, and running MD calculations. Finally, we investigated *13-cis, 15-anti* configuration stability by adding additional structures: Asp85, HOH401, HOH406 to L state system, freezing all atoms, except few, then running structure optimization, and observing configuration changes.

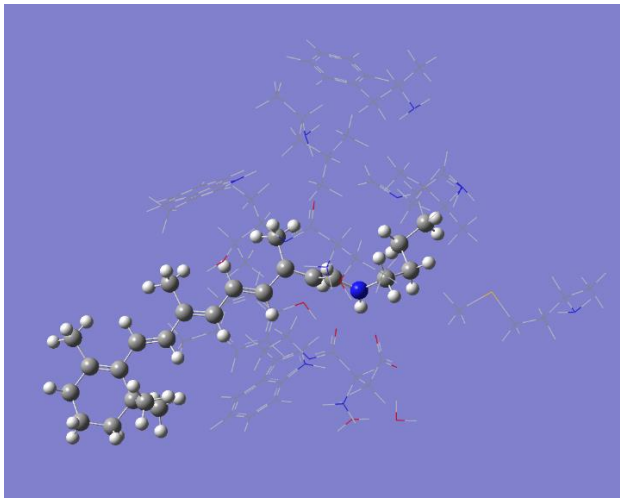


Fig.1. Bacteriorhodopsin active center (retinal)

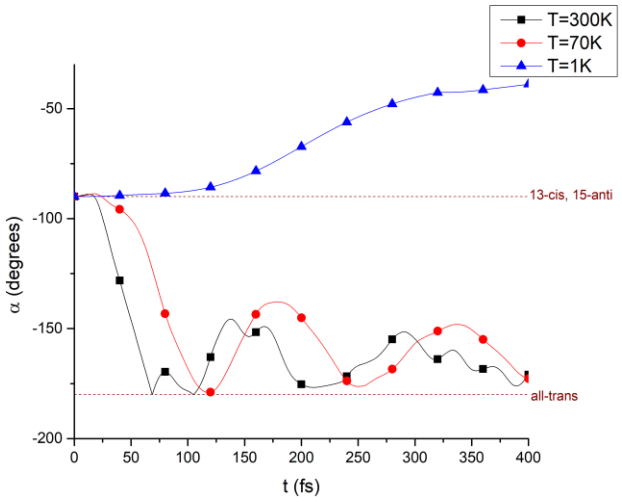


Fig. 2. Retinal configuration change during MD calculations

MD calculations show, that retinal's *13-cis, 15-anti* configuration duration in vacuum is $\tau = 30$ fs at $T = 1\ K$, and with residues from protein: Trp86, Trp182, Tyr185, and Thr90 is $\tau = 130$ fs at $T = 1\ K$. When we added residues: Phe219, Leu93, Val20, and Met20 duration of *13-cis, 15-anti* configuration became $\tau = 60$ fs at $T = 1\ K$. This work final conclusion is that stability of configuration depends on residues from protein, and right residues must be recognized in order to increase stability of configuration.

Computations were performed on resources at the supercomputer "VU HPC" Saulėtekis of Vilnius University in Faculty of Physics.

[1] B.P. Kietis, M. Macernis, J. Sulskus, L. Valkunas, Lith. J Phys. 50, 4, (2010).
[2] C. Wickstrand, et al., Bacteriorhodopsin: Would the real structural intermediates please stand up?, Biochim. Biophys. Acta (2014), http://dx.doi.org/10.1016/j.bbagen.2014.05.021
[3] Ernst OP, Lodowski DT, Elstner M, Hegemann P, Brown LS, Kandori H. Microbial and animal rhodopsins: structures, functions, and molecular mechanisms. Chem Rev. 2014;114(1):126-163. doi:10.1021/cr4003769
[4] Babitzki G, Mathias G, Tavan P. The infrared spectra of the retinal chromophore in bacteriorhodopsin calculated by a DFT/MM approach. J Phys Chem B. 2009 Jul 30;113(30):10496-508. doi: 10.1021/jp902432e. PMID: 19580300.

INFLUENCE OF LAYERED DOUBLE HYDROXIDE ON POLYADDITION OF AROMATIC ISOCYANATE AND MACRODIOL

Gytautė Sirgėdaitė, Paulina Nemaniutė, Dalia Bražinskienė, Svajus J. Asadauskas

Department of Chemical Engineering and Technology, FTMC, Vilnius, Lithuania
gytaute.sirgedaite@ftmc.lt

Layered double hydroxides (LDH), hydrotalcites in particular, represent a major and versatile class of 2D materials, which can be used to encapsulate drugs, flavors and other functional components in various matrices [1]. Consequently, LDH finds innovative uses in diverse polymer applications. However, its usage in polyurethane (PUR) might be complicated, because LDH contains hydrated moieties, which might react with isocyanates and disrupt polymerization. In this study, hydrotalcite LDH as $Mg_XAl_2(OH)_2]_{(2+X)}CO_3$ (x=4-6) with relatively low water contents (<0.5% wt. loss in 2 hrs at 105°C) was incorporated into PUR by mixing it in a diluted OH-terminated prepolymer and curing with aromatic isocyanate. The prepolymer was produced in ethyl acetate by chain extending the ether-ester macrodiol of 2700 g/mol, synthesized from adipic acid and diethylene glycol, with hexamethylene diisocyanate at 1:0.3 mol. ratio [2]. Polymerization was carried out by mixing the prepolymer with a trifunctional aromatic isocyanate (prediluted with 25% wt. ethyl acetate with or without LDH) at 1.4 mol. excess. Three blends were studied at 50°C:

- no LDH (60% wt. prepolymer, 32.5% wt. ethyl acetate and 7.5% wt. isocyanate);
- 1.8% LDH (59% wt. prepolymer, 31.7% wt. ethyl acetate, 1.8% wt. LDH and 7.5% wt. isocyanate) and
- 6% LDH (56% wt. prepolymer, 31.5% wt. ethyl acetate, 6% wt. LDH and 7.5% wt. isocyanate).

In every mixture, the isocyanate was preheated and added as the last component immediately before testing. The mixtures were agitated for 0.5-1 min and poured into a capillary Cannon-Fenske viscometer of 500 size (orifice of 2 mm ID), equilibrated at 50°C. The rate of isocyanate polyaddition to the OH-terminated prepolymer was monitored by measuring kinematic viscosity using an adapted ASTM D445 procedure [3].

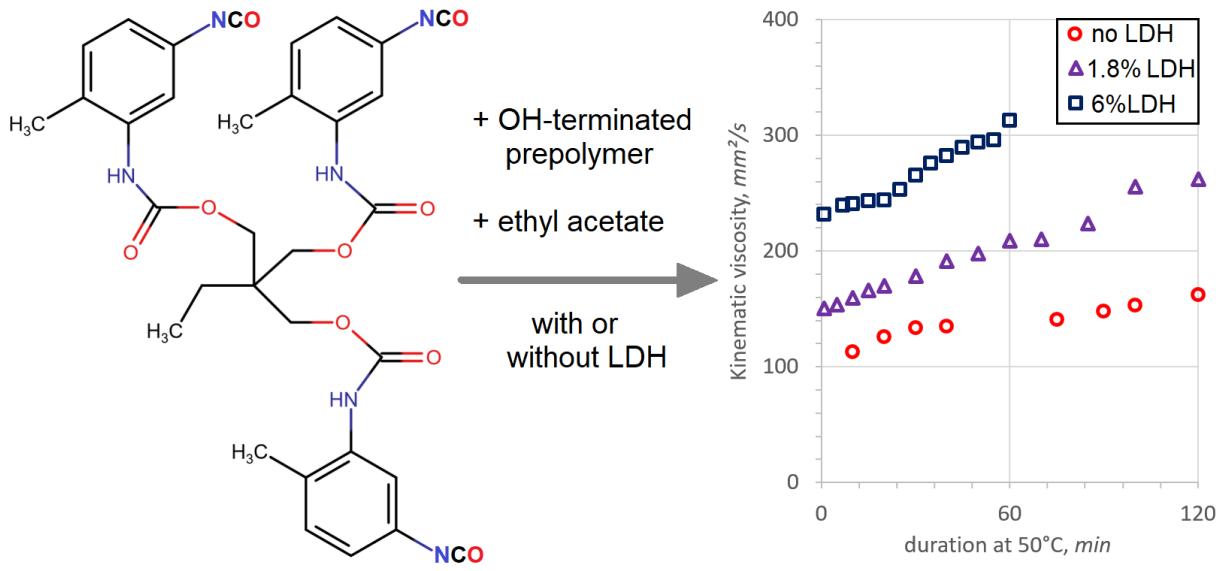


Fig. 1. Polyaddition of trifunctional aromatic isocyanate (left) to prepolymer, leading to viscosity increase and effects of LDH inclusion (right).

The results show, Fig. 1, that viscosity builds up gradually due to the ongoing polyaddition. Inclusion of 1.8% wt. LDH increases the viscosity by nearly 50%, retaining this ratio through the course of polyaddition. Higher amounts of LDH increase viscosity further, as in case of 6% wt. LDH. Nevertheless, the rate of polyaddition remains similar, which implies that LDH addition does not change polymerization mechanism significantly. However, H_2O concentration in LDH should be carefully considered, because the tested hydrotalcite had relatively low moisture levels.

Conclusion. Addition of hydrotalcite LDH into polyurethane matrix increases viscosity but should not significantly affect polymerization mechanisms, which makes it possible to develop PUR plastics with innovative functions.

Acknowledgment. This study was carried out under project TERMINUS, funded by the European Union under Horizon 2020. Call H2020-NMBP-ST-IND-2018. Grant Agreement: 814400. Clariant Inc. is gratefully acknowledged for the free sample of hydrotalcite LDH.

[1] N.B. Allou, P. Saikia, A. Borah et al., Hybrid nanocomposites of layered double hydroxides: an update of their biological applications and future prospects. Colloid Polym Sci, vol. 295, pp. 725–747 (2017) DOI 10.1007/s00396-017-4047-3
[2] S. Mačiulytė, A. Strakšys, S. Asadauskas, Influence of aliphatic moieties in diisocyanates on chain extension kinetics of adipate macrodiols. Proc. Baltic Polymer Symp. pg 40, Vilnius (2019) DOI: 10.5281/zenodo.3813463
[3] ASTM D445. Standard Test Method for Kinematic Viscosity of Transparent and Opaque Liquids. American Soc. for Testing Materials, Conshohocken, Pennsylvania, USA.

SYNTHESIS AND INVESTIGATION OF MESO-FORMYL BODIPY MODIFIED WITH PHENYL RINGS AT 2,6-POSITIONS

Rokas Žvirblis[1], Aurimas Vyšniauskas[2], Jelena Dodonova-Vaitkūnienė[1]

[1] Institute of Chemistry, Faculty of Chemistry and Geosciences, Vilnius University, Naugarduko str. 24, Vilnius, Lithuania

[2] Center for Physical Sciences and Technology, Saulėtekio av. 3, Vilnius, Lithuania

rokas.zvirblis@chgf.stud.vu.lt

Cellular viscosity is a crucial parameter that controls diffusion-mediated processes, such as protein interactions, signal transduction, transport of small organic molecules and others. Distortions in viscosity of the cell have been linked to multiple pathologies: diabetes, Alzheimer's disease, and atherosclerosis [1]. Fluorescent viscosity probes are a promising tool that could allow an effective way to measure cellular viscosity, significantly contributing to the elucidation of the mentioned diseases. *Meso*-phenyl BODIPY dyes are widely used as viscosity sensing probes because of their photostability and excellent photophysical properties. The main mechanism of their action is a non-radiative relaxation by rotation of the phenyl ring after the dye is excited with light. In more viscous media the rotation is suppressed leading to the increase of the fluorescence lifetime. Because *meso*-phenyl BODIPY dyes have mono-exponential lifetimes they can be used in FLIM (*fluorescence lifetime imaging viscosity*) to map cellular viscosity [1]. On the other hand, it has been noticed that *meso*-phenyl BODIPY also shows sensitivity to environmental polarity [2], which makes it more difficult to produce accurate measurements. Thus, we sought out to create a selective viscosity probe that would be based on the same BODIPY platform containing its great properties but bearing a formyl- rotating group. The introduction of the aldehyde group instead of the phenyl ring produces a change in the photophysical mechanism of the fluorophore, its rotation around C-C bond creates steric hindrances causing the bending of the dipyrrin scaffold, which means that in a low-viscosity environment the dye relaxes by a nonradiative manner [3]. One such fluorophore was reported as a successful probe for cellular viscosity [3] but its emission was green which is not the best option for use in biological samples. Red-emitting fluorophores are sought out because they offer better penetration of biological objects and decrease the probability of autofluorescence [4].

Thus, herein we report a *meso*-formyl BODIPY that is modified with phenyl rings at the 2,6-positions of the BODIPY scaffold to extend the conjugation of the system and move its fluorescence to longer wavelengths. Comparison of fluorescence lifetimes in solvent mixtures of different polarity and viscosity provides us with the conclusion that *meso*-formyl BODIPY $(Ph)_2$ is insensitive to differences of environmental polarity, but it also loses its sensitivity to viscosity when the probe is additionally modified with phenyl rings at the 2,6-positions (Fig. 1). This might be caused by both electronic effects and steric hindrance produced by the phenyls on the boron-dipyrromethene scaffold.

In conclusion, maintaining *meso*-formyl BODIPY sensitivity to viscosity while at the same time extending its conjugation is a complicated problem that needs to be tackled by both theoretical calculations and experimental investigations.

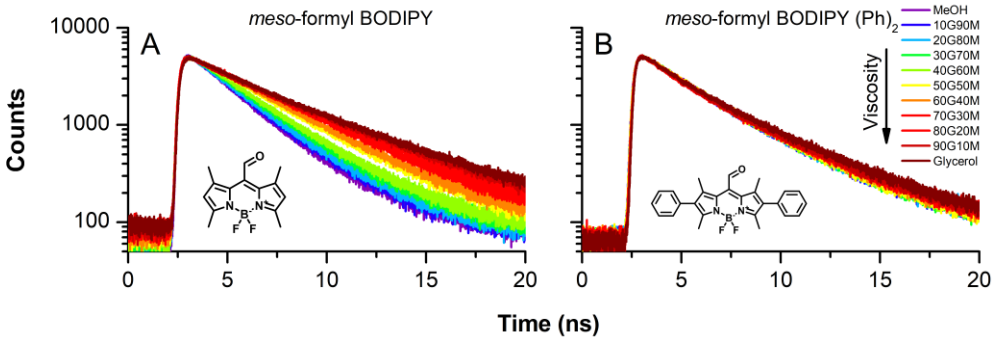


Fig. 1. Comparison of fluorescence lifetimes of *meso*-formyl BODIPY (A) and *meso*-formyl BODIPY $(Ph)_2$ substituted with phenyl rings (B) in glycerol/methanol mixtures of increasing viscosity.

RŽ thanks to European Social Fund for funding this project (No. 09.3.3-LMT-K-712-24-0103) under the grant agreement with Lithuanian Academy of Sciences.

[1] M. K. Kuimova, "Mapping viscosity in cells using molecular rotors", Phys. Chem. Chem. Phys. 2012, 14, pp. 12671-12686.

[2] A. Polita, S. Toliautas, R. Žvirblis, and A. Vyšniauskas, "The effect of solvent polarity and macromolecular crowding on the viscosity sensitivity of a molecular rotor BODIPY-C_{10}", Phys. Chem. Chem. Phys., 2020, 22, pp. 8296-8303.

[3] H. Zhu, J. Fan, M. Li, J. Cao, J. Wang, and X. Peng, "A "Distorted-BODIPY"-Based Fluorescent Probe for Imaging of Cellular Viscosity in Live Cells", Chem. Eur. J., 2014, 20, pp. 4691-4696.

[4] E. C. Jensen, "Use of Fluorecent Probes: Their Effect on Cell Biology and Limitations", The Anatomical Record, 2012, 295, 12, pp. 2031-2036.

P7-16

DID NOT PARTICIPATE

.

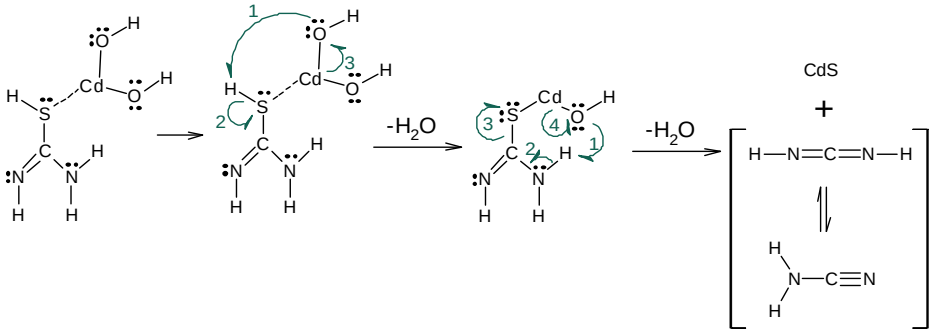
STUDY OF FORMATION OF CADMIUM SULFIDE LAYERS ON POLYPROPYLENE FILM USING DIFFERENT CADMIUM SALTS

Mindaugas Matijūnas, Rasa Alaburdaitė

Department of Physical and Inorganic Chemistry, Kaunas University of Technology, Lithuania
mindaugas.matijunas@ktu.edu

Cadmium sulfide (CdS) is a semiconductor that is often used in solar cells, flat screens, optical devices, and logical gates [1]. Polypropylene (PP) is a cheap hydrophobic thermoplastic that is nontoxic, quite rigid, and widely used [2]. The main idea of this experiment is to deposit thin layers of CdS onto PP film in order to get the benefits of both materials, which would be very favorable towards making flexible electronics.

The PP films (thickness 150 μm) were pretreated with a solution of H_2SO_4/H_3PO_4 (1:1), saturated with CrO_3 in a glass reactor for 25 min at 90°C. To synthesize CdS, three different cadmium salts ($CdSO_4$, $Cd(CH_3COO)_2$, $CdCl_2$) were used in mixture with thiourea [3]. Reaction took place via chemical bath deposition at 70°C and 90°C. Ammonium buffer was added while performing the reaction with $CdSO_4$ and $CdCl_2$. The formation of CdS can be described by the following reaction [3]:



In all cases yellow-colored CdS layers with an orange tint were observed deposited onto polypropylene. The concentration of cadmium salts had little influence on the reaction. $CdCl_2$ performed noticeably worst. The concentration of thiourea had a major influence on the reaction and the lack of it made the color of CdS darker and more transparent. The addition of ammonium buffer had a significant influence on the reaction: a thicker layer of CdS was observed, as well as a deeper yellow-orange color. The reaction performed better at a higher temperature. Each reaction reaches equilibrium after around 3 hours.

[1] B. G. An, H. R. Kim, Y. W. Chang, J.G. Park, J. C. Pyun, Photosensors-based on cadmium sulfide (CdS) nanostructures: a review, J. Korean Ceram. Soc. **58**, 631–644 (2021).
[2] H. A. Maddah, Polypropylene as a Promising Plastic: A Review, Am. J. Polym. Sci. **6**(1), 1-11 (2016).
[3] J. A. García-Valenzuela, Simple Thiourea Hydrolysis or Intermediate Complex Mechanism? Taking up the Formation of Metal Sulfides from Metal–Thiourea Alkaline Solutions, Comments Inorg.Chem. **37**, 99-115 (2017).

AIR QUALITY ASSESSMENT IN RELATION WITH INCREASING CONTRIBUTION OF TRANSPORT-RELATED BLACK CARBON

Agnė Minderytė[1,2], Julija Pauraite[1], Steigvilė Byčenkienė[1]

[1] Department of Environmental Research, Center for Physical Sciences and Technology, Lithuania
[2] Faculty of Physics, Vilnius university, Lithuania
agne.minderyte@ftmc.lt

European governments have been encouraging drivers to buy diesel vehicles rather than gasoline-powered ones since the 1990s. The reason for this was higher diesel fuel efficiency and lower CO_2 emissions in diesel exhaust, although it emits higher levels of particulates including black carbon (BC) [1]. In IPCC report Global Warming 1.5 °C black carbon (BC) was presented as the only component of aerosol particles that has a positive effect on atmospheric thermal balance [2]. Moreover, BC raises a threat to air quality and human health. Due to the formation during combustion processes, BC aerosol particles are small (around 200 nm) with porous surface and can adsorb various combustion-derived toxic compounds. Due to small radius, the particles can penetrate through lungs into other organs and cause serious health problems such as DNA damage, oxidative stress, pneumonia [3]. Currently there are no regulatory terms which control BC mass concentration levels. However, it is crucial to identify prevailing BC sources and develop mitigation strategies for the purpose of improving air quality and minimizing personal exposure of the public to atmospheric pollutants.

In this study the measurements were deployed in Vilnius (urban background site) using an Aerosol Chemical Speciation Monitor (ACSM) (Aerodyne Research Inc., USA) and a 7-wavelength Aethalometer (Model AE31 Spectrum, manufactured by Optotek, Slovenia). Aethalometer model was used to determine the quantitative contribution of fossil fuel and biomass combustion to the mass concentration of black carbon aerosol particles. This model uses source-specific absorption Angstrom exponent (AAE) values, which depend on various site-specific parameters, such as: common sources of pollution, fuels used, meteorology [4]. Therefore, the determination of individual values of the AAE for the urban environment is important in order to perform a qualitative separation of the origin of sources and to assess the contribution of pollution sources.

The study provides a quantitative assessment of pollution associated with diesel vehicles and points out that from 2014 to 2020 with an increase in the number of diesel vehicles of as much as 83.9%, a 1.3-fold increase in BC_{tr} (transport-related BC emission) mass concentration and 3.6-fold increase in BC_{tr} light absorption coefficient. Furthermore, a combination of the most suitable AAE_{tr} and AAE_{wb} (for transport exhaust and biomass burning emission, respectively) values for urban background environment was statistically established based on the correlation criteria between BC and trace pollutants. Regarding the negative impacts of BC on human health and the thermal balance of the atmosphere, the results of this study address air quality issues and seek possible measures to combat air pollution.

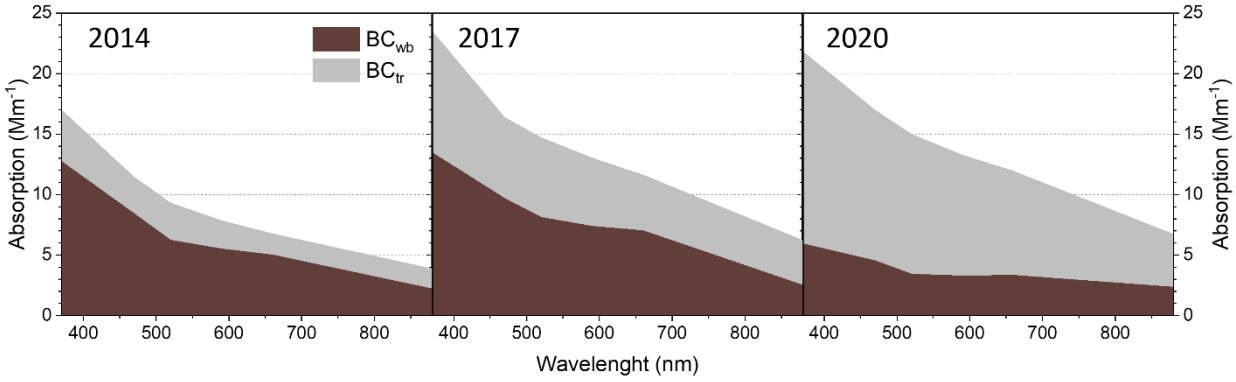


Fig. 1. Absorption coefficients of BC_{tr} and BC_{wb} as a function of wavelength for 2014, 2017 and 2020.

[1] S. C. Anenberg *et al.*, Global air quality and health co-benefits of mitigating near-term climate change through methane and black carbon emission controls, Environ. Health Perspect., **120**, 6, 831–839 (2012).

[2] IPCC, "Global Warming of 1.5 °C. An IPCC special report on the impacts of global warming of 1.5 °C above pre-industrial levels and related global greenhouse gas emission pathways, in the context of strengthening the global response to the threat of climate change" (2018). [Online]. Available: https://report.ipcc.ch/sr15/pdf/sr15_spm_final.pdf.

[3] S. Rovelli *et al.*, "Toxic trace metals in size-segregated fine particulate matter: Mass concentration, respiratory deposition, and risk assessment," Environmental Pollution, **266**, 115242 (2020).

[4] J. Sandradewi, A. S. H. Prévôt, E. Weingartner, R. Schmidhauser, M. Gysel, and U. Baltensperger, "A study of wood burning and traffic aerosols in an Alpine valley using a multi-wavelength Aethalometer," *Atmospheric Environment*, **42**, 1, 101–112 (2008).

INTERMOLECULAR STRUCTURE AND NMR PARAMETERS IN BINARY MIXTURES OF TRIFLUORACETIC ACID AND N, N–DIMETHYLFORMAMIDE MODELLED BY QM/MD APPROACHES

Greta Majauskaitė[1], Kęstutis Aidas[1],

[1] Institute of Chemical Physics, Faculty of Physics, Vilnius University, Lithuania
Greta.majauskaite@ff.stud.vu.lt

Carboxylic acids are strongly associating compounds, whose intermolecular structures can vary from cyclic dimers to chain-type associates [1]. These complexes exist in a dynamic equilibrium that is characteristic of each specific acid. Leonardo W. Reeves' study focused on the formation of hydrogen bonds in modified acetic acids and their mixtures with different polar solvents and revealed a strong dependence of some NMR parameters on the molar composition of the mixture [2]. It has been observed that the difference between the chemical shift of the acidic proton of trifluoroacetic acid (TFA) in pure liquid and the mixture with N, N-dimethylformamide (DMF) is as high as 4 ppm. In contrast, the chemical shift of the acidic proton of pure acetic acid is virtually insensitive to the amount of DMF in the mixture. The reason for this difference can be due to changes at the molecular level when the hydrogens of the methyl group of the acetic acid are replaced by fluorines. This substitution can affect the dynamical equilibrium between molecular aggregates in pure acid and its mixture with DMF. Also, DMF is a good proton acceptor, which can lead to the formation of hydrogen bond aggregates between TFA and DMF molecules. Changing equilibrium between various intermolecular aggregates induced by changing the composition of the mixture could lead to such a drastic increase in chemical shift.

This study aims to identify which of the occurring changes in the intermolecular structure of trifluoracetic acid and its mixture with N, N – dimethylformamide led to this strong increase in chemical shift of the acidic proton between neat TFA and the TFA-DMF mixture with the molar ratio of 1:1.

To achieve this goal further computational scheme was implemented. MD simulations were carried out for both systems using an OPLS-AA force field. NPT ensemble was used to reach thermodynamic equilibrium and stable density of the system at the temperature of 298 K and pressure of 1 atm. The production run was performed in the NVT ensemble at the same temperature for 2 ns. After that, intermolecular structure analysis was performed using the geometrical definition of a hydrogen bond. This was followed by quantum mechanics/molecular mechanics calculations of the ^{1}H NMR shielding constant of the acidic proton for both systems.

Our results show that by far the dominating form of intermolecular aggregates in neat TFA was that of the cyclic type – 60% overall, and especially cyclic trimers the population of which was as high as 48.5% on average. Interestingly, this constitutes a major qualitative difference compared to neat acetic acid, which is mainly composed of linear type chain aggregates, and even the cyclic structures that are formed are mostly dimers [3]. Moreover, our calculations revealed that the intermolecular structure of the TFA-DMF mixture changes drastically. All TFA molecular aggregates between TFA molecules are virtually broken, and instead, hydrogen-bonded TFA-DMF complexes are forming. The NMR shielding constants calculated for the acidic proton in neat TFA and the TFA-DMF mixture were computed to be equal to 21.64 (±0.12) and 20.26 (±0.12) ppm, respectively, was predicting that chemical shift of the acidic proton is by around 1.4 ppm in the TFA-DMF mixture than in the neat TFA. The predicted difference of the chemical shifts is considerably underestimated as compared to the corresponding experimental result. This discrepancy is likely caused due to the prolific proton transfer between TFA and DMF molecules in the mixture – an effect that was not accounted for in our model.

Computations were performed on the computational facilities provided by the High-Performance Computing Center "HPC Saulėtekis" at Vilnius University, Lithuania.

[1] Wu, J., 2014. Gaussian analysis of Raman spectroscopy of acetic acid reveals a significant amount of monomers that effectively cooperate with hydrogen bonded linear chains. Phys. Chem. Chem. Phys., 16(41), pp.22458-22461.

[2] Reeves, L., 1961. Hydrogen bonding in solutions of substituted acetic acids. Can, Journ. of Chem, 39(8), pp. 1711–1720.

[3] D. Lengvinaite, K. Aidas, L. Kimtys, 2019. Molecular aggregation in liquid acetic acid: Insight from molecular dynamics/quantum mechanics modeling of structural and NMR properties, Phys. Chem. Chem. Phys. 21, pp.14811–14820. https://doi.org/10.1039/c9cp01892a.

INTERMOLECUAR STRUCTURE AND NMR SPECTRA OF AQUEOUS MIXTURES OF [C_4mim][BF_4] IONIC LIQUID: A QM/MD STUDY

Greta Majauskaitė[1], Kęstutis Aidas[1],

[1] Institute of Chemical Physics, Faculty of Physics, Vilnius University, Lithuania
Greta.majauskaite@ff.stud.vu.lt

Ionic liquids (IL) are substances composed of organic molecular cations and organic or inorganic anions with high chemical, electrochemical and thermal stability [1]. With the development of "green" chemistry, ionic liquids are becoming very attractive for a variety of applications, but their high viscosity is a barrier to wider use. One of the easiest ways to reduce IL viscosity is to dilute it with water [2]. The prospect of modulating the properties of such a sustainable solvent simply by changing the proportion of water in the solvent has received considerable attention [3]. Therefore, it is important to gain an understanding of the effect of water on the properties of the aqueous IL mixtures at the molecular level. Experimental NMR measurements spectra could potentially reveal important information concerning the intermolecular structure of these systems. It has been recently observed that the ^{1}H NMR chemical shift of water molecules in the aqueous mixtures of imidazolium ionic liquids is strongly dependent on the composition of the mixture [4]. In particular, the ^{1}H NMR chemical shift of water was seen to decrease monotonically with the increasing molar fraction of the 1-butyl-3-methyl-imidazolium tetrafluoroborate ([C_4mim][BF_4]) IL. These observations are qualitatively different as compared to the imidazolium IL containing hydrophilic anions where non-monotonic dependence of the ^{1}H NMR chemical shift of water was recorded [4-5]. This study aims to model the most important peculiarities of the intermolecular structure of the [C_4mim][BF_4] IL and its aqueous mixtures using molecular dynamics simulations and QM/MM calculations of the NMR parameters.

In this work, MD simulations were performed for the following systems of IL and its mixtures with water: 1) pure ionic liquid: 500 ion pairs; 2) IL-water: 4:1 molar ratio (500 ion pairs, 125 water molecules); 3) IL-water: 1:1 molar ratio (500 ion pairs, 500 water molecules); 4) IL-water: 1:4 molar ratio (500 ion pairs, 2500 water molecules). The systems were first equilibrated in the isothermal-isobaric (NPT) ensemble, and the production run was performed in the canonical ensemble (NVT) simulations for all simulated systems.

Based on the MD simulations performed in the NPT ensembles, the modeled dependence of the density on the composition of the aqueous mixtures of [C_4mim][BF_4] IL was predicted which was found to be in very good qualitative and reasonable quantitative agreement with the corresponding experimental data. It was found that – as the molar fraction of water in the mixture increases – water tends to coordinate the $[BF_4]^-$ anion rather than the $[C_4mim]^+$ cation. A significant effect of water on the coordination pattern of the $[C_4mim]^+$ cation was only observed when the molar fraction of the IL in the mixture decreases to 0.20. Prolific formation of hydrogen bonds between water molecules is also observed, even when the molar fraction of water is as low as 0.20. The intermolecular structure of the [C_4mim][BF_4]/water mixtures is thus considerably different as compared to that of the imidazolium IL with hydrophilic anions where water-anionic aggregates prevail [5]. Interestingly, the local distribution of anions around the ring of the imidazolium cations was found to be virtually unaffected by the water molecules, and more pronounced changes were seen only when the molar fraction of the IL in the mixture decreases to 0.20. Based on these results, we can conclude that the intermolecular structure of the [C_4mim][BF_4] IL is quite stable and resistant to the effects caused by dilution with water. This leads to the conclusion that it is possible to reduce the viscosity of this IL considerably while maintaining the properties of "pure" IL well enough. The results of the modeling of NMR parameters are underway and they will be presented in the poster session of the conference.

This work is supported by the European Social Fund under measure no. 09.3.3.-LMT-K-712-25-0222 “Development of Competencies of Scientists, other Researcher,s and Students through Practical Research Activities.” Computations were performed on the computational facilities provided by the High-Performance Computing Center “HPC Saulėtekis” at Vilnius University, Lithuania.

[1] Villanueva, M., Coronas, A., García, J. and Salgado, J., 2013. Thermal Stability of Ionic Liquids for Their Application as New Absorbents. Industrial & Engineering Chemistry Research, 52(45), pp.15718-15727.

[2] Seddon, K., Stark, A. and Torres, M., 2000. Influence of chloride, water, and organic solvents on the physical properties of ionic liquids. Pure and Applied Chemistry, 72(12), pp.2275-2287.

[3] Rebelo, L., Najdanovic-Visak, V., Visak, Z., Nunes da Ponte, M., Szydlowski, J., Cerdeiriña, C., Troncoso, J., Romaní, L., Esperança, J., Guedes, H.and de Sousa, H., 2004. A detailed thermodynamic analysis of [C4mim][BF4] + water as a case study to model ionic liquid aqueous solutions. Green Chem., 6(8), p.369-381

[4] Bystrov, S., Matveev, V., Egorov, A., Chernyshev, Y., Konovalov, V., Balevičius, V. and Chizhik, V., 2019. Translational Diffusion in a Set of Imidazolium-Based Ionic Liquids [bmim]+A– and Their Mixtures with Water. The Journal of Physical Chemistry B, 123(43), pp.9187-9197.

[5] Lengvinaitė, D., Kvedaraviciute, S., Bielskutė, S., Klimavicius, V., Balevicius, V., Mocci, F., Laaksonen, A., and Aidas, K., 2021. Structural Features of the [C4mim][Cl] Ionic Liquid and Its Mixtures with Water: Insight from a 1H NMR Experimental and QM/MD Study. The Journal of Physical Chemistry B, 125(48), pp.13255-13266.

P7-21

DID NOT PARTICIPATE

.

DERIVATION OF A COVALENT RADII TABLE FROM OPEN CRYSTALLOGRAPHIC DATA

Eglė Šidlauskaitė[1], Antanas Vaitkus[1], Andrius Merkys[1]

[1] Sector of Crystallography and Chemical Informatics, Institute of Biotechnology, Life Sciences Center, Vilnius University, Lithuania
egle.sidlauskaite@gmc.vu.lt

Crystallography allows to determine the exact positions of atoms that constitute crystal structures [1]. Crystal structure determination methods, however, are unable to capture chemical bonding. In practice, two atoms are considered to be connected by a chemical bond if the calculated distance between them is smaller or equal to the sum of their covalent radii. This distance is called a covalent bond length.

Covalent radii tables which are often used to determine chemical bonds between atoms are created by statistically analysing lengths of observed chemical bonds. The most popular covalent radii tables [2] are derived using data from the Cambridge Structural Database [3] which is distributed under a proprietary license and therefore restricts the usage and spread of such derivative datasets. Due to this, there was a clear need to develop a completely independent workflow that allows covalent radii tables to be automatically calculated using open crystallographic datasets such as the Crystallography Open Database [4].

Method used in this research is based on the determination of the van der Waals gap – an interval within the interatomic distance distribution that separates peaks formed by covalent interactions from those formed mainly by van der Waals interactions. This interval contains no interatomic distance observations and thus corresponds to the lowest density region in the distribution [5]. In order to identify the lowest density region, a Gaussian distribution mixture model can be applied to the histogram of interatomic distances.

In the current study, a tool for automated determination of covalent radii from interatomic distances was created. Comparison of derived results with selected published covalent radii tables (Figure 1) displays reasonable deviations (up to 0.5 Å) for most atom types. Further research is focused on methods that would help to reduce these deviations that are primarily influenced by the quality of the input data, scarcity of observations in rare atom contact classes and interatomic contacts that involve chemical elements which rarely participate in covalent bonds.

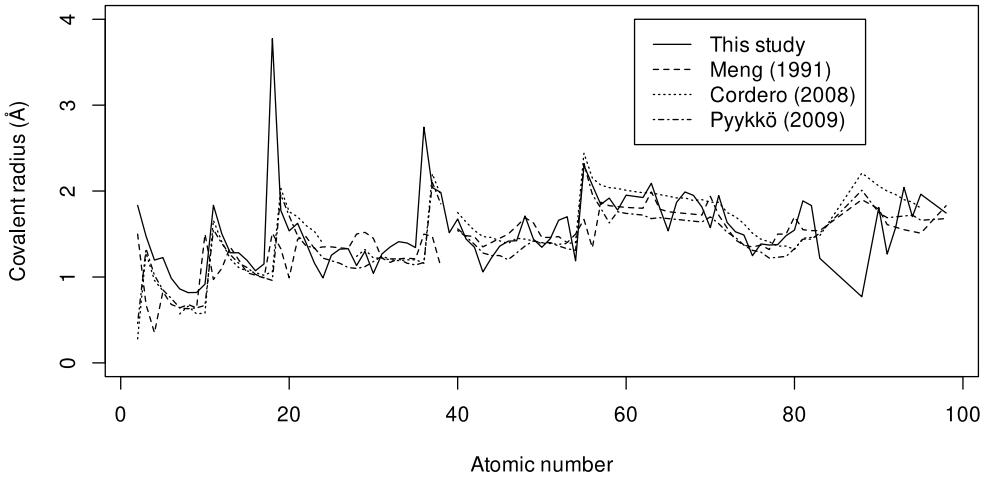


Fig. 1. Comparison of covalent radii in selected covalent radii tables.

Additional analysis of the input crystallographic data revealed that unmodelled solvent molecules, unmarked disordered structures as well as human errors in crystal structures often lead to abnormal interatomic distance observations. To address this, a set of quality criteria such as compatibility between the declared and calculated properties, use of standard experimental environment conditions, reasonable crystal structure density, etc. were determined to more easily identify crystallographic structures that are suitable for covalent radii derivation calculations. Application and further development of these criteria is part of an ongoing investigation.

[1] S. Gražulis, A. Merkys, A. Vaitkus et al., Computing stoichiometric molecular composition from crystal structures, Journal of Applied Crystallography **48**(1), 85-91 (2015). https://doi.org/10.1107/s1600576714025904

[2] B. Cordero, V. Gómez, A. E. Platero-Prats et al., Covalent radii revisited, Dalton Transactions (21), 2832-2838 (2008). https://doi.org/10.1039/b801115j

[3] C. R. Groom, I. J. Bruno, M. P. Lightfoot et al., The Cambridge Structural Database, Acta Crystallographica, Section B: Structural Science, Crystal Engineering and Materials **72**(2), 171-179 (2016). https://doi.org/10.1107/S2052520616003954

[4] S. Gražulis., A. Daškevič, A. Merkys et al., Crystallography Open Database (COD): an open-access collection of crystal structures and platform for world-wide collaboration, Nucleic Acids Research **40**, D420-D427 (2012). https://doi.org/10.1093/nar/gkr900

[5] S. Alvarez, A cartography of the van der Waals territories, Dalton Transactions **42**(24), 8617-8636 (2013). https://doi.org/10.1039/C3DT50599E

INVESTIGATION OF MULTIELEMENTAL CONTENTS OF PM_1 IN INDOOR AND OUTDOOR AIR

Audrė Kalinauskaitė[1], Inga Garbarienė[1], Agnė Minderytė[1], Julija Pauraite[1], Vadimas Dudoitis[1], Lina Davulienė[1], Kristina Plauškaitė-Šukienė[1], Vitalij Kovalevskij[1], Mindaugas Gaspariūnas[1], Steigvilė Byčenkienė[1]

[1]Department of Environmental Research, Center for Physical Sciences and Technology, Lithuania
audre.kalinauskaite@ftmc.lt

Air pollution is the single largest environmental health risk in Europe [1, 2], as well as a complex problem causing diverse challenges in the field of management and mitigation of harmful pollutants [3]. Indoor air pollution is the main problem for people living in urban areas because they spent almost 90% of their daily time indoor [4]. In 2019, the World Health Organization revealed that indoor air pollution killed the lives of 3.8 million people exposed to air pollution [5].

Concentration and outdoor/indoor (O/I) ratio of trace metals in the outdoor/indoor environments are presented. The concentrations of 17 elements, including Al, Si, P, Cl, K, Ca, Sc, Ti, V, Cr, Mn, Fe, Co, Ni, Cu and Zn in PM_1 (PM_1 – particulate matter, particle with aerodynamic diameter < 1 μm) were determined (Fig. 1). Trace elements, which are presented in this research as the constituents of PM_1, are emitted mainly by anthropogenic activities (power generation, industry and transport sectors) [3]. The combustion of fuels is the main source of sulphur (in the form of sulphur dioxide (SO_2)) if it is enriched with this element [3].

The aim of this study is to examine the O/I ratios of these trace elements during November 2020 – July 2021. Outdoor PM_1 filter samples (PTFE and PCTE) were collected using a low volume sampler (SVEN LECKEL, LVS6) with sampling frequency 2-3 times a week located on the roof of a 4-floor building (Center for Physical Sciences and Technology, FTMC (Vilnius, urban background site)) and indoor. The quantitative analysis of multielemental contents in PM_1 was performed using the Particle-Induced X-ray emission analysis detector CANBERRA SL30165 and the analyzer CANBERRA DSA1000.

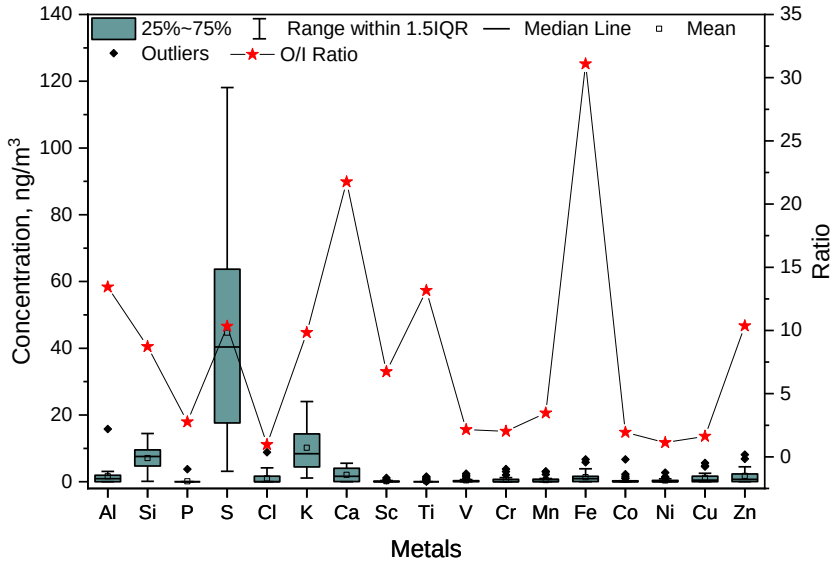


Fig. 1. Average mass concentrations of elements in indoor air (boxes and whiskers) and ratios of mass concentration of outdoor to indoor (O/I) air (stars with lines) (in measurement period 14/11/2020 - 17/07/2021).

Based on the results, the aerosol particles of PM_1 containing higher amounts of Al, Si, S, K, Ca, Ti, Fe and Zn are more effectively trapped by air filters, therefore these elements are detected in much lower concentrations in indoor air. Accordingly, the O/I ratio of these elements are the highest. The average mass concentrations of all elements in indoor air fluctuate from 0.15 ng/m^3 (phosphorus, P) to 44.67 ng/m^3 (sulphur, S).

The study of PM_1 constituents can provide an additional information about sources of air pollution. Comprehensive knowledge about air pollutants and their constituents, their transportation and transformation in the atmosphere is necessary in order to reduce their impact on human health, ecosystems and the climate [3].

This research was funded by a grant (No. S-MIP-20-28) from the Research Council of Lithuania.

[1] S. S. Lim, T. Vos, A. D. Flaxman et al., A comparative risk assessment of burden of disease and injury attributable to 67 risk factors and risk factor clusters in 21 regions, 1990–2010: a systematic analysis for the Global Burden of Disease Study 2010, The Lancet **380** (9859), 2224–2260 (2012).
[2] WHO, Burden of disease from Ambient Air Pollution for 2012 — Summary of results, World Health Organization (2014).
[3] EEA, Air quality in Europe — 2016 report, EEA Report No 28/2016, European Environment Agency (2016).
[4] J. A. Leech, W. C. Nelson, R. T. Burnett et al., It's about time: A comparison of canadian and american time–activity patterns, Journal of Exposure Science & Environmental Epidemiology **12**, 427–432 (2002).
[5] WHO, Household Air Pollution and Health (2021).

STYDY OF MELT FLOW INDEX FOR POST-CONSUMER MIXED POLYOLEFINS AFTER ADDITIONAL FILTRATION

Tetiana Tortykh[1], Oleg Shyniruk[1], Arkadiy Petukhov[1]

[1] Department of Chemical Technology of Composition Materials, National Technical University of Ukraine «Igor Sikorsky Kyiv Polytechnic Institute», Kyiv, Ukraine.
tortykh.tetiana@lll.kpi.ua

The production of plastic virgin materials is growing and has now reached 367 million tons per year and it will create more and more waste each year. The dominated plastic is the thermoplastic types of polypropylene (PP) (21%) and low-and linear low-density polyethylene (LDPE and LLDPE) (18%) [1]. The problem of increasing waste streams will only grow. The leading position in post-consumer waste is occupied by packaging. There are more than 40% of packaging waste, which is much higher than other types of waste in Europe. 29.5 million tons of post-consumer waste were collected [2].

Mechanical recycling is the most common and economical method available for recycling post-consumer plastic waste and involves sorting, grinding, washing, and extrusion of the material [3] but still, a lot of materials go to the landfills. With mechanical recycling possible to obtain new products from plastic waste, for example, replacing wood or concrete products, thereby reducing the percentage of plastic waste and at the same time reducing CO_2 emissions.

Post-consumer waste often ends up on production lines with large capacities for further granulation. For efficient and continuous granulation of this material, the most common extruder is used with a laser filtration system for deep cleaning of contaminants (wood, aluminum, copper, PA, *etc*.). In such cases, a "by-product" is formed from self-cleaning filters, the base of which consists of polyolefins but contains a large number of contaminants. The volumes of this raw material average 1% per ton of finished granulate. The material forms lumps from the filters, which can be crushed into a smaller fraction for easier processing material.

It is necessary to achieve stability in properties starting from the melt flow index (MFI) for the production of quality products from filtered material with impurities. Despite the fact that MFI is an empirically defined parameter with certain limitations, it is still one of the most popular parameters in the plastics industry for distinguishing various grades of polymers [4].

The basic raw materials from post-consumer packaging include LDPE, LLDPE, MDPE, HDPE, PP fractions with more than 10% contamination. Due to a large amount of visible contamination, the material was processed on a granulation line with a 300 μm filter mesh. The temperature was selected in accordance with the fact that the material heats up gradually as it moves along the cylinder from the first to the last zone and does not undergo destruction.

The obtained granule was suitable for carrying out the MFI test. To obtain an average melt flow index, 25 tests were made from the selected sample. Test conditions were chosen with temperature – 190 ºC; load – 5 kg. The results of the MFI test are shown in Figure 1.

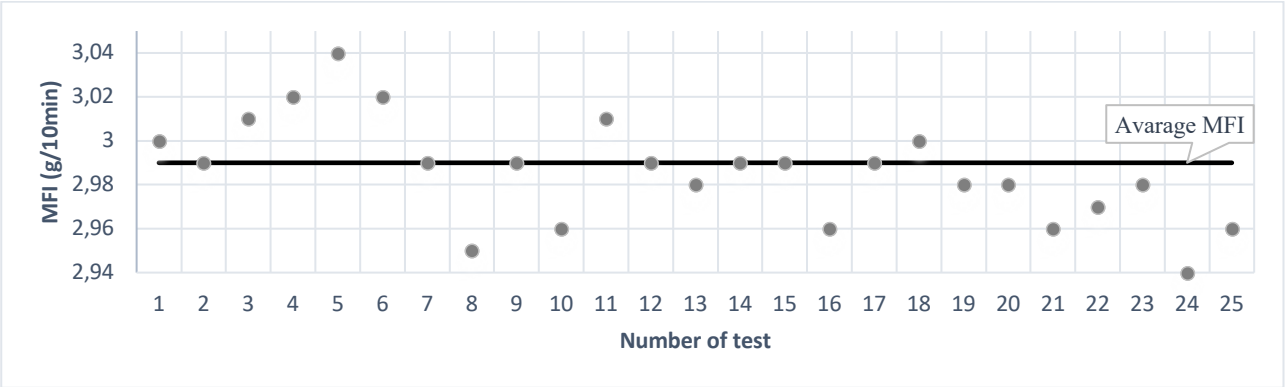


Fig. 1. The result of the melt flow index for post-consumer packaging.

The average value of the melt flow index is 2.99 g/10 min. Small deviations from the average MFI indicate that the homogenization of the polymer was successful and this material can be used for further testing to confirm the possibility of using this raw material in the manufacture of various products. Using this raw material, we can reduce the amount of burning and disposal of polymer waste.

[1] J. N. Hahladakis, C. A Velis, R. Weber, E. Iacovidou, P. Purnel An overview of chemical additives present in plastics: Migration, release, fate and environmental impact during their use, disposal and recycling. Journal of Hazardous Materials, 344, 179-199 (2018) doi: 10.1016/j.jhazmat.2017.10.014
[2] Plastics the Facts 2021 Available at: https://plasticseurope.org/knowledge-hub/plastics-the-facts-2021/
[3] S.M. Al-Salem Recycling and recovery routes of plastic solid waste (PSW): a review. Waste Manag.; 29: 2625-2643 (2009)
[4] A.V. Shenoy, D.R. Saini, Melt flow index: more than just a quality control rheological parameter. Part I. Advances in Polymer Technology 6 (1), 1-58 (1986)

EFFECTS OF WOOD BIOFUEL ASH ON THE CHEMICAL COMPOSITION AND QUALITY OF MAIZE GROWN

Ieva Bagamulskytė[1], Kristina Bunevičienė[2],

[1] Faculty of chemical technology, Kaunas university of technology, Lithuania
[2] Institute of Agriculture, Lithuanian Research Centre for Agriculture and Foresty, Lithuania
ieva.bagamulskyte@ktu.edu

Biofuels are a form of renewable energy. For this reason, it is one of the rapidly growing sources of energy. One disadvantage that makes biofuels unattractive is the accumulation of biofuel combustion products - ash. Only a small part of them is used in the construction industry [1], for immobilization/removal of toxic elements from wastewater and contaminated soils [2], as well as to produce products based on nanostructured aluminosilicates. Most ash is disposed of in landfills [3]. This is a very uneconomical and useless solution and requires the recycling or reuse of this waste. One possible solution is to use biofuel ash for soil improvement purposes. Biomass ash is enriched in nutrients (K, P, Ca, Mg) and minerals (quartz, calcite, etc.) [4]. In addition to these properties, biofuel ash has very high basicity (pH >12.5) and therefore is an effective means of neutralizing infertile acidic soils [5]. This solution would increase the area of fertile land, as acid soils occupy approximately 70% of the world's potentially arable land [6]. Neutralizing acidic soils would make it possible to grow raw materials for high-quality food and feed production. It should be noted, that in acidic soils the mobility and availability of toxic elements to plants increases [7], but this problem can be avoided by using biofuel ash.

This experiment was performed in the summer of 2021. The experiment was made in the soil, which pH ~ 4. The soil was taken from Lithuanian Research Center for Agriculture and Forestry (LAMMC), Vėžaičiai branch fields. The experiment was made in LAMMC, Institute of Agriculture, Agrobiology laboratory in controlled climate chambers (Fig. 1b). The experiment included the following treatments: 1) 0 %; 2) 1.25%; 3) 2.5 %; 4) 5 % and 5) 10% ash in soil mixture. The ash was mixed with the soil and maize (Fig. 1a) was sown. The experiment lasted 40 days. Maize biomass and root contents were calculated after harvest (Fig. 1c). Also, were determined the compositions of micro- and macroelements (Na, Mg, K, Ca, Fe, Al, P, B, Cr, Co, Ni, Zn, Cu, Pb) in soil and plants with ICP-MS.

The results obtained in this research showed that fertilization with wood biofuel ash in acidic soils increases the yield of maize biomass, as well as the concentration of toxic elements in plants, but does not adversely affect plant quality.



a b c

Fig. 1. Germination of maize (a), controlled climate chambers (b), maize after harvest (c)

[1] F. C. Silva, N. C. Cruz, L. A. C. Tarelho et al., Use of biomass ash-based materials as soil fertilisers: Critical review of the existing regulatory framework, Journal of Cleaner Production **214**, 112-124 (2019).
[2] L. Tosti, A. van Zomeren, J. R. Pels et al., Assessment of biomass ash applications in soil and cement mortars, Chemosphere **223**, 425-437 (2019).
[3] S. Voshell, M. Makela, O. Dahl, A review of biomass ash properties towards treatment and recycling, Renewable and Sustainable Energy Reviews **96**, 479-486 (2018).
[4] M. Freire, H. Lopes, L. A. C Tarelho, Critical aspects of biomass ashes utilization in soil: Composition, leachability, PAH and PCDD/F, Waste Management **46**, 304-315 (2015).
[5] J. Yliniemi, H. Nugteren, M. Illikainen et al., Lightweight aggregates produced by granulation of peat-wood fly ash with alkali activator, International Journal OF Mineral Processing **149**, 42-49 (2016).
[6] M. Bian, M. Zhou, D. Sun et al., Molecular approaches unravel the mechanism of acid soil tolerance in plant, The Crop Journal **1**, 91-104 (2013).
[7] C. Merino-Gergichevich, M. Reyes-Diaz, J. Guerrero et al., Physiological and nutritional responses in two highbush blueberry cultivars exposed to deficiency and excess of boron, Journal of Soil Science and Plant Nutrition **17**, 307-318 (2017).

SYNTHESIS AND INVESTIGATION OF PHENANTHROIMIDAZOLE DERIVATIVES FOR ORGANIC LIGHT EMITTING DIODES

Lukas Graibus, Rita Butkutė, Juozas Vidas Gražulevičius

Department of Polymer Chemistry and Technology, Kaunas University of Technology, Kaunas, Lithuania
lukas.graibus@ktu.edu

Technology of organic light emitting diodes (OLED) is currently considered to be the most promising technology for the transformation of electricity into light. OLEDs are used in the fabrication of displays of various electronic devices and in lighting appliances [1]. Compounds exhibiting thermally activated delayed fluorescence (TADF) are currently considered to be the most promising emitters of OLEDs. TADF emitters can be synthesized from low-cost organic reagents without the use of rare metals or toxic elements [2, 3]. They usually consist of donor and acceptor moieties. Due to low-cost synthesis, blue emission, bipolar charge transporting properties, and excellent thermal stability, donor-acceptor phenanthroimidazole derivatives are promising as emitters and hosts for emissive layers of OLEDs [4].

In this presentation we report on the synthesis and investigation of new donor-acceptor type bipolar, blue-emitting phenanthroimidazole derivatives.

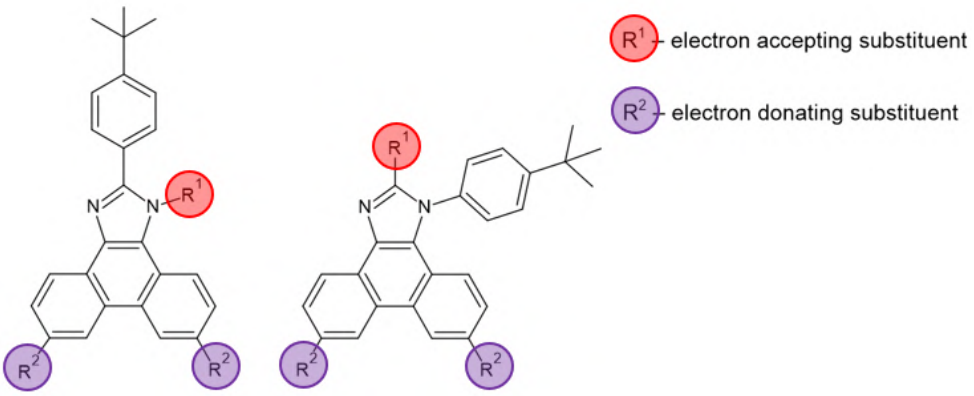


Fig. 1. Structures of phenanthroimidazole-based compounds containing both electron donating and accepting moieties.

The synthesized derivatives were characterized by ^{1}H and ^{13}C NMR, IR spectroscopy, mass spectrometry. The thermal, optical, photophysical, electrochemical and photoelectrical properties of the materials will be presented.

Acknowledgement. This project has received funding from the Research Council of Lithuania (LMT), project Nr. 09.3.3.-LMT-K-712-25-0025.

[1] H. Chen, J. Lee, B. Lin, S. Chen, S. Wu, Liquid crystal display and organic light-emitting diode display: present status and future perspective, Light: Science & Applications, Vol. 7, 17168, 2047-7538/18 (2018), doi: 10.1038/lsa.2017.168.

[2] M. J. A. Talite, H. T. Lin, Z. C. Jiang, T. N. Lin, H. Y. Huang, E. Heredia, A. Flores, Y. C. Chao, J. L. Shen, C. A. J. Lin, Solid-state, ambient-operation thermally activated delayed fluorescence from flexible, non-toxic gold-nanocluster thin films: towards the development of biocompatible light-emitting devices, Nanotechnology, 27, 345701 (2016), doi: 0.1088/0957-4484/27/34/345701.

[3] K. Yamaguchi, T. Matsushima, A. S. D. Sandanayaka, Y. Homma, N. Uchida, C. Adachi, Enhanced Operational Durability of Thermally Activated Delayed Fluorescence-Based Organic Light-Emitting Diodes with a Triazine Electron Transporter, Chemistry Europe, 26, 5598–5602 (2020), doi: 10.1002/chem.201905345.

[4] S. Ye, S. Zhuang, B. Pan, R. Guo, L. Wang, Imidazole derivatives for efficient organic light-emitting diodes, Journal of Information Display, Vol. 21, No. 3, 173–196 (2020), doi: 10.1080/15980316.2020.1802357.

ADJUSTING ELECTROLYTE FOR HYDROGEN EVOLUTION SUPPRESSION IN NA-ION AQUEOUS BATTERIES

Nadežda Traškina[1], Jurgis Pilipavičius[1], Jurga Juodkazytė[1], Linas Vilčiauskas[1]

[1]Center for Physical Sciences and Technology (FTMC), Saulėtekio al. 3, LT-10257 Vilnius, Lithuania
nadezda.traskina@ftmc.lt

In the era of continuously rising demand for large-scale energy storage systems the scientific attention has shifted to safer and cheaper alternatives to Li-ion batteries – rechargeable aqueous batteries. [1] Na-ion aqueous batteries, despite their environmental benignity and compatibility with highly ionically conductive electrolytes, suffer from intrinsically narrow electrochemical stability window (1.23V) limited by both oxygen (OER) and hydrogen (HER) evolution reactions. [2] The latter raises a bigger challenge due to the hydrogen/anode material redox potentials overlapping and results in poor cycling stability. Several strategies have been established in attempt to suppress the undesirable effects of hydrogen evolution. One of them, increasing pH to shift the HER potential, might have a deteriorating effect on most of electrode active materials. [3] Another approach utilizes water-in-salt electrolytes which increase the aqueous electrolyte stability through forming an ion-conducting solid-electrolyte interphase and reducing the overall amount of free water on the electrode. [4] However, there is no reported satisfactory HER inhibition for common non-toxic and cheap salts (perchlorate, nitrate, acetate, sulfate and etc.) which increases battery price, hence, compromises perspectives of stationary applications. A more appealing way to eliminate the unbounded water is by introducing hybrid aqueous/nonaqueous electrolytes, where nonaqueous electrolyte is preferably represented by a highly polar aprotic solvent. [1] DMSO has been reported to prevent water decomposition in aqueous zinc batteries due to strong solvation structure alteration (Fig.1). [5]

The aim of this work is to investigate the effect of the electrolyte composition on HER potential and cycling stability of $NaTi_2(PO_4)_3$ based anodes. The electrolytes were prepared by varying the salt, its concentration, aprotic solvent and its mole fraction in final electrolyte. The HER potential of prepared electrolytes was evaluated by cycling voltammetry (CV). The cycling stability of $NaTi_2(PO_4)_3$ based anodes in those electrolytes was investigated by charge/discharge galvanostatic cycling in three-electrode bottom mount flat sample beaker cells.

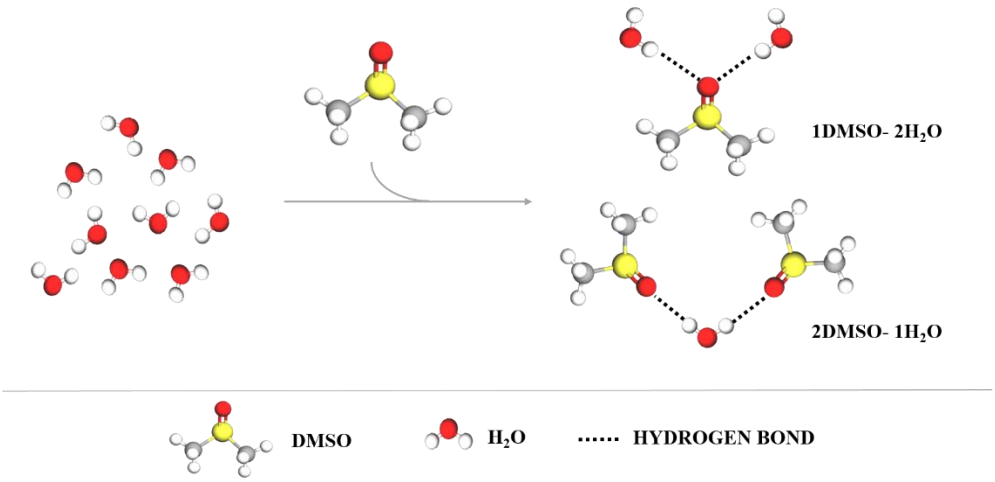


Fig. 1. Hydrogen bonding between water and DMSO molecules.

[1] Q. Nian, X. Zhang, Y. Feng et al., Designing Electrolyte Structure to Suppress Hydrogen Evolution Reaction in Aqueous Batteries, ACS Energy Letters **6 (6),** 2174-2180 (2021).
[2] Liu, Z.; Huang, Y.; Huang, Y.; Yang, Q.; Li, X.; Huang, Z.; Zhi, C. Voltage issue of aqueous rechargeable metal-ion batteries. Chem. Soc. Rev. **49 (1)**, 180−232 (2020).
[3] Luo, J. Y.; Cui, W. J.; He, P.; Xia, Y. Y. Raising the cycling stability of aqueous lithium-ion batteries by eliminating oxygen in the electrolyte. Nat. Chem. **2 (9)**, 760−765 (2010).
[4] Suo, L., Borodin, O., Wang, Y. et l, "Water-in-Salt" Electrolyte Makes Aqueous Sodium-Ion Battery Safe, Green, and Long-Lasting. Adv. Energy Mater. **7, 1701189** (2017)
[5] Cao, L.; Li, D.; Hu, E et al. Solvation Structure Design for Aqueous Zn Metal Batteries. J. Am. Chem. Soc. **142 (51)**, 21404−21409 (2020).

MICROGRANULAR STARCH ACETATES AND CROSS-LINKED STARCH ACETATES FOR ADSORPTION OF ALKYL PARABENS

Karolina Aleknaite, Laura Peciulyte, Deimante Rosliuk, Ramune Rutkaite

Department of Polymer Chemistry and Technology, Kaunas University of Technology, Kaunas, Lithuania
karolina.aleknaite@ktu.edu

Over the past several decades, there is extensive use of cosmetic and personal care products (CPCPs). The occurrence of CPCP residues in domestic sewage, municipal waste water and waste water treatment systems is inevitable. The monitoring results showed their ambient accumulation exhibiting an increasing trend during the past few years. Among the observed constituents of CPCP residuals, parabens are a group of compounds of concern because of their popularity as additives. Due to their potential toxicity and estrogen-mimicking property, the presence of parabens also poses a potential threat to the stability of microbial communities in a biological treatment system as well as in the ecological environment [1]. Hence, there is a need for search for new ways to additionally eliminate those contaminants.

In this study the microgranular starch acetate (SA) and cross-linked starch acetate (CSA) were synthesized and tested as a potential sorbents for removal of alkyl parabens from aqueous medium. Preparation of CSA has been achieved via two - step reaction approach (see Fig. 1). SA microgranules were obtained by reacting potato starch granules with acetic anhydride using aqueous NaOH solution as a catalyst and further cross-linked with epichlorohydrin. Otherwise, starch granules can be first cross-linked with epichlorohydrin and then reacted with acetic anhydride. In both cases the dually-modified starch derivatives with the same degree of substitution of acetyl groups of 0.2 and 0.4 were obtained.

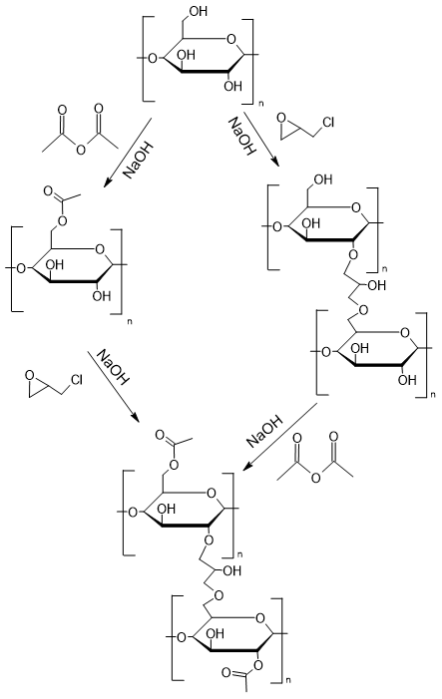


Fig. 1. Synthesis scheme for preparation of SA and CSA

The adsorption of alkyl parabens, namely methylparaben, ethylparaben and propylparaben, on SA and CSA microgranules in water has been investigated by employing the equilibrium adsorption method. It was found that adsorption of parabens on SA and CSA proceeded quickly during the first 10 min. The Langmuir, Freundlich and Dubinin–Radushkevich adsorption models were used to describe the adsorption isotherms and the main parameters of adsorption models such as the Langmuir sorption capacity (Q_L), the Freundlich constant (n_F) and the Dubinin-Radushkevich adsorption energy (E_{DR}) values were calculated and revealed that adsorption occurred due to physical forces.

Acknowledgment. This research was funded by the European Social Fund under the measure No 09.3.3-LMT-K-712 “Development of Competences of Scientists, other Researchers and Students through Practical Research Activities”.

[1] C. Haman et al., Occurrence, fate and behavior of parabens in aquatic environments: A review: Water Research 68, 1-11 (2015)

VISCOSITY VARIATION DURING ADDITION OF POLYLYCOLS TO TRIFUNCTIONAL ISOCYANATE

Paulina Nemaniutė[1], Marijus Jurkūnas, Dalia Bražinskienė, Svajus J. Asadauskas

[1] Department of Chemical Engineering and Technology, FTMC, Vilnius, Lithuania
paulina.nemaniute@ftmc.lt

Polyurethanes (PUR) are among the most widely used polymers due to the versatility of their properties. In order to perform pouring, filling, curing and other manufacturing operations properly, viscosity of the polymer blend has to be carefully controlled, especially when the polymer mixture is being exposed to the new surfaces. It might be expected for the viscosity to increase during polyaddition reaction, but previously, when an ether-ester macrodiol had been mixed with polyglycols and reacted with an isocyanate, a highly unusual drop in viscosity had been observed during early stages of polymerization [1]. In this study, instead of complex mixtures, two simple polyalkylene glycols were investigated for their viscosity variation during the addition reaction with a trifunctional isocyanate. Polyethylene glycol (PEG) of 400 g/mol and polypropylene glycol (PPG) of 2000 g/mol were reacted with a trifunctional adduct of hexamethylene -1,6-diisocyanate (HDI3, CAS 3779-63-3). The isocyanate was used at 1.4 mol excess, therefore HDI3 contents were higher than those of PEG. Before blending, the components were preheated to 50°C and their viscosities measured under different shear rates using Anton Paar MCR 302 rheometer with a concentric cylinder system [1]. Individually, PPG and HDI3 did not show much dependence on shear, recording 102.9, 102.2 and 102.1 mPa·s at 50°C under 1 s^{-1}, 10 s^{-1} and 100 s^{-1} for PPG and 481.9, 481.7 and 481.4 for HDI3 respectively. PEG was thinning much faster with higher shear, resulting in 34.7, 30.2 and 29.5 mPa·s respectively. With both polyglycol and isocyanate preheated separately, they were blended together and the viscosity measurements were started within 1 min. Two mixtures were tested:

- "PPG+HDI3" (containing 78.7% wt. PPG plus 21.3% wt. HDI3), and
- "PEG+HDI3" (containing 42% wt. PEG plus 58% wt. HDI3).

Theoretically, the initial values of the blend viscosity should have been quite similar for both PUR mixtures, assuming semilog dependence between the components and no polymerization, Fig. 1.

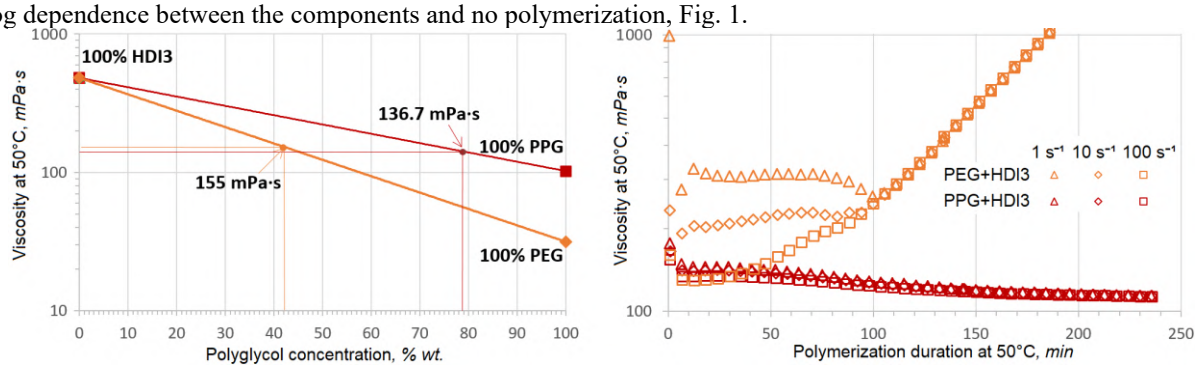


Fig. 1. Theoretically expected viscosities of the initial PUR mixtures at 50°C (left) and experimentally measured viscosities during their polyaddition reaction at 50°C (right)..

Measured initial viscosities under 100 s^{-1} shear rate nearly matched the predicted values. This suggests that semilog relationships might still be valid when predicting viscosities of non-reactive blends. However, viscosities of the PEG mixture appeared highly dependent on shear rate, showing many times higher magnitude than in case of individual components. When comparing the measurements of the same PEG mixture under 1 s^{-1} and 10 s^{-1}, the values barely fit within the same order. In contrast, the PPG mixture did not show much shear thinning. Nevertheless, both mixtures thinned down during early stages of polymerization. PEG mixture eventually rebounded and its viscosity started increasing, while that of PPG mixture did not increase within 4 hrs. This might imply that the PPG polymerization is much slower compared to PEG, in agreement with previous studies [2], but the absence of the viscosity increase alone cannot implicate that PPG doesn't react. With progressing polyaddition viscometric trends eventually become Newtonian-like. However, the initial stages, which often are extremely important during manufacturing, could be very perplexing.

Conclusion. Viscosity variation of polyglycol and isocyanate blends might be highly complex and demonstrate a reduction in viscosity despite ongoing polymerization. The drop in viscosity might be related to a gradual depletion of hydroxyl groups, but more testing is needed to assess this effect.

Acknowledgment. This study was carried out under project TERMINUS, funded by the European Union under Horizon 2020. Call: H2020-NMBP-ST-IND-2018. Grant Agreement: 814400.

[1] P. Nemaniutė, M. Jurkūnas, D. Bražinskienė et al. Viscosity Variation During Addition of Ester and Ether Macrodiols to Isocyanates. Proc. of 22nd Conf. Advanced Materials and Technologies, ISSN 2669-1930, pg 175, Palanga, 26 August 2021

[2] S. Mačiulytė, A. Strakšys, S. Asadauskas, Influence of aliphatic moieties in diisocyanates on chain extension kinetics of adipate macrodiols.. Proc. Baltic Polymer Symp. pg 40, Vilnius (2019) DOI: 10.5281/zenodo.3813463

BINDING OF ASTAXANTHIN TO BOVINE SERUM ALBUMIN AND ITS INFLUENCE ON CAROTENOID TRANSPORT TO ADIPOCYTES – ECD SPECTROSCOPY AND RAMAN IMAGING STUDIES

Joanna Janus[1], Aleksandra Kołodziejczyk[1], Aleksandra Wajda[1], Krzysztof Czamara[2], Agnieszka Kaczor[1]

[1]Faculty of Chemistry, Jagiellonian University, 2 Gronostajowa Str., 30-387 Krakow, Poland
[2]Jagiellonian Centre for Experimental Therapeutics (JCET), Jagiellonian University, 14 Bobrzynskiego Str., 30-348 Krakow, Poland
aleksandra.kolodziejczyk@student.uj.edu.pl, joanna.janus@doctoral.uj.edu.pl

Obesity and obesity-related comorbidities including hypertension, diabetes or cardiovascular diseases pose a significant health problem in developed and developing countries. In obesity, the adipose tissue rapidly expands and its functions become disrupted, leading to inflammation [1]. Carotenoids, such as astaxanthin (AXT), are among natural compounds that show a protective effect against inflammation [2]. AXT is a widespread carotenoid, present especially in many aquatic organisms, such as salmon or shrimps [3]. AXT as a superpotent antioxidant and an anti-inflammatory agent may be an important factor in prevention and treatment of chronic diseases and related conditions [2].

AXT molecule consists of 40 carbon atoms which construct a polyene chain and two terminal ionone rings. The presence of chromophore–conjugated double bonds and two chiral centers gives AXT its distinctive spectroscopic properties and makes it an interesting subject for chiroptical studies [2]. Within the organism AXT is transported in a bound state, forming complexes with plasma proteins [4]. Due to its lipophilic properties, AXT binds to lipid membranes and is stored mainly in lipid droplets of adipocytes [5].

In this work, we use AXT chiral properties to observe changes in the carotenoid structure occurring due to its binding to bovine serum albumin (BSA). ECD spectra of AXT in tetrahydrofuran (THF) and conjugated to BSA in phosphate-buffered saline (PBS) (Fig. 1) show significant changes in AXT structure in the presence of protein.

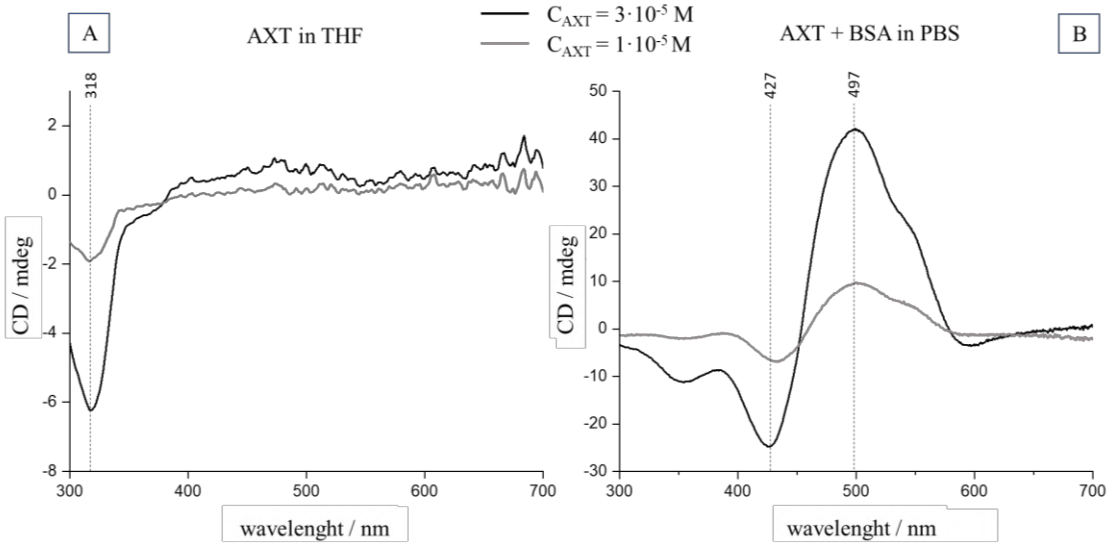


Fig. 1. ECD spectra of AXT in THF (A, **monomer**) and AXT conjugated to BSA in PBS (B, **aggregate**).

The analysis of obtained spectra indicates that AXT binds to BSA forming aggregates, which is visible as an appearance of the exciton couplet in the ECD spectra (Fig.1B). We presume that the binding of astaxanthin to serum protein may facilitate carotenoid transport to adipocytes, which is going to be examined using Raman microscopy.

Keywords: astaxanthin, bovine serum albumin, electronic circular dichroism, Raman imaging, adipocytes

Acknowledgements: This work was supported by the National Science Centre Poland (project no. 2020/37/B/ST4/01168 to A.K.)

[1] G. S. Hotamisligil, Inflammation and metabolic disorders, Nature **444**, 860-867 (2006).
[2] B. Kim, C. Farruggia, C. S. Ku, T. X. Pham, Y. Yang, M. Bae, C. J. Wegner, N. J. Farrel, E. Harness, Y. K. Park, S. I. Koo. J. Y. Lee, Astaxanthin inhibits inflammation and fibrosis in the liver and adipose tissue of mouse models of diet-induced obesity and nonalcoholic steatohepatitis, The Journal of Nutritional Biochemistry **43**, 27-35 (2017).
[3] R. T. Lorenz, G. R. Cysewski, Commercial potential for Haematococcus microalgae as a natural source of astaxanthin, Trends in Biotechnology **18**, 160-167 (2000).
[4] X. Li, G. Wang, D. Chen, Y. Lu, β-carotene and astaxanthin with human and bovine serum albumins, Food Chemistry **179**, 213-221 (2015).
[5] E. Guaranton, C.E. Yazidi, N. Cardinault, M.J. Amiot, P. Borel, J.F. Landrier, Purified low-density lipoprotein and bovine serum albumin efficiency to internalise lycopene into adipocytes, Food and Chemical Toxicology **46,** 3832-3836 (2008)

INFLUENCE OF TEMPERATURE ON FORMATION OF $BiVO_4$ PHOTOANODE

Laura Michailova[1*], Irena Savickaja[2], Vidas Pakštas[2], Jurga Juodkazytė[2], Milda Petrulevičienė[2]

[1] Institute of Chemistry, Faculty of Chemistry and Geosciences, Naugarduko str. 24, LT-03225 Vilnius University, Lithuania

[2] Center for Physical Sciences and Technology, Department of chemical engineering and technology Saulėtekio av. 3, LT-10257 Vilnius, Lithuania

laura.michailova@chgf.stud.vu.lt

Bismuth vanadate ($BiVO_4$) is one of the most promising photoanode materials for photoelectrochemical (PEC) water splitting, production of valuables chemicals and purification of wastewater. In addition to its moderate band gap (2.4-2.6eV) and ability to absorb visible light [1], bismuth vanadate is not toxic and can be formed using various synthesis techniques such as sol-gel, hydrothermal, electrochemical, etc. Synthesis method and conditions play crucial role in the formation of coatings morphology, oxygen vacancies and other defects. $BiVO_4$ suffers from fast charge recombination between excited electron and holes, what leads to decrease of efficiency of PEC systems. Charge recombination could be due to many factors, such as defects, oxygen vacancies, grain boundaries, particle size, etc., therefore careful optimization of synthesis is necessary [2]. In this work bismuth vanadate was synthesized using sol-gel approach and dip-coating technique. We investigated how annealing temperature influences formation and PEC performance of bismuth vanadate. XRD, SEM analysis was used for structure and morphology evaluation, respectively. Photoelectrochemical activity of the coatings was evaluated using cyclic voltammetry (CV), electrochemical impedance spectroscopy (EIS) and Mott-Schottky analysis.

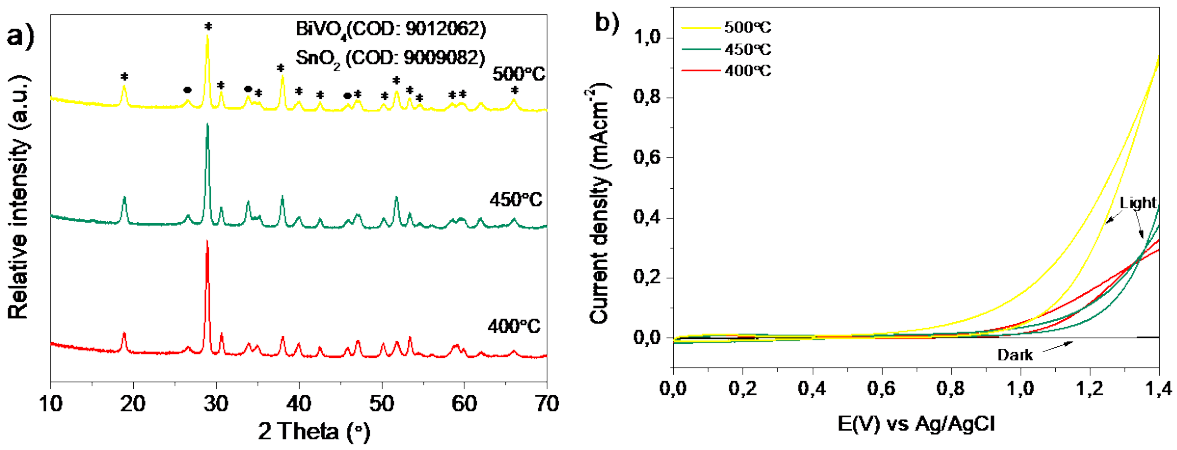


Fig. 1. a) XRD spetra of $BiVO_4$ coatings annealed at different temperatures; b) Cyclic voltammograms of $BiVO_4$ coatings recorded in 0.5 M Na_2SO_4 solution in the dark and under light illumination (100 mW/cm^2); potential scan rate 50 mV/s.

XRD results (Fig. 1a) showed that tetragonal structure of $BiVO_4$ is already formed at 400°C. Values of FWHM (full width at half maximum) of peak at 2Θ=28,9º are very similar for all samples, implying identical crystallinity and similar size of crystallites. SEM analysis showed that different annealing temperature leads to formation of different morphology of coatings. CV results confirmed that annealing temperature has strong influence to photoelectrochemical activity of the films (Fig. 1b). The highest photocurrent (~0.9 mAcm^{-2}) was obtained in the case of coating annealed at 500°C, whereas samples annealed at 400°C and 450°C yielded photocurrent of 0.3-0.4 mA cm^{-2}. EIS investigations and Mott-Schottky analysis were performed for deeper analysis of the synthesized coatings.

[1] D.T.T. Trinh, W. Khanitchaidecha et al., Synthesis, characterization and environmental applications of bismuth vanadate, Research on Chemical Intermediates **45**, 5217–5259 (2019).

[2] K.Karthik, K.R Sunaja Devi et al., Photocatalytic activity of bismuth silicate heterostructures synthesized via surfactant mediated sol-gel method, Materials Science in Semiconductor Processing **102**, 104589 (2019).

Acknowledgment: This research was funded by the M-ERA.NET project "Multiscale computer modelling, synthesis and rational design of photo(electro)catalysts for efficient visible-light-driven seawater splitting" (CatWatSplit), Ref. Number: project8168, under a grant agreement Nr. S-M-ERA.NET-21-3 with the Research Council of Lithuania(LMTLT).

SEASONAL VARIATION OF MICROPLASTIC ABUNDANCE AND CHARACTERISTICS IN SEWAGE SLUDGE

Sonata Pleskytė[1,2], dr. Ieva Uogintė[2]

[1]Department of Analytical and Environmental Chemistry, Vilnius University, Lithuania
[2]Department of Environmental Research, Center For Physical Sciences And Technology, Lithuania
sonata.pleskyte@ftmc.lt

In 1907 the invention of Bakelite brought about a revolution in materials by presenting synthetic plastic into daily life [1]. By the end of the 20th century, plastics had been found to be serious and permanent polluters of many environmental fields: from the highest mountain Everest to the bottom of the ocean Mariana Trench. According to Europe plastic organization data, in 2020 world plastic production reached 367 million metric tons [2]. Pollution by plastic litter has become a global environmental issue and a growing concern for scientists.

Plastics can be described as synthetic material made from a wide range of organic polymers. Microplastic particles (MPs) are defined as plastics with sizes <5 mm. There exist two main types of MPs. Primary is engineered micro-sized plastics while secondary can be generated via the degradation of larger plastic products [3]. MPs pollution characteristics may change according to seasonal variations. The newest research data has suggested that there is a significant difference in MPs abundance during the dry and wet seasons [4]. To better understand the impact of seasonal variation in microplastic characteristics more studies are required.

In 2021 more than 2000 scientific articles have been published on the topic of "Microplastic toxicity". MPs are complex materials containing not only various polymers but also hazardous additives (stabilizers, flame retardants, plasticizers). These chemicals can leach from the MPs surface in the organisms, increasing the potential for toxic or carcinogenic effects: oxidative stress, reduced immune functions, a disorder of reproductive activity, or cancer in marine biota [5]. Moreover, MPs surface morphology may act as a significant vector for toxic organic pollutants such as HCB or DTT, heavy metals, or even pathogens [6].

MPs are widely spread in natural environments, including marine, freshwater, sediment, and terrestrial environments. However, studies on MPs pollution in terrestrial environments are still limited and not fully investigated. There are many different sources of MPs pollution in soils. Major pathways of MPs include agricultural applications (pesticides, organic fertilizers), plastic films, and sewage sludge from wastewater treatment plants (WWTP). There was reported that sewage sludge containing a high amount of MPs may be the cause of negative impact on germination and growth of some floral species [7]. MPs from soils could be transferred to air or water as well as accumulate in soils for decades.

This work presents the identification and characterization of MPs in sewage sludge from the WWTP. The sewage sludge samples were collected in each season. We focused on MPs with sizes <1 mm and analyzed the concentration, classification, and morphological characteristics of MPs obtained from sewage sludge.

Research on microplastic properties in sewage sludge from WWTP emphasizes that more attention should be paid to sludge-based MPs pollution. Sewage sludge analysis could help to minimize pollution sources of MPs and improve our environment.

Acknowledgment: This research is funded by the European Social Fund under the No 09.3.3-LMT-K-712 “Development of Competencies of Scientists, other Researchers, and Students through Practical Research Activities” measure. (Grant No. 09.3.3-LMT-K-712-19-0112).



[1] American Chemical Society National Historic Chemical Landmarks. Bakelite: The World’s First Synthetic Plastic. Internet access: http://www.acs.org/content/acs/en/education/whatischemistry/landmarks/bakelite.html [seen: 2022 – 01 – 14].
[2] Garside M. 2020. Global plastic production 1950-2020, *Statista* [interactive], [seen: 2022-01-14]. Internet access: https://www.statista.com/statistics/282732/global-production-of-plastics-since-1950/.
[3] Shim W.J., Thomposon R.C. 2015. Microplastics in the Ocean, *Archives of Environmental Contamination and Toxicology* 69(3): 265–268. DOI: 10.1007/s00244-015-0216-x.
[4] Wang G., Lu J., Li W., Ning J., Zhou L., Tong Y., Liu Z., Zhou H., Xiayihazi N. 2021. Seasonal variation and risk assessment of microplastics in surface water of the Manas River Basin, China, *Ecotoxicology and Environmental Safety* 208: 111477. DOI: 10.1016/j.ecoenv.2020.111477.
[5] Guzzetti E., Sureda A., Tejada S., Faggio C. 2018. Microplastic in marine organism: Environmental and toxicological effects, *Environmental Toxicology and Pharmacology* 64: 164–171. DOI: 10.1016/j.etap.2018.10.009.
[6] Hahladakis J.N., Velis C.A., Weber R., Iacovidou E., Purnell P. 2018. An overview of chemical additives present in plastics: Migration, release, fate and environmental impact during their use, disposal and recycling, *Journal of Hazardous Materials* 344: 179–199. DOI: 10.1016/j.jhazmat.2017.10.014.
[7] Sol D., Laca Amanda, Laca Adriana, Díaz M. 2020. Approaching the environmental problem of microplastics: Importance of WWTP treatments, *Science of the Total Environment* 740: 140016. DOI: 10.1016/j.scitotenv.2020.140016.

ELECTROCHEMICAL IMAGING OF SACCHAROMYCES CEREVISIAE BY SCANNING ELECTROCHEMICAL MICROSCOPY

Kasparas Kižys[1], Wojciech Nogala[2], Inga Morkvėnaitė-Vilkončienė[1]

[1] Center for Physical Sciences and Technology, Department of Chemical Engineering and Technology, Lithuania
[2] Institute of Physical Chemistry, Polish Academy of Sciences, Poland
kasparas.kizys@ftmc.lt

Scanning electrochemical microscopy (SECM) becomes a popular tool for imaging the redox reactions and determining the reaction rates at the surface of interest using ultramicroelectrode (UME) as a probe [1]. SECM in feedback mode has an advantage, such as higher resolution than other modes. However, the UME at this mode is positioned at a close distance from the surface of interest. Therefore, the sample and/or UME can be damaged. The *Saccharomyces cerevisiae* cells have become an attractive object of research due to the fact that it is relatively easy to grow and handle them [2]. *Saccharomyces cerevisiae* cells are round shaped with a diameter of ~5 µm, while the usually used UME active diameter is 25 µm. Due to the difference in sizes, we can image only a group of these cells [3].

In our study, yeast cells, *Saccharomyces cerevisiae,* were immobilized on the glass surface by poly-L-lysine and then scanned with SECM using ferrocene methanol as a redox mediator. In parallel, optical microscopy was used for electrode aiming during the experiment, and the electrochemical and optical images were obtained.

These results are promising for future visualization of singular yeast cell imaging with smaller electrodes.

[1] A. Ramanavičius, I. Morkvėnaitė-Vilkončienė, A. Kisieliūtė, J. Petronienė, A. Ramanavičienė, Scanning electrochemical microscopy based evaluation of influence of pH on bioelectrochemical activity of yeast cells − Saccharomyces cerevisiae, Colloids and Surfaces B: Biointerfaces **149**, 1-6 (2017).

[2] J. Rožėnė, I. Morkvėnaitė-Vilkončienė, I. Bružaitė, A. Dzedzickis, Arūnas Ramanavičius, Yeast-based microbial biofuel cell mediated by 9,10-phenantrenequinone, Electrochimica Acta **373**, 159-168 (2021).

[3] I. Morkvėnaitė-Vilkončienė, A. Ramanavičienė, A. Ramanavičius, 9,10-Phenanthrenequinone as a redox mediator for the imaging of yeast cells by scanning electrochemical microscopy, Sensors and Actuators, B: Chemical **228**, 200-206 (2016).

POLYDOPAMINE AND POLYPYRROLE APPLICATION IN YEAST BIOFUEL CELLS: A SHORT POLYMER SYNTHESIS FOR BETTER FUNCTION

Viktorija Reinikovaite[1], Eivydas Andriukonis[1,2], Arūnas Ramanavičius[1,2]

[1] Department of Physical Chemistry, Faculty of Chemistry and Geosciences, Vilnius University, Naugarduko st. 24, LT-03225, Vilnius, Lithuania;
[2] Laboratory of Nanotechnology, State Research Institute Center for Physical Sciences and Technology, Sauletekio ave 3, LT-10257 Vilnius, Lithuania;
viktorija.reinikovaite@chgf.stud.vu.lt

In this study, we investigated two conducting polymers (polydopamine (PDA) and polypyrrole (Ppy)) for yeast cell modification to improved charge transfer across yeast cell membrane/wall. This could potentially help to advance the design of yeast-based microbial fuel cells. Modification utilizing Ppy was based on our previous reports [1]. However, concerns in reduced cell viability over 24 hour modification [2] led us to test shorter modification times. Various modification times with PDA were also examined. The modification with PDA was attempted to control by manipulating incubating buffer basicity from pH 5.0 to 7.5 [3]. Chemically formed PDA was optically evaluated by utilizing UV/VIS spectrophotometry and FTIR spectroscopy. For subsequent analysis we constructed a controlled flow-through system with a free flowing yeast cells to imitate a part of simplified commercial microbial fuel cell system. The modified cells with both conducting polymers were evaluated electrochemically by subjecting cells to three electrode flow-through system using amperometry and in two electrode microbial biofuel cell using potentiometry. Yeast cell modifications with both conducting polymers increased charge transfer efficiency from cells towards electrodes. Yeast cells, which undergo rather short incubation in polymerization bulk solutions, generated higher electrical current compared to long modification time and PDA modified cells generated 5 – 6 times more power density.

[1] Andriukonis, E.; Stirke, A.; Garbaras, A.; Mikoliunaite, L.; Ramanaviciene, A.; Remeikis, V.; Thornton, B.; Ramanavicius, A. Yeast-Assisted Synthesis of Polypyrrole: Quantification and Influence on the Mechanical Properties of the Cell Wall. *Colloids Surf. B Biointerfaces* **2018**, *164*, 224–231.

[2] Andriukonis, E.; Ramanaviciene, A.; Ramanavicius, A. Synthesis of Polypyrrole Induced by [Fe(CN)6]3− and Redox Cycling of [Fe(CN)6]4−/[Fe(CN)6]3−. *Polymers* **2018**, *10* (7), 749.

[3] Yang, S. H.; Kang, S. M.; Lee, K.-B.; Chung, T. D.; Lee, H.; Choi, I. S. Mussel-Inspired Encapsulation and Functionalization of Individual Yeast Cells. *J. Am. Chem. Soc.* **2011**, *133* (9), 2795–2797.

INFLUENCE OF SOLVENT POLARITY ON STOBER PARTICLES SIZE

Pavlo Sivolapov[1], Oleksiy Myronyuk[1], Denis Baklan[1], Valentyn Svidersky[1]

[1]Chemical Technology Faculty, National Technical University of Ukraine "Igor Sikorsky Kyiv Polytechnic Institute", Ukraine.

pavlo.sivolapov@gmail.com

One of the current promising surface texture forming materials is nanosized silicon dioxide. An important requirement for the synthesis of SiO_2 particles lays in ensuring uniformity of their sizes [1]. Among the known methods for regulating the size of silica nanoparticles (varying of reagent concentrations or temperature during synthesis), the effect of solvent polarity has been insufficiently studied [2].

The aim of this work is to describe the dependence of the effect of solvent polarity on particle sizes obtained during Stober synthesis.

SiO_2 particles were obtained by Stober synthesis in this research. 1.5 ml of TEOS, 1.7 ml of NH3, 1 ml of deionized water and 50 ml of solvent pair were used for this purpose. After reaction mixture had been held on a magnetic stirrer at 40 °C 1 ml of TEOS was added and the reaction was proceeded for 2 hours. After washing, the resulting system was dried.

The polarity of the solvent was varied by adding miscible liquids with various HSP parameters to the main solvent (isobutanol). The effect of 3 additional solvents was studied: THF (polar), ethyl acetate (polar) and xylene (non-polar). Content of these liquids was 25, 33, 66, 75, 100 wt. % in relation to the amount of alcohol.

It was found, that increase of the co-solvent content led to size growth of nanosilica particles obtained in it (Table 1). Compositions with tetrahydrofuran shows the largest particles of silica (from 470 to 1455 nm) were formed in its presence, regardless of its content. Presence of ethyl acetate provides a similar case, but the particles formed in this system (from 536 to 1413 nm) are slightly inferior in comparison to obtained in THF ones. Adding of 33 wt. % of non-polar xylene to alcohol led to formation of the smallest particles with an average size of 226 nm. At the same time in the presence of 66 wt. % xylene were obtained particles with an average size of 1083 nm, which is the highest value for all studied systems with this content of co-solvent.

Table 1 – minimum, average (mid) and maximum particle sizes of SiO_2

Solvent content, wt. %	Particle size, nm								
	Isobutanol – THF			Isobutanol – Ethyl Acetate			Isobutanol - Xylene		
	min	mid	max	min	mid	max	min	mid	max
25	451	697	1231	368	650	1355	107	271	426
33	323	470	699	354	629	1178	38	226	494
66	545	887	1306	311	547	758	485	1083	1658
75	367	736	1259	339	536	695	-	-	-
100	965	1455	1898	583	1413	2108	-	-	-

Thus, the use of a polar solvent makes it possible to obtain larger particles with a uniform distribution, in contrast to the non-polar one.

[1] P. G. Pramila, M. Jaroniec, Renaissance of Stöber method for synthesis of colloidal particles: New developments and opportunities, Journal of Colloid and Interface Science, 584, 838-865 (2021).

[2] A. Kharchenko, O. Myronyuk, L. Melnyk, P. Sivolapov, Analysis of methods of regulation of silicon dioxide particles size obtained by the Stober method, Technology Audit and Production Reserves, 2(3(40), 9–16 (2017).

CHITOSAN-CLAY-BASED COMPOSITES FOR SORPTION OF Cs, Co, Eu FROM AQUEOUS SOLUTIONS

Karolina Karalevičiūtė[1,2], Galina Lujanienė[2]

[1] Department of Analytical and Environmental Chemistry, Faculty of Chemistry and Geosciences, Vilnius University, Lithuania

[2] Department of Environmental Research, Center for Physical Sciences and Technology, Lithuania

karolina.karaleviciute@chgf.stud.vu.lt

Chitosan is the most widely used biodegradable, environmentally friendly, inexpensive and non-toxic material in nature. Chitosan is a cationic polymer that can be used in wastewater treatment to remove toxic and hazardous pollutants, heavy metals and other contaminants from water. Chitosan with characteristic functional groups such as amino and hydroxyl groups can be used as an adsorbent in water treatment by adsorption [1]. A common method to improve the mechanical and barrier properties of chitosan is to add nano-sized reinforcing elements to the chitosan chains. The use of clay as an adsorbent is due to the peculiarities of its structure and its economic availability and ubiquity [2]. Chitosan-clay composites are a very successful means of removing pollutants from water.
The aim of this study was to synthesise chemically modified chitosan-clay composites and use them for the sorption of Cs^{+}, Co^{2+} and Eu^{3+} from aqueous solutions.

In this study, chitosan powder was dissolved in 100 ml of an aqueous solution of acetic acid (1%, v/v) using a magnetic stirring plate at 90°C and 150 rpm for 1 hour, and the solution was then cooled to room temperature. Chitosan-clay nanocomposites were prepared by mixing chitosan with natural clay of local origin with a particle size of 1-4 µm and two commercially available minerals - montmorillonite K10 and zeolite. The resulting composites were chemically modified in various ways.

The composites obtained were used for the sorption of caesium, cobalt and europium. The adsorption of Cs^{+}, Co^{2+} and Eu^{3+} on the composites was investigated as a function of pH and initial concentration [3].

[1]Ahmad N., Sultana S., Khan M.Z., Sabir S. 2020. Chitosan Based Nanocomposites as Efficient Adsorbents for Water Treatment, Modern Age Waste Water Problems: 69–83. DOI: 10.1007/978-3-030-08283-3_4.

[2] Neji A.B., Jridi M., kchaou H., Nasri M., Dhouib Sahnoun R. 2020. Preparation, characterization, mechanical and barrier properties investigation of chitosan-kaolinite nanocomposite, Polymer Testing 84(October 2019): 106380. DOI: 10.1016/j.polymertesting.2020.106380.

[3] Zhang H., et al. 2021. Sorption behavior of Eu(III) on Tamusu clay under strong ionic strength: Batch experiments and BSE/EDS analysis, Nuclear Engineering and Technology 53(1): 164–171. DOI: 10.1016/j.net.2020.06.009.

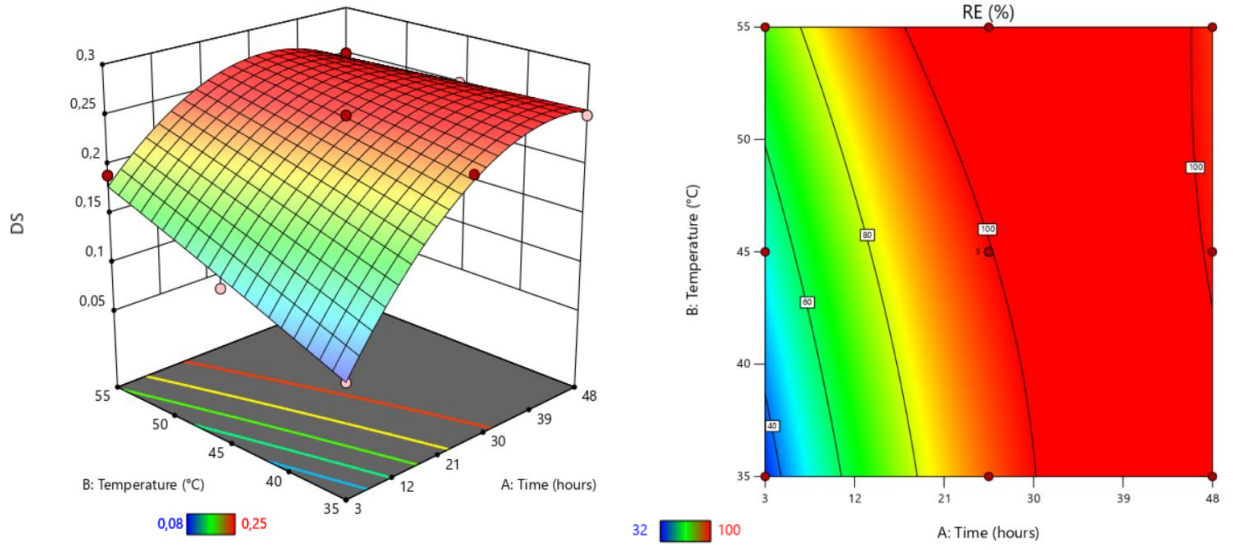
SYNTHESIS AND USE OF CATIONIC POTATO STARCH FLOCCULANTS FOR WASTEWATER SLUDGE SEPARATION

Karolina Almonaityte*, Joana Bendoraitiene, Diana Masiulionyte, Ramune Rutkaite

Department of Polymer Chemistry and Technology, Kaunas University of Technology, Lithuania
** karolina.almonaityte@ktu.lt*

Disposal of sludge produced from municipal wastewaters is an increasingly significant worldwide environmental problem. The materials used to separate the sludge often contaminate the sludge and make its further use more difficult. Coagulation/flocculation has been confirmed as an effective method and applied widely in water and wastewater treatment plants [1]. However, when using large amounts of inorganic coagulants some metals can remain in the treated water, e.g., aluminum, which can cause Alzheimer's disease [2]. Furthermore, synthetic organic flocculants are not biodegradable or degrade slowly, resulting in the formation of toxic degradation products that can cause carcinogenic effects when ingested. For more than half a century, the scientists have been looking for ways to replace synthetic flocculants with biodegradable polymer derivatives that are obtained from renewable resources. Modified starch flocculants could be a suitable alternative to fully or partially replacing synthetic ones. Increasingly, researchers are studying dual systems based on starch derivative flocculants, thus reducing sewage sludge contamination, and improving its continued use as fertilizer and biofuel [3].

The aim of this study was to obtain cationic starches (CS) using CaO in cationization reaction and to evaluate the biodegradability and flocculation properties of CS in sewage sludge separation. CS were obtained by etherification of native potato starch with 3-chloro-2-hydroxypropyl trimethylammonium chloride using NaOH and CaO. The optimization of synthesis conditions to obtain CS derivatives with the best flocculation properties in the model system was conducted with the assistance of the Design Expert 13 software. Analysis of variance (ANOVA) was used in the analysis of the output data. The dependencies of the reaction efficiency (RE) and the degree of substitution (DS) on the reaction temperature and time were evaluated (Fig.1).



a b

Fig. 1. The dependence of the DS of CS (a) and RE (b) on the temperature and duration of the reaction.

Flocculants are used to increase sludge dewatering efficiency. The interaction of flocculant and sludge results in clusters of sludge particles and formation of flakes. Moreover, the dose of flocculant significantly influences the content of dry solids in dewatered sludge. CS derivatives had flocculation properties similar to synthetic flocculants in the separation of sewage sludge as it was revealed by jar test. However, in sedimentation and filtration efficiency studies, dual systems with an anionic synthetic flocculant were used to achieve high efficiency. The sedimentation rate using synthetic flocculant was 148 a.u., meanwhile CS in combination with an anionic flocculant yielded sedimentation rate of 114 a.u.

It was revealed that biodegradable CS derivatives synthesized using CaO can partially replace the synthetic non-biodegradable flocculants, thereby reducing sewage sludge contamination, but they are not inferior to synthetic ones in terms of their efficiency.

[1] H. Wei, B.Q. Gao, J. Ren, A.M. Li, H. Yang. Coagulation/flocculation in dewatering of sludge: a review. Water Res., **143**, 608-631 (2018).
[2] V. Rondeu, D. Commenges, H. Jacqmingadda, J.F. Dartgues Relation between aluminum concentrations in drinking water and Alzheimer's diseases: an 8-year follow-up study Am. J. Epidemiol., **152**, 59-66 (2000).
[3] M. Lapointe, B. Barbeau. Dual starch–polyacrylamide polymer system for improved flocculation. Water Research **124**, 202-209 (2017).

INFLUENCE OF AMINO ACIDS ON THE PROPERTIES OF LIQUID FERTILIZERS

Goda Gudinskaitė, Rasa Šlinkšienė, Rasa Paleckienė

Faculty of Chemical Technology, Kaunas University of Technology, Lithuania
goda.gudinskaite@ktu.lt

Fertilizers are substances that are incorporated into the soil to improve plant growth and development. Fertilizers work in two ways: by supplying the minerals needed by plants and by improving the structure of the soil. Liquid fertilizers are used and produced for primary and secondary fertilization, foliar fertilization, pre - sowing seed treatment [1,2].

Amino acids are efficient in increasing yield and quality. In addition, they are most effectively absorbed through foliage of a plant. The effectiveness of the action of amino acids is observed when they are used prophylactically or to restore a plant after stress factors [3]. The amino acids sprayed on the leaves enter a plant through the leaf buds and enter the nitrogen metabolism cycle. They have a positive effect on respiratory, photosynthetic, circulatory activity and accelerate protein synthesis. One of the functions of proteins is to transfer substances from one tissue to another, therefore fertilizers containing amino acids intensify metabolism and promote plant growth and yield formation, reduce the amount of nitrates in plant production.

A sample of 100 g of liquid fertilizer was produced. The components are mixed, and the temperature is measured and recorded throughout the process. Add accurately weighed copper sulphate (7.48 g) to the calculated volume of water (54.58 g) and stir until all is dissolved. Zinc sulphate (17.94g) is then added. The raw material is granular, large particles of ZnSO4 are difficult to dissolve, so it is grounded before the addition. Stir until everything is dissolved. After an accurately weighed quantity of manganese sulphate (20.0g) is added, the solution becomes cloudy and warm, then it clarifies over time with constant stirring. Particles dissolve slowly and solution warms to 29 ° C. The solution is blue in color with copper sulphate.

Table 1. Physical properties of manufactured liquid fertilizers

Sample No.	pH	Density, g/cm^3	Viscosity , mm^2/s	Crystallization temperature, °C
1	4,5	1,428	5,698	6,45

Attempts were made to add up to 3 percent L - proline to the prepared liquid fertilizers with microelements. Proline contains specially selected amino acids, which promote the formation of rhizomes in plants, participate in the accumulation of nitrogen, stimulate the germination of pollen and seeds, regulate the circulation of water in the plant, so the plants recover more easily during droughts.

Table 2. Physical properties of manufactured liquid fertilizers with the addition of amino acids

Sample No.	Amino acid additive content,%	pH	Density, g/cm^3	Viscosity, mm^2/s	Crystallization temperature, °C
1	0,5	1,9	1,424	5,01	-2,8
	1,0	1,7	1,417	4,48	+3,5
	1,5	1,8	1,416	4,92	+4,3
	2,0	1,6	1,420	5,57	+1,7
	2,5	1,7	1,420	4,97	+3,2
	3,0	1,6	1,419	5,24	+3,6

In conclusions, liquid fertilizers with the addition of amino acids are more acidic, the density and viscosity are reduced. The higher the amino acid content, the lower the pH. The produced liquid fertilizer with the addition of amino acids is stable, there is no sediment, so it can be used to fertilize plants.

[1] A. M. Sviklas, R. Paleckienė, R. Šlinkšienė, Sudėtinės trąšos (2008).
[2] NARIMANI, Hekmat, et al. Study on the effects of foliar spray of micronutrient on yield and yield components of durum wheat. Archives of Applied Science Research, 2010, 2.6: 168-176. 6. MITA (2019).
[3] R. Jonytė, Amino rūgščių ir fitohormonų poveikis augalams.

CHARACTERIZATION OF MN-BASED PHOSPHATE FRAMEWORKS AS AQUEOUS NA-ION BATTERY CATHODES

Davit Tediashvili,[1,2] Linas Vilčiauskas[2]

[1] Institute of Chemistry, Faculty of Chemistry and Geosciences, Vilnius University, Lithuania
[2] Center for Physical Sciences and Technology, Sauletekio al. 3, LT-10257 Vilnius, Lithuania
Davit.Tediashvili@ftmc.lt

Aqueous Na-ion batteries offer one of the viable alternatives for conventional Li-ion batteries, especially when it comes to stationary energy storage. In this field the advantages of Li-ion technologies, such as high power/ energy density are of lesser concern, while the cost and operational safety are of a paramount importance. However, the absence of stable, high-voltage electrode materials remains one of the problems to be solved.

Mn-based materials are considered to be among the most suitable not only due to relative abundance and low cost, but also high voltage and multiple redox states, which could potentially yield high energy density [1]. With a general formula of $Na_3M_2(PO_4)_3$, NASICON-structured materials are exceptional due to their unique framework structure providing fast Na-ion transport and high stability. Despite a few successful reports in organic media, application of these materials in water-based systems is limited due to unfavourable aqueous chemistry [2,3].

Here we report operational and degradation study of $Na_3MnTi(PO_4)_3$ (NMTP), $Na_3MnPO_4CO_3$ (NMCP) and $Na_4Mn_3(PO_4)_2P_2O_7$ (NMPP) in conventional, as well as rotating ring-disc (RRDE) electrochemical set-ups. The results show that the significant part of long-term electrochemical activity and capacity retention of Mn-based materials can be attributed to the formation of new Mn species resulting from the dissolution of original material, observed as a shift of operating potential in conventional cells. RRDE results show capacity fade of the cathode is related to electrochemical, as well as electrochemically-induced chemical dissolution of these materials. Results also indicate that significant amount of manganese is still present on the electrode, however, it becomes electrochemically inaccessible and does not contribute to charge capacity.

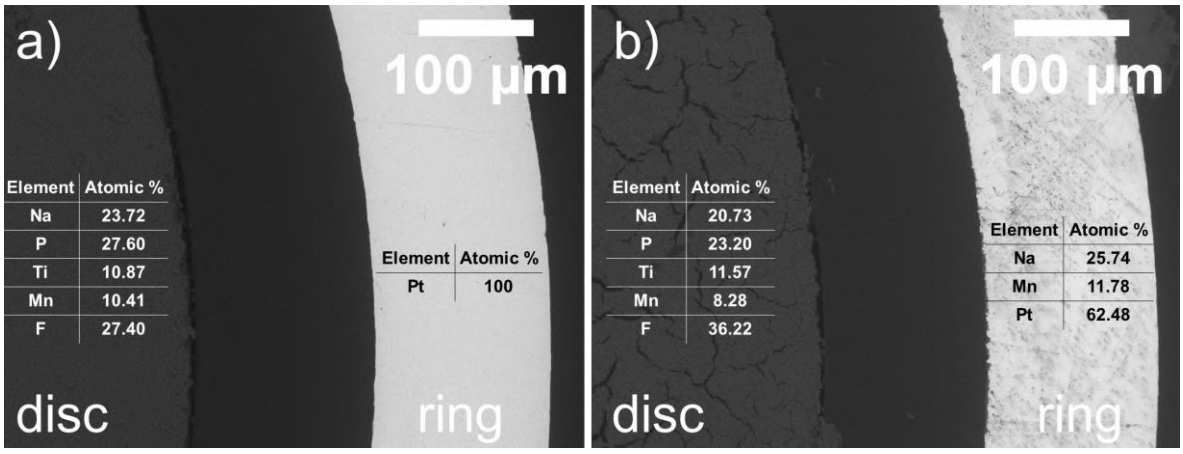


Fig. 1. SEM micrographs of RRDE setup with NMTP (a) before and (b) after cycling. The results of elemental composition analysis are shown on tables

Acknowledgements:

This project has received funding from the European Regional Development Fund (Project No. 01.2.2-LMT-K-718-02-0005) under grant agreement with the Research Council of Lithuania (LMTLT)

[1] Thackeray, M. M. *et al.* The quest for manganese-rich electrodes for lithium batteries: Strategic design and electrochemical behavior. *Sustain. Energy Fuels* **2**, 1375–1397 (2018).
[2] Guo, X. *et al.* Design principles for aqueous Na-ion battery cathodes. *Chem. Mater.* **32**, 6875–6885 (2020).
[3] Gao, H., Li, Y., Park, K. & Goodenough, J. B. Sodium extraction from NASICON-structured Na3MnTi(PO4)3 through Mn(III)/Mn(II) and Mn(IV)/Mn(III) redox couples. *Chem. Mater.* **28**, 6553–6559 (2016).

3D COATED GOLD(NICKEL, MOLYBDENUM)/TITANIUM CATALYST FOR THE GLUCOSE OXIDATION

Augustas Antanaitis, Aldona Balčiūnaitė, Loreta Tamašauskaitė-Tamašiūnaitė, Eugenijus Norkus

Department of Catalysis, Center for Physical Sciences and Technology, Saulėtekio Ave. 3, LT-10257, Vilnius, Lithuania
augustas.antanaitis@stud.vilniustech.lt

With the upcoming energy crisis in today's world, it is in the best interest to develop an alternative, renewable energy source. The glucose oxidation reaction is widely used in fuel cells because it is one of the most abundant clean fuels available from the decomposition of polysaccharides such as starch and cellulose. Also, glucose is a safe, non-toxic energy source with high chemical energy released during oxidation. Noble metals such as Pt and Au can effectively catalyze the oxidation reaction of glucose; however, Pt and Au are very expensive.

The aim of the work was to form a much cheaper and still effective catalyst for glucose oxidation reaction by electroplating 3D structure metal nickel-molybdenum (Ni-Mo) foam on a titanium plate (1 cm^2) and gilding it with a low amount of gold particles. Nickel-molybdenum 3D coatings were made by electrochemical deposition on titanium plate under time and current density conditions of 50 $mAcm^{-2}$ for 3 minutes and 500 $mAcm^{-2}$ for another 3 minutes, from a solution that contained 0.5 M nickel and 0.01 M molybdenum ions. Gold particles were deposited on Ni-Mo foam by immersion of NiMo/Ti electrode into 1 mM $HAuCl_4$ solution for 10 seconds. Coating surface morphology and composition were inspected using scanning electron microscopy, X-ray diffraction, energy-dispersive X-ray spectroscopy, and inductively coupled plasma optical emission spectroscopy. The cyclic voltammetry method was used to compare and evaluate the electrocatalytic activity of prepared electrodes for the glucose oxidation reaction. The cyclic voltammograms were recorded in 0.1 M NaOH and 0.01 M glucose solution in a potential range from -0.9 to 0.7 V vs. Ag/AgCl, at a potential scan rate of 50 mV s^{-1} and temperature of 25 °C. Research showed that the prepared 3D Au(NiMo)/Ti catalysts had higher electrocatalytic activity for glucose oxidation reaction than Ni-Mo foam.

Acknowledgment. This project has received funding from European Social Fund (project No 09.3.3-LMT-K-712-19-0138) under grant agreement with the Research Council of Lithuania (LMTLT).

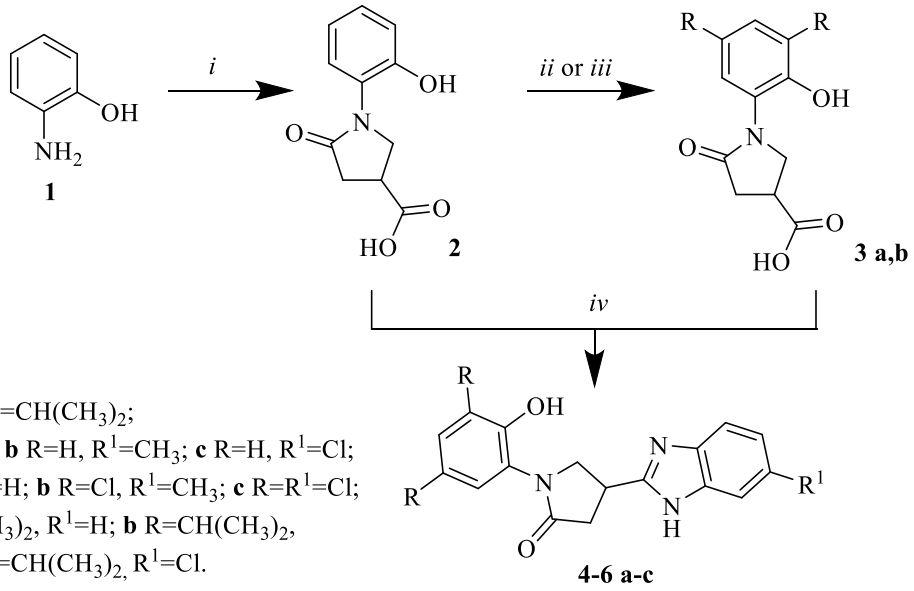
SYNTHESIS OF NEW 1,3-DISUBSTITUTED PYRROLIDINONES WITH BENZIMIDAZOLE MOIETY

Monika Bertašiūtė[1], Vytautas Mickevičius[1]

[1] Department of Organic Chemistry, Kaunas University of Technology, Kaunas, Lithuania
monika.bertasiute@ktu.lt

Interest in the synthesis of biologically active compounds is not diminishing - effective drugs, field plant protection and growth regulators are being sought. Amino acids, their derivatives and cyclization products occupy an important place among these compounds. Some γ-amino acids and their cyclization products - 2-pyrrolidinone derivatives - are used in the treatment of cancer, atherosclerosis, diabetes, and mental disorders [1-3]. Benzimidazoles form an important class of heterocyclic compounds with a wide variety of biological properties. Variously functionalized benzimidazoles have antiparasitic, antimicrobial and anticancer effects. They is also used as a medicine to treat diseases of the gastrointestinal tract [4,5].

The aim of this work is to synthesize compounds containing 2-pyrrolidinone and benzimidazole moieties.



3a R=Cl; **b** R=CH(CH$_3$)$_2$;
4a R=R^1=H; **b** R=H, R^1=CH$_3$; **c** R=H, R^1=Cl;
5a R=Cl, R^1=H; **b** R=Cl, R^1=CH$_3$; **c** R=R^1=Cl;
6a R=CH(CH$_3$)$_2$, R^1=H; **b** R=CH(CH$_3$)$_2$,
R^1=CH$_3$; **c** R=CH(CH$_3$)$_2$, R^1=Cl.

Reaction conditions: *i*) itaconic acid, water, reflux, 3 h; *ii*) 80% sulfuric acid, propan-2-ol, 50°C, 4 h *iii*) 6N HCl, hydrogen peroxide, 1 h *iv)* 6N HCl corresponding to *o*- phenilenediamine, reflux, 20 h.

Fig. 1. Synthesis of 1,3-disubstituted pyrrolidinones 2-6.

1-Substituted pyrrolidine-3-carboxylic acid **2** was synthesized from the reaction of 2-aminophenol **1** and itaconic acid in water at reflux. As an intermediate in this reaction, *N*-substituted *β*,*γ*-amino acid is formed, which is immediately cyclized to pyrrolidine-3-carboxylic acid **2**. Compound **2** was further used for the synthesis of new pyrrolidine-3-carboxylic acids **3 a,b**. Compound **3a** was obtained by chlorinating compound **2** with hydrochloric acid in a presence of hydrogen peroxide, and compound **3b** having **2** isopropyl groups in the aromatic substituent was synthesized by alkylation of compound **2** with 2-propanol in 80% sulfuric acid. In the next step of this work, we synthesized 9 compounds **4−6 a-c** having a benzimidazole moiety in their structure. Reactions were performed by condensing 1-substituted pyrrolidine-3-carboxylic acid **2, 3 a,b** with various *o*-phenylenediamines in 6 N HCl at reflux. The structure of the synthesized compounds was confirmed by microanalysis and NMR spectroscopy data.

[1] Z. Hosseinzadeh, A. Ramazani, K. Hosseinzadeh, N. Razzaghi-Asl, F. Gouranlou, Current Organic Synthesis, **15**, 166 (2018).
[2] R. Thangam, V. Suresh, M. Rajkumar, et al., Phytotherapy Research, **27**, 1664 (2013).
[3] B. Balandis, G. Ivanauskaitė, J. Smirnovienė, K. Kantminienė, D. Matulis, V. Mickevičius, A. Zubrienė, Bioorganic Chemistry, **97**, 103658 (2020).
[4] V. Strelčiūnaitė, K. Anusevičius, I. Tumosienė, J. Šiugzdaitė, I. Jonuškienė, I. Ramanauskaitė, V. Mickevičius, Heterocycles, **92** (2016).
[5] Gopakumar Kavya, Akhil Sivan, Exploring the Versatility of Benzimidazole Scaffolds as Medical Agents: A Brief Update, **3**, 29 (2021).

COPPER NICKEL CATALYSTS MODIFIED WITH GOLD AND PLATINUM NANOPARTICLES FOR DIRECT BOROHYDRIDE FUEL CELLS

Žana Činčienė, Aldona Balčiūnaitė, Loreta Tamašauskaitė-Tamašiūnaitė, Jūratė Vaičiūnienė, Eugenijus Norkus

Department of Catalysis, Center for Physical Sciences and Technology, Sauletekio Ave. 3, LT-10257, Vilnius, Lithuania, zana.cinciene@ftmc.lt

One of the renewable energy sources is fuel cells, which convert chemical energy directly into electricity. When developing new or improving existing fuel cells, much attention is paid to the search for new efficient catalysts that would increase the efficiency of fuel cells and enable the development of new catalyst formation technologies. As is already known, precious metal catalysts such as platinum, gold, and their alloys effectively catalyze the catalytic oxidation of sodium borohydride. Still, the cost of the catalysts is very high and a cheaper alternative is being sought.

This work aims to form efficient and inexpensive nanostructured catalysts and compare their activity with each other. Copper-nickel (Cu-Ni) foams were prepared by electrochemical deposition ($I_{deposition}$=1.5 Acm^{-2}, $t_{deposition}$= 3, 6 and 9 min) on the titanium (Ti) surface. The electrolyte contained 0.5 M Ni^{2+} ions, and 0.01 M Cu^{2+} ions. Cu-Ni foams were additionally decorated with small amounts of gold (AuNPs) and platinum (PtNPs) nanoparticles for electrooxidation of sodium borohydride ($NaBH_4$).

AuNPs and PtNPs were deposited on Cu-Ni foam (noted (Au(Cu-Ni)/Ti and Pt(Cu-Ni)/Ti) by it immersion in 1 mM $HAuCl_4$ or 1 mM H_2PtCl_6 solution at a temperature of 25 ° C for 1 min, respectively. The morphology and composition of the prepared catalysts were investigated using scanning electron microscopy, X-ray diffraction, and inductively coupled plasma optical emission spectroscopy. The electrocatalytic activity of the designed Cu-Ni foams, Au(Cu-Ni)/Ti, and Pt(Cu-Ni)/Ti catalysts was evaluated in terms of borohydride oxidation using cyclic voltammetry by recording cyclic voltammograms in a 0.05 M $NaBH_4$ solution in an alkaline medium in the potential range from -1.2 to 0.6 V vs. Ag/AgCl at an electrode potential scan rate of 10 mV s^{-1}.

The study showed that the prepared Au(Cu-Ni)/Ti and Pt(Cu-Ni)/Ti catalysts exhibit a higher electroactivity for borohydride oxidation in an alkaline medium than pure 3D metal Cu-Ni foam.

Acknowledgment. This project has received funding from European Social Fund (project No 09.3.3-LMT-K-712-19-0138) under grant agreement with the Research Council of Lithuania (LMTLT).

SOLID SOLUTION FORMATION AMONG METHYL 4-HALOGENBENZOATE DERIVATIVES - EXPERIMENTAL AND COMPUTATIONAL INVESTIGATION

Kristaps Saršūns[a*], Toms Reķis[a], Agris Bērziņš[a]

[a] Faculty of Chemistry, University of Latvia, Jelgavas iela 1, Riga, Latvia
kristaps.sarsuns@lu.lv

Solid solutions (SS) are single multicomponent phases for which the constituent component ratio can vary in continuum. In last decade, research of solid solutions has increased significantly and has become common in crystal engineering. While analysing solid solutions and their molecular packing, more and more attention is paid to structural aspects that promotes and are responsible for the formation of solid solutions in two-component systems. Both geometric and chemical aspects, such as molecule dimensions, symmetry, and intermolecular interactions, are important in understanding solid state properties of all these phases [1].

Several methyl 4-halogenbenzoates (M4RB) derivatives (Fig. 1) were selected as model compounds because of their chemically similar structures, in which the different atom (R) may not significantly affect the dominant intermolecular interactions [2].

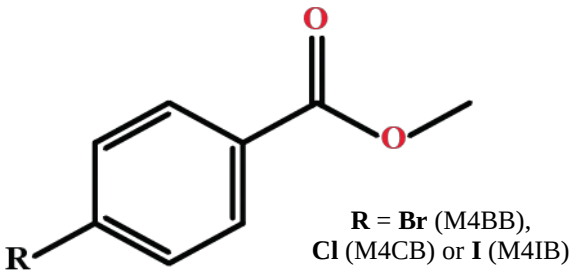


Fig. 1. Molecular structure of methyl 4-halogenbenzoate derivatives.

In this study we explore solid solution formation in methyl 4-halogenbenzoate derivative systems, namely methyl 4-bromobenzoate : methyl 4-chlorobenzoate / methyl 4-iodobenzoate. Solid solutions have been identified and characterized using PXRD and thermal methods of analysis. Their composition limits are summarized in respective phase diagrams, while computational calculations were carried out to identify possible factors which could be used in prediction of the formation of solid solutions between chemically similar molecules [3].

Acknowledgements

This work has been supported by the European Social Fund, project "Strengthening of the capacity of doctoral studies at the University of Latvia within the framework of the new doctoral model", identification No. 8.2.2.0/20/I/006 and University of Latvia foundation through "Mikrotīkls" doctoral scholarship in the field of natural and medical sciences.

[1] Lusi, M. Engineering Crystal Properties through Solid Solutions. *Crystal Growth & Design*, **2018**, *18(6)*, 3704-3712.
[2] Kenry, Chen, C., Liu, B. Enhancing the performance of pure organic room-temperature phosphorescent luminophores. *Nature Communications*, **2019**, *10(1)*, 2111.
[3] C. Gervais, R. F. P. Grimbergen, I. Markovits, G. J. A. Ariaans, B. Kaptein, A. Bruggink, Q. B. Broxterman, *J. Am. Chem. Soc.*, **2004**, *126 (2)*, 655-662.

PHOTOCATALYTIC PROPERTIES OF $Sr_{0.9}La_{0.1}TiO_3$ AND $Sr_{0.25}Ca_{0.25}Na_{0.25}Pr_{0.25}TiO_3$NANO-SIZED POWDERS

Milana Kudus[1], Annu Sharma[2], Nikola Kanas[3], Subramshu Bhattacharya[2], Maria Uzelac[1], Stevan Armaković[1], Sanja J. Armaković[1]

[1] University of Novi Sad, Faculty of Sciences, Novi Sad, Serbia
[2] Nanofunctional Materials Technology Centre, IIT Madras, India
[3]Centre of Sensor Technologies, Institute BioSense, University of Novi Sad, Serbia
kudusmilana17@gmail.com

Water pollution seems to be a significant issue nowadays. Among many different approaches for water purification, photocatalysis (Fig. 1) starts representing a promising chemical waste-water treatment [1]. In this study, $Sr_{0.9}La_{0.1}TiO_3$ and $Sr_{0.25}Ca_{0.25}Na_{0.25}Pr_{0.25}TiO_3$ nano-sized powders were tested as photocatalysts for removing organic pollutants from water. Metoprolol (MET) is a widely used β-blocker that was detected in a surface water of rivers, in a concentration varying from 3 ng/cm^3 to 4.9 μg/cm^3 [2].

Performances of these two photocatalysts were examined for removing MET from the water under simulated Solar irradiation (SSI), UV, and LED irradiation. The concentration of MET was determined by HPLC-DAD analysis [3]. Results show a decrease of MET concentration from water up to 17% and 20% for 240 min under SSI by $Sr_{0.25}Ca_{0.25}Na_{0.25}Pr_{0.25}TiO_3$ and $Sr_{0.9}La_{0.1}TiO_3$, respectively. Improved efficiency of 30% MET removal was achieved by UV irradiation for both photocatalysts.

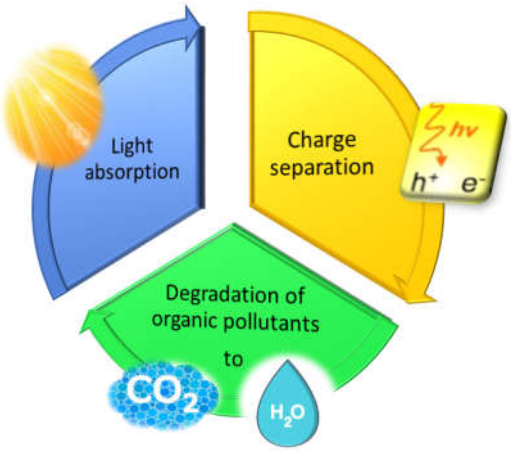


Fig. 1 General process of water purification based on photocatalysis

Chemical Oxygen Demand (COD) test was used to determine the amount of oxygen necessary to oxidize organic matter in samples in which photocatalysis have taken place for 240 min. Comparing the results of HPLC and COD, it was found that the studied materials are highly efficient in removing MET and intermediates formed during the degradation. The high mineralization degree, 27% with $Sr_{0.9}La_{0.1}TiO_3$ and 19% with $Sr_{0.25}Ca_{0.25}Na_{0.25}Pr_{0.25}TiO_3$ under UV light, indicates non-selective efficiency in removing organic pollutants.

All of the obtained results indicate a significant potential for future practical applications.

[1] J. Shi, L. Guo, ABO_3-based photocatalysts for water splitting, Progress in Natural Science: Materials International, **22**, 592-615, (2012).
[2] E-J Van den Brandhof, M. Montforts, Fish embryo toxicity of carbamazepine, diclofenac and metoprolol, Ecotoxicology and Environmental Safety, **73**, 1862-1866, (2010).
[3]S.J. Armaković, M. Grujić-Brojčin, M.Šćepanović et al. Efficiency of La-doped TiO_2 calcined at different temperatures in photocatalytic degradation of β-blockers, Arabian Journal of Chemistry, **12**, 5355-5369, (2019).

.

QUANTIFICATION OF FLAVANONES FROM THE FRESH FRUITS PARTS OF *CITRUS XPARADISI* L USING DIFFERENT EXTRACTION AND HYDROLYSIS METHODS

Jolita Stabrauskienė[1,2], Jurga Bernatonienė[1,2], Mindaugas Marksa[3]

[1]Department of Drug Technology and Social Pharmacy, Lithuanian University of Health Sciences, Lithuania
[2]Institute of Pharmaceutical Technologies, Lithuanian University of Health Sciences, Lithuania
[3]Department of Analytical and Toxicological Chemistry, Lithuanian University of Health Sciences, Lithuania
jolita.stabrauskiene@lsmu.lt

Flavonoids can be found in different chemical forms; one of the essential flavonoid groups in grapefruit (*Citrus xparadisi.* L) flavanones naringin, and his aglycone-naringenin with high biological activity, antioxidants, anti-inflammatory, metabolic diseases, antivirus, neuroprotective, and antitumor effects[1], [2].

The main aim of this study was to obtain the highest yields of naringin and naringenin from fresh grapefruit parts (*albedo*, *flavedo*, and *segment epidermis*) through various extraction and hydrolysis methods.

The grapefruit were collected from the local market. Fruit parts were separated into *flavedo*, *albedo*, and *segmental parts*, then fragmented and frozen in a freezer (18 ± 0,9 °C) until extracted. Flavanones were extracted at ratio 1:10 with solvent 50 and 70% ethanol (v/v) using different methods: Ultrasound-Assisted Extraction Bath (UAE)[3], Ultrasound-Assisted Extraction using an ultrasonic homogenizer (UAE*), and Heat Reflux Extraction (HRE). UAE was combined with acidic, alkaline, and thermal hydrolysis[4].

The samples were centrifuged for 10 minutes at 4000 rpm. The extracts were filtered through PVDF syringe filters (pore size of 0.22 µm) before HPLC analysis.

After applying different extraction methods, detected that using UAE with optimal conditions (processing time of 20 min, ethanol 70% (v/v), t°-50°C) obtained the highest extraction of naringin in a sample from the *albedo* part (17,39 ± 0,87 mg/g). The HR extraction increases naringenin by two times more from the *albedo* (UAE naringenin 4,63 ± 0,23 µg/g; HR naringenin 12,6 ± 0,63 µg/5) and shows better results from the *segmental part* (UAE naringenin- not found; HR naringenin 35,80 ± 1,79 µg/g; UAE* naringenin 7,40 ± 0,37 µg/g).

However, when compared to UAE without hydrolysis and UAE combined with an acid, alkaline, and thermal hydrolysis, the use of thermal hydrolysis from the *albedo* part increased naringin from (17,45 ± 0,87 mg/g to 25,05 ± 1,25 mg/g) and in *segmental* part, from 5,26 ± 0,708 mg/g to 11,07 ± 1,25 mg/g. Meanwhile, acidic and thermal hydrolysis have significantly increased naringenin from the *segmental* part (UAE- not found; alkaline-not found; acidic 1,12 ± 0,056 µg/g; thermal 4,21 ± 0,21µg/g). Therefore, the UAE method with thermal hydrolysis shows better results for naringin and naringenin extraction from the *albedo* and *segmental* parts compared to all hydrolysis methods.

[1] D. Barreca *et al.*, "Citrus Flavones: An Update on Sources, Biological Functions, and Health Promoting Properties," *Plants*, vol. 9, no. 3, p. 288, Feb. 2020, doi: 10.3390/plants9030288.

[2] M. A. Alam, N. Subhan, M. M. Rahman, S. J. Uddin, H. M. Reza, and S. D. Sarker, "Effect of Citrus Flavonoids, Naringin and Naringenin, on Metabolic Syndrome and Their Mechanisms of Action," *Advances in Nutrition*, vol. 5, no. 4, pp. 404–417, Jul. 2014, doi: 10.3945/an.113.005603.

[3] M. K. Khan, M. Abert-Vian, A.-S. Fabiano-Tixier, O. Dangles, and F. Chemat, "Ultrasound-assisted extraction of polyphenols (flavanone glycosides) from orange (Citrus sinensis L.) peel," *Food Chemistry*, vol. 119, no. 2, pp. 851–858, Mar. 2010, doi: 10.1016/j.foodchem.2009.08.046.

[4] I. A. Ribeiro, J. Rocha, B. Sepodes, H. Mota-Filipe, and M. H. Ribeiro, "Effect of naringin enzymatic hydrolysis towards naringenin on the anti-inflammatory activity of both compounds," *Journal of Molecular Catalysis B: Enzymatic*, vol. 52–53, pp. 13–18, Jun. 2008, doi: 10.1016/j.molcatb.2007.10.011.

NOTES

NOTES

NOTES

NOTES

NOTES

NOTES

OPEN READINGS 2022 ORGANIZERS

Faculty of Physics

OPTICA Advancing Optics and Photonics Worldwide | STUDENT CHAPTER VILNIUS UNIVERSITY

EPS Young Minds

SPIE. STUDENT CHAPTER VILNIUS UNIVERSITY

CENTER FOR PHYSICAL SCIENCES AND TECHNOLOGY

MAIN SPONSOR

OPTICA Advancing Optics and Photonics Worldwide | Formerly OSA

SPONSORS

LIGHT CONVERSION

EKSPLA

BROLIS

EKSMA OPTICS

Altechna

OPTOMAN IBS HERO

WOP WORKSHOP OF PHOTONICS

TERAVIL

femtika

bioanalizės sistemos

HOLTIDA

OPTOGAMA

MONO SPEKTRA

LIDARIS LIDT Service

BTC ENERGY LT

Cumulatis

TELE2